ICMUSTED

International Conference on Multidisciplinary Sciences and Technological Developments (ICMUSTED 2024)

PROCEEDINGS BOOK

December 13-15, 2024

Erzurum, Türkiye

Supporters

International Conference on Multidisciplinary Sciences and Technological Developments (ICMUSTED 2024)

Onsite – Online (Hybrid) Conference

December 13-15, 2024 | Erzurum, Türkiye

Editor-in-Chief

Yunus Kaya

Editors

Erman Kadir Oztekin

Hamdullah Ozturk

Intan Helina Hasan

Nurhafizah Hasim

Selahattin Kosunalp

Umit Yildirim

Papers reviewed by at least two reviewers presented at the International Conference on Multidisciplinary Sciences and Technological Developments (ICMUSTED 2024) are included in this proceedings book. The full responsibility for all papers presented at ICMUSTED 2024 and published in this proceedings book belongs solely with the respective authors of the papers.

Dear Participants,

We would like to thank all of you for your participation and interest in the International Conference on Multidisciplinary Sciences and Technological Developments (ICMUSTED 2024), which was held as Onsite/Online (Hybrid) in Erzurum, Türkiye on December 13-15, 2024.

ICMUSTED 2024 was organized for the first time this year with the support of Bayburt University (Türkiye) and SMA Customs Consultancy (Türkiye).

The aim of ICMUSTED 2024 is to provide an international forum for researchers, academics, people in industry, and students to consider the latest research results and to present and discuss their ideas, theories, technologies, systems, tools, applications, work in progress. In this regard, participants will experience all theoretical and practical problems and technological developments that arise in multidisciplinary topics.

Onsite and online presentations were made by invited speakers and other participants within the scope of the ICMUSTED 2024. ICMUSTED 2024, where 237 oral presentations prepared by 567 participants from 29 different countries, took place and opened a direction to new cooperation opportunities.

Therefore, we would like to thank Prof. Dr. Mutlu Turkmen (Rector of Bayburt University, Türkiye), the invited speakers and all other participants, the members of the scientific committee, the session chairs, and all those who contributed to make this conference a great success.

Hope to see you at the next ICMUSTED.

Best Regards,

On behalf of the ICMUSTED 2024 Organizing Committe
Organizing Committee Chairman
Assoc. Prof. Dr. Yunus Kaya

COMMITTEES

Organizing Committee

Conference Chairman

Assoc. Prof. Dr. Yunus Kaya, Bayburt University, Türkiye

Members

Prof. Dr. Jorge Montanari, National University of Hurlingham, Argentina

Assoc. Prof. Dr. Selahattin Kosunalp, Bandirma Onyedi Eylul University, Türkiye

Assoc. Prof. Dr. Umit Yildirim, Bayburt University, Türkiye

Asst. Prof. Dr. Erman Kadir Oztekin, Bayburt University, Türkiye

Asst. Prof. Dr. Hamdullah Ozturk, Gaziantep Islam Science and Technology University, Türkiye

Dr. Emine Keles Ozgenc, Trakya University, Türkiye

Dr. Intan Helina Hasan, Universiti Putra Malaysia, Malaysia

Dr. Nurhafizah Hasim, Universiti Teknologi Malaysia, Malaysia

Secretary

Asst. Prof. Dr. Meltem Kizilca Coruh, Ataturk University, Türkiye

Ins. Enes Ozgenc, Trakya University, Türkiye

Scientific Committee

Prof. Dr. Ahmet Cansiz, Istanbul Technical University, Türkiye

Prof. Dr. Alyani Ismail, Universiti Putra Malaysia, Malaysia

Prof. Dr. Devendra Mohan, Guru Jambheshwar University of Science and Technology, India

Prof. Dr. Federico Gobbo, University of Amsterdam, Netherlands

Prof. Dr. Grigor Yordanov Mihaylov, University of Telecommunications and Post, Bulgaria

Prof. Dr. Jorge Montanari, National University of Hurlingham, Argentina

Prof. Dr. Mehmet Ertugrul, Karadeniz Technical University, Türkiye

Prof. Dr. Mohd Nizar Hamidon, Universiti Putra Malaysia, Malaysia

Prof. Dr. Teodor Iliev, University of Ruse "Angel Kanchev", Bulgaria

Prof. Dr. Ugur Cem Hasar, Gaziantep University, Türkiye

Prof. Dr. Zehra Can, Bayburt University, Türkiye

Assoc. Prof. Dr. Adem Korkmaz, Bandirma Onyedi Eylul University, Türkiye

Assoc. Prof. Dr. Bora Goktas, Bayburt University, Türkiye

Assoc. Prof. Dr. Fatih Yilmaz, Bayburt University, Türkiye

Assoc. Prof. Dr. Gokhan Komur, Bayburt University, Türkiye

Assoc. Prof. Dr. Gokhan Ozturk, Ataturk University, Türkiye

Assoc. Prof. Dr. Halim Kovaci, Ataturk University, Türkiye

Assoc. Prof. Dr. Kubilay Demir, AISOFT Software Corporation, Türkiye

Assoc. Prof. Dr. Mustafa Tolga Yurtcan, Ataturk University, Türkiye

Assoc. Prof. Dr. Mourad Hebali, University of Mustapha Stambouli Mascara, Algeria

Assoc. Prof. Dr. Selahattin Kosunalp, Bandirma Onyedi Eylul University, Türkiye

Assoc. Prof. Dr. Umit Yildirim, Bayburt University, Türkiye

Assoc. Prof. Dr. Yunus Kaya, Bayburt University, Türkiye

Assoc. Prof. Dr. Yusuf Esmer, Bayburt University, Türkiye

Asst. Prof. Dr. Erdal Igman, Bayburt University, Türkiye

Asst. Prof. Dr. Erman Kadir Oztekin, Bayburt University, Türkiye

Asst. Prof. Dr. Hamdullah Ozturk, Gaziantep Islam Science and Technology University, Türkiye

Asst. Prof. Dr. Ibrahim Cengiz, Ataturk University, Türkiye

Asst. Prof. Dr. Latif Akcay, Bayburt University, Türkiye

Asst. Prof. Dr. Meltem Kizilca Coruh, Ataturk University, Türkiye

Asst. Prof. Dr. Mustafa Alptekin Engin, Bayburt University, Türkiye

Asst. Prof. Dr. Mustafa Ozdemir, Bayburt University, Türkiye

Asst. Prof. Dr. Ramazan Simsek, Bayburt University, Türkiye

Asst. Prof. Dr. Sebahat Oztekin, Bayburt University, Türkiye

Asst. Prof. Dr. Yahya Yasin Yılmaz, Bayburt University, Türkiye

Asst. Prof. Dr. Zeynep Ozturk, Erzurum Technical University, Türkiye

Dr. Ahmad Marzuki, Sebelas Maret University, Indonesia

Dr. Emine Keles Ozgenc, Trakya University, Türkiye

Dr. Fouzia Benoudjit, M'hamed Bougara University, Algeria

Dr. Hafize Hasar, Gaziantep Directorate of Provincial Agriculture and Forestry, Türkiye

Dr. Intan Helina Hasan, Universiti Putra Malaysia, Malaysia

Dr. Lawal Mohammed Bello, Bayero University Kano, Nigeria

Dr. Maria Natalia Calienni, University of Padova, Italy

Dr. Norhazren Izatie Mohd, Universiti Teknologi Malaysia, Malaysia

Dr. Nurhafizah Hasim, Universiti Teknologi Malaysia, Malaysia

Dr. Paula Lorena Bucci, University of Valladolid, Spain

Dr. Victoria Guglielmotti, Institute of Medical Physics & Max Planck Center for Physics and Medicine - FAU, Germany

TOPICS

Agriculture, Forestry, and Aquaculture

Architecture, Planning, and Design

Education Sciences

Engineering

Fine Arts

Health Sciences

Law

Philology (Language and Literature)

Research & Development and Technological Developments

Science and Mathematics

Social, Humanities, and Administrative Sciences

Sport Sciences

Theology

INVITED SPEAKERS

Prof. Dr. Devendra Mohan

Guru Jambheshwar University of Science and Technology
(Haryana, India)

Professor Dr. Devendra Mohan received his Doctoral degree in Physics from Maharshi Dayanand University Rohtak in year 1991.Presently he is senior most Professor of the Department of Physics at Guru Jambheshwar University of Science & Technology Hisar (Haryana), INDIA-125001. He has served the University in the capacity of varous positions like Chairperson of Department of Physics (November 6, 2004 to January 13, 2006, November 1, 2007 to November 30 2009, December 1, 2012 to November 30,2015), Dean of Faculty of Physical Sciences and Technology (September 1, 2017 to December 31, 2020), Member Finance Committee, Member University Court, Member Academic Council Member Executive Council and Member of Faculty of Physical Sciences, CBLU Bhiwani.

He has been the co-ordinator of varions research projects like from Department of Atomic Energy-Mumbai, Department of Science and Technology-New Delhi, University of Grants Commission- New Delhi and Instrument Research Design and establishment-Dehradun. He received DST Young Scientist award in the form of a project in Year 1992. He has been Associate of International Centre for Theoretical Physics (ICTP), Trieste, Italy from January 1995 to December 1998.

Also, he is active member of Indian Laser Association-Indore and member of Optical Society of India. He has organized a number of National and International symposia/Conferences in the area of Photonics and Materials Science for providing a common platform to the scientists to deliberate their research. More than 25 research students received their PhD under his guidance and around 05 students are still working in his group.

He has Developed e-PG Pathshala Modules for various topics of Physics under UGC initiative particularly Atomic and Molecular Physics, Fiber Optics and Nonlinear Optics. Around 110 research papers in International journal of Repute and monograms for the students.

Prof. Dr. Federico Gobbo

University of Amsterdam (Amsterdam, Netherlands)

Federico Gobbo is full professor at the University of Amsterdam by special appointment in Interlinguistics and Esperanto. He has been Visiting Professor at the University of Turin in Italy and at the Nanjing University in China. He participates in various EU-funded projects (MIME, LITHME, and APPLY). He got his PhD in Computer Science, defended in 2009 at the University of Insubria (Varese-Como, Italy), with a dissertation on constructive adpositional grammars (CxAdGrams). His main research interests are language policy and planning, constructive linguistics, philosophy of ideas.

Dr. Maria Natalia Calienni
University of Padova (Padova, Italy)

Maria Natalia Calienni is an Argentine biotechnologist who earned her PhD in Nanotechnology in 2019 from the University of Quilmes. She is currently a postdoctoral fellow in Professor Pasut's lab at the University of Padova, Italy. Previously, she worked as a researcher affiliated with her country's National Science Council and the University of Hurlingham, Argentina. She has also conducted research stays abroad at the Institute of Biotechnology of the Czech Academy of Sciences and the University Magna Graecia of Catanzaro, Italy. Her research focuses on nanotechnology-based strategies for developing treatments for skin diseases.

Dr. Paula Lorena Bucci
University of Valladolid (Valladolid, Spain)

Paula Lorena Bucci is a scientist specializing in chemical engineering and biotechnology. She holds a Ph.D. in Chemical Engineering from the National University of La Plata in Argentina and a B.Sc. in Biotechnology from the National University of Quilmes. She is currently a Marie Sklodowska-Curie Postdoctoral Research Fellow at the University of Valladolid in Spain.

Her research focuses on the sustainable use of industrial by-products and the development of bioactive compounds for pharmaceutical and cosmetic applications. She has done extensive work on ferulic acid extraction from brewery waste grain and nanoencapsulation for therapeutic uses, especially in skin rejuvenation and anti-inflammatory treatments.

Throughout her career, she has had the opportunity to publish her work in peer-reviewed journals, present at international conferences and collaborate on interdisciplinary projects. Teaching and mentoring are also an important part of her professional journey; she enjoys guiding the scientific development of undergraduate and Ph.D. students. Her ultimate goal is to contribute to innovative and sustainable solutions that improve both human health and environmental protection.

Dr. Ahmad Marzuki

Sebelas Maret University (Kota Surakarta, Indonesia)

Dr. Ahmad Marzuki holds a Bachelor's degree in Theoretical Physics from Diponegoro University, Semarang, Indonesia (1996). He earned his PhD in Optical Materials from the University of Leeds, UK, in 2003, with a thesis on Ion-Exchanged Neodymium-Doped Fluoroaluminate Glasses for Optical Amplification. Currently, Dr. Marzuki serves as a lecturer at Sebelas Maret University, specializing in Optics and Optoelectronics. He is actively involved in the Optics and Photonics Research Group and has contributed to significant research efforts in optical instrumentation, such as fiber-optic sensors for landslide detection and ventilators for COVID-19 patients. His work extends into optical materials, focusing on the synthesis of tellurite and fluoride glasses for laser applications. Dr. Marzuki's research and patents emphasize innovation in optical systems, including devices like landslide early warning systems and tellurite glass compositions for IR laser hosts. Beyond research, he has played a crucial role in organizing multidisciplinary academic events, such as the International Conference on Science and Applied Science. Notable accomplishments include several patents, publications in journals like Materials Research Express and Journal of Luminescence, and awards for innovation and academic leadership. His continued focus on optical technologies underscores his commitment to advancing the field of applied physics and photonics.

Dr. Victoria Guglielmotti

Institute of Medical Physics & Max Planck Center for Physics and Medicine – FAU (Erlangen, Germany)

Victoria Guglielmotti holds a degree in materials engineering from the National University of Mar del Plata in Argentina. She completed her PhD at the University of San Martín in Argentina, with extensive collaborations with the Max Planck Institute for Medical Research in Stuttgart and the Humboldt University of Berlin in Germany. Currently, she is doing a postdoc on the Max Planck Zentrum for Physics and Medicin, in Erlangen, Germany, studing the effects of cellular memory.

ICMUSTED 2024 PROGRAM

Friday, December 13, 2024

Conference Opening

Conference Hall (Necip Fazil Kisakurek Cultural Center, Erzurum)

09:15 – 09:30		Registration and Tea/Coffee Service
09:30 – 11:30	Opening Ceremony	Asst. Prof. Dr. Erman Kadir Oztekin – On Behalf of the Organizing Committee
	Opening Session	Hollow Gaussian Beam and Its Role in Optical Limiting Invited Speaker – Prof. Dr. Devendra Mohan Human-Machine Communication Strategies: The Case of Esperanto Invited Speaker – Prof. Dr. Federico Gobbo Cannabidiol-Loaded Lipid Nanoparticles for the Potential Treatment of Skin Diseases: Design and Characterization Invited Speaker – Dr. Maria Natalia Calienni Brewer's Spent Grain as a Sustainable Source of Ferulic Acid for Cosmetic and Pharmaceutical Innovations Invited Speaker – Dr. Paula Lorena Bucci Highly Transparent Bi_2O_3-PbO Glasses for Gamma Radiation Shielding Applications Invited Speaker – Dr. Ahmad Marzuki Development of Biomimetic Electrodes for Real-Time Monitoring of Cell Adhesion via Electrochemical Impedance Spectroscopy Invited Speaker – Dr. Victoria Guglielmotti

Onsite Session

Conference Hall (Necip Fazil Kisakurek Cultural Center, Erzurum)

	Onsite Session – 1 (in Turkish and English) Head of Session: Asst. Prof. Dr. Erman Kadir Oztekin
11:30 – 12:15	Design of MOF Immobilized Graphene Sponge for Sustainable Water Treatment System Applications *Aysenur Karakas*[*], *Kader Dagci Kiransan*
	Instructors' Opinions on the Use of Balkan Composers' Solo Piano Works in Piano Education *Hamza Serdar Turan*[*], *Sirin Akbulut Demirci*
	A Hybrid Model for Plant Disease Detection Based on Deep Learning *Tolga Aydin*, *Zainab Fadhil Abbas*[*]
	Comparison of Aerodynamic Properties of Three Airfoils Used in Small-Scale Vertical Axis Wind Turbines

	Erman Kadir Oztekin[*], *Elyasa Aydin*
12:15 – 13:30	Lunch (Aksu Cag Kebab)

Online Sessions

Virtual Hall 1

	Online Session – 1 (in Turkish) Head of Session: Assoc. Prof. Dr. Yusuf Esmer
13:30 – 15:00	The Link Between Technological Innovations and Total Quality Management: A Study on Turk Food Industry *Adnan Kara, Yusuf Esmer*[*]
	The Role of Rituals in Social Repair after Natural Disasters *Sonyel Oflazoglu Dora*[*], *Tutku Doksoz*
	Investigation of the Factors Influencing the Disaster Preparedness of Vocational Health Services Students *Sevil Ozcan*[*], *Perihan Ogdum*
	Expression, Alternative Polyadenylation Process and Epigenetic Regulation of MRPS16 Gene in Breast Cancer *Shams Sarimammadli, Tolga Acun*[*]
	Increased Climate Change and Its Effects on Insect Populations *Gokce Ustundag*[*]
	Evaluation of Ecosystem Services Provided by Trees in Edirne Baris Park Using the i-Tree Eco Model *Irem Nur Keles*[*], *Emine Keles Ozgenc*
	Upcycling Aircraft Scrap: Transforming Aviation Heritage into Functional Design *Deniz Ordulu*[*], *Mehmet Kenan Yildirim*
	Analytical Treatments for the Zig-Zag Optical Lattices in Quantum Physics *Bahadir Kopcasiz*[*]
15:00 – 15:15	Break
	Online Session – 2 (in Turkish) Head of Session: Assoc. Prof. Dr. Murat Colak
15:15 – 16:45	Urban Green Infrastructure and Stormwater Management *M. Burak Karakaya*[*], *Zeynep Eren*
	Thermal Kinetic Behaviour of 2-Methyl-1, 3-Dioxoisoindoline-5-Carboxylic Acid *Hatice Bayrakceken*[*], *Ozlem Gundogdu, Nurhan Horasan*
	Design, Prototyping, and Experimental Investigation of a Crash Box with Lattice Geometry *Erman Zurnaci*[*], *Mahmut Can Turk*
	Shunt Reactor Conservator Analysis: Under Full Vacuum and Buckling

	Conditions *Dogan Koyun*[*], *Cagri Aksakal, Ahmet Feyzioglu*
	Evaluating Count Regression Models Under Varying Dispersion: A Simulation Study of Poisson, Negative Binomial, and COM-Poisson Residuals *Sima Atalay*[*], *Hatice Tul Kubra Akdur*
	Investigation of Low Temperature Behaviour of Boron Added Rosin Compound *Merve Gulfer Bozdemir*[*], *Hacer Yesilcicek, Seref Oruc*
	Acetabular Liner Material Selection in Artificial Hip Joints Using Computer Aided Software (CES) Program *Zeynep Gerdan*[*]
	Investigation of the Modification Effect of Solidification Time and Sr Addition in Casting of Al12Si Alloy *Murat Colak*[*]
16:45 – 17:00	Break
— Online Session – 3 (in Turkish) Head of Session: Asst. Prof. Dr. Ramazan Simsek	
	Harmonic Analysis in Power Transformers by Performing Experiments and Using Developed Hybrid Heuristic Algorithms *Mehmet Zile*[*]
	Design and Production of High Mechanical Durability Vacuum Circuit Breaker with Insulation Class up to 36 kV *Arif Ucer, Mehmet Yuksel*[*], *Mustafa Cetin, Ramazan Karaaslan*
	Reduction of DC-Link Capacitor Current by Phase Shifting Method *Deniz Sahin*[*], *Bulent Dag*
17:00 – 18:30	The Influence of Rotor Magnet Height and Stator Position on Acoustic Performance in BLDC Blowers *Ahmet Arif Kose*[*]
	Optimizing Thermal Paste Application for Improved Cost Efficiency and Performance in BLDC Motor Production *Engin Mert Nayir*[*]
	Parametric Design and 3D Production of Door Hinges for Electric Vehicles *Erman Zurnaci*[*], *Ilker Ismail Soran*
	Electric Motor Attachment Point Target Setting for a HVAC *Murat Isik*[*]
	Addressing Acoustic Comfort in Electrified Vehicles: High-Frequency Noise Mitigation in BLDC Motors *Murat Isik*[*]
18:30 – 18:45	Break

Online Session – 4 (in Turkish)
Head of Session: Asst. Prof. Dr. Ramazan Simsek

18:45 – 20:15	Resolving NVH Challenges in BLDC HVAC Systems *Murat Isik*[*]
	In-Depth Analysis of Web and API Vulnerabilities: OWASP Top 10 and Security Strategies *Simge Sengul*[*], *Durmus Ozkan Sahin*
	Impacts of Mining Activities on Ecosystem Services: Environmental and Socioeconomic Perspectives *Enes Ozgenc*[*], *Emine Keles Ozgenc, Gunay Yildiz Tore*
	Criteria Affecting Online Shopping Site Selection and Choosing the Best Alternative *Zeynep Sude Cigdem*[*], *Nagihan Karsli, Emine Dadasoglu, Seyma Emec*
	Ergonomic Problems in the Textile Industry Determining Priorities with Multi-Criteria Decision Making *Zeynep Bora*[*], *Mujde Arslan, Kubra Deniz, Seyma Emec*
	Some Fertility Properties of Soils Due to Good Agricultural Practices *Mustafa Demir*[*], *Erdihan Tunc, Omer Celik, Nevzat Aslan, Hafize Hasar*
	A Study on Dominant Eigenvalues *Ramazan Simsek*[*]

Virtual Hall 2

Online Session – 5 (in English)
Head of Session: Dr. Intan Helina Hasan

13:30 – 15:00	Electronic and Optical Properties of Inorganic Perovskites: A DFT Study for Solar Energy Conversion *Lakhdar Benahmedi*[*], *Anissa Besbes, Radouane Djelti*
	An Optimization of Organic Solar Cell Using SCAPS-1D Simulation Based on Genetic Algorithm *Samia Moulebhar*[*], *Chahrazed Bendenia, Hanaa Merad-Dib, Souhila Bendenia, Sid Ahmed Khantar, Sarra Merabet*
	Enhancing Stability and Thermal Conductivity of Nanofluids: Insights into Advanced Formulations for Energy Systems *Sanae Bayou*[*], *Chouki El moujahid, Tarik Chafil*
	Influence of Connector Forces on the Multi-Directional Configuration of a Hexagonal Modular Floating Structure *Nur Hanani Ahmad Azlan*[*], *Nik Mohd Ridzuan Shaharuddin, Arifah Ali*
	Experimental Study of the Effect of the Rotating Grooved Tube on Adjacent

	Tubes in a Linear Tube Bundle *Ismail Drai*[*], *Tayeb Yahiaoui, Rachid Sahnoun, Habib Merouane, Omar Imine*
	Fractional Brownian Motion-Based Fractal Analysis of EEG Signals for Evaluating Neural Complexity in Alzheimer's Disease *Hadj Abdelkader Benghenia*[*], *Hadj Slimane Zine-Eddine, Hadj Ali Bakir*
	Molecular Structure of Hydroxyapatite bonded PDMS Composite with Enhanced Mechanical Properties – Experimental and Molecular Dynamic Simulation *Chellaiah Ayyanar, Sumit Pramanik*[*]
	Effect of Ground Granulated Blast-Furnace Slag on the Workability of Recycled Self-Compacting Concrete *Boubakeur Asmaa*[*], *Menadi Belkacem*
15:00 – 15:15	Break
Online Session – 6 (in English) Head of Session: Dr. Intan Helina Hasan
15:15 – 16:45	Viable Medical Supply Chains: A Comprehensive Literature Review *Beren Gursoy Yilmaz*[*], *Omer Faruk Yilmaz*
	Robust Optimization Model for Resilient Medical Supply Chain Network Design Under Demand Uncertainty *Omer Faruk Yilmaz, Beren Gursoy Yilmaz*[*]
	Performance Study of the Anode and Cathode Pressure for Fuel Cell System Regulated by PID Conventional and PID Optimized by Intelligent Algorithm Under Variable Load Demand *Sabah Kabache*[*], *Hicham Bouregba*
	Enhanced Fault Detection in Electrical Machines Using Modified Stator Current Signal Analysis *Azeddine Ratni*[*], *Djamel Benazzouz, Mohammed Tsebia*
	Photovoltaic-Hydroelectric-Diesel Power Storage Hybridization System Integrated in Algeria *Lahouasnia Nasreddine*[*]
	The Improvement of Load Unbalance Detection Through Space Vector Transform *Lahouasnia Nasreddine*[*], *Deghboudj Thamir*
	Contribution of Artificial Intelligence to Dynamic Industrial Risk Assessment: Towards Predictive and Secure Management *Imane Aila*[*], *Samia Chettouh, Djamel Haddad*
	Stability Analysis of the Pitch Angle Control Using MPPT of Large Wind Turbines Using Artificial Neuronal Network Controller Strategies *Hicham Bouregba*[*], *Sabah Kabache*
16:45 – 17:00	Break

	Online Session – 7 (in English) Head of Session: Dr. Mohd Hafizuddin Ab Ghani
17:00 – 18:30	Optimization of Drilling Performance in Natural Fiber Composites Using Taguchi and Desirability Function Methods *Mustapha Arslane*[*], *Mohamed Slamani, Abdelmalek Elhadi, Salah Amroune*
	Efficient Drilling Path Optimization in CNC Machining Using Genetic Algorithms and TSP Methodology *Mustapha Arslane*[*], *Mohamed Slamani, Abdelmalek Elhadi, Salah Amroune*
	Parametric Study of a Domestic Solar Water Heating System for Hot Water Supply *Ahmed Remlaoui*[*], *Driss Nehari*
	Study and Analysis of the Efficiency of a Photovoltaic Panel Using Phase Change Material *Taieb Nehari*[*], *Mohamed Serier, Zahra Assala Zehouani, Mohammed Hadjadj, Ahmed Remlaoui*
	Assessing Heat Transfer Efficiency in Building Brick: The Influence of Phase Change Materials and EPS Insulation as Passive Cooling Techniques *Zahra Assala Zehouani*[*], *Taieb Nehari, Mohamed Hadjadj*
	Challenges of Concentrated Solar Power in MENA Region, Case Study: Algeria *Mohamed Teggar*[*]
	Impact of Soil-Structure Interaction on Dynamic Amplification Factor: A Seismic Response Analysis for Multi-Degree-of-Freedom Systems *Leyla Bouaricha*[*]
	Evaluation of Mechanochemical and Thermal Performance of Sisal and Flax Fiber Mat Reinforced Epoxy Based Laminated Hybrid Composites *Ravi Chitra Kishor, Sumit Pramanik*[*]
18:30 – 18:45	Break
	Online Session – 8 (in English) Head of Session: Dr. Nurhafizah Hasim
18:45 – 20:15	Numerical Study of the Diffused Chamber Shapes of Aerostatic Thrust Bearing *Faiza Ghezali*[*]
	Numerical Evaluation of Spanswise Elliptical Film Cooling Hole *Faiza Ghezali*[*]
	Enhanced Photovoltaic Performance through Dual-Absorber Design: A Simulation Study of CIGS/CZTS Solar Cells *Sarra Merabet*[*], *Chahrazed Bendenia, Souhila Bendenia, Hanae Merad, Samia Moulebhar, Sid Ahmed Khantar*
	Finite Element Analysis of the Biomechanical Behavior of a Human Tibia

	Subjected to Mechanical Impact *Hadjer Benamar*[*], *Noureddine Djebbar, Wahid Oudad*
	A Computational Approche of Interface Damage in Biocomposites Based on PLA/Cellulosic Plant Fibers *Bouchra Achour*[*], *Allel Mokaddem, Bendouma Doumi, Abdelkader Ziadi, Lahcen Belarbi, Ahmed Boutaous*
	Chlorine Liquefaction Process at the ADWAN Company, Algeria *Chahrazed Bendenia*[*], *Souhila Bendenia, Hanaa Merad-Dib, Samia Moulebhar, Sarra Merabet, Sid Ahmed Khantar*
	Thermographic Assessment of Materials for Improved Comfort *Ivana Salopek Čubrić, Laure Maurice, Goran Čubrić*[*], *Antonija Petrov*
	Band Gap Alignment Analysis: Comparing the Ginley Method and XPS in ZrO2|V2O5 Type I Junctions *Abdelmounaim Chetoui*[*], *Ilyas Belkhettab, Youcef Messai*

Saturday, December 14, 2024

Online Sessions

Virtual Hall 1

Online Session – 9 (in English) Head of Session: Asst. Prof. Dr. Mustafa Alptekin Engin
09:00 – 10:30	Environmental Challenges and Geochemical Approaches for the Prediction of Mining Waste *Hanae Chat*[*], *Farida Salmoun*
	Design Dual-Band Microstrip Patch Antenna by Using a Rectangular Hole *Hassan Aldeeb*[*]
	Numerical Study of a Compressible Flow in a Convergent-Divergent Transonic Diffuser *Habib Merouane*[*], *Rachid Sahnoun, Ismail Drai*
	Numerical Investigations on the Effect of Isothermal Multi-Jets in Air Curtains with LES Approach *Rachid Sahnoun*[*], *Ismail Drai, Habib Merouane*
	Synthesis and Structural Refinement of Bismuth-Based Pyrochlore Oxides *Rafik El Arslene Dra*[*], *Amira Ghislaine Dra, Lynda Amel Chaabane*
	Evaluation of Structural and Optical Properties of Pristine and Cu-Doped Zno Thin Films *Khemissi Lahouel*[*], *Meriem Gasmi, Abdecharif Boumaza, Abdelkader Djeloul*
	The Influence of Nanofluids (Tio2, Sio2, Tio2/Sio2) on Asphaltenes Precipitation *Billel Zahaf*[*], *Issam Bouyahyaoui*

	Turbulent and Heat Transfer Investigation of Artificially Roughened Solar Air Heater with Curved Absorber Plate *Boucif Zina*[*], *Zerrouki Abdelwahhab, Abdelkader Filali, Ahmed Remlaoui*
10:30 – 10:45	Break
Online Session – 10 (in English) Head of Session: Assoc. Prof. Dr. Selahattin Kosunalp
10:45 – 12:15	Pyrolysis Temperature Effect on the Properties of Polyaniline Based Nitrogen Doped Carbon Supports for PEM Fuel Cells *Emine Oner, Ayse Bayrakceken*[*]
	Co@Pt/C Based Gas Diffusion Electrodes Prepared by Magnetron Sputtering for PEM Fuel Cells *Sonnur Kurtulus, Ayse Bayrakceken*[*]
	Effect of Thermal Treatment on the Electrical and Optical Properties of Al-Doped ZnO Thin Films for Solar Cell Applications *Mahdia Toubane*[*], *Asma Bessaad, Djedjiga Haouanoh, Fayrouz Benhaoua, Razika Tala-Ighil*
	Real-Time in Situ X-Ray Diffraction Analysis of Metal Oxide Nanoparticles: Structural Evolution and Phase Transitions *Abdelmalik Zemieche*[*], *Loubna Chetibi, Djamel Hamana, Slimane Achour*
	Use of Recycled Polyethylene Terephthalate Strips in Soil Improvement *Lina Zaidi*[*], *Fatima Zohra Benamara, Messaouda Bencheikh*
	Comprehensive Examination of the Properties and Applications of Smart Perovskites Materials *Saadiya Benatmane*[*], *Montaha Affane, Sabria Terkhi, Samira Ziane*
	Effect of Physical Treatment of Orange Peel Powder on the Mechanical Properties of Biocomposites Based on Polylactic Acid *Atmane Yahiaoui*[*]
	Prediction of Arias Intensity of Earthquake Acceleration Recorded in Soft Soil Sites *Aouari Issam*[*], *Benahmed Baizid, Rouabeh Aicha*
12:15 – 12:30	Break
Online Session – 11 (in English) Head of Session: Assoc. Prof. Dr. Selahattin Kosunalp
12:30 – 14:00	Impact of Cutting Parameters on Part Surfaces in Machining *Souad Meftah*[*]
	Effect of Durability Indicators of Precast Concrete on Mechanical Behavior in Hot Climate *Ben Ammar Ben Khadda*[*]

	Study of Optical Properties of NiO Thin Films Prepared by Lemon Peel Extracts *Imane Djouabi*[*], *Mahdia Toubane, Nadia Boukherroub*
	Damping Modification Factors Assessment for Displacement and Acceleration Spectra Considering Epicentral Distance and Site Conditions Effects *Abdelhamid Abdelmalek*[*], *Benahmed Baizid*
	Comparative Analysis of the Stability and Seismic Performance of a Reinforced Concrete Structure Using Two Bracing Systems *Bachir Bouderba*[*], *Abdelhamid Abdelmalek*[*]
	Drag Estimation and Validation of a USV Catamaran Hull Using Maxsurf Resistance and Towing Tank Testing *Muhammad Harith Danial Azlan, Nik Mohd Ridzuan Shaharuddin*[*]
	Synthesis and Characterization of Co_3O_4-rGO for Photodegradation of Dyes *Muhammad Saeed*[*], *Asif Nisar*
	Removal of Safranine O by Adsorption Using Commercial Activated Carbon Doped with Fe3O4 Nanoparticles *Asmaa Ouali*[*], *Salima Attouti, Nadia Douara*
14:00 – 14:15	Break
	Online Session – 12 (in English) Head of Session: Dr. Nurhafizah Hasim
14:15 – 15:45	Digital Transformations in the Oil and Gas Industry *Farhad Yusifov*[*]
	Optimizing Renewable Energy Integration in Radial Distribution Systems Considering Uncertainties in Power Generation *Bendriss Badreddine*[*], *Samir Sayah, Abdellatif Hamouda*
	Mitigating Emissions of Ship Exhausts for Maritime Sustainability *Atallah Ghribi, Mohamed Teggar*[*]
	2D Moving Objects Localization in Video Surveillance Based on Fast-ICA Algorithm for Background Subtraction and Local Yezzi Algorithm for Level Sets Models *Abderrahmane Naoum*[*], *Meriem Boumehed, Belal Alshaqaqi, Abdelkrim Meche*
	Analysis of Functionally Graded Materials Plates (FGM-P) Using Refined High Order (RHSDT) *Merdaci Slimane*[*], *Hadj Mostefa Adda, Bouchafa Ali*
	Predictive Modelling of Material Degradation Using Machine Learning *Tomislav Rolich, Ivana Salopek Čubrić*[*]
	Robust EEG Signal Prediction via Advanced Deep Learning and Ensemble Strategies *Mouissat Rabah Abderrahmane, Hakkoum Khaoula Nour El Houda*[*], *Hamza*

	Cherif Lotfi
	Biomechanical Assessment of Caries Effects on Tooth Stability in the Alveolar Bone <u>*Ali Merdji*</u>*, *Laid Aminallah, Ali Benaissa, Noureddine Della, Sandipan Roy*
15:45 – 16:00	Break
Online Session – 13 (in English) Head of Session: Dr. Nurhafizah Hasim
16:00 – 17:30	Therapeutic Potential of *Pistacia Lentiscus* Essential Oil: Antioxidant, Anti-Inflammatory, and Antimicrobial Activities <u>*Fatima Djenad*</u>*, *Sabiha Achat, Sabrina Idir, Yasmine Achat, Tassadit Sahki*
	Exploring the Biocompatibility of *Lepidium Sativum* Seeds Polysaccharide and Its Potential Therapeutic Properties <u>*Yasmine Achat*</u>*, *Khalef Lefsih, Lila Boulekbache, Fatima Djenad, Siham Beddar, Sabrina Idir*
	Anethum Graveolens L. Seeds in Algeria: An Important Source of Bioactives Compounds with Nutritional and Health Significance <u>*Nour El Houda Belabas*</u>*, *Younes Douffa, Nadjat Azzi, Amel Barkat, Haifaa Laroui, Thoraya Guemmaz, Fatima Zerargui, Karima Saffidinne, Abderrahmane Baghiani*
	Inula Viscosa: Total Antioxidant Capacity and Radical Scavenging Activity of Aqueous Extract <u>*Nadjat Azzi*</u>*, *Nour El Houda Belabas, Younes Douffa, Amel Barkat, Haifaa Laroui, Thoraya Guemmaz, Fatima Zerargui, Karima Saffidine, Abderrahmane Baghiani*
	Classification MRI Images of Depressed Subjects Using Artificial Neural Network Classifier <u>*Mansouria Sekkal*</u>*, *Samia Moulebhar*
	Novel Isoxazolines from (E)-α-Atlantone via [3+2] Cycloaddition Reactions: Experimental Insights, Docking Analysis, and Quantum Investigation <u>*Houria Raji*</u>, *Abdellah Zeroual**, *Ahmed Chekroun, Haydar Mohammad-Salim, Asad Syed, Ali H. Bahkali, Jesús Vicente de Julián-Ortiz, Ahmed Benharref*
	Whole Genome Sequencing of a Bacteriocinogenic *Enterococcus Faecium* Strain Isolated from Bottarga: Genomic Traits and Characterization of the Enterocins Clusters <u>*Abdelkader Fathallah*</u>*, *Mohamed Selim Kamoun, Chaima Hkimi, Kais Ghedira, Mohamed Salah Abbassi, Salah Hammami*
	In Vitro Antioxidant Potential of Methanolic and Aqueous Extracts from a *Chenopodiaceae* Family Plant <u>*Khalil Kaouane*</u>*, *Hamza Kemchache, Hanane Khither, Soraya Madoui*

17:30 – 17:45	Break

<table>
<tr><td colspan="2" align="center">Online Session – 14 (in English)
Head of Session: Dr. Nurhafizah Hasim</td></tr>
<tr><td rowspan="8">17:45 – 19:15</td><td>Toxic Plants Used in Folk Medicine and Their Impact on Nutrition and Food Security in Oran, Algeria
<i>Ali Khalfa[*], Fatima Bensalah, Sofiane Bouazza, Mounir Chihab, Farid Bennabi, Walid Khitri</i></td></tr>
<tr><td>Nutritional Strategies for Enhanced Recovery in Burn Patients
<i>Ali Khalfa[*], Fatima Bensalah, Sofiane Bouazza, Mounir Chihab, Farid Bennabi, Walid Khitri</i></td></tr>
<tr><td>Laying Rate and Characteristics of Plymouth Rock Hen Eggs in Oasis Family Farms in the Adrar Region, Southwest Algeria
<i>Abderrahmen Boubekeur[*], Mohammed Souddi</i></td></tr>
<tr><td>Anti-Diabetic Properties of Kombucha Made from Dried Coffee Peel: Flavonoid Content and Inhibitory Activity Against α-Glucosidase
<i>Meysin Anjliany[*]</i></td></tr>
<tr><td>Eco-Friendly Adsorption of Polyphenols from Olive Mill Wastewater Using Biochar Derived from Olive Mill Solid Waste
<i>Kawtar Ezzahi[*], Imad Rabichi, Nabil Rochdi, Rachid Idouhli, Mohamed Hafidi, Abdelaziz Bacaoui, Abdelghani Yaacoubi, Loubna El Fels</i></td></tr>
<tr><td>Optimizing Biochar Preparation for Eco-friendly Adsorption of Polyphenols and Organic Compounds in Pilot-Scale: An Application of Doehlert Designs
<i>Imad Rabichi[*], Kawtar Ezzahi, Chaima Sekkouri, Fatima Ezahra Yaacoubi, Karima Ennaciri, Loubna El Fels, Mohamed Hafidi, Abdelaziz Bacaoui, Abdelrani Yaacoubi</i></td></tr>
<tr><td>Detection of <i>Citrobacter Sp</i> in Tilapia Fish (<i>Oreochromis Sp</i>) and Tank Water and Its Antibiotic Resistance Pattern
<i>Romeissa Derdachi[*], Sabrine Boucetta</i></td></tr>
<tr><td>Priming with Chitosan Nanospheres Encapsulating Magnetite-Gibberellic Acid Elicit Tolerance Against Cadmium Toxicity in Wheat Seedlings
<i>Arruje Hameed[*], Alia Ambreen, Tahir Farooq, Amjad Hameed</i></td></tr>
</table>

19:15 – 19:30	Break

<table>
<tr><td colspan="2" align="center">Online Session – 15 (in English)
Head of Session: Asst. Prof. Dr. Sebahat Oztekin</td></tr>
<tr><td rowspan="2">19:30 – 21:00</td><td>Antibiotic Therapy and Antibiotic Residues Detection in Tilapia Fish <i>Oreochromis Sp</i> (Linnaeus, 1758)
<i>Romeissa Derdachi[*], Sabrine Boucetta</i></td></tr>
<tr><td>Priming with Chitosan Nanospheres Encapsulating Magnetite-Gibberellic Acid Elicit Tolerance Against Cadmium Toxicity in Wheat Seedlings</td></tr>
</table>

	Arruje Hameed[*], *Alia Ambreen, Tahir Farooq, Amjad Hameed*
	Assessment of Physico-Chemical and Biological Parameters in Poultry Manure Composting and the Biodegradation of Antibiotic Residues *Jihane Baghor*[*], *Mohamed Hafidi, Loubna El Fels*
	Valorization of Agricultural Wastes from *Rosa Canina*: Cellulose Extraction and Physico-Chemical Characterization *Fatma Bhiri*[*], *Fatma Kallel, Amir Bouallegue, Samira Abidi, Gmar Bensidhom, Semia Ellouz Chaabouni, Aida Ben Hassen Trabelsi*
	Critical Factors Governing the Activation Process of Olive Residue-Derived Activated Carbons for Enhanced Pollutant Removal *Abdelaziz Ounas, Imad Rabichi*[*], *Zaina Izeghiri, Abdelaziz Bacaoui, Abdelrani Yaacoubi*
	Examining the Impact of Biochar and Irrigation with Treated Wastewater on Soil Physicochemical Characteristics and Plant Growth (*Zea Mays*) *Asma Dahani*[*], *Elmostapha Outamamat, Khalid Oufdou, Mohamed Hafidi, Loubna El Fels*
	Evaluation of Rapid Alert System for Food and Feed (RASFF) Data for Pesticide Residues in Fresh Fruits and Vegetables from Türkiye in 2024 *Sebahat Oztekin*[*]
	Synbiotic Water Kefir Production and Investigation of Certain Quality Parameters *Sebahat Oztekin*[*]

Virtual Hall 2

	Online Session – 16 (in English) Head of Session: Dr. Nurhafizah Hasim
09:00 – 10:30	Effective Corrosion Protection of Aluminium Alloys with Polymeric Material *Meryem Imane Amrane*[*], *Wahiba Amrane, Chaimaa Boucherit*
	Preliminary Evaluation of Local Medicinal Plant Extract from Anacardiaceae Family *Fouzia Benoudjit*[*], *Hania Guechetouli, Lylia Naili*
	Exploring Phenolic Composition and Antioxidant Potential Using Ferric Reducing Power Assay of a Medicinal Plant from Khenchela Region in Crude Extract *Bouaita Rayene*[*], *Djemil Randa, Bouhalit Samira, Boutellaa Saber, Zineb Bouamrane, Teouallbia Youssra*
	Natural Antifungal Cream Based on Garlic Macera *Meryem Allioua*[*], *Ahmed Yacine Mazari, Waffa Bouali*
	Correlation and Agreement Between the Body Mass Index, Waist Circumference, Body Fat Index and Body Fat with the Waistto-Height Ratio in Algeria Adults *Salima Taleb*[*], *Fatma Klaa, Djihad Menia*

	Draft Genome Sequence of *optrA*-Positive *Enterococcus Feacium* Strain Isolated from Turkey in Tunisia: The Resistome, Virulome, and Mobilome *Sana Lengliz*[*], *Hajer Kilani, Faten Ghodhbane-Gtari, Meher Gtari, Mohamed Salah Abbassi*
	Phytochemical Analysis and Antibacterial Activity Assessment of Hydroethanolic Extracts from the Aerial Parts of a Wild Medicinal Plant in the Mila Region *Zineb Bouamrane*[*], *Hakima Belattar, Saber Boutellaa, Mouna Menakh, Nedjla Derbal, Manel Ferkhi, Rayene Bouaita*
	Bioactive Potential of Nettle Aerial Parts: Phenolic Content, Antioxidant Activity, and Anti-inflammatory Properties *Hamza Kemchache*[*], *Khalil Kaouane, Soraya Madoui, Hanane Khither*
10:30 – 10:45	Break
	Online Session – 17 (in English) Head of Session: Dr. Nurhafizah Hasim
10:45 – 12:15	Enhanced Pechini Sol-Gel Synthesis of NiO Nanoparticles Using Eruca Sativa Extract: Photocatalytic and Antibacterial Applications *Hayet Missouni*[*], *Djanette Blizak Meriem, Souheyla Toubal, Imane Djouabi*
	Algerian Lemon Balm: Chemical Composition and Antioxidant Capacity of Hydroethanolic Extract from the Aerial Parts *Nedjla Derbal*[*], *Hakima Belattar, Zineb Bouamrane*
	A Descriptive Study of Pathologically Confirmed Patients with Breast Cancer in the Region of Bejaia, Algeria *Mostaphaoui Yasmine*[*], *Menad Rafik, Moudilou Elara N'tima, Bencharif Chahla*
	Visceral Leishmaniasis and Poverty in the Middle East and North Africa Region *Mohammed-Yassine Takzima*[*], *Mohamed Echchakery, Mohamed Hafidi, Loubna El Fels*
	Phenolic Content and Antioxidant Activity of Ethyl Acetate Extract of *Pistacia Atlantica* Seeds *Younes Douffa*[*], *Nadjat Azzi, Nour El Houda Belabas, Haifaa Laroui, Thoraya Guemmaz, Karima Saffidine, Fatima Zerargui, Abderrahmane Baghiani*
	Phytochemical Analysis, Anti-Inflammatory, and Analgesic Activities of a Cypress Methanolic Extract *Thoraya Guemmaz*[*], *Nour El Houda Belabas, Nadjat Azzi, Younes Douffa, Haifaa Laroui, Fatima Zerargui, Karima Saffidine, Abderrahmane Baghiani*
	Antioxidant Activity of Two Date Fruits Cultivar in First Ripening Stage *Amel Barkat*[*], *Hayat Trabsa, Abderahmane Baghiani, Abdelnacer Agli*
	Impact of Early Maladaptive Schemas on Perceived Stress and Moderating Role of Resilience in Nursing Students *Ilham Rhzali*[*], *Hanane Khalki, Samira Boulbaroud, Fatima-Zahra Azzaoui*

12:15 – 12:30	Break

<table>
<tr><td colspan="2" align="center">Online Session – 18 (in English)
Head of Session: Dr. Nurhafizah Hasim</td></tr>
<tr><td rowspan="8">12:30 – 14:00</td><td>1,3-Dipolar Reaction Study by Means of Density Functional Theory Approaches
<i>Boulanouar Messaoudi</i>[*]</td></tr>
<tr><td>Synthesis, Biological Activity, and Enantioseparation of Iminonaringenine
<i>Mohamed Nadjib Rebizi</i>[*], <i>Salah-Eddin Rahmani</i></td></tr>
<tr><td>Molecular Pharmacology of Anti-Rheumatic Biomolecules: A Review
<i>Sara Ouari</i>[*], <i>Nadia Benzidane, Noureddine Bribi</i></td></tr>
<tr><td>α-Amylase and Antifungal Activity of a Medicinal Plant from Algeria Ammoides
<i>Roumeila Zerrouk</i>[*], <i>Sihem Boudermine, Tarek Boudiar</i></td></tr>
<tr><td>Exploring Arthropods as an α-Chitin and β-Chitin Sources for Circular Economy Applications
<i>Samia Elouali</i>[*], <i>Samira Benali, Jean-Marie Raquez, Mohammed Rhazi</i></td></tr>
<tr><td>Tuning the Plasmonic Properties of Gold Nanoparticles via Nd:YAG Laser Ablation in Liquid for Ethylene Glycol Sensing Application
<i>Latifatul Aisyah Nabila, Nurul Hidayat</i>[*], <i>Ahmad Taufiq</i></td></tr>
<tr><td>An Interior-Point Methods for Linear Complementarity Problem Based on a New Hyperbolic Kernel Function
<i>Youssra Bouhenache</i>[*], <i>Wided Chikouchee</i></td></tr>
<tr><td>Investigation of Structural, Electronic, Magnetic, and Elastic Characteristics of New KTaSn Half-Heusler Compound for Spintronic Devices
<i>Sabir Makhlouf</i>[*], <i>Malika Labidi, Abdelaziz Amara</i></td></tr>
</table>

14:00 – 14:15	Break

<table>
<tr><td colspan="2" align="center">Online Session – 19 (in English)
Head of Session: Asst. Prof. Dr. Mustafa Alptekin Engin</td></tr>
<tr><td rowspan="4">14:15 – 15:45</td><td>Structural and Mechanical Properties of Zinc-Strontium-Lithium Phosphate Glass Doped with Carboxymethyl Cellulose
<i>Siti Norfariza Farhana Binti Mohd Razak, Nur Hazwani Binti Mohd Yusoff, Nurhafizah Binti Hasim</i>[*], <i>Nur Hidayah Binti Ahmad, Norshahirah Binti Mohamad Saidi, Mohd Fuad Bin Mohamad</i></td></tr>
<tr><td>Some Physical Properties of Sn95X5 (X = Zn, Cd, Sb, and Ag) Alloys Rapidly Solidified by Melt Spinning Technique
<i>Teysir Alzamil</i>[*]</td></tr>
<tr><td>The Cauchy Problem of Ostrovsky Equation in Anisotropic Gevrey Spaces
<i>Feriel Boudersa</i>[*], <i>Abdellaziz Mennouni</i></td></tr>
<tr><td>The Combined Effects of Concave-Convex Nonlinearities to a New Class of Fractional Kirchhoff-Schrodinger-Poisson Systems</td></tr>
</table>

	Hamza Boutebba[*]
	Theoretical Study of Legendre Polynomials and Block-Pulse Functions Operational Matrix Algorithm and Its Application to the Stochastic Equation *Sara Youcef Achira*[*]
	Schrodinger Equation Approximate Eigensolutions for the Generalized Cornell Plus Inverse Trigonometric Scarf-Type Potential *Amal Ladjeroud*[*], *Badredine Boudjedaa*
	On the p-Variation and Lax-Friedrichs Scheme *Aimen Daoudi*[*], *Stéphane Junca*
	Global Asymptotic Stability of Nonlinear Difference Equations Using Semi-Cycle Analysis *Seyma Yesilusta*[*]
15:45 – 16:00	Break
Online Session – 20 (in English) Head of Session: Asst. Prof. Dr. Mustafa Alptekin Engin
16:00 – 17:30	Analysis Study of the Polymeric Materials Weldability by Friction Stir Welding Process *El Bahri Ould Chikh*[*], *Abdelnour Zaim, Laid Aminallah*
	Impact of Ground Motion Selection Strategies on the Seismic Response of Reinforced Concrete Structure *Abdelhamid Abdelmalek*[*], *Bouderba Bachir, Benahmed Baizid*
	Hybrid and Floating Photovoltaic Systems: Insights into Efficiency, Challenges, and Future Potential *Zulkifli Mohd Yusop*[*], *Siti Atirah Ibrahim, Muhamad Zalani Daud, Mohd Afifi Jusoh*
	Breast Cancer Detection Using a Hexagonal Slotted Microstrip Patch Antenna with an Electromagnetic Signal *Souheyla Ferouani*[*], *Bouchra Moulfi, Fatima Zahra Moussa, Safaa Moulfi*
	A Frequency-Reconfigurable Pentagonal Microstrip Antenna Array *Khouloud Mohammed Belhadj*[*], *Souheyla Ferouani, Djalal Ziani Kerarti*
	Elliptical Pin Fin Heat Sink: Passive Cooling Control *Fatima Zohra Bakhti*[*], *Mohamed Si-Ameur*
	Experimental Investigation of a High-Order Technique Combined with Electrical Signal Analysis for Fault Detection in Electrical Drives *Azeddine Ratni*[*], *Djamel Benazzouz, Ali Damou, Mohammed Tsebia*
	Nanocrystalline NiO Thin Films: Optical Characteristics *Djanette Meriem Blizak*[*]
17:30 – 17:45	Break

Online Session – 21 (in English) **Head of Session: Asst. Prof. Dr. Mustafa Alptekin Engin**	
17:45 – 19:15	K-Fold Cross-Validation for Enhancing Predictive Accuracy of Gradient Boosting Machine for Blasting Induced Fly Rock *Mohammed Bouhannache*[*], *Hamza Cheniti*
	Prediction of Penetration Resistance for Fine-Grained Soils Using Artificial Neural Networks *Haseeb Ullah Kashif*[*], *Naveed Ahmad*
	Recycling Construction Waste to Obtain a Cellular Insulation Material *Fayrouz Benhaoua*[*], *Djalila Aoufi, Nacira Stiti, Younes Lamri, Abdelouaheb Djeddou, Mahdia Toubane, Razika Tala-Irgil*
	Separation of Benzene – Cyclohexane Mixture Using Intensified Extraction Process by Pyridinium-Based Ionic Liquids *Mohammed Djamel Eddine Allali*[*], *Hassiba Benyounes, Nesrine Amiri*
	Performance Evaluation of PV/Wind/Wave Hybrid System for Green Hydrogen Generation for Kuala Terengganu, Malaysia *Mohd Afifi Jusoh*[*], *Mohd Zamri Ibarahim, Zulkifli Mohd Yusop, Muhamad Zalani Daud, Aliashim Albani, Muhammad Syarifuddin Yahya*
	Nano Terahertz Patch Antenna for Wireless Body Area Network Applications *Bouchra Moulfi*[*], *Souheyla Ferouani, Fatima Zahra Moussa, Safaa Moulfi*
	Slotted Miniature Patch Antenna for Wi-Fi 5 and Wi-Fi 6 Applications *Fatima Zahra Moussa*[*], *Souheyla Ferouani, Bouchra Moulfi*
	Machine Learning Based Weather Type Classification *Mustafa Alptekin Engin*[*], *Latif Akcay*
19:15 – 19:30	Break
Online Session – 22 (in English) **Head of Session: Asst. Prof. Dr. Mustafa Alptekin Engin**	
19:30 – 21:30	A Historiography Study: Sudanese Historians During and After the Anglo-Egyptian *Maab Ahmed*[*]
	The Impact of Digitalization on Business Management: A Case Study of SMEs in Tirana, Albania *Anxhela Bakiasi*[*], *Mariglend Pepmarku*
	Maternal Perceptions of Psychosocial Support and Family Well-Being: Exploring Connections *Nino Kitoshvili*[*]
	Communication in Fashion Media – Analysis and Comparision *Martina Hendija, Ivana Salopek Čubrić*[*]

	Exploring the Relationship Between Organizational Justice and Job Satisfaction: The Case of the Banking Sector in Albania *Petrit Dollani*, Arjola Hoti*
	The Administration's Liability for Errors Committed by Artificial Intelligence *Ahmed Merah**
	The Use of Artificial Intelligence in Teaching German as a Foreign Language: Potencials, Challenges, and Perspectives *Marisa Janku, Daniel Leka**
	Exploring Style: An in-Depth Analysis of Robert Frost's Poem "The Road Not Taken" *Fakiha Arain**
	Doing Applied Linguistics (2011) by Nicholas Groom and Jeannette Littlemore: A Critical Review *Om Kumar*, Shan E. Zehra*
	First-Principles Investigation on the Structural, Optoelectronic, and Photovoltaic Properties of Perovskite Oxide *Rekia Larbi*, Sahnoun Omar, Sahnoun Mohamed*

Sunday, December 15, 2024

Online Sessions

Virtual Hall 1

Online Session – 23 (in English) Head of Session: Asst. Prof. Dr. Latif Akcay	
09:00 – 10:30	Enhancing Self-Cleaning and Optical Properties in Erbium/Neodymium Co-Doped Lithium Niobate Tellurite Glass with Silver Nanoparticles for Laser Host Application *Nurhafizah Hasim**
	A Singular Fractional Elliptic Problem with an Absorption Term *Hanaa Achour*, Sabri Bensid*
	Munckenhoupt Weights and Homogeneous Besov Spaces Associated with No-Negative Self-Adjoint Operators *Romaissa Chichoune**
	Water Balloon Parachute: Synergy Between Generative AI, Design Thinking Process, and Project Based Learning in Physics and Mathematics *Siti Salwa Alias*, Raihanah Maisarah Roslan, Nuramilin Aishah Mohd Roslan, Muhammad Shafiq Izuddin Sazali, Arif Aiman Mohd Zulkarnain, Nor Ezzaty Ahmad, Nor Ain Husein*
	Decay Rate of Timoshenko System with Only Microtemperature Effects and No

	Thermal Diffusivity *Brahim Kilani*[*], *Marwa Boudeliou*
	DFT Computations of Schiff Base Ligand and Its Ni(II) and Cu(II) Complexes *Zakia Messasma*[*]
	Optical Parameter of New Glasses Base Antimony Oxide *Hanane Bouden*[*]
	Plasmonic Optimization of Laser-Ablated Gold Nanoparticles for Ethylene Glycol Detection *Ana Mardiana, Nandang Mufti, Nurul Hidayat*[*]
10:30 – 10:45	Break

Online Session – 24 (in English)
Head of Session: Asst. Prof. Dr. Latif Akcay

	Removal Pharmaceutical Wastewater Using Green Hydrothermal Synthesised Nanostructured Zinc Oxide Photocatalyst *Nur Aqilah Kamaludin, Nur Nabila Abd Aziz, Siti Salwa Alias*[*], *Juan Matmin, Nik Ahmad Nizam Nik Malek*
	Defining Priorities of the Polar Research Institute Using ANP Decision Support Tool *Ozgun Oktar*[*], *Burcu Ozsoy*
	Effect of (Al, Ag, and F) Dopants on Morphological and Electrical Properties of ZnO Thin Films *Djedjiga Haouanoh*[*], *Mahdia Toubane, Razika Tala Ighil*
10:45 – 12:15	Electrical Conductivity Characterization of $Bi_4V_2O_{11}$ Doped with Sulfur Prepared by Hydrothermal Process *Abdelmajid Agnaou*[*], *Wafaa Mhaira, Rachida Essalim, Fabrice Mauvy, Mustapha Zaghrioui, Tatiana Chartier, Maati Alga, Mohamed Zamama, Abdelaziz Ammar*
	High-Sensitivity Surface Plasmon Resonance Based Sensor for HIV Detection *Mohamed Esseddik Ouardi*[*], *Kada Abdelhafid Meradi, Fatima Tayeboun*
	Total Polyphenol Content and Antioxidant Activity of Date Palm Seeds in Adrar Region of Algeria *Omar Fandougouma*[*], *Khadidja Djaafri, Halima Kina*
	Exploring Piperazine Derivatives: Novel Insights and Therapeutic Prospects in Cancer Research *Ikram Bouziane*[*], *Yousra Mdarhri, Fatima Zohra Lenda, Mohamed Chabbi*
	A Novel Corrosion Inhibitor for Carbon Steel Revealed by Gravimetric Analysis *Benhadria Naceur*[*], *Tarik Attar, Abbes Benchadli, Esma Choukchou-Brahama*
12:15 – 12:30	Break

Online Session – 25 (in English)

	Head of Session: Asst. Prof. Dr. Latif Akcay
12:30 – 14:00	Jet-Vortex Above-Bit Arrangement for Drilling Production Wells *Denys Panevnyk*[*]
	Clay-Hydrochar Composites: A Sustainable Material for Solar Photocatalysis of Methylene Blue *Jalila Hanyny*[*], *Zaina Izghri, Abdelrani Yaacoubi, Layla El Gaini, Abdelaziz Bacaoui*
	Design and Characterization of Topical Nanosystems for Photodynamic Therapy *Daniela Maza Vega*[*], *R. Daniel Cacciari, Cristian Lillo, Silvia Del Valle Alonso, María Jimena Prieto, Fernando Alvira, Paula Caregnato, Mónica C. Gonzalez, Jorge Montanari*
	Elaboration and Characterization of PVA-g-PAA Graft Copolymers and PVA-g-PAA/Fe_2O_3: CuO Composites *Radja Megherbi*[*], *Hadjer Addou, Halima Benallou, Amina Arbaoui, Mohamed Karmaoui*
	Luminescence Enhancement in Eu^{3+}, Sm^{3+} Co-Doped $Li_2B_4O_7$ Phosphor *Rekia Belhoucif*[*], *Abdelkader Lalmi Benmaiza, Lyes Benharrat*
	Characterization of Pristine Bismuth Manganite Thin Films Deposited on Glass Substrates by Sol Gel Technique *Ouiza Allouane*[*], *Mahdia Toubane, Ryma Ben-Mammar, Katia Ayouz, Redouane Douali, Nadir Beldjoudi*
	Green Synthesis of Tin Oxide (SnO2) Nanoparticles from Ficus Carica Leaf Extract for Murexide Degradation *Toubal Badreddine*[*]
	Green Synthesis of Zinc Oxide Nanoparticles: An Eco-Friendly Approach *Asma Bessaad*[*], *Bedreddine Toubal, Mahdia Toubane, Kaouther El Kourd*
14:00 – 14:15	Break
	Online Session – 26 (in English) Head of Session: Asst. Prof. Dr. Latif Akcay
14:15 – 15:45	Impact of Different Immobilization Techniques on Probiotic Viability *Tanja Krunic*[*]
	Supported Nickel Catalyst: Exploring Advanced Hybrid Material with Synergistic Properties *Wahiba Amrane*[*], *Mohamed Karmaoui*
	Phenolic Compounds in Solanum Tuberosum Peel and Their Antioxidant Activities and FTIR Spectroscopy *Tassadit Sahki*[*], *Fatiha Brahmi, Fatima Djenad, Yasmine Achat, Lila Makhlouf-Boulekbache, Khodir Madani*

	Investigation of Structural and Optical Characteristics of Fe-Doped ZnO Nanoparticles Co-Precipitation Method *Roguai Sabrina*[*]
	Spray Deposition and Characterization of Cerium Oxide Thin Films as Optically Passive Counter Electrodes for Electrochromic Devices *Abdellatif El-Habib*[*], *Samir Haloui, Abdessamad Aouni, Mustapha Diani, Mohammed Addou*
	Green Synthesis of Magnesium Oxide Nanoparticles: The Influence of Lanthanum and Eucalyptus Extract *Fares Chabira*[*], *Toubane Mahdia, Tala-Ighil Razika, Ismail Pir, Mohamed Bououdina*
	Output Voltage Regulation of an LLC Resonant Inverter Based on Control *Chaimaa Youcef Achira*[*], *M'hamed Helaimi*
	Performance Comparison of RISC-V and TTA Processors for Ascon *Latif Akcay*[*], *Mustafa Alptekin Engin*
15:45 – 16:00	Break
Online Session – 27 (in English) Head of Session: Dr. Nurhafizah Hasim
16:00 – 17:30	Heat Transfer Analysis of Rotating Casson Blood-based Carbon Nanofluid in Channel *Wan Nura'in Nabilah Noranuar, Ahmad Qushairi Mohamad*[*], *Lim Yeou Jiann, Sharidan Shafie*
	Analysing Transmission Dynamics of Chagas Disease with Diapause and Developmental Delays *Manel Sbia*[*], *Tewfik Mahdjoub*
	Superhydrophobic Coating Based on Nanostructured ZnO Thin Films *Zehira Belamri*[*]
	Multiscale Modeling of Structural Stability and Mechanical Properties of $TeAuF_4$ (Te = Na, K, Rb) Materials *Ishak Mebarkia*[*]
	Nanoemulsions: Formulation Strategies and Characterization Techniques *Yousra Mdarhri*[*], *Ikram Bouziane, Mohamed Chabbi*
	Thermal Analysis of Low-Density Polyethylene Composites Reinforced with Copper and Zinc *Mohamed Belhamiani*[*], *Jihad Guendouz, Wahid Oudad*
	Thermal Stress Effects on Structures Repaired with Composite Patches: A Numerical Analysis *Laid Aminallah*[*], *Ali Merdji, El Bahri Ould Chikh, Ismail Drai*

	Advancing Clinical Diagnosis Through High-Resolution Ophthalmic Imaging with Deep Learning Innovations *Rania Saoudi*[*]
17:30 – 17:45	Break
	Online Session – 28 (in English) Head of Session: Asst. Prof. Dr. Sebahat Oztekin
17:45 – 19:45	Combustion Efficiency and Environmental Characteristics of Olive Pomace Fuel Systems *Zaina Izghri*[*], *Imad Rabichi, Jalila Hanyny, Abdelaziz Ounas, Fatima Ezzahra Yaacoubi, Chaima Sekkouri, Karima Ennaciri, Abdelaziz Bacaoui, Abdelrani Yaacoubi*
	Preliminary Observations on the Habitat of Two Mediterranean Endemic Birds in Algeria *Amira Bouderbala*[*], *Mohcen Menaa, Salah Telailia, Lamia Boutabia*
	Insecticidal Potential of Basil Essential Oil (*Ocimum Basilicum* L.) *Nacira Amara*[*], *Sabrina Amara, Souad Touati, Hadjer Guettaf, Ichrak Rahali*
	Exploring the Relationship Between Polyphenol Content and Antioxidant Activity in Mustard Seed and Its By-Products: An in Vitro Study *Siham Beddar*[*], *Hafid Boudries, Meriem Amrane-Abider, Yasmine Achat, Fatima Djenad, Sabrina Idir*
	Curcumin-Based Nanocomposite for the Bioactive Coloration of Cotton *Hassam Mehmood, Arruje Hameed, Tahir Farooq*[*]
	Urban Sustainability Through Vertical Farming: A Review of Techniques and Benefits *Zeenat Khan*[*], *Daud Khan*
	Scale Insects in Orange Orchards of Guelma Province, Algeria: Diversity, Abundance, and Climatic Influences *Omar Khaladi*[*], *Amira Bouderbala*
	Green Synthesis of Silver Nanoparticles Mediated by Essential Oil: Characterization and Antifungal Activity Against Plant Pathogens *Laila Reklaoui*[*], *Abdellatif El-Habib, Samir Haloui, Zine El Abidine Bzazou Elouazzani, Abderazzak Rfaki, Hassan Ghazal, Haiat Essalmani, Said Barrijal*
	Validation of Pandanus *Amaryllifolius* Phytochemicals Compound as Reducing Agent in Green Synthesis of Ag-Doped ZnO by Computational Method *Siti Rashidah Abdol Razid, Siti Salwa Alias*[*], *Juan Matmin, Fazira Ilyana Abdul Razak*
	Production of Vegan and Reduced-Calorie Mayonnaise Using Aquafaba and Pectin Derived from Fruit Waste *Sebahat Oztekin*[*]

* : Corresponding Author

_ : Presenter

Summary of Sessions

Friday, December 13, 2024		
Conference Hall	*Virtual Hall 1*	*Virtual Hall 2*
Opening Session	Online Session – 1	Online Session – 5
Onsite Session – 1	Online Session – 2	Online Session – 6
	Online Session – 3	Online Session – 7
	Online Session – 4	Online Session – 8

Saturday, December 14, 2024	
Virtual Hall 1	*Virtual Hall 2*
Online Session – 9	Online Session – 16
Online Session – 10	Online Session – 17
Online Session – 11	Online Session – 18
Online Session – 12	Online Session – 19
Online Session – 13	Online Session – 20
Online Session – 14	Online Session – 21
Online Session – 15	Online Session – 22

Sunday, December 15, 2024
Virtual Hall 1
Online Session – 23
Online Session – 24
Online Session – 25
Online Session – 26
Online Session – 27
Online Session – 28

CONTENTS

Hollow Gaussian Beam and Its Role in Optical Limiting

Devendra Mohan[1]

[1]Department of Physics, Guru Jambheshwar University of Science and Technology, Hisar 25001, India
Corresponding author: Devendra Mohan (e-mail: vand66@yahoo.com)

Abstract

Hollow Gaussian beams are a distinctive class of laser beams characterized by a ring-shaped intensity profile, with minimal or zero intensity at the center and a peak intensity at a specific radial distance. This unique profile results from tailored beam shaping optics and phase modulation. These beams have significant implications for optical limiting, a process critical for protecting optical systems against high-intensity laser pulses. Their low center intensity reduces the likelihood of nonlinear damage, while the ring-shaped intensity distribution enables uniform interaction with nonlinear optical materials. Such beams are optimized for materials transitioning from linear to nonlinear regimes, such as in nonlinear absorption or scattering processes. Hollow Gaussian beams also mitigate localized heating effects, ensuring better thermal management and enhancing material durability. Furthermore, they allow higher power handling by distributing intensity over a larger area, preventing damage to optical limiters. These attributes make hollow Gaussian beams highly effective in optical limiting applications, particularly in systems requiring enhanced energy distribution and high-power laser handling capabilities.

Keywords: Hollow Gaussian beams, Optical limiting, Nonlinear optics, Thermal management, Beam shaping

Human-Machine Communication Strategies: The Case of Esperanto

Federico Gobbo[1]

[1]Amsterdam Center for Language and Communication, University of Amsterdam, Amsterdam, Netherlands
Corresponding author: Federico Gobbo (e-mail: f.gobbo@uva.nl)

Abstract

Human-machine communication (HMC) is the field investigating the creation of meaning among humans and machines and it challenged anthropocentrism in the studies of communication since its beginning. Moreover, the emergence of generative artificial intelligence (AI) technologies introduced a new dimension of challenges faced by HMC. This talk focuses on the case of Esperanto and its community of practice facing such challenges; in particular, how are Esperantists – i.e., activists or simple enthusiasts of Esperanto – reacting to generative AI technologies, which are fascinating and threatening at the same time. The Esperanto community, although specific in its sociolinguistic characteristics, may be useful to understand the prototypical reactions towards the new challenges of HMC in general, beyond cultural background specifics and local situations.

Keywords: HMC, AI, Generative AI

Cannabidiol-Loaded Lipid Nanoparticles for the Potential Treatment of Skin Diseases: Design and Characterization

Maria Natalia Calienni[1,2,3,4], Magalí Di Meglio[2,3,4], Ana Sanguinetti[2,3,4], Merlina Corleto[3,5], Paulo Maffia[3,5], Jorge Montanari[2,3,4]

[1]Dept. of Pharmaceutical and Pharmacological Sciences, University of Padova, Padova, Italy
[2]Laboratory of Nanosystems for Applications in Biotechnology, National University of Hurlingham, Hurlingham, Argentina
[3]National Council for Scientific and Technical Research (CONICET), Buenos Aires, Argentina
[4]Scientific Research Commission of the Province of Buenos Aires, La Plata, Argentina
[5]Laboratory of Biotechnological Applications and Microbiology, National University of Hurlingham, Hurlingham, Argentina
Corresponding author: Maria Natalia Calienni (e-mail: marianatalia.calienni@unipd.it)

Abstract

Cannabidiol (CBD) has emerged as a potential therapeutic agent for various skin conditions, including bacterial infections and cancer. Despite the availability of CBD-based products on the market, achieving effective delivery of CBD into the deeper layers of the skin remains a challenge, primarily due to the barrier posed by the stratum corneum, the outermost layer of the skin. Additionally, the therapeutic potential of CBD remains underexplored due to two major limitations: its instability and poor water solubility. Consequently, encapsulation within nanoparticulate systems has gained attention as a promising strategy to protect and enhance the efficacy of CBD formulations. The objectives of this work were to formulate CBD within different lipid carriers for topical application and to evaluate their stability, interaction with the skin, antibacterial activity, and *in vitro* antitumor effect. Solid lipid nanoparticles and nanostructured lipid carriers loaded with CBD were prepared and characterized in terms of their physicochemical properties, colloidal stability, protection of the antioxidant capacity of CBD, and CBD retention over time. Skin penetration was assessed using an *in vitro* human skin model. Antibacterial activity was evaluated against *Staphylococcus aureus*, and antitumor efficacy was tested using the SK-Mel-28 human melanoma cell line. Three nanoformulations exhibited optimal size and reproducibility and were selected for further analysis. The formulations were stable, they effectively protected CBD, successfully delivered it to deep skin layers, and exhibited antibacterial and antitumor effects *in vitro*. Although further studies are needed, these nanoformulations show promising potential for the treatment of skin diseases and conditions.

Keywords: Cannabidiol, CBD, Solid lipid nanoparticles, Nanostructured lipid carriers, Skin

Brewer's Spent Grain as a Sustainable Source of Ferulic Acid for Cosmetic and Pharmaceutical Innovations

Paula Lorena Bucci[1], Miquel Martínez-Navarrete[2], Francisco J. Marti Quijal[3], Ana Melero[2], Danilo Cantero[4], Raúl Muñoz[1]

[1]Department of Chemical Engineering and Environmental Technology, Institute of Sustainable Processes, University of Valladolid, 47011Valladolid, Spain
[2]Department of Pharmacy and Pharmaceutical Technology and Parasitology, University of Valencia, Burjassot, 46100 Valencia, Spain
[3]Research Group in Innovative Technologies for Sustainable Food (ALISOST), Department of Preventive Medicine and Public Health, Food Science, Toxicology and Forensic Medicine, Faculty of Pharmacy and Food Sciences, University of Valencia, Burjassot, 46100 Valencia, Spain
[4]Department of Chemical Engineering and Environmental Technology, The Institute of Bioeconomy University of Valladolid, 47011Valladolid, Spain
Corresponding author: Paula Lorena Bucci (e-mail: paulalorena.bucci@uva.es)

Abstract

Brewer's spent grain (BSG), the primary by-product of the brewing industry, is a lignocellulosic material rich in ferulic acid (FA), a potent natural antioxidant. While the decomposition of BSG poses significant environmental challenges, such as greenhouse gas emissions and malodors, its high FA content offers a promising avenue for sustainable valorization. FA exhibits potent antioxidative, anti-inflammatory, and regenerative properties, including inhibition of melanogenesis, promotion of angiogenesis, and acceleration of wound healing. However, its therapeutic application is constrained by rapid oxidation and low stability.

This study evaluated the extraction of FA from BSG using chemical, enzymatic, and hydrothermal hydrolysis methods. Hydrothermal treatment proved most effective, achieving encapsulation efficiencies of 97–98% when FA was incorporated into ultra-deformable liposomes (ULs), an advanced delivery system designed to enhance stability and skin permeability. FA-loaded ULs were tested across in vivo, in vitro, and ex vivo models, demonstrating effective human skin permeation in Franz diffusion cell assays. Nano-encapsulation extended FA's shelf life to 188 days and significantly enhanced its bioactivity compared to its free form.

The antioxidant and regenerative properties of FA_ULs were confirmed using human keratinocytes (HaCaT), dermal fibroblasts (HDF), and a 3D reconstructed epidermis model. Encapsulated FA reduced reactive oxygen species (ROS) by 94% in HaCaT and HDF cells and promoted wound healing, with over 50% closure achieved within 6 hours and complete closure within 24 hours. In vivo assessments using an Oxazolone-Induced Delayed-Type Hypersensitivity model in Swiss CD1 mice corroborated the anti-inflammatory effects, including reduced ear thickness, decreased cytokine expression, and lower bioluminescence signals.

These findings highlight the potential of BSG as a sustainable source of high-value bioactives and FA_ULs as a novel platform for cosmetic and pharmaceutical applications targeting skin protection, regeneration, and inflammation management.

Keywords: Brewer's spent grain, Ferulic acid, Hydrothermal hydrolysis, Ultra-deformable liposomes, Skin

Highly Transparent Bi_2O_3-PbO Glasses for Gamma Radiation Shielding Applications

Ahmad Marzuki[1], Selvina Ariyanti[1], Cari[1], Ari Handono Ramelan[1], Lita Rahmasari[2], Nurhafizah Binti Hasim[3], Idris Kabalci[4]

[1]Department of Physics, Sebelas Maret University, 57126 Surakarta, Indonesia
[2]Department of Physics Education, Sebelas Maret University, 57126 Surakarta, Indonesia
[3]Advanced Optical Material Research Group, Department of Physics, Faculty of Science, Universiti Teknologi Malaysia, Skudai, 81310 Johor, Malaysia
[4]Faculty of Engineering, Usak University, 64200 Usak, Türkiye
Corresponding author: Ahmad Marzuki (e-mail: amarzuki@mipa.uns.ac.id)

Abstract

This study investigates the fabrication and characterization of heavy metal oxide glasses containing Bi_2O_3 and PbO, intended for use in gamma radiation shielding applications. The glasses were prepared using the meltquenching method. The quality of the resulting glasses, in terms of crystallinity and transparency, was assessed using X-ray diffraction (XRD), Differential Scanning Calorimetry (DSC), and UV-Vis Spectrophotometry. Gamma radiation shielding properties, including linear attenuation coefficient (LAC), effective atomic number (Zeff), electron density (Neff), half-value layer (HVL), mean free path (MFP), and exposure buildup factors (EBF) at different gamma photon energies, were simulated using XCOM and phy-X/PSD software, based on the glass composition and density. The results showed that glasses with higher concentrations of either PbO or B_2O_3 offer better gamma radiation shielding effectiveness. To address potential crystallization issues associated with these high concentrations, the addition of glass-forming compounds, such as boron oxide (B_2O_3) and phosphorus pentoxide (P_2O_5), can help minimize crystallization.

Keywords: Gamma shielding, radiation shielding, Heavy metal oxide glass, XCOM, Phy-X/PSD

Development of Biomimetic Electrodes for Real-Time Monitoring of Cell Adhesion via Electrochemical Impedance Spectroscopy

Victoria Guglielmotti[1,2], Emil Fuhry[1], Diego Pallarola[2], Kannan Balasubramanian[1]

[1]Department of Chemistry, School of Analytical Sciences Adlershof (SALSA) & IRIS Adlershof, Humboldt University of Berlin, Berlin 10099, Germany
[2]Institute of Nanosystems, National University of General San Martin, San Martin 1650 Province of Buenos Aires, Argentina
Corresponding author: Victoria Guglielmotti (e-mail: victoria.guglielmotti@fau.de)

Abstract

Cell adhesion plays a crucial role in regulating various cellular processes such as proliferation, survival, migration, and gene expression. Therefore, having effective analytical tools to investigate cell interactions is of highest importance for the development of therapeutic strategies. Biosensors have emerged as promising tool for studying cell behaviour due to their simplicity of operation, enhanced sensitivity, and cost-effectiveness, making them highly attractive for medical diagnosis applications. In particular, electrochemical impedance-based devices have demonstrated significant potential for investigating cell adhesion. One notable advantage is the ability to monitor changes in a label- free, instantaneous, and non-destructive manner. However, the majority of sensors developed have been limited to stiff and opaque devices with non-homogeneous distribution of ligands, posing challenges for accurate analysis. To address this limitation, my approach focused on the development of electrodes capable of mimicking specific properties of the cellular environment. By combining Electrochemical Impedance Spectroscopy (EIS) techniques with these engineered electrodes, it becomes possible to study the cellular response to different stimuli in biomimetic conditions, real-time and with high sensitivity. I particularly focus on two key extracellular properties: the homogeneous distribution of adhesive ligands and the stiffness of the extracellular matrix. By decorating micro-ITO-electrodes with homogenous arrays of gold nanoparticles and modifying them with specific adhesive ligands it is possible to mimic the nanoscale organization of the extracellular matrix proteins. On the other hand, by coating soft-transparent-polymers, like PDMS, with graphene it is possible to fabricate highly sensitive electrodes, maintaining the mechanical properties of the underlayer substrate and its transparency. Finally, real-time monitoring of the cell adhesion kinetics and cell-cell interaction progression can be obtained by analysing the impedance on broad a range of frequencies over time.

Keywords: Electrochemical biosensing, Cell adhesion, Nanofabrication, Graphene, AFM

Design of MOF Immobilized Graphene Sponge for Sustainable Water Treatment System Applications

Aysenur Karakas[1], Kader Dagci Kiransan[1]

[1]Department of Chemistry, Science Faculty, Ataturk University, Erzurum, Türkiye
Corresponding author: Aysenur Karakas (e-mail: aysenur-krkass1@hotmail.com)

Abstract

Solar steam generator systems are considered as an efficient and environmentally friendly technology for obtaining potable water from salty and wastewater using solar energy. However, the efficient operation of this system depends on the photothermal material used to transport water quickly and effectively and also on providing high photothermal conversion. In this study, a homogeneous sponge material was obtained by homogeneously doping MnZn-MOFs structure into the graphene sponge (GrS) structure. The fact that the MnZn-MOF/GrS material is prepared in a short time using simple techniques without requiring expensive devices and equipment is of great economic importance. The use of the MnZn-MOF/GrS material prepared in this way as a photothermal material in the solar steam generator system was investigated. It is shown in Figure 1 that the prepared MnZn-MOF/GrS is both very light and very resistant and flexible to mechanical stresses. Thus, both the uniformity will be disrupted by the homogeneous doping of MnZn-MOFs into the uniform GrS material structure and a more balanced transportation of water is provided due to the homogeneous doping of MOFs into the GrS pores. However, since the photothermal properties of Gr and MnZn-MOFs will be combined, it was determined that a high evaporation efficiency of 3.05 kg/m2h and approximately 86% thermal efficiency were obtained under 1 sunlight.

Keywords: MnZn-MOF, Graphene sponge, Solar stream generatore

1. INTRODUCTION

With the rapid increase in the world population, increasing industrialization and the environmental problems caused by these, fresh water scarcity has become one of the most important and fundamental global challenges [1, 2]. When we consider that although 71% of the world's surface is covered with water, only 2.5% of it is fresh water, the magnitude of the problem becomes clear [3]. There are many efforts to find solutions to eliminate the water scarcity that exists now and is predicted to become an even more serious problem in the future. Among these solutions, solar energy stands out as the cleanest and most inexhaustible renewable energy source. It emerges as a promising technology for obtaining fresh water from waste and salt water using solar energy [4–6].

However, since conventional solar steam generation systems heat wastewater in bulk, the use of optical concentrators, which are quite costly to maintain, is required. In addition, since the energy loss in these systems is high, the energy efficiency is quite low [7, 8]. Therefore, increasing the efficiency in solar steam generator systems is among the most researched topics by scientists in recent years. When recent studies are examined, it is observed that the designs of floating evaporators in solar steam generator systems have become widespread [9–14]. Previous studies have shown that nanoparticles and carbon-based materials that can float on the water surface and have high photothermal conversion efficiency are widely used in solar steam generator systems [15–19]. For example, a plasmonic film prepared by Deng's group using gold nanoparticles was reported to have 44% conversion efficiency when used as a photothermal material in a solar steam generator system [20]. Similarly, a photothermal material prepared by adding aluminum nanoparticles was shown by Zhu and Grunu to be effective in obtaining drinkable water, especially from salty water [21]. However, the fact that nanoparticles lose their photothermal activity due to their easy aggregation and that the synthesis procedures are time-consuming and costly restrict their use for this purpose.

On the other hand, carbon-based materials such as graphene and graphene oxide [22–24], carbon nanotube [25], carbon black [26], wood [27], carbonized cork [28], etc. are very promising candidates for solar steam generator systems due to their high sunlight absorption properties and environmental friendliness. Although the photothermal conversion efficiency of some of these materials exceeds 80% under a single sunlight, the photothermal efficiency of these raw materials decreases due to reasons such as the complexity of their pure production, their

easy decomposition and decay (wood gigb). Therefore, efforts to develop new rational photothermal materials by doping carbon-based materials with different materials have accelerated.

For example, a single-walled carbon nanotube (SWCN) film that can be combined with plasmonic Au nanorods was prepared by Yan et al. Although the prepared film has a stable structure and high evaporation performance, its high cost, complicated manufacturing process and use of precious metal Au have limited its practical use [29]. Hu et al. prepared carbon nanotube modified flexible wood membranes (F-Wood/CNTs) to improve water transport performance. It was determined that this material exhibited low solar evaporation performance due to both the complicated processes in the preparation process and the irregular structure of the wood and its sensitivity to deterioration [30]. Yuan et al. produced a hybrid film containing MoS2 nanolayers and single-walled carbon nanotubes and determined that the sunlight adsorption capacity was 82% and the photothermal conversion was low compared to similar materials [31]. Wang et al. prepared flexible photothermal fabric consisting of polymeric nanofiber matrix and inorganic carbon black nanoparticles. However, in the salt removal experiments of the photothermal fabric material, it was determined that its structural stability decreased and the evaporation efficiency decreased significantly after salt adsorption [32]. Furthermore, a double-layer solar vapor generator consisting of bacterial nanocellulose (BNC) film modified with polydopamine (PDA) nanoparticles was prepared by Singamaneni et al. and it was determined that it had a photothermal conversion efficiency of only 78% under 1 sun [33].

However, it has been observed that the flexible photothermal materials mentioned above require complex preparation processes and expensive metals and have relatively low evaporation efficiencies. It has also been stated that they are not sufficient for salt and heavy metal removal applications, especially in solar steam generator systems prepared in this way.

At this point, the design of carbon-based materials that can float on the water surface, have a flexible structure, have a fast water carrying capacity and high photothermal performance, are low-cost and can be prepared using simple methods has gained importance. At this point, the modification of graphene sponges with 3D porous structures with different materials to further improve their high photothermal efficiency and water carrying capacity has been among the topics that have been intensively researched in recent years.

In this context, due to their adjustable 3D structures, their practical synthesis and their easy compatibility with carbon-based materials, the high photothermal performance of MOFs has made these materials among the sought-after materials for solar steam generator systems. [34, 35]. MOFs have proven to be valuable templates or precursor materials in new material designs due to their controllable surface areas, high porosity and flexible composition. It is known that MOFs or their derivatives are widely used in many disciplines including catalysis [36, 37], gas storage and separation [38], oil/water separation [39], and sensors [40]. Among the MOF structures, MnZn-MOF stands out as a promising material for solar steam generator systems due to its ability to be synthesized using the solvothermal method, which is a simple and environmentally friendly technique, its non-toxicity, and its high photothermal activity due to the easy electron delocalization of Mn and Zn atoms. In addition, it has been determined that the MnZn-MOF structure can be prepared in different morphological structures by changing the reaction conditions, which will make them interact more easily with different materials and will cause the prepared composite materials to exhibit high mechanical, electrical and photochemical activity [35].

In this study, MnZn-MOF structure with low bandgap energy and high light absorption feature was prepared using an easy-to-apply, environmentally friendly and low-cost technique. The prepared MnZn-MOF structures were added to GrS by foaming and drying method, which is a low-cost, scalable and environmentally friendly method, and homogeneous MnZn-MOF/GrS flexible material was obtained. In literature reviews, it was determined that a flexible, homogeneous and uniform material containing MnZn-MOF and GrS has not yet been used in solar steam generators. It was determined that the prepared MnZn-MOF/GrS material exhibited high thermal efficiency (86% under 1 sunlight) and evaporation performance (3.06 kg/m2h under 1 sunlight) due to the high light absorption of both graphene structures and MnZn-MOF structures due to its homogeneous structure and the fact that the MnZn-MOF structure contributed to the increase in controlled water carrying capacity by reducing the hydrophobic character of GrS.

2. MATERIAL AND METHOD

2.1. Chemical Synthesis of GO

Graphene oxide (GO) was synthesized by a modification of the chemical method known in the literature as the Hummers method. In the modified Hummers method, the graphite powder was first extracted and then the pre-oxidation of graphite was performed. Details are presented in our previous studies. To prepare the GO dispersion, the GO solid was dispersed in water with the help of a sonicator (Bandelin Sonorex Digitec 160/640 W) and 7.0 mg/mL GO aqueous dispersion was prepared. It was determined that this homogeneous GO dispersion was stable for several weeks and there was no precipitation.

2.2. Synthesis of ZnMn-MOF

First, 0.55 g of zinc nitrate hexahydrate ($Zn(NO_3)_2$ 6. H_2O) and 0.2 g of manganese II chloride tetrahydrate (MnCl2 4. H2O) were dissolved in 30 mL of methanol. This solution was called solution A. Then, 4 g of 2-methylimidazole was dissolved in 30 mL of methanol in a separate container and this solution was called solution B. Then, solution A was added dropwise to solution B. The prepared mixture was dispersed in an ultrasonicator for 20 minutes to ensure that the chemical reaction took place. After mixing at a constant speed for another 20 minutes after dispersion, the resulting MOF structure was centrifuged and removed from the mixture and washed with pure water and ethanol at least three times to remove impurities. Then, MnZn-MOF was prepared by drying at 60°C (Figure 1(a)).
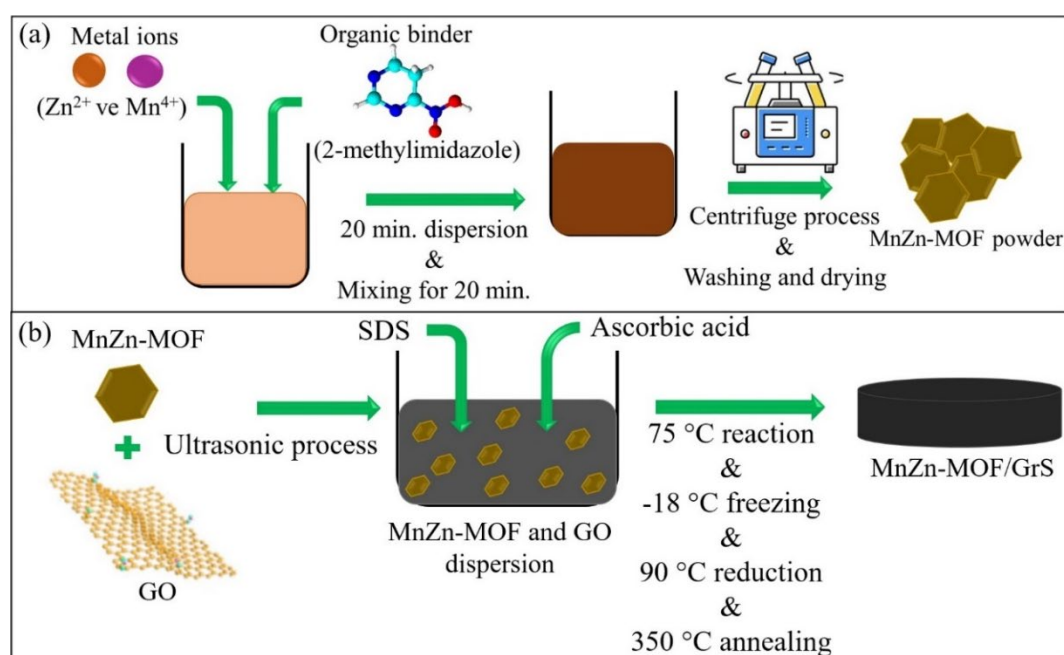
Figure 1. (a) Representative representation of the synthesis of MnZn-MOF. (b) Representative representation of the preparation of MnZn-MOF/GrS

2.3. Preparation of MnZn-MOF/GrS Material

When preparing GrS materials, a regular porous structure is achieved by foaming. The amount of surface active material used for foaming and the foaming time affect the pore size. However, when the pore sizes are too large, the resistance life of the sponge material to water decreases due to the rapid transport of water. For these reasons, it is aimed to provide a more controlled and longer water carrying capacity by adding the MnZn-MOF structure to the GrS structure, controlling the pore sizes and reducing the water carrying speed. Accordingly, in order to obtain flexible, durable and homogeneous MnZn-MOF/GrS, different amounts (10 mg, 15 mg, 20 mg and 30 mg) of MnZn-MOF were added to 50 mL of GO aqueous dispersion (7 mg mL-1) containing 450 mg ascorbic acid (as reducing agent) and 2 mL sodium dodecylsulfate (SDS) (for foaming) (50% by weight) and stirred at 2500 rpm for 30 min, and foaming was carried out to obtain a porous structure. The preparation procedure presented here is only the conditions used for GrS synthesis. The prepared foamed dispersions were poured into the reaction vessel and reacted at 75 °C for 3 h to obtain graphene hydrogel sponges (GHS). The prepared GHSs were completely frozen at -18°C for approximately 6 hours and then brought to room temperature, dried at 90°C for approximately 3 hours and washed with pure water 1-3 times to remove excess ascorbic acid. Then, after annealing at 350°C for 2 hours, MnZn-MOF/GrS material with different MnZn-MOF content was prepared (Figure 1(b)).

MnZn-MOF/GrS with different compositions were prepared by adding 10 mg, 15mg, 20mg, 25mg and 30mg MnZn-MOF. Since the materials obtained here with different compositions were intended to be used as photothermal materials in the solar steam generator system, the most suitable MnZn-MOF/GrS material was determined by looking at their mechanical resistance to water.

3. RESULTS

3.1. Structural and Morphological Characterization of MnZn-MOF/GrS

It is known that the physical properties of composite sponge materials prepared by adding different materials change after long-term use. In order to minimize this effect; the synthesized MOFs were added to the GO dispersion during the sponge preparation process and were placed in the voids formed by the foaming process. Thus, it was predicted that the MOFs would effectively adhere to the composite structure since they would provide pore formation appropriate to their own dimensions. The preparation process designed in this way aimed to prevent the migration of MOFs from the composite sponge structure.
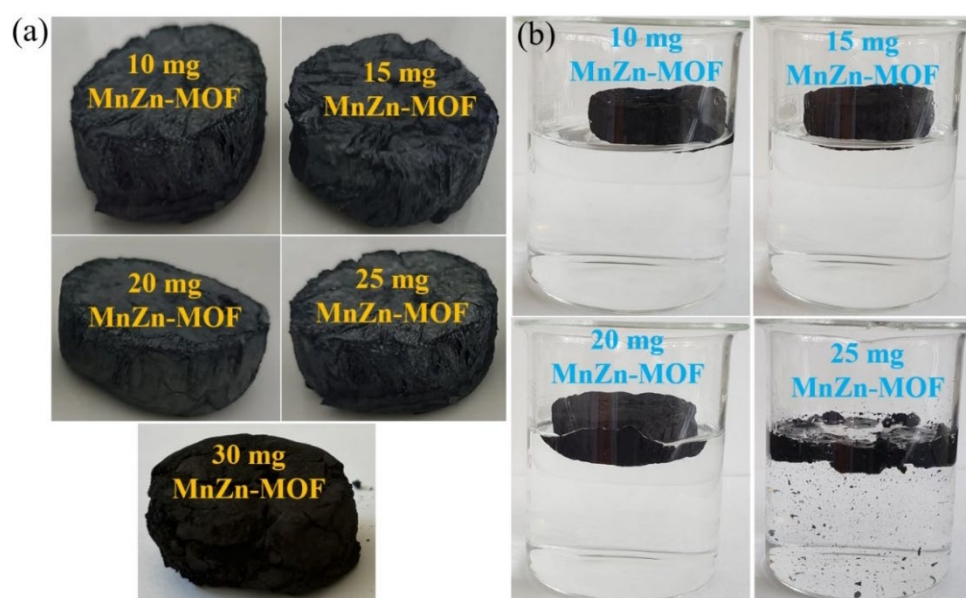
Figure 2. (a) Digital camera photographs of MnZn-MOF/GrS composite materials prepared by adding different amounts of MnZn-MOF, (b) photographs showing their resistance to water.

Digital camera images of MnZn-MOF/GrS materials prepared by adding different amounts of MnZn-MOF are presented in Figure 2(a). While it was determined that MnZn-MOF/GrS prepared by adding 10, 15, 20 and 25 mg of MnZn-MOF were successfully prepared, it was determined that when added 30 mg, the dense addition of ZnMn-MOF prevented the 3D arrangement of GO plates and the 3D structure was disrupted. Thus, the maximum amount of MnZn-MOF was determined as 25 mg to prepare a flexible, mechanically durable and self-supporting MnZn-MOF/GrS material. It has been shown that the material prepared with 30 mg MnZn-MOF doping is quite brittle and mechanically weak.

The aim of the optimizations presented here is to prepare MnZn-MOF/GrS material that is both mechanically and water resistant and can adsorb water in a balanced manner. Since the prepared MnZn-MOF/GrS are intended to be used in solar steam generators, it is planned that their structures will remain intact after long-term treatment with water and that they will adsorb water slowly and balancedly compared to GrS, which are known to be quite hydrophobic. In this direction, the water adsorption amounts and water resistance properties of MnZn-MOF/GrS materials prepared with different amounts of MnZn-MOF doping were determined by keeping them in water for 30 minutes (Figure 2(b)). It was observed that the composite material prepared with 10, 15 and 20 mg MnZn-MOF addition was quite stable against water for 30 minutes, whereas the composite sponge containing 25 mg MnZn-MOF was not resistant to water and its structure was broken down. Thus, when the obtained results were evaluated, it was determined that the most suitable composite for solar steam generator application was the material prepared with 20 mg MnZn-MOF addition.

It was shown that MnZn-MOF/GrS-3 prepared under optimum conditions was light enough to be carried by dried thin flower branches (Figure 3(a)) and quite flexible against mechanical pressures (Figure 3(b)–(d)). It was

also shown that its initial height of 2.0 cm (Figure 3(b)) returned to the same size after a 250 g weight pressure (Figure 3(c)) was applied (Figure 3(d)). Thus, it was revealed that MnZn-MOF/GrS is quite light, highly resistant to mechanical stresses and its structure is quite flexible.

Figure 3. Images showing that MnZn-MOF/GrS (a) is extremely light, (b)–(d) flexible and resistant to mechanical stresses

The morphological properties of the prepared composite material were determined using the FESEM technique. When the FESEM image of MnZn-MOF is examined in Figure 4(a), it is determined that its morphological structure is in the rhombic dodecahedron structure and that it grows homogeneously. In the SEM image of GrS (Figure 4(b)), the porous structure formed by the 3-dimensional arrangement of graphene layers is clearly observed. In the FESEM image of MnZn-MOF/GrS, the presence of MnZn-MOF structures embedded between the pores of GrS is remarkable (Figure 4(c)). In addition, it is observed that the MnZn-MOF structures are located especially at the corner edges within the GrS structure. When the EDX spectrum of MnZn-MOF was examined, the presence of C (50.19%), O (35.22%), Mn (5.27%), Zn (8.02%) and N (1.31%) atoms originating from the organic molecule used in the MOF synthesis were determined (Figure 4(d)). Thus, it was shown that the GS structure was successfully prepared by doping MnZnMOF.
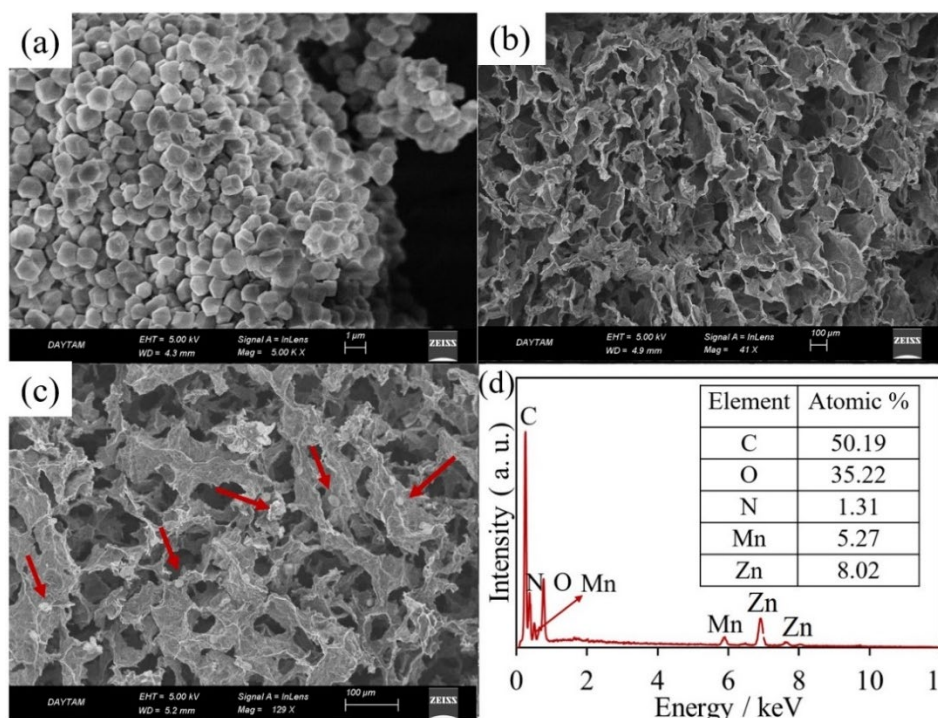
Figure 4. FESEM images of (a) MnZn-MOF, (b) GrS, (c) MnZn-MOF/GrS. (d) EDX spectrum of MnZn-MOF/GrS

XRD spectra of GrS, MnZn-MOF powder and MnZn-MOF/GrS are presented in Figure 5(a). When the XRD spectrum of GrS is examined, it is observed that the peak corresponding to the 002 diffraction of graphene layers occurs at 25.4°. When the XRD spectrum of MnZnMOF powder was examined, it was determined that the peaks corresponding to the diffraction points 011 (7.3°), 002 (10.3°), 112 (12.7°), 222 (18.0°), 233 (24.6°), 134 (26.7°) and 311 (35.1°) were formed, in accordance with previous studies. When the XRD spectrum of MnZnMOF-GrS was examined, it was observed that the peaks belonging to both GrS and MnZn-MOF powder were formed, thus it was determined that the proposed composite structure was successfully prepared.

Raman spectra of GrS and MnZn-MOF/GrS are shown in Figure 5(b). In the Raman spectrum of GS, it was observed that the G band (1618 cm-1) corresponding to the characteristic ring vibration of the graphene structure and the D band (1425 cm-1) originating from the defects in the graphene structure were formed, while in MnZn-MOF/GrS, in addition to the D and G bands in the GS structure, it was observed that peaks corresponding to the geometric vibrations T2g at 460 cm-1 and A1g at 725 cm-1 were formed in the MnZn-MOF structure (REF). The D/G ratio for graphene-containing materials provides information about the surface defect densities of the prepared materials. In this context, the D/G ratios for GrS and MnZn-MOF/GrS were determined as 1.38 and 1.17, respectively. The lower D/G ratio obtained for MnZn-MOF/GrS was attributed to the decrease in the defect ratio by placing MnZn-MOFs in the defective regions (regions containing oxygenated functional groups) of the GrS structure while preparing the composite material. Thus, it was determined that the proposed composite structure was prepared successfully.
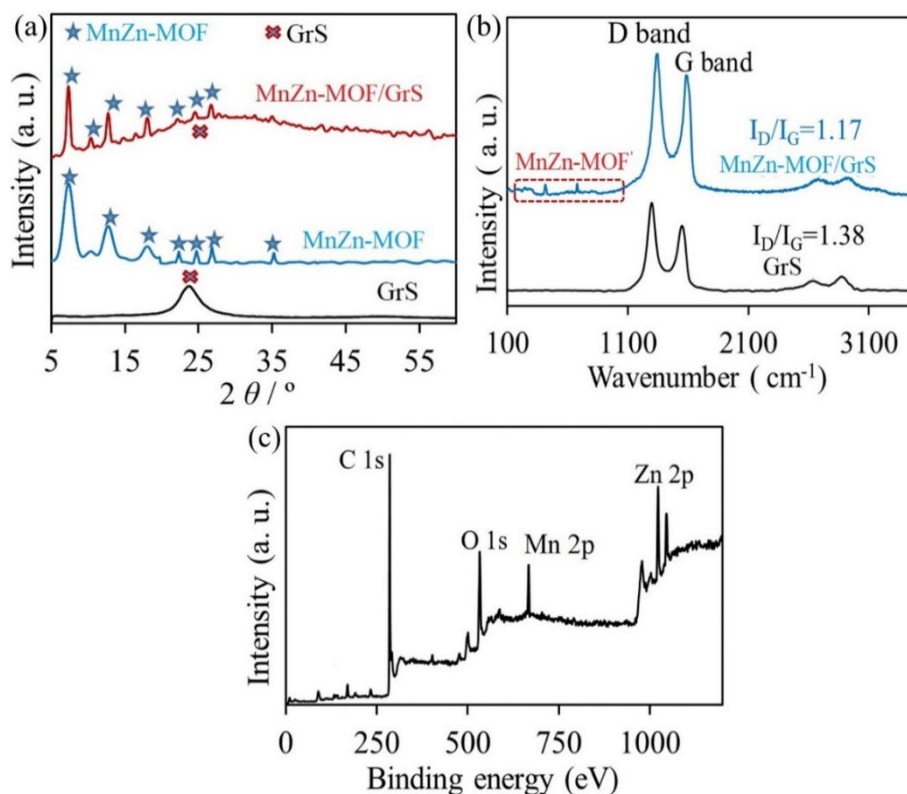
Figure 5. (a) XRD spectra of MnZn-MOF/GrS, MnZn-MOF and GrS. (b) Raman spectra of MnZn-MOF/GrS and GrS. (c) XPS spectrum of MnZn-MOF/GrS

The structural analysis of the prepared MnZn-MOF/GrS was performed using the XPS technique (Figure 5©). In the XPS analysis, it was determined that the chemical structure contained C (51.67%), O (34.25%), Mn (6.30%), Zn (9.04%) and a small amount of N (0.81%) atoms. It was reported that the N atom originated from the N 1s peak (399 eV) in the MOF structure. Since C and O elements are present in both the GrS structure and the MOF structure, it was determined that their atomic percentage was higher than the other elements.

3.2. Determination of Photothermal Performance of MnZn-MOF/GrS

The solar energy vapor energy generation system classically consists of 5 basic components. The first of these is the experimental system with water inside and prepared photothermal materials, which is insulated against heat conduction outside, the second is a sunlight source, the third is a thermal camera to monitor and record heat changes, the fourth is an analytical precision balance to measure the amount of evaporated water, and finally the computer support system used to determine the vapor generation rate over time. The picture of this system is shown in Figure 6.

Water evaporation rates for MnZn-MOF/GrS materials were determined using the prepared experimental setup (Figure 6). Graphs showing the evaporation amounts over time when MnZn-MOF/GrS and GrS were used as photothermal materials and when no photothermal material was used are presented in Figure 6(d). For the analysis, changes in the 60-minute time period were monitored and measurements were started with 30 mL of

water volume. Water evaporation rates (kg/m2h) were determined for each different material against time. Evaporation amounts were calculated using the Apps Acpa program [41]. When sunlight was sent directly to the water surface without using any photothermal material, it was observed that there was a certain level of evaporation due to the heat energy of sunlight, albeit small (Figure 6(d), red dashed lines). It was observed that there was a significant increase in vapor formation performance compared to GrS for the system where both sunlight was turned on and the prepared MnZn-MOF/GrS was used as photothermal material (Figure 6(d), green solid lines). Vapor formation performances for GrS and MnZn-MOF/GrS were determined as 1.79 and 3.1 kg/m2h, respectively. The approximately 2-fold increase in the evaporation rate by modifying the MnZn-MOF structure to GrS was attributed to the high light absorption of MOF structures and the ability to convert the energy they absorb into thermal energy at a high rate. In addition, it was concluded that MnZn-MOF/GrS, compared to GrS with hydrophobic characteristics, transmits water to the upper parts more quickly and steadily, contributing to more vapor formation per unit time.
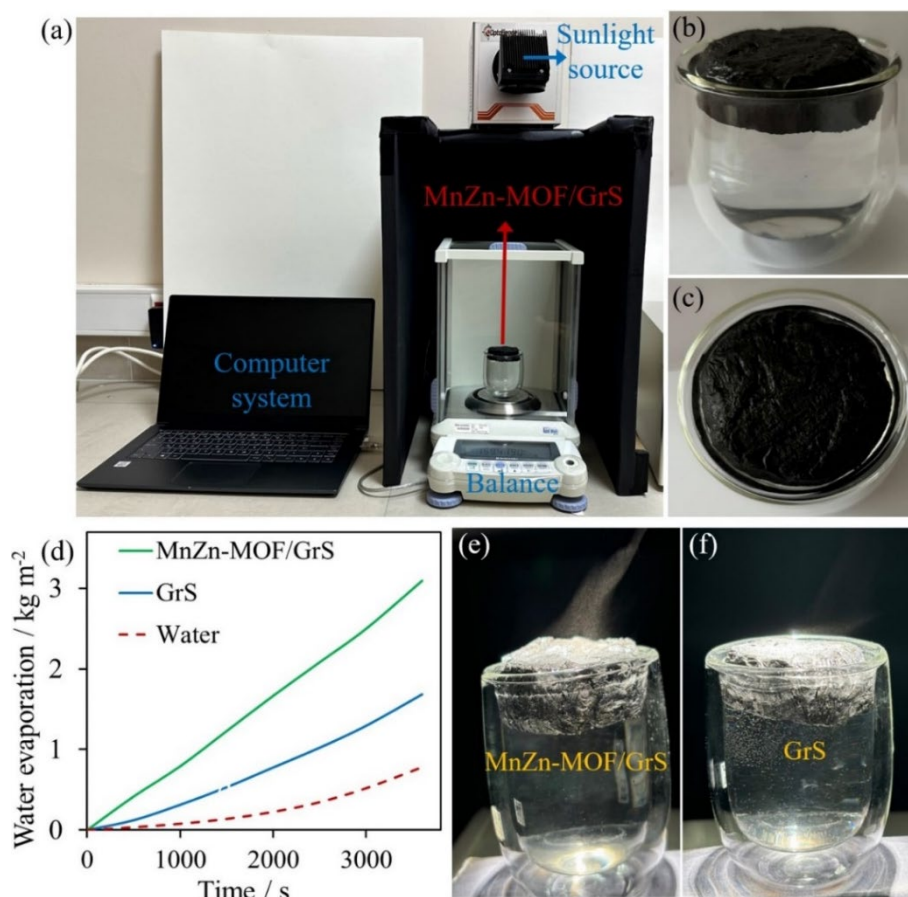
Figure 6. (a) Photograph of the system where MnZn-MOF/GrS is used as a photothermal material. Photographs of the prepared photothermal MnZn-MOF/GrS material (b) from the side, (c) from above. (d) Graphs showing the water evaporation amounts of MnZn-MOF/GrS and GrS materials in the dark and under sunlight over time. (e) Photographs of MnZn-MOF/GrS and (f) GrS under sunlight at 40 s

Figure 6(e) and f show photographs of MnZn-MOF/GrS and GrS obtained under sunlight at 40 s. When the photographs were examined, it was observed that the amount of vapor formed on the GrS surface was very low in the same period, while a noticeable increase was determined in the vapor formation performance of MnZn-MOF/GrS to GrS. It was observed that MnZn-MOF/GrS formed vapor more intensively, which was proportional to their vapor formation performance.

3.3. Monitoring Temperature Changes During Irradiation for MnZn-MOF/GrS Material

Under optimum conditions for MnZn-MOF/GrS material, during 100 seconds of irradiation (1 kW m^{-2} under 1 sunlight), temperature changes on the surfaces and within the system were recorded and monitored with a thermal camera.

Thermal camera images obtained as a result of different irradiation times of MnZn-MOF/GrS are presented in Figure 7. When thermal camera images are examined, it is observed that the surface temperature increases by approximately 10 °C (from 25 °C to 35 °C) in a short period of 10 s, while it reaches 42 °C in 25 s, 53 °C in 45 s and 61 °C in 60 s. This situation is attributed to the fact that the prepared photothermal material absorbs sunlight very effectively and also converts it into thermal energy effectively. When the irradiation continued, it was determined that the surface temperature reached approximately 61 °C in 60 s. Thus, it was observed that MnZn-MOF/GrS absorbed sunlight faster than GrS and converted it into thermal energy, and the surface temperature was higher at the end of the same irradiation time. When GrS and MnZn-MOF/GrS were compared with each other, the increase in surface temperatures, as well as their vapor generation performance, was higher in MnZn-MOF/GrS, which was attributed to the fact that the electrons of the Mn and Zn atoms in the MnZn-MOF/GrS material structure were delocalized to the empty orbitals they had, and the coordinated covalent bonds in the MOF structure reduced the rigidity of the structure, causing a large amount of the absorbed energy to be converted into thermal energy and relaxing, and the contribution of the Mn atoms to electron transfer.
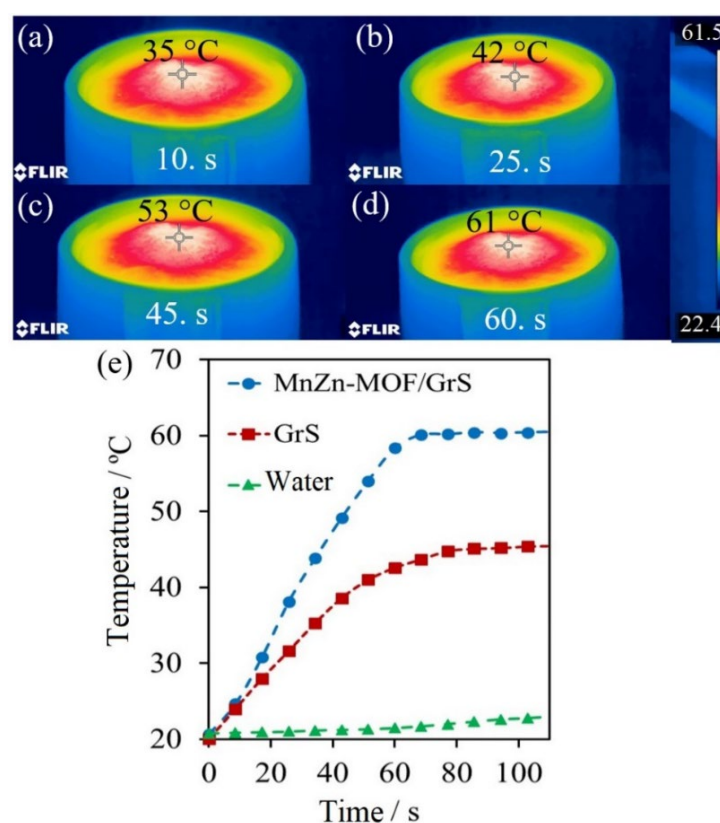
Figure 7. Thermal camera images showing surface temperatures of MnZn-MOF/GrS after (a) 10 s, (b) 25 s, (c) 45 s and (d) 60 s irradiation. (d) Graphs showing changes in surface temperatures after irradiation of MnZn-MOF/GrS, GrS and direct water surface for 100 s

In Figure 7(e), the changes in the surface temperatures of the prepared MnZn-MOF/GrS, GrS and direct water surfaces were compared and presented during the 100 s irradiation period. While it was observed that the surface temperature of the direct water increased from 21 °C to 23 °C after 100 s irradiation, this increase was higher in the system where photothermal materials were used. The increase in surface temperature for GrS (from 21 °C to 47 °C) is attributed to the photothermal activity of the direct graphene structures, while the increase in surface temperature for MnZn-MOF/GrS material is attributed to the coordinated covalent bonds in the MOF structure, which reduce the rigidity of the structure, convert a large amount of the absorbed energy into thermal energy, and relax and contribute to the electron transfer of Mn atoms, as well as to the graphene structures.

Heat conversion efficiencies for GrS and MnZn-MOF/GrS were calculated using equation 1 and equation 2 as 47% and 85%, respectively. It was suggested that the MOF structures incorporated into the structure contribute to the increase in the evaporation rate by reducing heat losses. The high evaporation efficiency for the MOF modified material was attributed to the high solar light absorption and thermal energy conversion properties of the MOF structures. In addition, it has been shown that MOF structures homogeneously doped into the GrS structure increase efficiency by acting as a barrier to prevent heat losses.

$$\eta = \frac{m \cdot h_{LV}}{l} \qquad (1)$$

$$m_{su} \cdot h_{su} = m_{sm} \cdot h_{sm} \qquad (2)$$

4. CONCLUSION

In summary, a new material was produced by homogeneously doping the MnZn-MOF structure into the porous 3D structured GrS. In the characterization studies carried out using different structural and morphological techniques, it was confirmed that MnZn-MOF was homogeneously doped into the GrS. When the MnZn-MOF/GrS prepared in this way was used as a photothermal material in the solar vapor generator system, it was determined that it had a very balanced water carrying capacity and a very high photothermal performance due to the MnZn-MOFs doped into the structure. It was determined that MnZn-MOF/GrS exhibited approximately 2.5 times higher photothermal performance than GrS with a steam generation performance of 3.05 kg/m2h under 1 sun light and a thermal conversion of 86%.

Acknowledgments

References

[1]   J. Bartram, C. Brocklehurst, M. Fisher, R. Luyendijk, R. Hossain, T. Wardlaw, and B. Gordon, "Global monitoring of water supply and sanitation: history, methods and future challenges," *Int. J. Environ. Res. Public Health*, vol. 11, no. 88, art. no.137, 2014.

[2]   M. Elimelech and W.A. Phillip, "The future of seawater desalination: energy, technology, and the environment," *Science*, vol. 333, no. 6043, pp. 712–717, 2011.

[3]   S. L. Postel, G. C. Daily, and P. R. Ehrlich, "Human appropriation of renewable fresh water," *Science*, vol. 271, no. 5250, pp. 785–788, 1996.

[4]   S. W. Sharshir, G. Peng, N. Yang, M. O. A. El-Samadony, and A. E. Kabeel, "A continuous desalination system using humidification-dehumidification and a solar still with an evacuated solar water heater," *Appl. Therm. Eng.*, vol. 104, pp. 734–742, 2016.

[5]   H. Li, Y. He, Z. Liu, Y. Huang, and B. Jiang, "Synchronous steam generation and heat collection in a broadband Ag@TiO2 core-shell nanoparticle-based receiver," *Appl. Therm. Eng.*, vol. 121, pp. 617–627, 2017.

[6]   Z. Deng, J. Zhou, L. Miao, C. Liu, Y. Peng, L. Sun, and S. Tanemura, "The emergence of solar thermal utilization: solar-driven steam generation," *J. Mater. Chem.*, vol. 5, no. 17, pp. 7691–7709, 2017.

[7]   A. Lenert and E. N. Wang. "Optimization of nanofluid volumetric receivers for solar thermal energy conversion," *Sol. Energy*, vol. 86, no. 1, pp. 253–265, 2012.

[8]   G. Ahmadi, D. Toghraie, A. Azimian, and O. A. Akbari, "Evaluation of synchronous execution of full repowering and solar assisting in a 200mW steam power plant, a case study," *Appl. Therm. Eng.*, vol. 112, pp. 111–123, 2017.

[9]   H. Ghasemi, G. Ni, A. M. Marconnet, J. Loomis, S. Yerci, N. Miljkovic, and G. Chen, "Solar steam generation by heat localization," *Nat. Commun.*, vol. 5, art. no. 4449, 2014.

[10]   L. Zhang, B. Tang, J. Wu, R. Li, and P. Wang, "Hydrophobic light-to-heat conversion membranes with self-healing ability for interfacial solar heating," *Adv. Mater.*, vol. 27, no. 33, pp. 4889–4894, 2015.

[11]   G. Ni, G. Li, Svetlana V. Boriskina, H. Li, W. Yang, T. Zhang, and G. Chen, "Steam generation under one sun enabled by a floating structure with thermal concentration," *Nat. Energy*, vol.1, art. no. 16126, 2016.

[12]   S. Ma, C. P. Chiu, Y. Zhu, C. Y. Tang, H. Long, W. Qarony, X. Zhao, X. Zhang, W. H. Lo, and Y. H. Tsang, "Recycled waste black polyurethane sponges for solar vapor generation and distillation," *Appl. Energy*, vol. 206, pp. 63–69, 2017.

[13]   J. Li, M. Du, G. Lv, L. Zhou, X. Li, L. Bertoluzzi, C. Liu, S. Zhu, and J. Zhu, "Interfacial solar steam generation enables fast-responsive, energy-efficient, and low-cost offgrid sterilization," *Adv. Mater.*, vol. 30, no. 49, art. no. 1805159, 2018.

[14]   X. Li, J. Li, J. Lu, N. Xu, C. Chen, X. Min, B. Zhu, H. Li, L. Zhou, S. Zhu, T. Zhang, and J. Zhu, "Enhancement of interfacial solar vapor generation by environmental energy," *Joule*, vol. 2, no. 7, pp. 1331–1338, 2018.

[15] L. Zhou, Y. Tan, D. Ji, B. Zhu, P. Zhang, J. Xu, Q. Gan, Z. Yu, and J. Zhu, "Self-assembly of highly efficient, broadband plasmonic absorbers for solar steam generation," *Sci. Adv.*, vol. 2, no. 4, 2016.

[16] M. Zhu, Y. Li, F. Chen, X. Zhu, J. Dai, Y. Li, Z. Yang, X. Yan, J. Song, Y. Wang, E. Hitz, W. Luo, M. Lu, B. Yang, and L. Hu "Plasmonic wood for high-efficiency solar steam generation," *Adv. Energy Mater.*, vol. 8, no. 4, art. no. 1701028, 2017.

[17] J. Yang, Y. Pang, W. Huang, S.K. Shaw, J. Schiffbauer, M.A. Pillers, X. Mu, S. Luo, T. Zhang, Y. Huang, G. Li, S. Ptasinska, M. Lieberman, and T. Luo, "Functionalized graphene enables highly efficient solar thermal steam generation," *ACS Nano*, vol. 11, no. 6, pp. 5510–5518, 2017.

[18] Y. Ito, Y. Tanabe, J. Han, T. Fujita, K. Tanigaki, and M. Chen, "Multifunctional porous graphene for high-efficiency steam generation by heat localization," *Adv. Mater.*, vol. 27, no. 29, pp. 4302–4307, 2015.

[19] C. Chen, L. Zhou, J. Yu, Y. Wang, S. Nie, S. Zhu, and J. Zhu, "Dual functional asymmetric plasmonic structures for solar water purification and pollution detection," *Nano Energy*, vol. 51, pp. 451–456, 2018.

[20] Z. Wang, Y. Liu, P. Tao, Q. Shen, N. Yi, F. Zhang, Q. Liu, C. Song, D. Zhang, W. Shang, and T. Deng, "Bio-inspired evaporation through plasmonic film of nanoparticles at the air-water interface," *Small*, vol. 10, no. 16, pp. 3234–3239, 2014.

[21] L. Zhou, Y. Tan, J. Wang, W. Xu, Y. Yuan, W. Cai, S. Zhu, and J. Zhu, "3D self-assembly of aluminium nanoparticles for plasmon-enhanced solar desalination," *Nat. Photon.*, art. no. 10393, 2016.

[22] Q. Jiang, L. Tian, K.-K. Liu, S. Tadepalli, R. Raliya, P. Biswas, R. R. Naik, and S. Singamaneni, "Bilayered biofoam for highly efficient solar steam generation," *Adv. Mater.*, vol. 28, no. 42, pp. 9400–9407, 2016.

[23] X. Hu, W. Xu, L. Zhou, Y. Tan, Y. Wang, S. Zhu, and J. Zhu, "Tailoring graphene oxidebased aerogels for efficient solar steam generation under one sun," *Adv. Mater.*, vol. 29, no. 5, art. no. 1604031, 2016

[24] X. Zhou, F. Zhao, Y. Guo, Y. Zhang, and G. Yu, "A hydrogel-based antifouling solar evaporator for highly efficient water desalination," *Energy Environ. Sci.*, vol. 11, no. 8, pp. 1985–1992 , 2018.

[25] Y. Wang, L. Zhang, and P. Wang, "Self-floating carbon nanotube membrane on macroporous silica substrate for highly efficient solar-driven interfacial water evaporation," *ACS Sustain. Chem. Eng.*, vol. 4, no. 3, pp. 1223–1230, 2016

[26] G. Xue, K. Liu, Q. Chen, P. Yang, J. Li, T. Ding, J. Duan, B. Qi, and J. Zhou, "Robust and low-cost flame-treated wood for high-performance solar steam generation," *ACS Appl. Mater. Interfaces*, vol. 9, no. 17, pp. 15052–15057, 2017

[27] N. Xu, X. Hu, W. Xu, X. Li, L. Zhou, S. Zhu, and J. Zhu, "Mushrooms as efficient solar steam-generation devices," *Adv. Mater.*, vol. 29, no. 28, art. no. 1606762, 2017.

[28] W. Xu, X. Hu, S. Zhuang, Y. Wang, X. Li, L. Zhou, S. Zhu, and J. Zhu, "Flexible and salt resistant janus absorbers by electrospinning for stable and efficient solar desalination," *Adv. Energy Mater.*, vol. 8, no. 14, art. no. 1702884, 2018

[29] Y. B. Yang, X. D. Yang, L. N. Fu, M. C. Fu, M. C. Zou, A. Y. Cao, Y. P. Du, Q. Yuan, and C. H. Yan, "Two-dimensional flexible bilayer janus membrane for advanced photothermal water desalination," *ACS Energy Lett.*, vol. 3, pp. 1165–1171, 2018.

[30] C. J. Chen, Y. J. Li, J. W. Song, Z. Yang, Y. D. Kuang, E. Hitz, C. Jia, A. Gong, F. Jiang, J. Y. Zhu, B. Yang, J. Xie, and L. B. Hu, "Highly flexible and efficient solar steam generation device," *Adv. Mater.*, vol. 29, art. no. 1701756, 2017

[31] X. D. Yang, Y. B. Yang, L. N. Fu, M. C. Zou, Z. H. Li, A. Y. Cao, and Q. Yuan, "An ultrathin flexible 2D membrane based on single-walled nanotube-MoS2 hybrid film for highperformance solar steam generation," *Adv. Funct. Mater.*, vol. 28, art. no. 1704505, 2018.

[32] Y. Jin, J. Chang, Y. Shi, L. Shi, S. Hong, and P. Wang, "A highly flexible and washable nonwoven photothermal cloth for efficient and practical solar steam generation," *J. Mater. Chem.*, vol. 6, pp. 7942–7949, 2018

[33] Q. S. Jiang, H. G. Derami, D. Ghim, S. S. Cao, Y. S. Jun, and S. Singamaneni, "Polydopamine-filled bacterial nanocellulose as a biodegradable interfacial photothermal evaporator for highly efficient solar steam generation," *J. Mater. Chem.*, 5 18397–18402, 2017.

[34] H. Furukawa, K. E. Cordova, M. O'Keeffe, and O. M. Yaghi, "The chemistry and applications of metal-organic frameworks," *Science*, vol. 341, no. 6149, art. no. 974, 2013.

[35] H.-C. Zhou, J. R. Long, and O. M. Yaghi, "Introduction to metal-organic frameworks," *Chem. Rev.*, vol. 112, no. 2, pp. 673–674, 2012

[36] X. Li, Y. Fang, X. Lin, M. Tian, X. An, Y. Fu, R. Li, J. Jin, and J. Ma, "MoF derived Co3O4 nanoparticles embedded in N-doped mesoporous carbon layer/MWCNT hybrids: extraordinary bi-functional electrocatalysts for OER and ORR," *J. Mater. Chem.*, vol. 3, no. 33, pp. 17392–17402, 2015.

[37] K. Shen, X. Chen, J. Chen, and Y. Li, "Development of MOF-derived carbon-based nanomaterials for efficient catalysis," *ACS Catal.*, vol. 6, no. 9, pp. 5887–5903, 2016.

[38]   S. J. Yang, T. Kim, J. H. Im, Y. S. Kim, K. Lee, H. Jung, and C. R. Park "Mof-derived hierarchically porous carbon with exceptional porosity and hydrogen storage capacity," *Chem. Mater.*, vol. 24, no. 3, pp. 464–470, 2012.

[39]   A. Banerjee, R. Gokhale, S. Bhatnagar, J. Jog, M. Bhardwaj, B. Lefez, B. Hannoyer, and S. Ogale, "MOF derived porous carbon-Fe3O4 nanocomposite as a high performance, recyclable environmental superadsorbent," *J. Mater. Chem.*, vol. 22, no. 37, pp. 19694–19699, 2012.

[40]   X.-H. Zhao, S.-N. Ma, H. Long, H. Yuan, C. Y. Tang, P. K. Cheng, and Y. H. Tsang, "Multifunctional sensor based on porous carbon derived from metal-organic frameworks for real time health monitoring," *ACS Appl. Mater. Interfaces*, vol. 10, no. 4, pp. 3986–3993, 2018.

[41]   http://apps.acpa.org/applibrary/EvaporationRate/

Instructors' Opinions on the Use of Balkan Composers' Solo Piano Works in Piano Education

Hamza Serdar Turan[1], Sirin Akbulut Demirci[2]

[1]Department of Music, Kocaeli University, Kocaeli, Türkiye
[2]Department of Music Education, Bursa Uludag University, Bursa, Türkiye
Corresponding author: Hamza Serdar Turan (e-mail: h.serdarturan@gmail.com)

Abstract

Balkan geography is a region where different cultures and historical richness intersect, reflecting this richness in the field of music and hosting many composers. The aim of this study is to determine the use of solo piano works of Balkan composers in undergraduate piano education. For this purpose, semi-structured interviews were conducted with nine instructors who teach piano at the undergraduate level. The instructors were selected from nine different institutions, including three faculties of fine arts, three faculties of education, and three conservatories, to make the data obtained from the research comprehensive. The data obtained from the research were analyzed with NVivo 10, and certain themes, categories, and codes were identified. Considering the findings, it was determined that the works of Balkan composers are generally not included in piano education. Among the reasons for not including these works, it was concluded that there were issues such as a lack of resources, limited awareness of the composers, and insufficient weekly lesson hours. In addition, it was concluded that only one of the nine lecturers took part in academic studies related to Balkan composers and their works, while the others did not take part in any artistic and educational activities. However, it was stated that including the works of Balkan composers in piano education would provide many cognitive, affective, and psychomotor contributions to students. Finally, suggestions such as including the works of Balkan composers in the course curriculum, increasing printed and electronic resources, and increasing artistic activities were made for the dissemination of the use of Balkan composers' works in piano education.

Keywords: Balkan composers, Music education, Piano education

A Hybrid Model for Plant Disease Detection Based on Deep Learning

Tolga Aydin[1], Zainab Fadhil Abbas[1]

[1]Department of Computer Engineering, University Ataturk University, Erzurum, Türkiye
Corresponding author: Zainab Fadhil Abbas (zainabfadel51@gmail.com)

Abstract

Precise detection of plant diseases is done in the early stages in successful crop rearing, as they menace the yielding of crops with great promise [1]. In this paper, we introduce a novel diagnosis using four pre-trained Convolutional Neural Network models, namely ResNet-50, VGG-19, VGG-16, and Inception V3 on the PlantVillage dataset. Among those four, ResNet-50 presented the best accuracy of 82.74% and AUC of 79.13%, hence could be considered the best for hybridization with other models to further improve its overall performance. Then, by merging this best performing model, ResNet-50 with each of the other three models one after another, three hybrid models were formed: We prove through experiments that these hybrid models have higher classification accuracies by effectively utilizing the strengths of both networks. Among the models put to test, the most effective hybrid model was that of ResNet-50 and Inception V3 with an accuracy of 99.60%, AUC also at 99.98%. This proves that adding various feature extraction capacities makes the detection of plant diseases robust.

Keywords: Plant disease, CNN, Deep learning, Pre trained models, RecNet50

1. INTRODUCTION

Plant diseases pose a big challenge to agriculture; they affect both the quality and quantity of yield. Like any other living organism, plants pass through certain developmental stages where a plant becomes highly susceptible to certain diseases. Such diseases will drastically reduce crop yields and farmers' net incomes [2]. It therefore goes without saying that early detection becomes one of the most critical elements in fighting against plant diseases to limit economic damages in agricultural productivity for food security. Early identification allows farmers to take appropriate preventative measures, thereby reducing probable crop losses that can be incurred and sustain farming. Traditionally, diseases in plants are diagnosed by experts in agriculture through ocular examination [3]. Limitations to ocular diagnosis include the fact that this is a laborious task, time-consuming, and prone to human error. In remote areas where agriculture can be more viable, skilled experts cannot be made available with full certainty; hence, the use of manual diagnostic processes would not be quite feasible. These are several challenges that define the need for automated plant disease detection systems to be quite accurate and efficient enough to enable farmers in decision-making on a real-time basis [4].

Recent trends in machine learning, specifically deep learning, have shown great promise in classifying plant diseases based on image processing. It has been documented that CNNs are very appropriate in image processing tasks; therefore, they perform outstandingly in the detection and classification of plant diseases [5]. Where CNNs can learn such complicated information from photos themselves, which lets them find out whether a plant leaf is healthy or diseased with outstanding accuracy. The currently used deep learning models have a series of drawbacks concerning the amount of training parameters required, the high computational power they demand, and the restricted classification accuracy they provide when applied for plant disease detection [6].

This is done to adapt four state-of-the-art pre-trained CNN models to the classification of plant diseases: ResNet-50, VGG-19, VGG-16, and Inception V3. Pre-trained models are of especial benefit because they permit better generalization, even when trained with rather small datasets like PlantVillage [7]. This is because they use a learned feature from the major datasets for pre-training and therefore take advantage of the learned features. While doing so, the fine-tuning process of the models for plant disease classification aims at achieving a higher level of accuracy by reducing the time taken for training up the models and the computer resources needed in the process [8].

Every single one of the pre-trained models that were utilized in this investigation possesses distinctive qualities that render it appropriate for particular endeavors. For example, ResNet-50 is used to solve the problem of vanishing gradients through residual learning. It enables going deeper without losing network performance. On the one hand, VGG-19 and VGG-16 were called very user-friendly and efficient models to extract features

hierarchically from an image. On the other side, Inception V3 combined a big set of features using different filter sizes with parallel processing. Because of this diversity, these designs are particularly well-suited for combination, as each model might bring different key strengths to bear on the classification task.

This further ascertains the potentials of hybrid models, considering encouraging outcomes that these different individual models have produced. Three hybrid architectures are produced by combining the best performing model, ResNet-50, with each of the remaining models, consisting of VGG-19, VGG-16, and Inception V3. It is apparent that hybrid model development is driven by the need to realize better classification performance if the characteristics of diverse architectures can be combined. A hybrid approach tries to collect a combined set of feature vectors salvaged from multiple models in an attempt to concatenate them, so as to further improve the accuracy and robustness of plant disease classification.

This approach can solve the current bottlenecks in plant disease detection systems. The main objective of the project will be flexible, efficient, and scalable identification of diseases in plants. This work will be achieved by building an efficient hybrid model that combines the power of different CNN architectures. This will not only contribute to the development of agricultural technologies but also assist farmers, especially in low-input areas, by providing them with a user-friendly tool for early disease diagnosis. The long-term objective is to enhance agricultural productivity with minimal economic loss due to plant diseases, hence helping to ensure global food supply security.

3. LITERATURE REVIEW

The table below summarizes the previous studies in terms of researcher(s) and techniques used and methodology and key findings and accuracy metrics and dataset details, and contribution/objective.

Table 1. Literature review summary

Research	Techniques Used & Methodology	Key Findings & Accuracy Metrics	Dataset Details	Contribution/ Objective
[9]	Improved YOLOv5l model, Convolutional Block Attention Module (CBAM)	mAP of 80.10%, improved detection accuracy	Custom cucumber leaf dataset	Early detection of cucumber leaf diseases, improved model over YOLOv5
[10]	Convolutional Neural Networks (CNNs), MobileNet	CNN: 89% accuracy; MobileNet: 96% accuracy	Public dataset (unspecified)	Effective use of DL models in early plant disease detection
[11]	Modified YOLOv8, EIoU loss and α-IoU loss	Accuracy of 89.9% on 3175 images	Rice leaf images collected in the field	Improved rice leaf disease detection using modified loss functions
[12]	Bibliometric analysis, AI-based ML and DL algorithms	Analysis of 109 publications from Scopus	Scopus database	Impact of unexpected weather on agricultural output
[13]	Eight DL models, new CNN model	Improved accuracy across rice, wheat, and maize datasets	Rice, wheat, maize datasets	Improved food grain disease recognition with new DL model
[14]	Convolutional Neural Network (CNN)	95% accuracy	Rice leaf images	Effective detection of rice diseases using CNN
[15]	VGG19, DenseNet201, ResNet152V2, Vision Transformer (VIT)	Best accuracy: DenseNet201 at 98.77%	Betel leaf dataset	Detection of betel leaf diseases using multiple DL models
[16]	Custom CNN, Google Colab, single-board computers	Evaluated using Raspberry Pi, NVIDIA GPUs, Google Coral Dev	Healthy and unhealthy plant images	Comparison of performance on different hardware for plant health detection
[17]	Integrated DL Framework (IDLF),	99.58% accuracy with RegNetY080 + Random Forest	Wheat plant dataset	Ensemble DL for wheat disease classification

	ensemble learning, pre-trained networks			
[18]	DL-based web application for apple leaf diseases	Identification of various diseases (e.g., Alternaria, Leaf Spot)	Apple leaf image dataset	Early identification of apple leaf diseases to boost production
[19]	Krill Herd-based Random Forest (KHbRF)	Improved detection accuracy	PlantVilla image dataset	Optimization of crop disease detection using KHbRF
[20]	Pre-trained CNNs (AlexNet, VGG16, VGG19), Transfer Learning	Best performance: AlexNet at 96.63% accuracy	PlantVillage dataset	Enhanced plant disease detection using pre-trained CNNs
[21]	CNN, CNN-SVM, DNN (Deep Ensemble)	Best accuracy: 99.98%	Potato leaf images	Detection of four types of potato diseases using DL ensemble
[22]	Pre-processing, feature extraction, feature selection, RGB conversion	Evaluation on sensitivity, specificity, accuracy	Paddy leaf dataset	Automated leaf disease detection focusing on paddy leaves
[23]	MobileNetV3Small, E-GreenNet Framework	Accuracy: 0.96% - 1.00%	Plant composite, PlantVillage, DRLI datasets	Deep learning framework for plant disease classification
[24]	Embedded systems, IoT, cloud platforms, ML, DL	Survey and real-time IoT-based detection	Various IoT and cloud platforms	Comprehensive survey on real-time plant disease detection

2. MATERIAL AND METHOD

The proposed methodology consists of two major phases: training individual CNN models and generating hybrid models from the best-performing one.

2.1. Non-Hybrid Model Training

Four pre-trained models—ResNet-50, VGG-19, VGG-16, and Inception V3—were trained on the PlantVillage dataset, which contains images of plant leaves with various diseases. The training methodology followed a standard process of loading and labelling the dataset, splitting the data into training and testing sets, augmenting the data, and fine-tuning each pre-trained model to fit the dataset. Specifically, the steps were as follows:

- The dataset was loaded from a specified directory, and labels were assigned based on folder names.
- The data was split into an 80:20 ratio for training and testing.
- Image augmentation techniques were applied to enhance data diversity, which included resizing images to 224x224x3, converting grayscale to RGB, and other preprocessing techniques.
- Each pre-trained model was fine-tuned by freezing the lower layers and replacing the final fully connected layers with custom layers suitable for the number of classes in the PlantVillage dataset.
- The training parameters in each used model, which basically are learning rate, batch size, and number of epochs, are optimized to efficiently converge. The starting learning rate was 0.0001, with a batch size of 32, while the maximum number of epochs was 10. Each of these four pre-trained models is further trained separately using the above methodology: ResNet-50, VGG-19, VGG-16, and Inception V3. This ensured the realization of distinctive capabilities of each architecture in classifying plant diseases.

ResNet-50 turned out to be the best among the four models, with the highest performance at 82.74% regarding accuracy and 79.13% for the AUC. Because of the superior performance, ResNet-50 turned out to be the ideal candidate for creating hybrid models with a view to improving further the accuracy and robustness of the detection.

2.2. Hybrid Model Development

Since ResNet-50 yielded the highest performance among the independent models, the hybrid models were created by combining ResNet-50 independently with the other models, VGG-19, VGG-16, and Inception V3. The methodology for the development of the hybrid models was as follows:

- Features extracted from the fully connected layers of both ResNet-50 and the secondary models - VGG-19, VGG-16, or Inception V3 - were then concatenated. For example, features from the last fully connected layer of ResNet-50 were combined with that of the last fully connected layer of VGG-16 to obtain a comprehensive feature set comprising a wide range of discriminative properties from the input data.

Classifier Training: After these feature vectors were combined, training would be necessary with such a classifier on these combined features for the prediction of the class related to the disease. The multi-class SVM here was trained by concatenating the feature vectors through the training set. In this way, allowing the model to take advantage of the strength of each of the other models.

Training: Similar to the training of the non-hybrid models, the hybrid model was then trained with the concatenated feature set.

Evaluation Metrics: Standard performance metrics were used to evaluate the performance of both individual and hybrid models. The following are accuracy, precision, recall, F1 score, AUC, and the confusion matrix. It can be observed that, compared to the independent ResNet-50 model, hybrid models improve the classification for better accuracy and AUC. Among them, the best performing hybrid model involves the combination of ResNet-50 with Inception V3. The flowchart for the proposed models is presented in Figure 1.
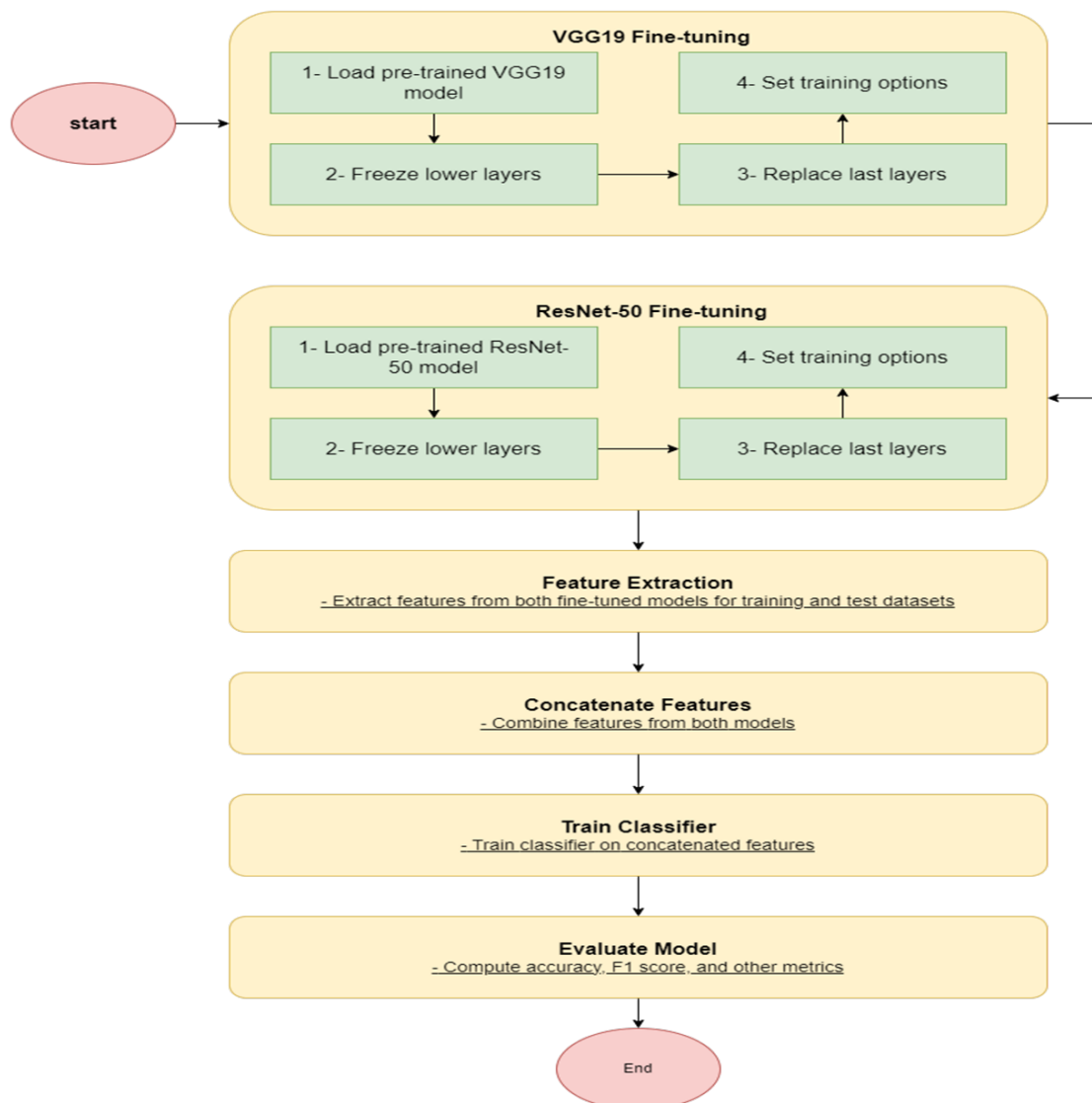
Figure 1. The flowchart for the proposed models

2.3. Dataset

The dataset that will be used in this effort is one of the well-known resources of plant diseases; it is the PlantVillage dataset. It consists of over 20.6k images of healthy and diseased plant leaves, representing 14 disease categories and 1 category of the healthy ones. Figure 2 below shows both a healthy and diseased image of representative plant leaf-providing complete representation of common plant diseases. As such, each image is titled with the specific type of plant and its disease; hence, this dataset best suits supervised learning model training applications.

The dataset covers a wide variety of conditions, including different disease manifestations across multiple plant species, which makes it a valuable resource for deep learning-based classification tasks. Images were collected under controlled conditions to ensure consistency, yet they reflect significant diversity in color, shape, and texture. This diversity presents realistic challenges that help improve the robustness of trained models.

The PlantVillage dataset serves as the foundational input for training both individual and hybrid models, allowing the network to learn distinguishing features between healthy and diseased leaves. Its diversity and comprehensiveness make it suitable for developing robust models for real-world plant disease detection. Some samples of the dataset used in the study.is shown in Figure 2.
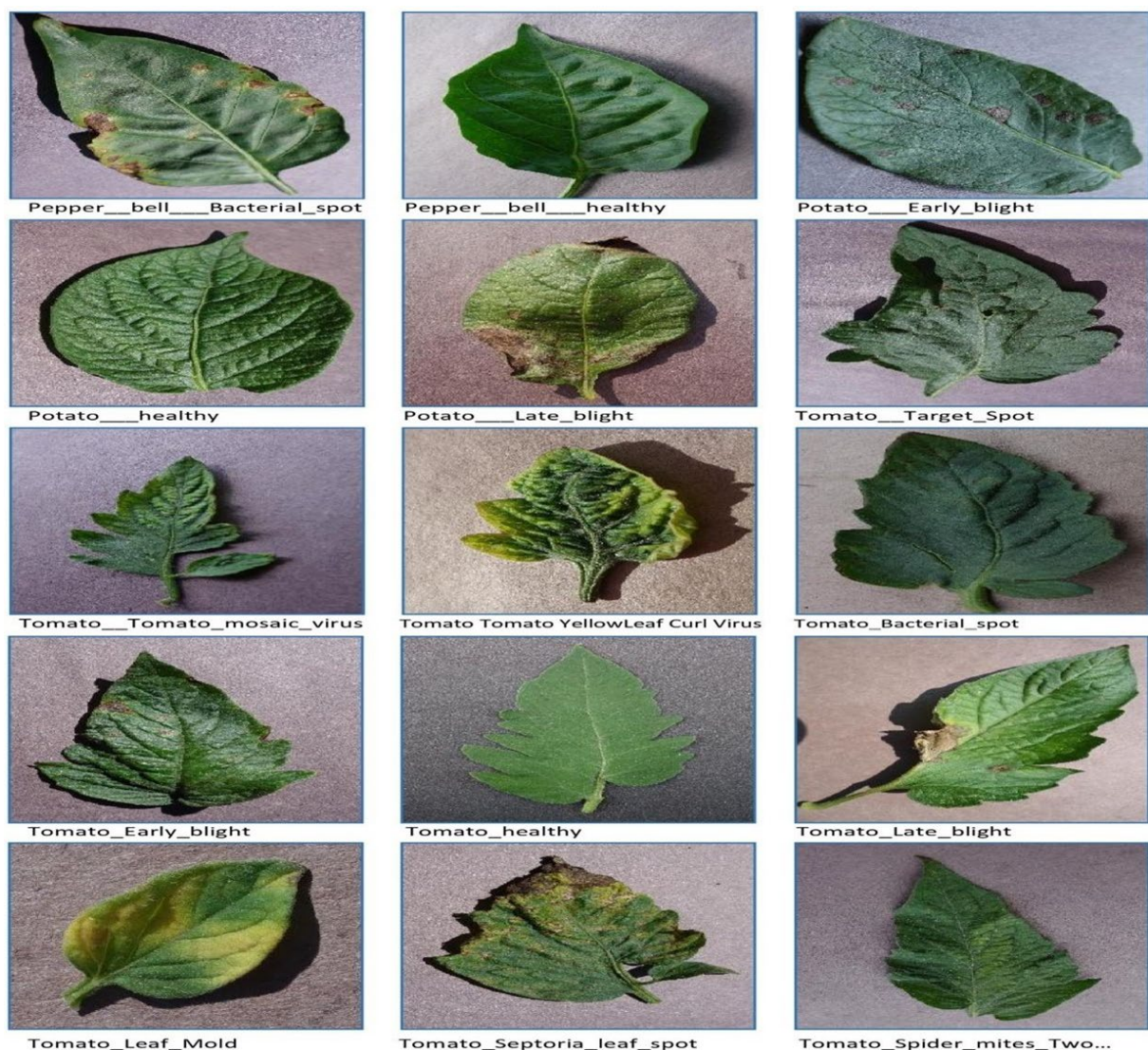
Figure 2. Some samples of the dataset used in the study

2.2. Fine-Tuning Technique

One of the most important techniques employed in the fine-tuning of pre-trained models for this particular study of plant disease detection is fine-tuning. Fine-tuning in CNN takes a model that was pre-trained on a huge dataset,

say ImageNet, and restructures it to suit the very particular dataset used in this study. In this regard, the process of fine-tuning is summarized as follows:

- Retains the first few layers of a pre-trained network that capture general features such as edges and textures. These are often frozen during training, as the learned weights are not updated.
- The last, more task-specific layers of the model are replaced by new layers with a number of classes equal to that in the PlantVillage dataset.

These added layers are then trained, and the whole model is fine-tuned by using a smaller learning rate in order to adjust weights throughout the network without significantly altering the earlier learned features.
Fine-tuning allows the model to leverage those features learned from the large-scale general dataset in this specific case of plant disease classification problems more precisely and much more effectively.

3. RESULTS

The performances of both non-hybrid and hybrid models will be done in two stages: first, each of the pre-trained models was evaluated, and second, the performance evaluation of a hybrid model with a different architecture combined with ResNet-50, namely VGG-19, VGG-16, and Inception V3.

3.1. Non-Hybrid Model Results

Each of the four pre-trained CNN models, namely ResNet-50, VGG-19, VGG-16, and Inception V3, was subjected to individual examination in plant disease classification. All models underwent exactly the same training methodology on the PlantVillage dataset for training and fine-tuning. Each model was trained and fine-tuned using the same method on the same PlantVillage dataset. The following key metrics-Accuracy, Precision, Recall, F1 Score, and AUC-were implemented to investigate the performance of these strategies. Results can be seen in the Table 1 below.

This conclusively made ResNet-50 the best individual model, with an accuracy of 85.30%, hence making it a very suitable candidate for hybridization. Inception V3 had an accuracy of 72.00%, which might be called moderate, and VGG-16 and VGG-19 recorded accuracies in the 60s, hence portraying a larger gap in performance. These varying performances by these models when applied individually to the task of plant disease detection commerce.

Table 2. Comparison of non-hybrid models performance

Model	Accuracy	Precision	Recall	F1 Score	AUC
ResNet-50	85.30%	84.75%	83.90%	84.32%	82.40%
Inception V3	72.00%	70.50%	69.00%	69.74%	68.30%
VGG-16	63.25%	62.10%	61.20%	61.64%	60.45%
VGG-19	67.50%	66.20%	65.40%	65.79%	64.95%

3.2. Hybrid Model Results

The latter step involved the development of hybrid models. ResNet-50, which was the topmost model, was combined with each of the other models, namely VGG-19, VGG-16, and Inception V3. Each hybrid model was evaluated again on the basis of the metrics discussed above. The following table enumerates the performance results of each hybrid model in terms of accuracy, precision, recall, F1 score, and AUC, showing that hybrid models outperform those that are non-hybrid.

Table 3. Comparison of hybrid models performance

Model	Accuracy	Precision	Recall	F1 Score	AUC
ResNet-50 & VGG-19	99.52%	99.52%	100%	99.75%	92.80%
ResNet-50 & VGG-16	98.74%	95.71%	97.24%	92.80%	92.80%
ResNet-50 & Inception V3	99.60%	99.13%	98.21%	98.66%	99.98%

Model 1: ResNet-50 & VGG-19: Results with ResNet-50 combined with the VGG-19 model returned an accuracy of 99.52% on the test set. Precision was 99.52%, while Recall was perfect at 100%, thus showing that this model can recognize all positive instances without any false negatives. With regard to F1, which is indicative of balance between Precision and Recall, it reaches as much as 99.75%, meaning a very excellent overall performance. The AUC also fared similarly well, posting a value of 92.80% to reflect a high degree of separability between classes.

Model 2: ResNet-50 & VGG-16: The accuracy in the second model, with ResNet-50 and VGG-16, is 98.74%. Although slightly lower than Model 1, this has also resulted in a very good performance. The precision will be 95.71%, and the Recall is 97.24%, which gives an F1 Score of 92.80%. The AUC value also turns out to be the same as that of the first model, which can be interpreted to mean that the capability of the model in distinguishing classes is highly effective, though the performance metrics went down by a margin.

Model 3: The model that married ResNet-50, and Inception V3 architectures combined returned an accuracy of 99.60% pants. Precision was 99.13%, and Recall was 98.21%, thus yielding the value of F1 Score to 98.66%, which was the best of the three models. The AUC value for this model was 99.98%, the best across systems and indicating a very good performance on class discrimination.

3.3. Comparison of Model Performance

The results depicted that the overall performance of ResNet-50 and Inception V3 works best for the classification tasks in terms of accuracy and AUC, i.e., distinguishing between classes. Model 1 (ResNet-50 & VGG-19) performed almost equally in terms of accuracy and F1 Score but Model 3 slightly outperformed the result regarding the precision and recall. Model 2, on the other hand, lost momentum a bit more compared to the other two models, with a drop in performance a bit clearer, especially at Precision.
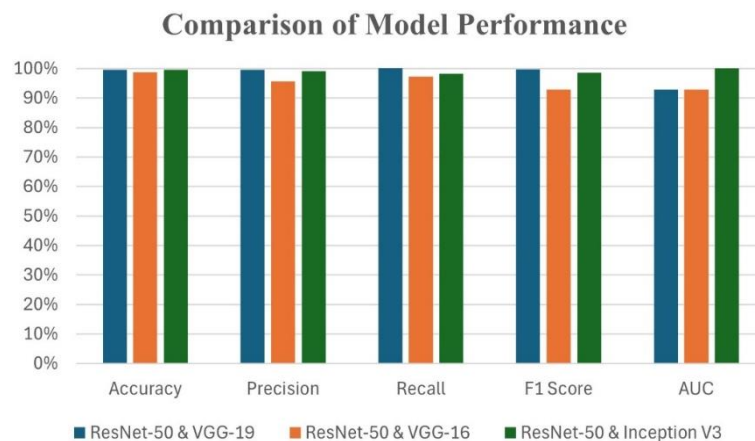
Figure 3. Comparison of hybrid models performance

4. CONCLUSION

This research provides an effective solution for the detection of plant diseases through the use of hybrid CNN models. Accordingly, four pre-trained models were trained: ResNet-50, VGG-19, VGG-16, and Inception V3. These aforementioned models showed that ResNet-50 was the best among them. Hybrid models were then developed to further enhance disease-detecting results. Among the hybrids developed, the highest accuracy and AUC values were found when ResNet-50 was combined with Inception V3, proving that hybridization can expand robustness and efficiency in the plant disease classification system.

This hybrid model delivered superior accuracy and also demonstrated the effective detection of multiple plant diseases, well equipped for agricultural monitoring. This study opens a very promising avenue for the monitoring of agricultural diseases in the future. The practical applications will definitely be pursued in the real world by farmers and agricultural experts. Further work may include additional network combinations, for which, after testing these hybrid approaches on their datasets, the described hybrid approach can be better revealed in its effectiveness.

References

[1]   M. Agarwal, A. Singh, S. Arjaria, A. Sinha, and S. Gupta, "ToLeD: Tomato leaf disease detection using

convolution neural network," *Procedia Computer Science*, vol. 167, pp. 293–301, 2020.

[2]   K. Ahmed, T. R. Shahidi, S. M. I. Alam, and S. Momen, "Rice leaf disease detection using machine learning techniques," in *2019 International Conference on Sustainable Technologies for Industry 4.0 (STI)*, 2019.

[3]   M. S. Al-Gaashani, F. Shang, M. S. Muthanna, M. Khayyat, and A. A. Abd El-Latif, "Tomato leaf disease classification by exploiting transfer learning and feature concatenation," *IET Image Processing*, vol. 16, no. 3, pp. 913–925, 2022.

[4]   T. Ashraf, and Y. N. Khan, "Weed density classification in rice crop using computer vision," *Computers and Electronics in Agriculture*, vol. 175, art. no. 105590, 2020.

[5]   J. Basavaiah and A. Arlene Anthony, "Tomato leaf disease classification using multiple feature extraction techniques" *Wireless Personal Communications*, vol. 115, no. 1, pp. 633–651, 2020.

[6]   A. Batool, S. B. Hyder, A. Rahim, N. Waheed, and M. A. Asghar, "Classification and identification of tomato leaf disease using deep neural network," in *2020 International Conference on Engineering and Emerging Technologies (ICEET)*, 2020.

[7]   J. Chen, J. Chen, D. Zhang, Y. Sun, and Y. A. Nanehkaran, "Using deep transfer learning for image-based plant disease identification," *Computers and Electronics in Agriculture*, vol. 173, art. no. 105393, 2020.

[8]   G. Gangadevi and C. Jayakumar, "Review of deep learning architectures used for identification and classification of plant leaf diseases," in *Artificial Intelligent Techniques for Wireless Communication and Networking*, R. Kanthavel, K. Ananthajothi, S. Balamurugan, and R. Karthik Ganesh Eds. 2022, pp. 75–90.

[9]   S. M. Omer, K. Z. Ghafoor, and S. K. Askar, "Lightweight improved yolov5 model for cucumber leaf disease and pest detection based on deep learning," *Signal, Image and Video Processing*, vol. 18, no. 2, pp. 1329–1342, 2024

[10]   M. M. Khalid and O. Karan, "Deep learning for plant disease detection," *International Journal of Mathematics, Statistics, and Computer Science*, vol. 2, pp. 75–84, 2024.

[11]   D. Trinh, A. Mac, K. Dang, H. Nguyen H. Nguyen, and T. Bui, "Alpha-EIOU-YOLOv8: An improved algorithm for rice leaf disease detection," *AgriEngineering*, vol. 6, no. 1, pp. 302–317, 2024.

[12]   A. Bonkra, S. Pathak, A. Kaur, and M. A. Shah, "Exploring the trend of recognizing apple leaf disease detection through machine learning: a comprehensive analysis using bibliometric techniques," *Artificial Intelligence Review*, vol. 57, no. 2, art. no. 21, 2024.

[13]   D. S. Joseph, P. M. Pawar, and K. Chakradeo, "Real-time plant disease dataset development and detection of plant disease using deep learning," *IEEE Access*, vol. 12, pp. 16310–16333, 2024.

[14]   P. Kulkarni and S. Shastri, "Rice leaf diseases detection using machine learning," *Journal of Scientific Research and Technology*, vol. 2, no. 1, pp. 17–22, 2024.

[15]   S. Kusuma and K. R. Jothi, "Early betel leaf disease detection using vision transformer and deep learning algorithms," *International Journal of Information Technology*, vol. 16, no. 1, pp. 169–180, 2024.

[16]   G. Routis, M. Michailidis, and I. Roussaki, "Plant disease identification using machine learning algorithms on single-board computers in IoT environments," *Electronics*, vol. 13, no. 6, art. no. 1010, 2024.

[17]   H. Catal Reis and V. Turk, "Integrated deep learning and ensemble learning model for deep feature-based wheat disease detection," *Microchemical Journal*, vol. 197, art. no. 109790, 2024.

[18]   S. Kumar, R. Kumar, M. Gupta, and A. J. Obaid, "Deep learning-based web application for real-time apple leaf disease detection and classification," in *2024 International Conference on Advancements in Smart, Secure and Intelligent Computing (ASSIC)*, 2024.

[19]   L. N. B. Srinivas, A. M. Viswa Bharathy, S. Kumar Ramakuri, A. Sethy, and R. Kumar, "An optimized machine learning framework for crop disease detection," *Multimedia Tools and Applications*, vol. 83, no. 1, pp. 1539–1558, 2024.

[20]   P. Dey, T. Mahmud, S. R. Nahar, M. S. Hossain, and K. Andersson, "Plant disease detection in precision agriculture: Deep learning approaches," in *2024 2nd International Conference on Intelligent Data Communication Technologies and Internet of Things (IDCIoT)*, 2024.

[21]   H. Paul, S. Ghatak, S. Chakraborty, S. K. Pandey, L. Dey, D. Show, and S. Maity, "A study and comparison of deep learning based potato leaf disease detection and classification techniques using explainable AI," *Multimedia Tools and Applications*, vol. 83, no. 14, pp. 42485–42518, 2024.

[22]   R. K. Dubey and D. K. Choubey, "An efficient adaptive feature selection with deep learning model-based paddy plant leaf disease classification," *Multimedia Tools and Applications*, vol. 83, no. 8, pp. 22639–22661, 2024.

[23]   T. S. Adekunle, M. O. Lawrence, O. O. Alabi, A. A. Afolorunso, G. N. Ebong, and M. A. Oladipupo, "Deep learning technique for plant disease detection," *Computer Science and Information Technologies*, vol. 5, no. 1, pp. 55–62, 2024.

[24]   A. Morchid, M. Marhoun, R. El Alami, and B. Boukili, "Intelligent detection for sustainable agriculture: A review of IoT-based embedded systems, cloud platforms, DL, and ML for plant disease detection," *Multimedia Tools and Applications*, vol. 83, pp. 70961–71000, 2024.

Comparison of Aerodynamic Properties of Three Airfoils Used in Small-Scale Vertical Axis Wind Turbines

Erman Kadir Oztekin[1], Elyasa Aydin[1]

[1]Department of Mechanical Engineering, Bayburt University, Bayburt, Türkiye
Corresponding author: Erman Kadir Oztekin (e-mail: ermanoztekin@bayburt.edu.tr)

Abstract

Small-scale vertical axis wind turbine (VAWT) can be used to meet the energy needs of rural areas or to provide part of the energy need of a family through renewable means. VAWTs operate at lower noise levels and are considered much safer to use. It is not easy to predict the torque and power outputs of the VAWTs since angle of attack of their blades is constantly changing with respect to the air flow direction. VAWTs are relatively easy to manufacture, especially their blades, and their production costs are low. VAWTs are classified into two groups: Darrieus type and Savonius type. Darrieus type turbines are powered by the lift force acting on their blades. Their blades are constructed by using different types of airfoils. This study examines the lift and drag properties of three distinct airfoil types, FX 66, SD 7032, and SG 6043, in two dimensions. These airfoils mostly preferred in H-blade design. Airfoils were simulated using computational fluid dynamics (CFD). Drag and lift forces and coefficients are calculated in order to compare characteristics of these airfoils.

Keywords: Airfoil, Vertical axis, Wind turbine, Lift, Drag

1. INTRODUCTION

Wind turbines can be classified in various ways. The most common classification is based on the turbine's axis of rotation relative to the direction of the wind. They can also be classified according to the type of aerodynamic forces acting on the turbine blades and the power produced [1]. Wind turbines (WTs) are produced in smaller sizes, especially for rural areas and individual uses which can be called small-scale WT. The power produced by the turbine depends on the scale of the turbine body. WTs are generally divided into two types, vertical (VAWT) and horizontal axis wind turbines (HAWT), according to their rotation axes. While HAWTs are not preferred in urban areas, VAWTs are preferred [2, 3]. This is because HAWTs are relatively less effective and their use poses safety problems. VAWTs are simpler to manufacture, so their small-scale production can easily be used in urban and rural settings. VAWTs require self-start mechanism but can extract more wind energy from per rotation. VAWT can be categorized into two groups based on design: Savonius type and Darrieus type. The design of Savonius type VAWT consists of two half cylinders facing opposite directions. Darrieus offer superior aerodynamic performance, lower costs, and a simpler design than the Savonius. So far the improvements have been done on the design of VAWT regarding blade design, aerodynamic performance, and modelling [4, 5].

The blades of Darrieus type of turbine use lift force while rotating in the vertical direction. The Darrieus type consist of blades with airfoil cross-section. H-blades are easier to design and manufacture than curved blades, and their performance is superior to conventional designs. Working principle and schematic view of the H-blades Darrieus type wind turbine can be seen from Figure 1.
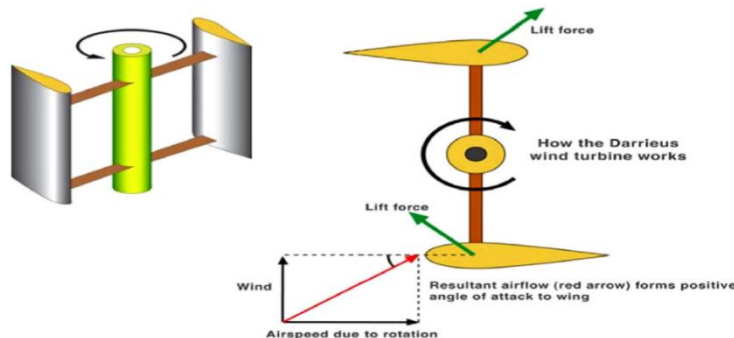
Figure 1. H-design Darrieus type turbine with lift force acting on the blades [1]

The sum of the pressure and shear forces acting on the entire surface of a airfoil moving in the airflow is equal to the net aerodynamic force. Aerodynamic forces are called drag force, which is parallel to the direction of motion of the flow, and lift force, which is perpendicular to the direction of motion of the flow. The expression for the complete drag force can be given as:

$$F_D = C_D A \frac{\rho}{2} V^2 \qquad (1)$$

where C_D is the coefficient A is the frontal area of the vehicle, ρ is the density of the fluid and V is the speed of the object relative to the fluid. Similarly, the expression for the lift force can be given as:

$$F_L = C_L A \frac{\rho}{2} V^2 \qquad (2)$$

where C_L is the coefficient and A is the airfoil surface. In both expression coefficients contain all complex dependencies and are calculated experimentally or numerically.

2. MATERIAL AND METHOD

Two-dimensional computational fluid dynamics (CFD) analysis was performed using the ANSYS Fluent program in this inquiry. Since they serve as the foundation for CFD and allow us to simulate intricate turbulent flows, the Reynolds-Averaged Navier-Stokes Equations (RANS) have played a significant role in this breakthrough. Applications of the RANS model include marine solutions, aerospace and aeronautical engineering, industrial and automotive solutions, and more. The standard k-ε turbulence model consists a set of equations which can be applied to a large number of turbulent applications.

Three different geometry used in the analyses. FX 66, SD 7032, and SG 6043 type airfoils are meshed and analysed for their aerodynamic characteristics in 2D. For this study, only the aerodynamic performance at zero-degree angle of attack were investigated for three profiles. It is known that some wings can create lift even when horizontal [1]. The air assumed to approach an airfoil with the velocity of 40 km/h (11.1 m/s). The chord length of airfoil is taken as 100 mm for all profiles. The schematic view of the FX 66 airfoil can be seen from Figure 2. No-slip wall conditions for the surfaces were defined. The same boundary conditions were defined in all analyses.
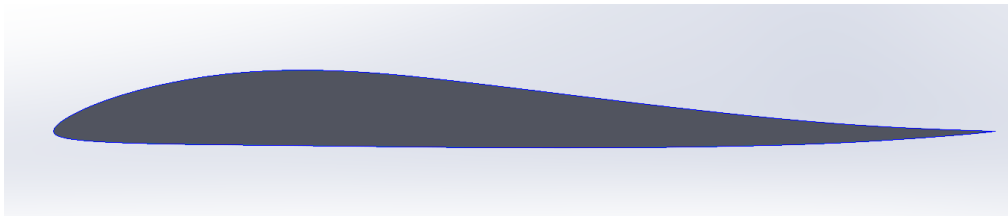
Figure 2. 2D view of FX 66 airfoil
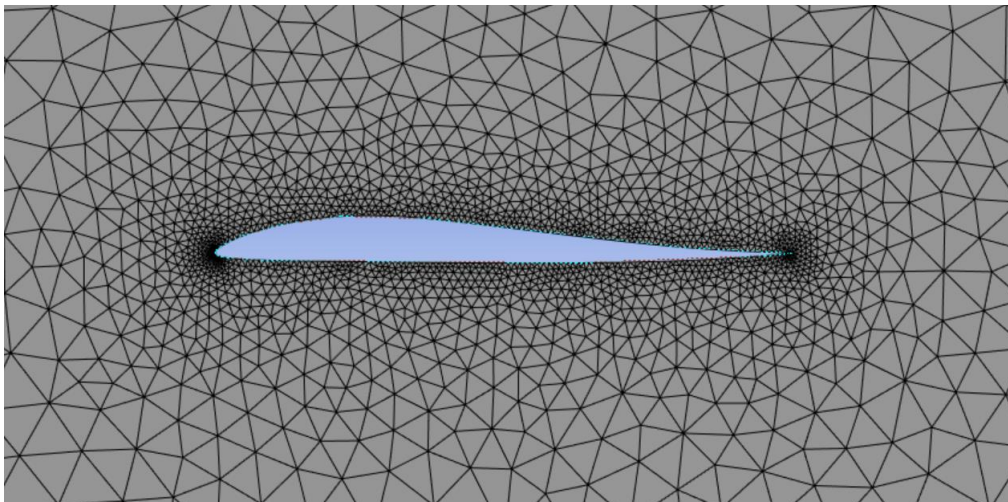
Figure 3. 2D mesh of FX 66 airfoil

Comparison of aerodynamic properties of three airfoils used in small-scale
vertical axis wind turbines
ICMUSTED 2024

Triangles method was applied to mesh fluid around airfoil. Moreover, dense mesh was applied to the edges of the airfoil in order to get more accurate results from the surface of the airfoil [6]. For all types maximum mesh skewness value is less than 0.6. The mesh profile around the airfoil can be seen from Figure 3.

3. RESULTS

Table 1 shows lift and drag coefficients and forces for three airfoils.

Table 1. Lift and drag characteristics of airfoils. C_L and C_D are coefficients and F_L and F_D are forces acting on the surface of the airfoil

FX 66		SD 7032		SG 6043	
C_L	0.81581	C_L	4.3324	C_L	7.32756
F_L	0.49968 (N)	F_L	2.65361 (N)	F_L	4.48813 (N)
C_D	0.28314	C_D	0.31781	C_D	0.36945
F_D	0.17342 (N)	F_D	0.19465 (N)	F_D	0.22629 (N)

Pressure distribution at zero-degree of angle of attack for three airfoils are presented in Figure 4, Figure 5 and Figure 6.
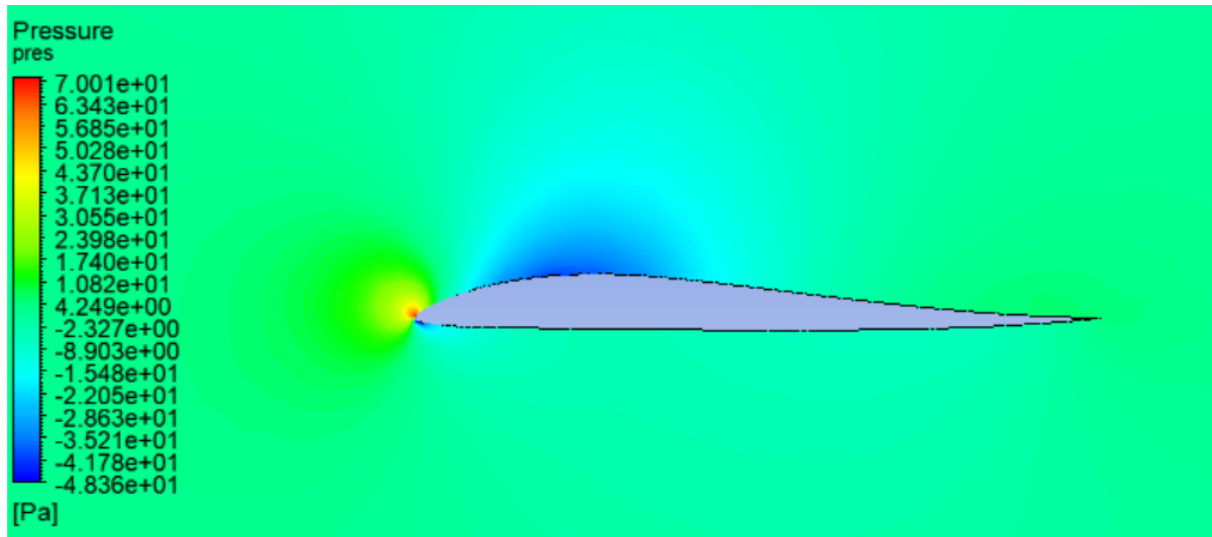
Figure 4. Pressure distribution around FX 66
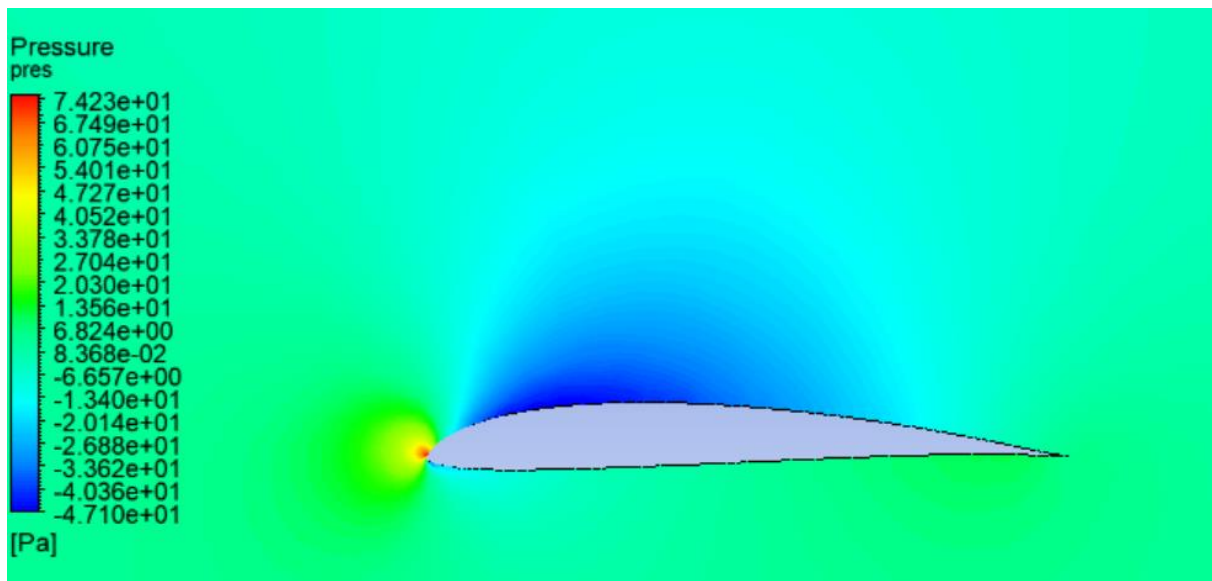
Figure 5. Pressure distribution around SD 7032
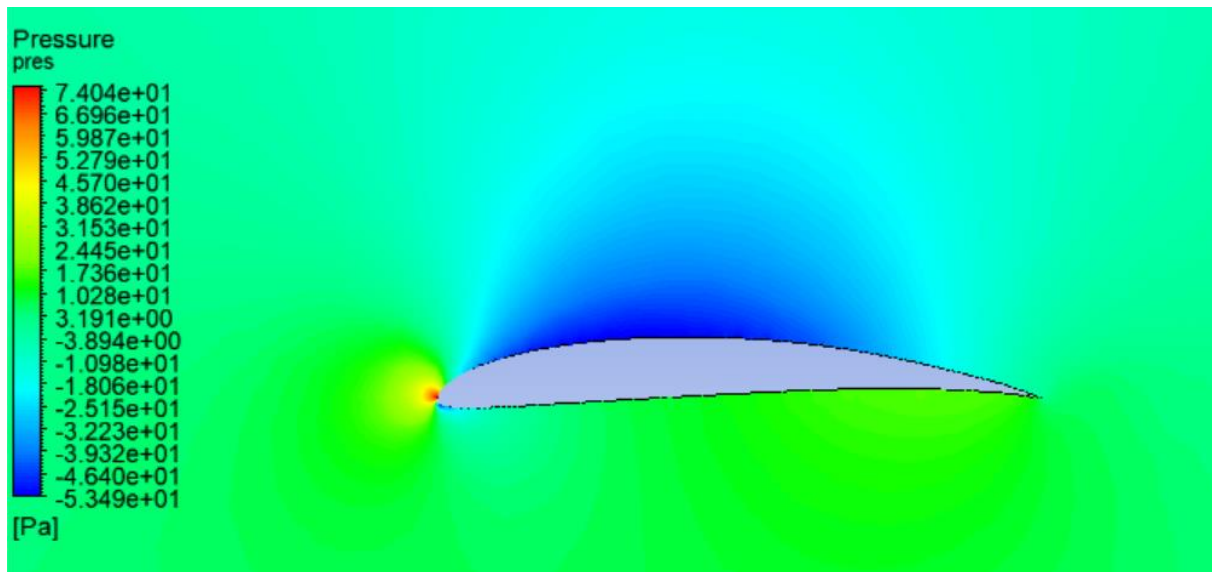
Figure 6. Pressure distribution around SG 6043

4. CONCLUSION

VAWTs can be used to harness energy from wind. Since H-type wind turbines are relatively easier and less costly to manufacture, they can be produced on a small scale in urban areas. The following inferences can be made with the results obtained here.

- Thier performance can be improved by using different airfoils.
- Some airfoils can create better lift even at horizontal position. It seen from the results that SD 7032 and SG 6043 has wider low-pressure on their top surface.
- The performance of 3D structure is not easy to analyse since the degree of the attack angle changes during rotation.

References

[1] R. Kumar, K. Raahemifar, and A. S. Fung, "A critical review of vertical axis wind turbines for urban applications," *Renewable and Sustainable Energy Reviews*, vol. 89, pp. 281–291, 2018.

[2] N. A. Ahmed and M. Cameron, "The challenges and possible solutions of horizontal axis wind turbines as a clean energy solution for the future, " *Renewable and Sustainable Energy Reviews*, vol. 38, pp. 439–460, 2014.

[3] Z. Simic, J. G. Havelka, and M. Bozicevic Vrhovcak, "Small wind turbines – A unique segment of the wind power market," *Renewable Energy*, vol. 50, pp. 1027–1036, 2013.

[4] G. J. van der Veen, J. W. van Wingerden, P. A. Fleming, A. K. Scholbrock, and M. Verhaegen, "Global data-driven modeling of wind turbines in the presence of turbulence," *Control Engineering Practice*, vol. 21, no. 4, pp. 441–454, 2013.

[5] Y. A. Katsigiannis and G.S. Stavrakakis, "Estimation of wind energy production in various sites in Australia for different wind turbine classes: A comparative technical and economic assessment," *Renewable Energy*, vol. 67, pp. 230–236, 2014.

[6] K. A. H. Al-Gburi, F. B. I. Alnaimi, B. A. J. Al-Quraishi, E. S. Tan, and A. K. Kareem, "Enhancing savonius vertical axis wind turbine performance: A comprehensive approach with numerical analysis and experimental investigations," *Energies*, vol. 16, no. 10, art. no. 4204, 2003, doi: 10.3390/en16104204.

The Link Between Technological Innovations and Total Quality Management: A Study on Turk Food Industry

Adnan Kara[1], Yusuf Esmer[2]

[1]Department of International Trade and Business Administration, Bayburt University, Bayburt, Türkiye
[2]Department of Management Information Systems, Bayburt University, Bayburt, Türkiye
Corresponding author: Yusuf Esmer (e-mail: yesmer@bayburt.edu.tr)

Abstract

In this study, it is aimed to determine the relationship between technological innovations and TQM based on the Turk food industry. For this purpose, it was deemed appropriate to use thematic analysis, one of the qualitative research techniques, in the study. Within the scope of thematic analysis, a 5-stage path was followed and word frequency analysis, clustering analysis and word tree mapping techniques were used in the data analysis process with Nvivo 15 software program. As a result of the analysis, it was determined that the innovation strategies of the companies in the study included concepts, words and expressions within the scope of TQM principles, and the relationship between technological innovation and TQM was confirmed.

Keywords: Quality, TQM, Technological innovation, Thematic analysis

1. INTRODUCTION

Quality is an issue that businesses deal with both statistically and managerially. Especially production enterprises look at quality from both aspects. While the statistical aspect of quality focuses on outputs such as zero defects, waste and product durability, the managerial aspect of quality focuses on antecedents such as process improvement, training and development. While the production unit focuses on statistical outputs for quality in enterprises, the management unit focuses on managerial antecedents. In this context, Total Quality Management (TQM) is a quality approach that is designed to bring together the different understandings of quality in all units of the organization. In other words, TQM is a management philosophy that promotes an organizational culture that aims to achieve customer satisfaction through continuous improvement [1, 2].

Technological innovations such as information technologies, robotic systems and automation have led to changes in the understanding of TQM in enterprises. While businesses gain benefits such as speed, agility and standardization in production, they are exposed to drawbacks such as maintenance costs, control and data entry processes, and failures [2]. Innovation is defined by the European Commission as *"the renewal and expansion of the product range and related markets, the creation of new production, supply and distribution methods, the introduction of changes in management, business organization and working conditions and business skills"* [3]. According to [4], in many respects TQM can be seen as laying the foundations for a cultural environment that fosters innovation. Implementation of TQM contributes to the achievement of beneficial effective innovation by leading to changes in the organizational structure and making it flexible. TQM concepts such as formalization and empowerment can create the necessary balance between autonomy, discipline and control and provide a solid foundation for the development of incremental innovations and eventually radical innovations [4]. Based on these judgments, the effects of the skills acquired by enterprises on total quality are the main subject of the research, and this study aims to examine the relationship between technological innovations and TQM based on the Turk food industry.

2. MATERIAL AND METHOD

In the study, content analysis was used within the scope of qualitative research method, and content analysis was carried out with thematic analysis technique. Thematic analysis is used to make sense of the data in a data set and to identify certain themes and sub-themes. In the research, thematic analysis was used to categorize the data in the context of innovation and TQM and to reveal the relationships and differences between the concepts. A 5-stage method was followed in the thematic analysis. In the first stage, the websites, reports and news content of 8 companies (Eti, Ulker, Arcelik, Ford Otosan, Türkiye Is Bankasi, Tirsan, Turkcell, Netas) operating in Türkiye and whose innovation strategies were identified were analyzed. In the second stage, the data obtained from

company reports were coded according to the themes related to innovation and TQM. In the third stage, the coded
data were analyzed and similar themes were brought together to form larger themes. In the fourth stage, the
relationships between the themes were examined. In the last stage, the themes and relationships were interpreted.
Thematic analysis was conducted with Nvivo 15 software program and word frequency analysis, clustering
analysis and word tree mapping techniques were used.

3. RESULTS

The results of the cluster analysis of the concepts related to TQM included in the expressions of innovation
strategies of the companies included in the research sample are given in Figure 1. The concepts related to TQM
were transformed into graphs in groups according to the relationships between them. Within the employee
involvement group, the words expectation, solution, knowledge, value, change, experience and time are included.
Continuous improvement group includes the words training, development, empowerment, improvement, culture,
service and errors. Risk management includes the words standard, mentorship, learning, market, performance,
plan, competition and strategy. The productivity group includes the words savings, production, processes, talent,
management, vision, efficiency, and productive.

Figure 1. Cluster analysis findings

The word graph created according to the frequency and weight of the words in the innovation strategies of the research sample companies is shown in Figure 2. It is seen that innovation, new product and novelty are the most repeated words with the highest weights. On the other hand, it is understood that concepts such as customer, investment, difference, project, big data, cyber security, knowledge are less frequently repeated.

Figure 2. Word frequency and weight graph

The sentences related to quality in the innovation strategies of the research sample companies were analyzed with the word tree technique and the findings are shown in Figure 3.

Figure 3. Word tree

In the word tree in Figure 3, it is seen that the goals to increase quality and expressions related to production are predominant. It is also understood that the concepts related to the quality management system are also at the forefront.

4. CONCLUSION

TQM is a management system that aims to create an organizational culture open to innovation and technology and is closely related to the concept of technological innovation [5]. In this context, the relationship between technological innovations and TQM was investigated in Turk food industry companies. The results of the research are as follows: The technological innovation strategies of the companies include many concepts such as value, knowledge, education, culture, competition, strategy, production and savings within the scope of TQM principles of employee participation, continuous improvement, risk management and efficiency. This result shows that companies develop and implement innovation strategies related to TQM. It is seen that the most frequently repeated words in the innovation strategies of the companies and the words with the highest weights are innovation, new product and novelty. This result shows that companies prioritize technological innovation and give importance to innovation. It is concluded that quality development, quality management system and production related statements are predominant in the innovation strategies of the companies. This result shows that companies give importance to quality management system, quality improvement and production along with innovation. As a result,

it is thought that this study is important in terms of revealing the link between technological innovation and TQM based on the concepts and words in the innovation expressions of companies and will contribute to the literature.

References

[1]   G. K. Kanji, *Measuring Business Excellence*, London and New York: Routledge, 2002.

[2]   P. Moura E Sá and A. Abrunhosa, "The role of TQM practices in technological innovation: The Portuguese footwear industry case," *Total Quality Management & Business Excellence*, vol. 18, no. 1–2, pp. 57–66, 2007.

[3]   European Commision, *Green Paper on Innovation*, 1995.

[4]   J. Zeng, C. A. Phan, and Y. Matsui, "The impact of hard and soft quality management on quality and innovation performance: An empirical study," *International Journal of Production Economics*, vol. 16, pp. 216–226, 2015.

[5]   A. Yuksel, "A new look at the relationship between total quality management and innovation: Innovative literacy," *ASBIDER-Akademi Sosyal Bilimler Dergisi*, vol. 10, no. 30, pp. 231–241, 2023.

The Role of Rituals in Social Repair after Natural Disasters

Sonyel Oflazoglu Dora[1], Tutku Doksoz[1]

[1]Department of Business Administration, Hatay Mustafa Kemal University, Hatay, Türkiye
Corresponding author: Sonyel Oflazoglu Dora (e-mail: oflazoglusonyel@gmail.com)

Abstract

Recovery and adaptation processes in post-disaster periods cannot be explained only by physical and economic factors. This process also requires a deep understanding of social and cultural dynamics. Rituals and place-memory relations play an important role in post-disaster social recovery and adaptation. Rituals symbolize individuals and communities mourning together, showing solidarity and participating in the reconstruction process (Turner 1969). This is in line with Nora's (1989) concept of 'places of memory'. Moreover, rituals allow communities to develop adaptability and resilience in the process of reconstruction after a disaster. Within the scope of the study, the functions of rituals performed after natural disasters on society and their unifying power in post-disaster processes were examined. Qualitative research method was used in the study. The sample of the research is Hatay, which was affected by the February 6 Kahramanmaras earthquake and attracts attention with its multicultural structure. Using participant observation and in-depth interview techniques, a total of 14 people were interviewed and participant observation was made in 6 religious-cultural ritual ceremonies. According to the results of the research; we observed that even if the ritual places were destroyed, the rituals continued to be held in the same places by adapting the "old" form in social memory to the "new" order. Again, as a result of participant observation, we observed that some changes (due to capacity inadequacies such as space and physical conditions) occurred in the rituals, but the continuation of these rituals in some way instils a sense of "hope" and "the possibility of re-existence" in both those who stayed and those who left, and the socially restorative role of this feeling is among the most important results we have reached.

Keywords: Post-disaster trauma, Ritual, Collective identity, Collective memory

Investigation of the Factors Influencing the Disaster Preparedness of Vocational Health Services Students

Sevil Ozcan[1], Perihan Ogdum[2]

[1] Environmental Health Programme / Medical Services and Technics Department, Aydin Vocational School of Health Services, Aydin Adnan Menderes University, Aydin, Türkiye
[2] Medical Secretary and Documentary Programme / Medical Services and Technics Department, Aydin Vocational School of Health Services, Aydin Adnan Menderes University, Aydin, Türkiye
Corresponding author: Sevil Ozcan (e-mail: sozcan@adu.edu.tr)

Abstract

This cross-sectional study was conducted on 623 students who are studying in eight different programs at Aydin Adnan Menderes University (ADU), Aydin Vocational School of Health Services (AVSHS) in 2023-2024 academic calendar. A questionnaire consisting of 34 questions and two parts was used in the study. In the first part, 14 questions were asked about the socio-demographic characteristics of the participants, whether they had experienced a disaster or not, and their status related to disaster preparedness, and in the second part, a 20-question "Disaster Preparedness Status Scale (DPSS)" was used. The surveys were administered face-to-face by the researchers to student volunteers. Frequency, percentage, mean, homogeneity, skewness and kurtosis, and Cronbach alpha reliability coefficients of the data were calculated. In addition, Pearson correlation test was used to evaluate whether there is a correlation between Disaster Preparedness Status (DPS) depending on some socio-demographic characteristics. As a result of the analysis of the obtained data, the reliability coefficient of the questionnaire was $\alpha = .91$ and the mean DPS score was 2.29. A statistically significant correlation was found between the mean DPS scores of the participants and their age, division of education, perceived income status, loss of a relative as a result of a disaster, having received disaster training, having a disaster plan, and having a disaster bag ($p = .01$). In addition, there was no statistical difference ($p > .05$) between the mean DPS scores of students from 11 provinces where the February 6, 2023 earthquake occurred (earthquake victims) and students from other provinces (non-earthquake victims).

Keywords: Disaster preparedness, Earthquake victims, University student, Health education

Expression, Alternative Polyadenylation Process and Epigenetic Regulation of MRPS16 Gene in Breast Cancer

Shams Sarimammadli[1], Tolga Acun[1]

[1]Department of Molecular Biology and Genetics, Zonguldak Bülent Ecevit University, Zonguldak, Türkiye
Corresponding author: Tolga Acun (e-mail: tolgaacun@yahoo.com)

Abstract

MRPS16 (mitochondrial ribosomal protein S16) protein is overexpressed in gliomas and promotes tumor development, migration and invasion by activating the PI3K/AKT/Snail pathway. Besides, suppression of MRPS16 expression inhibits tumor growth. In small intestinal neuroendocrine tumors (SI-NETs), an alternative mRNA with a shorter 3'-UTR region is formed due to the alternative polyadenylation (APA) site in the 3'-UTR region with the phenomenon known as UTR-APA. As it is well known, UTR regions are target sites for miRNAs and/or antisense RNAs and play an important role in post-transcriptional regulation. Considering the association of MRPS16 gene with some cancer pathways and cancer types, it is important to reveal the role of the MRPS16 gene in breast carcinogenesis. By using an in silico tool (UALCAN), we found that MRPS16 expression was significantly higher in breast cancer patients (n=1097) than in normals (n=114) (P= 1.62e-12). Similar results were also obtained with Bc-GenExMiner in silico tool, which analyze DNA microarray and RNA-seq datasets. Besides, we also found that overexpression of MRPS16 gene negatively affected survival values in breast cancer patients. According to the Ensembl genome browser, the MRPS16 gene has two isoforms. We showed that both isoforms, including the one that undergoes the UTR-APA process in SI-NET samples, were expressed in breast cancer cell lines and do not going through the UTR-APA process. Our in silico analysis revealed that the methylation level of the MRPS16 promoter region was significantly lower in triple-negative breast cancer samples than in normals (P=1.29e-08). We are currently analyzing the promoter methylation status of MRPS16 gene in breast cancer cell lines. We suggest that MRPS16 expression may have prognostic significance and could be regulated by epigenetic mechanisms in breast cancer.

Keywords: MRPS16, Breast cancer, APA, Promoter methylation, Expression

Increased Climate Change and Its Effects on Insect Populations

Gokce Ustundag[1]

[1]Veterinary Medicine Department, Zonguldak Bülent Ecevit University, Zonguldak, Türkiye
Corresponding author: Gokce Ustundag (e-mail: gokce.ustundag1@gmail.com)

Abstract

One of the most important ecological problems we face worldwide today is climate change caused by global warming. In addition to affecting all living things on earth, climate changes will inevitably affect insects, the largest living group on earth with more than one million species. Changes in humidity, CO_2 and temperature with the effect of climate changes will cause changes in the development time, reproduction, reproduction and behavior of insects. The fact that the body temperature of insects, which are cold-blooded creatures, is generally the same with the ambient temperature is a positive feature for insects, and their distribution areas will expand with the increase in the number of offspring of insects and the acceleration of their development. This situation, which is in favor of insects, will lead to serious economic losses in agricultural products, especially with the proliferation of some agricultural pest insect species in agricultural lands, in parallel with the increase in the number of these creatures. In addition, the increase in the number of disease-carrying insects will also pose a serious threat to public health.

Keywords: Climate, Insect, Population

Evaluation of Ecosystem Services Provided by Trees in Edirne Baris Park Using the i-Tree Eco Model

Irem Nur Keles[1], Emine Keles Ozgenc[1]

[1]Department of Landscape Architecture, Trakya University, Edirne, Türkiye
Corresponding author: Irem Nur Keles (e-mail: kelesiremnur43@gmail.com)

Abstract

Cities face serious environmental problems due to population growth and expansion. Environmental hazards such as air pollution, heat waves, and flooding are the most significant problems. Urban green spaces, which provide nature-based solutions to these problems, play a crucial role in increasing the environmental resilience of cities. Urban green spaces like parks, squares, and tree-lined streets provide ecosystem services and environmental, economic, and social benefits. In this study, the ecosystem services of urban trees in Baris Park, located in the Sukrupasa neighborhood, one of the densely populated areas of Edirne, were assessed. Using the i-Tree Eco v.6 models, the contributions of trees in the park, such as carbon storage and sequestration, air pollution reduction, and runoff prevention, were quantitatively analyzed from an environmental and economic perspective. The study identified 844 trees of 24 different species in Baris Park. The annual environmental benefits of the trees were calculated as follows: 567.3 kg of air pollutant removal, 606.90 tonnes of carbon storage, 40.24 tonnes of oxygen production, and 393.36 m³ of runoff reduction. These results show that the right choice of tree species and density in urban green spaces is essential to maximize city ecosystem services. The study highlights the contribution of urban green spaces to cities' environmental and economic sustainability. It provides valuable information for local authorities to optimize the benefits of urban green spaces.

Keywords: Air pollution removal, Ecosystem services, Edirne, Urban park, Urban trees

1. INTRODUCTION

More than half of the world's population lives in cities, and this proportion is expected to reach 68% by 2050 [1]. Increasing urbanization increases the demand for living space. It leads to environmental, economic, and social problems such as replacing natural vegetation with artificial surfaces, soil sealing, reduction of biodiversity, pollution, urban heat island effect, and increased greenhouse gas risks [2–6]. In this context, green infrastructure is recognized as an important tool to mitigate habitat fragmentation and climate change impacts. It is being recognized at the global policy level for providing multiple ecosystem services to urban communities [7]. Urban forests and trees are key components of green infrastructure and provide people with social, economic, health, and visual aesthetic benefits through provisioning, regulating, and cultural ecosystem services [8, 9]. Urban trees can potentially improve urban areas' environmental quality by reducing air pollution and contributing to the carbon balance of the atmosphere through carbon capture and storage [9–11]. For example, the annual economic benefits of urban trees in the USA have been estimated at USD 1.5–13 billion [3]. Species selection is critical to improving the effectiveness of these services; choosing the right tree species can increase the diversity and effectiveness of the ecosystem services provided [12].

Reducing urban air pollution is one of the most effective nature-based solutions, particularly through urban vegetation such as parks, street trees, green roofs, and walls. Green infrastructure supports optimal urban environmental conditions by removing air pollutants and improving air quality [13, 14]. In this context, identifying and valuing urban ecosystem services is an important step that should be integrated into urban planning decision support tools.

Ecosystem services models have become an effective tool for analyzing the benefits of urban forests and trees. The i-Tree Eco model was developed in the USA to value the ecosystem services provided by urban trees and has been adopted by many countries. This model enables the quantification of various environmental services such as carbon storage, air pollution reduction, water flow regulation, and energy efficiency [15–19]. Many studies have analyzed the services provided by urban trees and forests. Nowak, et al. [16] analyzed the urban forest structure and associated ecosystem services and values in Syracuse, New York. Selmi, et al. [18] using the i-Tree Eco model

in green spaces in Strasbourg, France, found that urban trees remove 88 tonnes of pollutants per year. Similarly, Paoletti, et al. [20], investigated the potential of urban trees to reduce air pollutants in the Cascine Park in Florence, Italy. Tugluer and Gul [21], emphasized the importance of tree inventories in determining the ecosystem services provided by urban trees by using the UFORE model to evaluate the environmental services provided by street trees in Isparta.

Although the inputs and outputs of the i-Tree model vary depending on the individual application, it generally requires the user to define a study area and detailed tree inventory data on land use and different tree species in that area (i-Tree Eco Field Guide, 2019). It is easy for developed countries, such as the USA, to find tree inventory data for a specific area [22]. However, it is difficult to find information on tree inventory in Turkey and requires determination of tree inventories through field studies. There is still a deficiency in evaluating the ecosystem services of public open green areas, especially in cities such as Edirne, which are subject to rapid population growth and intense visitor flows. The lack of data on tree inventory requires more comprehensive field studies in this field. However, although the ecosystem services provided by urban trees play a critical role in improving the urban environment, they are often overlooked in planning and policy processes.

The main objective of this study is to evaluate the carbon sequestration, storage, and air pollution mitigation potential of urban trees in Baris Park in the Sukrupasa Neighbourhood of Edirne using the i-Tree Eco model. The study aims to contribute to optimizing urban green infrastructure and developing sustainable urban policies. In this way, it aims to raise awareness about the ecosystem services provided by urban trees and provide concrete recommendations for creating sustainable and resilient cities.

2. MATERIAL AND METHOD

2.1. Material

The study area is Baris Park (Golet Park), located in the Sukrupasa Neighbourhood, which is one of the largest settlements of Edirne province and has a population of approximately 40,700 people. The neighborhood is a densely built-up area, and Baris Park is an important image point for the residents and the city. The park offers recreational opportunities to the neighborhood and the city, creates an intensive usage area, and stands out as one of the largest parks in the city center with a size of 47,879 m² (Figure 1).

The construction of Baris Park in the 2000s increased the development area in the Sukrupasa Neighbourhood and provided recreational opportunities and green space access for the existing population. In addition to various seating areas and different tree species, the park includes walking path, children's playground, a café and an artificial pond. These elements make the park a valuable urban green space for the neighborhood, both environmentally and socially.
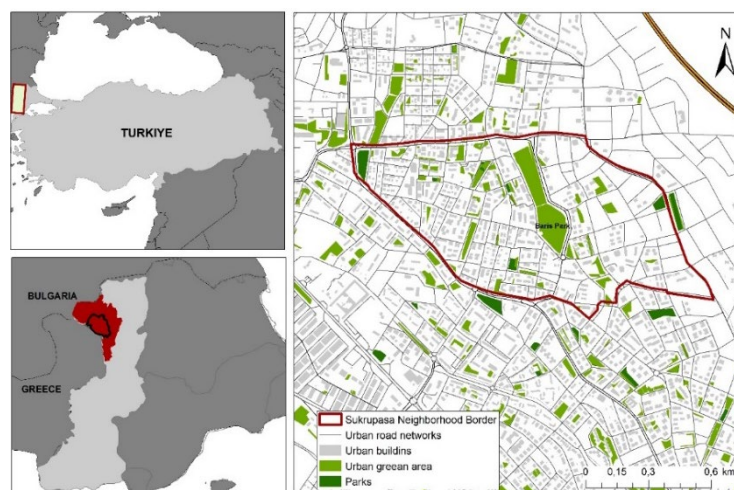
Figure 1. Geographical location of the work area

2.2. Method

In this study, the ecosystem services urban trees in Baris Park provided were assessed using the i-Tree Eco software. The i-Tree model, developed by the United States Department of Agriculture (USDA) Forest Service to

analyze the benefits of urban forests, uses specific parameters to estimate the value of ecosystem services provided by vegetation (www.itreetools.org) i-Tree Eco has functions such as carbon storage and sequestration, removal of air pollutants and determining the monetary value of these services. Using the dry deposition technique quantifies the capacity of plant species to remove air pollutants during periods without precipitation. Furthermore, the quantitative analysis of environmental services is carried out by integrating tree data (number of trees, species, stem diameter, height, canopy cover, etc.), local environmental data (hourly meteorological and air pollution data), and geographical location information (latitude and longitude) [23, 24]. Within the scope of this study, the analyses were carried out using the i-Tree Eco v6 tool.

In the first stage of the study, a tree inventory was created as a result of field studies. The species and general characteristics of the trees in Baris Park were determined, and these data were used to evaluate carbon storage, air pollution removal, and other ecosystem services. Location information of trees, individual tree canopy characteristics (species, stem diameter, height, crown size, health status), and weather and air pollution data were collected by the i-Tree field guide. The study area was divided into parcels, and the data collected from these parcels were transferred to the i-Tree Eco model. In the second stage, land inventory data were inputted into the model, and carbon storage and sequestration were calculated based on measured tree information. Air pollution removal estimates were carried out using a hybrid model based on broadleaf and multi-layered crown braid. The model inputs were supplemented with local air pollution data obtained from the Edirne meteorological station. The data collection process was completed in March 2024, and 844 trees were included in the inventory. All collected data was sent to the US Forest Service through the i-Tree database and approved for the analysis processes.

3. RESULTS

3.1 Tree Features in the Baris Park

As a result of the field studies carried out in Baris Park, a total of 844 trees and 24 different species were identified. Two species, which are found intensively, make up 63.1% of the park's canopy. The dominant species in the park are *Cedrus deodora* (63.2%), *Prunus cerasifera* (10.4%), *Cedrus atlantica* (6%), *Robinia pseudoacacia* (5.7%) and *Ligustrum japonicum* (3.2%) (Table 1, Figure 2).

The top 10 species with the highest importance value are listed in Table 1. Other species with significance values below 1% are as follows: *Betula pubescens* (4), *Melia azedarach* (4), *Prunus x yedoensis* (4), *Quercus ilex* (4), *Robinia viscosa* (3), *Cupressus cashmeriana* (2), *Cupressus sempervirens* (2), *Malus x robusta* (2), *Prunus cerasus* (2), *Abies pinsapo* (1), *Acer buergerianum* (1), *Gleditsia triacanthos* (1), *Hesperomannia arborescens* (1), and *Platanus orientalis* (1).

When the trunk diameter of the trees in the park was analyzed, it was determined that 40% of them were between 30.5-45.7 cm and 50% were between 45.7-61 cm (Figure 3, Figure 4). It was observed that most of the trees were in good crown condition, and the number of trees with inadequate or poor crown health was found to be very few.

Table 1. The most important species in Baris Park trees

Species	Number of trees	Percent of population (%)	Percent of leaf area (%)	Importance value
Cedrus deodara	534	63.3	59.9	123.1
Prunus cerasifera	88	10.4	13.2	23.6
Cedrus atlantica	51	6.0	6.7	12.7
Robinia pseudoacacia	48	5.7	6.6	12.2
Ligustrum japonicum	27	3.2	2.4	5.6
Prunus subhirtella	23	2.7	2.7	5.4
Cedrus libani	11	1.3	1.6	2.9
Prunus serrulata	13	1.5	1.2	2.8
x Hesperotropsis	6	0.7	1.2	1.9
Ulmus americana	11	1.3	0.3	1.6
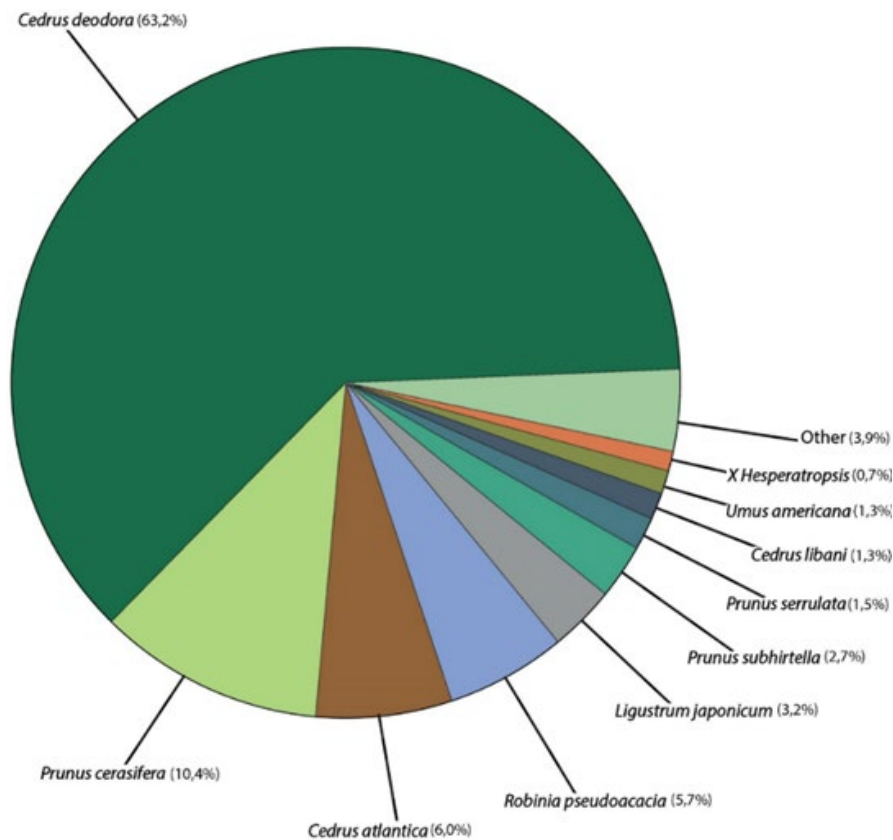
Figure 2. Tree species composition in Baris Park
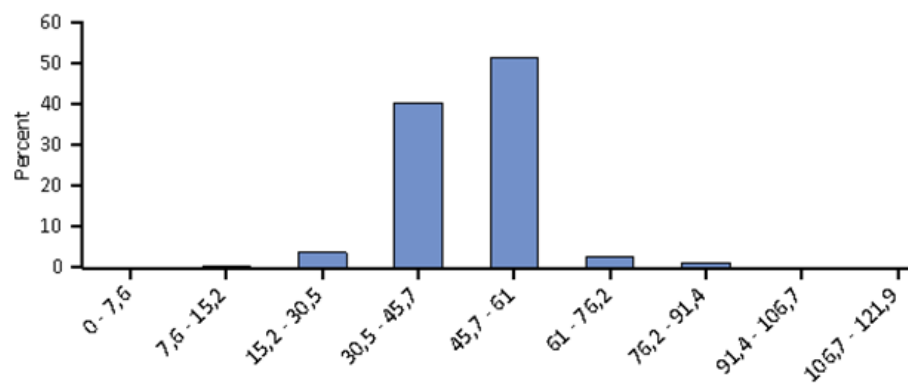
Figure 3. Percent of tree population by diameter class
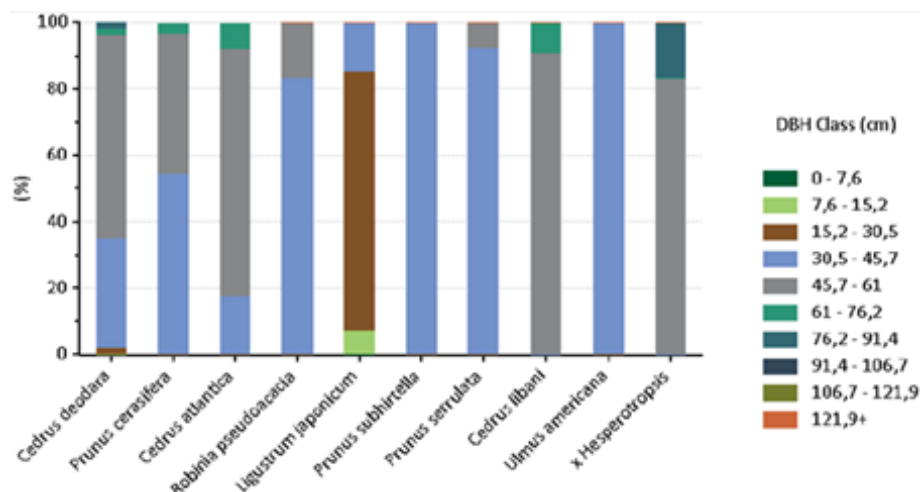
Figure 4. Species distribution by DBH class (cm)

3.2 Assessment of Ecosystem Services of Trees

3.2.1 Carbon sequestration and storage

Urban trees have the potential to mitigate the effects of climate change by removing carbon from the atmosphere and storing it within their structure. This process affects the amount of carbon stored and sequestered each year, depending on factors such as the size and health of the trees [22, 25].

According to the analyses conducted in Baris Park, the trees in the park sequester approximately 15.09 metric tonnes of carbon per year, the monetary value of which is calculated as 13,500 TL. In addition, it was determined that 606.9 metric tonnes of carbon is stored in the park (Figure 5, Table 2). These trees are estimated to produce an average of 40.24 tonnes of oxygen annually. Urban trees significantly contribute to air quality through carbon sequestration and storage, lowering air temperature, directly removing pollutants, and reducing energy consumption. These effects also reduce emissions of air pollutants from energy sources [22].
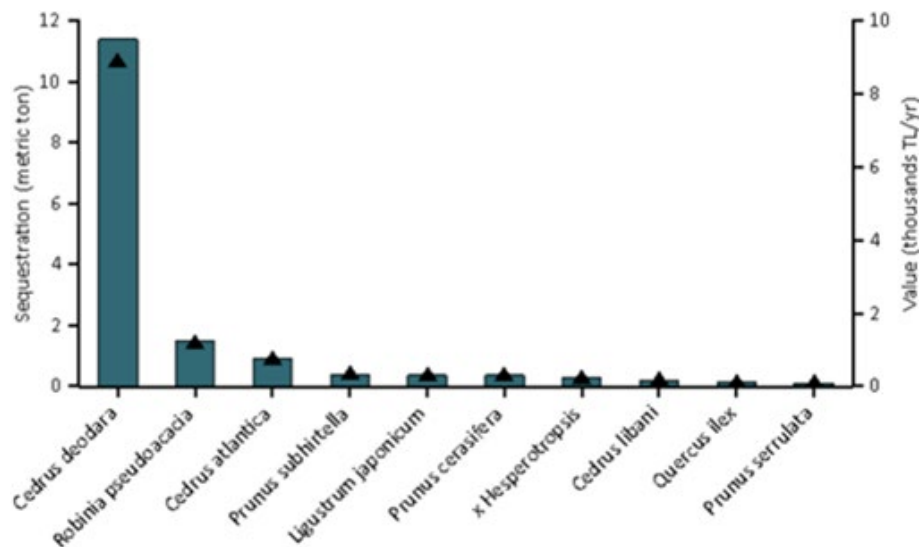
Figure 5. Estimates of annual gross carbon sequestration for tree species with the highest sequestration, Baris Park trees

Trees act as important carbon sinks; their leaves absorb CO_2 from the atmosphere and store it as carbon in biomass. As the tree grows, the amount of carbon stored increases [16]. In Baris Park, the two species with the largest contribution in terms of carbon storage are *Cedrus deodora* (360.25 tonnes) and *Prunus cerasifera* (84.01 tonnes) (Figure 6). Similarly, *Cedrus deodora* stands out with 10.65 tonnes/year and *Robinia pseudoacacia* with 1.38 tonnes/year in carbon sequestration capacity.
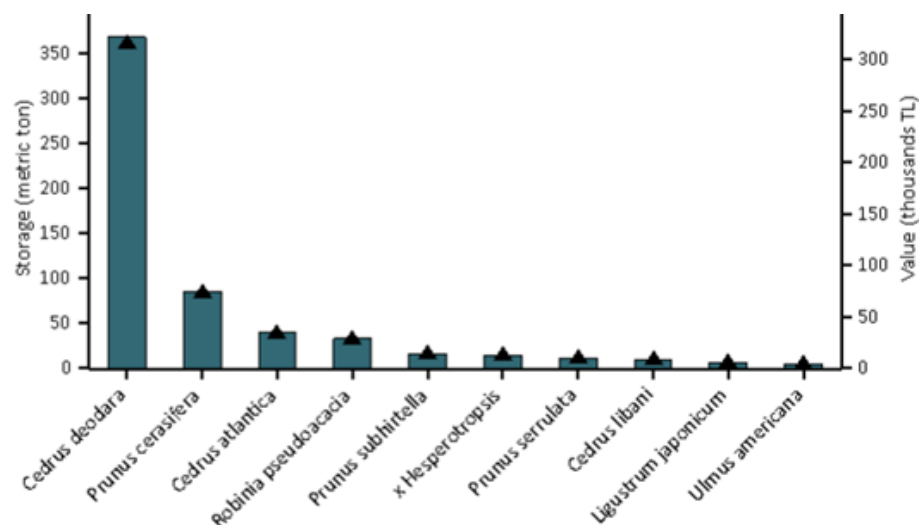
Figure 6. Estimated carbon storage for tree species with the highest storage, Baris Park trees

Table 2. Benefits summary of trees by species

	Trees Number	Canopy Cover (m²)	Leaf Area (m²)	Carbon Storage		Gross Carbon Sequestration		Avoided Runoff		Pollution Removal	
				(metric ton)	(TL)	(metric ton/yr)	(TL/yr)	(m³/yr)	(TL/yr)	(metric ton/yr)	(TL/yr)
Cedrus deodara	534	28346.0	160255.0	360.25	321255.13	10.65	9499.04	235.48	2177.26	0.34	68784.89
Prunus cerasifera	88	7152.2	35316.3	84.01	74919.20	0.35	309.00	51.89	479.82	0.07	15158.53
Cedrus atlantica	51	3066.4	17870.5	38.91	34694.59	0.87	772.20	26.26	242.79	0.04	7670.42
Robinia pseudoacacia	48	3444.5	17545.8	32.42	28910.47	1.38	1235.08	25.78	238.38	0.04	7531.02
Ligustrum japonicum	27	1215.4	6452.0	6.32	5632.98	0.35	309.22	9.48	87.66	0.01	2769.33
Prunus subhirtella	23	1581.5	7248.9	15.95	14224.95	0.38	335.52	10.65	98.49	0.02	3111.39
Cedrus libani	11	727.7	4166.0	9.70	8651.67	0.20	176.40	6.12	56.60	0.01	1788.15
Prunus serrulata	13	1007.4	3332.4	11.70	10434.86	0.10	87.89	4.90	45.27	0.01	1430.33
x Hesperotropsis	6	480.5	3155.5	14.84	13234.18	0.25	223.69	4.64	42.87	0.01	1354.42
Ulmus americana	11	365.2	802.5	4.78	4264.82	0.09	84.70	1.18	10.90	0.00	344.44
Other	32	2181.9	11556.3	28.02	24994.73	0.47	425.21	16.98	157.01	0.02	4960.18
Total	844	49568.7	267701.2	606.90	541217.58	15.09	13457.95	393.36	3637.05	0.57	114903.1

3.2.2 Improving air quality

The effects of trees on reducing each air pollutant are shown in Figure 7. The most significant improvement was observed in PM2.5, PM10, and O_3 concentrations. Especially in the removal of PM2.5, which is one of the most dangerous air pollutants, it was determined that the trees in the park made a significant contribution. Studies reveal that air pollution removal may vary depending on the amount of tree cover, pollution concentration, growing season length, and evergreen species' leaf area [23]. In this context, species with larger leaf areas and longer leaf life span, such as *Quercus ilex,* have an advantage in terms of particulate matter capture capacity. These species are predicted to greatly reduce PM2.5 concentration and minimize human exposure. The total air pollution removal of trees in Baris Park was estimated to be 567.3 kg/year, which includes the removal of pollutants such as (particulate matter smaller than 2.5 microns (PM2.5)), (particulate matter smaller than 10 microns and larger than 2.5 microns (PM10)), (ozone (O_3)), (sulfur dioxide (SO_2)), (nitrogen dioxide (NO_2)) and carbon monoxide (CO)). The results of the study show that the pollution removal capacity of Baris Park is consistent when compared with similar studies conducted in other regions [26].
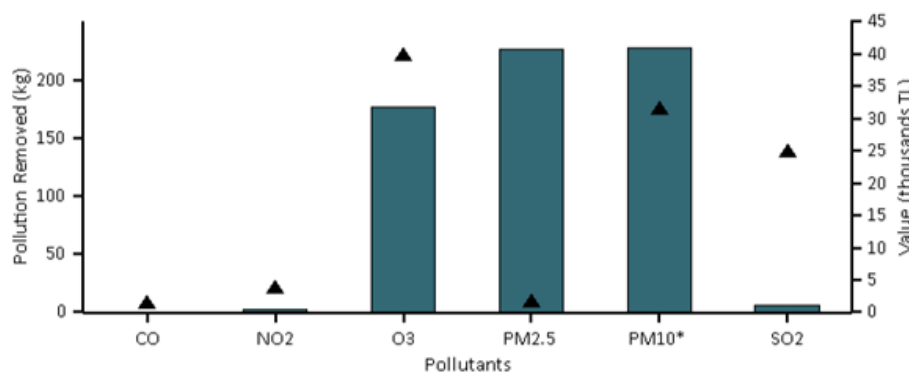
Figure 7. Annual pollution removal by urban trees, Baris Park trees

The economic value of air pollution reduction in the study area varies according to the type of pollutant. Accordingly, the values per tonne are calculated as TL 2,119 for carbon monoxide (CO), TL 144,318 for ozone (O_3), TL 21,538 for nitrogen dioxide (NO_2), TL 7,844 for sulfur dioxide (SO_2), TL 5,012,137 for PM2.5 and TL 234,657 for PM10. The main sources of PM2.5 are anthropogenic activities such as road transport and the combustion of fuels used for home heating (EPA, 2019). Air pollution is closely linked to urbanization, and urban trees have the potential to improve local air quality by altering the accumulation and dispersion rates of pollutants [27]. In the study area, PM2.5 and PM10 are among the highest removal rates, suggesting that the densely developed park is important in improving the city's air quality.

3.2.3 Oxygen production

Oxygen production is one of the most frequently emphasized ecosystem services for urban trees. Annual oxygen production is directly related to the amount of carbon sequestered by a tree, and this value is often estimated based on gross carbon sequestration [28]. Trees remove carbon from the atmosphere through photosynthesis, extract

carbon from the air, separate carbon atoms from oxygen atoms, and return it to the atmosphere as oxygen [25]. The annual oxygen production of the trees in Baris Park was calculated to be approximately 40.24 metric tonnes (Table 3). According to the data shown in Table 3, oxygen production is directly proportional to plant leaf area, which is related to the size and vigor of the trees.

Table 3. The top 20 oxygen production species at the study site

Species	Oxygen (metric ton)	Gross carbon sequestration (kg/yr)	Number of trees	Leaf area (ha)
Cedrus deodara	28.41	10651.93	534	16.03
Robinia pseudoacacia	3.69	1384.98	48	1.75
Cedrus atlantica	2.31	865.92	51	1.79
Prunus subhirtella	1.00	376.24	23	0.72
Ligustrum japonicum	0.92	346.75	27	0.65
Prunus cerasifera	0.92	346.50	88	3.53
x Hesperotropsis	0.67	250.84	6	0.32
Cedrus libani	0.53	197.81	11	0.42
Qurecus ilex	0.31	117.55	4	0.26
Prunus serrulata	0.26	98.55	13	0.33
Betula pubescens	0.25	95.46	4	0.19
Ulmus americana	0.25	94.98	11	0.08
Robinia viscosa	0.20	75.82	3	0.10
Melia azedarach	0.16	60.45	4	0.06
Cupressuss cashmeriana	0.10	37.41	2	0.06
Gleditsia triacanthos	0.09	32.75	1	0.04
Prunus cerasus	0.04	15.92	2	0.07
Platanus orientalis	0.03	12.98	1	0.02
Prunus x yedoensis	0.03	11.24	4	0.07
Malus x robusta	0.02	7.54	2	0.04

3.2.4 Avoided runoff

One of the important ecosystem services urban trees provide is managing runoff. Runoff is a problem in urban areas. Trees, a nature-based solution, intercept runoff and help reduce the amount of water that reaches the ground and forms surface runoff. The portion of rainfall that does not infiltrate into the ground becomes surface runoff [25]. Trees and shrubs play an important role in improving water quality by reducing runoff. Trees and shrubs in the study area were found to reduce 393.36 cubic meters of runoff per year. Cedrus deodora was the most effective species in providing this service. The total cost of ecosystem services provided by trees and shrubs in the park was determined to be TL 3637 (Table 4, Figure 8).

Table 4. Avoided Runoff Effects of Trees by Species

Species	Trees Number	Leaf area (ha)	Avoided runoff (m3/yr)	Avoided runoff value (tl/yr)
Cedrus deodara	534	16.026	235.48	2177.26
Prunus cerasifera	88	3.532	51.89	479.82
Cedrus atlantica	51	1.787	26.26	242.79
Robinia pseudoacacia	48	1.755	25.78	238.38
Ligustrum japonicum	27	0.645	9.48	87.66
Prunus subhirtella	23	0.725	10.65	98.49
Cedrus libani	11	0.417	6.12	56.60
Prunus serrulata	13	0.333	4.90	45.27
x Hesperotropsis	6	0.316	4.64	42.87
Ulmus americana	11	0.080	1.18	10.90
Other	32	1.154	16.98	157.01
Total	844	26.770	393.36	3637.05
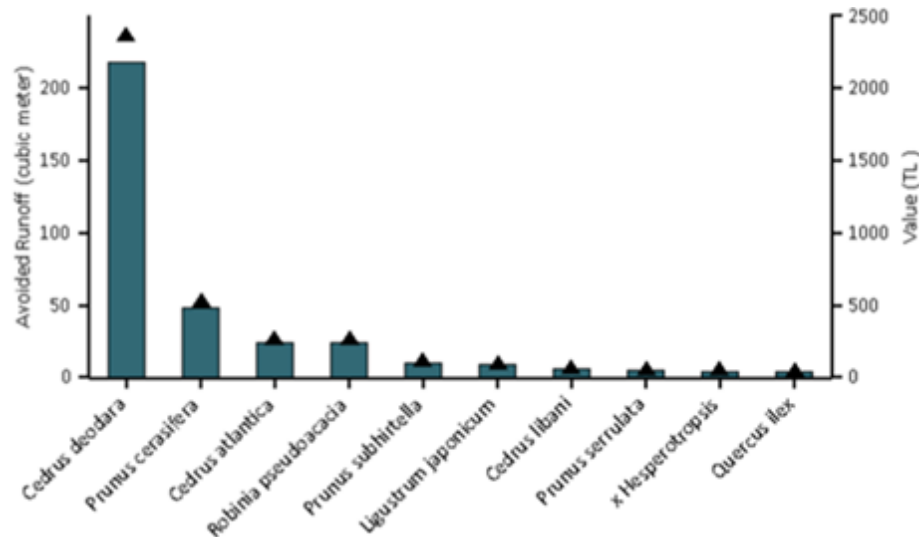
Figure 8. Avoided runoff for species with the greatest overall impact on runoff, Baris Park trees

4. CONCLUSION

This study aimed to draw attention to the environmental and economic benefits of urban vegetation by quantifying the ecosystem services provided by trees in Baris Park in the Sukrupasa Neighbourhood of Edirne. The findings revealed that park trees play important roles in ecosystem services such as carbon sequestration and storage, air pollution removal, and oxygen production. *Cedrus deodora*, the dominant species in the park, was the highest contributor to these services. However, additional research is needed to better understand the potential of different tree species in critical services such as air pollution removal.

The results provide a strategic roadmap for the sustainable management of urban green infrastructure. Planting strategies that take into account characteristics such as pollution sensitivity, site adaptation, and maintenance requirements of various tree species are expected to increase the resilience and benefits of urban ecosystems. It is also emphasised that strategic management of parks and green spaces can increase carbon sequestration capacity, improve air quality, and transform these services into social benefits. It also draws attention to the potential to increase carbon sequestration through strategic management of green infrastructure in urban areas in Edirne.

The i-Tree model used in the study is an effective tool for quantitative analysis of the ecosystem services provided by urban trees. By fitting the model with local field data and environmental observations, the model reveals the relationship between tree structure and ecosystem services in detail. However, the accuracy of the model results depends on the quality of the data inputs and modeling processes. Therefore, providing local air pollution and meteorological data is crucial to improve the reliability of the results. Despite the global applicability of the i-Tree model, the study reiterates the need for adaptation to local conditions. This research provides managers and urban planners with a scientific guide for tree species selection to improve air quality and optimize environmental benefits. In particular, evaluating characteristics such as leaf surface area, which effectively removes pollutants such as PM2.5, will inform planning processes. The research also contributes to creating healthier and sustainable cities by providing concrete evidence for local planners to understand the effects of urban vegetation on air quality and public health.

In conclusion, this study brings to the forefront the understanding of the value of urban green infrastructure, the sustainable management of ecosystem services, and the role of urban vegetation in combating climate change. The research is an important reference for integrating biodiversity into sustainable urban planning in line with the 2030 Agenda of the United Nations Sustainable Development Goals. In this context, it is envisaged that the measures to protect, enhance, and increase urban vegetation's benefits will guide policymakers, urban planners, and researchers.

References

[1]   U. Nations, *World Urbanization Prospects: The 2003 Revision*, UN, 2004.

[2]   R. Rasoolzadeh, N. Mobarghaee Dinan, H. Esmaeilzadeh, Y. Rashidi, M. V. Marcu, and S. M. M. Sadeghi, "Carbon sequestration and storage of urban trees in a polluted semiarid city," *Forests,* vol. 15, no. 9, art. no. 1488, 2024.

[3]   D. J. Nowak, S. Hirabayashi, A. Bodine, and E. Greenfield, "Tree and forest effects on air quality and human health in the United States," *Environmental Pollution,* vol. 193, pp. 119–129, 2014.

[4]   C. Nyelele, C. N. Kroll, and D. J. Nowak, "Present and future ecosystem services of trees in the Bronx, NY," *Urban Forestry & Urban Greening,* vol. 42, pp. 10–20, 2019.

[5]   L. V. Pinto, M. Inácio, C. S. S. Ferreira, A. D. Ferreira, and P. Pereira, "Ecosystem services and well-being dimensions related to urban green spaces–A systematic review," *Sustainable Cities and Society,* vol. 85, art. no. 104072, 2022.

[6]   Z. Cimburova and D. N. Barton, "The potential of geospatial analysis and Bayesian networks to enable i-Tree Eco assessment of existing tree inventories," *Urban Forestry & Urban Greening,* vol. 55, art. no. 126801, 2020.

[7]   J. D. Sjöman *et al.*, "Expectations of i-Tree Eco as a tool for urban tree management in Nordic cities," *Frontiers in Sustainable Cities,* vol. 5, art. no. 1325039, 2024.

[8]   D. Nowak, D. Crane, J. Stevens, R. Hoehn, J. Walton, and J. Bond, "A ground-based method of assessing urban forest structure and ecosystem services," *Arboriculture & Urban Forestry,* vol. 34, no. 6, pp. 347–358, 2008.

[9]   R. Rasoolzadeh, N. Mobarghaee Dinan, H. Esmaeilzadeh, Y. Rashidi, and S. M. M. Sadeghi, "Assessment of air pollution removal by urban trees based on the i-Tree Eco Model: The case of Tehran, Iran," *Integrated Environmental Assessment and Management,* 2023.

[10]   F. Salbitano, *Guidelines on Urban and Peri-Urban Forestry*, Fao, 2016.

[11]   J. Ma *et al.*, "Spatial variation analysis of urban forest vegetation carbon storage and sequestration in built-up areas of Beijing based on i-Tree Eco and Kriging," *Urban Forestry & Urban Greening,* vol. 66, art. no. 127413, 2021.

[12]   G. Churkina, R. Grote, T. M. Butler, and M. Lawrence, "Natural selection? Picking the right trees for urban greening," *Environmental Science & Policy,* vol. 47, pp. 12–17, 2015.

[13]   M. Vashist, T. V. Kumar, and S. K. Singh, "Assessment of air quality benefits of vegetation in an urban-industrial region of India by integrating air monitoring with i-Tree Eco model," *CLEAN–Soil, Air, Water,* vol. 52, no. 7, art. no. 2300198, 2024.

[14]   Y. Yao, Y. Wang, Z. Ni, S. Chen, and B. Xia, "Improving air quality in Guangzhou with urban green infrastructure planning: An i-Tree Eco model study," *Journal of Cleaner Production,* vol. 369, art. no. 133372, 2022.

[15]   R. Pace, P. Biber, H. Pretzsch, and R. Grote, "Modeling ecosystem services for park trees: Sensitivity of i-tree eco simulations to light exposure and tree species classification," *Forests,* vol. 9, no. 2, art. no. 89, 2018.

[16]   D. J. Nowak, R. E. Hoehn, A. R. Bodine, E. J. Greenfield, and J. O'Neil-Dunne, "Urban forest structure, ecosystem services and change in Syracuse, NY," *Urban Ecosystems,* vol. 19, pp. 1455–1477, 2016.

[17]   A. Russo, F. J Escobedo, and S. Zerbe, "Quantifying the local-scale ecosystem services provided by urban treed streetscapes in Bolzano, Italy," *AIMS Environmental Science,* vol. 3, no. 1, pp. 58–76, 2016.

[18]   W. Selmi, C. Weber, E. Rivière, N. Blond, L. Mehdi, and D. Nowak, "Air pollution removal by trees in public green spaces in Strasbourg city, France," *Urban Forestry & Urban Greening,* vol. 17, pp. 192–201, 2016.

[19]   A. Himes, K. Puettmann, and B. Muraca, "Trade-offs between ecosystem services along gradients of tree species diversity and values," *Ecosystem Services,* vol. 44, art. no. 101133, 2020.

[20]   E. Paoletti, T. Bardelli, G. Giovannini, and L. Pecchioli, "Air quality impact of an urban park over time," *Procedia Environmental Sciences,* vol. 4, pp. 10–16, 2011.

[21]   M. Tugluer and A. Gul, "Kent ağaçlarının çevresel etkileri ve değerinin belirlenmesinde UFORE modelinin kullanımı ve Isparta örneğinde irdelenmesi," *Turkish Journal of Forestry,* vol. 19, no. 3, pp. 293–307, 2018.

[22]   R. Sharma, B. R. Bakshi, M. Ramteke, and H. Kodamana, "Quantifying ecosystem services from trees by using i-tree with low-resolution satellite images," *Ecosystem Services,* vol. 67, art. no. 101611, 2024.

[23]   Y. Yousofpour, L. Abolhassani, S. Hirabayashi, D. Burgess, M. S. Sabouni, and M. Daneshvarkakhki, "Ecosystem services and economic values provided by urban park trees in the air polluted city of Mashhad," *Sustainable Cities and Society,* vol. 101, art. no. 105110, 2024.

[24]   A. Yarnvudhi, N. Leksungnoen, P. Tor-Ngern, A. Premashthira, S. Thinkampheang, and S. Hermhuk, "Evaluation of regulating and provisioning services provided by a park designed to be resilient to climate change in Bangkok, Thailand," *Sustainability,* vol. 13, no. 24, art. no. 13624, 2021.

[25]   D. Bidolakh, P. Lakyda, V. Myroniuk, Y. Hayda, and S. Pidkhovna, "Assessment and representation of Urban Trees Ecosystem Services: a case study in Pryzamkovyi Park," *Folia Forestalia Polonica,* vol. 65, no. 2, pp. 104–116, 2023.

[26]   G. Kacmaz, M. O. Alkan, H. Cobankaya, and D. Sen, "Assessment of ecosystem services provided by street trees: Burdur (Türkiye) city center," *Ege Universitesi Ziraat Fakultesi Dergisi,* vol. 60, no. 2, pp. 221–234, 2023.

[27]   E. Riondato, F. Pilla, A. S. Basu, and B. Basu, "Investigating the effect of trees on urban quality in Dublin by combining air monitoring with i-Tree Eco model," *Sustainable Cities and Society,* vol. 61, art. no. 102356, 2020.

[28]   D. J. Nowak, R. Hoehn, and D. E. Crane, "Oxygen production by urban trees in the United States," *Arboriculture and Urban Forestry,* vol. 33, no. 3, art. no. 220, 2007.

Upcycling Aircraft Scrap: Transforming Aviation Heritage into Functional Design

Deniz Ordulu[1], Mehmet Kenan Yildirim[2]

[1]Industrial Design Department, Yeditepe University, Istanbul, Türkiye
[2]Mechanical Engineering Department, Marmara University, Istanbul, Türkiye
Corresponding author: Deniz Ordulu (deniz.ordulu@skyart.com)

Abstract

When aircraft reach the end of their life, some parts like engines, cockpit components, and composite materials cannot be melted down and are considered scrap. While aluminum panels and landing gear can be recycled, other parts with unique shapes or strong materials are turned into everyday items or special design pieces. This upcycling process keeps the industrial strength and unique history of these parts alive, giving them a second life in creative or functional designs. This approach supports environmental sustainability and creates valuable, distinctive products with a story to tell. The cowling is the part that surrounds and protects an aircraft's engine, made from metal or composite materials. It helps improve airflow and engine performance. With its removable structure and eye-catching design, the cowling is ideal for turning into creative and functional products. This project focuses on turning scrap aircraft parts into high-value furniture. A cowling was redesigned as a reception desk that is both functional and stylish, with customizable features. The process transformed scrap material into a high-value product ready for export. The cowling's original texture and history were preserved while making it into a practical and visually appealing piece of furniture. 3D models and technical drawings were created using computer-aided design software to verify durability and stability. Additionally, virtual tests were conducted to optimize the design and ensure its functionality and safety before moving to production. The final product highlights sustainability, aesthetics, and storytelling. It shows how parts from the aviation industry can be turned into useful and visually interesting furniture, preserving industrial heritage and adding value through sustainable design. By reusing the cowling, this project combines creativity, engineering, and history, turning low-value scrap into a valuable export product.

Keywords: Upcycle design, Aircraft cowling, Sustainability, Aviation heritage, High-value products

1. INTRODUCTION

When airplanes reach the end of their service life, certain components, such as engines, cockpit systems, and composite materials, are classified as scrap due to their complex structures and resistance to conventional recycling. In aviation design, the emphasis on sustainability involves using recycled and renewable materials to reduce the environmental impact of manufacturing and end-of-life disposal. This ensures that components such as composite materials are not only effective in performance but also in minimizing their ecological footprint [1]. However, these materials hold untapped potential for upcycling, turning discarded industrial waste into innovative, high-value products. When considering the global recycling industry, the demand for advanced recycling is also a necessity. One of the key materials in this transformation is often scrap aluminum [2], which is abundantly found in scrap aircraft. This project focuses on this transformation by repurposing an aircraft cowling—a durable engine covering with both structural integrity and visual appeal—into a premium reception desk. This study showcases how scrap materials can be reimagined, not only to create functional designs but also to contribute to economic and environmental sustainability.

The cowling was chosen for its robust material properties and distinctive aesthetic, making it ideal for creative reuse. The project followed a step-by-step process beginning with concept development. Initial stages involved preserving the cowling's industrial character while adapting its form to suit a contemporary furniture design. Using computer-aided design (CAD) tools, 3D models and technical drawings were developed to optimize the concept. Virtual tests analyzed durability, stability, and ergonomic suitability, ensuring the design met both functional and aesthetic requirements.

Subsequent stages integrated these technical analyses with ergonomic considerations, resulting in a refined and practical design. Prototyping played a critical role in verifying structural safety and functionality before moving

into production. The final product successfully balanced storytelling, industrial heritage, and sustainability, turning a low-value scrap material into a high-value export product.

The following sections of this study will delve into each phase of the process in detail. The design concept will be elaborated, highlighting the creative approach to upcycling and the techniques used for testing and refinement. Upcycling is a sustainable and eco-friendly way to reduce waste and minimize the environmental impact of discarded materials. By transforming these materials into innovative products, we can contribute to a circular economy where resources are reused and repurposed, extending their lifecycle and reducing waste [3]. Furthermore, the challenges of integrating sustainability into industrial design will be discussed, along with the project's broader implications for environmental and economic impact. This introduction sets the foundation for exploring the full potential of upcycling in industrial design and its contribution to sustainable practices.

2. MATERIAL AND METHOD

Skyart Aviation Design and Engineering, known for transforming scrap aircraft parts into high-value furniture projects through upcycling, was approached by an aviation enthusiast client. The request was to design a reception desk for a therapy center's entrance area. This desk needed to be both functional and visually striking, while also offering personal spaces for users. It had to accommodate up to five people at the same time, provide wireless charging for their phones, and include personalized lighting similar to the systems used in aircraft cabins. To create a striking and elegant reception bar, the cowling part was selected as the centerpiece due to its expansive surface area and perfectly suited shape.

In the initial phase, it was necessary to select an aircraft cowling of appropriate dimensions for the project. Among the various sizes available in the inventory, the A300 cowling (Figure 1) was identified as the most suitable in terms of diameter and height and approved for use in the design. The selected cowling was accurately recreated as a 3D model in a computer environment (Figure 2). Collaborating with the industrial design team, concepts were developed to meet the project requirements and the client's stylistic expectations, ensuring both aesthetic appeal and functionality. The design concept evolved into utilizing a semi-circular cowling shape. Decisions regarding color, material, and maintaining ergonomic dimensions were integrated into the design as the process advanced. The first step involved cutting the cowling part.

Figure 1. Scrap A300 cowling
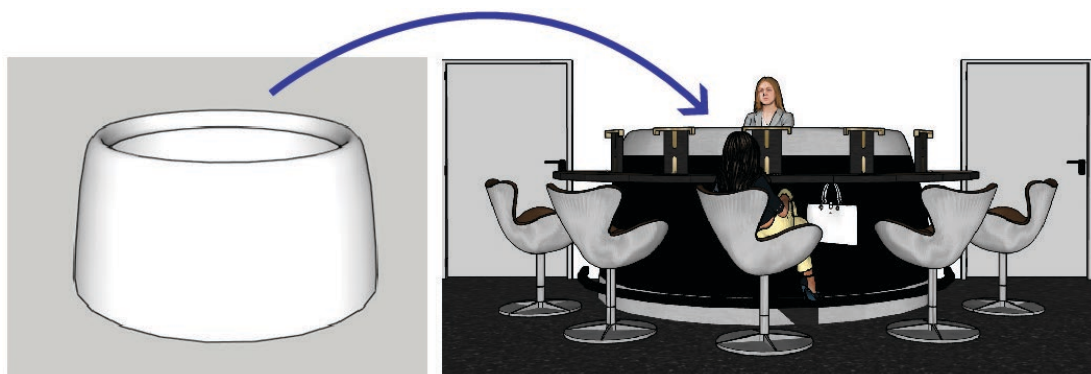
Figure 2. 3D concept model of the cowling

The cowling piece is inherently symmetrical only along one axis in terms of height. However, the cut needed to be made on the axis perpendicular to this symmetry. This ensured that the cowling's height peaked at the central point where the staff would stand, gradually lowering as it extended to the right and left (Figure 3), creating a cohesive design.

Cutting the cowling was a meticulous process requiring skill and precision. A qualified metalworker was essential to achieve a clean and precise cut. Using a level, the center of the cowling was identified, and guiding lines were drawn to ensure equal heights on both sides (Figure 4).

Figure 3. Cowling's symmetry point

Figure 4. Cutting phase

The cowling piece consists of different materials across its surfaces. The top layer is aluminum, while the body features a honeycomb structure. The honeycomb body is cylindrically formed, and the aluminum piece is curved in a C-shape, serving as a flush cover that overlaps the honeycomb structure at the top. This design leaves a gap between the inner and outer honeycomb layers. The aluminum and honeycomb materials are riveted together using titanium fastening components within the cowling. As seen in the internal structure of the cowling (Figure 5), the titanium-reinforced components at the top and bottom secure the assembly. This ensures the materials maintain their forms and remain firmly in place.

One of the key focal points of the design is a wooden furniture section located at the concave side of the cowling, where a staff member stands to manage computer operations and filing tasks. The other focal point is a bar table on the convex side of the cowling, featuring customer seating areas arranged side-by-side, centered around the standing staff member.

Figure 5. Inside of the cowling

To ensure functionality and interaction, the design accommodates the exchange of files and eye contact between the seated customers and the standing staff member. This is achieved by carefully determining the chair height and angles. The cowling's height is 1450 mm, which could potentially obstruct interaction. The ergonomic dimensions used in this design are informed by DIN 92419 standards of ergonomics. To ensure ergonomic compatibility and user comfort, the design process followed the DIN 92419 standard [4], which provides detailed guidelines on dimensions and seating heights essential for creating ergonomic workspaces. This standard played a crucial role in ensuring that the reception desk design maintained user-friendly proportions, promoting comfort and ease of use for both staff and visitors. To address this, the chairs were designed to be taller, with suspension mechanisms enabling vertical adjustments for comfort. A bar footrest (Figure 6) was integrated into the design to enhance comfort while seated, ensuring that the user's legs don't dangle uncomfortably.

Another client requirement was to ensure that the components within the staff member's workspace remained hidden from the customers' view, maintaining an isolated and focused area. Additionally, the dimensions of the cowling, the width of the table, and the distance introduced by the furniture behind the staff created a physical separation. This ensured limited interaction, preventing prolonged conversations and keeping the environment professional and task-oriented (Figure 7). While customers enjoy a communal seating arrangement, the staff member's workspace remains a private zone, enabling them to carry out their responsibilities efficiently within a dedicated and organized space.
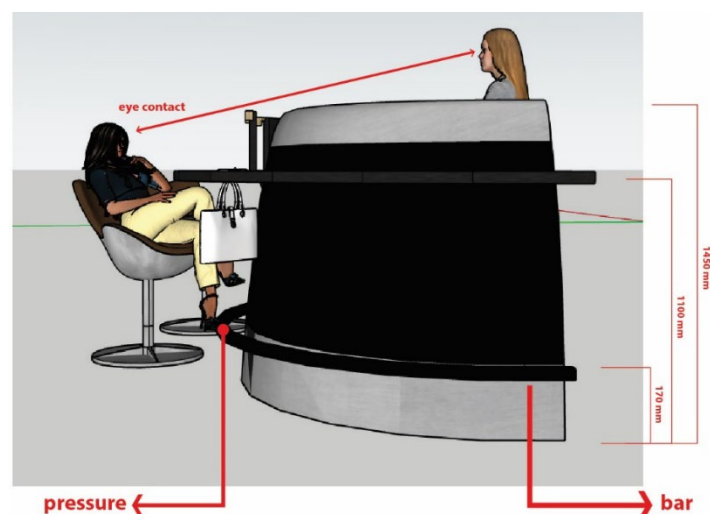
Figure 6. Dimensions
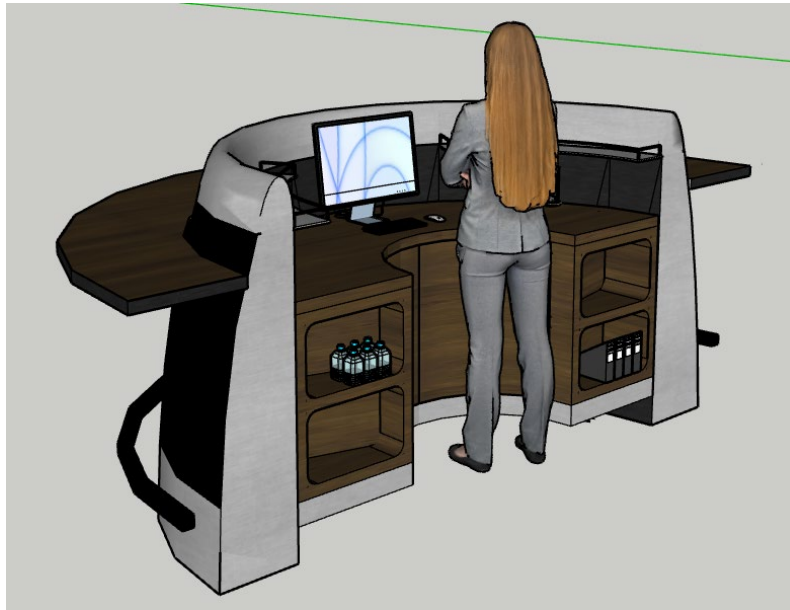
Figure 7. The space where the staff is positioned

The customer seating area features a customizable lighting and charging unit (Figure 8). This unit also incorporates the initials of the client's company, "HT," as part of its silhouette design. Toggle switches positioned on the unit allow for light control, while magnetic wireless charging provides a convenient way to charge phones.

The customer's table, positioned 1100 mm above the ground, and the footrest bar, located 170 mm above the floor, needed to be securely attached to the cowling surface to ensure stability. Designed to support the weight of five individuals leaning or resting their feet, these elements required careful engineering to achieve both strength and aesthetic integration. The honeycomb material used in the cowling is not suitable for direct mounting due to its structural characteristics [5]. While it is favored in aircraft parts for its lightweight and high strength, its hexagonal structure provides impact resistance, thermal insulation, and aerodynamic efficiency. However, it is prone to damage when drilled, making direct attachments unfeasible.

To address this, the hollow structure within the cowling was utilized. The mounting solution involved creating components that extend vertically inside the cowling to distribute the load from the table and footrest to the ground (Figure 9). This internal support system ensures that the mounting elements remain hidden, preserving the clean and seamless aesthetic of the design.
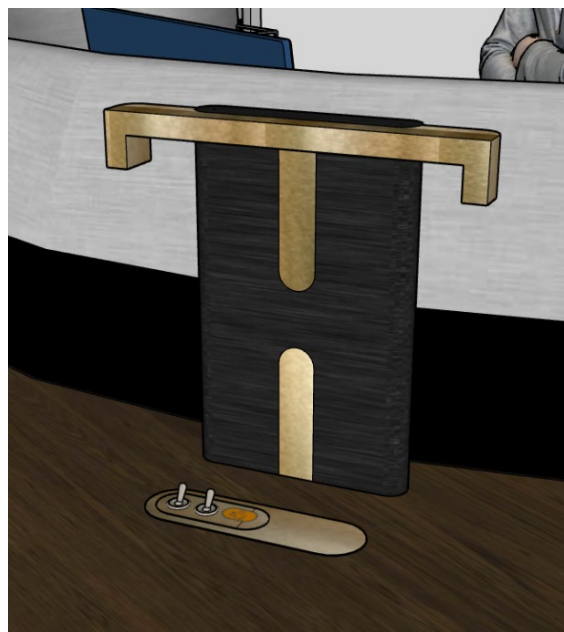
Figure 8. Personal unit
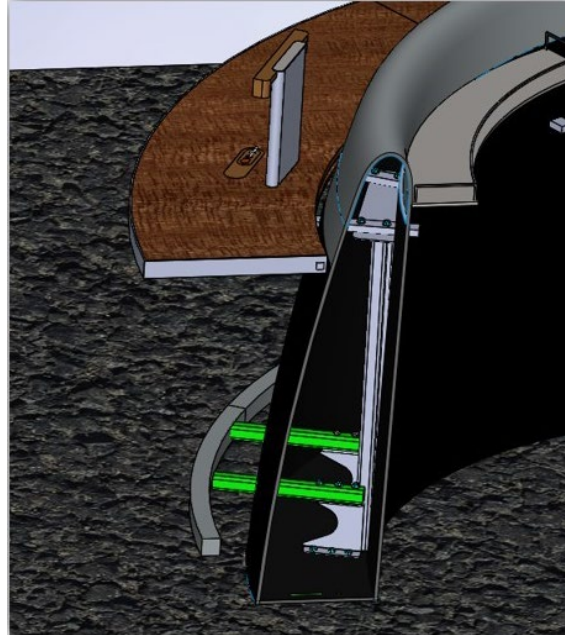
Figure 9. Mounting elements

The cowling is a large structure, and no additional intervention points are available on its sides for load distribution. Through computer-aided analyses (Figure 10), it was determined that the load of five individuals must be distributed across at least four support points. Based on these findings, the support components were strategically positioned, and the mounting details were finalized. A second round of load distribution analysis was conducted to validate the design. Following the analysis, production drawings were prepared, and the finalized design proceeded to the manufacturing phase (Figure 11).

The cowling's curved surface presented challenges during assembly, requiring various adjustments for proper alignment. Access to the inner sections of the cowling was made possible through service panels integrated into the interior surface, allowing mounting details to be addressed from within. With meticulous craftsmanship, the components were modified with minor revisions to ensure a seamless fit to the surface, allowing the assembly process to move forward. The open side surfaces of the cowling were first molded with wood to create forms for the metal, then covered with stainless steel, achieving a clean and polished finish.
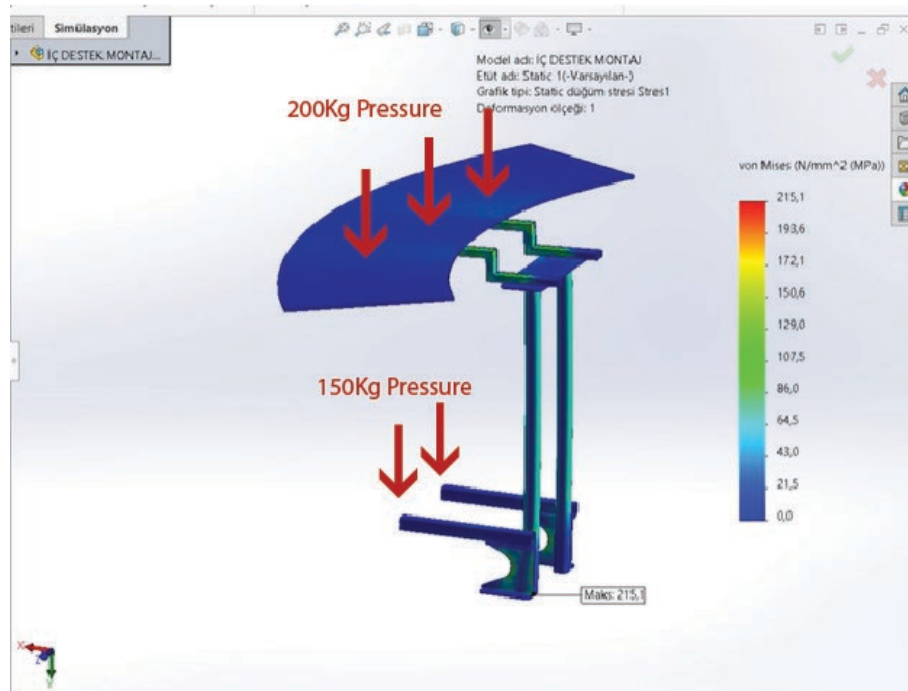
Figure 10. Computer-aided analyses

Figure 11. Production phase

3. RESULTS

The discarded cowling part was transformed into an aesthetically pleasing industrial design product, reflecting an aviation theme, in line with the client's requirements. Due to the cowling's curved and organic surface and the honeycomb material's limited resistance to direct attachment and weight support, the design incorporated hidden, durable components to ensure effective weight distribution. These components were meticulously planned, tested using computer-aided analysis, and adjusted to fit the surface perfectly through trial methods where necessary. The final product was created with both functionality and aesthetics in mind. The low-value scrap piece was successfully converted into a high-value product, which was subsequently exported.

4. CONCLUSION

The cowling part has been transformed from a discarded aircraft component into a high-value export product, serving as a valuable example of advanced recycling while also referencing sustainability. The scrap cowling, which was unsuitable for recycling through melting or breaking down and could no longer perform its original function, has been revived and presented to the client in its new, much more impressive form. It has become both an aesthetic and functional product, a testament to the collaboration between industrial design and engineering. The aviation theme has been integrated into everyday life in a creative and usable way.

References

[1]   T. Matutyte, *Upcycling: A New Frontier in Aviation Sustainability*, 2023.
[2]   Aerospace Manufacturing and Design (AMD). (2010, Jul. 02). *AFRA targets 90% recyclability of global fleet by 2016* [Online]. Available: https://www.aerospacemanufacturinganddesign.com/news/aerospace-manufacturing-design-afra-recyclability-amd-070210/
[3]   A. Filippatos, D. Markatos, G. Tzortziniz, K. Abhyankar, S. Malefaki, M. Gude, and S. Pantelakis, "Sustainability-driven design of aircraft composite components," *Aerospace*, vol. 11*, no. 1, art. no. 86, 2024, doi: 10.3390/aerospace11010086.
[4]   DIN 92419.Ergonomics-Workplace Design for Seated Work. *Deutsches institut für normung e.V.* [Online]. Available: https://www.din.de
[5]   C. Guler and G. Ulay, "Petekli (hpneycomb) kompozit levhalar," *Mobilya Dekorasyon Dergisi*, p. 86, May-Jun. 2009.

Analytical Treatments for the Zig-Zag Optical Lattices in Quantum Physics

Bahadir Kopcasiz[1]

[1]Department of Mathematics, Faculty of Arts and Sciences, Bursa Uludag University, Bursa, Türkiye
Corresponding author: Bahadir Kopcasiz (e-mail: bkopcasz@gmail.com)

Abstract

This paper investigates the widely used zig-zag optical lattice prototype for cold bosonic atoms. This prototype generally represents nonlinear waves in plasma physics and fluid mechanics. A new version of the generalized exponential rational function method (nGERFM) is utilized to discover diverse soliton solutions. The nGERFM facilitates the generation of multiple solution types, including singular, shock, singular periodic, exponential, combo trigonometric, and hyperbolic solutions in mixed forms. To gain a deeper understanding of the dynamic behavior of the solutions, analytical results are supplemented with numerical simulations. These obtained outcomes provide a foundation for further investigation, making the solutions useful, manageable, and trustworthy for the future development of intricate nonlinear issues. This study's methodology is reliable, strong, effective, and applicable to various nonlinear partial differential equations (NLPDEs). As far as we know, this type of research has never been conducted to such an extent for this equation before. The Maple software application is used to verify the correctness of all obtained solutions.

Keywords: Zig-zag model, nGERFM, Soliton

Urban Green Infrastructure and Stormwater Management

M. Burak Karakaya[1], Zeynep Eren[2]

[1]Tekman District National Education Directorate, Erzurum, Türkiye
[2]Ataturk University, Engineering Faculty, Environmental Engineering Department, 25240 Erzurum, Türkiye
Corresponding author: M. Burak Karakaya (e-mail: m.burak.karakayaa@gmail.com)

Abstract

In recent years, with the rapid increase in urbanisation, awareness on the sustainability of water resources and environmental impacts has increased. In this context, rainwater harvesting systems and urban green infrastructure applications are of great importance for both the protection of water resources and the adaptation of urban areas to climate change. Rainwater harvesting and urban green infrastructure are two critical topics for sustainability in modern cities. These methods aim both to use water resources more efficiently and to reduce the environmental footprint of cities. The widespread adoption of these practices in the future will play an important role in tackling global challenges such as water scarcity and climate change. Rainwater harvesting is the process of collecting water from roofs, roads and other hard surfaces, collecting it and making it usable. These systems support local water supplies and prevent flooding by preventing water from going directly into the ground or into the sewerage system. Collected rainwater can be used for garden irrigation, filling toilet reservoirs and even as drinking water after some filtration processes. This method offers a sustainable solution, especially in regions with water scarcity. Rainwater Harvesting and Storage Methods In rainwater harvesting systems, two main methods can be mentioned as underground and above ground, cistern method and tank method. These applications have a strategic importance in terms of both combating climate change and providing resilience to cities. This study presents detailed solutions that bring a sustainable approach to the use of green infrastructure systems and stormwater management.

Keywords: Stormwater, Green infrastructure, Sustainable water management

Thermal Kinetic Behaviour of 2-Methyl-1, 3-Dioxoisoindoline-5-Carboxylic Acid

Hatice Bayrakceken[1,2], Ozlem Gundogdu[3], Nurhan Horasan[4]

[1]Chemical Engineering Department, Ataturk University, Erzurum, Türkiye
[2]Nanoscience and Nanoengineering Department, Ataturk University, Erzurum, Türkiye
[3]Food Processing, Kaman Vocational School, Ahi Evran University, 40360 Kirsehir, Türkiye
[4]Department of Science, Science Faculty, Ataturk University, 25240 Erzurum, Türkiye
Corresponding author: Hatice Bayrakceken (e-mail: hatbay@atauni.edu.tr)

Abstract

Determination of the thermochemical properties of isoindole-1,3-dione used in the synthesis of polymers, drugs and biological solid support materials is important in terms of method and application safety during the production stages. After synthesizing new organic compounds, it is necessary to be purified and determine their physical and chemical properties. In addition, reaction kinetics and safety are also important in synthesis and production. Content and purity are determined at each stage of the synthesis process. When the final product is isolated, properties such as purity, stability, polymorphism, melting, and reactivity should also be checked. One of the procedures performed for this purpose is thermal analysis (TG) and Differential scanning calorimetry (DSC) measurement. Thermal analysis can be used to study, predict and control steps in the production of organic compounds. TG analyses are more important, especially in the industrial sector, which includes the synthesis of polymeric substances. In this study, phthalimide derivative 2-methyl-1,3-dioxo isoindoline-5-carboxylic acid was synthesized and its thermal decomposition kinetics were investigated. It has been studied using four different heating rates in the air environment. As a result of the thermal analysis, it was observed that the decomposition was single-step for these four heating rates. The kinetic parameters were calculated by means of the model-free isoconversional method for reliable estimation. Flynn-Wall-Ozawa (FWO), Kissinger-Akahira-Sunose (KAS) and Starink (STK) models were used from the data obtained from the decay curves. The activation energies (Ea) of 2-methyl-1,3-dioxo isoindoline-5-carboxylic acid were calculated by applying three different models.

Keywords: 2-methyl-1, 3-dioxoisoindoline-5-carboxylic acid, Thermal decomposition, TG-DSC, Kinetic model, KAS-FWO

1. INTRODUCTION

Aromatic polyimides are widely used for various polymer applications, such as composite materials, coatings and membranes [1, 2]. One of the aromatic polyimides used for this purpose is isoindole-1,3-dione (phthalimide) [3, 4]. Isoindolin-1,3-dion, (phthalimide) is also found as a functional group in the structure of many compounds and a good many of these compounds has biological activity [5, 6]. These compounds are sedative hypnotic, hypoglycemic, antimalarial, antiandrogenic, hypolipidemic, antitumor, antiangiogenic, antiviral, anticonvulsant, antipsychotic, anti-inflammatory, herbicide and insecticides [6–8]. Synthesis of N-substituted phthalimide derivatives has gained importance by using Thalidomide, one of the isoindolin-1,3-dion derivatives, for the treatment of epilepsy [7, 8].
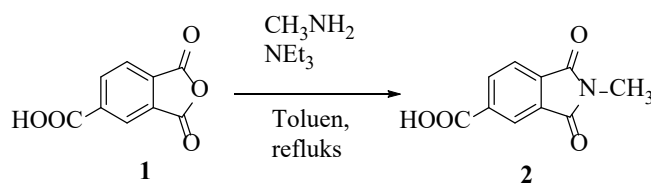
Figure 1. Synthesis of 2-methyl-1, 3-dioxoisoindoline-5-carboxylic acid

Reaction kinetics and safety are also important in synthesis and production. Content and purity are determined at each stage of the synthesis process. When the final product is isolated, properties such as purity, stability, polymorphism, melting, and reactivity should also be checked. One of the procedures performed for this purpose is thermal analysis (TG) and Differential scanning calorimetry (DSC) measurement. Thermal analysis can be used

to study, predict and control steps in the production of organic compounds. TG analyzes are more important, especially in the industrial sector, which includes the synthesis of polymeric substances. DSC measurement allows us to detect endothermic and exothermic effects, to measure transition and reaction enthalpies, to determine temperatures and heat capacity that characterize other effects [9, 10]. Thermal stability of synthesized organic materials can be easily found by TG and DSC methods [11].

N-methyl phthalimide are heterocyclic compounds used as intermediates in organic synthesis or as a building block for plastics and dyes. Also, the compounds known as N-alkyl phthalimides are used as intermediates in the production of nitro N-alkyl phthalimides [12, 13]. These nitro N-alkyl phthalimides are starting reactants for making a number of different organic dianhydrides and polyimides as shown by Heath et al. [14].

In this study, the thermal behavior of the phthalimide derivative 2-methyl-1,3-dioxoisoindoline-5-carboxylic acid (or N-methyl-phthalimide-5-carboxylic acid) was investigated using TG, DTG and DSC analysis results.

2. MATERIAL AND METHOD

Thermal analysis of the synthesized organic matter was performed on a Netzsch STA 409 PC Luxx brand device. The temperature was increased up to 800 K in a controlled manner using the desired heating rate. Analyses were made in the temperature range of 300-800 K and approximately 10 mg of substance was used. Experiments were done using an alumina pan. Empty alumina crucible was used as reference material. Air environment was used in experiments. Four different heating rates were studied at 1, 2.5, 5 and 10 min^{-1}. While choosing these heating rates, it has been taken into account that the highest heating rate is ten times the lowest heating rate. DTG graphics were derived from the obtained TG data. In addition, DSC experiments were performed simultaneously with TG analyses at the same heating rates. Data from these thermal analysis experiments were used in the FWO, KAS and STK models.

The KAS method is mathematically expressed by Eq. (1).

$$\ln\left(\frac{\beta}{T^2}\right) = \ln\left(\frac{AR}{E_a G(\alpha)}\right) - \frac{E_a}{RT}$$

(1)

Activation energy can be found if $\ln\left(\frac{\beta}{T^2}\right)$ versus 1/T is plotted using this equation. FWO, which is the other method used in the calculations, is expressed by the equation below.

$$\log(\beta) = \ln\left(\frac{AE_a}{RG(\alpha)}\right) - 2.315 - 0.4567\frac{E_a}{RT}$$

(2)

The 1/T plot against β according to Eq. (2) will be sufficient to find the activation energy. The linear equation of the Starink model is given below.

$$\ln\left(\beta/T^{1.92}\right) = -10008\left(E_a/RT\right) + C$$

(3)

3. RESULTS

The thermal behavior of the synthesized material was investigated at four different heating rates. Figures 2–4 show the TG DTG and DSC of this material, respectively. Thermal kinetic calculations can be performed in single and multiple steps. As can be seen from this figure, the thermal decomposition of 2-methyl-1,3-dioxoisoindoline-5-carboxylic acid occurred in a single step. DTG curves of 2-methyl-1,3-dioxoisoindoline-5-carboxylic acid are given in Figure 3. In both figures, it can be seen how seriously the decomposition temperatures are affected by the heating rate. These temperatures according to the heating rate are given in Table 1. Conversion values (α) for each temperature were calculated from the TG data. Conversion values include eight conversion values between 0.1 and 0.9. Kinetic parameters were calculated according to these two methods. Using the KAS method, E_a for 2-methyl-1,3-dioxoisoindoline-5-carboxylic acid was obtained between 0.1-0.9 values of the converted fraction at 0.1 intervals from the slope in Figure 6. Slope $-E_a/R.E_a$ and correlation coefficients (R^2) for these calculations are

given in Table 1. E_a was also determined by the FWO method. Here, a linear fit curve for $\ln\beta$ versus 1000/T (Figure 7) was simultaneously obtained. The graph of the third method, STK, is given in Figure 8.
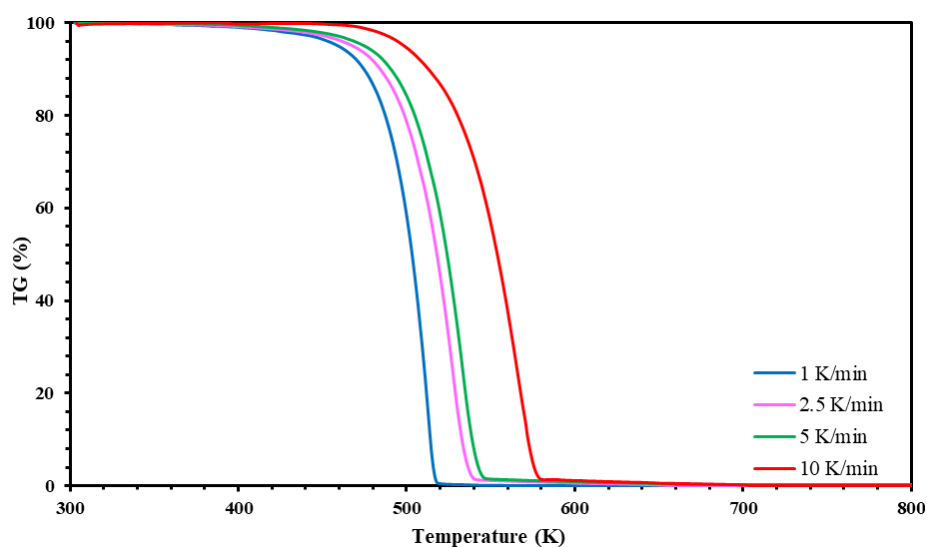
Figure 2. TG curves of 2-methyl-1,3-dioxoisoindoline-5-carboxylic acid at different heating rates
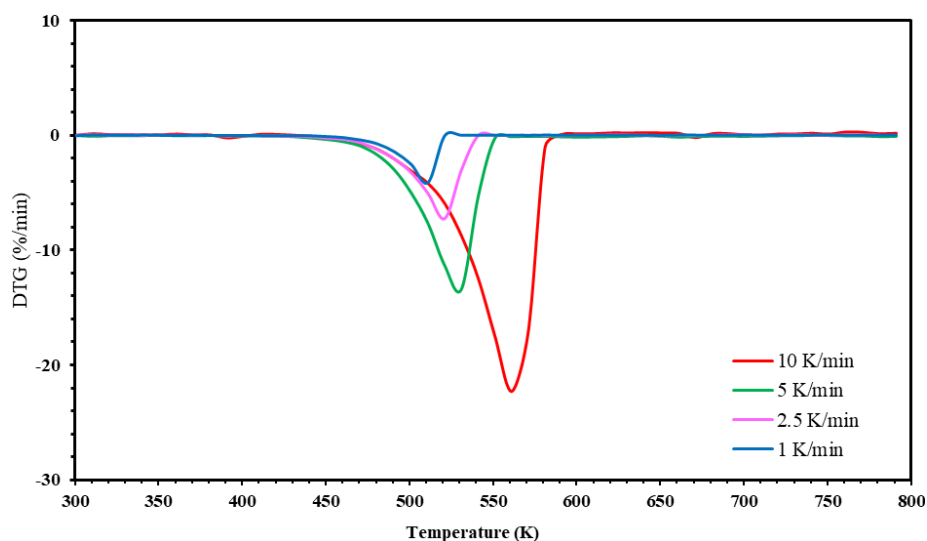
Figure 3. DTG curves of 2-methyl-1,3-dioxoisoindoline-5-carboxylic acid at different heating rates
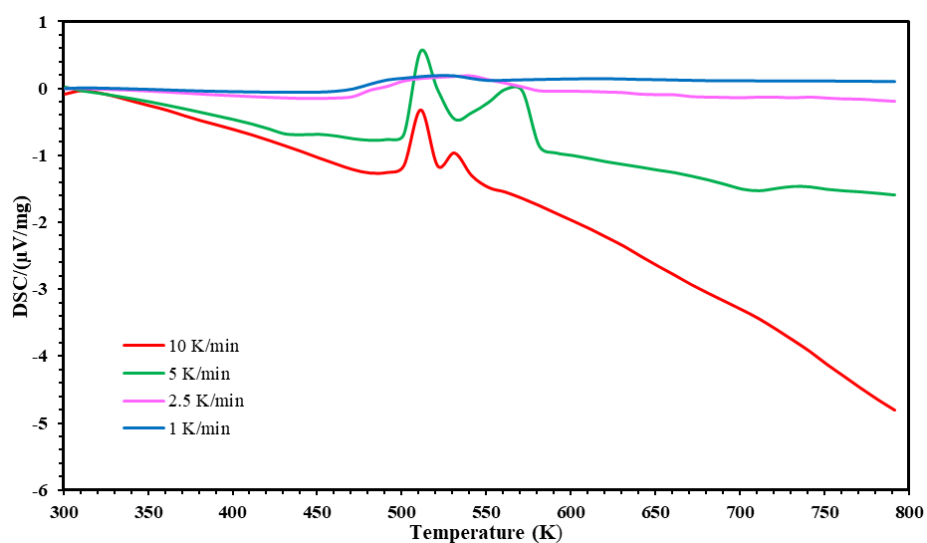
Figure 4. DSC curves of 2-methyl-1,3-dioxoisoindoline-5-carboxylic acid at different heating rates
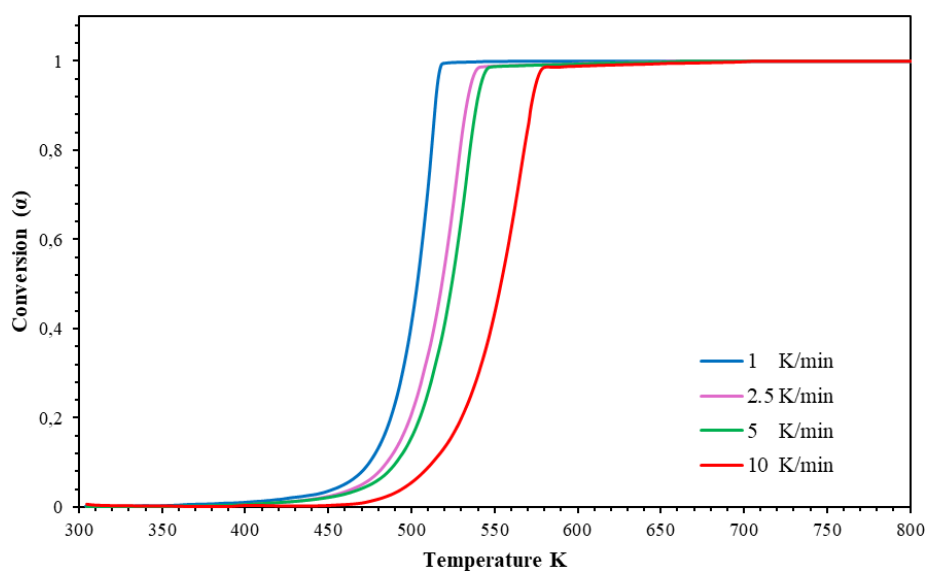
Figure 5. Conversion curve of 2-methyl-1,3-dioxoisoindoline-5-carboxylic acid at different heating rates
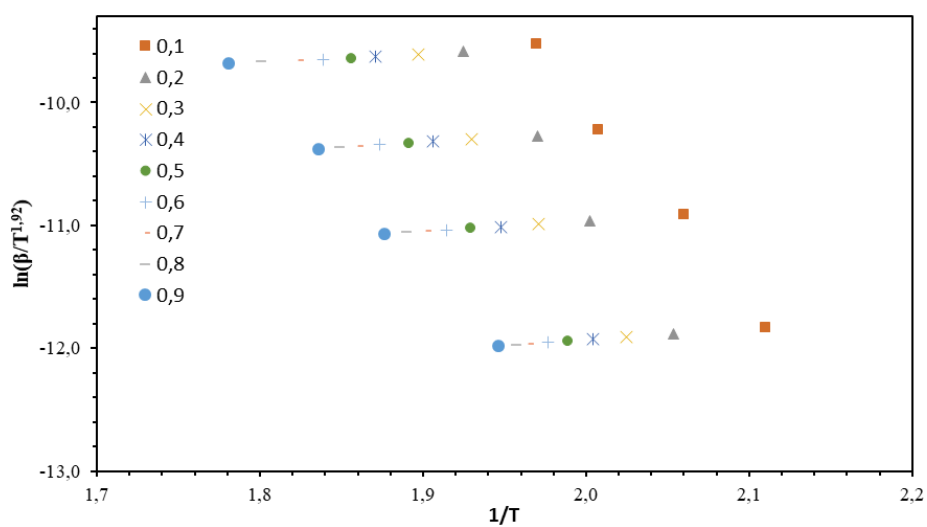
Figure 6. KAS plot of 2-methyl-1,3-dioxoisoindoline-5-carboxylic acid for different values of conversion
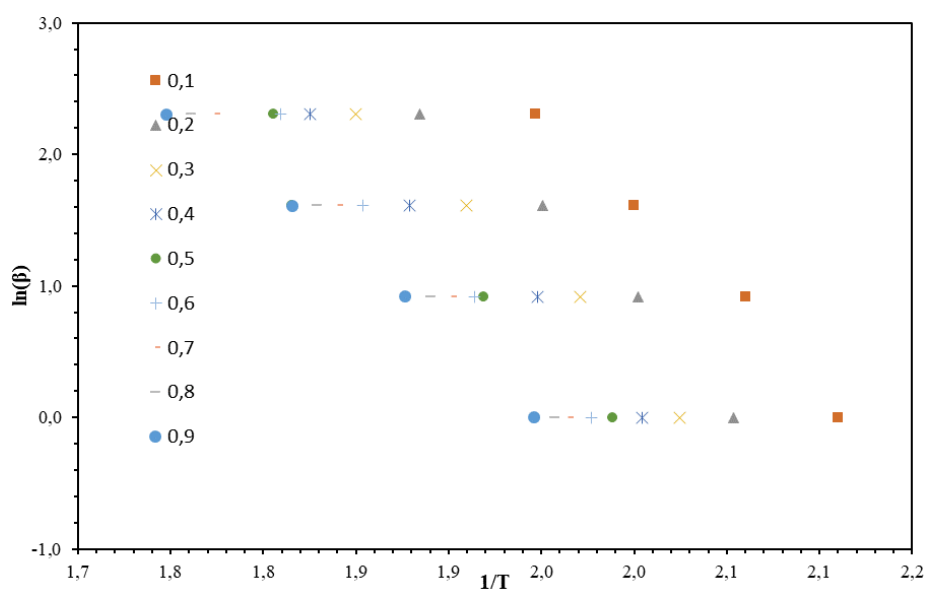
Figure 7. FWO plot of 2-methyl-1,3-dioxoisoindoline-5-carboxylic acid for different values of conversion
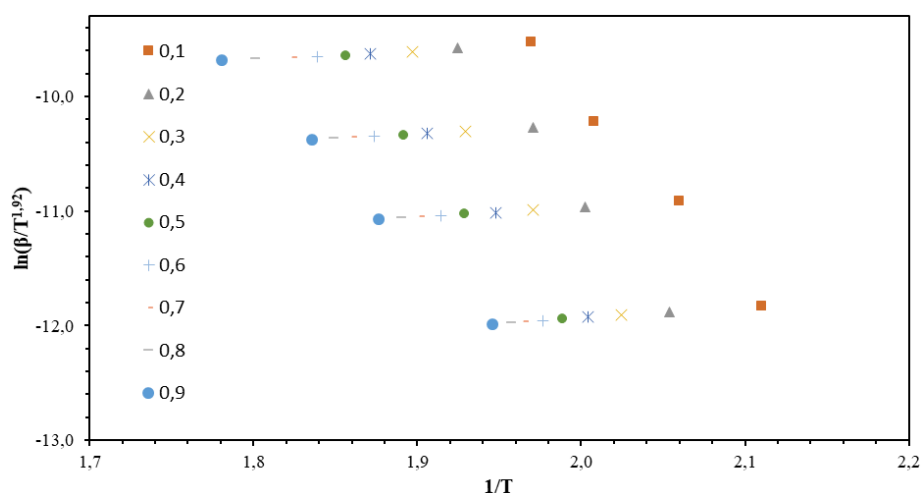
Figure 8. STK plot of 2-methyl-1,3-dioxoisoindoline-5-carboxylic acid for different values of conversion

Table 1. Activation energies from KAS, FWO and STK methods for the decomposition of 2-methyl-1,3-dioxoisoindoline-5-carboxylic acid

	KAS			FWO			STK		
α	E_a (kJ mol^{-1})	R^2	A (min^{-1})	E_a (kJ mol^{-1})	R^2	A (min^{-1})	E_a (kJ mol^{-1})	R^2	A (min^{-1})
0.1	102.45	0.9935	13.67	102.15	0.9652	25.864	133.00	0.9958	21.96
0.2	96.60	0.9928	11.501	97.15	0.9676	23.956	150.10	0.9961	25.21
0.3	93.63	0.9939	10.41	94.39	0.9653	22.944	148.31	0.9973	24.19
0.4	94.01	0.9938	9.7063	96.09	0.9654	22.32	142.28	0.9978	22.35
0.5	90.75	0.9948	9.2608	91.72	0.9624	21.885	144.41	0.9962	22.55
0.6	88.09	0.9965	8.4822	89.05	0.9574	21.118	137.74	0.9949	20.75
0.7	86.86	0.9964	8.0677	88.05	0.9585	20.763	135.12	0.9962	19.93
0.8	84.89	0.9951	7.4955	86.38	0.9597	20.271	123.54	0.9985	17.09
0.9	83.84	0.9956	7.1128	85.33	0.9568	19.902	117.27	0.9974	15.45
Average	91.24	0.9947	9.5229	92.26	0.9620	22.1137	136.86	0.9967	21.05

4. CONCLUSION

The thermal decomposition of 2-methyl-1,3-dioxoisoindoline-5-carboxylic acid in air atmosphere at four heating rates (1, 2.5, 10, and 20 K min^{-1}) was investigated using the simultaneous TG- DTG measurements. KAS, FWO and STK methods were used to study thermal degradation. The activation energy E_a was calculated as 91.24, 92.26 and 136.86 kJ/mol, respectively. The correlation coefficient (R^2) of both models was calculated quite high. In particular, the correlation coefficient (R^2) of the STK method is quite high. The thermal stability of 2-methyl-1,3-dioxoisoindoline-5-carboxylic acid was determined to be up to 440.3 K.

References

[1]   C. J. Guo, Z. Sun, S. L. Xia, and Y. H. Wang, "A preliminary inquiry into the conformation of the side chains on polyimide film and the mechanism of the vertical alignment of liquid crystals induced by polyimides with side chains," *Liquid Crystals*, vol. 39, pp. 721–728, 2012.

[2]   S. Xia, L. Yi, Z. Sun, and Y. Wang. "The effect of phthalimide side chains on the thermal stability and rubbing   resistance of polyimide used as a liquid crystal vertical alignment layer," *Journal of Polymer Research*, vol. 20, 2013.

[3]   D. R. Barn and J. Richard Morphy, "Solid-phase synthesis of cyclic imides," J*ournal of Combinatorial Chemistry*, vol. 1, pp. 151–156, 1999.

[4]   M. H. Norman, D. J. Minick, and G. C. Rigdon, "Effect of linking bridge modifications on the antipsychotic profile of some phthalimide and isoindolinone derivatives," *Journal of Medicinal Chemistry*,vol. 39, pp. 149–157, 1996.

[5]   X. Collin and J. Robert, "Original article new anti-inflammatory N-pyridinyl (alkyl) phthalimides acting as

tumour necrosis factor-a production inhibitors," *Eur. J. Med. Chem.*, vol. 36, pp. 639–449, 2001.

[6] M. Y. Chang, S. T. Chen, and N. C. Chang, "A synthesis of racemic thalidomide," *Synthetic Communications*, vol. 33, pp. 1375–1382, 2003.

[7] B. D. Vu, N. M. Ho Ba, and D. C. Phan, "Facile synthesis of thalidomide," *Organic Process Research and Development*, vol. 23, pp. 1374–1377, 2019.

[8] B. Grabowska, K. Hodor, K. Kaczmarska, A. Bobrowski, Z. Kurleto-Koziol, and C. Fischer, "Thermal analysis in foundry technology: Part 2. TG–DTG–DSC, TG–MS and TG–IR study of the new class of polymer binders BioCo," *Journal of Thermal Analysis and Calorimetry*, 2019.

[9] R. Bottom, "Thermogravimetric analysis," in *Principles and Applications of Thermal Analysis*, P. Gabbott, Eds.: Blackwell Publishing, 1963, pp. 187–118.

[10] K. Sekiguchi, I. Hımuro, I. Horıkoshi, T. Tsukada, and T. Okamoto, "NII-Electronic library service," *Chemical Pharmaceutical Bulletin*, vol. 17, pp. 191–199, 1969.

[11] N. V. Sadavarte, S. S. Patil, C. V. Avadhani, and P. P. Avadhani, "New organosoluble aromatic poly(esterimide)s containing pendent pentadecyl chains: Synthesis and characterization," *High Performance Polymers*, vol. 25, pp. 735–743, 2013.

[12] D. A. Kirby, "The Characterization of N-methylphthalimide," *NMP*, vol. 8, pp. 36–38.

[13] P. Das, and P. Tiwari, "Thermal degradation kinetics of plastics and model selection," *Thermochimica Acta*, vol. 654, pp. 191–202, 2017.

[14] R. Heath, U.S. Patent 19, 1975

Design, Prototyping, and Experimental Investigation of a Crash Box with Lattice Geometry

Erman Zurnaci[1], Mahmut Can Turk[2]

[1]Mechanical Engineering Department, Engineering and Architecture Faculty, Kastamonu University, Kastamonu, Türkiye
[2]Yazmaksan Thermoblock Heating Systems Inc., Ferizli, Sakarya, Türkiye
Corresponding author: Erman Zurnaci (e-mail: ermanzurnaci@kastamonu.edu.tr)

Abstract

The design of automobile chassis is important regarding vehicle safety and crash management. Crash boxes are used in the front part of the automobile chassis to protect the integrity of the automobile and to ensure passenger safety in the event of a possible accident. Crash boxes are designed in different geometries to absorb the maximum amount of energy generated in the event of a collision. Lattice structures are frequently preferred for engineering components that require high mechanical strength and lightness. The mechanical behavior of lattice structures varies depending on the unit cell geometry and size. Therefore, different strength properties can be obtained by designing the configuration of the lattice cell geometry. In addition, these developed structures can be easily produced by fused deposition modeling (FDM). This study examines the mechanical performance of crash boxes with different lattice geometries. In the study, crash boxes with two different lattice geometries were designed and produced with three-dimensional manufacturing methods, and experimental tests were carried out. The mechanical performance of the developed designs was compared with the performance of the crash box with a conventional design. The results showed that the crash boxes with a hexagonal lattice structure increased the energy absorption performance, reduced the crushing resistance, and improved the stress distribution.

Keywords: Crash box, Lattice structures, Structural optimization, Numerical analysis, 3D printing

1. INTRODUCTION

Crash boxes are used on the chassis of vehicles to control collisions and minimize possible accident risks in transportation vehicles where human safety is important, such as highways, railways, and the defense industry [1–3]. Crash boxes are designed to absorb kinetic energy in the initial stages of a frontal collision without damaging the chassis [4]. Crash boxes, especially used in cars and trains, are connection elements that absorb the impact energy that occurs in the event of an accident and ensure that the impact force is transmitted to the vehicle at a minimum level. Crash boxes absorb the impact energy by undergoing plastic deformation during the collision, thus reducing the impact force affecting the entire vehicle [5]. Due to their critical role, many studies have been conducted to improve crash boxes. Since crash boxes are replaceable structural elements, they can be repaired at a lower cost than other components of vehicles. The crash box is the most important component that provides crash resistance in vehicles [1].

Crash resistance is defined as the ability of a structure to resist loading under a certain intensity and sustain low damage for dynamic loads [6]. In automotive engineering terms, crashworthiness is the ability of a vehicle to protect occupants from serious injury or death in the event of an accident [7]. Due to this function, crash boxes are of great importance in automobiles. In recent years, studies have gained importance to reduce the weight of vehicles together with the targets of low carbon dioxide emissions. Researchers use various methods to lighten the different components of automobiles. Structural optimization is an excellent method to improve mechanical strength by considering the design parameters [8–10].

In this study, the effect of lattice structures in the design of crash boxes was investigated to reduce the weight and increase the impact energy absorption capacity of the crash boxes. The effect of different lattice geometries on the crash strength was investigated. Experimental and numerical tests were carried out for the different designs developed, and the designs' weight/mechanical strength performance was compared.

1.1. Crash Boxes

Crash boxes are generally manufactured in rectangular prism and conical structures and are placed between the front bumper beam and the chassis (Figure 1). Crash boxes can be manufactured in different geometries, including quadrilateral and hexagonal. Honeycomb structures are especially highly resistant to vertical crushing loads [11]. However, they become less resistant to lateral loads after the initial breaking load. To prevent this weakness, hexagonal crash boxes are filled with different filling materials [12, 13].
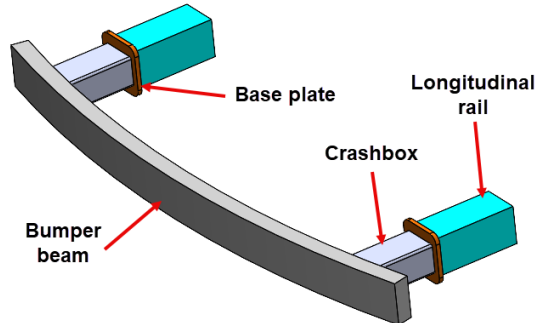
Figure 1. Crash box on a vehicle chassis

The lattice structure is preferred in many design applications (aviation, biological engineering, mechanical engineering, etc.) due to its excellent properties, such as lightness, high specific strength and stiffness, and improved thermal conductivity [14]. Lattice structures can also be redesigned to suit the field of use. In other words, each unit cell and each support in the lattice structure can be set as a design variable and functionally optimized to meet specific customized requirements, meaning that the mechanical properties of lattices can be controlled more flexibly than foams and honeycombs [15]. Therefore, it can be concluded that lattice structures perform better than foam structures and honeycombs [16]. Due to their superior energy-absorbing properties and load-carrying capacity, 3D lattice core structural components are widely used as energy-absorbing elements in crashworthiness applications [17]. Studies have shown that lattice structures have improved mechanical properties, especially those competitive with low-density honeycomb forms [18, 19].

2. MATERIAL AND METHOD

2.1. Crash Box Design

In this study, three different crash box designs were made. The first design (Figure 2a) has a flat cylindrical structure representing the traditional crash box (Model 1). The second design (Model 2) has the same dimensions, but a lattice structure is obtained by creating hexagonal cavities in the crash box body (Figure 2b). The third design (Model 3) is designed in a lattice structure (Figure 2c). All the crash tubes are 90 mm long and 48 mm in diameter, and the wall thickness differs for each design. In order to compare the designs realistically, the wall thicknesses of the designs were determined differently to obtain models with equal weights.

a) Model 1	b) Model 2	c) Model 3
t = 1.2 mm	t = 2 mm	t = 2 mm
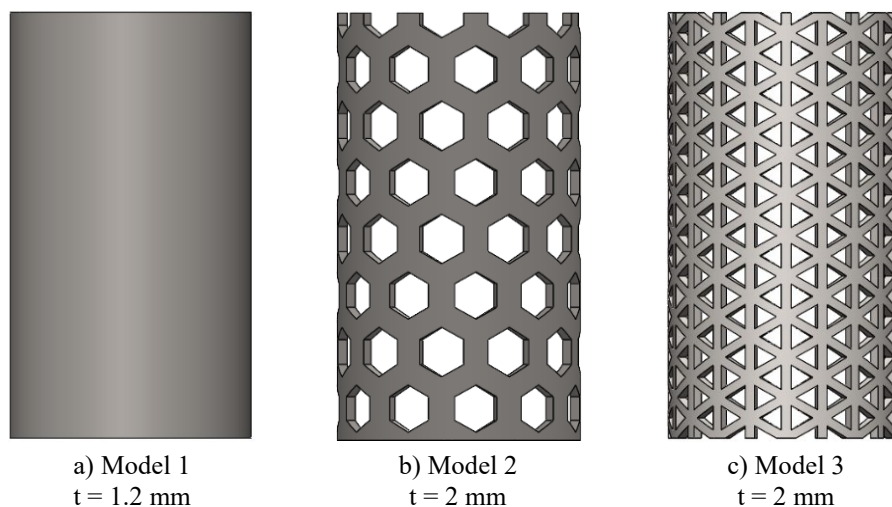
Figure 2. Crash box models

2.2. Numerical Analysis

The solid models of the three different crash boxes were created using Solidworks software. Then, the stress distributions in the models were examined with the finite element method. Thus, the effect of design features on the stress distribution was compared. AISI 1020 material was assigned for the crash boxes in the analysis. Fixed support was applied to the models from the bottom base so that it would be fixed on each axis. The meshing process was applied to the models, creating finite element models (Figure 3a). Then, an 80 N planar load was applied from the top of the models (Figure 3b). As a result of numerical analysis, the stress distributions in the models were determined (Figure 4).

a)   b)
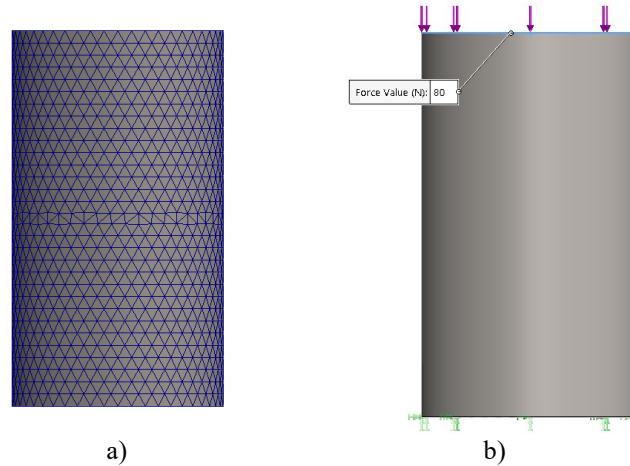
Figure 3. a) Numerical analysis finite element model and b) load scenario

Model 1   Model 2   Model 1
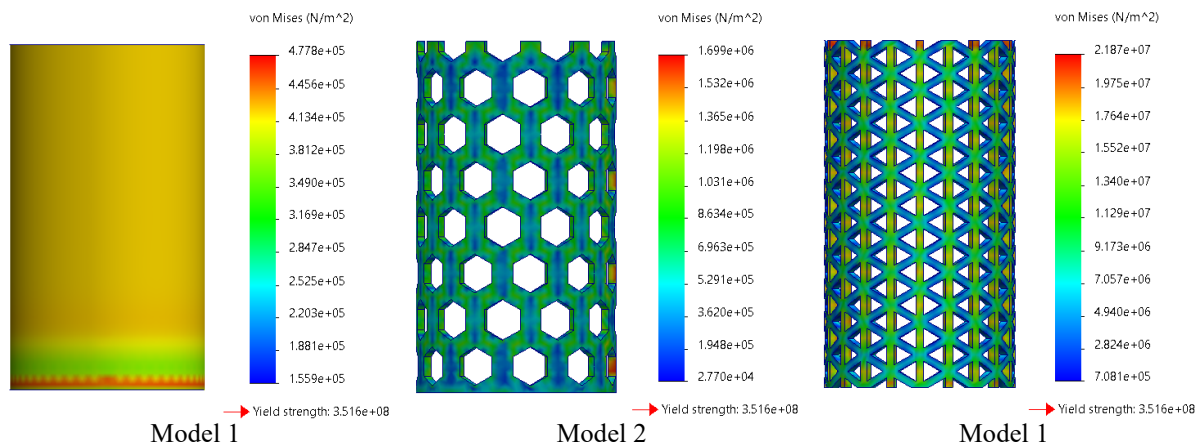
Figure 4. Stress distribution was calculated for different designs as a result of numerical analysis

When Figure 4 is examined, it is seen how the stresses are distributed in the model. Model 1 shows high stress spreading throughout the crash box. The blue regions symbolizing the low-stress value are almost nonexistent. In Models 2 and 3, it is seen that the stress spreads throughout the body. Especially in Model 2, the stress values calculated on the body remained at low levels. The numerical analysis results show that the lattice body geometry successfully reduces the stress and spreads it throughout the crash box.

2.3. Prototype Production

Models of crash boxes will be produced with a three-dimensional production technique, prototypes will be prepared, and experimental tests will be carried out. For this purpose, three-dimensional models of crash box designs were produced on a Creality Ender 3 S1 model 3D printer operating with the fused deposition technique (Figure 5). For production, solid models of crash boxes were converted to STL format and then transferred to Ultimaker Cura slicing software to determine three-dimensional production parameters. Production was carried out by transferring g-codes containing production parameters to the three-dimensional printer. All prototypes were produced at room temperature. Three-dimensional production parameters are given in Table 1.
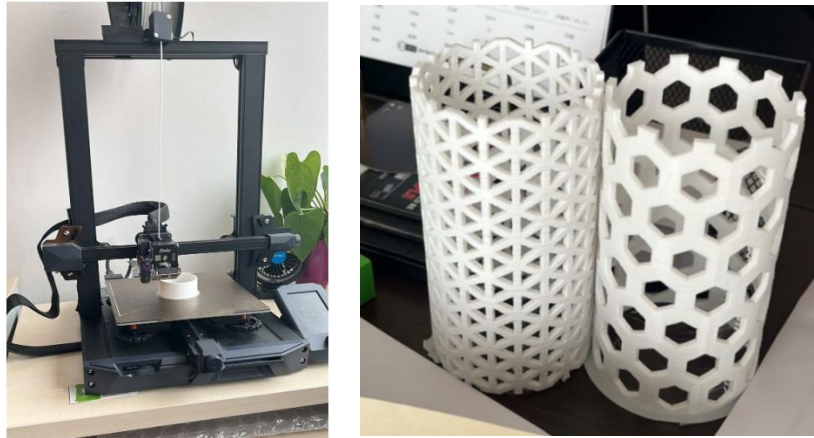
Figure 5. Production of crash box prototypes with a 3D printer

Table 1. 3D printing parameters

Parameter Type	Parameter Value
Filament material	PLA
Filament color	White
Filament diameter	1.75 mm
Layer thickness	0.2 mm
Nozzle diameter	0.4 mm
Nozzle temperature	210º
Bad temperature	60º
Infill density	100%
Infill pattern	Lines
Printing speed	50 m/s

3. RESULTS

3.1. Experimental Analysis of Prototypes

Experimental compression tests were conducted to determine the crushing behavior of the crash box prototypes produced with the three-dimensional manufacturing method under quasi-static load. Both the deformation behavior of the samples was observed, and the mechanical performance was measured using the compression test. The experiments were carried out at a 1 mm/min speed in the 10 kN Shimadzu Autograph AGS-X testing machine located in the Kastamonu University Central Research Laboratory. The tests were terminated with the occurrence of permanent deformation. The deformations in the samples after the experimental test are shown in Figure 6.

Model 1   Model 2   Model 3
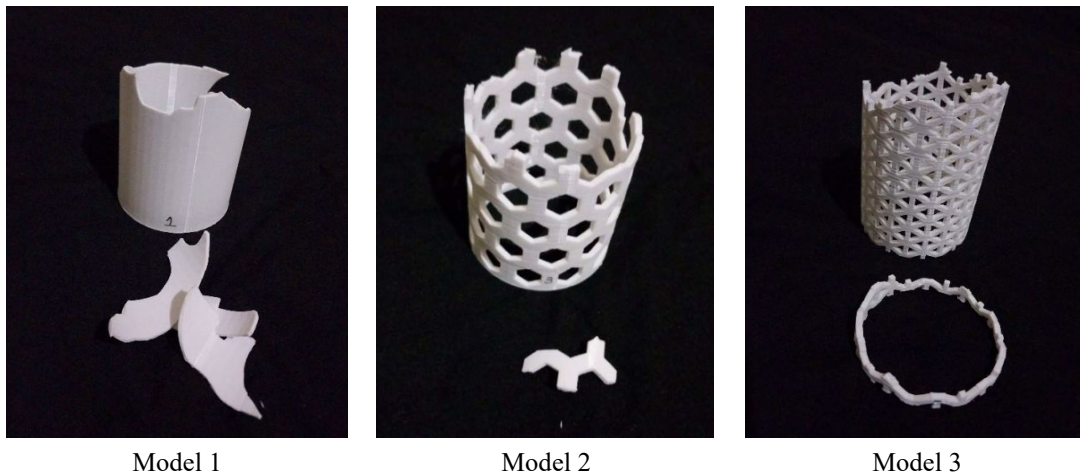
Figure 6. Deformation of samples as a result of experimental test

Model 1 showed a more brittle deformation behavior under deformation load due to its solid body structure, and fractures occurred in the upper part of the crash box. While a small piece broke off from the Model 2 crash box, the upper part of the Model 3 crash box broke off.

Force-displacement curves of the prototypes were created to examine the experimental test results (Figure 7). Using these curves, the maximum crushing resistance of the designs was determined. The crushing resistance gives the maximum force value the models can resist before breaking. This value was determined as a performance criterion to be used to evaluate the models. The area under the force- displacement curves shows the amount of energy absorbed by the models. The results obtained were used to compare the designs (Table 2).
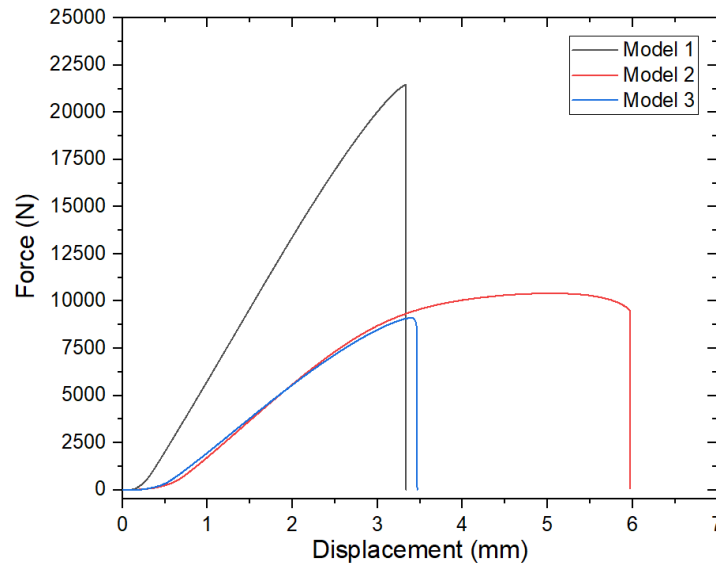
Figure 7. Force- displacement curves of the models

Table 2. Experimental test results

	Weight (g)	Max Force (kN)	Absorbed Energy (J)
Model 1	17.54	21.44	35.61
Model 2	17.88	10.41	41.09
Model 3	17.13	9.10	15.63

4. CONCLUSION

Experimental test results provide important information about the mechanical strength performance of the models. Although the weights of the models are approximately the same, there are significant differences between their mechanical responses. While the Model 1 crash box absorbed 35.61 J of energy until the first fracture, the Model 3 crash box was able to absorb less than half of the energy (15.63 J) despite approximately the same deformation value. The Model 2 crash box, despite its flatter crushing resistance, has become the design that absorbs the most impact energy by absorbing 41.09 J of energy. When the numerical and experimental analysis results are evaluated, it is revealed that the hollow lattice structure with hexagonal geometry increases the energy absorbing capacity of the crash box while improving the stress distribution. In addition, despite the low crushing resistance of Model 3, its high absorbing capacity can also prevent sudden accelerations in the event of a crash.

Acknowledgments

References

[1]   N. A. Z. Abdullah, M. S. M. Sani, M. S. Salwani, and N. A. Husain, "A review on crashworthiness studies of crash box structure," *Thin-Walled Struct.*, vol. 153, art. no. 106795, Aug. 2020, doi:

10.1016/j.tws.2020.106795.

[2]   A. Ciampaglia, D. Fiumarella, C. Boursier Niutta, R. Ciardiello, and G. Belingardi, "Impact response of an origami-shaped composite crash box: Experimental analysis and numerical optimization," *Compos. Struct.*, vol. 256, art. no. 113093, Jan. 2021, doi: 10.1016/j.compstruct.2020.113093.

[3]   G. Wang, Y. Zhang, Z. Zheng, H. Chen, and J. Yu, "Crashworthiness design and impact tests of aluminum foam-filled crash boxes," *Thin-Walled Struct.*, vol. 180, art. no. 109937, Nov. 2022, doi: 10.1016/j.tws.2022.109937.

[4]   A. Ciampaglia, L. Patruno, and R. Ciardiello, "Design of a Lightweight Origami Composite Crash Box: Experimental and Numerical Study on the Absorbed Energy in Frontal Impacts," *J. Compos. Sci.*, vol. 8, no. 6, art. no. 224, Jun. 2024, doi: 10.3390/jcs8060224.

[5]   Y. Xiang, T. Yu, and L. Yang, "Comparative analysis of energy absorption capacity of polygonal tubes, multi-cell tubes and honeycombs by utilizing key performance indicators," *Mater. Des.*, vol. 89, pp. 689–696, Jan. 2016, doi: 10.1016/j.matdes.2015.10.004.

[6]   S. A. Meguid, M. S. Attia, and A. Monfort, "On the crush behaviour of ultralight foam-filled structures," *Mater. Des.*, vol. 25, no. 3, pp. 183–189, May 2004, doi: 10.1016/j.matdes.2003.10.006.

[7]   E. Mahdi, A. S. Mokhtar, N. A. Asari, F. Elfaki, and E. J. Abdullah, "Nonlinear finite element analysis of axially crushed cotton fibre composite corrugated tubes," *Compos. Struct.*, vol. 75, no. 1–4, pp. 39–48, Sep. 2006, doi: 10.1016/j.compstruct.2006.04.057.

[8]   P. G. Anselma, C. B. Niutta, L. Mainini, and G. Belingardi, "Multidisciplinary design optimization for hybrid electric vehicles: component sizing and multi-fidelity frontal crashworthiness," *Struct. Multidiscip. Optim.*, vol. 62, no. 4, pp. 2149–2166, Oct. 2020, doi: 10.1007/s00158-020-02603-6.

[9]   X. An, Y. Gao, J. Fang, G. Sun, and Q. Li, "Crashworthiness design for foam-filled thin-walled structures with functionally lateral graded thickness sheets," *Thin-Walled Struct.*, vol. 91, pp. 63–71, Jun. 2015, doi: 10.1016/j.tws.2015.01.011.

[10]   E. Zurnacı and H. Gökkaya, "The effect of core configuration on the compressive performance of metallic sandwich panels," *Mater. Tehnol.*, vol. 53, no. 6, pp. 859–864, Dec. 2019, doi: 10.17222/mit.2019.023.

[11]   Z. Li, Q. Yang, R. Fang, W. Chen, and H. Hao, "Crushing performances of Kirigami modified honeycomb structure in three axial directions," *Thin-Walled Struct.*, vol. 160, art. no. 107365, Mar. 2021, doi: 10.1016/j.tws.2020.107365.

[12]   A. De Biasio, H. Ghasemnejad, S. Srimanosaowapak, and J. W. Watson, "Development of multi aluminium foam-filled crash box systems to improve crashworthiness performance of road Service vehicle," *Eur. J. Mech. - A/Solids*, vol. 109, art. no. 105433, Jan. 2025, doi: 10.1016/j.euromechsol.2024.105433.

[13]   F. Djamaluddin, "Optimization of foam-filled crash-box under axial loading for pure electric vehicle," *Results Mater.*, vol. 21, art. no. 100505, Mar. 2024, doi: 10.1016/j.rinma.2023.100505.

[14]   M. E. Korkmaz, M. K. Gupta, G. Robak, K. Moj, G. M. Krolczyk, and M. Kuntoglu, "Development of lattice structure with selective laser melting process: A state of the art on properties, future trends and challenges," *J. Manuf. Process.*, vol. 81, pp. 1040–1063, Sep. 2022, doi: 10.1016/j.jmapro.2022.07.051.

[15]   G. Dong, Y. Tang, and Y. F. Zhao, "A survey of modeling of lattice structures fabricated by additive manufacturing," *J. Mech. Des.*, vol. 139, no. 10, Oct. 2017, doi: 10.1115/1.4037305.

[16]   C. Pan, Y. Han, and J. Lu, "Design and optimization of lattice structures: A review," *Appl. Sci.*, vol. 10, no. 18, art. no. 6374, Sep. 2020, doi: 10.3390/app10186374.

[17]   M. Tafazoli and M. D. Nouri, "Investigation of the experimental, statistical and optimisation of 3D printed lattice core sandwich panel energy absorber with novel configuration using response surface method," *Int. J. Crashworthiness*, vol. 27, no. 1, pp. 261–272, Jan. 2022, doi: 10.1080/13588265.2020.1786913.

[18]   G. W. Kooistra, V. S. Deshpande, and H. N. G. Wadley, "Compressive behavior of age hardenable tetrahedral lattice truss structures made from aluminium," *Acta Mater.*, vol. 52, no. 14, pp. 4229–4237, 2004, doi: 10.1016/j.actamat.2004.05.039.

[19]   E. Zurnaci and H. K. Ozdemir, "Investigation of the compressive strength, energy absorption properties and deformation modes of the reinforced core cell produced by the FDM method," *Gazi J. Eng. Sci.*, vol. 9, no. 1, pp. 1–11, Apr. 2023, doi: 10.30855/gmbd.0705047.

Shunt Reactor Conservator Analysis: Under Full Vacuum and Buckling Conditions

Dogan Koyun[1], Cagri Aksakal[1], Ahmet Feyzioglu[2]

[1]General Electric, Kocaeli, Türkiye
[2]Faculty of Science, Business and Enterprise, University of Chester, United Kingdom
Corresponding author: Dogan Koyun (e-mail: dogan.koyun@ge.com)

Abstract

Shunt reactors, indispensable components in power systems, play a pivotal role in voltage regulation and power factor improvement. These reactors, often situated in harsh environments, are subject to various operational stresses, including thermal cycling, vibration, and pressure fluctuations. The conservator, a crucial component of the reactor system, serves to maintain the insulating oil level and mitigate the effects of pressure variations. Under normal operating conditions, the conservator is subjected to a partial vacuum. However, in certain scenarios, such as during maintenance or fault conditions, the conservator may experience full vacuum. Furthermore, the conservator's cylindrical shape makes it susceptible to buckling under external loads or internal pressure differentials.

In this context, the function and design of conservators are explored in detail, including the materials used and the factors influencing their design. The effects of full vacuum on the conservator, including stress distribution, material properties, and potential failure modes, are comprehensively analyzed. Theoretical and computational methods used to evaluate the buckling behavior of cylindrical shells under various loading conditions are elaborated. The use of finite element analysis (FEA) to simulate complex stress and deformation patterns within the conservator under full vacuum and buckling conditions is demonstrated. Furthermore, the influence of material properties such as Young's modulus, Poisson's ratio, and yield strength on conservator behavior is discussed extensively. Experimental techniques used to validate analytical models and assess the actual performance of conservators under simulated operating conditions are also included in the study.

This study provides a comprehensive understanding of the challenges associated with the design and analysis of shunt reactor conservators. By addressing critical conditions such as full vacuum and buckling, the necessary knowledge and expertise for ensuring the safe and reliable operation of these components are highlighted. The findings obtained carry significant importance for the sustainability and reliability of power systems.

Keywords: Shunt reactor, Conservator, Power systems, Full vacuum, Buckling analysis

Evaluating Count Regression Models Under Varying Dispersion: A Simulation Study of Poisson, Negative Binomial, and COM-Poisson Residuals

Sima Atalay[1], Hatice Tul Kubra Akdur[2]

[1]Graduate School of Natural and Applied Sciences, Gazi University, Ankara, Türkiye
[2]Department of Statistics, Gazi University, Ankara, Türkiye
Corresponding author: Sima Atalay (e-mail: sima.kucukdilek@gazi.edu.tr)

Abstract

The Conway-Maxwell Poisson (COM-Poisson) regression model is a flexible alternative to Poisson regression, effectively managing count data that shows overdispersion or underdispersion. The standard Poisson regression assumes that the mean and variance of the response variable are equal, a condition often violated in real-world datasets. When the variance significantly exceeds or falls below the mean, Poisson regression may produce inaccurate results. COM-Poisson regression addresses this by introducing an extra parameter, ν, which allows the variance to vary independently from the mean. In the COM-Poisson model, the parameter λ controls the mean, while the dispersion parameter ν adjusts the variance. When $\nu=1$, the model reduces to the standard Poisson distribution. For $\nu > 1$, the model handles underdispersion, where data points are closer together than in a typical Poisson model. For $\nu < 1$, it captures overdispersion, where the variance exceeds the mean, which is common in many datasets. The flexibility of the COM-Poisson model makes it useful in various fields such as healthcare (disease counts or hospital admissions), transportation (vehicle or accident counts), and insurance (claim frequencies). In these areas, COM-Poisson regression provides a more accurate and reliable approach than the Poisson regression, which may lead to errors if the variance is not properly accounted for. In this study, we conducted a simulation study to assess the performance of three count regression models (Poisson, Negative Binomial, and Conway-Maxwell-Poisson (COM-Poisson)) under various dispersion conditions. For each model, we generated synthetic datasets reflecting different dispersion levels (underdispersion, overdispersion, and equidispersion) to explore the accuracy and robustness of model fitting and residual behavior. Shapiro-Wilk tests were applied to raw and quantile residuals from each model to evaluate their adherence to normality. The results provide insights into each model's suitability across diverse data structures, highlighting the COM-Poisson model's flexibility for handling varying dispersion. A real data application was also presented to show the usefulness of the COM-Poisson regression model in practice.

Keywords: Com-Poisson regression, Over-dispersion, Under-dispersion, Residual analysis

Investigation of Low Temperature Behaviour of Boron Added Rosin Compound

Merve Gulfer Bozdemir[1], Hacer Yesilcicek[2], Seref Oruc[2]

[1]Department of Civil Engineering, Faculty of Engineering and Architecture, Erzurum Technical University, Türkiye
[2]Department of Civil Engineering, Faculty of Technology, Karadeniz Technical University, Türkiye
Corresponding author: Merve Gulfer Bozdemir (e-mail: merve.ozcan@erzurum.edu.tr)

Abstract

In cold climatic regions, one of the most important problems in asphalt pavements is thermal cracking. Thermal cracks occur on the pavement surface when the asphalt pavement exceeds its tensile strength, and this adversely affects the life of the pavement. Thermal cracks are closely related to the properties of the asphalt binder. For this reason, binders are modified with many different additives. The aim of this study is to determine the effect of the boron added rosin compound synthesized in the laboratory on the low temperature behaviour of the original asphalt binder. The low temperature behavior of asphalt binders can be determined by Fraass breaking point and BBR experiments. Since the Frass breakpoint test is an empirical test, the BBR test is needed to obtain more accurate results. In this study, original binder (by weight) was modified by adding 1% and 3% additives. The original and modified asphalt binders Fraass break point and BBR tests were applied. The BBR test was carried out at –6 and –12 °C. The Fraass breaking point test was applied up to the temperature of the first cracking. The effect of the additive on the low temperature behavior of the asphalt binder was investigated comparatively with two experiments. According to the results obtained, it was observed that the binder modified with 1% additive compared to the base binder increased its resistance against cracks. However, it was stated that high amount of additives increased the hardness of the binder and decreased its ductility. By determining the low temperature behavior of the binder with two experiments in the study, the region where the asphalt binder will be applied can be selected. In addition, the low temperature PG level of the modified binder can be determined by the BBR test.

Keywords: Asphalt modification, Additive, Thermal cracking, BBR, Fraass breaking point

1. INTRODUCTION

Flexible road pavements have a complex structure consisting of aggregate, asphalt binder and air. Asphalt, which is generally used as a binder in flexible pavements, has an important place in terms of road pavement performance, although it is used at low rates such as 5–7%. Asphalt binder shows different behaviors depending on climatic conditions due to its viscoelastic property. In cold climatic regions, one of the most important problems in asphalt pavements is thermal cracking. Thermal cracks occur on the pavement surface when the asphalt pavement exceeds its tensile strength, and this adversely affects the life of the pavement. Thermal cracks are closely related to the properties of the asphalt binder. In order to reduce these deteriorations and improve asphalt pavement performance, binder modifications are made by adding many different additives to the asphalt binder [1–3]. In order to improve the properties of asphalt binder, various polymers [4, 5], nano and nano composite materials [6–8], oil-based materials [9, 10] and waste materials [11, 12] is used.

There are studies in which boron element, which is found as a compound in nature, is used as a modifier in asphalt. It has been determined that the boron element cannot adhere directly to the asphalt binder and that it is a good modifier in asphalt by synthesizing it with another substance [13]. In recent years, studies have shown that boron and resin types are synthesized and used as a new additive [14, 15]. The aim of this study is to determine the effect of the boron added rosin compound synthesized in the laboratory on the low temperature behaviour of the original asphalt binder.

2. MATERIAL AND METHOD

In this study, penetration degree 50/70 asphalt cement (PG 64-16) obtained from Turkish Petroleum Refinery (Izmit) was used.

Rosin is a natural resin obtained from pine trees by evaporating the terpene components in fresh liquid resin [16]. The rosin properties used in this study are given in Table 1.

Table 1. Properties of the rosin

Purity	95–97% min.
Molar mass	302.45 g/mol
Melting temperature	72-75 °C
Specific gravity	1.06–1.07 g/cm^3

Boron oxide is an odorless, hard, glassy chemical substance obtained by dehydration of boric acid [17]. The properties of boron oxide are given in Table 2.

Table 2. Properties of the boron oxide

Components	Amount
B_2O_3	98.00% min.
SO_4	500 ppm max
Cl	10 ppm max.
Fe	35 ppm max.
+0.315 mm [size]	%75.00 min.

2.1. Preparation of the BORB Modified Binders

Boron oxide and rosin compound (BORB) additive was synthesized in the laboratory environment, considering the methods used in previous studies [14, 15, 18–20].

The additive is dark in color and solid at ambient temperature. This synthesis additive can be produced industrially with a short production process. The general view of the boron oxide and resin compound (BORC) synthesis additive is given in Figure 1.

Figure 1. Visual of BORB additive

BORB synthesis additive was added separately at the rates of 1% and 3% (based on binder weight) to the asphalt binder, which became fluid at 150 ± 5 °C. Modified asphalts were produced using a high shear mixer at 2000 rpm for 30 minutes at 150 ± 5 °C. The description of the asphalt binders is shown in Table 3.

Table 3. The description of the asphalt binders

Sample Content	Code
Asphalt binder	BA
Asphalt binder + %1 BORB	BA1
Asphalt binder + %3 BORB	BA3

2.2. Fraass Breaking Point Test

Fraass breaking point allows measuring the brittleness of asphalt binders at low temperatures (subzero) [21]. According to TS EN 12593, 0.40 g of asphalt binder is placed on a steel sheet with equal thickness on all sides and the sheet is cooled at a constant rate. The sheet metal plate with the sample on it is placed in the device and when the desired low temperatures are achieved with dry ice, the sample is stretched at regular intervals. The temperature at which the first cracking begins on the sample surface is determined as the Fraass breaking point of the binder.

2.3. Bending Beam Rheometer (BBR) Test

With the BBR test, the deflection amount and creep characteristics of the binder at low temperatures under constant load at a certain temperature are determined. Long-term aged binders obtained from the RTFOT + PAV experiment are used for this experiment. The BBR test was carried out at –6 and –12 ºC. the creep stiffness (S) and creep rate (m-value) are obtained at the end of the BBR test. Low creep hardness and high creep rate are required to reduce the formation of thermal cracks that occur at low temperatures. A maximum hardness of 300 MPa and a minimum m value of 0.300 are required to minimize low temperature cracking.

3. RESULTS

3.1. Results of Fraass Breaking Point Test

Fraass breaking point test results of base and modified asphalts are given in Figure 2. Looking at the experimental data, it can be said that the resistance of pure asphalt to cracking at low temperatures has generally increased thanks to the synthesis additive.
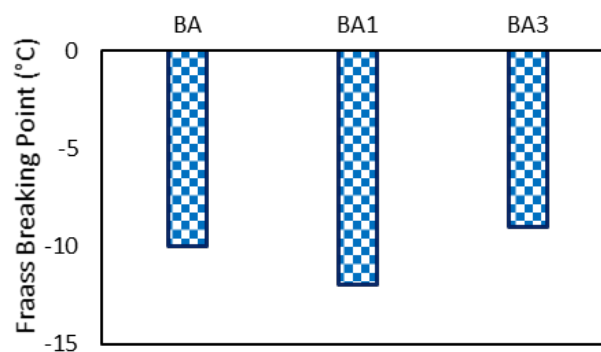
Figure 2. Fraass breaking point test results

3.2. Results of BBR Test

Bending beam rheometer (BBR) test was applied to the binders aged for a long time with the PAV test, and the results obtained from the test are expressed graphically in Figure 3(a) and 3(b). BBR test was applied to binders at –6 ºC and –12 ºC to determine their resistance to cracking at low temperatures.

(a)   (b)
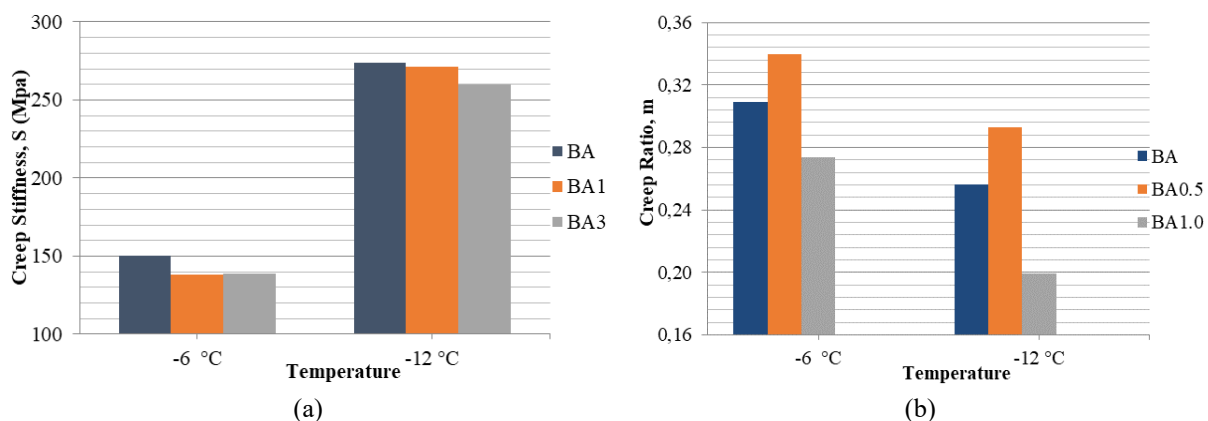
Figure 2 Properties of PAV-aged asphalt binders samples; (a) S and (b) m-value

When Figure 3 is examined, it is seen that the creep stiffness and creep rate values of the modified binder with 1% additive at –6 ºC meet the specification limits, but the modified binders with 3% additive cannot meet the creep rate requirement. It has been determined that 1% synthesis additive does not negatively affect the rheological properties of the base binder at low temperatures.

4. CONCLUSION

In this study, a new additive containing rosin and boron oxide, namely BORC, was chemically synthesized. Fraass breaking point and BBR experiments were carried out to determine the behavior of BORC synthesis additive at low temperatures and the results obtained were summarized as follows:

- From the Fraass breaking point test results, it was determined that the resistance of pure asphalt to cracking at low temperatures increased with the use of low amounts of synthesis additive in the binder.
- From the BBR results, it was determined that as the amount of synthesis additive increased, the performance at low temperatures was negatively affected and the potential for thermal crack formation increased. However, it was stated that 1% synthesis additive did not adversely affect the rheological properties of the pure binder at low temperatures and showed better performance than the pure binder at low temperatures.

BBR test results support each other with the Frass breaking point test results, showing that high amounts of additives increase the hardness and reduce the ductility of the binder.

Acknowledgments

References

[1] T. Geckil, "Siyah karbonun bitumlu sicak karisimlarin ozelliklerine etkisinin arastirilmasi," Ph.D. thesis, Firat University, Elazig, Türkiye, 2008.

[2] M. Arabani, S. Mirabdolazimi, and A. Sasani, "The effect of waste tire thread mesh on the dynamic behaviour of asphalt mixtures," *Construction and Building Materials*, vol. 24, pp. 1060–1068, 2010.

[3] M. Yildırim, "Farkli dogal asfaltlarin bitum ve bitumlu sicak karisimlarin ozelliklerine etkisi," M.Sc. thesis, Firat University, Elazig, Türkiye, 2014.

[4] B. Yilmaz, "Bor icerikli katkiyla modifiye edilen asfaltin performans ozelliklerinin arastirilmasi," Ph.D. thesis, Karadeniz Technical University, Trabzon, Türkiye, 2016.

[5] A. O. Adeboje, W. K. Kupolati, E. R. Sadiku, and J. M. Ndambuki, "Characterization of modified crumb rubber concrete," *International Journal of Sustainable Development and Planning (IIETA)*, vol. 15, no. 3, pp. 377–383, 2020.

[6] H. Yao, Q. Dai, and Z. You, "Chemo-physical analysis and molecular dynamics (MD) simulation of moisture susceptibility of nanohydrated lime modified asphalt mixtures," *Constr. Build. Mater.*, vol. 101, no. 1, pp. 536–547, 2015.

[7] C. Fang, R. Yu, S. Liu, and Y. Li, "Nano materials applied in asphalt modification: A review," *J. Mater. Sci. Technol.*, vol. 29, no. 7, pp. 589–594, 2013.

[8] N. Yusoff, A. Breem, H. Alattug, A. Hamim, and J. Ahmad, "The effects of moisture susceptibility and Ageing Conditions on Nano-Silica/Polymer Modified Asphalt Mixtures," *Constr. Build. Mater.*, vol. 72, pp. 139–147, 2014.

[9] A. C. X. Portugal, L. C. F. Lucena, A. E. F. L. Lucena, D. B. Costa, and K. A. Lima, "Rheological properties of asphalt binders prepared with maize oil," *Construction and Building Materials*, vol. 152, pp. 1015–1026, 2017.

[10] M. T. Rahman, M. N. A. Aziz, M. R. Hainin, and W. A. W. A. Bakar, "Impact of bitumen binder: Scope of bio-based binder for construction of flexible pavement," *Jurnal Teknologi*, vol. 70, no. 7, pp. 105–109, 2014.

[11] A. Kumandas, E. Cavdar, N. Sahan, B. V. Kok, E. B. Pancar, and S. Oruc, "Investigation of rutting and low temperature cracking behavior of reactive ethylene terpolymer and waste cooking oil modified bitumen," *Turkish Journal of Civil Engineering*, vol. 35, no. 4, pp. 1–26, 2024.

[12] M. Garcia-Morales, P. Partal, F. J. Navarro, F. Martinez-Boza, C. Gallegos, N. Gonzales, and M. E. Munoz, "Viscous properties and microstructure of recycled EVA modified bitumen," *Fuel*, vol. 83, pp. 31–38, 2004.

[13] M. Yilmaz, B. V. Kok, N. Kuloglu, and T. Alatas, "Elastomer türü polimerler ile modifiye edilmiş bitümlü bağlayıcıların depolama stabilitelerinin ve reolojik özelliklerinin incelenmesi," *DEU Muhendislik Fakultesi Fen ve Muhendislik Dergisi*, vol. 15, no. 1, pp. 67–77, 2013.

[14] J. Gao, Y. Liu, and L. Yang, "Thermalstability of boron-containing phenol formaldehyde resin," *Polymer Degradation and Stability*, vol. 63, no. 1, pp. 19–22, 1999.

[15] P. Deng, Y. Shi, Y. Liu, Y. Liu, and Q. Wang, "Solidifying process and flame retardancy of epoxy resin cured with boron-containing phenolic resin," *Applied Surface Science*, vol. 427, Part A, pp. 894–904, 2018.

[16] H. Wang, X. Liu, B. Liu, J. Zhang, and M. Xian, "Synthesis of rosin-based flexible anhydride-type curing agents and properties of the cured epoxy," *Polymer International*, vol. 58, no. 12, pp. 1435–1441, 2009.

[17] I. Tore and N. Ay, "The characterization and production of amorphous boron oxide," in *International Boren Symposium*, 2004, Eskisehir, Türkiye.

[18] W. Zhang, C. Liu, Y. Ying, and W. Dong, "The preparation and characterization of boron-containing phenolic fibers," *Materials Chemistry and Physics*, vol. 121, pp. 89–94, 2010.

[19] D. Arslan, M. Guru, M. K. Cubuk, and M. Cubuk, "Improvement of bitumen and bituminous mixtures performances by triethylene glycol based synthetic polyboron," *Construction and Building Materials*, vol. 25, no. 10, pp. 3863–3868, 2011.

[20] D. Arslan, M. Guru, and M. K. Cubuk, "Performance assessment of organic-based synthetic calcium and boric acid modified bitumens." *Fuel*, vol. 102, pp. 766–772, 2012.

[21] F. Orhan, *Bitumlu Karisimlar Laboratuvari Calismalari*, Ankara, Karayollari Genel Mudurlugu, 2005.

Acetabular Liner Material Selection in Artificial Hip Joints Using Computer Aided Software (CES) Program

Zeynep Gerdan[1]

[1]Department of Biomedical Engineering, Istanbul Beykent University, Istanbul, Türkiye
Corresponding author: Zeynep Gerdan (e-mail: zeynepgerdan@beykent.edu.tr)

Abstract

Depending on the developments in materials science, there is a very large pool of materials that engineers can use in any product design, including thousands of materials in the main groups of metals, ceramics, glass, polymers and composites. With the studies carried out, material properties continue to be improved day by day and it is also known that a new material is offered to the use of engineers. For this reason, the use of information management systems, i.e. computer-aided software, is also important in terms of controlling the existing information and monitoring up-to-date information in material selection. The importance of material selection and the development of new materials for the needs in the field of biomedical engineering is also increasing.

In this study, material selection studies for acetabular liner in artificial hip replacements were performed with the computer-aided software named CES Selector. In the study, alternative materials were identified in accordance with the requirements and technical specifications of the products and the evaluation process mechanisms and the best material selection process were explained. Alternative materials were determined for acetabular liner in artificial hip joints.

Keywords: Material selection, CES selector, Biomedical, Artificial hip joint acetabular liner

1. INTRODUCTION

In general terms, design is the blending of analysis, synthesis, material selection, measurement and control methods to solve the problem in order to meet a basic need. In engineering design, on the other hand, it covers all activities from the determination of the physical principles of any technical system, the selection of the elements that provide these principles, their assembly and the preparation of part drawings [1, 2]. For this reason, the first and most important step in engineering design is the selection of materials suitable for the intended use of the part [3,4]. The basic selection method based on the physical properties and performance characteristics of materials in the light of information obtained from material manufacturers, suppliers and standards. The steps of material selection by this method can be listed as analysis of the required properties of materials, selection of candidate materials, development of candidates and selection of the material that best fits the required properties [1–4].

There is a large inventory of materials used in engineering systems to ensure performance and economy. When newly developed materials such as alloys and coatings are added to these basic materials, the range of products expands and the selection of appropriate materials becomes increasingly complex [5–10]. For this reason, there is a need for a knowledge management system in order to control the available information and to follow the current information in material selection. The use of computer systems where material properties are stored allows the designer to easily access faster and large capacity material data. Material selection is done in various methods. Ashby and Dargie have conducted various studies on the first one, the sieving method. For the sieving method, Ashby and Granta Design introduced the graphical interface program [11]. It is possible to see where the material groups are located for the two existing features with the graphs drawn between two features called Ashby Diagrams. As a second method, knowledge-based systems are available, but the complexity and information-intensive nature of these methods has limited their use [12]. There are many studies in the literature that use different material selection methods for material selection. Unlike many programs used in the literature, the computer-aided material selection program named CES Selector makes the selection by considering the mechanical, physical, chemical properties of the material as well as the cost and formability. There are studies in the literature where material selection was successfully performed using this program [13, 14]. To date, there have been many studies on this topic in a wide variety of fields such as aerospace [15], automotive [16], energy [17], etc. Especially for biomedical engineering applications, this topic has attracted more attention from scientists as it is directly related to human health. The choice of material for implants depends on various factors such as the

location of the implant, the expected lifetime of the implant and the patient's medical history. One of the most commonly chosen materials for dental and orthopedic implants is titanium due to its biocompatibility, corrosion resistance, light weight, strength and ability to integrate with bone, i.e. osseointegration. Another material candidate is cobalt-chromium alloy, which is often used for orthopedic implants such as hip and knee prostheses due to its strength, durability, good wear and corrosion resistance. Where low friction is needed where joint prostheses are used, polyethylene can be an alternative due to its low coefficient of friction. Ceramics are another category of material of choice, especially for dental and hip prostheses, due to their good biocompatibility and wear resistance. Of course, the materials used as tissue replacements in the human body are not limited to the material candidates mentioned above. There are dozens of material candidates that can be preferred as implant materials, and there are ongoing research and development efforts to reach a better material for a specific need. There are many studies in the literature on the determination of the most suitable implant materials with the help of numerical techniques such as the finite element method [18].

Total hip arthroplasty (THA) is a successful surgical operation that aims to reduce pain, restore joint function and improve mobility and overall quality of life in patients with hip pain [19, 20]. In this operation, the damaged parts of the hip joint are replaced with an artificial joint called a prosthesis in many painful hip diseases such as osteoporosis, fractures and damage due to falls, rheumatoid arthritis. The prosthesis allows the damaged parts of the femoral head, neck or acetabulum of the hip to be replaced artificially. The choice of material to be used in these operations is very important for the patient's quality of life [21–23]. In this study, the CES Selector software developed by Ashby and Granta Design was used to select materials for the acetabular liner in artificial hip prostheses. The aim of this study was to take advantage of the wide range of products of the CES Selector program and to compare the results obtained with alternative materials used today.

2. MATERIAL AND METHOD

There are also different methods for material selection. The most commonly used methods are; searching for the relevant product from the material database, making a selection on the desired property comparison graphs and determining the materials that meet the specified selection criteria by elimination method and making a selection based on weighted properties. In this study, the selection procedure based on the specified limit values will be used. For this, first the Selection tab and then the material database is determined. Using the material database data, the material selection process is continued by entering graphs or certain boundary conditions depending on the properties. Afterwards, the selection process is continued by determining the required limit values of the material from the limit section in the software. The material database consists of many sub-headings such as biocompatibility, physical properties, mechanical properties, thermal properties, etc. that may be required. In this section, considering the place where the material will be used, all desired minimum and maximum boundary conditions values are determined and the alternative materials are sorted accordingly. According to the given boundary conditions, material selection is made by comparing alternative materials depending on their weighted properties. Figure 1 shows a visual representation of hip prosthesis components.
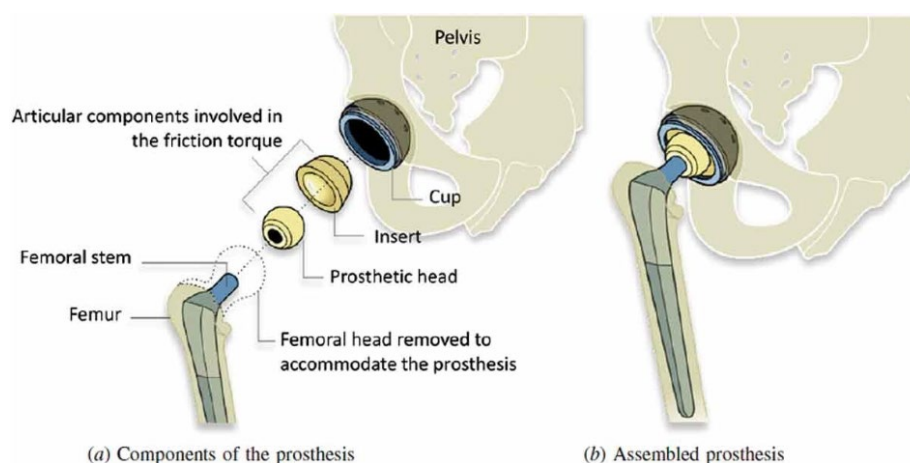
Figure 1. Illustration of hip replacement components [24]

In general, the materials used for hip replacement can be divided into four main categories: metallic materials, ceramic materials, polymers and composite materials. Metallic materials have been preferred in biomedical applications for many years due to their biocompatibility and bio inert nature. Metallic materials are generally used in implants for load-bearing parts of the body. The most widely used metallic materials in this context are titanium

and its alloys (Ti-6Al-4V), cobalt-chromium alloys and stainless steel [25]. However, although these materials have advantages such as high mechanical strength, biocompatibility and corrosion resistance, they also have various disadvantages. The high density and stress protection effect of these materials can be disadvantages. There is also the risk of metallic wear particles causing tissue reactions. Metallic implants have some limitations such as allergies, staining of metals and failure of implants and wear [26, 27].

The other materials, ceramics, are inorganic and non-metallic solid materials containing metal, non-metal or semi-metal atoms formed by ionic and covalent bonds, which are considered strong bonds [28]. The brittle structure and high elastic modulus of ceramics, their difficulty in processing and low mechanical strength make them not ideal for bone fracture fixation [29]. Commonly used ceramic materials are alumina, zirconia and calcium phosphate derivatives [30]. Polymers, which consist of very long chain molecules formed by the successive addition of monomers, are widely used in artificial joints together with metals. In orthopedic applications, such as hip and knee prostheses, a polymer bearing and a sliding metal spherical component are commonly used [31]. In these prostheses, non-degradable polymers are generally preferred. While the advantages of polymers are low abrasion and friction resistance, biocompatibility and good tensile strength, they have disadvantages such as the formation of debris as a result of osteolysis and the disintegration of the cement over time in cemented prostheses [32, 33]. Composite materials are materials formed by the combination of at least two or more different materials without dissolving in each other. They offer high strength-to-weight ratio, high modulus-to-weight ratio, high modulus-to-weight ratio, good damage tolerance, excellent fatigue resistance and corrosion resistance, provided that they can be processed into desired shapes at an acceptable cost and quality [2]. Composite materials can be one of the most difficult materials to machine due to their inherent inhomogeneity, the abrasive nature of the reinforcements and their anisotropic nature, resulting in high tool wear and subsurface damage [33, 34]. Today, polymers are widely used in a wide variety of applications due to their advantages. In hip joint prostheses, polymer-metal approaches are currently used, where the polymer is usually used as an acetabular liner made of ultra-high molecular weight polyethylene (UHMWPE) and cobalt-chromium-molybdenum (Co-Cr-Mo) is used as the femoral head. However, due to the poor mechanical properties of UHMWPE, it causes wear of the acetabular liner, leading to inflammation and osteolysis [35].

As a result of the evaluation of the properties required for the Acetabular Liner in Artificial Hip Joints and the examination of the available materials, it will be the most appropriate process to select all materials, which gives the opportunity to select all of the alternative material groups. After selecting the appropriate database for selection, the selection process will continue by entering the minimum and maximum limit values for other properties required from the material. In the researchers conducted, it was determined that the hip bone properties have a tensile strength of 100–200 MPa, compressive strength between 130–230 MPa, and modulus of elasticity between 10–20 MPa. In addition, it was determined that it has low brittleness and medium abrasion resistance properties [36]. Based on these values, the boundary condition values determined for the material and used for selection are given in Table 1.

Table 1. Properties used in material selection

Attribute	Constraints
Density (kg/m^3)	$\leq$ 2.5e3
Tensile strength (MPa)	$\geq$ 100
Compressive strength (Mpa)	130 to 230
Poisson's ratio	$\geq$ 0.3
Fracture toughness $\left(MPa \cdot \sqrt{m} \right)$	$\geq$ 1
RoHS (EU) compliant grades?	✓
Medical grades? (USP Class VI, ISO 10993)	✓
MRI safe	Safe

If desired, a range of values can be specified for the material properties, or it is sufficient to write the required minimum or maximum value as shown in Table 1. We can explain some of the material properties selected in the table as follows. RoHS specification normally comply with European Restriction on Hazardous Substances (RoHS) legislation. Grades with concentrations of prohibited substances greater than the following weight % (of the homogeneous material) are not compliant; 0.1% Lead, 0.1% Mercury, 0.01% Cadmium, 0.1% Hexavalent chromium (chromium xxx or Cr6+), 0.1% Polybrominated biphenyls (PBB), 0.1% Polybrominated diphenyl ether (PBDE). If Medical grades "yes", it is believed there are commercially available medical grades within this material specification. It does not mean that all grades of this material are for medical use — usually only a minority will be. Indication of whether it is safe to use the material in a magnetic resonance (MR) environment.

3. RESULTS

Alternative materials were determined according to the limit values and properties entered in the program. Figure 2 gives an example of comparison graphs based on material properties and the position of the selected materials among material groups. In the image; comparison graphs of tensile strength, compressive strength, fracture toughness against density, and tensile and compressive strength against fracture toughness are given.
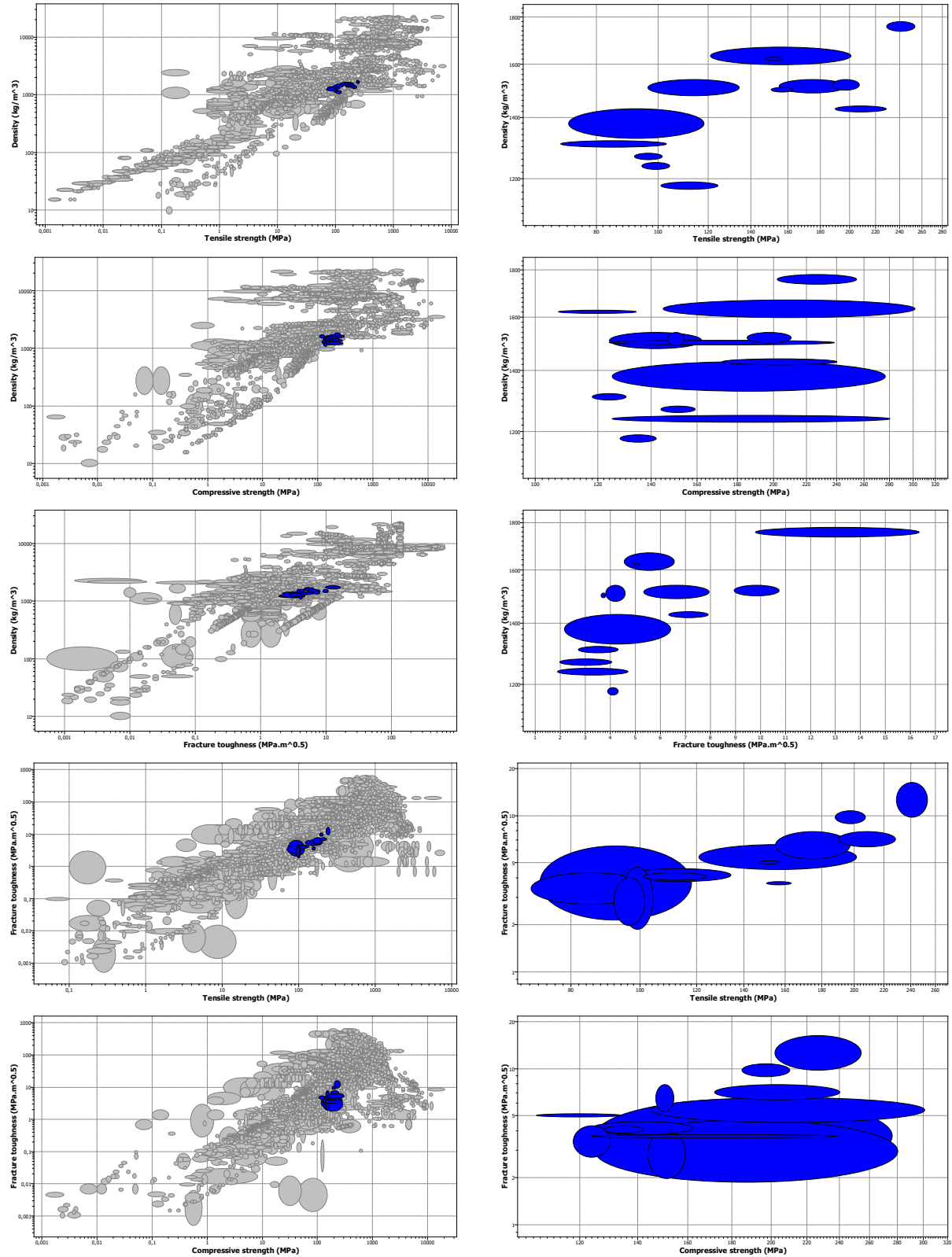
Figure 1. Representation of selected materials in material properties comparison graphs

In Figure 2, the position of the materials in all materials is determined in the comparison graphs of the properties determined for the relevant product. Table 2 lists the materials selected according to the properties determined.

Table 2. Materials and their properties in accordance with the specifications set in the CES program

Material Name	Density (kg/m³)	Tensile Strength (MPa)	Compressive Strength (MPa)	Fracture Toughness $\left(MPa \cdot \sqrt{m}\right)$	Poisson's Ratio	RoHS (EU) Compliant Grades?	Medical Grades? (USP Class VI, ISO 10993)	MRI Safe
PA transparent	1170–1190	101–124	128–142	3.89–4.3	0.385–0.401	✓	✓	Safe
PBT (30% glass fiber	1480–1540	96.5–134	124–162	3.81–4.58	0.349–0.363	✓	✓	Safe
PEEK (30% carbon fiber)	1420–1440	190–228	172–240	6.34–7.89	0.43–0.45	✓	✓	Safe
PEEK (30% glass fiber)	1490–1540	155–197	147–154	5.34–7.93	0.39–0.41	✓	✓	Safe
PEEK (unfilled)	1300–1320	70.3–103	118–130	2.73–4.3	0.39–0.41	✓	✓	Safe
PEI (unfilled)	1260–1280	91.9–101	144–159	1.99–4.03	0.385–0.401	✓	✓	Safe
PI (unfilled)	1330–1430	72.4–118	125–276	2.16–6.4	0.385–0.401	✓	✓	Safe
PPS (40% glass fiber)	1600–670	121–201	145–301	4.56–6.54	0.34–0.364	✓	✓	Safe
PSU	1230–1250	94.4–104	125–280	1.89–4.69	0.388–0.404	✓	✓	Safe
TPU(r) (40% long glass fiber)	1500–1540	188–207	185–210	8.95–10.7	0.346–0.36	✓	✓	Safe
TPU(r) (60% long glass fiber)	1740–1780	229–253	202–254	9.81–16.3	0.328–0.342	✓	✓	Safe
LCP (30% carbon fiber)	1490–1510	151–163	124–238	3.64–3.79	0.4–0.43	✓	✓	Safe
LCP (30% glass fiber)	1620	147–157	107–134	4.95–5.13	0.45–0.47	✓	✓	Safe

As seen in Table 2, according to the limit values entered in the program, the 13 materials listed in Table 2 appear as alternatives. At this stage, detailed selection process will be started for materials. In this context, all materials should be evaluated in detail.

Polyamide (PA) is one of the most widely used thermoplastics characterized by good mechanical, electrical and thermal properties and exhibits high electrical and temperature resistance. Polyamides are named in different forms such as PA6, PA66, PA11, PA12 and PA46 depending on the monomer [37]. It is hygroscopic and absorbs modest amounts of water. Moisture absorption can lead to small but significant dimensional changes, expanding parts beyond their size specifications, causing interruptions in processes or destroying the product. Direct measurement of these small size changes is often tedious [38].

Polymides (PI), also called polymides, thermoplastics or thermosets, are the most heat-resistant polymers [39]. They have high thermal and dimensional stability, low dielectric constants, exceptional mechanical strength and excellent chemical inertness [40]. PI have attracted attention in the medical sector due to these outstanding

properties and efficient production methods. Their suitability for harsh environments and robust treatment methods are in line with biomedical needs [41].

Thermoplastic polyurethane (TPU) is a polymer material with excellent physical and chemical property belonging to the class of polyurethane plastics, which is recognized for various properties such as high strength and toughness, transparency, excellent absorption resistance and resistance to oil, water and abrasion, and acid and alkali resistance [42]. Technically classified as thermoplastic elastomers, these polymers consist of linear segmented block copolymers composed of rigid and flexible segments. Crystallization in the rigid segments of TPU acts as physical crosslinking and reinforcement contributing to good performance properties. The soft segments contribute to the high flexibility of TPU [43]. TPU can be used in medical materials, automotive industry, electronics, coatings and sporting goods [44].

Polysulfones (PSFs, PSUs) are a high temperature resistant, rigid polymer composed of aryl and sulfonyl groups. Their inherent high bond dissociation energy makes them resistant to hydrolysis in both acidic and basic environments and at high temperatures. They are biocompatible and have the capacity to retain endotoxins. They are amorphous, translucent and have low creep, electrical insulating properties and self-extinguishing ability [45].

Polyphenylene sulfide (PPS) [46] is a linear semi-crystalline thermoplastic polymer with repeating thiophenyl units and is widely used as a specialty engineering plastic. PPS has outstanding thermal resistance and its thermal deformation temperature is 260 °C. The long-term use temperature is about 200 °C. At the same time, PPS also has excellent creep, fatigue and chemical resistance. Therefore, PPS as structural parts is widely used in automotive, aerospace and other fields. However, the main disadvantage of pure PPS is brittleness, which causes poor impact toughness.

Polyphenylene sulfide (PPS) is a linear semi-crystalline thermoplastic polymer composed of repeating thiophenyl units. It has widespread use as an engineering plastic. PPS has a very high thermal resistance. It undergoes thermal deformation at 260 °C. In addition, PPS has exceptional creep, fatigue and chemical resistance. Therefore, PPS as a structural component is widely used in many fields. Besides, the main disadvantage of pure PPS is its brittleness. This brittleness results in poor impact toughness [47].

4. CONCLUSION

In this study, CES Selector was used to investigate alternative polymer materials for Acetabular Liner. A total of 13 different materials were identified. By examining the mechanical properties of these materials, the most suitable material was tried to be determined according to various criteria. The findings obtained from this study can be summarized as follows:

- CES software serves as an effective tool in material selection. CES Selector has identified alternative materials that have not previously been considered or widely used in the construction of artificial hip Acetabular liners. These materials can be listed as PA, PBT, PEEK, PEI, PI, PPS, PSU, TPU, and LCP. Although each of them has advantages and disadvantages, they have the potential to be an alternative.
- In terms of mechanical properties, certain polymers such as PEEK, PI, PPS, PSU, TPU, and LCP emerge as worthy candidates, especially where long-term durability is important.
- In terms of fracture toughness, all materials have satisfactory values, but TPU polymer stands out. Also PI polymer is considered to be a better choice.
- But as a result of all evaluations, different materials come to the fore, and at this stage, manufacturability and availability criteria must be put into effect for the final decision.

References

[1]   M. Ashby, H. Shercliff, and D. Cebon, *Materials Engineering, Science, Processing and Design*, 3rd. Elsevier, 2007.
[2]   F. Findik, S. C. Okumus, and M. Colak, *Malzeme Secimi ve Uygulamalari*, Seckin Yayinevi, 2018.
[3]   S. Sapuan, "A knowledge-based system for materials selection in mechanical engineering design," *Materials Design*, pp.687-695, 2001.
[4]   R. Amen and P. Vomacka, "Case-based reasoning as a tool for materials selection," *Materials Design*, vol. 22, pp. 353–358. 2001.
[5]   M. F. Ashby, Y. J. Bréchet, D. Cebon, and L. Salvo, "Selection strategies for materials and processes," *Materials & Design*, vol. 25, no. 1, pp. 51–67, Feb. 2004.
[6]   M. Bovea, and R. Vidal, "Materials selection for sustainable product design: A case study of wood based

furniture eco-design," *Materials Desing*, vol. 25, pp. 111–116, 2004.

[7]   F. Giudice, R.G. La, and A. Risitano, "Materials selection in the life cycle design process: A method to integrate mechanical and environmental performances in optimal choice," *Materials & Method*, vol. 26, pp. 9–20, 2005.

[8]   A. Balakrishna, D. Rao, J. Srinivas, and P. Satish, "Computer aided material selection processes in concurrent engineering using neural networks," *J. Inst. Eng. (India): Mech. Eng. Div.*, vol. 88, pp. 20–23, 2007.

[9]   E. Karana, P. Hekkert, and P. Kandachar, "Material considerations in product design: A survey on crucial material aspects used by product designers," *Materials Design*, pp.1081–1089, 2008.

[10] P. S. Ramalhete, A.M.R. Senos, and C. Aguiar, "Digital tools for material selection in product design," *Materials and Design*, vol. 31, no. 5, pp. 2275–2287, 2010.

[11] X. F. Zha, "A web-based advisory system for process and material selection in concurrent product design for a manufacturing environment," *Int. J. Adv. Manuf. Technol.*, vol. 25, no. 3–4, pp. 233–43, 2005.

[12] U. G. Y. Abeysundara, B. Sandhya, and G. Shabbir, "A matrix in life cycle perspective for selecting sustainable materials for buildings in Sri Lanka," *Build Environ.*, vol. 44, pp. 997–1004, 2008.

[13] F. Findik, M. Colak, and S. Aslanlar, "Materials selection for car bumper with a conventional method as well as CES selector software," in *1st International Conference on Engineering and Natural Sciences (ICENS 2015)*, 2015, pp. 199–208,.

[14] A.T. Şensoy, M. Çolak, "Optimal material selection for total hip implant: A finite element case study," *Arabia Journal for Science and Engineering*, 2019.

[15] Z. Huda and P. Edi, "Materials selection in design of structures and engines of supersonic aircrafts: A review," *Materials & Design*, vol. 46, pp. 552–560, 2013.

[16] S. W. Burande and D. V. Bhope, "Review on material selection, tailoring of material properties and ageing of composites with special reference to applicability in automotive suspension," *Materials Today-Proceedings*, vol. 46, pp. 520–527, 2021.

[17] I. A. Rauf and P. Rezai, "A review of materials selection for optimized efficiency in quantum dot sensitized solar cells: A simplified approach to reviewing literature data," *Renewable & Sustainable Energy Reviews*, vol. 73, pp. 408–422, 2017.

[18] K. K. Alaneme, S. A. Kareem, B. N. Ozah, H. A. Alshahrani, and O. A. Ajibuwa, "Application of finite element analysis for optimizing selection and design of Ti-based biometallic alloys for fractures and tissues rehabilitation: A review," *Journal of Materials Research and Technology-Jmr&T*, vol. 19, pp. 121–139, 2022.

[19] M. Anger, T. Valovska, H. Beloeil, P. LirkJoshi, G. P. Van de Velde, M. and M. Bonnet, "PROSPECT guideline for total hip arthroplasty: A systematic review and procedure-specific postoperative pain management recommendations," *Anaesthesia*, vol. 76, no. 8, pp. 1082–1097, 2021.

[20] X. Ren, L. Ling, L. Qi, Z. Liu, W. Zhang, Z. Yang, and Z. Li, "Patients' risk factors for periprosthetic joint infection in primary total hip arthroplasty: A meta-analysis of 40 studies," *BMC Musculoskeletal Disorders*, vol. 22, pp. 1–17, 2021.

[21] L. Guo, S. A. Naghavi, Z. Wang, S. N. Varma, Z. Han, Z. Yao, L. Wang, L. Wang, and C. Liu, "On the design evolution of hip implants: A review," *Materials & Design*, vol. 216, 2022.

[22] J. Szczesiul and M. Bielecki, "A review of total hip arthroplasty comparison in FNF and OA patients," *Advances in Orthopedics*, vol. 2021, no. 1, 2021.

[23] S. P. Vajapey, J. Morris, D. Li, N. G. Greco, M. Li, and A. I. Spitzer, "Outcome reporting patterns in total hip arthroplasty: a systematic review of randomized clinical trials," *JBJS Reviews*, vol. 8, no. 4, art. no. e0197, 2020.

[24] C. KN, N, S. Bhat, M. Zuber, and B. S. Shenoy, "Evolution of different designs and wear studies in total hip prosthesis using finite element analysis: A review," *Cogent Engineering*, vol. 9, no. 1, 2022.

[25] M. Chandrasekaran, "Forging of metals and alloys for biomedical applications," in *Metals for Biomedical Devices*, Mitsuo Niinomi, Eds. Cambridge: Woodhead, 2010, pp. 293–310.

[26] N. Eliaz, "Corrosion of metallic biomaterials: A review," *Materials*, vol. 12, no. 3, art. no. 407, 2019.

[27] S. Krishnakumar, and T. Senthilvelan, "Polymer composites in dentistry and orthopedic applications-A review," *Materials Today: Proceedings*, vol. 46, pp. 9707–9713, 2021.

[28] A. T. Guner and C. Meran, "Ortopedik implantlarda kullanilan biyomalzemeler," *Pamukkale Universitesi Muhendislik Bilimleri Dergisi*, vol. 26, no. 1, pp. 54–67, 2020.

[29] T. Kim, C. W. See, X. Li, and D. Zhu, "Orthopedic implants and devices for bone fractures and defects: Past, present and perspective," *Engineered Regeneration*, vol. 1, pp. 6–18, 2020.

[30] A. Pasinli, "Biyomedikal uygulamalarda kullanilan biyomalzemeler," *Makine Teknolojileri Elektronik Dergisi*, vol. 4, no. 4, pp. 25–34, 2004.

[31] T. Kim, C. W. See, X. Li, and D. Zhu, "Orthopedic implants and devices for bone fractures and defects: Past, present and perspective," *Engineered Regeneration*, vol. 1, pp. 6–18, 2020.

[32] M. R. Senra and M. D. F. V. Marques, "Synthetic polymeric materials for bone replacement," *Journal of Composites Science*, vol. 4, no. 4, art. no. 191, 2020.

[33] N. Filip, I. Radu, B. Veliceasa, C. Filip, M. Pertea, A. Clim, and I. L. Serban, "Biomaterials in orthopedic devices: current issues and future perspectives," *Coatings*, vol. 12, no. 10, art. no. 1544, 2022.

[34] C. R., Dandekar and Y. C. Shin, "Modeling of machining of composite materials: A review," *International Journal of Machine Tools and Manufacture*, vol. 57, pp. 102–121, 2012.

[35] A. Fouly, I. A. Alnaser, A. K. Assaifan, and H. S. Abdo, "Evaluating the performance of 3D-printed PLA reinforced with date pit particles for its suitability as an acetabular liner in artificial hip joints," *Polymers*, vol. 14, no. 16, art. no. 3321, 2022.

[36] T. Ceyhan, and N. Kose, "Ortopedide biyomalzeme kullanimi: Genel bilgiler ve tanimlar," *TOTBID Dergisi*, vol. 10, no. 2, pp. 79–82, 2011.

[37] S. Krishna, I. Sreedhar, and C. M. Patel, "Molecular dynamics simulation of polyamide-based materials– A review," *Computational Materials Science*, vol. 200, art. no. 110853, 2021.

[38] L. Monson, M. Braunwarth, and C. W. Extrand, "Moisture absorption by various polyamides and their associated dimensional changes," *Journal of Applied Polymer Science*, vol. 107, no. 1, pp. 355–363, 2008.

[39] D. J. Liaw, K. L. Wang, Y. C. Huang, K. R. Lee, J. Y. Lai, and C. S. Ha, "Advanced polyimide materials: Syntheses, physical properties and applications," *Progress in Polymer Science*, vol. 37, no. 7, pp. 907–974, 2012.

[40] M. Bruma, M. D. Damaceanu, and R. D. Rusu, "Study of thin films made from aromatic polymers containing six-member imide rings," *High Performance Polymers*, vol. 24, no. 1, pp.31–39, 2012.

[41] G. Yilmaz, Z. Gerdan, and M. Colak, "Exploring alternative polymer materials for joint liners: A software-guided material selection," *Engineering Research Express*, vol. 6, no. 4, art. no. 045539, 2024.

[42] L. Wan, C. Deng, H. Chen, Z. Y. Zhao, S. C. Huang, W. C. Wei, and Y. Z. Wang, "Flame-retarded thermoplastic polyurethane elastomer: From organic materials to nanocomposites and new prospects," *Chemical Engineering Journal*, vol. 417, art. no. 129314, 2021.

[43] N. A. Ahad, "A Recent blend of thermoplastic polyurethane (TPU)," in *International Conference on Sustainable Materials (ICoSM 2020)*, 2020, p. 012045.

[44] Y. Yao, M. Xiao, and W. Liu, "A short review on self-healing thermoplastic polyurethanes," *Macromolecular Chemistry and Physics*, vol. 222, no. 8, art. no. 2100002, 2021.

[45] V. Athipatla, "Polysulfones and their applications," *Journal of High School Science*, vol.7, no. 2, 2023.

[46] L. Zhao, Y. Yu, H. Huang, X. Yin, J. Peng, J. Sun, and L. Wang, "High-performance polyphenylene sulfide composites with ultra-high content of glass fiber fabrics," *Composites Part B: Engineering*, vol. 174, art. no. 106790, 2019.

[47] Y. Deng, Y. Yang, Y. Ma, K. Fan, W. Yang, and G. Yin, "Nano-hydroxyapatite reinforced polyphenylene sulfide biocomposite with superior cytocompatibility and in vivo osteogenesis as a novel orthopedic implant," *RSC Advances*, vol. 7, no. 1, pp. 559–573, 2017.

Investigation of the Modification Effect of Solidification Time and Sr Addition in Casting of Al12Si Alloy

Murat Colak[1]

[1]Electronics and Automation Department, Bayburt University, Bayburt, Türkiye
Corresponding author: Murat Colak (e-mail: mcolak@bayburt.edu.tr)

Abstract

Eutectic composition is formed with the addition of Si around 12% to aluminium alloys. During solidification of eutectic Al-Si alloys, eutectic Si crystals are seen in a lamellar structure and thick. However, it is known that these lamellar crystals can be converted into fiber-like structure by modification. Modification process can be applied by various methods such as rapid cooling, alloy addition, mechanical processes. In this study, the effect of modification on the microstructure without the addition of master alloy and solidification time will be examined. Al12Si alloy was cast without addition and with 0.2% Sr effect. In the experiments, a model designed to produce gradually different solidification times was used. After the test specimens were prepared metallographically, microstructure images were taken and the structure of Si crystals was evaluated. The changes in the porosity and microstructure of the sample due to solidification time and Sr modification were determined.

Keywords: Al12Si casting, Solidification time, Sr addition, Modification

1. INTRODUCTION

Aluminium alloys are widely used in many sectors due to their light weight, high strength-to-weight ratio and corrosion resistance [1–3]. The widespread use of aluminium alloys increases the quality requirements. The factors affecting the casting quality of aluminium casting alloys are quite diverse. According to the research in the literature, various factors such as alloy addition, chemical composition, casting temperature, microstructure, porosity and casting process can be determinative. Alloy addition plays a critical role in determining the mechanical properties, fluidity and microstructure of the cast alloy [4, 5].

Modification is the change in the size and distribution of eutectic silicon grains in the structure by adding alkaline metals to Al-Si alloys. The modification process can be by element addition, rapid solidification, vibration applied during solidification, high pressure effect and heat treatment. Modification of the casting structure is the transformation of the eutectic Si structure from lamellar to fiber-like [6–9]. The most practical and widespread application of the modification process is through element addition, and the most effective modifications can be made with Na, Sr, and Sb [6, 8]. However, in industrial applications, only Na and Sr have strong effects at low densities [8–10]. The initial effects of Na and Sr are very beneficial, but the effects of sodium are temporary due to oxidation and vapor pressure losses. In addition, the percentage elongation and castability of the alloys modified with strontium are higher than those modified with sodium [3]. In a study, it was found that the addition of Sr not only affects the eutectic transformation of Si crystals but also changes the structure of α-Al dendrites in a positive way and the effect is more pronounced at increasing cooling rates [11]. Strontium is usually added to liquid aluminium in the form of Al10Sr master alloys containing 10% Sr. The incorporation of rare earth elements into aluminium alloys can lead to improvements in alloy properties (corrosion resistance and mechanical properties, such as strength) [12]. It has also been shown that adding rare earth elements to aluminium alloys improves mechanical properties by changing the microstructure of the alloy [13–15]. These additions can improve the grain structure of the alloy, inhibit recrystallisation and affect the precipitation process, ultimately improving the comprehensive mechanical properties of the alloy [16, 17].

Rare earth elements are known to act as surface-active elements in the alloy, contributing to the improvement, purification, and modification of the properties of the aluminium alloy, thus enhancing its mechanical and physical properties [18]. In addition, adding rare earth elements has been reported to refine the grain size and change the eutectic solidification mode of Al-Si alloys [10, 19]. There are fundamental differences in the solidification of modified and unmodified alloys. These differences arise from the growth mode of eutectic silicon. While unmodified silicon solidifies in the form of plates at slow cooling rates, with modification, silicon changes from a plate structure to a rod structure. The modification process slows down the growth of silicon crystals in the eutectic,

stabilises the silicon-matrix growth rates and thus forms a thin lamella structure. In unmodified alloys, eutectic silicon is first nucleated by aluminium. In the form of dendritic, the silicon continuously migrates from the interface in front of the aluminium into the liquid. However, with the modification process, the silicon does not grow in front of the aluminium. For these solidification forms, it is stated that unmodified alloys solidify from inside to outside and modified alloys solidify from outside to inside [20, 21].

In a study investigating the effect of the modification process on the solidification conditions and porosity formation in the alloy, it was observed that the porosity formed in structures without the addition of a modifier were small, irregular, and clustered in the inter-dendritic regions. However, it was stated that the porosity in the modified structure were spherical in shape and located in the inter-dendritic regions [22]. In addition, another study found that Na and Sr additions had a beneficial effect on porosity and casting defects [23]. In this study, it was aimed to investigate the modification effect of master alloy addition and solidification time on microstructure. In this context, Al12Si alloy was cast without and with 0.2% Sr addition into sand moulds prepared with a model with different solidification times. Density measurements, porosity and microstructure of the castings were investigated depending on Sr and solidification time.

2. MATERIAL AND METHOD

In order to investigate the effect of modifier addition and solidification time on the casting of aluminium alloys in sand moulds, the geometry with dimensions and solid model image presented in Figure 1 was used.
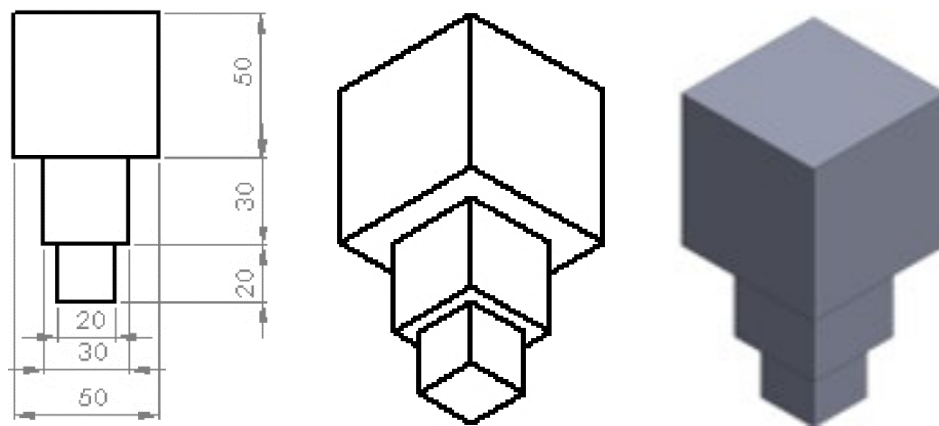
Figure 1. Model image and dimensions

Moulds were prepared from green mould sand with 2 models made in accordance with the dimensions in Figure 1. The solid model image of the mould ready for casting is presented in Figure 2. Since the castings will be made without the addition of modifier and after the addition of 0.2% Sr, sand moulds were prepared accordingly. No riser was used in the moulding in order to investigate the feeding efficiency with the addition of modifier and the shrinkage model at the top of the casting.
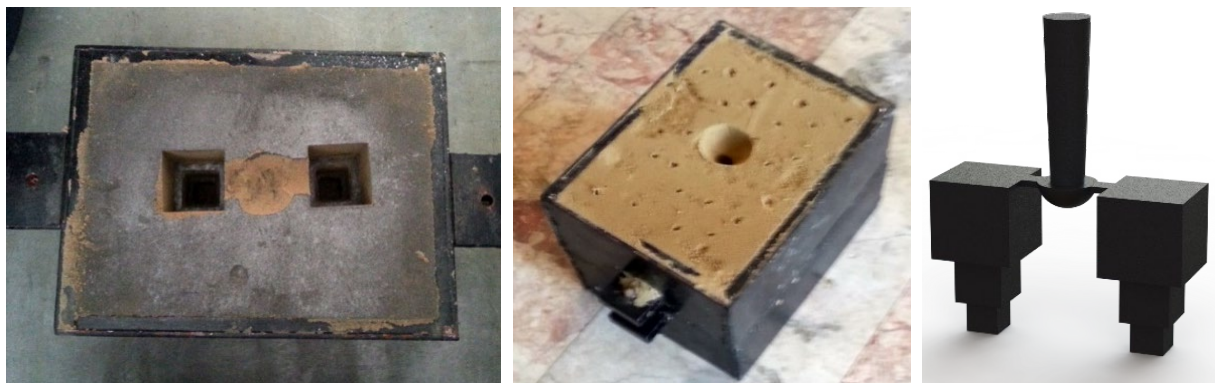
Figure 2. Mould image ready for casting, solid model image after casting

The melting processes were carried out in an electric resistance furnace in a SiC based crucible with a melting capacity of 8 kg aluminium. After melting, nitrogen cleaning was carried out with the help of a graphite lance immersed in the crucible at approximately 720 ºC in order to purify the liquid metal from dissolved hydrogen gas.

After this process, the liquid metal was covered with a commercial powder flux and the slag layer was cleaned by scraping the slag layer from the surface of the liquid metal at 700 ºC in the crucible. After this process, Al10Sr master alloy was added to the molten alloy to add 0.2 wt% Sr and castings were made.

Density measurements were made according to Archimedes' principle to determine the amount of porosity in the inner cross-sections of the cast specimens under varying casting conditions and accordingly the feeding ability. Afterwards, samples were taken for microstructure investigations at different section thicknesses as shown in Figure 3.
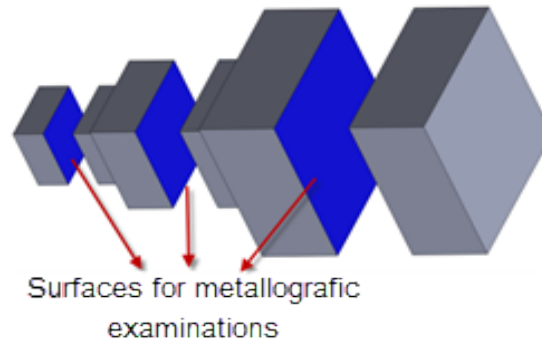
Figure 3. Microstructure examination surface of the test specimen

The cast specimens were subjected to metallographic grinding and polishing after cutting. For the microstructure investigations of the cast specimens, they were grinded with 180, 400, 800, and 1200 grit abrasives respectively and then polished on felt with 6 and 3μm diamond paste suspension. After polishing, microstructure photographs of the samples were taken with an optical microscope and a digital camera. In addition, SolidCast casting simulation software was used to determine the solidification time of the sample at different stages.

3. EXPERIMENTAL RESULTS AND EVALUATION

3.1. Chemical Analysis Results

Firstly, chemical analysis tests were performed on the test samples. Chemical analysis tests were analysed by optical spectrometer according to EN 1706 standard. In this method, combustion is created on the surface with the arc sent on the part with the optical emission spectrometer (OES) device. According to the wavelengths emitted from the surface, the elements in the sample can be seen. The chemical compositions of the samples obtained from the castings are presented in Table 1.

Table 1. Chemical composition results of the test samples (%wt)

Alloy	Si	Fe	Cu	Mn	Mg	Zn	Ti	B	Sr	Al
Al12Si	11.832	0.231	0.013	0.019	0.255	0.009	0.008	0.002	0.007	Rem.
Al12Si + Sr	11.946	0.214	0.012	0.021	0.257	0.008	0.012	0.005	0.196	Rem.

When the chemical composition values presented in Table 1 are examined, it was determined that the Etial 140 equivalent alloy containing 12% Si met the standard values and 0.196% Sr was obtained in the experiments with 0.2% Sr content.

3.2. Solidification Time Modelling Results

The solidification time variation in varying sections of the model was determined by SolidCast Casting simulation software and the results are presented in Figure 4. As seen in Figure 4, the solidification of the model varied between 3.2 minutes and 4.3 minutes and there was not much difference in solidification time. This situation is also thought to be due to the high thermal conductivity of the casting alloy, the slow cooling in the sand moulds and the small cross-sectional differences. When the results were analysed, the solidification times of the castings from thin section to thick section were 3.2 minutes, 4.1 minutes and 4.3 minutes respectively. There was only 25% difference in solidification time between the bottom section with the lowest thickness and the thickest section.

Solidification time 4.3 mins.   Solidification time 4.1 mins   Solidification time 3.2 mins.
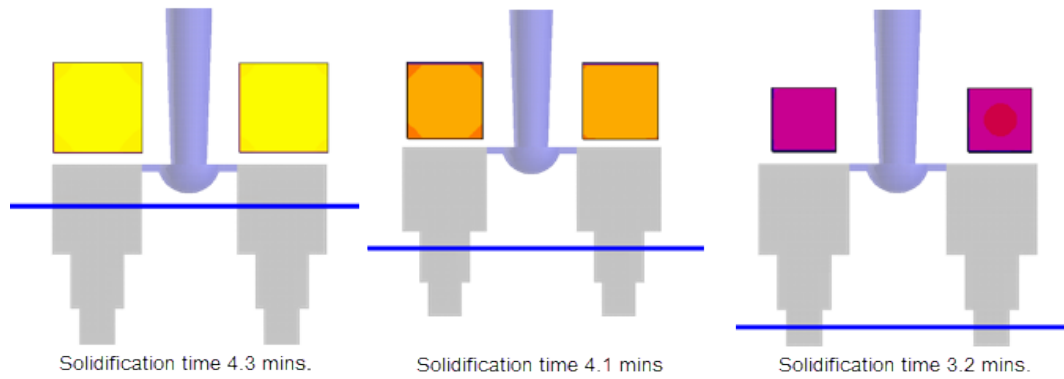
Figure 4. Solidification time determined by SolidCast programme in model sections

3.3. Density Measurement and Porosity Results

The results of density measurement and % porosity values obtained from each stage of the test specimens according to Archimedes' principle are presented in Table 2. In porosity calculations, the reference density value was taken into account as 2.68 gr/cm^3.

Table 2. Density and porosity measurement results of cast samples

Sample Name		Weight on Air (gr)	Weight in Water (gr)	Experimental Density (gr/cm^3)	Theoretical Density (gr/cm^3)	Porosity %
Al12Si	Bottom	12.32	7.62	2.62	2.68	2.37
	Middle	36.34	22.40	2.60	2.68	2.90
	Top	128.66	78.84	2.58	2.68	3.81
Al12Si + Sr	Bottom	12.54	7.84	2.66	2.70	1.36
	Middle	36.78	22.98	2.66	2.70	1.46
	Top	131.08	81.82	2.66	2.70	1.62

When the results given in Table 2 were compared, it was observed that there was an increase in density values and a decrease in porosity amounts with the addition of Sr. While the average density value was 2,6 gr/cm^3 in Al12Si casting without addition, this value was determined as 2,66 gr/cm^3 with Sr addition. While the porosity values were determined as 3.02% on average in the Al12Si casting, it was determined as 1.48% in the Sr added casting. In addition, density values increased depending on the solidification rate in modifier added castings and thin sections. Sr addition also decreased the porosity values formed in the interior of the casting. This can be attributed to the fact that the castings can be fed for a longer period of time due to the decrease in the grain size and the reduction of voids between the dendrites caused by the formed microstructure. Also, it is seen that the thin section lower part contains less porosity than the upper parts. This is thought to be due to the completion of solidification in a shorter time. In order for solidification to start and growth to continue, the liquid metal can transfer its heat from the mould walls to the atmosphere faster depending on its modulus. Fast solidification facilitates nucleation. Under fast solidification conditions, the casting structure results in a finer grained structure. In this case, the liquid flow in the feed zone between the dendrites is facilitated and a shorter dendritic lattice is formed. Thus, it is known that by shortening the liquid flow distance between dendrites, the feedability capacity increases and porosity formation decreases [24, 25].

3.4. Microstructure Investigations

The microstructure of the castings without Al12Si addition and with Sr addition were examined at each solidification stage. Figure 5 shows sample microstructure pictures taken at 200 magnification.

When the microstructure pictures given in Figure 5 are examined, it is determined that the eutectic Si structure in the casting is transformed from lamellar structure to fiber-like structure with the addition of Sr modifier master alloy added into the liquid metal. In addition, it is seen that the porosity formation in the casting structure decreases with the modification process. This is thought to be due to the fundamental differences in the solidification of modified and unmodified alloys. While unmodified silicon solidifies in the form of sheets at slow cooling rates, with modification, silicon changes from sheet structure to rod structure. The modification process slows down the

growth of silicon crystals in the eutectic, balances the silicon-aluminium growth rates and thus forms a thin lamellar structure [7, 21].

In a study investigating the effect of the modification process on the solidification conditions and porosity formation of the alloy, it was observed that the porosity formed in the structures without the addition of modifier were small, irregular and clustered in the inter-dendrite regions [9]. In addition, in a different study, it was found that porosity and casting defects decreased with Na and Sr additions [23]. In a study examining the effect of modifier addition on feedability, it was reported that the addition of Sr not only affects the eutectic transformation of Si crystals, but also positively changes the structure of α-Al dendrites and the effect is more pronounced at increased cooling rates [11].

Al12Si   Al12Si + Sr

Bottom

Middle

Top
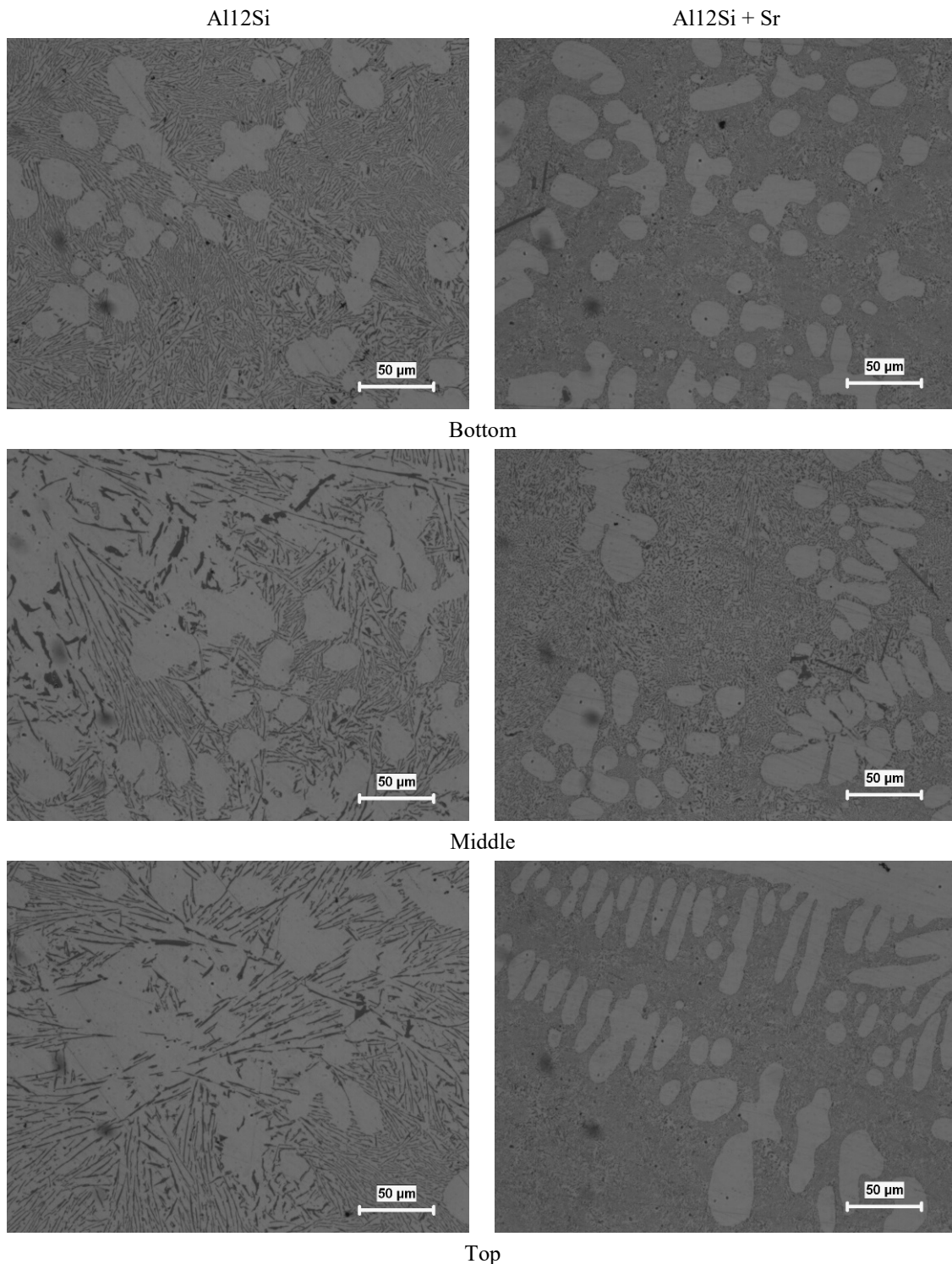
Figure 5. Microstructure pictures

4. CONCLUSION

The results obtained from the study in which the effect of modifier addition with different section thicknesses and at different solidification times were examined are summarised below;

- With the addition of modifier using Al10Sr master alloy, eutectic Si crystals formed in the microstructure were transformed from lamellar to fiber shape. It was understood that the addition of modifier to affect 0.2% Sr was sufficient for the modification process.
- The solidification time of the castings from thin section to thick section was 3.2 minutes, 4.1 minutes and 4.3 minutes respectively.
- It was observed that the density values increased and the amount of porosity decreased with the addition of Sr. While the average density value was 2.6 gr/cm^3 in Al12Si casting without Sr addition, this value was determined as 2.66 gr/cm^3 with Sr addition.
- Porosity values were found to be 3.02 % in Al12Si casting with Sr addition and 1.48 % in Sr addition. In addition, the lower part of the thin section contains less porosity than the upper parts.
- The grain size varies depending on the solidification time and it was determined that the grain structure resulting from the addition of modifiers became smaller. In thin section regions, finer grain size is formed due to rapid solidification.

References

[1]   M. H. Kadhim, N. A. Latif, M.A. Harimon, A. A. Shamran, and D. R. Abbas, "Effects of side-groove and loading rate on the fracture properties of aluminium alloy AL-6061," *Materialwissenschaft und Werkstofftechnik*, vol. 51, no. 6, pp. 758–765. 2020.

[2]   B. Stojanović, M. Bukvic, and I. Epler, "Application of aluminum and aluminum alloys in engineering," *Applied Engineering Letters Journal of Engineering and Applied Sciences*, vol. 3, no. 2, pp. 52–62, 2018.

[3]   E. Uslu, M. M. Dag, and M. Colak, "Design and manufacturing of reduced pressure test machine for determination of liquid aluminum quality in casting," *Turkish Journal of Electromechanics and Energy*, vol. 8, no. 3, 2023.

[4]   A. M. A. Mohamed, F. H. Samuel, A. M. Samuel, H. W, Doty, and S. Valtierra, "Influence of tin addition on the microstructure and mechanical properties of Al-Si-Cu-Mg and Al-Si-Mg casting alloys," *Metallurgical and Materials Transactions A*, vol. 39, pp. 490–501, 2008.

[5]   M. Durmus, D. Dispinar, M. Gavgali, E. Uslu, and M. Colak, "Evaluation of Fe content on the fluidity of A356 aluminum alloy by new fluidity ındex," *International Journal of Metalcasting*, pp. 1-15, 2024.

[6]   J. Kim, J. Choi, C. Lee, and E. Yoon, "A study on the variation of solidification of A356 aluminum alloys with Sr addition," *Kluwer Academic Publishers*, pp. 1395–1397, 2000.

[7]   J. G. Kaufmann and E. L. Rooy, *Aluminum Alloy Castings, Properties, Processes, and Applications,* ASM International, American Foundry Society, USA, 2005.

[8]   G. K. Sıgworth, "Theoretical and partical aspects of the modification of aluminium-silicon alloys," *A.F.S. Transactions,* vol. 66, 1983.

[9]   N. Kanani, G. R. Abbaschican, and F. L. Gainesuille, "Modification of –aluminium silicon alloys," *Aluminium*, vol. 8, art. no. 505, 1984.

[10]   K. Nogita, S.D. Mcdonald, and A.K. Dahle, "Aluminium phosphide as a eutectic grain nucleus in hypoeutectic Al-Si alloys," *Mater. Trans,* vol. 45, pp. 323–326, 2004.

[11]   Z. Chen and R. Zhang, "Effect of strontium on primary dentrite and eutectic temperature of A357 aluminium alloy," *China Foundry*, vol. 7 no. 2, pp. 149–152, 2010.

[12]   A. Kania, R. Nowosielski, A. Gawlas-Mucha, and R. Babilas, "Mechanical and corrosion properties of Mg-based alloys with Gd addition," *Materials*, vol 12, no. 11, art. no. 1775, 2019.

[13]   J. Wang and F. Li, "Effect of Sm+ Er and heat treatment on as-cast microstructure and mechanical properties of 7055 aluminum alloy," *Materials*, vol. 16, no. 13, art. no. 4846, 2023.

[14]   T. Qin, B. Fan, J. Yu, C. Bu, and J. Zhang, "Effect of erbium micro-additions on microstructures and properties of 2024 aluminum alloy prepared by microwave sintering," *Crystals*, vol. 14, no. 4, art. no. 382, 2024.

[15]   Y. Xia, D. Wang, J. Jia, J. Wu, Z. Wang, X. Li, and J. Huang, "An investigation on the precipitated phases and mechanical properties of cerium modified 2024 aluminum alloy," *Materialwissenschaft und Werkstofftechnik*, vol. 51, no. 9, pp. 1267–1273, 2020.

[16]   C. Liu, Y. Liu, Y. Ma, W. Liu, and Y. Yang, "Effects of CeO2 on the microstructure and properties of 2A12 porous aluminum," *SN Applied Sciences*, vol. 1, no. 1, art. no. 111, 2019.

[17] J. Xue, J. Wang, Y. Han, P. Li, and B. Sun, "Effects of CeO2 additive on the microstructure and mechanical properties of in situ TiB2/Al composite," *Journal of alloys and compounds*, vol, 509, no. 5, pp. 1573–1578, 2011.

[18] H. Zhao, Y. Song, M. Li, and S. Guan, "Grain refining efficiency and microstructure of Al–Ti–C–RE master alloy," *Journal of Alloys and Compounds*, vol. 508, no. 1, pp. 206–211, 2010.

[19] M. Li, Z. Shi, X. Wu, H. Wang, and Y. Liu, "Study of the microstructure and crack evolution behavior of Al-5Fe-1.5 Er alloy," *Materials*, vol. 12, no. 1, art. no. 172, 2019.

[20] S. G. Shabestarı and F. Shahrı, "Influence of modification, solidification conditions and heat treatment on the microstructure and hechanical properties of A356 aluminum alloy," *Kluwer Academic Publishers*, pp. 2023–2032, 2004.

[21] L. Lu and A. K. Dahle, "Grain refinement effiency and mechanism of aluminium carbide in Mg-Al alloys," *Scripta Materialia*, vol. 53, no. 5, pp. 517–522, 2005.

[22] E. N. Pan, H. S. Chiou, and G. J. Liao, "Effects of modification and solidification conditions on the feedeing behaviour of A356 Al alloy," *AFS Transactions*, vol. 99, pp. 605–621, 1991.

[23] L. Lua, K. Nogita, and A. K. Dahle, "Combining Sr and Na additions in hypoeutectic Al Si foundry alloys," *Materials Science and Engineering A,* vol. 399, pp. 244–253, 2005.

[24] W. Kurz and D. J. Fisher, *Fundamentals of Solidification*, 3rd ed. Switzerland-Germany-UK-USA: Trans Tech Publications,1989.

[25] D. A. Porter and K. E. Easterling, *Phase Transformations in Metals and Alloys*, 3rd ed. Boca Raton, FL: CRC Press, 2009.

Harmonic Analysis in Power Transformers by Performing Experiments and Using Developed Hybrid Heuristic Algorithms

Mehmet Zile[1]

[1]Department of Motor Vehicles and Transportation Technology-Aircraft Technology, Tusas Kazan Vocational School, Gazi University, Ankara, Türkiye
Corresponding author: Mehmet Zile (e-mail: mehmetzile@gazi.edu.tr)

Abstract

In this study, a hybrid heuristic algorithm has been developed by combining firefly optimization with ant colony optimization. Power transformer tests have been carried out at Kahramankazan Transformer Center. The data from the transformer has been synchronized with the PIC microcontrollers and transferred to the computer by a fast and secure sampling via the USB port. The harmonic analysis of the power transformers has been determined using the developed hybrid heuristic algorithm and computer program. The developed algorithm is coded using C# programming language. Power transformer harmonic analysis has been created using the Microsoft SQL Server 2017 database. An interface written in Visual Studio programming language has been designed to present analog signals in a digital format to the user. The data obtained from experimental studies have been compared with the data obtained from the developed algorithm and computer program. The accuracy and success of the developed hybrid algorithm and computer program have been tested in the real system. The data obtained showed that the system was successful. Thus, the harmonic analysis of the transformers has been performed by the algorithm, software, and hardware.

Keywords: Electric machines, Heuristic algorithms, Power system harmonics

1. INTRODUCTION

Harmonics in power transformers occur harmonics due to various reasons. At the beginning of these, nonlinear magnetic and electrical circuits come. If the non-linear circuit is the magnetic circuit of the generator, the voltage produced by the generator will be harmonic because it is sinusoidal [1, 2]. If the non-linear circuit belongs to the transformer, the user voltage connected to the secondary side will also be harmonic. If the user's magnetic or electrical circuit is linear but the voltage supplying this user is not sinusoidal, the current drawn by this user will also be harmonic. The harmonic or harmonic voltage on the source side due to the effect of a non-linear circuit occurs [3, 4]. Current and voltage harmonics cause parallel and series resonance to increase harmonic levels. It causes a decrease in efficiency in energy transmission, weakening of insulation in electrical facilities, and decreasing the useful life of system elements [5, 6]. Capacities placed to correct the power factor can be damaged by high currents due to serial or parallel resonance events. In the case of parallel resonance, the source generating the harmonic at the resonance frequency encounters a high-value impedance. When harmonic sources are often modeled as current sources, the harmonic currents flowing from the parallel arms and parallel arm voltages increase. Parallel resonance occurs in different ways. The first conceivable form arises when a capacity is connected to the same bus bar as the harmonic generating source. In this case, a parallel resonance occurs between the harmonic source and the capacity. Due to the serial resonance effect, the impedance of the connected capacity parallel to the load will be very low at high frequencies. Resistive load may not be taken into consideration. Serial resonance may occur between the transformer's inductance, and the installed capacity to correct the power factor. In the series resonance circuit, high capacity capacities but low harmonic voltages are observed. Due to the harmonic currents, the machines, and the transformers become hot. In addition, the depreciation windings of the generators act in such a way that they reduce and eliminate the harmonics occurring in one-phase or two-phase short circuits. They become very hot and cause additional losses in the generators [7, 8]. Harmonic currents cause additional voltage drops over various circuit impedances. Since the frequencies of harmonic currents are equal to the normal network frequency of 50 Hz, the voltage drops occurring on the generator, transformer, and line reactance against these currents increase in proportion to the harmonic frequencies. Consequently, the waveform of the voltage is distorted. Harmonic voltages in transformers increase hysteresis and eddy currents and increase losses. Harmonic currents also increase copper losses. This is especially important in power transformers. Therefore, the power of the transformer should be increased. This increases the cost of the transformer. In this study, experiments are carried out for harmonic analysis of power phase transformers in different connection

forms. Short circuit and idle working tests, sensitivity, and field tests were performed in different connection types of power transformers [9, 10].

2. HARMONICS IN POWER TRANSFORMERS

Harmonics Have important effects on the power transformers. If the power transformers are loaded on an asymmetrical load, and the load current contains a direct current component, the magnetic circuit of the transformer will go to saturation. Also, all harmonic component levels of the excitation current will increase. The harmonic equivalent circuit of power transformers is given in Figure 1.
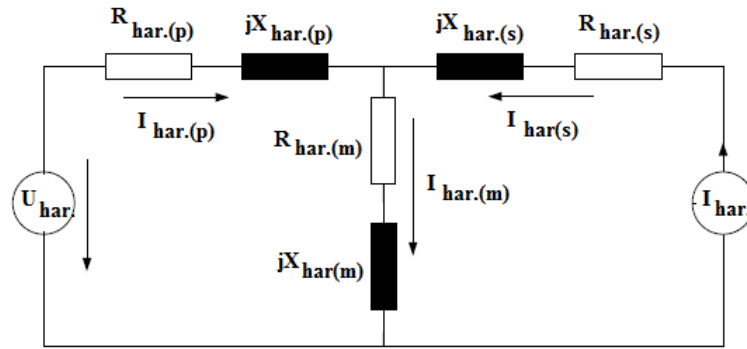
Figure 1. The harmonic equivalent circuit of the power transformer

$R_{har. (p)}$ and $R_{har. (s)}$ are the primary and secondary harmonic equivalent resistance values. $X_{har. (p)}$ and $X_{har. (s)}$ are the primary and secondary harmonic equivalent reactance values. $R_{har. (m)}$ is magnetic resistance. $X_{har. (m)}$ is magnetic reactance. The total power transformer loss is given in Equation (1).

$$P_{TL} = \sum_{har=1}^{har=har_{max}} \left(3 \cdot I_{har(p)}^2 \cdot R_{har(p)} + 3 \cdot I_{har(s)}^2 . R_{har(s)} \right) \tag{1}$$

The high voltage and high current harmonics are caused by series and parallel resonance between the network and the capacity heat and even destroy capacities. Harmonics have the property of disrupting or destroying the operating characteristics of the relays. Digital relays and software are very sensitive to sampled data and zero transitions. The harmonic effects therefore make the relays prone to error. In cases where the harmonic voltage level is less than 20%, the result is mostly negative. The electromagnetic relays are less sensitive to high-grade harmonics [11, 12]. The harmonic effects of impedance measurement are very important. The distance relays have a working principle based on the measurement of the impedance value corresponding to the main frequency. When the error occurs, a measurement error may occur, especially with the third harmonic effect. In the short circuits that occur through the resistance, the high harmonic components will emerge. The current will flow through a high-value resistance. In this case, the relay will probably not be able to work. If the fault is not through a resistor, and the metallic short circuit, the main harmonics of current and voltage gain importance. Therefore, the current transformer's secondary current deteriorates. When a high-value electromotive force occurs in the secondary winding, the non-linear current flowing from the excitation impedance of the relay transformer causes a single-order harmonic distortion. When the core reaches saturation, the harmonic generation source will be the second and third harmonic components of the relay transformer voltage [13, 14]. It is possible to avoid the above-mentioned design problems by selecting the correct device that meets the system requirements. Especially in systems with distance protection based on digital protection systems, it is very important to filter current and voltage waveforms. Under normal system conditions, the insensitivity of the protective devices' means that the harmonics in the power system do not cause any problems except the error conditions. In power transformers, in practice, the first moments of the magnetizing current during the commissioning of the transformer have high harmonic components. When these component values occur, the systems that protect the transformer are activated to prevent the circuit breaker from being opened. Because of the very high amplitude currents during the energized, the relay tends to signal an error. The harmonics in the transformers can be prevented using low core flux density. This results in more conductive material in the core region and therefore more cost. It is not economical to design and operate transformers at lower flux density. Triple harmonic currents and voltages in the lines are prevented using the transformer's star or triangular connections. Using a triangular connection in the primary or secondary winding; when one of the transformer windings is connected to the triangle, the triple harmonic voltages are highly avoided [11, 15]. Therefore, one of the transformer windings must be connected to the triangle to avoid triple

harmonic voltages. In addition to the primary and secondary windings, a third winding is connected to the transformers. This winding is called a tertiary or stable winding. Therefore transformers equipped with tertiary windings are called three-winding transformers. The tertiary dressing is usually tied to the triangle and the ends of the taps are not removed outside the tank. The third harmonic magnet flows in the tertiary winding connected to the triangle. As a result, the core flux and the impulses are almost in the form of a sine wave. Using a star/triangular grounding transformer; the third harmonic voltages in the two windings of the star/star transformer are avoided using a star/triangular grounded transformer. Using a closed triangle connection style provides a path for the third harmonic current. The flux and electromotor force waves remain in the form of a sine wave.

3. DEVELOPED HYBRID HEURISTIC ALGORITHMS

In the generated hybrid algorithm, mathematical modeling of ant and firefly colony behavior has been performed. This method has been used to solve the continuous and discontinuous problems in the analysis of harmonics in the transformer by simulating the natural behavior of ants and fireflies. The hybrid optimization produced is an optimization technique that evaluates the light intensity of fireflies, following paths used by ants between food sources and nests. Studies on ants revealed that many ant species did not have visual abilities. Again, it was understood that the communication of ants with each other was done by chemical secretions produced in their bodies and named pheromones [16, 17]. According to environmental conditions, ants determine the paths between food supply and house. The ants living in the colonies send an ant to the food source as a pioneer ant to find food. This ant tries to find the proper source of food. As ants progress, they store a certain amount of pheromones. They leave the pheromones and store on the way they choose to food [18–20]. They help them choose the way to the next ants. The first way pioneer ants have found may not be the shortest path. When the ants have to choose one of the many paths, they prefer the path where the trace amount is dense. If the shortest route to the food source is no longer the shortest route due to environmental conditions, colony members begin their work to find a new shortest route. The fact that fireflies are single genera and attract each other is the basis of this hybrid algorithm. All fireflies are single-genus, so there is no male and female distinction. All fireflies are attracted by other fireflies. The attractiveness of fireflies is directly proportional to their brightness [21–23]. So the brighter a firefly is, the more attractive it is. The brighter firefly attracts the less bright [24–26]. At the same time, the distance decreases the luster and reduces the charm. If there is a firefly brighter than a firefly, this firefly will move towards the bright one. If there are no more bright fireflies, they move in random directions [27–29]. The insight of fireflies can be considered as the target function of our heuristic algorithm. The hybrid harmonic analysis algorithm developed in power transformers is given in Figure 2.

Two species of the same size have been used. In particular, a single set of ants of one type has been used in single cluster fireflies of another type. In the first stage of the algorithm, populations have been randomly generated for both species. In each generation, Ant Colony and Firefly Optimization have produced solutions in parallel. Solutions obtained using two populations are listed according to the degree of restriction violation. For each problem, the algorithm is assigned a random vector for each ant. Here, all solutions for each variable represent the candidate group of values. A pheromone is added for each variable in each ant. The pheromone has been reduced by a constant factor to prevent early convergence. Some pheromones are discarded from the components of the candidate groups and modified to enhance good solutions. When the pheromone is updated after an iteration, the next iteration begins by changing the paths of the ants. In power transformers, a current harmonic measurement test was performed at idle and load. In this experiment, the losses of the power transformers in idle and load operations were measured. In power transformers, odd-numbered harmonics are important. Even-numbered harmonics are not seen due to the constructive properties of the transformer. In the experiment, the connection of the current transformers on the dimension circuit of the energy transformer which is working in idle and load conditions is made from the secondary ends to the heterodyne analyzer.

4. PERFORMING EXPERIMENTS

Current and voltage harmonics 3-5-7 and 9 are measured with this device. The measured current and voltage values for harmonics are compared with the guaranteed current and voltage values given for this transformer. Experimental connection diagrams for harmonic measurement are given in Figure 3.
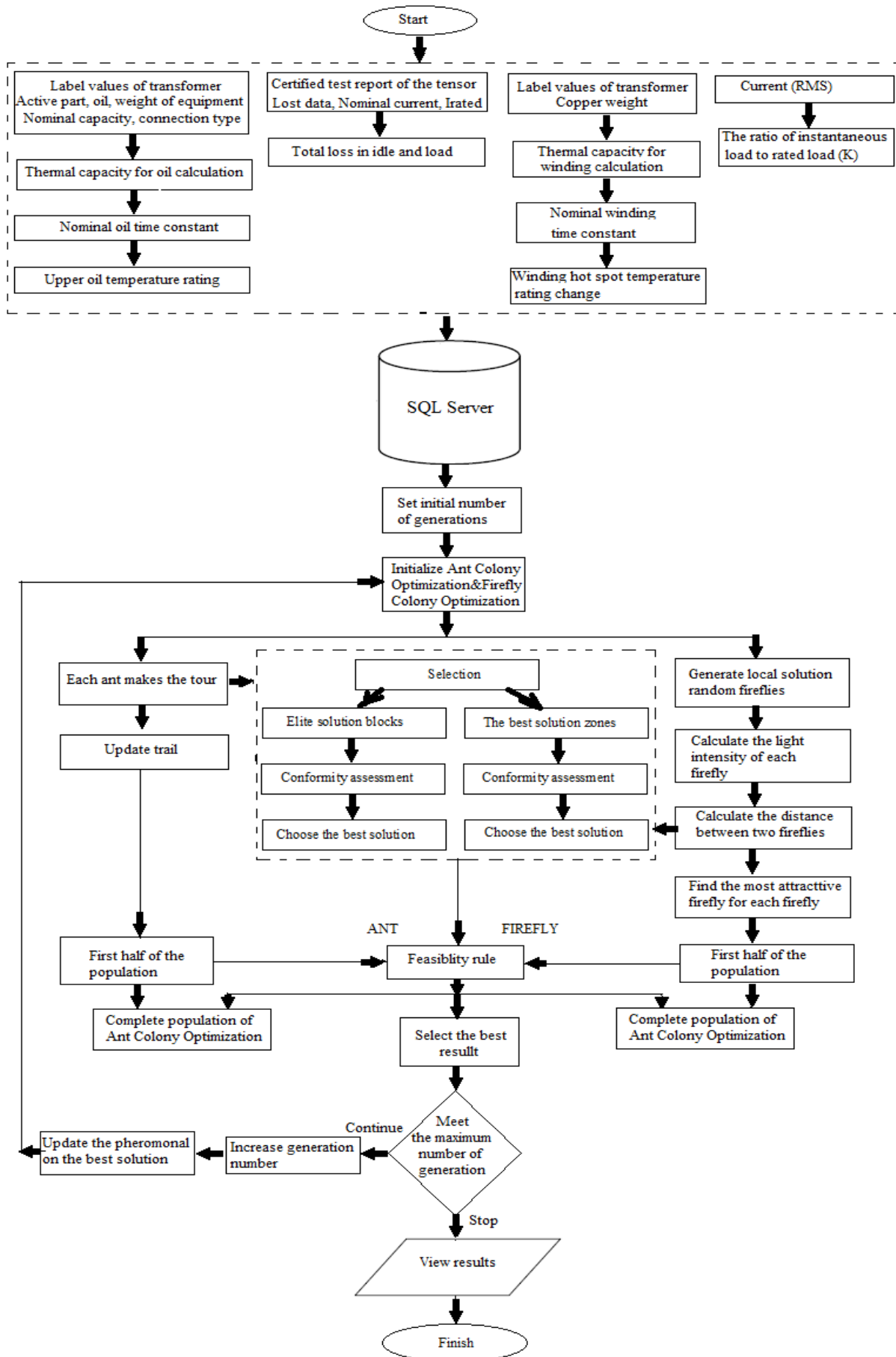
Figure 2. The hybrid harmonic analysis algorithm developed in power transformers
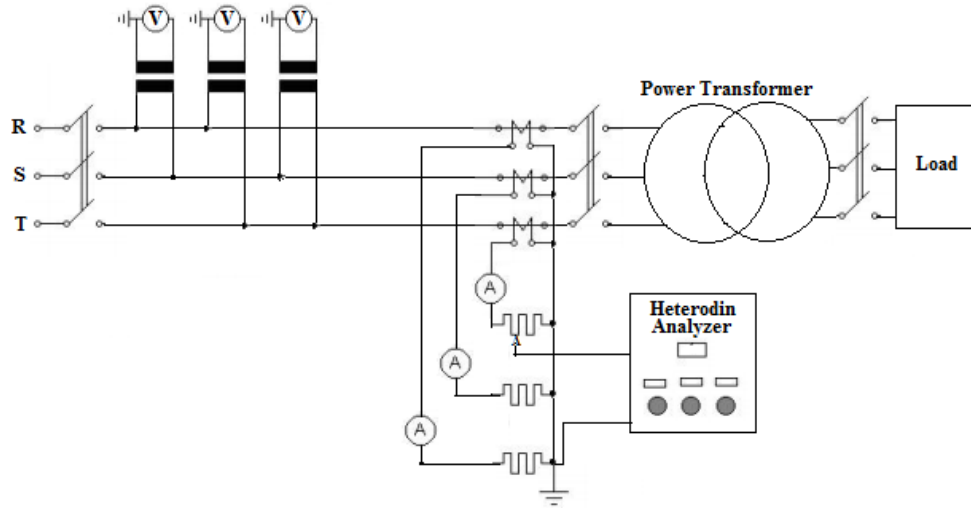
Figure 3. Experimental connection diagrams for harmonic measurement

The transformer parameters are given in Table 1.

Table 1. Transformer parameters

Transformer power	1600 kVA
Transformer primary voltage	31.5 kV
Transformer secondary voltage	0.4 kV
Rated current	29.1 A
Short circuit voltage (%)	% 6.2
Short circuit current	480 kA

The measured values of the load harmonic voltage are given in Table 2.

Table 2. The measured value of the load harmonic voltage

Harmonic Seq.	Measurement	Harmonic Seq.	Measurement
h2	0.10-0.18	h11	0.09-0.47
h3	0.12-0.27	h13	0.12-0.34
h4	0.04-0.14	h15	0-0
h5	0.89-1.55	h17	0.13-0.38
h6	0.04-0.14	h19	0.08-0.19
h7	0.98-1.41	h23	0.08-0.19
h9	0.10-0.19	h25	0.08-0.19

The measured values of the load harmonic current are given in Table 3.

Table 3. The measured value of the load harmonic current

Harmonic Seq.	Measurement	Harmonic Seq.	Measurement
h2	1.0-2.4	h11	0.46-2.37
h3	0.47-0.98	h13	0.52-0.97
h4	0.04-0.11	h15	0-0
h5	8.1-16.2	h17	0.21-0.98
h6	0.01-0.27	h19	0.21-0.98
h7	3.98-8.71	h23	0-0
h9	0-0	h25	0-0

The measured total harmonic deviation of the transformer current is given in Figure 4.
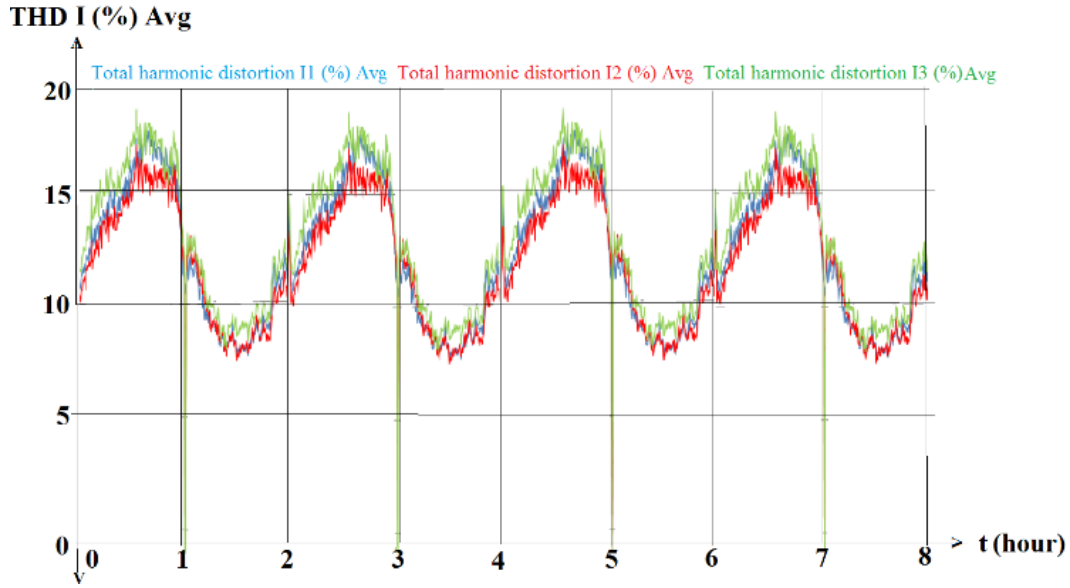
Figure 4. Measured total harmonic deviation of transformer current

The measured total harmonic deviation of transformer voltage is given in Figure 5.
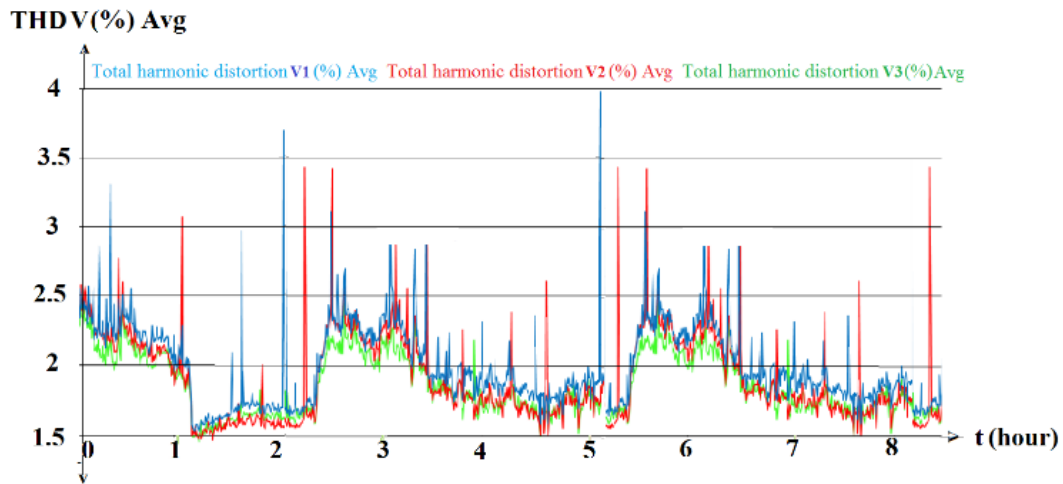
Figure 5. Measured total harmonic deviation of transformer voltage

5. DATA FROM THE DEVELOPED ALGORITHM

The values of the load harmonic voltage obtained from the algorithm are given in Table 4. The values of the load harmonic current obtained from the algorithm are given in Table 5. The total harmonic deviations of transformer currents obtained from the cerated algorithm are given in Figure 6. The total harmonic deviation of transformer voltage obtained from the algorithm is given in Figure 7.

Table 4. The value of the load harmonic voltage obtained from the algorithm

Harmonic Seq.	Algorithm	Harmonic Seq.	Algorithm
h2	0.09-0.19	h11	0.08-0.45
h3	0.11-0.25	h13	0.10-0.32
h4	0.03-0.13	h15	0-0
h5	0.87-1.52	h17	0.12-0.36
h6	0.03-0.13	h19	0.07-0.18
h7	0.97-1.40	h23	0.07-0.18
h9	0.09-0.18	h25	0.07-0.18

Table 5. The value of the load harmonic current obtained from the algorithm

Harmonic Seq.	Algorithm	Harmonic Seq.	Algorithm
h2	1.1-2.3	h11	0.42-2.30
h3	0.46-0.97	h13	0.50-0.90
h4	0.03-0.13	h15	0-0
h5	8.0-16.4	h17	0.20-0.90
h6	0.02-0.26	h19	0.20-0.90
h7	3.90-8.70	h23	0-0
h9	0-0	h25	0-0
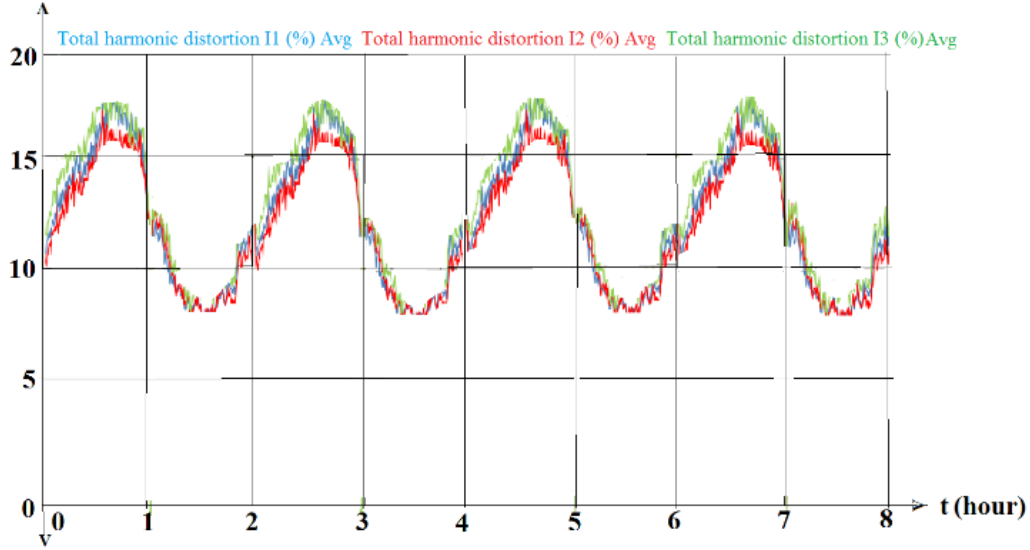
Figure 6. The total harmonic deviation of transformer current obtained from the algorithm
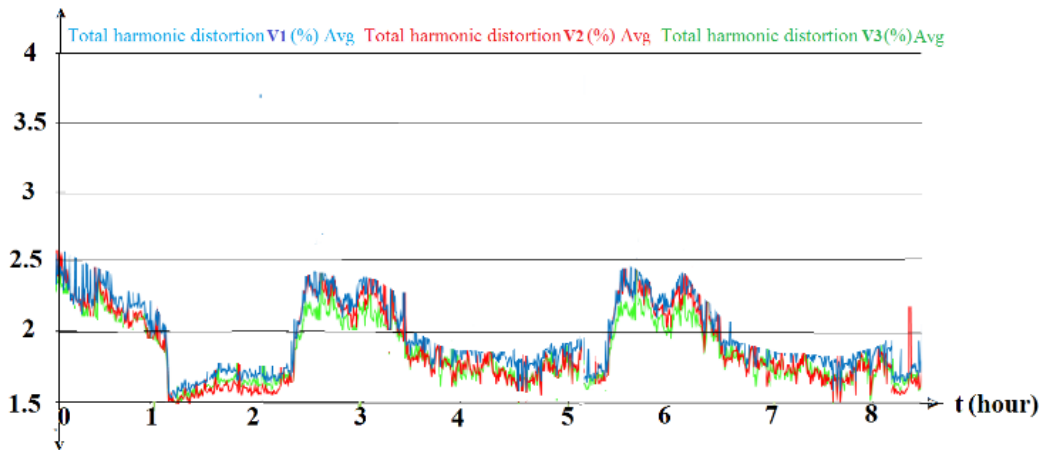
Figure 7. The total harmonic deviation of transformer voltage obtained from the algorithm

6. ACCURACY ANALYSIS OF THE GENERATED HYBRID ALGORITHM

A comparison of the values obtained from the algorithms with the current values obtained from the measurements is given in Table 6. Harmonic experiments have been performed on the power transformers to test the accuracy of the algorithms. The data obtained from these experiments and the results obtained from the algorithms have been compared. It shows that the developed hybrid optimization can provide faster and better solutions than other Ant and Firefly Optimization.

Table 6. Comparison of the values obtained from the algorithms with the harmonic current values obtained from the measurements

Harmonic Seq.	Ant Colony O. Value	Firefly O. Value	Hybrid O. Value	Measured Value
h2	1.8-2.6	1.3-2.5	1.1-2.3	1.0-2.4
h3	0.6-1.2	0.5-1.1	0.46-0.97	0.47-0.98
h4	0.09-0.19	0.07-0.16	0.03-0.13	0.04-0.11
h5	8.7-18.2	8.4-17.5	8.0-16.4	8.1-16.2
h6	0.08-0.36	0.06-0.3	0.02-0.26	0.01-0.27
h7	4.80-9.9	4.6-9.2	3.90-8.70	3.98-8.71
h9	0-0	0-0	0-0	0-0

7. HARMONIC ANALYSIS COMPUTER PROGRAM

The interface of the created transformer harmonic analysis program is given in Figure 8.
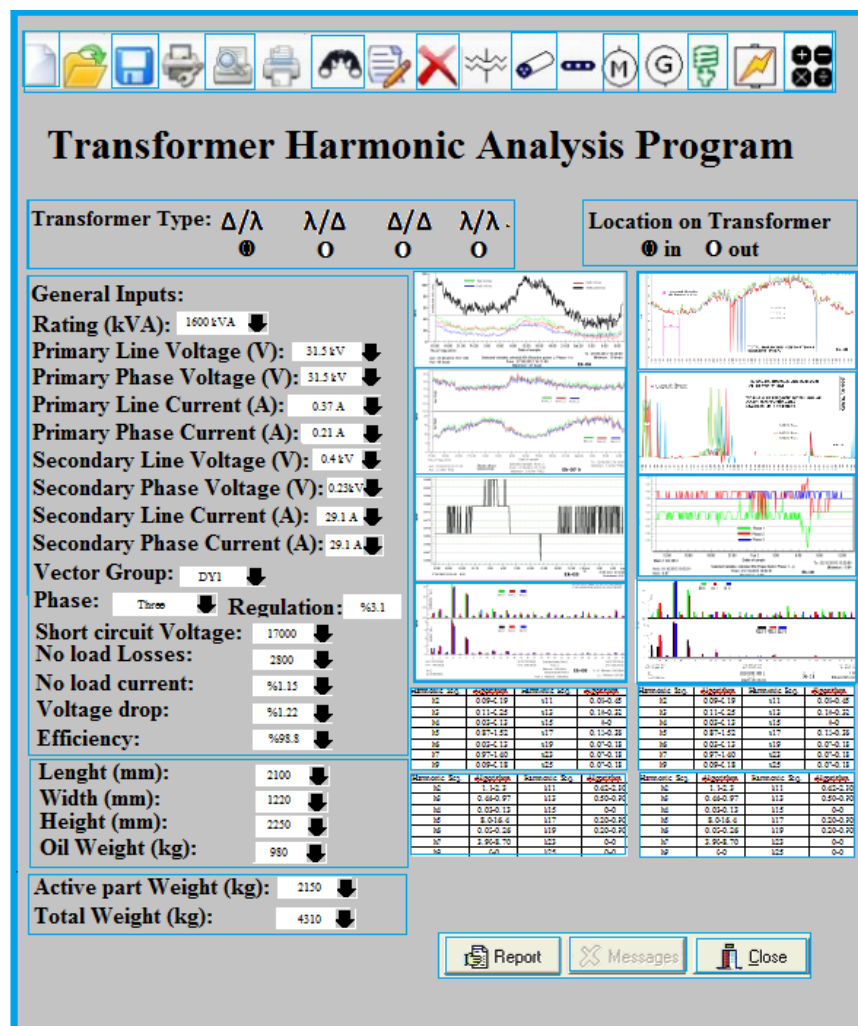
Figure 8. The interface of the created transformer analysis program

Using the Matlab 2018 and Visual Studio 2017 package programs, a computer program for harmonic analysis in power transformers in different connection types has been created. There is a hybrid algorithm created in the infrastructure of the computer program. The introduction screen consists of three main sections. In the first section, all the electrical parameters of the transformer are entered. In the second section, all dimensions and weights of the transformer are entered. In the third chapter, the current and voltage harmonic values and signals of the

transformer are taken. The values obtained from the computer program and the values obtained from the experiments have been compared. It is understood that the accuracy of the values obtained from the program is appropriate.

8. CONCLUSIONS

Firefly Optimization has been used in the local search to find the optimal solution for determining the harmonics in power transformers. In the global search, Ant Colony Optimization has been used. The best solution has been obtained from Ant Colony Optimization. The fastest solution has been obtained from Firefly Optimization. In this study, a hybrid combination strategy has been developed using these two evolutionary algorithms. To minimize the increasing convergence times due to a large number of variables and repetitions, the least number of ants and fireflies has been used. The hybrid optimization developed for the determination of transformer harmonics has been seen to be the most suitable and fastest solution according to Firefly Optimization and Ant Colony Optimization. The hybrid optimization results obtained from the algorithm are very close to the actual value obtained from the harmonic experiments performed on the power transformer in different connection types. By using the developed Ant and Firefly hybrid optimization algorithm, Matlab 2018, and Visual Studio 2017 package programs, a computer program has been created that performs harmonic analysis in power transformers. The current and voltage harmonic values of the transformer have been estimated by entering all electrical parameters, dimensions, and weights of the power transformer. It has been seen that the results are good compared to the values obtained from the power transformer tests. By this study, it is possible to predict the current and voltage harmonic values that may occur in power transformers.

References

[1]   N. Pjevalica, N. Petrovic, V. Pjevalica, and N. Teslic, "Experimental detection of transformer excitation asymmetry through the analysis of the magnetizing current harmonic content," *Elektronika Ir Elektrotechnika*, vol. 22, no. 2, pp 43–48, 2016.

[2]   E. Cazacu, L. Petrescu, and V. Ionita, "Derating of power distribution transformers serving nonlinear industrial loads," in *2017 International Conference on Optimization of Electrical and Electronic Equipment (OPTIM) & 2017 Intl Aegean Conference on Electrical Machines and Power Electronics (ACEMP)*, Brasov, 2017, pp. 90–95.

[3]   J. P. Srividhya, D. Sivakumar, and T. Shanmathi, "A Review on causes, effects, and detection techniques of harmonics in the power system," in *IEEE International Conference on Computation of Power, Energy Information and Communication*, pp. 680–686, 2016.

[4]   F. Z. Peng, "Harmonic sources and filtering approaches", *IEEE Trans. on Industry Applications Magazine*, vol. 7, pp. 18–25, 2016.

[5]   J. C. Das, *Power System Harmonics and Passive Filter Designs*, 1st ed. United States of America: Wiley-IEEE Press., 2015.

[6]   P. S. Moses and M. A. S. Masoum, "Three-phase asymmetric transformer aging considering voltage-current harmonic interactions, unbalanced nonlinear loading, magnetic couplings, and hysteresis," *IEEE Transactions on Energy Conv.*, vol. 27, no. 2, pp. 318–327, 2012.

[7]   S. B. Sadati, A. Tahani, M. Jafari, and M. Dargahi, "Derating of transformers under non-sinusoidal loads," in *11th International Conferenec on Optimization of Electrical and Electronic Equipment, OPTIM*, 2008, pp.263–268.

[8]   Sh. Taheri, A. Gholami, I. Fofana and H.Taheri, "Modeling and simulation of Transformer loading capability and hot spot temperature under Harmonic Conditions," Electric Power Systems Research, vol. 86, pp. 68–75, May 2012.

[9]   A. Elmoudi, M. Lehtonen, and H. Nordman, "Effect of harmonics on transformers loss of life," in *IEEE conference 2006*, Canada, 2016.

[10]   L. Chengjun and Y. Rengang, "Calculation and analysis of transformer's harmonic loss", *Power System Protection and Control*, 2008.

[11]   T. Shun and X. Xiangning, "Comparing transformer derating computed using the harmonic loss factor FHL and K factor," *Advanced Technology of Electrical Engineering and Energy*, 2008.

[12]   M. Marzband and A. Shaikholeslami, "A program for harmonic modeling of distribution network transformers and determination of loss in the transformers and the amount of decrease of their life," in *International Conference on Power Electronics, Drives, and Energy Systems, 2006 (PEDES '06)*, New Delhi: IEEE, 2006, pp. 1–6.

[13]   A. Elmoudi, M. Lehtonen, and H. Nordman, "Effect of harmonics on transformers loss of life," in *Conference Record of the 2006 IEEE International Symposium on Electrical Insulation*, Espoo, Finland: IEEE, 2006, pp. 408–411.

[14] F. De La Rosa, *Harmonics and Power Systems*, Boca Raton, London NY: Taylor & Francis Group, 2006.

[15] L. Chengjun and Y. Rengang, "Calculation and analysis of transformer's harmonic loss," *Power System Protection and Control*, 2008.

[16] R. Laptik and D. Navakauskas, "Application of ant colony optimization for image segmentation," *Elektronika Ir Elektrotechnika*, vol. 80, no. 8, pp. 13–18, 2017.

[17] R. Laptik, "Ant system initial parameters distribution," *Elektronika Ir Elektrotechnika*, vol. 110, no. 4, pp. 85–88, 2011.

[18] R. Laptik, "Ant system with distributed values of pheromone evaporation," *Elektronika Ir Elektrotechnika*, vol. 18, no. 8, pp. 69–72, 2012.

[19] M. Dorigo and T. Stutzle, "Ant colony optimization,", *The MIT Press*, pp 33–41, 2004.

[20] C. Fernandes, V. Ramos, and A. C. Rosa, "Self-regulated artificial ant colonies on digital image habitats," *International Journal of Lateral Computing,* vol. 1, no. 2, pp. 1–8, 2005.

[21] X. S. Yang, S. S. S. Hosseini, and A. H. Gandomi, "Firefly algorithm for solving non-convex economic dispatch problems with valve loading effect," *Applied Soft Computing*, vol. 12, pp. 1180–1186, 2012.

[22] A. H. Gandomi, X. S Yang, and A. H. Alavi, "Mixed variable structural optimization using firefly algorithm," *Computers & Structures*, vol. 89, pp. 2325–2336, 2011.

[23] K. S. Lee and Z. W. Geem, "A new structural optimization method based on the harmony search algorithm," *Computers & Structures*, vol. 82, pp. 781–798, 2004.

[24] X. S. Yang, "Firefly algorithms for multimodal optimization" in *Stochastic Algorithms: Foundations and Applications, SAGA 2009, Lecture Notes in Computer Science*, 5792. Berlin: Springer Verlag, 2009, pp. 169–178.

[25] M. K. Sayadi, R. Ramezanian, and N. Ghaffari-Nasab, "A discrete firefly meta-heuristic with local search for makespan minimization in permutation flow shop scheduling problems," *Int. J. of Industrial Engineering Computations,* vol. 1, pp. 1–10, 2010.

[26] L. dos Santos Coelho, D. L. de Andrade Bernert, and V. C. Mariani, "A chaotic firefly algorithm applied to reliability-redundancy optimization," in *2011 IEEE Congress on Evolutionary Computation (CEC'11)*, 2011, pp. 517–521.

[27] S. M. Farahani, B. Nasiri, and M. R. Meybodi, "A multiswarm based firefly algorithm in dynamic environments," in *Third Int. Conference on Signal Processing Systems (ICSPS2011)*, Yantai, China, 2011, pp. 68–72.

[28] J. Senthilnath, S. N. Omkar, and V. Mani, "Clustering using firefly algorithm: performance study," *Swarm and Evolutionary Computation*, vol. 1, no. 3, pp. 164–171, 2011.

[29] X. S. Yang, "Multiobjective firefly algorithm for continuous optimization," *Engineering with Computers*, 2012, doi: 10.1007/s00366-012-0254-1.

Design and Production of High Mechanical Durability Vacuum Circuit Breaker with Insulation Class up to 36 kV

Arif Ucer[1], Mehmet Yuksel[2], Mustafa Cetin[1], Ramazan Karaaslan[1]

[1]EFG Electric Energy Inc., Diyarbakir, Türkiye
[2]Dicle University, Institute of Science, Electrical and Electronics Engineering Department, Diyarbakir, Türkiye
Corresponding Author: Mehmet Yuksel (e-mail: mehmet.yuksel@efgelektrik.com)

Abstract

High voltage circuit breakers are the important switching devices in electrical transmission and distribution networks. Besides switching under normal operating conditions, they also protect the network by interrupting power within the desired time during fault conditions. The distribution infrastructure in our country is not of the desired quality. As a result, faults occur more frequently than standard levels, causing excessive strain on the circuit breakers and leading to a shorter lifespan. For this reason, the project aimed at designing and manufacturing high mechanical durability vacuum circuit breakers. Vacuum circuit breakers are highly preferred due to their ability to extinguish arcs that may occur during opening and closing, their lack of harmful gases, and ease of operation and maintenance. The design of the circuit breaker aimed to reduce potential fault points and enhance durability. Thus, it was planned to produce a circuit breaker with higher durability than standard requirements. A design and production of circuit breakers capable of operating at voltages up to 36 kV in a vacuum environment compliant with standards was carried out.

Keywords: Circuit breakers, High voltage, Fault protection, Vacuum circuit breakers, Arc extinguishing

1. INTRODUCTION

Vacuum circuit breaker is today the dominant technology worldwide for Medium Voltages up to 52kV and is seen as the main candidate to replace SF6 circuit breakers at higher voltages. Vacuum switching technology was introduced into service in the late 1960's and since that time millions of vacuum circuit breakers have been manufactured. Today it is estimated that over a thousand vacuum circuit breakers will be manufactured worldwide annually.

On the other hand, maintaining safety and reliability of this huge system is very difficult challenge for the energy control and management system who needs powerful, resistant and reliable tools in order to interfere to the necessary area of the network under high electric energy.

There is no doubt, one of these tools used in electric power network is circuit breakers. The circuit breaker instantaneously breaks the electric current which flows in a high voltage transmission line in case of applying any control action or if there is any fault. To perform this duty, the circuit breakers must be both a good conductor and a good isolator, also they must change from the closed to open position in a very short period of time and not cause overvoltage during this rapid change [1].

Nowadays, the circuit breakers constitute the most important part of both transmission and distribution networks owing to their current breaking ability under load condition [2]. In particular, while the SF6 circuit breaker have to be used at the high voltage transmission lines due to their high-power switching capacity, the vacuum circuit breaker which is relative new technology is preferred to the SF6 circuit breaker in a distribution network due to its switching efficiency [3].

2. MATERIAL AND METHOD

2.1. Working Principle of Vacuum Circuit Breakers

This type of circuit breakers uses the arc extinction ability and high insulating strength of the 10-7 - 10-5 Torr vacuum. Generally, they include two contacts in a vacuum tube with a pressure of approximately 10-3 N/m2 [4]. One of these is moveable contact. The arc formed during interruption is very diffuse and burns in evaporated

contact material. It consists of a large number of independent arcs burning in parallel. Each arc carries about 100A and moves freely about the contact surfaces.

2.2. Development and Modification Process

The 36 kV 1250A side mechanism vacuum circuit breaker which has been produced in EFG factory is presented in Figure 1. In the standard regarding circuit breakers, the mechanical life of the breaker is required to be at least 2,000 cycles in idle. However, it is often encountered that existing circuit breakers fail under load with a very low number of switching cycles. Therefore, it is extremely important that the mechanical strength of circuit breakers is high. For this purpose, some measures were taken to ensure that the circuit breaker developed in the project has high mechanical strength. One of these is that the switching mechanism has a gear structure. The number of components is reduced with the gear mechanism, reducing the possibility of failure. The target is for the vacuum circuit breaker to have a minimum of 13,000 idle switching times. This value is 30% more than the value specified in the standard.

Figure 1. 36 kV 1250A side mechanism vacuum circuit breaker

2.3. Method of Gear Working at Vacuum Circuit Breaker

Two gear shaft groups are designed for vacuum circuit breaker spring installation mechanisms. The first of these is the manual spring setting group, the other is the motorized spring setting group. The purpose of these two gear groups is to start the closing spring loading process by transferring movement to the Z10 gear group. The closing spring is loaded by the spring loading lever movement. The vacuum breaker mechanism design is shown in Figure 2.
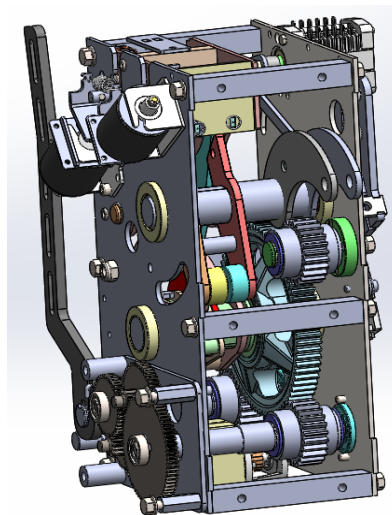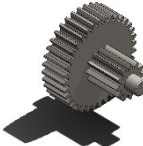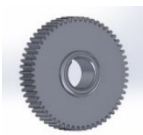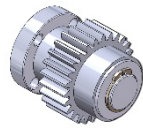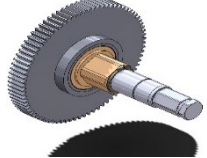
Figure 2: Vacuum breaker mechanism design

2.4 Material of Gear

Gears and gear groups designed for vacuum circuit breakers are coated with manganese phosphate. The hardness levels of the gears are between 36-58 HRC. The gear definitions and explanations used in the mechanism are given in Table 1.

Table 1. Gear material features and definitions

Material Code / Name (in Turkish)	Visual	Explanation
H40mtl00018 / Z2 Motor Baglanti Disli Grubu		Z2 _Helical_gear / 1 pcs Zp _pinion shaft / 1 pcs
Hm40mtl00019 / Z4 Motor Aktarma Disli Grubu		Z4 gear / 1 pcs Zp _pinyon_shaft / 1 pcs
Hm40mtl00020 / Z6 Motor Ara Disli Grubu		Z6 gear / 1 pcs Zp_pinyon_shaft / 1 pcs
Hm40mtl00021 / Z8 Motor Cikis Dislisi		Z8 gear / 1 pcs
Ym40ksc00001 / S4 Disli Tutma Komplesi		Z9 / 1 pcs HK 2512 INDIA / 2 pcs / 1 pcs
Ym50ksc00003 / S5 Disli Kurma Kolu Mili Komplesi		Z9 gear / 1 pcs HK 2512 INDIA/ 2 pcs
Ym50ksc00002 / S6 Disli Motor Cikis Mili Komplesi		Z9 / 1 pcs HK 2512 INDIA / 2 pcs
Hm40mtl00022 / Z10 Ana Mil Disli Grubu		Z10 / 1 pcs HK 3016 INDIA / 1 pcs HK 6012 INDIA / 1 pcs

3. RESULTS

The prototype of the mechanism design has been manufactured. The prototype of this mechanism has been tested according to the M1 class TS EN 62271-100 article 6.101 standard. Thus, the mechanical strength tests have yielded positive results. In addition, assembly analysis of the gears was performed using the simulation module of the Solidworks program. As a result of these analyses, mechanical strength lives were calculated and weak points were identified.

4. CONCLUSION

Gear groups designed for vacuum circuit breakers ensured that the system operated more stably. This minimized adverse conditions such as breakage, buckling and stretching in mechanisms. However, the cost of the mechanism

and the number of materials used have increased with this gear group. In subsequent studies, a more compact spring-loading mechanism can be designed by reducing the number of gears and other auxiliary materials.

Acknowledgments

References

[1]   A. A. Razi-Kazemi ans K. Niayesh, "Condition monitoring of high voltage circuit breakers: past to future," *IEEE Transactions on Power Delivery,* vol. 36, no. 2, pp. 740–750, 2020.

[2]   D. Dufournet, "AC high-voltage circuit breakers," *IEEE Switchgear Committee Portland,* vol. 22, no. 5, pp. 190–201, 2017.

[3]   S. Ochi, K. Kagawa, G. A. Calhoon, and K. Beamer, "Vacuum circuit breaker technology vacuum interrupters – How they work"*, Neta World*, vol. 21, no. 5, pp. 87–96, 2010.

[4]   S. Uzel, "Design and implementation of a compact 36 KV 1250 A. Front mechanism vacuum circuit breaker", *Nevsehir Bilim ve Teknoloji Dergisi,* vol. 8, no. 1, pp. 26–32, 2019.

[5]   M. C. Toplamacioglu, S. Uzel, O. Aladag, and S. Keskintas, "Development and modifications of 36 KV 1250A front mechanism vacuum circuit breaker for 5000 cycles test," *Ulusoy Electric Company*, vol. 8, no. 1, pp. 26–32, 2019.

Reduction of DC-Link Capacitor Current by Phase Shifting Method

Deniz Sahin[1], Bulent Dag[1]

[1]Graduate School of Natural and Applied Sciences, Gazi University, Ankara, Türkiye
Corresponding author: Deniz Sahin (denizshn1994@gmail.com)

Abstract

This paper describes the reduction of the DC-link capacitor current by creating a phase difference between the carrier waves of two three-phase voltage source inverters (VSIs) driving two permanent magnet synchronous motors (PMSM). There is a voltage fluctuation at the input of the VSI inverters due to pulsating current and input impedance. The DC-link capacitor minimizes this fluctuation by decreasing the input impedance. Most of the pulsating current source is the DC-link capacitor current and the average current source is the battery. Since the DC-link capacitor has equivalent series resistance (ESR), there is a temperature rise on the DC-link capacitor reducing its operating life. In addition, the volume of the DC-link capacitor is directly related to the current flowing through it. Inserting phase difference between the carrier waves of the VSIs, reduces harmonics of the input current and so the DC-link capacitor current. As RMS value of the DC-link capacitor decreases, volume of the DC-link capacitor current decreases and its life-time increases. The PWM signals of the VSIs are generated using the space vector pulse width modulation (SVPWM) algorithm. To analyze the DC-link capacitor current, the input current of the VSIs is analyzed using the double Fourier series method. The magnitude of the harmonics of the DC-link capacitor current is simulated using MATLAB. In addition, the PLECS is used to simulate PMSMs. Simulation results and mathematical models show that, inserting phase difference between the carrier waves of the VSIs, the DC-link capacitor current is reduced by almost 50%.

Keywords: PMSM, VSI, SVPWM, Phase difference, Carrier waves

The Influence of Rotor Magnet Height and Stator Position on Acoustic Performance in BLDC Blowers

Ahmet Arif Kose[1]

[1]Test & Validation, VALEO Automotive, Bursa, Türkiye
Corresponding author: Ahmet Arif Kose (e-mail: ahmet-arif.kose.ext@valeo.com)

Abstract

Brushless DC (BLDC) blower motors play an important role in making the vehicle cabin comfortable, especially in heating, ventilation, and air conditioning (HVAC) systems. These motors help to move the air around and keep the temperature and air quality at the right level inside the cabin. As there are more electric vehicles (EVs) on the road and cars are getting better at blocking sound, the noise inside the cabin has gone down. While this makes driving more comfortable, it also means that sounds from parts like the blower can be heard more clearly, so controlling noise is becoming more important. Because of this, controlling and reducing noise from these systems has become more important and is a key part of designing today's vehicles. This study looks at how the height of rotor magnets and their position compared to the stator affect the noise produced by the motor. The research tries to understand how these design choices influence the sound made by the blower motor. By studying these factors, the research hopes to find ways to make the motor design better and reduce the noise it makes. The results could help in making quieter motors, which would make the ride more comfortable in both regular cars and electric vehicles. As noise, vibration, and harshness (NVH) control becomes more important, especially with more electric cars on the road, this study is expected to give helpful information to the car industry, helping to make driving more enjoyable for everyone. This research employs design of experiments (DOE) methodology to systematically investigate the impact of rotor magnet height and stator position on acoustic performance.

Keywords: Brushless DC, Design of experiments, Noise, vibration, and harshness, Heating, ventilation, and air conditioning

Optimizing Thermal Paste Application for Improved Cost Efficiency and Performance in BLDC Motor Production

Engin Mert Nayir[1]

[1]Test & Validation, VALEO Automotive, Bursa, Türkiye
Corresponding author: Engin Mert Nayir (e-mail: mert.nayir@valeo.com)

Abstract

In the production of brushless DC (BLDC) motors for automotive heating, ventilation, and air conditioning (HVAC) systems, the printed circuit board assembly (PCBa) is an important part that controls the motor's functions. Thermal paste is applied between the PCBa and heatsink to help with heat dissipation and keep the motor from overheating. At first, we were using more thermal paste than necessary, which led to higher costs and longer production times. So we had to decrease it. To improve this, we tested whether we could reduce the amount of thermal paste without affecting the motor's performance. In the first round of tests, we used the standard amount of paste, then gradually decreased it by 60% in later trials. Even with less paste, the motor stayed within safe temperature limits. By using less thermal paste, we were able to cut material costs. The application process also became quicker which made our production more efficient. So the study proved itself. Test results show that applying less thermal paste during the production is not only a more cost-effective approach but also more efficient. Reducing thermal paste amount helped lower the costs, speed up production, and minimized waste. These changes have made the manufacturing process faster. It means it is improving both cost and sustainability.

Keywords: BLDC motor, Thermal paste, Cost Efficiency, Thermal management, PCBa

Parametric Design and 3D Production of Door Hinges for Electric Vehicles

Erman Zurnaci[1], Ilker Ismail Soran[2]

[1]Mechanical Engineering Department, Engineering and Architecture Faculty, Kastamonu University, Kastamonu, Türkiye
[2]Mechanical Engineering, Kastamonu University, Kastamonu, Türkiye
Corresponding author: Erman Zurnaci (e-mail: ermanzurnaci@kastamonu.edu.tr)

Abstract

Electric vehicles are emerging as an environmentally friendly solution in today's world, where the effects of global warming are increasing. One of the most important parameters affecting the range of electric vehicles is their weight. To increase the range, manufacturers prefer low-weight but high-strength components in the production of electric cars. This study aims to develop an easily manufacturable but lightweight door hinge that can be used as a door hinge in small-scale electric vehicles. Parametric design methods and topology optimization were used to design a new hinge. Numerical analyses were performed to determine the mechanical performance of the structure during the development phase. The prototypes of the new and conventional hinge designs were realized on a 3D printer. The developed design reduced the conventional weight of the hinge by 24.43%. The study also showed that parametric design methods can develop lighter automobile components.

Keywords: Electric vehicle, Door hinge, Structural design, Topology optimization, Numerical analysis

1. INTRODUCTION

Today, many researches are being conducted on the production of electric vehicles at optimum costs. In order to reduce the need for raw materials during production, overcome environmental concerns and increase vehicle range by reducing weight, automobile manufacturers are experimenting with innovative approaches. Recent studies show that the mechanical strength of structural components can be improved, especially through design optimization [1–3]. Reducing component weight without compromising mechanical strength is one of the most important engineering problems. Reducing the weight of automobiles and increasing efficiency has become a significant focus of research in this area. The automotive industry is focusing on the study of composite-based automobile components to cope with the need for increased strength and lightweight components and parts, as they can provide higher strength, more excellent resistance, and higher fatigue life [4]. A ten percent reduction in vehicle weight has been shown in studies to save 6 to 8 percent of fuel for a conventional vehicle [5]. Lightweighting is a more important issue for electric vehicles, which are heavier than internal combustion vehicles [6]. The main reason for the weight of electric vehicles is the lithium battery, which in some cases can reach 700 kilograms or 30 percent of the vehicle's weight [7]. This results in a car body about 284 kilograms heavier than conventional vehicles. This problem shows the importance of reducing the weight of electric vehicle components.

Albak (2019) lightened the brake pedal by 11% compared to the initial design with the structural optimization study he carried out for the Formula SAE vehicle brake pedal made of aluminum 7075-T6 material. Although there is a 6% increase in the stress value of the improved design, it is stated that this value remains within acceptable limits in terms of strength [8]. Topaç et al. (2020) developed the mechanical design of the rear axle-chassis connection bracket using topology optimization. They used response surface methodology (RSM) to reduce stresses in critical regions of high stress. With the final design they developed and optimized, they reduced the mass of the bracket by 63% [9]. Cavazzuti et al. (2011) used parametric design and topology optimization techniques to reduce the chassis weight of the Ferrari F458 Italia model vehicle. In the optimization phase, they optimized to reduce the chassis weight without weakening the chassis in terms of structural stiffness, modal response, and crashworthiness. The study demonstrated the effectiveness of topology optimization in reducing the weight of structural components [10]. In their study, Petrov et al. (2020) performed optimization for vehicle door hinges. They also used the characteristics of various production types, such as milling, casting, and additive manufacturing, as optimization criteria. In the study, they aimed to determine the most efficient manufacturing method and structural optimization for hinges. Using the finite element method, the researchers reduced the structural weight of the hinge [11].

Studies in the literature have shown that parametric design methods are an effective technique for optimizing structural components. It is also possible to reduce the weight of components by using optimization methods. This study aims to reduce the hinge weight of electric vehicles. With the help of topology optimization techniques and numerical analysis, the load distribution on the hinge was determined. A new hinge design was realized by utilizing the results obtained.

2. MATERIAL AND METHOD

2.1. Hinge Design

This project aims to redesign each vehicle's conventional and suitable door hinge. For this purpose, hinge optimization will aim to reduce the weight of the hinge and, at the same time, maintain its mechanical strength. Firstly, a conventional design will be made, and a new hinge design will be realized by evaluating the results of numerical analyses to be performed on this design. First, the hinge designs commonly used in the industry were examined for conventional designs that can be used as a basis. Some of the hinge models taken as a basis for the model are given in Figure 1.

Tesla Model Y   Ford Granada

Chevrolet Camaro

Nissan Genuine   Ford Ranger

Figure 1. Front door hinges of different brands and models

A two-piece design was chosen for the hinge model. Many companies use two-piece hinges. The two-piece design provides ease of manufacturing as well as ease of assembly. The conventional hinge design and hinge components selected for this study are given in Figure 2. The dimensions of the hinge design were determined with reference to the dimensions of the reference hinge models. The dimensions of the conventional hinge design are given in Figure 3.

Upper part   Hinge   Lower part
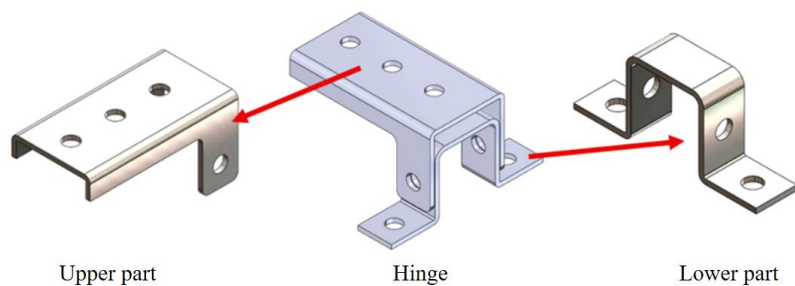
Figure 2. Conventional hinge design and hinge components
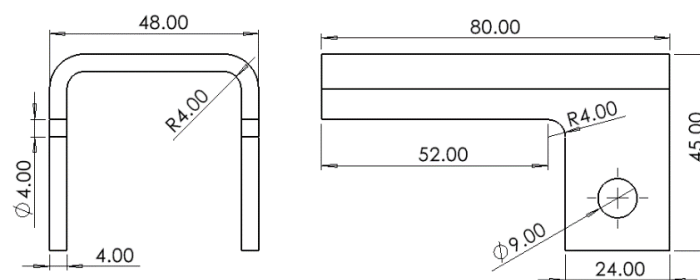
Figure 3. Dimensions of the conventional hinge design

2.2. Numerical Mechanical Analysis

To improve the hinge design, it is first necessary to determine how the design behaves under mechanical load. Because the stress and strain occurring on the hinge are guided by the characteristics of the design. Using the finite element numerical analysis method, the mechanical changes occurring on a part can be determined [12]. Solidworks software was used to numerically determine the behavior of the upper and lower parts of the hinge under load. AISI 1020 steel was selected as the hinge material in the analysis.

The holes in the upper part of the hinge to be fixed to the car body are defined as fixed hinges in the analysis. Then, since the part will be connected to the door through the upper holes, the door's weight is defined on these holes. A force of 350 N was determined at 500 mm offset from the axes of the holes (Figure 4a). The analyses performed in this scenario caused very high deformation in the hinges, resulting in unrealistic results. For this reason, 350 N was applied to the upper part of the hinge through the holes where the door will be connected (Figure 4b). The force of 350 N simulates the weight of the door. With this analysis, the deformations occurring in the door were calculated.

(a)   (b)
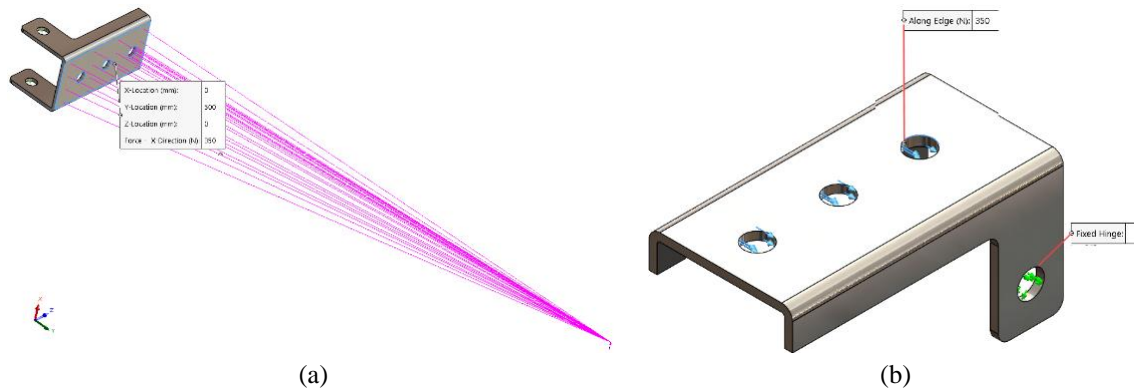
Figure 4. Determination of pin connection and load values of the hinge

First, the design's finite element (mesh) model was created (Figure 5a). Then, stress (Figure 5b), deformation (Figure 5c), and strain analyses (Figure 5d) were applied to the model. When the analysis results were evaluated, it was observed that the stress increased at the point where the upper part of the hinge was connected to the car body. Deformation analysis shows that the highest displacement occurs at the ends of the hinge. In addition, strain occurrences were also observed in the upper parts of the hinge.

(a)   (b)

(c)   (d)
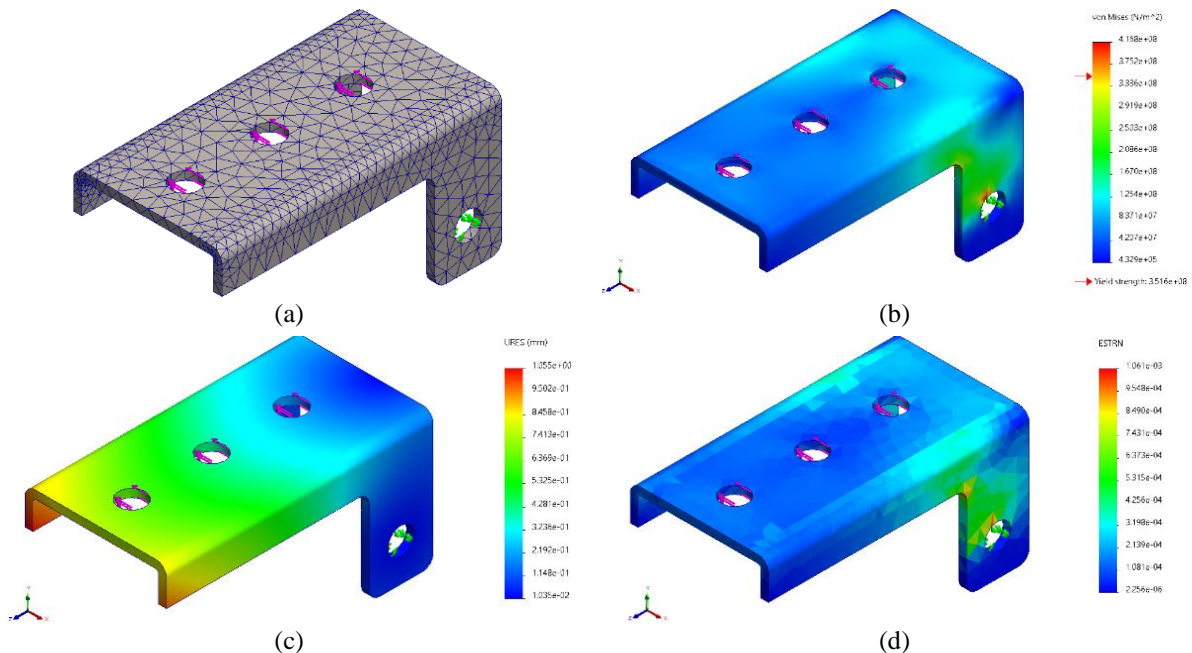
Figure 5. Analysis of hinge using finite element method

2.3. Topology Optimization

The increasingly evident effects of global warming have led to more significant consideration of environmental concerns in production [13]. These concerns have contributed to the widespread use of electric vehicles. Automotive manufacturers are researching to develop lighter vehicles to reduce fuel consumption. The production of lighter cars is possible through the development of lightweight components. Engineers use various structural optimization methods to reduce weight without reducing mechanical strength. Structural optimization methods ensure that automobile parts give the optimum result in size, weight, manufacturability, and cost.

Topology optimization is a structural optimization method used in many different fields. The basis of topology optimization is to find the optimum material distribution according to a structure's design and boundary constraints [14]. In this study, topology optimization was performed on the upper and lower parts of the hinge under predetermined load conditions. In the figure obtained from the analysis, the yellow-colored regions indicate the regions that should remain in the model, and the blue areas indicate the regions that can be removed (Figure 6).

(a)

(b)
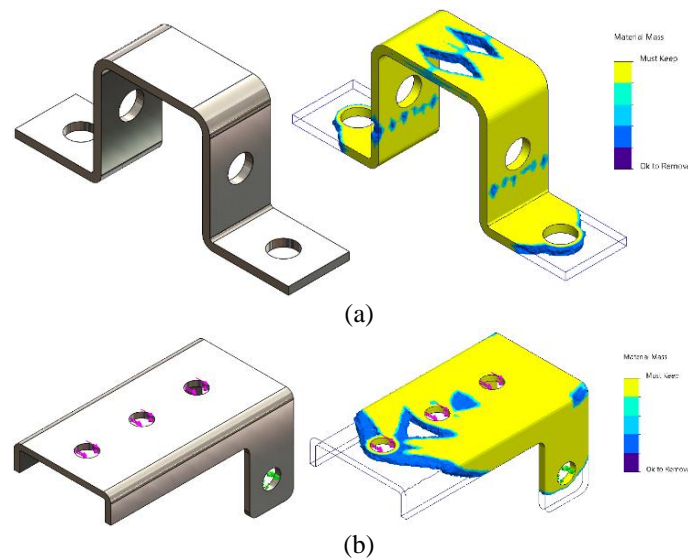
Figure 6. Topology optimization results: (a) Hinge lower part and (b) hinge upper part

Using the topology optimization results, the final model of the hinge design was developed. A parametric design study was carried out under static load conditions for the selected parameters of the developed model. Solidworks software Design Study module was used for the parametric design (Figure 7). Design constraints and objective functions were determined under static load conditions for the four parameters selected in the model. Then, the optimum design dimensions were calculated by analyzing 108 different design scenarios. The three-dimensional model of the determined optimum design is given in Figure 8.
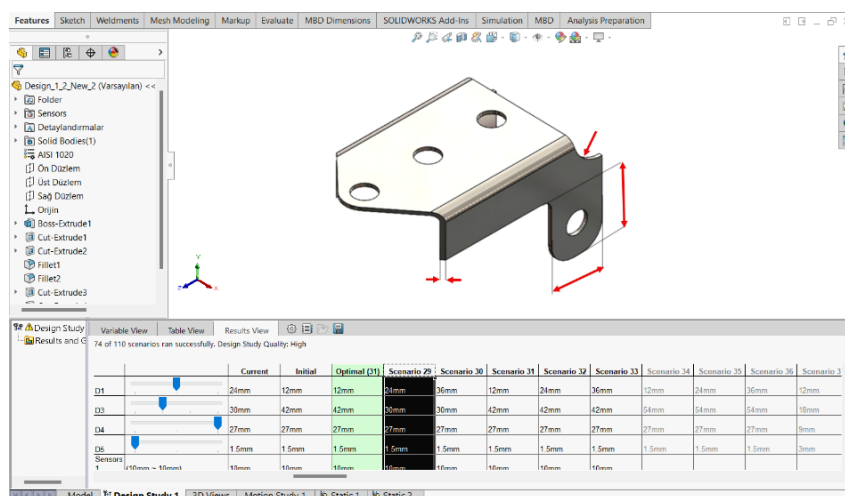
Figure 7. Determination of dimensions by parametric design method

(a) Lower part   (a) Upper part
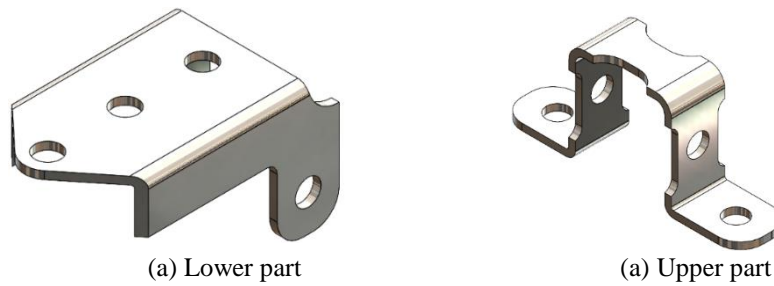
Figure 8. Optimized hinge design parts

2.4. Comparison of Models Using Numerical Analysis

Numerical static analyses were again performed to determine the effects of the developed design on the mechanical performance of the hinge and to compare it with the conventional design. The results of the analysis made it possible to evaluate the contribution of the developed design to the performance. The analysis results in Figures 9 and 10 show the effect of the optimized design on the stress and displacement values. As a result of the studies performed, the stress changes and displacement amounts in the conventional and optimized hinge designs under the same load conditions were calculated. The effect of the design developed by using these values on these criteria is shown in Table 1. The optimized design decreased the stress value in the lower part by approximately 13% while increasing it in the upper part by 20%. In addition, the optimized design decreased the displacement value in the lower part by approximately 7% while increasing it in the upper part by 5%.
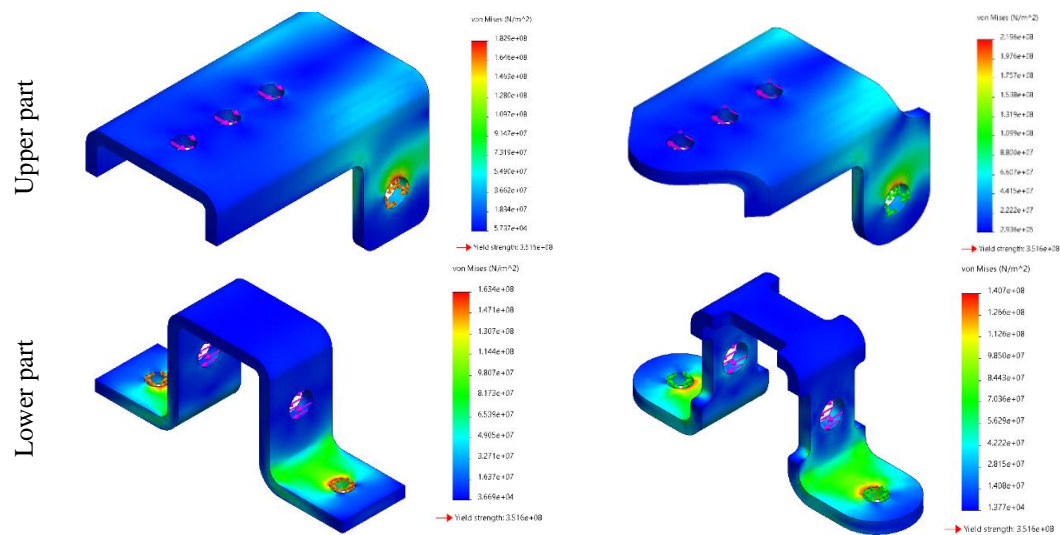
Figure 9. Results of stress analysis
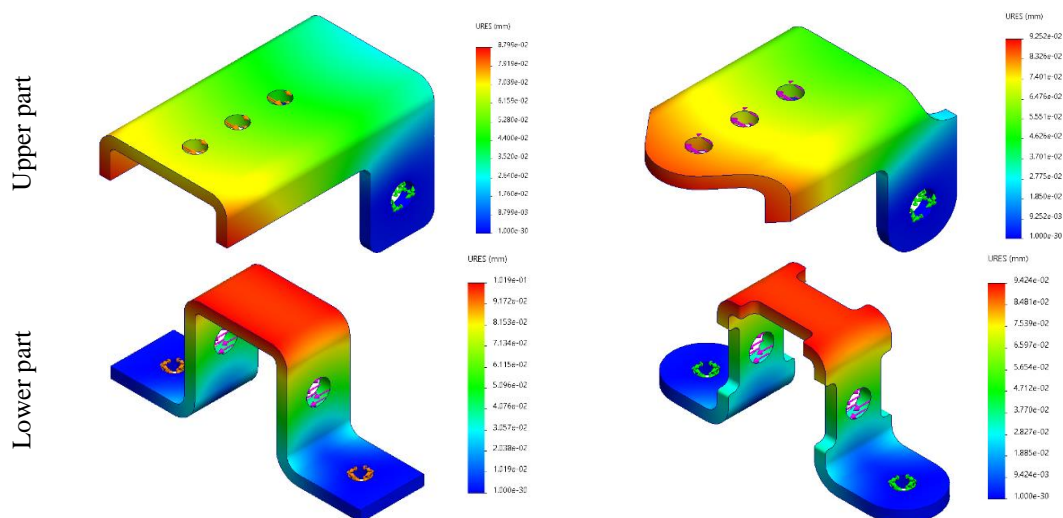
Figure 10. Results of displacement analysis

Table 1. Comparison of analysis results

	Stress (MPa)		Displacement (mm)	
	Lower part	Upper part	Lower part	Upper part
Conventional design	163.41	182.87	0.102	0.088
Optimized design	140.70	219.56	0.094	0.093
Change (%)	-13.89	+20.06	-7.84	+5.68

2.5. Prototype Samples Production

The prototype sample production of this new hinge design will be carried out with a three-dimensional manufacturing technique, and the manufacturability performance of the design will be evaluated. For this purpose, three-dimensional (3D) models of conventional and improved hinge prototypes were produced on a Creality Ender 3 S1 model 3D printer working with the melt deposition (FDM) technique (Figure 11). For this, the solid models of the hinges were converted into STL format. Then, they were transferred to Ultimaker Cura slicing software, and three-dimensional production parameters were determined. Then, the software g-codes were transferred to the three-dimensional printer, and production was realized. The production parameters are given in Table 2.
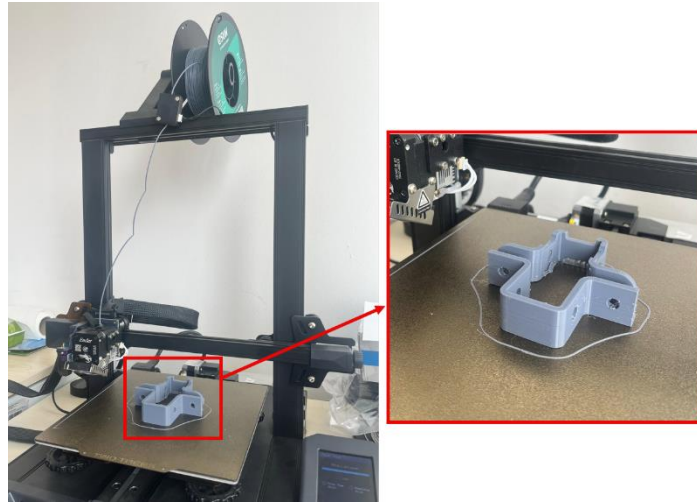
Figure 11. Three-dimensional printer production of hinge prototypes

Table 2. Three-dimensional printing parameters

Parameter Type	Value
Filament material	PLA
Filament diameter	1.75 mm
Layer thickness	0.2 mm
Nozzle diameter	0.4 mm
Nozzle temperature	210º
Bad temperature	60º
Infill density	100%
Infill pattern	Lines
Printing speed	50 m/s

3. RESULTS

The samples produced with the three-dimensional production technique are given in Figure 12. After prototype production, the weights of the samples were measured and compared. Thus, it is aimed to determine how much weight savings the developed design provides in the conventional hinge model. The developed design reduced the hinge weight by 24.43% (Table 3). Although the specimens are made of plastic material, weight reduction is achieved in terms of volume, and approximately the same amount of savings can be achieved by producing models made of metal material.

(a) Conventional design model

(b) Optimized design model
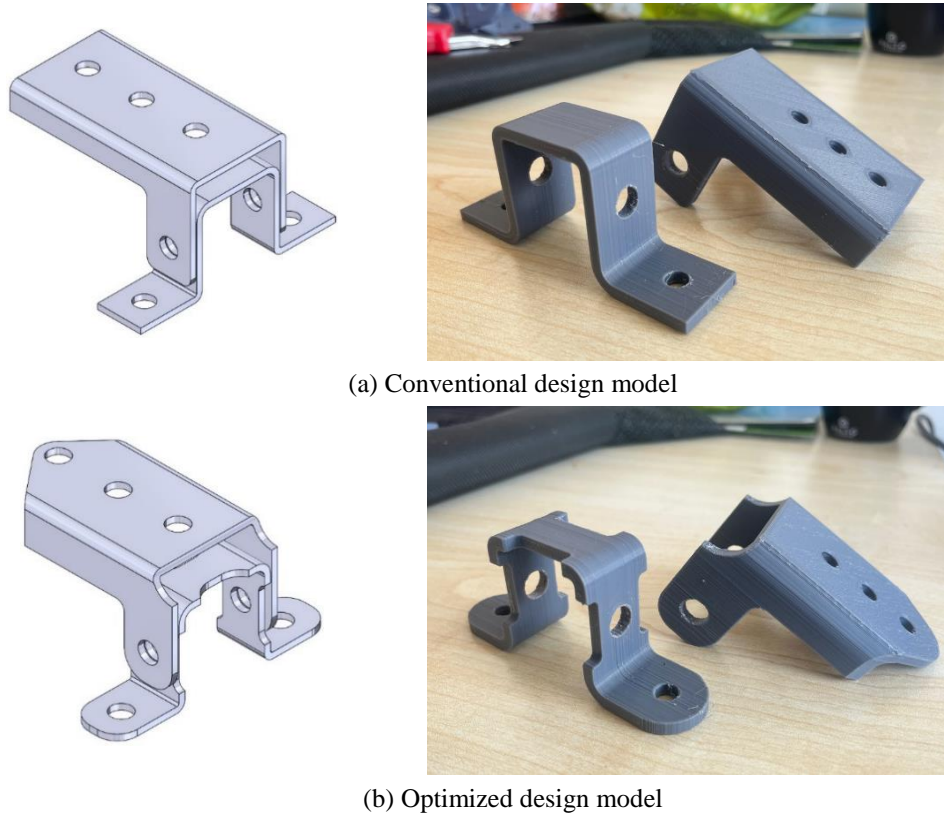
Figure 12. Model and prototype views of conventional and improved design

Table 3. Model weights

	Conventional Design	Optimized Design	Total Weight
Upper part	31.40 gr	18.17 gr	49.57 gr
Lower part	24.30 gr	13.16 gr	37.46 gr
		Change	12.11 gr

4. CONCLUSION

This study developed a new hinge for electric vehicles using the topology optimization method without compromising mechanical strength. Since lightweight is the primary criterion in this study, cost increase and mechanical strength increase within certain limits are considered negligible. In topology optimization, the design variables are defined as the regions where unloading is desired, stress is defined as the constraint, and weight is defined as the optimization objective. As a result of the topology optimization, a new hinge design was realized. The new hinge design was lightened by 24.43% compared to the conventional design.

Topology optimization and parametric design results have shown that it is possible to produce a lighter hinge. In addition, more robust components can be produced by using metal or carbon-doped filaments in three-dimensional printers that have more advanced features and can be produced at high temperatures. This will make it possible to produce more complex automobile components.

Acknowledgments

References

[1]   G. Sun, G. Li, S. Zhou, H. Li, S. Hou, and Q. Li, "Crashworthiness design of vehicle by using multiobjective

robust optimization," *Struct. Multidiscip. Optim.*, vol. 44, no. 1, pp. 99–110, 2011, doi: 10.1007/s00158-010-0601-z.

[2] J. Zhang, L. Ning, Y. Hao, and T. Sang, "Topology optimization for crashworthiness and structural design of a battery electric vehicle," *Int. J. Crashworthiness*, vol. 26, no. 6, pp. 651–660, Nov. 2021, doi: 10.1080/13588265.2020.1766644.

[3] E. Zurnacı and H. K. Özdemir, "Investigation of the compressive strength, energy absorption properties and deformation modes of the reinforced core cell produced by the FDM method," *Gazi J. Eng. Sci.*, vol. 9, no. 1, pp. 1–11, Apr. 2023, doi: 10.30855/gmbd.0705047.

[4] A. Wazeer, A. Das, C. Abeykoon, A. Sinha, and A. Karmakar, "Composites for electric vehicles and automotive sector: A review," *Green Energy Intell. Transp.*, vol. 2, no. 1, p. 100043, Feb. 2023, doi: 10.1016/j.geits.2022.100043.

[5] S. Kobayashi, S. Plotkin, and S. K. Ribeiro, "Energy efficiency technologies for road vehicles," *Energy Effic.*, vol. 2, no. 2, pp. 125–137, May 2009, doi: 10.1007/s12053-008-9037-3.

[6] A. Cimprich, K. Sadayappan, and S. B. Young, "Lightweighting electric vehicles: Scoping review of life cycle assessments," *J. Clean. Prod.*, vol. 433, art. no. 139692, Dec. 2023, doi: 10.1016/j.jclepro.2023.139692.

[7] A. Parvanta, *Smart Weight-Loss Program for Electric Vehicle*, Continental AG.

[8] E. I. Albak, "Optimum design of brake pedal using topology optimization method intended for weight reduction on the formula SAE car," *Uluslararası Muhendis. Arastirma ve Gelistirme Derg.*, pp. 328–334, Jan. 2019, doi: 10.29137/umagd.467057.

[9] M. M. Topaç, M. Karaca, B. Aksoy, U. Deryal, and L. Bilal, "Lightweight design of a rear axle connection bracket for a heavy commercial vehicle by using topology optimisation: A case study," *Mechanics*, vol. 26, no. 1, pp. 64–72, Feb. 2020, doi: 10.5755/j01.mech.26.1.23141.

[10] M. Cavazzuti, A. Baldini, E. Bertocchi, D. Costi, E. Torricelli, and P. Moruzzi, "High performance automotive chassis design: A topology optimization based approach," *Struct. Multidiscip. Optim.*, vol. 44, no. 1, pp. 45–56, Jul. 2011, doi: 10.1007/s00158-010-0578-7.

[11] R. Petrov, P. Cvetkov, A. Maksimov, and O. Klyavin, "On the problem of optimizing the door hinge of electro car by generative design methods," *Int. J. Mech.*, vol. 14, Jul. 2020, doi: 10.46300/9104.2020.14.15.

[12] F. H. Dar, J. R. Meakin, and R. M. Aspden, "Statistical methods in finite element analysis," *J. Biomech.*, vol. 35, no. 9, pp. 1155–1161, Sep. 2002, doi: 10.1016/S0021-9290(02)00085-4.

[13] P. M. Vitousek, "Beyond global warming: Ecology and global change," *Ecology*, vol. 75, no. 7, pp. 1861–1876, Oct. 1994, doi: 10.2307/1941591.

[14] M. P. Bendsøe and O. Sigmund, "Topology optimization by distribution of isotropic material," in *Topology Optimization*, Berlin, Heidelberg: Springer Berlin Heidelberg, 2004, pp. 1–69, doi: 10.1007/978-3-662-05086-6_1.

Electric Motor Attachment Point Target Setting for a HVAC

Murat Isik[1]

[1]Valeo Thermal Systems, Bursa, Türkiye
Corresponding author: Murat Isik (e-mail: murat.isik@valeo.com)

Abstract

This study addresses the challenge of minimizing vibrations transmitted through heating, ventilation, and air conditioning (HVAC) systems, particularly those caused by imbalance-related orders in a brushless direct current (BLDC) motor used in electric vehicles. These vibrations are primarily transmitted through the motor's mounting points on the HVAC structure, leading to tactile vibrations at critical locations, such as the steering wheel, during operation. The BLDC motor, operating within a speed range of 800 to 5000 rpm, generates centrifugal forces due to unbalanced components, which amplify vibrations at specific motor speeds. Investigation revealed that the dynamic stiffness of the HVAC attachment points was comparable to the stiffness of the motor's vibration isolation material, resulting in inadequate vibration decoupling and poor filtration performance. To address these issues, impact testing was conducted to identify weak dynamic stiffness points in the HVAC structure. Based on the findings, structural reinforcements were implemented by designing and applying 3D-printed brackets to improve the stiffness of the attachment points. These modifications increased the dynamic stiffness to exceed the required threshold of being at least ten times higher than the isolation material's stiffness, leading to improved vibration isolation. Additionally, unbalance in the blower unit was corrected, further reducing vibrations transmitted to tactile points. Post-rework testing demonstrated significant improvements, including enhanced filtration performance of the motor's isolation material and reduced steering wheel vibrations during AC operation. This research highlights the importance of optimizing the dynamic stiffness of HVAC components and incorporating modal design criteria to ensure effective vibration isolation. The findings emphasize the role of early-phase structural reinforcement and design optimization in improving the noise, vibration, and harshness (NVH) performance and overall comfort in electric vehicles.

Keywords: Dynamic stiffness, Attachment point, Design criteria, Target setting, NVH

Addressing Acoustic Comfort in Electrified Vehicles: High-Frequency Noise Mitigation in BLDC Motors

Murat Isik[1]

[1]Valeo Thermal Systems, Bursa, Türkiye
Corresponding author: Murat Isik (e-mail: murat.isik@valeo.com)

Abstract

The electrification trends in the automotive industry are introducing new challenges in noise, vibration, and harshness (NVH) management. Among these, high-frequency noise issues have become a critical concern, particularly in components of BLDC (Brushless DC) motors. This study addresses a specific high-frequency noise problem associated with the sidewalls of a thin-walled, stamped cover component used in a BLDC motor. The issue emerged as a customer complaint regarding noise levels exceeding promised thresholds, significantly impacting acoustic comfort. Root cause analysis revealed that the interaction between the cover sidewalls and the heatsink was the primary source of the problem. Weak frictional interfaces and insufficient stiffness in the sidewall structure contributed to low damping of modal behavior, particularly around 4 kHz. Experimental rework on the interface between the sidewalls and the heatsink achieved a noise reduction of 5–6 dB(A), confirming the critical role of structural stiffness in mitigating the issue. This paper emphasizes the importance of improving stiffness in the sidewall design to address the modal and damping weaknesses. The findings underline the broader implications of NVH challenges in automotive electrification, where integration dynamics and component-level compliance often diverge. By resolving these issues, this study contributes to enhancing the acoustic comfort of both passengers and pedestrians in electric vehicles, aligning with the evolving standards of automotive NVH performance.

Keywords: Integration, Brushless direct current motor, Noise and vibration, High frequency

Resolving NVH Challenges in BLDC HVAC Systems

Murat Isik[1]

[1]Valeo Thermal Systems, Bursa, Türkiye
Corresponding author: Murat Isik (e-mail: murat.isik@valeo.com)

Abstract

Electrification trends in the automotive industry have intensified noise, vibration, and harshness (NVH) challenges, particularly in heating, ventilation, and air conditioning (HVAC) systems, which play a critical role in passenger comfort and regulatory compliance. This research investigates two prominent acoustic issues in brushless direct current (BLDC) blower systems: low-frequency vibration and high-frequency whistle noise. Both problems arise from unique root causes yet significantly impact system performance, durabilit and customer satisfaction. Low-frequency vibration, linked to modal mismatches, was analyzed using advanced techniques such as operational deflection shapes analysis, fast fourier transform (FFT) and order analysis. These methods pinpointed the system's first modal frequency at 33.667 Hz and the decoupling resonance frequency above 42 Hz. The resultant bending motions in the BLDC fan induced undesirable pumping actions, leading to noise levels of 28.08 decibels at 62.5 Hz. Implementing a locking mechanism to stabilize the decoupling interface achieved a 12-decibel noise reduction, bringing levels down to 16.3 decibels. Additionally, a high-frequency whistle noise near 6 kHz was identified and attributed to leakage within the blower system. Root cause analysis and targeted improvements successfully eliminated this issue, enhancing the system's acoustic profile. These findings underscore the necessity of addressing NVH issues at both component and system integration levels to meet evolving electrification standards. By combining modal and leakage-focused solutions, this study provides a roadmap for optimizing HVAC system design to reduce mechanical instabilities and enhance acoustic performance. The research highlights the importance of comprehensive NVH assessments to ensure both operational reliability and customer satisfaction in electrified vehicle platforms.

Keywords: Low frequency, High frequency, Whistle noise, Noise and vibration, Leakage

In-Depth Analysis of Web and API Vulnerabilities: OWASP Top 10 and Security Strategies

Simge Sengul[1], Durmus Ozkan Sahin[1]

[1]Department of Computer Engineering, Ondokuz Mayis University, Samsun, Türkiye
Corresponding author: Simge Sengul (e-mail: wsimgesen@gmail.com)

Abstract

This study examines web and API vulnerabilities within the scope of the current open web application security project (OWASP) Top 10 list published by OWASP. The study details the most common vulnerabilities encountered in modern software development processes, explaining the possible effects and exploitation methods of these vulnerabilities. In addition, effective protection strategies that can be used to prevent such vulnerabilities and ensure system security are included. The aim of the study is to contribute to software developers, system administrators and security experts to adopt a security-focused approach by increasing their awareness of vulnerabilities.

Keywords: Owasp top 10, Web security, API vulnerabilities, Security strategies, Cybersecurity risks

1. INTRODUCTION

Web security is increasingly important in the digital world. Today, many individuals and organizations communicate, share data, and conduct commercial transactions via digital platforms. However, this situation also brings with it various security threats [1, 2]. According to studies in the literature, it is known that cyber-attacks cause not only financial losses but also reputational damage and data breaches. In particular, attacks such as distributed denial of service (DDoS) [3], phishing [4, 5], and application programming interface (API) exploits [6] in recent years have revealed how serious the consequences of neglecting web security can be. In this context, the importance of security has become critical for both individuals and institutions.

Web security is a fundamental requirement to not only prevent threats but also to ensure that all interactions on digital platforms occur safely and smoothly [7]. Web applications and APIs play a critical role in transporting data and performing transactions. However, these systems have many vulnerabilities that can be targeted by cyber attackers [7]. These vulnerabilities can be exploited by malicious individuals and lead to serious security breaches. Therefore, raising awareness about current threats and defence methods in the field of web security is of great importance, especially for software developers, system administrators and security experts. Failure to take security measures can not only cause financial losses for organizations, but also compromise users' personal data.

Today, security vulnerabilities are not only caused by technical deficiencies, but also by human errors caused by malicious individuals. Social engineering techniques such as phishing attacks compromise users' security and provide access to critical information [8, 9]. Being aware of such attacks and increasing security awareness play a role as important as technical defences. In addition, API security is also of particular importance. APIs, which are widely used to exchange data between web and mobile applications, create attractive targets for attackers when they are misconfigured or inadequately protected. In this context, API security has become an integral part of web security, and robust measures must be taken to close security gaps. In this study, threats to web security will be addressed and strategies that can be implemented to increase security will be discussed.

1.1. Related Works

In [10], security vulnerabilities disclosed by OWASP in 2013 are discussed. The article provides an in-depth analysis of the security flaws encountered in user authentication and session management processes in web applications, explaining the causes of these vulnerabilities and their potential impacts. Additionally, it presents secure user authentication methods and robust session management strategies, offering solutions and implementation recommendations to prevent such security flaws.

In [11], the difficulties of ensuring the security of information-based systems that provide services today are discussed. It is emphasized that basic security principles such as confidentiality, integrity and availability are of great importance, especially in areas such as database management systems, mobile vehicle networks, cloud computing and the Internet of Things. These principles must be protected in order for systems to operate healthily and provide uninterrupted service to their users. The article includes the security problems of each system and solution techniques for these problems, and also discusses the threats that internet users are exposed to and solution suggestions against these threats.

In [12], researcher conducted to increase the security of web applications are presented. With the widespread use of the Internet, the security of web applications containing sensitive information has become important. In the study, vulnerabilities in web applications were examined and how the integrity of web applications could be compromised in case of exploitation of these vulnerabilities was discussed. In addition, security solutions to prevent these vulnerabilities were investigated and in line with the obtained results, a unique system that protects the integrity of web applications was developed. This system detects the web application whose integrity was compromised as a result of an attack or unauthorized operation, automatically restores the integrity and generates warnings about the attacks. The developed system was presented under the name WUBKU and licensed under GPL version 3 and opened to everyone.

In [13], web-based automated testing tools are compared based on 20 different criteria. It examines which tools can provide more effective results in software testing processes. The study aims to provide guidance in the selection of these tools and to make a comprehensive evaluation based on different criteria.

In [14], a benchmark is proposed to evaluate and compare static analysis tools with respect to their capability to detect vulnerabilities in web applications. The proposed benchmark tests five free PHP static analysis tools on 134 WordPress plugins, considering real-world development scenarios with different budgets and goals. The experimental results reveal that the most effective solution varies depending on the application scenario and the type of vulnerability detected, emphasizing that these factors are critical for the design of the benchmark and future static analysis tools.

In [15], different types of technologies used to analyse security vulnerabilities in web applications and web services are discussed, along with the advantages and disadvantages of each type. The article emphasizes that web application security testing requires careful thought and planning due to the immature state of the tools and the industry. It is noted that selecting the right tools involves several stages, considering factors such as the development environment, business needs, and the complexity of the application. This analysis at Foundstone was done in collaboration with major banks and telecommunications companies worldwide.

In [16], it is discussed that the rapid development phases and extremely short delivery times of web applications make it difficult to eliminate security vulnerabilities. It is examined how software testing techniques, especially fault injection and runtime monitoring, can be applied to web applications. The proposed mechanisms are implemented on web application vulnerability and error scanner (WAVES), a black-box testing framework used for automatic web application security assessment. WAVES is tested in real-world scenarios and compared with other tools.

In [17], it is emphasized that the services provided by the Internet have an important place at every level of society, but at the same time, they bring many security risks. Attackers carry out various attacks by targeting web pages and online services. Although there are theoretical studies in the literature on cyber-attacks against web services, studies on the detection and technical analysis of these attacks are limited. In the study, a real attack example made by hacking a web page was examined and analysed in detail.

1.2. Motivation and Contributions

When the current literature is examined, it is seen that studies on web and API security generally address the vulnerabilities within the scope of OWASP Top 10 at a theoretical level, but practically applicable protection strategies and current attack scenarios in the real world are not sufficiently examined. This deficiency creates a significant gap in terms of security practices and defence mechanisms, and the main purpose of this study is to fill this gap and develop practical solution suggestions by going beyond theoretical knowledge. The main points that distinguish this study from other studies can be summarized as follows:

- Current Approach: Provides a comprehensive analysis of the vulnerabilities in the OWASP Top 10 list in a holistic manner in the context of web and API, both theoretically and practically.

- Focus on Protection Strategies: Unlike many studies in the literature, it offers concrete suggestions not only about what the vulnerabilities are, but also how these vulnerabilities can be prevented.
- Real Attack Examples: It includes important cyber-attacks that have occurred in recent years and emphasizes the practical effects and importance of these vulnerabilities.
- Dynamic Structure: The study is designed to be open to expansion when the OWASP Top 10 2025 update is published and is a resource that can be updated with future developments.

With these contributions, the study aims to increase awareness of web and API security and pioneer solution-oriented approaches in both academic and practical applications.

1.3. Organizations

The remaining parts of the study are summarized as follows: Section 2 explores the OWASP Top 10 risks in web security, providing a detailed overview of the most critical vulnerabilities. In Section 3, the real-world impacts of these risks are examined, highlighting their consequences on web applications and organizations. Section 4 focuses on general prevention strategies, offering practical solutions to mitigate web security threats. Finally, Section 5 concludes the paper by summarizing the findings and proposing directions for future research."

2. OWASP Top 10 in Web Security

This study aims to analyse OWASP Top 10 vulnerabilities and determine effective protection strategies against these vulnerabilities. The research was conducted based on current cybersecurity reports, academic publications, and OWASP's official documentation. During the study, the OWASP 2021 Top 10 vulnerability list was examined [18]. Figure 1 shows the evolution of the OWASP Top 10 list over the years in web application security. The 2021 version focuses on modern threats by combining some categories and adding new ones compared to the 2017 version. These changes once again show that security should be considered a key priority in software development processes [18].
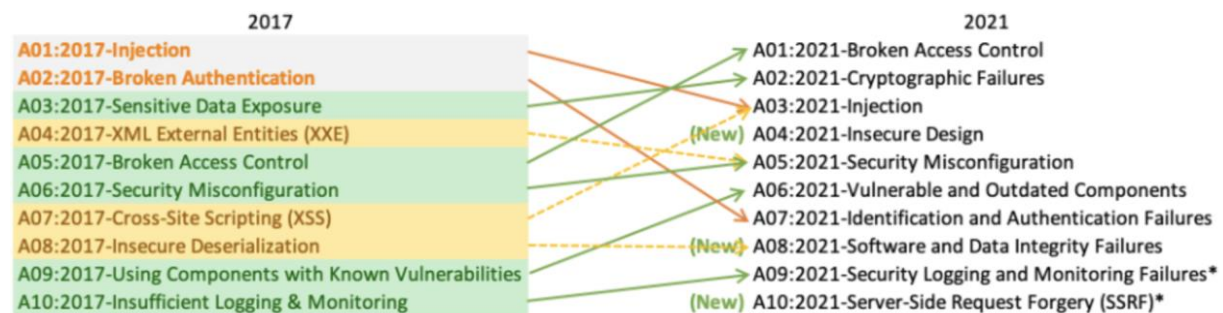
Figure 1. OWASP top 10 list: Yearly changes [18]

2.1. What is OWASP?

OWASP is a non-profit organization run by a global community of web and software security experts. Founded in 2001, OWASP works to promote secure software development processes, provide guidance to developers, and draw attention to application security risks [18]. OWASP provides application security standards, tools, training materials, and guides, primarily the OWASP Top 10. The OWASP Top 10 lists the most common and critical security vulnerabilities in web and API applications, identifying priority areas to focus on in software development processes. This list is updated regularly as the nature of cyber threats changes and is an essential resource for software security professionals [18].

The open source tools and guides provided by OWASP enable both individuals and organizations to increase security awareness on topics such as secure coding, vulnerability analysis, and risk management. For this reason, OWASP is considered an indispensable guide in the software security ecosystem.

2.2. Vulnerabilities

In this section, the vulnerabilities in the OWASP top 10 list will be discussed.

2.2.1. Broken Access Control (BAC)

BAC refers to security vulnerabilities that occur when an application fails to properly manage users' access rights. When access control mechanisms are not implemented correctly, attackers can perform unauthorized actions, access confidential information, or manipulate other users' data [1, 9]. This vulnerability can occur both horizontally (accessing resources of other users with the same privilege level) and vertically (unauthorized access to higher privilege levels). BAC is a key component of application security. Properly designed and implemented access control mechanisms are critical to ensuring the security of user data and systems. Examples of this vulnerability are as follows:

- Bypassing Authorization Checks (URL Manipulation): The user can access another user's profile by changing the URL, even though he/she should only be able to access her own profile. An example is given as follows:

  GET /user/12345/profile
  GET /user/67890/profile # Profile of unauthorized user

  If the application does not check the authorization of this request, the attacker can access other users' information.

- Unauthorized Access to Admin Functions: An attacker can gain access to administrative features despite being an unauthorized user. An example is given as follows:

  GET /admin/delete-user?user=12345

  If the system does not check for admin privileges, the attacker can use administrator functions.

- Direct Access to Hidden Areas: Some applications do not fully protect pages that are hidden from the menu. For example, an attacker could access the application's admin panel by:

  https://example.com/admin

  If authorization checks are not performed on these areas that are removed from the menu, the attacker can gain access.

- JSON Web Token (JWT) Manipulation: By changing the isAdmin flag in the JWT, an unauthorized user can introduce himself/herself as an administrator. An example is given as follows:

  { "username": "user", "isAdmin": false}
  { "username": "user", "isAdmin": true}

  The token in the first line can be changed as in the second line. If the system does not verify these changes, the attacker can perform operations on the system with admin authority.

2.2.2. Cryptographic Failures

Cryptographic Failures are incorrect practices related to encryption and protection of sensitive data. This vulnerability occurs when data is not securely encrypted or when weak encryption algorithms are used. Cryptography is an important security mechanism used to protect data from unauthorized access [18]. If data is not encrypted properly or encryption keys are not securely managed, this allows attackers to access or modify the data. Such errors typically occur in data transmission, databases, session management, and storage of encrypted information. Examples of this vulnerability are as follows:

- Use of Weak Encryption Algorithms: An application may use old and easy-to-break encryption algorithms. For example, old algorithms such as data encryption standard (DES) are now vulnerable to modern cryptographic attacks.
- Transmission of Data Without Encryption: Another common example of a cryptographic error is when sensitive data is transmitted unencrypted over an unsecured channel. If a web application sends users' credit card information over HTTP instead of HTTPS, that information is transmitted unencrypted over the network and can be intercepted by malicious actors.
- Insecure Storage of Encryption Keys: Encryption keys are critical information used in encryption and decryption operations. When keys are not stored properly, attackers can obtain these keys and decrypt data. If

an application stores encryption keys in plain text in a configuration file, a malicious attacker can obtain this file and use the keys to access the encrypted data.

- Missing or Improperly Implemented Two-Factor Authentication (2FA): 2FA is an important method to increase account security. However, poor implementation of these mechanisms due to cryptographic errors can lead to user accounts being compromised. An app transmits verification codes sent over SMS without encryption, and an attacker can obtain this code by intercepting the message.
- Weak Key Management: Failure to properly manage encryption keys can compromise the security of the system. This is especially true if old keys are still being used or keys are not periodically changed. If a banking application is still encrypting with a key pair that was created 10 years ago, attackers can eventually decipher that key and access old data.

2.2.3. Injection

Injection vulnerability refers to the ability of attackers to insert malicious data into an application, causing the application to disrupt its normal operation or produce unexpected results. Such vulnerabilities usually arise from data received from users being transmitted to a system, database, command line, or other external component without being sufficiently validated or sanitized. Attackers can exploit this gap to "inject" malicious code into the application system [1, 9]. Injection types are typically associated with web applications, but can also be applied to a variety of systems, such as APIs, databases, command lines, and even operating systems. Examples of this vulnerability are as follows:

- SQL Injection: SQL injection occurs when user data is incorrectly included in a SQL query. This vulnerability allows an attacker to exfiltrate or manipulate data by sending malicious SQL commands to the database. Suppose an application uses the following SQL query to authenticate username and password:

    *SELECT * FROM users WHERE username = 'user_input' AND password = 'password_input';*

    If the user enters a value like ' OR 1=1 -- in the user_input field, the query becomes as follows.

    *SELECT * FROM users WHERE username = '' OR 1=1 --' AND password = '';*

    This gives access to all users' information in the database, since 1=1 will always be true, and the password verification part is disabled by commenting it out with --.

- Command Injection: Command injection allows an attacker to execute external commands (such as operating system commands) by injecting them into the system. This type of attack is typically done by providing input data to the application to execute external commands. For example, suppose an application passes a file path it receives from the user to an operating system command.

    system("cat " + user_input);

    An attacker can enter the command file.txt; rm -rf /# in the user_input field: This command will display the contents of file.txt and then delete all system files.

- XPath Injection: XPath injection occurs when data obtained from the user is uncontrollably included in XPath expressions in queries to XML databases. Attackers can perform malicious operations on the database by manipulating XPath queries. Suppose an XML query is as follows:

    /search?query=<user_input>

    If an attacker enters ' OR '1'='1 in the user_input field, the XPath query will query */search?query=' OR '1'='1*. In this case, it can return all records in the database, allowing the attacker to obtain the information.

- Lightweight Directory Access Protocol (LDAP) Injection: LDAP injection means that LDAP queries are constructed with user input, which allows unauthorized individuals to access directory data.
- Operating System Command Injection: Operating system command injection occurs when an application that runs external commands does not properly validate user input. An attacker can run malicious commands on the operating system.

2.2.4. Insecure Design

Insecure Design is the disregard of the security requirements of the software at the initial design stage. This type of vulnerability is difficult to detect and fix the existence of security vulnerabilities after the application or system starts operating, since security is not considered at the initial stage of the system. Insecure design is caused by the lack of security measures in basic structural areas such as the architecture of the application, data flow, user management or interaction of the components [18]. As a result, vulnerabilities may not be noticed in the early stages, but a malicious attacker can target these vulnerabilities and cause significant security breaches in the system. Examples of this vulnerability are as follows:

- Storing Passwords in Plain Text: Many applications may store user passwords in plain text instead of securely encrypting them. This is due to the lack of secure encryption methods in the design phase. An application stores user passwords in plain text in a database and verifies this password on every login. In this case, an attacker who gains access to the database can easily obtain all user passwords.
- Mismanaged User Roles and Permissions: When user roles and permissions are not properly defined in the application design, users may access data or operations beyond their authorization. An application allows all users to access the admin panel, but all users can perform administrative operations, even though only certain roles should have this access. This is a vulnerability resulting from a design flaw.
- Poorly Defined API Security: APIs are the gateways to the outside world for an application. However, when API security is not adequately considered during the design phase, APIs can be vulnerable to external attacks. An application may not add authentication or authorization to API endpoints, allowing anyone to access those endpoints. This can lead to APIs being misused due to insecurity.
- Incorrect Authentication and Session Management: Failure to use secure authentication methods in application design or poor design in session management can lead to attackers gaining unauthorized access. An application does not manage users' login times and does not implement secure session management. In this case, an attacker can access data in the system by stealing others' active sessions.
- Weak Database Security: Databases are the heart of most applications. When weak database security is implemented during the design phase, attackers can gain access to the database and cause major security breaches. If encryption is not used in the database design, the database is exposed to the outside. In this case, attackers can access the database and take the entire database out.
- Incorrect Data Validation and Filtering: Data validation and filtering are fundamental components of application security. If the application does not adequately validate the data coming from the users, malicious data inputs can enter the system. A web application simply accepts the data entered by the user and processes the data sent out without filtering it. This leaves it open to attacks such as SQL injection and cross-site scripting (XSS).

2.2.5. Security Misconfiguration

Security Misconfiguration is when an application, server, database, or network infrastructure is not configured properly to ensure security. This is often caused by errors such as incorrect or incomplete configurations, failure to change default settings, or leaving unnecessary services open. Security misconfiguration can create vulnerabilities throughout the system, allowing attackers to access systems, exfiltrate data, or perform exploitation [18]. In general, the existence of this type of vulnerability occurs when developers, system administrators, and security experts do not take security measures into account during the configuration phases and do not follow best practices. Examples of this vulnerability are as follows:

- Using Default Passwords and Settings: Many applications use default passwords or configurations during installation. If these settings are not changed, attackers can easily gain access to the systems. A database management system or application server will continue to use the default username and password that came with the installation (for example: admin/admin). In this case, attackers can easily gain access to the system using the default information.
- Unnecessary Services and Ports Open: When unnecessary services and ports are left open on servers or application systems, attackers can target these vulnerabilities. Any unnecessary service or open port creates a potential attack surface. A web server should only be accessed via HTTP, but unnecessary services such as FTP or telnet can be left enabled. Attackers can infiltrate the system by targeting these services.
- Missing Security Headers: Many web applications use security headers to allow browsers and users to interact more securely. However, missing these headers can lead to a security vulnerability in an application. A web application's HTTP response headers may not include important security headers such as Strict-Transport-Security or Content-Security-Policy, allowing attackers to perform XSS or other attacks on the application.
- Incorrect Error Messages and Detailed Error Logs: An application may provide error messages that provide a lot of information about security vulnerabilities. This allows an attacker to understand the internals of the application and target potential weaknesses. A web application may provide detailed error messages to the user

(for example: "Database connection failed") after a failed login attempt. This may allow an attacker to learn about the database structure and search for vulnerabilities.

- Misconfigured Cloud Services: Cloud-based services and infrastructures can be quite vulnerable to security misconfigurations. Misconfigured cloud services can lead to data being exposed publicly or unauthorized access. A company stores database backups on cloud storage services but has not properly configured access permissions for that data. As a result, the data becomes publicly available and attackers can access it.
- Missing or Misconfigured Web Application Firewall: A web application firewall (WAF) is used to block threats to web applications. However, incorrect configuration of this firewall can allow malicious traffic to pass through. A web application's WAF is configured to block traffic from specific IP addresses only, but this IP filtering is done incorrectly, and attackers use this incorrect configuration to gain access to the system.

2.2.6. Vulnerable and Outdated Components

Vulnerable and Outdated Components refers to the presence of outdated or vulnerable components (libraries, frameworks, software, etc.) used in an application or system. These components can often be software that is not updated, old versions, or libraries with discovered vulnerabilities. Such components can seriously weaken the security level of the application and provide potential attack surfaces to attackers [18]. The outdated nature of the components used in a software can lead to the emergence of security vulnerabilities. In particular, neglecting software updates and patches makes it easier for cyber attackers to exploit these vulnerabilities. The use of such components can have serious negative effects on database security, user information, and overall application security. Examples of this vulnerability are as follows:

- Old and Outdated Libraries: Many web applications use third-party libraries and frameworks. However, older versions of these libraries may have security vulnerabilities. A web application uses an older version of jQuery (for example, 1.x). This version has vulnerabilities such as XSS. An attacker can use these vulnerabilities to run malicious code on the application.
- Old Software Versions: Many applications may rely on older versions of software, such as operating systems, database management systems, or web servers. Over time, this software stops receiving security updates, and vulnerabilities become exposed. A company's web application uses Apache HTTP Server version 2.2.x. This version has several vulnerabilities and no longer receives security updates. This allows attackers to target older versions of Apache.
- Old Framework and API Versions: Many software applications are developed using different frameworks and APIs. Older versions of the framework may have security vulnerabilities compared to newer versions. An application is using an older version of the Ruby on Rails framework (for example, 3.x). Known vulnerabilities in that version could allow the application to be compromised. Also, older versions of the framework may not comply with modern security standards.
- Vulnerable Plugins and Modules: Many applications gain functionality through plugins or modules. If these plugins are not updated, they can contain security vulnerabilities. If WordPress, a content management system (CMS), uses outdated plugins, these plugins can be targeted by attackers. For example, an outdated version of a plugin like Yoast SEO may have XSS vulnerabilities.
- Third Party Software with Vulnerabilities: Many applications provide functionality using third-party software and services. However, this software can also become outdated and have security vulnerabilities over time. If a payment processor uses an outdated version of its API and that version has a known SQL injection vulnerability, attackers may be able to access payment data.

2.2.7. Identification and Authentication Failures

Identification and Authentication Failures are security vulnerabilities that occur when a system does not correctly identify and verify the identities of its users. These types of errors occur when the system makes mistakes when identifying the user or verifying the identities of users. This can allow an attacker to gain unauthorized access to the system or to exploit the credentials of others [18]. Authentication is one of the basic security steps required for a user to log in to the system. This process, in which a user enters the correct credentials to access the system, also aims to prevent unauthorized access. Authentication errors occur when users use incorrect or weak authentication methods, leak or misuse their credentials. Examples of this vulnerability are as follows:

- Weak Password Policies: Many applications do not require strong user passwords. Weak passwords make it easier for attackers to take over accounts. A user signs up for a website with a simple password like "12345" and logs into the system using that password. Such weak passwords can be easily cracked using brute force attacks on the user account in question.

- Storing Passwords in Plain Text: Many applications store user passwords in plain text in a database instead of storing them securely. In this case, if an attacker gains access to the database, all user passwords can be easily obtained. A web application stores user passwords in plain text in a database instead of encrypting them. In a database breach, attackers can easily obtain and use these passwords.
- Many apps only authenticate with a username and password combination, but don't use additional security layers like two 2FAs. This makes accounts more prone to abuse. A banking app that accepts only a username and password as a login, doesn't require a second verification via an SMS verification code or mobile app as an additional layer of security. This allows attackers to easily access accounts if they get their hands on the username and password.
- Reuse of Personally Identifiable Information: Many users use the same credentials to log into multiple services. This means that a data breach on one platform can compromise a user's account on other platforms. A user uses the same password on an e-commerce site to access their bank account. A data breach on an e-commerce site can also give access to the attacker's bank account.
- Sending Authentication Data over Insecure Connections: Many applications send user information over insecure connections for authentication purposes. This can lead to malicious people intercepting the data. When a user logs in, they send their password and username over the HTTP protocol. Attackers can easily intercept this information by monitoring it on the network.

2.2.8. Software and Data Integrity Failures

Software and Data Integrity Failures are security vulnerabilities that occur as a result of the violation of the integrity of software and data. Such errors refer to situations where software or data is changed, deleted, or corrupted by malicious actors or faulty software updates, rather than by authorized persons. Software and data integrity is critical to ensuring the integrity and security of the system. Such errors allow an attacker to install malicious software (e.g., malware) or manipulate data [18]. Software and data integrity errors are often caused by insecure software updates, weak signing and verification mechanisms, incorrect configurations, and exploits. Such vulnerabilities allow attackers to install malware, manipulate data, and cause the system to operate unexpectedly. Examples of this vulnerability are as follows:

- Malware Injection: When users download a fake, malicious version of a software update or package, it compromises data integrity and threatens the security of the system. An attacker distributes a fake file that appears to be an update for popular software, thus injecting malware (for example, a virus or ransomware) onto a user's device. The user downloads and installs the update, believing it to be the correct one.
- Weak Software Signing: If software updates or files are not protected with a verifiable digital signature, the software could be tampered with or counterfeited. This poses a serious threat to the security of the software. An application releases software updates without verifying them with a digital signature. An attacker modifies the update and installs their own malware. Users install the update thinking they are downloading it safely.
- Weak Data Communication Security: If the data is not encrypted during data transmission or the encryption is weak, and the data is not transported securely, this can compromise the integrity of the software. A banking application does not use encryption to transmit user account information. By monitoring this data over the network, an attacker can access user information and modify the data.
- Unsafe Software Updates: Many applications get their updates from untrusted sources. This could allow a malicious actor to modify the update and distribute malware on the system. A web application downloads software updates from an untrusted server. An attacker gains access to the update server and delivers a malicious update package instead of the original software.
- Data Manipulation by Exploiting Security Vulnerabilities: When software does not perform strict enough data validation and integrity checks, it is possible for data to be altered or corrupted. This leads to insecure data processing. An online store does not sufficiently check the accuracy of the data sent by the user when processing payment information. By changing payment data, an attacker gets the product for free or manipulates the money transfer.

2.2.9. Security Logging and Monitoring Failures

Security Logging and Monitoring Failures are when a system fails to properly record or monitor security events. These types of failures make it difficult to detect and respond appropriately to potential security breaches and attacks. Security logs are critical for tracking and analyzing when, where, and how a system is attacked. Monitoring and logging failures allow cyberattacks to continue unnoticed and allow attackers to do more damage to the system [18]. These failures often occur due to insufficient logging, incorrectly configured logs, failure to record certain events, or inaccessibility of logs. Additionally, these failures make it easier for malicious attackers to enter a system and operate undetected for long periods of time. Examples of this vulnerability are as follows:

- Insufficient Event Logs: Many security events are not recorded in log files. This makes it difficult to track down network attacks, system errors, and anomalies in user behavior. A web application records only login and logout actions, but does not record activities where users perform significant actions (such as transferring funds or updating personal data). This prevents an attacker from detecting their actions once they have infiltrated the system.
- Neglect of Access Control and Log Files: Without access control and proper protection of log files, attackers can access these files and manipulate the logs. This creates the risk of deleting or changing the record of events. An organization allows public access to the system log. An attacker can access the log file and hide the vulnerability in the system. This disables monitoring and detection mechanisms.
- Weak Incident Monitoring and Alerting System: Some systems are not configured to send an alert when certain security events occur. This can allow an attack to proceed unnoticed. When a network attack (such as a DDoS attack) occurs, no automatic alert is sent to system administrators or the security team. Therefore, the attack proceeds undetected.
- Inadequate Storage of Logs: Logs may be deleted or not retained after a certain period of time. This prevents past security events from being reviewed and analyzed. Security logs are only retained for 30 days on a system. During this time, an attack occurs, but since the event history is older than 30 days, those events are lost and cannot be analyzed retrospectively.
- Logs Provide Insufficient or Misleading Data: Logs record only basic events, omitting security-critical information or presenting misleading data. This prevents vulnerabilities from being detected. An application records the time users log in to the system, but does not record important details such as IP address, type of device used, or browser information. This makes it difficult to understand how attackers entered the system.

2.2.10. Server-Side Request Forgery (SSRF)

SSRF is a type of cyber-attack in which an attacker sends a malicious request to a server, which allows the attacker to compromise the server. In an SSRF attack, the attacker causes the target server to send requests to systems outside of itself, such as devices on the local network or other servers on the Internet. This often bypasses the server's own security boundaries, allowing the attacker to perform malicious activities on the internal network or on external systems [18]. SSRF typically occurs when a web application processes URLs received from users. Such situations can allow the attacker to send requests to the application to a target of its own choosing. In this way, the system itself is used as a "tool" and the attacker can exploit the application's privileges and network access. Examples of this vulnerability are as follows:

- Internal Network Discovery: If a web application allows users to send HTTP requests to external URLs, an attacker can target services on the local network. This can help identify systems that are not exposed, such as a company's internal database or admin panel. If a user enters a URL such as "http://localhost:8080/admin," the application targets that request. If the application can send requests to internal systems, not just external systems, an attacker can gain access to the admin panel or other sensitive services on the local network.
- Cloud Metadata Service: Many cloud service providers offer a "metadata" service that provides information about the environment of the servers themselves. SSRF attacks can send requests to these services, allowing an attacker to access this sensitive data. In cloud platforms such as AWS, Google Cloud, or Azure, servers provide access to metadata information. By targeting this metadata service with SSRF requests from the server, an attacker can obtain, for example, AWS EC2 instance credentials or other sensitive data.
- Port Scanning: SSRF allows an attacker to scan the externally open ports of a server and discover what services are running on the network. This can be used to discover internal systems. An attacker can send requests to the ports where a web application is running by entering URLs such as "http://127.0.0.1:80". The application can detect other services on the internal network and send requests to those ports. This allows the attacker to discover open ports on internal systems.
- Sending Requests to Unwanted URLs: SSRF also allows attackers to send requests to unwanted URLs (malicious websites or fake systems). This can be used for malicious purposes such as data exfiltration or phishing attacks. The attacker sends a malicious URL to an HTTP endpoint on the target system, which is somehow redirected to an external resource and sends data to the attacker's malicious server. In this case, the attacker can steal information from the target system.

3. REAL-WORLD IMPACTS OF OWASP TOP 10 RISKS

This section delves into the real-world impacts of the vulnerabilities listed in the OWASP Top 10, providing an in-depth analysis of the potential damages and risks associated with each security flaw in web applications.

BAC leads to serious security vulnerabilities resulting from weak authorization controls in the system. Such vulnerabilities can allow attackers to gain unauthorized access to users' personal and sensitive information, which leads to data leaks and privacy violations. In addition, unauthorized access can lead to data manipulation, which means changing or deleting other people's data, which jeopardizes the reliability of the system. BAC allows attackers to take over the entire system by gaining access to administrative functions, which leads to loss of control of the entire system. Finally, such vulnerabilities can lead to the misuse or deletion of critical system components, which can lead to service interruption and operational disruptions [18].

Cryptographic failures can cause serious damage that can lead to serious security breaches. Weaknesses in encryption methods can allow attackers to obtain personal data, financial information, and credentials, which can lead to major data breaches. In addition, when users' credentials are stolen, fake identities can be created, which leads to identity theft. Attacks on payment information and bank accounts in particular can cause financial losses, as attackers can misuse this information to create major financial losses. Finally, a company's reputation can be seriously damaged by a security breach due to encryption errors. Such breaches undermine customer trust and negatively affect the company's reputation [18].

Injection vulnerabilities can cause serious damage to systems. Attackers can use these vulnerabilities to inject malicious commands, queries, or data, and as a result, gain full control over the database, system, or application. Such attacks can result in the seizure, modification, or deletion of sensitive data. For example, as a result of a SQL injection attack, an attacker can steal all user information in the database or corrupt the database. In addition, thanks to injection vulnerabilities, attackers can perform unauthorized system operations, which can damage critical system components. Such attacks can also disrupt the operation of the application and lead to service interruptions, which can cause financial losses and reputational damage. In short, injection vulnerabilities mean attacks that threaten the security of the system and seriously compromise the integrity and confidentiality of data [18].

Insecure Design can cause many damages by causing serious security vulnerabilities. Such vulnerabilities can cause users' personal data, financial information or confidential data to be compromised by attackers. In addition, user accounts and credentials can be stolen to perform fraudulent transactions or payment information can be misused. DoS attacks can be carried out on the system due to poor design, which can cause the application or service to become inaccessible or cause performance problems. Breaches due to security vulnerabilities damage the reputation of the business and undermine customer trust. Finally, poor security design can lead to financial losses, fraud and legal penalties, which cause businesses to suffer serious financial losses. Therefore, it is critical to prioritize security measures during the design phase [18].

Security Misconfiguration can lead to serious security vulnerabilities caused by incorrect configuration of the system. Incorrectly configured security settings can allow attackers to gain unauthorized access to the system and access critical data. In addition, leaving unnecessary services open or using weak passwords can become targets for potential attackers. These situations can lead to data breaches, system crashes, and service interruptions. Security misconfigurations can damage the reputation of businesses, cause loss of customer trust, and result in penal sanctions for non-compliance with legal regulations. Therefore, correct configuration of systems and continuous auditing are of great importance [18].

Vulnerable and Outdated Components pose serious security risks due to the use of outdated and vulnerable components. Such components can lead to the theft of user data and allow attackers to gain unauthorized access to systems. In addition, uncontrolled operations can be performed on web applications or APIs by exploiting vulnerabilities. Security breaches damage the reputation of companies and cause them to lose customer trust. In addition, data security breaches can result in legal penalties and sanctions imposed by regulatory bodies. Therefore, it is of great importance that the components used are up-to-date and secure [18].

Authentication and authorization errors can seriously weaken the security of a system and cause various damages. Such errors can allow attackers to gain unauthorized access to the system and cause user accounts to be compromised. In particular, weak passwords, lack of authentication or data breaches can compromise account security and lead to identity theft. Theft of personal information can lead to misuse of users' identities and data breaches. In addition, authentication vulnerabilities in financial systems carry the risk of causing serious financial losses by targeting bank accounts or payment systems. Such damages clearly show how important it is to protect system security with strong authentication mechanisms [18].

Software and Data Integrity Failures can lead to serious security risks and damage. Malware can cause data corruption or modification, leading to data loss and loss of trust. In addition, attackers can take over the entire

software through malware or updates and harm users. Such attacks can lead to theft of personal and financial data, theft of banking information, or identity theft. Security vulnerabilities damage the reputation of companies and cause loss of user trust. In addition, data breaches can expose companies to legal sanctions and cause heavy financial losses. This has serious consequences for both individuals and institutions [18].

Security Logging and Monitoring Failures can cause serious security vulnerabilities and cause great harm. Undetected attacks allow attackers to cover their tracks using logging errors and operate unnoticed for long periods of time, which can lead to serious data breaches and cyberattacks. Insufficient or incorrect logs can cause security teams to make incorrect analyses and misleading security decisions, which leads to continued weak defenses. If security incidents are not recorded or monitored, attacks cannot be detected and more damage occurs because they cannot be intervened in a timely manner. In addition, attackers can evade security reviews by manipulating log files, which can lead to theft or damage of user data. Such deficiencies seriously endanger the security of systems and users [18].

SSRF is a dangerous vulnerability where attackers trick a server into sending requests on their behalf, and it can cause serious damage. Such attacks allow attackers to access sensitive information, typically located on internal networks, obtain unauthorized data, and discover internal services. SSRF can compromise servers, allowing them to bypass authentication processes or exfiltrate sensitive information. Additionally, attackers can use SSRF to deploy malware, manipulate security configurations on the system, or perform chain attacks on other systems. Therefore, SSRF vulnerabilities pose a significant threat not only to the targeted server, but to the entire network and connected systems [18].

4. GENERAL PREVENTION STRATEGIES FOR WEB SECURITY

This section explores general prevention strategies for enhancing web security, offering a comprehensive overview of methods and best practices designed to mitigate vulnerabilities and protect web applications from potential threats.

A number of security measures should be implemented to protect against BAC. First, the user's authorizations should be verified for each request; this ensures that each user can only access the permitted resources. In addition, directory and URL protection mechanisms should be added to prevent direct access to confidential or critical resources. In this way, attackers are prevented from unauthorized access to sensitive data in the system. Token validation is a critical step to ensure the security of JWT or similar authentication methods, in particular, because secure session management can be provided through these methods. Regular tests and audits should be conducted to maintain the effectiveness of access control mechanisms, and vulnerabilities should be detected and closed. Finally, access to all resources should be denied by default, and only authorized users should be able to access these resources. Such measures greatly increase the security of access controls in the system [18].

To protect against cryptographic failures, it is very important to use strong and up-to-date encryption algorithms. Secure encryption methods such as AES-256 should be preferred for data encryption. In addition, web applications and APIs should provide secure data transmission using SSL/TLS methods such as the HTTPS protocol for secure data transmission. Safe storage of encryption keys is also a critical step; keys should be stored in environmental variables or hardware secure modules (HSM). In addition, the implementation of secure authentication methods such as 2FA is necessary to increase user security. In addition, periodic key changes should be made and old keys should be retired. These measures play a fundamental role in preventing cryptographic errors and developing secure data transmission and storage applications. Using the right cryptographic methods helps to ensure the security of data as well as prevent possible data breaches [18].

Injection is one of the most common and dangerous vulnerabilities for web applications and APIs. A number of security measures should be taken to protect against such vulnerabilities. First of all, prepared statements should always be used to prevent SQL injections. This method defines database queries independently of user data, thus preventing attackers from injecting malicious commands. In addition, any data coming from the user should be validated and sanitized before being used; this includes steps such as sanitizing special characters. User input should be secured using escape characters before being directly added to commands or database queries. When receiving data through APIs, secure and validated API methods should always be used, thus ensuring that data coming from outside is processed correctly. Finally, software security tests should be performed regularly and audits should be performed against potential vulnerabilities. These measures are critical to prevent injection vulnerabilities and ensure the security of the system [18].

To protect against Insecure Design vulnerabilities, security should be a priority from the beginning of the software development process. During the design phase, authentication and authorization requirements should be securely determined and managed. API security should also be designed correctly from the beginning; elements such as authentication, authorization, and data encryption should be considered. Encrypting and storing sensitive data securely is critical to preventing data breaches. In addition, data from the user should be correctly verified and sanitized when necessary. Insecure design can be prevented with these precautions from the beginning; a secure design plays an important role in ensuring the security of the software and helps prevent possible security breaches. Therefore, secure design practices are indispensable to maximize the security of the software [18].

To protect against security misconfiguration, it is critical that system configurations are done correctly and reviewed regularly. First, default passwords and configurations should definitely be changed after installation, as these settings can often be weak and predictable. Closing unnecessary services and ports on servers makes the system more secure against attacks. Using security headers in web applications completely increases the security level of the application. Error messages and logs should only contain necessary information and should not provide too much information to the user, thus not helping potential attackers. The security of cloud services should also be carefully configured and regularly audited. In addition, WAF should be configured correctly and effective protection should be provided to block malicious traffic. These measures are very important to prevent major threats that security misconfigurations can cause and should be reviewed continuously [18].

Weak and outdated components can seriously weaken the security of an application and invite various types of attacks. To prevent these risks, all software, libraries, APIs, and frameworks used by the application should be regularly updated and the latest security patches should be applied. In addition, old and unused components should be removed from the system and only secure, up-to-date versions should be used. Every component used should be inspected for security vulnerabilities and any identified vulnerabilities should be fixed immediately. Third-party software and services should also be subject to ongoing security audits as they may pose a security risk. Components should also be regularly evaluated for compliance with security best practices and industry standards. These measures play a critical role in ensuring software security and preventing potential vulnerabilities [18].

Identification and verification errors are one of the most critical security vulnerabilities of a system, and such errors can endanger a large number of users and companies, leading to serious financial and reputational damage. Strong password policies should be implemented to protect against such errors. Users should be encouraged to choose strong, complex passwords and to change their passwords at regular intervals. Passwords should be stored securely and encryption structures such as *bcrypt* or *scrypt* should be used in this process. The use of multi-factor authentication (MFA) increases security by allowing users to verify their identities not only with username and password, but also with additional security factors such as SMS, mobile application verification or biometric data. In addition, it is of great importance that authentication data is sent over secure connections such as HTTPS. Storing and managing user information securely ensures that authentication information is protected and not disclosed to third parties. These measures make authentication processes more secure and minimize potential risks [18].

Various protection methods should be implemented to prevent software and data integrity errors. Protecting software updates with digital signatures ensures that only secure and verified software is installed. Using strong encryption algorithms during data transmission ensures that data is transported securely. Software updates should only be obtained from secure sources and verification procedures must be performed. By adopting the secure software development life cycle (SDLC), security vulnerabilities can be prevented from the very beginning during software development stages. In addition, continuous monitoring and auditing should be carried out to protect the integrity of software and data, and suspicious activities should be detected quickly. Such measures prevent major security risks by creating the foundations of a secure and robust system [18].

Security Logging and Monitoring Failures pose a critical risk in cybersecurity, and eliminating such errors makes systems more secure. In order to prevent these risks, it is of great importance to store logs securely; log files should be kept in a secure environment and only authorized persons should be allowed to access them. Automatic monitoring and alert systems should be established that can instantly detect security events and send alerts to administrators. In addition, log files should be structured correctly to include all critical security events, and the details of the events should be recorded completely. Regularly examining logs helps detect potential threats, while long-term storage of events allows analysis of past attacks and better precautions to be taken. These precautions increase the security of systems and minimize potential threats [18].

Various measures should be taken to protect against SSRF attacks. Input validation and filtering ensure that URLs from the user are limited to a safe and specified list, ensuring that external requests go through a rigorous validation

process. Restricting access to local and internal resources includes ensuring that the server only accepts requests from external networks and blocking access to internal IPs such as "localhost" or "127.0.0.1". Especially in cloud environments, measures should be taken to restrict access to metadata services, preventing attackers from accessing these sensitive services. All data received from the user should be carefully cleaned and checked for malicious data. In addition, all external requests should be logged in detail and monitored regularly. Abnormal or suspicious requests can be quickly detected and intervened to minimize potential damage. These measures are critical to preventing the effects of SSRF attacks and improving system security [18].

5. CONCLUSION AND FUTURE WORKS

Examining the OWASP Top 10 vulnerabilities and developing protection strategies is a critical step to increase the security of modern web applications. In our study, each security vulnerability included in the OWASP Top 10 2021 version was examined in detail and effective protection methods that can be applied against these vulnerabilities were analysed. In addition, the effects of the vulnerabilities on both individual users and organizations were emphasized and supported by practical examples and solution strategies. This study serves as a guide for software developers, security experts and organizations. As part of future studies, it is aimed to examine the security vulnerabilities that will be included in the new list and develop protection strategies when the 2025 version of the OWASP Top 10 is announced. The 2025 update will reflect new types of vulnerabilities or changes in the priorities of existing vulnerabilities along with rapidly changing technological trends and cyber threats. In this context, in our study, a comparison will be made between the 2025 list and previous versions, and in-depth analyses will be performed on the evolution of vulnerabilities and how organizations can adapt to these changes. In addition, applicable protection methods and sector-based strategies for new vulnerabilities will be developed and integrated into the scope of the current study. This process will ensure that our work remains up-to-date and provides more effective solutions against future threats.

References

[1]   M. Aydos, C. Aldan, E. Coskun, and A. Soydan, "Security testing of web applications: A systematic mapping of the literature," *Journal of King Saud University-Computer and Information Sciences*, vol. 34, no. 9, pp. 6775–6792, 2022.

[2]   M. Bruno, P. Ibañez, T. Techera, D. Calegari, and G. Betarte, "Exploring the application of process mining techniques to improve web application security," in *2021 XLVII Latin American Computing Conference (CLEI)*, 2021, pp. 1–10.

[3]   A. Singh and B. B. Gupta, "Distributed denial-of-service (DDoS) attacks and defense mechanisms in various web-enabled computing platforms: issues, challenges, and future research directions," *Int. J. on Semantic Web and Information Systems (IJSWIS)*, vol. 18, no. 1, pp. 1–43, 2022.

[4]   E. Benavides, W. Fuertes, S. Sanchez, and M. Sanchez, "Classification of phishing attack solutions by employing deep learning techniques: A systematic literature review," in *Developments and Advances in Defense and Security: Proceedings of MICRADS 2019*, 2020, pp. 51–64.

[5]   L. M. Abdulrahman, S. H. Ahmed, Z. N. Rashid, Y. S. Jghef, T. M. Ghazi, and U. H. Jader, "Web phishing detection using web crawling, cloud infrastructure and deep learning framework," *Journal of Applied Science and Technology Trends*, vol. 4, no. 01, pp. 54–71, 2023.

[6]   A. S. Buyukkayhan, C. Gemicioglu, T. Lauinger, A. Oprea, W. Robertson, and E. Kirda, "What's in an exploit? An empirical analysis of reflected server XSS exploitation techniques," in *23rd International Symposium on Research in Attacks, Intrusions and Defenses (RAID 2020)*, 2020, pp. 107–120.

[7]   A. D. J. Domínguez-García, X. Limón, J. Ocharán-Hernández, and J. C. Pérez-Arriaga, "Security testing for web applications: A Systematic Literature Review," in *2023 11th International Conference in Software Engineering Research and Innovation (CONISOFT)*, 2023, pp. 82–91.

[8]   S. Venkatesha, K. R. Reddy, and B. R. Chandavarkar, "Social engineering attacks during the COVID-19 pandemic," *SN Comput. Sci.*, vol. 2, pp. 1–9, 2021.

[9]   W. Syafitri, Z. Shukur, U. Asma'Mokhtar, R. Sulaiman, and M. A. Ibrahim, "Social engineering attacks prevention: A systematic literature review," *IEEE Access*, vol. 10, pp. 39325–39343, 2022.

[10]   D. Aydogdu and M. Gunduz, "Web uygulamlama guvenligi aciklikari ve guvenlik cozumleri uzerine bir arastirma," *Uluslararasi Bilgi Guvenligi Muhendisligi Dergisi*, vol. 2, no. 1, pp. 1–7, 2016, doi: 10.18640/ubgmd.56836.

[11]   E. Iren and O. Can, "Bilgi sistemlerinde guncel guvenlik problemleri ve onerilen cozumler," *TUBAV Bilim Dergisi*, vol. 10, pp. 27–42, 2017.

[12]   D. Aydogdu, "Web uygulama saldirilarina yonelik otomatik tespit ve duzeltme sistemi," M.S. thesis, Gazi Univ., 2015.

[13]   R. Samli and Z. Orman, "A comprehensive overview of web-based automated testing tools," *Ileri*

Muhendislik Calismalari ve Teknolojileri Dergisi, vol. 4, no. 1, pp. 13–28, 2023.

[14]   P. Nunes, I. Medeiros, J. C. Fonseca, N. Neves, M. Correia, and M. Vieira, "Benchmarking static analysis tools for web security," *IEEE Trans. Reliab.*, vol. 67, no. 3, pp. 1159–1175, 2018, doi: 10.1109/TR.2018.2839339.

[15]   M. Curphey and R. Arawo, "Web application security assessment tools," *IEEE Security & Privacy*, vol. 4, no. 4, pp. 32–41, 2006.

[16]   Y. W. Huang, C. H. Tsai, T. P. Lin, S. K. Huang, D. T. Lee, and S. Y. Kuo, "A testing framework for web application security assessment," *Comput. Netw.*, vol. 48, no. 5, pp. 739–761, 2005.

[17]   I. Kara, "Web Hackleme(Hacking) Saldirilari," *Ejovoc (Electronic Journal of Vocational Colleges)*, vol. 10, pp. 1–6, 2020.

[18]   Owasp. [Online]. Available: https://owasp.org/www-project-top-ten/ (Last access date: December 5, 2024)

Impacts of Mining Activities on Ecosystem Services: Environmental and Socioeconomic Perspectives

Enes Ozgenc[1], Emine Keles Ozgenc[2], Gunay Yildiz Tore[3]

[1]Environmental Health Program, Vocational School of Health Services, Trakya University, Edirne, Türkiye
[2]Department of Landscape Architecture, Faculty of Architecture, Trakya University, 22030, Edirne, Türkiye
[3]Department of Environmental Engineering, Tekirdag Namik Kemal University, Tekirdağ, Türkiye
Corresponding author: Enes Ozgenc (e-mail: enesozgenc@trakya.edu.tr)

Abstract

Although mining activities are an important element of economic development worldwide, they are notable for their negative impacts on ecosystems, the environment, and society. In this study, an assessment has been made to reduce the mining sector's environmental, ecological, and social damage. In particular, environmental impacts caused by mining activities, such as habitat loss, biodiversity decline, pollution of water resources, air pollution, and soil degradation, were evaluated. It also focused on the social and economic consequences of these processes on local communities. The research assesses existing policies and technologies to promote sustainable mining practices and strengthen fair management approaches in the sector. The study examines green technology, waste management strategies, and innovative rehabilitation techniques to reduce environmental impacts. In addition, community engagement, fair sharing mechanisms, and assessment of long-term social impacts are considered critical elements in mitigating the negative impacts of mining activities on society. The findings provide a roadmap for better management of future mining practices. This roadmap recommends adopting a mining approach that balances environmental, social, and economic considerations in line with sustainable development goals. The study provides guidance for policymakers, industry leaders, and researchers and aims to contribute to a sustainable transformation of the mining sector. In this context, recommendations are presented for reshaping the sector in a more equitable, sustainable, and environmentally friendly framework at the global level.

Keywords: Biodiversity, Ecosystem, Habitat loss, Mining, Social impacts

1. INTRODUCTION

Mining has been recognized throughout history as one of the cornerstones of economic development and industrial progress [1]. In every period of human history, the extraction and utilization of natural resources have been key elements in increasing the welfare of societies and, with the industrial revolutions, technological progress [2]. Today, many sectors, such as industry, construction, energy, electronics, and transportation, rely on raw materials from mining [3]. For example, critical minerals such as lithium and cobalt are essential for renewable energy technologies and electric vehicle batteries [4]. However, traditional resources, such as coal and iron, remain the basic building blocks of industrial production. However, as great as the economic importance of mining activities is, their environmental and social impacts are just as deep and widespread [5].

The mining sector involves processes that directly damage ecosystems and the environment [6]. These processes result in impacts such as deforestation, habitat loss, soil degradation, pollution of water resources, and air pollution. This leads to a reduction in biodiversity in natural areas and negatively affects the functioning of ecosystems and ecosystem services. The damage caused by mining activities, especially to water resources and groundwater systems, has serious consequences on the environment and the social dimension. Local communities face water access challenges, health problems, and reduced livelihoods. In addition, air pollution and toxic wastes cause serious public health problems in residential areas close to mining sites [7].

Mining brings with it a complex set of issues that are not only environmental but also social. Often, these activities lead to the destruction of the habitats of local communities, forced migration, and cultural loss [8]. The inability of local populations to benefit fairly from economic returns and their exclusion from decision-making processes is a major problem that deepens social inequalities. Moreover, the mining sector, especially in developing countries, fails to mitigate environmental and social impacts due to weak governance and inadequate oversight mechanisms. This makes it difficult to achieve sustainable development goals at both local and global levels [5,9].

Today, global challenges such as climate change, depletion of natural resources, and increased environmental awareness further emphasize the need to adopt sustainable practices in the mining sector [10]. International frameworks such as the United Nations Sustainable Development Goals (SDGs) and the Paris Agreement have made the principles of environmental responsibility, social inclusion, and fair economic benefit sharing a priority for all sectors, including mining. In this context, approaches such as green mining, circular economy, and just transition provide an important foundation for building a sustainable mining future. Green mining aims to reduce the ecological footprint by using environmentally friendly technologies, while circular economy principles emphasize the efficient use of resources and the reuse of waste [11].

This study aims to address the mining sector's environmental, ecological, and social impacts and provide recommendations to promote sustainable and equitable practices in the sector. The study's main objectives include evaluating the environmental impacts of mining activities, assessing technological and policy innovations that can mitigate these impacts, and ensuring more active participation of local communities in the processes. In particular, the research seeks to answer the following questions: How can mining activities be aligned with global sustainability goals? Which technologies and policy mechanisms can most effectively minimize environmental and social damage? How can communities be ensured to benefit equitably from resources and participate in decision-making processes?

This study also aims to provide a roadmap for a transformation in the mining sector that prioritizes sustainability and social justice. The study's findings guide policymakers, industry leaders, and researchers, contributing to developing strategies that maximize the economic benefits of mining while minimizing its environmental and social harms. In this context, the study aims to be an important resource for reshaping the mining sector to be in line with global sustainable development goals and transform it into a more environmentally friendly, equitable, and responsible structure.

2. THE RELATIONSHIP BETWEEN MINING ACTIVITIES AND THE SERVICES PROVIDED BY ECOSYSTEMS

Mining activities have far-reaching, often permanent, and complex impacts on ecosystem services (Fig. 1). Ecosystem services are defined as the natural processes and functions that support human life and well-being and are generally divided into four main categories: Supporting, regulating, provisioning, and cultural services [12]. These services rely on ecosystems to sustain basic biological and physical processes [13], but mining interferes with these processes directly or indirectly, weakening the capacity and impairing the functionality of ecosystems [14]. Supporting services such as soil formation, nutrient cycling, and habitat provision are severely affected by mining activities. Open-cast mining operations, in particular, require the extraction of surface soils over large areas. This disrupts soil structure, increasing erosion, reducing soil fertility, and limiting the capacity of ecosystems to perform their basic functions. In addition, destroying natural areas around mining sites leads to habitat loss and ecosystem fragmentation, reducing biodiversity [15]. Habitat fragmentation can lead to habitat loss for many species, disruption of ecological interactions between species, and, in some cases, local extinctions [16].

Regarding regulatory services, mining damages natural processes that regulate water and air quality [17]. Open pits and underground mining activities often cause acid mine drainage, which leads to contamination of surrounding water sources. This chemical process leads to heavy metals and other toxic substances being introduced into water bodies, threatening aquatic ecosystems. In addition, pumping out groundwater resources during mining operations can lead to a lowering of the water table and a reduction in freshwater resources [18]. Air pollution is another major problem related to mining. Dust emissions, greenhouse gas emissions, and releasing toxic gases into the atmosphere undermine local and global climate regulation functions [19].

In the context of provisioning services, mining activities threaten the sustainable use of agricultural production, fisheries, and water resources. The expansion of mining sites leads to a reduction in agricultural land, while water resources contaminated by mining waste become insufficient to meet irrigation and drinking water needs. Especially in developing regions, this overlap between mining and agriculture poses critical food security challenges. In addition, fisheries and other aquaculture production are severely affected by water pollution from mining [20].

Though often less recognized, impacts on cultural services have profound and long-term social consequences for communities. Mining activities lead to the destruction of natural areas of aesthetic, spiritual, and cultural value, undermining their social and cultural functions for human communities [21]. Indigenous peoples and traditional communities, in particular, are disproportionately affected by the destruction of natural areas. Many of these areas are not only a source of livelihood for these communities but also part of their cultural identity, rituals, and

traditional wisdom [22]. For example, the destruction of a mountain considered sacred due to mining activity not only creates a physical loss but also deeply shakes the spiritual fabric and cultural ties of the community.

These impacts on ecosystem services disrupt environmental and biological balances and threaten human well-being, economic sustainability, and social justice. Ecosystem services should be seen as benefits provided by nature and vital elements supporting societies' economic, social, and cultural foundations [23, 24]. Therefore, protecting ecosystem services should be a priority in planning and managing mining activities. Sustainable mining practices should aim to protect the functioning of ecosystems and support the livelihoods and well-being of communities affected by mining [6]. Adopting innovative technologies, strong environmental regulations, and collaborating with local communities are key strategies for sustaining ecosystem services and minimizing mining activities' impacts [5, 25].
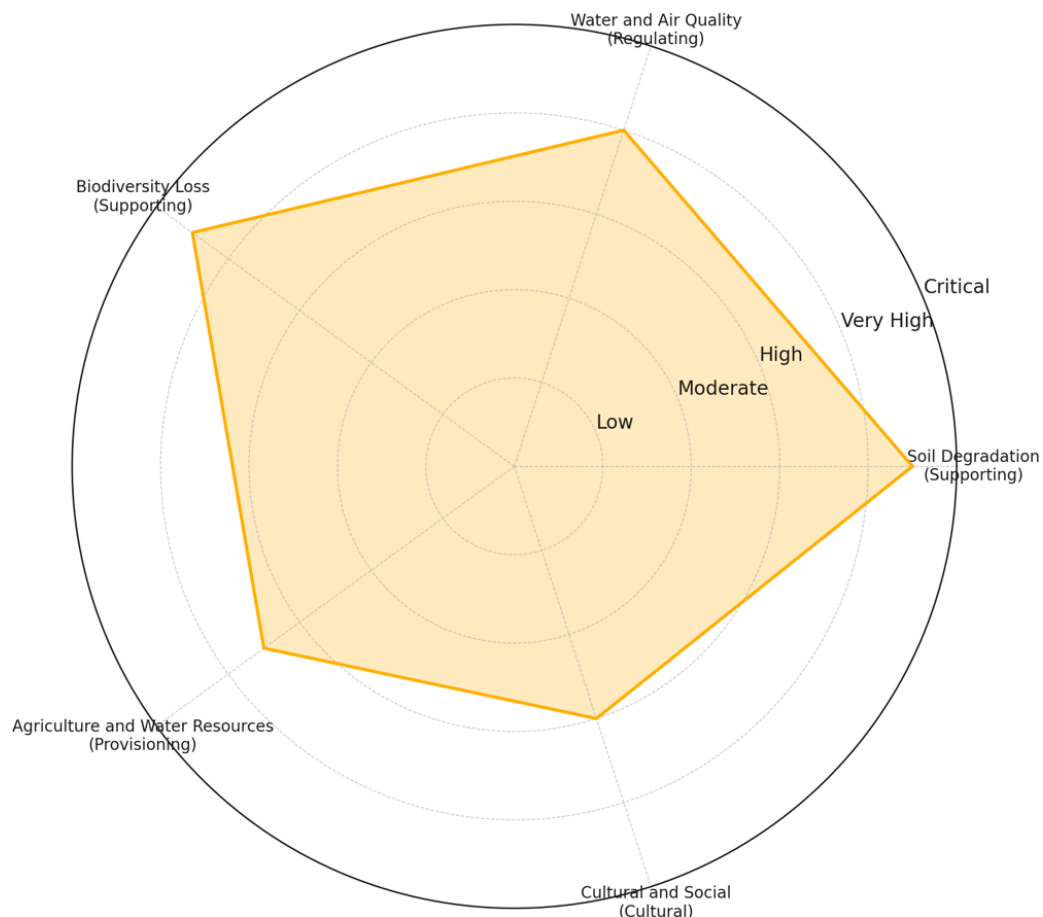
Figure 1. Impacts of mining activities on different ecosystem services

The radar plot reveals the impacts of mining activities on ecosystem services in different categories and severity levels. One of the highest impact levels is observed in the *Soil Degradation and Habitat Loss* category. This is particularly related to methods like open pit mining, which degrade soil over large areas and destroy habitats. Damage to these services, which support the basic functions of ecosystems, leads to irreversible losses in biodiversity and ecosystem resilience. The category *Impacts on Water and Air Quality* highlights the negative impacts of mining activities on regulating services. Acid mine drainage and introduction of other pollutants into water bodies threaten aquatic ecosystems, while dust and greenhouse gas emissions undermine air quality and climate regulation functions. Similarly, the category *Loss of Biodiversity* indicates that habitat destruction and pollution increase species extinction risk and disrupt the ecological balance. The category *Impacts on Agricultural and Water Resources* highlights the impacts of mining on food security and water resources. Loss of agricultural land and contaminated water resources threaten both ecosystem services and the livelihoods of communities dependent on these services. In the *Cultural and Social Impacts* category, the loss of aesthetic and cultural values of natural areas stands out. Mining weakens the social fabric, especially by negatively affecting local and indigenous communities' spiritual and cultural ties. Overall, the graph shows that the impacts of mining activities on ecosystem services are at high levels across a broad spectrum. These impacts are not only limited to environmental damage but also have complex consequences that threaten human well-being, livelihoods, and

cultural heritage. Therefore, the protection of ecosystem services and mitigation of these impacts should be prioritized in the planning of mining processes.

3. MINING-RELATED CONCERNS AND SOME SOLUTIONS WAY

3.1. How Can Mining Activities Be Harmonised with Global Sustainability Goals?

Harmonising mining activities with global sustainability goals is possible by integrating environmental, social and economic factors. In this context, adopting circular economy principles in mining processes is an important starting point. Recycling waste and reusing by-products contribute to minimising environmental impacts by reducing resource consumption. At the same time, international regulations, standards, and certification processes can be applied to minimise the environmental impact of mining activities. For example, promoting environmentally friendly methods such as 'Green Mining,' reducing carbon emissions, and promoting practices that protect biodiversity can align the sector with global sustainability goals [26, 27].

3.2. Which Technologies and Policy Mechanisms Can Most Effectively Minimize Environmental and Social Harm?

Innovative technologies and comprehensive policy mechanisms play a critical role in minimising environmental and social damage. The energy efficiency of equipment and processes used in mining operations can be improved to minimize environmental damage. For example, machinery powered by renewable energy sources can significantly reduce carbon emissions. In addition, water management technologies can minimise water consumption by making it possible to treat and reuse water used in mines. In terms of policies, strong environmental regulations, comprehensive impact assessment processes for mining permits, and post-mining rehabilitation plans can be made mandatory. On the social dimension, mechanisms to involve communities in decision-making and social impact assessments are effective policy tools [28, 29].

3.3. How Can Communities Be Ensured to Benefit Fairly from Resources and Participate in Decision-Making Processes?

Policies and practices that increase local participation and inclusiveness are necessary to ensure communities benefit equitably from mining activities and participate in decision-making processes. 'Stakeholder Engagement' models encourage open dialogue and cooperation between mining companies, local governments, and communities. These mechanisms provide transparent and fair processes that consider the needs and expectations of communities. At the same time, financial mechanisms such as a 'Natural Resource Fund' can be established to ensure equitable distribution of resource revenues. These funds guarantee investment in the basic needs of communities, such as health, education, and infrastructure. Special protection measures in accordance with international law should be taken to protect indigenous peoples' cultural and spiritual sites, and their traditional knowledge and experience should be integrated into decision-making processes. In this way, communities can reap economic benefits and sustainably protect their social and cultural assets [30, 31].

4. CONCLUSION

Although mining is one of the fundamental building blocks of economic development and industrial production, it has serious and extensive impacts on ecosystem services. These activities threaten many ecosystem services, such as soil degradation, habitat loss, reduced water and air quality, reduced biodiversity, and damage to agricultural resources. In addition, social concerns such as loss of cultural and social values, loss of livelihoods of local communities, and deepening social inequalities are among the impacts of mining. These impacts jeopardise environmental balance, human well-being, food security, and sustainable development goals. A multifaceted approach is required to manage mining activities sustainably, protect ecosystem services, and safeguard the rights of communities. Applying circular economy principles, adopting technological innovations, and implementing effective environmental regulations are critical in this process. In addition, involving communities affected by mining activities in decision-making processes, reducing social inequalities, and equitably distributing resource revenues should be among the cornerstones of sustainable mining practices. Future mining practices should be reshaped to protect ecosystem services and maximise social benefits. To this end, strong cooperation between stakeholders should be ensured, scientific research and innovation should be supported, and local communities' traditional knowledge and experience should be integrated into the processes. Furthermore, prioritising post-mining rehabilitation works is vital to support nature's regenerating capacity. In conclusion, the mining sector has the potential to contribute to a sustainable future by minimising both environmental and social impacts. However, decisive policies, strong regulations, and broad public participation are essential to achieve these goals. This study

presents the impacts of mining on ecosystem services while providing a roadmap for sustainable and equitable mining practices. With the right strategies and a comprehensive vision, the mining sector can achieve a positive transformation in terms of environmental responsibility and social welfare.

References

[1] M. Mohsin, Q. Zhu, S. Naseem, M. Sarfraz, and L. Ivascu, "Mining industry impact on environmental sustainability, economic growth, social interaction, and public health: an application of semi-quantitative mathematical approach," *Processes*, vol. 9, no. 6, art. no. 972, 2021.

[2] H. Jie, I. Khan, M. Alharthi, M. W. Zafar, and A. Saeed, "Sustainable energy policy, socio-economic development, and ecological footprint: The economic significance of natural resources, population growth, and industrial development," *Utilities Policy*, vol. 81, art. no. 101490, 2023.

[3] T. Igogo, K. Awuah-Offei, A. Newman, T. Lowder, and J. Engel-Cox, "Integrating renewable energy into mining operations: Opportunities, challenges, and enabling approaches," *Applied Energy*, vol. 300, art. no. 117375 2021.

[4] G. Calvo and A. Valero, "Strategic mineral resources: Availability and future estimations for the renewable energy sector," *Environmental Development*, vol. 41, art. no. 100640, 2022.

[5] O. Agboola, D. E. Babatunde, O. S. I. Fayomi, E. R. Sadiku, P. Popoola, L. Moropeng, A. Yahaya, and O. A. Mamudu, "A review on the impact of mining operation: Monitoring, assessment and management," *Results in Engineering*, vol. 8, art. no. 100181, 2020.

[6] A. S. Worlanyo and L. Jiangfeng, "Evaluating the environmental and economic impact of mining for post-mined land restoration and land-use: A review," *Journal of Environmental Management*, vol. 279, art. no. 111623, 2021.

[7] M. M. Dehkordi, Z. P. Nodeh, K. S. Dehkordi, R. R. Khorjestan, and M. Ghaffarzadeh, "Soil, air, and water pollution from mining and industrial activities: sources of pollution, environmental impacts, and prevention and control methods," *Results in Engineering*, art. no. 102729, 2024.

[8] X. T. Tiamgne, F. K. Kalaba, and V. R. Nyirenda, "Mining and socio-ecological systems: A systematic review of Sub-Saharan Africa," *Resources Policy*, vol. 78, art. no. 102947, 2022.

[9] A. O. Noah, P. Adhikari, B. O. Ogundele, and H. Yazdifar, "Corporate environmental accountability in Nigeria: an example of regulatory failure and regulatory capture," *Journal of Accounting in Emerging Economies*, vol. 11, no. 1, art. no. 70, 2021.

[10] R. Marimuthu, B. Sankaranarayanan, S. M. Ali, A. B. L. de Sousa Jabbour, and K. Karuppiah, "Assessment of key socio-economic and environmental challenges in the mining industry: Implications for resource policies in emerging economies," *Sustainable Production and Consumption*, vol. 27, art. no. 814, 2021.

[11] H. Hatayama, "The metals industry and the Sustainable Development Goals: The relationship explored based on SDG reporting," *Resources, Conservation and Recycling*, vol. 178, art. no. 106081, 2022.

[12] R. S. De Groot, M. A. Wilson, and R. M. Boumans, "A typology for the classification, description and valuation of ecosystem functions, goods and services," *Ecological Economics*, vol. 41, no. 3, art. no. 393, 2002.

[13] N. Rangel-Buitrago, D. González-Fernández, O. Defeo, W. Neal, and F. Galgani, "Rethinking plastic entrapment: Misconceptions and implications for ecosystem services in coastal habitats," *Marine Pollution Bulletin*, vol. 205, art. no. 116665, 2024.

[14] I. I. Kayode-Edwards and P. O. Isibor, "Arctic benthic habitat alterations," in *Arctic Marine Ecotoxicology*, Springer, 2024.

[15] R. Kumar, K. Mourya, S. Hota, M. Nogiya, S. Verma, V. Naik, S. Kumar, A. Barman, and R. Meena, "Impact of stone mining on soil properties," in *Ecological Impacts of Stone Mining: Assessment and Restoration of Soil, Water, Air and Flora*, Springer, 2024.

[16] D. A. Driscoll, D. Armenteras, A. F. Bennett, L. Brotons, M. F. Clarke, T. S. Doherty, A. Haslem, L. T. Kelly, C. F. Sato, and H. Sitters, "How fire interacts with habitat loss and fragmentation," *Biological Reviews*, vol. 96, no. 3, art. no. 976, 2021.

[17] J. Guo, K. Tu, L. Chou, Y. Zhang, S. Wei, X. Zhang, H. Yu, and W. Shi, "Deep mining of reported emerging contaminants in China's surface water in the past decade: Exposure, ecological effects and risk assessment," *Water Research*, vol. 243, art. no. 120318, 2023.

[18] B. Rezaie and A. Anderson, "Sustainable resolutions for environmental threat of the acid mine drainage," *Science of the Total Environment*, vol. 717, art. no. 137211, 2020.

[19] G. Richard and T. C. Odubo, "Impacts of artisanal mining on air quality and one health," in *Air Pollutants in the Context of One Health: Fundamentals, Sources, and Impacts*, Springer, 2024.

[20] M. C. Jackson, D. J. Woodford, and O. L. Weyl, "Linking key environmental stressors with the delivery of provisioning ecosystem services in the freshwaters of southern Africa," *Geo: Geography and Environment*, vol. 3, no. 2, art. no. e00026, 2016.

[21] J. E. Gordon, R. Crofts, M. Gray, and D. Tormey, "Including geoconservation in the management of protected and conserved areas matters for all of nature and people," *International Journal of Geoheritage and Parks*, vol. 9, no. 3, art. no. 323, 2021.

[22] S. N. Kativu and P. Oskarsson, "Our own law is making us beggars': Understanding experiences of governed, mine-side communities in Mutoko district, Zimbabwe," *The Extractive Industries and Society*, vol. 8, no. 4, art. no. 101003, 2021.

[23] N. Hariram, K. Mekha, V. Suganthan, and K. Sudhakar, "Sustainalism: An integrated socio-economic-environmental model to address sustainable development and sustainability," *Sustainability*, vol. 15, no. 13, art. no. 10682, 2023.

[24] R. Boldy, T. Santini, M. Annandale, P. D. Erskine, and L. J. Sonter, "Understanding the impacts of mining on ecosystem services through a systematic review," *The Extractive Industries and Society*, vol. 8, no. 1, art. no. 457, 2021.

[25] A. Kinyondo and C. Huggins, "State-led efforts to reduce environmental impacts of artisanal and small-scale mining in Tanzania: Implications for fulfilment of the sustainable development goals," *Environmental Science & Policy*, vol. 120, art. no. 157, 2021.

[26] L. Hamraoui, A. Bergani, M. Ettoumi, A. Aboulaich, Y. Taha, A. Khalil, C. M. Neculita, and M. Benzaazoua, "Towards a circular economy in the mining industry: Possible solutions for water recovery through advanced mineral tailings dewatering," *Minerals*, vol. 14, no. 3, art. no. 319, 2024.

[27] R. Balanay and A. Halog, "Charting policy directions for mining's sustainability with circular economy," *Recycling*, vol. 1, no. 2, art. no. 219, 2016.

[28] F. Sánchez and P. Hartlieb, "Innovation in the mining industry: Technological trends and a case study of the challenges of disruptive innovation," *Mining, Metallurgy & Exploration*, vol. 37, no. 5, art. no. 1385, 2020.

[29] M. T. Andersen and J. Noailly, "Environmental regulations in the mining sector and their effect on technological innovation, " 2022.

[30] H. Yu, I. Zahidi, C. M. Fai, D. Liang, and D. Ø. Madsen, "Elevating community well-being in mining areas: The proposal of the mining area sustainability index (MASI)," *Environmental Sciences Europe*, vol. 36, no. 1, art. no. 71, 2024.

[31] M. Conde and P. Le Billon, "Why do some communities resist mining projects while others do not?," *The Extractive Industries and Society*, vol. 4, no. 3, art. no. 681, 2017.

Criteria Affecting Online Shopping Site Selection and Choosing the Best Alternative

Zeynep Sude Cigdem[1], Nagihan Karsli[1], Emine Dadasoglu[1], Seyma Emec[1]

[1]Industrial Engineer, Erzurum Technical University, Erzurum, Türkiye
Corresponding author: Zeynep Sude Cigdem (e-mail: zeynepcigdemm700@gmail.com)

Abstract

The internet is widely used today as a significant communication tool, with one of the key applications being online shopping platforms, which enable consumers to purchase products through digital platforms instead of physical stores. Online shopping has profoundly changed consumer purchasing habits and impacted industry dynamics. This study aims to determine the ranking of the best online shopping sites by surveying 10 participants from different regions of Turkey who have made at least one online purchase. The goal is to identify which criteria consumers prioritize in online shopping and rank the best online shopping sites based on these criteria. In line with this objective, a survey was conducted to determine the relative importance of different criteria in online shopping, using the analytic hierarchy process (AHP) method. The results revealed that price is the most important criterion for consumers, followed by campaign opportunities and product variety. Based on the criterion weights obtained from the AHP method, a ranking of online shopping sites was made using the technique for order preference by similarity to ideal solution (TOPSIS) method. As a result, A1 online shopping site was identified as the most suitable alternative. The selection of A1 as the best alternative highlights the critical role that user experience, accessibility, reliability, and services provided by the site play in shaping consumer preferences. This study aims to provide an essential resource for evaluating and improving online shopping platforms, and the findings are expected to guide both academic research and the e-commerce sector. By scientifically analyzing the factors affecting the online shopping experience, this research seeks to enhance the understanding of consumer expectations and provide valuable data for improving the performance of online shopping sites.

Keywords: AHP, Online shopping site selection, Shopping criteria, TOPSIS

1. INTRODUCTION

The internet has become one of the most widespread communication tools in contemporary society. By providing access to unlimited information, it offers significant opportunities across various fields. This clearly underscores the fact that the internet is an indispensable communication channel in the modern age. Online shopping websites, in particular, stand out as one of the most notable examples of this expansive platform. Online shopping creates a virtual environment that overcomes the limitations of physical stores, offering a broad range of products to both buyers and sellers. Through user-friendly interfaces, immediate access to desired products is facilitated, while the availability of various alternatives enhances the ease of shopping.

The pandemic period has made in-person shopping more challenging. Social distancing rules and restrictions have directed many individuals towards online shopping platforms. During this time, virtual storefronts replaced the experiences offered by physical stores, and consumers were able to access a wide range of products across different categories with ease, thanks to user-friendly interfaces [1]. However, this convenience of online shopping has also brought about some challenges for consumers. In this context, the study has identified ten key criteria influencing the online shopping process, drawing from the opinions of three individuals who actively use online shopping sites and the relevant literature. These criteria have served as a foundation for improving customer experience and evaluating the performance of online shopping platforms. The identified criteria are: access to customer service (k1), shipping fee (k2), shipping speed (k3), price (k4), product evuluation (k5), campaisns (k6), product image (k7), website conveni ence (k8), product diversity (k9), and product technical information (k10). Based on these criteria, four websites were selected. In order to prevent unfair competition and adhere to privacy principles, these websites will be referred to as A1, A2, A3, and A4 in this report.

The objectives of this study are as follows:

- To determine the weights of the selected criteria—such as access to customer service, shipping cost, shipping speed, product images, product specifications, product reviews, product variety, website usability, promotions, and price based on surveys conducted with individuals living in different regions of Turkey who have made at least one online purchase. Additionally, to rank the best online shopping websites within the framework of these criteria.
- To contribute to the literature by introducing the identified criteria and expanding the scope of existing research in the field of online shopping, thereby facilitating academic contributions and enabling a deeper exploration of factors affecting the performance of online shopping websites and user satisfaction.
- To support the development of online shopping platforms by contributing to the sustainable growth of businesses in the e-commerce environment and to provide strategic recommendations for businesses by examining the factors influencing customer satisfaction.

In this study, a roadmap was developed to achieve the established objectives, and several steps were followed. First, a brainstorming session was conducted with a decision-making team consisting of three individuals to identify the criteria and online shopping websites. Subsequently, the analytic hierarchy process (AHP) method was used to assign weights to the criteria, and the technique for order preference by similarity to ideal solution (TOPSIS) method was applied to rank the online shopping site alternatives. While AHP determines the relative importance of the criteria, TOPSIS ranks the alternatives based on their proximity to the ideal solution. The study employed these two methods together to rank and analyze the best online shopping websites. Furthermore, the integration of AHP and TOPSIS methods in the evaluation of online shopping platforms presents a methodological innovation, enabling more comprehensive results through the simultaneous assessment of various criteria. This research, adopting an interdisciplinary approach, aims to contribute to the industry, develop customer-oriented strategies, and improve the user experience.

Within the scope of this study, considering the literature examining criterion selection under topics such as e-commerce and online shopping, the studies between the years (2010-2024) are as follows:

The impact of the COVID-19 pandemic on e-commerce was investigated. Using canonical correlation analysis, models and hypotheses were tested based on data collected during selected months (February, May, and October) of the pandemic from 16 e-commerce platforms. The results indicate a strong relationship between independent variables (e.g., technical specifications of websites, site access sources) and dependent variables (e.g., website usage statistics), consistent across different periods [1]. The AHP method was employed to evaluate the relative importance of criteria in selecting online shopping platforms from the perspective of young consumers. A total of 7 main criteria and 23 sub-criteria were analyzed [2]. The classification of 26 main criteria and 26 sub-criteria using the AHP method was examined, followed by an interpretation of the identified criteria [3]. Open-ended survey questions were administered to 182 participants. The responses were analyzed descriptively using the statistical package for the social sciences (SPSS) method, and the scope of the AHP method was weighted accordingly. The findings highlight the preferences influencing the selection of online shopping platforms [4]. Twenty criteria and 9 sales strategies, encompassing 5 main and 15 sub-criteria, were identified. While the criteria priorities were determined using the Analytic Network Process (ANP), the strategies were ranked comparatively using TOPSIS, ELECTRE, and VIKOR methods. The findings revealed that "product" is the most significant main criterion influencing e-commerce activities, with "product diversity" being the most critical sub-criterion [5]. A face-to-face survey was conducted with 418 students to identify the factors influencing usability and success in e-commerce platforms. The collected data were analyzed using the SPSS method [6]. Factors influencing customer satisfaction in e-commerce were explored from the perspectives of infrastructure/interface providers and managers. Based on expert opinions and feedback from seven industry experts, a total of 18 criteria (4 main and 14 sub-criteria) were evaluated using the AHP method [7]. The concept of e-commerce and the usability of active e-commerce sites in Turkey were discussed. This quantitative study collected data through surveys to assess the usability of these platforms [8]. The aim was to develop a scientifically grounded approach to understanding the purchasing decision process of e-commerce customers. The research also sought to transfer e-commerce practices between Austria and Turkey and contribute to the development of the field. In-depth interviews were conducted within the dimensions of affordability, usefulness, accessibility, speed, comfort, convenience, and cost. The data were analyzed statistically, and the findings were interpreted accordingly [9]. Virtual store websites were ranked according to customer preferences using the Fuzzy TOPSIS method. Four decision-makers evaluated the websites of four virtual stores based on criteria such as design, product diversity, customer service, and information richness. Uncertainties in the evaluation process were modeled using triangular fuzzy numbers [10]. Issues, disruptions, and successes associated with e-services in the retail, private, and public sectors were investigated. The findings highlight the importance of a well-executed e-transformation process for successful e-commerce activities. The results were evaluated using statistical analysis methods [11].

Our difference from the articles and thesis studies examined is that the survey results were applied to 10 people of different genders (5 girls and 5 boys) from different regions of the country, and AHP and TOPSIS methods were used together.

2. MATERIAL AND METHOD

Our study began as a preliminary investigation, with a brainstorming session involving three individuals who actively engage in online shopping, discussing the challenges they face during the online shopping process. During this brainstorming process, we aimed to identify the criteria that consumers pay attention to while shopping online, and based on this, determine which online shopping website is most preferred and the criteria influencing that preference.

In line with this objective, the methods applied in our study were determined by reviewing previous research on this topic in the literature. The gaps identified in the theses and articles examined were used to shape the approach. The reason for selecting these methods was to ensure the accuracy and validity of the survey results by subjecting them to two stages, thereby minimizing errors.

In our study, the data obtained from the surveys were used to calculate the criterion weights using the AHP method, while the ranking of alternatives was conducted using the TOPSIS method. Through this approach, we aim to determine which criteria are more important in online shopping and, based on this, identify which online shopping site is most preferred. The methods mentioned above are explained in detail below, along with the reasons for their selection.

2.1. AHP

AHP is a mathematical calculation method used for measurement and decision-making, and it is one of the most commonly used multi-criteria decision-making methods in the literature in recent years. The main reason for its popularity is its simplicity and ease of understanding for decision-makers. In literature review, studies [2] and [4] have used this method to calculate criterion weights. However, no findings were found indicating that these criterion weights had an impact on the selection or ranking of any shopping sites. The steps for applying the AHP method are as follows [12]:

Step 1: Creation of the Hierarchical Structure: The decision hierarchy is initially formed by setting the criteria at the middle level and the alternatives at the lowest level.

Step 2: Pairwise Comparison Matrices (A) and Determination of Priorities: The goal is to create an (n×n) pairwise comparison matrix to determine the relative importance of the criteria and sub-criteria among themselves (Equation 1).

$$\left[1 \cdots a_{n1} \vdots \ddots \vdots \frac{1}{a_{n1}} \cdots 1 \right] (n \times n) \tag{1}$$

The relative importance of each criterion in terms of its contribution to the objective and the superiority of each goal in terms of the criteria are determined using the pairwise comparison method, as presented in Table 1.

Table 1. Pairwise comparison scale

Numerical Value	Definition
1	Both elements are equally important, or there is no preference between them.
3	The first element is slightly more important or slightly more preferred than the second.
5	The first element is significantly more important or significantly more preferred.
7	The first element is much more important or much more preferred than the second.
9	The first element is extremely more important or extremely more preferred than the second.
2, 4, 6, 8	Intermediate values that represent compromises between the main levels of importance.

Step 3: Determination of the Eigenvector (Relative Importance Vector): After the pairwise comparison matrix is created, the next step is to calculate the eigenvector, which represents the importance of each element in the matrix relative to the others. The eigenvector of the matrix with dimensions n×1 is determined as follows:

$i = 1, 2, 3, \ldots\ldots, n$ and $j = 1, 2, 3, \ldots\ldots, n$ as follows;

$$b_{ij} = \frac{a_{ij}}{\sum\limits_{i=1}^{n} a_{ij}} \quad \text{and} \quad w_i = \frac{\sum\limits_{j}^{n} b_{ij}}{n} \tag{2}$$

To determine the percentage importance distribution of the criteria, it is necessary to calculate the column vectors $W = [w_i]_{nx1}$. The column vector W is obtained from the arithmetic average of the row elements of the matrix formed by the b_{ij} values specified in Equation (2).

2.2. TOPSIS Method

TOPSIS is a technique developed by Hwang and Yoon (1981) for multi-criteria decision-making (MCDM) processes. This method evaluates solution alternatives based on the concepts of the shortest distance to the positive-ideal solution and the farthest distance to the negative-ideal solution. The application process begins with the identification of decision criteria and alternatives. Then, the positive-ideal and negative-ideal solutions are defined. The distance of each alternative to these solutions is calculated, and the best alternative is selected. TOPSIS provides decision-makers with a systematic and objective approach to make decisions in complex situations, and it is widely used in various fields such as engineering, business, and environmental sciences [5]. The TOPSIS method consists of 8 steps, which are explained in detail below:

Step 1: Identification of goals and definition of evaluation criteria.

Step 2: Construction of the Decision Matrix (D): In the decision matrix, the alternatives $(a_1 \ldots a_n)$ are listed vertically, and the characteristics of each alternative according to each criterion $(y_{1k} \ldots y_{nk})$ are listed next to them. The creation of the decision matrix is given in Equation 3.

$$D = \begin{bmatrix} y_{11} & y_{12} & \cdots & y_{1k} \ y_{21} & y_{22} & \cdots & y_{2k} \cdots & \cdots & \cdots & \cdots y_{n1} & y_{n2} & \cdots & y_{nk} \end{bmatrix} \tag{3}$$

Step 3: Creation of the Normalized Decision Matrix (R): The matrix is normalized by taking the square root of the sum of the squares of the scores or characteristics corresponding to the criteria in the decision matrix. Equation 4 is used for the normalization process, and at the end of the normalization, the R matrix, as shown in Equation 5, is obtained.

$$r_{ij} = \frac{y_{ij}}{\sqrt{\sum\limits_{i=1}^{n} y_{ij}^2}}, \quad i = 1, 2, \ldots\ldots, n \text{ and } j = 1, 2, \ldots\ldots, k \tag{4}$$

$$R = \begin{bmatrix} r_{11} & r_{12} & \cdots & r_{1k} \ r_{21} & r_{22} & \cdots & r_{2k} \cdots & \cdots & \cdots & \cdots r_{n1} & r_{n2} & \cdots & r_{nk} \end{bmatrix} \tag{5}$$

Step 4: Creation of the Weighted Normalized Decision Matrix (V): Let W_i represent the weight of each jth criterion. The relative weight values of the elements in the normalized decision matrix are determined according to the importance assigned to the criteria, based on the objective.

$$W = \begin{bmatrix} w_{11} & w_{12} & \cdots & w_{1k} \ w_{21} & w_{22} & \cdots & w_{2k} \cdots & \cdots & \cdots & \cdots w_{n1} & w_{n2} & \cdots & w_{nk} \end{bmatrix} \tag{6}$$

Then, the elements in each column of the R matrix, as given in Equation 5, are multiplied by the corresponding W_{ij} : values, as shown in Equation 6, to construct the V matrix, as presented in Equation 7.

$$V = \begin{bmatrix} v_{11} & v_{12} & \cdots & v_{1k} \ v_{21} & v_{22} & \cdots & v_{2k} \cdots & \cdots & \cdots & \cdots v_{n1} & v_{n2} & \cdots & v_{nk} \end{bmatrix} \tag{7}$$

Step 5: Creation of the Ideal (A*) and Negative Ideal (A-) Solutions: The positive ideal solution consists of the best performance values from the weighted normalized decision matrix, while the negative ideal solution consists of the worst values. The ideal solutions can be calculated using Equations 8 and 9.

$$A^* = \left(max\ v_{ij} \mid j \in I \right), \left(min\ v_{ij} \mid j \in J \right) \tag{8}$$

$$A^- = \left(min\ v_{ij} \mid j \in I \right), \left(max\ v_{ij} \mid j \in J \right) \tag{9}$$

In both formulas, I represents the benefit (maximization) and J represents the cost (minimization) values. The values obtained from Equation 6 are expressed as $A^* = \{v1^*, v2^*, \ldots, vk^*\}$ and the values obtained from Equation 7 are expressed as $A^- = v_1^-, v_2^-, \ldots, v_k^-$.

Step 6: Calculation of Separation Measures: The separation (distance) between the alternatives is measured. The distance of each alternative from the positive-ideal solution is calculated as shown in Equation 10.

$$S_i^* = \sqrt{\sum_{j=1}^{n} (v_{ij} - v_j^*)^2} \tag{10}$$

Similarly, the distances from the negative-ideal solution are calculated as shown in Equation 11.

$$S_i^* = \sqrt{\sum_{j=1}^{n} (v_{ij} - v_j^-)^2} \tag{11}$$

Step 7: Calculation of Relative Closeness to the Ideal Solution: The relative closeness to the ideal solution (C_i^*) is calculated using Equation 12.

$$C_i^* = \frac{S_i^-}{S_i^- + S_i^*} \qquad 0 \le C_i^* \le 1 \tag{12}$$

Step 8: The alternatives are ranked according to their relative closeness to the ideal solution (C_i^*) values. The alternative with the maximum C_i^* value is selected.

With the successful completion of this project, we aim to pave the way for new studies in this field within the literature and ensure that regulations made in the online shopping sector, considering the criteria identified in this study, help maintain market vitality.

2.3. Case Study

A decision-making team of three experts specializing in online shopping has been formed. The team has identified 10 criteria that are crucial for customers when shopping online. These criteria and their explanations are as follows:

- Customer Service Access: The availability and accessibility of customer service channels (such as phone, email, social media) positively affect customer loyalty.
- Shipping Cost: The transportation cost required for the delivery of purchased products. Shipping cost is one of the factors that directly influence consumer behavior and purchasing decisions.
- Shipping Speed: The time elapsed from order placement to delivery. Delivery speed significantly impacts customer satisfaction and can enhance a company's competitive advantage.
- Product Images: Providing detailed visual materials that ensure the products meet customer expectations. Visual elements play a decisive role in the consumer's decision-making process.
- Product Technical Information: A critical factor influencing consumers' purchasing decisions in online shopping. This information ensures clear understanding of the product's features, uses, and performance. Detailed and accurate technical information increases customer trust and positively impacts potential purchase intentions.

- Product Reviews: Opinions and ratings from customers who have previously purchased the product provide valuable information and build trust for potential buyers. Product reviews influence brand perception and customer loyalty.
- Product Variety: Refers to the wide range of products offered by the shopping platform to meet consumer needs, including various models, colors, or functionalities. Diversification contributes to market share growth by providing more choices for customers.
- Website Usability: The user-friendly interface and easy navigation features of the website. Usability has a significant impact on customer experience and transaction continuity.
- Promotions: Discounts, special offers, or promotions presented to consumers. These incentives are designed to attract consumer interest, increase sales volume, and enhance brand awareness.
- Price: The financial value of the products offered to the customer. Pricing strategies are one of the most critical factors influencing the sustainability of businesses in competitive markets.

The hierarchical table for the criteria explained above is as follows:
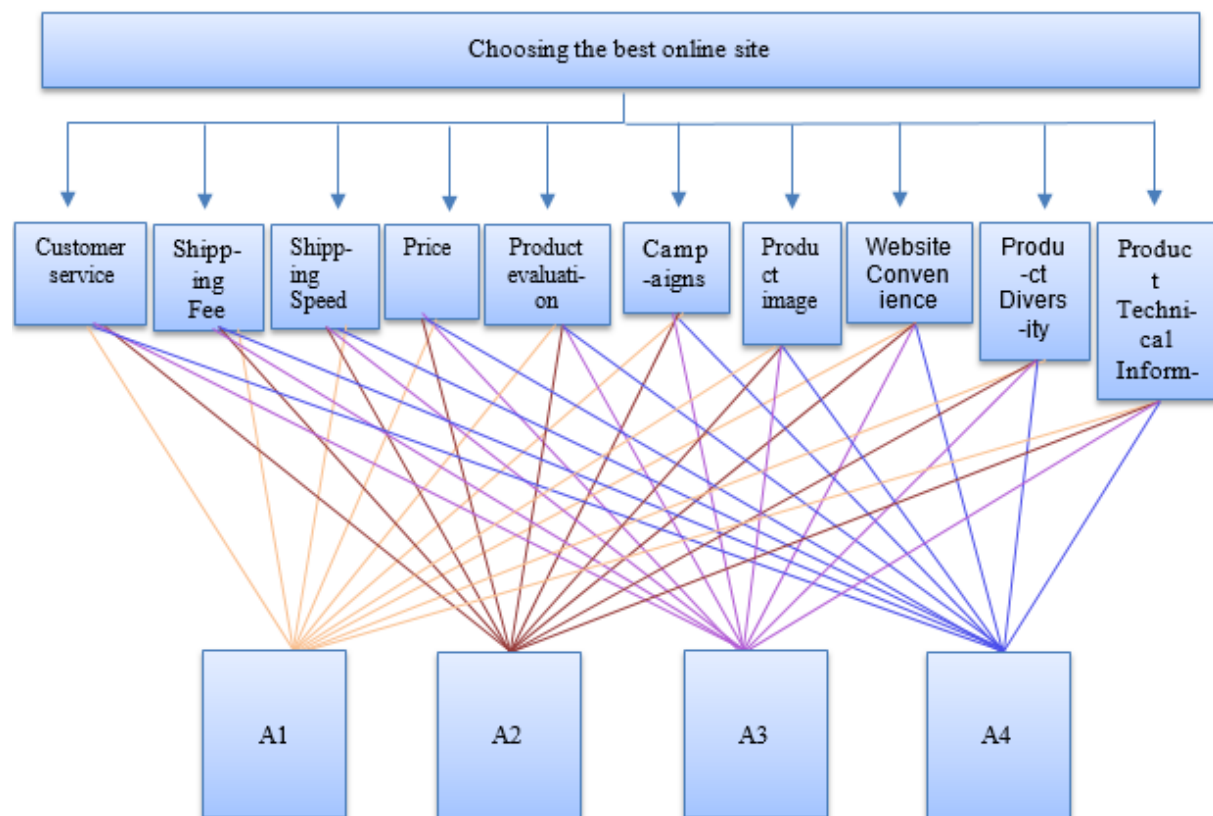
Figure 1. Decision problem hierarchy

The AHP method was used to calculate the weights of the identified criteria, followed by the application of the TOPSIS method to rank the online shopping site alternatives.

3. RESULTS

In this section, the 10 decision-makers evaluated the criteria using the Saaty scale, and pairwise comparison matrices were obtained. The obtained pairwise comparison matrices were then combined. Using the equations provided in Section 2, the values in the combined pairwise comparison matrix were normalized. The resulting normalized pairwise comparison matrix is presented in Table 2. Subsequently, the weights for each criterion were calculated and are presented in Table 3.

Based on these criterion weights. the priority ranking obtained through survey studies is as follows: price (k10) > campaign (k9) > product variety (k7) > website usability (k8) > product reviews (k6) > product technical information (k5) > product images (k4) > shipping speed (k3) > shipping cost (k2) > customer service accessibility (k1). This ranking indicates that. in the consumer shopping experience. price and campaign opportunities are the most decisive factors. followed by the importance of product variety and website usability. Additionally,

informational factors such as product reviews. technical details. and images play a supportive role in the decision-making process. Logistics and service-oriented factors. such as shipping speed. cost. and customer service accessibility. are of lower priority.

Table 2. Normalized pairwise comparison matrix

Criteria/Criteria	k1	k2	k3	k4	k5	k6	k7	k8	k9	k10
k1	0.016805	0.003563	0.004162	0.00424	0.006404	0.007665	0.009959	0.01268	0.016883	0.047541
k2	0.104706	0.022203	0.006365	0.005495	0.008055	0.008923	0.00989	0.012236	0.021534	0.057496
k3	0.093052	0.080387	0.023047	0.005797	0.007168	0.007681	0.010258	0.014738	0.016986	0.055413
k4	0.124447	0.126886	0.124853	0.031402	0.00744	0.011044	0.012655	0.014004	0.022744	0.06759
k5	0.09442	0.099173	0.115691	0.15187	0.035981	0.009931	0.011463	0.015423	0.022225	0.070529
k6	0.108155	0.122748	0.148021	0.140264	0.178726	0.049329	0.013668	0.017206	0.025853	0.078178
k7	0.111541	0.14839	0.148511	0.164028	0.207477	0.238564	0.066101	0.018441	0.029161	0.073599
k8	0.086928	0.119021	0.102568	0.147079	0.15302	0.188045	0.235106	0.065591	0.017914	0.065756
k9	0.112222	0.11625	0.152971	0.155666	0.182532	0.215127	0.255571	0.412825	0.112746	0.065994
k10	0.147723	0.161379	0.17381	0.194159	0.213197	0.263692	0.375329	0.416855	0.713955	0.417904

Table 3. Criterion weights and ranking of importance

Criteria	Criteria Weights
k1	0.01299
k2	0.02569
k3	0.031453
k4	0.054307
k5	0.062671
k6	0.088215
k7	0.120581
k8	0.118103
k9	0.17819
k10	0.3078

In the second phase of the study. the TOPSIS method was used to rank the alternatives. The equations from Step 2 were utilized during the application of the TOPSIS method. The 10 identified decision alternatives were evaluated under the established criteria. and comparison matrices were generated. The consolidated decision matrix was then normalized and presented in Table 4. Subsequently. the normalized matrix values were multiplied by the criterion weights determined by the AHP method to obtain the weighted decision matrix. which is shown in Table 5.

Table 4. Normalized decision matrix

	k1	k2	k3	k4	k5	k6	k7	k8	k9	k10
A1	0.303551	0.295805	0.292249	0.31821	0.298062	0.322789	0.289484	0.348961	0.288458	0.332346464
A2	0.24656	0.269146	0.250026	0.256456	0.254074	0.254129	0.274726	0.259575	0.329731	0.279508673
A3	0.265219	0.238231	0.256514	0.224071	0.23957	0.215829	0.200975	0.196007	0.161686	0.18364805
A4	0.18467	0.196819	0.20121	0.201263	0.208294	0.207253	0.234815	0.195456	0.220124	0.204496813

Table 5. Weighted normalized decision matrix

	k1	k2	k3	k4	k5	k6	k7	k8	k9	k10
A1	0.003943	0.007599	0.009192	0.017281	0.01868	0.028475	0.034906	0.041213	0.051401	0.102296309
A2	0.003203	0.006914	0.007864	0.013927	0.015923	0.022418	0.033127	0.030657	0.058755	0.086032826
A3	0.003445	0.00612	0.008068	0.012169	0.015014	0.019039	0.024234	0.023149	0.028811	0.056526907
A4	0.002399	0.005056	0.006329	0.01093	0.013054	0.018283	0.028314	0.023084	0.039224	0.06294416

The positive ideal and negative ideal distances for each alternative were calculated. Then, the relative closeness values of the alternatives to the ideal were computed. Table 5 presents the relative closeness value and ranking of the alternatives in relation to the ideal.

Table 6. Weighted normalized decision matrix

Alternative	C_i^*	Ranking
A1	1.515534578	1
A2	1.354276953	2
A3	0.670532156	4
A4	0.67485061	3

Upon examining Table 6. it can be observed that. considering the 10 established criteria. the best online shopping site is A1, followed by A2, A4, and A3 in that order.

4. CONCLUSION

This study provides an academic framework for evaluating and improving the performance of online shopping platforms. The identified criteria offer important insights for customer-oriented improvements in the online shopping sector. The combined use of AHP and TOPSIS methods allows for more comprehensive analyses in decision-making processes. Price emerges as the most important criterion. with A1 being identified as the most suitable alternative. According to the findings. while price is the primary criterion. A1 is determined to be the best alternative. This indicates that. in consumers' shopping decisions. not only the price but also the platform's features. user experience. and services play a crucial role. The selection of A1 as the best alternative highlights the importance of factors such as accessibility. reliability. and user-friendly design in shaping consumer preferences.

The results of the research provide not only recommendations for the improvement of existing online shopping platforms but also offer a new perspective for understanding sectoral competition and analyzing user preferences. Future studies aim to build upon this research. adapting to the innovations of the current era. with the goal of contributing valuable insights to the literature on online shopping and e-commerce.

In future studies. the evolution of results can be examined by increasing the number of alternatives and criteria. Additionally, findings obtained using various decision-making methods (DMM) can be compared and analyzed. In this context. the generalizability and accuracy of the study can be tested with more comprehensive datasets and new methodological approaches. This will enable a better understanding of how decision-making processes can be grounded on stronger foundations and how different results may emerge under varying conditions

Acknowledgments

References

[1] R. Nacar and K. Ozdemir, "E-ticaret pazaryeri web sitelerinin dinamikleri: Covid-19 pandemi surecindeki degisim," *Eskisehir Osmangazi Universitesi Iktisadi ve Idari Bilimler Dergisi*, vol. 16, no. 1, pp. 205–226, 2021.

[2] Z. Yilmaz, "Determining criteria weights at online shopping website selection from the perspective of young people," *Uluslararasi Yonetim Iktisat ve Isletme Dergisi*, vol. 17, no. 2, pp. 438–465, 2021.

[3] E. Cavlak, "Online alisveris sitesi tercihinde etkili olan kriterlerin belirlenmesine ve onceliklendirilmesine yonelik bir karar modeli," M.S. thesis, Istanbul Technical University, Istanbul, Türkiye, 2012.

[4] T. Bayir, "B2c online alışveriş sitelerinin seçim kriterlerinin AHP yöntemi ile belirlenmesi," *Kesit Akademi Dergisi*, vol. 6, no. 25, pp. 641–653, 2020.

[5] E. E. Nebati, "Cok kriterli karar verme yaklaşımı ile e-ticarette strateji secimi: Perakende sektorunde bir arastirma," *International Journal of Advances in Engineering and Pure Sciences*, vol. 34, no. 4, pp. 580–602, 2022.

[6] Y. T. Ulger and M. Toksari, "E-ticaret sitelerinin kullanılabilirligi ve basarisini etkileyen faktorlerin belirlenmesi," *Giresun Universitesi Iktisadi ve Idari Bilimler Dergisi*, vol. 6, no. 2, pp. 116–128, 2020.

[7] H. Razani, "E-ticaret alanında müşteri memnuniyeti takibini etkileyen faktörlerin AHS yöntemi ile

değerlendirilmesi," M.S. thesis, Bahcesehir University, Istanbul, Türkiye, 2020.

[8] E. Ozmen, G. E. Karaman, and E. Karaman, "E-ticaret sitelerinin kullanılabilirliginin degerlendirilmesine yonelik olcek gelistirme ve uygulama," *Gazi Universitesi Sosyal Bilimler Dergisi*. vol. 5, no. 12, pp. 74–91, 2018.

[9] M. Albayrak, "Elektronik ticaretin gelisimi ve internetin tuketici satin alma karar surecine etkisi: Salzburg-Ankara ornegi," M.S. thesis, Balikesir University, Balikesir, Türkiye, 2015.

[10] S. Dundar, F. Ecer, and S. Ozdemir, "Fuzzy TOPSIS yöntemi ile sanal magazalarin web sitelerinin degerlendirilmesi," *Atatuk Universitesi Iktisadi ve Idari Bilimler Dergisi*, vol. 21, no. 1, pp.287–305, 2007.

[11] E. Yildirim, "Türkiye'de perakende ticaret yapan firmalarda E-ticaretin uygulanabilirligi uzerine bir arastirma," M.S. thesis, Gazi University, Ankara, Türkiye, 2010.

[12] A. Supciller and O. Capraz, "AHP-TOPSIS yontemine dayali tedarikci seçimi uygulamasi," *Istanbul University Econometrics and Statistics e-Journal*. vol. 13, pp. 1–22, 2011.

Ergonomic Problems in the Textile Industry Determining Priorities with Multi-Criteria Decision Making

Zeynep Bora[1], Mujde Arslan[1], Kubra Deniz[1], Seyma Emec[1]

[1]Industrial Engineering, Erzurum Technical University, Erzurum, Türkiye
Corresponding author: Zeynep Bora (zeynepbora.2003@gmail.com)

Abstract

Ergonomic problems are a critical issue that can have significant negative effects on worker health and productivity when ignored in the design of working environments, and the textile sector is one of the industry areas where these problems are most experienced. This study aims to prioritize ergonomic problems in the textile sector. In this context, common ergonomic problems such as posture disorders, repetitive movements and inappropriate work tools were identified and a hierarchical model was established. For the identified problems, bilateral comparisons were made between decision makers and the analytical hierarchy process (AHP) was analyzed. As a result of the calculations made with AHP, weights were determined for each ergonomic problem and the priority order of the problems was established. According to the results obtained, the priority ranking of ergonomic problems is as follows: noise, low salary, ventilation, irregularity of machine maintenance, communication problem, repetitive movements, occupational health and safety literacy, hygiene and the employee lifting weight in a risky way. In this way, it has been revealed which are the most critical ergonomic problems. The results contribute to the development of strategies to improve worker health and productivity by determining which areas ergonomic improvements should focus on. This study aims to provide an important reference for improving ergonomic conditions in the textile industry

Keywords: Ergonomics, Multi-criteria decision Making, Textile industry

1. INTRODUCTION

In addition to being an important source of employment worldwide, the textile industry is a dynamic and fast-changing sector. Production processes in this area have a number of challenges that directly affect the health and efficiency of the workforce. Long working hours, repetitive movements and inappropriate workstation design can have negative consequences on the physical and psychological health of employees. In this context, the application of ergonomics is of critical importance in terms of both increasing occupational safety and ensuring employee satisfaction.

Ergonomics aims to optimize people's interactions with business environments. The main elements in the textile industry, such as the use of machines and the organization of work areas, are the areas in which ergonomic principles should be applied. While ergonomic designs increase the comfort of workers, they also increase productivity. Employees working in a comfortable environment both reduces work accidents and increases productivity.

However, multi-criteria decision-making (MCDM) methods are extremely useful for solving the complex problems faced by textile enterprises. MCDM facilitates the process of making constructive and rational choices between different alternatives. This process allows many criteria such as cost, time, occupational safety and environmental factors to be evaluated together. Thus, businesses can develop sustainable solutions both economically and socially.

The textile industry is increasingly turning to adopt the principles of ergonomics in order to increase the efficiency of work processes and worker health. Ergonomics aims to meet the physical, cognitive and emotional needs of the workforce, taking into account human factors in the design of work environments [1]. In particular, physical difficulties and prolonged sessions in the textile production process can cause health problems for employees [2]. In this context, ergonomic adjustments play a critical role in reducing frequent discomfort (e.g., back and neck pain) [3] and thus improves workforce efficiency [4].

Research on ergonomics shows that considering ergonomic design in processes such as sewing machines, fabric cutting and dyeing, it provides significant improvements in production speed and quality control [5]. In addition, MCDM methods help to put ergonomic design decisions on a rational foundation in the textile industry. MCDM allows a large number of factors to be evaluated between different alternatives, from occupational safety to cost-effectiveness [6]. This type of systematic approach serves as an important guideline for textile businesses to aim to both increase employee satisfaction and optimize business processes [7]. At the same time, the adoption of ergonomic designs in the textile industry and their integration with multi-criteria decision-making processes has the potential to improve occupational health while also increasing the competitiveness and sustainability of enterprises [8].

As a result, the integration of ergonomics and multi-criteria decision-making methods in the textile industry has become a decisive factor in the improvement of business processes and the protection of employee health. By bringing these two disciplines together, it is possible to contribute to the sustainability of the sector and raise the living standards of the employees. Future research should aim to focus on how to optimize ergonomic design decisions more effectively with MCDM processes.

2. MATERIAL AND METHOD

2.1. Analytical Hierarchy Process (AHP) Methods and Steps

The AHP is a systematic technique used to evaluate a number of alternatives in complex decision-making situations and determine the most appropriate option. AHP helps decision makers create a hierarchy by analyzing their preferences. In this article, the steps of the AHP method, a detailed description of each step, the formulas and the meanings of the terms in the formulas will be discussed.

Step 1. Defining the Problem and Creating the Hierarchy: In this first step, it is important to clearly identify the problem to be decided and to establish a hierarchy for it.

- Purpose: It is necessary to determine the goal of the decision-making process. This allows you to understand why the decision was made and what results are expected.
- Criteria and Sub-Criteria: It should be determined which criteria will be evaluated in line with the purpose. Criteria are the necessary factors for the successful decision to be made. At this stage, it is also possible to divide the criteria into sub-criteria.
- Alternatives: A list of options to be evaluated should be created. These alternatives will be evaluated according to the determined criteria.

Step 2. Creating a Comparison Matrix: It is necessary to create a matrix by making comparisons between criteria or alternatives. This matrix shows the relative superiority of alternatives over each other.

- Comparison Scale: AHP usually uses a scale between 1 and 9. This scale refers to the degrees of importance of alternatives or criteria relative to each other. For example, 1 is of equal importance, while 9 indicates that an alternative is definitely more important.
- Matrix Format: In the created comparison matrix, the relationship of each alternative with others is indicated. This matrix forms the basis of the decision-making process.

Step 3. Normalization: Normalization is done to express more clearly the relative importance of each element relative to each other. It is normalized by dividing by the sum of the elements in each column (Equation 1).

$$b_{ij} = \frac{a_{ij}}{\sum_{i=1}^{n} a_{ij}} \tag{1}$$

Where a_{ij}, i. the value of the alternative j. as a result of comparing it with the alternative. b_{ij} is the normalized form of a_{ij}. This process determines the ratio of each alternative in the total, making the comparison matrix more meaningful.

Step 4. Calculation of Weights: The weight of each alternative is calculated by taking the row averages of the normalized matrix.

$$w_i = \frac{\sum_{j}^{n} b_{ij}}{n} \tag{2}$$

Here w_i is i. weight of the alternative and n is total number of alternatives.

This stage determines how important each of the alternatives is and shows which alternatives take precedence in the decision-making process.

2.1. Case Study

In this study, ergonomic problems experienced by employees in a textile factory operating in Erzurum were detected. 9 most important criteria have been selected from these problems. These criteria are:

- k1 - Ventilation: Inadequate ventilation in the working environment can negatively affect the respiratory health of employees while reducing labor efficiency.
- k2 - Sound: High levels of noise exposure reduces the work concentration of employees and can cause health problems such as hearing loss in the long run.
- k3 - Hygiene: The inadequacy of hygienic conditions increases the spread of infectious diseases and puts employee health and work continuity at risk.
- k4 - Occupational Health and Safety Literacy: The low level of knowledge of employees on occupational health and safety may lead to an increase in occupational accidents by limiting their capacity to notice and prevent hazards.
- k5 - Low Salary: Low wages given to employees cause loss of motivation and negatively affect organizational commitment in the long run.
- k6 - Communication Problem: Communication deficiencies in the workplace reduce organizational performance by causing coordination problems and disruption of business processes.
- k7 - Employee's Risky Weight Lifting: Weight lifting with non-ergonomic methods is an important risk factor that leads to musculoskeletal disorders and work accidents.
- k8 - Irregularity of Machine Maintenance: Failure to maintain machines regularly causes both disruptions in production processes and employee safety to be compromised.
- k9 - Repeated Movements: Performing the same movements all the time causes repetitive difficulties on the musculoskeletal system, causing loss of labor and health problems.

It was evaluated using the Hour scale by 3 randomly selected employees. Then, using the AHP method, the weights of my criteria were calculated and the order of importance were found.

3. RESULTS

The binary comparison matrices obtained by 3 employees working in the textile factory as a result of the evaluation of 9 criteria are combined. The combined binary comparison matrix is given in Table 1.

Table 1. Combined pairwise comparison matrix

criterion/ criterion	k1	k2	k3	k4	k5	k6	k7	k8	k9
k1	1	0.368403	2.620741	1.747161	1.144714	1.44225	3.556893	1.44225	1.21644
k2	2.714418	1	3.036589	3.556893	0.854988	1.817121	3.476027	1.587401	2.620741
k3	0.381571	0.329317	1	2.289428	0.255436	0.793701	0.793701	0.456671	0.829827
k4	0.572357	0.281144	0.43679	1	0.464159	1.817121	0.746901	0.678604	0.90856
k5	0.87358	1.169607	3.914868	2.154435	1	2.620741	3.634241	2	1.44225
k6	0.693361	0.550321	1.259921	0.550321	0.381571	1	2.289428	0.629961	1.587401
k7	0.281144	0.287685	1.259921	1.338866	0.275161	0.43679	1	0.584804	0.629961
k8	0.693361	0.629961	2.18976	1.473613	0.5	1.587401	1.709976	1	2.466212
k9	0.822071	0.381571	1.205071	1.100642	0.693361	0.629961	1.587401	0.40548	1

The values in the combined pairwise comparison matrix were normalized using the equations in step 3 given in Section 2. The resulting normalized pairwise comparison matrix is given in Table 2.

Table 2. Normalized pairwise comparison matrix

criterion/ criterion	k1	k2	k3	k4	k5	k6	k7	k8	k9
k1	0.124504	0.07371	0.154857	0.114859	0.205537	0.118752	0.189251	0.164169	0.095772
k2	0.337956	0.20008	0.179429	0.233831	0.153516	0.149618	0.184948	0.180691	0.206335
k3	0.047507	0.06589	0.059089	0.150508	0.045864	0.065352	0.04223	0.051982	0.065334
k4	0.071261	0.056251	0.025809	0.06574	0.083341	0.149618	0.03974	0.077244	0.071532
k5	0.108764	0.234015	0.231325	0.141633	0.179553	0.215786	0.193367	0.227656	0.113551
k6	0.086326	0.110108	0.074447	0.036178	0.068512	0.082338	0.121813	0.071707	0.124979
k7	0.035004	0.05756	0.074447	0.088018	0.049406	0.035964	0.053207	0.066567	0.049598
k8	0.086326	0.126042	0.12939	0.096876	0.089776	0.130703	0.090982	0.113828	0.194169
k9	0.102351	0.076345	0.071206	0.072357	0.124495	0.05187	0.084461	0.046155	0.078732

Then, with the help of the equations in step 4, the weights were calculated for each criterion and their importance levels were found. The importance ranking of the criteria is presented in Table 3.

Table 3. Criteria weights and order of importance

Criterion	Criterion Weights	Order of Importance
k1	0.137934	3
k2	0.202934	1
k3	0.065973	8
k4	0.071171	7
k5	0.18285	2
k6	0.086268	5
k7	0.056641	9
k8	0.117566	4
k9	0.078663	6

k2 - Sound (Weight: 0.202934): Noise, a high priority problem, can disrupt employees' concentration, causing distraction and work accidents. Long-term exposure can lead to hearing loss.
- Recommendation: In order to reduce the noise level, sound insulation should be applied, ear protective equipment should be provided to employees, and maintenance periods should be increased for machine noise.

k5 - Low Salary (Weight: 0.18285): Low salary of employees can cause loss of motivation, job dissatisfaction and high labor cycle.
- Recommendation: Salary policies should be reviewed and performance-based reward systems should be developed. Additional social benefits can be provided to reduce the economic concerns of employees.

k1 - Ventilation (Weight: 0,137934): Inadequate ventilation causes employees to experience respiratory problems and decrease in work efficiency.
- Recommendation: Ventilation systems in the working environment should be modernized and natural ventilation opportunities should be increased.

k8 - Irregularity of Machine Maintenance (Weight: 0,117566): Failure to maintain the machines regularly may lead to work accidents with malfunctions. In addition, this situation causes disruptions in production.
- Recommendation: Regular machine maintenance protocols should be established and planned maintenance processes should be closely followed.

k6 - Communication Problem (Weight: 0,086268): Lack of communication at work can disrupt team coordination and cause work accidents and disruptions in processes.

- Recommendation: Employees should be given trainings to improve their communication skills, open communication policies should be applied and in-team meetings should be organized.

k9 - Repetitive Movements (Weight: 0,078663): Employees performing the same movements all the time can lead to musculoskeletal disorders.
- Recommendation: Workstations should be ergonomically redesigned, regular breaks and stretching exercises should be encouraged.

k4 - Occupational Health and Safety Literacy (Weight: 0.071171): The lack of sufficient knowledge of the employees may cause the hazards not to be noticed and prevented.
- Recommendation: Occupational health and safety trainings should be given to employees on a regular basis and awareness should be increased.

k3 - Hygiene (Weight: 0.065973): In environments where hygiene is insufficient, infectious diseases may increase and employee health may be at risk.
- Recommendation: Cleaning policies in accordance with hygiene standards should be applied in the working areas and access to individual hygiene products should be provided.

k7 - Employee's Risky Weight Lifting (Weight: 0.056641): Lifting weights with the wrong methods can lead to musculoskeletal system disorders and work accidents.
- Recommendation: Employees should be trained about weight lifting techniques, and physical strain should be minimized by providing load-carrying equipment.

Although occupational health and safety measures have been taken in the textile sector, raising employee awareness is a critical step. For this purpose, regular occupational health and safety trainings should be given, and safety warnings should be constantly reminded through posters, brochures and digital screens. Thus, the safety culture can be made a part of daily business life. Among the ergonomic problems, sound stands out as the most important problem. Solving this problem will improve employee health and productivity and reduce occupational accidents. In addition, low salaries can negatively affect employee motivation; therefore, policies that will increase employee loyalty should be implemented. A safe and efficient working environment can be provided by considering factors such as physical factors, especially ventilation, machine maintenance and ergonomic design.

4. CONCLUSION

In this study, multi-criteria decision making (MRP) methods were used to evaluate the ergonomic risks of textile workers and to determine priority problems. Within the scope of the study, ergonomic problems encountered by the employees during work such as sound, hygiene, irregularity of machine maintenance, repetitive movements and risky weight lifting were determined and bilateral comparisons between decision makers for the determined problems and the AHP were analyzed. The results of the study revealed that factors such as noise and low salary were primary problems; accordingly, it was suggested to improve working conditions and apply ergonomic design.

For future studies, it is recommended to carry out extensive analyzes covering different production units in the textile sector and to integrate the MCDM method with other decision support systems. In addition, by including technological innovations in the studies, real-time monitoring of ergonomic risks to which workers are exposed and dynamic determination of solutions can be ensured. Such studies will contribute to the creation of safer and more efficient working environments in the sector

Acknowledgments

References

[1]   P. O. Pablos, M. D. Lytras, A. Visvizi, and X. Zhang, "Human factors and ergonomics in manufacturing & service industries," *Human Factors & Ergonomics in Manufacturing & Service Industries*, vol. 29, no. 1, 2019.
[2]   M. I. Khan, A. Hamid, and A. Mahmood, "Ergonomics in textile industry: A review," *Textile Progress*, vol. 53, no. 4, pp. 245–282, 2021.

[3]   R. Bhandari, A. Gupta, and P. Kumar, "Work-related musculoskeletal disorders among textile workers: A review," *Occupational Medicine*, 2020.

[4]   S. Pheasant and D. Steffen, *Bodyspace: Anthropometry, Ergonomics and the Design of Work*, 3rd ed. Boca Raton: CRC Press, 2019.

[5]   P. G. Dempsey, W. A. Dempsey, and Y. Wu, "The relationship between ergonomics and productivity in the global textile industry," *Ergonomics*, 2021.

[6]   H. R. Zardari, M. A. Khanzada, and S. Ali, "Multi-criteria decision analysis in textile industry: A review," *Journal of Textile Engineering & Fashion Technology*, 2018.

[7]   A. Marinelli, B. Fabiano, and G. De Marco, "Integrating ergonomics into decision making processes: A study in the textile industry," *Applied Ergonomics*, 2022.

[8]   A. Sharma, R. Gupta, and A. Sahu, "Sustainable practices in textile manufacturing: A study on ergonomics and environmental impact," *Sustäten Erstäten und Erworten*, 2023.

Some Fertility Properties of Soils Due to Good Agricultural Practices

Mustafa Demir[1], Erdihan Tunc[1], Omer Celik[2], Nevzat Aslan[3], Hafize Hasar[4]

[1]Biology Department, Gaziantep University, 27310 Gaziantep, Türkiye
[2]Department of Plant Production, Faculty of Applied Sciences, Mus Alpaslan University, 49250 Mus, Türkiye
[3]Department of Soil Science and Plant Nutrition, Siirt University, Siirt, Türkiye
[4]Gaziantep Directorate of Provincial Agriculture and Forestry, Ministry of Agriculture and Forestry of Republic of Türkiye, 27090 Gaziantep, Türkiye
Corresponding author: Mustafa Demir (e-mail: mustdem@gmail.com)

Abstract

Human survival depends on supplemented food and relevant resources in ever-expanding local and global populations. For this goal, several factors including variations in climate, loss in biodiversity, degradation in land, pollution and salinization, depletion of water resources, and any possible rise in the production of agricultural goods pose a significant role in supplying human needs in the future. Good agricultural practices (GAP) can be a useful approach for improving quality, healthy, and safe foods for consumers. Besides, it is an approach that supports sustainable, environmentally friendly agriculture due to actions taken to protect the health of workers and the quality and health of soils on farms where production is made. Different from previous studies [6–10], in this study, we statistically examine for the first time in the literature the effect of GAP on some fertility properties of soils.

Keywords: Good agricultural practices, Fertility properties, Soil, Statistical analysis

1. INTRODUCTION

It is extremely important for human survival in today's growing world to continuously supplement food and relevant resources to ever-expanding local and global populations. To meet such a need, several factors including variations in climate, loss in biodiversity, degradation in land, pollution and salinization, depletion of water resources, and any possible rise in the production of agricultural goods produce a potential risk in meeting human needs in the future. Present conventional farming applications or practices can only benefit and be durable provided that processing of post-harvesting and crop production technologies are properly implemented. Additionally, pressure on local and global economies as well as drastic changes in climate conditions put an impetus on new ways of alternative, cost-effective, and energy-efficient and sustainable agricultural practices. Specifically, sustainability in agriculture proves efficient resource allocation to accommodate the changing needs of humans in addition to keeping up environmental quality and preserving natural resources such as crop diversity, effective management of water resources, and subsidization of nutrients and pests in proper amounts. Good agricultural practices (GAP) based agricultural production is an approach aimed at producing quality, healthy, and safe foods for consumers. Besides, it is an approach that supports sustainable, environmentally friendly agriculture due to actions taken to protect the health of workers and the quality and health of soils on farms where production is made [1, 2]. In Türkiye, GAP started with the publication of the "Regulation on Good Agricultural Practices" in the Official Gazette No. 25577 dated 08.09.2004 [3, 4], and as of 2023, the number of certified producers reached 8,045, the agricultural area under certified production reached 3,726,514, and the certified production amount reached 6,119,846 tons [5].

There are various papers or articles dealing with the GAP in the literature. In the study [6], the authors evaluated the effect of the perception of official national programs on the development of the GAP (mainly oriented on integrated plant production) and examined any potential barriers to the implementation of such practices. It is noted that social and environmental awareness, higher material security, and attitude toward pro-market all influence in different amounts the motivation in putting such national programs [6]. Besides, in the study [7], authors investigated any possible advantages that the GAP program can bring to farmers, mainly focusing on hazelnut production for farmers in Kocaali province, Sakarya, Türkiye. It is observed that the majority (more than 65%) of hazelnut producers harvest hazelnuts over long distances of around 30 years and that the education level of hazelnut farmers following the GAP is higher than the education level of those using traditional agricultural practices. The main reason for such a difference is noted to be an interest in getting financial support provided by

the government for the GAP program. From this study, it is also noteworthy that hazelnut farmers following the GAP, in comparison with hazelnut farmers not following the GAP program, more consciously use agricultural drugs and first-aid cabinets as well as wearing a face mask. On the other hand, in the study, the authors focused on assessing the relationship between inputs and outputs and economic analysis of the peach and cherry farmers in the Canakkale province of Türkiye, following the GAP program and not following it [8]. The results revealed that the efficiency of energy usage for peach and cherry farmers following the GAP program is higher than for those not following it, showing a definite advantage of the GAP program on the production of peach and cherry in the region where the study was conducted. Additionally, in the study [9], the authors show the possibility of improving amaranth production through the development and promotion of better varieties through GAP programs. Moreover, in the study [10], the authors aimed to evaluate the contribution of the GAP program on invertebrates, especially focusing on differences between soil types. It is noted that implementation of the GAP program improves litter and soil invertebrate abundance while modifying faunal composition.

When recent studies in the literature are examined [6–10], it is observed that there are no scientific studies on the effects of GAP applications on the protection of soil quality and health, which is an important requirement in the production of these foods on a global scale. Different from previous studies [6–10], in this study, we statistically examine for the first time in the literature the effect of GAP on some fertility properties of soils.

2. MATERIAL AND METHOD

2.1. Soil Samples and Preparing for Analyses

After harvesting, a total of 100 soil samples were taken from 20 different garlic fields, 10 of which were conventional (CNA) and 10 of which were implemented with GAP, randomly selected in the Araban Plain (Gaziantep, Southeastern Türkiye). The soil samples, which were placed in plastic bags, were immediately brought to the Gaziantep University Soil Ecology Laboratory, dried in the air, and sieved with a 2 mm sieve.

2.2. Methods

To determine the organic carbon content (SOC) of the soils, the titrimetric method [11], which is recommended for soils with low SOC contents [12], was used. Soil organic matter (SOM) was determined by multiplying SOC, which was assumed to contain 58%, by the Van Bemmelen factor (1.724) [12]. pH and electrical conductivity (EC, dS/m) contents of the soils were determined in the prepared soil-water (1:2.5) saturation sludge utilizing a multimeter (Consort C5020, Turnhout, Belgium) [13]. Inorganic carbonate (IC, %) contents were determined by a method recommended for soils low in organic matter and MnO_2 and using a Scheibler calcimeter (Eijelkamp M1.08.53.D, The Netherlands) [14]. Soil texture was determined by the Bouyoucos method [15]. Plant-available phosphorus (P, mg.kg-1) contents were determined by reading the absorbance values of the extracts obtained by extraction of soil samples with ammonium bicarbonate ($NaHCO_3$) through a spectrophotometer (UV-1280, Shimadzu Corporation, Japan) [16]. Total nitrogen (N, %) in soils was determined by the Kjeldahl method [17].

2.3. Quality of Analyses

Analyses of each parameter of each sample were performed three times and arithmetic averages were taken. UME RM 9908a was used for SOM and IC, and UME RM 9918c (TÜBİTAK, Ankara) was used for EC as reference material. In this study, the arithmetic average of SOM, IC, and EC analyses repeated three times corresponded to 95.5%, 92.2% and 98.9% of the reference value, respectively.

2.4. Statistical Analyses

SPSS Statistics (Version 27, IBM, USA) was used for normality tests of the obtained data, and Jamovi Desktop (Version 2.6.13, Jamovi Project) and Minitab (Version 19, Minitab Ltd., Coventry, UK) were used for Sample T-Test and correlation analyses.

3. RESULTS AND DISCUSSION

As a result of the analyses, some descriptive statistical values and sample T-test results obtained in CNA and GAP soils are summarized in Table 1. These findings, which are consistent with the results of previous studies [18–20] conducted in the region, showed that both CNA and GAP soils have low SOM and high lime contents developed from calcareous and gypsum bedrock under dry and hot climatic conditions [21–23].

However, in terms of average contents, IC and sand contents were found to be higher in GAP (38.23% and 24.41%, respectively), while clay, P_{av}, and TN contents were found to be higher in CNA (17.26%, 54.36% and 26.72%, respectively) ($p < 0.05$).

Table 1. Statistical results (p refers to the Pearson correlation coefficient value. * designates a result when $p < 0.05$; ** designates a result when $p < 0.01$; *** designates a result when $p < 0.001$; and n.s. refers to a non-significant result)

		Min.	Q1	Mean	±StD	Med.	Q3	Max.	Kurt	Skew	CV (%)	p
pH	CNA	7.19	8.16	8.11	0.33	8.19	8.24	8.31	9.10	-2.96	4.05	n.s.
	GAP	8.04	8.17	8.29	0.16	8.33	8.37	8.50	-0.98	-0.42	1.90	
EC (dS/cm)	CNA	0.11	0.17	0.23	0.15	0.20	0.21	0.64	8.32	2.78	64.43	n.s.
	GAP	0.10	0.14	0.17	0.07	0.15	0.19	0.35	2.61	1.68	42.48	
IC (%)	CNA	2.27	5.54	9.22	6.63	6.50	10.35	24.06	1.91	1.49	71.94	*
	GAP	5.51	11.09	14.93	5.20	17.36	18.60	19.51	-0.69	-1.01	35.83	
Clay (%)	CNA	52.16	54.16	56.19	3.28	56.20	57.21	62.45	0.05	0.62	5.83	***
	GAP	30.23	46.09	46.49	6.26	48.09	49.53	52.09	5.91	-2.22	13.46	
Silt (%)	CNA	15.50	19.60	20.12	2.18	20.61	21.52	22.86	1.17	-1.06	10.84	n.s.
	GAP	17.42	20.12	22.17	3.01	21.64	23.48	27.57	-0.08	0.33	13.59	
Sand (%)	CNA	16.84	20.84	23.69	3.87	23.88	27.02	28.34	-0.84	-0.40	16.33	***
	GAP	24.49	28.74	31.34	4.89	31.35	32.43	42.20	2.13	0.98	15.60	
P_{av} (mg/kg)	CNA	34.00	66.50	89.40	37.41	77.50	116.5	154.0	-0.54	0.54	41.85	**
	GAP	18.00	24.50	40.80	27.96	36.00	44.50	114.0	6.15	2.29	68.54	
SOM (%)	CNA	0.95	1.05	1.17	0.22	1.10	1.12	1.64	1.62	1.61	19.20	n.s.
	GAP	0.97	1.02	1.11	0.13	1.09	1.17	1.34	-0.44	0.67	11.26	
TN (%)	CNA	0.10	0.10	0.12	0.02	0.11	0.13	0.14	-0.84	0.73	14.44	***
	GAP	0.08	0.08	0.09	0.01	0.09	0.09	0.09	-0.03	-0.13	6.13	

Especially the high IC in GAP is probably related to the differences between CNA and GAP in the irrigation method preferred by the producer. In contrast to CNA, where lime can be easily washed away with wild irrigation, the authors in the study [24] reported that producers adopting GAP prefer drip irrigation in terms of product, cost and environment. The high IC contents of the regional soils have been associated with the main rock contents consisting of limestone and gypsum as well as low rainfall amounts [22]. On the contrary, in the study conducted in Araban, it was reported that IC contents in pistachio orchards with dry farming were significantly lower than those in wheat fields with irrigated farming [19]. Nitrogen in soils is the most important element that determines the quality and productivity of soils in agricultural areas and thus limits plant growth and the amount of agricultural products. Higher TN contents in CNA than GAP are associated with higher nitrogen fertilizer use in conventional agriculture. In a previous study, it was reported that producers' use of inorganic fertilizers, pesticides or organic fertilizers decreased with GAP preference [25].

4. CONCLUSION

It was determined that GAP had significant effects on some physical and chemical properties of soils. In particular, IC and sand contents increased, while clay, P_{av}, and TN contents decreased. It was found that it did not have significant effects on pH, EC, and silt contents, which have significant effects on the general characteristics of the region's soils. GAP did not create a significant difference in SOM, which is one of the important indicators of soil quality and health.

References

[1] A. N. T. Wardani and D. H. Darwanto, "The impact of GAP-SOP on the production and technical efficiency of garlic in Temanggung regency," *Agro Ekonomi*, vol. 29, no. 2, pp. 299–309, 2019.
[2] C. Yildirim, H. Turkten, V. Ceyhan, E. Atis, M. Hasdemir, H. E. Salali, Y. Akyuz, and F. Gungor, "Exploring opportunity cost of conversion to eco-friendly farming system: the case of Samsun and Adana provinces of Turkey," *Environment, Development and Sustainability*, vol. 23, no. 2, pp. 1447–1460, 2021.
[3] G. Aydin Eryilmaz, O. Kilic, and I. Boz, "Türkiye'de organik tarım ve iyi tarım uygulamalarının ekonomik, sosyal ve çevresel sürdürülebilirlik açısından değerlendirmesi," *Yuzuncu Yil Tarim Bilimleri Dergisi*, vol. 29, no. 2, pp. 352–361, 2019.
[4] Resmi Gazete, *Iyi Tarim Uygulamalarina Iliskin Yonetmelik,* 2004.

[5] TOB, *Iyi Tarım Uygulamaları İstatistikleri (Bolge-Il-Uretici-Alan) 2007-2019*, 2020.

[6] M. Pink, M. Niewiadomski, K. Grochola, and A. Gorczyca, "Producers' perception of the benefits of farm certification: The case of the national good agricultural practices programme," *Sustainability (Switzerland)*, vol. 16, no. 18, pp. 1–20, 2024.

[7] M. Tuccar, S. Turhan, and A. Cansev, "Evaluation of good agricultural practices in Turkey: Perspective from hazelnut producers," *Journal of Agricultural Faculty of Bursa Uludag University*, vol. 36, no. 1, pp. 227–243, 2022.

[8] B. Aydin and D. Akturk, "Energy use efficiency and economic analysis of peach and cherry production regarding good agricultural practices in Turkey: A case study in Canakkale province," *Energy*, vol. 158, pp. 967–974, 2018.

[9] J. Ochieng, P. Schreinemachers, M. Ogada, F. F. Dinssa, W. Barnos, and H. Mndiga, "Adoption of improved amaranth varieties and good agricultural practices in East Africa," *Land Use Policy*, vol. 83, pp. 187–194. 2019.,

[10] J. C. Bedano, A. Domínguez, R. Arolfo, and L. G. Wall, "Effect of Good Agricultural Practices under no-till on litter and soil invertebrates in areas with different soil types," *Soil and Tillage Research*, vol. 158, pp. 100–109, 2016.

[11] A. Walkley and I. A. Black, "An examination of the Degtjareff method for determining soil organic matter, and a proposed modification of the chromic acid titration method," *Soil Science*, vol. 37, no. 1, pp. 29–38, 1934.

[12] D. W. Nelson and L. E. Sommers, "Total carbon, organic carbon, and organic matter," in *Methods of Soil Analysis Part 3. Chemical Methods*, D. L. Sparks, A. L. Page, P. A. Helmke, R. H. Loeppert, P. N. Soltanpour, M. A. Tabatabai, C. T. Johnston, and M. E. Sumner, Eds.: SSSA Book Series No:5, 1996, pp. 961–1010.

[13] L. A. Richard, "Diagnosis and ımprovement of saline and alkaline soils," in *Soil Science Society of America Journal* (vol. 18, issue 3), United States Department of Agriculture Handbook No. 60, United States Government Printing Office, 1954.

[14] L. E. Allison and C. D. Moodie, "Carbonate," in *Methods of Soil Analysis, Part 2: Chemical and Microbiological Properties*, A. G. Norman, Ed.: American Society of Agronomy Inc., 1965, pp. 1379–1396.

[15] G. J. Bouyoucos, "The hydrometer as a new method for the mechanical analysis of soils," *Soil Science*, vol. 23, no. 5, pp. 343–354, 1927.

[16] S. R. Olsen, C. V. Cole, F. S. Watanabe, and L. A. Dean, "Estimation of available phosphorus in soils by extraction with sodium bicarbonate," *United States Departement of Agriculture Circular*, vol. 939, pp. 1–19, 1954.

[17] J. M. Bremner, "Nitrogen-total," in *Methods of Soil Analysis Part 3. Chemical Methods-SSSA Book Series 5*, D. L. Sparks, Ed.: SSSA Book Series, 1996, pp. 1085–1121.

[18] E. Tunç, A. Özkan, and M. A. Çelik, M. A. "Determination of the K-Factor of arable land in Yavuzeli and Araban/Gaziantep Province," *The Journal of International Social Research*, vol. 6, no. 28, pp. 432–440, 2013.

[19] E. Tunc, M. S. Tekin, M. Demir, and T. Tsegai, "Halophytic species in natural areas close to agricultural areas of Araban (Gaziantep, Turkey)," *Journal of Agricultural Chemistry and Environment*, vol. 9, pp. 48–58, 2020.

[20] E. Tunc, A. T. Tsegai, and S. Celik, "Analysis of spatial-temporal changes of agricultural land use during the last three decades in the Araban district of Turkey using remote sensing," *Geomatics and Environmental Engineering*, vol. 15, no. 1, pp. 111–123, 2021.

[21] H. Avcı and M. Yaman, "Concentrations, accumulation, and interactions of redoximorphic metals (Fe, Mn) between other elements in plants grown on wastewater-irrigated and control soils," *Water, Air, and Soil Pollution*, vol. 225, no. 4, art. no. 1926, 2014.

[22] M. Demir, E. Tunc, S. Thiele-Bruhn, O. Celik, A. T. Tsegai, N. Aslan, and S. Arslan, "Status, sources and assessment of potentially toxic element (PTE) contamination in roadside orchard soils of Gaziantep (Türkiye)," *International Journal of Environmental Research and Public Health*, vol. 20, art. no. 2467, 2023.

[23] E. Tunc and M. Demir, "Investigation of total carbon and nitrogen content of Gaziantep agricultural soils," *The International Journal of Energy & Engineering Sciences*, vol. 6, no. 2, pp. 13–22 2021.

[24] M. Dagtekin, M. E. Bilgili, and A. Beyaz, "The effects of good agricultural practises on energy use effectiveness on mandarin production and environmental," *Erwerbs-Obstbau*, vol. 61, no 1, pp. 55–60, 2018.

[25] B. Aydin, D. Akturk, E. Ozkan, H. Hurma, and M. A. Kiraci, "Comparative energy use efficiency and economic analysis of apple production in Turkey: Case of thrace region," *Erwerbs-Obstbau*, vol. 61, no. 1, pp. 39–45, 2019

A Study on Dominant Eigenvalues

Ramazan Simsek[1]

[1]Department of Mathematics and Science Education, Faculty of Education, Bayburt University, Bayburt, Türkiye
Corresponding author: Ramazan Simsek (e-mail: rsimsek@bayburt.edu.tr)

Abstract

Eigenvalues and eigenvectors are very important, especially on matrices, on vectors and in solving equation systems. They also have an important function in solving differential equation systems used in statistics and engineering science. In this study, first of all, the definition of eigenvalues and eigenvectors will be given, and what dominant eigenvalues and eigenvectors correspond to will be given. Finally, for $k \in \mathbb{N}$, the convergence of the vector sequence $A^k x$ obtained with the help of a certain number of iterations, where $x \in \mathbb{R}^n$ is the linear combination of the eigenvectors of the matrix of type A, $n \times n$, will be examined with the help of dominant eigenvalues.

Keywords: Mathematic, Matrix, Eigenvalues, Dominant eigenvalues, Eigenvectors

1. INTRODUCTION

In this section, firstly a brief definition of eigenvalues and eigenvectors given. For more information see references [1–6].

Definition 1.1.1: Let V be a vector space of dimension n and let $L : V \to V$ be a linear transformation. If for any non-zero $x \in V$,

$$L(x) = \lambda x. \tag{1}$$

The number λ satisfying equality L is called the eigenvalue of the linear transformation. Non-zero values of $x \in V$ satisfying Equation (1) are called eigenvectors corresponding to the eigenvalue λ of the linear transformation [3–6]. For the general properties of linear transformations defined on vector spaces and the eigenvalues being real numbers or complex numbers, see references [3, 4].

Definition 1.1.2: Let A be a square matrix of type $n \times n$ for the determinant equation,

$$|A - \lambda I| = 0 \tag{2}$$

the non-zero number λ satisfying the equality is called the eigenvalue of matrix A. Corresponding to a non-zero number λ,

$$Av = \lambda v \text{ and } (A - \lambda I)v = 0 \tag{3}$$

the non-zero vector $v \in \mathbb{R}^n$ is called an eigenvector [2–4].

Definition 1.1.3: Obtained with the help of Equation (2) in Definition 1.1.2

$$|A - \lambda I| = \begin{vmatrix} a_{11} - \lambda & a_{12} & \cdots & a_{1n} \\ a_{21} & a_{22} - \lambda & \cdots & a_{2n} \\ \vdots & \vdots & \vdots & \vdots \\ a_{n1} & a_{n1} & \cdots & a_{nn} - \lambda \end{vmatrix} = 0 \tag{4}$$

Equation (4) is called the characteristic equation (polynomial) of the matrix. It is obvious that the roots of this equation are given by the eigenvalues of the matrix [2–6]. With the help of the type of matrix we can easily see that it is a determinant,

$$b_n \lambda^n + b_{n-1} \lambda^{n-1} + ... + b_1 \lambda + b_0 = 0, \tag{5}$$

gives the nth order polynomial. According to the fundamental theorem of algebra, the polynomial obtained by Equation (5) has at most n different roots. This shows that it can have n eigenvalues. These roots can be real numbers, multiple real numbers and complex numbers [3–6]. In addition, eigenvectors are found with the help of Equation (3) for each eigenvalue of λ_i obtained from Equation (5).

2. MATERIAL AND METHOD

Definition 2.1.1: If A be a square matrix of type $n \times n$ is similar to a diagonal matrix $D,$ then for a suitable matrix $P,$

$$D = P^{-1}AP = PAP^{-1}. \tag{6}$$

Here, the elements of the diagonal matrix D on the diagonal correspond to n different eigenvalues of the matrix $A.$ P is a matrix formed by writing the eigenvectors $x_i \in \mathbb{R}^n$ corresponding to the eigenvalues λ_i for $i = 1, 2, ..., n$ and satisfying Equation (3) as columns [2].

Theorem 2.1.1: Similar matrices have the same eigenvalues [3].

Proof: It is obvious from the definition and determination properties of similar matrices.

Theorem 2.1.2: The necessary and sufficient condition for A be a square matrix of type $n \times n$ to be similar to a diagonal matrix D is that matrix A has n linearly independent eigenvectors [3].

The elements forming the main diagonal of the matrix D mentioned in Theorem 2.1.2 are the n eigenvalues λ_i of the matrix $A.$ With the help of linearly independent eigenvectors $x_1, x_2, ..., x_n$ corresponding to the eigenvalues $\lambda_1, \lambda_2, ..., \lambda_n,$ the matrix P with columns $x_j, j = 1, 2, ..., n,$ respectively, is obtained [3]. In this case we can state the following theorem.

Theorem 2.1.3: A square matrix A of type $n \times n$ is diagonalisable if all roots of the characteristic polynomial are real and different from each other [1–6].

Proof: It is easily shown from the definitions of linear independence, characteristic polynomial and eigenvector.

3. RESULTS

Definition 3.1.1: Let A be a real valued matrix of type $n \times n$ whose eigenvalues $\lambda_1, \lambda_2, ..., \lambda_n \in \mathbb{R}$ are real numbers. The biggest eigenvalue by absolute value is called the dominant eigenvalue of matrix A [3].

Example 3.1.1: The eigenvalues of matrix $A = \begin{bmatrix} -5 & 6 & -14 \\ 0 & 1 & 2 \\ 0 & 0 & 3 \end{bmatrix}$ are −5, 1, 3. In this case, the dominant eigenvalue of A is −5 since it is $|-5| > 1$ and $|-5| > 3$. There may also be more than one dominant eigenvalue.

Let the real values of $\lambda_1, \lambda_2, ..., \lambda_n \in \mathbb{R}$ be the eigenvalues of a real-valued matrix A of type $n \times n.$ In this case, let $x_1, x_2, ..., x_n$ be the linearly independent eigenvectors corresponding to these eigenvalues respectively. Then by Theorem 2.1.3 A is a diagonalisable matrix. Also, the set $S = \{x_1, x_2, ..., x_n\}$ is a base of $\mathbb{R}^n.$ In this case, we can write the vector $x \in \mathbb{R}^n$ as combination of vectors in S as follows.

$$x = c_1 x_1 + c_2 x_2 + ... + c_n x_n. \tag{7}$$

For $k \in \mathbb{N}$ with the help of the vector $x \in \mathbb{R}^n$ obtained by Equation (7),

$$Ax, A^2 x, ..., A^k x, ... \tag{8}$$

we can write the sequence. We can write this sequence more clearly as follows.

$$\left. \begin{aligned} Ax &= c_1 A x_1 + c_2 A x_2 + ... + c_n A x_n = c_1 \lambda_1 x_1 + c_2 \lambda_2 x_2 + ... + c_n \lambda_n x_n \\ A^2 x &= c_1 \lambda_1 A x_1 + c_2 \lambda_2 A x_2 + ... + c_n \lambda_n A x_n = c_1 \lambda_1^2 x_1 + c_2 \lambda_2^2 x_2 + ... + c_n \lambda_n^2 x_n \\ &\quad\quad\quad\quad\quad\quad \vdots \\ A^k x &= c_1 \lambda_1^k x_1 + c_2 \lambda_2^k x_2 + ... + c_n \lambda_n^k x_n \\ &\quad\quad\quad\quad\quad\quad \vdots \end{aligned} \right\} \tag{9}$$

Let λ_n be the dominant eigenvalue of matrix A. In this case for $\forall i < 1$, $|\lambda_n| > |\lambda_i|$, and $\left| \dfrac{\lambda_i}{\lambda_n} \right| < 1$ we find,

$$A^k x = c_1 \lambda_1^k x_1 + c_2 \lambda_2^k x_2 + ... + c_n \lambda_n^k x_n = \lambda_1^k \left(c_1 \left(\frac{\lambda_1}{\lambda_n} \right)^k x_1 + c_2 \left(\frac{\lambda_2}{\lambda_n} \right)^k x_2 + ... + c_n x_n \right). \tag{10}$$

Finally for $k \to \infty$,

$$A^k x \to \lambda_n^k c_n x_n \tag{11}$$

is obtained. Thus, the convergence of the sequence obtained by Equation (8) can be given by the following theorem.

Theorem 3.1.1: Let A be a diagonalisable matrix of type $n \times n$ with all eigenvalues real and dominant eigenvalue λ_n. In this case,

i.   If $|\lambda_n| < 1$ the sequence of vectors $A^k x$ converges to zero for any vector x.

ii. If $|\lambda_n| > 1$ the sequence of vectors $A^k x$ is not convergent.

iii. If $|\lambda_n| = 1$ converged limit value of the sequence of vectors $A^k x$ is an eigenvector corresponding to the eigenvalue λ_n.

4. CONCLUSION

In this study, it is shown where the sequence of vectors $Ax, A^2 x, ..., A^k x, ...$ obtained from a diagonalisable matrix A converges with the help of the dominant eigenvalue based on different real eigenvalues. Similar results can be obtained when the matrix A has a real eigenvalue and a folded eigenvalue, provided that this folded eigenvalue is the dominant eigenvalue. Again, using the concept of norm in complex numbers, the convergence of the vector sequence can be investigated.

References

[1]   F. Basar, *Lineer Cebir*, 3rd ed. Istanbul: Surat Universite Yayinları, 2012.
[2]   H. Keles, *Lineer Cebire Giris I*, 2nd ed.: Bilal Ofset, 2015.
[3]   B. Kolman and D. R. Hill, *Uygulamalı Lineer Cebir*, O. Akin, Cev. Ed. Ankara: Palme Yayincilik, 2011.
[4]   A. Sabuncuoglu, *Lineer Cebir*, Ankara: Nobel Yayinları, 2008.
[5]   R. Kaya, *Lineer Cebir*, Anadolu Universitesi Egitim, Saglik ve Bilimsel Arastirma Calismaları Vakfi Yayinları No: 40, 1993.

[6]   *Dominant eigenvalue* [Online]. Available: https://www.sciencedirect.com/topics/mathematics/dominant-eigenvalue

Electronic and Optical Properties of Inorganic Perovskites: A DFT Study for Solar Energy Conversion

Lakhdar Benahmedi[1], Anissa Besbes[1], Radouane Djelti[1]

[1]Laboratory of Technology and Properties of Solids, Abdelhamid Ibn Badis University, Mostaganem, Algeria
Corresponding author: Lakhdar Benahmedi (e-mail: Lakhdar.benahmedi@gmail.com)

Abstract

This study presents a comprehensive density functional theory (DFT) investigation of novel inorganic perovskites for solar cell applications, employing the Wien2k software. The structural, electronic, and optical properties of the perovskites were systematically analyzed using the generalized gradient approximation (GGA) and the modified Becke-Johnson (mBJ) exchange-correlation functional. The optimized lattice parameters for the perovskite structures were found to be approximately 4.12 Å, indicating good agreement with experimental and theoretical values. Electronic structure calculations reveal a direct band gap of approximately 1.75 eV, which is within the optimal range for photovoltaic applications. The calculated optical properties, including the absorption coefficient and dielectric function, demonstrate strong absorption in the visible range, making these materials suitable for solar energy harvesting. Additionally, the effective masses of electrons and holes were found to be 0.22 m_e and 0.31 m_e, respectively, suggesting efficient charge carrier mobility. To evaluate the photovoltaic performance, solar cell devices were simulated using the SCAPS-1D software, incorporating the studied perovskites as the absorber layer. The simulated power conversion efficiencies (PCE) reached up to 18.5%, highlighting the potential of these materials in next-generation solar cells. This work provides valuable insights into the potential of inorganic perovskites as efficient and stable materials for solar energy conversion, contributing to the ongoing development of sustainable energy technologies.

Keywords: Density functional theory, Inorganic perovskites, Wien2k, Solar cell, Photovoltaic efficiency

An Optimization of Organic Solar Cell Using SCAPS-1D Simulation Based on Genetic Algorithm

Samia Moulebhar[1], Chahrazed Bendenia[1], Hanaa Merad-Dib[1], Souhila Bendenia[1], Sid Ahmed Khantar[1], Sarra Merabet[1]

[1]Faculty of Sciences and Technology, University Abd El Hamid Ibn Badis, 27000 Mostaganem, Algeria
Corresponding author: Samia Moulebhar (e-mail: samia.moulebhar.etu@univ-mosta.dz)

Abstract

In simulation, it is often difficult to identify the relevant values for material properties. In this context, we have proposed an approach to optimise the efficiency of organic solar cells, a promising technology in the renewable energy sector, using genetic algorithms. Our method identifies the objective functions to be maximised by taking into account the interactions between different parameters, such as the thickness of the active layer, the electron transport layers (ETL) and the hole transport layers (HTL), as well as the doping of these layers. The results of our study show that optimum performance is achieved with active layer, ETL and HTL thicknesses of 100.86 nm, 79.9 nm and 20.24 nm, respectively, and dopings of 8.71E+21 cm^{-3} for the active layer, 9.90E+21 cm^{-3} for the HTL and 9.49E+21 cm^{-3} for the ETL. Analysis using SCAPS-1D software confirms that these parameter values enable optimum performance to be achieved. After optimisation using genetic algorithms, the power conversion efficiency (PCE) was improved by 39% compared with previous work. This study highlights the effectiveness of our hybrid approach for improving the performance of organic solar cells, with strong agreement between the results obtained using genetic algorithms and SCAPS-1D. This opens up some promising prospects for the future of organic solar cells.

Keywords: Organic solar cell, SCAPS-1D, GA, Optimization, Efficiency

Enhancing Stability and Thermal Conductivity of Nanofluids: Insights into Advanced Formulations for Energy Systems

Sanae Bayou[1], Chouki El moujahid[1], Tarik Chafil[1]

[1]Chemical Engineering and Resources Valorisation Group, Faculty of Sciences and Techniques, Abdelmalek Essaadi University, Tangier, Morocco
Corresponding author: Sanae Bayou (e-mail: bayousanae@gmail.com)

Abstract

Nanofluids, consisting of nanoparticles dispersed in base fluids, have gained significant attention for their potential in improving heat transfer performance in energy and industrial applications. This work provides a comprehensive overview of nanofluid stability, formulation strategies, and thermophysical property characterization, focusing on key aspects of their development and analysis. The stability of nanofluids is critical to their performance and is addressed through methods such as zeta potential analysis, sedimentation studies, and particle size distribution measurements. Various approaches to enhance stability, including surface functionalization, the use of dispersants, and optimization of formulation parameters, are explored. In addition, the thermophysical properties of nanofluids, including thermal conductivity, viscosity, and specific heat capacity, are systematically analyzed. Characterization techniques such as the transient hot-wire method and rheological studies are discussed, highlighting the factors influencing property enhancement, such as nanoparticle type, size, concentration, and base fluid composition. This presentation offers a holistic view of the formulation and characterization processes necessary for the development of high-performance nanofluids. It aims to provide a foundation for researchers and industry professionals interested in harnessing nanofluids for advanced thermal management systems and energy-efficient technologie.

Keywords: Nanotechnology, Thermal conductivity, Nanofluids, Materials characterization

Influence of Connector Forces on the Multi-Directional Configuration of a Hexagonal Modular Floating Structure

Nur Hanani Ahmad Azlan[1], Nik Mohd Ridzuan Shaharuddin[1,2], Arifah Ali[1]

[1] Department of Aeronautics, Automotive and Ocean Engineering, Faculty of Mechanical Engineering, Universiti Teknologi Malaysia, Johor Bahru, Malaysia
[2] Marine Technology Centre, Institute for Vehicle System and Engineering, Universiti Teknologi Malaysia, Johor Bahru, Malaysia
Corresponding author: Nur Hanani Ahmad Azlan (e-mail: nhanani4@gmail.com)

Abstract

The preliminary design of a hexagonal modular floating structure (HMFS) system comprises four configurations: U-shaped, VP-shaped, VV-shaped and centre layout which connect three hexagonal modules that form a network of connectors. The connector force plays a crucial role in determining the configuration of the connector network, as it must endure the forces generated by wave motion. This paper outlines the establishment of the HMFS connector network and the determination of the impact of the connector horizontal force using four types of configurations. In order to propose design concepts for HMFS configurations, simulation was conducted for regular waves in the following directions: 0º, 30º, 45º, 60º, 85º, and 90º. The analysis takes into account the influences of various wave directions and HMFS configurations on the connector forces. The analysis indicated that the connector force in the centre configuration and VV-shaped configuration is higher than the load in the other two HMFS configurations. The VV-shaped configuration, which has hexagonal vertices oriented towards wave direction, experiences a greater connector force than the VP-shaped configuration, which aligns its hexagonal parallel side with the wave directions.

Keywords: Hexagonal floating structure, Connector force, Connector arrangement, Module arrangement

Experimental Study of the Effect of the Rotating Grooved Tube on Adjacent Tubes in a Linear Tube Bundle

Ismail Drai[1,3], Tayeb Yahiaoui[2,3], Rachid Sahnoun[1], Habib Merouane[1], Omar Imine[2,3]

[1]Department of Mechanical Engineering, Mustapha Stambouli University, Mascara, Algeria
[2]Department of Mechanical Engineering, University of Science and Technology USTO, Oran, Algeria
[3]Department of Mechanical Engineering, LASP Laboratory for Aeronautics and Propulsive Systems, Mnaouer, Oran, Algeria
Corresponding author: Ismail Drai (e-mail: ismail.drai@gmail.com)

Abstract

In an experimental study conducted in the mechanical engineering workshop at the University of Mascara, a bundle of tubes was investigated. Fifteen tubes were arranged in line within a subsonic wind tunnel, with one of the tubes being grooved and capable of rotating at various speeds. The objective was to analyze the distribution of the pressure coefficient around the tubes in different configurations, comparing the results between bundles composed solely of non-grooved tubes and those that included a grooved tube, both in fixed and rotating modes. These tube bundles are widely used in numerous industrial applications. However, they can be susceptible to various types of damage or issues, including cracks, which can affect their performance and durability. Therefore, it is essential to regularly monitor the condition of the tube bundles to detect any signs of damage and implement preventive maintenance measures to avoid failures. This experimental study has enhanced the understanding of the performance and behavior of tube bundles, thereby facilitating the identification of potential cracking risks and the establishment of appropriate preventive measures to ensure their integrity and optimal functioning.

Keywords: Rotating tube, Grooved tube, Flow morphology, Tube bundle, Fluid dynamics, Aerodynamic forces

Fractional Brownian Motion-Based Fractal Analysis of EEG Signals for Evaluating Neural Complexity in Alzheimer's Disease

Hadj Abdelkader Benghenia[1,2], Hadj Slimane Zine-Eddine[2], Hadj Ali Bakir[3,4]

[1]Department of Electronics and Telecommunications, Faculty of science and technology, Ain Temouchent University Belhadj Bouchaib, Algeria
[2]Biomedical Engineering Laboratory, Faculty of Technology, Abou Bekr Belkaid University, 13000 Tlemcen, Algeria
[3]Faculty of Technology, Hassiba Benbouali University of Chlef, Algeria
[4]Laboratory of Signals, Systems, Artificial Intelligence Laboratory Chlef, Algeria
Corresponding author: Hadj Abdelkader Benghenia (e-mail: hadjabdelkader.benghenia@univ-temouchent.edu.dz)

Abstract

Alzheimer's disease (AD) disrupts neural complexity and connectivity, leading to progressive cognitive decline. Electroencephalogram (EEG) signals offer a non-invasive method to analyze these changes in brain activity. This study employs Fractional Brownian motion (FBM) methods—FBM1, FBM2, and FBM3—to perform fractal analysis of EEG signals, quantifying neural complexity in individuals with AD compared to healthy controls. EEG data were collected, preprocessed to remove artifacts, and analyzed using FBM1 for basic Hurst exponent estimation, FBM2 for extended time-series scaling, and FBM3 for multifractal spectrum extraction. The results reveal a significant reduction in fractal dimensions and complexity metrics in Alzheimer's patients, highlighting impaired neural dynamics and connectivity. These findings underscore the potential of FBM-based fractal analysis as a diagnostic and monitoring tool for Alzheimer's disease.

Keywords: Alzheimer's disease, Electroencephalogram, Fractional Brownian motion, Fractal analysis, Neural complexity

1. INTRODUCTION

Alzheimer's disease (AD) is one of the most prevalent neurodegenerative disorders worldwide, characterized by progressive cognitive decline and memory impairment. Affecting millions of individuals, AD poses significant challenges in both diagnosis and treatment due to its complex pathophysiological mechanisms and gradual onset. At its core, the disease disrupts neural connectivity, impairs information processing, and alters the dynamic organization of brain networks. Understanding these alterations is critical for advancing early detection and improving therapeutic interventions [1–3].

Electroencephalogram (EEG) signals, which non-invasively capture the electrical activity of the brain, provide a valuable tool for studying neural dynamics in Alzheimer's disease. EEG analysis offers insights into the underlying changes in brain function, particularly in the synchronization and complexity of neural signals. However, traditional approaches, such as spectral analysis, often fail to fully characterize the complex, non-linear, and dynamic nature of brain activity. This limitation has driven the exploration of advanced analytical techniques capable of capturing the inherent complexity of neural signals [4–6].

Fractal analysis has emerged as a promising approach to studying the intricate properties of EEG signals. Fractals describe structures or signals that exhibit self-similarity and scaling properties, meaning that patterns repeat at different scales. In the context of neural activity, fractal properties reflect the balance between randomness and order in brain signals, which is a fundamental aspect of cognitive function. Alzheimer's disease is associated with disruptions in this balance, leading to decreased neural complexity and impaired brain network dynamics [7, 8]. Among fractal analysis methods, Fractional Brownian motion (FBM) has gained significant attention due to its ability to quantify the stochastic and self-similar properties of time-series signals. FBM is a mathematical model that generalizes Brownian motion by incorporating long-range dependencies and variability in scaling behavior. FBM-based methods, including FBM1, FBM2, and FBM3, offer a detailed framework for analyzing neural complexity in EEG signals. FBM1 focuses on estimating the Hurst exponent, a parameter that reflects the persistence or randomness of the signal. FBM2 extends the analysis by evaluating the scaling behavior of the signal

Fractional brownian motion-based fractal analysis of EEG signals for evaluating neural complexity in alzheimer's disease

ICMUSTED 2024

across different time scales, while FBM3 provides a multifractal spectrum to capture heterogeneity in signal dynamics [9].

In this study, we leverage FBM-based fractal analysis to investigate the neural complexity of EEG signals in individuals with Alzheimer's disease. By applying FBM1, FBM2, and FBM3 to EEG data collected from Alzheimer's patients and healthy controls, we aim to identify changes in fractal properties that reflect the disease's impact on brain function. Specifically, we hypothesize that Alzheimer's patients will exhibit reduced fractal dimensions, altered scaling behaviors, and a narrower multifractal spectrum compared to controls, indicative of impaired neural dynamics and connectivity.

The implications of this work are twofold. First, it enhances our understanding of the alterations in neural complexity associated with Alzheimer's disease, providing a new perspective on the disease's pathophysiology. Second, it highlights the potential of FBM-based fractal analysis as a diagnostic tool for early detection and monitoring of Alzheimer's disease progression. By bridging the gap between mathematical modeling and clinical application, this study contributes to the growing field of computational neuroscience and its role in addressing neurodegenerative disorders.
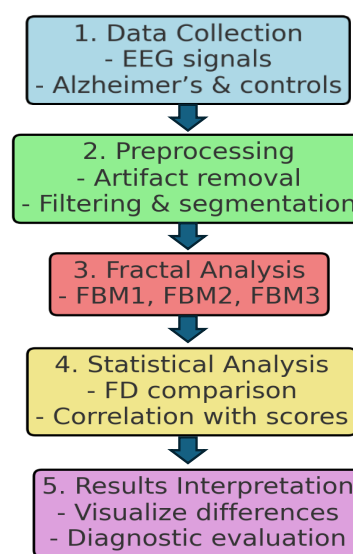
Figure 1. Workflow for fractal analysis of EEG signals using FBM methods for neural complexity assessment in Alzheimer's disease

2. MATERIAL AND METHOD

2.1. Data Collection

Table 1. OpenNeuro dataset ds004504 description

Participant Group	Number of Participants	Description	EEG Details and Recording Protocol
Alzheimer's Disease	36	Participants diagnosed with Alzheimer's disease based on clinical criteria.	Resting-state, eyes-closed EEG recordings using 19 scalp electrodes. Clinical EEG system following standard protocols for data quality.
Frontotemporal Dementia	23	Participants diagnosed with Frontotemporal Dementia, a type of neurodegenerative disorder.	Resting-state, eyes-closed EEG recordings using 19 scalp electrodes. Clinical EEG system following standard protocols for data quality.
Healthy Controls	29	Age-matched healthy individuals with no history of neurological disorders.	Resting-state, eyes-closed EEG recordings using 19 scalp electrodes. Clinical EEG system following standard protocols for data quality.

OpenNeuro Dataset ds004504: This dataset comprises resting-state, eyes-closed EEG recordings from 88 participants, including 36 diagnosed with Alzheimer's disease, 23 with Frontotemporal Dementia, and 29 healthy

Fractional brownian motion-based fractal analysis of EEG signals for evaluating neural complexity in alzheimer's disease

ICMUSTED 2024

controls. The data were collected using a clinical EEG system with 19 scalp electrodes, adhering to standard protocols to ensure data quality [10].

2.2. Preprocessing

The preprocessing of EEG signals is a critical step to ensure high-quality data for fractal analysis. The raw EEG recordings are visually inspected to identify major artifacts such as eye blinks, muscle movements, line noise (50/60 Hz), and other distortions. Segments with significant artifacts are flagged for further processing or exclusion to maintain data quality. Advanced techniques are applied to eliminate artifacts. Independent component analysis (ICA) is used to separate EEG signals into independent components. Physiological artifacts, such as eye blinks and muscle noise, are identified and rejected by analyzing spatial and temporal patterns. Automated methods, such as amplitude thresholding or z-score-based algorithms, are employed to detect and remove high-amplitude noise that may affect signal integrity. To retain relevant neural activity while eliminating noise, filtering is applied. A bandpass filter with a range of 0.5–40 Hz is used. The low cutoff (0.5 Hz) removes slow drifts caused by electrodermal activity or equipment-related noise, while the high cutoff (40 Hz) excludes high-frequency noise from muscle activity or equipment interference. Notch filtering at 50/60 Hz is optionally applied to remove line noise based on the recording environment.

The EEG signals are divided into 2-second non-overlapping epochs to enable detailed analysis. These segments are carefully reviewed to ensure they are free of residual artifacts and suitable for further processing. Re-referencing is performed to improve signal clarity and reduce noise. The linked mastoid reference is commonly used to enhance the signal-to-noise ratio, while the average reference combines all electrode signals to create a mean baseline, providing a uniform reference for all channels. Each epoch is corrected by subtracting the mean value of a pre-stimulus or resting interval. This step removes slow fluctuations and establishes a consistent baseline across all epochs. Additional noise reduction is achieved through spatial filtering, such as Common Average Referencing (CAR) or Laplacian filtering, which enhances the spatial resolution of EEG signals. Automatic noise rejection is also applied to identify and remove noisy epochs exceeding predefined amplitude thresholds (e.g., $\pm 100\ \mu V$).

A final visual inspection of the preprocessed data is conducted to ensure artifacts have been effectively removed and the signals are of high quality. Metrics such as signal-to-noise ratio (SNR) and variance are calculated to confirm the preprocessing efficacy. The clean, preprocessed EEG data are then exported in standard formats such as (.edf), (.mat), or (.csv) for further fractal analysis. Metadata, including electrode positions, sampling rates, and preprocessing steps, are included to ensure reproducibility and transparency. This thorough preprocessing pipeline ensures that the EEG signals are artifact-free and ready for accurate analysis of neural complexity using FBM-based fractal methods.

2.3. Fractal Analysis: FBM1, FBM2, and FBM3

Fractal analysis using FBM is a powerful method for evaluating the neural complexity of EEG signals. This approach examines scaling properties, self-similarity, and randomness in time-series data, with three distinct methods: FBM1, FBM2, and FBM3, each offering unique insights into EEG signal characteristics.

Fractal analysis begins with the examination of the Hurst exponent (FBM1), which quantifies the persistence or randomness in EEG signals. The Hurst exponent (HHH) measures how future signal values depend on past values. If $H > 0.5H$, the signal is persistent, indicating long-range dependencies and higher neural complexity. If $H < 0.5$, the signal exhibits anti-persistence, suggesting frequent changes in direction and lower complexity. If $H = 0.5$, the signal resembles white noise with no memory. The Hurst exponent is computed using techniques such as rescaled range (R/S) analysis, detrended fluctuation analysis (DFA), or wavelet-based methods [11].

FBM2 extends the analysis by investigating the scaling properties of EEG signals across multiple time scales. It examines how signal variance changes as a function of time window size, capturing long-range correlations and dependencies in the signal. Log-log plots of variance against time window length are generated, and the slope of this plot provides the scaling exponent. This analysis highlights the interaction of neural processes across temporal scales, reflecting network-level behavior. The scaling exponent is particularly useful for understanding how Alzheimer's disease impacts long-range connectivity and neural dynamics [12].

FBM3 introduces multifractal spectrum analysis to capture heterogeneity in EEG signal dynamics. Unlike monofractal methods (FBM1 and FBM2), FBM3 examines variations in fractal dimensions within the signal, providing a more detailed picture of neural complexity. The multifractal spectrum is computed for different

Fractional brownian motion-based fractal analysis of EEG signals for evaluating neural complexity in alzheimer's disease

ICMUSTED 2024

moments, characterizing the diversity of scaling exponents in the signal. A broader spectrum indicates richer neural dynamics and higher complexity, while a narrower spectrum reflects reduced variability and lower complexity. Techniques such as the wavelet transform modulus maxima method or multifractal detrended fluctuation analysis are commonly employed [13].

3. RESULTS

The analysis of EEG signals using FBM1, FBM2, and FBM3 revealed significant differences in neural complexity between Alzheimer's disease (AD) patients and healthy controls. The Hurst exponent (H), derived through FBM1 (Figure 2), showed a marked reduction in AD patients, particularly in the lower frequency bands (δ and θ). This reduction indicates diminished persistence and disrupted long-range temporal correlations in their neural activity. In contrast, higher frequency bands (α and β) displayed relatively stable H values, though slight reductions were observed in the frontal cortex, reflecting subtle impairments in those regions.
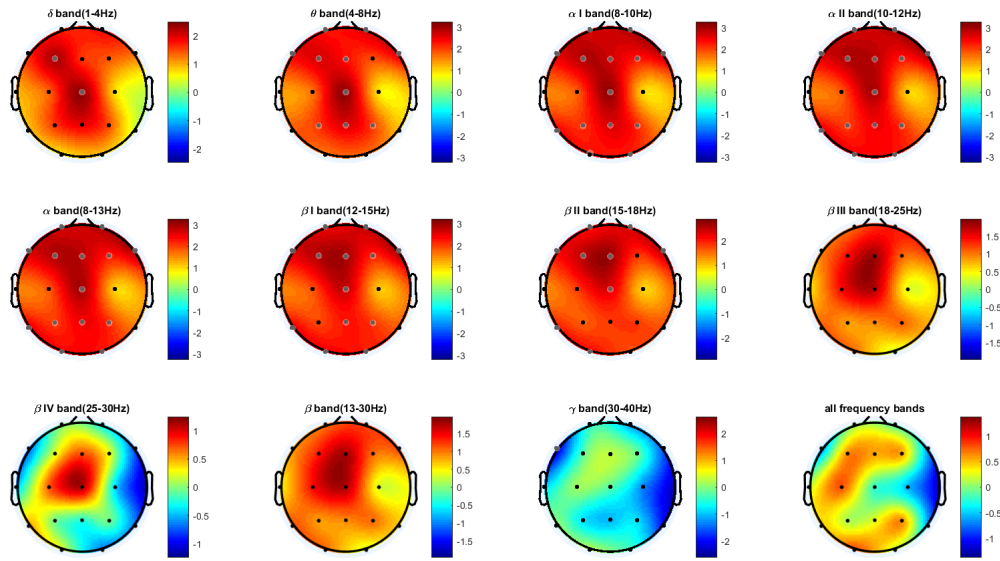
Figure 2. FBM1

FBM2 scaling analysis (Figure 3) highlighted altered scaling properties in Alzheimer's patients across multiple frequency bands. In the δ and θ bands, reduced scaling exponents in the frontal and parietal regions pointed to disrupted neural coordination, while higher variability in the β and γ bands suggested inconsistent activity in these high-frequency oscillations. These changes further emphasize the breakdown in hierarchical neural processes in Alzheimer's disease.

Figure 3. FBM2

Fractional brownian motion-based fractal analysis of EEG signals for evaluating neural complexity in alzheimer's disease

ICMUSTED 2024
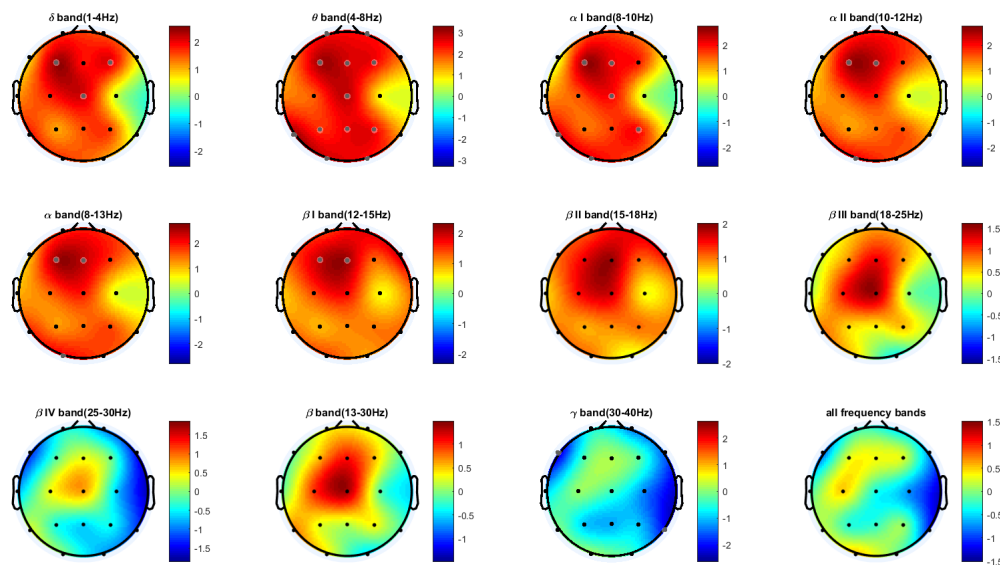
FBM3 analysis (Figure 4) revealed a narrowing of the multifractal spectrum (Dmax−Dmin) in AD patients, signifying reduced heterogeneity in their neural dynamics. The most pronounced changes were observed in the α and β bands, which are critical for cognitive functions such as memory and attention. This reduction in multifractal complexity reflects a loss of variability and adaptability in the brain's neural networks, consistent with cognitive decline associated with AD.
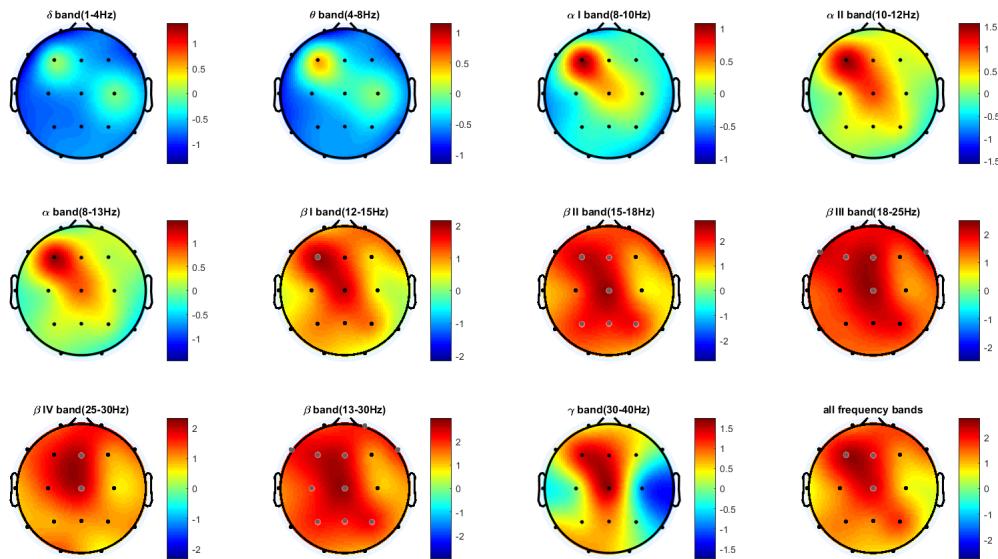
Figure 4. FBM3

Regionally, the most significant alterations were found in the frontal and temporal areas, as illustrated in Figures 2, 3, and 4. These findings align with the known pathological impacts of Alzheimer's disease on these regions. Collectively, the results demonstrate that reduced fractal dimensions, altered scaling properties, and narrower multifractal spectra are key markers of the diminished neural complexity and connectivity characteristic of Alzheimer's disease. These results provide compelling evidence for the utility of FBM-based fractal analysis as a tool for detecting and monitoring neural dysfunction in AD.

4. DISCUSSION

The findings from this study provide significant insights into the alterations in neural complexity associated with Alzheimer's disease (AD) using FBM-based fractal analysis. The reduced Hurst exponent (H) observed in FBM1 reflects a decline in long-range temporal correlations and persistence in neural signals, particularly in the lower frequency bands (δ and θ). These changes are consistent with impaired functional connectivity and disrupted communication within large-scale neural networks, a hallmark of Alzheimer's pathology. The relative stability of H in higher frequency bands (α and β) suggests that these oscillatory activities may be less affected in the earlier stages of the disease, though subtle regional impairments in the frontal cortex were observed.

FBM2 scaling analysis revealed significant disruptions in the hierarchical organization of neural processes, with altered scaling exponents particularly evident in the frontal and parietal regions. These regions are critical for executive functions and cognitive control, which are commonly compromised in Alzheimer's patients. The variability in scaling properties across different frequency bands highlights the differential impact of AD on neural dynamics, with the most pronounced effects in the low-frequency bands critical for long-range connectivity and global integration.

FBM3 multifractal analysis further emphasized the loss of complexity in Alzheimer's patients, as evidenced by the narrowing of the multifractal spectrum. This reduction in multifractal width suggests a loss of heterogeneity in neural signal dynamics, reflecting diminished adaptability and robustness of the brain's neural networks. The most significant changes were observed in the α\alphaα and β bands, which are closely associated with memory and attentional processes. These findings underscore the role of multifractal properties as sensitive markers of cognitive decline and neural degeneration in AD.

Regionally, the most affected areas were the frontal and temporal lobes, consistent with the known progression of Alzheimer's pathology, which initially targets these regions before spreading to other areas of the brain. These

Fractional brownian motion-based fractal analysis of EEG signals for evaluating neural complexity in alzheimer's disease

ICMUSTED 2024

regional effects align with the observed cognitive impairments in memory, executive function, and attention, which are mediated by these brain regions.

Overall, the results demonstrate that FBM-based fractal analysis provides a comprehensive framework for quantifying neural complexity and capturing the subtle changes associated with Alzheimer's disease. The strong correlation between fractal metrics and cognitive scores highlights the potential of these methods as biomarkers for early diagnosis and monitoring of AD progression. Furthermore, the frequency- and region-specific nature of the findings offers valuable insights into the mechanisms underlying the disease, paving the way for more targeted therapeutic interventions.

Future studies should explore the integration of FBM-based metrics with other modalities, such as structural and functional neuroimaging, to provide a more holistic understanding of Alzheimer's pathology. Additionally, longitudinal studies could assess the utility of fractal metrics in tracking disease progression and evaluating the efficacy of therapeutic interventions. These findings reinforce the promise of fractal analysis as a diagnostic and research tool in the field of neurodegenerative diseases.

4. CONCLUSION

This study utilized Fractional Brownian Motion (FBM)-based fractal analysis to investigate the neural complexity of EEG signals in Alzheimer's disease (AD) patients. The analysis methods—FBM1, FBM2, and FBM3—provided critical insights into the changes in signal dynamics and complexity associated with the progression of AD. The results revealed significant alterations in fractal properties across multiple frequency bands, particularly in the δ, θ, and α bands. These alterations included reduced Hurst exponents, narrower multifractal spectra, and altered scaling exponents, all indicative of disrupted neural connectivity and diminished signal complexity in Alzheimer's patients compared to healthy controls. Regionally, the most pronounced changes were observed in the frontal and temporal regions, consistent with the known pathological impact of AD on these areas. The findings highlight the potential of fractal analysis as a diagnostic tool for detecting and monitoring Alzheimer's disease. The significant correlations between fractal metrics and cognitive scores suggest that neural complexity metrics could serve as biomarkers for disease progression. The ability of FBM-based methods to capture frequency- and region-specific changes in neural dynamics makes them particularly valuable for understanding the impact of neurodegeneration on brain function. In conclusion, fractal analysis using FBM1, FBM2, and FBM3 provides a robust framework for quantifying neural complexity and offers promising avenues for early diagnosis, monitoring, and understanding of Alzheimer's disease. Future studies should aim to integrate fractal analysis with other modalities, such as neuroimaging and genetic data, to enhance diagnostic accuracy and unravel the multifaceted nature of AD pathology.

References

[1]   R. Hoghoughi, "Assessing the impact of educating people regarding Alzheimer's disease in Alzheimer's association," Doctoral dissertation, California State University, Northridge, 2022.
[2]   R. Vinay and N. Biller-Andorno, "A critical analysis of national dementia care guidances," *Health Policy*, vol. 130, art. no. 104736, 2023.
[3]   A. P. Porsteinsson, R. S. Isaacson, S. Knox, M. N. Sabbagh, and I. Rubino, "Diagnosis of early Alzheimer's disease: Clinical practice in 2021," *The Journal of Prevention of Alzheimer's Disease*, vol. 8, pp. 371–386, 2021.
[4]   J. Dauwels, F. Vialatte, and A. Cichocki, "Diagnosis of Alzheimer's disease from EEG signals: Where are we standing?," *Current Alzheimer Research*, vol. 7, no. 6, pp. 487–505, 2010.
[5]   G. G. Yener and E. Başar, "Biomarkers in Alzheimer's disease with a special emphasis on event-related oscillatory responses," *Supplements to Clinical Neurophysiology*, vol. 62, pp. 237–273, 2013.
[6]   B. Jelles, P. Scheltens, W. M. Van der Flier, E. J. Jonkman, F. L. da Silva, and C. J. Stam, "Global dynamical analysis of the EEG in Alzheimer's disease: frequency-specific changes of functional interactions," *Clinical Neurophysiology*, vol. 119, no. 4, pp. 837–841, 2008.
[7]   Z. J. Lau, T. Pham, S. A. Chen, and D. Makowski, "Brain entropy, fractal dimensions and predictability: A review of complexity measures for EEG in healthy and neuropsychiatric populations," *European Journal of Neuroscience*, vol. 56, no. 7, pp. 5047–5069, 2022.
[8]   F. M. Smits, C. Porcaro, C. Cottone, A. Cancelli, P. M. Rossini, and F. Tecchio, "Electroencephalographic fractal dimension in healthy ageing and Alzheimer's disease," *Plos One*, vol. 11, no. 2, art. no. e0149587, 2016.
[9]   P. Potgieter, "The fractal geometry of Brownian motion," Doctoral dissertation, University of South Africa, 2004.

Fractional brownian motion-based fractal analysis of EEG signals for evaluating neural complexity in alzheimer's disease

ICMUSTED 2024

[10]   A. Miltiadous, K. D. Tzimourta, T. Afrantou, P. Ioannidis, N. Grigoriadis, D. G. Tsalikakis, and A. T. Tzallas, "A dataset of EEG recordings from: Alzheimer's disease, frontotemporal dementia and healthy subjects," *OpenNeuro*, vol. 1, art. no. 88, 2023.

[11]   C. J. Stam, "Nonlinear dynamical analysis of EEG and MEG: Review of an emerging field," *Clinical Neurophysiology*, vol. 116, no. 10, pp. 2266–2301, 2005.

[12]   K. Linkenkaer-Hansen, V. V. Nikouline, J. M. Palva, and R. J. Ilmoniemi, "Long-range temporal correlations and scaling behavior in human brain oscillations," *Journal of Neuroscience*, vol. 21, no. 4, pp. 1370–1377, 2001.

[13] E. A. Ihlen, "Introduction to multifractal detrended fluctuation analysis in Matlab," *Frontiers in Physiology*, vol. 3, art. no. 141, 2012.

Molecular Structure of Hydroxyapatite bonded PDMS Composite with Enhanced Mechanical Properties – Experimental and Molecular Dynamic Simulation

Chellaiah Ayyanar[1], Sumit Pramanik[1]

[1]Functional and Biomaterials Engineering Laboratory, Department of Mechanical Engineering, College of Engineering and Technology, SRM Institute of Science and Technology, Kattankulathur, Kancheepuram, Chennai, 603203, Tamil Nadu, India
Corresponding author: Sumit Pramanik (e-mail: sumitprs@srmist.edu.in)

Abstract

This research developed a mechanical property of polydimethylsiloxane (PDMS) elastomer mixing with 2wt% nanohydroxyapatite (HA) porous ceramic using conventional method. A series of tensile tests was conducted to evaluate the physical performance of the conventional composites compared to the PDMS specimen. Here, PDMS/HA showed highest stress and elongation. An efficiency obtained based on tensile elongation recovery up to 80% depending upon the HA contained in PDMS composite. Finally, the molecular structure of pure PDMS and HA was compared the result shows that the energies of HA has remarkably reinforced by being filled with a low volume faction of calcium nanoparticles. In addition, this material is easy to make bonding in favorable of optical and mechanical properties. Here, molecular dynamic (MD) simulation technique is used for getting closer insight into the structural background of physical properties of PDMS/HA. The main subject of this paper is an analysis of relationship between the PDMS/HA cross-linking mechanism and its properties. Thus, the present advanced composite exhibited remarkable crack recovery upon unloading conditions could be potential for smart coating applications.

Keywords: PDMS, HA Conventional method, Simulation, Performance, Mechanism

1. INTRODUCTION

A component of the widely recognized organosilicon group of silicones is polydimethylsiloxane, also widely known as PDMS. With its transparent, flexible, and biocompatible qualities, PDMS becomes the most popular silicone based polymers [1]. In recognition of this, polymers are utilized in numerous applications and are frequently encountered in synthetic fibers, plastic bags, paints, glues, lenses, and biomedical equipment [2–5]. Furthermore, the polymeric industry has expanded rapidly and has become among the largest [6].

However, considering its inadequate mechanical qualities, including low strength and elasticity modulus, a number of PDMS applications might be affected. Bulk changes that produce PDMS composites with customized characteristics are one method of getting around this restriction. These changes can be accomplished through altering the pre-polymer composition and by incorporating free molecules (nano or microparticles) [7].

Adding physiologically active nanosized hydroxyapatite to the matrix is one way to enhance the bioactivity and binding characteristics of polymers like PDMS to bone tissues [8]. A novel class of nanostructured biomaterials is represented by the resulting PDMS/HA composite of nanosized hydroxyapatite and polydimethylsiloxane (n-HA/PDMS). While HA encourages bioactivity, PDMS provides the necessary mechanical qualities, potentially resulting in good physical and biological properties for such composites [9]. Bioabsorbable bioactive areas in PDMS are made more conducive to tissue development by the addition of HA [10].

The mechanical characteristics of the PDMS have garnered increasing attention in recent years due to microfluidic devices through simulation studies besides experimental. A unique probe of the mechanisms governing crystallization, such as the water exchange associated with the constituent cations (Ca^{2+} in hydroxyapatite), which has been demonstrated to be the rate-limiting step to crystal growth from aqueous solution of ionic crystals, can be obtained through molecular dynamics (MD) [11] simulations of mineral-water interfaces. Of the polymers in the organosilicone group, polydimethylsiloxane or PDMS is the most frequently used as an elastomeric polymer [12, 13].

Molecular structure of hydroxyapatite bonded PDMS composite with   ICMUSTED 2024
enhanced mechanical properties – Experimental and molecular dynamic
simulation

Therefore, main objective of this research work is to determine the mechanical properties of HA incorporated into PDMS, modes of adsorption on phosphorus surface, their adsorption ability and the active sites of this molecules using Molecular dynamic simulation. A considering property such as cross linking/bonding effect, bond length, bond angle, torsion angle and quantum chemical parameters such as energy of deformation at the geometry optimized using materials studio.

2. MATERIALS AND METHODS

Materials used for PDMS and PDMS/HA composites have already been described in our previous reports [14, 15]. Briefly in the present work, Part A as a resin and Part B as a hardener of silicone formulation of 1:1 (w/w) ratio were weighed according to the mixing ratio provided by the manufacturer. Then, 2 wt% HA were added to the freshly prepared resin and hardener mixture (i.e., PDMS) separately. A desired amount of the HA powder was ultrasonically dispersed in a mixture of Ecoflex PDMS resin and hardener for the preparation of the conventional technique. The porous bioactive ceramic nanopowder was used as an additive in the PDMS composite as bioactive materials. Ecoflex PDMS, $CH_3[Si(CH_3)_2O]nSi(CH_3)_3$, was mixed with porous HA ceramic powder to prepare the composite.

The chemical structures and interactions of PDMS, HA, and their composite system PDMS/HA were investigated in the present research using modeling and molecular dynamics (MD) simulations. By examining the materials' molecular activity under various circumstances, these simulations offer insights into their dynamics and structural characteristics. Materials Studio 2020 (version 20.1), a complete molecular simulation software suite, was used to prepare the molecular structures for PDMS, HA, and the PDMS/HA composite. The program offers resources for creating, displaying, and refining molecular structures. The structures were built using the chemical information that was accessible, and stable configurations were achieved by minimizing energy. To investigate the dynamic behavior of the systems at the atomic level, molecular dynamics simulations were run. Force fields likely the COMPASS force fields, depending on the simulation setup were used to simulate the interactions between atoms and molecules in these simulations. Depending on the simulation setting, MD simulations were usually conducted in NVT or NPT ensembles (constant volume and temperature or constant pressure and temperature).

3. RESULTS AND DISCUSSION

3.1. Mechanical Property

To determine the elongation of the prepared composite material, the static tensile properties of pristine PDMS are compared with conventional PDMS/HA composite as depicted in Figure 1. The flexibility at 1.8 MPa ultimate tensile strength (UTS) of PDMS/HA was 1385%, which is expressively sophisticated than that of pristine PDMS of 725%, as mentioned in Figure 1. The minimum strength of 0.52 MPa obtained by the PDMS is also performed for this study work. Therefore, it is an asset noting that all the prepared polymer-based materials' elongation showed more than 600% compared to the existed PDMS-based nanocomposites, indicating the elastomeric behavior. The static tensile results also indicate that PDMS/HA was much flexible related to pure PDMS, suggesting a good bonding structure interaction. Depending on the level of flexibility and stretching required for various wearable technology applications, elongation is required during stretching. The mechanical properties had been improved compared to the neat samples by further cross-linking with noncovalent bonds. The improvement in mechanical properties, especially, elongation of mechanical property of polymer compared to the neat polymer, had also been reported by several researchers.
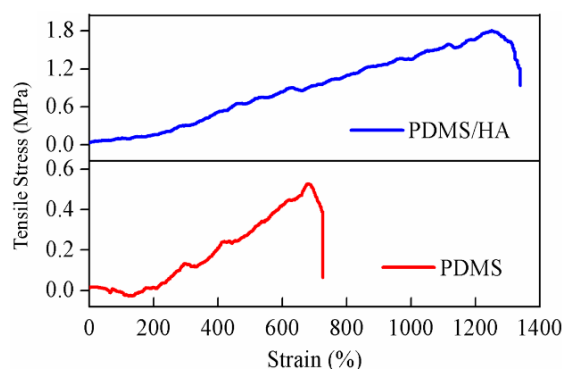
Figure 1. Mechanical properties of PDMS and its composite

Molecular structure of hydroxyapatite bonded PDMS composite with   ICMUSTED 2024
enhanced mechanical properties – Experimental and molecular dynamic
simulation

3.2. Structural Properties

In this research work, the convergence was assessed in the geometry optimization of PDMS/HA as shown in Figure 2. From the molecular properties results were obtained PDMS as well as HA tends to converge and get stable gradually with an increase of optimization step, thus the PDMS/HA model established for geometry optimization simulation. The changing structure of the PDMS/HA molecules after Vamp Process reveals a changed in bond length, bond angle and torsional effects as shown in Table 1.
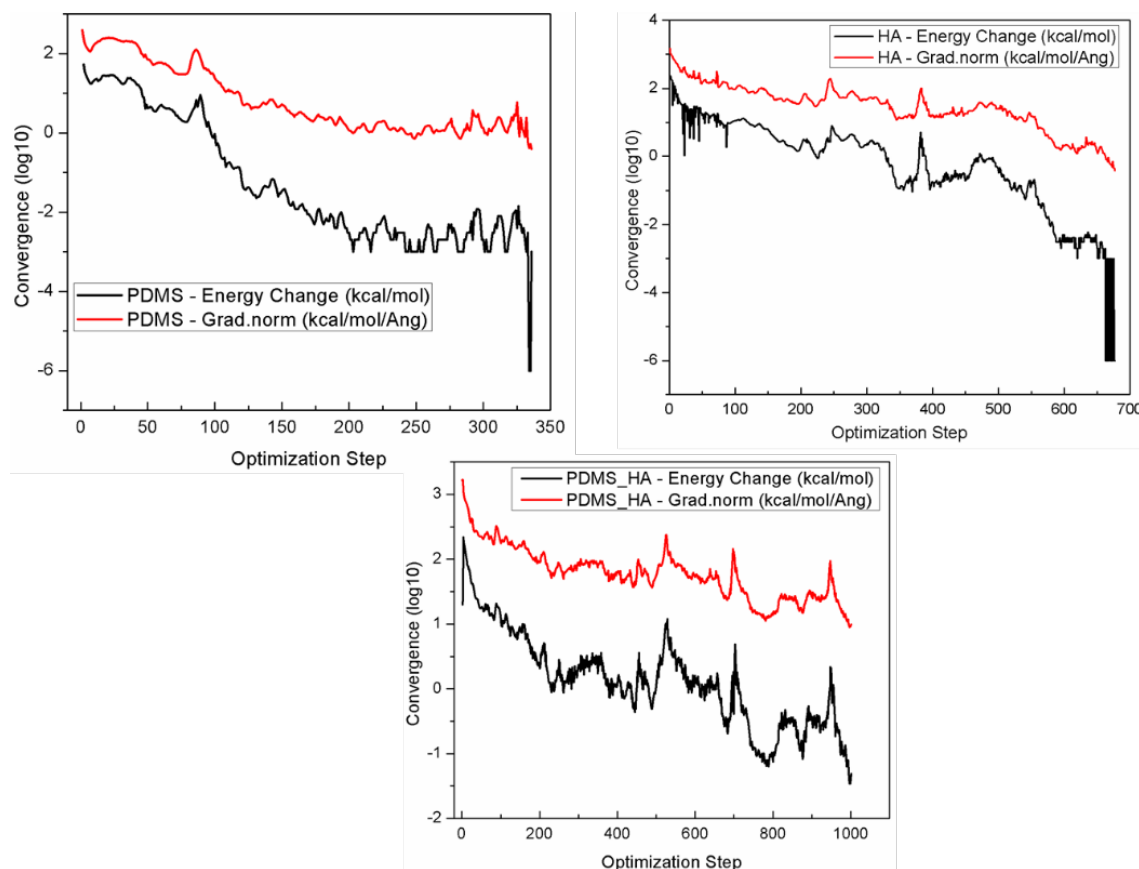
Figure 2. Convergence obtained from PDMS/HA after geometry optimization run

Table 1. Chemical structure parameters obtained from PDMS/HA after vamp run

Atom	Bond Length (Å)	Bond Angle (°)	Max Twist Angle (°)
C42	1.94	156.80	284.92
H61	1.14	100.86	337.88
O29	1.37	134.18	354.83
Si41	5.69	160.85	222.83
P8	1.84	150.05	239.74
Ca40	2.40	150.24	180.00

3.3. Mechanism of Cross Linking

Crosslinking involves are chemical reaction between polymer chains to link together. Polymeric chains are un-cross linked are freer to move around than polymers that are linked together through crosslinking [16]. Cross linked chains should behave quite differently. Chains do not flow as much under stresses like pulling and swell as much in a solvent as unbound chains, which improves chemical/solvent resistance for making a stronger/tougher coating or binder between two materials. Crosslinking is the process of chemically joining two or more molecules by a covalent bond as shown in Figure 3. Modification involves attaching or cleaving chemical groups to alter the solubility or other properties of the original molecule. The PDMS and HA chemical reaction has mentioned in below Equation 1. Cross-linking process simulation was conducted by creating bonds

Molecular structure of hydroxyapatite bonded PDMS composite with enhanced mechanical properties – Experimental and molecular dynamic simulation

ICMUSTED 2024

between reactive sites in close proximity. The bonds will be created between a pair of sites with the smallest distance among possible pairs and then to create new possible pairs between materials. The system is relaxed by another circle of molecular mechanics (MM) and MD to remove any unfavorable interactions due to the formation of new bonds.

$$\left(C_2H_6OSi\right)_n + Ca_{10}\left(PO_4\right)_6\left(OH\right)_2 = \left(C_2H_4OSi\right)_n Ca_{10}\left(PO_4\right)_6 + 2H_2O \tag{1}$$
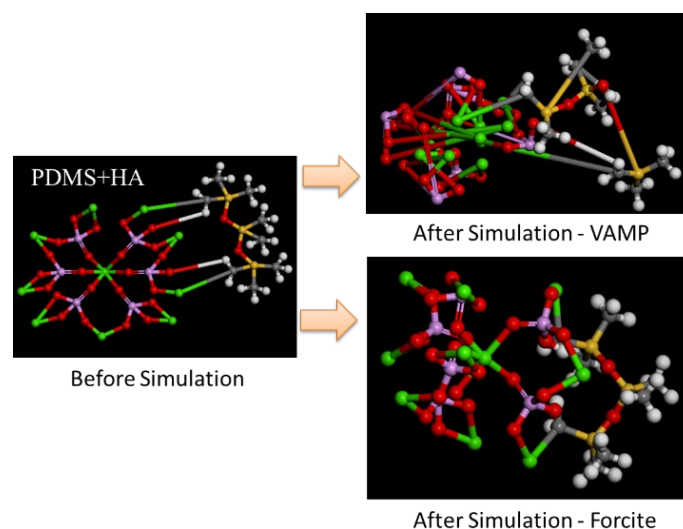
Figure 3. Cross linking effect of PDMS/HA

The method for modelling polymer systems of PDMS creates chain growth as shown in Figure 4. The way the system is created results in a more natural model with greater amorphous characteristics, but still possessing a degree of molecular structure. Polymer-based cross linking molecules are packed into a periodic cell to a specified density manually or by an algorithm such as *Amorphous Cell* from *Materials Studio*. Once this is done, final cross linking can be completed through residual, un-reacted functional groups, followed by electron density, potential effect and molecular dynamics (MD) to relax the molecular structure.
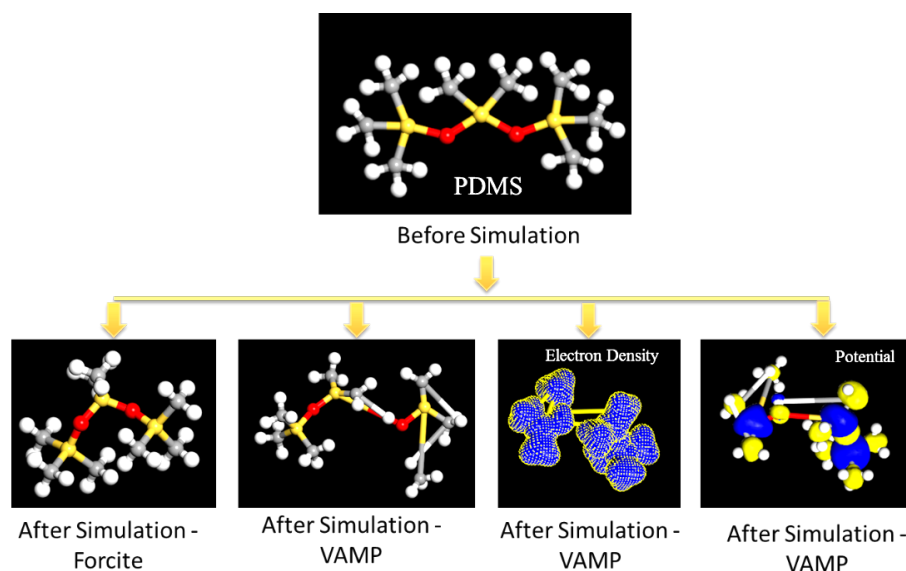
Figure 4. Cross linking effect of PDMS simulation

The method for modelling porous bioceramic systems of HA creates chemical structure as shown in **Figure 5**. Energy minimization is performed followed over 1,000 steps of MD simulation to relax the system, which was then analyzed in order to identify the reactive sites in close proximity. Once this is done, final cross linking can be completed through residual, un-reacted functional groups, followed by electron density, potential effect and molecular dynamics (MD) to relax the molecular structure using forcite and VAMP methods.

Molecular structure of hydroxyapatite bonded PDMS composite with
enhanced mechanical properties – Experimental and molecular dynamic
simulation
ICMUSTED 2024
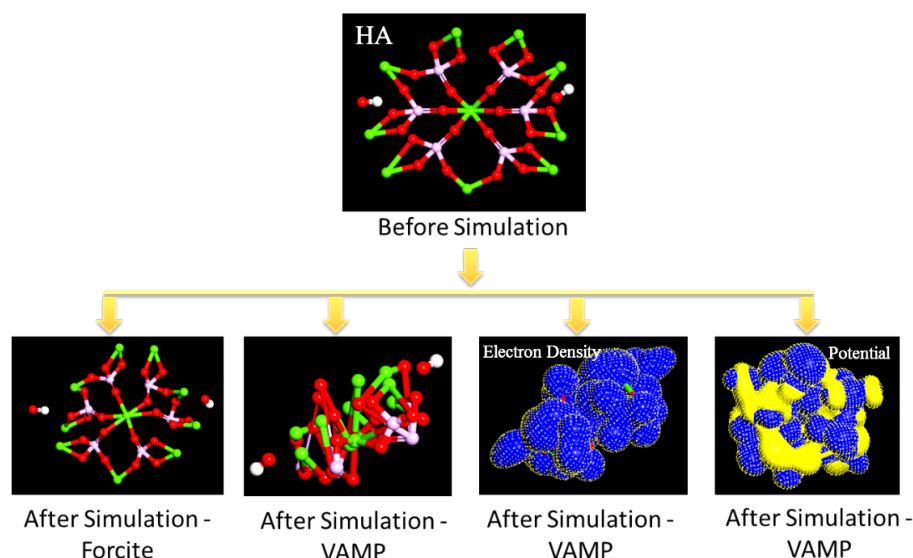
Figure 5. Cross linking effect of HA simulation

3. CONCLUSIONS

A porous bioceramic (HA) with advanced PDMS nanocomposite thin film has been invented in the current research work. The reaction between HA and PDMS through crosslinking mechanism via hydrogen bonds has been noticed. The structural and mechanical analyses have been carried out to determine the mechanical performance for all the samples. Despite highest elongation shown by PDMS/HA composite, the conventional composite has exhibited as best mechanical property performance up to 80% compared with pristine PDMS material. The results showed that the total energy PDMS and HA explosive increased with the increasing of time, which indicates that the compatibility and stability of explosive was strong. Besides, the energy changes in order to illustrating that the intermolecular interaction energy between PDMS and HA crystal surface is stronger. The results seem to indicate that energies of PDMS/HA depend in the major extend on the crosslinking proportion and the particular network topology of the molecular structure. Finally, the effect of cross linking between PDMS and HA has been performed with proper bond length, bond angle and torsion angle also obtained from chemical molecular structure.

References

[1]   S. Fanse, Q. Bao, Y. Zou, Y. Wang, and D. J. Burgess, "Effect of crosslinking on the physicochemical properties of polydimethylsiloxane-based levonorgestrel intrauterine systems," *International Journal of Pharmaceutics*, vol. 609, art. no. 121192, 2021.

[2]   S. Damodara, D. George, and A. K. Sen, "Single step fabrication and characterization of PDMS micro lens and its use in optocapillary flow manipulation," *Sensors and Actuators B: Chemical*, vol. 227, pp. 383–392, 2016.

[3]   A. S. Cruz-Félix, A. Santiago-Alvarado, J. Márquez-García, and J. González-García, "PDMS samples characterization with variations of synthesis parameters for tunable optics applications," *Heliyon*, vol. 5, no. 12, art. no. e03064, 2019.

[4]   J. A. Smith, S. Li, E. Mele, A. Goulas, D. Engstrøm, and V. V. Silberschmidt, "Printability and mechanical performance of biomedical PDMS-PEEK composites developed for material extrusion," *Journal of the Mechanical Behavior of Biomedical Materials*, vol. 115, art. no. 104291, 2021.

[5]   W. Qian, X. Hu, W. He, R. Zhan, M. Liu, D. Zhou, and Y. Huang, "Polydimethylsiloxane incorporated with reduced graphene oxide (rGO) sheets for wound dressing application: Preparation and characterization," *Colloids and Surfaces B: Biointerfaces*, vol. 166, pp. 61–71, 2018.

[6]   M. Arshad, M. Zubair, S. S. Rahman, and A. Ullah, "Polymers for advanced applications," in *Polymer Science and Nanotechnology, Elsevier*, pp. 325–340, 2020.

[7]   M. P. Wolf, G. B. Salieb-Beugelaar, and P. Hunziker, "PDMS with designer functionalities properties, modifications strategies, and applications," *Progress in Polymer Science*, vol. 83, pp. 97–134, 2018.

[8]   M. T. Choy, C.-Y. Tang, L. Chen, W.-C. Law, C.-P. Tsui, and W. W. Lu, "Microwave assisted-in situ synthesis of porous titanium/calcium phosphate composites and their in vitro apatite-forming capability," *Composites Part B: Engineering*, vol. 83, pp. 50–57, 2015.

Molecular structure of hydroxyapatite bonded PDMS composite with enhanced mechanical properties – Experimental and molecular dynamic simulation

ICMUSTED 2024

[9]   L. Fang, P. Gao, and Y. Leng, "High strength and bioactive hydroxyapatite nano-particles reinforced ultrahigh molecular weight polyethylene," *Composites Part B: Engineering*, vol. 38, no. 3, pp. 345–351, 2007.

[10]   F. Abbasi, H. Mirzadeh, and A. A. Katbab, "Modification of polysiloxane polymers for biomedical applications: a review," vol. 50, no. 12, pp. 1279–1287, 2001.

[11]   S. Xiong, S. Chen, S. Jin, and C. Zhang, "Molecular dynamics simulations on dihydroxylammonium 5, 5′-bistetrazole-1, 1′-diolate/hexanitrohexaazaisowurtzitane cocrystal," *RSC Advances*, vol. 6, no. 5, pp. 4221–4226, 2016.

[12]   J. Jakoubková, and L. Kalvoda, "Molecular dynamics simulations of poly (dimethylsiloxane) elasticity," *Acta Physica Polonica A*, vol. 134, no. 3, pp. 857–858, 2018.

[13]   A. Sharfeddin, A. A. Volinsky, G. Mohan, and N. D. Gallant, "Comparison of the macroscale and microscale tests for measuring elastic properties of polydimethylsiloxane," *Journal of Applied Polymer Science*, vol. 132, no. 42, pp. 1–6, 2015.

[14]   C. Ayyanar, and S. Pramanik, "Effect of graphene on self-healing performance of hydroxyapatite/polydimethysiloxane composites," *Materials and Manufacturing Processes*, vol. 38, no. 9, pp. 1068–1080, 2023.

[15]   C. Ayyanar, S. Rakshit, K. Sarkar, and S. Pramanik, "Unprecedented approach of fabrication and analysis of a bioactive PDMS/hydroxyapatite/graphene nanocomposite scaffold with a vascular channel to combat carcinogenesis," *ACS Applied Bio Materials*, vol. 7, no. 5, pp. 3388–3402, 2024.

[16]   Y. Mo, H. Zhang, and J. Xu, "Molecular dynamic simulation of the mechanical properties of PI/SiO$_2$ nanocomposite based on materials studio," *Journal of Chemical and Pharmaceutical Research*, vol. 6, pp. 1534–1539, 2014.

Effect of Ground Granulated Blast-Furnace Slag on the Workability of Recycled Self-Compacting Concrete

Boubakeur Asmaa[1], Menadi Belkacem[1]

[1]Civil Engineering, University of Blida 1, Blida, Algeria
Corresponding author: Boubakeur asmaa (e-mail: asmaaboubekeur27@gmail.com)

Abstract

In the current state of the world, pollution is increasing very rapidly. One of its main reasons is the production of a large quantity of cement, which results in the release of CO_2 into the environment, as well as the deposition of construction and demolition waste on land, leading to soil pollution. To address this major issue, it is important to reduce the use of cement by replacing it with cementitious additives such as slag and by using recycled aggregates to replace natural aggregates. The present study aims to investigate the effect of granulated blast furnace slag (GGBFS) on the workability of recycled self-compacting concrete (RSCC). Coarse natural aggregates (CNA) were replaced by coarse recycled concrete aggregates (CRA) at rates of 50% and 100%, while fine natural aggregates (FNA) were partially substituted at 50% by fine recycled concrete aggregates (FRA). Fresh state tests were conducted, including slump tests, V-funnel flow time tests, L-box tests, and sieve stability tests. The experimental results show that the combined use of GGBFS in RSCC mixes met the EFNARC requirements for filling capacity, passing ability, and resistance to segregation.

Keywords: Ground granulated blast-furnace slag, Recycled aggregates, Recycled self-compacting concrete, Workability

Viable Medical Supply Chains: A Comprehensive Literature Review

Beren Gursoy Yilmaz[1], Omer Faruk Yilmaz[1]

[1]Department of Industrial and Systems Engineering, University of Florida, Gainesville, USA
Corresponding author: Beren Gursoy Yilmaz (e-mail: gursoyyilmazb@ufl.edu)

Abstract

The concept of viability has become increasingly prominent in recent years, driven by the inadequacies of the existing frameworks, particularly following the disruptions caused by the pandemic. This growing focus on viability, especially within the context of medical supply chains (MSC), has garnered significant attention in the literature as researchers seek to address the challenges of ensuring continuous medical products delivery. This study conducts a comprehensive review of 516 research papers retrieved from academic databases, including Google Scholar, Scopus and ScienceDirect, employing selection criteria to assess studies for developing viable MSC networks. Furthermore, the review examines the interconnections between viability, resilience, robustness, and sustainability to identify the key drivers of this emerging concept. The findings reveal an increasing emphasis on viability within MSC research while also exposing critical gaps in the existing literature. By identifying these gaps, this study contributes to a deeper understanding of viable MSC network problems and provides valuable insights for future research.

Keywords: Literature review, Viability, Medical supply chain, Resilience, Sustainability

1. INTRODUCTION

Viability, in the context of supply chains, refers to the ability of a system to sustain itself and adapt in dynamic environments by redesigning structures and replanning operations to ensure long-term functionality. This concept underscores the importance of adaptability, resilience, and long-term operational effectiveness in the face of disruptions [1]. Its significance has grown in response to increasing global uncertainties, including economic volatility, natural disasters, and public health crises. Notably, the COVID-19 pandemic revealed the urgent need for supply chains to maintain continuity while balancing efficiency and resilience, highlighting viability as a critical framework for addressing this challenge [2].

Among supply chains, medical supply chains (MSCs) hold a particularly vital role in ensuring the timely delivery of essential medical resources, especially during global crises. The pandemic exposed significant vulnerabilities in traditional MSC frameworks, underscoring the necessity for more adaptable and sustainable systems [3]. This heightened criticality has brought the concept of viability to the forefront, emphasizing the need to enhance adaptability, manage demand surges, and maintain flexibility to navigate uncertainties. These capabilities are indispensable for supporting healthcare systems during emergencies, such as pandemics or natural disasters, while ensuring seamless operations under unexpected conditions [4].

Viability in MSCs is deeply intertwined with the concept of resilience, robustness, and sustainability [5]. Resilience in this context emphasizes the ability of MSCs to recover quickly from disruptions, such as sudden demand surges for critical medical supplies during a pandemic and restore functionality without compromising healthcare outcomes [6]. Robustness highlights the capacity of MSCs to endure external shocks, such as logistical delays or supply shortages, while maintaining acceptable levels of performance [7]. Sustainability further extends the scope by integrating environmental, economic, and social dimensions, fostering MSC designs that support durable and equitable healthcare systems [8]. By synthesizing these concepts, viability provides a comprehensive framework that enables MSCs to address the challenge of ensuring operational continuity and promoting broader societal goals. This integrative perspective is essential for designing MSCs capable of thriving under both stable and adverse conditions, thereby safeguarding public health [9].

Despite their importance, the design and operation of viable MSCs encounter unique challenges. Regulatory constraints, the perishable nature of medical products, significant variability in demand, and ethical considerations further complicate their management. Additionally, ensuring equitable resource distribution while maintaining operational efficiency highlights the complexity of achieving viability in MSCs [10]. These challenges necessitate

a deeper exploration of the factors driving viability in MSCs and the development of tailored methodologies to address their specific characteristics [11].

To this end, this paper provides a comprehensive review of the literature on viable MSCs, categorizing studies by problem domains, methodologies, and key concepts. It aims to address gaps in the existing literature by examining the interconnections between viability, resilience, robustness, and sustainability. To achieve this objective, the research focuses on two critical questions:

- RQ1: How can the concept of viability be effectively integrated into MSCs networks, and what methodologies have been employed to enhance viability?
- RQ2: What are the problem types in MSC viability, and how are these challenges interconnected with concepts such as resilience, robustness, and sustainability?

These research questions guide the analysis and provide a framework for understanding the complexities of viable MSCs in both theoretical and practical contexts.

The remainder of this paper is organized as follows: Section 2 outlines the research methodology, including the review process and selection criteria for relevant papers. Section 3 presents the review results, offering a comprehensive analysis of the MSC viability literature. Finally, Section 4 concludes the paper by summarizing the key findings and providing recommendations for future research.

2. RESEARCH METHODOLOGY

To understand the state-of-the-art research on MSCs viability, a comprehensive literature review is conducted using the Scopus, Google Scholar, and Science Direct databases. The review is structured around the keywords "medical AND supply AND chain AND viability," ensuring the retrieval of studies explicitly addressing the concept of viability within MSCs. This systematic approach facilitates the identification of relevant research articles, conference papers, and other academic contributions, enabling an in-depth review of the challenges, methodologies, and advancements in this field.
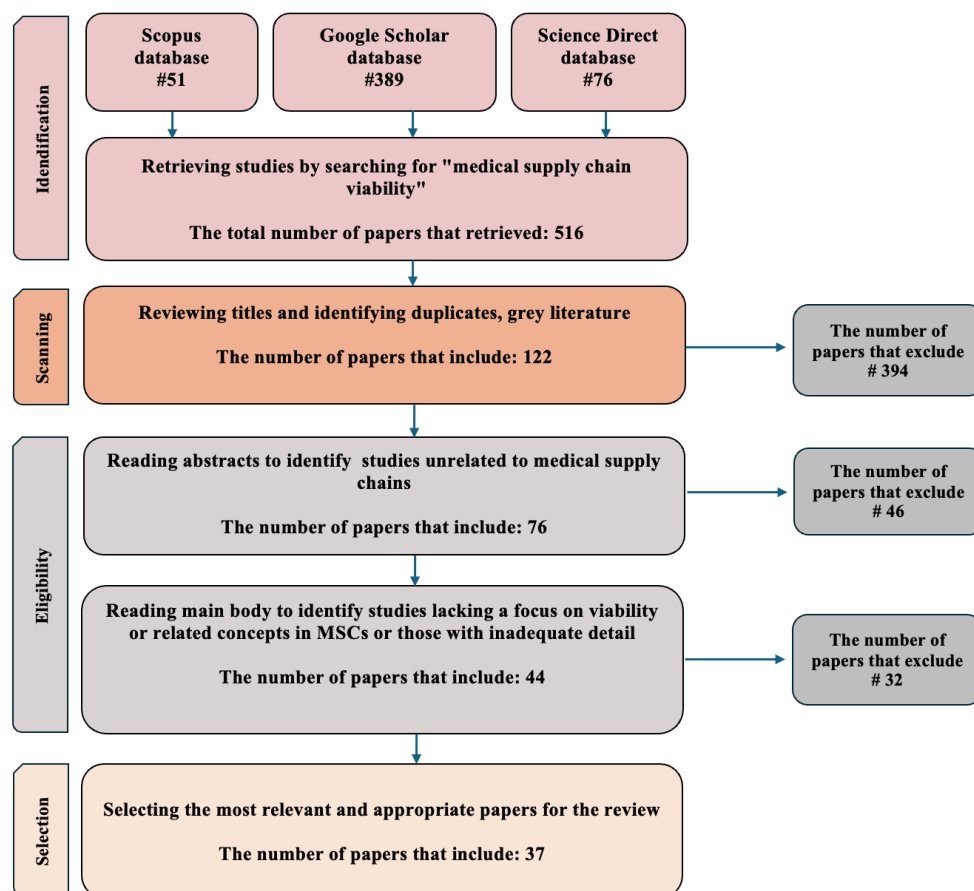
Figure 1. Research methodology flow

The selection of papers for this study follows clearly defined inclusion and exclusion criteria to ensure both relevance and rigor. Studies are included if they focus on MSCs and address viability or its related dimensions, such as resilience, robustness, and sustainability. The review prioritizes peer-reviewed articles, conference proceedings, and book chapters published within the last two decades, with exceptions for foundational works offering significant theoretical insights. Only studies published in English and retrieved from reputable academic databases are considered, with Scopus, Google Scholar, and Science Direct serving as the primary sources. Additionally, freely accessible studies are included to promote broader usability and accessibility.

Exclusion criteria include studies that focus on non-MSC without transferable insights, lack a meaningful discussion on viability or related concepts, or provide insufficient methodological or contextual details. Grey literature, such as blogs or opinion pieces, and duplicate studies, is also excluded. By applying these criteria, this review ensures the inclusion of high-quality, relevant, and accessible contributions to the understanding of viable MSC networks. Figure 1 illustrates the research methodology flow, detailing the selection criteria as well as the number of papers excluded and included during the review process.

3. RESULTS

This section presents the findings obtained from the literature review. Through the applied research methodology, 37 studies are selected and analysed. Figure 2 illustrates the distribution of these studies across years, highlighting the increasing focus on viability in recent research. A significant portion of these studies are published after 2020, a trend largely driven by the outbreak of the COVID-19 pandemic. The pandemic exposes critical gaps in the existing literature and underscores the inadequacy of traditional approaches in ensuring supply chain resilience, catalysing the emergence of "viability" as a prominent concept in academic research [12].
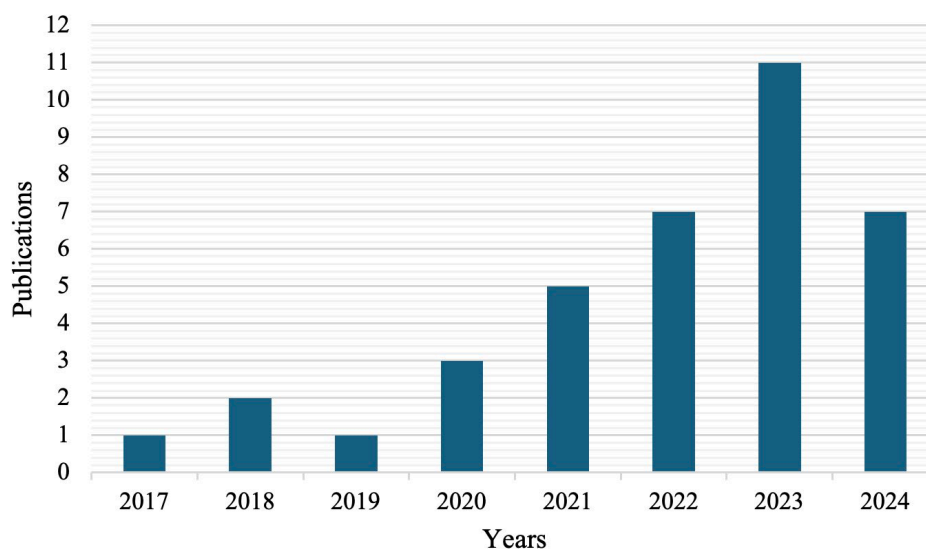
Figure 2. Number of publications across years

Figure 3 categorizes the reviewed studies based on the types of problems they address in either deterministic or uncertain environments. As shown in the figure, network design problems emerge as the most extensively studied area, followed by distribution planning and inventory management. This finding underscores the critical importance of designing resilient and viable MSC networks, particularly in the face of disruptions. Among the studies addressing uncertainty, network design problems dominate, with significant attention given to uncertainties such as demand, and capacity. This highlights the foundational role of network design in MSC viability, as it directly influences the system's ability to adapt to and recover from unexpected events [13]. In addition to network design, inventory planning, supplier selection, and distribution planning also receive substantial attention under uncertain conditions. These studies emphasize the need for efficient resource allocation and flexible operational strategies to address variability and maintain continuity in supply chain operations [14, 15]. Addressing uncertainty in these areas ensures that MSCs can respond effectively to dynamic challenges and disruptions.

Beyond these core problem domains, other areas such as forecasting, blockchain applications, and comprehensive literature reviews also appear in the reviewed studies. Forecasting studies focus on improving demand predictions, while blockchain applications aim to enhance supply chain transparency and traceability under complex conditions

[16, 17]. Literature reviews provide a structured synthesis of existing knowledge, identifying trends and gaps to guide future research on viable and resilient MSC networks [18].
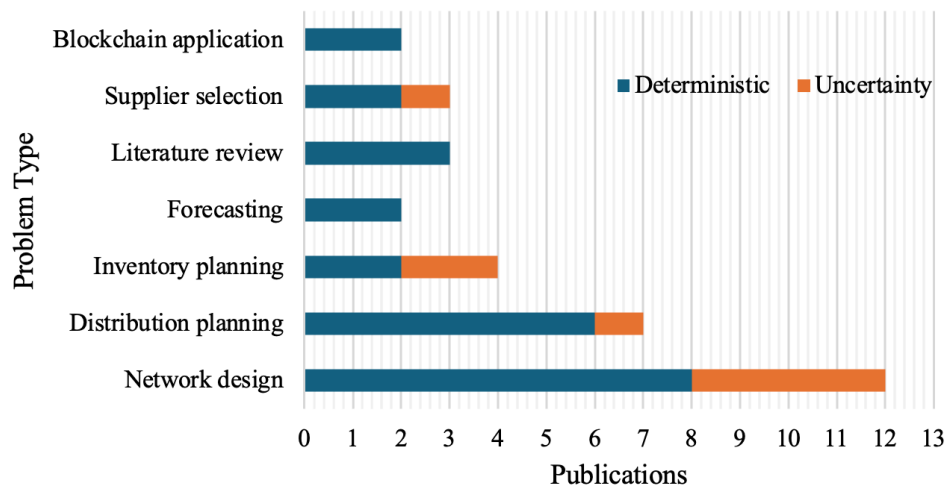
Figure 3. Number of publications by problem types

Figure 4 illustrates the solution methods employed to address the identified problems. Optimization models, such as mixed-integer linear programming (MILP) and robust optimization, emerge as the most commonly utilized methods, accounting for 39% of the reviewed studies. These are followed by metaheuristic approaches, representing 19% of the employed methodologies. Among the metaheuristics, genetic algorithms and particle swarm optimization are particularly prominent due to their effectiveness in solving large-scale and complex problems.
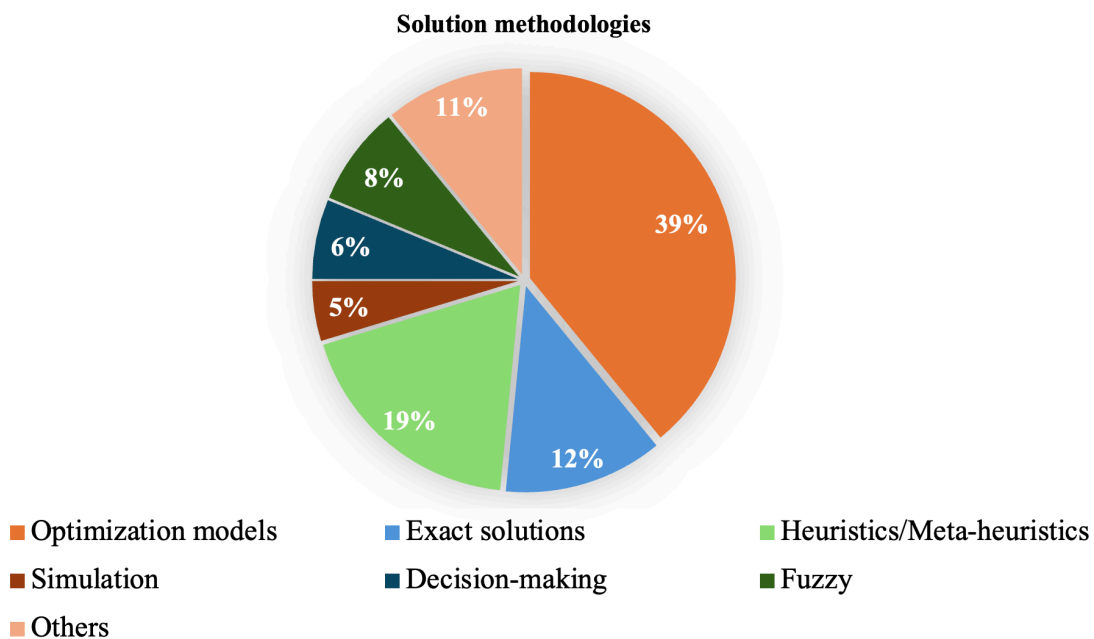
Figure 4. Number of publications by solution methodologies

Additionally, other methods, such as simulation, multi-criteria decision-making techniques, and exact solution methods like branch-and-bound, are also employed to a lesser extent, depending on the problem's requirements. This diversity in solution methods reflects the complexity of the addressed problems, highlighting the need for both precision and computational efficiency in supply chain research.

Figure 5 highlights the keywords commonly addressed in studies related to MSC viability. As shown in the figure, resilience emerges as the most frequently associated concept with viability. Other prominent terms include pandemic, sustainability, and robustness, reflecting their integral role in the discourse on supply chain viability. This prominence arises from the inherent interconnections between these concepts and the multifaceted nature of supply chain viability.

Figure 5. Number of publications by related keywords

As noted above, resilience refers to a supply chain's ability to recover from disruptions, such as natural disasters or pandemics, and return to its baseline or initial state. In contrast, viability adopts a broader perspective, emphasizing the capability to maintain operations and meet customer demands even during prolonged crises. This is achieved through the dynamic adaptation and reconfiguration of supply chains in response to changing conditions, ensuring long-term survival and functionality. Furthermore, while resilience primarily focuses on the economic performance and recovery of individual supply chains, viability integrates resilience and sustainability by considering both economic and societal dimensions. This comprehensive approach addresses not only the sustainability of individual supply chains but also the resilience of interconnected supply networks [19]. The frequent association of pandemic-related terms underscores the critical lessons learned from recent global crises, such as COVID-19, which highlighted the importance of balancing resilience, sustainability, and robustness in MSC management [20].

Ultimately, the interplay of these concepts highlights the necessity of adopting a holistic framework that ensures supply chain functionality and adaptability in both immediate and long-term scenarios, thereby contributing to the broader viability discussion in MSC [21].

4. CONCLUSION AND FUTURE RESEARCH

This study provides a comprehensive literature review analysis of the emerging concept of viability in MSCs, examining its relationship with related concepts such as resilience, robustness, and sustainability The findings emphasize the critical need for adaptable, long-term, and operationally sustainable MSC frameworks, especially in response to disruptions such as the COVID-19 pandemic. Despite significant advancements in the field, several research gaps and future directions are identified, offering opportunities to further develop the concept of viability in complex and uncertain environments.

One promising direction for future research is incorporating uncertainties in various parameters, such as supply disruptions and transportation delays, to provide a more comprehensive approach to addressing operational challenges. Additionally, including deep uncertainty, such as unknown-unknowns, helps better reflect real-world situations. Furthermore, the development of multi-stage stochastic models could capture the evolving needs of MSCs across different disaster phases, including preparation, immediate response, recovery, and long-term rebuilding efforts, ensuring adaptability across various scenarios.

Another promising avenue for future research lies in applying emerging methodologies, such as artificial intelligence and machine learning algorithm, to enhance the prediction and mitigation of risks in MSCs. These methodologies enable more accurate demand forecasting, optimize inventory management, and improve the efficiency of distribution networks, thereby enhancing overall supply chain viability. Moreover, by integrating optimization techniques with machine learning and leveraging real-time data, future studies could develop innovative, adaptive, and data-driven solutions for managing complex and unpredictable MSC environments. Additionally, as environmental sustainability gains prominence, research on green logistics and sustainable procurement practices in MSCs is likely to increase, particularly in developing frameworks that balance environmental, economic, and social goals.

The complexity of modern MSCs also underscores the need for a holistic approach to network design. Future studies could investigate how multi-tiered supply networks and inter-organizational collaboration influence MSC

viability, focusing on both short- and long-term strategies for improving supply chain survivability. The integration of collaborative, cross-functional decision-making processes could further enhance the viability of MSCs, particularly in response to large-scale crises. Additionally, research could explore multi-objective optimization problems, where the simultaneous consideration of conflicting goals, such as minimizing cost, reducing risk, and ensuring service levels, can guide decision-making processes. Developing models that balance these objectives can lead to more resilient and viable MSCs, enabling them to adapt to changing conditions while maintaining optimal performance.

In conclusion, while significant progress has been made in understanding and advancing MSC viability, much work remains. By addressing the identified research gaps, future studies can contribute to the development of more effective, adaptable, sustainable and viable MSCs, ensuring their continued functionality in both stable and disruptive environments.

Acknowledgments

References

[1]   D. Ivanov, "Supply chain viability and the COVID-19 pandemic: a conceptual and formal generalisation of four major adaptation strategies," *International Journal of Production Research*, vol. 59, no. 12, pp. 3535–3552, 2021.

[2]   E. Cumbler, M. Wittig, N. Jacobson, H. McClain, A. Treat, J. Radin, and E. Harry "Contingency planning for health care worker masks in case of medical supply chain failure: Lessons learned in novel mask manufacturing from COVID-19 pandemic," *American Journal of Infection Control*, vol. 49, no. 10, pp. 1215–1220, 2021.

[3]   M. U. Farooq, A. Hussain, T. Masood, and M. S. Habib, "Supply chain operations management in pandemics: A state-of-the-art review inspired by COVID-19," *Sustainability*, vol. 13, no. 5, 2021.

[4]   M. Alizadeh, M. S. Pishvaee, H. Jahani, M. M. Paydar, and A. Makui, "Viable healthcare supply chain network design for a pandemic," *Annals of Operations Research*, vol. 328, no. 1, pp. 35–73, 2023.

[5]   D. Ivanov, "Viable Supply Chain Model: Integrating agility, resilience and sustainability perspectives – lessons from and thinking beyond the COVID-19 pandemic," *Annals of Operations Research*, vol.319, pp. 1411–1431, 2022.

[6]   O. F. Yilmaz, F. B. Yeni, B. Gursoy Yilmaz, and G. Ozcelik, "An optimization-based methodology equipped with lean tools to strengthen medical supply chain resilience during a pandemic: A case study from Turkey," *Transportation Research Part E: Logistics and Transportation Review*, vol. 173, art. no. 103089, 2023.

[7]   R. Lotfi, R. M. Shafiei, M. G. Komeleh, F. G. Pasha, and M. Ferasat, "Vaccine supply chain network design by considering viability, robustness and risk," *Journal of Engineering Research*, in press, 2023.

[8]   R. Lotfi, H. Hazrati, S. S. Ali, S. M. Sharifmousavi, A. Khanbaba, and M. Amra, "Antifragile, sustainable and agile healthcare waste chain network design by considering blockchain, resiliency, robustness and risk," *Central European Journal of Operations Research*, in press, pp.1–34, 2023.

[9]   G. Caggia, J. Fondrevelle, and A. C. Cagliano, "Viability and resilience in the personal protective equipment supply chain. The impacts of Covid-19," *IFAC-PapersOnLine*, vol. 58, no. 19, pp. 1132–1137, 2024.

[10]   R. Lotfi, N. Mardani, S. S. Ali, S.M. Pahlevan, and S. M. R. Davoodi, "A robust and risk-averse medical waste chain network design by considering viability requirements," *RAIRO-Operations Research*, vol. 58, no. 2, pp. 1473–1497, 2024.

[11]   Z. Hussaini, A. Nemati, and M. M. Paydar, "A multi-period multi-season multi-objective mathematical model for guaranteeing the viability of supply chains under fluctuations: a healthcare closed-loop supply chain application," *Annals of Operations Research*, in press, pp. 1–46, 2023.

[12]   K. M Lavassani, Z. M. Boyd, B. Movahedi, and J. Vasquez, "Ten-tier and multi-scale supply chain network analysis of medical equipment: random failure & intelligent attack analysis," *International Journal of Production Research,* vol. 61, no. 24, pp. 8468–8492, 2023.

[13]   R. Lotfi, B. Kargar, A. Gharehbaghi, and G. W. Weber, "Viable medical waste chain network design by considering risk and robustness," *Environmental science and pollution research*, vol. 29, pp. 79702–79717, 2022.

[14]   O. Rostami, M. Tavakoli, A.Tajally, and M. GhanavatiNejad, "A goal programming-based fuzzy best–worst method for the viable supplier selection problem: a case study," *Soft Computing*, vol. 27, no. 6, pp.

2827–2852, 2023.

[15] S. Zaoui, C. Foguem, D. Tchuente, S. Fosso-Wamba, and B. Kamsu-Foguem, "The viability of supply chains with interpretable learning systems: The case of COVID-19 vaccine deliveries," *Global Journal of Flexible Systems Management*, vol. 24, no. 4, pp. 633–657, 2023.

[16] Y. Zhang and D. Wang, "Integrating blockchain technology and cloud services in healthcare: A security and privacy perspective," *Proceedings of the Indian National Science Academy*, vol. 89, no. 4, pp. 837–850, 2023.

[17] R. Agrawal and K. P. Patil, "Blockchain Technology for Medical Records Security Using Fit Viability Approach," in *2nd International Conference on Advancement in Computation & Computer Technologies (InCACCT)*, Gharuan, India, 2024, pp. 805–810.

[18] T. K. Dasaklis and G. T. Tsoulfas, "The Future of Healthcare Supply Chains: Integrating Industry 4.0 Technologies for Improved Resilience and Sustainability," in *Hospital Supply Chain: Challenges and Opportunities for Improving Healthcare,* F. Jawab, Eds. Cham: Springer Nature Switzerland, 2024, pp. 533–551.

[19] D. Ivanov, A. Dolgui, J. Blackhurst, and T.M. Choi, "Toward supply chain viability theory: from lessons learned through COVID-19 pandemic to viable ecosystems," *International Journal of Production Research*, vol. 61, no. 8, pp. 2402–2415, 2023.

[20] J. O. Onyango, "Supply chain solutions for essential medicine availability during COVID-19 pandemic," *Journal of Humanitarian Logistics and Supply Chain Management*, vol. 14, no. 1, pp. 118-133, 2024.

[21] D. Ivanov and A. Dolgui, "Viability of intertwined supply networks: extending the supply chain resilience angles towards survivability. A position paper motivated by COVID-19 outbreak," *International journal of production research*, vol. 58, no. 10, pp. 2904–2915, 2020.

Robust Optimization Model for Resilient Medical Supply Chain Network Design Under Demand Uncertainty

Omer Faruk Yilmaz[1], Beren Gursoy Yilmaz[1]

[1]Department of Industrial and Systems Engineering, University of Florida, Gainesville, USA
Corresponding author: Beren Gursoy Yilmaz (e-mail: gursoyyilmazb@ufl.edu)

Abstract

Recent global crises, particularly the COVID-19 pandemic, have exposed significant vulnerabilities in medical supply chains (MSCs), underscoring the necessity for resilient strategies to manage demand fluctuations and disruptions. This study addresses the resilient MSC network design problem under demand uncertainty. To tackle this problem, a robust optimization model is proposed, aiming to maximize the total quantity of medical products delivered to hospitals. The model incorporates supplier and warehouse opening and allocation decisions using a risk-averse approach that ensures reliable delivery while managing operational costs. Small-sized instances of the problem are solved using GAMS 24.7/CPLEX. Computational results reveal that increasing the the level of robustness enhances the MSC resilience but leads to higher costs due to additional resource allocation. These findings provide strategic insights into designing MSC networks that balance cost-effectiveness and resilience, ensuring uninterrupted delivery of critical medical supplies during crises.

Keywords: Medical supply chain network design, Resilience, Robust optimization model, Demand uncertainty

1. INTRODUCTION

In recent years, ensuring the resilience of medical supply chains (MSCs) has become a critical priority due to the increasing frequency and severity of global disruptions, such as pandemics, natural disasters, and geopolitical conflicts. The COVID-19 pandemic, in particular, exposed significant weaknesses in existing MSC structures, as unprecedented surges in demand led to shortages of essential medical products and delayed deliveries [1]. Unlike other supply chains, MSCs directly impact human lives, as they are responsible for the delivery of life-saving medicines, equipment, and supplies to healthcare facilities [2]. The time-sensitive and high-stakes nature of medical products, combined with stringent regulatory requirements and cold chain logistics, adds a layer of complexity to MSC operations that is less pronounced in other industries. Ensuring the uninterrupted availability of high-demand medical products from suppliers is crucial to prevent delays or gaps in meeting healthcare needs, as any disruption can have severe consequences for patient outcomes [3]. These challenges have underscored the imperative to enhance the flexibility of MSCs to address sudden demand fluctuations and supply disruptions, highlighting the critical role of resilience in maintaining continuity of healthcare services [4].

Resilience in supply chains refers to the ability to withstand and recover from disruptions by adapting to changes and returning to stable operational performance [5]. In the context of MSCs, resilience ensures the availability of vital medical products even under adverse conditions, thereby maintaining hospital operations and patient care when demand or supply conditions fluctuate unexpectedly during disruptions [6].

Recent literature emphasizes the importance of resilience-focused MSC design to address uncertainty in healthcare logistics, proposing various methodologies [7]. For example, [8] developed optimization and simulation models for MSC network design that consider resilience against disruptions. Similarly, [9] introduced a multi-objective robust optimization model for designing the MSC network under disruption. A novel hybrid meta-heuristic algorithm was employed to handle this problem. This approach incorporated budget uncertainty and risk mitigation strategies to improve the sustainability and resilience of the SC. [10] devised a multi-objective distributionally robust optimization model to enhance MSC resilience, emphasizing the role of early warning systems and contingency planning. Furthermore, [11] explored procurement strategies to strengthen resilience in healthcare SC, focusing on effective resource allocation and planning practices to ensure supply continuity. In a related study, [12] offered emergency strategies to minimize costs and maximize profits in a resilient MSC network during pandemics. They formulated an optimization model and utilized digital twins to address disruptions. [13] developed a multi-objective linear programming model to design resilient MSC that balance cost, environmental impact, and social needs. Likewise, [14] proposed multi-objective optimization model for the vaccine SC network

design problem, concentrating on resilience strategies against disruptions. Their study highlighted the importance of these strategies in reducing emissions and enhancing overall SC performance.

While these contributions advance the understanding of MSC resilience, traditional approaches are limited in handling the full scope of uncertainty affecting healthcare logistics. Demand uncertainty, in particular, remains a significant challenge for MSCs due to unpredictable fluctuations and supply risks that disrupt delivery timelines and product availability [15]. To address these challenges, robust optimization has gained attention as a promising approach. Unlike conventional models that assume deterministic environment, robust optimization generates solutions that perform reliably across a range of potential outcomes, enhancing MSC resilience by preparing for worst-case conditions. By accounting for demand variability, robust optimization models mitigate critical shortages, enabling MSCs to maintain service levels even when demand deviates from expected values [16, 17].

Therefore, this study proposes a robust optimization model for designing a resilient MSC network under demand uncertainty. The model integrates supplier and warehouses opening decisions with allocation decisions to design a resilient MSC network capable of adapting to uncertain demand conditions. By embedding robustness into the model, this approach ensures that the MSC can withstand demand uncertainties, minimizing the risk of shortages and maintaining continuity of service during disruptions. The problem is solved using the GAMS 24.7/CPLEX solver for small-sized instances. The study provides decision-makers with a strategic insight to mitigate risks and ensure the continuity of medical services, contributing to the overall sustainability and resilience of the MSC.

The remainder of this paper is organized as follows: Section 2 presents the materials and methods, including the problem description and robust optimization model. Section 3 provides a detailed analysis of the computational results. Finally, Section 4 presents the conclusions, along with recommendations for future research directions.

2. MATERIAL AND METHOD

2.1. Problem Description

This study develops a robust optimization model to design a resilient medical supply chain (MSC) capable of effectively responding to demand uncertainty during disruptions. The MSC is structured as a two-echelon network, comprising product flows from suppliers to warehouses and then from warehouses to hospitals, as illustrated in Figure 1. The network includes a set of potential suppliers S, a set of potential warehouses W, and a set of hospitals K with variable demands for essential medical products. The objective of the model is to maximize the total quantity of medical products delivered to hospitals while ensuring that total costs remain within a predefined budget.
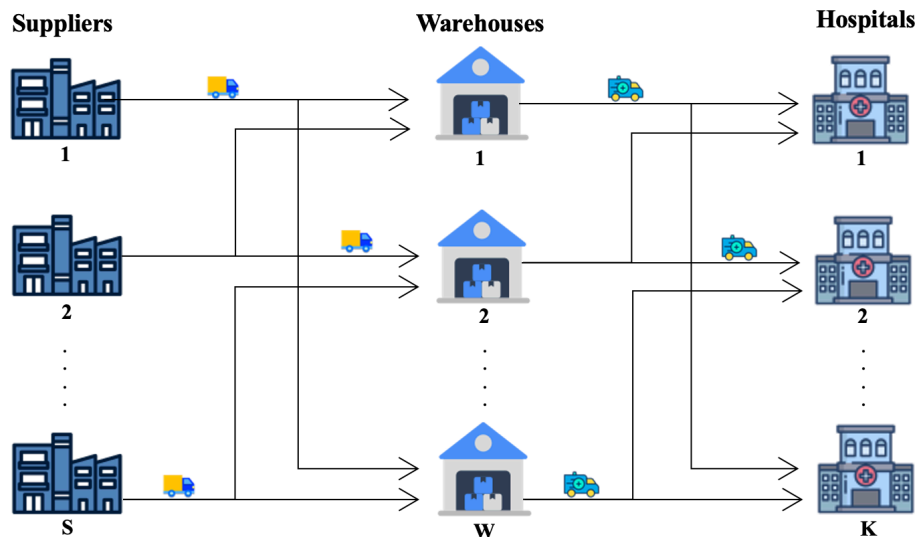
Figure 1. Medical supply chain structure

The model addresses demand uncertainty, which can arise from unexpected events such as pandemics or natural disasters. Demand fluctuations due to these disruptions may lead to critical shortages of essential medical products, adversely affecting patient care and hospital operations. The proposed methodology incorporates robustness to enhance the MSC's resilience and operational efficiency, enabling it to manage demand variability effectively while balancing costs with reliable service delivery during disruptions.

The MSC design problem is formulated based on the following assumptions:

- The MSC design is considered for a one-year planning horizon.
- The quantity of medical products delivered must complies with regulatory limits and healthcare standards.
- All parameters, aside from demand, are known in advance.
- The model considers disruption risks solely in terms of demand for medical products.
- Distances between suppliers, warehouses, and hospitals are assumed to be independent of each other and fixed over the planning period.

2.2. Robust Optimization Model

This section presents the optimization model, including its notations, indices, parameters, and decision variables.

Sets:
S: Set of possible suppliers
W: Set of possible warehouses
K: Set of hospitals

Indices:
s: Index of possible supplier $\left(s \in S\right)$

w: Index of the possible warehouse $\left(w \in W\right)$

k: Index of the demand points, i.e., hospitals $\left(k \in K\right)$

Parameters:
b_{sw} : The distance from the supplier s to the warehouse w

d_{wk} : The distance from the warehouse w to the hospital k

a_s : The opening cost of the supplier s

e_w : The opening cost of the warehouses w

T_k : The demand of the hospital k

g: The shortage cost

C_s : The capacity of the supplier s

C_w' : The capacity of the warehouse w

f: The transportation cost for per mile

v: The total budget limit

Γ : The level of robustness associated with the number of hospitals faced with demand uncertainty

Decision variable:
y_s : If the supplier s is opened 1, otherwise 0

z_w : If the warehouse w is opened 1, otherwise 0

x_{sw} : The number products delivered from the supplier s to the warehouse w

x_{wk}' : The number of products delivered from the warehouse w to the hospital k

p, q_k : Auxiliary non-negativity variables for robust counterpart

The nominal model:

$$z = \max \sum_{w \in W} \sum_{k \in K} x_{wk}' \tag{1}$$

Subject to

$$\sum_{s \in S} a_s y_s + f \left(\sum_{s \in S} \sum_{w \in W} b_{sw} x_{sw} + \sum_{w \in W} \sum_{k \in K} d_{wk} x_{wk}' \right)$$
$$+ \sum_{k \in K} g \left(T_k - \sum_{w \in W} x_{wk}' \right) + \sum_{w \in W} e_w z_w \leq v \tag{2}$$

$$\sum_{w \in W} \sum_{l \in L} x_{sw} \le c_s y_s \quad \forall s \in S \tag{3}$$

$$\sum_{s \in S} \sum_{l \in L} x_{sw} \le c_w^{'} z_w \quad \forall w \in W \tag{4}$$

$$\sum_{s \in S} x_{sw} - \sum_{k \in K} = 0 \quad \forall w \in W \tag{5}$$

$$\sum_{w \in W} x_{wk} - T(k) = 0 \quad \forall k \in K \tag{6}$$

$$s_{sw} \ge 0 \text{ and integer}; \quad \forall s \in S \text{ and } \forall w \in W \tag{7}$$

$$x_{wk}^{'} \ge 0 \text{ and integer}; \quad \forall w \in W \text{ and } \forall k \in K \tag{8}$$

$$y_s \in \{0,1\} \quad \forall s \in S \tag{9}$$

$$z_w \in \{0,1\} \quad \forall w \in W \tag{10}$$

Equation (1) depicts the objective function, which seeks to maximize the total delivered products to hospitals. Constraint (2) ensures that the overall cost does not surpass the total budget limit set to sustain critical operations within the MSC. In order to realize the [18] approach in terms of demand uncertainty, overall cost is given in Constraint (2) and the demand is represented in with unsatisfied amounts. That being the case, the maximization of amount of delivered products as determined as objective function instead of the minimization of overall cost. Constraint (3) guarantees that the capacity of all utilized suppliers remains within limits, while Constraint (4) imposes similar restrictions on capacity of all opened warehouses. Constraint (5) and (6) is formulated to maintain delivered products equilibrium across MSC stages. Constraints (7 to 10) impose sign and binary restrictions.

The robust counterpart:

The constraints presented below are formulated based on the studies conducted by [18] and [19], demonstrating the incorporation of combined interval and polyhedral uncertainty sets into the model to represent demand uncertainty. To integrate these constraints into the nominal model to generate the robust counterpart, constraints (12 to 14) need to be added to the model, while constraint (2) must be replaced by constraint (11).

$$\sum_{s \in S} a_s y_s + f\left(\sum_{s \in S} \sum_{w \in W} b_{sw} x_{sw} + \sum_{w \in W} \sum_{k \in K} d_{wk} x_{wk}^{'}\right)$$
$$+ \sum_{k \in K} g\left(T_k - \sum_{w \in W} x_{wk}^{'}\right) + \sum_{w \in W} e_w z_w + p\Gamma + \sum_{k \in K} q_k \le v \tag{11}$$

$$p + q_k \ge T_k^{'} \quad \forall k \in K \tag{12}$$

$$p \ge 0 \tag{13}$$

$$q_k \ge 0 \quad \forall k \in K \tag{14}$$

$$\left\{T \in Z^{|K|} : T_k - T_k^{'} \le T_k \le T_k + T_k^{'}\right\} \quad \forall k \in K \tag{15}$$

In the formulation, Γ utilized to quantify the number of hospitals subject to demand increases. Auxiliary non-negativity variables, p and q_k are introduced for the robust counterpart, following the approach outlined by [18]. The parameter Γ ranges from 0 and $|K|$ where higher values indicate increased protection through conservative solutions. When $\Gamma = |K|$, it signifies that the demand of all hospitals is affected by the pandemic. Essentially Γ, can gauge the contagious impact of pandemic. Here, $T_k^{'}$ in constraint (12) denotes the extent to which the nominal demand values can deviate from the expected value. Constraint (15) defines the demand deviation interval for the robust counterpart, ensuring the model's feasibility against uncertainty. Overall, the proposed model mitigates the

impact of uncertainty stemming from the pandemic by striking a balance between the measurement parameter and the PoV at an acceptable cost, i.e. the price of robustness.

3. RESULTS

In this section, a numerical example is presented to validate the proposed model using hypothetical data. The example considers three potential suppliers, three potential warehouses, and ten hospitals. Each supplier has a capacity of 20 units, while each warehouse has a capacity of 25 units. The opening costs for the suppliers are 15, 10, and 20, respectively, while the opening costs for the warehouses are 10, 20, and 15. The shortage cost per unit is set at 5, and the transportation cost per mile is 2. The total budget for the system is constrained to 300,000. Distances between suppliers and warehouses, as well as between warehouses and hospitals, are detailed in Table 1. The analysis is performed using GAMS 24.7/CPLEX software on a computer equipped with a 2.50 GHz processor and 16 GB of RAM. Two critical aspects, conservativeness and tractability, are emphasized while solving the robust counterpart of the nominal model. The results are interpreted in terms of these aspects.

Table 1. Distances

Suppliers	Warehouses		
	1	2	3
1	5	12	20
2	3	21	14
3	12	5	8

Warehouses	Hospitals									
	1	2	3	4	5	6	7	8	9	10
1	19	9	12	22	10	7	18	29	30	37
2	7	15	8	26	15	10	38	42	18	6
3	19	29	47	10	24	16	9	13	8	11

A computational study is conducted to examine the impact of the uncertainty parameter on the price of robustness using the proposed robust optimization model. Since the price of robustness is directly linked to the probability of constraint violation (PoV), the results are observed until a predefined probability limitation is reached. The PoV value is computed using the formula $\text{PoV} = e^{-\Gamma^2/2|K|}$ [17], where K represents the number of hospitals potentially affected by crises. Crises, such as pandemic, lead to an increase in patient numbers, thereby escalating the demand for medical products. Figure 2 illustrates the relationship between the PoV and the uncertainty parameter (Γ) which quantifies the number of hospitals subject to demand increases. The figure reveals that PoV decreases as the value of the uncertainty parameter increases. This suggests that as more hospitals are affected by demand variations, the model becomes capable of accounting for a broader range of scenarios, ensuring that constraints remain feasible with a certain probability. Notably, when the uncertainty parameter reaches $\Gamma = 10$, the PoV stabilizes at 0.01 and does not decrease further. This behaviour occurs because $\Gamma = 10$ represents the worst-case scenario, covering all hospitals within the affected by the disruption. Beyond this point, further increases in the uncertainty parameter have no impact on the PoV, as all possible demand variations have already been accounted for.
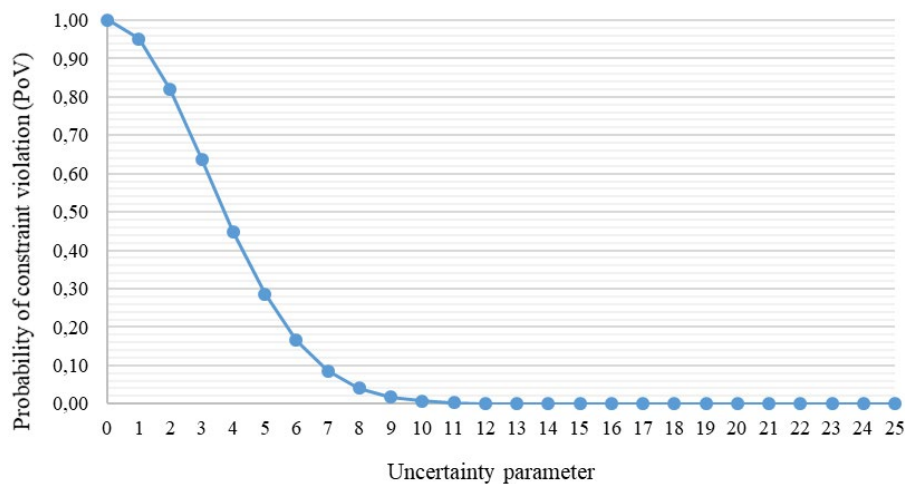
Figure 2. The probability of constraints violation with respect to the uncertainty parameter

Table 2 presents the computational results for different values of the uncertainty parameter Γ. The CPU times shown in the last column demonstrate the model's computational efficiency, indicating that robust solutions are obtained within reasonable time frames, even as Γ increases. This highlights the tractability of the proposed robust optimization model. For all values of Γ, all suppliers and warehouses are utilized to meet demand, showcasing the system's capacity utilization. This consistent utilization reflects the network's robustness in maintaining supply chain functionality, even under heightened uncertainty. Additionally, the objective function values decrease as Γ increases, reflecting the trade-off between balancing costs and ensuring greater robustness.

Table 2. Computational results

Uncertainty Parameter (Γ)	Objective Function (Z)	Utilized Suppliers (S)	Opened Warehouses (W)	CPU Time (sec)
0	16969	1,2,3	1,2,3	1.15
1	10374	1,2,3	1,2,3	4.18
2	9384	1,2,3	1,2,3	5.30
3	8384	1,2,3	1,2,3	6.64
4	7598	1,2,3	1,2,3	7.79
5	7284	1,2,3	1,2,3	7.98
6	7160	1,2,3	1,2,3	8.01
7	7100	1,2,3	1,2,3	9.02
8	7080	1,2,3	1,2,3	10.04
9	7054	1,2,3	1,2,3	11.07
10	7028	1,2,3	1,2,3	13.10

The changes in the objective function and price of robustness values are further analyzed in Figures 3 and 4. Figure 3 shows a substantial decline in objective function values as Γ increases from 0 to 5. This behavior indicates that increasing Γ enhances the network's robustness to demand uncertainty, as the model prioritizes solutions that mitigate vulnerability to disruptions. However, beyond $\Gamma = 5$, the changes in objective function values become negligible, suggesting that the system reaches a point of diminishing returns. This plateau reflects that additional investments in robustness beyond this threshold offer limited improvements in cost-effectiveness or resilience, making such measures less justifiable from a cost perspective.

Similarly, Figure 4 depicts exponential growth in the price of robustness values as Γ increases up to 5 with deviations reaching approximately 53% from the nominal value. The rise indicates that achieving higher levels of conservativeness in the model incurs substantially higher costs. Beyond $\Gamma = 5$, the price of robustness values stabilizes, aligning with the plateau observed in the objective function. This stabilization underscores that while the network remains capable of delivering products effectively, the cost of additional robustness becomes disproportionate to its benefits. These results highlight the importance of identifying an optimal balance between maximizing product deliveries and managing associated costs.
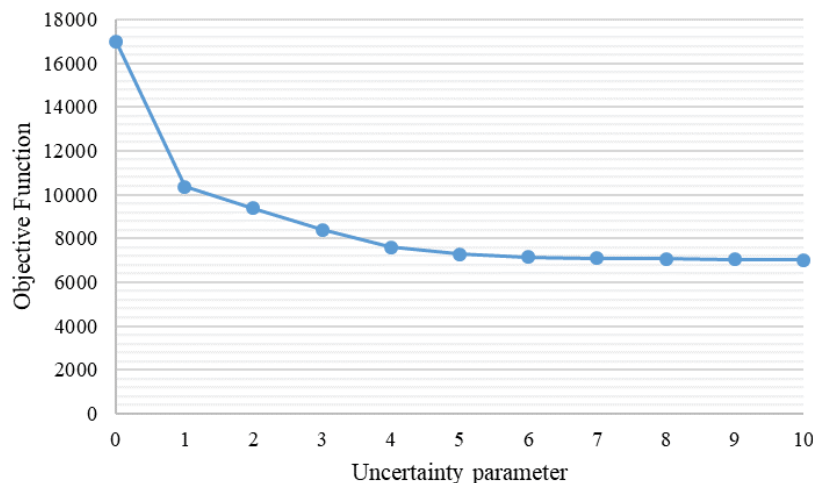
Figure 3. The objective function considering the uncertainty parameter
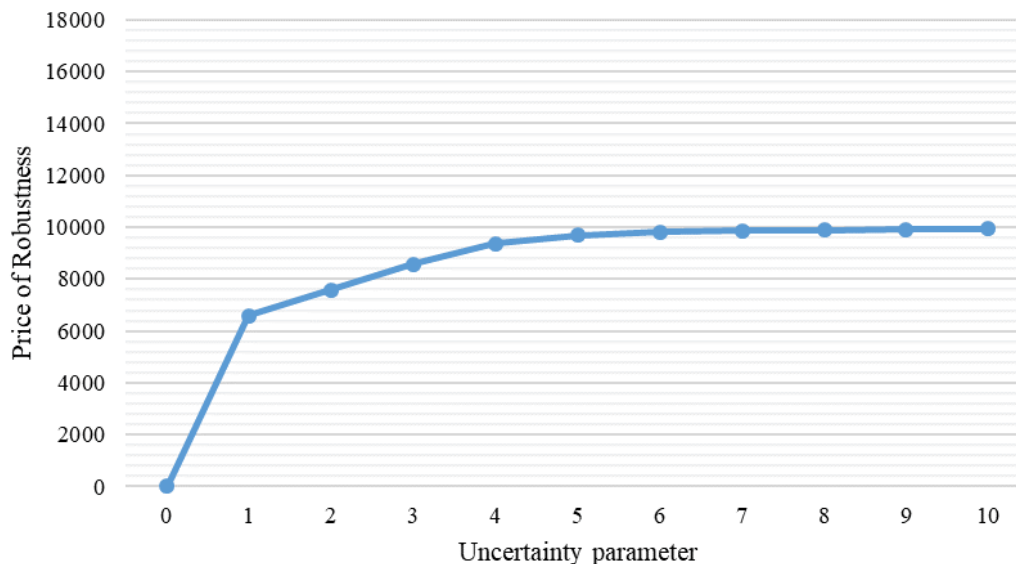
Figure 4. The price of robustness with respect to the uncertainty parameter

Notably, between $\Gamma = 5$ and $\Gamma = 10$, the minimal variation in both objective function and price of robustness values underscores the diminishing returns of higher Γ values. These results demonstrate that while increasing Γ enhances the network's resilience to uncertainty, excessive conservativeness can impose significant costs without yielding proportional benefits. Consequently, decision-makers must carefully assess the trade-offs between robustness and cost efficiency to ensure a sustainable and resilient supply chain.

4. CONCLUSION

This study addresses the resilient MSC design problem under demand uncertainty. A robust optimization model is developed to mathematically represent the problem, accounting for worst-case scenarios to ensure solutions meet requirements even under extreme conditions. The problem is solved using GAMS 24.7/CPLEX solver, resulting in optimal decisions for opening suppliers and warehouses, as well as allocating medical products to meet hospital demands. The findings emphasize the importance of balancing cost efficiency and robustness in MSC design. Furthermore, the results demonstrate that the system accommodates increased demand during crises, preventing supply shortages while ensuring operational reliability.

The robust optimization model effectively captures the trade-off between cost and robustness. By adjusting the robustness parameter (Γ), decision-makers can control the level of conservatism in the model. A higher Γ value provides greater protection against demand uncertainty but may lead to higher costs due to increased resource allocation. Overall, this model provides a strategic tool for designing a MSC network that is both cost-effective and resilient to demand uncertainties, ensuring the continuous delivery of essential medical supplies to hospitals during critical times.

To guide future research and address the limitations observed in this study, several suggestions are proposed. Firstly, incorporating multiple types of uncertainties, such as capacity, transportation delays, and fluctuating resource availability, can enhance the model's applicability to real-world scenarios. Secondly, extending the robust optimization framework to consider multi-objective decision-making, including quality assurance and environmental sustainability, could provide a more comprehensive evaluation of trade-offs. Thirdly, developing metaheuristic algorithms can support solving large-scale MSC problems with greater computational efficiency while maintaining solution quality. Last but not least, integrating advanced data analytics and machine learning techniques can improve demand forecasting and decision-making processes by identifying trends and patterns in MSC operations. By addressing these directions, future studies can build upon the findings of this research, further enhancing the robustness and practicality of MSC network designs.

Acknowledgments

References

[1]   M. Alizadeh, A. R. Kalantari Khalil Abad, H. Jahani, and A. Makui, "Prevention of post-pandemic crises: A green sustainable and reliable healthcare supply chain network design for emergency medical products," *Journal of Cleaner Production*, vol. 434, art. no. 139702, Jan. 2024.

[2]   F. Goodarzian, A. A. Taleizadeh, P. Ghasemi, and A. Abraham, "An integrated sustainable medical supply chain network during COVID-19," *Engineering Applications of Artificial Intelligence*, vol. 100, art. no. 104188, 2021.

[3]   P. Ma, Y. Gong, and M. Jin, "Quality efforts in medical supply chains considering patient benefits," *European Journal of Operational Research*, vol. 279, no. 3, pp. 795–807, 2019.

[4]   O. F. Yilmaz, F. B. Yeni, B. Gursoy Yilmaz, and G. Özçelik, "An optimization-based methodology equipped with lean tools to strengthen medical supply chain resilience during a pandemic: A case study from Turkey," *Transportation Research Part E: Logistics and Transportation Review*, vol. 173, art. no. 103089, May 2023.

[5]   D. Ivanov, "Two views of supply chain resilience," International Journal of Production Research, vol.62, no.11, pp. 4031–4045, Sep. 2024.

[6]   B. Ojo, "Enhancing The Resilience Of The Healthcare Supply Chain Against Pandemics And Bioterrorism," *International Journal of Engineering and Advanced Research Technology (IJEART),* vol. 15, pp. 13–33, 2024.

[7]   A. Dixit and P. Dutta, "Thematic review of healthcare supply chain in disasters with challenges and future research directions," *International Journal of Disaster Risk Reduction*, vol.100, art. no. 104161, Jan. 2024.

[8]   J. Lozano-Diez, J. Marmolejo-Saucedo and R. Rodriguez-Aguilar, "Designing a resilient supply chain: An approach to reduce drug shortages in epidemic outbreaks," *EAI Endorsed Transactions on Pervasive Health and Technology*, vol. 6, no. 21, 2020.

[9]   A. Hasani, H. Mokhtari, and M. Fattahi, "A multi-objective optimization approach for green and resilient supply chain network design: a real-life case study," *Journal of Cleaner Production*, vol. 278, art. no. 123199, 2021.

[10]   C. Ash, C. Diallo, U. Venkatadri, and P. VanBerkel, "Distributionally robust optimization of a Canadian healthcare supply chain to enhance resilience during the COVID-19 pandemic," *Computers & Industrial Engineering,* vol. 168, art. no. 108051, 2022.

[11]   A. Spieske, M. Gebhardt, M. Kopyto, and H. Birkel, "Improving resilience of the healthcare supply chain in a pandemic: Evidence from Europe during the COVID-19 crisis," *Journal of Purchasing and Supply Management*, vol. 28, no. 5, art. no. 100748, Dec. 2022.

[12]   Z. Lv, L. Qiao, A. Mardani, and H. Lv, "Digital twins on the resilience of supply chain under COVID-19 pandemic," *IEEE Transactions on Engineering Management*, vol. 71, pp. 10522–10533, 2024.

[13]   A. Moadab, G. Kordi, M.M. Paydar, A. Divsalar, and M. Hajiaghaei-Keshteli, "Designing a sustainable-resilient-responsive supply chain network considering uncertainty in the COVID-19 era," *Expert Systems with Applications*, vol. 227, art. no. 120334, 2023.

[14]   E. Torshizi, A. Bozorgi-Amiri, and F. Sabouhi, "Resilient and sustainable global COVID-19 vaccine supply chain design considering reverse logistics," *Applied Soft Computing*, vol. 151, art. no. 111041, 2024.

[15]   F. Betto and P. Garengo, "A circular pathway for developing resilience in healthcare during pandemics," *International Journal of Production Economics*, vol. 266, art. no. 109036, 2023.

[16]   A. Hasani and A. Khosrojerdi, "Robust global supply chain network design under disruption and uncertainty considering resilience strategies: A parallel memetic algorithm for a real-life case study," *Transportation Research Part E: Logistics and Transportation Review*, vol. 87, pp. 20–52, 2016.

[17]   G. Ozcelik, O.F. Yilmaz, and F. B. Yeni, "Robust optimisation for ripple effect on reverse supply chain: an industrial case study," *International Journal of Production Research*, vol. 59, no. 1, pp. 245–264, 2021.

[18]   D. Bertsimas and M. Sim, "The Price of Robustness." *Operations Research*, vol. 52, no. 1, pp. 35–53, 2004.

[19]   M. Toloo and E. K. Mensah, "Robust Optimization with Nonnegative Decision Variables: A DEA Approach," *Computers & Industrial Engineering,* vol. 127, pp. 313–325, 2019.

Performance Study of the Anode and Cathode Pressure for Fuel Cell System Regulated by PID Conventional and PID Optimized by Intelligent Algorithm Under Variable Load Demand

Sabah Kabache[1], Hicham Bouregba[2]

[1]Coating, Materials, and Environment laboratory, Physics Department, University of Boumerdes, Algeria
[2]Mechanical, Energy, and Engineering Laboratory, Faculty of Technology, M'Hamed Bougara University, Boumerdes, Algeria
Corresponding author: Sabah Kabache (e-mail: s.kabache@univ-boumerdes.dz)

Abstract

In a proton exchange membrane fuel cell (PEMFC) system, precise pressure control on the anode (H2) and cathode (O2) sides is essential, especially during load variations. Improper pressure regulation can lead to imbalances that damage the fuel cell stack's sensitive membranes. This study introduces a dual-control strategy combining a conventional PID controller with an AG-optimized version to ensure stable membrane pressure within acceptable limits. The approach was validated on a 5 kW PEMFC stack model under 50 A current fluctuations, using Matlab/Simulink simulations. The results demonstrated that conventional regulation with AG-optimized gains effectively mitigated load-induced disturbances, achieving excellent performance in terms of response time, overshoot, and stability. Performance was further confirmed by metrics such as integral absolute error (IAE), integral time absolute error (ITAE), and integral square error (ISE).

Keywords: PEMFC, Hydrogen pressure, Conventional regulation, PID tuned by AG algorithm, Oxygen regulation

1. INTRODUCTION

Fuel cells (FC) are stationary systems that enable the direct conversion of hydrogen's electrochemical energy into electrical power. This innovative technology has garnered significant attention in both industrial and research domains. Among the various fuel cell types, the proton exchange membrane fuel cell (PEMFC) is especially noteworthy for its potential in stationary and mobile applications. Its advantages include a lightweight structure, high power density, and efficient operation at lower temperatures compared to other fuel cell technologies [1].

Several recent studies in the scientific literature have investigated various linear and nonlinear control strategies for the modelling and regulation of fuel cells. Prominent research works in this area include: Andrés Moran Doran et al. [2] present a hybrid control scheme utilizing neural networks for modelling and managing fuel cell systems. The study underscores the significance of accounting for variables beyond reactant supply to enhance fuel cell performance. It reveals that a neuro-PID controller alone is insufficient for voltage stabilization and requires an inverse model control for effective operation. Kai Ou et al. [3] propose a feedforward fuzzy-PID controller aimed at regulating the oxygen excess ratio in PEM fuel cell systems. This approach successfully manages the oxygen excess ratio while minimizing parasitic power losses. The study highlights the integration of PID and fuzzy logic to achieve straightforward and efficient air flow control. Nicu Bizon et al. [4] introduce a strategy for fuel savings in PEMFC systems by switching to a load-following mode for fuelling regulators. This method significantly enhances fuel consumption efficiency, achieving reductions of 14-29% compared to conventional commercial strategies.

Proportional-integral-derivative (PID) controllers continue to be one of the most commonly employed solutions in process control, valued for their straightforward design and effectiveness. Nevertheless, conventional PID parameter tuning typically depends on heuristic or empirical approaches, which may result in less-than-optimal performance, particularly in complex or dynamically changing environments [5]. The optimization of PID parameters has become a critical focus for enhancing the performance of control systems. Genetic Algorithm (GA) has emerged as a promising technique to address this challenge. GA is an optimization approach inspired by the principles of natural selection and genetic evolution, enabling an effective exploration of the solution space to identify the optimal set of parameters [6].

Performance study of the anode and cathode pressure for fuel cell system   ICMUSTED 2024
regulated by PID conventional and PID optimized by intelligent algorithm
under variable load demand

The novelty of this study, introduced a hybrid approach that combines the PID controller with an optimized Genetic Algorithm (GA) to develop an adaptive law. This integration improves the controller's adaptability, allowing it to maintain high performance and effectively manage the complex nonlinear behavior of the fuel cell (PEMFC), as well as handle load disturbances arising from fluctuations in load demand. The performance of the optimized PID controller (PID-GA) is compared with that of the conventional PID controller to enhance gas consumption efficiency and stabilize power output at rated levels during load variations. The primary focus of this work is on maintaining pressure stability at the terminals of the membranes for both oxygen and hydrogen, as fluctuations in these pressures directly impact the system's lifespan and efficiency. The transient performance of the proposed adaptive PID controller is evaluated against that of the classical PID controller (PID-C) using various performance indices.

This work is distributed across several essential parts to comprehensively address the design, modeling, control, and analysis of the fuel cell system. The introduction provides an overview of the problem, objectives, and the significance of the study. The second section, system design and model building, is subdivided into five parts: fuel cell system design, which outlines the system architecture; modeling of the fuel cell system, focusing on mathematical and simulation approaches; output voltage model, detailing the relationships governing voltage generation; dynamic gas transport model, addressing the transport dynamics of reactant gases; and power conditioning, which describes the methods for stabilizing and optimizing power output. The third section, control of the fuel cell system, includes PID control tuned by GA for optimized performance and fuel flow control to enhance efficiency and stability. The fourth section presents simulation results and discussion, analyzing the outcomes and validating the proposed methods. Finally, the conclusion summarizes the key findings and highlights future directions for research.

2. SYTEM DESIGN AND MODEL BUILDING

The aim of this article is to create a pressure control strategy for the anode and cathode of a fuel cell that is better suited to real-world technical applications. This strategy intends to improve fuel cell control systems, especially those with high power capacities. To accomplish this, a 5 kW fuel cell system has been developed as part of the research.

2.1. Fuel Cell System Design

A PEM fuel cell system, illustrated in Figure 1, operates by utilizing hydrogen and oxygen, which require humidification before being supplied to the stack. To prevent membrane flooding, the heat generated during operation must be dissipated, typically through natural or forced cooling mechanisms. Therefore, a conventional fuel cell system comprises a range of auxiliary components such as hydrogen storage tanks, pressure regulators, humidifiers, air filters, heat exchangers, compressors, water separators, relief valves, pumps, and water tanks, among others. These components are essential for maintaining optimal operation and ensuring system efficiency [9, 10].
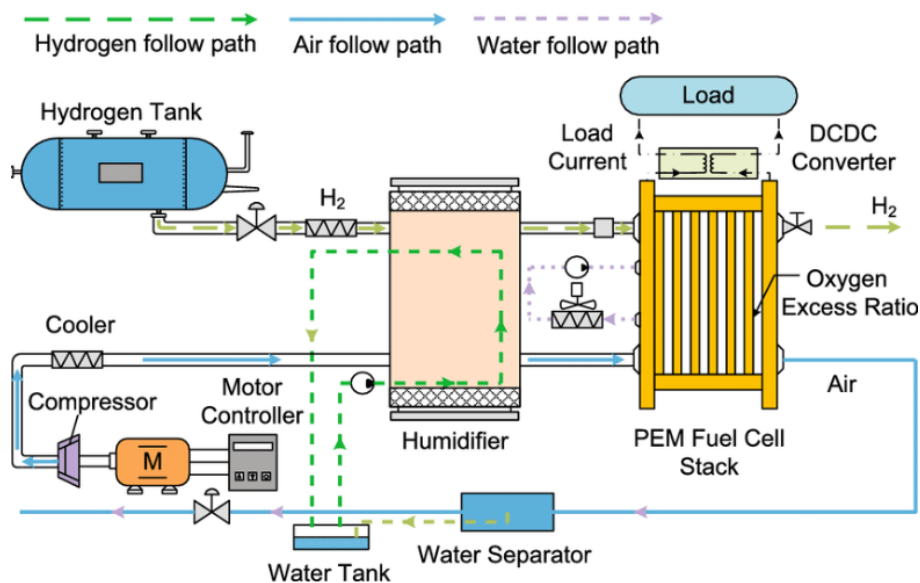
Figure 1. Fuel cell system [9]

Performance study of the anode and cathode pressure for fuel cell system   ICMUSTED 2024
regulated by PID conventional and PID optimized by intelligent algorithm
under variable load demand

2.2. Modelling of the Fuel Cell System

The mathematical model of the fuel cell system incorporates several components, including the stack, anode and cathode gas supply system, and hydrothermal management system [10]. To clearly present and explain key system characteristics and facilitate controller design, the following assumptions are made in the development of the fuel cell system's mathematical model.

- It is assumed that all gases behave as ideal gases and follow the ideal gas law.
- The focus is solely on changes in gas inflow and outflow, with the assumption of a uniform distribution of gas composition throughout the system.
- The relative humidity of the air entering the cathode is set at 0.7, and the stack temperature is maintained at 65 °C.
- Nitrogen permeation from the cathode to the anode is considered negligible.

This paper provides an in-depth analysis of a 5 kW fuel cell stack consisting of 35 individual cells, each with an active surface area of 232 cm². The total output voltage of the stack exceeds 19 V, which corresponds to approximately 0.53 V per cell, and it is capable of delivering a maximum current of 300 A. The study is particularly focused on evaluating the system's performance during H2/air operation, utilizing pure hydrogen at the anode and ambient air at the cathode. The investigation aims to assess the stack's efficiency, stability, and response to varying load conditions, with a specific emphasis on optimizing the fuel cell's performance and longevity under real-world operational scenarios [11, 12]. Relevant parameter values are given in Table 1.

Table 1. PEMFC model's parameters

Parameters	Value	Unit
T	353	K
N_{fc}	35	
t_m	175×10^{-4}	cm
F	96485	C kmol^{-1}
R	8.31415	J kmol^{-1} K^{-1}
K_{O2}	2.11e-5	Kmol S^{-1} atm
K_{H2}	4.22e-5	Kmol S^{-1} atm
τ_{O2}	3.37	(s)
τ_{H2}	6.47	(s)
ξ_1	-0.944	
ξ_2	0.00354	
ξ_3	8×10^{-8}	
ξ_4	-1.96×10^{-4}	

2.3. Output Voltage Model

Figure 1 illustrates the fuel cell as an electrochemical device that efficiently converts the chemical energy stored in hydrogen into electrical power. The fuel cell operates based on an electrochemical redox reaction [13], which facilitates the interaction between hydrogen and oxygen to generate electricity, water, and heat. This process is summarized by the following overall chemical equation:

$$2H_2 + O_2 \rightarrow 2H_2O + \text{Heat} + \text{Energy} \tag{1}$$
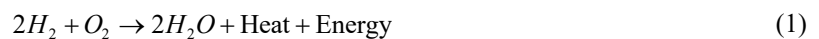
The output voltage of the fuel cell can be expressed using the following equation [14].

$$V_{FC} = E_{Nerst} - V_{act} - V_{ohm} - V_{conc} \tag{2}$$

E_{Nerst}, is the reversible open-circuit voltage, it is described by the Nerst equation as:

Performance study of the anode and cathode pressure for fuel cell system   ICMUSTED 2024
regulated by PID conventional and PID optimized by intelligent algorithm
under variable load demand

$$E_{Nerst} = 1.229 - 8.5 \times 10^{-4}(T_{fc} - 298.15) + 4.3085 \times 10^{-5} \times T_{fc}\left[\ln(P_{H_2}) + 0.5(P_{O_2})\right] \tag{3}$$

Where, PH2 hydrogen pressure (atm), PO2 Oxygen pressure (atm) and T Absolute temperature (K). V_{act} denotes the activation voltage drop, as expressed in the Tafel equation as:

$$V_{act} = \xi_1 + \xi_2 T + \xi_3 T \ln(C_{O_2}) + \xi_4 T \ln I_{FC} \tag{4}$$

Here, IFC denotes the fuel cell current (A), and ξ_i (where $i = 1$- 4) represent parametric coefficients corresponding to each cell model. CO2 denotes the concentration of dissolved oxygen at the interface of the cathode catalyst, which can be determined through the following calculation:

$$C_{O_2} = \frac{P_{O_2}}{5.08 \times 10^6 \exp^{\left(\frac{-498}{T}\right)}} \tag{5}$$

The total ohmic voltage loss, often denoted as V_{ohm}, can be formulated as:

$$V_{ohm} = I R_{mem} \tag{6}$$

Where R_m the membrane resistance is determined by dividing the thickness, t_{mem}, by the conductivity σ_{mem} as described by the following equation.

$$R_{mem} = \frac{t_{mem}}{\sigma_{mem}} \tag{7}$$

V_{conc} represents the concentration voltage drop, which is defined as:

$$V_{conc} = -B \ln\left(1 - \frac{J}{J_{max}}\right) \tag{8}$$

Where, J_{max} is the maximum current density of the cell, J (A/cm^2) represents the actual current density of the cell and B is a parametric coefficient, which depends on the cell and its operation state. When NFC fuel cells are linked in series, the fuel cell stack's output voltage is determined by:

$$V_{stack} = N_{FC} V_{FC} \tag{9}$$

The characteristic curve for this model is presented as follows:
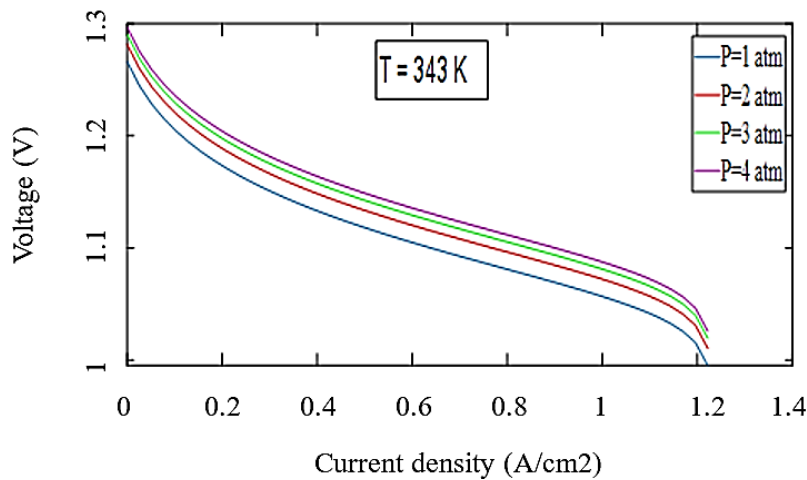
Figure 2. Characteristic curve of output voltage

Performance study of the anode and cathode pressure for fuel cell system   ICMUSTED 2024
regulated by PID conventional and PID optimized by intelligent algorithm
under variable load demand

2.4. Dynamic Gas Transport Model

The hydrogen partial pressure can be determined by considering the input flow rate and the current of the fuel cell, establishing a functional relationship between these variables [15]:

$$P_{H2} = \left[(1/K_{H2})/1 + \tau_{H2}S \right] \times \left(q_{H2}^{in} - 2K_r I \right) \tag{10}$$

In this context, q_{H2} represents the input hydrogen flow, while K_r signifies the hydrogen flow that is consumed. This consumption can be mathematically expressed as follows:

$$K_r = \frac{N_{fc}}{4F} \tag{11}$$

Using identical methods, the oxygen partial pressure is articulated as:

$$P_{H2} = \left[(1/K_{O2})/1 + \tau_{O2}S \right] \times \left(q_{O2}^{in} - K_r I \right) \tag{12}$$

where in q_{O2} is the input oxygen flow, and K_r is the hydrogen flow which is consumed, and can be expressed as:

$$K_r = \frac{N_{fc}}{2F} \tag{13}$$

Equations (13) and (15) delineate the correlation between the current of the fuel cell and the partial pressures of hydrogen and oxygen, respectively. As the load initiates current flow, both hydrogen and oxygen reactants rise, leading to a corresponding decrease in their partial pressures.

2.5. Power Conditioning

The fuel cell operates at a low output voltage within a wide range (18 ~ 36 V). To convert this DC power to a higher voltage and connect it to the load, appropriate power converters are necessary. This paper proposes using a boost converter. A single-phase pulse width modulated (PWM) H-bridge inverter is employed to convert the DC power into high-voltage AC (120 V). Four insulated gate bipolar transistor (IGBT) diode pairs are configured as switches in two arms of the inverter [16].

The inverter receives a variable DC input, while the load voltage and frequency remain fixed at 120 V and 50 Hz, respectively. The inverter stage must be controlled to compensate for variations in the stack output. A straightforward approach is to adjust the modulation index, m, to modify the PWM gating signals, which control the on/off times of the four IGBTs in the inverter (Figure 1).

For this purpose, a PID controller is designed and tuned, and the dimensions of the DC/DC converter components are provided in the table below.

Table 2. Converter parameters

Parameters		Values
DC/DC components	Inductance	L = 6.725e-3 H
	Capacity	C = 1.68e-4 F
	Duty cycle	D = 0.24
Regulator gains	Proportional gain	K_p = 0.1
	Integral gain	K_i = 60

3. CONTROL OF THE FUEL CELL SYSTEM

3.1. PID Tuned by GA

This study, utilize the Genetic Algorithm (GA) to optimize the gains of the Proportional-Integral-Derivative (PID) controller, aiming to improve the performance of a dynamic system. By incorporating GA into PID tuning, our

Performance study of the anode and cathode pressure for fuel cell system
regulated by PID conventional and PID optimized by intelligent algorithm
under variable load demand

ICMUSTED 2024

goal is to determine the optimal gains that ensure stability, faster transient response, and robustness in the face of varying load demands. This innovative approach has the potential to significantly enhance control strategies for complex systems. Through comprehensive analysis, we demonstrate the efficacy and adaptability of the GA-based PID tuning method. The convergence of the algorithm is visually validated in Figure 3, highlighting its effectiveness [18].
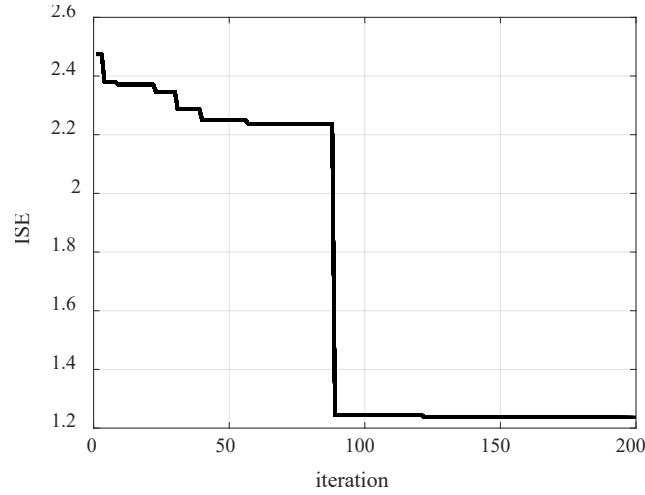
Figure 3. Convergence integral square error

The tuning parameters of genetic algorithm are presented in the table below:

Table 3. GA parameters

Parameters	Description
$N_{Var} = 3$	Number of regulation parameters (K_p, K_i, K_d)
$L_b = [0\ 0\ 0]$	Lower bound of algorithm research
$U_b = [100\ 100\ 100]$	Highly bound of algorithm research
$P_{size} = [50\ to\ 200]$	Population size
$ISE\ /\ OTAE = 0$	Objective function

3.2. Fuel Flow Control

The theoretical voltage of the cell is highly sensitive to the partial pressures of both hydrogen and oxygen. To maintain these pressures at constant levels, we propose calculating the fuel flow of the PEMFC using a proportional-integral-derivative controller (Figure 4), which will regulate the fuel flow through an actuator.
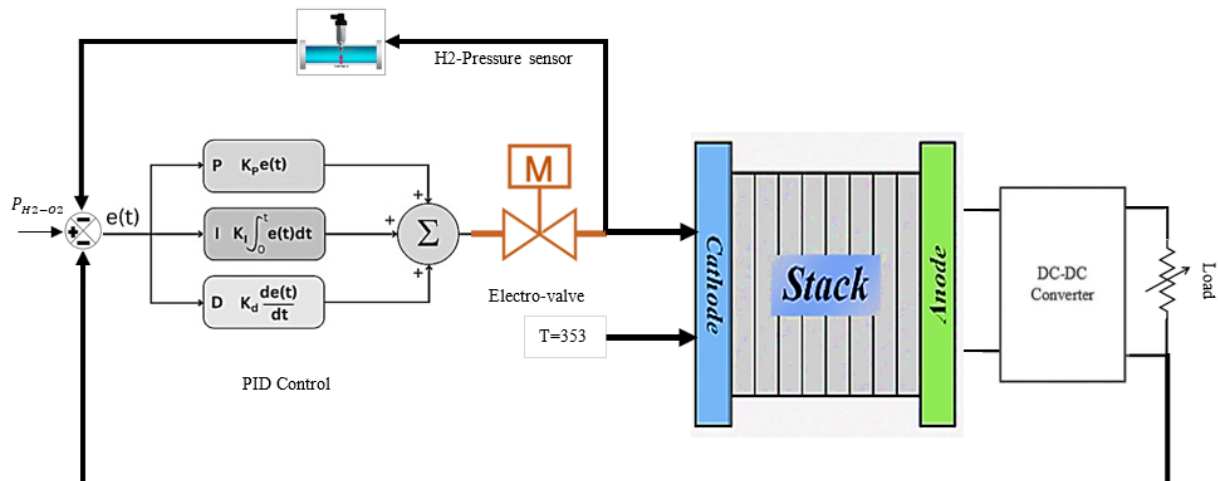
Figure 4. Pressure control loop of hydrogen and oxygen using PID and optimized PID controller

Performance study of the anode and cathode pressure for fuel cell system   ICMUSTED 2024
regulated by PID conventional and PID optimized by intelligent algorithm
under variable load demand

The trial-and-error method and tuned gains by PSO algorithm are used to calculate the controller gains, which presented in the table below for current loop regulation, H2 and O2 pressure loops as follows:

Table 4. Manuel regulation parameters

Parameters		Values
Current regulator		$K_p = 15$
		$K_i = 10$
Hydrogen regulator	Manuel regulation	$K_p = 1.9$
		$K_i = 1$
		$K_d = 0.15$
	GA tuning	$K_p = 11.3$
		$K_i = 15.5$
		$K_d = 23.2$
Oxygen regulator	Manuel regulation	$K_p = 2$
		$K_i = 1.5$
		$K_d = 0.2$
	GA tuning	$K_p = 12.2$
		$K_i = 17.8$
		$K_d = 47.2$

4. SIMULATION RESULT AND DISCUSSION

As part of the modeling study in Matlab Simulink, the objective was to assess the performance of the "PEMFC" fuel cell. We investigated the impact of load variations while maintaining constant pressure. This setup is essential for understanding the intricate interactions between load and pressure, offering valuable insights into the system's performance. The analysis of the simulation results, including hydrogen pressure, oxygen pressure, DC voltage, and power consumption, are presented in this focus.

The variation in load is outlined as follows:
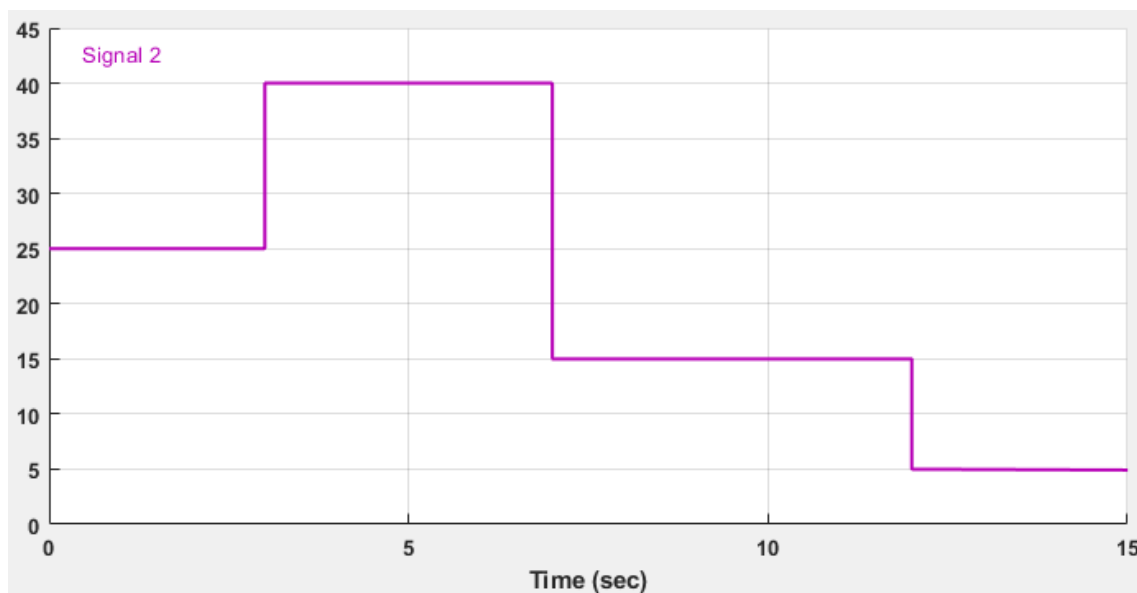
Figure 5. Load profile

The performance analysis is conducted based on three critical parameters in the control chain: H2 pressure, O2 pressure, and, as illustrated in Figure 6 and Figure 7, respectively. Proper control of these parameters is essential

Performance study of the anode and cathode pressure for fuel cell system   ICMUSTED 2024
regulated by PID conventional and PID optimized by intelligent algorithm
under variable load demand

for ensuring the longevity of the fuel cell and its components, while also maintaining high energy efficiency. The Figure 8 presented the control of DC voltage by the DC/DC inverter at the load terminal is essential for a best efficiency and saved power.
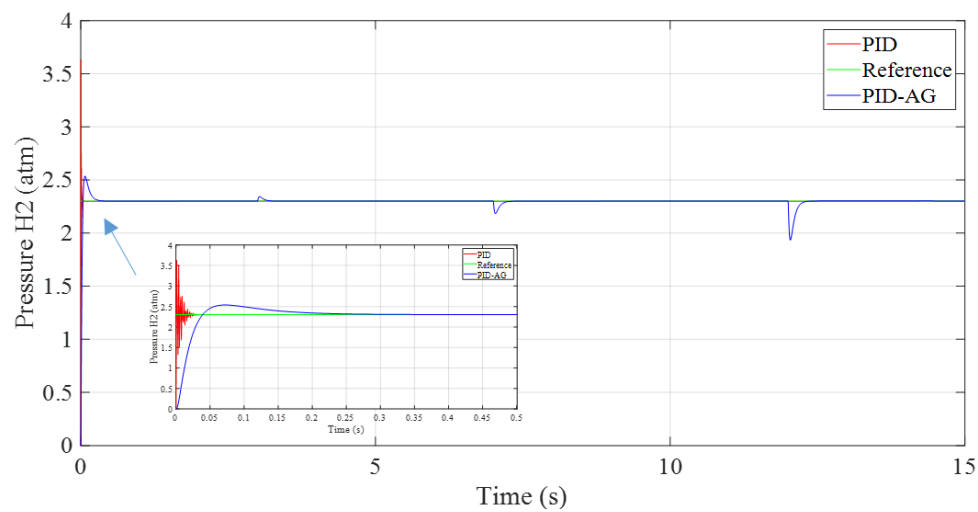
Figure 6. H2 pressure profile
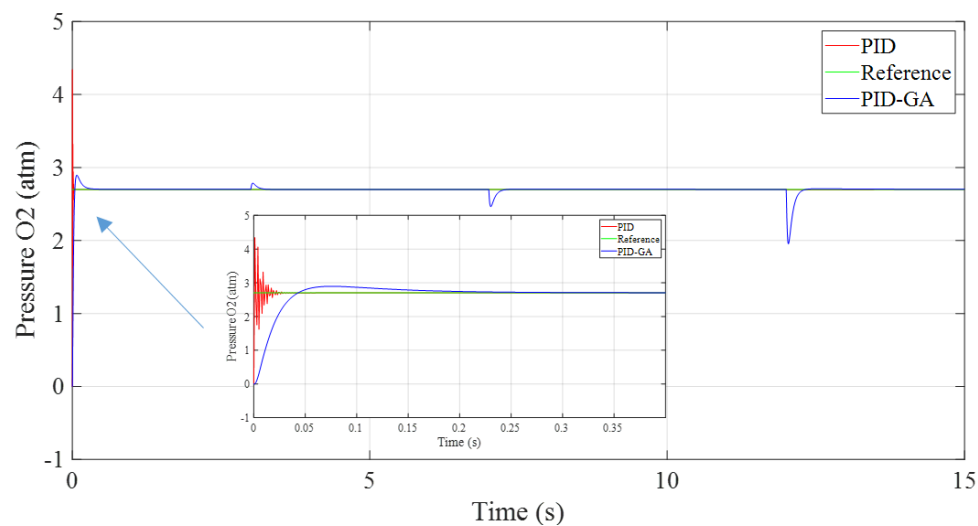
Figure 7. O2 pressure profile
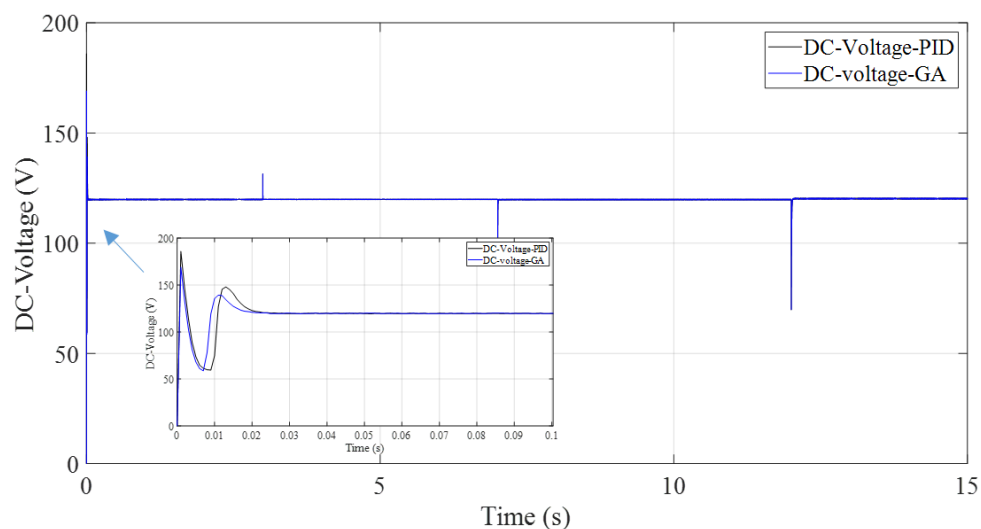
Figure 8. DC-Voltage profile

Performance study of the anode and cathode pressure for fuel cell system regulated by PID conventional and PID optimized by intelligent algorithm under variable load demand

ICMUSTED 2024
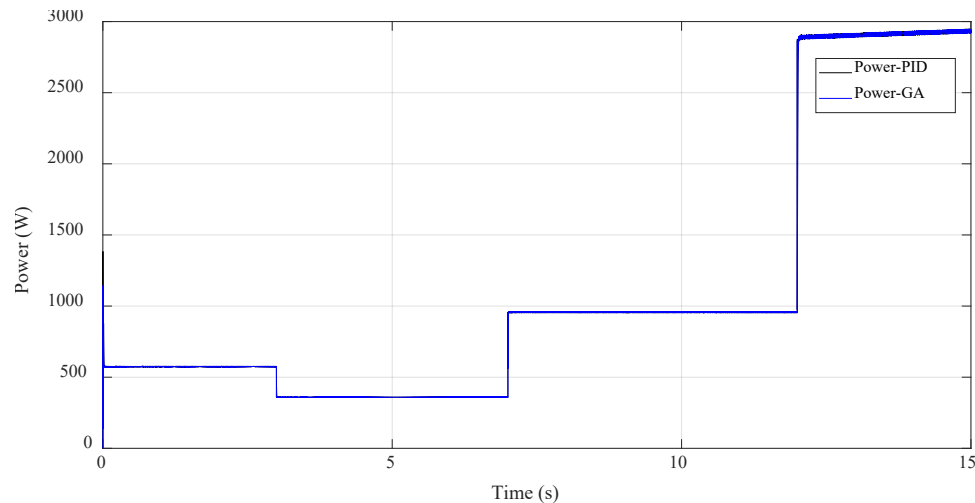
Figure 9. Power rate

The performance analysis based on the PID and PID tuned by GA are presented in the table below.

Table 5. Analyses performance for tuned and manually PID regulation

Parameters		Performances	
Hydrogen pressure	Manuel regulation	Response time (s)	0.05
		Overshoot (%)	2%
		Stability	0.01
	GA tuned	Response time (s)	0.03
		Overshoot (%)	TDR
		Stability	0.003
Oxygen pressure	Manuel regulation	Response time (s)	0.3
		Overshoot (%)	0%
		Stability	0.024
	GA tuned	Response time (s)	0.2
		Overshoot (%)	TDR
		Stability	0.011

The specified characteristics for conventional PID pressure regulation of hydrogen and oxygen—response times of [0.05 s-0.3 s] for H_2 and O_2, respectively, an overshoot range of [2%-0%], and stability values between [0.01-0.024]—highlight the system's high efficiency and reliability for fuel cell applications. The swift response time allows for quick adaptation to demand fluctuations, thereby minimizing component stress and protecting the fuel cell membrane from potential damage. Precise control, evidenced by the minimal overshoot, ensures stable operation by limiting pressure fluctuations around the setpoint. Furthermore, the tight stability parameters guarantee consistent performance, contributing to the system's durability and enhanced operational efficiency. Overall, these features underscore a well-designed pressure regulation system that maintains optimal hydrogen pressure, reduces risks, and promotes the fuel cell's long-term efficiency and reliability.

The GA-tuned PID regulator outperforms conventional PID regulation across critical performance metrics. Its faster response time and remarkably tight stability, maintained at 0.003, ensure rapid adjustments and minimal deviation from the setpoint, significantly enhancing system responsiveness and operational stability. Additionally, the GA-tuned PID's capability to achieve a "Transient Damped Regime" with minimal overshoot demonstrates its precise control, effectively reducing the likelihood of system instability. These advancements collectively result in superior pressure regulation, greater efficiency, and improved reliability in fuel cell operations when compared to traditional PID regulation.

Performance study of the anode and cathode pressure for fuel cell system   ICMUSTED 2024
regulated by PID conventional and PID optimized by intelligent algorithm
under variable load demand

To enhance the study and improve the accuracy of the regulated system, we evaluated the controller's stability relative to its reference using several key performance indicators: Integral absolute error (IAE), integral time absolute error (ITAE), and integral square error (ISE). The results are summarized in the table below.

Table 6. Stability analyses of steady state

Parameters		IAE	Itae	ISE
PID tuned regulator	Hydrogen pressure	0.003	0.005	0.0012
	Oxygen pressure	0.011	0.0013	0.0002
	DC voltage	0.021	0.045	0.006
PID manual regulation	Hydrogen pressure	0.01	0.037	0.0016
	Oxygen pressure	0.024	0.028	0.0037
	DC voltage	0.023	0.05	0.0078

The comparison between PID-tuned regulation and manual PID regulation across various control scenarios demonstrates notable improvements in stability and performance. For hydrogen pressure, oxygen pressure, and DC voltage control, the PID-tuned regulator consistently achieves lower stability index values (IAE, ITAE, and ISE) than manual regulation. This reflects enhanced control precision and reduced oscillations, emphasizing the effectiveness of PID tuning, particularly when augmented by optimization techniques such as PSO. These findings highlight the critical role of optimized control strategies in achieving superior stability and performance across diverse scenarios, ultimately boosting system efficiency and reliability.

4. CONCLUSION

This study explores the dynamic modeling, control, and simulation of Proton Exchange Membrane Fuel Cells (PEMFC). We begin by introducing the dynamic model of the PEMFC, derived from existing literature, and incorporating key evolutions in physical parameters. Next, we detail the methodology for calculating hydrogen and oxygen flow rates. Subsequently, we propose a control strategy using Proportional Integral (PI) controllers for the DC-DC boost converter. The effectiveness of this strategy across a wide operational range is validated through simulations performed in Matlab/Simulink. The simulation results for the hydrogen and oxygen pressure control loops, utilizing both conventional PID controllers and GA-tuned PID controllers, were analyzed. The findings reveal that parameter tuning via the GA algorithm significantly improves system performance. This enhancement is demonstrated through performance indices such as Integral Absolute Error (IAE), Integral Time Absolute Error (ITAE), and Integral Square Error (ISE), particularly in mitigating load variation peaks. Such optimization ensures stable and consistent pressure at the PEMFC membrane terminals, further enhancing the system's reliability and efficiency.

References

[1]   G. Bhansali and R. Kumar, "Design analysis and dynamic control of PEM fuel cell for standalone applications," in *2014 IEEE Students' Conf. Electr. Electron. Comput. Sci. SCEECS 2014*, 2014, doi: 10.1109/SCEECS.2014.6804455.

[2]   Y. Li, X. Zhao, S. Tao, Q. Li, and W. Chen, "Experimental Study on Anode and Cathode Pressure Difference Control and Effects in a Proton Exchange Membrane Fuel Cell System," *Energy Technol.*, vol. 3, no. 9, pp. 946–954, 2015, doi: 10.1002/ente.201500077.

[3]   F. Gonzatti, M. Miotto, and F. A. Farret, "Proposal for Automation and Control of a PEM Fuel Cell Stack," *J. Control. Autom. Electr. Syst.*, vol. 28, no. 4, pp. 493–501, 2017, doi: 10.1007/s40313-017-0322-2.

[4]   R. Geethanjali and R. Sivakumar, "Design of intelligent controller for PEM fuel cell," in *ICONSTEM 2017 - 3rd IEEE Int. Conf. Sci. Technol. Eng. Manag.*, pp. 1050–1053, 2017, doi: 10.1109/ICONSTEM.2017. 8261316.

[5]   H. Marzougui, A. Kadri, M. Amari, and F. Bacha, "Improvement of energy management algorithm for fuel cell electrical vehicle with fuzzy logic," in *2017 18th Int. Conf. Sci. Tech. Autom. Control Comput. Eng. STA 2017 - Proc.*, pp. 212–217, 2017, doi: 10.1109/STA.2017.8314963.

[6]   Y. Zhu, J. Zou, C. Peng, Y. Xie, and L. Li, "Modelling and fuel flow control of PEMFC considering over-pressure case," in *2017 Chinese Autom. Congr. CAC 2017*, pp. 2222–2225, 2017, doi: 10.1109/CAC.2017. 8243143.

[7]   Y. Qi, M. Thern, M. Espinoza-Andaluz, and M. Andersson, "Modeling and control strategies of proton

Performance study of the anode and cathode pressure for fuel cell system regulated by PID conventional and PID optimized by intelligent algorithm under variable load demand

ICMUSTED 2024

exchange membrane fuel cells," *Energy Procedia*, vol. 159, pp. 54–59, 2019, doi: 10.1016/j.egypro.2018.12.017.

[8]   A. Morán-Durán, A. Martínez-Sibaja, J. P. Rodríguez-Jarquin, R. Posada-Gómez, and O. S. González, "PEM fuel cell voltage neural control based on hydrogen pressure regulation," *Processes*, vol. 7, no. 7, art. no. 434, 2019.

[9]   Y. Rao, Z. Shao, A. H. Ahangarnejad, E. Gholamalizadeh, and B. Sobhani, "Shark Smell Optimizer applied to identify the optimal parameters of the proton exchange membrane fuel cell model," *Energy Convers. Manag.*, vol. 182, pp. 1–8, 2019, doi: 10.1016/j.enconman.2018.12.057.

[10]   H. C. Nejad, M. Farshad, E. Gholamalizadeh, B. Askarian, and A. Akbarimajd, "A novel intelligent-based method to control the output voltage of Proton Exchange Membrane Fuel Cell," *Energy Convers. Manag.*, vol. 185, pp. 455–464, 2019, doi: 10.1016/j.enconman.2019.01.086.

[11]   H. Deng, Q. Li, Y. Cui, Y. Zhu, and W. Chen, "Nonlinear controller design based on cascade adaptive sliding mode control for PEM fuel cell air supply systems," *Int. J. Hydrogen Energy*, vol. 44, no. 35, pp. 19357–19369, 2019, doi: 10.1016/j.ijhydene.2018.10.180.

[12]   Y. Cao, Y. Li, G. Zhang, K. Jermsittiparsert, and N. Razmjooy, "Experimental modeling of PEM fuel cells using a new improved seagull optimization algorithm," *Energy Reports*, vol. 5, pp. 1616–1625, 2019, doi: 10.1016/j.egyr.2019.11.013.

[13]   M. K. Singla, A. S. Oberoi, and P. Nijhawan, "Trends so far in hydrogen fuel cell technology: State of the art," *Int. J. Adv. Trends Comput. Sci. Eng.*, vol. 8, no. 4, pp. 1146–1155, 2019, doi: 10.30534/ijatcse/2019/23842019.

[14]   H. He, S. Quan, and Y. X. Wang, "Hydrogen circulation system model predictive control for polymer electrolyte membrane fuel cell-based electric vehicle application," *Int. J. Hydrogen Energy*, vol. 45, no. 39, pp. 20382–20390, 2020, doi: 10.1016/j.ijhydene.2019.12.147.

[15]   T. Pangaribowo, "Modeling of control system for hydrogen and oxygen gas flow into pemfc based on load demand by using fuzzy controller," *Int. J. Adv. Trends Comput. Sci. Eng.*, vol. 1, no. 4, pp. 606–611, 2020, doi: 10.30534/ijatcse/2020/8491.42020.

[16]   A. Polak, "Simulation of fuzzy control of oxygen flow in PEM fuel cells," *Energies*, vol. 13, no. 9, pp. 15–25, 2020, doi: 10.3390/en13092372.

[17]   H. Yuan, H. Dai, W. Wu, J. Xie, J. Shen, and X. Wei, "A fuzzy logic PI control with feedforward compensation for hydrogen pressure in vehicular fuel cell system," *Int. J. Hydrogen Energy*, vol. 46, no. 7, pp. 5714–5728, 2021, doi: 10.1016/j.ijhydene.2020.11.089.

[18]   H. Rezk, M. Aly, and A. Fathy, "A novel strategy based on recent equilibrium optimizer to enhance the performance of PEM fuel cell system through optimized fuzzy logic MPPT," *Energy*, vol. 234, art. no. 121267, 2021, doi: 10.1016/j.energy.2021.121267.

Enhanced Fault Detection in Electrical Machines Using Modified Stator Current Signal Analysis

Azeddine Ratni[1], Djamel Benazzouz[1], Mohammed Tsebia[2]

[1]Solid Mechanics and Systems Laboratory, University of Boumerdes, Boumerdes, Algeria
[2]Signals and Systems Laboratory, University of Boumerdes, Boumerdes, Algeria
Corresponding author: Azeddine Ratni (e-mail: a.ratni@univ-boumerdes.dz)

Abstract

This paper presents an efficient signal processing approach for detecting mechanical faults in induction motors using electrical signals. Unlike traditional fault detection methods, which typically require multiple sensors (e.g., line current and voltage), the proposed approach simplifies the system by utilizing only a single current sensor. A mathematical modification is applied to the stator current signal, which improves the ability to extract key information regarding the motor's behavior and enhances the accuracy of fault detection. This modification is specifically designed to detect faults such as broken rotor bars at an early stage, ensuring proactive maintenance. An electrical model of the induction machine is also introduced, with simulation results provided to validate the theoretical assumptions. The findings show that the stator current signal analysis, along with the applied mathematical modification, is highly effective in identifying abnormal operating conditions, making it a valuable tool for predictive maintenance in industrial applications. This method minimizes the number of sensors required while maintaining high reliability in fault detection.

Keywords: Motor diagnostics, Stator current signal, Condition monitoring, Signal processing, Broken rotor bars

Photovoltaic-Hydroelectric-Diesel Power Storage Hybridization System Integrated in Algeria

Lahouasnia Nasreddine[1]

[1]Electromechanical Department, Badji Mokhtar University, Annaba, Algeria
Corresponding author: Lahouasnia Nasreddine (e-mail: hnasro114@gmail.com)

Abstract

The evolution of hybrid microgrid energy system (HMGES) technology carefully delivers the hybrid system concept in a controlled way to solve energy problems with both optimal design and management strategy. The latter not only acquires the merit of regional sources, but also mitigates the transport of energy in a well-qualified manner. It also preserves and guarantees the quality and reliability of energy services. In addition, the merging of the (EMC) into the hybrid microgrid (HMG) system makes it possible to improve and maximise both solar photovoltaic (PV) and storage sources (ESS). This study confirms that the new, accurate formulation of online fuel consumption per kWh, compared to existing literature, is successfully tested in the proposed energy management system and can be applied in future analogous studies.

Keywords: Solar energy, Hybrid system, PV panel, Diesel generator

1. INTRODUCTION

Worldwide energy consumption is closely linked to population. The growth in the world's population and industrial activity in developing countries have led to an explosion in energy requirements. Excessive use of fossil fuels to meet these needs is the main cause of emissions of polluting gases, whose pollution is responsible for global warming and climate change [1]. The transport sector currently accounts for almost a third of global CO_2 emissions. Renewable energies are an alternative to fossil fuels because of their low impact on the environment. Unfortunately, to date, the power installed by renewable energies has not been able to compete with today's large power plants because of their intermittent and fluctuating nature. It is therefore essential to use storage facilities to ensure continuity of energy supply [2]. These renewable energy sources and the associated storage facilities therefore form a hybrid system.

Among the most promising systems for using renewable energy are multi-source systems. For isolated or remote regions, the cost of extending the electricity grid is prohibitive, and the additional cost of fuel supply increases radically with isolation [3]. This concept excludes large interconnected grids in which the sources can also be of several types. The combination of renewable energy sources such as wind, photovoltaic or small hydroelectric power stations can provide a complement or an alternative to the diesel generators generally used to generate electricity in isolated regions. Multi-source systems are generally designed to meet an energy need ranging from simple lighting to the complete electrification of villages or small islands [4].

In remote areas, energy needs are mainly met by diesel generators (DG). The disadvantages of DG outweigh its advantages. To illustrate this point, it is very difficult to supply remote sites with indeterminate load demand, particularly due to the high cost of refuelling because of the distance involved. Subsequently, the cost of electricity is up to ten times higher than in urban areas. To overcome these problems, more reliable, credible and well-managed sources of electricity are needed in remote areas to reduce fuel costs (FCcost), fuel consumption (FC) and CO_2 emissions. Therefore, an eligible renewable energy (RE) system is proposed as a solution to meet load energy needs as well as to reduce environmental problems arising from the combustion of DG distributed generation fuel [5, 6].

Photovoltaic electricity was initially developed for autonomous applications without connection to a network, for example for telecommunications satellites or for isolated homes. It is now found in applications of various powers such as calculators, watches and other objects of everyday use. Indeed, this electricity produced by individual photovoltaic cells can power various systems without difficulty. More recently, with the emergence of photovoltaic installations connected to the distribution network, photovoltaics have experienced significant development as a means of producing electricity [7].

The hybrid microgrid energy system (HMGES) technology stems from the smart microgrid concept. It employs an optimal strategy to minimize energy losses, leading to efficient resource utilization, reduced energy transmission, and maintained quality and reliability of energy services. Additionally, the energy management control (EMC) strategy used in the HMGES is sophisticated. It effectively maximizes the utilization of photovoltaic (PV) and pumped storage hydroelectric (PSH) sources. The EMC strategy operates intelligently and efficiently to meet energy demands under various conditions [8].

As far as this study is concerned, solar energy is the most favourable because it provides clean, sustainable energy. However, it has a correlative relationship with variable weather conditions, which means that it cannot be used as the sole energy source for stand-alone systems. As a result, the HMGES and solar energy (SE) precisely improve energy reliability in remote areas. It ensures the cohesion and continuity of energy supply services in terms of cost-effective maintenance and operation. In addition, it is a combination of a conventional DG source and a solar PV source linked to an energy storage system (ESS). As a result, it not only minimises sulphur (SOX), carbon (COX) and nitrogen (NOX) emissions, but also offers cost-effective maintenance and operation compared with the diesel system [9–11].

2. Model Description

For long-term investment, the project must satisfy both financial and technical aspects. It should also authentically meet the energy requirements of the load. This is primarily influenced by two factors: the consumers and the various energy sources (PV, DG, and PSH). The main objective of the hybridization is illustrated through both Equation (1) and Figure 1.

$$P_{LOAD}(t) = P_{DG}(t) + P_{PV}(t) + P_{PHS}(t) \qquad (1)$$

The hybrid microgrid system integrates photovoltaic (PV) panels, DG, and pumped storage hydroelectric (PSH) systems to ensure a reliable and continuous energy supply. Each component plays a crucial role in the overall performance and efficiency of the system. The PV panels harness solar energy, the diesel generators provide backup power during low solar periods, and the PSH system stores excess energy for later use.

The goal is to achieve an optimal balance between these sources, ensuring that the energy supply meets the demand while minimizing costs and environmental impact. The mathematical model, represented by Eq. (1), and the system configuration, depicted in Figure 1, provide a comprehensive framework for analyzing and optimizing the hybrid system's performance.
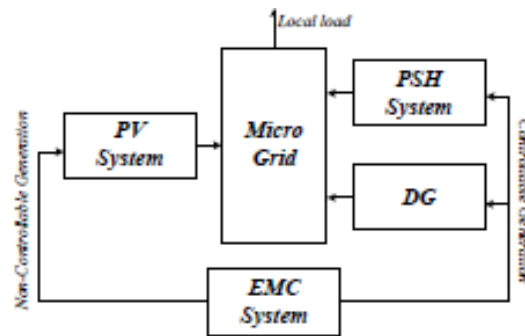
Figure 1. The hybrid microgrid energy system HMGES model

2.1. PV Array

The PV array is an essential component of the HMGES. The output power from the PV array is used to meet the load demands and, in the case of excess power, to pump water to the upper tank. The PV output power (P_{PV}) is calculated using Equation (2), which takes into account the incident irradiance (G_{IIR}). In this study, the SunPower SPR-305-WHT module type is utilized.

$$P_{PV} = P_{STC} \frac{G_{IIR}}{G_{STC}} \left(1 + k\left(T_c - T_a\right)\right) \qquad (2)$$

- Calculation of PV Output Power: The PV output power can be determined using the following equation,

$$P_{PV} = P_{rated} \frac{G_{IIR}}{G_{STC}} \tag{3}$$

Where:
- P_{PV} is the PV output power.
- P_{rated} is the rated power of the PV module (305 W for the SunPower SPR-305-WHT).
- G_{IIR} is the incident irradiance.
- G_{STC} is the standard test condition irradiance (typically 1000 W/m²).

This equation allows us to estimate the power output of the PV array based on the available solar irradiance, enabling efficient energy management within the hybrid system.

2.2. Diesel Generator

When the solar and ESS sources are unable to meet the energy demands, the diesel generator (DG) functions as a backup source to enhance the reliability of the power production. The type of DG needed is determined by factors such as peak load, FC, and transportation costs. The DG is characterized by its efficiency and fuel consumption rate.

- Calculation of Diesel Generator Fuel Consumption: The FC of the DG can be calculated using Equation (3), which is the traditional method,

$$FC = a \cdot P_{DG} + b \tag{4}$$

Where:
- FC is the fuel consumption in liters per hour (liter/h).
- P_{DG} is the power output of the diesel generator in kilowatts (kW).
- (a) and (b) are coefficients that depend on the specific DG model and its efficiency.

This equation allows for the estimation of the DG's fuel consumption based on its power output, which is crucial for optimizing the overall energy management and ensuring cost-effective operation within the hybrid system.

This method involves using Matlab to model the DG's performance and obtain a more accurate equation for fuel consumption based on various operational parameters. This approach aims to improve the precision of fuel consumption estimates, thereby optimizing energy management and reducing operational costs in the hybrid system. The resulting equation, Equation (4), provides a detailed and specific relationship between the DG's power output and its fuel consumption, tailored to the particular characteristics of the DG used in the system.

$$FC_{2(t)} = a\left(e^{(bP_{DG(t)})}\right) + c\left(e^{(dP_{DG(t)})}\right) \tag{5}$$

With, $a = 23.4$, $b = -2.20e - 6$, $c = 24.52$, and $d = 4.52e - 6$.
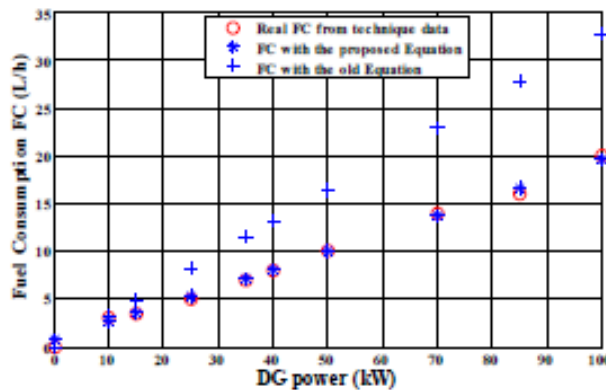
Figure 2. FC for different DG power

2.3. Energy Storage System

The PSH system has the potential to serve as an effective ESS in isolated areas. Its state of charge (SOC) efficiency can reach up to 80%. This system operates by converting excess power into gravitational energy. When needed, water is released from an upper reservoir to pass through pipes to drive a turbine generator. Equation (6) and Equation (7) represent the pump and turbine output power, respectively [10].
Pump Output Power:

$$P_{pump} = \eta \cdot g \cdot Q \cdot h \tag{6}$$

Where:
- p_{pump} is the pump output power.
- ρ is the density of the fluid.
- g is the acceleration due to gravity.
- Q is the flow rate of the fluid.
- h is the height difference between the upper and lower reservoirs.

Turbine Output Power:

$$P_{turbine} = \eta \cdot \rho \cdot g \cdot Q \cdot h \tag{7}$$

Where:
- $p_{turbine}$ is the turbine output power.
- η is the efficiency of the turbine.

These equations describe the power generation process in the PSH system, illustrating how excess energy is stored and later utilized to generate electricity when needed.

2.4. EMC Strategy

The EMC collects data from the HMGES to determine an economically accurate strategy, such as starting the DG or utilizing the energy stored in the PSH system. It aims to increase the reliability of the entire system by providing uninterrupted energy to customers under different climate conditions. The EMC strategy guarantees the performance and effectiveness of the HMG by reducing both the economic costs and the CO_2 emissions associated with DG fuel consumption.

The control strategy procedure is summarized in a flowchart depicted in Figure 3. This flowchart outlines the steps involved in decision-making and ensures the optimal operation of the hybrid system, thereby maximizing efficiency and minimizing environmental impact.
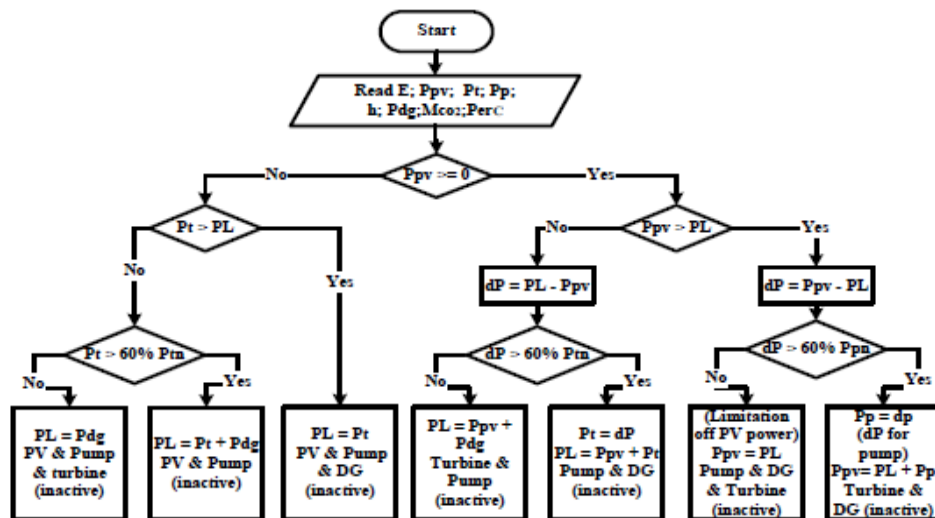
Figure 3. Algorithm flowchart

3. RESULTS AND DISCUSSION

3.1. Solar Irradiation Profiles

Figure 4.a presents different solar irradiation profiles obtained from the site. The data consists of three selected days: the first day with high solar irradiation density (rich), the second day with regular solar irradiation (normal), and the third day with the lowest solar irradiation density (poor). These profiles are acquired from the Renewable Energy weather station of the Research Unit-Medium Saharan (URER-MS).

- PV Power Output: The corresponding output PV power is depicted in Figure 4.b, derived from the available solar irradiation data. It illustrates the variation in PV power generation based on the solar irradiation levels throughout the selected days.
- Power Requirements Profile: Figure 4(c) illustrates the power requirements profile for supplying domestic loads, as well as additional power for agricultural demands. This profile reflects the energy needs of the system under consideration, encompassing both residential and agricultural consumption patterns.

The analysis of these results allows for a comprehensive understanding of the performance and dynamics of the hybrid micro-grid energy system, enabling informed decision-making and optimization strategies to meet energy demands effectively while maximizing efficiency and reliability.
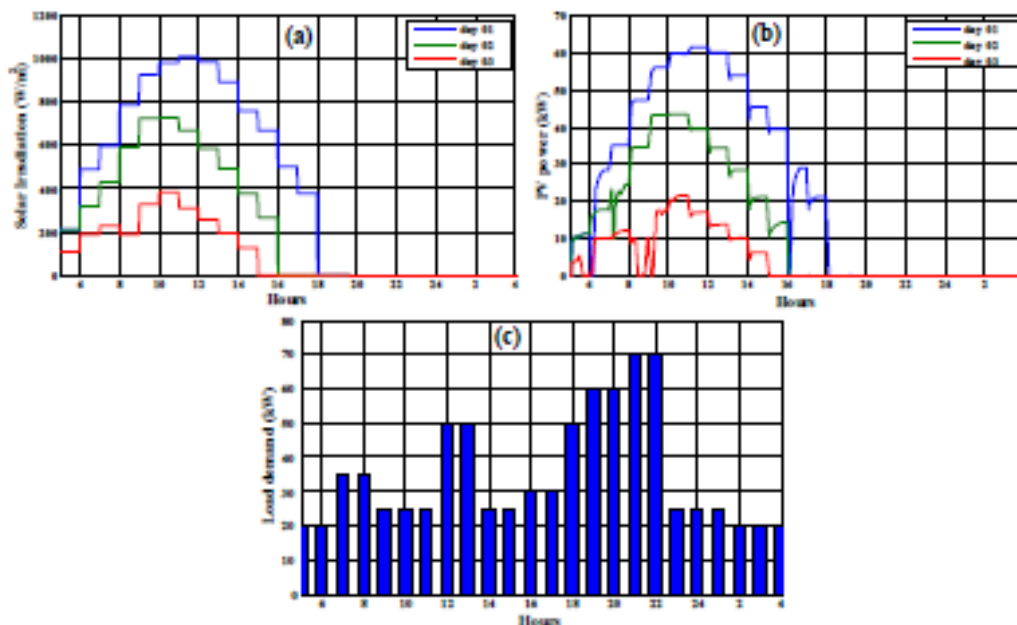
Figure 4. The three selected days solar irradiation data; the three selected days PV output power during 24 hours, the load demands profile

3.2. PSH System

The PSH system is integrated into the available sources of the HMGES to enhance production flexibility. When the results indicate that the PV source alone is insufficient to meet energy demands, the PSH turbine is activated.

- PSH Operation Modes: Figure 5 illustrates the characteristics of the PSH system in both charge and discharge modes. In the discharge mode, represented by the output PSH power, the PSH system provides the required supply, rendering the diesel generator (DG) inactive. Conversely, if the PSH system cannot meet the supply demands, the DG is activated to cover the deficit, minimizing reliance on the DG and its associated drawbacks.
- Output Power Comparison: Figure 6 presents the output power of both the PSH system and the DG. It demonstrates the interplay between these two energy sources, highlighting the dynamic adjustment of the system to optimize energy production while minimizing reliance on conventional diesel generation.

This integrated approach ensures a more resilient and efficient energy supply, with the PSH system acting as a complementary resource to the PV source, thereby reducing reliance on fossil fuel-based generation and enhancing overall system reliability.
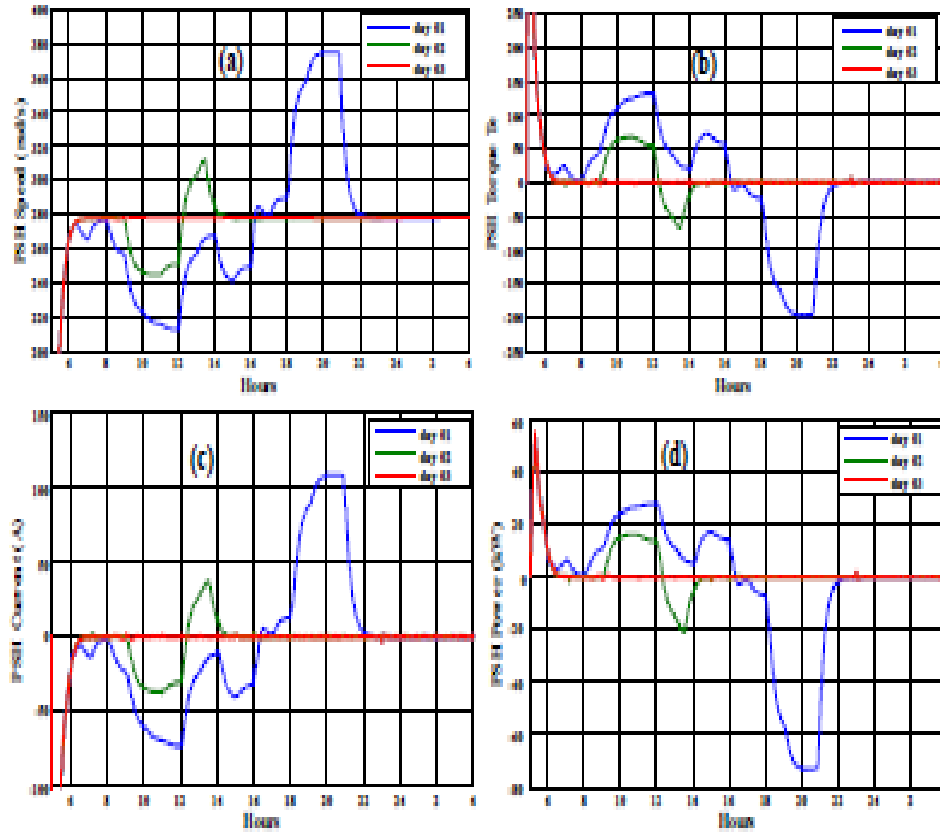
Figure 5 (a) The speed (rad/s), (b) torque, (c) current, and (d) the output power PSH system characteristics
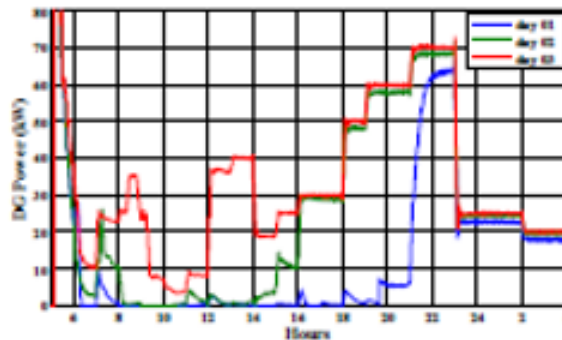
Figure.6 The output power produced by DG during the selected days

3.3 CO2 Gas Emission Analysis

The emission of CO2 gas (Figure 7(a)) is directly proportional to the output energy of the DG, its running time, and its FC (Figure 7(b)). Consequently, both the DG output power and the FC are influenced by factors such as the solar penetration of the site, the SOC of the PSH system, and the effectiveness of the EMC strategy.

3.4. Impact of EMC Strategy

The EMC strategy plays a crucial role in minimizing CO2 emissions and reducing FC costs (Figure 7(c)). By optimizing the operation of the hybrid microgrid energy system (HMGES), the EMC strategy effectively regulates the usage of the DG and coordinates its operation with other available energy sources, such as the PV array and the PSH system. This results in reduced reliance on the DG, leading to lower CO2 emissions and decreased FC costs, ultimately contributing to a more sustainable and cost-effective energy production process.

Through the integration of renewable energy sources, efficient energy storage systems, and intelligent control strategies, the HMGES demonstrates its potential to mitigate environmental impacts and optimize economic performance, paving the way for a more sustainable energy future.
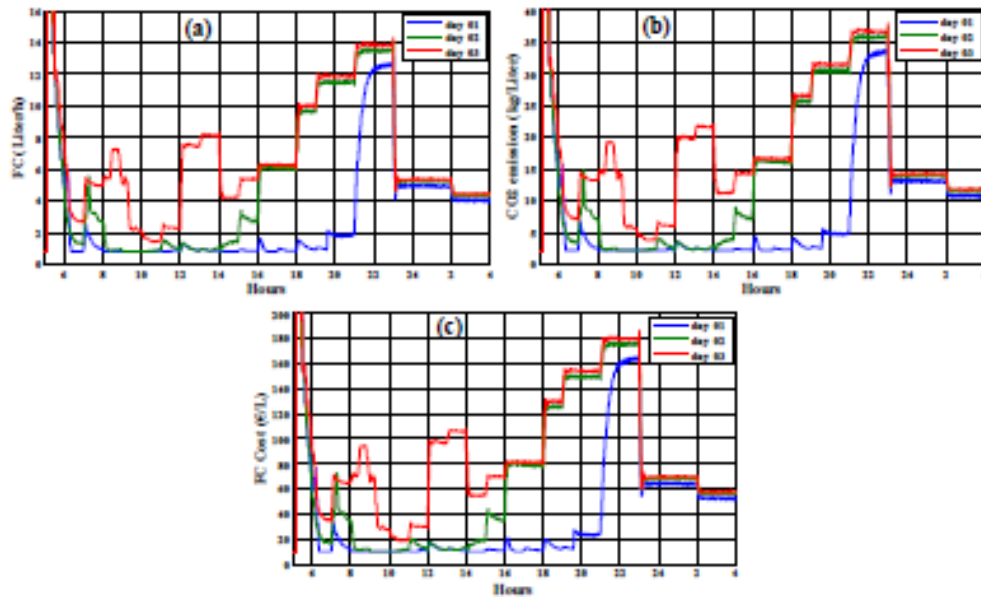
Figure 7. (a) FC (liter/h) of DG during the selected days, (b) CO2 emission (kg/L) of DG during the selected days, and (c) the FC cost(ε/L) of DG during the selected days

3.5 Optimal Power Generation by HMGES

Figure 8 illustrates the optimal power generation by the hybrid micro-grid energy system (HMGES) over a 24-hour period under different profiles of solar irradiation. Daytime Operation (Sunrise to Sunset): During daytime hours, the PV array takes the lead in supplying energy, harnessing solar irradiation from sunrise to sunset. This reduces reliance on the DG and minimizes fuel consumption and CO2 emissions during daylight hours.

Nighttime Operation: As solar irradiation decreases at night, the PV array's output diminishes, and the PSH turbine system covers the energy demands. The PSH system helps to minimize DG fuel consumption and CO2 emissions by providing energy storage and discharge capabilities during periods of low solar generation.

DG Backup: In cases where neither the PV array nor the PSH system can meet the energy demands, especially during nighttime, the DG takes the lead to ensure uninterrupted energy supply. However, its operation is minimized to reduce fuel consumption and CO2 emissions, with preference given to renewable energy sources whenever possible.
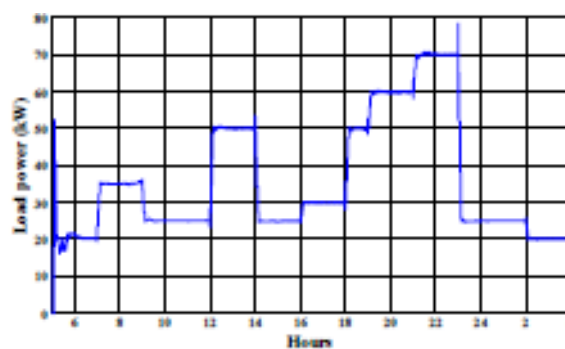
Figure 8. The total power produced by the HMGES for the different profiles for solar irridiations

4. CONCLUSION

The work carried out in this dissertation concerns the dimensioning of autonomous multi-source systems to supply homes in the southern Algeria region. To this end, a multi-source electrical system was chosen, initially consisting of a photovoltaic field, a diesel generator, a battery pack and a domestic load. The generator was later replaced by a wind turbine, transforming the system into a multi-source renewable energy system. These systems look set to undergo significant development, mainly as a result of the growing desire to diversify production methods and to be more environmentally friendly.

References

[1]   M. Pouresmaieli, M. Ataei, A. N. Qarahasanlou, and A. Barabadi, "Integration of renewable energy and sustainable development with strategic planning in the mining industry," *Results in Engineering*, vol. 20, 2023.

[2]   A. I. Osman, L. Chen, M. Yang, G. Msigwa, M. Farghali, S. Fawzy, D. W. Rooney, and P-S. Yap "Cost, environmental impact, and resilience of renewable energy under a changing climate: a review" *Environmental Chemistry Letters*, vol. 21, pp. 741–764, 2023.

[3]   A. Abdulkarim, N. Faruk, E. Alozie, H. Olagunju, R. Y. Aliyu, A. L. Imoize et al., "Advances in the design of renewable energy power supply for rural health clinics, case studies, and future directions," *Clean Technologies*., vol. 6, no. 3, doi:10.3390/cleantechnol6030047

[4]   M. de Witt, C. Chung, and J. Lee "Mapping Renewable Energy among Antarctic Research Stations" *Sustainability*, vol. 16, no.1, Dec 2023.

[5]   Kouton Jeffrey, "Information Communication Technology development and energy demand in African countries," *Energy*, vol. 189, art. no. 116192, 2019.

[6]   M. Khalid, "Smart grids and renewable energy systems: Perspectives and grid integration challenges," *Energy Strategy Reviews*, vol. 51, art. no. 101299, 2024.

[7]   A.M Bagher, M. Mahmoud, A. Vahid, and M. Mohsen. "Types of solar cells and application," *American Journal of Optics and Photonics*. vol. 3, no. 5, pp. 94–113, 2015.

[8]   D. R. Nair, M. G. Nair, and T. Thakur "A Smart Microgrid System with Artificial Intelligence for Power-Sharing and Power Quality Improvement," *Energies*, vol. 15, no. 15, art. no. 5409, 2022.

[9]   A. M. de Morais, S. de Morais Hanriot, A. de Oliveira, M. A. M. Justino, O. S. Valente, and J. R. Sodré, "An assessment of fuel consumption and emissions from a diesel power generator converted to operate with ethanol," *Sustainable Energy Technology Assessments*, vol. 35, pp. 291–297, Jun. 2019.

[10]   M. U. Hassan, M. Humayun, R. Ullah, B. Liu, and Z. Fang, "Control strategy of hybrid energy storage system in diesel generator based isolated AC micro-grids," *Journal of Electrical Systems Information Technology*, vol. 5, no. 3, pp. 964–976, 2016.

[11]   M. Gharibi and A. Askarzadeh, "Size and power exchange optimization of a gridconnected diesel generator-photovoltaic-fuel cell hybrid energy system considering reliability, cost and renewability," *International Journal of Hydrogen Energy*, vol. 44, no. 47, pp. 25428–25441, 2019.

The Improvement of Load Unbalance Detection Through Space Vector Transform

Lahouasnia Nasreddine[1], Deghboudj Thamir[2]

[1]Electromechanical Department, Badji Mokhtar University, Annaba, Algeria
[2]Department, Yahia Fares University, Medea, Algeria
Corresponding author: Lahouasnia Nasreddine (e-mail: hnasro114@gmail.com)

Abstract

Advances in the design and manufacture of rotating machines have resulted in more and more efficient machines. As their mass power is constantly increasing, they have to cross several critical speeds while speeding up and slowing down. The inevitable machining and mounting faults then cause significant vibration problems. Industrial manufacturers and operators seek to eliminate them to increase the life of the machines, to optimize their performance and to ensure their regularity of operation. One of the most important vibration problems is due to imbalances which cause generally synchronous vibrations. An unbalance corresponds to the non-coincidence of the main axis of inertia and the center of inertia with the axis of rotation.

Keywords: Fault detection, Load unbalance, Space vector

1. INTRODUCTION

Rotating machines are massively present in many industrial installations. There are many failures that can be encountered on a rotating machine. Given the importance of these rotating machines in certain devices, it is necessary to learn about their mechanical state, in order to be able to make the right decisions about their mechanical state at the right time. One of the means of monitoring the mechanical state of a rotating machine is the collection and analysis of its vibrations. The vibrations captured, collected and analyzed can provide information on the state of a system, in particular on the state of a rotating machine or certain elements of it [1, 2].

The diagnosis of electric machines and specifically asynchronous motors represent a scientific and economic issue motivated by the objectives of dependability and continuity of service of electric drives [2]. In order to prevent faults likely to occur in the engines, which are the main component and the weak link in the electrical process controls in time, predictive maintenance is essential on the operator's part. To date, the diagnosis and detection of faults have mobilized many researchers [1, 3]. There is no miracle solution to the problem of monitoring electrical machines and it should not be forgotten that it is a set of techniques used simultaneously which makes it possible to draw up a reliable and robust diagnosis, and which is able to reduce the rate of false alarms.

One of the most popular methods for diagnosing faults in asynchronous machines is the power spectral density (PSD) [4]. These faults can be detected by the presence of additional spectral components or the increase in amplitude of the spectral components already existing in the spectrum of signals analyzed [5]. However, in several industrial applications, such as in cement plants, the motor is subject to variations in the load torque. If the frequencies of variation of the load torque are similar to the frequencies of the real faults, the same spectral components due to the real faults can appear in the spectrum of the signals analyzed even when the engine is in its healthy state.

Time-frequency transforms, such as the Wigner-Ville distribution [6] and the short time fourier transform (STFT) [7] can be used to analyze the induction motor signals. Nevertheless, these techniques provide constant resolution for all frequencies due to the same window length use for analysis of the entire signal. The Hilbert-Huang transform (HHT) on the other hand is a time-frequency analysis technique based on empirical mode decomposition (EMD). HHT offers great reliability, as in the case of [8]. Like HHT, the wavelet transform (WT) is a time-scale analysis method suitable for both stationary and non-stationary signals. The WT, offering a multi-resolution analysis, is very suitable for fault diagnosis. Thus, the WT has been used not only for bearings, but for gears [9], mechanical unbalances [10] and shafts [11]. However, using the WT is a little complicated because of the critical parameters that must be chosen, such as the mother wavelet, the filter order, and the decomposition level. Wavelet packet transform (WPT) is an enhancement of the multi-resolution analysis (MRA) [12, 13], since it allows the decomposition of all frequency sub-bands. Thus, WPT applications are widely used in signal processing in several

fields. WPT coefficients can be used directly as indicators or characteristics, since they contain consistent information about defects [14].

The application of these single-phase methods presents numerous disadvantages, as they often ignore crucial information provided by the three-phase system, which is frequently essential for the diagnosis of induction motors (IM). Furthermore, the stator current spectrum may contain high-frequency harmonics that have not been adequately filtered during current acquisition, which can be compounded by measurement noise. These factors can result in a reduction in the resolution of incipient failure signatures, thereby limiting the ability to detect early defects.

This paper presents a solution to the aforementioned shortcomings and offers two primary contributions. The initial contribution addresses the enhancement of early load unbalance detection capabilities in three-phase IM, taking into account the multicomponent nature of the stator currents and processing the entirety of the information provided by the three-phase induction motor using current space vector (CSV). The second contribution is the detection of phase modulation and the provision of a broader range of failure-related frequencies. The tools used for fault analysis and diagnosis are based on the use of spectra via the Power Spectral Density and the wavelet transform. To carry out this study, the article is structured into four parts:

The first part is devoted to the state of the art in asynchronous machine fault diagnosis. The various faults that can affect the correct operation of the asynchronous machine and the different methods of detecting and diagnosing these faults are described. The second part is devoted primarily to the modelling of the machine in case of load unbalance. Thus, the study is carried out for the case of the machine supplied by an unbalanced load in order to study the effect of the fault on the diagnosis. Secondly, the detection of the fault using PSD and wavelet signal processing methods for the stator current. The third part is devoted to describe the Wavelet transform in order to use it for the detection of the fault. In the fourth part, the characterization of the effect of the fault is performed by evaluating the energy in frequency bands obtained by wavelet analysis and by spectral analysis of the stator current. Finally, a general conclusion is presented, summarizing the results obtained and outlining future prospects for improving this work.

2. THE UNBALANCE FAULT

2.1. Fault Description

An unbalance is caused by an incorrect spatial distribution of the rotating masses, resulting in a discrepancy between the axis of inertia and the axis of rotation. During rotation, this causes a centrifugal force on the rotor. This leads to significant radial vibration at the frequency of rotation. There are several factors that contribute to the appearance of unbalance, but the most common are:

- Non-homogeneity of materials: cast iron pump rotors are characterized by the presence of cavities, called "cast iron blowholes" or "sand holes", formed during the molding process.
- Manufacturing and assembly tolerances: play or looseness can lead to unbalance in the rotating part.
- Physical changes to a rotor in operation: Even if a part is reasonably well balanced at the time of manufacture, thermal deformation, corrosion and wear, or fouling of the rotor can alter its original balance.

The value of an unbalance is the product of the unbalance mass m, in grams, and the distance r, in millimeters, separating it from the shaft axis (in the case of rigid bearings, the axis of rotation is the shaft axis) [5]. Thus, for example, a mass of 10 grams at a radius of 20 millimeters from the shaft axis gives an unbalance value equal to 200 g.mm is equivalent to
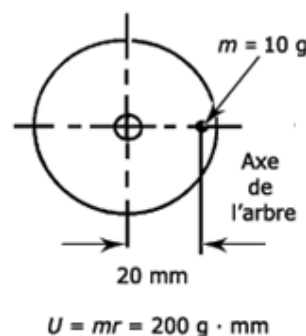
Figure 1. Unbalance value

The value of the unbalance produced by a given mass increases as the distance separating this mass from the shaft axis increases [5]. This mass undergoes a centrifugal force that induces torque oscillations at particular frequencies often related to the mechanical motor speed, generating peaks in the stator current spectrum at specific frequencies [15].

$$f_{defect} = f_s \pm k f_{rot} \tag{1}$$

Where f_s is the stator supply frequency, f_{rot} is the rotational frequency, and k = 1, 2, 3 ... .

2.2. Current Space Vector

The space vector transformation is derived from the symmetric component transformation, also known as the Fortescue transformation. A brief history of symmetric component transformations and their link to the space vector transformation is given in this section. Symmetric components were introduced in 1918 by Fortescue [16]. Fortescue's transformation, applicable to the phasors of sinusoidal functions, allows the analysis of asymmetric three-phase systems under sinusoidal conditions. Later, Lyon took up Fortescue's transformation and modified it so that it could be applied to time-dependent quantities, whatever the conditions (sinusoidal or not):

$$\begin{bmatrix} ip(t) \\ in(t) \\ i0(t) \end{bmatrix} = \frac{2}{3} \begin{pmatrix} 1 & a & a^2 \\ 1 & a^2 & a \\ \frac{1}{2} & \frac{1}{2} & \frac{1}{2} \end{pmatrix} \tag{2}$$

Where j is the square root of (-1), and the 2/3 normalization coefficient is chosen to maintain the amplitudes between the three phase systems before and after transformation.

If the quantities in the initial system $i_1(t)$, $i_2(t)$, and $i_3(t)$ are real values, the direct and inverse components of the Lyon transformation and are complex conjugates of each other. These quantities therefore carry the same information and are redundant. In fact, to fully describe the three real scalar quantities of the original three-phase system, only one complex scalar quantity and one real scalar quantity are sufficient. Moreover, since the machine is supposed to be star wired, the sum of the stator three currents is zero and the instantaneous zero-sequence vector is zero for all time. Thus, the original three-phase system can be described only by the positive-sequence component $i_p(t)$ that we will note $i(t)$ in the rest as follows [17]:

$$i(t) = \frac{3}{2} \left[i_1(t) + a i_2(t) + a^2 i_3(t) \right] \tag{3}$$

Where $a = e^{-j\frac{2\pi}{3}}$ since our system is balanced.

2.3. Load Unbalances Effect on Current Space Vector

With the presence of mechanical faults in the asynchronous machine, the apparition of load torque variations can happen [6] which can be expressed as follows:

$$\Gamma(t) = \Gamma c [1 + \Delta\Gamma] \text{ with } \Delta\Gamma \lll 1 \tag{4}$$

where, Γ_c is the constant part of load torque and $\Delta\Gamma(t)$ is torque variations induced by the defect.

In order to detect effectively this type of defects using stator currents, it is necessary to determine the signature of this mechanical phenomenon in the currents. In this purpose, we will use space vector for the magneto-motive force (MMF) and permeance wave approach already used in [5] for a single-phase current.
The space vector of the stator MMF generated only by the power supply F_S is given by:

$$F_S(t) = F_S e^{j(2f_s t - p)} \tag{5}$$

Where F_S is a constant complex number. This MMF induces a balanced system of three phase currents in the rotor, generating itself a rotor MMF. The authors of [5] showed that in the case of torque variations of Equation (4), the rotor MMF becomes:

$$F_R(t, \theta) = F_R e^{j\left(2f_s t + \frac{p_c}{J}\int_{t_0}^{t}\int_{t_0}^{v}\Gamma(u)dudv - p\right)} \tag{6}$$

Where F_R constant complex number and J the mechanical system total inertia. We can obtain the stator current space vector $i(t)$ using the stator voltage equation:

$$i(t) = \frac{V(t)}{R_s} - \frac{1}{R_s}\frac{d(t)}{dt} \tag{7}$$

$V(t)$ is the space vector of the supply voltages deduced from the magnetic flux and R_s is the stator resistance of the machine. Consequently, we can express the stator current space vector in a general form as follows:

$$i(t) = I_S e^{j2f_s t} + I_R^{\Phi} e^{j\left(2f_s t + \frac{p_c}{J}\int_{t_0}^{t}\int_{t_0}^{v}\Gamma(u)dudv - p\right)} \tag{8}$$

The term $I_S(t)$ results from the stator MMF and not modulated. In addition, the term $I_R^{\Phi}(t)$, which is a direct consequence of the rotor MMF shows phase modulation due to the considered load torque oscillations.

The findings of this qualitative study indicate that load unbalance is the primary cause of phase modulations in the corresponding space vector stator current. It is therefore appropriate to employ techniques developed in the field of signal processing in order to develop effective detectors for this kind of phenomenon. The following paragraph will present the fundamental principles of these signal-processing methods.

3. WAVELET TRANSFORM

The wavelet transform is a powerful signal processing tool [18], it is based on the decomposition of a signal into a family of scale wavelets and different positions. These wavelets are obtained by dilating or contracting a mother wavelet and translating it along the time axis. Signal analysis methods have been developed for stationary signals, that is, the characteristics do not vary over time.

Continuous and discrete wavelet transforms are different applications. The continuous transform makes it possible to more precisely locate events temporally and frequently [18]. It is therefore rather used to analyze transients or temporal events. The discrete transform on the other hand allows an efficient calculation and is used for compression or stretching. As part of this work, we will only use discrete wavelet transforms [18].

3.1. Wavelet Packet Decomposition

When using wavelets on a signal it splits it into detail and approximation. The approximation is then decomposed into approximation and detail of second level, and the process is repeated. For n-level decompositions, there are (n + 1) ways to split the signal. The WPD is an improvement of the discrete wavelet transform (DWT), it splits detail (Di) and approximation (Ai) simultaneously which leads to more than 2^{2n-1} different decompositions of the signal. This offers a richer range of possibilities for signal analysis. There is no redundant information in the decomposed frequency bands. It is an efficient analysis approach based on multi-resolution, which makes it an excellent method for fault diagnosis [19].

3.2. Energy of Wavelet Decomposition

After the extraction of stator current fundamental, we can detect the fault by observing and comparing decomposition energy associated with each decomposition level node or node which contains defect information of the monitored motor. The energy at level j is defined by [20]:

$$E_j = \sum_{n=1}^{N} \left| d_j(n) \right|^2 \tag{9}$$

Where j is the decomposition level, N is the total number of samples in the signal and d_j denotes the detail signal at level j. The energy of the decomposition levels contains the information of an asynchronous motor signals, the plot of these values can be used to diagnose faults.

4. EXPERIMENTAL RESULTS

4.1. Experimental Setup

To demonstrate the superiority of the space vector approach compared to single-phase analysis, a data set of mechanical unbalance faults is used. The data was obtained via the experimental setup machinery diagnosis system, which comprises a 0.37 kW, 0.8 A, one-pole pair, three-phase star-connected induction machine, which is supplied by an inverter at a frequency of 26 Hz.

The data set is captured using three current sensors and Dspace1104 acquisition system with a sampling frequency $f_e = 10$ kHz. The set is connected to a computer for viewing and processing acquired signals as illustrated in Figure 2.

Figure 2. Experimental setup (composed of a 0.37 kW induction machine supplied by an inverter)

4.2. Results in Healthy State

By comparing the amount of energy of single phase and space vector currents presented in Figure 4, a remarkable difference between the two spectrums is noticeable. By observing Figure 5 that presents a phase current as well as current space vector PSD spectrums, we can understand the origin of this phenomenon. In fact, some additional components are present in the single-phase spectrum (see arrows), these components are the result of small phase shifts and amplitude unbalances. In contrast, space vector current is not affected by these components and therefore does not generate any more parasitic phenomena that may hide incipient load unbalance.
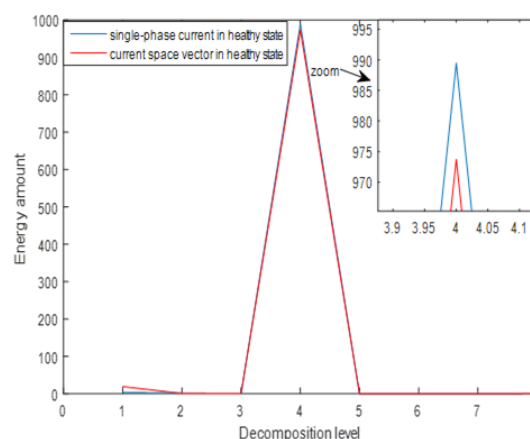
Figure 4. Wavelet packet decomposition energy in single-phase and current space vector in healthy state
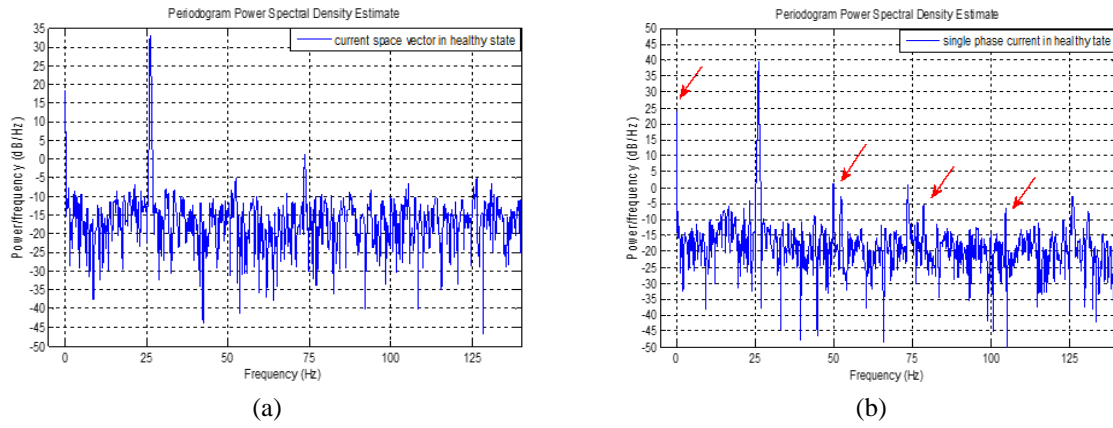
Figure 5. Power spectral density (a) current space vector and (b) single-phase current

4.3. Results at Low Load Unbalance Level

Furthermore, if we compare healthy single phase WPD spectrum with current space vector in case of 0.5g load unbalance (Figure 6), we notice that single phase WPD spectrum in healthy case is slightly higher than current space vector with 0.5g load unbalance. Therefore, by relying on single-phase signal analysis, we will not be able to detect incipient load unbalance (0.5g); this is clear in figure 7 on 0 Hz, 106 Hz and 126 Hz components, where we can see that these components in single-phase spectrum are higher than in the case of current space vector with a 0.5g load unbalance.

From these observations, we can conclude that one of the current space vector contributions is the increase of the signal resolution, by eliminating additional components present in single-phase signal even in healthy condition that may hide incipient load unbalance (0.5g). In the following, and in order to prove the proposed technique, only the current space vector will be analyzed in healthy and faulty conditions.
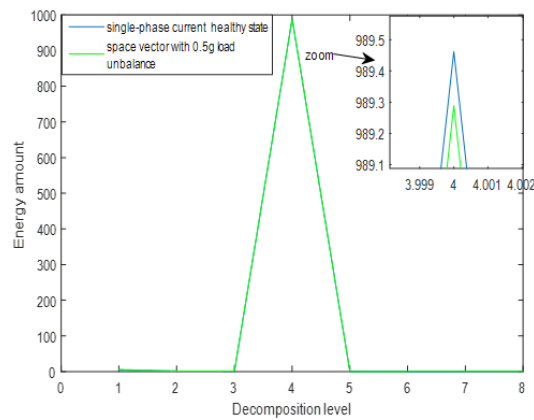
Figure 6. Decomposition energy of single-phase current in healthy state and CSV with 0.5g load unbalance
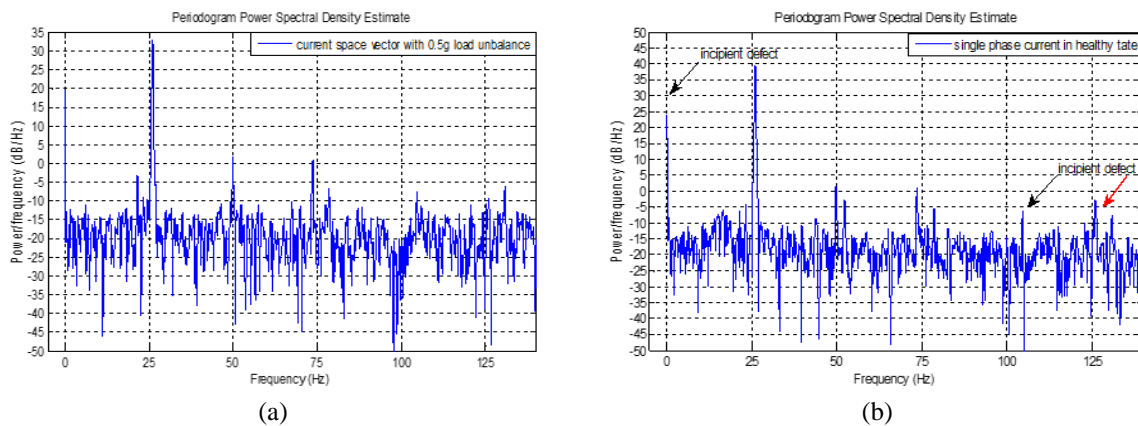
Figure 7. (a) CSV spectrum with 0.5g load unbalance and (b) PSD of single-phase current in healthy case

4.4. Results at Higher Load Unbalance Levels

Now the same process is applied but only for current space vector in order to detect higher load unbalance levels, tests are conducted with 5g load unbalance. The WPD and PSD spectrums for current space vector in healthy and faulty states are presented in Figure 8 and Figure 9 respectively.

A fluctuation of the energy amount is clearly visible between healthy and faulty states, demonstrating the presence of a defect. Also, on the PSD graph (Figure 9), during the appearance of a load unbalance, an increase of about 2 dB of sidebands at frequencies 0 Hz, 78Hz, 106 Hz and 130Hz is noticed compared to healthy state(which is equivalent to $f_{defect} = f_s \pm nf_r$ where n = 1, 2, 3 respectively. This result is in perfect agreement with single-phase analysis.

Another interesting point concerning the use of wavelet packet decomposition is the ability to detect the defect severity, and distinguish clearly between the different load unbalance levels as illustrated in Figure 10.
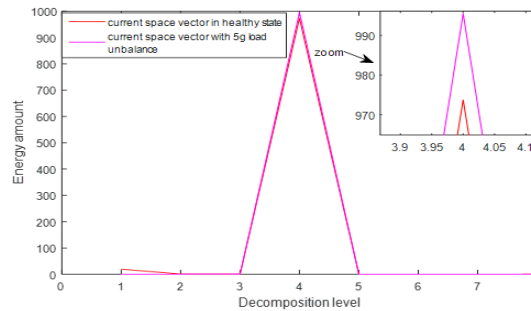
Figure 8 Decomposition energy of current space vector in healthy and faulty case

(a)   (b)
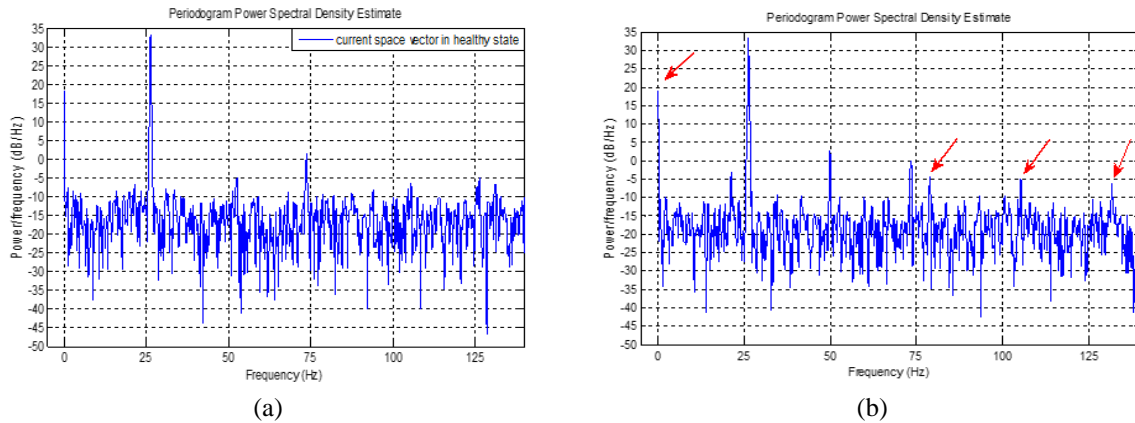
Figure 9. (a) CSV spectrum in healthy state and (b) PSD spectrum of CSV with 2g load unbalance
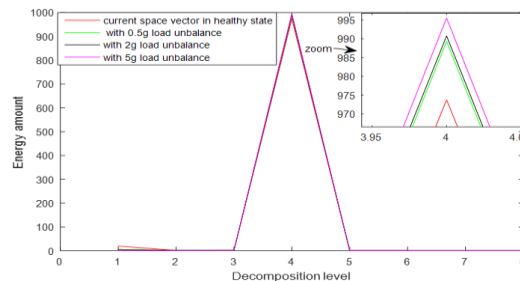
Figure 10. Energy decomposition levels corresponding to different load unbalance levels

4. CONCLUSION

This paper examines the phenomenon of load unbalance in induction motors through the ictilization of stator current monitoring techniques. The objective of this study is to apply the current space vector and to extract its advantages in comparison to a single-phase analysis. The results demonstrated that utilizing current space vector for the analysis of induction machine signals offers significant advantages over the use of a single-phase current.

The processing of all the information provided by the three-phase system is therefore required. The utilization of a current space vector facilitates the attainment of identical outcomes to those achieved through single-phase analysis with regard to load unbalance detection, albeit with enhanced precision.

References

[1]   S. Gawde, S. Patil, S Kumar, P. Kamat, K. Kotecha, and A Abraham   "Multi-fault diagnosis of industrial rotating machines using data-driven approach: A review of two decades of research," *Engineering Applications of Artificial Intelligence*, vol. 123, Part A, art. no. 106139, Aug. 2023.

[2]   J. Chen, C. Lin, D. Peng, and H. Ge, "Fault diagnosis of rotating machinery: A review and bibliometric analysis," *IEEE Access*, vol. 8, no. 1, 224985–225003, 2020.

[3]   R. Issa, G. Clerc, M. Hologne-Carpentier, R. Michaud, E. Lorca, C. Magnette, and A. Messadi, "Review of fault diagnosis methods for induction machines in railway traction applications," Energies, Vol.17, no.11, 2024.

[4]   C. Jordi, R. Luis, O. Juan, R.G Javier, and G.E Antonio "Fault detection in induction machines using power spectral density in wavelet decomposition," *IEEE Transactions on Industrial Electronics*. vol 55, pp. 633–643, 2008.

[5]   N. Lahouasnia, M.F Rachedi, D. Drici, and S. Saad, "Load unbalance detection improvement in three-phase induction machine based on current space vector analysis," *Journal of Electrical Engineering and Technology*, vol. 15, pp. 1205–1216, 2020.

[6]   P. Singru, V. Krishnakumar, D. Natarajan, and A. Raizada "Bearing failure prediction using Wigner-Ville distribution, modified Poincare mapping and fast Fourier transform," *Journal of Vibroengineering*, vol. 20, no.1, 2018.

[7]   F. K. Choy, J. Wei, and W. Ruiwei "Identification of bearing and gear tooth damage in a transmission system," *Tribology Transactions*, vol. 52, no.3, pp. 303–309, 2009.

[8]   H. Liu, X. Wang, and C. Lu, "Rolling bearing fault diagnosis under variable conditions using hilbert-huang transform and singular value decomposition," *Mathematical Problems in Engineering*, vol. 2014, no. 1, art. no. 765621, 2014.

[9]   S. S. Kulkarni, A. K. Bewoor, and R. B. Ingle, "Vibration signature analysis of distributed defects in ball bearing using wavelet decomposition technique," *Noise & Vibration Worldwide*, vol. 48 no.1–2, pp. 7–18, 2017.

[10]   F. R, Gomaa, k. M. khader, and M. A. Eissa, "Fault diagnosis of rotating machinery based on vibration analysis," *International Journal of Advanced Engineering and Global Technology*, vol. 04, no. 01, 2016.

[11]   A. Umbrajkaar and A. Krishnamoorthy, "Shaft misalignment prediction on basis of discrete wavelet transform," *International Journal of Mechanical Engineering and Technology (IJMET),* vol. 9, no.7, pp. 336–344, 2018

[12]   H. S. Kumar, P. Srinivasa Pai, N. S. Sriram, and G. S. Vijay "Selection of Mother Wavelet for Effective Wavelet Transform of Bearing Vibration Signals" *Advanced Math Research*, vol. 1039, pp. 169–176, 2014.

[13]   M. Rhif, A.B. Abbes, I.R. Farah, B. Martínez, and Y. Sang "Wavelet transform application for/in non-stationary time-series analysis: A review" *Applied Science*, vol. 9, no.7, 2019.

[14]   Q. Huang, Y. Yin, and G. Yin, "Automatic classification of magnetic tiles internal defects based on acoustic resonance analysis," *Mechanical Systems and Signal Processing*, vol. 60–61, pp 45–58, 2015.

[15]   G. Cablea, P. Granjon, and C. Bérenguer, "Method for computing efficient electrical indicators for offshore wind turbine monitoring," in *11th International Conference on Condition Monitoring and Machinery Failure Prevention Technologies, CM 2014 / MFPT 2014*, Manchester, UK, 2014.

[16]   G. K. Yamamoto, C. da Costa, and JS. da Silva Sousa, "A smart experimental setup for vibration measurement and imbalance fault detection in rotating machinery," *Case Study on Mechanical Systems and Signal Processing*, vol. 4, pp. 8–18, 2016.

[17]   M. Salah, K. Bacha, and A. Chaari, "Comparative investigation of diagnosis media for induction machine mechanical unbalance fault," *ISA Transactions*, vol. 52, pp. 888–899, 2013.

[18]   E. Gómez-Luna, D.E. Cuadros-Orta, J.E. Candelo Becerra, and J.C. Vasquez "The development of a novel transient signal analysis: A wavelet transform approach," *Computation*, vol. 12, no. 9, art. no. 178, 2024.

[19]   D. Bianchi, E. Mayrhofer, M. Gröschl, G. Betz, and A. Vernes, "Wavelet packet transform for detection of single events in acoustic emission signals," *Mechanical System and Signal Processing*, vol. 64–65, pp 441–451, 2015.

[20]   D. Drici, H Merabt, S Aouabdi, and A Boudiaf "Detection of broken bar fault in squirrel cage induction motor using wavelet packet analysis," *Electrotechnica Electronica Automatica*, vol. 64, no. 3, pp. 60–67, 2018.

Contribution of Artificial Intelligence to Dynamic Industrial Risk Assessment: Towards Predictive and Secure Management

Imane Aila[1], Samia Chettouh[1], Djamel Haddad[1]

[1]Laboratory of Research in Industrial Prevention, Institute of Health and Safety, Universiy of Chahid Mostepha Ben Boulaid-Batna 2, Batna, Algeria
Corresponding author: Imane Aila (e-mail: imane.aila@univ-batna2.dz)

Abstract

Dynamic industrial risk assessment is a crucial process for ensuring safety and continuity of operations in industrial facilities. As technology advances, artificial intelligence (AI) is emerging as a key solution to significantly enhance, automate, and improve this process, making it more efficient. Because of its ability to process huge quantities of data in real-time, AI can continuously analyze and monitor operational conditions, identifying potential risks before they become real threats. Moreover, AI can anticipate failure trends, offering a faster, more preventive response. This study explores the contribution of AI to dynamic industrial risk assessment, highlighting its role in predicting incidents, optimizing risk responses, reducing costs, improving reliability, and enhancing overall risk management. The results show that AI promotes more accurate, reactive, and proactive risk assessment, reducing the frequency of accidents and production interruptions while optimizing productivity. However, the implementation of AI in these critical environments must be accompanied by robust cybersecurity measures to ensure that infrastructures are protected against cyberattacks and potential vulnerabilities. In the future, the successful integration of AI into risk assessment will depend on close collaboration between AI experts and industrial safety specialists to develop solutions that are safe, effective, and resilient in the face of future technological challenges.

Keywords: Dynamic risk assessment, AI, Incident prediction, Industrial safety, Infrastructure resilience

Stability Analysis of the Pitch Angle Control Using MPPT of Large Wind Turbines Using Artificial Neuronal Network Controller Strategies

Hicham Bouregba[1], Sabah Kabache[2]

[1]Energetics, Mechanics & Engineering Laboratory, Faculty of Technology, M'Hamed Bougara University of Boumerdes, Algeria
[2]Coating, Materials and Environment Laboratory, Department of Physics, M'Hamed Bougara University of Boumerdes, Algeria
Corresponding author: Hicham Bouregba (e-mail: mr.bouregbahicham@gmail.com)

Abstract

Reducing the environmental impact necessitates a boost in renewable energy conversion systems. Wind energy is regarded as one of the most essential energy sources. For this purpose, the high wind variations in the high-power energy conversion chain require robust and reliable control. This research aims to implement a regulation based on artificial neuronal network (PI-ANN) toward a blade orientation mechanism to improve the stability of energy conversion. On the other hand, an energy maximization technique is integrated into the control system. A developed program in Matlab estimates the turbine performance with two different strategies, namely the maximum power point tracking (MPPT) technique and the Pitch control mechanism. The proposed control improved more stability of energy conversion, were employed. They are compared with the conventional controller (PI-C). This comparison is made to distinguish the most robust regulator against wind speed variations. The different performance indices showed that the controller PI-ANN has an excellent response, with a mean absolute error (MAE) equal 0.455, which PI-C equal 0.495 whereas the mean relative error (MRE) equal 0.222 and 0.243, respectively.

Keywords: MPPT, Pitch control, Neuronal network, Wind turbine generator, Modelling system

1. INTRODUCTION

Energy plays a crucial role in socioeconomic development, sustainable growth, and improving the quality of human life. In the coming decades, energy demand will rise due to the growth of the global population and economic activity [1]. In recent years, wind energy has experienced rapid and consistent growth. Over the next 30 years, it is projected to account for 18% of global electricity generation. As environmental concerns have increased, the popularity of renewable energy has surged. One of the most significant challenges facing wind energy today is maximizing the energy output of wind farms, which relies on optimizing the power generated by each wind turbine within the park [2].

However, wind turbines (WTs) generate power that is directly proportional to the cube of the wind speed [3]. This leads to significant variability, especially as wind speed fluctuates constantly and unpredictably. Wind turbines cannot produce constant power indefinitely. To address this, variable-speed wind turbines employ strategies such as the maximum power point tracking (MPPT) technique and pitch control mechanism. MPPT optimizes power output in the second and third operating zones of the system. Pitch control is designed to protect wind turbines from strong winds by adjusting the blade orientation. To achieve this, a system is needed that can optimize the power extracted from the wind when the turbines are operating in different zones. The variable mode of operation also helps mitigate the effects of the intermittent nature of wind power, which can otherwise place unnecessary strain on mechanical components [4].

The scientific literature includes studies that have utilized the pitch angle control approach. Other research focuses on turbine power maximization techniques with various controllers. For instance, P. Venkaiah et al. developed a fuzzy-anticipation PID controller for pitch control of horizontal axis wind turbines, utilizing an electro-hydraulic pitch actuation system [5]. Chiung Hsing Chen et al, implements a fuzzy hybrid control of the caged synchronous generator of a low-power wind turbine by controlling the stall angle using recurrent neural network (RNN) [6]. Amirhossein Asgharnia et al, recommends using sophisticated controllers like FPID and FOFPID to improve pitch control performance [7]. Tauseef Aized et al. examined how wind speed data can be collected, how a wind-driven water pumping system can be designed, and how the design can be analyzed under a variety of wind conditions in

Pakistan [8]. An FDI system for a 4.8 MW wind turbine was developed by Ayoub El Bakri et al., which was described using numerous Takagi-Sugeno (T-S) models [9]. When a PMSG is constructed in Matlab, some study employs artificial neural network(ANN)-based pitch control for MPPT in wind turbines.

The existing studies in the technical literature are insufficient to fully address the wind conversion chain. Ensuring optimal control and better protection of wind turbine infrastructure remains a significant challenge. It is highly recommended to use control systems based on artificial intelligence with various strategies to tackle these issues. On the other hand, the regulation mechanism based on conventional controllers is sensitive to wind variations, leading to a loss of control and reduced reliability of the conversion system [10]. In this study, Xiaodong Sun et al. addressed the weaknesses of the conventional regulator across various research areas. In the first study, the standard proportional-integral (PI) speed loop was replaced with a sliding mode controller to enhance steady-state performance [11]. In a second study, researchers compared the efficiency of the proposed technique with that of the conventional low-speed sensorless approach through a series of experiments using PMSG. The proposed low-speed sensorless system was demonstrated to be successful in the experiments [12]. This article presents a sensorless approach for controlling permanent-magnet synchronous motors. The proposed technique has been experimentally tested and compared to the standard PLL under various conditions. This innovative approach demonstrated excellent steady-state performance while reducing speed, angular, and transient oscillations.

In the present work, a performance study based on ANN monitoring is conducted. The results of the ANN controller are compared with those of the conventional controller to improve the stability of the pitch angle mechanism and limit the output power to the rated value under full load conditions.

The hybridization of the ANN controller with the traditional PI controller approach is then used to develop an adaptive law. As a result, the scaling factors are automatically adjusted based on the correction factor generated from the gain scheduling PI approach. This enhances the flexibility of the controller, allowing it to maintain high performance and optimally manage the highly nonlinear behavior of the turbine, as well as the load disturbances caused by wind speed variations. The transient performance of the proposed adaptive ANN controller is compared with that of the classical PI controller (PI-C) using two performance indices: Mean absolute error (MAE) and mean relative error (MRE).

The article is divided into five sections. The first section describes the methodology. The second section provides a brief description of the WT model. A simplified mathematical model is derived in the third section. The fourth section outlines the different types of controllers, including pre-existing proportional-integral controllers and their control techniques. Finally, the last section presents a comparison of the performance results of the different types of controllers (PI-C, PI-ANN) applied to a high-power wind turbine.

2. METHODOLOGY AND DESCRIPTIONS

In the presence of severe disturbances, the performance of fixed-gain controllers does not accurately predict the system's response, such as in cases of short circuits and wind speed variations. While the fixed gain of the PI controller ensures excellent steady-state performance at a specific operating point, the converter's operating point constantly changes due to the plant's dynamic behavior. As a result, it is not uncommon for the controller to exhibit poor transient performance. Figure 1 illustrates the proposed artificial intelligence controller integrated into the wind turbine conversion chain for predicting performance.
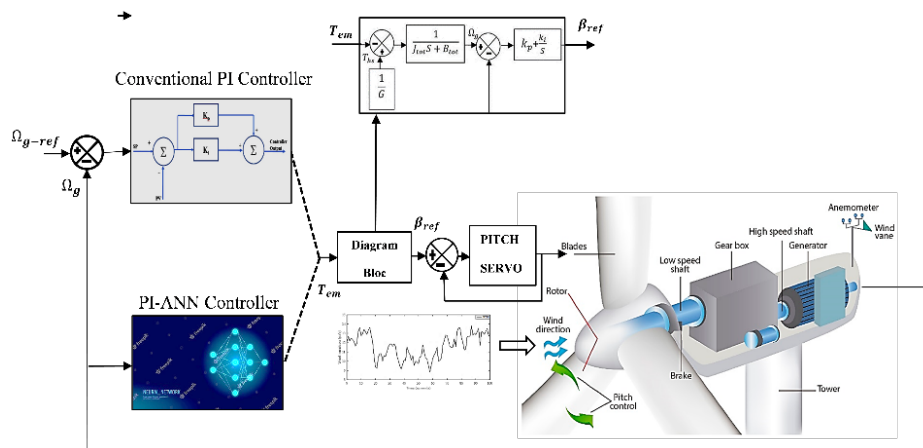
Figure 1. Bloc diagram of suggested pitch control using regulators

The five-step workflow is described as follows:

- The relative wind data is simulated based on a Nikita's model at the predicted capacities of the high-power wind turbines, which are collected in a first step.
- The turbine's modeling contains two masses, and the second phase involves using a simulation tool to depict the energy performance.
- Integration of control technique for extracting the maximum power and pitch control mechanism for the third operation zone based on a linear PI controller is planned in the third step.
- The synthesis of artificial neuronal network is based on software simulation.
- The fifth step is to examine the wind turbine's performance parameters

Two control systems are combined in a high-power three-bladed WT. This system incorporates pitch control, and the maximum power point (MPP) approach is used to extract the maximum possible power from the wind. The doubly fed induction generator (DFIG) provides greater flexibility for connection to the electrical grid. The four zones in which a variable-speed wind turbine operates are as follows:

Zone 1: The wind speed is lower than starting inertia turbine condition that mean the importance of the turbine's inertia, resulting in no power being provided.

Zone 2: The wind turbine operates in partial load mode when the wind speed varies between the startup speed (Vd) and the nominal speed (Vn). In this zone, the pitch control mechanism is set to a fixed angle of $\beta = 2°$. The power ranges between synchronous speed (Ωs) and $0.7\ \Omega s$. Here, the wind speed generates kinetic energy to drive the turbine, allowing it to maintain power levels higher than the generator's operating requirements. This zone uses MPPT algorithms to maximize power transfer.

Zone 3: The wind turbine works when the MPPT method with pitch control is used. The speed of the generator (Ωg) controlled when the wind speed (WS) is between the nominal value (Vn) and the maximum value (Vmax). The speed generator exceeds ($1.3\ \Omega s$) above the nominal speed, this decreases the blade angle. Therefore, it requires regulation of the turbine speed to provide a supportable power level.

Zone 4: The wind turbine is operating under mechanical locking caused by the high-speed generator. On the other hand, the blade angle exceeds the saturation states $\beta = \beta max$.

3. MODELING SYSTEM

Figure 2 illustrates a conventional variable-speed wind turbine, which consists of an aerodynamic system, a gearbox, and a generator. The components that contribute to transmitting mechanical torque to the axis of rotation are collectively referred to as the powertrain or mechanical transmission system. Mechanical modeling can vary in complexity, with some models incorporating as many as six masses, depending on the intricacy of the system being modelled [13].
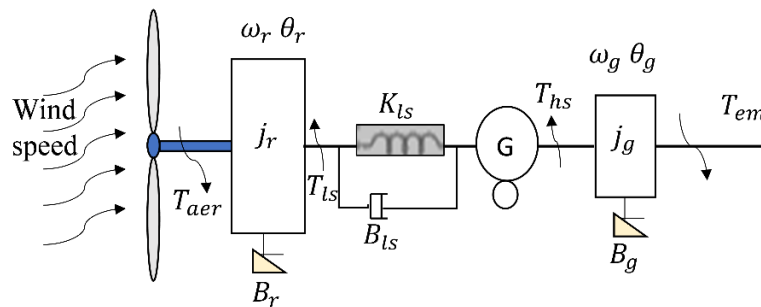
Figure 2. Wind turbine dynamics

The model's simplifying assumptions are as follows:

- The blades' flexible modes are thought to be high enough to be ignored, while the flexible modes are found in the slow shaft's flexible element. The fast shaft, on the other hand, is regarded as indefinitely stiff.
- The inertia of the gearbox and the slow shaft is integrated with that of the rotor (Jr), which represents the whole.
- The inertia of the hub can be ignored because it accounts for only 1% of the total inertia of the turbine. The inertia of the fast shaft connected to the generator is represented by (Jg).

- The torsion of the turbine axis, in terms of stiffness constancy, can be calculated analytically, provided that its geometric shape is known.
- The torsional forces of the blades, hub, multiplier, and slow shaft are all included in the total elasticity coefficient (Kls) of the slow shaft.
- Viscous friction on the bearings of the drive unit is taken into account by the coefficients (Kr) and (Kg).
- The inertia of the turbine is substantially equal to that of the blades.

For the rotor's aerodynamic power capture, the non-linear expression is [14]:

$$P_{aer} = \frac{1}{2} \rho.\pi.R^2 C_p\left(\lambda,\beta\right).v^3 \tag{1}$$

where, C_p: Power coefficient, v: Wind speed (m.s^{-1}), R: Rotor radius (m), and ρ: Air density (kg.m^3). The blade pitch angle (β) and the tip-speed ratio (λ) both have an impact on the power coefficient.

$$\lambda = \frac{R.\Omega_t}{v} \tag{2}$$

where, Ω_t: Turbine speed (rad.s^{-1}). According to the following equation, the power coefficient is proportional to the aerodynamic torque coefficient, profiting from a partnership.

$$P_{are} = \Omega_t.T_{are} \tag{3}$$

Where, T_{aer}: Aerodynamic torque (N.m). The following equation is used to determine the aerodynamic torque expression:

$$T_{are} = \frac{1}{2} \rho.\pi.R^3.C_{aer}\left(\lambda,\beta\right).v^2 \tag{4}$$

$$C_{aer}\left(\lambda,\beta\right) = \frac{C_p\left(\lambda,\beta\right)}{\lambda} \tag{5}$$

The power coefficient (Cp) for a 2 MW wind turbine is presented in the equation below [15].

$$C_p\left(\lambda,\beta\right) = c_1\left(c_2\frac{1}{R} - c_3\beta - c_4\beta^x - c_5\right)e^{-c_6\frac{1}{R}} \tag{6}$$

$$\frac{1}{R} = \frac{1}{\lambda+0.08\beta} - \frac{0.035}{\beta^3+1} \tag{7}$$

where, $C_1 = 0.5$, $C_2 = 116$, $C_3 = 0.4$, $C_4 = 0$, $C_5 = 5$, $C_6 = 21$, and $x = 0$. The dynamic response of the rotor driven at a speed (Ωr) by the aerodynamic torque (Taer) is shown in the equation below:

$$j_r\frac{d\Omega_r}{dt} = T_{aer} - T_{ls} - B_r.\Omega_t \tag{8}$$

where, j_r: Rotor inertia (kg.m^2), T_{ls}: Low speed shaft torque (N.m), and B_r: Rotor external damping (N.m.rad^{-1}.s). The high-speed shaft torque (T_{hs}) drives the generator, while the generator electromagnetic torque brakes it (T_{em}).

$$j_g\frac{d\Omega_g}{dt} = T_{hs} - T_{em} - B_g.\Omega_g \tag{9}$$

where, Ω_g: Generator speed (rad. s^{-1}), j_g: Generator inertia (kg.m^2), T_{hs}: High speed shaft torque (N.m), T_{em}: Electromagnetic torque (N.m), and B_g: Generator external damping (N.m.rad^{-1}.s). The rotor is slowed down by the low-speed shaft torque (T_{ls}). Because of the discrepancy between (Ω_t) and (Ω_{ls}) which occurs from torsion and friction effects.

$$T_{ls} = B_{ls}\left(\theta_t - \theta_{ls}\right) + K_{ls}\left(\Omega_t - \Omega_{ls}\right) \tag{10}$$

where, B_{ls}: Low speed shaft stiffness (N.m.rad^{-1}.s), K_{ls}: Low speed shaft damping (N.m.rad^{-1}.s), θ_t: Rotor turbine position, and θ_{ls}: Low speed position. By applying the Laplace transformation, is obtained:

$$\Omega_t = \frac{1}{j_r S + B_r}\left(T_{aer} - T_{ls}\right) \tag{11}$$

$$\Omega_g = \frac{1}{j_g S + B_g}\left(T_{hs} - T_{em}\right) \tag{12}$$

Using an ideal gearbox and transmission ratio, the following equations may be derived (G).

$$G = \frac{T_{ls}}{T_{hs}} = \frac{\Omega_g}{\Omega_{ls}} = \frac{\theta_g}{\theta_{ls}} \tag{13}$$

It is possible to represent the turbine as a single mass by using equations (10) and (13) with a completely stiff low-speed shaft:

$$J_{tot}\frac{d\Omega_t}{dt} = T_{aer} - T_{tot} - B_{tot}.\Omega_t \tag{14}$$

with

$$\begin{cases} J_{tot} = j_r + G^2.j_g \\ B_{tot} = B_r + G^2.B_g \\ T_{tot} = G.T_{em} \end{cases} \tag{15}$$

where: T_{tot}: Generator torque in the rotor side (N.m), J_{tot}: Turbine total inertia (kg.m^2), G: Gearbox ratio, B_{tot}: Turbine total external damping (N.m.rad^{-1}.s). The total inertia, friction coefficient, and torque of the generator returned to the slow shaft are represented by the parameters (Jtot), (Btot), and (Ttot). The generator's inertia is frequently disregarded in favor of the rotor. The last equations allow the block diagram of the turbine model Figure 3 to be created.
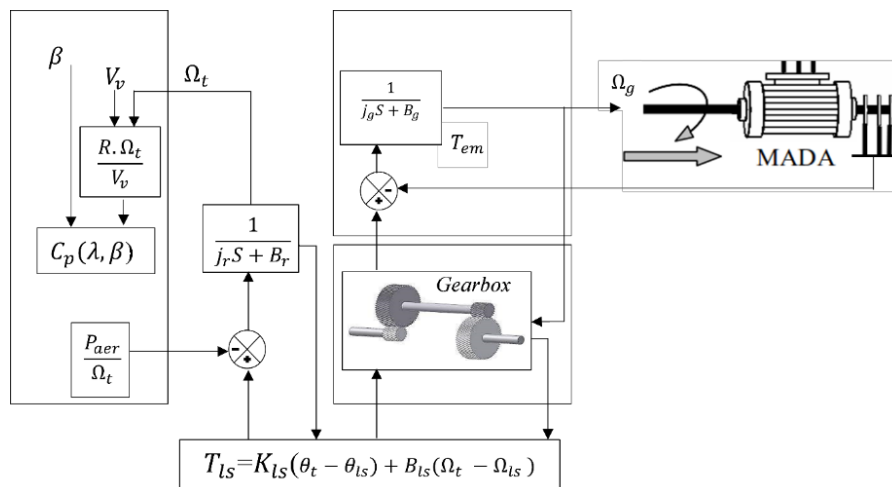
Figure 3. The aerodynamic model's block diagram

This study employs two different techniques. The turbine has developed its pitch control mechanism and MPPT technique. Figure 4 illustrates the use of various controllers to evaluate their contribution to the wind energy conversion system (WECS) [16].
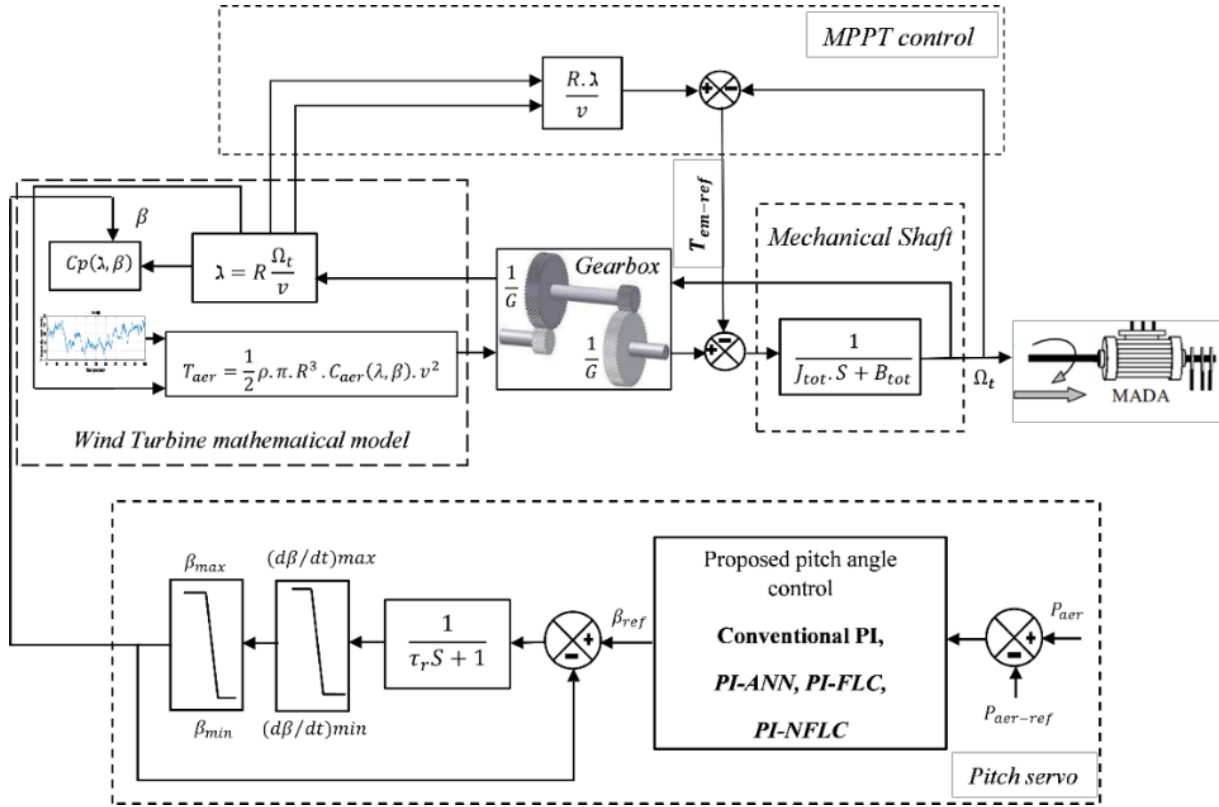
Figure 4. Diagram of a variable pitch control based DFIG

3.1. MPPT Control

To achieve better results, the system must utilize the MPPT approach while operating at variable wind speeds. In this study, a control strategy called tip speed ratio (TSR) control, based on the PI controller, is employed. When the TSR is set to its optimal value and the wind speed is measured at that point, the rotor's optimal speed can be expressed as [17]:

$$\Omega_{t-opt} = \frac{v.\lambda_{opt}}{R} \tag{16}$$

The regulator uses rapid dynamic speed adjustments to generate electromagnetic torque, ensuring a steady-state reference value for the rotor's constant speed:

$$P_{aer\_ref} = \frac{1}{2\lambda_{opt}^3} C_{p\_max} \rho \pi R^5 \Omega_t^3 \tag{17}$$

3.2. Pitch Control

The variable pitch system consists of a controller and an actuator. The actuator, which is a nonlinear system, provides servo control for the blade's rotation. The output signal of the height controller can be considered as a dynamic system with both an amplitude and a saturation point.

The goal is to ensure that the rotor captures the maximum amount of wind at all times. The blades can adjust their pitch angle to align with the wind direction. The explanatory diagram for pitch angle regulation in wind energy conversion systems is shown in Figure 5, as follows [18]:

In Zone 02, the blade angle is fixed, the rotor speed remains steady, and the specific speed is at its optimal value. In Zone 03, it is crucial to control the blade angle to prevent damage to the structure. This zone begins at a maximum speed supported by the generator, which is more than 30% above the synchronization speed. The variation of the blade angle controls the aerodynamic torque, which remains constant as the wind turbine produces power. The following is a description of its dynamic behavior [19]:

$$\frac{d\beta}{dt} = \frac{1}{\tau_r}\beta + \frac{1}{\tau_r}\beta_{ref} \qquad (18)$$

where β, βref are respectively the actual and given pitch angles, τ_r is the actuator time constant. Normally, beta ε (0°; 90°), The rate of change of pitch angle is within -10°/s; +10°/s.
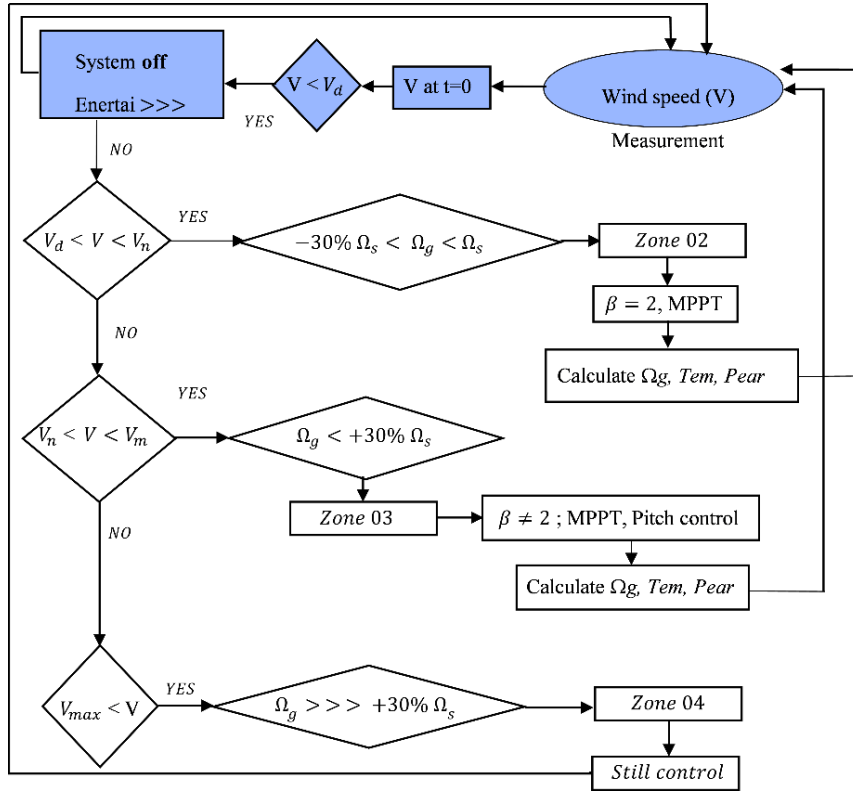
Figure 5. Operating diagram of a wind turbine generator

3. CONTROLLER DESIGN

3.1. Proportional-Integral Controller

Because of its straightforward design, the PI controller is the type of controller that finds the most use in industrial settings. It causes the angle of the blades to change based on how fast the rotor is moving, which is an error in pitch control [20]. In the Laplace domain, the conventional PI control is defined as:

$$\Delta\beta(S) = K_p \Delta\Omega_t(S) + K_i \frac{1}{S}\Delta\Omega_t(S) \qquad (19)$$

Eq. (19) may also be stated in the s-domain to provide the result shown below:

$$\Delta\Omega_t(S)[S - A] = B\Delta\beta(S) + D\Delta v_w(S) \qquad (20)$$

The closed-loop transfer function T(s) is found by substituting Eq. (19) with Eq. (20):

$$T(S) = \frac{\Delta\Omega_t(S)}{\Delta v_w(S)} = \frac{D_S}{S^2 + \left(-A - BK_p\right)S + \left(-BK_i\right)} \qquad (21)$$

The stability condition is the first factor to consider while choosing PI gains. For a stable closed-loop system, the denominator roots should be negative or the polynomial coefficients should be positive: (-A-BKp > 0) and (-BKi > 0). Finding the right controller gains is done by comparing the denominator to the standard form, which is written as:

$$S^2 + 2\xi\omega_n S + \omega_n^2 \tag{22}$$

Where ξ is the damping ratio and ω_n is the undamped natural frequency. Thus, K_i and K_p are given by:

$$\begin{cases} K_i = -\dfrac{\omega_n^2}{B} \\ K_p = -\dfrac{A}{B} - \dfrac{2\xi\omega_n}{B} \end{cases} \tag{23}$$

There is a link between B and the angle of the blades and the partial derivative of the turbine torque. the angle of the torque curve changes considerably from one equilibrium point to the next. Because of this, choosing this equilibrium point as the operating point is a challenging task that must be performed in order to get good results.

3.2. Artificial Neural Network Controller

A multi-layer perceptron-type (MLP) non-recurrent network model is chosen for identification and control. Different techniques can be used with one or more hidden layers, in which each neuron in one layer is connected to those in the next layer. The neurons in the various hidden levels have sigmoid, tangential, or logarithmic activation functions. At the same time, those of the output layer are linear. Due to the internal feedback loop, the RNN is robust to various environmental conditions and wind torque perturbations, allowing it to perform nonlinear dynamic mapping. Furthermore, the RNN outperforms other frequently used NNs in terms of speed and efficiency, making it ideal for real-time control and identification applications [21]. As illustrated in Figure 6, The RNN the type MLP has two inputs in the input layer, twenty-five neurons in the first hidden layer, ten neurons in the second hidden layer with "logsig" function in both layers. One output neuron in the output layer with "pureline" function, is employed to approximate the dynamics of the generator.
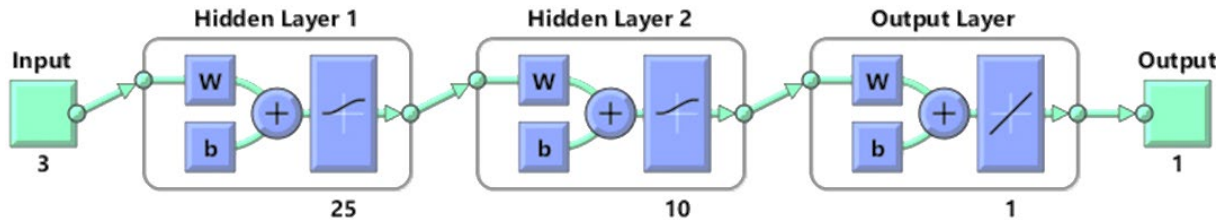
Figure 6. RNN topology

The activation function is a LogSig:

$$f(x) = \frac{1}{1 + e^{-x}} \tag{24}$$

Neuron output identification:

$$O_j = f\left(\sum_{i=1}^{N} x_j . \omega_{ij} + \omega_{bj}\right) \tag{25}$$

Update of synaptic weights:

$$\omega_{ij}(n+1) = \omega_{ij}(n) + \mu.e.f'\left(\sum_{i=1}^{N} x_j.\omega_{ij} + \omega_{bj}\right)x_j \tag{26}$$

Bias update:

$$\omega_{ij}(n+1) = \omega_{ij}(n) + \mu.e.f'\left(\sum_{i=1}^{N=2} x_j.\omega_{ij} + \omega_{bj}\right)x_j \tag{27}$$

By increasing the number of interconnecting weights and neurons in the hidden layer, the RNN approximation's accuracy may be greatly improved. By choosing proper connection weights and a reasonably high number of

neurons in the hidden layer, the approximation error may be greatly decreased to arbitrarily small over a compact set.

The appropriate model of two input and one-output Neuron PI controller is created according to the aforementioned configuration, as illustrated in Figure 7.
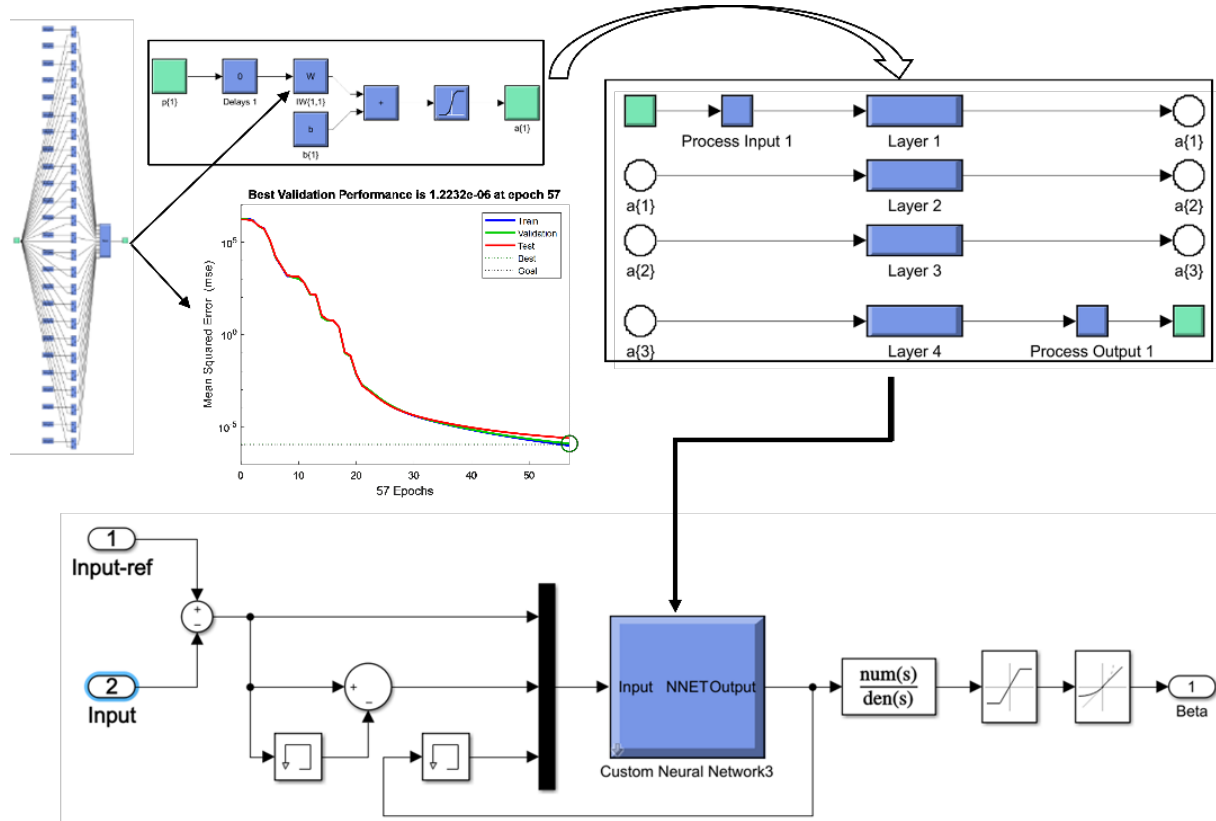
Figure 7. Variable pitch mechanism is controlled using a PI-ANN model

4. RESULTS AND DISCUSSION

The proposed artificial intelligence controller is used to regulate the variation of the pitch angle. A two-mass turbine model was developed and simulated in the Matlab/Simulink environment. This was done to demonstrate its ability to effectively control mechanical speed to extract maximum power using the "MPPT" technique and mitigate the effects of strong wind disturbances using the "Pitch" technique. The characteristics of a 2 MW three-bladed wind turbine model, as presented in the table below, are used in this study [22].

Table 1. Simulation parameters

Parameters of Turbine	Units	Ratings
Nominal turbine power rating P_n	(MW)	2.5
Rated wind speed V	(m/s)	12
Cut in speed	(m/s)	03
Cut out speed	(m/s)	25
The radius of the blades R	(m)	40
Multiplier gain G		95
Turbine inertia j	(kg.m^2)	6.3 10^6
Damping coefficient ξ		0.707
Air Density ρ	(kg/m^3)	1.225
Friction coefficient f_v		10^{-3}
K_p		$-A/B - 2\xi\omega_n/B$
K_i		$K_i = -\omega_n^2/B$

The wind speed selected using the Nichita model, as shown in Figure 8, has an average value of 11 m/s, with minimum and maximum values of 9.5 m/s and 13 m/s, respectively. This approach was adopted to ensure that the selected wind speed remains consistently around the nominal speed throughout the entire simulation period [13].
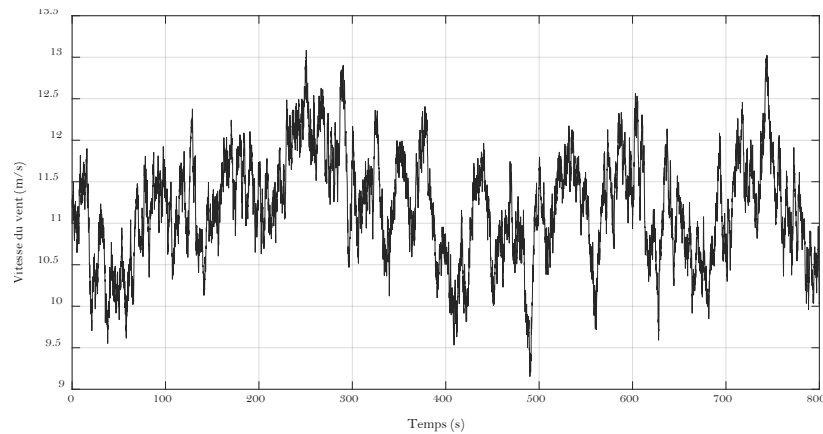
Figure 8. Wind speed rang

To demonstrate the effectiveness of the techniques used (MPPT, Pitch) based on artificial regulation, various mechanical parameters were extracted, such as the pitch angle, generator rotor speed, relative speed, electromagnetic torque, and turbine power.

Performance analysis of generator speed with MPPT and pitch technique: The unpredictable evolution of wind speed necessitated the implementation of generator speed control to maintain it at the maximum value supported by the machine. We implemented a blade orientation mechanism (Pitch) while extracting the maximum power using the MPPT technique within the nominal operating range, as shown in Figures 9 and 10.
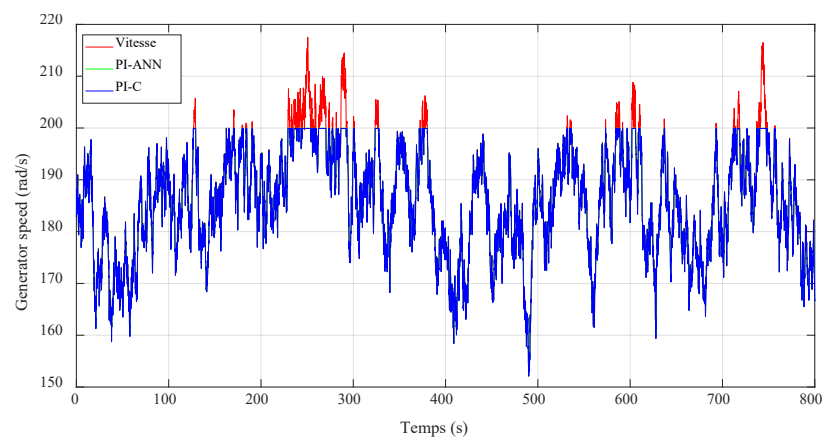
Figure 9. Generator speed controlled by "MPPT and pitch" mechanisms
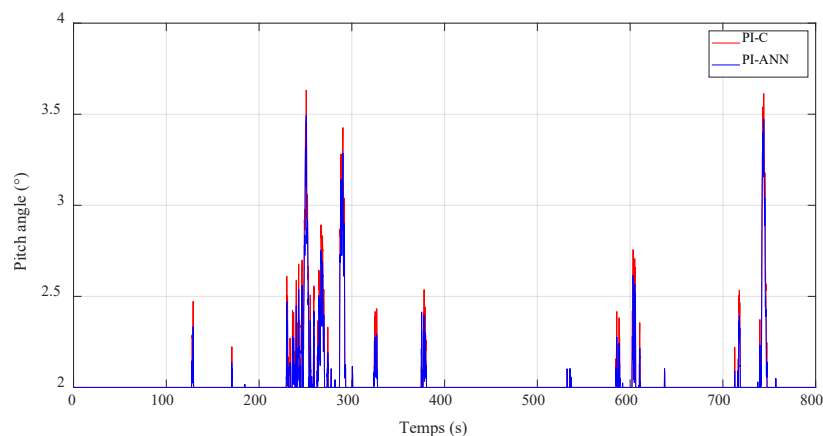
Figure 10. Pitch angle variation

The generator used in this type of wind turbine is called a DFIG, which provides a wider speed variation range, from 1200 rpm up to a maximum value of 1900 rpm (200 rad/s), with a synchronization speed of 1500 rpm (157 rad/s).

The blade orientation mechanism in Figure 1 shows its objective when the wind exceeds the maximum supported wind speed (12 m/s) for a pitch angle of 2°. On the other hand, this variation occurs over different time periods, ranging from 120 s to 750 s, as shown in Figure 10. The peaks of the variations reach a maximum value of 3.6°. Furthermore, the benefits of the MPPT technique, with mechanical speed control, are evident, as it adjusts proportionally with the variation in wind speed.

We will deepen our results by studying the tracking error between the wind profile and the different control laws to demonstrate the regulation performance as presented in the following table.

Table 2. Steady state analysis

Regulators	Mean Absolut Error	Mean Relative Error (%)
Conventional regulation (PI-C)	0.495	0.243
Neuronal regulation (PI-ANN)	0.455	0.222

The integration of artificial intelligence in the blade regulation has a notable influence on the tracking of the setpoint using the MPPT technique, as demonstrated by two indices: The MAE and the mean relative absolute error (MRAE). The maximum error value is given by the conventional controller (0.243%). The neural controller shows a noticeable improvement with an error of (0.222%), as shown in the figure above. This improvement helps extract even more energy from the wind and enhances the system's efficiency.
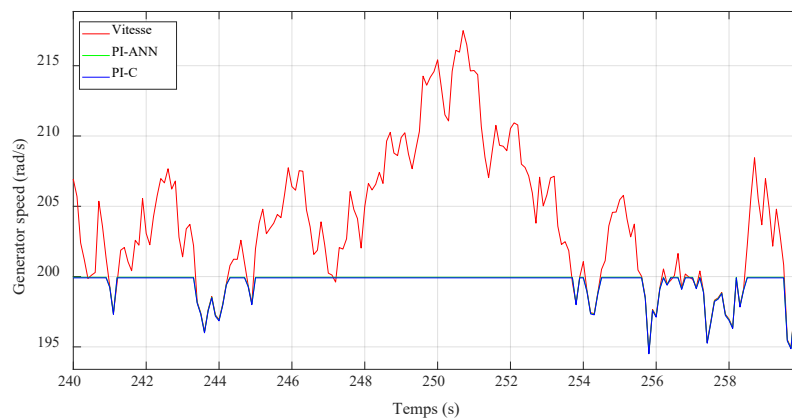
Figure 11. The enhancement of setpoint tracking by MPPT in the generator speed

The influence of artificial intelligence helps the blade orientation mechanism improve their stability while minimizing sensitivity to wind variations. The peak opening and closing of the blade angle in response to violent wind fluctuations were lower compared to other controllers, which allows the angle (beta=2) to approach and extract the maximum power. The variation in the pitch angle is shown in the figure above.
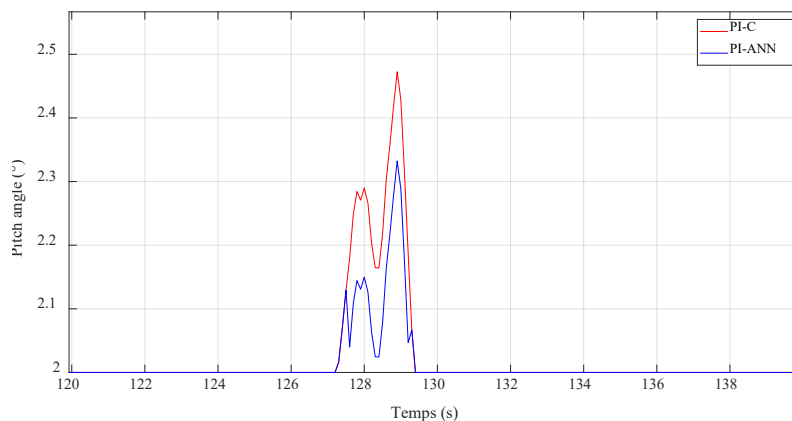
Figure 12. The enhancement of setpoint tracking by pitch

Performance analysis of artificial intelligence on other parameters: We estimate the analysis in this section of some interesting parameters such as the relative speed (λ) and the mechanical power of the system.

The performance of the relative speed presented in Figure 13 is proportional to the variation in the turbine speed. Their stability around the setpoint proves the effectiveness of the optimal exploitation of wind energy by the turbine blades. The importance of this requires analysis to understand the influence of integrating artificial intelligence in the blade control.
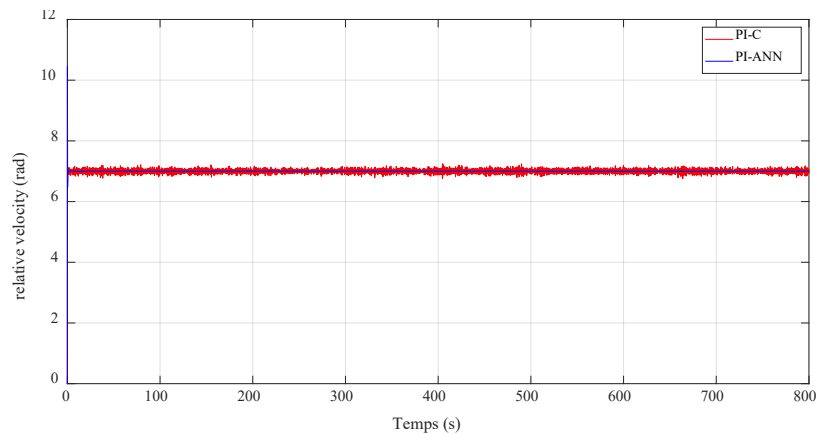
Figure 13. Relative speed

The performance of the latter is analyzed using different regulation criteria such as response time, stability, and overshoot, which are presented in the table below:

Table 3. Performance of the relative speed

Stability Conditions	Transient Study	MAE	MRE (%)
Stability (Steady state)	Conventional regulator	0.05	0.707
	Neuronal regulator	0.004	0.051

The integration of artificial intelligence has proven its notable influence on the relative speed, with a very short damped transient regime and an insignificant overshoot, as well as stability around the setpoint. The setpoint tracking is evaluated by different indices, which are MAE and MRE. Unfortunately, the conventional controller gives a small percentage (0.7%) compared to the artificial regulation. The neural controller reduces sensitivity to wind variation with better stability (0.051%), demonstrating its predictive capability, as shown in the Figure 14. This allows us to say that the conventional controller is fragile in the face of disturbing wind variations, while artificial regulation proves stability under undesirable conditions.
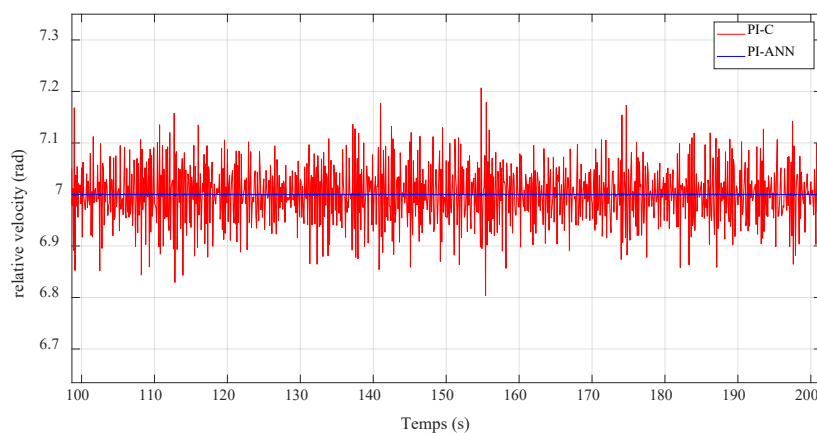
Figure 14. The enhancement of the relative speed

Finally, the performance of the controllers used for setpoint tracking and robustness against wind variations is projected onto the relative speed regulation presented in Figure 14, and the extracted power is presented in Figure

15. The ANN controller provides good setpoint tracking, leading to effective extraction of the available energy in the wind, followed by the conventional controller.
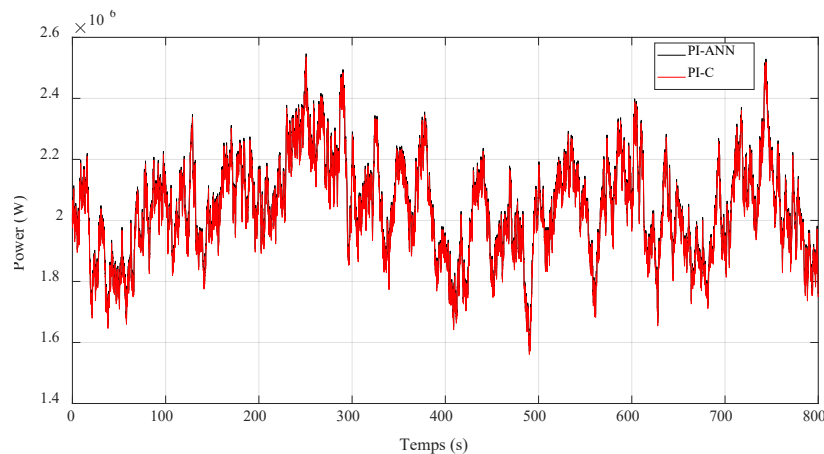
Figure 15. Power rate evolution

5. CONCLUSION

This paper deals with the design of a pitch angle controller based on an adaptive artificial intelligence control, aiming at enhancing the power quality and reducing the mechanical loads when the wind system operates at the above rated wind speeds. The necessary results are summarized as follows:

- Firstly, two of the aforementioned controller responses (PI-C, PI-ANN) were evaluated in terms of robustness and precision, utilizing a variable wind speed and turbulent wind speed profile. This last was selected using Nichita's model, and has a value of 11 m/s on average, with minimum and maximum values of 9 and 13.5 m/s, respectively.
- The MAE, MRE, the two performance indices used in the study to judge the principal parameters that are analyzed of the WTs under wind speed fluctuations, as well as generator rotor speed, relative speed and aerodynamic torque.
- The pitch activity of the conventional controller (PI-C) is still acceptable, and the pitch angle actuator is requested at a lower level than the neuronal network controller (PI-ANN).
- The aerodynamic torque oscillations are analyzed by the performance indices, which are summarized in Table 2. Neuronal control (PI-ANN) provides the best results since it has fewer oscillations and dispersion of variability around the average than another controller. As a result, the suggested controller can reduce the mechanical stresses imposed on the turbine and gearbox.
- The results indicate that the proposed controller (PI-ANN) can both achieve an accurate regulation of the generator speed and electrical power and give the best mitigation of the mechanical load effects compared with the other controllers. The tests reveal that conventional controllers give almost the same results and can be adopted as the second choice.

References

[1]   M. N. Uddin and H. Wen, "Development of a self-tuned neuro-fuzzy controller for induction motor drives," *IEEE Trans. Ind. Appl.*, vol. 43, no. 4, pp. 1108–1116, 2007, doi: 10.1109/TIA.2007.900472.

[2]   W. Siddique *et al.*, "Evaluation of thermal performance factor for solar air heaters with artificially roughened channels," *Arch. Mech. Eng.*, vol. 68, no. 2, pp. 195–225, 2021, doi: 10.24425/ame.2021.137048.

[3]   N. Ozturk, A. Dalcali, E. Celik, and S. Sakar, "Cogging torque reduction by optimal design of PM synchronous generator for wind turbines," *Int. J. Hydrogen Energy*, vol. 42, no. 28, pp. 17593–17600, 2017, doi: 10.1016/j.ijhydene.2017.02.093.

[4]   E. Chavero-Navarrete, M. Trejo-Perea, J. C. Jáuregui-Correa, R. V. Carrillo-Serrano, and J. G. Ríos-Moreno, "Expert control systems for maximum power point tracking in a wind turbine with PMSG: State of the art," *Appl. Sci.*, vol. 9, no. 12, 2019, doi: 10.3390/app9122469.

[5]   P. Venkaiah and B. K. Sarkar, "Hydraulically actuated horizontal axis wind turbine pitch control by model free adaptive controller," *Renew. Energy*, vol. 147, pp. 55–68, 2020, doi: 10.1016/j.renene.2019.08.127.

[6]   C. H. Chen, C. M. Hong, and T. C. Ou, "Hybrid fuzzy control of wind turbine generator by pitch control

using RNN," *Int. J. Ambient Energy*, vol. 33, no. 2, pp. 56–64, 2012, doi: 10.1080/01430750.2011.630754.

[7]   A. Asgharnia, R. Shahnazi, and A. Jamali, "Performance and robustness of optimal fractional fuzzy PID controllers for pitch control of a wind turbine using chaotic optimization algorithms," *ISA Trans.*, vol. 79, pp. 27–44, 2018, doi: 10.1016/j.isatra.2018.04.016.

[8]   T. Aized, S. Muhammad, S. Rehman, and S. Kamran, "Design and analysis of wind pump for wind conditions in Pakistan," vol. 11, no. 9, pp. 1–18, 2019, doi: 10.1177/1687814019880405.

[9]   A. El Bakri and I. Boumhidi, "Fuzzy model-based faults diagnosis of the wind turbine benchmark," *Procedia Comput. Sci.*, vol. 127, pp. 464–470, 2018, doi: 10.1016/j.procs.2018.01.144.

[10]   R. F. Nayeh, H. Moradi, and G. Vossoughi, "Multivariable robust control of a horizontal wind turbine under various operating modes and uncertainties: A comparison on sliding mode and H$_\infty$ control," *Int. J. Electr. Power Energy Syst.*, vol. 115, 2018, art. no. 105474, 2020, doi: 10.1016/j.ijepes.2019.105474.

[11]   S. Prasad, S. Purwar, and N. Kishor, "Non-linear sliding mode control for frequency regulation with variable-speed wind turbine systems," *Int. J. Electr. Power Energy Syst.*, vol. 107, pp. 19–33, 2019, doi: 10.1016/j.ijepes.2018.11.005.

[12]   X. Sun, J. Cao, G. Lei, Y. Guo, and J. Zhu, "Speed sensorless control for permanent magnet synchronous motors based on finite position set," *IEEE Transactions on Industrial Electronics*, vol. 67, no. 7, pp. 6089–6100, 2020.

[13]   S. Tang, D. Tian, J. Fang, F. Liu, and C. Zhou, "Individual pitch controller characteristics analysis and optimization under aerodynamic imbalanced loads of wind turbines," *Energy Reports*, vol. 7, pp. 6489–6500, 2021, doi: 10.1016/j.egyr.2021.09.114.

[14]   X. Yuan and Y. Li, "Control of variable pitch and variable speed direct-drive wind turbines in weak grid systems with active power balance," *IET Renewable Power Generation*, vol. 8, no. 2, pp. 119–131, 2014, doi: 10.1049/iet-rpg.2012.0212.

[15]   J. E. Sierra-Garcia, M. Santos, and R. Pandit, "Engineering applications of artificial intelligence wind turbine pitch reinforcement learning control improved by PID regulator and learning observer," *Eng. Appl. Artif. Intell.*, vol. 111, art. no. 104769, 2022, doi: 10.1016/j.engappai.2022.104769.

[16]   A. Mezache and F. Soltani, "A novel threshold optimization of ML-CFAR detector in Weibull clutter using fuzzy-neural networks," vol. 87, pp. 2100–2110, 2007, doi: 10.1016/j.sigpro.2007.02.007.

[17]   J. Vinod and B. K. Sarkar, "Francis turbine electrohydraulic inlet guide vane control by artificial neural network 2 degree-of-freedom PID controller with actuator fault," *Proceedings of the Institution of Mechanical Engineers, Part I: Journal of Systems and Control Engineering*, vol. 238, no. 8, 2020, doi: 10.1177/0959651820973797.

[18]   H. Erol, "Sustainable Energy, grids and networks stability analysis of pitch angle control of large wind turbines with fractional order PID controller," *Sustain. Energy, Grids Networks*, vol. 26, art. no. 100430, 2021, doi: 10.1016/j.segan.2021.100430.

[19]   A. B. Moreira, T. A. S. Barros, V. S. C. Teixeira, and E. Ruppert, "Power control for wind power generation and current harmonic fi ltering with doubly fed induction generator," *Renew. Energy*, vol. 107, pp. 181–193, 2017, doi: 10.1016/j.renene.2017.01.059.

[20]   A. Thakallapelli, S. Ghosh, S. Kamalasadan, and P. D. E. Engineering, "Sensorless real-time reduced order model-based adaptive maximum power tracking pitch controller for grid connected wind turbines," *Electr. Power Syst. Res.*, vol. 194, art. no. 107115, 2021, doi: 10.1016/j.epsr.2021.107115.

[21]   X. Yin, Z. Jiang, and L. Pan, "Recurrent neural network based adaptive integral sliding mode power maximization control for wind power systems," *Renew. Energy*, vol. 145, pp. 1149–1157, 2020, doi: 10.1016/j.renene.2018.12.098.

[22]   F. Bounifli, A. E. L. Moudden, A. Wahabi, and A. Hmidat, "Vector control of a doubly-fed induction generator by using a classical PI and a fuzzy PI controllers," *World Journal of Innovative Research*, vol. 1, no. 2, pp. 18–24, 2016.

Optimization of Drilling Performance in Natural Fiber Composites Using Taguchi and Desirability Function Methods

Mustapha Arslane[1], Mohamed Slamani[1], Abdelmalek Elhadi[1], Salah Amroune[1]

[1]Laboratory of Materials and Mechanics of Structures (LMMS), Faculty of technology, University of M'sila, University Pole, Road Bourdj Bou Arreiridj, 28000 M'sila, Algeria
Corresponding author: Mustapha Arslane (e-mail: mustapha.arslane@univ-msila.dz)

Abstract

Drilling natural fiber-reinforced composites presents unique challenges due to their heterogeneous structure, leading to issues such as delamination, poor hole quality, and material damage. This study focuses on optimizing drilling parameters_ spindle speed, feed rate, and drill type_ to improve key metrics like delamination, circularity, and cylindricity in hybrid jute/palm fiber-polyester composites. Employing the Taguchi method and Desirability Function Analysis (DFA), the investigation utilizes a 25-run orthogonal array to identify the optimal settings for each drill type. Analysis of variance (ANOVA) highlights feed rate as the dominant factor affecting hole quality, with spindle speed playing a secondary role. The optimized parameters significantly enhance drilling performance, particularly with solid carbide drills, which outperform others in maintaining precision and minimizing defects. This comprehensive multi-response optimization offers a pathway to improving the machining of natural composites for various industrial applications.

Keywords: Drilling optimization, Natural fiber composites, Taguchi method, Desirability function analysis, Delamination, Hole quality

Efficient Drilling Path Optimization in CNC Machining Using Genetic Algorithms and TSP Methodology

Mustapha Arslane[1], Mohamed Slamani[1], Abdelmalek Elhadi[1], Salah Amroune[1]

[1]Laboratory of Materials and Mechanics of Structures (LMMS), Faculty of technology, University of M'sila, University Pole, Road Bourdj Bou Arreiridj, 28000 M'sila, Algeria
Corresponding author: Mustapha Arslane (e-mail: mustapha.arslane@univ-msila.dz)

Abstract

Optimizing drilling paths in CNC machining is critical to reducing production time and improving operational efficiency. This research integrates the Traveling Salesman Problem (TSP) framework with a Genetic Algorithm (GA) to minimize both the travel distance and machining time in drilling operations. By considering the varying machining times at different drilling points and the distances between them, this study presents an approach that identifies near-optimal drilling sequences. The proposed solution led to a 20% reduction in total machining time, demonstrating the effectiveness of advanced computational techniques in complex manufacturing environments. These findings contribute to ongoing improvements in manufacturing efficiency and precision.

Keywords: CNC machining, Drilling path optimization, Genetic algorithm, Traveling salesman problem, Machining time reduction, Manufacturing efficiency

Parametric Study of a Domestic Solar Water Heating System for Hot Water Supply

Ahmed Remlaoui[1], Driss Nehari[1]

[1]Applied Hydrology and Environment Laboratory, University of Ain Temouchent, 46000 Ain-Temouchent, Algeria

Corresponding author: Ahmed Remlaoui (e-mail: ahmed.remlaoui@univ-temouchent.edu.dz)

Abstract

This paper presents a parametric study of a domestic solar water heating system (SDHW) aimed at fulfilling household hot water needs. The system's performance is analyzed using the Solar Advisor Model (SAM) under various climatic conditions in Ain Temouchent. The study examines five key parameters: the collector area, storage tank volume, and outlet water temperature. The analysis shows that the highest energy production occurs in July, reaching 210 kWh, with a solar fraction of 0.65. Auxiliary heat demand ranged from 16 kWh to 153 kWh, while delivered heat varied between 145 kWh and 242 kWh. Several scenarios were tested, with solar fractions ranging from 0.60 to 0.65. Results indicate that increasing the collector area boosts the solar fraction, while larger tank volumes and higher outlet water temperatures tend to lower it. The study emphasizes the importance of optimizing these parameters for improved system efficiency.

Keywords: SDHW, SAM, Climatic conditions, Energy production, Solar fraction, System efficiency

Study and Analysis of the Efficiency of a Photovoltaic Panel Using Phase Change Material

Taieb Nehari[1], Mohamed Serier[2], Zahra Assala Zehouani[1], Mohammed Hadjadj[1], Ahmed Remlaoui[2]

[1]Structure Intelligent laboratory, University of Ain Temouchent-Belhadj Bouchaib, 46000 Ain-Temouchent, Algeria
[2]Applied Hydrology and Environment Laboratory, University of Ain Temouchent-Belhadj Bouchaib, Ain-46000 Temouchent, Algeria
Corresponding author: Taieb Nehari (e-mail: taieb.nehari@univ-temouchent.edu.dz)

Abstract

The growing global demand for sustainable energy solutions has increased interest in photovoltaic (PV) technology. However, the efficiency of photovoltaic panels decreases significantly with rising temperatures, posing a critical challenge in optimizing their performance. This stady studies an innovative cooling strategy for photovoltaic panels using phase change materials (MCP). The study focuses on the performance of a single MCP which is the RT-25, evaluating its effectiveness in maintaining optimal temperatures of photovoltaic panels. In addition, the impact of fins on thermal regulation efficiency is explored by integrating fins into the MCP-based cooling system. This research contributes to the field of renewable energy by providing a viable solution to improve the performance and sustainability of photovoltaic systems, thus promoting the adoption of more efficient and sustainable energy practices.

Keywords: Phase change material, Latent heat, Thermal regulation, Photovoltaic cell

Assessing Heat Transfer Efficiency in Building Brick: The Influence of Phase Change Materials and EPS Insulation as Passive Cooling Techniques

Zahra Assala Zehouani[1], Taieb Nehari[1], Mohamed Hadjadj[1]

[1]Department of Mechanical Engineering, University of Ain Temouchent Belhadj Bouchaib, Ain Temouchent, Algeria
Corresponding author: Zahra Assala Zehouani (e-mail: assala.zehouani@univ-temouchent.edu.dz)

Abstract

Passive cooling techniques offer an eco-friendly approach to reducing energy use in buildings, standing as a viable alternative to conventional, energy-intensive cooling systems. The increasing energy demands for maintaining comfortable indoor environments and powering various devices in buildings further highlight the necessity for such energy-efficient strategies. This study used a dynamic heat transfer model to assess the effectiveness of combining two passive methods—phase change materials and EPS insulation—within clay bricks. Initially, three different PCMs were positioned at the brick's centerline, while the cavities remained air-filled. Then, EPS insulation was integrated into the cavities to evaluate the combined effect of both methods. The findings revealed that Capric acid outperformed the other PCMs. Although utilizing a single passive method provides clear benefits in improving thermal performance and energy efficiency, the combined use of PCMs and EPS insulation revealed further advantages. Specifically, incorporating Capric acid at the brick's centerline, along with EPS insulation in the cavities, resulted in a significant reduction in inner surface temperature by approximately 3.9°C and a decrease in heat flux by around 35% compared to traditional bricks. Furthermore, the combined approach delayed the peak heat flux by 2h, demonstrating its potential to improve building performance and reduce overall energy consumption.

Keywords: Phase change material, EPS insulation, Building brick, Energy consumption

Challenges of Concentrated Solar Power in MENA Region, Case Study: Algeria

Mohamed Teggar[1]

[1]LMe Laboratory, Department of Mechanical Engineering, University Amar Telidji, Laghouat, Algeria
Corresponding author: Mohamed Teggar (e-mail: m.teggar@lagh-univ.dz)

Abstract

Concentrated solar power is a key for deployment of renewable energy worldwide. The Middle East and North Africa (MENA) region can power the world due to being in the solar belt of high solar energy potential. Concentrated solar power deployment in MENA region is discussed in this study with particular focus on Algeria. Concentrated solar power deployment is not as developed as solar PV in the country though planned programs. This study aims to discuss the reasons behind this low deployment of CSP in MENA region in general and particularly in Algeria. Available data are analysed and discussions are presented to find out the main barriers against proper deployment of CSP in the region. The investigation revealed that availability of fossil fuel sources, low local cost of fuel-fired power, and excessive water consumption of CSP plants are the main challenges of CSP deployment in the country. However, exportation prospects particularly with recent initiation of a project of submarine line to export clean electricity to Europe would increase the interest in CSP in the future.

Keywords: Concentration, Deployment, Power, Solar energy

Impact of Soil-Structure Interaction on Dynamic Amplification Factor: A Seismic Response Analysis for Multi-Degree-of-Freedom Systems

Leyla Bouaricha[1]

[1]Department of Civil Engineering and Architecture, Faculty of Sciences and Technology, University of Khemis, 44225 Miliana, Algeria
Corresponding author: Leyla Bouaricha (e-mail: l.bouaricha@univ-dbkm.dz)

Abstract

The interaction between a structure, its foundation, and the underlying soil has been a subject of interest and research for many years. Analyzing the behavior of a structure such as a building, taking into account soil-structure interaction, involves evaluating the combined response of the superstructure, its foundation, and the surrounding soil under dynamic excitation, including seismic excitation. On the other hand, the dynamic amplification factor (DAF) is an important parameter in the design of structures and bridges. This factor (DAF), which is defined as the ratio of the amplitude of vibratory response to static response, is normally used to describe the dynamic effect. In this work, we examined the effect of soil-structure interaction on the calculation of the dynamic amplification factor for different structures modeled by systems with one or more degrees of freedom, taking into account the effect of damping. The results of this work show that soil-structure interaction should be considered during the seismic design of the structure, especially since studies conducted in this context have highlighted the beneficial or detrimental effect of this consideration.

Keywords: Soil-structure interaction, Degree of freedom, Loading, Earthquake, Amplification factor

Evaluation of Mechanochemical and Thermal Performance of Sisal and Flax Fiber Mat Reinforced Epoxy Based Laminated Hybrid Composites

Ravi Chitra Kishor[1], Sumit Pramanik[1]

[1]Functional and Biomaterials Engineering Laboratory, Department of Mechanical Engineering, College of Engineering and Technology, SRM Institute of Science and Technology, Kattankulathur, Chennai 603203, Tamil Nadu, India

Corresponding author: Sumit Pramanik (e-mail: sumitprs@srmist.edu.in)

Abstract

The demand for environmental friendly materials has encouraged the development of natural fiber-reinforced polymer composites. Sisal and flax fibers are familiar for their excellent strength-to-weight ratios, renewable nature and low cost, have emerged as viable reinforcements in polymer matrices. Hybrid composites, which combine two or more type fibers, use the unique features of each type fiber to improve overall performance of the hybrid composite. Sisal fibers have great tensile strength and stiffness while, the flax fibers are more impact resistant and flexible. In the present study, the mechanical and thermal properties of hybrid composites consist of sisal and flax fiber mats are reinforced with a volume fraction of 50% in the epoxy resin using hand lay-up technique followed by hot compression. Fourier transform infrared (FTIR) analysis shows a prominent peak at 3694 cm^{-1}, indicating (N–H) and O–H stretching and a peak shown at 2005 cm^{-1} which originates from C=O stretching of carboxyl groups or ester group of hemicelluloses. The elongation of the C–C–O–C bond could be seen by examining the peaks at 1313 cm^{-1}. In addition, the peak at 1095 cm^{-1} attributed to the stretching of the aliphatic ring (C-O-C). Thermogravimetric analysis (TGA) showed initial degradation at 135 °C and 235 °C, and the further showed a significant decomposition starting at $250 - 260$ °C due to hemicellulose and cellulose degradation. The composite hardness test result, 8 layers of sisal and flax fibers with epoxy have a 35.83 HRB hardness value, which is slightly higher than the other layered composites. More research needs to be done to find a better fiber matrix ratio that can improve heat and dynamic properties in future.

Keywords: Sisal fiber, Flax fiber, Hardness, FTIR, Thermogravimetric analysis, Limb

1. INTRODUCTION

Presently, worldwide worry is the increasing incidents of vascular diseases, dislocations and trauma injuries to the amputees. Prosthetic devices are the replaceable parts of those who lost their limbs. These are the most important prosthesis devices that disabled people can bring back to a normal comfortable life [1]. Human legs have a major loss in accidents and more than 20% of people miss their residual lower limb and it is very common in recent years. To function and activate the missing part, prosthetic devices were designed to rectify these processes. Lower limb prostheses are of two types. Below the hip and above the knee of the human leg part is called transfemoral. Below the hip and above the foot of the human part is called transtibial [2, 3].

In this context, natural fibers could be used in various applications and have received more scope by replacing synthetic fibers in modern technology. Low cost, lightweight, and renewability are some advantages of natural fibers over synthetic fibers. Natural fibers are used in construction, automobiles and biomedicine for their good mechanical and functional characteristics in polymer composites with excellent their biocompatibility, biodegradability and high specific strength [4–7]. In the agriculture market, globally natural fibers are available in large numbers because their food sustainability and health improvement have great significance as well as poverty removal [8].

Recently, natural fibers are mostly used in lower limb prosthetic lower limbs. The multicellular leaf fiber known as Sisal comes from the Agave plant family and it is the 6th biggest production of fiber in the world. Brazil, China, Kenya and Tanzania are the major places of sisal production; among these Brazil is its major producer. In India, more than 3000 hectares and generating 5000 quintals were produced and Odisha is the major production state [9]. A robust sisal plant produces 200-250 leaves over 10-12 years and it is harvested for 2-2.5 years after planting. From the second year to the twelfth year, growers may sell leaves. Composite materials used in vehicle components, roofing, panelling, carpets, bags, and polishing cloth could be made from sisal leaf fibre [10].

On the other hand, flax fiber comes from Linaceae plants and in India, it is produced majorly in the Himalayas, where winters and Summers in Europe. Temperature between 10 and 27 °C and with relative humidity of 30% to 95% in cloudy conditions, the plant flourishes. It is 25-50 mm long fiber, silky, flexible, glossy and pale yellow. Flax fibre is stronger, sharper, and stiffer than cotton, making it suitable for linen. Fabrics and high-quality home textiles use 70% linen. Substandard fibres fill and reinforce thermoplastic composites. Linen is a classic for bed linen, furniture, and home décor [11, 12].

The chemical, mechanical and also thermal properties of the polymer and its composites depend on their functional bonding. The C-C symmetric stretching at 1520 cm^{-1} was associated with the stretching of aromatic rings in lignin. The overall chemical qualitative information and the standard vibrational modes are well matched. The development of lignin modes in comparison with cellulose cites for the better thermal stability of the composite in a calculation to sisal fibers [13]. Flax and jute fiber mixtures with different amounts of multiwalled carbon nanotube (MWCNT) show clear patterns in the peak features from the Fourier transform infrared (FTIR) study, which suggests that the molecular structure or chemical bonds have changed. In the overall combinational work, these differences might change how the MWCNTs and fiber grid interact and how much they interact. It is important to understand these details to create and make jute and flax hybrid materials that are specifically used for things like car parts, building supplies, and medical equipment [14].

According to the thermogravimetric analysis, the composite without carbon fiber (CF) experienced a weight loss of 11.09%, while the composite with CF experienced a decrease of 7.45%. The thermal stability of the polymethyl methacrylate(PMMA)-based sisal/PMMA composites improved by the inclusion of CF was demonstrated [15]. At a temperature of 100 – 130 °C, resulting in substantial weight loss and lignin degradation, composite commences the degradation of a flax/polyester. Plain glass/polyester composites decompose at 180 – 190 °C and flax fiber/glass fiber (GF) hybrid polyester composites disintegrate rapidly. The thermal stability of the hybrid composite was greater to that of complete flax-polyester composites [16].

Among various mechanical properties, hardness is very important for thepropsthetic material since it requires for close contact with the skin and soft tissues besides structural supports. The three-layer sisal core with the implementation of carbon nanotube (CNT) sandwich composites resulted in an increase in their microhardness from 44.7 HRB to 59.6 HRB indicated by the investigation. 2% chitosan, 3% sisal layer, and 2% glass fiber were the highest from the microhardness test, while the same trend was observed in four-layer composites. However, the hardness values of the four-layer sisal fiber core sandwich composites decreased [17]. They determined microhardness within 1 to 50 µm using the Vickers hardness test apparatus with 10 s dwell duration, 100 grains indentation burden, and 50 µm/s speed. The coir-based sample exhibited superior hardness in comparison to the wood-based sample [18].

From the existed reported materials, no composites showed desired mechanical, chemical as well as thermal properties close to the skin or muscle tissue besides mechanical strength. Therefore, this present study mainly aims to identify the mechanochemical and thermal properties of hybrid composites of sisal and flax fibers with epoxy to develop a new generation biomaterials for the prosthetic limb device. The mechanical properties of the hybrid composite were evaluated through the microhardness test. Rockwell hardness, FTIR spectroscopy, and thermogravimetric analysis (TGA) were studied to evaluate the performance of the laminated hybrid composite with different types of layered materials such as sisal and flax in the epoxy matrix.

2. MATERIALS AND METHODS

2.1. Materials

Sisal and flax fibers were purchased in M/s Fiber Region Pvt Ltd., Valasravakkam, Chennai are shown in Figure 1. Epoxy Resin (LY556) and Hardener (HY951) were purchased from M/s Herenba Instruments and Engineers, Ambattur, Chennai. All the other consumables (viz., brush, mug, stirrer, and glove) were purchased from the local sources.
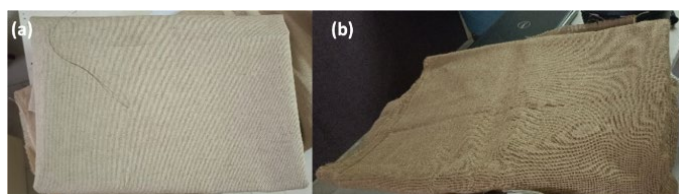
Figure 1. (a) Sisal and (b) flax fiber mat

Table 1. Properties of fibers (Information given from the supplier and verified in [19])

Material	Density (g/cm^3)	Elastic Modulus (GPa)
Sisal Fiber	1.45	22
Flax Fiber	1.45	60-80

2.2. Fabrication of Composites

To create laminates, fibers are layered between 300×300 mm steel mould plates, which were cleaned and coated with released agents. Initially, flax and sisal fiber mats are cut into 300×300 mm sizes. The epoxy and hardener were combined at a ratio of 10:1 and are shown in Figure 2. Different kinds of layers were created with the fibers of flax and sisal laminated alternatively with epoxy by 4, 8, 12, and 16 layers. The process was done by producing consistent composite laminates. Air entrapment was prevented by allowing the resin to run completely over the fiber mat for 30 min before compression. Then, the steel mould containing composite layers was kept for hot compression at 80 °C under 50 MPa for 8 hrs.
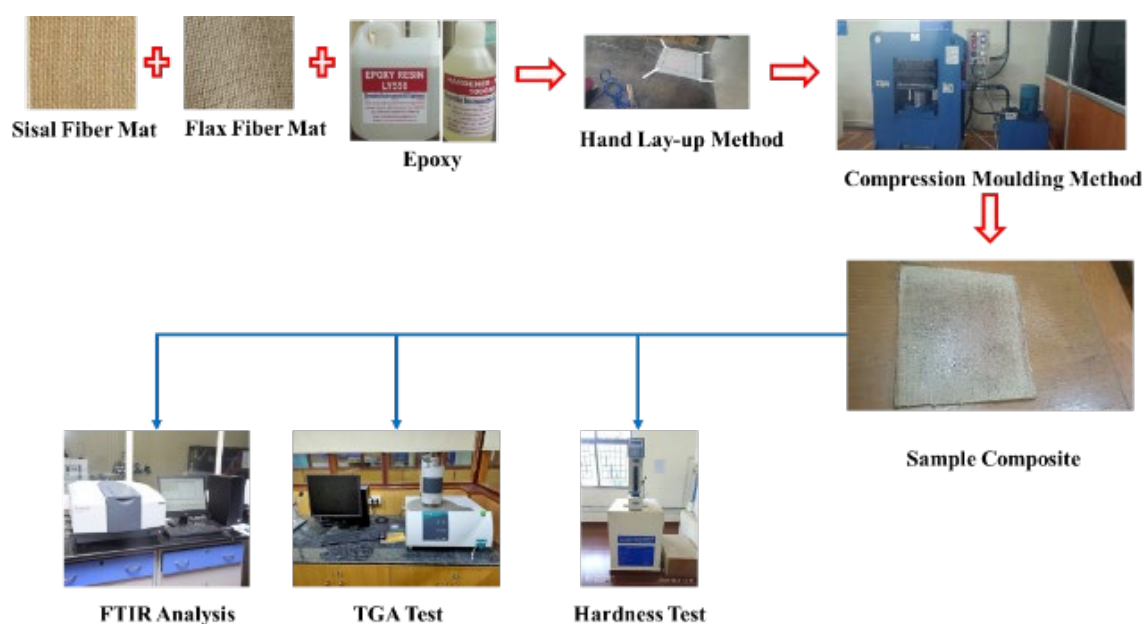
Figure 2. Sample preparation and testing

3. CHARACTERIZATIONS

3.1. FTIR Analysis

FTIR analysis, hybrid composites of sisal and flax fibers were obtained in the wave number range of 4000-400 cm^{-1} in ATR mode at a resolution of 4 cm^{-1} using a twin beam IR spectrophotometer (Shimadzu IRTracer 100, Shimadzu Corporation, Japan.) at room temperature [20]. Figure 3 shows the sample of sisal and flax fiber with epoxy composite for FTIR test.

Figure 3. Specimen for FTIR analysis

3.2. TGA

Thermal stability has been investigated by TGA curves for the hybrid composites of sisal and flax fibers using a thermogravimetry analyzer (STA 2500 Regulus, Netzsch-, Germany). Nitrogen gas atmosphere was used for the

TGA tests. 4.1 g to 9.9 g were heated at the rate of 10 °C/min up to 800 °C in this method. Measurement was carried out twice, to ensure reproducibility [21].

3.3. Rockwell Hardness Test

Since the prosthetic material must come into close contact with the skin and soft tissues in addition to providing structural support, hardness is one of the most crucial mechanical characteristics. Thus, Rockwell hardness could be more suitable compared to the other hardness method. Here to investigate the thin laminate hybrid composite materials, indentation was made at 60 kgf for 10 s dwell time with steel ball indenter of 1.5875 mm diameter using a Digital Rockwell Harness Tester (Rockwell RH-150DX, Chennai Metco, India). The indentation geometry was then, measured under optical microscope to calculate the indentation area and finally the hardness value in HRB scale. To deliver exact results, the surface of the specimen was polished finely and taken at least three identical specimens and each specimen was indented at 7 points. ASTM standard E18 (1984) method was followed for hardness test [22].

4. RESULTS AND DISCUSSION

4.1. FTIR Analysis

In FTIR spectroscopy, the samples undergoing infrared light is used to observe the chemical imprint. It identifies the composition by understanding the effects of infrared on sisal and flax natural fibers combination of lignocellulosic fibers. FTIR spectra are used to study hydrogen bonds in chemical composition, cellulose and structure of natural fibers. Lignocellulosic materials are similar to the lignocellulosic fibers chemical composition, although they change in appearance [23]. The FTIR spectra of the different layered laminated hybrid composites of sisal and flax fiber with epoxy are depicted in Figure 4.

The Figure 4 shows a prominent peak at 3694 cm^{-1}, indicating the presence of secondary amine (N–H) and O–H stretching. Another prominent peak shows at 2005 cm^{-1} which originates from C=O stretching of carboxyl groups or ester group of hemicelluloses. The elongation of the C–C–O–C bond could be seen by examining the peaks at 1313 cm^{-1}. In addition, the peak at 1095 cm^{-1} attributed to the stretching of the aliphatic ring (C-O-C). The complete chemical qualitative information matches the standard vibrational modes [24, 25]. The development of lignin modes in comparison with cellulose mentions the better thermal stability of the hybrid composites. The the presence of more large amount of secondary amine (N–H) and O–H stretching peaks along with the aliphatic ring (C-O-C) stretching peak clearly indicates the amount of excess fibers in the laminated hybrid composites.
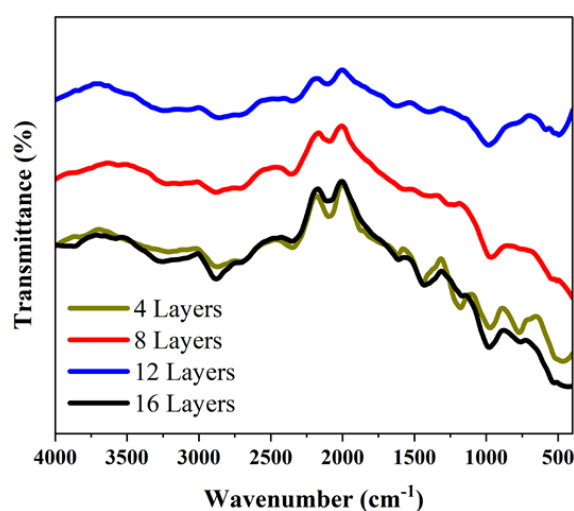
Figure 4. FTIR analysis of sisal and flax fiber with epoxy composite

4.2. Thermogravimetric Analysis

TGA was conducted to evaluate the thermal stability of sisal and flax fibers with epoxy composites. The relationship between mass loss (%) and temperature (%) of composite materials with different number of layers (4, 8, 12, and 16 layers). Figure 5 shows X-axis indicates the temperature range from room temperature to 800

°C. Y axis represents the mass loss percentage of the composite, as it decomposes or degrades when subjected to increasing temperatures.
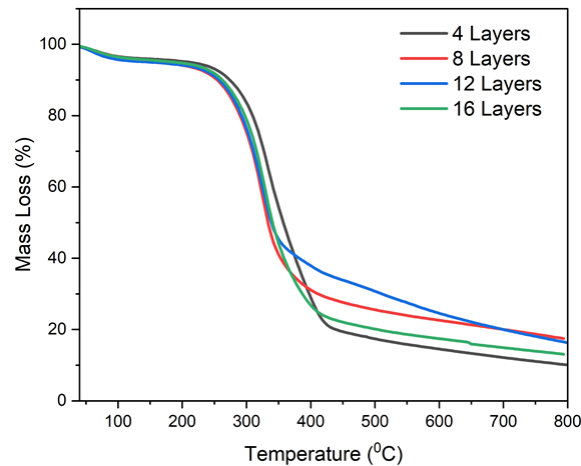
Figure 5. Thermogravimetric analysis of sisal and flax fiber with epoxy composite

Each curve corresponds to the thermal degradation behaviour material with a specific number of layers (viz., 4 layers in black, 8 layers in red, 12 layers in blue, and 16 layers in green colours). The thermal stability of sisal and flax fibers composites under nitrogen atmosphere has been conducted using a simultaneous thermal analysis instrument. The fibres were tested at different temperatures, including 135 and 235 °C, and the results showed significant decomposition starting at 250–260 °C. The sisal and flax fibers composites are thermally stable up to 135 °C, with no significant weight loss observed during isothermal heating. TGA indicates the best thermal stability of 8-layered laminated hybrid composite compared to the other composites.

4.3. Hardness Test

The hardness of a material measures its resistance to deformation under the compressive force used by a sharp item [26] as shown in Figure 6. Table 2 shows the hardness test result for the different layers of sisal and flax fibers with epoxy. A comparison of hardness values of the laminated hybrid composites with different numbers of alternate layers of sisal and flax fiber in epoxy matrix is also depicted in in Figure 7. From the results, 8 layers of sisal and flax fibers with epoxy have a 35.83 HRB hardness value, which is slightly higher than the other layered composites can be seen in Figure 7. 4 layers have a 35.51 HRB hardness value, 12 layers have a 30.88 HRB hardness value and 16 layers have a 28.93 HRB hardness value. This is because hybrid fiber composites resistance to diffusion is more due to the availability of fibers arranged alternatively. The hardness result indicates that the surface mechanical property of 8-layered laminated hybrid composites is best which corroborates our thermal stability effect.
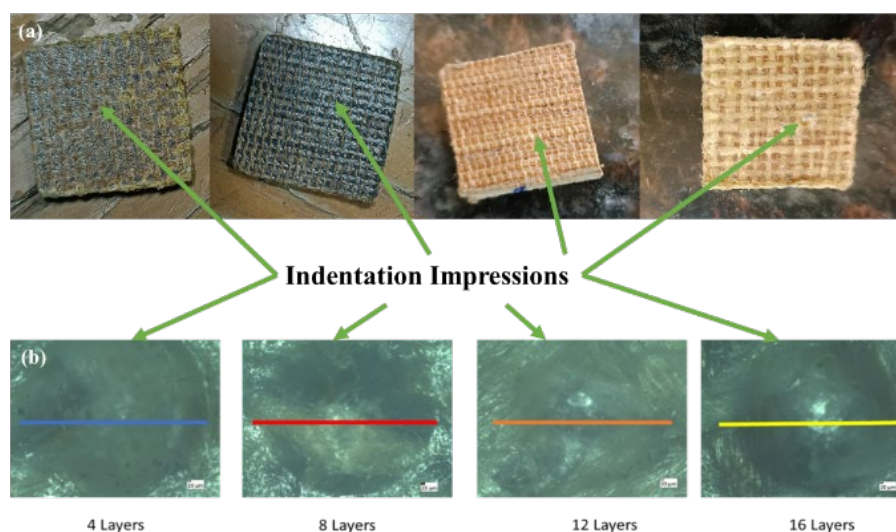
Figure 6. (a) Indentation impression during hardness test and (b) dimension length measurement after the indentation impression

Evaluation of mechanochemical and thermal performance of sisal and flax
fiber mat reinforced epoxy based laminated hybrid composites

ICMUSTED 2024

Table 2. Hardness values of sisal and flax fibers with epoxy laminated hybrid composites

Sl. No.	Composites	Average Diameter – D (mm)	Hardness (HRB)
1	4 Layers	1.77	35.51
2	8 Layers	1.762	35.83
3	12 Layers	1.898	30.88
4	16 Layers	1.961	28.93
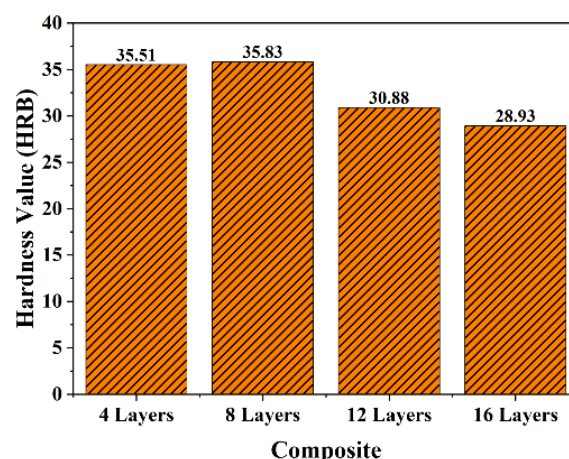
Figure 7. Comparison of hardness values of the laminated hybrid composites with different numbers of alternate layers of sisal and flax fiber in epoxy matrix

5. CONCLUSIONS

Sisal and flax fiber mats with epoxy hybrid composites have good mechanical, thermal and chemical bonding qualities. FTIR identifies that the fibers and matrix have better load transfer by strong chemical reactions and keep structure truthfulness. The thermogravimetric analysis results show that the material was impartially constant at high temperatures. The initial degradation at 135 and 235 °C, the results showed significant decomposition starting at 250–260 °C due to hemicellulose and cellulose degradation. 8 layers of sisal and flax fibers with epoxy have a 35.83 HRB, the material is best for uses where the mild strength and stiffness are needed. These results show that the laminated hybrid composite consisting alternate layer of sisal and flax fiber with epoxy-reinforced composites could be used environmentally friendly option in the medical as well as structural industries. In future, further research will be done to obtain the other thermomechanical, physical, degradation and biocompatible properties.

References

[1]   S. Kumar, S. Bhowmik, and V. K. Mahakur, "Thermo-mechanical and degradation properties of naturally derived biocomposites for prosthesis applications: Analysis of the interface pressure and stress distribution on the developed socket," *Proceedings of the Institution of Mechanical Engineers, Part E: Journal of Process Mechanical Engineering*, vol. 237, no. 5, pp. 1999–2015, 2023.

[2]   M. Asif, M. I. Tiwana, U. S. Khan, W. S. Qureshi, J. Iqbal, N. Rashid, and N. Naseer, "Advancements, trends and future prospects of lower limb prosthesis," *IEEE Access*, vol. 9, pp. 85956–85977, 2021.

[3]   O. S. Yarmoshevych, N. E. Nesterchuk, I. O. Mykhailova, O. V. Semenchuk, E. A. Dovnich, and O. Y. Sierkov, "Current trends in the rehabilitation of patients with lower limb amputation," *Art of Medicine*, vol. 3, no. 31, pp. 275–280, 2024.

[4]   C. S. Malalli and B. Ramji, "A comprehensive study on biomaterials and their application in prosthesis," *Journal of Jilin University*, vol. 41, no. 11, pp. 1195–212, 2022.

[5]   S. S. Todkar and S. A. Patil, "Review on mechanical properties evaluation of pineapple leaf fiber (PALF) reinforced polymer composites," *Composites Part B: Engineering*, vol. 174, art. no. 106927, 2019.

[6]   J. K. Odusote and A. Oyewo, "Mechanical properties of pineapple leaf fiber reinforced polymer composites for application as a prosthetic socket," *Journal of Engineering Technology,* vol. 7, no. 1, pp. 125–139, 2016.

[7]   A. I. Campbell, S. Sexton, C. J. Schaschke, H. Kinsman, B. McLaughlin, and M. Boyle, "Prosthetic limb sockets from plant-based composite materials," *Prosthetics and Orthotics International*, vol. 36, no. 2, pp. 181–189, 2012.

[8]   H. Takagi, "Review of functional properties of natural fiber-reinforced polymer composites: thermal insulation, biodegradation and vibration damping properties," *Advanced Composite Materials*, vol. 28, no. 5, pp. 525–543, 2019.

[9]   D. Lilargem Rocha, L. U. D. Tambara Júnior, M. T. Marvila, E. C. Pereira, D. Souza, and A. R. G. de Azevedo, "A review of the use of natural fibers in cement composites: concepts, applications and Brazilian history," *Polymers*, vol. 4, no. 10, art. no. 2043, 2022.

[10]   P. K. Miniappan, S. Marimuthu, S. D. Kumar, G. Gokilakrishnan, S. Sharma, C. Li, and M. Abbas, "Mechanical, fracture-deformation, and tribology behavior of fillers-reinforced sisal fiber composites for lightweight automotive applications," *Reviews on Advanced Materials Science*, vol. 62, no.1, art. no. 20230342, 2023.

[11]   M. Preisner, W. Wojtasik, A. Kulma, M. Żuk, and J. Szopa, "Flax fiber," in *Kirk-Othmer Encyclopedia of Chemical Technology*, D. E. Akin, Eds. Russell Research Center: ARS-USDA, vol. 11, 2000, pp. 588–623.

[12]   A. Lefeuvre, A. Bourmaud, L. Lebrun, C. Morvan, and C. Baley, "A study of the yearly reproducibility of flax fiber tensile properties," *Industrial Crops and Products*, vol. 50, pp. 400–407, 2013.

[13]   D. Sundeep, E. K. Varadaraj, S. D. Ephraim, C. C. Sastry, and A. G. Krishna, "Mechanical, morphological and thermal analysis of unidirectional fabricated sisal/flax hybrid natural fiber composites," *Surface Topography: Metrology and Properties*, vol. 10, no. 1, art. no. 015028, 2022.

[14]   T. Sathish, "Performance enhancement on hybrid composite using multiwall carbon nanotubes for prosthetic sockets," *Interactions*, vol. 245, no. 1, pp. 1–11, 2024.

[15]   H. Sosiati, N. D. M. Yuniar, D. Saputra, and S. Hamdan, "The influence of carbon fiber content on the tensile, flexural, and thermal properties of the sisal/pmma composites," *Evergreen*, vol. 9, no. 1, pp. 32–40, 2022.

[16]   S. H. Mahmud, M. W. Akram, M. F. Ahmed, and M. A. B. Habib, "Preparation and investigation of mechanical and physical properties of flax/glass fabric reinforced polymer hybrid composites," *Journal of Textile Science and Technology*, vol. 9, no. 3, pp. 165–182, 2023.

[17]   S. Arumugam, J. Kandasamy, A. U. Md Shah, M.T. Hameed Sultan, S. N. A. Safri, M. S. Abdul Majid, and F. Mustapha, "Investigations on the mechanical properties of glass fiber/sisal fiber/chitosan reinforced hybrid polymer sandwich composite scaffolds for bone fracture fixation applications," *Polymers*, vol. 12, no. 7, art. no. 1501, 2020.

[18]   N. Kumari and K. Kumar, "Orthopedic application of plant-based composites: a case on orthotic calipers," *Plant and Animal Based Composites*, vol. 13, art. no. 71, 2021.

[19]   C. Meenakshi and A. Krishnamoorthy, "Study on the effect of surface modification on the mechanical and thermal behaviour of flax, sisal and glass fiber-reinforced epoxy hybrid composites," *Journal of Renewable Materials*, vol. 7, no. 2, pp. 153–169, 2019.

[20]   A. E. Bekele, H. G. Lemu, and M. G. Jiru, "Experimental study of physical, chemical and mechanical properties of enset and sisal fibers," *Polymer Testing*, vol. 106, art. no. 107453, 2022.

[21]   S. Rajaram, K. Venkatesan, I. Jenish, and G. B. Bhaskar, "Study of mechanical properties on abaca/sisal fibre–reinforced epoxy resin–based hybrid composites," *Biomass Conversion and Biorefinery*, vol. 14, no. 12, pp. 13431–13444, 2024.

[22]   S. Senkathir, S. Pramanik, and M. Mukherjee, "Evaluation of process parameters for poly (ether ether ketone) to poly (ether ether ketone) friction welded joint," *Proceedings of the Institution of Mechanical Engineers, Part J: Journal of Engineering Tribology*, vol. 236, no. 2, pp. 266–273, 2022.

[23]   K. S. Salem, V. Naithani, H. Jameel, L. Lucia, and L. Pal, "Lignocellulosic fibers from renewable resources using green chemistry for a circular economy," *Global Challenges*, vol. 5, no. 2, art. no. 2000065, 2021.

[24]   V. Titok, V. Leontiev, S. Yurenkova, T. Nikitinskaya, T. Barannikova, and L. Khotyleva, "Infrared spectroscopy of fiber flax," *Journal of Natural Fibers*, vol. 7, no.1, pp. 61–69, 2010.

[25]   P. Garside and P. Wyeth, "Identification of cellulosic fibres by FTIR spectroscopy differentiation of flax and hemp by polarized ATR FTIR," *Studies in Conservation*, vol. 51, no. 3, pp. 205–211, 2006.

[26]   K. Venkatesan and G. Bhaskar, "Evaluation and Ccomparison of mechanical properties of natural fiber abaca-sisal composite," *Fibers and Polymers*, vol. 21, pp. 1523–1534, 2020.

Numerical Study of the Diffused Chamber Shapes of Aerostatic Thrust Bearing

Faiza Ghezali[1]

[1]Structural and Solid Mechanics Laboratory, Department of Mechanical Engineering, University Djillali Liabes, Sidi Bel Abbes, Algeria
Corresponding author: Faiza Ghezali (faiza.ghezali4@gmail.com)

Abstract

This article aims to analyse The influences of the air film thickness on the mass flow rate for different types of chamber shapes on performance characteristics of aerostatic thrust bearings at ultra-high speed spindles under various operating conditions. The analyse the effect of several configurations are studied using the computational fluid dynamics approach to evaluate the inertia effect and load capacity of aerostatic bearings. The obtained results show that there are many differences in performance behaviours of the aerostatic thrust bearing caused by different geometry of chamber shapes. The pressure distribution and mass flow rate were analyzed for the case in different shapes and the pressure depression, gas vortices, and the turbulent intensity which is all weakened with decreasing air film thickness. Further analysis represents that the load capacity of the aerostatic thrust bearing slightly decreases with increasing rotational speeds of the spindle.

Keywords: Chamber shapes, Aerostatic bearing, Film thickness, Rotational speeds

Numerical Evaluation of Spanswise Elliptical Film Cooling Hole

Faiza Ghezali[1]

[1]Structural and Solid Mechanics Laboratory, Department of Mechanical Engineering, University Djillali Liabes, Sidi Bel Abbes, Algeria
Corresponding author: Faiza Ghezali (faiza.ghezali4@gmail.com)

Abstract

This paper presents a numerical investigation of the film-cooling performance of a elliptical film-cooling hole in comparison with a fan-shaped hole. The elliptical shaped hole is designed to increase the lateral spreading of coolant on the cooling surface. The film-cooling performance of the elliptical hole is evaluated at a density ratio of 1.75 and the range of the blowing ratio of 0.5 to 2.5. The simulations were performed using three dimensional Reynolds averaged Navier–Stokes analysis with the SST k-ω model. This model consists of all internal flow passages and cooling hole rows at the leading edge. The numerical results obtained of the fan shaped hole show very good agreement with the experimental data. For the blowing ratio of 0.5, the elliptical film-cooling hole shows a similar cooling performance as the fan-shaped hole. However, as the blowing ratio increases, the elliptical film -cooling hole shows greatly improved lateral spreading of the coolant and the cooling performance in terms of the film-cooling effectiveness in comparison with the fan-shaped hole.

Keywords: Film-cooling, SST k-ω model, Elliptical hole, Fan shaped hole, Film-cooling effectiveness

Enhanced Photovoltaic Performance through Dual-Absorber Design: A Simulation Study of CIGS/CZTS Solar Cells

Sarra Merabet[1], Chahrazed Bendenia[1], Souhila Bendenia[1], Hanae Merad[1], Samia Moulebhar[1], Sid Ahmed Khantar[1]

[1]Faculty of Science and Technology, University Abd elhamid Ibn badis, Mostaganem, Algeria
Corresponding author: Sarra Merabet (e-mail: sarra.merabet.etu@univ-mosta.dz)

Abstract

Copper Indium Gallium Selenide (CIGS) is a prominent material in the field of thin-film solar cells, renowned for its high absorption coefficient, adjustable bandgap, and excellent optoelectronic properties. These characteristics enable CIGS to achieve remarkable efficiencies in converting solar energy into electricity, making it a leading candidate for sustainable energy solutions. However, to further enhance performance and reduce reliance on toxic elements, the incorporation of Copper Zinc Tin Sulfide (CZTS) has emerged as a viable strategy. CZTS offers similar advantages while being composed of abundant, non-toxic materials, thus addressing environmental concerns.In this study, we present a numerical simulation of a solar cell structure utilizing a double absorber layer configuration comprising Copper Indium Gallium Selenide (CIGS) and Copper Zinc Tin Sulfide (CZTS). The architecture incorporates Zinc Oxide (ZnO) as the electron transport layer (ETL) and Cadmium Sulfide (CdS) as the buffer layer, aiming to optimize photovoltaic performance. Using SCAPS software, we achieved a maximum open-circuit voltage (VOC) of 0.7221 V, a short-circuit current density (JSC) of 43.83 mA/cm², and a fill factor (FF) of 84.56%. These parameters culminated in an impressive power conversion efficiency (η) of 26.77%. The results indicate that the use of a double absorber layer significantly enhances the performance of the solar cell, highlighting its potential for advancing thin-film photovoltaic technologies.

Keywords: Absorber layer, SCAPS-1D, CIGS, CZTS, Efficiency

Finite Element Analysis of the Biomechanical Behavior of a Human Tibia Subjected to Mechanical Impact

Hadjer Benamar[1], Noureddine Djebbar[1], Wahid Oudad[1]

[1]Department of Mechanical Engineering, Belhadj Bouchaib University, 46000 Ain Temouchent, Algeria
Corresponding author: Hadjer Benamar (e-mail: hadjerbenamar92@gmail.com)

Abstract

The tibia is an important bone in the lower limb has a central shaft known as the diaphysis with two ends named the epiphyses. It plays a crucial role in weight-bearing and locomotion. It is the second longest bone in the human body, the longest being the femur. The tibia is the bone most frequently fractured in collisions, caused by falls or car accidents, due to its thinness. It is essential to understand the distribution of stresses and the structural behaviour of the tibia to ensure its protection. Safety tests are quite costly and require expensive space and equipment. These expensive tests can be replaced by less expensive simulations using validated finite element models. In this study, FEM was used to investigate how the tibia reacts to mechanical impacts. The aim was to determine the intensity and distribution of stresses in the bone. The analysis involved simulating real-life scenarios in which the tibia may be struck by projectiles, such as stones or other objects. By examining the effects of impacts at different velocities, ranging from low to high, the study was able to assess how the tibia reacts under different conditions. This comprehensive approach enabled a detailed understanding of how different impact shapes and velocities influence the damage potential and fracture risk of the tibia.

Keywords: Biomechanics, Tibia, Impact, Velocity, Finite element analysis

A Computational Approche of Interface Damage in Biocomposites Based on PLA/Cellulosic Plant Fibers

Bouchra Achour[1], Allel Mokaddem[2], Bendouma Doumi[2,3], Abdelkader Ziadi[1], Lahcen Belarbi[4], Ahmed Boutaous[5]

[1]Smart Structures Laboratory, Mechanical Engineering Department, University of Ain Temouchent, Algeria
[2]Laboratory of Instrumentation and Advanced Materials, Nour Bachir El-Bayadh University Center, BP 900 Route Aflou, 32000 El Bayadh, Algeria
[3]Department of Physics, Faculty of Sciences, Dr Tahar Moulay University of Saida, 20000 Saida, Algeria
[4]Applied Chemical Laboratory, Ain Temouchent University, Algeria
[5]Department of Materials Technology, Faculty of Physics, University of Science and Technology Mohamed Boudiaf, Oran, Algeria
Corresponding author: Bouchra Achour (e-mail: bouchraachour6@gmail.com)

Abstract

The use of natural fibers has seen a significant rise across various industrial sectors, notably in automotive engineering and civil construction, due to their eco-friendly properties such as biodegradability, recyclability, and negligible environmental impact. This study investigates the influence of raffia, alfa, and sisal fibers on the damage characteristics of biocomposite materials. Specifically, composites of raffia/ polylactic acid (PLA), alfa/PLA, and sisal/PLA were subjected to identical mechanical shear stress conditions to assess their performance. To evaluate interface damage, which includes both fiber and matrix degradation, a genetic algorithm based on the Weibull distribution was applied. The findings reveal that raffia/PLA and alfa/PLA composites demonstrate superior mechanical properties compared to sisal/PLA, as shown by the varying levels of interface damage among the tested materials. These results align closely with Cox's theoretical model, which posits that higher fiber Young's modulus enhances interface resistance. Additionally, our data, visualized using a red cloud representation, correspond well with findings from Antoine Le Duigou, Bodros, and other researchers, all indicating that natural fibers significantly improve the mechanical and physical properties of composite materials.

Keywords: Alfa, Interface, PLA, Raffia; Shear damage, Sisal

Chlorine Liquefaction Process at the ADWAN Company, Algeria

Chahrazed Bendenia[1], Souhila Bendenia[1], Hanaa Merad-Dib[1], Samia Moulebhar[1], Sarra Merabet[1], Sid Ahmed Khantar[1]

[1]Faculty of Sciences and Technology, University Abd El Hamid Ibn Badis, Mostaganem 27000, Algeria
Corresponding author: Chahrazed Bendenia (e-mail: bendenia.chahrazed@yahoo.com)

Abstract

As an inexhaustible brut material, chlorine is the object of great interest in the world industrial and economic growth. It is used in several fields such as water treatment, medicine, health, electronics, etc. Its production and handling are subject to rigorous procedures of which the liquefaction process is part. In this perspective, our present work is devoted to a study on the liquefaction technique of chlorine carried out at the level of the company ADWAN Chemicals Company Algeria. This process is performed out with a set of equipment among which the heat exchangers which constitutes an indispensable role because it favors the heat transfer between two fluid bodies without mixing them. Subsequently, the fundamental parameters of the HE-162 calandria-tube heat exchanger were calculated from the real data of its installation. The obtained results showed us that the highest thermal efficiency of the operated device is correlated with the operation mode of the countercurrent type exchanger. So, the HE-162 heat exchanger treated here is highly efficient for its essential role in the liquefaction circuit and particularly that of chlorine.

Keywords: Chlorine gas, Process, Liquefaction, ADWAN company, Exchanger, Heat

Thermographic Assessment of Materials for Improved Comfort

Ivana Salopek Čubrić[1], Laure Maurice[2], Goran Čubrić[3], Antonija Petrov[3]

[1]Department of Textile Design and Management, University of Zagreb Faculty of Textile Technology, Zagreb, Croatia
[2]National School of Chemical and Technological Arts Engineers, Toulouse, France
[3]Department of Clothing Technology, University of Zagreb Faculty of Textile Technology, Zagreb, Croatia
Corresponding author: Goran Čubrić (e-mail: goran.cubric@ttf.unizg.hr)

Abstract

This study investigates the moisture management properties of different knitted fabrics used in sportswear, focussing on their wetting speed, wetting surface and drying time. Fourteen polyester-based fabrics, including conventional and recycled types, were tested under different environmental conditions using a frame and a semi-permeable cellophane film to simulate skin contact. The results show that the moisture absorption and drying properties of the individual fabrics are very different. Certain samples, such as F5 and F10, exhibit better moisture transport and faster drying. Samples made from recycled polyester, such as F14, showed a smaller wetting surface areas, indicating differences in moisture management compared to conventional polyester. The results underline the importance of material selection based on specific sports requirements and emphasise that fast moisture absorption and efficient drying are crucial for athletic performance and comfort. This study provides valuable insights for optimising fabric selection in the development of high-performance sportswear development.

Keywords: Polyester material, moisture management, thermography

1. INTRODUCTION

Clothing is a fundamental human necessity, and throughout history, people have adapted their clothing to their needs. Every day, people are confronted with a range of challenging environmental conditions. In these situations, clothing primarily serves to protect the body from external factors. Based on their specific functions and characteristics, garments can be categorized into several types, including workwear, protective clothing, uniforms, clothing for casual purpose, specialised clothing, and sportswear. Sportswear, in particular, plays a significant role in everyday life. When purchasing or designing sportswear, it is important to focus on the comfort properties - both thermophysiological and sensorial - to ensure that it remains appropriate for as long as possible during use [1–3].

In order not to hinder athletes in their activities, active clothing is often made from very light materials. This type of clothing must not restrict or hinder movement and must often fulfil additional requirements that are specific to the sport in question. It can also have a major impact on performance. The thermodynamic, aerodynamic, and hydrodynamic characteristics of the material used, as well as the structure, design, and finish of the material, all have an impact on the performance of sportswear [4–6].

Infrared thermography (IRT) can be used as a diagnostic tool to detect the presence of moisture in the cavities of fabrics. IRT uses of an infrared camera that can detect thermal radiation and create colour images, known as thermograms [7]. A thermogram contains temperature data, and one of the main advantages is that it allows us to visualise temperature differences across the object detected, using colour differences that relate to a colour-temperature scale [8].

In the field of textile engineering, thermography can be used to monitor the production process, textile material properties, clothing comfort, failure and product development. Researchers confirmed that thermography is a great tool for evaluating the efficiency of clothing interventions and has great potential for evaluating regional or whole-body patterns for targeted clothing [9-11].

The objective of this study is to determine the most optimal fabric regarding the humidity that athletes can have during the use of these sportswear. The optimal fabric sought must allow moisture to spread quickly through the fabric and allow it to dry very quickly.

2. MATERIAL AND METHOD

For this study 14 fabrics were selected. These fabrics are all made as knitted fabrics, i.e. the structure of fabric is built-up from the loops. Such structure ensures greater body fit and increases the perspiration what is very important for sportswear. The overview of fabrics used is given in Table 1.

Table 1. Materials

Sample ID	Material Description		
	Yarn Composition	Fabric Structure	Fabric Surface Mass, g/m^2
F1	100% polyester	Double jersey mesh	105
F2	100% polyester	Double jersey mesh	152
F3	100% polyester	Double jersey mesh	192
F4	100% polyester	Double jersey plated mesh	157
F5	100% polyester	Plated double jersey	136
F6	100% polyester	Double jersey mesh	155
F7	100% polyester	Interlock	151
F8	100% polyester	Double jersey mesh	145
F9	91% polyester + 9% elastan	Single jersey	178
F10	92% polyester + 8% elastan	Single jersey	197
F11	84% polyester + 16% elastan	Single jersey	180
F12	87% polyester + 13% elastan	Single jersey	141
F13	100% polyester, recycled yarn	Single jersey	130
F14	100% polyester, recycled yarn	Single jersey	185

2.1. Method

In the experimental part of the research, the fabrics were tested for wetting time, wetting surface, wetting speed and drying time. In order to do so, the following protocol was used:

- The fabric to be studied was placed on the shee so that it does not touch the table but is not stretched so as not to deform the stitch. The fabric was wedged using clips and the dial was placed on top (Figure 1).

Figure 1. Setting up the fabric for the tests with the frame

- Using a precision pipette, 0.5 mL of distilled water was taken and applied to the fabric.
- The fabric wetting time was measured using a stopwatch.
- Subsequently, after the distilled water was spread through the fabric, the dimensions of the water stain formed on the fabric were measured and expressed as the surface area.
- The wetting speed was calculated using noted data and expressed in mm/s.
- Using the TESTO 872 thermal camera, the progress of the drying of the fabric was monitored every 10 min. The fabric is defined to be dry at the moment when the color of whole fabric surface on a thermographs image

is even. For the analysis of thermograms, a TESTO IRSoft v4.8 software was used. The images, to verify the presence of water are shown in Figure 2 (examples for the fabric F10).
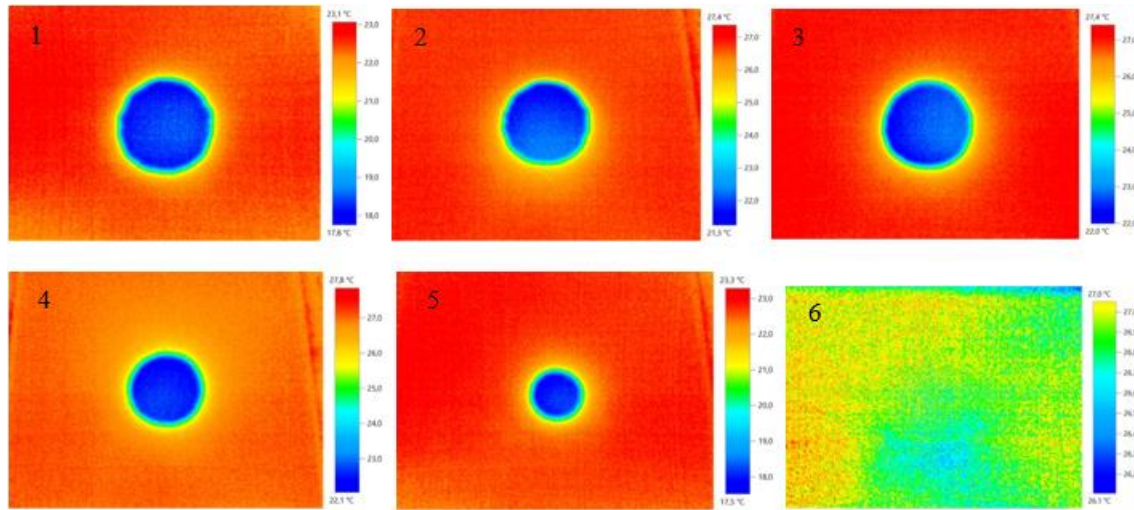
Figure 2. Pictures taken with the thermal camera TESTO 872 on the F10 sample

Figure 2 shows three phases in the drying of the fabrics:

- A wet phase, corresponds to the first 10 minutes of drying (image no 1)
- A static phase where the temperature of the task in the middle remains constant (images no 2, 3, and 4)
- A drying phase with a large reduction in the size of the water stain until it disappears (images no 5 and 6).

A second protocol was carried out which aims to simulate human skin and therefore to look at the effect that this can have on the tissue. To achieve this, a semi-permeable cellophane film was used. This cellophane film was placed on a flat support (Figure 3). The materials were placed on the cellophane film and the same experiment was carried out as before.

Figure 3. Semi-permeable cellophane film with the samples to be analyzed

To improve the data obtained when using cellophane as an imitation of skin, this experiment was carried out six times, i.e.:

- Three times with the air conditioning set at 21°C in order to have a uniform temperature throughout the room (room temperature is 24 ± 2 ºC and relative humidity was 39.5%) and

- Three without air conditioning (room temperature is 30 ± 2 ºC and relative humidity was 40.3%).
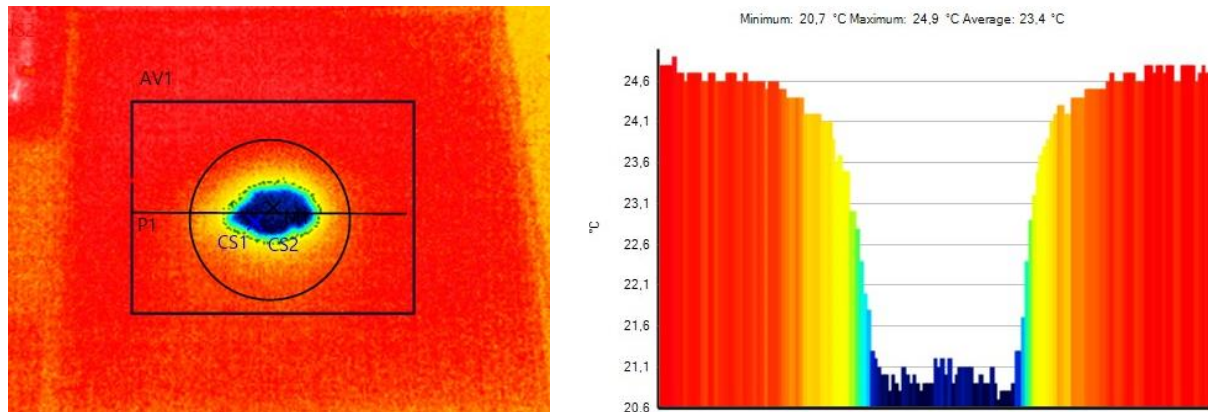
Figure 4. Thermogram and graphical presentation of the testing results TESTO IRSoft v4.8 software

3. RESULTS

The results of the measurements are shown in Figures 5 – 12. Figure 5 shows the results for the wetting speed on the frame (X and Y-direction). The results show considerable variability between the samples. The wetting speeds in the X-direction range from 10.12 mm/s to 134.69 mm/s, while in the Y-direction they range from 8.93 mm/s to 118.37 mm/s. Sample F11 exhibited the lowest wetting speed in both directions, indicating a lower moisture absorption capacity, closely followed by samples F9, F3 and F4. In contrast, sample F5 showed the highest wetting speed in both the X and Y-directions, clearly standing out from the other samples. This indicates that F5 has a more open or porous structure that allows moisture to spread rapidly across the surface of the fabric. These properties make F5 particularly suitable for applications that require efficient moisture transport.
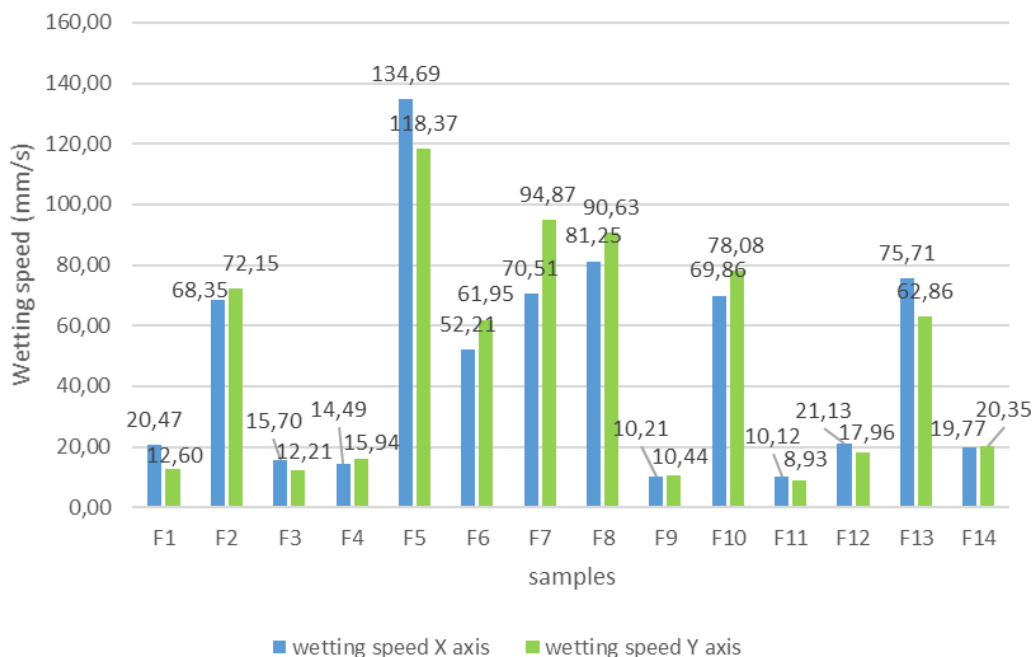
Figure 5. Wetting speed for samples on the frame in X-direction (horizontal) and Y-direction (vertical)

Figures 6 and 7 show the results of the wetting speed on the semi-permeable cellophane film with air conditioning and without air conditioning in the X and Y-directions. The results of the wetting speed with air conditioning (Figure 6) range from 2.37 mm/s to 131.74 mm/s in the X-direction, while the results in the Y-direction range from 3.88 mm/s to 127.13 mm/s. Sample F10 is characterized by the highest wetting speed in both directions, while conversely sample F2 has the lowest wetting speed.

When comparing the results of the wetting speed on the frame and the wetting speed on the semi-permeable cellophane film with air conditioning, it is clear that the lowest value observed on the semi-permeable cellophane

is significantly lower than the lowest value measured on the frame. In addition, there are substantial variations between the X-direction and Y-direction results. There is no consistent or linear trend indicating that one direction always has a higher speed than the other does. The lower wetting speeds observed on the semi-permeable cellophane film with air conditioning indicate slower moisture absorption compared to the frame tests. Although air conditioning generally accelerates evaporation, the semi-permeable cellophane film retains moisture to the fabric and prevents it from spreading as quickly as on the frame. This results in slower wetting, even under air conditioning.
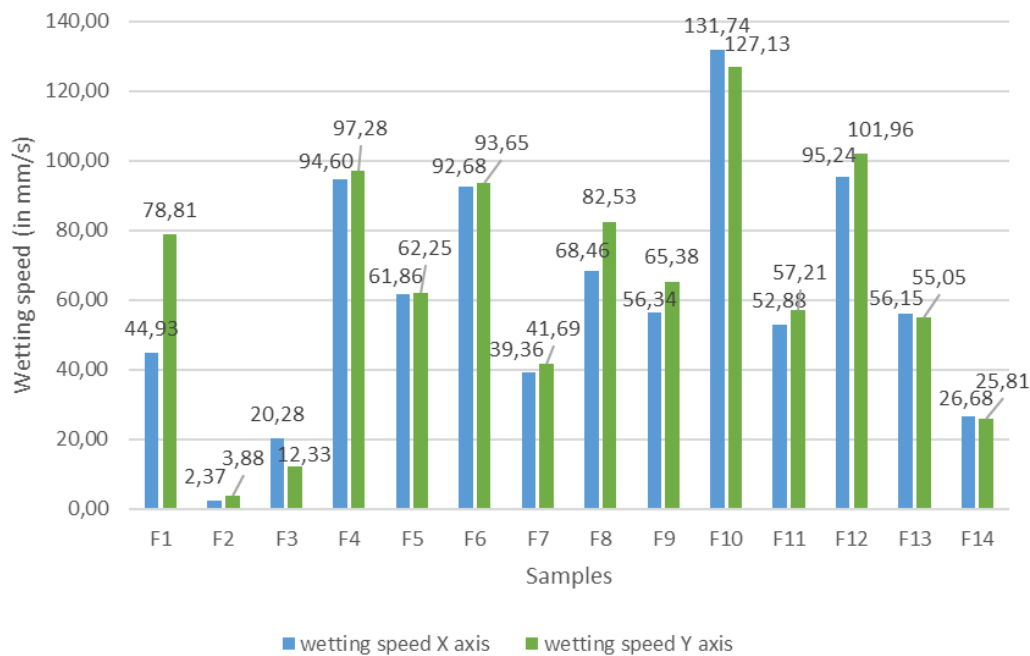
Figure 6. Wetting speed for samples on the semi-permeable cellophane film in X-direction (horizontal) and Y-direction (vertical) with air conditioning
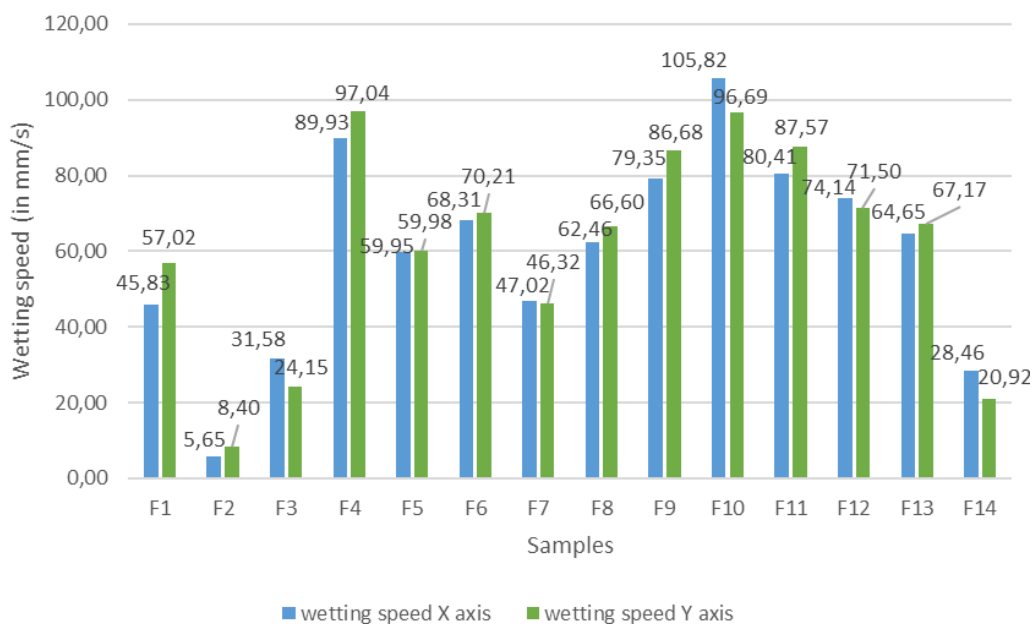
Figure 7. Wetting speed for samples on the semi-permeable cellophane film in X-direction (horizontal) and Y-direction (vertical) without air conditioning

The results shown in Figure 7 for the wetting speed on the semi-permeable cellophane film without air conditioning follow a similar trend to the results with air conditioning. Again, sample F10 showed the highest wetting speed in both directions, with a value of 105.82 mm/s in the X-direction and 96.69 mm/s in the Y-direction, which are slightly lower values compared to the results with air conditioning. Sample F2 was also characterised by the lowest

wetting speed, with values of 5.65 mm/s in the X-direction and 8.40 mm/s in the Y-direction. These values are slightly higher than the values measured under air conditioning, indicating a faster wetting speed of this sample in non-air-conditioned environments. While the results for the wetting speed on the semi-permeable cellophane film without air conditioning are generally similar to those with air conditioning, some samples without air circulation show a slightly faster wetting speed, as observed for samples F2, F3, F7, etc. This indicates that the wetting speed on the semi-permeable cellophane film without air conditioning is slightly faster than that with air conditioning. This suggests that the lack of air conditioning may result in faster moisture uptake for certain fabrics, possibly due to differences in humidity or fabric behaviour under less controlled environmental conditions.

Figure 8 shows the wetting speed in the X-direction for measurements on the frame and on the semi-permeable cellophane film, both with and without air conditioning. The first observation is that sample F5 achieves the highest wetting speed in the tests with the frame. However, the results of the tests with the semi-permeable cellophane film, both with and without air conditioning, are notably lower and differ from each other. These values are considerably inferior compared to those obtained on the frame. A similar trend can be observed for sample F10. The results clearly show that the measurements on the frame differ drastically from those carried out on the semi-permeable cellophane film. This discrepancy indicates a lack of uniformity in the results. The values of individual measurements are not consistently higher than those of the others, and there are noticeable large variations across all three conducted measurements. These variations may indicate the complexity of the interactions between the materials and the environment, particularly in relation to the use of the cellophane film, which may not provide a stable or predictable barrier to wetting.
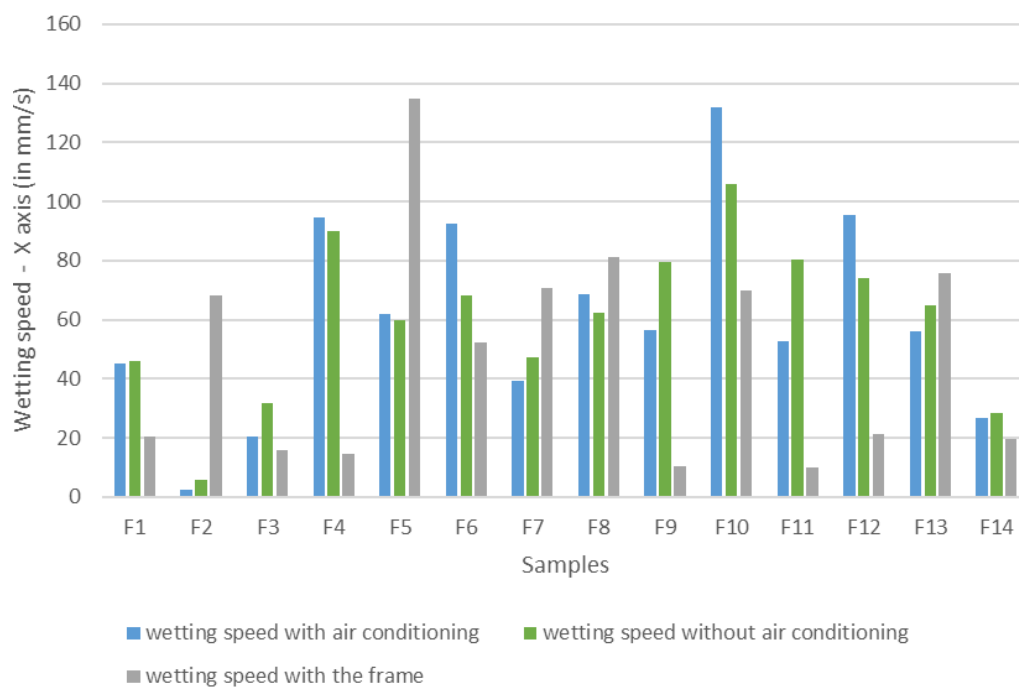
Figure 8. Wetting speed in X-direction (horizontal) for the measurements with the frame and with semi-permeable cellophane film with air conditioning and without air conditioning

Figure 9 shows the wetting speed in the Y-direction for tests carried out on the frame and on the semi-permeable cellophane film, both with and without air conditioning. The results are generally consistent with those observed in the X-direction and show similar trends. Again, the results are not uniform and vary considerably depending on the sample and test conditions. One notable observation is the considerable differences between the results obtained on the frame and those obtained on the semi-permeable cellophane. The values show considerable variation, with some results being either much higher or much lower compared to the results obtained on the semi-permeable cellophane film. Sample F5 again stood out as it showed high wetting speed in the X-direction, as did sample F10, which showed similar behaviour in both directions. These differences indicate that the test method — whether on the frame or one the semi-permeable cellophane film — has a significant influence on the wetting speed, which is probably due to the differences in the behaviour of the fabric when it is placed on the frame and not in contact with the semi-permeable surface.
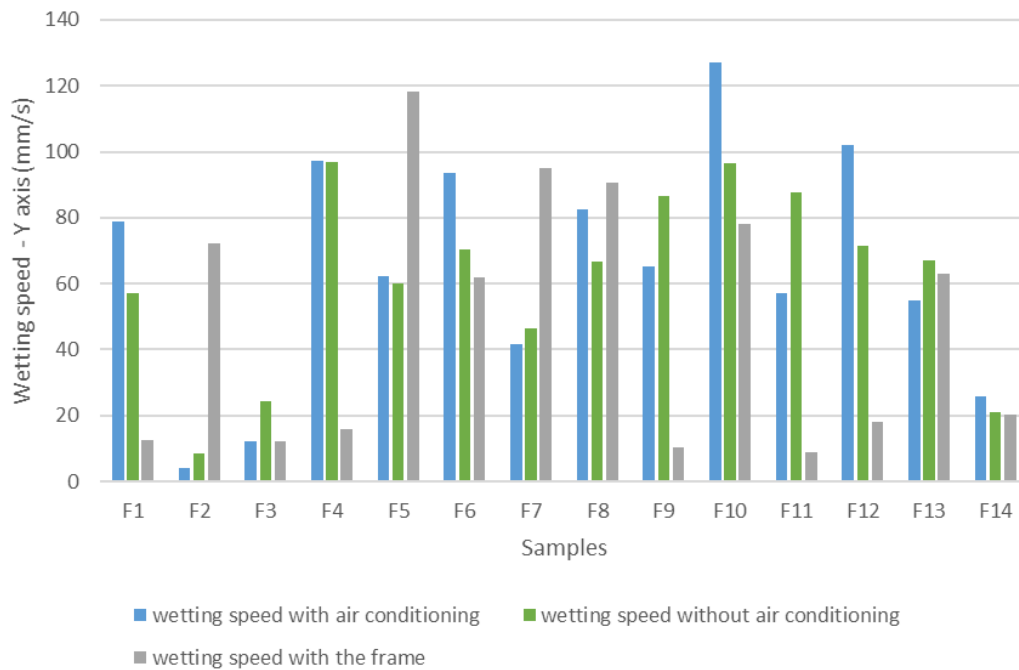
Figure 9. Wetting speed in Y-direction (vertical) for the measurements with the frame and with semi-permeable cellophane film with air conditioning and without air conditioning

Figure 10 shows the results of the drying times for the tests carried out on the frame and on the semi-permeable cellophane film, both with and without air conditioning. The drying times with air conditioning range from 54 minutes to 110 minutes, while without air conditioning they range from 73 minutes to 113 minutes. It can be seen that the drying time with air conditioning is generally shorter, as the air circulation accelerates evaporation by promoting more efficient moisture removal. Sample F3 was the slowest drying material. It took 110 minutes with air conditioning and 113 minutes without air conditioning when tested on the semi-permeable cellophane film. This result is not surprising considering that F3 has one of the highest fabric masses (192 g/m²). Materials with greater mass tend to retain more moisture, which leads to longer drying time as the water needs more time to evaporate from the denser structure. The results for drying times on the frame ranged from 30 minutes to 90 minutes, which is considerably faster compared to the tests carried out on the semi-permeable cellophane film. This difference can be explained by the fact that the material is raised on the frame and is not in direct contact with the surface (unlike on the semi-permeable cellophane, which simulates skin contact). This arrangement allows for better air circulation around the material, which promotes evaporation as the liquid has more paths to escape, including the underside of the material. Sample F1 had the shortest drying time. It only took 30 minutes on the frame and just under an hour when tested on the semi-permeable cellophane film with air conditioning. This result is consistent with the fact that F1 has the lowest fabric mass (105 g/m²) of all the samples tested. Lighter fabrics naturally hold less moisture and therefore dry faster. The lower mass reduces the total amount of water absorbed by the material, which means that less time is needed for complete evaporation.

The results for the wetting time under all three conditions are shown in Figure 11. The data are relatively consistent, with a few samples standing out clearly. The results for the wetting time on the semi-permeable cellophane film with air conditioning range from 0.55 seconds to 14.96 seconds, with samples F2 and F3 showing the most noticeable deviations. Sample F2 had the longest wetting time of 14.96 seconds, followed by F3 with a much shorter time of 2.82 seconds. This corresponds to a difference of approximately 81.1% between the two samples. Sample F10 had the shortest wetting time of 0.55 seconds, although it had the highest mass of all samples tested (197 g/m²). The short wetting time of sample F10, despite its higher mass, could be due to the fabric structure and surface properties. A denser or thicker fabric, although having a greater mass, may limit the amount of liquid that initially penetrates the fabric, resulting in faster surface absorption but not deeper penetration. The composition of the fabric could also play a role in this rapid initial absorption phase. In the tests without air conditioning on the semi-permeable cellophane film, the wetting times varied between 0.70 seconds and 6.85 seconds. Once again, samples F2 and F3 stood out, with F2 showing a notably longer wetting time. This indicates that fabric properties such as fibre composition and fabric structure have a greater influence on these results than the ambient conditions. The results for the wetting time on the frame showed a smaller range with times from 0.49 seconds to 4.31 seconds and were the shortest under all three conditions. The samples with the longest wetting times were F9 (4.31 seconds), F11 (3.36 seconds) and F12 (2.84 seconds), suggesting that certain fabric structures may retain moisture longer when not in contact with a surface that simulates skin. In contrast, sample F5 had the shortest wetting time,

indicating its superior ability to quickly absorb and distribute moisture over the surface. These results illustrate the influence of both the material composition and the test conditions on the wetting time. The fabrics tested on the frame dried faster due to better air circulation around the fabric, allowing moisture to dissipate more quickly. The presence of the semi-permeable cellophane film, which simulates skin contact, slowed down the wetting process by trapping moisture on the fabric surface and prolonging the wetting time, especially for samples such as F2 and F3.
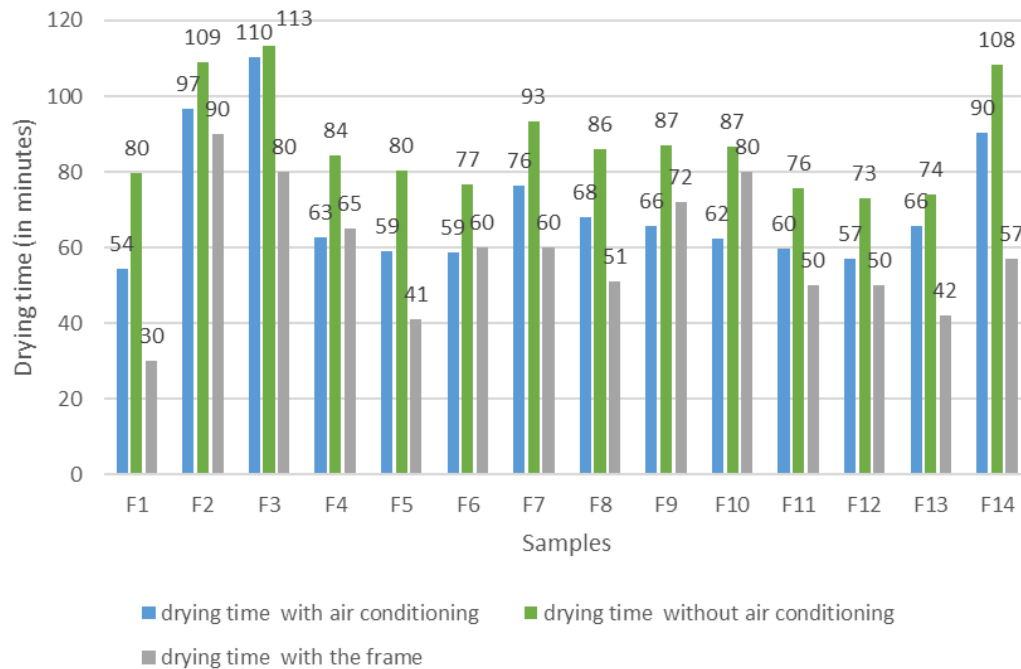
Figure 10. Drying time for the measurements with the frame and with semi-permeable cellophane film with air conditioning and without air conditioning
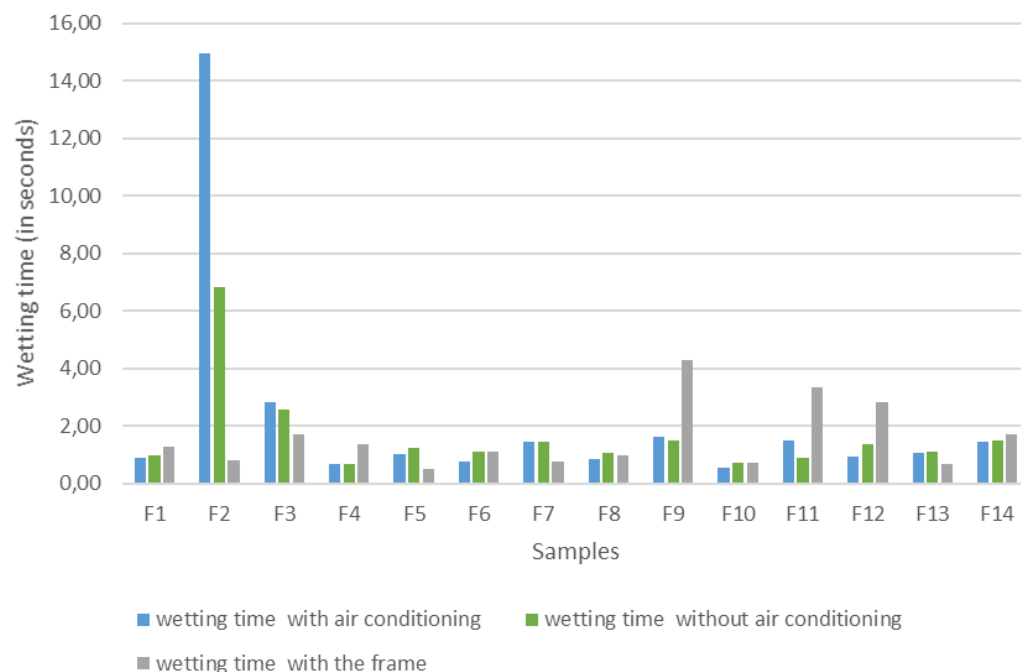
Figure 11. Wetting time for the measurements with the frame and with semi-permeable cellophane film with air conditioning and without air conditioning

Figure 12 shows the results of the wetting surface area on the frame and on the semi-permeable cellophane film, both with and without air conditioning. The graph shows that the wetting surface area in the tests with the semi-permeable cellophane film is greater overall than in the results with the frame, regardless of the air conditioning.

The results vary considerably depending on the sample tested. One notable observation is that sample F14 consistently had the smallest wetting surface area on the semi-permeable cellophane, both with and without air conditioning. With air conditioning, a surface area of 1108.72 mm² was measured, while without air conditioning it was slightly smaller at 878.33 mm². This sample was made from recycled polyester, which could significantly affect the wetting behaviour. Recycled polyester fibres may have different surface tensions or structural properties than conventional polyester fibres, which may reduce their ability to absorb and release moisture, resulting in a smaller wetting surface area. On the other hand, samples F12 and F11 had the largest wetting surface areas on the semi-permeable cellophane tests. Under air conditioning, F11 had a surface area of 4281.47 mm², while F12 reached 5023.14 mm² without air conditioning. These large wetting areas indicate that these fabrics have a higher ability to retain and release moisture, possibly due to their fibre composition and structure, which allows for deeper moisture penetration and slower evaporation. In the tests on the frame, the wetting surface areas were generally much smaller, with sample F1 having the smallest surface area of only 326.73 mm². This represents a significant reduction compared to the semi-permeable cellophane tests. This is probably due to the fact that the fabric is raised on the frame and is not in contact with a surface that simulates the skin. This allows moisture to dissipate more freely so that it does not accumulate and spread over a larger area. Interestingly, sample F8 had the largest wetting surface area when tested on the frame, with a surface area of 5329.71 mm². This was not only the largest value in the frame tests, but also the largest surface area measured under all three test conditions. This could be due to the structure of the fabric, which probably facilitates rapid surface absorption and the distribution of moisture over a large area.
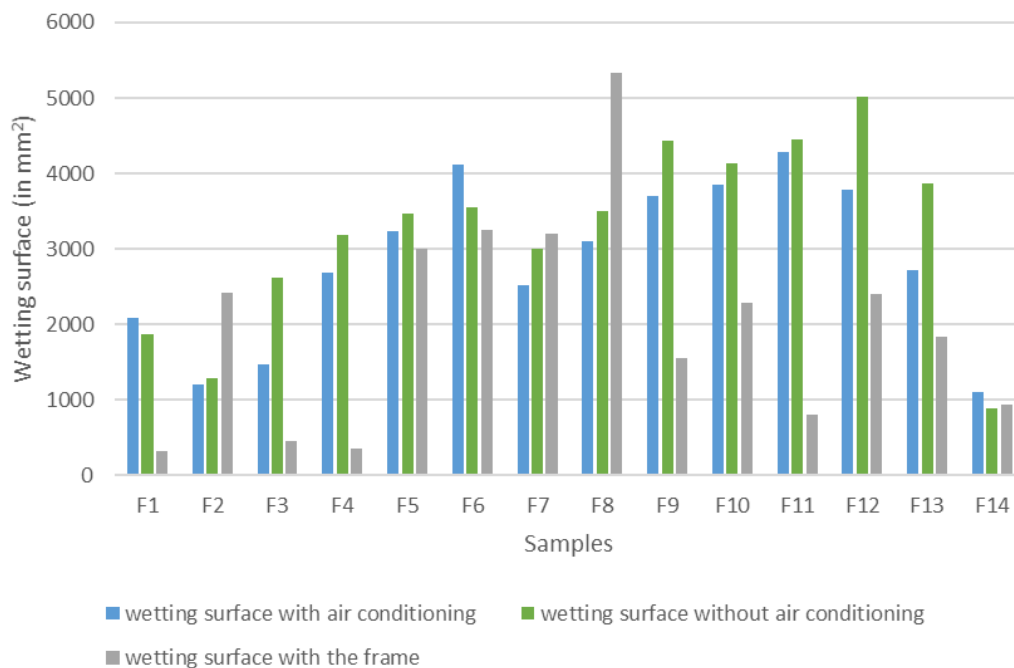
Figure 12. Wetting surface for the measurements with the frame and with semi-permeable cellophane film with air conditioning and without air conditioning

The results indicate that the test method (frame vs. semi-permeable cellophane) and the different conditions (with or without air conditioning) have a significant influence on the wetting surface. Materials tested on semi-permeable cellophane film tend to have larger wetting areas, which is due to the simulated skin contact that retains moisture on the material. In addition, the composition and structure of the fabrics, especially recycled compared to conventional polyester, play an important role in the ability to wick and retain moisture. The results highlight the complexity of moisture management in sports textiles and the importance of both material selection and environmental factors in their performance.

4. CONCLUSION

The experiments conducted provide valuable insights into the moisture management properties of various sports materials under different conditions and test methods. The results show that both the structure and the composition of the materials significantly influence the wetting speed, the wetting surface and the drying time. The materials tested on the semi-permeable cellophane consistently showed longer drying times and larger wetting surface areas compared to the materials tested on the frame, reflecting the effects of direct contact with a skin-simulating surface.

This suggests that under real-world conditions, where materials are in constant contact with the skin, moisture is likely to be retained for longer, particularly for materials with greater mass or more compact structures. In particular, materials such as F5 and F10 showed excellent moisture absorption, with faster wetting speeds and shorter drying times. These materials are well suited to sports applications where fast moisture absorption and drying are critical to maintaining comfort and performance. Conversely, materials such as F2 and F3, which have a longer wetting time and slower drying, are less suitable for high performance sportswear, but could be used in situations where moisture retention is an advantage. The influence of recycled polyester was particularly evident in samples such as F14, where the wetting surface area was consistently smaller. This suggests possible differences in moisture management between recycled and conventional polyester that need to be considered when selecting sustainable materials for sportswear.

Overall, the results emphasise the importance of selecting materials with suitable moisture management properties based on the specific requirements of each sport. Faster drying, higher wicking speed and efficient moisture distribution are key factors that have a direct impact on athletes' comfort and performance, especially during high-intensity activities where effective sweat management is crucial. The study emphasises the need for careful consideration of both material properties and environmental conditions in the development of high performance sportswear.

Acknowledgments

References

[1] I. Ziemele, I. Šroma, and A. Kakarane, "Comfort in sportswear," *Key Engineering Materials*, vol. 762, pp. 402–407, 2008.

[2] I. Salopek Čubrić, G. Čubrić, I. Katić Križmančić, and M. Kovačević, "Evaluation of changes in polymer material properties due to aging in different environments," *Polymers,* vol. 14, art no. 1682, 2022.

[3] J. I. Priego Quesada, F. P. Carpes, R. R. Bini, R. Salvador Palmer, P. Pérez-Soriano, and R. M. Cibrián Ortiz de Anda, "Relationship between skin temperature and muscle activation during incremental cycle exercise," *Journal of Thermal Biology*, vol. 48, pp. 28–35, 2015.

[4] J.I. Priego Quesada, "Assessment of sport garments using infrared thermography," in *Application of Infrared Thermography in Sports Science*, New York: Springer, Cham; 2017, pp. 159–183.

[5] K. Krstović, V.M. Potočić Matković, I. Salopek Čubrić, and G. Čubrić, "Physical-mechanical properties of knitted fabric for swimsuits," *Tekstilec*, vol. 65, no. 3, pp. 181–193, 2022.

[6] M. Hassan, K. Qashqary, H.A. Hassan, E. Shady, M. Alansary, et al., "Influence of sportswear fabric properties on the health and performance of athletes, " *Fibres & Textiles in Eastern Europe*, vol. 20, no. 4. pp. 82–88, 2012.

[7] F. Ring and K. Ammer, "The technique of infrared imaging in medicine Infrared imaging," in *Infrared Imaging*, IOP Publishing Ltd, 2015, pp. 7–14.

[8] M.Raccuglia, C. Heyde, A. Lloyd, S. Hodder, and G. Havenith, "The use of infrared thermal imaging to measure spatial and temporal sweat retention in clothing," *Intenational journal Biometeorology*, vol. 63, pp. 885–894, 2019.

[9] D. Fournet, B. Redortier, and G. Havenith, "Can body-mapped garments improve thermal comfort for sport in the cold?," *Extreme Physiology & Medicine,* vol. 4, no. 1, 2015.

[10] I. Salopek Čubrić, and G. Čubrić, "Body-mapping based on thermographic measurements under different influencing factors," *Sigurnost, v*ol. 63, no.2, pp. 143–154, 2021.

[11] D. Rojas-Valverde, P. Tomás-Carús, R. Timón, N. Batalha, B. Sánchez-Ureña, R. Gutiérrez-Vargas, and G. Olcina, "Short-term skin temperature responses to endurance exercise: a systematic review of methods and future challenges in the use of infrared thermography," *Life*, vol. 11, art. no. 1286, 2021.

Band Gap Alignment Analysis: Comparing the Ginley Method and XPS in ZrO2|V2O5 Type I Junctions

Abdelmounaim Chetoui[1], Ilyas Belkhettab[1], Youcef Messai[2]

[1]Research Center in Semiconductors Technology for Energetics (CRTSE), Merveilles, Algiers, Algeria
[2]Laboratory for the Study of Surfaces and Interfaces of Solid Matter (LESIMS), Badji Mokhtar University, 23000 Annaba, Algeria
Corresponding author: Abdelmounaim Chetoui (e-mail: chetoui_mounaim@yahoo.fr)

Abstract

The determination of band edge positions is crucial across various fields. Here, we compare different methods for assessing band edge alignment, focusing on the ZrO2|V2O5 heterojunction. X-ray diffraction (XRD) analysis revealed orthorhombic V2O5 and ZrO2 in both monoclinic and tetragonal phases. Absorption spectra indicated near-band edge values of 2.07 eV for V2O5, 4.9 eV for ZrO2, and 2.12 eV for ZrO2|V2O5, with corresponding band gaps (via the Tauc method) of 2.32, 5.16, and 2.35 eV. Down-conversion photoluminescence (PL) spectra for pure and junction materials are explored, while ZrO2's up-conversion confirmed its band gap (~5.14 eV) aligning closely with the Tauc result. The band gap alignment of ZrO2|V2O5 was determined using the Sanderson method and X-ray photoelectron spectroscopy (XPS). This study emphasizes an in-depth photoluminescence analysis to confirm the heterojunction type by probing hydroxyl radical (HO•) production.

Keywords: Type I heterojunction, Photoluminescence, Hydroxyl radical, Band edges, XPS, Semiconductors

1. INTRODUCTION

Understanding the characteristics and behavior of materials, particularly their band edge potentials (BEP), is crucial for applications in electronics [1], photonics [2], photocatalysis [3], electrolysis [4], and energetics. BEP estimation is key in determining a semiconductor's redox ability and efficiency in photocatalytic processes, such as pollutant degradation or water splitting [5]. In heterojunctions, BEP alignment governs carrier transport, recombination, and generation, affecting device performance across applications like LEDs, photovoltaic devices, and tunneling systems.

Accurate BEP prediction, essential for optimizing material junctions, was first introduced by Butler and Ginley in 1978, relying on Mulliken's electronegativity and Sanderson's relation for calculation [6]. Although density functional theory (DFT) provides good BEP estimates, the Ginley approach remains a simpler alternative, though it may not suit all materials [7]. For instance, its application to g-C3N4 has yielded discrepancies with experimental results, where XPS proved more reliable but prone to errors for materials with similar band positions.

This research aims to conduct a comparative study for band gap alignment using Ginley approach and XPS analysis. Using a ZrO2|V2O5 Type I heterostructure, we established a link between its alignment by the previously mentioned methods.

2. MATERIAL AND METHOD

All reagents and solvents were purchased from commercial suppliers (Sigma-Aldrich) and used as received, without further purification. The samples were synthesized using a solvothermal method followed by annealing.

2.1. Synthesis of V_2O_5

The hydrothermal method was used to prepare the V_2O_5 material was by dissolving 4.64 g of ammonium metavanadate (NH_4VO_3) in 60 ml of ethylene glycol (EG), stirred for 1h at 80 °C. The resulting mixture was placed into a Teflon-lined stainless steel autoclave, kept at 200 °C for 24h, and then naturally cooled to room temperature. The precipitate was annealed at 550 °C for 6h.

2.2. Synthesis of ZrO2

Zirconium oxide was obtained by a simple precipitation method. Therefore, an appropriate mass of zirconium(IV) oxychloride octahydrate ($ZrOCl_2.8H_2O$) was dissolved in deionized water, mixed with ammonium hydroxide (NH_4OH, 30%) until reaching a pH=10. Subsequent stirring was performed during 1h at room temperature. The precipitate was then washed, dried overnight at 80 °C and annealed at 550 °C for 6h (rate of 2°C min^{-1}).

2.3. Synthesis of ZrO2/V2O5 Junction

The $ZrO_2|V_2O_5$ heterojunction was obtained by a facile chemical method. Firstly, a solution of $ZrOCl_2.8H_2O$ (10^{-3} M, 20 ml) was precipitated in the presence of NH_4OH (pH=10) under stirring for 1h at room temperature. The precipitate was then rinsed several times with deionized water. The obtained precipitate was dispersed in 40 ml of deionized water, and appropriate amount of the previously prepared V_2O_5 was added to this suspension. The mixture was stirred for 1h at 100°C to ensure good miscibility. After being dried overnight at 80 °C, the powder was annealed at 550 °C for 6h (2°C min^{-1}).

3. RESULTS

3.1. XRD Analysis

The X-ray diffraction (XRD) patterns for the synthesized samples are presented in Figure 1. The XRD pattern of V2O5 confirms the formation of a pure material with an orthorhombic structure, corresponding to the Pmn21 space group (PDF-ICCD: 72-0598) [8]. In the case of ZrO2, the XRD analysis revealed the presence of two crystalline phases: the monoclinic phase (m-ZrO2) with the P21/c space group, and the tetragonal phase (t-ZrO2) with the P42/nmc space group. These crystal structures were verified using standard reference data (PDF-ICCD: 83-0944 for m-ZrO2 and PDF-ICCD: 79-1764 for t-ZrO2) [9]. The XRD pattern of the ZrO2|V2O5 heterostructure confirms the coexistence of V2O5, m-ZrO2, and t-ZrO2 phases. The phase composition, calculated using the XPowder software, indicates a qualitative weight percentage (%wt) of approximately 10.2% for V2O5, 83% for m-ZrO2, and 6.8% for t-ZrO2.
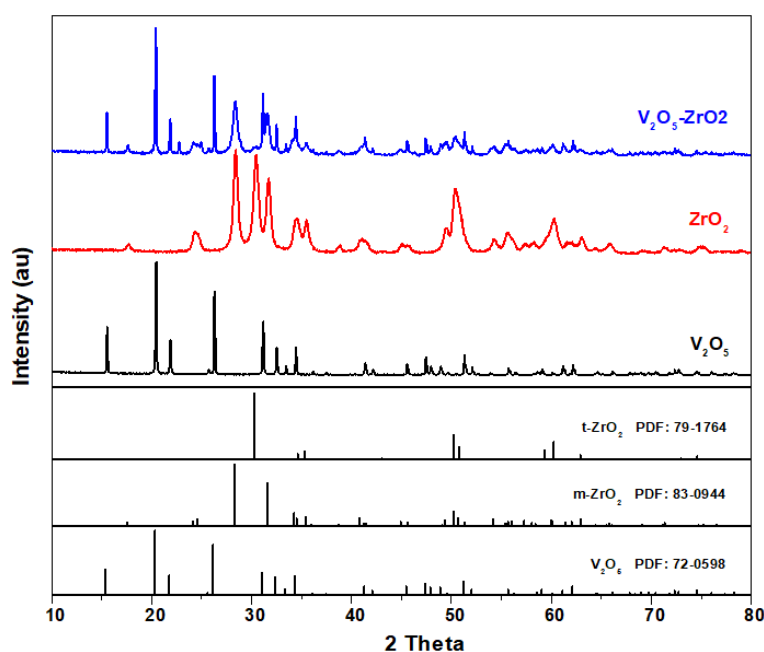
Figure 1. The XRD patterns of V_2O_5, ZrO_2 and $ZrO_2|V_2O_5$

The estimated crystallite size (C_s) for all the samples was calculated using the Debye-Sherrer equation:

$$C_s = \frac{k\lambda}{\beta \cos(\theta)}$$

(1)

where k is the Sherrer constant (k=0.89), λ is the X-ray wavelength ($\lambda = 0.154$ nm), β is the Full Width at Half Maximum (FWHM) of a given (hkl) peak at θ value, θ is the half of the scattering angle. A summary of the extracted structural parameters is presented in Table 1.

Table 1. Some structural parameters of the synthesized materials

Samples	Crystalline Phase	Phase Structure	Weight of Phase (%Wt)	Crystallite Size (nm)
V_2O_5	V_2O_5	Orthorhombic	100	74
ZrO_2	m-ZrO_2	Monoclinic	70.25	16
	t-ZrO_2	Tetragonal	29.75	
ZrO_2|V_2O_5	V_2O_5	Orthorhombic	10.2	64
	m-ZrO_2	Monoclinic	83.0	15
	t-ZrO_2	Tetragonal	06.8	

The average crystallite size of the pure V2O5 sample was calculated to be 74 nm, while the crystallite size of pure ZrO2 was determined to be 16 nm. Notably, upon the formation of the ZrO2|V2O5 heterojunction, the crystallite size of V2O5 decreased to 64 nm, whereas the crystallite size of ZrO2 remained unchanged. This reduction in V2O5 crystallite size may be attributed to the introduction of additional defects by ZrO2 during heterojunction formation [10].

3.2. Optical Properties

The estimation of the optical band gap was done by considering the direct allowed transition behavior for the studied materials using the Tauc relation:

$$\left[F(R)h\nu \right]^2 = A\left(h\nu - E_g \right) \tag{2}$$

where F(R) being the Kubelka-Munk function, E_g is the band gap and is determined by the linear extrapolation of the linear part of the Tauc plot to the energy axis. The estimated band gaps are depicted in Figure 2.
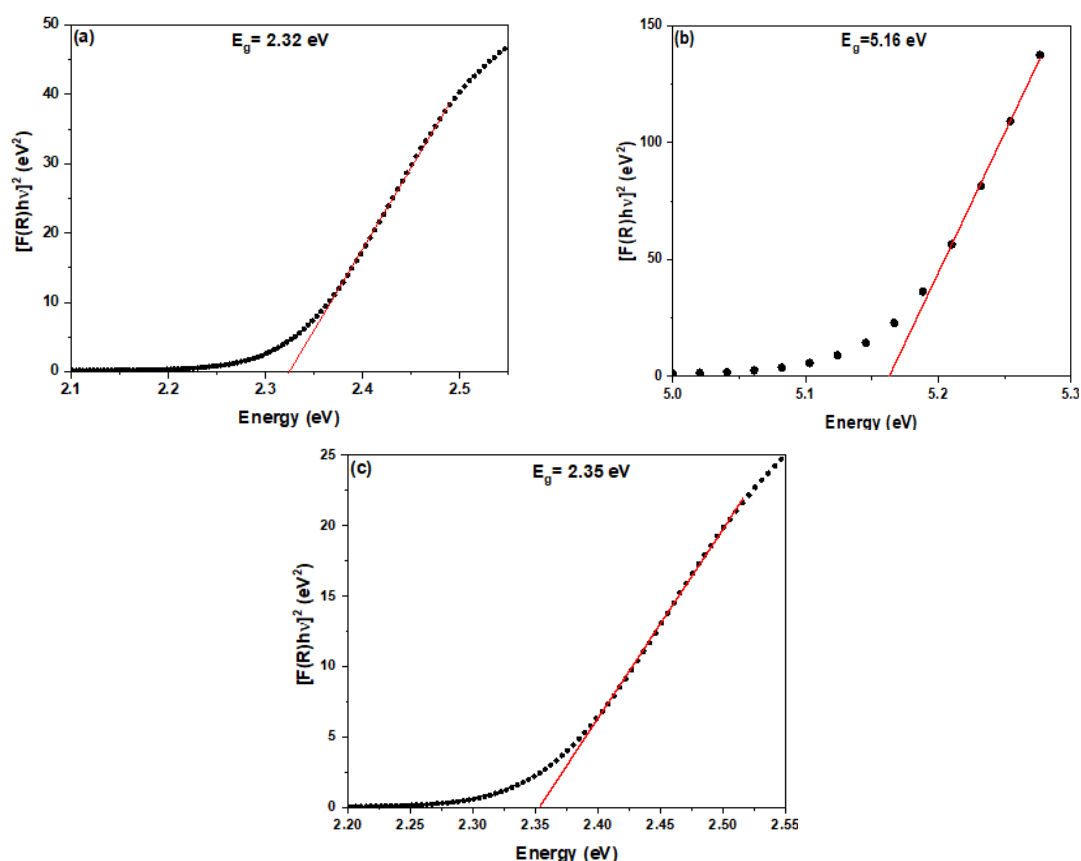
Figure 2. The band gap estimation for: a) V_2O_5, b) ZrO_2, and c) ZrO_2| V_2O_5

The calculated band gaps for V_2O_5 and ZrO_2 were found to be in good agreement with the values of 2.3 eV and 5.1 eV, respectively, reported in the literature [11]. The estimated band gap of the ZrO_2|V_2O_5 structure was found to be ~ 2.35 eV. As can be noticed, the band gap of ZrO_2|V_2O_5 junction is between ZrO_2 and V_2O_5, which confirms the electronic coupling of these latter [12].

3.3. Determination of the Band Gap Alignment

In order to get a preliminary insight into the band alignment of the ZrO$_2$|V$_2$O$_5$ heterostructure, it is worthwhile to estimate the band edge potentials (BEP). The calculation of the BEP is performed using the following Sanderson relation [13]:

$$\chi = \left[\chi^a(A)\chi^b(B)\chi^c(C) \right]^{\frac{1}{a+b+c}} \tag{3}$$

where, χ denotes the Mulliken's electronegativity of the A$_a$B$_b$C$_c$ compound. We define a, b, and c as the number of atoms for the elements A, B, and C, respectively. The Mulliken electronegativities for Zr, V, and O have been determined as 3.53 eV, 3.63 eV, and 7.53 eV, respectively. The calculated electronegativities of ZrO$_2$ and V$_2$O$_5$ were found to be 5.84 and 6.11 eV, respectively. The conduction band (CB) and the valence band (VB) potentials are calculated using Butler and Ginley relations [6]:

$$E_{CB} = \chi - E^e - E_g/2 \tag{4}$$

$$E_{VB} = E_{CB} + E_g \tag{5}$$

where, E^e is the energy of free electrons vs. standard hydrogen electrode (SHE, 4.5 eV), and E_g is the optical band gap of the material. By considering the previously calculated band gaps, the band potentials of each material were estimated to:

- ZrO$_2$ $\begin{cases} E_{CB} = -1.25\,\text{eV} \\ E_{VB} = 3.93\,\text{eV} \end{cases}$

- V$_2$O$_5$ $\begin{cases} E_{CB} = 0.45\,\text{eV} \\ E_{VB} = 2.77\,\text{eV} \end{cases}$

Thus, the corresponding potential energy diagram of the two materials with respect to vacuum level is shown in Figure 3. The alignment between the standard hydrogen electrode (SHE) and the vacuum level was established using the following relation [14]:

$$E_{SHE} = -E_{vac} - 4.5 \tag{6}$$
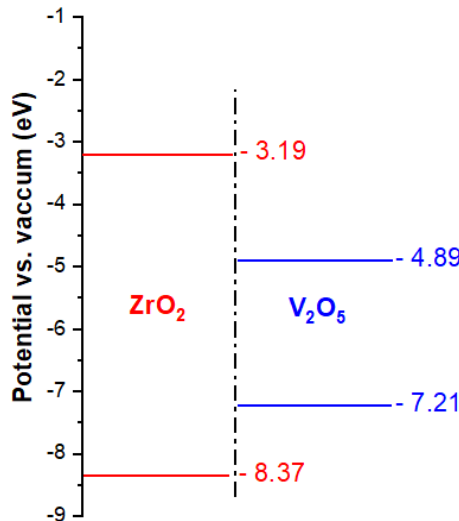
Figure 3. The potential energy diagram for the ZrO$_2$|V$_2$O$_5$ heterostructure

The calculations of band edge potentials revealed that the possible heterostructure achievable through the combination of these two materials is a Type I (straddling) junction. This kind of junction is known for its inability to separate the photogenerated charge carriers, but it could be efficient for optoelectronic applications. In order to push the investigation further, we deemed necessary to perform some XPS measurements, which are presented in detail in the section below.

3.4. XPS Measurements

In addition to its customary role in surface composition analysis to a depth of approximately 10 nanometers and in ascertaining the chemical state of elements in relation to their environment, X-ray Photoelectron Spectroscopy (XPS) proves to be a potent instrument for investigating the alignment of band gaps in heterostructures. Subsequently, we delve into the determination of the band offset of the $ZrO_2|V_2O_5$ heterojunction through fundamental XPS measurements.
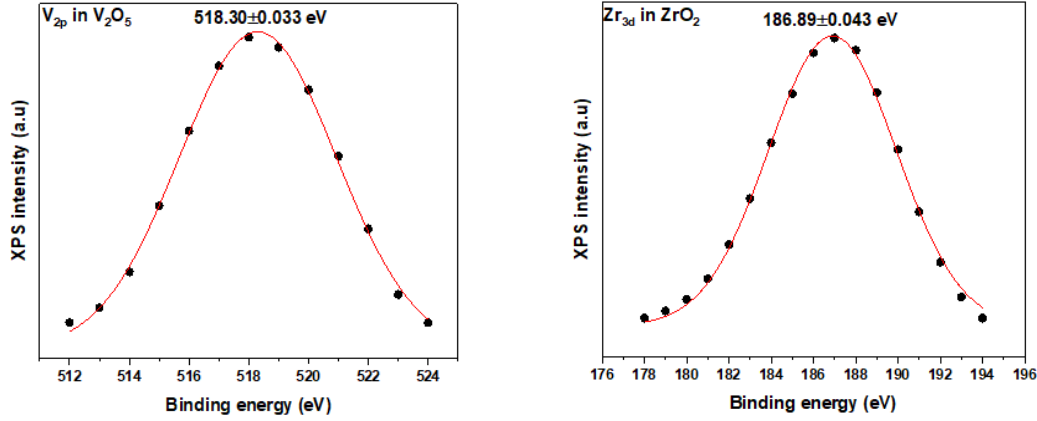
Figure 4. The core-level (CL) of: a) V_{2p} in single V_2O_5, and b) Zr_{3d} in single ZrO_2
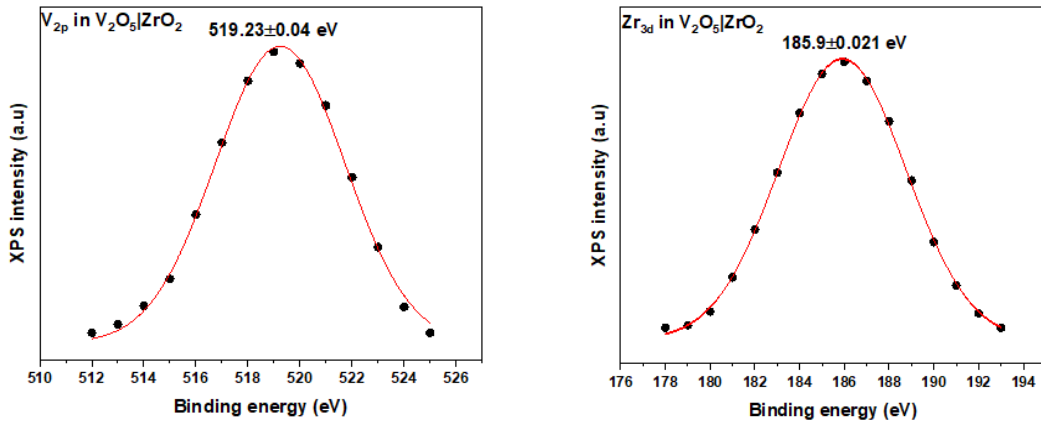
Figure 5. The core-level (CL) of: a) V_{2p}, and b) Zr_{3d} in the junction
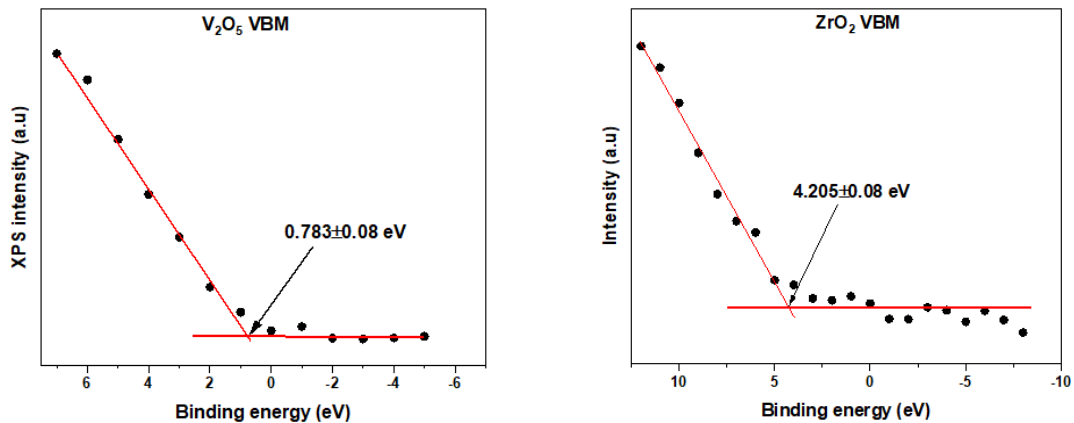
Figure 6. The VBM measurements for: a) V_2O_5, and b) ZrO_2

By adopting the methodology introduced by Kraut et al., one can employ the following expression to ascertain the valence band offset (VBO) [15]:

$$\Delta E_V = \left(E_{V_{2p}}^{ZrO_2 - V_2O_5} - E_{Zr_{3d}}^{ZrO_2 - V_2O_5} \right) - \left(E_{V_{2p}}^{V_2O_5} - E_{VBM}^{V_2O_5} \right) + \left(E_{Zr_{3d}}^{ZrO_2} - E_{VBM}^{ZrO_2} \right) \tag{7}$$

where, the first term: $\Delta E_{CL} = E_{V_{2p}}^{ZrO_2 - V_2O_5} - E_{Zr_{3d}}^{ZrO_2 - V_2O_5}$, represents the energy difference between V_{2p} CL of V_2O_5 and Zr_{3d} CL in ZrO_2 in the $ZrO_2|V_2O_5$ heterojunction. The experimental spectra corresponding to the parameters outlined in equation (7) are showcased in Figures 4, 5, and 6. The ΔE_{CL} quantity is determined to be approximately 333.33 eV, leading to an estimated valence band offset (VBO) of around 1.50 eV. As a result, the conduction band offset (CBO) can be estimated using the subsequent expression,

$$\Delta E_C = E_g^{ZrO_2} - \Delta E_V - E_g^{V_2O_5} \tag{8}$$

where, $E_g^{V_2O_5}$ and $E_g^{ZrO_2}$ correspond to the band gaps of V_2O_5 and ZrO_2, respectively. Subsequently, the conduction band offset (CBO) of the $ZrO_2|V_2O_5$ heterostructure was established to be approximately 1.35 eV. Taking into account the relative VBM positions of both materials, and by taking the E_g values into consideration, the flat-band diagram of the studied heterostructure can be presented as shown in Figure 8.
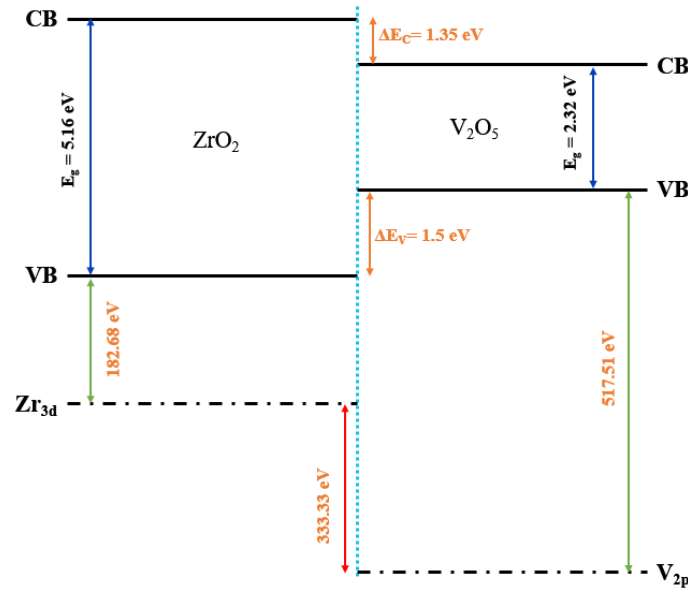
Figure 7. The energy band diagram of $ZrO_2|V_2O_5$ heterojunction obtained via XPS

4. CONCLUSION

In the present work, the V_2O_5, ZrO_2, and $ZrO_2|V_2O_5$ materials were successfully synthesized by the solvothermal method. The structural analysis indicates that V_2O_5 exhibits an orthorhombic structure, while ZrO_2 crystallizes in two distinct phases, namely, the monoclinic phase (m-ZrO_2) and the tetragonal phase (t-ZrO_2). The quantitative weight percentages (%wt) of each phase were averaged to 70.25% and 29.75% for the monoclinic and tetragonal phases, respectively. The near-band edges of V_2O_5, ZrO_2, and $ZrO_2|V_2O_5$ were found to be 2.07, 4.9, and 2.12 eV, respectively. The different approaches used for the determination of the band gap alignment, namely, the Sanderson method and XPS, were in good agreement. The Ginley approach indicated that the combination of ZrO_2 and V_2O_5 could shape a type I heterojunction. The Ginley approach was then endorsed by the XPS investigation.

References

[1]   J. F. Wager, "Transparent electronics: Schottky barrier and heterojunction considerations," *Thin Solid Films*, vol. 516, no. 8, pp. 1755–1764, Feb. 2008, doi: 10.1016/J.TSF.2007.06.164.

[2]   D. W. Prather, A. Sharkawy, and S. Shi, "Heterostructure photonic crystals: Theory and applications," *Appl. Opt.*, vol. 41, no. 34, pp. 7245–7253, Dec. 2002, doi: 10.1364/AO.41.007245.

[3]   X. He, T. Kai, and P. Ding, "Heterojunction photocatalysts for degradation of the tetracycline antibiotic: a review," *Environ. Chem. Lett.*, vol. 19, no. 6, pp. 4563–4601, Aug. 2021, doi: 10.1007/S10311-021-01295-8.

[4]   Z. Li, M. Hu, P. Wang, J. Liu, J. Yao, and C. Li, "Heterojunction catalyst in electrocatalytic water splitting," *Coord. Chem. Rev.*, vol. 439, art. no. 213953, Jul. 2021, doi: 10.1016/J.CCR.2021.213953.

[5]   T. Suzuki, H. Watanabe, Y. Oaki, and H. Imai, "Tuning of photocatalytic reduction by conduction band engineering of semiconductor quantum dots with experimental evaluation of the band edge potential,"

Chem. Commun., vol. 52, no. 36, pp. 6185–6188, Apr. 2016, doi: 10.1039/C6CC01166G.

[6] M. A. Butler and D. S. Ginley, "Prediction of flatband potentials at semiconductor-electrolyte interfaces from atomic electronegativities," *J. Electrochem. Soc.*, vol. 125, no. 2, pp. 228–232, Feb. 1978, doi: 10.1149/1.2131419/XML.

[7] Y. Wu, M. K. Y. Chan, and G. Ceder, "Prediction of semiconductor band edge positions in aqueous environments from first principles," *Phys. Rev. B*, vol. 83, art. no. 235301, 2011, doi: 10.1103/PhysRevB.83.235301.

[8] N. M. Anjan Kumar, S. Mukherjee, S. Ramesh, A. Mondal, V. Mahalingam, and N. Kamaraju, "Photoexcited ultrafast dynamics of free carriers and polarons in v2o5microparticles through time-resolved nondegenerate pump probe spectroscopy," *J. Phys. Chem. C*, Dec. 2022, doi: 10.1021/ACS.JPCC.2C06894/SUPPL_FILE/JP2C06894_SI_001.PDF.

[9] Y. Zhou, L. Liu, G. Li, and C. Hu, "Insights into the Influence of ZrO2 Crystal Structures on Methyl Laurate Hydrogenation over Co/ZrO2 Catalysts," *ACS Catal.*, vol. 11, no. 12, pp. 7099–7113, Jun. 2021, doi: 10.1021/ACSCATAL.1C00632/SUPPL_FILE/CS1C00632_SI_001.PDF.

[10] Y. Zou *et al.*, "Scalable and facile synthesis of V2O5 nanoparticles via ball milling for improved aerobic oxidative desulfurization," *Green Energy Environ.*, vol. 6, no. 2, pp. 169–175, Apr. 2021, doi: 10.1016/J.GEE.2020.10.005.

[11] A. Badreldin *et al.*, "Surface microenvironment engineering of black V2O5 nanostructures for visible light photodegradation of methylene blue," *J. Alloys Compd.*, vol. 871, p. 159615, Aug. 2021, doi: 10.1016/J.JALLCOM.2021.159615.

[12] F. Dong *et al.*, "In situ construction of g-C3N4/g-C3N 4 metal-free heterojunction for enhanced visible-light photocatalysis," *ACS Appl. Mater. Interfaces*, vol. 5, no. 21, pp. 11392–11401, Nov. 2013, doi: 10.1021/AM403653A/SUPPL_FILE/AM403653A_SI_001.PDF.

[13] M. Mousavi, A. Habibi-Yangjeh, and M. Abitorabi, "Fabrication of novel magnetically separable nanocomposites using graphitic carbon nitride, silver phosphate and silver chloride and their applications in photocatalytic removal of different pollutants using visible-light irradiation," *J. Colloid Interface Sci.*, vol. 480, pp. 218–231, Oct. 2016, doi: 10.1016/J.JCIS.2016.07.021.

[14] G. Xiao, X. Wang, D. Li, and X. Fu, "InVO4-sensitized TiO2 photocatalysts for efficient air purification with visible light," *J. Photochem. Photobiol. A Chem.*, vol. 193, no. 2–3, pp. 213–221, Jan. 2008, doi: 10.1016/J.JPHOTOCHEM.2007.06.027.

[15] E. A. Kraut, R. W. Grant, J. R. Waldrop, and S. P. Kowalczyk, "Semiconductor core-level to valence-band maximum binding-energy differences: Precise determination by x-ray photoelectron spectroscopy," *Phys. Rev. B*, vol. 28, no. 4, p. 1965, Aug. 1983, doi: 10.1103/PhysRevB.28.1965.

Environmental Challenges and Geochemical Approaches for the Prediction of Mining Waste

Hanae Chat[1], Farida Salmoun[1]

[1]Department Chemistry, University Abdelmalek Essaadi, Tager, Morocco
Corresponding author: Hanae Chat (hanae.chat@etu.uae.ac.ma)

Abstract

Mining, while essential for economic prosperity and social development, generates significant amounts of waste throughout its various stages. This waste, including tailings, sludge, and waste rock, often contains sulfur-bearing minerals. When exposed to oxygen, water, and microbial activity, this waste can produce acid mine drainage (AMD), leading to the acidification of mine effluents and the solubilization of metals. This process increases the environmental availability of potentially toxic metals. However, in the presence of neutralizing minerals, such as carbonates, the acidity generated by sulfide oxidation can be partially or completely neutralized. AMD is a major source of water pollution, causing the loss of aquatic organisms, altering soil structure, and impairing vegetation growth. Furthermore, the heavy metals released during this process pose a significant risk to human health due to their toxicity and bioaccumulation in food chains. Understanding the geochemical behavior of mine waste and its prediction are critical challenges for the effective rehabilitation of mining sites. This prediction is based on multi-scale tests conducted in laboratories or in the field, such as static tests, column leaching tests, weathering cells, and in situ experiments. Static tests provide a quick evaluation of neutralization and acidification potentials, offering a preliminary overview of the type of mine drainage. Complementarily, kinetic tests provide detailed information on mineral reactivity and the release rates of chemical species, enabling a deeper understanding of the mechanisms involved. Reliable AMD prediction requires consideration of several key aspects: (i) a rigorous sampling strategy and the textural properties of the waste, such as mineral liberation and association, and (ii) scale effects during kinetic tests. The geochemical behavior of mine waste is influenced by intrinsic factors, such as particle size, mineralogy, and chemical composition, as well as extrinsic factors, including test dimensions, rinsing frequency, liquid-to-solid ratios, and climatic conditions.

Keywords: AMD, Waste mining, Static tests, Kinetic tests

Design Dual-Band Microstrip Patch Antenna by Using a Rectangular Hole

Hassan Aldeeb[1,2]

[1]Electrical and Electronic Engineering Department, Misurata University, Misurata, Libya
[2]Research Scholar at Electrical Engineering Department, Colorado School of Mines, USA
Corresponding author: Hassan Aldeeb (e-mail: haldeeb@mines.edu)

Abstract

Patch antennas are used in different types of equipment for transmitter and receiver signals that operate at high frequencies many devices such as mobiles, wireless devices and satellites, because they have different features like small size, directivity, space-saving, and efficiency. By using this kind of antenna, wireless communications are remarkable and rapid development, to be used in the medical, industrial, educational, military and the Internet of Things and other applications.

We designed a dual-band frequencies patch antenna in this paper, by using a new approach, by making a rectangular hole in the patch antenna microstrip, we got it a dual-band antenna in one layer. Our This patch antenna was designed to work at 3.8 GHz for the first band and the second band is 6 GHz, and it works in the open frequencies field. The values of the attenuation (S_{11}) are equal to -42 dB for the first band and -32 dB for the second band, which are good and suitable values for both frequencies, and the same for the radiation patterns such as gain, radiation efficiency, and directivity.

Keywords: Microstrip patch antenna, Antenna, Dual-band, Advanced design system

1. INTRODUCTION

Different type of Patch antennas become demand for using in wireless communication and its application field, and many studies and research have done. These antennas are designed in many different frequencies and shapes, but most of them work on one frequency band.

Patch antenna is designed for different wireless applications, like Wi-Fi, Wi-MAX, RF energy harvesting, Cognitive radio, GSM, Radar, and ultra-wideband. In [1], they designed the antenna by making many different slots in the patch antenna with different lengths, sizes, and dimensions using microstrip line fading. They may obtain different frequencies at which this antenna works.

Malisuwan et al. [2], had designed a patch antenna that use in satellite communications, it operates on the Ku frequency, and modified the design by making the antenna in the shape of the letter E, so they got an antenna with with a bandwidth starting from 150MHz to 250MHz. Kaburcuk et al. [3], were designed the antenna to operate at dual frequency bands worked at 24 and 28 GHz, and the feed line was modified in three different dimensions to feed the antenna and to get the alignment between the input and the antenna. Some of these antennas are designed to work in the fifth-generation band. They explain the 5G bands, which work above 6 GHz according to the Federal Communication Commission (FCC) [4–6]. Sim et al. [7], designed a patch antenna in the shape of a ring to operate at the frequency of 2.4GHz, and their results matched the simulation with a narrow band, and the return loss was less than 30dB. By making different grooves in the patch antenna and different places and lengths, they obtain different bands of frequencies, which work at frequencies from 2.18 GHz to 2.41 GHz [8]. Wali et al. [9], had a new compact microstrip slot antenna with a Y-shaped design, their results show two available bands with –10 dB band S at 2.7 GHz and band C at 5 GHz. They designed a patch antenna Some researchers to work on the S-Band frequency and they got the desired results for the antenna to work so it can be used for applications such as GSM850, GSM900, DCS, PCS, UMTS, WWAN. [10–12].

2. ANTENNA DESIGN THEORY

Many advantages have microstrip patch antennas such as compatibility with integrated circuits, low cost, and easy to fabricate, but at the same time, it has some drawbacks, including narrow bandwidths and low gain [13]. It has different kinds of shapes and several ways to feed.

Fig. 1 shows a Microstrip patch antenna at FR4 board with two metal strips (patch), one on the top and the other on the ground with a dielectric sheet separated between them. In our research, we designed the antenna on an FR4 board with a fed line that has a 50 Ω input impudence, $H = 60$ mil, $\varepsilon_r = 4.25$, Cond. $= 5.813e7$, $T = 0.5$ mil, and $\tan \delta = 0.02$.
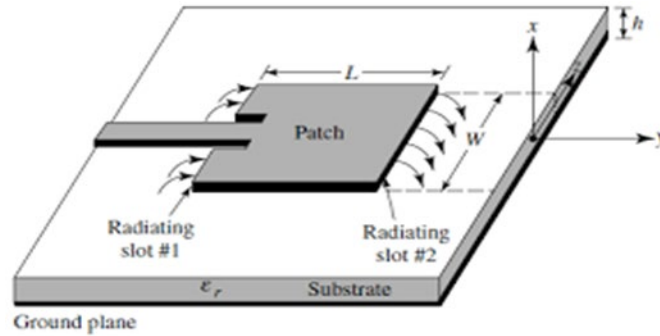
Figure 1. Microstrip patch antenna

Our proposed antenna has been designed to work as a dual-band microstrip patch antenna as shown in Fig. 2, by using Advanced Design System (ADS) software, which we need to calculate the width and length of the patch and dimensions of the feeding line.
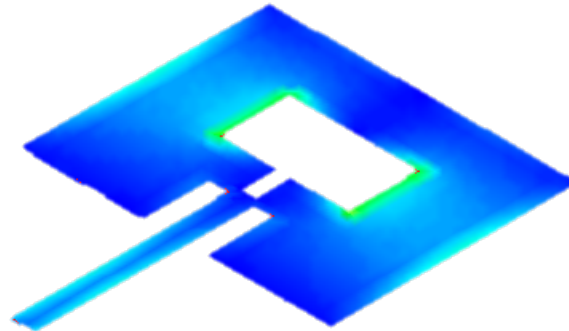
Figure 2. Dimensions of proposed antenna

To calculate the width W of the antenna from the equation [14].

$$W = \frac{c}{2f_c\sqrt{\frac{\varepsilon_r + 1}{2}}} \tag{1}$$

Where: W = Patch antenna width, $c =$ Speed of light, $f_c =$ Center frequency, and $\varepsilon_r =$ Dielectric constant of the substrate. The microstrip antenna length (L) is determined as following

$$L = \left(L_{eff} - 2\Delta L\right) \tag{2}$$

Where: $L_{eff} =$ The effective length of the patch and $\Delta L =$ The extended length.

$$L_{eff} = \frac{c}{2f_c\sqrt{\varepsilon_{reff}}} \tag{3}$$

$$\Delta L = h(0.412)\frac{\left(\varepsilon_{reff} + 0.3\right)\left(\frac{W}{h} + 0.264\right)}{\left(\varepsilon_{reff} - 0.258\right)\left(\frac{W}{h} + 0.8\right)} \tag{4}$$

ε_{eff} is the value of the effective dielectric constant, and can be calculated from the following equation:

$$\varepsilon_{reff} = \frac{\varepsilon_r + 1}{2} + \left(\frac{\varepsilon_r - 1}{2}\right) \cdot \frac{1}{\sqrt{1 + 12\dfrac{h}{W}}} \qquad (5)$$

Where h is the height of the substrate. The patch antenna is designed on a ground plan with width W_g and length L_g, which can be calculated from these equations:

$$W_g = 6h + W \qquad (6)$$

$$L_g = 6h + L \qquad (7)$$

3. SIMULATION RESULTS

By using the questions from (1) to (7), we get our patch antenna was designed on a dual band, the first band is 3.8 GHz, and the other band is 6 GHz, the antenna dimensions for both frequencies were obtained by optimizing the design to specific goals, as shown in Table 1.

Fig. 3 shows the layout of a circuit we designed in ADS, using the dimensions we calculated for both frequencies 3.8 GHz and 6 GHz as shown in Table 1, and the simulation results are shown in Fig. 4.

Table 1. Antenna design dimensions

Parameters	Values (3.8 GHz)	Values (6 GHz)
Impedance (Z_0)	50 Ω	50 Ω
Dielectric constant (ε_r)	4.25	4.25
Height of substrate	1.6 mm	1.6 mm
Copper Thickness	0.013 mm	0.013 mm
Loss tangent (δ)	0.002	0.002
Width of the patch (W)	38.6 mm	16 mm
Length of the patch (L)	30 mm	12 mm
Ground plane width (W_g)	48.2 mm	25.6 mm
Ground plane length (L_g)	39.6 mm	21.6 mm
Feeding width (W_f)	3.24 mm	1.62 mm
Feeding length (L_f)	23 mm	9.6 mm
Gap width (W_s)	2.24 mm	0.79 mm
Gap length (L_s)	8.2 mm	3.3 mm

In the simulation results, we had some good outcomes, where we got the dual band as we designed, the first one at 3.84 GHz with around -42 dB return loss, and the second band at 5.97 GHz which approximately is equal to the frequency designed with a decent return loss at -32 dB.

Fig. 5 depicts a 3D simulated radiation pattern for the proposed antenna configuration at 3.8GHz with a maximum gain of 3.6 dBi, a directivity of 7.74 dBi, and a radiation efficiency was about 38.54%. In comparison to the second frequency at 6GHz, where the gain was at 3.3 dBi, the directivity was 6.5 dBi, and the radiation efficiency was 47.89%.
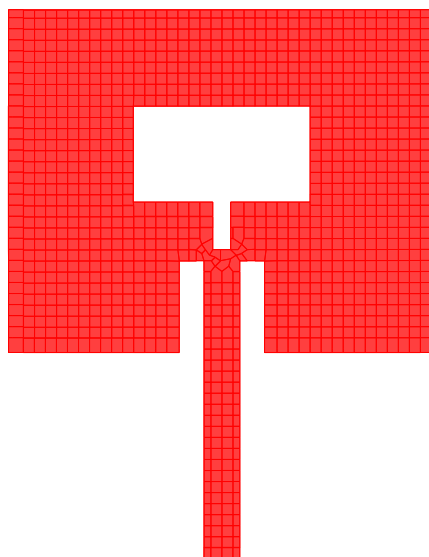
Figure 3. A layout of the patch antenna
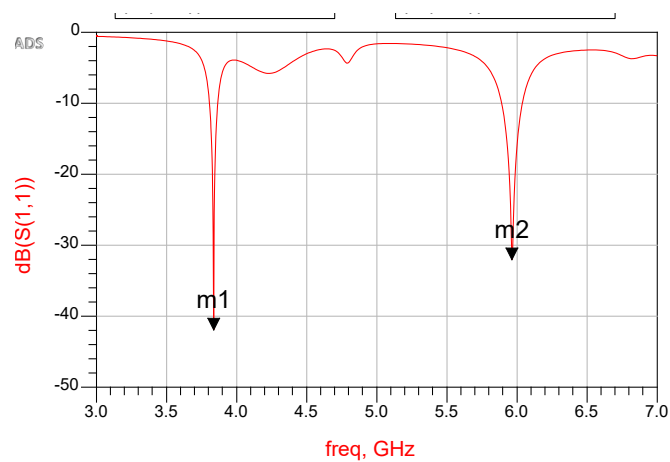
Figure 4. Simulation results from ADS

The following figures compare the parameters between the two bands that the patch antenna was designed to work with. Fig. 6 shows the gain and directivity at 3.8 GHz and 6 GHz. Figs. 7 and 8 show the Radiation Intensity and Electric Far Field at 3.8 GHz and 6 GHz.
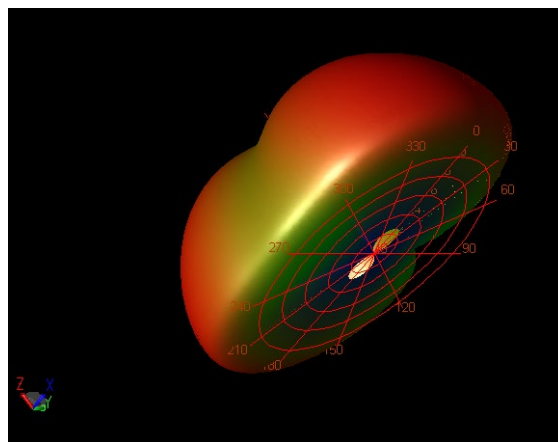
Figure 5. A 3D radiation pattern from ADS
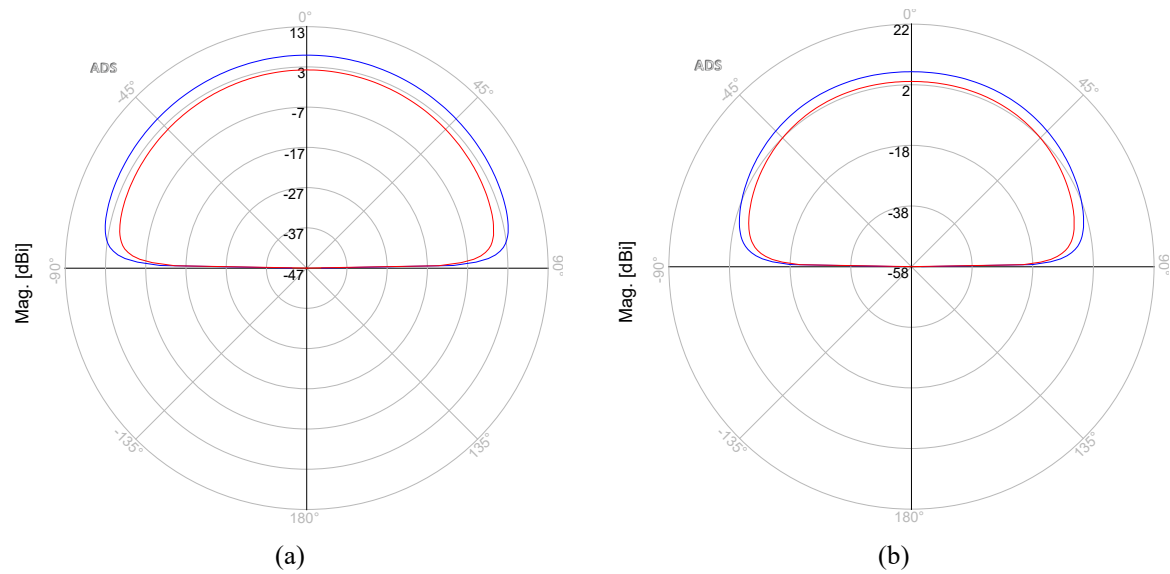
Figure 6. Gain, directivity, (a) 3.8 GHz, (b) 6 GHz
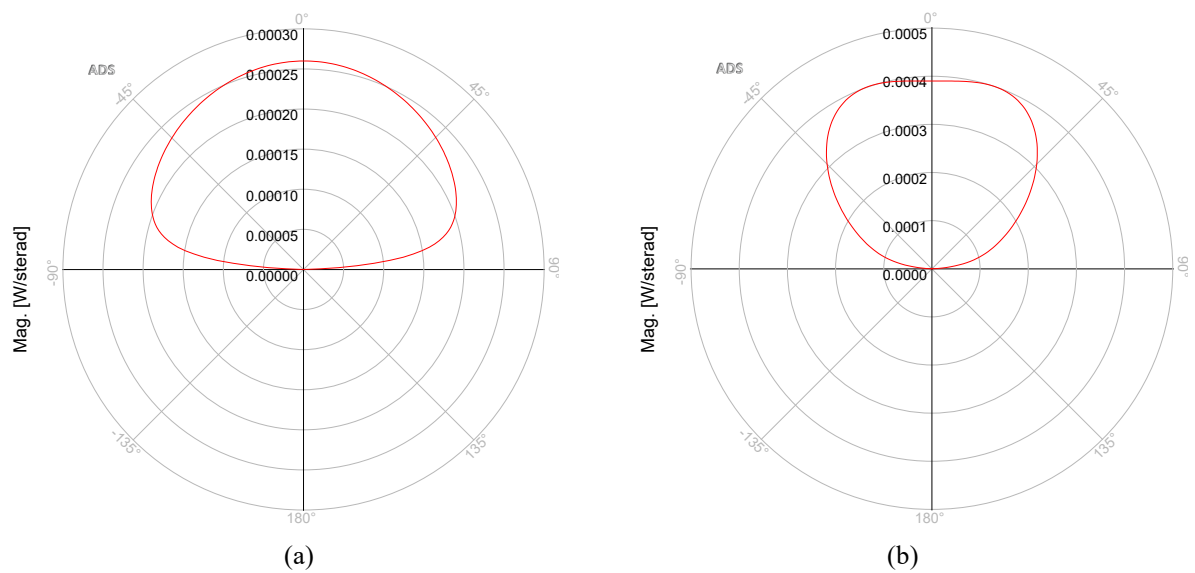
Figure 7. Radiation intensity, (a) 3.8 GHz, (b) 6 GHz
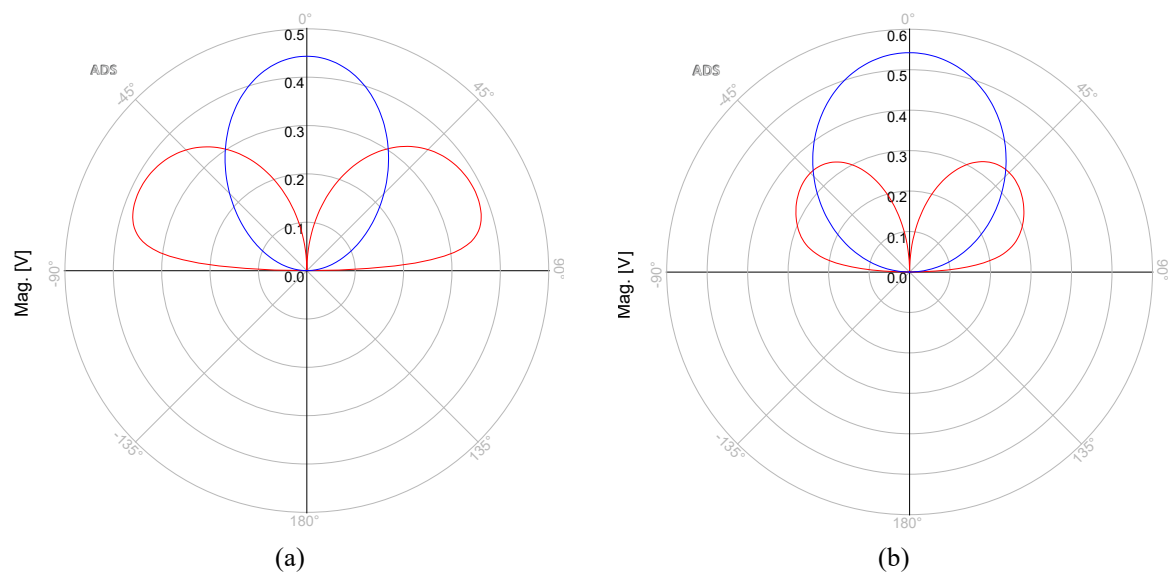
Figure 8. Electric far field, (a) 3.8GHz, (b) 6 GHz

4. CONCLUSION

In this research paper, we designed a microstrip patch antenna for dual-band frequencies at 3.84GHz and 6GHz by making a rectangular hole inside. In the simulation results for this antenna in ADS software, we got the return loss (S11) values for both bands were about -42 dB and -32 dB, respectively. We got a good result for the radiation efficiency, the radiation pattern for both bands, gains, and directivities. Thus, we designed a dual-band microstrip patch antenna with a new approach (Rectangular Hole) to get a dual-band patch antenna.

References

[1]   V. Bankey and N. A. Kumar, "Design and performance issues of microstrip antennas," *International Journal of Scientific and Engineering Research*, vol. 6, no. 3, pp. 1572–1580, 2015.

[2]   S. Malisuwan, J. Sivaraks, N. Madan, and N. Suriyakrai, "Design of microstrip patch antenna for Ku-band satellite communication applications," *International Journal of Computer and Communication Engineering*, vol. 3, no. 6, pp. 413–416, 2014.

[3]   F. Kaburcuk, G. Kalinay, Y. Chen, A. Z. Elsherbeni, and V. Demir, "A dual-band and low-cost microstrip patch antenna for 5G mobile communications," *ACES Journal*, vol. 36, no. 7, pp. 824–829, Oct. 2021.

[4]   "Global update on 5G spectrum," [Online]. Available: https://www.qualcomm.com/media/documents/files/spectrum-for-4g-and-5g.pdf

[5]   Available: https://www.5gamericas.org/wpcontent/uploads/2019/07/5G_Americs_Spectrum_Recommen dations_for_the_U.S_Final.pdf

[6]   "America's 5G future," [Online]. Available: https://www.fcc.gov/5G

[7]   C. Sim, M. Chang, and B. Chen, "Microstrip-fed ring slot antenna design with wideband harmonic suppression," *IEEE Transactions on Antennas and Propagation*, vol. 62, no. 9, pp. 4828–4832, Sep. 2014.

[8]   O. Ossa-Molina and F. López-Giraldo, "A simple model to compute the characteristic parameters of a slotted rectangular microstrip patch antenna," *Electronics*, vol. 11, no. 1, art. no. 129, 2022.

[9]   O. Rawia, G. Said, A. Gharsallah, and R. Tchanguiz, "Analysis and design of a new dual band microstrip patch antenna based on slot matching Y-shaped," *Journal of Engineering Research*, vol. 11, no. 2, pp. 89–97, 2015, doi: 10.24200/tjer.

[10]   G. T. Bharathy, G. Bhargavi, S. Bhavanisankari, and T. Tamilselvi, "Rectangular microstrip patch antenna design and simulation for single S-band frequency using ADS," in *Proceedings of International Conference on Smart Structures and Systems-ICSSS'18*, 2018, pp. 66–71.

[11]   A. K. Al-Azzawi, "New design approach of a "2.4 GHz" slotted rectangular patch antenna with a wideband harmonic suppression," *Arabian Journal for Science and Engineering*, Apr. 2021.

[12]   P. Sharma and D. Kumar, "Design and optimization of dual band antenna with DGS for IoT applications," *International Journal of Advance Research, Ideas and Innovations in Technology*, vol. 5, no. 1, pp. 601–603, Feb. 2019.

[13]   C. A. Balanis, Antenna Theory; Analysis and Design, 3rd edition, New York: Wiley and Sons, 2005.

[14]   N. C. Okoro and L. I. Oborkhale, "Design and simulation of rectangular microstrip patch antenna for X-band application," *Umudike Journal of Engineering and Technology*, pp. 1–8, 2019.

Numerical Study of a Compressible Flow in a Convergent-Divergent Transonic Diffuser

Habib Merouane[1], Rachid Sahnoun[1], Ismail Drai[1]

[1]Department of Mechanical Engineering, University of Mustapha Stambouli Mascara, Algeria
Corresponding authors: Habib Merouane (e-mail: merouanehabib@yahoo.fr)

Abstract

We present in this work a numerical simulation of a convergent-divergent nozzle similar to a rocket/ramjet nozzle where air flows inside this convergent-divergent nozzle. The role of this study is to identify and characterize the behavior of the fluid inside this nozzle for different flow regimes where the intensity of turbulence and the Mach number have varied. The RANS approach is adopted for our study with the application of the first-order turbulence model. The finite volume method is chosen for the resolution of the discretized equations by using a CFD calculation code. The coupled algorithm is adopted to treat the coupling between pressure and velocity. The results obtained numerically are compared with the experimental.

Keywords: Compressible flow, Convergent, Convergent divergent, Transonic diffuser, Rocket, Nozzle

Numerical Investigations on the Effect of Isothermal Multi-Jets in Air Curtains with LES Approach

Rachid Sahnoun[1], Ismail Drai[1], Habib Merouane[1]

[1]Department of Mecanic, University Mustapha Stambouli, Mascara, Algeria
Corresponding author: Rachid Sahnoun (e-mail: r_sahnoun@yahoo.fr)

Abstract

This work focuses on the analysis of the turbulent intensity of the flow field resulting from planar jets applied in air curtains systems, which are used in various industry sectors. The air curtains allow realizing cellular containment. Hence, the main objective is to improve the quality of confinement's separation by air curtains. In order to achieve this target, the jet flow must be as laminar as possible. Numerical LES investigations are carried out in this study. A jet impingement against a flat and a smooth surface without recirculation has been used for this assessment. The WALE (Wall Adapting Local Eddy) structure models the subgrid-scale tensor. First, the configuration of air curtain with a single jet and then with a twin-jet are investigated. Result comparisons to available experimental measurements have been performed and good agreements have been noticed. The study is then extended for the first time to air curtain configurations with more than two planar jets. The configuration of the triple jet indicates a lower turbulence level than the single jet and the twin-jet ones. This improves the confinement's separation quality. However, increasing the number of jets highlights a limit because the turbulence decrease will be not significant beyond a certain number of jets taking into account the operating conditions. In this study, an effective process shows that, the four jets configuration is considered as the better compromise under the considered operating conditions.

Keywords: Multi-jets, LES approach, Plan curtain, Planar jet, Turbulence

Synthesis and Structural Refinement of Bismuth-Based Pyrochlore Oxides

Rafik El Arslene Dra[1], Amira Ghislaine Dra[2], Lynda Amel Chaabane[3]

[1]Department of Energy and Process Engineering, Djillali Liabes University, Sidi Bel Abbes, Algeria
[2]Department of Biology Sciences, Djillali Liabes University, Sidi Bel Abbes, Algeria
[3]Physical-Chemistry of advanced materials Laboratory (LPCMA), Djillali Liabes University, Sidi Bel Abbes, Algeria
Corresponding author: Rafik El Arslene Dra (e-mail: dra.rafik@gmail.com)

Abstract

the aim of this work is the synthesis of an advanced material in the form of a pyrochlore-like solid solution $Bi_{1,5-x}Ca_xSb_{1,5}CuO_{7-\delta}$ by conventional ceramic solid-state reaction with $0 \leq x \leq 0.4$. Samples were characterised by X-ray powder diffraction (XRPD), scanning electron microscopy (SEM) and electrical conductivity measurements. The formation of a single pyrochlore phase was confirmed for all x fractions, in particular that of the x=0.2 fraction, by Rietveld refinement. The variation in electrical resistivity as a function of x of all the samples, measured using a four-probe device at room temperature, indicates that these samples remain insulators. Electrical conductivity measurements at high temperature and different frequencies, using a two-electrode device, revealed a maximum electrical conductivity of 4.7×10^{-3} S.cm-1 achieved at $x = 0.2$, generating an activation energy of 0.14 eV, making them favourable candidates as solid electrolytes in fuel cells. For this fraction in particular, structural refinement by Rietveld of the X-ray diffractogram of the corresponding powder confirmed the typical cubic space group Fd-3m with a cell parameter of a = 10.4089(1) Å.

Keywords: Pyrochlore, Solid solution, Bismuth, Rietveld refinement, Electrical conductivity

Evaluation of Structural and Optical Properties of Pristine and Cu-Doped Zno Thin Films

Khemissi Lahouel[1,2], Meriem Gasmi[1,2], Abdecharif Boumaza[1,2], Abdelkader Djeloul[1,2]

[1]Laboratory of Structures, Proprieties and Inter Atomic Interactions (LASPI2A), Faculty of Science and Technology, University of Abbes Laghrour, Khenchela 40000 Algeria
[2]Department of Matter Sciences, University of Abbes Laghrour, Khenchela, Algeria
Corresponding author: Khemissi Lahouel (e-mail: lahouel.khemissi@gmail.com)

Abstract

Zinc oxide (ZnO), is the material versatile inorganic compound with exceptional characteristics, including a wide band gap 3.10-3.37 eV, high chemical stability, a broadened radiation absorption spectrum, high photostability with the molecular formula ZnO, high exciton binding energy of 60 meV, high piezoelectric constant, low dielectric constant. This material can therefore be utilized in a wide range of technological applications, such as photodetectors, photocatalytic, optoelectronic, gas sensors, solar cells, piezoelectric devices, and UV light. Several techniques have been employed to create ZnO thin films like sol-gel (deep coating, spin coating), spray pyrolysis, chemical vapor deposition, electrochemical deposition, metal organic CVD (MOCVD), DC magnetron sputterin. In the current investigation, we employed the ultrasonic spray pyrolysis (USP) procedure to prepare thin film samples, which is a relatively easy, and low-cost technique that doesn't require complex equipment, to further expound at 450 °C, layers of pure and Cu-doped ZnO with atomic concentrations of 1, and 3% were applied to glass substrates, X-ray diffraction, SEM, EDS, and UV-visible spectroscopy were used to analyzes these layers.

Keywords: Ultrasonic spray pyrolysis, ZnO thin film, X-ray diffraction

The Influence of Nanofluids (Tio2, Sio2, Tio2/Sio2) on Asphaltenes Precipitation

Billel Zahaf[1], Issam Bouyahyaoui[1]

[1]Process Engineering Department, Faculty of Hydrocarbons & Chemistry, University M'Hamed Bougara, 35000 Boumerdes, Algeria
Corresponding author: Billel Zahaf (e-mail: zahafbillel10@gmail.com)

Abstract

Asphaltenes are the heavy and polar fraction of crude oil, it causes undesirable precipitation problems in crude oil mining, transportation and refining. One of the parameters that influence the precipitation of asphaltenes is the viscosity, therefore our research is based on decreasing this parameter of asphaltene crudes using nanofluids depending on the structure of asphaltenes. Firstly, we determined the viscosity of asphaltene crude as a function of the shear rate and then in the presence of nanofluids with the oil studied. The viscosity measurements were carried out in solutions (heptane/toluene) containing 20 g/L of the vacuum residue oil in toluene and nanofluids of (TiO2, SiO2 and the melange TiO2/SiO2 with the same ratio). The results obtained show that the nanofluids significantly decrease the viscosity of asphaltenic vacuum residue oil especially.

Keywords: Asphaltenes, Vacuum residue, Precipitation problems, Nanofluids, Viscosity

Turbulent and Heat Transfer Investigation of Artificially Roughened Solar Air Heater with Curved Absorber Plate

Boucif Zina[1], Zerrouki Abdelwahhab[2], Abdelkader Filali[3], Ahmed Remlaoui[4]

[1]Djilali Liabes University, Sidi bel abbes, Algeria
[2]Center of Research in Mechanics CRM, Constantine, Algeria
[3]Chemical Engineering Department, Imperial College London, South Kensington, London SW7 2AZ, United Kingdom
[4]Applied Hydrology and Environment Laboratory, University of Ain Temouchent-Belhadj Bouchaib, Algeria
Corresponding author: Boucif Zina (boucif.zin@gmail.com)

Abstract

Many attempts are being made to investigate the different design configurations of solar air heaters (SAHs) in order to enhance the heat transfer rate without increasing the power required by the pump. In this paper, instead of an absorber flat plate, a curved absorber plate) having triangular artificial roughness with semi-circular nooks is employed in order to conduct a comparative study. The main objective of this investigation is to improve the heat transfer with minimum pressers drop, and determination of the optimum value of pitch that provides the best thermo-hydraulic performance. The technique uses the concept of providing a curved heat plate at fixed value of ratio of depth curved (e/D = 0.12) with different geometrical parameters of the ribs, the geometrical parameters of the artificial roughness having semi-circular nooks such as the roughness pitch ratio (P/e =7.14, 10.70, 14.28 and 17.86) for several *Re* number varied between 3800 to 18000. An imposed uniform heat flux is considered, and the flow and energy equations are solved with the association of two transport equation for the kinetic turbulence energy *k* and the dissipation rate ε with the selected RNG k-ε turbulent model. Obtained results indicates that the increased the Nusselt number (Nu) by approximately 55.94% compared to the regular one and Thermo-Hydraulic Performance (THPP) strongly depends on the different investigated geometrical parameters and Re number. The best solar air heater performance could be obtained for *P/e* = 14.28, *e/D* = 0.042.

Keywords: Solar air heater, Curved absorber plate, Artificial roughness, THPP, Heat transfer, Friction factor
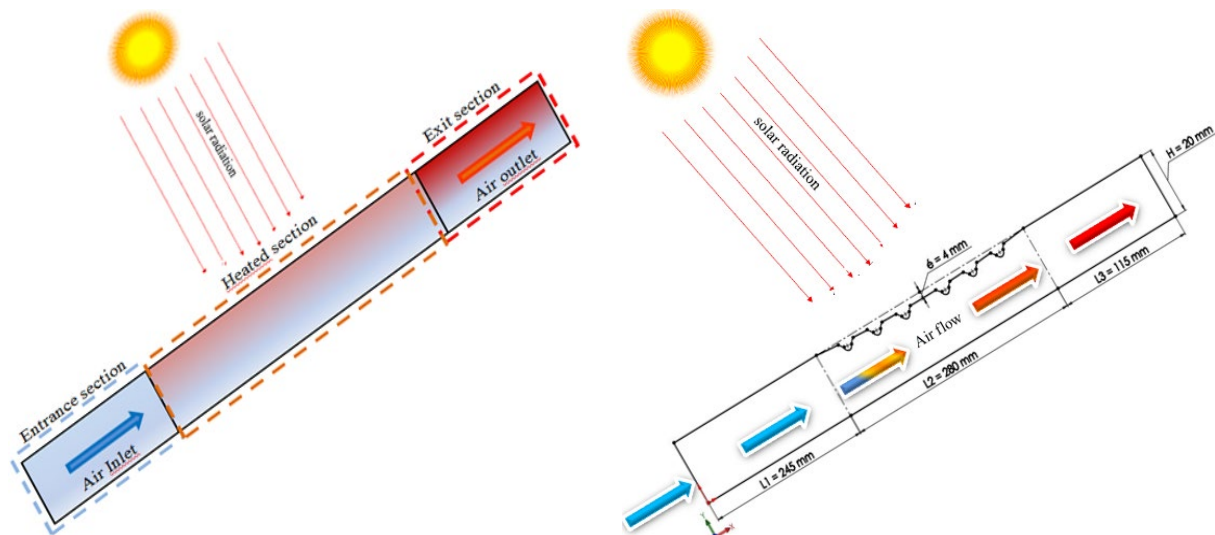
Figure 1. Configurations of solar air heart

Pyrolysis Temperature Effect on the Properties of Polyaniline Based Nitrogen Doped Carbon Supports for PEM Fuel Cells

Emine Oner[1], Ayse Bayrakceken[1,2]

[1]Chemical Engineering Department, Ataturk University, Erzurum, Türkiye
[2]Nanoscience and Nanoengineering Department, Ataturk University, Erzurum, Türkiye
Corresponding author: Ayse Bayrakceken (e-mail: ayse.bayrakceken@gmail.com)

Abstract

In this study, polyaniline is used as the nitrogen source for doping carbon black. Aniline is polymerized over the carbon black via chemical oxidative polymerization and carbon to nitrogen ratio (C/N) was set to 1:1. Then the composites were pyrolyzed at four different pyrolysis temperatures such as 600, 700, 800, and 900 °C. These nitrogen doped support materials were used in order to synthesize Pt based electrocatalysts by using microwave irradiation technique. Physical characterization was used to determine the structural and morphological properties of the supports and the electrocatalysts. The polymer electrolyte membrane (PEM) fuel cell test was used to determine the activity of the electrocatalysts. It was observed that the properties of the materials and also the performance of the PEM fuel cell significantly affected by the pyrolysis temperature.

Keywords: PEM fuel cell, Electrocatalyst, Polyaniline, Carbon support, Nitrogen doping

1. INTRODUCTION

Among alternative fuels, hydrogen is the most efficient and useful energy carrier. Hydrogen is seen as the solution to future energy problems worldwide. Hydrogen energy and fuel cells are seen as the most promising clean, alternative energy source of the future, as they have low or zero carbon emissions and environmental pollution due to the production of hydrogen from non-renewable or renewable energy sources. Fuel cell is the power generation element that converts the chemical energy of the fuel and oxidant provided externally to the system directly into usable energy in the form of electricity and heat. Fuel cell technology has become the focus of attention for many researchers due to its advantages such as producing high-efficiency energy from the fuel used, having no moving parts, requiring little maintenance, and being easily used in mobile applications. There are six types of fuel cells that can be preferred according to the utilization area and conditions in which they will be used, and one of them is the polymer electrolyte membrane (PEM) fuel cells. PEM fuel cells seem to be a promising choice in energy conversion due to their outstanding properties including low operating temperature and high power density. Commercialization of these systems are dealing with the decrease of the cost of the components [1].

Electrocatalysts used in these fuel cells are mostly carbon supported platinum group metals (PGM) which improve the sluggish oxygen reduction reaction. In order to decrease the cost of the PGM based catalysts and increase the activity of the electrocatalysts different routes are followed. One promising way is the modification of the carbon support with the heteroatom doping to provide new active sites [2]. Among the other heteroatoms nitrogen seem to be a good candidate for doping of carbon due to their comparable atomic sizes and also strong covalent bonding ability [3]. There are different types of nitrogen precursors for doping and among them polyaniline is a promising precursor which is a nitrogen containing conducting polymer.

In this study, nitrogen doping of carbon black is achieved by using the polymerized aniline over carbon black and pyrolysing them at different temperatures such as 600, 700, 800, and 900 °C.

2. MATERIAL AND METHOD

2.1. Synthesis of Nitrogen Doped Carbon Materials and Electrocatalysts

For material synthesis at a C/N ratio of 1:1, first HCl was placed in a beaker mud aniline was added. The mixture was stirred in an ultrasonic bath for 30 minutes and carbon black was added and stirred at room temperature for 5 h. HCl was placed in a separate beaker and APS was added. The second solution was added dropwise to the first solution during vigorous stirring. The polymerization process took place in an ice bath with temperature control

for 10 h. It was ensured that the temperature did not exceed 5 °C. The mixture was then filtered and washed with alcohol and deionized water. It was dried in the oven at 80 °C for 24 h. The structures obtained in the synthesis were pyrolyzed in an Ar gas atmosphere at pyrolysis temperature values of 600, 700, 800, and 900 °C.

Electrocatalysts were synthesized by using microwave irradiation technique. In this method, ethylene glycol was used as solvent and also reducing agent. A domestic microwave oven was used as microwave source for the reduction of Pt ions to its metallic form.

2.2. Characterization of the synthesized materials

Synthesized materials were characterized by using elemental analysis, SEM images, BET analysis, and electrochemically by PEM fuel cell tests.

3. RESULTS

Elemental analysis results of the nitrogen doped carbon support materials are given in Table 1. As can be seen from table that the nitrogen content is getting decreased as the pyrolysis temperature increase.

Table 1. Elemental analysis results of the support materials

Pyrolysis Temperature (°C)	C (%)	H (%)	N (%)	O (%)
600	59.31	1.16	5.01	0.08
700	53.20	0.57	3.76	0.10
800	66.60	0.38	3.47	0.29
900	70.40	0.30	2.45	0.22

Figure 1 shows the SEM images of plain Vulcan and nitrogen-doped carbon structures. The change that occurs when nitrogen is added to the plain Vulcan structure is evaluated. C/N structures show spherical-like nanostructures resulting from the formation of core-shell nanoparticles. In addition, the fiber-like structure of polyaniline (PANI) is clearly observed in the images of nitrogen-doped supports.

C/N 1:1 600 °C   C/N 1:1 700 °C

C/N 1:1 800 °C   C/N 1:1 900 °C

C/N 1:1 800 °C   C/N 1:1 900 °C

Plain Vulcan
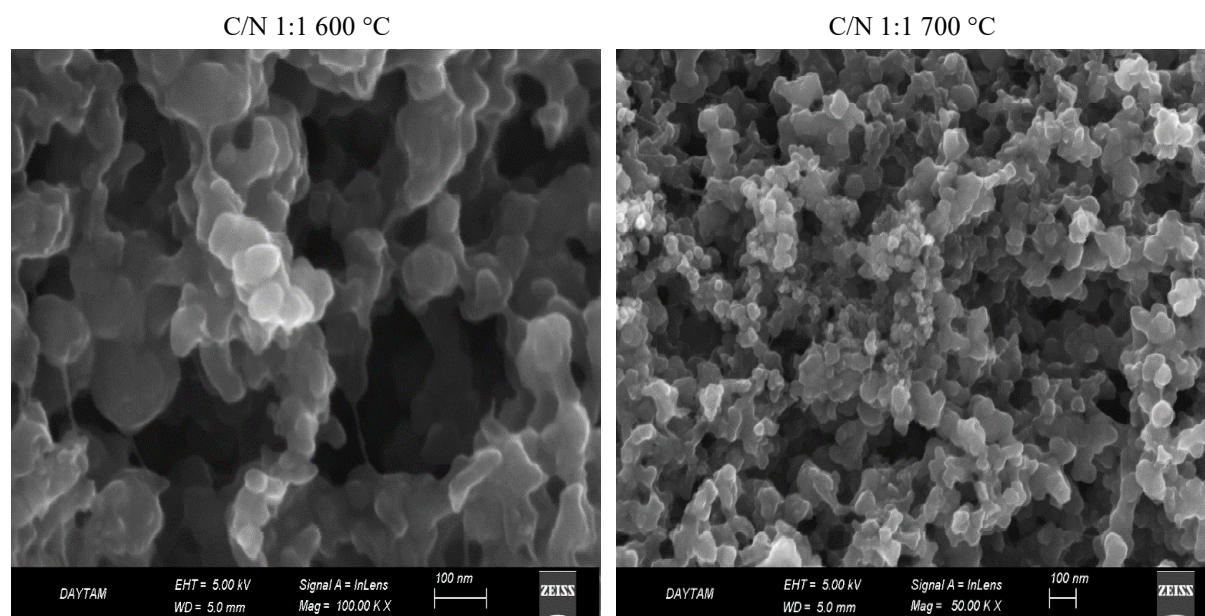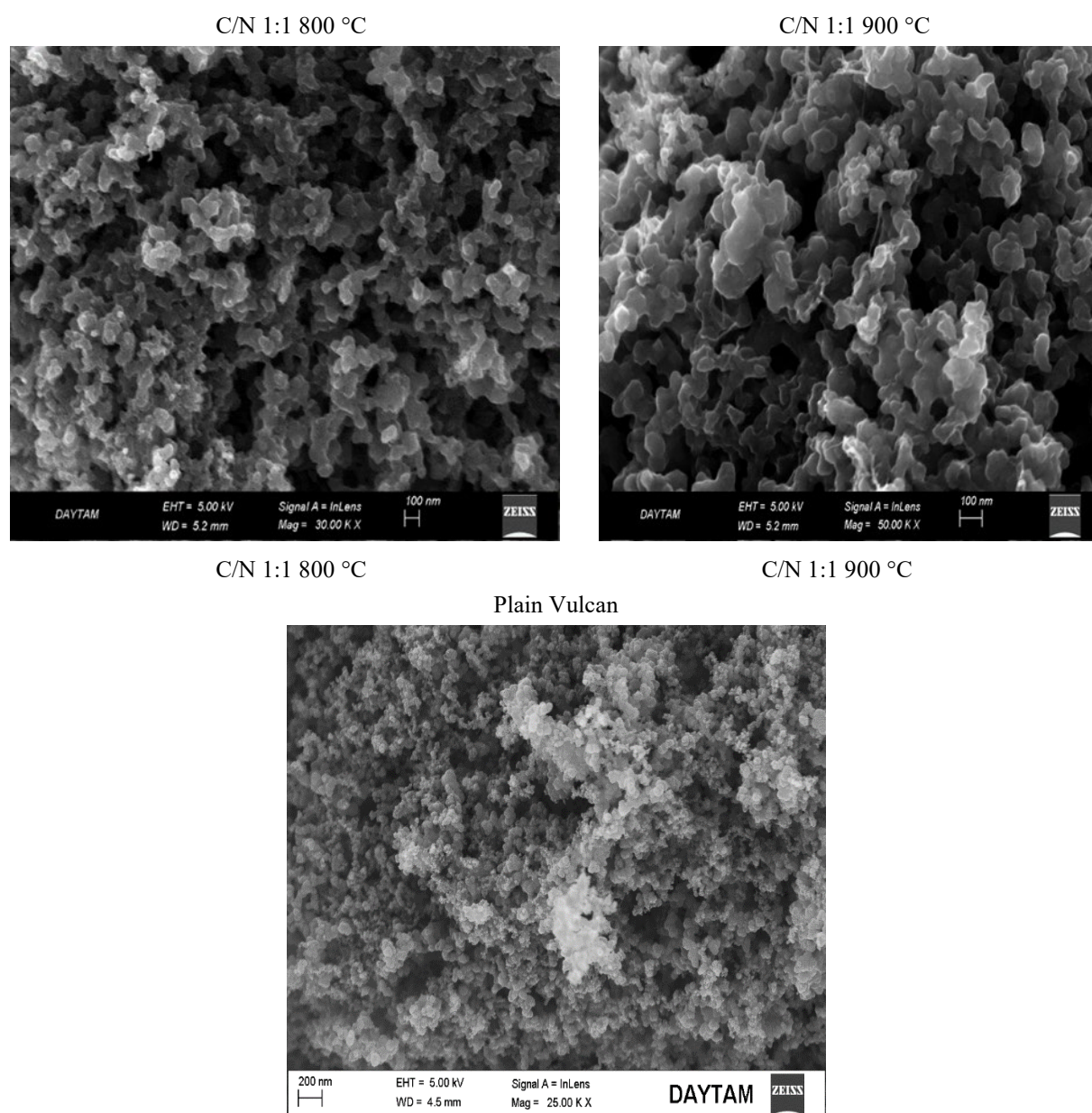
Figure 1. SEM images of Vulcan and nitrogen doped support materials

Nitrogen adsorption/desorption analysis is used to get structural information about the support materials. Structural properties are summarized in Table 2. It was observed that the BET surface area of the support materials are getting decreased with an increase in pyrolysis temperature.

Table 2. BET analysis results of the support materials

Pyrolysis Temperature (ºC)	BET Surface Area (m²/g)	Average Pore Diameter (nm)	BJH Pore Volume (cm³/g)
600	150.67	4.71	0.45
700	110.44	5.73	0.43
800	91.52	6.68	0.41
900	81.05	6.80	0.41

PEM fuel cell performance results are summarized in Table 3. As can be seen from table that the best PEM fuel cell performance was obtained for the pyrolysis temperature of 900 ºC.

Table 3. PEM fuel cell performance results of the electrocatalysts

Catalyst	Current Density @0.6 V (mA/cm^2)	Power Density @0.6 V (W/cm^2)
600	183.45	0.11
700	111.56	0.07
800	176.87	0.11
900	421.54	0.25

4. CONCLUSION

Nitrogen doped carbon black support materials were obtained by using polyaniline as nitrogen source. After the polymerization of aniline over carbon black pyrolysis temperature was changed in between 600 to 900 ºC. The nitrogen content decreased significantly with an increase in pyrolysis temperature. the best PEM fuel cell performance was obtained for the pyrolysis temperature of 900 ºC. These results showed the importance of pyrolysis temperature on the properties and also the activity of the elecetrocatalysts.

Acknowledgments

References

[1]   F. Barbir, *Pem Fuel Cells: Theory and Practice*, 2nd ed. Academic Press, 2012.
[2]   H. Tao, Y. Gao, N. Talreja, F. Guo, J. Texter, C. Yan, et al., "Two-dimensional nanosheets for electrocatalysis in energy generation and conversion," *Journal of Materials Chemistry A*, vol. 5, pp. 7257–7284, Mar. 2017.
[3]   D. Higgins, P. Zamani, A. Yu, and Z. Chen, "The application of graphene and its composites in oxygen reduction electrocatalysis: A perspective and review of recent progress," *Energy & Environmental Science*, vol. 9, pp. 357–390, Jan. 2016.

Co@Pt/C Based Gas Diffusion Electrodes Prepared by Magnetron Sputtering for PEM Fuel Cells

Sonnur Kurtulus[1], Ayse Bayrakceken[1,2]

[1]Chemical Engineering Department, Ataturk University, Erzurum, Türkiye
[2]Nanoscience and Nanoengineering Department, Ataturk University, Erzurum, Türkiye
Corresponding author: Ayse Bayrakceken (e-mail: ayse.bayrakceken@gmail.com)

Abstract

In this study, in order to reduce the amount of Pt/C electrocatalysts which are commonly used in the proton exchange membrane (PEM) fuel cells, thin film coatings were formed on different amounts of Pt/C surfaces of gas diffusion electrodes with different amounts of transition metals using the magnetron sputtering method. It is aimed to reduce the use of platinum for the gas diffusion layer, the most costly component of fuel cell systems, and to increase performance and reduce costs by using cheaper metals. In this aspect, firstly gas diffusion electrode was prepared by spraying the ink of Pt/C based solution over the gas diffusion layer. Then magnetron sputtering of Co metal was used to prepare thin film of Co over the Pt/C coated gas diffusion electrode. In order to determine the effect of the amounts of Pt/C and Co coated on the gas diffusion layer, Pt/C amount and also sputtering time were changed. This two layer gas diffusion electrode was then characterized physically by using characterization techniques. These gas diffusion electrodes were electrochemically characterized by using the PEM fuel cell test. Significant performance changes were observed for the gas diffusion electrodes having different amounts of Pt/C and Co.

Keywords: PEM fuel cell, Electrocatalyst, Gas diffusion electrode, Magnetron sputtering, Thin film

1. INTRODUCTION

Proton exchange membrane (PEM) fuel cells are the devices that are suitable for portable and mobile applications. The commercialization of these energy conversion devices will be achieved by decreasing the cost of the components mainly which depends on electrocatalyst cost. Carbon supported platinum based electrocatalysts are the promising ones as the hydrogen oxidation reaction (HOR) and oxygen reduction reaction (ORR) electrocatalysts which are occurred the anode and cathode sides of the PEM fuel cells, respectively. Mostly platinum based carbon supported electrocatalysts are used for PEM fuel cells. The financial burden of platinum, one of the expensive metals used in catalysts, is one of the biggest obstacles to fuel cell technology. In addition to the metal used as a catalyst, various support materials can also be developed. Various metals are actively used in catalysts, and the rarity or cost of the metal used can be a problem for the system. Platinum group metals (PGM) are the alternatives as the electrocatalysts such as platinum (Pt), ruthenium (Ru) or palladium (Pd) are known as PGMs, non-platinum group metals are lower cost and have no supply problems, such as cobalt (Co), nickel (Ni), copper (Cu) and iron (Fe). Scientists aim to reduce the cost burden brought by platinum by bringing together cheaper metals.

The limiting factor at the heart of fuel cell systems is the oxygen reduction (ORR) mechanism that operates on the cathode side. Platinum is used on both the anode and cathode sides of the fuel cell system and is one of the main cost drivers. Experiments with various combinations of inexpensive metals (Fe, Co, Cu, Ni, etc.) have attempted to overcome the limitations of the ORR mechanism and increase activity for the cathode side. Studies on inexpensive metals in particular show that cobalt and nickel are among the most important options. Even just a few examples of catalysts developed using inexpensive metals show that bimetallic catalysts are promising. In studies conducted, scientists have found various innovative approaches to improve the distribution of platinum on the surface and its surface-specific activity. In the literature, platinum was developed as a monolayer catalyst and by placing all platinum atoms on the particle surface, minimum platinum usage in the mass of the nanoparticle was achieved [1]. It was observed that it can have twice the activity compared to the platinum/carbon (Pt/C) structure.

Magnetron sputtering is preferred for controlled and uniform distribution of nanoparticles of platinum or bimetallic materials on a substrate with low Pt loading and homogeneous particle distribution, which improves both metal

utilization and ORR activity of the electrocatalyst. Sputtering has found wide application in fuel cell electrocatalysis, ranging from Pt deposition on carbon-based supports, metal oxides and oxide-carbon composites to the fabrication of bimetallic catalysts and membrane electrode assemblies (MEAs) which are the heart of the fuel cells [2].

In this study, firstly Pt/C based gas diffusion electrodes were prepared by using spray method and then in order to decrease the amount of Pt/C a cheap metal, Co, was sputtered via magnetron sputtering over this electrode.

2. MATERIAL AND METHOD

Gas diffusion electrodes (GDEs) with different platinum loadings were prepared by spraying commercially purchased Tanaka catalyst (Pt/C, 67%) over gas diffusion layers (GDLs). Platinum loading amounts were changed between 0.05 and 0.4 mg Pt cm^{-2} in an increasing direction. Then, thin film coatings of Co metal was applied to the prepared GDEs by Magnetron Sputtering method for 60 and 300 seconds (Figure 1). These electrodes were used as cathode side and anodes side was obtained only by using commercial Tanaka catalyst. Physical and electrochemical characterizations of the prepared electrodes were investigated.
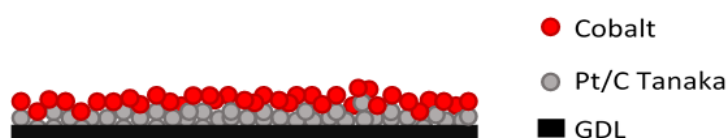
Figure 1. Schematic representation of GDE preparation

3. RESULTS

The morphological changes of the GDEs were investigated by using SEM. SEM images of the corresponding electrodes are given in Figure 2. From SEM images at different magnifications, it was observed that the layer on the GDL became more distinct and a denser surface was formed due to the increasing amount of Pt on the catalyst surface. This situation was more evident in the samples prepared by magnetron sputtering with cobalt metal for 60 seconds. It was observed that less cobalt metal was distributed evenly on the surface and into the pores compared to the samples coated for 300 seconds. From SEM analyses, it was observed that the amount of metal deposited on the surface increased as the duration of the treatment with magnetron sputtering application increased.
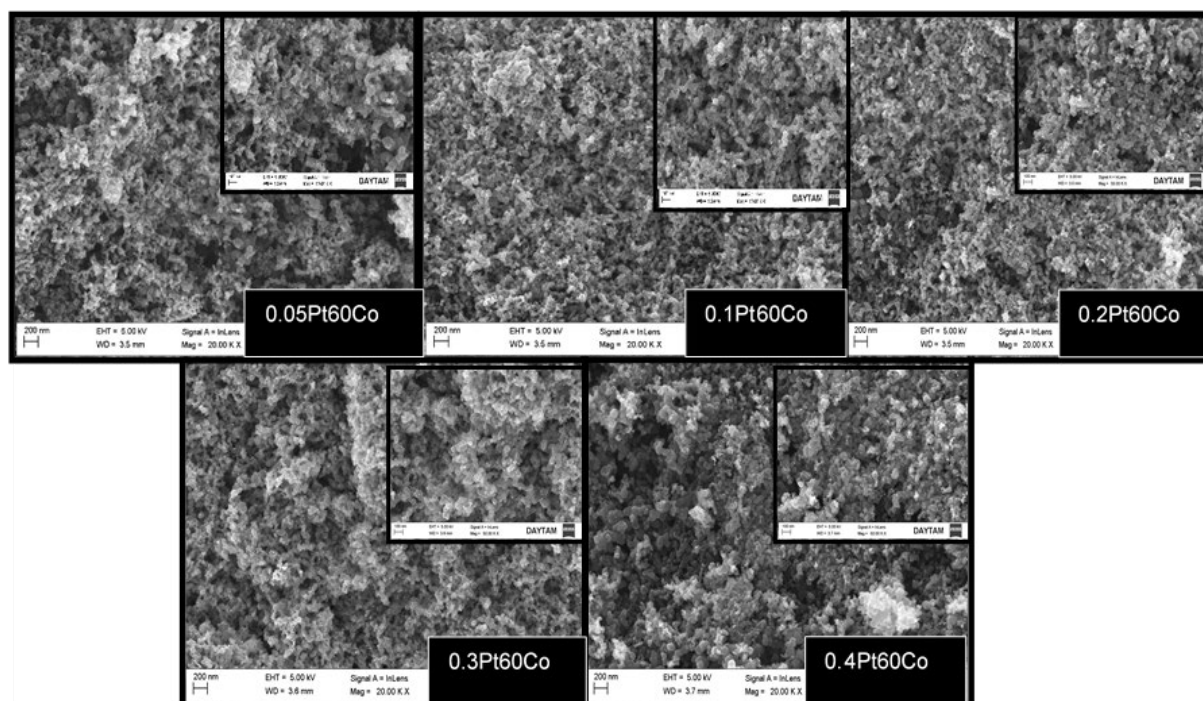
(a)
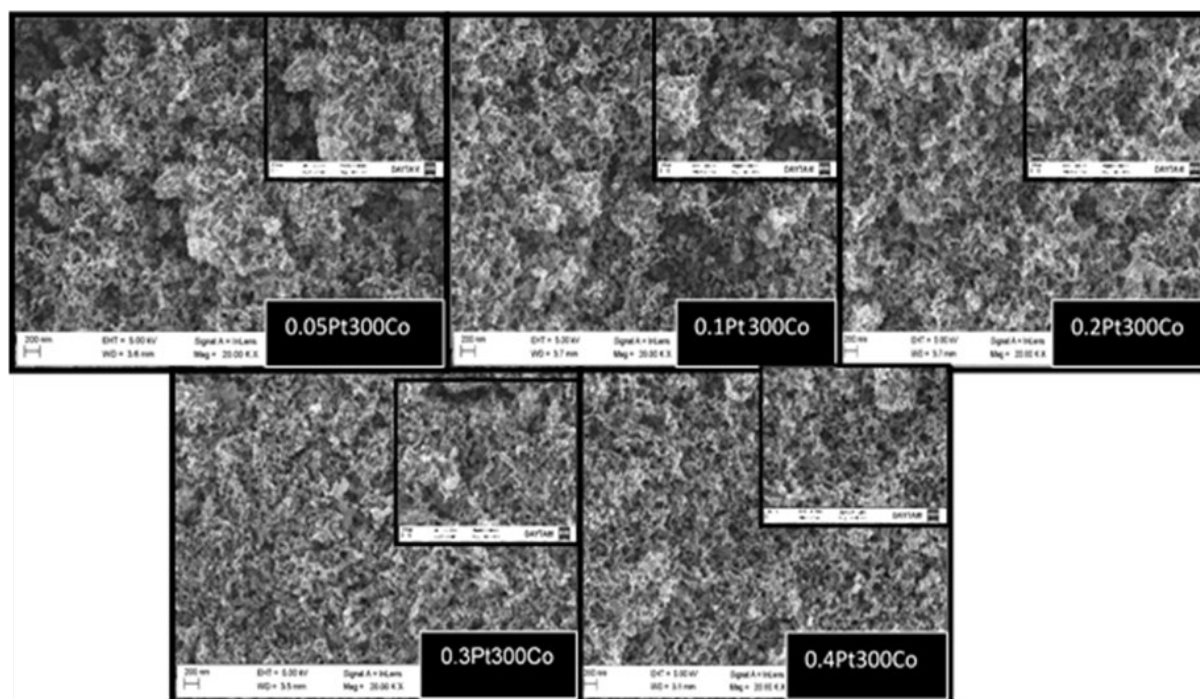
(b)

Figure 2. SEM images of GDEs a) 60 seconds and b) 300 seconds

By sputtering the GDL surface for 60 and 300 seconds using the magnetron sputtering method, contact angle measurements were taken to obtain information about the hydrophilicity or hydrophobicity of samples containing different platinum amounts. The contact angles of the electrode surfaces coated with a thin film of cobalt metal for 60 seconds and 300 seconds are given in Figure 3. In the contact angle measurement analyses, it was observed that the samples coated with cobalt 60 seconds film exhibited hydrophilic behaviour by giving results below 90°. The highest contact angle belongs to the sample containing the least platinum and it was observed that the hydrophilicity behaviour increased with the increase in the amount of platinum. The contact angle measurement of the surface containing the commercial catalyst Tanaka (for 0.4 mg Pt cm^{-2}) was obtained as 168.40° and the contact angle values decreased as the amount of metal coated on the surface increased. The samples coated with cobalt metal for 300 seconds film exhibited more hydrophilic behaviour than the samples coated with 60 seconds thin film by giving results below 90°, and it was determined with lower contact angle results.
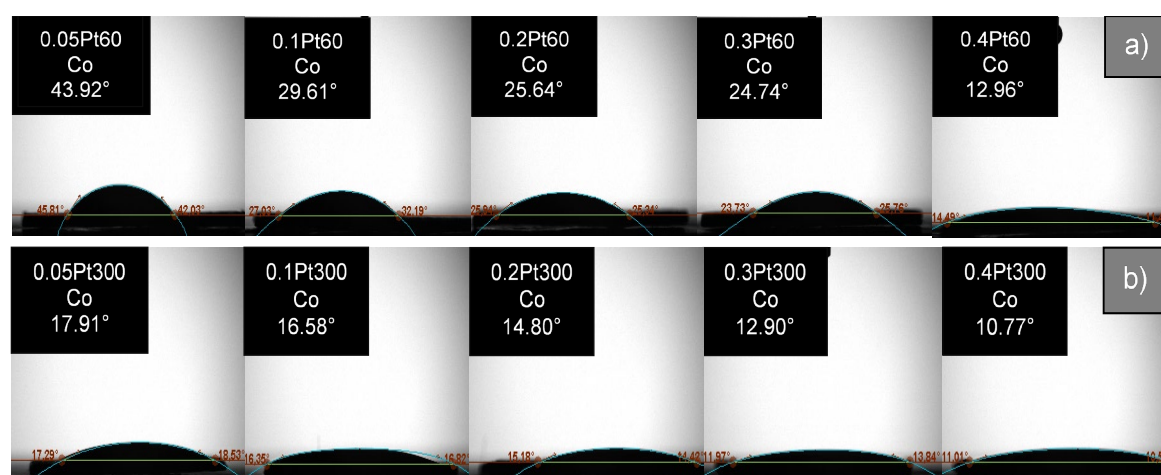
Figure 3. Contact angle measurements of GDEs a) 60 seconds and b) 300 seconds

PEM fuel cell performance tests were also performed to the prepared GDEs. The current densities at 0.6 V obtained for the electrodes prepared at different sputtering times, 60 and 300 seconds, are tabulated in Table 1. It was observed that the lower Pt loadings showed higher performances than the GDE prepared with commercial catalyst.

In 60 seconds, the loading up to 0.2 mgPtcm^{-2} and for 300 seconds the loading up to 0.1 mgPtcm^{-2} showed better performances.

Table 1. Current densities @0.6 V for the prepared GDEs

GDE	0.05 mgPtcm^{-2} (mAcm^{-2})	0.1 mgPtcm^{-2} (mAcm^{-2})	0.2 mgPtcm^{-2} (mAcm^{-2})	0.3 mgPtcm^{-2} (mAcm^{-2})	0.4 mgPtcm^{-2} (mAcm^{-2})
Tanaka	173.6	246.4	413.6	635.6	697.9
60Co	286.1	392.9	583.9	487.9	540.3
300Co	248.1	331.2	398.4	550.3	612.6

4. CONCLUSION

In this study, it was showed that GDEs can be prepared successfully by using magnetron sputtering. The properties and also the electrochemical behaviour of the GDEs are changing significantly depending on the sprayed Pt/C amount and also sputtering time. These parameters have to be optimized in order to get a better performing PEM fuel cell.

Acknowledgments

References

[1] J. Zhang, Y. Mo, M. B. Vukmirovic, R. Klie, K. Sasaki, and R. R. Adzic, "Platinum monolayer electrocatalysts for O2 reduction: Pt monolayer on Pd (111) and on carbon supported Pd nanoparticles," *The Journal of Physical Chemistry B*, vol. 108, no. 30, pp. 10955–10964, Jun. 2004.

[2] M. S. Çögenli, S. Mukerjee, A. B. Yurtcan, "Membrane electrode assembly with ultra low platinum loading for cathode electrode of PEM fuel cell by using sputter deposition," *Fuel Cells*, vol. 15, no. 2, pp. 288–297, Apr. 2015.

Effect of Thermal Treatment on the Electrical and Optical Properties of Al-Doped ZnO Thin Films for Solar Cell Applications

Mahdia Toubane[1], Asma Bessaad[2], Djedjiga Haouanoh[1], Fayrouz Benhaoua[1], Razika Tala-Ighil[1]

[1]Research Unit on Materials Processes & Environment, University M'hamed Bougara of Boumerdes, 35000 Boumerdes, Algeria
[2]Department of Material Sciences, University of Algiers 1, Benyoucef Benkhedda, Algeria
Corresponding author: Mahdia Toubane (e-mail: m.toubane@univ-boumerdes.dz)

Abstract

This study concerns the experimental results of Al doped ZnO layers deposited on glass substrates using the sol-gel method. We will discuss the experimental results on the influence of two parameters (Annealing time and temperature) on the various properties of the deposited layers, including structural, optical, and electrical properties, with a focus on conductivity. Annealing temperature T (400 °C, 450 °C, and 500 °C) for 1 hour, with a dopant concentration of 6% Al. ii) Annealing time t (1 hour and 1 hour 30 minutes) at an annealing temperature T = 500 °C with a dopant concentration of 6% Al. X-ray diffraction (XRD) analysis indicates that the deposited films crystallize within the hexagonal wurtzite type structure with a preferential growth orientation along (002) plane. All deposited layers show a transmission above 80%, with the maximum transmission of approximately 95% obtained at an annealing temperature of 500 °C for 1 hour and 30 minutes. This makes it advantageous for use as a transparent layer in thin-film solar cells. We observe that thermal treatment has a negligible effect on the variation of the bandgap energy, with a maximum value of 3.28 eV at (Tr = 500 °C, t = 1 hour and 30 minutes) and a minimum value of 3.271 eV at (Tr = 450 °C, t = 1 hour). The electrical results show that annealing temperature improves the conductivity of our samples Al-doped ZnO layers under light exposure; however, it has a negligible effect in darkness. In contrast, a negative effect is observed with increased annealing time.

Keywords: Zinc oxide, Aluminum, Optical properties, Electrical conductivity, Photovoltaic

Real-Time in Situ X-Ray Diffraction Analysis of Metal Oxide Nanoparticles: Structural Evolution and Phase Transitions

Abdelmalik Zemieche[1], Loubna Chetibi[1,2], Djamel Hamana[1,2], Slimane Achour[1,2]

[1]Laboratory of Advanced Materials Technology, National Polytechnic School of Constantine, Algeria
[2]Phase Transformation Laboratory, University of Constantine 1, Algeria
Corresponding author: Abdelmalik Zemieche (e-mail: mailkzemieche@gmail.com)

Abstract

This study investigates the structural evolution and phase transitions of metal oxide nanoparticles using real-time in situ X-ray diffraction (XRD). In situ XRD enables the monitoring of dynamic structural changes in metal oxides as they undergo heating, cooling, or chemical reactions, providing valuable insights into phase stability and transformation mechanisms. Metal oxide nanoparticles, such as MnO_x and NiO_x, were synthesized using a green synthesis method and subsequently analyzed under varying temperature conditions, ranging from room temperature to 1000 °C. The use of real-time in situ XRD allowed for the precise tracking of crystallographic changes, including phase transitions and the formation of intermediate structures. The results reveal the onset of phase changes at specific temperature ranges, with the nanoparticles exhibiting transitions from amorphous to crystalline phases, as well as changes in crystallite size and lattice parameters. Notably, the study captures the transformation from metastable phases to thermodynamically stable phases as a function of temperature, shedding light on the complex behavior of metal oxide nanoparticles under thermal stress. These findings have significant implications for optimizing the synthesis and thermal treatment of metal oxides for applications in catalysis, energy storage, and electronic devices. This work demonstrates the potential of in situ XRD as a powerful tool for understanding the real-time behavior of nanomaterials under operational conditions.

Keywords: In situ XRD, Metal oxide nanoparticles, Phase transitions, Structural evolution, Real-time analysis

Use of Recycled Polyethylene Terephthalate Strips in Soil Improvement

Lina Zaidi[1], Fatima Zohra Benamara[1], Messaouda Bencheikh[1]

[1]Laboratory of Civil and Hydraulic Engineering (LGCH), Department of Civil Engineering and Hydraulics,
University May 8, 1945 Guelma, Algeria
Corresponding author: Lina Zaidi (e-mail: linazaidi68@gmail.com)

Abstract

Waste is the product of all companies and industrial enterprises. The reduction and recycling of waste is justified first of all from an environmental and economic point of view. Indeed, this problem can be reduced by finding applications for recycled waste in the field of civil engineering and this as lightweight backfilling materials in geotechnical works and thus contribute to the preservation of natural resources. In this work, we modeled a mechanically stabilized earthen wall (MSE) in finite elements using the PLAXIS 2D software, the backfill of which is composed of a mixture of sand and recycled waste at different percentages (Plastic fiber PET 0.3%, 0.7%, 1%, and 2%).The results obtained from this numerical study were compared and interpreted to confirm the effectiveness of the substitution of recycled waste for sand used as backfill adjacent to retaining structures.

Keywords: Recycled waste, Retaining wall (MSE), Contiguous embankments, 2D PLAXIS, Stability

Comprehensive Examination of the Properties and Applications of Smart Perovskites Materials

Saadiya Benatmane[1,2], Montaha Affane[1], Sabria Terkhi[1], Samira Ziane[1]

[1]Department of Science and Technology, Faculty of Sciences and Technology, Abdelhamid Ibn Badis University, 27000 Mostaganem, Algeria
[2]Laboratory of Modelling and Simulation of Materials Science, Djillali Liabes University of Sidi Bel-Abbes, 22000 Sidi Bel-Abbes, Algeria
Corresponding author: Saadiya Benatmane (e-mail: saadia.benotmane@univ-mosta.dz)

Abstract

Materials science has been instrumental in the development of innovative technologies aimed at tackling economic and ecological sustainability challenges. Among advanced materials, cubic nitride perovskites stand out for their potential to contribute to a cleaner environment, ample clean energy, sanitized water, and resources for industrial and growing populations. These eco-friendly smart materials exhibit properties that can be significantly modified under controlled conditions. Lead-free perovskites ceramics and their composites are gaining attention due to their simple stoichiometry, cost-effectiveness, ease of synthesis, eco-friendly characteristics, and wide-ranging applications.

This study provides a concise overview of the crystal structure and various properties such as piezoelectric, ferroelectric, magnetic, and multiferroic behaviors of perovskites nitride. It also aims to cover the progress of specific perovskites nitride and their composites, highlighting recent advances and applications in energy storage, energy scavenging via multi-layer ceramic capacitors, supercapacitors, solid-nitride fuel cells, piezoelectric actuators, transducers, sensors, and spintronics. Additionally, recent industrial developments based on these perovskites nitride are discussed, along with an evaluation of future perspectives on current advancements in the field.

The full-potential linearized augmented plane waves (FP-LAPW) method, which is based entirely on functional density theory (DFT), is used to investigate the structural, electronic, magnetic, optical, and elastic properties of perovskites ABN_3 This method also employs the Generalized Gradient Approximation (GGA) and a modified Beck Johnson TB-mBJ potential in the exchange correlation term. When the resulting structural properties were examined, the findings showed that our compounds are best stable when they are configured as ferromagnetic materials. The formation energy value demonstrated that these chemicals could be produced experimentally.

Additionally, the estimated band structures show that ABN_3 exhibits half-metallic behavior with an indirect band gap.

Keywords: Perovskites, Elastic properties, Optical properties, Density functional theory, Energy gap

Effect of Physical Treatment of Orange Peel Powder on the Mechanical Properties of Biocomposites Based on Polylactic Acid

Atmane Yahiaoui[1]

[1]Laboratory of Advanced Polymer Materials (LMPA), Department of Process Engineering, Faculty of Technology, University of Bejaia, 06000 Bejaia, Algeria
Corresponding author: Atmane Yahiaoui (e-mail: atmane.yahiaoui@univ-bejaia.dz)

Abstract

The incorporation of orange peel powder (OPP) into polylactic acid (PLA)-based biocomposites represents a promising approach to enhance the mechanical properties of these eco-friendly materials. This study examines the impact of various physical treatments of OPP on the mechanical performance of PLA/OPP biocomposites.

The physical treatments applied to OPP include grinding, sieving, and thermal treatment. These treatments aim to modify the particle size, size distribution, and surface properties of OPP to improve its interaction with the PLA matrix.

The results show that physically treated PLA/OPP biocomposites exhibit significant improvements in tensile strength and flexural modulus compared to untreated composites. Fine grinding of OPP, in particular, led to better dispersion and a reinforced interface between OPP and PLA, thus increasing the overall strength of the material.

Moreover, the thermal treatment of OPP helped to reduce its hygroscopicity, thereby minimizing the moisture effect on the mechanical properties of the biocomposites. This study highlights the importance of physical treatments of OPP to optimize the performance of PLA/OPP biocomposites, paving the way for potential applications in packaging and sustainable materials sectors.

Keywords: Fiber, Orange peel, Biocomposite, Physical treatment

Prediction of Arias Intensity of Earthquake Acceleration Recorded in Soft Soil Sites

Aouari Issam[1,2], Benahmed Baizid[2], Rouabeh Aicha[1,2]

[1]Civil Engineering Department, University Akli Mohand Oulhadj, Bouira, Algeria
[2]Laboratory of Development in Mechanics and Materials, Ziane Achour University, Djelfa, Algeria
Corresponding author: Aouari Issam (e-mail: i.aouari@univ-bouira.dz)

Abstract

Arias intensity is a measure used in seismology to quantify the shaking intensity of an earthquake at a specific location. It is particularly useful for assessing the potential impact of seismic activity on structures and infrastructure. The research presents the results of a detailed study of seismic motions recorded at soft soil sites in different regions of the world. By analyzing more than 8,000 accelerograms selected from the European strong motion database (ESM), the Arias intensity of ground acceleration (A_I) was estimated for soft soil sites. Prediction models for these quantities were proposed for the studied sites. A comparison of the various expressions used in the literature to estimate the Arias intensity of seismic motion was conducted, also revealing correlations between the obtained values and parameters related to the source (M_w), the target distance (R), and the local soil conditions (V_{s30}). The comparison of the predicted Arias intensity using the proposed formulas for motions recorded in soft soils during the same earthquake with prediction models from the literature that do not take site effects into account shows a significant difference. Thus, the proposed models can be used to determine the Arias intensity for the earthquakes recorded at soft soil sites.

Keywords: Arias intensity, Soft soil, ESM database, Moment magnitude

Impact of Cutting Parameters on Part Surfaces in Machining

Souad Meftah[1]

[1]Department of Mechanical Engineering, Faculty of Science and Technology, University of Mascara, Algeria
Corresponding author: Souad Meftah (e-mail: meftahsouad27@gmail.com)

Abstract

This experimental study investigates the effects of cutting parameters on the surface quality of machined parts made from aluminum alloy and bronze. Key milling process variables, including cutting speed, feed rate, and depth of cut, were analyzed to determine their impact on surface roughness and material hardness. The results reveal that higher feed rates and depths of cut lead to increased surface roughness, while higher cutting speeds produce smoother surfaces. Additionally, other factors such as the condition and power of the machine tool, cutting tool parameters, and material properties also significantly influence surface quality. This research provides practical insights for optimizing milling operations to achieve superior machined surfaces.

Keywords: Bronze and aluminum alloy, Milling processes, Surface roughness, Material hardness, Machining parameters

Effect of Durability Indicators of Precast Concrete on Mechanical Behavior in Hot Climate

Ben Ammar Ben Khadda[1]

[1]Civil and Hydraulic Engineering Department, University of Biskra, Algeria
Corresponding author: Ben Ammar Ben Khadda (e-mail: b.benammar@univ-biskra.dz)

Abstract

The durability of precast concrete structures now occupies a decisive position in the new European normative context on concrete and which requires an effective control of all factors likely to affect its behavior over time. Experience shows that the most important influencing factors in terms of durability and which must therefore be subject to continuous control. The objective of this experimental study is the search for the characterization of the open porosity of concrete using the capillary absorption test of healthy and steamed concretes that are subjected to accelerated carbonation and to establish the existing links between the open porosity characterized by the initial absorption and the compressive strength. To do this, six types of concrete based on two cements (CEMI 42.5 and CEMII/B 42.5) were tested, the W/C ratio varies from 0.4 to 0.6 and the influence of carbonation was studied. The results obtained show that carbonation is beneficial for concrete alone as long as it reduces its porosity and highlight the effects of the water/cement ratio on open porosity and finally we can deduce the theoretical relationships that link the compressive strength at 28 days and the initial absorption of concrete.

Keywords: Precast concrete, Carbonation, Initial absorption, Compressive strength, Durability

Study of Optical Properties of NiO Thin Films Prepared by Lemon Peel Extracts

Imane Djouabi[1], Mahdia Toubane[2], Nadia Boukherroub[2]

[1]Physical Science Department, Higher Normal School of Kouba, Vieux-Kouba, Algeirs, Algeria
[2]M'hamed Bougara University, 35000 Boumerdes, Algeria
Corresponding author: Imane Djouabi (e-mail: imane.djouabi@g.ens-kouba.dz)

Abstract

This study investigates the effect of lemon peel extracts, both fresh peel and dried peel on the optical properties of NiO thin films prepared via green synthesis method. Nickel acetate tetrahydrate and lemon peel extract were used as precursor and solvent respectively. The synthesis was conducted under ambient conditions. The homogeneous solution obtained was then deposited onto a cleaned glass substrate using dip-coating techniques.The films were initially dried at 400°C for 10 minutes to eliminate any solvent and residual organic compounds, with this process repeated several times. Finally, the as-deposited NiO thin films were annealed at 500°C for 1h. The as deposited thin films were charactherized by uv-visible spectroscopy which revealed a noticeable variation in transmittance. The obtained results show that fresh peel (FP-NiO) samples exhibit higher transparency compared to dried peel (DP-NiO) samples. This difference is attributed to variations in organic composition, influenced by the freshness of the lemon peel. Fresh lemon peel yields a greater concentration of bioactive compounds, which facilitates the formation of more uniform NiO structure characterized by enhanced transmittance. In contrast, the utilization of dried peel may result in a more compact NiO layer exhibiting diminished transparency due to alterations in chemical composition and particle arrangement. The band gap of both two samples were approximately the same about 4.32 eV.These results underscore the profound effect of the organic environment during the synthesis process on the Optical properties of NiO thin films, there by emphasizing the potential of natural extracts for the modulation of material characteristics in optoelectronic applications.

Keywords: NiO thin film, Lemon peel extract, Optical properties, Optoelectronic application

Damping Modification Factors Assessment for Displacement and Acceleration Spectra Considering Epicentral Distance and Site Conditions Effects

Abdelhamid Abdelmalek[1,2], Benahmed Baizid[1]

[1]Development Laboratory in Mechanics and Materials, University of Djelfa, Djelfa, Algeria
[2]Mechanical Engineering Materials and Structures Laboratory, Department of Civil, Mechanical and Transportation Engineering, Tissemsilt University, Tissemsilt, Algeria
Corresponding author: Abdelhamid Abdelmalek (e-mail: abdelmalek.abdelhamid@univ-djelfa.dz)

Abstract

Damping modification factors (DMFs) play a pivotal role in design codes, as they adjust structural responses to account for variations in damping ratios different from the conventional 5% assumed in dynamic analyses. Studies have shown that DMFs are influenced by damping ratios, structural periods, seismic characteristics, and site-specific conditions. However, the effects of ground motions aligned with code-based target spectra on DMFs remain underexplored. This research focuses on Eurocode-8 compatible ground motions selected for three soil categories: Rock, dense, and soft, considering the impact of epicentral distance. DMFs were derived from displacement and acceleration response spectra using dynamic analyses of single degree of freedom (SDOF) systems. The results revealed significant differences in DMF values for ground motions recorded at distances greater and less than 20 km, with acceleration-based DMFs consistently exceeding displacement-based DMFs. Sensitivity to soil categories was particularly notable for soil class B, as classified by Eurocode 8. Furthermore, the findings indicated that the DMF values provided in Eurocode-8 were generally non-conservative. These outcomes highlight the need to revise code provisions to account for critical parameters such as epicentral distance and soil categories, which have a substantial influence on DMFs.

Keywords: Damping modification factors, Epicentral distance, Response spectra, Site conditions

Comparative Analysis of the Stability and Seismic Performance of a Reinforced Concrete Structure Using Two Bracing Systems

Bachir Bouderba[1,2], Abdelhamid Abdelmalek[1,3]

[1]Department of Civil, Mechanical and Transportation Engineering, Tissemsilt University, Tissemsilt, Algeria
[2]Mechanical Engineering Materials and Structures Laboratory, Tissemsilt University, Tissemsilt, Algeria
[3]Development Laboratory in Mechanics and Materials, University of Djelfa, Djelfa, Algeria
Corresponding author: Bachir Bouderba (e-mail: bouderba.bachir@univ-tissemsilt.dz)

Abstract

This research conducts a comparative analysis of two distinct bracing systems implemented to enhance the stability and seismic performance of a reinforced concrete structure, aligned with Algerian seismic design codes. The analyzed structure features a ground floor and five upper stories. After an extensive review of existing literature, two bracing configurations were chosen for evaluation. Numerical simulations were performed to assess earthquake-induced impacts, focusing on shear force distribution and overall structural behavior. The comparative analysis revealed similar response patterns between the systems, although a significant difference of approximately 20% in shear force values was observed. These results underline critical disparities in efficiency, providing insights for selecting the most suitable bracing strategy. Future research should expand on this work by incorporating global standards like Eurocode 8, exploring taller structures, various loading conditions, and integrating sustainability principles to improve structural resilience in seismic zones.

Keywords: Bracing systems, Reinforced concrete, Seismic design, Structural stability, Earthquake simulation

Drag Estimation and Validation of a USV Catamaran Hull Using Maxsurf Resistance and Towing Tank Testing

Muhammad Harith Danial Azlan[1], Nik Mohd Ridzuan Shaharuddin[1,2]

[1]Department of Aeronautics, Automotive, and Ocean Engineering, Faculty of Mechanical Engineering, Universiti Teknologi Malaysia, Johor Bahru, Malaysia
[2]Marine Technology Centre, Institute for Sustainable Transport, Universiti Teknologi Malaysia, Johor Bahru, Malaysia
Corresponding author: Nik Mohd Ridzuan Shaharuddin (e-mail: nmridzuan@utm.my)

Abstract

This paper presents the resistance estimation of an unmanned surface vehicle (USV) catamaran hull using the Maxsurf Resistance package, validated with experimental data. The study evaluates the reliability of Maxsurf Resistance in predicting resistance and highlights potential discrepancies between computational and experimental methods. The hull form, based on the Stan Tender 1905 design, was split at the centerline, spaced apart, scaled to a 1-meter length, and analyzed computationally using Maxsurf Resistance. A physical model was fabricated, and towing tank tests were performed. Results showed 21% discrepancies between Maxsurf Resistance predictions and experimental data at highest tested speed. At higher speeds, discrepancies were attributed to software assumptions about wave-making resistance and hull geometry effects. These findings emphasize the need for experimental validation to complement analytical predictions, particularly for complex hydrodynamic interactions, and provide practical insights for optimizing USV catamaran performance.

Keywords: Catamaran hull, Maxsurf software, Ship resistance, Tank testing, Unmanned surface vehicle

1. INTRODUCTION

Unmanned surface vehicles (USVs) are increasingly utilized for various applications, including environmental monitoring and maritime operations, necessitating efficient and reliable hull designs [1]. In environmental monitoring, USVs are employed to measure water quality parameters, map ecosystems, and detect pollutants in real time, enabling effective environmental management and preservation efforts [2]. Meanwhile, in commercial maritime operations, USVs are utilized for tasks such as hydrographic surveys, offshore structure inspections, and shipping logistics, enhancing efficiency and cost-effectiveness while reducing environmental impact [3]. These diverse applications demand advanced hull designs that minimize hydrodynamic resistance, optimize fuel efficiency, and ensure stability under various operational conditions. Among USV configurations, catamarans are favoured due to their superior stability and lower resistance compared to monohull counterparts, especially at moderate speeds. The twin-hull design of catamarans provides a broader beam, enhancing stability and reducing the vessel's tendency to roll, which is particularly beneficial for operations requiring precise manoeuvring and the deployment of sensitive equipment [4, 5]. Furthermore, catamarans exhibit lower hydrodynamic resistance, which translates to improved fuel efficiency and longer operational range. This efficiency is critical for USVs, as it directly impacts their endurance and ability to cover larger areas without frequent refuelling. Accurate resistance estimation is critical in optimizing their performance, as resistance directly impacts fuel efficiency, speed, and operational range [6].

Analytical methods such as those offered by Maxsurf Resistance are widely used in the preliminary design stages due to their cost-effectiveness and time efficiency. MAXSURF employs empirical and theoretical models to estimate resistance based on hull geometry and operational parameters. Several studies have demonstrated the effectiveness of Maxsurf Resistance in estimating the resistance of various hull forms. For instance, [7] analyzed patrol boat hull resistance using Savitsky and Holtrop approaches from Maxsurf Resistance software, emphasizing the influence of internal design factors such as rudder and frontal area on hydrodynamic performance. Similarly, [8] applied Holtrop's regression-based method and Savitsky's mathematical model to evaluate fishing vessel resistance using Maxsurf Resistance. The study compares different hull designs and concludes that the monohull with a 30° dagger board fin has the lowest total resistance. The results suggest that both methods are reliable for resistance estimation, showing less than a 15% error. [9] explored the impact of flat hull shapes on resistance. Their research examines the effect of the shape and arrangement of the flat plates forming the hull on resistance,

using the comparator ship method and Maxsurf Resistance Software. The study concluded that the more closely the hull plate arrangement of a flat hull ship resembles that of a streamlined comparator ship, the closer the resistance experienced, with unevenness in the hull causing energy losses and higher resistance. [10] examined the resistance characteristics of a 19-ton airboat, focusing on its unique operational requirements. By employing advanced experimental and computational techniques, their study demonstrated how specific design adaptations can enhance performance in specialized vessels. Collectively, these works emphasize the utility of empirical and computational approaches in understanding and improving hull resistance, offering valuable frameworks for future research and design in maritime engineering.

On the other hand, the towing tank test is very common in estimating the ship resistance in scaled size. By directly measuring hydrodynamic forces acting on a scaled physical model, these tests provide invaluable validation for computational tools. Studies comparing experimental and computational resistance have demonstrated the importance of integrating both approaches to capture the full spectrum of hydrodynamic behaviour. Previous research on catamaran hulls has shown significant variations in wave-making resistance and flow separation patterns that are often oversimplified in analytical models. Therefore, this paper aims to validate the reliability of Maxsurf Resistance for a USV catamaran hull based on the Stan Tender 1905 design. By comparing the Maxsurf Resistance predictions with towing tank test results, this study identifies areas of agreement and deviation, providing insights into the strengths and limitations of Maxsurf Resistance for complex hull configurations.

2. METHODOLOGY

2.1. Hull Form Description

The Stan Tender 1905 is an ideal choice for developing USVs due to its versatile design, proven performance, robust construction, and ease of modification. Its operational efficiency and adaptability make it suitable for various USV applications. The 3D model of the Stan Tender 1905 was initially developed from the lines plan drawing obtained from [11]. Details on this vessel are shown in [12]. Figures 1(a) and 1(b) illustrate the developed original 3D model and the transformation of the monohull into the catamaran 3D hull, respectively. The original hull form scale was reduced by a factor of 18.5, then sliced at its centreline with a spacing of 0.195 meters. Detailed particulars of the newly designed catamaran hull are provided in Table 1.

| (a) | (b) |
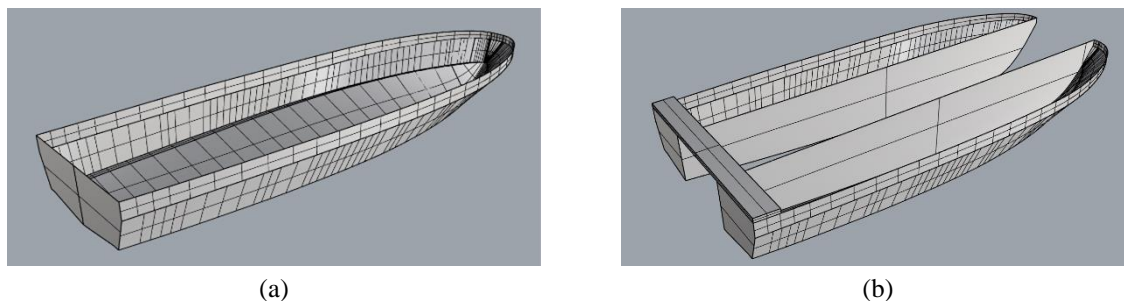
Figure 1. 3D model of the original and new catamaran hull transformation for USV: (a) Original hull form and (b) transformed hull form

Table 1. Catamaran hull data

Particulars	Parameter
Length overall (m)	1.050
Breadth (m)	0.525
Depth (m)	0.215
Draft (m)	0.104
Hull spacing$_{inside}$	0.195
Displacement (kg)	18.08

2.2. Maxsurf Modeler and Resistance Packages

Before estimating the resistance value, the modified hull form was exported to Maxsurf Modeler. In this software package, the frame of reference was set up and the hydrostatic data was generated. Figure 2 shows the model in Maxsurf Modeler, and Table 2 presents the hydrostatic data at its designed draft. The Maxsurf formatted 3D model was then exported to Maxsurf Resistance. The input parameters used in this software included the resistance estimation method, required speeds, and efficiency. In this research, the analytical calculation was performed using

the Molland Catamaran method with a default form factor value of 1.4. The efficiency was set to 70%, which is commonly used for electrical propulsion systems. The model was run at four speeds, starting from 0.5 m/s to 1.25 m/s at 0.25 m/s intervals.
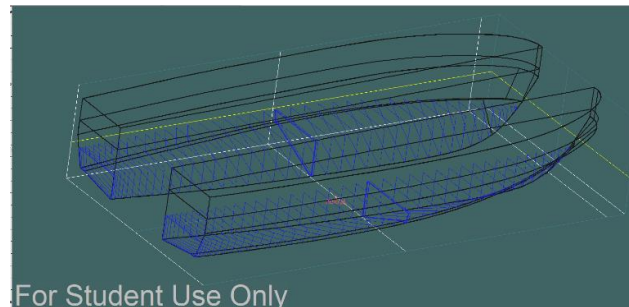
Figure 2. 3D model in Maxsurf models

Table 2. Catamaran hydrostatic data

Particulars	Parameter
Wetted Area	0.579
Max sect. area	0.023
Waterpl. Area	0.284
Prismatic coeff. (Cp)	0.782
Block coeff. (C_B)	0.326
Max Sect. area coeff. (Cm)	0.436
Waterpl. area coeff. (Cwp)	0.533

2.3. Model Tank Testing

The tank test was conducted at the Marine Technology Centre, Universiti Teknologi Malaysia. The towing tank facility measures 120 meters in length, 4 meters in width, and 2.5 meters in depth. The towing carriage can operate at speeds up to 2.5 m/s. The USV catamaran hull form was fabricated at a reduced scale factor of 18.5 from the original hull form. The model was constructed using 3D printer material, printed in sections, and then integrated into one complete hull. The accuracy of the fabricated hull adheres to the ITTC Recommendation on model making. Figure 3 shows the setup of the model under the towing carriage. The model is allowed to move in the heave direction and rotate about the y-axis (pitch direction). The resistance of the hull is measured in real time using a load cell located at its centre of gravity.

Figure 3. USV Catamaran model setup for resistance test

3. RESULTS AND DISCUSSION

The purpose of calculating ship resistance is to determine the friction between the fluid and the hull below the waterline, often referred to as drag or resistance. Accurate estimation of this resistance is crucial for determining the installed power required by the vessel. Figure 4 shows the resistance curve for both analytical and experimental approaches, indicating an error of 21% at speed of 1.25 m/s. This discrepancy is significant and warrants a detailed examination of the underlying causes. Several factors may contribute to this discrepancy. First, methods like slender body using Molland's incorporate adjustments for viscous drag but may generalize hull surface roughness or boundary layer development. This generalization can lead to underpredictions because it does not account for the specific characteristics of the hull surface. This factor can significantly affect the boundary layer development and, consequently, the drag experienced by the vessel. Analytical methods often rely on simplified assumptions

about flow dynamics, which might not fully capture the interference effects between the two hulls of a catamaran. These methods typically assume idealized flow conditions that do not account for complex interactions such as wave interference and turbulent flow between the hulls. Such interactions can significantly impact resistance, particularly at higher speeds where wave-making resistance becomes more pronounced.

Additionally, Maxsurf Resistance may underestimate the wave-cancellation effect between the hulls, especially at specific hull spacings or speeds. This effect occurs when the waves generated by one hull interfere with those generated by the other, potentially reducing the overall wave resistance. Figure 5 illustrates this phenomenon, where the wave pattern generated is underestimated in Maxsurf Resistance, leading to under predicted resistance values. This underestimation of wave-cancellation can result in significant under-predictions of total resistance, particularly at speeds where wave-making is a dominant factor. Furthermore, experimental works are often conducted in controlled environments with ideal water conditions and accurately fabricated hulls, resulting in lower drag compared to the assumptions in the software. To address these discrepancies, it is essential to complement computational predictions with experimental validation. Experimental tests provide empirical data that can help identify and correct the limitations of computational methods. By understanding the sources of discrepancies, engineers can refine computational models to better account for real-world conditions and complex hydrodynamic interactions. This combined approach of computational analysis and empirical testing is crucial for optimizing the performance and efficiency of USV catamaran hulls.
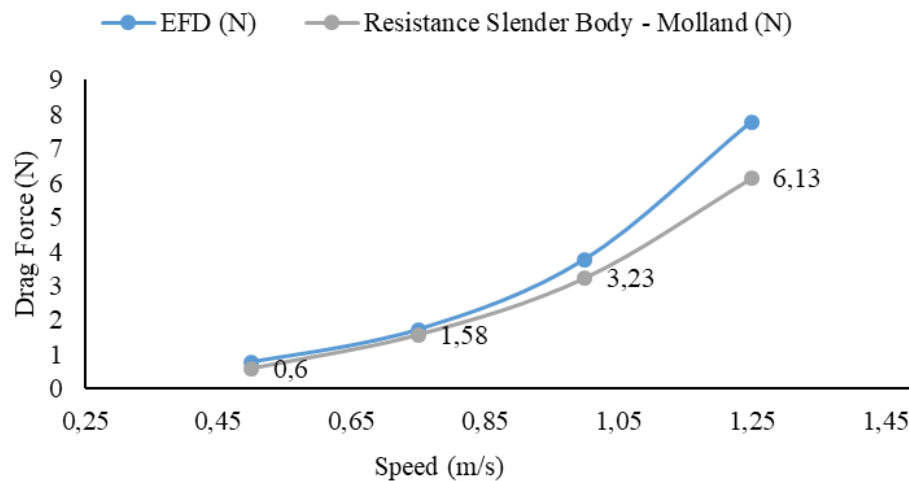
Figure 4. Resistance estimation for catamaran hull using Maxsurf Resistance

(a)

(b)
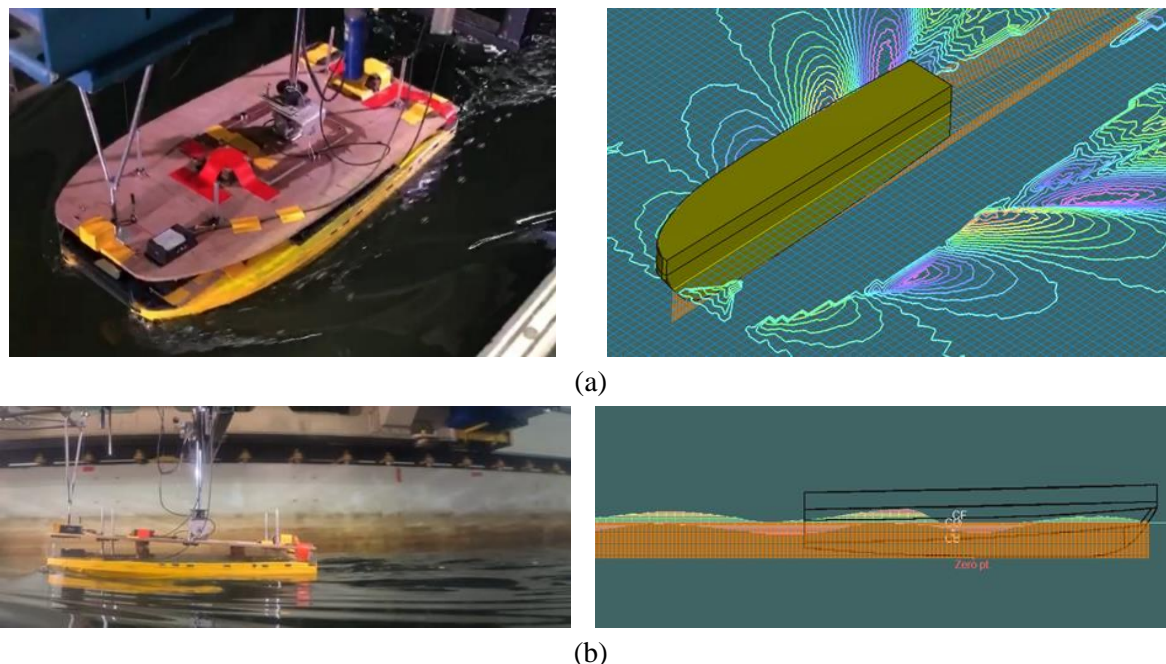
Figure 5. Wave generated pattern at towing speed of 1.0 m/s: (a) Perspective view and (b) side view

4. CONCLUSION

The study demonstrates that while Maxsurf Resistance provides a useful tool for predicting the resistance of USV catamaran hulls, there are notable discrepancies when compared to experimental data, particularly at higher speeds. These discrepancies highlight the limitations of the software in accurately modeling wave-making resistance and complex hull geometries. The research emphasizes the importance of experimental validation to complement analytical methods, ensuring more accurate and reliable predictions for optimizing the performance of USV catamarans. Therefore, there is a need to utilize a Computational Fluid Dynamics (CFD) approach in evaluating the resistance of the catamaran hull. Overall, the findings provide valuable insights for improving the design and efficiency of USV catamaran hulls through a combined approach of computational analysis and empirical testing.

Acknowledgments

References

[1]   X. Bai, B. Li, X. Xu, and Y. Xiao, "A review of current research and advances in unmanned surface vehicles," *Journal of Marine Science and Application*, vol. 21, pp. 47–58. 2022.

[2]   N. M. Zahari, P. Sankar, I. N. Ismail, M. H. Zawawi, N. N. Nashrudin, and N. A. Aziz, "A review of unmanned surface vehicle for water quality assessment application," *AIP Conference Proceedings*, vol. 2750, art. no. 050004, 2024.

[3]   L. F. Constantinoiu, M. Bernardino, and E. Rusu, "Autonomous shallow water hydrographic survey using a proto-type USV," *Journal of Marine Science and Engineering*, vol. 11, no. 4, art. no. 799, 2023, doi: 10.3390/jmse11040799.

[4]   Y. Xing-Kaeding and A. Papanikolaou, "Optimization of the propulsive efficiency of a fast catamaran," *Journal of Marine Science and Engineering*, vol. 9, no. 5, art. no. 492, May 2021.

[5]   T. Putranto, W. D. Aryawan, H. A. Kurniawati, D. Setyawan, and S. R. W. Pribadi, "Resistance and stability analysis for catamaran fishing vessel with solar cell in calm water," in *MATEC Web of Conferences*, 2018, vol. 159, p. 1059.

[6]   A. F. Zakki, A. Windyandari, D. Chrismianto, and R. Ilham, "On the development of catamaran hull form for fish processing vessel to support domestic fishing activities in Indonesia," *Nase More*, vol. 68, no. 3, pp. 175–188, 2021, doi: 10.17818/NM/2021/3.5.

[7]   M. A. Lutfi, R. A. Haikal, R. F. Firmansyah, and M. S. Maulana, "Analysis of the internal-design factor to the patrol boat: A study of hull resistance using Savitsky and Holtrop approaches," *IOP Conference Series: Earth and Environmental Science*, vol. 1278, art. no. 012014, 2023.

[8]   R. I. Julianto, A. R. Prabowo, N. Muhayat, T. Putranto, and R. Adiputra, "Investigation of hull design to quantify resistance criteria using Holtrop's regression-based method and Savitsky's mathematical model: A study case of fishing vessels," in *Proceedings of Universitas Sebelas Maret, Department of Mechanical Engineering*, Surakarta, Indonesia, 2022.

[9]   R. A. Nabawi, S. Syahril, and R. Refdinal, "The study of shape flat hull ship toward resistance," *TEM Journal*, vol. 11, no. 4, pp. 1669–1673, Nov. 2022, doi: 10.18421/TEM114-30.

[10]   J.-H. Pyun, H.-K. Yang, J.-H. Choo, I.-T. Kim, and S.-G. Ryu, "A study on characteristics of the ship resistance for the 19-ton class airboat," *Journal of Advanced Marine Engineering and Technology (JAMET)*, vol. 46, no. 5, pp. 224–229, 2022, doi: 10.5916/jamet.2022.46.5.224.

[11]   Boat Design Net. (2019). *Lines plan for 18 meter patrol boat* [Online]. Available: https://www.boatdesign.net/threads/lines-plan-for-18-meter-patrol-boat.60274/ (Accessed: 2024, Dec. 6).

[12]   Damen Shipyards Group. (2023). *Stan tender 1905 – High-speed crafts* [Online]. Available: https://www.damen.com/vessels/high-speed-crafts/stan-tenders/stan-tender-1905 (Accessed: 2024, Dec. 6).

Synthesis and Characterization of Co₃O₄-rGO for Photodegradation of Dyes

Muhammad Saeed[1], Asif Nisar[1]

[1]Department of Chemistry, Government College University Faisalabad, Pakistan
Corresponding author: Muhammad Saeed (e-mail: msaeed@gcuf.edu.pk)

Abstract

The growing issue of water contamination by synthetic dyes is a global concern. In this study, Co_3O_4-decorated reduced graphene oxide (Co_3O_4-rGO) is introduced as an efficient heterogeneous photocatalyst for the degradation of organic dyes. The successful synthesis of the Co_3O_4-rGO composite was confirmed using various spectroscopic techniques, including XRD, XPS, TEM, and FTIR. Following characterization, the photocatalytic performance of the Co_3O_4-rGO was evaluated for the degradation of methylene blue (MB) and methyl orange (MO). The composite demonstrated a photocatalytic efficiency of over 95% within 60 minutes, with an initial dye concentration of 200 mg/L. Biochemical Oxygen Demand (BOD) and Chemical Oxygen Demand (COD) measurements confirmed the degradation of both dyes. Additionally, the impact of factors such as catalyst reusability, catalyst dosage, and initial dye concentration on photocatalytic activity was examined. The photocatalytic degradation efficiency of Co_3O_4-rGO for MB was 2.13 times higher than Co_3O_4 and 3.43 times higher than rGO alone. Similarly, for MO, the degradation efficiency of Co_3O_4-rGO was 2.36 times and 3.56 times greater than Co_3O_4 and rGO, respectively. Therefore, Co_3O_4-rGO is demonstrated to be an effective and reusable photocatalyst for the degradation of these dyes in aqueous solutions.

Keywords: Methylene blue, Methyl orange, Co₃O₄-rGO, Photodegradation

Removal of Safranine O by Adsorption Using Commercial Activated Carbon Doped with Fe3O4 Nanoparticles

Asmaa Ouali[1], Salima Attouti[1], Nadia Douara[1]

[1] Chemical Engineering Department, University Abdelhamid Ibn Badiss University, Mostaganem, Algeria
Corresponding author: Asmaa Ouali (e-mail: asmaa.ouali.etu@univ-mosta.dz)

Abstract

Nanotechnology, a rapidly advancing field, is widely applied in various domains, particularly in environmental protection and pollutant removal through processes like adsorption. In this study, we synthesize Fe3O4 nanoparticles via the co-precipitation method and use them to dope commercial powdered activated carbon (PAC). The doped PAC is then employed to remove Safranine O dye from aqueous solutions through adsorption. We investigate the effects of key parameters such as initial dye concentration, pH, contact time, and PAC/Fe3O4 dose. Results show significant dye removal at pH 6, with a contact time of 60 minutes and a PAC dose of 2 g/L. The adsorption process was analyzed using Langmuir and Freundlich isotherm models to understand the underlying mechanism.

Keywords: PAC, Nanoparticles, Adsorption, Safranine O dye, Isotherme, Removal

Digital Transformations in the Oil and Gas Industry

Farhad Yusifov[1]

[1]Digital Transformation and E-Government, Institute of Information Technology, Baku, Azerbaijan
Corresponding author: Farhad Yusifov (e-mail: farhadyusifov@gmail.com)

Abstract

The article examines the state of the art of digital transformations in the oil and gas sector and analyzes trends in this field. Major digital solutions used in the oil and gas sector include artificial intelligence, machine learning, the internet of things, cloud computing, smart materials, big data, digital twins, robotization, drones, blockchain, and other digital ecosystems. The literature review shows that digital transformation is widely used to effectively organize oil and gas industry activities and increase management effectiveness. The reasons for the effectiveness of digital technologies include increasing production efficiency, lower production costs, faster management decision-making, improving the quality of applied solutions, etc. Taking into account its advantages and potential risks, the application of digital technologies, especially in a complex field such as the oil and gas industry, makes it necessary to conduct research in this field.

Keywords: Oil-gas industry, Digital transformation, Digital technology, Artificial intelligence

Optimizing Renewable Energy Integration in Radial Distribution Systems Considering Uncertainties in Power Generation

Bendriss Badreddine[1], Samir Sayah[1], Abdellatif Hamouda[2]

[1]Department of Electrical Engineering, QUERE Laboratory, Ferhat Abbas University, Algeria
[2]Optics and Fine Mechanics Institute, QUERE Laboratory, Ferhat Abbas University, Algeria
Corresponding author: Bendriss Badreddine (e-mail: badreddine.bendriss@univ-setif.dz)

Abstract

Integrating renewable energy sources (RES), such as wind turbines (WT) and solar photovoltaic (PV) systems, into Radial Distribution Systems (RDSs) has become increasingly essential due to its significant impact on improving system performance and reducing greenhouse gas emissions. This paper presents an effective method called grey wolf optimization (GWO) to determine the optimal locations for these RESs within the RDS. The power generation from WT and PV systems is highly unpredictable, depending on varying factors like wind speed and solar irradiance. To effectively handle these uncertainties, a probability density function is employed to accurately estimate the power output of the DGs using historical wind speed and solar irradiance data. The main objectives of this study are to significantly reduce power losses, improve voltage profiles, and enhance system stability. The proposed method is rigorously tested on the IEEE 69 bus RDS, demonstrating its high effectiveness through successful results.

Keywords: Wind turbines, Solar photovoltaic, Radial distribution systems, Uncertainties, Probability density function

Mitigating Emissions of Ship Exhausts for Maritime Sustainability

Atallah Ghribi[1], Mohamed Teggar[2]

[1]Department of Law, Amar Telidji University, 03000 Laghouat, Algeria
[2]Department of Mechanical Engineering, Amar Telidji University, 03000 Laghouat, Algeria
Corresponding author: Mohamed Teggar (e-mail: m.teggar@lagh-univ.dz)

Abstract

Emission from ships are governed by restricted international laws and specific conventions to limit their damage to the environment. The International Maritime Organization (IMO) of the United Nations concludes measures to reduce emissions from ship exhausts and engines. The latter use heavy oil fuels of great damage when burned, the ship exhausts release harmful emissions for living beings and contribute to depleting the ozone layer as well. Efforts for mitigation of these emissions are discussed herein. We have noted that the mentioned efforts of IMO represent an added value for protecting the global ecosystem, including the marine environment. However, they did not link compensation for damages of fossil fuels and damages of ship exhaust emissions. These emerging challenge should be addressed by the legislator for maritime sustainability.

Keywords: Maritime, Pollution, Ship, Exhaust, Emissions

2D Moving Objects Localization in Video Surveillance Based on Fast-ICA Algorithm for Background Subtraction and Local Yezzi Algorithm for Level Sets Models

Abderrahmane Naoum[1], Meriem Boumehed[2], Belal Alshaqaqi[3], Abdelkrim Meche[1]

[1]Signal and Image Laboratory, Department of Electronic, Faculty of Electrical Engineering, University of Science and Technology of Oran-Mohamed Boudiaf, Oran, Algeria
[2]Department of Second Cycle, Higher School of Electrical and Energetic Engineering of Oran, Oran, Algeria
[3]Institute of Maintenance and Industrial Safety, University Oran 2-Mohamed Ben Ahmed, Oran, Algeria
Corresponding author: Abderrahmane Naoum (e-mail: abderrahmane.naoum@univ-usto.dz)

Abstract

The localization of moving objects stands as an essential technology within the realm of intelligent system automation, including traffic monitoring, video surveillance, gesture recognition, object tagging, and vehicle navigation. In this work, we introduce an automated methodology designed to precisely identify moving objects within surveillance scenes. This methodology comprises two primary parts: global detection and fine localization. Global detection involves the utilization of a background subtraction algorithm to discern the presence or absence of a moving object using fast independent component analysis. On the other hand, for fine localization, we propose a novel method employing localized statistical models based on active contours. The proposed method is evaluated on the publicly available change detection datasets CDnet 2014 using performance parameters such as recall, precision and F-measure. Experimental results approve the method with real-time frame rate.

Keywords: Visual surveillance, Fast-ICA, Level Set, Yezzi model, 2D localization

1. INTRODUCTION

The Visual systems are broadly used for solving the shortage of visual information in the aforementioned localisation systems [1–3]. By handling images acquired by surveillance cameras, the location of a person or an object can be pinpointed continuously [4, 5]. That is, we do not merely intend to know that an object is present in the image, but we also require knowing where it is in the image. This location or positional information is usually referred to as the object's pose [6, 7].

As all the existing systems, this visual technology has its own pros and cons. It is characterised by the abundance of the visual information, which indicates the presence or absence of the object [2]. In indoor milieus, the person has no need to bear a device with him at all, which means that anyone entering a building can be located without using any wearable devices [8]. However, the tracked object has to be visible for the system, in other words [9] the surveillance cameras have to cover places where the localisation is necessary, which means that huge investments in infrastructure may be required.

Lately, visual surveillance in dynamic scenes has become one of the most research hotspots in computer vision. This is due to the increasing demand of accurate information for security of sensitive areas, traffic monitoring in cities and highways law enforcement, and military applications [10].

The substantial objective of this work is to explore a novel method for localizing moving objects in 2D environments, with the intention of advancing the development of an Automatic Video-Surveillance (AVS) system. This approach encompasses the utilization of a background subtraction algorithm to isolate foreground pixels from the background image using fast independent component analysis [11] and employing algorithm based on level sets models to localise the detected objects in 2D space [12, 13]. This proposed technique is particularly tailored for relatively uncontrolled settings. Additionally, it does not require external training data and offers efficient solutions to: object movement, non-stationary background, splitting/merging objects, occlusions, disappeared object, camouflage, ghosts, shadow and moving camera [14–16]. Indeed, the proposed Independent Component Analysis (ICA)-based background subtraction technique effectively segments and filters foreground

2D moving objects localization in video surveillance based on fast-ICA   ICMUSTED 2024
algorithm for background subtraction and local Yezzi algorithm for level sets
models

objects even amidst substantial environmental changes, rendering it suitable for both indoor and outdoor surveillance applications [11, 17, 18].

The localization algorithm, based on local Yezzi model, employs temporal object localization principles rather than relying solely on spatial cues to discern the presence, location, and actions of subjects in a 2D scene. This approach offers the potential for other application layers to derive insights about these subjects. Leveraging the proposed ICA-based background subtraction technique addresses the challenge of initial curve placement in the image. Furthermore, it adjusts contour smoothness and object perimeter accuracy across varying shapes through a novel stopping criterion. Results are demonstrated across diverse and challenging indoor/outdoor sequences.

The remainder of this paper is organized as follows. The method is presented in section 2. In section 3 shows the experiments results and demonstrates the localization performance of the proposed system. The discussion of results is interpreted in section 4. Finally, the conclusion is drawn in section 5.

2. MATERIAL AND METHOD

With the increasing concerns regarding public and road safety, the implementation of sophisticated visual surveillance systems has become crucial to detect and locate potentially hazardous situations. Locating objects in 2D scenes requires two steps in this work. First, global detection via background subtraction using fast-ICA algorithm. Second, fine localization thru level set model by local Yezzi model. Figure 1 illustrates this two steps.
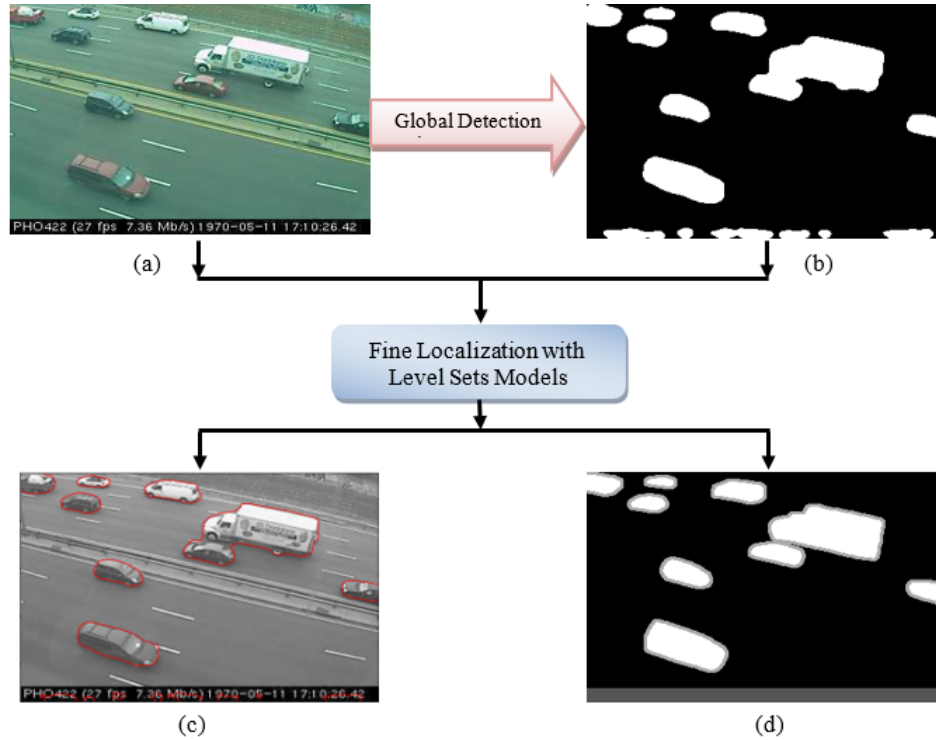
Figure 1. The proposed framework for locating moving objects: (a) Original image (turnpike_0_5fps (1031th) from low frame-rate), (b) foreground mask for initialisation, and (c) moving objects localization. (d) Segmentation result

2.1. Background Subtraction Method Based on the Fast-ICA Algorithm

Assuming that the video scenes are acquired by a stationary camera, the moving objects are considered independent from the background image [19]. Thus, to separate the motion objects, we apply a proposed background subtraction method based on the fast-ICA algorithm, which consists of four steps: pre-processing, training step, detection step, and post-processing [11, 20, 21]. Let's denote the reference background image by B of size $k = m \times n$, and any frame from the scene by F, the approximated foreground by F_g, the noise model by N, the data matrix by X, the de-mixing matrix by W, the denoising matrix by W^d and the filtered foreground by $F_g{}^d$. The main steps of our framework can be described in Algorithm 1.

2D moving objects localization in video surveillance based on fast-ICA algorithm for background subtraction and local Yezzi algorithm for level sets models

ICMUSTED 2024

Algorithm 1

- Initialization of: B, W, W^d and N
- While F is true:
    # pre-processing:
    # convert F from RGB to YCrCb
    # reshape the Y channel from matrix to row vector.
    - $B_V(1, [n \times (i - 1)] + j) = B(i, j)$;
    - $F_V(1, [n \times (i - 1)] + j) = F(i, j)$
    # construct the data matrix.
    - $X = [[B_V], [F_V]]$
    - $Result = W \times X$
    # the second row from Result represent objects detected.
    # construct the new data matrix.
    - $X = [[Result[1]], [N_V]]$
    - $Result = W^d \times X$
    # the second row from new Result represent the foreground.
    - $F_g = Result[1]$
    # reshape from row vector to matrix
    - $F_g(i, j) = F_g(1, [n \times (i - 1)] + j)$
    # post-processing: filtering and morphological transformation.
    - $F_g = F_g \times G(\mu, \sigma)$
    - $F_g = Open(F_g)$
    - $F_g = Close(F_g)$
    # create the binary foreground mask.
    - $F_g(i, j) = \begin{cases} 1 & if \quad F_g(i, j) > threshold \\ 0 & otherwise \end{cases}$
- End

2.2. 2D Localization of Moving Objects

The proposed localisation framework enables any region-based energy to be localized in a fully variational way. The significant improvement of localization within this framework is that objects that have complex aspect can be accurately located with localized energies, when the corresponding global energies fail [12]. The framework is also utilised to generate two localized energies' Chan-Vese and Yezzi. These are given as examples to show how any energy can be localized in a similar way [13]. In this study we use only Yezzi energy.
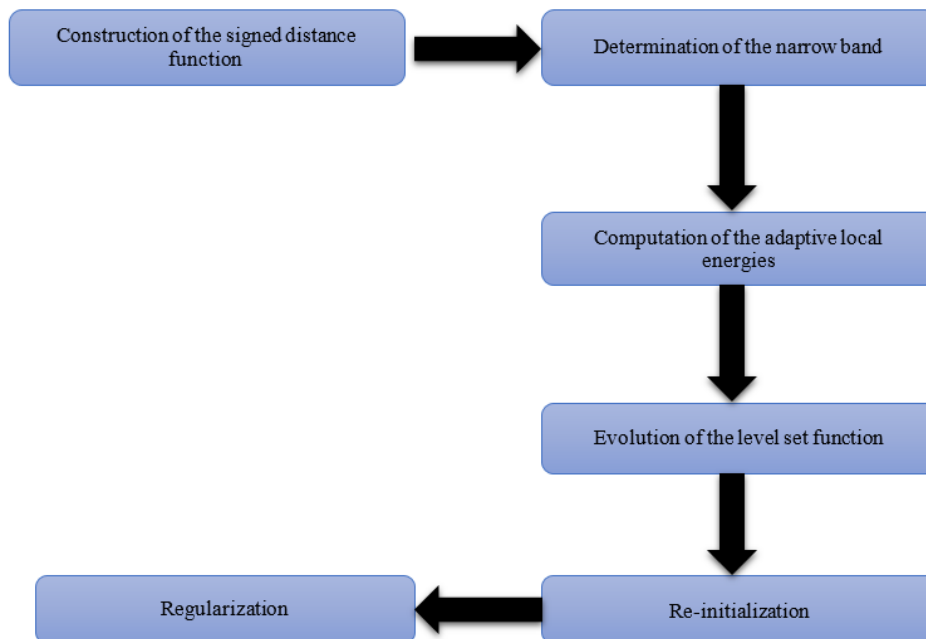
Figure 2. The main steps of the local-region based framework

2D moving objects localization in video surveillance based on fast-ICA   ICMUSTED 2024
algorithm for background subtraction and local Yezzi algorithm for level sets
models

The localization process relies on information from local interior and exterior regions along the contour rather than global regions. This means that interior and exterior regions will be distinguishable locally. Basing on this notion, a set of local regions around each point along the curve will be constructed, and meanwhile a family of local energies is computed. In order to optimize localized energies, each point moves to optimize the component of the energy added from its local region. Each point's component of the overall energy is computed by splitting the local neighbourhoods into local-interior and local-exterior using the evolving curve and a squared window function as described below. Consequently, the curve must evolve for all the points of the windows; however this increases the computation load. To reduce this load, without distorting the result, a thin or narrow band is determined just around the zero level set. Furthermore, to guarantee that ϕ remains as it was initialized, a re-initialization step is incorporated. We also propose to add up a regularization step that allows us on one hand to determine an automatic stopping criterion for reaching the object boundary, and on the other hand to arrange the weight of the curvature that enables the contour to smooth easily. The main procedure is illustrated by the diagram in Figure 2.

3. RESULTS

3.1. Test Sequences

Throughout this work, eleven-(11) test sequences from CDnet 2014 datasets; three-(03) indoor benchmark datasets and height-(08) outdoor benchmark datasets are used. Additionally, these test sequences encapsulate varying camera height, camera orientation and environmental conditions. These sequences were chosen to comprehensively evaluate the proposed technique in various scenarios and to illustrate how the local framework can enhance the performance of a given global energy. An overview of these datasets and the selected sequences are depicted in Table 1.

Table 1. Overview of the datasets and the selected sequences

Data-Set	Category	Selected Sequences	Frames of Sequence	Resolution
CD -net 2012	Baseline (Ba)	Office	2050	360×240
		PETS2006	1200	720×576
	Dynamic Background (DB)	Boats	7999	320×240
	Camera Jitter (CJ)	Traffic	1570	320×240
	Shadow (Sh)	Backdoor	2000	320×240
	Intermittent Object Motion (IOM)	Sofa	2750	320×240
	Thermal (Th)	LakeSide	6500	320×240
CD -net 2014	Bad Weather (BW)	Blizzard	7000	720×480
	Low Frame-Rate (LFR)	Turnpike_0_5_fps	1500	320×240
	Night Videos (NV)	winterStreet	1785	624×420
	Turbulence (Tu)	Turbulence0	5000	720×480

3.2. Main Evaluation Metrics

Three performance measures; Recall, Precision, and F-measure are utilized to measure how well our method matches the ground-truth:

$$\text{Recall} = \frac{TP}{TP + FN} \qquad (1)$$

$$\text{Precision} = \frac{TP}{TP + FP} \qquad (2)$$

$$F_{\text{measure}} = \frac{2 \times \text{Recall} \times \text{Precision}}{\text{Recall} + \text{Precision}} \qquad (3)$$

Where TP is true positives, TN is true negatives, FN is false negatives, and FP is false positives. Typically, there is a trade-off between Recall and Precision, Recall usually increases with the number of foreground pixels detected, which in turn may lead to a decrease in Precision. A good algorithm should attain as high a Recall value as possible without sacrificing Precision. F_{measure} is the harmonic mean between Recall and Precision (a large value of F_{measure} is better).

2D moving objects localization in video surveillance based on fast-ICA   ICMUSTED 2024
algorithm for background subtraction and local Yezzi algorithm for level sets
models

3.3. Quantitative Evaluation

In this section we presents a quantitative comparison between the local regions-based model of Yezzi against its global counterpart to illustrate how the local framework can enhance the performance of a given global energy. The results of this comparison are summarized in Table 2. Observing Table 2 reveals that the local model Yezzi consistently outperform its global counterpart in performance.

Table 2. Quantitative evaluation of the global model Yezzi with its local counterpart

Sequences	Metric Measures	Global Yezzi	Local Yezzi
Office	Recall	0.95	0.99
	Precision	0.73	0.91
	$F_{measure}$	0.82	0.95
PETS2006	Recall	0.97	0.98
	Precision	0.70	0.93
	$F_{measure}$	0.81	0.95
Boats	Recall	0.92	0.97
	Precision	0.69	0.90
	$F_{measure}$	0.78	0.93
Traffic	Recall	0.94	0.95
	Precision	0.80	0.91
	$F_{measure}$	0.86	0.93
Backdoor	Recall	0.93	0.97
	Precision	0.88	0.94
	$F_{measure}$	0.90	0.95
Sofa	Recall	0.96	0.98
	Precision	0.78	0.90
	$F_{measure}$	0.86	0.94
LakeSide	Recall	0.92	0.92
	Precision	0.80	0.90
	$F_{measure}$	0.85	0.91
Blizzard	Recall	0.96	0.98
	Precision	0.90	0.94
	$F_{measure}$	0.93	0.96
Turnpike_0_5_fps	Recall	0.95	0.98
	Precision	0.70	0.88
	$F_{measure}$	0.80	0.92
winterStreet	Recall	0.92	0.96
	Precision	0.63	0.80
	$F_{measure}$	0.74	0.87
Turbulence0	Recall	0.85	0.88
	Precision	0.89	0.96
	$F_{measure}$	0.87	0.92

As it can be seen from Table 2, the local model Yezzi exhibit higher accuracy compared to its global counterpart. This model achieves higher F-measure (from 0.92 to 0.96) except in category NightVideos (WinterStreet sequences about 0.87). This is due to the strong public illumination and lights of vehicles.

In order to simplify the comparison, recall, precision, and F-measure averaged over the all test sequences are given in Table 3.

Table 3. Average recall, precision, and $F_{measure}$ results

	Global Yezzi	Local Yezzi
Recall	0.93	0.96
Precision	0.77	0.90
$F_{measure}$	0.84	0.93

2D moving objects localization in video surveillance based on fast-ICA ICMUSTED 2024
algorithm for background subtraction and local Yezzi algorithm for level sets
models

Moving forward, Table 4 displays the processing time of the local Yezzi model on the aforementioned sequences. The resolutions of the sequences varied from 320×240 to 720×480. Consequently, the runtime of each algorithm is expected to increase with larger image sizes, whereas it will decrease with smaller sizes.

In our experiments, the local Yezzi model takes from 2 to 10 iterations per image to locate the object. This is owing to the use of the results detection of fast-ICA algorithm. The average frame rate of the algorithm is all about 29 fps for the sequences of (320×240) and nearly 20 fps for the sequences of (720×480). Hence, our proposed method demonstrates the capability to accurately detect moving objects in real-time frame speed.

Table 4. Processing speed of local Yezzi model

Sequences Resolution	Processing Speed (fps)
320×240	About 29
720×480	Nearly 20

3.4. Qualitative Evaluation

In this section, we conduct a subjective visual evaluation using a diverse range of indoor and outdoor scenarios. This qualitative assessment serves to reinforce the quantitative findings and highlights the advantages of employing this technique for locating movement in various scenarios. Figures 3 and 4 depict the results obtained by the localization algorithm outlined in Figure 1. In each figure, images (a) and (e) correspond to the original images, while images (b) and (f) represent the moving objects extracted by the ICA method for initializing the proposed fine localization stage. The results of this stage are depicted in images (c) and (g). Subsequently, images (d) and (h) contain the identified objects. The results presented in Figures 3 and 4 are further elaborated upon in Table 5.

Active contour methods face a significant challenge in their sensitivity to the initial contour placement provided by the user. To deal with this issue, our proposed model adopts a rapid initialization approach based on the Independent Component Analysis Method (ICA). This method is adaptive and capable of handling multimodal backgrounds. However, despite its advantages, there are certain drawbacks, as outlined in Table 5 and visually represented in Figures 3 and 4.

(a) Current image: Office (677)

(e) Current image: PETS2006 (992)
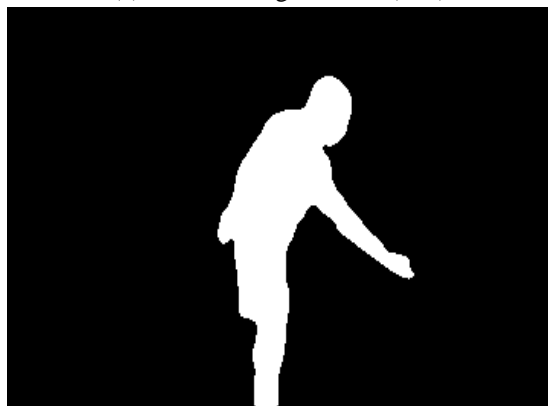
(b) Initial mask
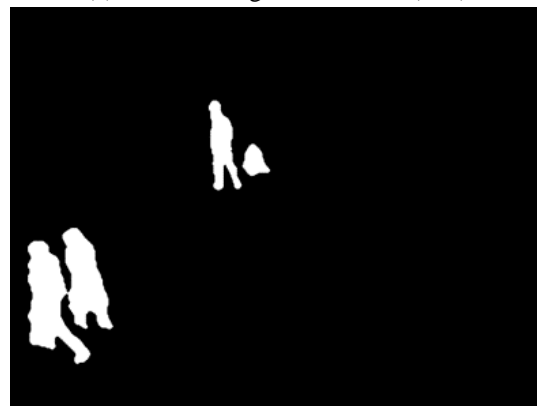
(f) Initial mask
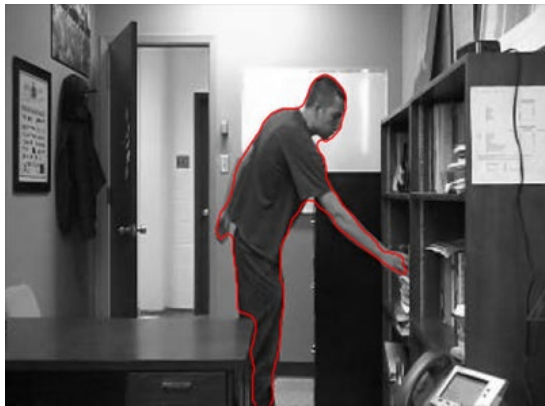
2D moving objects localization in video surveillance based on fast-ICA   ICMUSTED 2024
algorithm for background subtraction and local Yezzi algorithm for level sets
models

(c) Object localization

(g) Object localization

(d) Object segmentation
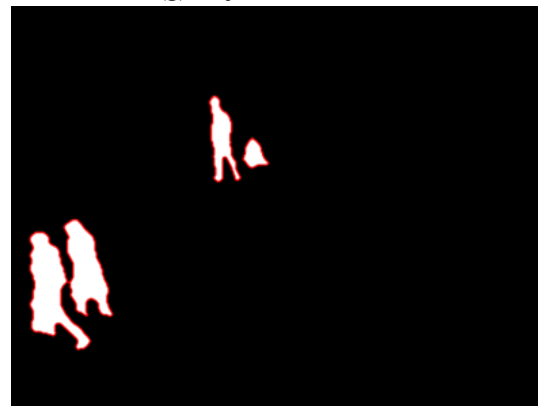
(h) Object segmentation

Figure 3. Samples results of moving object localization of indoor sequences

(a) Current image: Turnpike_0_5fps (874)

(e) Current image: Turbulence0 (2200)

(b) Initial mask

(f) Initial mask

2D moving objects localization in video surveillance based on fast-ICA
algorithm for background subtraction and local Yezzi algorithm for level sets
models

ICMUSTED 2024

<div align="center">(c) Object localization</div>

<div align="center">(g) Object localization</div>

<div align="center">(d) Object segmentation</div>
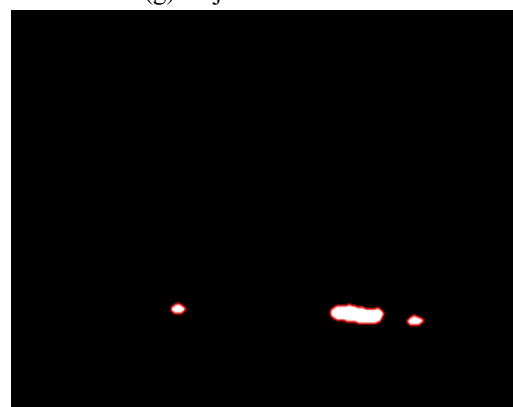
<div align="center">(h) Object segmentation</div>

Figure 4. Samples results of moving object localization of outdoor sequences

Table 5. Illustration of the localization results by local Yezzi model in various sequences

Sequence	Figure	Components of the Initial Mask	Localisation Results
Office	3	One person walking in an office trying to take a file. Small parts of this person doesn't appear behind a desk. Middle illumination in the office.	The person is well located. Several FP pixels are reduced.
PETS2006	3	Three persons walking in railway station. One person left a backpack (abandoned object).	The persons are correctly located. The abandoned object is tracked.
Turnpike (0.5 fps)	4	Vehicles captured with a low frame rate. Some isolated pixels at the bottom of the picture.	The vehicles are located. All the isolated pixels are eliminated. Major of FP pixels reduced.
Turbulence0	4	Three cars far from near-infrared camera at hot summer day. The scene is very large. Large distortion in frames caused by distance and high temperature.	The cars are successfully extracted, and the right location of each moving object is provided. Numerous FP pixels decreased.

4. CONCLUSION

In this paper, we present a novel technique tailored for robustly 2D localizing moving objects in uncontrolled environments. In addition to the conventional steps of image acquisition and digitization, our proposed framework comprises two main blocks. In this initial step, the presence or absence of an object is discerned by separating the motion regions from the background, facilitating the initialization of the localization process. This step is accomplished using the Fast-ICA technique. For the second step, we proposed a local regions-based level set model. This model generates different energies based on two well-known global energies, facilitating the

2D moving objects localization in video surveillance based on fast-ICA ICMUSTED 2024
algorithm for background subtraction and local Yezzi algorithm for level sets
models

localization of the global region. Additionally, the regularity of the level set function is intrinsically maintained by the proposed regularization term, which is linked to the automatic stopping criterion.

The final system exhibits localization recall, precision, and F-measure of, 96%, 90%, and 93%, respectively. These metrics indicate the strong performance of the proposed approach for various scenarios. Moreover, visual results demonstrate the algorithm's ability to efficiently and effectively extract target locations from inherently noisy data. In the future work, the utilization of multiple cameras provides additional data, such as object depth, a critical visual cue for scene comprehension (3D localization). Stereo vision enhances object localization by transitioning the problem from the 2D image domain to the 3D world domain. In our context, we are working to develop a robust stereo matching algorithm to accurately determine the real Euclidean size and distance of objects.

References

[1] D. R. Patrikar and M. R. Parate, "Anomaly detection using edge computing in video surveillance system: Review," *International Journal of Multimedia Information Retrieval*, vol. 11, pp 85–110, 2022.

[2] G. Sreenu and M. A. Saleem Durai, "Intelligent video surveillance: A review through deep learning techniques for crowd analysis," *Journal of Big Data*, vol. 6, art. no. 48, 2019.

[3] S. R. R. Sanches, A. C. Sementille, I. A. Aguilar, and V. Freire, "Recommendations for evaluating the performance of background subtraction algorithms for surveillance systems," *Multimedia Tools and Applications*, vol. 80, pp. 4421–4454, 2021.

[4] M. Gehrig , W. Aarents, D. Gehrig, and D. Scaramuzza, "DSEC: A stereo event camera dataset for driving scenarios," *IEEE Robotics and Automation Letters*, vol. 6, no. 3, pp.4947-4954 july 2021.

[5] J. Mo, Md J. Islam, and J. Sattar, "Fast direct stereo visual SLAM," *IEEE Robotics and Automation Letters*, vol. 7, no. 2, pp 778–785, Apr. 2022.

[6] Y. Li and Z. Wang, "RGB line pattern-based stereo vision matching for single-shot 3-D measurement," *IEEE Transactions on Instrumentation and Measurement*, vol. 70, 2021.

[7] Y. D Teja, "Static object detection for video surveillance," *Multimedia Tools and Applications*, vol. 82, pp. 21627–21639, 2023.

[8] G. Zhai, W. Zhang, W. Hu, and Z. Ji, "Coal mine rescue robots based on binocular vision: A review of the state of the art," *IEEE Access*, vol. 8, pp. 130561–130575, 2020.

[9] S. Paul and A. K. Pal, "An efficient surveillance video coding scheme for static camera based captured video data," in *International Conference on Signal Processing and Integrated Networks*, pp. 868–873, 2019.

[10] A. Krishna, N. Pendkar, and S. Kasar, "Advanced video surveillance system," in *International Conference on Signal Processing and Communication (ICPSC)*, pp. 558–561, 2021.

[11] N. Abderrahmane, M. Boumehed, B. Alshaqaqi, and M. Keche, "Efficient background subtraction method based on fast independent component analysis in video-surveillance," *Indonesian J. Elec. Eng. & Comp. Sci.*, vol. 32, no. 1, pp. 197–205, Oct. 2023.

[12] M. Boumehed, B. Alshaqaqi, A. Ouamri and M. Keche, "Moving objects localization by local regions based level set: Application on urban traffic," *J. Math Imaging Vis.*, vol. 46, pp. 258–274, 2013.

[13] M. Boumehed and B. Alshaqaqi, "New technique for extraction moving object based on active contours for intelligent visual surveillance applications," *International Review on Computers and Software (IRECOS)*, Jul. 2015.

[14] J. A. Yezzi, A. Tsai, and A. Willsky, "A fully global approach to image segmentation via coupled curve evolution equations," *Journal of Visual Communication and Image Representation*, vol. 13, pp. 195–216, 2002.

[15] C. Li, C. Kao, J. Gore, and Z. Ding, "Implicit active contours driven by local binary fitting energy," in *IEEE Computer Vision and Pattern Recognition*, 2007, pp. 1–7.

[16] J. Yuan, "Active contour driven by local divergence energies for ultrasound image segmentation," *IET Image Process*, vol. 7, pp. 252–259, 2013.

[17] A. Hyvärinen, "Independent component analysis: Recent advances," *Philosophical Transactions of the Royal Society A: Mathematical, Physical and Engineering Sciences*, vol. 371, no. 1984, art. no. 20110534, Feb. 2013.

[18] D. M. Tsai and S. C. Lai, "Independent component analysis-based background subtraction for indoor surveillance," *IEEE Transactions on Image Processing*, vol. 18, no. 1, pp. 158–167, Jan. 2009.

[19] N. Fakhfakh, L. Khoudour, E. M. El-Koursi, J. L. Bruyelle, A. Dufaux, and J. Jacot, "Background subtraction and 3D localization of moving and stationary obstacles at level crossings," in *2010 2nd International Conference on Image Processing Theory, Tools and Applications*, 2010, pp. 72–78.

[20] N. Abderrahmane, et al., "Moving objects detection in video-surveillance based on background subtraction method by fast-ICA algorithm," in *2nd International Conference on Engineering and Applied Natural*

2D moving objects localization in video surveillance based on fast-ICA algorithm for background subtraction and local Yezzi algorithm for level sets models

ICMUSTED 2024

Sciences, Oct. 2022, pp. 454–464.

[21] N. Abderrahmane, et al., "Evaluation of Real-Time Background Subtraction Technique for Moving Object Detection Using Fast-Independent Component Analysis in Video Surveillence," in *4th ICEANS*, Nov. 2022, pp. 122–132.

Analysis of Functionally Graded Materials Plates (FGM-P) Using Refined High Order (RHSDT)

Merdaci Slimane[1], Hadj Mostefa Adda[2], Bouchafa Ali[3]

[1]Department of Civil Engineering and Public Works, University Djillali Liabes of Sidi Bel Abbes, Algeria
[2]Department of Civil Engineering, University of Relizane, Algeria
[3]Department of Civil Engineering and Public Works, University Djillali Liabes of Sidi Bel Abbes, Algeria
Corresponding author: Merdaci Slimane (e-mail: slimanem216@gmail.com)

Abstract

Functionally graded materials (FGMs) are microscopically inhomogeneous spatial composite materials, typically composed of a ceramic-metal or ceramic-polymer pair of materials. Therefore, it is important to investigate the behaviors of engineering structures such as beams and plates made from FGMs when they are subjected to bending and thermal loads for appropriate design. Therefore, using an improved high order shear deformation theory based on more rigorous kinetics of displacements to predict the behaviors of functionally graded plates is expected to be more suitable than using other theories. In this paper, the improved the present study is used to investigate bending of functionally graded plates. The analytical solution of the rectangular plate in FGM subjected to static bending is obtained, using the different theories: Euler-Bernoulli theory (CPT), Timoshenko theory (FPT), theory sinusoidal of plates (high order theory) (SPT) and refined plate theory (RPT).

Keywords: Functionally graded materials, Static bending, Shear deformation theory, Refined high order

Predictive Modelling of Material Degradation Using Machine Learning

Tomislav Rolich[1], Ivana Salopek Čubrić[2]

[1]Department of Fundamental Natural and Engineering Sciences, University of Zagreb Faculty of Textile Technology, Zagreb, Croatia
[2]Department of Textile Design and Management, University of Zagreb Faculty of Textile Technology, Zagreb, Croatia
Corresponding author: Ivana Salopek Čubrić (e-mail: ivana.salopek@ttf.unizg.hr)

Abstract

Aging of textile materials involves the gradual degradation of their properties over time due to various internal and external factors. This process is influenced by elements such as UV radiation, temperature, humidity, mechanical wear, and chemical agents. Natural fibres like cotton are more susceptible to aging compared to synthetics, which are generally more resistant but still vulnerable over time. Key effects of aging include reduced strength, elasticity, colour changes, and tactile alterations. To assess aging, standardized tests simulate these factors in controlled conditions. For sportswear materials, particularly polyester (PET), while studies on aging are limited, this paper aims to develop a predictive model for material degradation over time.

Keywords: Machine learning, Predictive, Model, Material, Degradation, Property

1. INTRODUCTION

Aging of textile materials refers to the process of degradation or changes in material properties over time under the influence of various factors. The service life and quality of textile materials are affected by numerous internal and external factors, therefore, research into the aging of materials is very important for the longevity of a textile product. In general, materials made from natural fibres are more susceptible to aging compared to synthetic fibres. For example, cotton fibres can be relatively easily damaged over time by exposure to sunlight and moisture, causing loss of strength and discoloration. In contrast, synthetics are more resistant to many aging factors and are a common choice for making products used outdoors. However, even with this group of materials, degradation occurs under the influence of various factors.

Among the most important factors that affect the aging of textiles, UV radiation, temperature (heat), moisture, mechanical effects and chemical agents stand out in the first place. Their influence is possible in the following ways:

- UV radiation: Sunlight, especially UV rays, causes photooxidation of textile fibers, which leads to discoloration, fading and a decrease in the mechanical resistance of the fibers. This is most pronounced with natural materials such as cotton and wool.
- Temperature and humidity: Extreme temperatures can lead to thermal degradation of fibers, while high humidity can cause the appearance of mold or bacteria, especially in natural fibers. For example, wool is particularly susceptible to damage by moths.
- Mechanical damage: Wear and friction during wearing and product care cause fiber damage, which manifests itself in the formation of microcracks, yarn breakage and thinning of the material itself.
- Chemical agents: detergents, bleaches and various textile cleaning agents can accelerate the aging of textiles. Synthetic materials are more resistant to the action of chemical agents compared to materials made from natural fibers, but they can still show signs of degradation after long-term exposure to aggressive substances.

Because of the aging of textile materials, a decrease in strength and elasticity, a change in tactile characteristics and a change in colour are possible. Related to the decrease in strength, materials lose their original mechanical properties over time, become less resistant to the action of forces, the strength decreases, and it is easier for the material to tear. Elastane yarns in the structure of textile materials lose their elasticity over time, which often results in the deformation of the materials themselves and the objects made from them. Regarding the sense of touch, materials may become stiffer. Also, many materials, especially those exposed to UV rays, lose their original colour or turn yellowish over time. To assess the aging of textile materials, different test methods are used. Some of the

standard tests include simulation of UV radiation, mechanical wear and exposure to chemical agents. These tests help to assess how resistant the textile is to various influences over time. Aging can be carried out in laboratory conditions or by exposing the material to real aging in the open air or in specific conditions characteristic for the use of a particular material. Aging of textile materials is a natural process, but with proper maintenance and the use of quality fibres, it can be significantly slowed down. Understanding the factors that affect aging allows for better protection and a longer life for clothing and textile products.

In sportswear production, the most widely recognised and commonly used type of polyester is polyethylene terephthalate or PET. Polyester fibres lead in global production and consumption among synthetic fibres due to their elasticity, durability, ease of care, and resistance to wear, making them ideal for various applications. PET is also noted for its strong chemical resistance, particularly to acids, as well as its excellent resistance to cleaning solvents and bleaching agents [1,2]. Its recyclability is highly valued for ecological and sustainability purposes. While PET offers good resistance to UV radiation, extended sun exposure can cause degradation, leading to the breakdown of its molecular chains and structural damage. Standard PES fibres typically have a strength range of 30–70 cN/tex, and studies have shown that PET fibres exhibit lower tensile strength compared to standard PES fibres. PET's breaking elongation falls within the 20–30% range [3,4].

As far as the aging of sportswear material is concerned, the literature review indicated lack of studies covering this topic. Our previous studies in the field were focused on the investigation of tactile feeling of materials [5,6], physical-mechanical properties and their changes due to aging [7-9]. The future step, presented in this paper was to develop a model that will be used for the description and prediction of material properties due to aging.

2. MATERIAL AND METHOD

2.1. Materials

For this study was used a set of knitted materials intended to produce sportswear. The materials were subjected to weathering conditions that simulated typical use by football players. This process included static outdoor exposure, with the addition of artificial sweat. The weathering took place during the summer in the Mediterranean region, where the average air temperature was 31°C (with a 7.36% coefficient of variation), the average UV index was 8 (with a 14.49% variation), and the average humidity was 58% (with a 17.27% variation). All environmental data were tracked by the European Meteorological Center ECMWF using the HRES weather forecast model. A diluted acid sweat solution (pH 5.5) was applied to the fabric samples 15 minutes after sun exposure began. After each 2-hour simulated training session, the fabrics were washed at 30°C with phosphate-free detergent and air-dried.
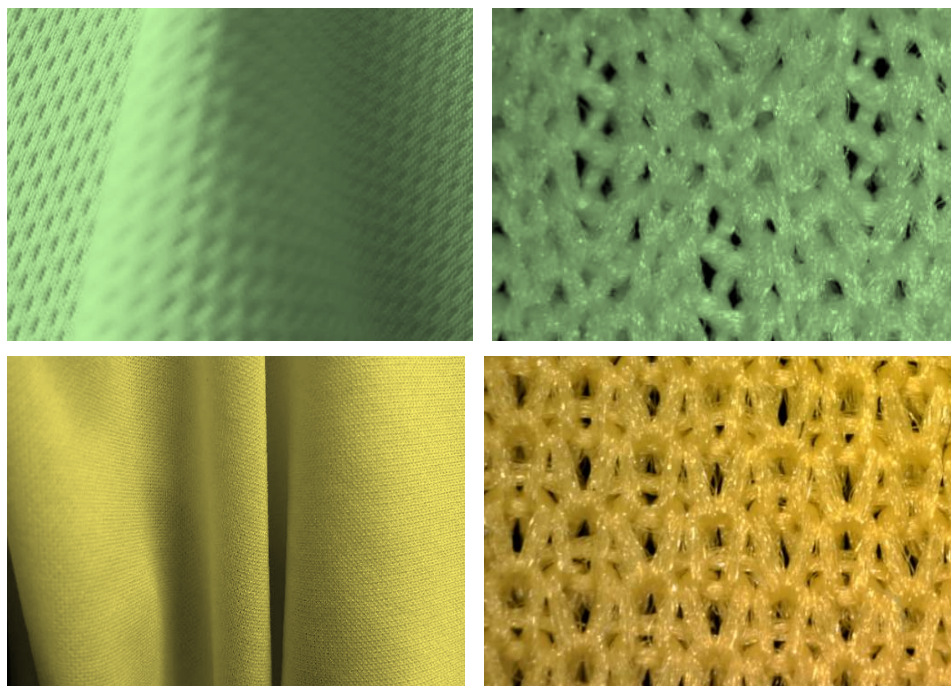
Figure 1. Illustration of the structure of the materials used: Image of material (on the left) and structure under magnification (on the right)

2.2. Instrumental Testing Methods

Both unaged and aged materials were tested for several physical-mechanical properties, i.e.:

- Thickness - D,
- Surface mass - m,
- Force at break in the course direction
- Breaking elongation in the course direction - epsB1,
- Force at break in the row direction - Fp2,
- Breaking elongation in the row direction - epsB2,
- Breaking force (ball burst method) - FB, and
- Pilling rating.

The overview of the testing equipment used is shown in Figure 2.

Thickness tester   Analytic scale   Tensile meter   Bursting tester   Wet and Dry Abrasion Tester
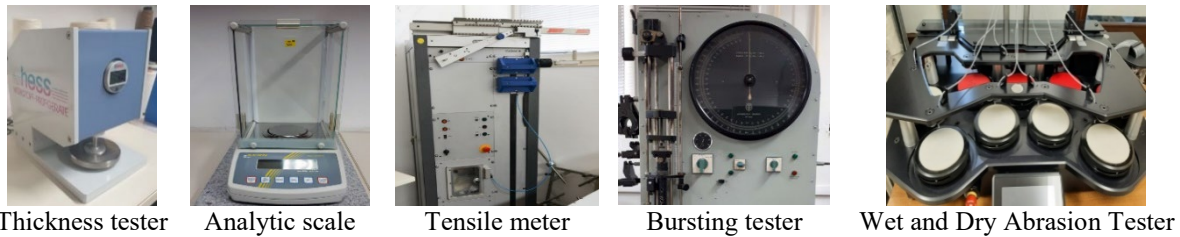
Figure 2. Testing devices used

Material thickness was determined according to EN ISO 5084:1996. The thickness of the specimen was measured as the distance between the reference plate on which the specimen rests and a parallel circular presser-foot that exerts a specified pressure on the area of the textile under test. For each material, 10 repetitions were made.

The surface mass of the material was measured according to the ISO 3801 standard, method 5, where a specimen size of 10 x 10 cm was cut and measured on an analytic scale with an accuracy of +/- 0.001 g.

The force at break and the breaking elongation are recorded according to ISO 13934-1. Using this method, a fabric test specimen with dimensions 200x50 mm is being prolonged with a constant elongation force, upon rupture. The measurements were conducted in the directions of courses and wales. For the measurement was used the tensile tester produced by Textechno company.

According to the standard ISO 13938-2 materials were measured on a burst tester using the 'ball burst test'. The test determined the force required for bursting the material.

The testing of material piling was performed using the AquaAbrasion – Wet and Dry Abrasion Tester, produced by James Heal. For the abrasion was used the standard woven woollen material. The diameter of the woven woolen felt base was 140 ± 5 mm. Normal-pressure of 9 kPa was used and the total number of cycles was 2500. After the abrasion, the specimens were photographed by digital microscope and appearance due to pilling was rated.

2.3. Model Development

The WEKA (Waikato Environment for Knowledge Analysis) software was used to develop the J48 classifier. WEKA is a data mining tool that offers various algorithms for data analysis and predictive modelling through a graphical interface. The dataset used in this study contains 70 instances and 19 attributes, with 5 classes (A, B1, B2, C1, C2), each class having 14 samples. The attributes include: thickness - D, surface mass - m, breaking force in the course direction - Fp1, breaking elongation in the course direction - epsB1, breaking force in the row direction - Fp2, breaking elongation in the row direction - epsB2, breaking force (ball burst method) - FB, pilling rating - OP, K, WT1, WT2, OMMC, W, VM, VS, TD, KM, NR, HG, and the output (class). The dataset has 5 classes: Class A corresponds to unaged samples, class B1 corresponds to samples after 12 training sessions and sun aging, class B2 corresponds to samples after 24 training sessions and sun aging, class C1 corresponds to samples after 12 training sessions and shade aging, and class C2 corresponds to samples after 24 training sessions and shade aging. The J48 algorithm was compared with the ZeroR model, which simply predicts the most represented class (A). However, in this case, all classes are equally represented. J48 should provide better results than the ZeroR model as it uses more advanced data analysis.

For the decision tree algorithm, the results can be graphically presented, as shown in Figure 3. At each leaf node, the corresponding class (A, B1, B2, C1, C2) is displayed, with the numbers in parentheses indicating the correct and incorrect classifications for that rule.
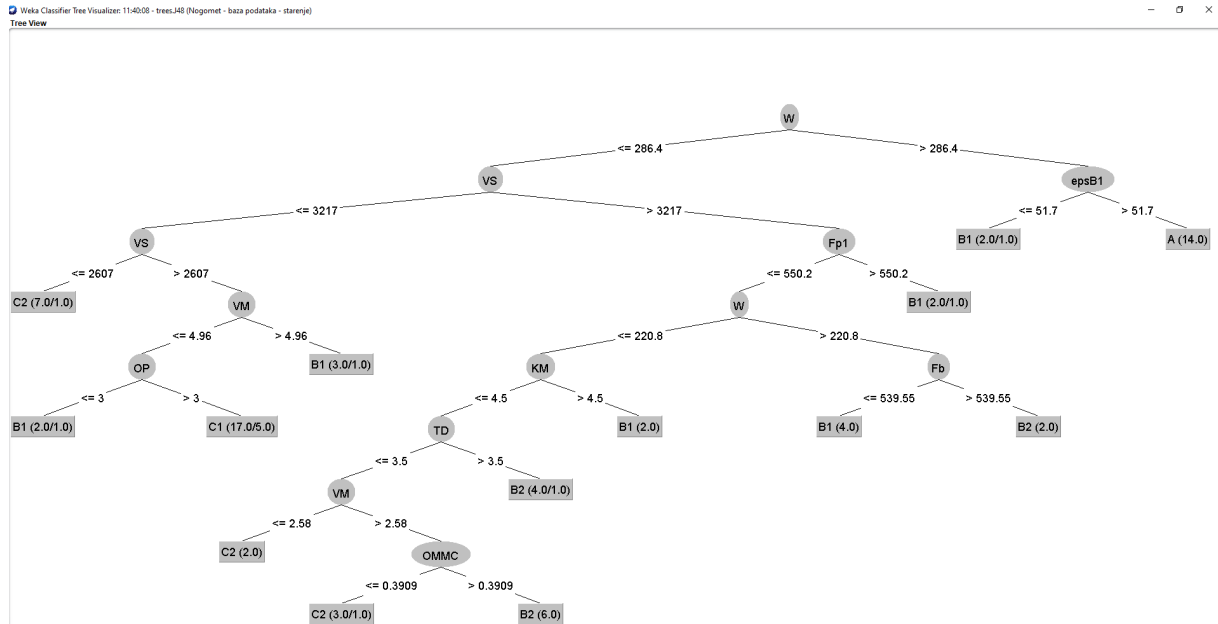
Figure 3. Graphical representation of the decision tree

The results will be presented for a dataset consisting of 70 instances, 19 attributes, and 5 classes. The description of the parameters in Table 2 is provided below:

TP – number of true positives
TN – number of true negatives
FP – number of false positives
FN – number of false negatives

$$TPR = \frac{TP}{TP + FN} \tag{1}$$

$$FPR = \frac{FP}{FP + TN} \tag{2}$$

$$\text{Precision} = \frac{TP}{TP + FP} \tag{3}$$

$$F = 2 \cdot \frac{\text{Precision} \cdot TPR}{\text{Precision} + TPR} \tag{4}$$

$$MCC = \frac{TP \cdot TN - FP \cdot FN}{\sqrt{(TP + FP) \cdot (TP + FN) \cdot (TN + FP) \cdot (TN + FN)}} \tag{5}$$

3. RESULTS AND DISCUSSION

The Matthews correlation coefficient (MCC) is a correlation coefficient between observed and predicted binary classifications, returning a value between -1 and +1. A coefficient of +1 represents perfect prediction, 0 is no better than random prediction, and -1 indicates complete disagreement between prediction and observation. The receiver operating characteristic (ROC) curve is a graphical plot illustrating the diagnostic ability of a binary classifier system as its discrimination threshold varies. The ROC curve is created by plotting the true positive rate (TPR)

against the false positive rate (FPR) at various threshold settings. A precision-recall curve area (PRC Area) is an area of a plot of Precision against TPR.

Table 1 presents the confusion matrix for the J48 algorithm. Table 2 shows detailed accuracy by class for the J48 algorithm. The confusion matrix for the J48 algorithm, shown in Table 1, can be interpreted as follows: 58 of the 70 instances were correctly classified, which is 82.86%, and 12 instances were incorrectly classified, which is 17.14%. By class, 14 cases were correctly classified in class A with 0 misclassifications, 11 cases were correctly classified in class B1 with 3 misclassifications, 11 cases were correctly classified in class B2 with 3 misclassifications, 12 cases were correctly classified in class C1 with 2 misclassifications, and 10 cases were correctly classified in class C2 with 4 misclassifications.

Table 1. Confusion matrix for the J48 algorithm

	Classified as				
	A	B1	B2	C1	C2
A	14	0	0	0	0
B1	0	11	1	2	0
B2	0	1	11	0	2
C1	0	2	0	12	0
C2	0	1	0	3	10

Table 2. Detailed accuracy by class for the J48 algorithm

Class	TP Rate	FP Rate	Precision	F	MCC	ROC Area	PRC Area
A	1.000	0.000	1.000	1.000	1.000	1.000	1.000
B1	0.786	0.071	0.733	0.759	0.696	0.945	0.813
B2	0.786	0.018	0.917	0.846	0.815	0.980	0.911
C1	0.857	0.089	0.706	0.774	0.716	0.946	0.700
C2	0.714	0.036	0.833	0.769	0.720	0.951	0.796
Weighted average	0.829	0.043	0.838	0.830	0.790	0.965	0.844

4. CONCLUSION

In this paper, a predictive model was developed to assess the degradation of sportswear materials, with a particular focus on polyester fabrics used in sportswear manufacturing. By analysing key aging factors such as UV radiation, temperature, humidity, and mechanical wear, it was found that these factors significantly impact the reduction of mechanical properties, elasticity, and changes in colour and texture of the materials. The study employed standardized tests to simulate the aging process in controlled laboratory conditions, ensuring reliable and repeatable results.

The developed model, based on the J48 algorithm, successfully classified material samples according to different stages of aging, with an accuracy of 82.86%. The model demonstrated solid predictive capability, particularly in classifying material samples that had undergone various simulated training sessions and environmental conditions. This approach enables better evaluation of material longevity and provides valuable insights for designing sportswear with improved resistance to aging.

Further research could focus on expanding the dataset to include other types of textile materials and applying additional machine learning algorithms to further improve prediction accuracy. Additionally, conducting tests under real-world usage conditions would allow for more precise modelling and prediction of the aging process in various environmental settings. The developed model makes a significant contribution to understanding the aging processes of textile materials and can serve as a tool for designing long-lasting materials, especially in the sportswear industry.

Acknowledgments

References

[1] S. G. Hayes and P. Venkatraman, *Materials and Technology for Sportswear and Performance Apparel*, 1st ed.: Taylor & Francis Group, 2016.

[2] B. L. Deopura, R. Alagirusamy, M. Joshi, and B. Gupta, *Polyesters and Polyamides*, 1st ed.: Woodhead Publishing Limited, 2008.

[3] R. Shishoo, *Textiles in Sport*, 1st ed.; E-Book; Woodhead Publishing Limited: Cambridge, 2005.

[4] R. Zhou, J. Yu, and J. Qin, "Comfort properties of modified knitted polyester fabrics," *Melliand International*, vol. 20, pp. 38–41, 2014.

[5] I. Salopek Čubrić, G. Čubrić, and A. Majumdar, "Sensory attributes of knitted fabrics intended for next-to-skin clothing," *Journal of Textile Institute*, vol. 114, pp. 757–762, 2023.

[6] I. Salopek Čubrić, G. Čubrić, and P. Perry, "Assessment of knitted fabric smoothness and softness based on paired comparison," *Fibers and Polymers*, vol. 20, pp. 656–667, 2019.

[7] I. Katić Križmančić, I. Salopek Čubrić, V. M. Potočić Matković, and G. Čubrić, "Changes in mechanical properties of fabrics made of standard and recycled polyester yarns due to aging," *Polymers*, vol. 15, art. no. 4511, 2023.

[8] A. Petrov, I. Salopek Čubrić, and G. Čubrić, "Influence of aging on the physical properties of knitted polymeric materials," *Polymers*, vol. 16, art. no. 513, 2024.

[9] I. Salopek Čubrić, G. Čubrić, I. Katić Križmančić, and M. Kovačević, "Evaluation of changes in polymer material properties due to aging in different environments," *Polymers,* vol. 14, art. no. 1682, 2022.

Robust EEG Signal Prediction via Advanced Deep Learning and Ensemble Strategies

Mouissat Rabah Abderrahmane[1], Hakkoum Khaoula Nour El Houda[2], Hamza Cherif Lotfi[2]

[1]Department of Applied Mathematics and Computer Science, Saint Petersburg State University, Saint Petersburg, Russia
[2]Department of Biomedical Engineering, University of Abou Bekr Belkaid, Tlemcen, Algeria
Corresponding author: Hakkoum Khaoula Nour El Houda (hakkoummkhaoulaanourelhouda32@gmail.com)

Abstract

This study investigates the effectiveness of advanced deep learning and ensemble strategies for predicting harmful brain activity from electroencephalogram (EEG) signals. The primary objective is to enhance predictive accuracy through the integration of three distinct models: HMS ResNet1D-GRU Inference, which combines ResNet and Gated Recurrent Unit (GRU) layers; Features + Head Starter (K + E + KE), focusing on custom feature extraction; and a traditional ResNet-based architecture adapted for time-series data. The methodology involves data acquisition from Parquet files, signal pre-processing with Butterworth filtering to reduce noise, and quantization using Mu-Law encoding for efficient data handling. Missing values in the EEG signals are imputed to maintain integrity. The ensemble approach aggregates the outputs of the three models to improve prediction robustness. The computational environment is optimized for performance using CUDA, leading to a leader board score of 0.32, which significantly exceeds that of individual models. This demonstrates the ensemble's ability to leverage the strengths of each component, resulting in enhanced predictive capabilities. Overall, the proposed methodology shows significant improvements in prediction accuracy for complex brain activities, highlighting its potential for applications in neurophysiological research and clinical diagnostics. Comparative analysis confirms that the ensemble approach outperforms existing single-architecture methods, underscoring the importance of model diversity and feature engineering. This work positions itself among the leading methodologies in EEG signal prediction, paving the way for future research in this domain.

Keywords: EEG, deep learning, ensemble learning, ResNet1d, GRU layers, Butterworth filters, Mu-Law encoding, CUDA

1. INTRODUCTION

Electroencephalogram (EEG) signals are vital for understanding brain activity, serving critical roles in both clinical diagnostics and neurophysiological research [1–3]. Over recent decades, a variety of methods have been developed to analyze EEG data, ranging from traditional statistical techniques to advanced machine learning approaches. Historically, analysis has relied on manual feature extraction from EEG signals, followed by the application of machine learning algorithms such as Support Vector Machines (SVM), k-Nearest Neighbors (k-NN), and Random Forests [4–6]. Early investigations predominantly employed traditional methods like autoregressive modelling [7] and time-frequency analysis [8]. However, these methods exhibited limitations in capturing complex patterns within high-dimensional EEG data, prompting a shift toward deep learning frameworks [9, 10].

While these advanced techniques have shown efficacy in specific contexts, they often necessitate substantial domain expertise for feature selection and data preprocessing [11, 12], and may struggle with generalizability across various datasets. Recent advancements in deep learning have revealed significant potential for EEG signal classification [13]. For example, studies using Convolutional Neural Networks (CNNs) have achieved notable success in identifying seizure activities [14–16]. Similarly, recurrent architectures such as Long Short-Term Memory (LSTM) networks have been employed to capture temporal dependencies in EEG signals, yielding promising results in diverse applications [17, 18]. Nonetheless, these approaches often utilize single-model architectures, which can constrain predictive performance due to their limited ability to generalize across different data scenarios [19, 20].

To overcome these challenges, ensemble learning strategies have emerged as a compelling alternative. By integrating multiple models, ensembles can harness the distinct strengths of each, resulting in improved predictive

accuracy [21–23]. This study proposes an ensemble approach that integrates three distinct models: a hybrid model combining ResNet and Gated Recurrent Unit (GRU) layers (HMS ResNet1D-GRU), a custom feature extraction model (Features + Head Starter [K + E + KE]), and a traditional ResNet architecture adapted for time-series data. This methodology enhances the robustness of predictions and underscores the pivotal role of feature engineering in optimizing model performance, ultimately providing effective predictions of harmful brain activity.

The proposed methodology encompasses several critical steps. Data acquisition and preprocessing techniques are detailed, including signal filtering and strategies for addressing missing values. Model architectures and training processes that form the basis of the ensemble approach are described. The results section offers a comparative analysis of individual model performances and the overall effectiveness of the ensemble strategy, along with insights into hyperparameter tuning and model contributions. A fundamental aspect of this methodology is the rigorous preprocessing of EEG data, which includes applying Butterworth filters to reduce noise and Mu-Law encoding for optimal data representation. Missing data are addressed through a robust imputation strategy, wherein NaN values are replaced with the mean signal value. By employing an ensemble of models, the approach aims to enhance the robustness and reliability of the classification process, with a specific focus on accurately predicting harmful brain activity.

This comprehensive framework establishes significant improvements in the classification of complex brain activities and the prediction of harmful brain activity [24], paving the way for more precise and reliable neurodiagnostic tools. Furthermore, this study has demonstrated promising results and high accuracy, which can significantly advance the medical field of brain activity assessment. Section 2 outlines the methodology, including data acquisition, model architecture, and training procedures. Section 3 presents the results and discusses the implications of the findings. Finally, Section 5 concludes the study, summarizing key contributions and potential avenues for further exploration.

2. MATERIAL AND METHOD

This section outlines the approach taken in this study, detailing the processes of data acquisition, pre-processing, model architecture, training, evaluation, and post-processing. The methodology aims to ensure robust analysis and accurate prediction of EEG signals related to brain activity. Each step is designed to maintain data integrity and enhance model performance, providing a systematic framework for the research:

2.1. Data Acquisition and Pre-Processing

The dataset utilized in this study comprises electroencephalogram (EEG) signals, which were derived from a publicly accessible repository hosted on Kaggle, specifically from the HMS - Harmful Brain Activity Classification competition. To ensure the consistency of the samples, the central 50 seconds of each EEG recording were selected for analysis (Figure 1). Missing data points within the signals, represented as NaN, were addressed by substituting these values with the mean of the respective channel. In cases where an entire channel consisted of NaN values, these were replaced with zeros to maintain data integrity.
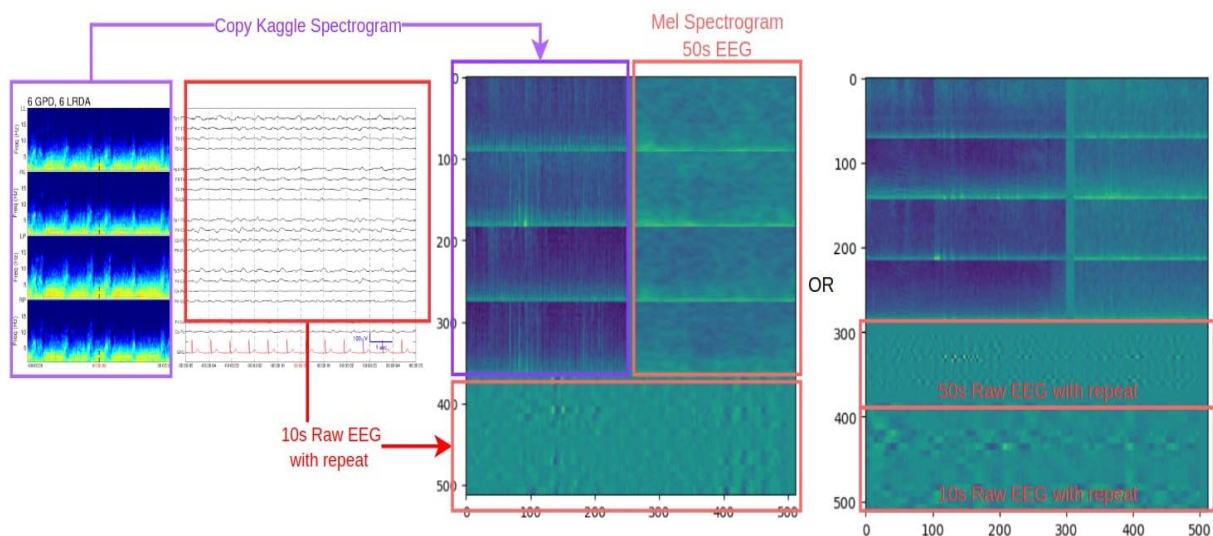
Note: The inputs here do not match. Just to demonstrate the idea.

Figure 1. Input EEG data

The EEG channels selected for this study included Fp1, T3, C3, O1, Fp2, C4, T4, and O2. These channels were chosen based on their relevance to the study's objectives and were used to construct the feature matrix that served as input to the machine learning model. To enhance the quality of the signals, a Butterworth bandpass filter was applied, with a low cut-off frequency of 0.5 Hz and a high cut-off frequency of 20 Hz. The filter was designed with an order of 6, allowing for effective noise reduction while preserving the essential characteristics of the EEG signals.

2.2. Model Architecture

The study employed a custom deep learning model, designated as resnet1d "gru", which integrates a one-dimensional ResNet architecture with Gated Recurrent Unit (GRU) layers. three distinct models were utilized and subsequently ensembled to predict harmful brain activity from EEG data. The models included:

2.2.1. HMS Resnet1d GRU Inference

A hybrid model combining ResNet and GRU layers designed to capture both spatial and temporal dependencies in the EEG signals.

2.2.2. Features + Head Starter [K + E + KE]

A model that emphasizes feature extraction using a custom head designed to aggregate and enhance the extracted features.

2.2.3. ResNet-Based Architecture

A traditional ResNet model adapted for time-series data, aimed at capturing intricate patterns in the EEG signals. In this study, the hybrid architecture was selected to leverage both the spatial and temporal characteristics of EEG signals. The model was configured with a series of convolutional kernels of sizes [3, 5, 7, 9, 11], and the final linear layer was set to a feature size of 304. The model's input consisted of sequences of EEG data spanning 50 seconds, sampled at 200 Hz, resulting in 10,000 time steps per sequence. The output of the model was designed to predict six distinct categories related to seizure activity and other brain states: seizure_vote, lpd_vote, gpd_vote, lrda_vote, grda_vote, and other_vote.

2.3. Training and Evaluation

The model training process was conducted using the Adam optimizer, with a batch size of 32. The learning rate and other hyperparameters were fine-tuned according to the specific requirements of the model. Cross-validation techniques were employed to ensure the generalizability and robustness of the model. Performance evaluation was carried out using the Kullback-Leibler (KL) divergence metric, which quantifies the divergence between the predicted probability distribution and the actual distribution of the target classes. This metric was chosen due to its sensitivity in detecting deviations in probability distributions, making it suitable for this classification task.

All computational experiments were performed in a CUDA-enabled environment with access to GPUs, provided through the Kaggle platform. PyTorch was utilized as the primary deep learning framework, given its efficiency and flexibility in handling complex neural network architectures. In detail shown in the Figure 2.

2.4 Post-Processing

Following model inference, the outputs were subjected to µ-law encoding, a form of quantization that reduces the dynamic range of the data while retaining key signal features. This post-processing step was critical in ensuring that the model's predictions were both accurate and interpretable. Additionally, a secondary bandpass filtering process was applied to the model's output to further refine the results. This filtering was focused on isolating the relevant frequency bands that correspond to the targeted brain activities, thereby enhancing the clarity and reliability of the final predictions.

2.5 Model Tuning and Hyperparameters

Significant effort was placed in hyperparameter tuning for each model to optimize performance while avoiding overfitting. The ensemble's final configuration was achieved after multiple iterations, balancing the contributions

of each model effectively. Techniques such as cross-validation and careful monitoring of loss curves were used to ensure that the models generalize well to unseen data.
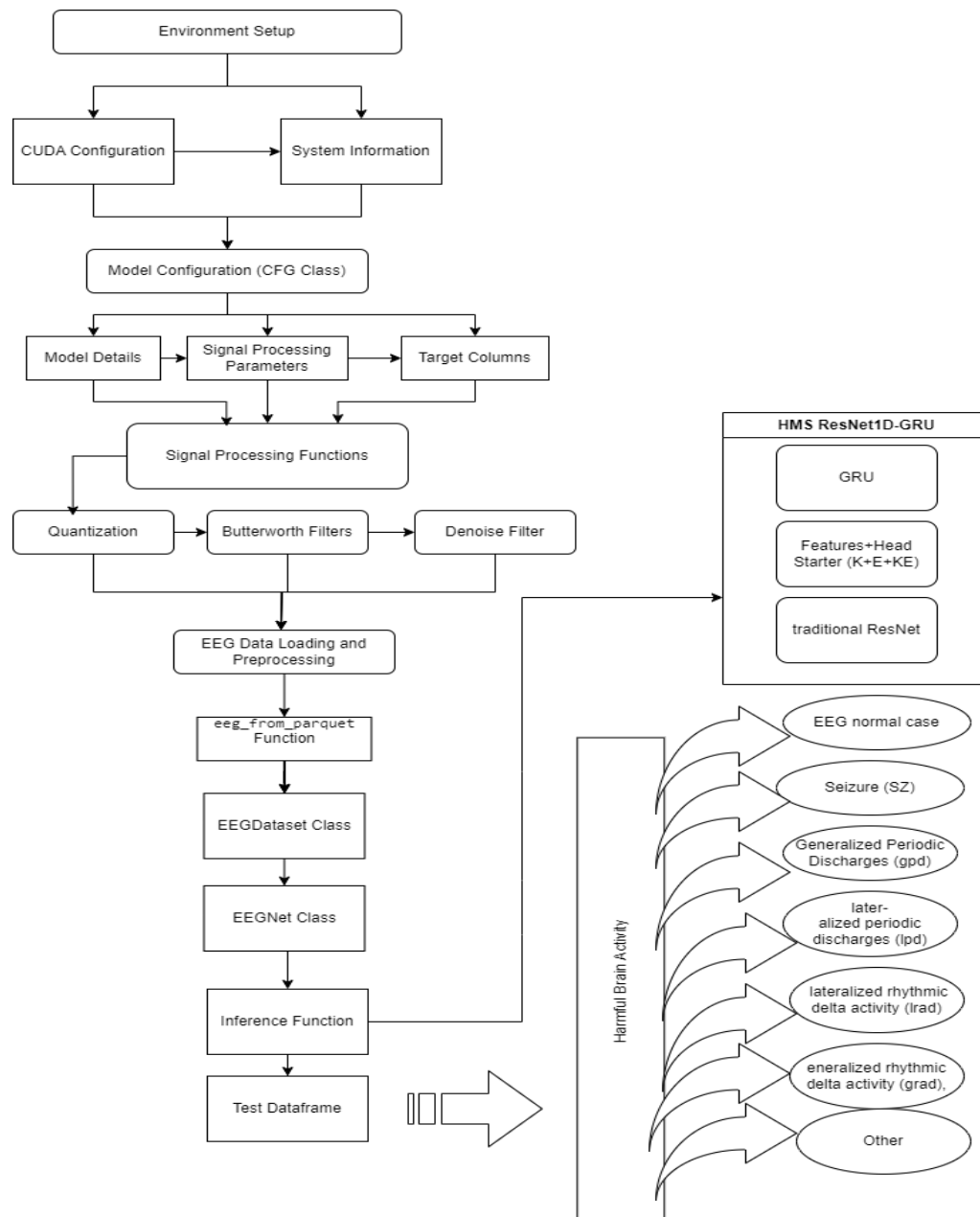
Figure 2. Method diagram of EEG data prediction: Harmful brain activity

3. RESULTS

This section presents the results of the modeling efforts, emphasizing both the ensemble performance and the contributions of individual models following data preprocessing. The accompanying figure illustrates the potential phase shift, indicated by the red box (Figure 3).

The ensemble approach, which integrates multiple models, aims to enhance prediction accuracy by leveraging their unique strengths. The method employed facilitated the presentation of distinctive results regarding the prediction of harmful brain activity, and focuses on seven key patterns of interest: EEG normal case, seizure (SZ), generalized periodic discharges (gpd), lateralized periodic discharges (lpd), lateralized rhythmic delta activity (lrad), generalized rhythmic delta activity (grad), and a category labeled as "other" as shown in Table 1. The discussion begins with the overall performance of the ensemble, followed by a detailed examination of each model's contribution, illustrating how their individual capabilities collectively resulted in improved predictive performance.
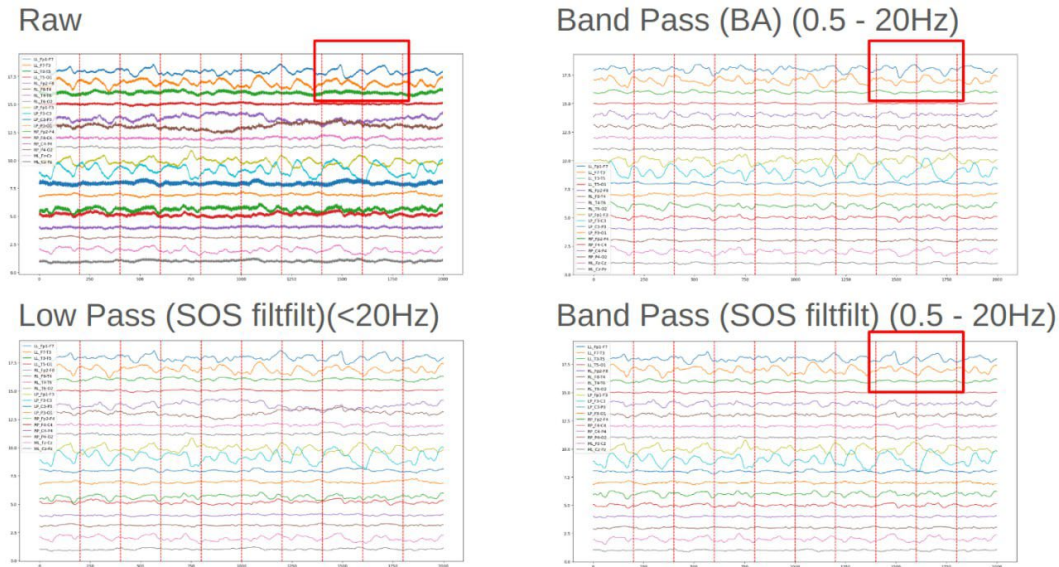
Figure 3. The potential phase shifts

Table 1. Harmful brain activity prediction

Classes	eeg_id	Seizure_vote	Lpd_vote	gpd_vote	lrad_vote	grad_vote	other_vote
Parameter Value	3911565283	0.3061	0.0517	0.004668	0.248397	0.056106	0.608518

3.1. Ensemble Performance

The ensemble of these models resulted in a Leaderboard (LB) score of 0.32. This performance was found to be superior when compared to the individual model scores, demonstrating the effectiveness of the ensemble method in improving predictive accuracy. The ensemble leveraged the diverse strengths of each model, leading to a more robust overall prediction.

3.2. Individual Model Contributions

3.2.1 HMS Resnet1d GRU Inference

This model's use of GRU layers was particularly beneficial in capturing the sequential nature of EEG signals. The ResNet layers further contributed to capturing complex patterns, making this model a strong individual performer.

3.2.2. Features + Head Starter [K + E + KE]

By focusing on handcrafted feature extraction, this model contributed unique high-level patterns that were crucial in improving the ensemble's performance. The custom head architecture provided an additional layer of feature aggregation that was beneficial in enhancing model output.

3.2.3. ResNet-Based Architecture

This model, adapted from the traditional ResNet for time-series classification, played a crucial role in capturing the finer details in the EEG signals. Its deep convolutional layers allowed for effective pattern recognition, complementing the other models in the ensemble.

4. DISCUSSION

This study presents a comprehensive examination of an ensemble approach combining three distinct deep learning models to enhance the prediction of harmful brain activity from EEG signals. The results icmonstrate a clear advantage of using ensemble strategies over traditional single-model architectures, with a leaderboard score of 0.32, which surpasses the performance of individual models. This aligns with findings from previous studies that

advocate for ensemble methods in various domains, emphasizing their robustness and predictive accuracy [22, 23].

Comparative analysis with previous studies reveals significant advancements in predictive capabilities through the proposed methodology. Earlier works have primarily relied on traditional machine learning techniques, such as SVM and k-NN, which, while effective, often fell short in their ability to capture complex temporal patterns inherent in EEG data [4, 6]. By integrating deep learning methods, particularly the hybrid ResNet1D-GRU model, this study effectively addresses these limitations, showcasing improved classification performance in identifying seizure activities and other brain states [14, 15].

The importance of feature extraction, highlighted by the Features + Head Starter model, echoes findings from past research that stress the role of domain-specific feature engineering in enhancing model performance [11, 12]. The unique feature aggregation capabilities of this custom model empowered the ensemble, demonstrating that tailored approaches can yield substantial improvements in classification tasks [9]. Each model within the ensemble contributed uniquely to the overall performance. The HMS ResNet1D-GRU model effectively captured sequential dependencies, a critical aspect when analyzing time-series data like EEG signals. This functionality aligns with the successes noted in studies employing LSTM networks for similar tasks [17, 18]. The ResNet-based architecture, adapted for time-series classification, further corroborates the findings of Nakagome et al. (2022), which emphasize the effectiveness of convolutional networks in recognizing intricate patterns within EEG data [19].

Despite these advancements, challenges persist in the field of EEG signal classification. One of the most significant challenges is the variability in EEG signals across different individuals and recording sessions, which can lead to diminished model performance when applied to new, unseen data [9, 25]. To address this, researchers have explored transfer learning and domain adaptation techniques, which have shown potential in enhancing the robustness and adaptability of EEG classifiers across different datasets [10, 13].

Another challenge was the complexity involved in tuning and managing the ensemble. Each model required careful hyperparameter tuning, and combining their outputs effectively posed additional difficulties. This highlights the need for more streamlined approaches to ensemble learning, potentially through automated machine learning (AutoML) techniques that can optimize model combinations with minimal manual intervention. Additionally, the risk of overfitting remains a concern, especially when dealing with complex models and smaller datasets. Future work should explore more robust methods for preventing overfitting, such as dropout or advanced regularization techniques.

The promising results of this study lay the groundwork for future research in neurophysiological diagnostics. Enhanced predictive accuracy in identifying harmful brain activities can lead to improved clinical tools for monitoring and diagnosing neurological disorders [24]. As deep learning methodologies continue to evolve, further exploration of hybrid models and ensemble strategies may unlock new avenues for research, particularly in real-time applications where timely and accurate predictions are critical.

This study not only demonstrates the efficacy of an ensemble learning framework for EEG signal analysis but also reinforces the significance of model diversity and tailored feature engineering in advancing predictive performance. The findings underscore the potential of this methodology to influence future research and clinical practices in the field of neurodiagnostics.

5. CONCLUSION

The present research successfully demonstrates the effectiveness of an ensemble learning approach to enhance the prediction of harmful brain activity from EEG signals. By integrating three distinct models—HMS ResNet1D-GRU Inference, Features + Head Starter (K + E + KE), and a ResNet-based architecture—this research achieved a notable leaderboard score of 0.32, surpassing the performance of individual models and traditional methods. The findings highlight the importance of model diversity and tailored feature engineering in improving predictive accuracy. Each model contributed unique strengths, effectively capturing both temporal and spatial dependencies within EEG data. This ensemble approach not only addresses the limitations of earlier single-model techniques but also sets a precedent for future research in neurophysiological diagnostics. Despite the advancements achieved, challenges remain, particularly regarding the variability in EEG signals across individuals and the complexity of managing ensemble models. Future work should focus on refining these methods, exploring transfer learning and domain adaptation techniques, and developing automated approaches for model optimization. Ultimately, this research underscores the potential of ensemble learning frameworks in clinical settings, paving the way for more

accurate and reliable detection of harmful brain activities. The implications of these findings extend beyond academic research, offering valuable insights into the development of clinical tools for monitoring and diagnosing neurological disorders.

Acknowledgments

References

[1]   S. Benbadis, "The role of EEG in patients with suspected epilepsy," *Epileptic Disorders*, vol. 2, pp. 143–155, 2020.

[2]   C. Babiloni, "What electrophysiology tells us about Alzheimer's disease: a window into the synchronization and connectivity of brain neurons," *Neurobiology of Aging*, vol. 85, pp. 58–73, 2020.

[3]   M. Hallett, "Human brain connectivity: Clinical applications for clinical neurophysiology," *Clinical Neurophysiology*, vol. 131, pp. 1621–1651, 2020.

[4]   S. Jukic, "Comparison of ensemble machine learning methods for automated classification of focal and non-focal epileptic EEG signals," *Mathematics*, vol. 8, art. no. 1481, 2020.

[5]   P. Boonyakitanont, "A review of feature extraction and performance evaluation in epileptic seizure detection using EEG," *Biomedical Signal Processing and Control*, vol. 57, art. no. 101702, 2020.

[6]   S. I. Ben, "EEG epileptic seizure detection and classification based on dual-tree complex wavelet transform and machine learning algorithms," *The Journal of Biomedical Research*, vol. 34, pp. 151–161, 2020.

[7]   A. Subasi, "EEG signal classification using wavelet feature extraction and a mixture of expert model," *Expert Systems with Applications*, vol. 32, pp. 1084–1093, 2007.

[8]   C.-F. Lin, "Chaotic visual cryptosystem using empirical mode decomposition algorithm for clinical EEG signals," *Journal of Medical Systems*, vol. 40, pp. 1–10, 2016.

[9]   B. Garcia Santa Cruz, "Machine learning models for diagnosis and prognosis of parkinson's disease using brain imaging: General overview, main challenges, and future directions," *Frontiers in Aging Neuroscience*, vol. 15, art. no. 1216163, 2023.

[10]   K. He, "Deep residual learning for image recognition," in *IEEE Conference on Computer Vision and Pattern Recognition*, 2016, pp. 770–778.

[11]   M. M. Islam, "Human activity recognition using tools of convolutional neural networks: A state of the art review, data sets, challenges, and future prospects," *Computers in Biology and Medicine*, vol. 149, art. no. 106060, 2022.

[12]   D. Bone, "Signal processing and machine learning for mental health research and clinical applications [perspectives]," *IEEE Signal Processing Magazine*, vol. 34, pp. 196–195, 2017.

[13]   S. Aggarwal, "Review of machine learning techniques for EEG based brain computer interface," *Archives of Computational Methods in Engineering*, vol. 29, pp. 3001–3020, 2022.

[14]   F. Achilles, "Convolutional neural networks for real-time epileptic seizure detection," *Computer Methods in Biomechanics and Biomedical Engineering: Imaging & Visualization*, vol. 6, pp. 264–269, 2018.

[15]   T. Iešmantas, "Convolutional neural network for detection and classification of seizures in clinical data," *Medical & Biological Engineering & Computing*, vol. 58, pp. 1919–1932, 2020.

[16]   S. Raghu, "EEG based multi-class seizure type classification using convolutional neural network and transfer learning," *Neural Networks*, vol. 124, pp. 202–212, 2020.

[17]   G. Li, "Deep learning for EEG data analytics: A survey." Concurrency and Computation: Practice and Experience," *Concurrency and Computation: Practice and Experience*, vol. 32, art .no. e5199, 2020.

[18]   A. Sikka, "Investigating the temporal dynamics of electroencephalogram (EEG) microstates using recurrent neural networks," *Human Brain Mapping*, vol. 41, pp. 2334–2346, 2020.

[19]   S. Nakagome, "Deep learning methods for EEG neural classification," in *Handbook of Neuroengineering*, Singapore, Springer, 2022, pp. 1–39.

[20]   X. Wang, "Automated recognition of epilepsy from EEG signals using a combining space–time algorithm of CNN-LSTM," *Scientific Reports*, vol. 13, art. no. 14876, 2023.

[21]   Z. Wan, "A review on transfer learning in EEG signal analysis," *Neurocomputing*, vol. 421, pp. 1–14, 2021.

[22]   S. M. Usman, "A deep learning based ensemble learning method for epileptic seizure prediction," *Computers in Biology and Medicine*, vol. 136, art. no. 104710, 2021.

[23]   S. Bouazizi, "Enhancing accuracy and interpretability in EEG-based medical decision making using an explainable ensemble learning framework application for stroke prediction," *Decision Support Systems*, vol. 178, art. no. 114126, 2024.

[24] L. J. Hirsch, "American clinical neurophysiology society's standardized critical care EEG terminology," *Journal of Clinical Neurophysiology*, vol. 38, pp. 1–29, 2021.

[25] X. Zhang, "A survey on deep learning-based non-invasive brain signals: recent advances and new frontiers," *Journal of Neural Engineering*, vol. 18, art. no. 031002, 2021.

Biomechanical Assessment of Caries Effects on Tooth Stability in the Alveolar Bone

Ali Merdji[1,2], Laid Aminallah[1], Ali Benaissa[1], Noureddine Della[1], Sandipan Roy[3]

[1]Department of Mechanical Engineering, Faculty of Science and Technology, University of Mascara, Algeria
[2]Laboratory of Mechanics and Materials Physics (LMPM), Mechanical Engineering Department, University of Sidi Bel-Abbes, Algeria
[3]Department of Mechanical Engineering, SRM Institute of Science and Technology, 603203 Kattankulathur, India
Corresponding author: Ali Merdji (e-mail: merdji_ali@yahoo.fr)

Abstract

This study presents a numerical analysis of the impact of dental caries on the stability of the periodontal system using a 3D finite element method. The objective was to assess the stresses in the bone surrounding a tooth under dynamic mastication and combined loading conditions. A comparative analysis was conducted between infected and healthy periodontal systems. The infected tooth was modeled with a carious defect introduced in the coronal portion of the tooth. The equivalent von Mises interface stress values of the infected tooth were then compared to those of the healthy tooth. The 3D finite element analysis revealed that maximum stress concentrations primarily occurred at the cervical region of the root and in the alveolar bone. In the cortical bone, the stress was higher in the infected system compared to the healthy system, representing a 37.4% increase. In contrast, the stress increase in the trabecular bone was only 1.6% for the infected model. The concentration of stress at the cervical level may contribute to abnormal bone remodeling or bone loss, potentially leading to the loss of tooth attachment or damage to the surrounding bone. Our findings indicate that carious single-rooted teeth are more susceptible to apical root resorption than healthy teeth. The numerical approach presented here not only provides insight into the biomechanics of cariously infected teeth but can also be applied to evaluate the effectiveness of advanced restorative materials and treatment protocols.

Keywords: Dental caries, Biomechanics, Stress, Finite element method

Therapeutic Potential of *Pistacia Lentiscus* Essential Oil: Antioxidant, Anti-Inflammatory, and Antimicrobial Activities

Fatima Djenad[1], Sabiha Achat[1], Sabrina Idir[1], Yasmine Achat[1], Tassadit Sahki[1]

[1]Laboratory of Biomathematics, Biophysics, Biochemistry, and Scientometrics (L3BS), Department of Food Sciences, Faculty of Sciences of Nature and Life, University of Bejaia, 06000 Bejaia, Algeria
Corresponding author: Fatima Djenad (e-mail: fatima.djenad@univ-bejaia.dz)

Abstract

The Algerian climate supports the growth of a wide range of medicinal and aromatic plants, among which the mastic tree (*Pistacia lentiscus* L.) stands out due to its strong aromatic properties and evergreen foliage. This shrub has long been valued in traditional medicine, and its essential oils (E.O.) have become the focus of increasing scientific interest for their potential health benefits, particularly their antioxidant, antimicrobial, and anti-inflammatory effects. Our study aims to investigate the bioactive potential of *P. lentiscus* E.O. as a natural health product, exploring its suitability for applications in nutraceuticals, and functional foods.

The essential oil was extracted via hydrodistillation and subjected to various in vitro assays to evaluate its antioxidant activity using DPPH radical scavenging, hydrogen peroxide scavenging, and ferrous ion chelation methods. The oil's antimicrobial activity was tested against four bacterial strains: Gram-positive (*Staphylococcus aureus* and *Enterococcus faecalis*) and Gram-negative (*Escherichia coli* and *Salmonella enterica*). The anti-inflammatory potential was assessed through heat-induced hemolysis of human erythrocytes and BSA protein denaturation assays. The results showed strong antioxidant activity, with IC50 values of 63.26 ± 1.12 µg/ml for DPPH and 140 ± 0.93 µg/ml for hydrogen peroxide scavenging. The E.O. exhibited superior ferrous ion chelation activity (IC50 = 153.01 ± 1.29 µg/ml) compared to EDTA (IC50 = 187.19 ± 2.45 µg/ml). Anti-inflammatory tests revealed effective membrane stabilization (IC50 = 1.81 ± 0.07 mg/ml) and inhibition of protein denaturation (IC50 = 0.644 ± 0.1 mg/ml), comparable to diclofenac sodium. Antimicrobial assays showed notable efficacy, with *S. aureus* and *E. faecalis* exhibiting MICs below 0.03 mg/mL, while *E. coli* displayed a MIC of 0.08 mg/mL and *S. enterica* had a MIC of 0.37 mg/mL. These findings highlight the potential of *P. lentiscus* E.O. as a multifunctional agent with antioxidant, anti-inflammatory, and antimicrobial properties, offering valuable applications in health-promoting products.

Keywords: *Pistacia lentiscus*, Essential oil, Antioxidant activity, Anti-inflammatory, Antimicrobial properties

Exploring the Biocompatibility of *Lepidium Sativum* Seeds Polysaccharide and Its Potential Therapeutic Properties

Yasmine Achat[1], Khalef Lefsih[1,2], Lila Boulekbache[1], Fatima Djenad[1], Siham Beddar[1], Sabrina Idir[1]

[1]Laboratory of Biomathematics, Biophysics, Biochemistry, and Scientometrics (L3BS), Department of Food Science, Faculty of Nature and Life Sciences, University of Bejaia, 06000 Bejaia, Algeria
[2]Ecology, Biotechnology and Health Laboratory, University of Tizi Ouzou, Algeria
Corresponding author: Yasmine Achat (e-mail: yasmine.achat@univ-bejaia.dz)

Abstract

Polysaccharides are highly abundant molecules in nature with divers biologicals properties, influenced by their monosaccharide compositions and structure. Due to their non-toxic nature, biocompatibility, and medicinal benefits (e.g., anti-tumor, antioxidant, anti-diabetic), they have gained increasing interest. Polysaccharides may have different origins including plants. *Lepidium sativum L,* commonly known as garden cress; and as "Hab el Rashaad" in Arabic, was used by Persians in the form of vegetable and spice (leaves, seeds), and as a medicinal plant due to its composition of biologically active compounds (phenolic substances, polysaccharide). The aim of this work is the extraction and the evaluation of cytotoxicity of *Lepidium sativum* seeds polysaccharide (LSP). First, the powder obtained from the seeds was extracted with hot distilled water. The supernatant was precipitated with ethanol, and the obtained polysaccharide was lyophilized, with total sugar and proteins determined following Dubois and Bradford methods, respectively. The cytotoxicity of LS polysaccharide was assessed in-vitro using a haemolytic assay, and a viability test on human fibroblast cells. LSP solutions at different concentrations were tested on a 10% suspension of normal blood cells obtained from healthy volunteers, the hemolysis rate was calculated by measuring the absorbance. LSP solutions were also tested on fibroblast cells using a CCK8 Kit. The results showed that LSP is composed of 79% of total sugar, and 20% of proteins. The hemolytic activity was increasing as function of concentration increase, and LSP exhibited a maximum hemolytic rate of 9.2% at a concentration of 5mg/mL. LSP at 50μg/mL LSP had no negative impact on fibroblast cells, while 500μg/mL significantly enhanced cells proliferation. These findings suggest that *lepidium sativum* seeds polysaccharide exhibits a good biocompatibility with erythrocytes and fibroblasts, and a possible pro-proliferative effect indicating its potential for pharmaceutical applications.

Keywords: Polysaccharide, *Lepidium sativum*, Biocompatibility, Extraction

Anethum Graveolens L. Seeds in Algeria: An Important Source of Bioactives Compounds with Nutritional and Health Significance

Nour El Houda Belabas[1], Younes Douffa[1], Nadjat Azzi[1], Amel Barkat[2,3], Haifaa Laroui[1], Thoraya Guemmaz[1], Fatima Zerargui[1], Karima Saffidinne[1], Abderrahmane Baghiani[1]

[1]Laboratory of Applied Biochemistry, Department of Biochemistry, Faculty of Nature and Life Sciences, Farhat Abbas University of Setif 1, Setif 19000, Algeria
[2]Promoting Innovation in Agriculture in Arid Regions (PIAAR), Biskra, Algeria
[3]Department of Natural Sciences and Life, Faculty of Exact Sciences Natural and Life Sciences, University of Mohamed Khider, Biskra, Algeria
Corresponding author: Nour El Houda Belabas (e-mail: belabes.nouerlhouda@univ-setif.dz)

Abstract

The seeds of *Anethum graveolens* are well known for their food and nutritional attributes, as well as a wealth of natural phytochemicals, including secondary metabolites, essential oils, and antioxidants. his. Recently, much attention has been focused on dietary polyphenols, as they inhibits oxidation of biomolecules by scavenging free radicals or by inducing endogenous antioxidant enzymes thus protect humans from the onset of various chronic diseases. The objective of this study is to analyze the chemical composition of the ethanol extract obtained from seeds gathered in Setif, Algeria. Additionally, the antioxidant properties of these extract will be evaluated *in-vitro* by using H_2O_2 and OH scavenging assays. The phenolic components were extracted using the method of maceration. The assay of the phenolic compounds showed that the ethanol extract of *A. graveolens* seeds contained considerable amounts of polyphenols and flavonoids. In addition, the ethanolic extract showed antioxidant activity that was distinguished with $IC_{50} = 1.159 \pm 0.017$ mg/ml and $IC_{50} = 1.1 \pm 0.01$ mg/ml for H_2O_2 and OH assays, respectively. Finally, our findings emphasize the significance of *A. graveolens* seeds as a promising reservoir of advantageous health compounds that can used as a promising source of natural antioxidants.

Keywords: Oxidative stress, *Anethum graveolens* L, Polyphenols, Flavonoids, H_2O_2 and OH assays

Inula Viscosa: Total Antioxidant Capacity and Radical Scavenging Activity of Aqueous Extract

Nadjat Azzi[1], Nour El Houda Belabas[1], Younes Douffa[1], Amel Barkat[1,2], Haifaa Laroui[1], Thoraya Guemmaz[1], Fatima Zerargui[1], Karima Saffidine[1], Abderrahmane Baghiani[1]

[1]Laboratory of Applied Biochemistry, Department of Biochemistry, Faculty of Nature and Life Sciences, Ferhat Abbas University of Setif 1, 19000 Setif, Algeria
[2]Promoting Innovation in Agriculture in Arid Regions (PIAAR), Biskra, Algeria
Corresponding author: Nadjat Azzi (e-mail: noura196999@gmail.com)

Abstract

Medicinal plants contain natural antioxidants that neutralise free radicals, protecting the body's cells against oxidative stress. This helps prevent premature ageing and certain chronic diseases. The present study aimed to investigate the relationship between phenolic and flavonoids content and the antioxidant activity of the aqueous fraction (AqE) of the aerial parts of a medicinal plant. Aqueous extract was obtinated out by scale liquid-liquid extraction. Total polyphenols and flavonoids content were estimated using the Folin-Ciocalteu reagent and $AlCl_3$ methods, respectively. Antioxidant activity was performed using the total antioxidant capacity (TAC), nitric oxide (NO•) and hydroxyl (OH•) scavenging assays. The yield of Aqueous fraction obtained was 14.9%. Total polyphenols and flavonoid amounts were 106.16 ± 2.72 μg EGA/mg and 6.06 ± 0.22 μg EQ/mg of extract, respectively. AqE exhibited potentactivity in TAC ($EC_{50} = 47.69 \pm 0.73$ μg/ml), in NO radical scavenging ($IC_{50} = 2065.13 \pm 8.50$ μg/ml) and in OH radical scavenging ($IC_{50} = 3491.48 \pm 6.12$ μg/ml). As a conclusion, in the future in-depth study of *Inula viscosa*'s bioactive compounds and their free-radical scavenging mechanisms could enable the development of more targeted and effective natural treatments.

Keywords: *Inula viscosa*, Phenolic contents, Antioxidant activity, Radical scavenging activity

Classification MRI Images of Depressed Subjects Using Artificial Neural Network Classifier

Mansouria Sekkal[1], Samia Moulebhar[2]

[1]Electronics and Telecommunications Department, Faculty of Science and Technology, University of Ain Temouchent, Ain Temouchent 46000, Algeria
[2]Faculty of Sciences and Technology, University Abd El Hamid Ibn Badis, Mostaganem 27000, Algeria
Corresponding author: Mansouria Sekkal (e-mail: mansouria.sekkal@univ-temouchent.edu.dz)

Abstract

Depression is a mental illness that affects people of various ages. In our study, we have proposed intelligent methods based on artificial intelligence for the automatic diagnosis of depression. Specifically, we developed neural network classifiers utilizing MRI images collected in collaboration with several psychiatrists in Ain-Temouchent city. A total of 100 MRI images were gathered, divided into a training set of 75 cases and a test set of 25 cases. Multiple simulations were conducted to achieve optimal performance. The 'CLSI' classifier demonstrated the best performance, with a classification rate of 90%, an error rate of 10E-5, and 5 neurons in the hidden layer, highlighting the effectiveness of our methods.

Keywords: Depression, Artificial neural network, MRI, Machine learning, Classification

Novel Isoxazolines from (E)-α-Atlantone via [3+2] Cycloaddition Reactions: Experimental Insights, Docking Analysis, and Quantum Investigation

Houria Raji[1,2], Abdellah Zeroual[2], Ahmed Chekroun[1], Haydar Mohammad-Salim[3,4], Asad Syed[5], Ali H. Bahkali[5], Jesús Vicente de Julián-Ortiz[3], Ahmed Benharref[1]

[1]Natural Substances Chemistry Laboratory, Semlalia Faculty of Sciences, Cadi Ayyad University, Marrakech, Morocco
[2]Molecular Modelling and Spectroscopy Research Team, Faculty of Science, Chouaïb Doukkali University, P. O. Box 20, 24000 El Jadida, Morocco
[3]Molecular Topology and Drug Design Research Unit, Department of Physical Chemistry, Pharmacy Faculty, University of Valencia, Burjassot, 46100 Valencia, Spain
[4]Department of Chemistry, Faculty of Science, University of Zakho, Zakho, 42002 Duhok, Iraq
[5]Department of Botany and Microbiology, College of Science, King Saud University, P. O. Box 2455, 11451 Riyadh, Saudi Arabia
Corresponding author: Abdellah Zeroual (e-mail: zeroualabdellah2@gmail.com)

Abstract

In this study, we investigated the cycloaddition reaction of alpha atlantone 1 experimentally and theoretically, using three dipoles. The structure of the synthesized products was determined by proton and carbon-13 nuclear magnetic resonance (NMR) spectral analyses, as well as theoretically using density functional theory (DFT) with base 6-311G(d,p). In addition, an electronic localization function (ELF) analysis of the two reactants was carried out to illustrate the product formation process. Analysis of the reactivity indices and calculation of the activation energies of the transition states showed that this reaction is chemo- and stereoselective. Theoretical results are in good agreement with experimental data. In addition, a docking study was carried out to predict potential drugs against Covid-19 and HIV-1. Ligand-3 proved to be the most promising compound for both viruses, while Ligand-5 showed a more marked specificity for COVID-19. The P-3a product is a promising candidate for drug development where good skin permeation is crucial. However, the low solubility of these products will need to be optimized during formulation to ensure maximum absorption and efficacy.

Keywords: α-Atlantone, Isoxazolines, MEDT, ELF

Whole Genome Sequencing of a Bacteriocinogenic *Enterococcus Faecium* Strain Isolated from Bottarga: Genomic Traits and Characterization of the Enterocins Clusters

Abdelkader Fathallah[1], Mohamed Selim Kamoun[2,3], Chaima Hkimi[2,3], Kais Ghedira[2], Mohamed Salah Abbassi[1,3], Salah Hammami[1,4]

[1]Laboratory of Bacteriology, Tunisian Institute of Veterinary Research, University of Tunis El Manar, Tunis, Tunisia
[2]Laboratory of Bioinformatics, Biomathematics and Biostatistics (LR16IPT09), Pasteur Institute of Tunis, Tunis, Tunisia
[3]Higher Institute of Biotechnology of Sidi Thabet, University of Manouba, Ariana BP-66, Manouba 2010, Tunisia
[4]Research Laboratory "Antimicrobial resistance" LR99ES09, Faculty of Medicine of Tunis, University of Tunis El Manar, Tunis, Tunisia
Corresponding author: Abdelkader Fathallah (e-mail: a.fathallah@yahoo.fr)

Abstract

Enterococcus spp. genera is among Lactic Acid Bacteria, which are known to produce several substances and molecules used for biotechnological purposes or used as probiotic in livestock. During our study aiming to detect beneficial LAB isolates from bottarga, one *Enterococus faecium* strain showed large spectrum of inhibition against pathogenic bacteria, tolerance to salt bile, growth at acidic medium, production of caseinase, no phenotypic virulence factor, and no phenotypic susceptibility to antibiotics. Therefore, to further characterise this isolate, it was studied by Whole Genome Sequencing (WGS) (Financed by the GetGenome Tunisia project). Genetic traits of the isolate were determined by performing WGS using the HiSeq 2500 platform. Carbohydrate utilization and related genes were identified through the integration of KofamScan and KEGG the metabolic pathways identification. The carbohydrate-active enzymes (CAZyme) were investigated using the dbCAN3 server and based on the latest version of the Carbohydrate Active Enzymes Database (CAZy) with a coverage > 0.35 and an E-Value cut-off < 1e-15. WGS showed that the genome of the *E. faecium* strain has a size of 2,630,535 bp, with a GC content of 38.03%. The strain belonged to the sequence type ST722 not known as human clonal lineage. Annotations through the PGAAP tool revealed 2,521 predicted chromosomal genes (coding sequences (CDS)), from which 2,413 are coding CDS (Protein-coding genes with assigned function). The functional annotation of the strain whole genome through the KEGG database using KofaScan revealed a number of genes and pathways belonging to several major types of biological processes (pathways related to metabolic processe, carbohydrate metabolism, amino acid metabolism and nucleotide metabolism). The strain harbored three enterocins encoded by *entA*, *entB*, and *entX* genes. According to WGS findings and phenotypic traits, this isolate showed important traits enabling its application as probiotic or for biotechnological purposes.

Keywords: Bacteriocinogenic, *Enterococcus faecium*, WGS, Biotechnological applications

In Vitro Antioxidant Potential of Methanolic and Aqueous Extracts from a *Chenopodiaceae* Family Plant

Khalil Kaouane[1], Hamza Kemchache[1], Hanane Khither[1], Soraya Madoui[1]

[1]Department of biochemistry, University of Ferhat Abbas, Setif, Algeria
Corresponding author: Khalil Kaouane (e-mail: khalil.kaouane@univ-setif.dz)

Abstract

This study investigated the in vitro antioxidant activities of the methanolic and aqueous extracts of the leaves of a Xero-halophyte species belonging to the *Chenopodiaceae* family. This plant is widely distributed in both non-saline and saline areas, ranging from subhumid to arid regions of Southern Europe, the Eastern Mediterranean, and North Africa, including the Sahara in Algeria. The objectives of the research were to assess the radical scavenging activity of the extracts and determine the total phenolic and flavonoid contents. The results revealed that both methanol and aqueous extracts exhibited radical scavenging activity, as evidenced by the 1,1'-diphenyl-2-picryl-hydrazil (DPPH) assay at a concentration of 1 mg/mL. The methanol extract exhibited a percentage inhibition of 68.47%, while the aqueous extract achieved 49.88%. Furthermore, the methanol extract demonstrated superior ferrous ion chelating activity, with a percentage inhibition of 58.19%, compared to only 10.12% for the aqueous extract at the same concentration. The methanol extract showed a total phenolic content (40.749 ± 1.375 µgGAE/mg) and a total flavonoid content (16.462 ± 0.649 µgQE/mg), the aqueous extract showed a total phenolic content (15.83 ± 1.632 µgGAE/mg) and a total flavonoid content (8.149 ± 0.144 µgQE/mg).

Keywords: Chenopodiaceae, Total phenolic, Flavonoids, DPPH, Ferrous iron chelating

Toxic Plants Used in Folk Medicine and Their Impact on Nutrition and Food Security in Oran, Algeria

Ali Khalfa[1], Fatima Bensalah[1], Sofiane Bouazza[1], Mounir Chihab[1], Farid Bennabi[2], Walid Khitri[3]

[1]Department of Agri-Food, Faculty of Science and Technology, University of Ain Temouchent - Belhadj Bouchaib- Ain Temouchent, Algeria
[2]Department of Biology, Faculty of Science and Technology, University of Ain Temouchent - Belhadj Bouchaib- Ain Temouchent, Algeria
[3]Department of Pharmacy, Faculty of Medicine, University Oran 1, Oran, Algeria
Corresponding author: Ali Khalfa (e-mail: ali.khalfa@univ-temouchent.edu.dz)

Abstract

Since ancient times, humans have relied on plants for food, shelter, and remedies. Today, the practice of using plants for medicinal purposes, known as phytotherapy, enjoys significant popularity, reflecting a broader trend towards natural and holistic health solutions. However, this resurgence in the use of therapeutic plants has brought about several concerns, particularly regarding the free and often unregulated sale of these plants by non-specialized vendors. One major issue is the lack of botanical, analytical, and toxicological control over the plants being sold. Without proper regulation, there is no guarantee that the plants are safe or effective for their intended uses. This lack of oversight can lead to significant variability in the quality and safety of the products available to consumers. Another problem arises from the inconsistent naming and usage indications of the same plant species by different herbalists. Currently, plant intoxications are ranked fourth in cases of poisoning, following domestic drugs, household products, and cosmetics. This statistic highlights the pressing need for better regulation and control of the sale of medicinal plants. Our study aims to shed light on the public health risks posed by the unregulated sale of plants used in popular medicine and to underscore the necessity of implementing stringent regulatory measures. By establishing clear guidelines and controls for the sale and use of medicinal plants, we can protect public health and ensure that consumers can safely benefit from the therapeutic properties of these natural remedies. This regulation should include proper identification, quality assurance, and accurate labeling of medicinal plants to prevent misuse and accidental poisoning.

Keywords: Quality assurance, Phytotherapy, Medicinal plant, Natural remedies, Public health

Nutritional Strategies for Enhanced Recovery in Burn Patients

Ali Khalfa[1], Fatima Bensalah[1], Sofiane Bouazza[1], Mounir Chihab[1], Farid Bennabi[2], Walid Khitri[3]

[1]Department of Agri-Food, Faculty of Science and Technology, University of Ain Temouchent - Belhadj Bouchaib- Ain Temouchent, Algeria
[2]Department of Biology, Faculty of Science and Technology, University of Ain Temouchent - Belhadj Bouchaib- Ain Temouchent, Algeria
[3]Department of Pharmacy, Faculty of Medicine, University Oran 1, Oran, Algeria
Corresponding author: Ali Khalfa (e-mail: ali.khalfa@univ-temouchent.edu.dz)

Abstract

This study aims to identify and evaluate nutritional strategies that significantly enhance recovery outcomes for burn patients, focusing on how specific nutritional interventions aid in wound healing. Material and Methods: Included patients with second and third-degree burns admitted to specialized burn units. Nutritional Assessment: Baseline nutritional status was assessed using anthropometric measurements, serum protein levels, and micronutrient evaluations. Interventions: Protein Intake: High-protein diets and amino acid supplements to support tissue repair. Micronutrient Supplementation: Zinc, vitamin C, and vitamin A to aid collagen synthesis and immune function. Omega-3 Fatty Acids: Anti-inflammatory properties to reduce systemic inflammation. Enteral and Parenteral Nutrition: Based on the patient's condition and ability to ingest food orally. Monitoring and Evaluation: Regular monitoring of nutritional intake, metabolic needs, wound healing progress, and immune function markers. Results: Protein Supplementation: Patients on high-protein diets showed improved wound healing rates and muscle mass retention; Micronutrient Efficacy: Zinc, vitamin C, and vitamin A supplementation enhanced collagen formation and reduced infection rates; Omega-3 Fatty Acids: Reduced inflammatory markers and improved immune response were observed with omega-3 supplementation; Enteral vs. Parenteral Nutrition: Enteral nutrition was associated with better gastrointestinal function and fewer complications than parenteral nutrition. Discussion: Targeted nutritional strategies are crucial for burn patient recovery. Protein supplementation is vital for tissue repair and muscle preservation. Micronutrients like zinc, vitamin C, and vitamin A are essential for collagen synthesis and immune function, reducing infection rates. Omega-3 fatty acids manage systemic inflammation, aiding the recovery process. Enteral nutrition is preferable over parenteral nutrition due to its benefits in maintaining gut integrity and reducing infection risks. Conclusion: Effective nutritional strategies, including high-protein diets, targeted micronutrient supplementation, and omega-3 fatty acids, significantly enhance burn patient recovery. These interventions support wound healing, reduce infection rates, and improve immune response. Whenever feasible, enteral nutrition is recommended over parenteral nutrition.

Keywords: Nutritional strategies, Burn recovery, Protein supplementation, Micronutrient supplementation, Omega-3 fatty acids

Laying Rate and Characteristics of Plymouth Rock Hen Eggs in Oasis Family Farms in the Adrar Region, Southwest Algeria

Abderrahmen Boubekeur[1,2], Mohammed Souddi[2]

[1]Higher School of Saharan Agriculture, Adrar, Algeria
[2]Saharan Natural Resources Laboratory, Faculty of Natural and Life Sciences, University of Ahmed Draia, Adrar, Algeria
Corresponding author: Abderrahmen Boubekeur (e-mail: ma.boubekeur@esas-adrar.edu.dz)

Abstract

The aim of this study is to evaluate the productivity and characteristics of eggs of the Plymouth Rock hen introduced into oasis family farms in the wilaya of Adrar. 60 eggs, 5 eggs per month between October 2022 and September 2023, were collected and analyzed. The eggs were laid by 10 Plymouth Rock hens in a traditional family farm. Monthly laying rates were calculated from the first month of laying. The egg quality parameters studied included weights (whole weight, yolk weight, albumen, shell) and dimensions (length, large diameter). The shape index, yolk/white ratio and the proportion of white, yolk and shell were calculated. The average laying rate was $48.86 \pm 4.03\%$. The peak of egg production (77.42%) was noted in March, which corresponds to the 6th month of laying. The lowest rate (27.42%) was recorded in July. The eggs collected had an average weight of 46.79 ± 1.46 g. The largest eggs (weight > 50 g) were obtained during the cool months (temperature $\leq 30°C$) and the low weight eggs (weight ≤ 40 g) were produced in July and August, which coincide with the hot season. Weighing of different parts of the egg showed that the weight of albumen, yolk and shell were 27.28 ± 0.8 g, 14.93 ± 0.48 g and 4.57 ± 0.22 g respectively. The mean dimensions of the eggs were 48.8 ± 0.68 mm for length and 36.58 ± 0.38 mm for major diameter with mean shape index of 0.75 ± 0.006. The yolk/albumen ratio was 0.55 ± 0.01 and the proportions of yolk, albumen and shell were $31.92 \pm 0.27\%$, $58.38 \pm 0.37\%$ and $9.70 \pm 0.20\%$ respectively. High temperatures during the summer have negatively affected chicken productivity. In conclusion, high temperatures during the summer negatively affected chicken productivity.

Keywords: Adrar, Poultry farming, Oasis, Table eggs, Imported chickens

Anti-Diabetic Properties of Kombucha Made from Dried Coffee Peel: Flavonoid Content and Inhibitory Activity Against α-Glucosidase

Meysin Anjliany[1]

[1]Food Science and Technology, IPB University, Bogor, Indonesia
Corresponding author: Meysin Anjliany (e-mail: anjlianymeysin@apps.ipb.ac.id)

Abstract

Indonesia is rank 4th as the world's largest coffee producers. A significant coffee production volume leads to a substantial amount of waste in the form of coffee cherry husks. These husks contain several bioactive components and can be processed into tea. The processing of dried coffee peel into kombucha increase its phenolic and flavonoid content, which in turn enhances its α-glucosidase inhibitory activity. This study aims to determine the effects of dried coffee peel concentration and fermentation time on total α-glucosidase inhibitory activity, total phenolic and total flavonoid content in dried coffee peel kombucha. The results showed that dried coffee peel concentration, fermentation time, and their interaction significantly affected α-glucosidase inhibitory activity, total phenolic and total flavonoid content ($p < 0.05$). The highest total phenolic content 842.76 ± 10.84 µg GAE/mL and flavonoid content 0.087 mg QE/mL were obtained in kombucha fermented for four days with a dried coffee peel concentration of 3%. The highest α-glucosidase inhibitory activity $91.33 \pm 0.41\%$ was observed after eight days of fermentation with a dried coffee peel concentration of 3%. Overall, an 8-day kombucha fermentation with a 3% dried coffee peel concentration provided the best results regarding total phenolic content, total flavonoid content and α-glucosidase inhibitory activity.

Keywords: Coffee peel, Fermentation, Flavonoid, α-glucosidase

Eco-Friendly Adsorption of Polyphenols from Olive Mill Wastewater Using Biochar Derived from Olive Mill Solid Waste

Kawtar Ezzahi[1,2], Imad Rabichi[1,2], Nabil Rochdi[3,4], Rachid Idouhli[2], Mohamed Hafidi[1], Abdelaziz Bacaoui[2], Abdelghani Yaacoubi[2], Loubna El Fels[1]

[1]Laboratory of Microbial Biotechnologies Agrosciences and Environment (BioMAgE), Faculty of Sciences Semlalia, Cadi Ayyad University, PO Box 2390, 40000 Marrakesh, Morocco
[2]Laboratory of Applied Chemistry and Biomass (LCAB), Faculty of Sciences Semlalia, Cadi Ayyad University, PO Box 2390, 40000 Marrakesh, Morocco
[3]Laboratory of Innovative Materials, Energy and Sustainable Development (IMED-Lab), Cadi Ayyad University, PO Box 549, 40000 Marrakesh, Morocco
[4]Department of Physics, Faculty of Sciences Semlalia, Cadi Ayyad University, PO Box 2390, 40000 Marrakesh, Morocco
Corresponding author: Kawtar Ezzahi (e-mail: k.ezzahi.ced@uca.ac.ma)

Abstract

Olive Mill WasteWater (OMWW), a by-product of olive oil production, presents environmental challenges due to its potent pollutants. The heedless release of this effluent into the environment, particularly from smaller olive mills, bears the potential for profound ecological disruption. In response to this pressing environmental concern, an array of treatment modalities has been posited, each seeking to redress the toxicity inherent in OMWW and curtail its adverse environmental impact. This paper presents an innovative solution for addressing environmental challenges in olive oil production by converting Olive Stone (OS) into biochar (BC), which serves as an effective adsorbent for polyphenol recovery or removal from OMWW. The study highlights the pyrolysis process used to convert OS into biochar. Through a comprehensive research approach, we demonstrate the efficacy of successive biochar filtration as a pretreatment method for raw OMWW. Our findings reveal the significant enhancement of total suspended solids (TSS) and mineral matter (MM) removal from raw OMWW, achieving rates of approximately 86% and 75%, respectively. Additionally, a substantial reduction in total phenolic compounds (TP) and chemical oxygen demand (COD) by 52.34% and 40.90%, respectively, is observed. This study underscores the potential of biochar derived from OS as a sustainable tool for OMWW pretreatment, with notable contributions to pollutant removal and environmental impact mitigation. By transforming waste into a valuable resource, this approach exemplifies the transformative power of eco-friendly practices in reshaping industries and fostering a more sustainable future for olive oil production and wastewater management.

Keywords: Olive mill wastewater, Biochar, Polyphenol adsorption, Sustainable waste management

Optimizing Biochar Preparation for Eco-friendly Adsorption of Polyphenols and Organic Compounds in Pilot-Scale: An Application of Doehlert Designs

Imad Rabichi[1,2], Kawtar Ezzahi[2], Chaima Sekkouri[1], Fatima Ezahra Yaacoubi[1], Karima Ennaciri[1], Loubna El Fels[2], Mohamed Hafidi[2], Abdelaziz Bacaoui[1], Abdelrani Yaacoubi[1]

[1]Laboratory of Applied Chemistry and Biomass (LCAB), Faculty of Sciences Semlalia, Cadi Ayyad University, 40000 Marrakech, Morocco
[2]Laboratory of Microbial Biotechnologies Agrosciences and Environment (BioMAgE), Faculty of Sciences Semlalia, Cadi Ayyad University, 40000 Marrakech, Morocco
Corresponding author: Imad Rabichi (e-mail: i.rabichi.ced@uca.ac.ma)

Abstract

Olive oil production holds a pivotal role in the agroindustry of numerous countries in the Mediterranean basin, contributing to nearly 90% of global production [1]. However, the by-products generated during the extraction process pose significant challenges. Particularly in Africa, where basic production units are prevalent, these units produce a semi-liquid by-product known as olive mill wastewater (OMWW). Unfortunately, the common practice involves disposing of OMWW into evaporation ponds, leading to extended storage times. Over time, the organic load in these liquid effluents undergoes sedimentation, resulting in the formation of large quantities of olive mill waste sludge (OMWS). OMWS represents the most resistant and hazardous pollutant from olive oil extraction processes [2]. This study aims to assess the efficacy of optimizing the conversion of OMSW into biochar through pyrolysis. Our goal is to produce a first-class biochar, adhering to the IBI Standard with a Cog exceeding 60% these optimized conditions to the pilot scale, aiming to generate a substantial quantity of high-quality biochar. Finally, we use this Biochar for the treatment of OMWW and the preparation of Activated carbon. In Morocco, the disposal of olive mill wastewater poses a significant environmental challenge. This study pioneers an innovative approach to address this issue by converting olive OMSW into high-quality biochar. The process employs Response Surface Methodology, focusing on three key parameters: residence time, temperature, and the rate of heating. A Doehlert design and the desirability function are utilized for multicriteria optimization to achieve optimal results. The produced biochar is designed as an adsorbent with the specific purpose of recovering or removing polyphenols from OMWW. The experimental adsorption process is accurately represented by the nonlinear Freundlich isotherm model, supported by a high correlation coefficient ($R^2 = 0.9909$). The maximum achieved polyphenol adsorption is 23.23 mg/g, resulting in the removal of 92.23% of polyphenols, along with 65.46% of Total Organic Carbon and 80.84% of Chemical Oxygen Demand.

Keywords: Pilot-scale, Biochar production, Optimization, Olive mill wastewater, TOC

References

[1] I. Rabichi, F. E. Yaacoubi, C. Sekkouri, K. Ezzahi, K. Ennaciri, L. E. Fels, H. Mohamed, A. Baçaoui, and A. Yaacoubi, "Optimizing biochar preparation for eco-friendly adsorption of polyphenols and organic compounds in pilot-scale: An application of doehlert designs," *Biomass Conversion and Biorefinery*, 2024, doi: 10.1007/s13399-024-06031-0.

[2] I. Rabichi, C. Sekkouri, F.E. Yaacoubi, K. Ennaciri, Z. Izghri, T. Bouzid, L. El Fels, A. Baçaoui, and A. Yaacoubi, "Experimental and theoretical ınvestigation of olive mill solid waste biochar for vanillic acid adsorption using DFT/B3LYP analysis," *Water, Air, & Soil Pollution*, vol. 235, art. no. 369, 2024, doi: 10.1007/s11270-024-07183-5.

Detection of *Citrobacter Sp* in Tilapia Fish (*Oreochromis Sp*) and Tank Water and Its Antibiotic Resistance Pattern

Romeissa Derdachi[1,2,3], Sabrine Boucetta[1]

[1]Department of Nature and Life Sciences, University of August 20, 1955, Skikda, Algeria
[2]Laboratory of Interactions, Biodiversity, Ecosystems and Biotechnology, University of August 20, 1955, Skikda, Algeria
[3]Laboratory of Optimization of Agricultural Production in Subhumid Zones, University of August 20, 1955, Skikda, Algeria
Corresponding author: Romeissa Derdachi (e-mail: romaissaderdachi@gmail.com)

Abstract

Food-borne pathogens causing food-borne diseases are predominant worldwide. This study aimed to investigate the presence and antimicrobial susceptibility profile of *Citrobacter* in tilapia fish and tank water. Tank water was collected in a sterile tube, samples of the skin, gills, and intestines fish were diluted in sterile saline then the streak plate method was used to isolate the bacteria on xylose-lysine-desoxycholate (XLD) agar. The identification was done by morphological characteristics and biochemical tests such as citrate utilization test, catalase test, and cytochrome oxidase test. The drug-resistant pattern was determined by the Kirby-Bauer technique using five antibiotics: Tetracycline, gentamicin, ampicillin, ciprofloxacin, and erythromycin. The results showed the presence of *Citrobacter sp* in fish samples and tank water, the Kirby Bauer test showed that the strains were sensible to tetracycline, ciprofloxacin and gentamicin, and presented resistance to erythromycin and ampicillin. In conclusion, this study determined the presence of *Citrobacter sp* in the gills of tilapia fish and tank water, its presence may pose a health risk to human beings and may cause disease to susceptible individuals, especially immune-compromised consumers. Accordingly, proper hygienic measures from farm to fork and hygienic education for fish handlers/traders and consumers are required.

Keywords: *Citrobacter sp, Oreochromis sp*, Antibiotic resistance

Priming with Chitosan Nanospheres Encapsulating Magnetite-Gibberellic Acid Elicit Tolerance Against Cadmium Toxicity in Wheat Seedlings

Arruje Hameed[1], Alia Ambreen[1], Tahir Farooq[2], Amjad Hameed[3]

[1]Department of Biochemistry, Government College University Faisalabad, Pakistan
[2]Department of Applied Chemistry, Government College University Faisalabad, Pakistan
[3]Nuclear Institute for Agriculture and Biology (NIAB), P.O. Box 128, Jhang road Faisalabad, Pakistan
Corresponding author: Arruje Hameed (e-mail: arrujeh@yahoo.com)

Abstract

Wheat is an important cereal crop and staple food for Asian population. However, its yield is usually encumbered by the abiotic stress like temperature, water and salinity. The detrimental effects of abiotic stress on crop yield have been mitigated by the development of several stress management approaches during the last few decades. Recent studies have shown that nanotechnology may improve agricultural sustainability by encouraging plant growth and development in both stressful and non-stressful environments. Seed nanopriming has emerged as a promising approach modulating the morphological, physiological, and biochemical features in response to biotic and abiotic stresses. Nanospheres is an effective novel strategy for improving seed germination, seedling development and plant growth. In our study, the chitosan nanospheres encapsulating magnetite-gibberellic acid as priming agent showed great potential to mitigate Cd stress. The prepared nanospheres were characterized using X-ray diffraction (XRD), Fourier transform infrared spectroscopy (FTIR) and scanning electron microscopy (SEM). Priming with nanospheres boosted germination, antioxidant scavenging, nutrient absorption, and oxidative tolerance in both stressed and non-stressed conditions. Seed and seedling samples were collected and various biochemical parameters were analyzed to measure the effectiveness of the prepared nanopriming agent. The nanopriming induced a significant increase in enzymatic and non-enzymatic antioxidants enabling the seeds to resist the oxidative damage of Cd stress. The priming treatments also caused a significant reduction in MDA contents along with an increase in other important biomolecules including proteins, sugars and osmolytes etc. The nanopriming-mediated readjustments in physio-biochemical attributes in primed seeds positively influenced the germination and seedling development ensuring sustainable plant growth.

Keywords: Nanopriming, Nanospheres, Cadmium toxicity, Wheat

Antibiotic Therapy and Antibiotic Residues Detection in Tilapia Fish *Oreochromis Sp* (Linnaeus, 1758)

Romeissa Derdachi[1,2,3], Sabrine Boucetta[1]

[1]Department of Nature and Life Sciences, University of August 20, 1955, Skikda, Algeria
[2]Laboratory of Interactions, Biodiversity, Ecosystems and Biotechnology, University of August 20, 1955, Skikda, Algeria
[3]Laboratory of Optimization of Agricultural Production in Subhumid Zones, University of August 20, 1955, Skikda, Algeria
Corresponding author: Romeissa Derdachi (e-mail: romaissaderdachi@gmail.com)

Abstract

The use of antibiotics in aquaculture poses a threat to human health and the contamination of the environment with antibiotic residues and resistant organisms. This study aimed at the screening of doxycycline residues in tilapia fish. Alive tilapia fish were divided randomly into three groups, control group, group 2 treated with 50mg/kg doxycycline, and group 3 treated with 100mg/kg doxycycline. After 13 days of treatment samples of the liver and muscles were evaluated for the presence of doxycycline residues by diffusion method. Petri dishes poured with Muller Hinton agar were seeded with Bacillus subtilis, holes were formed in the agar and filled with 100µl of the extracts of different samples, Petri dishes were incubated for 24 hours at 37°C then the presence of inhibition zones was evaluated. The results showed no inhibition zones around the holes filled with the extracts of the liver and muscles; therefore, these samples did not contain doxycycline residues, which may indicate that the 13-day treatment period was not long enough for the antibiotic to accumulate in fish organs. In conclusion, this study determined the absence of doxycycline residues in tilapia fish after 13 days of therapy, nevertheless, we still cannot say that short-term use of antibiotics is safe. The research for natural alternatives is more reliable.

Keywords: Doxycycline, Antibiotic therapy, Antibiotic residues, *Oreochromis sp*

Priming with Chitosan Nanospheres Encapsulating Magnetite-Gibberellic Acid Elicit Tolerance Against Cadmium Toxicity in Wheat Seedlings

Arruje Hameed[1], Alia Ambreen[1], Tahir Farooq[2], Amjad Hameed[3]

[1]Department of Biochemistry, Government College University Faisalabad, Pakistan
[2]Department of Applied Chemistry, Government College University Faisalabad, Pakistan
[3]Nuclear Institute for Agriculture and Biology (NIAB), Jhang road Faisalabad, Pakistan
Corresponding author: Arruje Hameed (e-mail: arrujeh@yahoo.com)

Abstract

Wheat is an important cereal crop and staple food for Asian population. However, its yield is usually encumbered by the abiotic stress like temperature, water and salinity. The detrimental effects of abiotic stress on crop yield have been mitigated by the development of several stress management approaches during the last few decades. Recent studies have shown that nanotechnology may improve agricultural sustainability by encouraging plant growth and development in both stressful and non-stressful environments. Seed nanopriming has emerged as a promising approach modulating the morphological, physiological, and biochemical features in response to biotic and abiotic stresses. Nanospheres is an effective novel strategy for improving seed germination, seedling development and plant growth. In our study, the chitosan nanospheres encapsulating magnetite-gibberellic acid as priming agent showed great potential to mitigate Cd stress. The prepared nanospheres were characterized using X-ray diffraction (XRD), Fourier transform infrared spectroscopy (FTIR) and scanning electron microscopy (SEM). Priming with nanospheres boosted germination, antioxidant scavenging, nutrient absorption, and oxidative tolerance in both stressed and non-stressed conditions. Seed and seedling samples were collected and various biochemical parameters were analyzed to measure the effectiveness of the prepared nanopriming agent. The nanopriming induced a significant increase in enzymatic and non-enzymatic antioxidants enabling the seeds to resist the oxidative damage of Cd stress. The priming treatments also caused a significant reduction in MDA contents along with an increase in other important biomolecules including proteins, sugars and osmolytes etc. The nanopriming-mediated readjustments in physio-biochemical attributes in primed seeds positively influenced the germination and seedling development ensuring sustainable plant growth.

Keywords: Nanopriming, Nanospheres, Cadmium toxicity, Wheat

Assessment of Physico-Chemical and Biological Parameters in Poultry Manure Composting and the Biodegradation of Antibiotic Residues

Jihane Baghor[1], Mohamed Hafidi[1,2], Loubna El Fels[1]

[1]Laboratory of Microbial Biotechnology, AgroSciences and Environment, Department of Biology, Faculty of Sciences Semlalia, Cadi Ayyad University, 40000 Marrakesh, Morocco
[2]African Susainable Agriculture Research Institute (ASARI), Mohammed VI Polytechnic University (UM6P), 70000 Layoune, Morocco
Corresponding author: Jihane Baghor (e-mail: j.baghor@gmail.com)

Abstract

The expansion of the livestock industry is increasingly creating challenges in managing the vast amounts of waste it generates, which account for about 30% of global agricultural output. According to the FAO, global livestock waste production surpassed 5 billion tons annually by 2018. This growing volume of waste presents serious environmental, public health, and sustainability issues as the industry continues to grow. A significant portion of this waste contains pharmaceutical residues, particularly antibiotics from intensive farming. Estimates from the World Organization for Animal Health (OIE) and FAO suggest that up to 80% of all antibiotics sold globally are used in livestock production. The widespread use of antibiotics leads to contamination and antimicrobial resistance (AMR), disrupting ecosystems, spreading resistant bacteria, and weakening the effectiveness of antibiotics in treating infections. In this context, bioremediation strategies have gained momentum, with composting emerging as one of the most effective methods for treating antibiotic-laden waste. Composting not only helps reduce the volume of waste but also facilitates the degradation of antibiotics through the action of microbial communities. For composting to be successful, it is critical to manage key physicochemical parameters such as temperature, moisture, carbon-to-nitrogen (C/N) ratio, pH, and oxygen levels. These parameters directly influence microbial activity, ensuring efficient organic matter decomposition and contaminant breakdown. Additionally, routine monitoring of antibiotic concentrations using advanced analytical techniques is essential for assessing the progress of degradation and ensuring the compost produced is safe for reuse in agriculture. Our research tackles antibiotic contamination in livestock waste by studying the degradation pathways during composting, identifying key microorganisms and conditions for optimal breakdown. This will help improve bioremediation techniques, promoting sustainable waste management and reducing environmental and health risks.

Keywords: Livestock waste, Antibiotics, Composting, Bioremediation

Valorization of Agricultural Wastes from *Rosa Canina*: Cellulose Extraction and Physico-Chemical Characterization

Fatma Bhiri[1], Fatma Kallel[2], Amir Bouallegue[3], Samira Abidi[1], Gmar Bensidhom[1], Semia Ellouz Chaabouni[2], Aida Ben Hassen Trabelsi[1]

[1]Laboratory of Wind Energy Management and Waste Energy Recovery. Research and Technology Center of Energy, 2050 Hammam-Lif, Tunisia
[2]Laboratory of Plant Improvement and Valorization of Agricultural resource. National School of Engineering of Sfax. University of Sfax. 3038 Sfax, Tunisia
[3]Laboratory of Food Oral Processing, School of Food Science and Biotechnology. Zhejiang Gongshang University, 310018 Hangzhou, China
Corresponding author: Fatma Bhiri (e-mail: fatmabhiri@gmail.com)

Abstract

The hydro-distillation of *Rosa canina* results in a significant amount of waste, which raises environmental and economic concerns. However, by making use of these neglected agricultural wastes, we can not only address these challenges but also provide an attractive and sustainable raw material for green chemistry and energy generation. Therefore, the goal of this study is to extract cellulose from these wastes for the first time. To achieve this, various chemical pretreatments were employed, including defatting, hot water extraction, alkaline treatment, and bleaching. Chemical analysis of the starting material revealed that it contains 23.55% cellulose, 30.91% hemicelluloses, and 34.21% lignin. In order to demonstrate the removal of lignin and hemicelluloses from the fiber surface, a range of physical techniques were utilized, such as colorimetry, scanning electron microscopy (SEM), Fourier transform infrared spectroscopy (FTIR), X-ray diffraction (XRD) and thermogravimetry (TGA). The extracted cellulose showed a yield of 23.34%, a cellulose content of 80.42%, and an average diameter of 9.66 μm. In comparison to the raw material, the extracted cellulose displayed excellent whiteness (75.72), moderate crystallinity (56.34%), and improved thermal stability (Tmax= 350.41 °C). These results suggest that extracted cellulose shows promising potential for the preparation of bio-based materials.

Keywords: Agricultural wastes, Hydro-distillation, *Rosa canina*, Chemical pretreatments, Cellulose extraction

Critical Factors Governing the Activation Process of Olive Residue-Derived Activated Carbons for Enhanced Pollutant Removal

Abdelaziz Ounas[1], Imad Rabichi[1], Zaina Izeghiri[1], Abdelaziz Bacaoui[1], Abdelrani Yaacoubi[1]

[1]Laboratory of Applied Chemistry and Biomass (LCAB), Faculty of Sciences Semlalia, Cadi Ayyad University, 40000, Marrakech, Morocco
Corresponding author: Imad Rabichi (e-mail: rabichiimad20@gmail.com)

Abstract

Activated carbon derived from lignocellulosic biomass, such as olive pomace, has garnered significant attention for its potential in environmental applications, particularly in pollutant removal [1]. This study investigates the chemical activation of Moroccan olive pomace to prepare highly efficient activated carbons using an experimental design approach. The activation process involved impregnation with three acids and three bases, followed by carbonization under nitrogen at varying temperatures and residence times [2]. Key parameters, including activation temperature (T ºC), residence time (Ts), type of chemical agent, and impregnation ratio (chemical agent/olive pomace), were systematically explored to identify optimal conditions. The prepared activated carbons were characterized by their yield (13-69%) and their adsorption capacities for iodine (444-1100 mg/g), methylene blue (31-300 mg/g), and phenol (37-218 mg/g). The total effects of each parameter were visualized through response diagrams, providing insights into their influence on carbon properties. Findings were validated by testing the carbons for the removal of micropollutants such as 2.4-D, MCPA, and humic acid, with adsorption isotherms modeled using the Langmuir equation. An ultimate analysis of olive pomace composition justified its use as a precursor, while thermogravimetric analysis (TGA) monitored thermal decomposition behavior under various heating rates. This research underscores the potential of Moroccan olive pomace as a sustainable source for activated carbon production and offers valuable guidelines for optimizing chemical activation processes aimed at environmental applications.

Keywords: Biomass, Activated carbon production, Optimisation, Wastewater

References

[1]   I. Rabichi, F. E. Yaacoubi, C. Sekkouri, K. Ezzahi, K. Ennaciri, L. E. Fels, H. Mohamed, A. Bacaoui, and A. Yaacoubi, "Optimizing biochar preparation for eco-friendly adsorption of polyphenols and organic compounds in pilot-scale: An application of doehlert designs," *Biomass Conversion and Biorefinery*, 2024, doi: 10.1007/s13399-024-06031-0.

[2]   I. Rabichi, C. Sekkouri, F.E. Yaacoubi, K. Ennaciri, Z. Izghri, T. Bouzid, L. El Fels, A. Bacaoui, and A. Yaacoubi, "Experimental and theoretical investigation of olive mill solid waste biochar for vanillic acid adsorption using DFT/B3LYP analysis," *Water, Air, & Soil Pollution*, vol. 235, art. no. 369, 2024, doi: 10.1007/s11270-024-07183-5.

Examining the Impact of Biochar and Irrigation with Treated Wastewater on Soil Physicochemical Characteristics and Plant Growth (*Zea Mays*)

Asma Dahani[1], Elmostapha Outamamat[1], Khalid Oufdou[1], Mohamed Hafidi[1], Loubna El Fels[1]

[1]Laboratory of Microbial Biotechnologies, Agrosciences and Environment (BioMAgE), Labeled Research Unit-CNRST N4, Cadi Ayyad University, 40000 Marrakesh, Morocco
Corresponding author: Asma Dahani (asmadahani@gmail.com or a.dahani.ced@uca.ac.ma)

Abstract

Morocco places great importance on the reuse of wastewater due to the scarcity of water resources, particularly in arid and semi-arid areas. The government has implemented policies aimed at promoting the safe and sustainable reuse of treated wastewater in various sectors, including agriculture. This study focuses on the impact of irrigating treated wastewater and the use of biochar as a soil amendment on soil physicochemical characteristics, as well as the agro-physiological parameters of maize (*Zea mays*). To achieve this research objective, a greenhouse experiment was conducted on *Zea mays* plants. Various plots were treated with biochar at rates of 0%, 2%, and 3%, and irrigated with either treated wastewater or well water as a control. The results showed that the treated wastewater generally meets the quality standards for irrigation water. The evaluation of irrigating with wastewater and organic amendment using biochar (3%) improved the soil quality by enriching it with mineral elements and enhancing its water retention capacity. This had a positive impact on the performance of the mays plants, as evidenced by good results in both agronomic and physiological parameters. In conclusion, the co-application of biochar and irrigation with treated wastewater can be considered a promising approach in the field of agriculture, in order to combat water scarcity, and on the other hand, to improve the management of solid and liquid waste. However, it is necessary to establish monitoring systems to ensure compliance with irrigation water quality standards in order to prevent any contamination that may affect human and animal consumption.

Keywords: Wastewater, Irrigation, Biochar, Maize, Soil fertility

Evaluation of Rapid Alert System for Food and Feed (RASFF) Data for Pesticide Residues in Fresh Fruits and Vegetables from Türkiye in 2024

Sebahat Oztekin[1]

[1]Department of Food Engineering, Bayburt University, Bayburt, Türkiye
Corresponding author: Sebahat Oztekin (e-mail: ozakca.sebahat@gmail.com)

Abstract

In this study, the rapid alert system for food and feed (RASFF) database was analyzed to evaluate pesticide hazards in fresh fruits and vegetables originating from Türkiye in 2024. The assessment focused on identifying pesticide residues and compliance with safety regulations. Pesticide use in agriculture endangers human health, animals, and the environment. Acute exposure may cause respiratory irritation, dermatitis, and toxicity, as well as chronic issues such as congenital defects, infertility, neurotoxicity, and cancer. Data were analyzed to identify key trends, recurring pesticides, and non-compliance patterns in various product categories. Among the 272 reported pesticide instances, the most frequently detected residues were acetamiprid (20.95%), chlorpyrifos-methyl (16.54%), imazalil (8.08%), chlorpyrifos (5.88%), pyriproxyfen (4.77%), buprofezin (4.04%), diflubenzuron (3.67%), formetanate (2.94%), spirotetramat (2.94%) tebuconazole (2.57%) and indoxacarb (2.20%). A total of 134 notifications were recorded, primarily for fruits like pomegranates, mandarins, and lemons, as well as vegetables such as peppers and tomatoes. Of these, 71.64% were classified as border rejections, with 70.89% assessed as serious risks. Lemons (*Citrus limon, Citrus limonum*) contained imazalil (28.175 ± 14.088 ppm) and propiconazole (5.604 ± 2.802 ppm), far exceeding the allowable limits of 5.0 ppm and 0.01 ppm, respectively. Chlorpyrifos-methyl in citrus fruits (0.396 ± 0.198 ppm > 0.01 ppm) also exceeded limits. Sweet peppers contained spirotetramat (3.953 ± 1.977 ppm > 1.0 ppm), tebuconazole (1.461 ± 0.731 ppm > 0.6 ppm), sulfoxaflor (1.330 ± 0.665 ppm > 0.4 ppm), formetanate (0.458 ± 0.229 ppm > 0.01 ppm), and acetamiprid (1.270 ± 0.635 ppm > 0.3 ppm). The findings highlight the need for robust monitoring and stricter compliance to ensure safe agricultural exports from Türkiye, with recommendations to improve pesticide management in line with the European Union standards.

Keywords: RASSF, Pesticide residues, Fruits and vegetables, Türkiye

1. INTRODUCTION

The rapid alert system for food and feed (RASSF), was established by the European Union (EU) in 1979 under Regulation (EC) No 178/2002, to facilitate the rapid exchange of information regarding food and feed risks, including pesticide residues. Its main objective was to alert member states and international partners about unsafe food and feed, particularly when pesticide residues surpassed the maximum residue limits (MRLs). The portal enables swift communication of food safety hazards among EU authorities, helping to prevent unsafe food and feed from entering the market. Notifications on the portal are classified based on the risk severity and product distribution status, providing detailed information such as actions taken, case dates, hazard categories, risk assessments, notifying countries, and analytical findings [1]. In 2014, the European Commission launched the RASFF Consumers' Portal, which connected RASFF notifications to publicly available information regarding product recalls. By enabling swift communication, RASSF ensured the prompt removal of contaminated products from the market, thereby protecting consumer health. In pesticide residue monitoring, food products were analyzed for compliance, and any non-compliance was reported. These notifications included key details such as the type of pesticide, food product, origin country, detected residue levels, and the acceptable MRL. RASSF notifications were divided into three categories: alert notifications for critical risks requiring immediate action, information notifications for less urgent concerns, and border rejections for products failing EU border inspections [2].

Pesticides are agricultural chemicals used to protect crops from pests during cultivation and to prolong the shelf life of products after harvest. Their application in postharvest treatment is particularly important for imported goods, which can lead to higher pesticide concentrations and increased health risks for consumers. These varied chemical compounds are also employed in households to control pests, ensuring the quality of crops and reducing the spread of diseases carried by insects and rodents. However, their toxicity and environmental persistence pose significant risks. Excessive use, especially in postharvest treatments, can result in food contamination, elevated pesticide levels, and increased risks of poisoning and diseases in humans, ultimately impacting both health and the

environment [3, 4]. High pesticide residue levels compromise the quality of grapes and their processed products, posing health hazards to consumers. Monitoring and regulating these residues is crucial. In the European Union, Regulation 396/2005/EC sets MRLs for pesticides in consumable products, with MRLs for grapes typically ranging from 0.01 mg/kg to 5 mg/kg, depending on the pesticide [5]. Pesticides can be determined using common techniques such as capillary gas chromatography (GC) and high-performance liquid chromatography (HPLC), particularly in reversed-phase mode, and based on the quick, easy, cheap, effective, rugged, and safe (QuEChERS) methodology [3]. The QuEChERS method, when coupled with liquid chromatography-tandem mass spectrometry (LC–MS/MS) and gas chromatography-tandem mass spectrometry (GC–MS/MS), is the most commonly used procedure for pesticide analysis [5].

Certain pesticides, such as acephate and fludioxonil in blueberries, can damage the neurological system, kidneys, and liver, while bifenthrin in strawberries and other greens is linked to central nervous system tumors. Pesticides are associated with cancer, cardiovascular, and neurological diseases, underscoring the need for monitoring pesticide residues in food. Even organic farming, which avoids chemical pesticides, may be affected by contaminated soil or improperly labeled products, making residue detection vital for food safety [6]. For Türkiye, compliance with EU pesticide residue limits was vital, as the country was a significant exporter of fruits and vegetables to the European Union. Exceeding the MRLs could result in product rejections, financial losses, and stricter future inspections, posing challenges for the continuity of exports [2].

Fruits and vegetables, vital for nutrition, were cultivated through conventional, organic, and natural farming practices. Conventional farming significantly depended on the widespread application of agrochemicals, such as pesticides and fertilizers, to optimize agricultural output. In 2022, pesticide consumption hit 3.69 million metric tons, indicating a consistent increase in global agricultural pesticide usage from 1990 to 2022 [7]. Globally, approximately 2 million tons of pesticides are used annually, with herbicides, insecticides, and fungicides making up 47.5%, 29.5%, and 17.5%, respectively [6].

Given that the most commonly detected pesticides in Türkiye-based fruits and vegetables are acetamiprid, chlorpyrifos-methyl, imazalil, and chlorpyrifos, it would be beneficial to first provide an explanation of these substances. For example, acetamiprid is an insecticide commonly used to control pests, particularly aphids in pome fruit and protected tomatoes, as well as aphids and Colorado beetles in potatoes. Its systemic action and rapid effectiveness make it valuable for protecting crops from damage and disease transmission. The applicant proposes its use to promote healthy crop growth and yield while emphasizing the importance of proper application to minimize risks to beneficial insects and the environment [8]. Chlorpyrifos and chlorpyrifos-methyl are organophosphate insecticides that controls a variety of pests but poses risks to non-target organisms, including beneficial insects and humans [9]. Epidemiological, in vivo, and in vitro studies reveal that chlorpyrifos exposure harms the developing nervous system, reducing IQ in school-aged children at current exposure levels [10]. Imazalil is a fungicide used primarily to combat fungal diseases in fruits and vegetables, especially citrus and bananas, and is often applied postharvest to extend shelf life [11]. Although these pesticides play a vital role in managing agricultural pests, they also pose considerable concerns regarding their effects on health and the environment.

According to the 2024 RASSF notifications, Türkiye recorded the highest percentage of pesticide notifications in fruits and vegetables, accounting for 24.47%. Out of a total of 547 notifications regarding pesticide residues in these products, Türkiye was responsible for 134 notifications, highlighting its significant contribution to the overall figure. This situation highlights a significant disparity compared to other countries, with Türkiye contributing nearly a quarter of all notifications. Furthermore, Egypt ranked second with 12.98%, which is almost half the rate observed for Türkiye. Kenya, India, and Vietnam followed with 6.76%, 6.22%, and 4.57%, respectively, indicating the necessity of stricter controls on agricultural exports in these regions. Meanwhile, Spain and Italy recorded lower percentages, 3.11% and 1.83%, likely reflecting the influence of the European Union's stringent food safety and pesticide regulations [12]. Therefore, this study highlights the urgent need for effective management of pesticide residues, particularly in Türkiye. Updating agricultural practices and adopting sustainable pesticide strategies could greatly enhance compliance with international market standards.

2. MATERIAL AND METHOD

2.1. Extraction of the database

RASSF Dataset for pesticide residues in fresh fruits and vegetables from Türkiye in 2024 was extracted from RASSF Portal [12]. Each notification included detailed information, such as the case date, notification type (alert, border rejection, or information), notifying country, actions taken, risk decision, and pesticide concentration. Notifications concerning fruits and vegetables exported from Türkiye to the EU were identified by filtering for the

product's origin labeled as "Türkiye" and the hazard category designated as "pesticide residues," with further refinement for the product category using the keyword "fruits and vegetables" for the period from January 1, 2024, to December 14, 2024. A database containing all available information for the 134 notifications was created using Microsoft Office Excel (Microsoft, USA).

2.2. Analysis of RASFF data

The visualization of the number of notifications was created using bar charts in GraphPad Software (San Diego, USA).

3. RESULTS

The analysis of RASFF notifications in 2024 aimed to identify the types of notifications, notifying countries, risk decisions, analytical results and actions taken concerning fruits and vegetables from Türkiye.

Figure 1 represents the classification of pesticide notifications for fruits and vegetables originating from Türkiye in 2024, detailing the types of notifications, including border rejections, information notifications for attention, information notifications for follow-up, and alert notifications. The analysis of pesticide notifications reveals significant trends in the classification of alerts. The most common notification type was "border rejection," comprising 96 notifications (71.64%), indicating substantial health risks detected at border controls, leading to the refusal of contaminated products. Following this, there were 29 notifications categorized as "information notifications for attention" (21.64%), suggesting a need for closer inspection of certain products. "Information notifications for follow-up" accounted for 6 notifications (4.47%), pointing to instances that require further investigation, while "alert notifications" represented only 3 notifications (2.23%), highlighting serious market risks that necessitate immediate action. Overall, the predominance of border rejection notifications underscores the effectiveness of regulatory measures in preventing contaminated items from entering the market, while the lower percentages of alert and follow-up notifications indicate that most pesticide-related concerns are effectively addressed before reaching consumers.
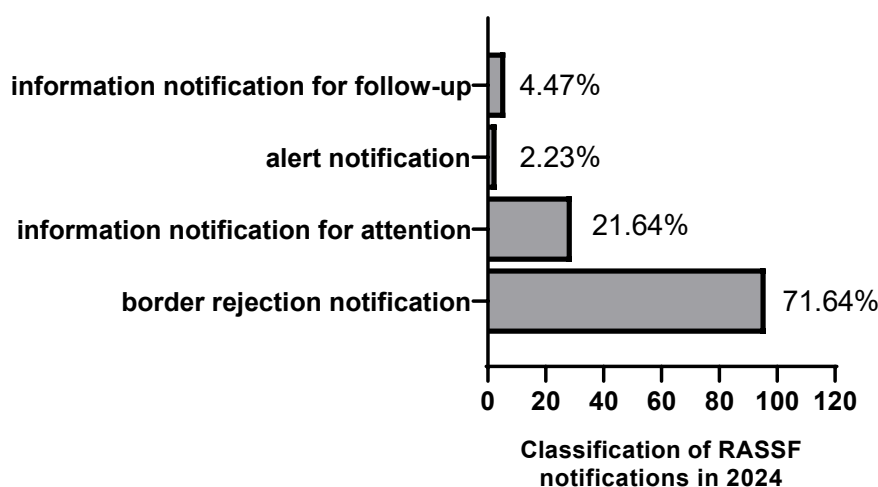
Figure 1. Classification of pesticide notifications for fruits and vegetables originating from Türkiye in 2024

Figure 2 shows the classification of risk decisions for pesticide notifications related to fruits and vegetables originating from Türkiye in 2024. The analysis of pesticide notifications reveals significant trends in risk classification and health concerns. Out of 134 notifications, the majority were categorized as "serious" risks (70.89%), indicating a substantial threat to health that necessitates immediate attention. This is followed by "potentially serious" notifications at 12.68%, suggesting that these cases may escalate if not properly managed. Notifications categorized as "potential risk" account for 9.70%, highlighting instances where caution is warranted but do not yet present a direct health threat. Additionally, 5.22% of notifications indicate "no risk," reflecting a small proportion of cases where pesticide residues are not deemed harmful, while only 1.49% are classified as "not serious." The predominance of serious and potentially serious notifications underscores the importance of rigorous monitoring and intervention strategies to safeguard public health, ensuring that most pesticide-related concerns are effectively addressed before reaching consumers.
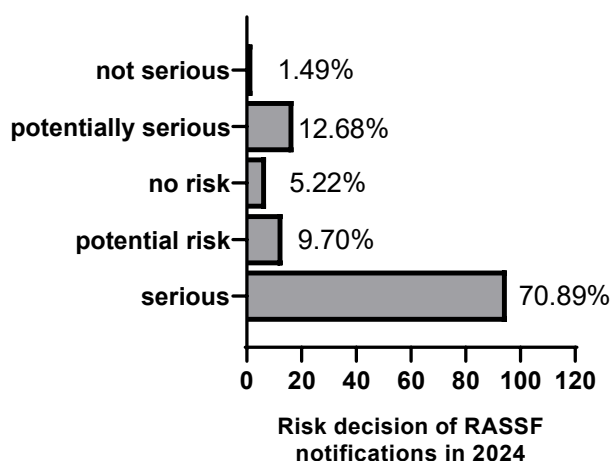
Figure 2. Classification of risk decisions for pesticide notifications related to fruits and vegetables originating from Türkiye in 2024

Figure 3 illustrates the notifying countries for pesticide notifications related to fruits and vegetables in 2024. The distribution of pesticide notifications by notifying country reveals notable trends in contamination sources among the 14 countries issuing a total of 134 notifications. Bulgaria is the most significant contributor, accounting for 58.21% of the notifications, highlighting a substantial concern regarding pesticide residues from this country. Germany follows with 11.94%, indicating a notable, albeit smaller, prevalence of pesticide issues. Croatia and Romania contribute 7.46% and 6.72%, respectively, suggesting considerable risks associated with these countries. Austria (3.73%) and Greece (2.99%) also report moderate levels of pesticide concerns, along with Poland (2.99%). Denmark accounts for 1.49%, while several other countries, including Cyprus, Finland, Latvia, Luxembourg, Norway, and Slovenia, each represent 0.75% of notifications. This data underscores the importance of monitoring pesticide use across these countries to ensure food safety and protect public health.
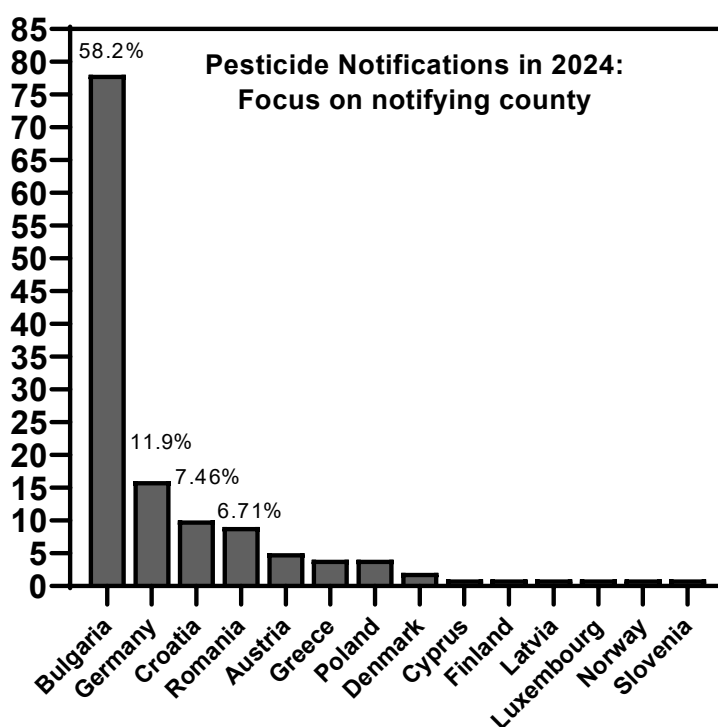
Figure 3. Pesticide notifications in 2024: Focus on notifying countries related to fruits and vegetables originating from Türkiye in 2024

Figure 4 presents the pesticide residues found in fruits and vegetables from Türkiye in 2024. The analysis of pesticide types detected reveals a diverse range of chemicals associated with notifications. Out of the 272 reported instances, the most commonly detected residues included acetamiprid (20.95%), chlorpyrifos-methyl (16.54%), imazalil (8.08%), chlorpyrifos (5.88%), pyriproxyfen (4.77%), buprofezin (4.04%), diflubenzuron (3.67%), formetanate (2.94%), spirotetramat (2.94%), tebuconazole (2.57%), and indoxacarb (2.20%). Acetamiprid is the

Evaluation of rapid alert system for food and feed (RASFF) data for pesticide residues in fresh fruits and vegetables from Türkiye in 2024

ICMUSTED 2024

most prevalent pesticide detected, accounting for 20.96% of detections, followed by chlorpyrifos-methyl at 16.54%, indicating significant concerns regarding these pesticides. Other notable pesticides include imazalil (8.09%) and chlorpyrifos (5.88%), reflecting further issues related to pesticide residues. Additionally, pyriproxyfen (4.78%), buprofezin (4.04%), and diflubenzuron (3.68%) present relevant contamination concerns.

Detection percentages decrease for formetanate and spirotetramat, each at 2.94%, while tebuconazole (2.57%) and indoxacarb (2.21%) also contribute to the overall pesticide profile. A range of other pesticides, including etoxazole (1.84%), pyrimethanil (1.84%), and various dithiocarbamates (1.47%), demonstrate lower detection rates. Several pesticides, such as cypermethrin, didecyldimethylammonium, emamectin, and metalaxyl, each account for 1.10%, while others, including sulfoxaflor, tebufenpyrad, propiconazole, and cadmium, are detected at 0.74%. A number of pesticides show minimal detection rates at 0.37%, including chlormequat, dimethoate, pirimiphos-methyl, cyflufenamid, cymoxanil, penconazole, tetraconazole, and trifloxystrobin. This comprehensive data highlights the need for ongoing monitoring of pesticide residues to ensure food safety and mitigate potential health risks associated with these chemicals.
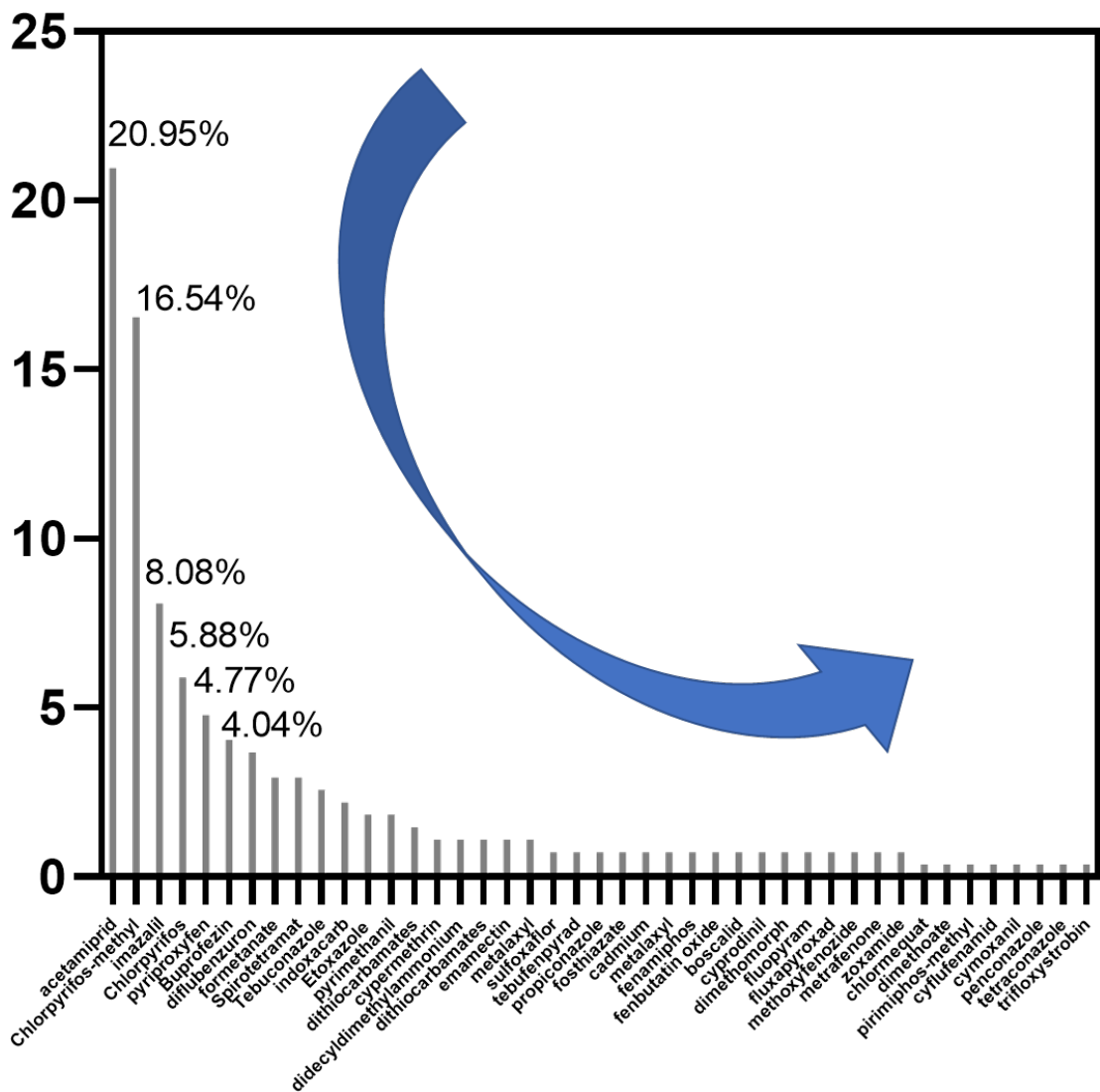
Figure 4. Pesticide residues in fruits and vegetables originating from Türkiye in 2024

Figure 5 shows the pesticide notifications in 2024 with the focus on fruits and vegetables originating from Türkiye. The analysis of pesticide notifications among various fruits reveals notable trends in contamination levels. Peppers and lemons lead the list, with 24.59% and 20.49% of notifications, respectively, indicating a higher prevalence of pesticide residues in these fruits. Pomegranate and tomato follow closely, each accounting for 10.66% of notifications. Other fruits, such as mandarin and grapes, have lower percentages at 7.38%. The notifications decrease further with pears (5.74%) and grapefruit (6.56%). Oranges and vine leaves show even lower rates at 4.92% and 4.10%, respectively. The least affected fruits include plums, cucumbers, cherries, apricots, nectarines,

quinces, and cowpeas, each contributing less than 1% to the total notifications. This data highlights the need for ongoing monitoring and regulation of pesticide use to ensure food safety.
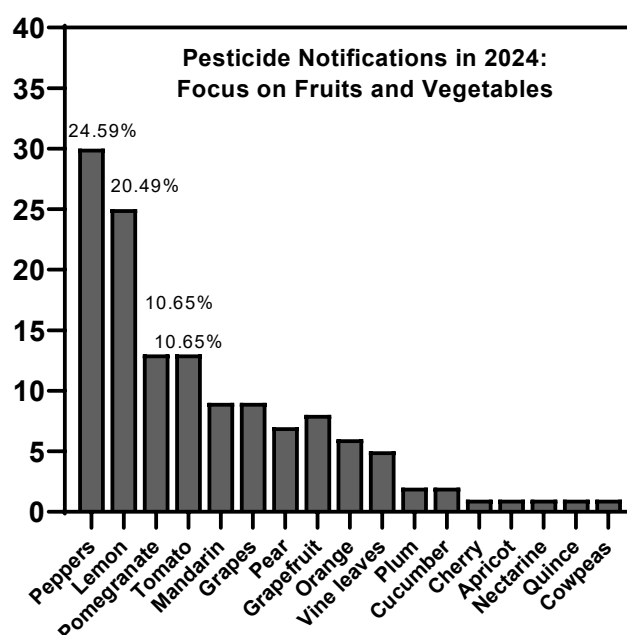
Figure 5. Pesticide notifications in 2024: Focus on fruits and vegetables originating from Türkiye in 2024

Table 1 presents the maximum residue levels of pesticides classified under the "border rejection" and "serious" categories, detected in fruits and vegetables from Türkiye in 2024.

Table 1. Maximum residue levels of pesticides in the "border rejection" and "serious" categories detected in fruits and vegetables from Türkiye in 2024

Fruit/Vegetables	Pesticide Category	Results	Maximum Residue Level (MRL)
Grapefruit	Buprofezin	0.034+/-0.017 mg/kg	0.01 mg/kg
	Chlorpyrifos-methyl	0.174+/-0.087 mg/kg	
		0.136+/-0.068 mg/kg	
		0.079 mg/kg	
		0.027+/-0.014 mg/kg	
		0.026+/-0.013 mg/kg	
	Chlorpyrifos	0.028 mg/kg	
	Metalaxyl	0.069+/-0.035 mg/kg	
Green plums	Chlorothalonil	0.024 mg/kg	0.01 mg/kg
Lemons (*Citrus limon, Citrus limonum*)	Chlorpyrifos-methyl	0.087+/-0.044 mg/kg	0.01 mg/kg
		0.065+/-0.033 mg/kg	
		0.063+/-0.032 mg/kg	
		0.028+/-0.014 mg/kg	
		0.028+/-0.014 mg/kg	
	Chlorpyrifos	0.091+/-0.046 mg/kg	
		0.028+/-0,014 mg/kg	
	Imazalil	28.175+/-14.088 mg/kg	5.0 mg/kg
		21.025+/-10.513 mg/kg	
		19.040+/-9.520 mg/kg	
		18.750+/-9.375 mg/kg	
		17.760+/-8.880 mg/kg	
		16.920+/-8.460 mg/kg	
		16.675+/-8.338 mg/kg	
		16.564+/-8.282 mg/kg	

		15.818+/-7.909 mg/kg	
		13.425+/-6.713 mg/kg	
	Prochloraz	2.445+/-1.223 mg/kg	0.03 mg/kg
		1.881+/-0.941 mg/kg	
		1.508+/-0.754 mg/kg	
		1.458+/-0.729 mg/kg	
		1.400+/-0.700 mg/kg	
		1.345+/-0.673 mg/kg	
Mandarin	Chlorpyrifos-methyl	0.053+/-0.027 mg/kg	0.01 mg/kg
		0.200+/-0.100 mg/kg	
Navel oranges	Buprofezin	0.057+/-0.029 mg/kg	0.01 mg/kg
	Chlorpyrifos-methyl	0.087+/-0.044 mg/kg	
		0.034+/-0.017 mg/kg	
	Chlorpyrifos	0.063+/-0.032 mg/kg	
	Propiconazole	0.101+/-0.051 mg/kg	
Oranges	Imazalil	19.550+/-9.775 mg/kg	4.0 mg/kg
Pomegranates	Tebuconazole	0.678+/-0.339 mg/kg	0.02 mg/kg
	Zoxamide	0.164+/-0.082 mg/kg	
	Cypermethrin	0.106+/-0.053 mg/kg	0.05 mg/kg
	Acetamiprid	0. 034 mg/kg	n/a
Peppers (other than sweet) (*Capsicum* spp.)	Acetamiprid	1.055+/-0.528 mg/kg	0.3 mg/kg
	Etoxazole	0.093+/-0.047 mg/kg	0.01 mg/kg
Sweet peppers	Acetamiprid	1.270+\-0.635 mg/kg	0.3 mg/kg
		1.270+\-0.635 mg/kg	
		1.242+-0.621 mg/kg	
		1.143+/-0.572 mg/kg	
		1.138+/-0.569 mg/kg	
		1.138+/-0.569 mg/kg	
		0.986+/-0.493 mg/kg	
		0.965+/-0.483 mg/kg	
		0.965+/-0.483 mg/kg	
		0.960 +/- 0.480 mg/kg	
	Buprofezin	0.373+/-0.187 mg/kg	0.01 mg/kg
	Chlorpyrifos-methyl	0.158+/-0.079 mg/kg	0.01 mg/kg
	Etoxazole	0.170+/-0.085 mg/kg	0.01 mg/kg
	Fenamiphos	0.088+/-0.044 mg/kg	0.01 mg/kg
	Flonicamid	0.900+/-0.450 mg/kg	0.3 mg/kg
	Formetanate	0.458+/-0.229 mg/kg	0.01 mg/kg
		0.450+/-0.225 mg/kg	
		0.386+/-0.193 mg/kg	
		0.203+-0.102 mg/kg	
		0.129+/-0.065 mg/kg	
	Pirimiphos-methyl	0.188+/-0.094 mg/kg	0.01 mg/kg
	Fosthiazate	0.086+-0.043 mg/kg	0.02 mg/kg
	Spirotetramat	3.953+\-1.977 mg/kg	1.0 mg/kg
		3.953+\-1.977 mg/kg	
		2.571+/-1.286 mg/kg	
		2.461+/-1.231 mg/kg	
		2.461+/-1.231 mg/kg	
	Sulfoxaflor	1.330+\-0.665 mg/kg	0.4 mg/kg
	Tebufenpyrad	0.426+/-0.213 mg/kg	0.01 mg/kg
	Tebuconazole	1.461+/-0.731 mg/kg	0.6 mg/kg

Evaluation of rapid alert system for food and feed (RASFF) data for pesticide residues in fresh fruits and vegetables from Türkiye in 2024

ICMUSTED 2024

4. CONCLUSION

Türkiye accounted for 134 of the 547 notifications on pesticide residues in 2024, with most classified as border rejections. Notably, lemons and sweet peppers exceeded permissible pesticide limits, highlighting safety concerns. Enhanced monitoring systems, stricter regulations, and alignment with European Union standards are essential to ensure consumer safety and improve export quality. Systematic data collection will also play a critical role in addressing these challenges and safeguarding public health.

References

[1]   RASFF, "The rapid alert system for food and feed, annual report 2012," in *Office for Official Publications of the European Communities*, Luxemburg, 2024.

[2]   RASSF, *The History of RASFF*, 2024.

[3]   J. Fenik, M. Tankiewicz, and M. Biziuk, "Properties and determination of pesticides in fruits and vegetables," *TrAC Trends Anal. Chem.*, vol. 30, no. 6, pp. 814–826, 2011.

[4]   G. Jurak, J. Bosnir, D. Dikic, A. M. Cuic, I. P. Prokurica, A. Racz, T. Jukic, D. Stubljar, and A. Starc, "The risk assessment of pesticide ingestion with fruit and vegetables for consumer's health," *Int. J. Food Sci.*, vol. 2021, no. 1, art. no. 9990219, Jan. 2021.

[5]   S. Grimalt and P. Dehouck, "Review of analytical methods for the determination of pesticide residues in grapes," *J. Chromatogr. A*, vol. 1433, pp. 1–23, 2016.

[6]   A. Balkrishna, A. Kumari, A. Kumar, V. Arya, A. Chauhan, N. K. Upadhyay, I. Guleria, R. Amarowicz, D. Kumar, and K. Kuca, "Biosensors for detection of pesticide residue, mycotoxins and heavy metals in fruits and vegetables: A concise review," *Microchem. J.*, vol. 205, art. no. 111292, 2024.

[7]   S. R. Department, "Agricultural consumption of pesticides worldwide from 1990 to 2022," 2024.

[8]   EFSA, "Peer review of the pesticide risk assessment of the active substance acetamiprid," *EFSA J.*, vol. 14, no. 11, art. no. e04610, 2016.

[9]   P. R. S. Soares, W. G. Birolli, I. M. Ferreira, and A. L. M. Porto, "Biodegradation pathway of the organophosphate pesticides chlorpyrifos, methyl parathion and profenofos by the marine-derived fungus aspergillus sydowii CBMAI 935 and its potential for methylation reactions of phenolic compounds," *Mar. Pollut. Bull.*, vol. 166, art. no. 112185, 2021.

[10]   A. Mie, C. Rudén, and P. Grandjean, "Safety of safety evaluation of pesticides: Developmental neurotoxicity of chlorpyrifos and chlorpyrifos-methyl," *Environ. Heal.*, vol. 17, pp. 1–5, 2018.

[11]   S. Oztekin and F. Karbancioglu-Guler, "Biological control of green mould on mandarin fruit through the combined use of antagonistic yeasts," *Biol. Control*, vol. 180, art. no. 105186, 2023.

[12]   RASSF, *RASSF Portal*, 2024.

Synbiotic Water Kefir Production and Investigation of Certain Quality Parameters

Sebahat Oztekin[1]

[1]Department of Food Engineering, Bayburt University, Bayburt, Türkiye.
Corresponding author: Sebahat Oztekin (e-mail: ozakca.sebahat@gmail.com)

Abstract

This study investigates the physicochemical, microbiological, and sensory properties of synbiotic water kefir made by incorporating Jerusalem artichoke (*Helianthus tuberosus* L.) powder and various wild berries (raspberry, blackberry, and blueberry). The high inulin content of Jerusalem artichoke offers prebiotic effects that promote gut health, while the probiotic properties of water kefir enable the formation of a functional beverage through the synergistic interaction of these components. The study focuses on developing a functional and healthy beverage by assessing its quality parameters, supporting digestive health, providing a natural and sustainable alternative, and catering to vegan diets with plant-based ingredients. Additionally, the project aims to produce a flavorful drink, increase consumer awareness of its health benefits, and introduce an innovative product to the functional beverage market. The results showed that Jerusalem artichoke-added synbiotic water kefirs contained higher lactic acid bacteria (> 8 log CFU/mL) and yeast (> 6 log CFU/mL) counts than that of the control groups, indicating that Jerusalem artichoke with fruits can be used as a suitable substrate for probiotic microorganisms. The addition of fruit juices/slices to this water kefir significantly increased the antioxidant activity however, the increased microbial activity in the synbiotic product slightly reduced the antioxidants. The sensory analysis indicated that Jerusalem artichoke-enriched synbiotic water kefir exhibited pronounced acidic, fruity, and alcoholic characteristics, which were further enhanced by the higher activity of lactic acid bacteria. When combined with wild berry juice, the 40/60 % v/v blend emerged as a consumer favourite. The incorporation of fruit moderated the aroma, resulting in a water kefir with a harmonious profile characterized by prominent symbiotic and fruity notes.

Keywords: Synbiotic, Water kefir, Fermentation, Probiotics, Prebiotics

1. INTRODUCTION

Water kefir is a non-dairy probiotic and fermented beverage made through the fermentation of water kefir grains in a sugar solution. It provides an important source of probiotics, prebiotics, and antioxidants, making it beneficial for vegans and individuals with dairy allergies or intolerances [1]. The original value of this research lies in its focus on the production of synbiotic water kefir using Jerusalem artichoke (*Helianthus tuberosus* L.) and various wild berry fruits (e.g., raspberry, blackberry and blueberry).

In the literature, the prebiotic effects of Jerusalem artichoke, known for its inulin-type fructans, which are polymers made up of fructose molecules, supporting gut health, are well-documented [2–4]. The typical composition of fresh Jerusalem artichoke tubers includes water (75–80% w/w) and total carbohydrates that make up to 22% of their weight, with 70–90% of these carbohydrates being inulin [5]. This polysaccharide serves as a prebiotic fiber, digestible by beneficial bacteria in the colon. In addition, water kefir contains probiotic bacteria (*Bifidobacterium* spp., *Lactobacillus* spp., *Lactococcus* spp., *Streptococcus* spp., *Acetobacter* spp., and *Gluconobacter* spp.) and various yeasts (*Candida, Hanseniaspora, Kloeckera,* and *Guehomyces*) and can support digestive health [1, 6]. However, limited studies have investigated the combination of Jerusalem artichoke with probiotic water kefir in synbiotic beverages [7].

While Jerusalem artichoke promotes the growth of beneficial bacteria in the digestive system due to its prebiotic fibers, fruits may enhance probiotic efficacy through their high antioxidant content [8, 9]. In a healthy gut microbiota, beneficial bacteria dominate, whereas dysbiosis, an imbalance between beneficial and harmful microorganisms, leads to an increase in harmful bacteria. This imbalance may cause digestive issues, weakened immunity, obesity, inflammation, and various chronic diseases. Dysbiosis is typically triggered by poor diet, antibiotic use, stress, and environmental factors, adversely affecting gut health. To address this issue, combinations of prebiotics and probiotics (synbiotics) have been proposed to prevent dysbiosis and improve gut flora [10].

Thus, the aim is to develop a healthy and functional synbiotic beverage, akin to soda but with added health benefits [11, 12]. This study seeks to address the gap in the literature by examining the physicochemical, microbiological, and sensory properties of synbiotic water kefir produced from Jerusalem artichoke and various wild berry fruits. The outcome will be an innovative functional beverage that supports gut health, strengthens the immune system, and enhances antioxidant activity. Additionally, utilizing Jerusalem artichoke will add economic value to local agricultural products and contribute to sustainable development by supporting local producers. Therefore, the findings of this study are expected to offer novel approaches for the development of synbiotic products, meet consumer expectations, and provide innovative solutions in the health sector from both scientific and industrial perspectives.

2. MATERIAL AND METHOD

Water kefir is produced by fermenting sugar- or fruit-enriched water using water kefir grains that contain lactic acid bacteria (LAB) and yeast. The fermentation process typically lasts 2–4 days, during which the microorganisms generate substances such as lactic acid, acetic acid, ethanol, CO_2, and aromatic compounds. Unlike milk kefir, where lactose is fermented, brown sugar is utilized in water kefir, resulting in an acidic, tangy, carbonated, and fruity flavour. As water kefir does not contain dairy-derived lactose or residues, it is particularly appealing to individuals with dairy allergies and vegan consumers [1, 13]. Hence, synbiotic water kefir made with Jerusalem artichoke and fruits could attract consumers seeking healthy and natural beverage options. By paying attention to factors such as hygiene, ingredient selection, and controlled fermentation during production, a high-quality and safe product can be achieved. The production steps for synbiotic water kefir are presented below:

2.1. Preparation of Fruit Juices

Fresh and undamaged fruits, including raspberry, blackberry, and blueberry, were sourced from local markets. Upon arrival at the laboratory, the fruits were washed and subsequently cut into smaller cubic pieces. The obtained juices were then simmered for 10 minutes and cooled to 25 ℃ [11].

2.2. Preparation Jerusalem Artichoke Powder

Jerusalem artichoke tubers were thoroughly washed under tap water, sliced, and dried at 60 ℃ for 10 hours. Once dried, they were ground into a fine powder [14].

2.3. Preparation of Water Kefir Grains

Water kefir grains (Büyüdanem water kefir culture) were obtained from Danem Dairy and Dairy Products Co., Ltd. The grains 5% (w/v) were incubated in a sterile 15% (w/v) brown sugar (molasses) solution at 25 ℃ using a shaking incubator, as described by Guzel-Seydim et al. [1]. The sugar solution was refreshed every 24 hours to maintain the vitality and freshness of the grains [1].

2.4. Water Kefir Fermentation

During the first fermentation step, water kefir grains (10% w/v) and dried Jerusalem artichoke powder were introduced into a sugary water solution (100 g/L) and fermented at 25 ℃ for 24–48 hours. In the subsequent fermentation phase, fruit juices were added to the mixture, which was then subjected to another 24–48 hours of fermentation (a total of 72 h fermentation) at the same temperature range (Figure 1). Following the fermentation process, the kefir was filtered and freeze-dried or stored at 4 °C for further analyses [1, 15, 16]. Additionally, a control sample of water kefir, without the inclusion of Jerusalem artichoke powder, was prepared.

The primary goal was to examine the effect of Jerusalem artichoke, the experimental design was adjusted accordingly. To isolate its impact, the effects of fruit and brown sugar were controlled. The groups were designed as follows:

- Control Group 1: Water kefir fermented with only brown sugar (water kefir grains + brown sugar)
- Experimental Group 1: Water kefir fermented with Jerusalem artichoke + brown sugar (water kefir grains + Jerusalem artichoke + brown sugar)
- Experimental Group 2: Water kefir prepared with fruit and brown sugar (water kefir grains + fruit + brown sugar)
- Experimental Group 3: Water kefir prepared with Jerusalem artichoke + fruit + brown sugar (water kefir grains + Jerusalem artichoke + fruit + brown sugar).

The control group and experimental groups allowed for the evaluation of the prebiotic effect of Jerusalem artichoke in the presence and absence of fruit juice while maintaining a clear comparison with groups that only used brown sugar. It helped in understanding the contribution of prebiotics from Jerusalem artichoke to the overall fermentation process and potential health benefits.
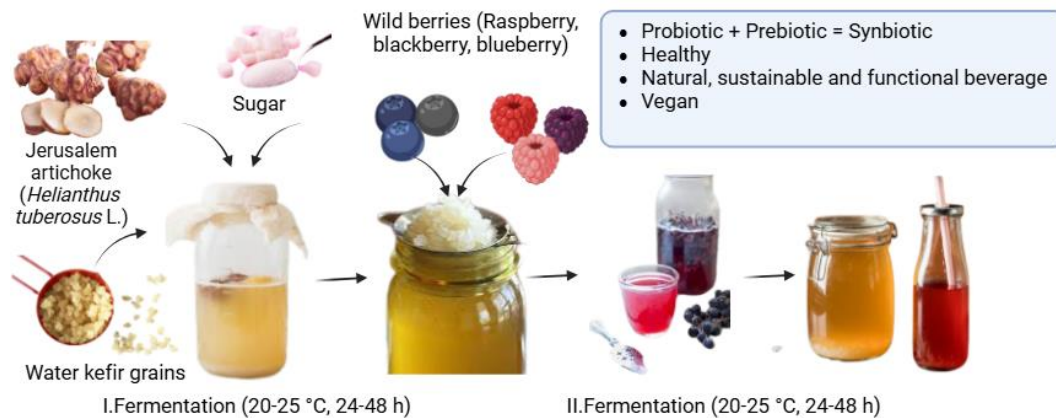
Figure 1. Synbiotic water kefir production steps

2.5. Microbiological Analyses

Microbiological analyses were conducted on synbiotic water kefir and control samples, focusing on yeast, *Lactobacillus* spp., and *Lactococcus* spp. counts. For this purpose, yeast counts were determined using the spread plate method on Dichloran Rose Bengal Chloramphenicol (DRBC) agar, followed by incubation at 25 ºC for 48 hours, with colony-forming units per milliliter (CFU/mL) counted. *Lactobacillus* and *Lactococcus* counts were performed using the pour plate method on Man-Rogosa-Sharpe (MRS) agar and M17 agar, respectively, with colonies counted after incubation at 37 °C for 48 hours, expressed as CFU/mL [17]. All analyses were repeated three times.

2.6. pH Measurement

The pH of the prepared water kefirs and control groups was measured using a digital pH meter [18].

2.7. Determination of Total Phenolic Content

The total phenolic content was determined using the Folin-Ciocalteu reagent according to the method by Slinkard & Singleton (1977). Samples of 100 µL were mixed with 0.75 mL of diluted (10-fold) Folin-Ciocalteu reagent (0.2 N). After allowing the samples to stand in the dark for 5 minutes, 750 µL of saturated Na_2CO_3 (6%) solution was added. The absorbance of the mixed samples was measured at a wavelength of 765 nm using a UV-vis spectrophotometer after incubation in the dark at room temperature for 90 minutes. Each sample was prepared in triplicate, and the results were expressed as mg of gallic acid equivalent (GAE) per 100 mg of sample.

2.8. Antioxidant Analysis

Antioxidant analyses of the fruit synbiotic water kefirs were performed using the DPPH (2,2-diphenyl-1-picrylhydrazyl) method. The assay utilized the DPPH radical reagent, with ascorbic acid serving as the positive control. In a microtiter plate, 100 microliters of the sample, calibration standard (2.5 mmol/L Trolox stock solution), positive control, and blank (ethanol) were pipetted in triplicate. For this purpose, 100 µL aliquots from each sample were added to 2.9 mL of a 120 µmol/L DPPH methanol solution. After incubating in the dark at 30 ºC for 30 minutes, the absorbance was measured at a wavelength of 517 nm, with the DPPH methanol solution used as a control. The results were calculated using the formula: DPPH radical scavenging activity (%) = 100 – (sample absorbance/control absorbance) × 100 [19].

2.9. Sensory Analysis

Sensory evaluation was performed by 20 trained panelists (18–38 years, 10 males and 10 females) experienced in assessing kefir drinks. The final product was evaluated based on appearance, color, aroma, sweetness, sourness, and acidity parameters using a total score of 10 points. From 1 (extremely disliked) to 10 (extremely liked), evaluations were based on predefined attributes such as Aroma/odor, attractiveness (taste), sweetness, acidity, sparkling (CO_2), turbidity, color, attractiveness (optical), and favor (overall acceptance) [11].

2.10. Statistical Analysis

Statistical analyses were performed using the SPSS software. One-way analysis of variance (ANOVA) was applied to determine statistically significant differences followed by a Tukey's multiple comparison test ($p < 0.05$).

3. RESULTS

After 72 hours of fermentation, the total phenolic content of water kefir samples showed a decreasing trend, while antioxidant activity increased with the fermentation and the addition of wild berry fruits.
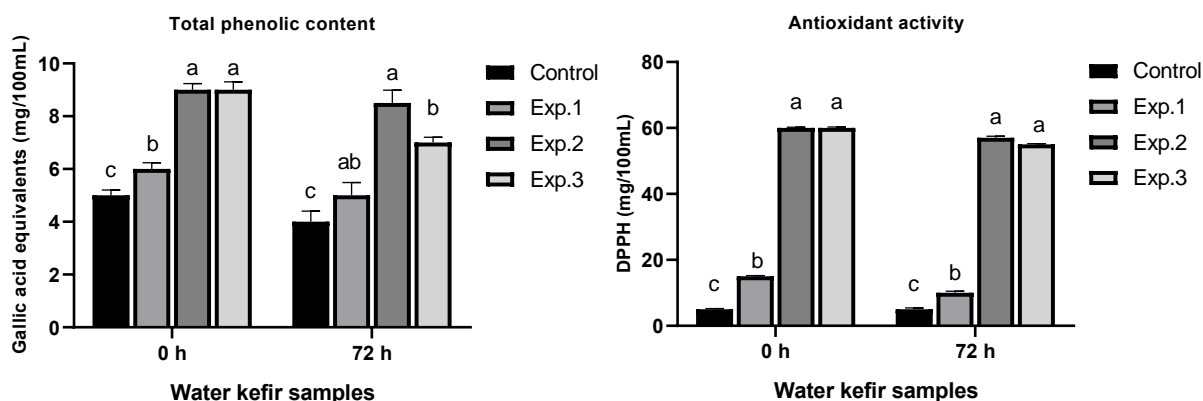
Figure 2. Total phenolic content and DPPH antioxidant activity of water kefir samples

The addition of Jerusalem artichoke was found to support the growth of *Lactobacillus* spp. (> 8 log CFU/mL), *Lactococcus* spp. (> 7 log CFU/mL), and yeast counts (> 6 log CFU/mL). It is possible that the increased growth of Lactobacillus resulting from the addition of Jerusalem artichoke suppressed yeast growth in the experimental group 1 and 2.
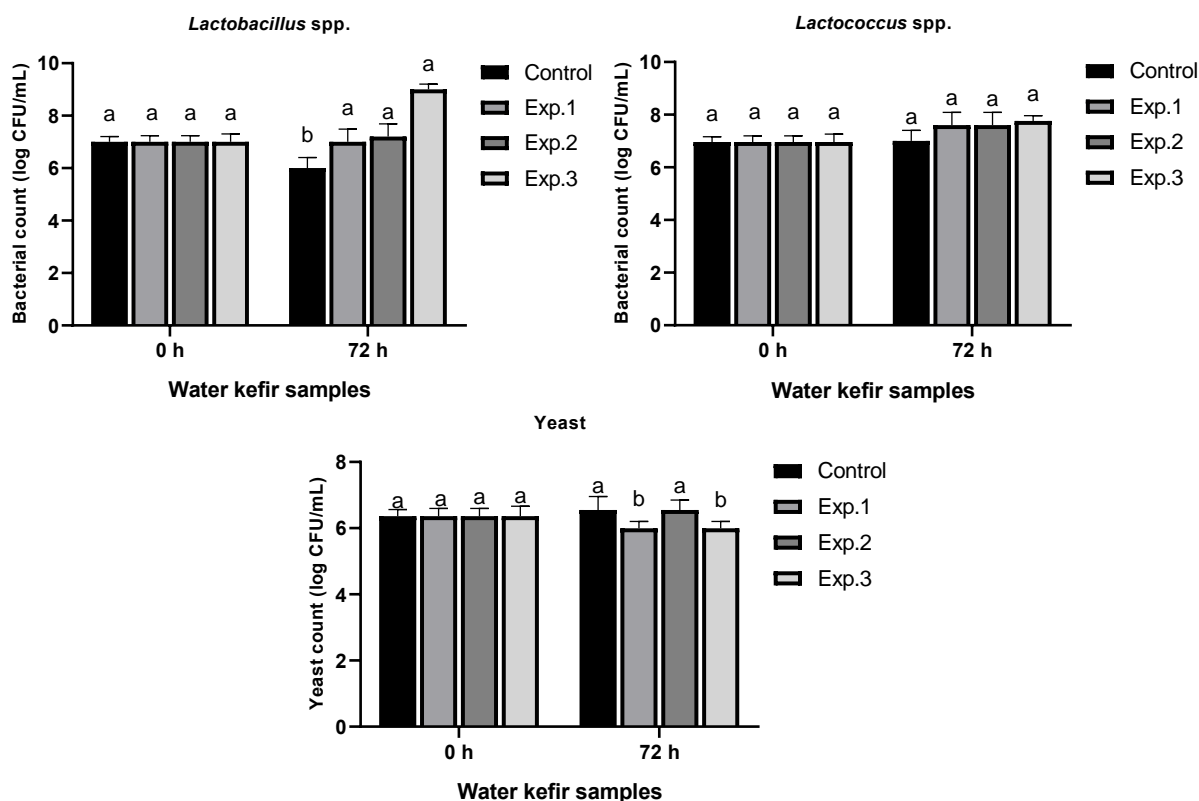
Figure 3. *Lactobacillus* spp., *Lactococcus* app., and yeast counts (log CFU/mL) of water kefir samples

The addition of Jerusalem artichoke resulted in increased microbial activity, which led to a reduction in pH, decreasing from 3.6 to 3.00 in experimental group 3, the most significant change observed. In experimental group

2, pH levels decreased from 3.63 to 3.59, while experimental group 1 saw a reduction from 6.96 to 4.00. The control group also experienced a decline in pH from 7.51 to 5.25.

In terms of sensory analysis, the highest overall acceptance was attributed to Experimental Group 3, which excelled in color, appearance, aroma, and taste.
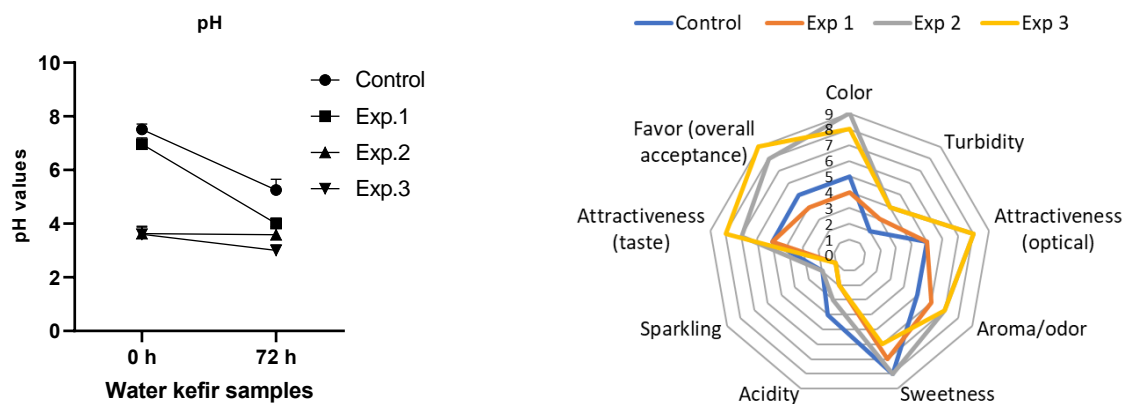
Figure 4. pH measurements and sensory analysis of produced water kefir samples

4. CONCLUSION

Jerusalem artichoke is an effective substrate for water kefir fermentation, making it a promising foundation for synbiotic beverage development. Its addition supported probiotic growth, resulting in higher lactic acid bacteria (> 8 log CFU/mL) and yeast (> 6 log CFU/mL) counts compared to controls. While the addition of wild berries enhanced antioxidant activity, a slight reduction was observed due to increased microbial activity. In water kefir enriched with Jerusalem artichoke and wild berry fruits, elevated microbial activity also led to a decreased pH of 3.00. This innovative beverage provides health benefits, functionality, and suitability for vegan diets. Further investigation is needed to determine the aroma compounds produced during fermentation.

References

[1] Z. B. Guzel-Seydim, C. Gokirmakli, and A. K. Greene, "A comparison of milk kefir and water kefir: Physical, chemical, microbiological and functional properties," *Trends Food Sci. Technol.*, vol. 113, pp. 42–53, 2021.

[2] N. S. Dias, J. F. S. Ferreira, X. Liu, and D. L. Suarez, "Jerusalem artichoke (Helianthus tuberosus, L.) maintains high inulin, tuber yield, and antioxidant capacity under moderately-saline irrigation waters," *Ind. Crops Prod.*, vol. 94, pp. 1009–1024, 2016.

[3] W. Li, J. Zhang, C. W. Yu, Q. Li, F. Dong, G. Wang, G. D. Gu, and Z. Y. Guo, "Extraction, degree of polymerization determination and prebiotic effect evaluation of inulin from Jerusalem artichoke," *Carbohydr. Polym.*, vol. 121, pp. 315–319, 2015.

[4] P. Ramnani, E. Gaudier, M. Bingham, P. van Bruggen, K. M. Tuohy, and G. R. Gibson, "Prebiotic effect of fruit and vegetable shots containing Jerusalem artichoke inulin: A human intervention study," *Br. J. Nutr.*, vol. 104, no. 2, pp. 233–240, 2010.

[5] I. A. Rubel, C. Iraporda, G. D. Manrique, D. B. Genovese, and A. G. Abraham, "Inulin from Jerusalem artichoke (Helianthus tuberosus L.): From its biosynthesis to its application as bioactive ingredient," *Bioact. Carbohydrates Diet. Fibre*, vol. 26, art. no. 100281, 2021.

[6] Z. Guzel-Seydim, J. T. Wyffels, A. C. Seydim, and A. K. Greene, "Turkish kefir and kefir grains: microbial enumeration and electron microscobic observation," *Int. J. Dairy Technol.*, vol. 58, no. 1, pp. 25–29, 2005.

[7] C. Iraporda, I. A. Rubel, G. D. Manrique, and A. G. Abraham, "Influence of inulin rich carbohydrates from Jerusalem artichoke (Helianthus tuberosus L.) tubers on probiotic properties of Lactobacillus strains," *LWT*, vol. 101, pp. 738–746, 2019.

[8] P. Markowiak and K. Śliżewska, "Effects of probiotics, prebiotics, and synbiotics on human health," *Nutrients*, vol. 9, no. 9, art. no. 1021, 2017.

[9] L. L. Tan, J. J. Ngiam, E. S. Z. Sim, P. L. Conway, and S. C. J. Loo, "Liquorilactobacillus satsumensis from water kefir yields α-glucan polysaccharides with prebiotic and synbiotic qualities," *Carbohydr. Polym.*, vol. 290, art. no. 119515, 2022.

[10] G. L. V. de Oliveira, A. Z. Leite, B. S. Higuchi, M. I. Gonzaga, and V. S. Mariano, "Intestinal dysbiosis and probiotic applications in autoimmune diseases," *Immunology*, vol. 152, no. 1, pp. 1–12, 2017.

[11] T. Esatbeyoglu, A. Fischer, A. D. S. Legler, M. E. Oner, H. F. Wolken, M. Kopsel, Y. Ozogul, G. Ozyurt, D. De Biase, and F. Ozogul, "Physical, chemical, and sensory properties of water kefir produced from Aronia melanocarpa juice and pomace," *Food Chem. X*, vol. 18, art. no. 100683, 2023.

[12] K.-H. Seo, D.-H. Kim, W. H. Yokoyama, and H. Kim, "Synbiotic effect of whole grape seed flour and newly isolated kefir lactic acid bacteria on intestinal microbiota of diet-induced obese mice," *J. Agric. Food Chem.*, vol. 68, no. 46, pp. 13131–13137, 2020.

[13] W. Randazzo, O. Corona, R. Guarcello, N. Francesca, M. A. Germana, H. Erten, G. Moschetti, and L. Settanni, "Development of new non-dairy beverages from Mediterranean fruit juices fermented with water kefir microorganisms," *Food Microbiol.*, vol. 54, pp. 40–51, 2016.

[14] B. Srinameb, S. Nuchadomrong, S. Jogloy, A. Patanothai, and S. Srijaranai, "Preparation of inulin powder from Jerusalem artichoke (Helianthus tuberosus L.) tuber," *Plant foods Hum. Nutr.*, vol. 70, pp. 221–226, 2015.

[15] F. A. Fiorda, G. V. D. Pereira, V. Thomaz-Soccol, S. K. Rakshit, M. G. B. Pagnoncelli, L. P. D. Vanderberghe, and C. R. Soccol, "Microbiological, biochemical, and functional aspects of sugary kefir fermentation-A review," *Food Microbiol.*, vol. 66, pp. 86–95, 2017.

[16] A. Gulitz, J. Stadie, M. Wenning, M. A. Ehrmann, and R. F. Vogel, "The microbial diversity of water kefir," *Int. J. Food Microbiol.*, vol. 151, no. 3, pp. 284–288, 2011.

[17] C. Gokirmakli, G. Satir, and Z. B. Guzel-Seydim, "Microbial viability and nutritional content of water kefir grains under different storage conditions," *Food Sci. Nutr.*, vol. 12, no. 6, pp. 4143–4150, 2024.

[18] AOAC, *Official Methods of Analysis of AOAC International*, 22nd ed., 2023.

[19] K. Mishra, H. Ojha, and N. K. Chaudhury, "Estimation of antiradical properties of antioxidants using DPPH assay: A critical review and results," *Food Chem.*, vol. 130, no. 4, pp. 1036–1043, 2012.

Effective Corrosion Protection of Aluminium Alloys with Polymeric Material

Meryem Imane Amrane[1,2], Wahiba Amrane[3], Chaimaa Boucherit[1]

[1]Department of Engineering Process, National Polytechnic School of Oran Maurice Audin (ENPO-MA), Oran, Algeria
[2]Macromolecular Physical Organic Chemistry Laboratory, Department of Chemistry, University of Djillali Liabes, Bel Abbes, Algeria
[3]Physical Chemistry Department, University of Science and Technology of Oran-Mohamed Boudiaf (USTO-MB), Oran, Algeria
Corresponding author: Meryem Imane Amrane (e-mail: ima_search@yahoo.fr)

Abstract

The corrosion protection of aluminium materials and its alloys is particularly suitable for different industrial chemical surface treatments. Many industries highly claimed chromium Cr (VI) over a certain period to achieve high resistance to corrosion. However, research toward alternative approaches has integrated more green inhibitors. Corrosion inhibition of metal materials has been the subject of previous work. Both natural polymeric and synthetic polymeric inhibitors have proven their efficiency. One key aspect of this study is to examine the variations of physical-chemical parameters in the pre-treatment baths and the relationships between them. On the other hand, we report a polyester resin synthesis by polycondensation of glycerol and ortho phthalic acid, and a corrosion inhibition evaluation for aluminium alloy materials was performed. The target resin was obtained. The ability to reduce corrosion in different corrosive media and concentrations was investigated.

Keywords: Corrosion inhibitors, Resin, Surface aluminium treatment, Conversion process

Preliminary Evaluation of Local Medicinal Plant Extract from Anacardiaceae Family

Fouzia Benoudjit[1,2], Hania Guechetouli[3], Lylia Naili[3]

[1]Laboratory of Coatings, Materials & Environment, M'hamed Bougara University, Boumerdes, Algeria
[2]Research Unit of Materials, Processes and Environment, M'hamed Bougara University, Boumerdes, Algeria
[3]Faculty of Sciences, Department of Chemistry, M'hamed Bougara University, Boumerdes, Algeria
Corresponding author: Fouzia Benoudjit (e-mail: f.benoudjit@univ-boumerdes.dz)

Abstract

The pink pepper tree is a perennial species that belongs to the Anacardiaceae family. It is known for its medicinal and therapeutic qualities. The plant has been traditionally used for its anti-inflammatory, antioxidant, and antimicrobial benefits, which have gained attention for its potential in treating various health issues. The objective of this work is to conduct a preliminary evaluation of a local pink pepper essential oil extracted through hydrodistillation, currently commercialized in Algeria. This essential oil was characterized using organoleptic and physicochemical properties to assess its quality and suitability for therapeutic use. Key parameters, including refractive index and acid value, were measured to determine compliance with standards. Rheological and spectroscopic analysis were also conducted to evaluate the viscosity and flow properties, and to provide detailed information about the chemical composition and functional groups of the studied essential oils, respectively. The results show that the pink pepper extract meets the required norms indicating the good quality of the product and presents a Newtonian behaviour. Furthermore, infrared spectroscopy analysis revealed the presence of various chemical groups such as alcohols, alkanes, alkenes, aldehydes, ethers, aromatics, and esters. These findings confirm the complexity of the essential oil's chemical composition, which supports its potential health benefits and therapeutic applications. This preliminary evaluation highlights the importance of further studies to explore the broader applications of pink pepper essential oil and its potential for commercialization in medicinal and cosmetic industries.

Keywords: Medicinal plant, Extract, Anacardiaceae, Characterization, Physicochemical properties

Exploring Phenolic Composition and Antioxidant Potential Using Ferric Reducing Power Assay of a Medicinal Plant from Khenchela Region in Crude Extract

Bouaita Rayene[1], Djemil Randa[1], Bouhalit Samira[1], Boutellaa Saber[2], Zineb Bouamrane[2], Teouallbia Youssra[3]

[1]Laboratory of Biotechnology, Water, Environment and Health, Department Cell Biology and Molacullar, University Abbes Laghrour, Khenchela, Algeria
[2]Laboratory of Science and Materials, Department of Biology, University Abdelhafid Bousouf, Mila, Algeria
[3]Laboratory of Biology, Department of Biology, Envirenement and Health,University, El-Oued, Algeria
Corresponding author: Bouaita Rayene (e-mail: bouaita.rayene@univ-khenchela.dz)

Abstract

Free radicals play a key role in the genesis of numerous diseases, which has stimulated research on natural antioxidants derived from medicinal plants. In recent years, research in this field has expanded significantly, with a proliferation of studies focusing on natural antioxidants, particularly polyphenols which are recognized for their strong antioxidant properties. In this context, the present study focuses on the identification and quantification of secondary metabolites in the leaves of a plant from Khenchela region. The primary objective of this study was to evaluate the antioxidant activity in Hydroethanolic extract of the leaves from a plant belonging to the Eleagnaceae family, prepared by maceration, using the FRAP (Ferric Reducing Antioxidant Power) method. The total polyphenol content was measured using the Folin-Ciocalteu method. Additionally, the aluminum chloride method was used to quantify the total flavonoid content, which indicated a significant presence of these antioxidants with 146,83µg GAE/mg of polyphenols and 53.9 µg QE/mg of flavonoids.. The antioxidant potential of the extract was further assessed using the (FRAP) assay, which evaluates the extract ability to reduce ferric ions, thereby providing an estimate of its overall antioxidant capacity. The results showed that the hydroethanolic extract exhibited notable antioxidant activity, with a value of (38.15 ± 0.18) µg/ml, compared to ascorbic acid (14.94 ± 0.36) µg/ml. In conclusion, the findings highlight the plant's potential as a rich source of natural antioxidants. This suggests that the bioactive compounds it contains could be further explored for their potential health benefits and applications in developing antioxidant-based therapies or supplements.

Keywords: Polyphenols, FRAP, Flavonoids, Eleagnaceae

Natural Antifungal Cream Based on Garlic Macera

Meryem Allioua[1], Ahmed Yacine Mazari[1], Waffa Bouali[2]

[1]Department of Sciences, Institute of Applied Sciences and Techniques (ISTA), Tlemcen, Algeria
[2]Department of Biology, Faculty of SNV-STU, Tlemcen University, Algeria
Corresponding author: Meryem Allioua (e-mail: mariaall260@yahoo.fr)

Abstract

With the increasing spread of fungal skin diseases and the increasing resistance of some of them to traditional treatments, it is essential to find effective and safe natural solutions. Our project to produce a natural antifungal cream based on garlic infusion is a pioneering initiative in this field, taking advantage of the unique therapeutic properties of garlic. It is known that garlic is very effective against fungi, thanks to its presence of allicin, a biologically active sulfur compound that has antifungal and antibacterial properties. The objective of our project is to create a natural antifungal using garlic macera and certain essential oils. We will use the antifungal and health-promoting properties of garlic as well as essential oils such as tea tree oil and citronella oil and clove oil. The antifungal product is made from natural ingredients, where the garlic is soaked to extract its active compounds, then carefully mixed with the cream and essential oils to ensure effectiveness and superior quality. The physicochemical, microbiological parameters and antifungal activity were analyzed and tested, and several experiments on the effectiveness of the antifungal cream are tested on voluntary people and to have the results it took at least more than 5 days for the effect to appear. This product aims to meet the needs of consumers looking for natural and healthy solutions for skin problems caused by fungi, offering a safe and effective alternative to commercial alternatives.

Keywords: Natural antifungal, Garlic macera, Essential oils, Active compounds, Natural ingredients

Correlation and Agreement Between the Body Mass Index, Waist Circumference, Body Fat Index and Body Fat with the Waistto-Height Ratio in Algeria Adults

Salima Taleb[1,2,3], Fatma Klaa[1], Djihad Menia[1]

[1]Department of Applied Biology, Faculty of Exact Sciences and Natural and Life Sciences, Echahid Cheikh Larbi Tebessi University, 12000 Tebessa, Algeria
[2]Water and Environment Laboratory, Echahid Cheikh Larbi Tebessi University, 12000 Tebessa, Algeria
[3]Laboratory of Nutrition and Food Technology (LNTA), University of Constantine 1, Algeria
Corresponding author: Salima Taleb (e-mail: taleb.salima@univ-tebessa.dz)

Abstract

To determine the correlation and diagnostic agreement of body mass index (BMI) with abdominal obesity (AO), fat mass %, fat mass index (FMI) and waist-to-height ratio (WHtR). A cross-sectional study was conducted from January 15 to March 15, 2022, at the diabetic center in Tebessa (east of Algeria). Were included during the period of the realization of our work, 200 patients having presented type 2 diabetes aged 18 years or more. The type of diabetes was confirmed by the patient's medical file. Anthropometric measurements: weight, height, waist circumference (WC) and hip circumference were performed for each patient. Body mass index (BMI), percentage body fat (BF%), body fat index (BFI) and WHtR were calculated. The prevalence of obesity was estimated according to BMI, WC, %BF, BFI and WHtR. Lin's correlation coefficient and Cohen's Kappa were used to determine the correlation and agreement between the five anthropometric measurements. According to the BMI, WC, BF%, BFI and WHtR criteria, the prevalence of obesity was 41.5%, 70.5% and 93.0%, 79%, 98% respectively; the prevalence of obesity was higher in women and in those under 10 years of diabetes duration. The correlation between BMI and WC, was poor as well as between BMI and BF and between BMI and WHtR, it was moderate between BF% and BFI as well as between BMI and BFI, with differences between men and women. Furthermore, the agreement between BMI and WC was poor, whereas the agreement between BMI and WHtR was low as well as between BMI and BFI. It was mild between BMI and BF%. The results regarding correlation and agreement are limited and suggest that they are not interchangeable measures, so it is necessary to evaluate the adequacy of using BMI alone for the diagnosis of obesity in Algeria.

Keywords: BMI, Waist circumference, BFI, %BF, Algeria

Draft Genome Sequence of *optrA*-Positive *Enterococcus Feacium* Strain Isolated from Turkey in Tunisia: The Resistome, Virulome, and Mobilome

Sana Lengliz[1,2], Hajer Kilani[1,3], Faten Ghodhbane-Gtari[4], Meher Gtari[4], Mohamed Salah Abbassi[1,3]

[1]Laboratory of Bacteriological Research, University of Tunis El Manar, Institute of Veterinary Research of Tunisia, Tunis 1006, Tunisia

[2]Laboratory "Materials, Molecules and Application LR11ES22", University of Carthage, Preparatory Institute for Scientific and Technical Studies, La Marsa 2078, Tunisia

[3]Research Laboratory "Antimicrobial Resistance" LR99ES09, University of Tunis El Manar, Faculty of Medicine of Tunis, Tunis 1006, Tunisia

[4]Department of Biological and Chemical Engineering, USCR Molecular Bacteriology and Genomics, University of Carthage, National Institute of Applied Sciences and Technology, Tunis, Tunisia

Corresponding author: Sana Lengliz (e-mail: lengliz_sana@yahoo.fr)

Abstract

Enterococcus spp have been emerged as important nosocomial pathogen causing severe infections. Treatments of multi-drug resistant enterococcal infections are a cause of concern especially for vancomycin- and linezolid resistant isolates. Livestock is well known as hot spot of antimicrobial resistant pathogens owing to prolonged excessive use or misuse of antibiotics. Among 69 enterococci isolates recovered from feces of healthy turkey in avian farms located in the north of Tunisia, high rates of multidrug resistant (MDR) isolates were observed. One *Enterococcus faecium* isolate showing MDR phenotype toward ampicillin, erythromycin, spiramycin, streptomycin, and linezolid was investigated. Whole genome sequencing of the strain was performed and the draft genome was analysed using appropriate softwares. The draft genome sequence of the *E. faecium* strain showed that the chromosome size is 2,956,417 bp, belonging to new sequence type (ST) of the pandemic high risk clonal complex CC17. The resitome was composed of several genes encoding resistance to linzolid (*optrA*), fenicols (*fexA*), aminoglycosides *(aac(6')*-Ii), tetracyclines (*tetM*, *tetL*), macrolides (*ermA*, *ermB*, *msrC*). The strain possessed an array of virulence genes implicated in several infectious process including *bepA-Entfm*-hosp, *ccpA*-Entfm-com, *acm*-Entfm-com, *bepA*-Entfm-com, *glsB1*-Entfm, *fnm*-Entfm-com, *scm*-Entfm-hosp, *fms14*-Entfm-hosp, *empB*-Entfm-com, *empA*-Entfm-hosp, *gls33*-Entfm, *glsB*-Entfm, *fms15*-Entfm-hosp, *fms13*-Entfm, *gls20*-Entfm, *sagA*-Entfm-hosp, and *efaAfm*. The mobilome of the strain was also rich and contained 3 plasmids, insertion sequences (*IS*fm1, *IS*Efa10) and an antimicrobial resistance genes-carriers transposon (*Tn*6009). These findings are alarming and highlight the ability of *E. faecium* to possess rich genetic pools encoding antimicrobial resistance and virulence which is a cause of concern for human and animal health. Further studies are required to decipher the resistome/virulome/mobilome of pathogenic bacteria of turkey colonizers.

Keywords*: Enterococcus faecium*, Healthy Turkey, WGS, Multutrug resistance, *optrA*

Phytochemical Analysis and Antibacterial Activity Assessment of Hydroethanolic Extracts from the Aerial Parts of a Wild Medicinal Plant in the Mila Region

Zineb Bouamrane[1], Hakima Belattar[1], Saber Boutellaa[1], Mouna Menakh[2], Nedjla Derbal[1], Manel Ferkhi[1], Rayene Bouaita[3]

[1]Laboratory of Natural Sciences and Materials (LSNM), Institute of Natural and Life Sciences, University Center Abdehafid Boussouf, Mila, Algeria
[2]Department of Biological and Agricultural Sciences, Institute of Natural and Life Sciences, University Center Abdehafid Boussouf, Mila, Algeria
[3]Laboratory of Biotechnology, Water, Environment, and Health, Khenchla, Algeria
Corresponding author: Zineb Bouamrane (e-mail: z.bouamrane@centre-univ-mila.dz)

Abstract

The exploration of natural products for therapeutic uses has intensified interest in wild medicinal plants, with *Ruta montana* being a notable subject due to its traditional medicinal applications. This study aimed to thoroughly evaluate the phytochemical composition and antibacterial efficacy of *R. montana*. Plant material was meticulously collected from the Mila region and subjected to maceration with 80% ethanol to produce a hydroethanolic extract. Phytochemical screening revealed the presence of key secondary metabolites, including flavonoids, leucoanthocyanins, tannins, steroids, and alkaloids. However, quinones and terpenoids were not detected. The antibacterial potential of the extract was assessed using the disk diffusion method against five bacterial strains: *Escherichia coli, Staphylococcus aureus*, *Pseudomonas aeruginosa*, *Klebsiella pneumoniae*, and *Bacillus subtilis*. Despite the presence of several potentially bioactive compounds, the extract exhibited no significant antibacterial activity against any of the tested strains. In conclusion, the study demonstrates that *R. montana* hydroethanolic extract is rich in various phytochemicals but lacks effective antibacterial properties. Future research should focus on optimizing extraction methods, exploring alternative solvents, and investigating other biological activities such as antioxidant potential. Additionally, identifying specific bioactive compounds in *R. montana* may uncover novel therapeutic applications and enhance the understanding of its medicinal potential.

Keywords: *Ruta montana*, Mila region, Phytochemical screening, Antibacterial potential

Bioactive Potential of Nettle Aerial Parts: Phenolic Content, Antioxidant Activity, and Anti-inflammatory Properties

Hamza Kemchache[1], Khalil Kaouane[1], Soraya Madoui[1], Hanane Khither[1]

[1]Departement of Biochemistry, University of Farhat Abbas Setif-1, Setif, Algeria
Corresponding author: Hamza Kemchache (e-mail: kemchacheh@gmail.com)

Abstract

The study aimed to evaluate the bioactive properties of a crude methanolic extract derived from the aerial parts of nettle, focusing on its phenolic content, antioxidant activity, and anti-inflammatory potential. Total polyphenol content was determined using the Folin-Ciocalteu reagent and $ALCL_3$ method for the total flavonoid content, while anti-inflammatory activity was assessed through the inhibition of protein denaturation assay. Antioxidant capacity was measured using the Iron chelating assay. The results revealed an extraction yield of $10.955 \pm 0.94\%$, with significant amounts of bioactive compounds: total phenolic content of 31.875 ± 2.17 µg GAE/mg extract and flavonoid content of 3.06 ± 0.117 µg RE/mg extract. Moreover, the extract exhibited remarkable anti-inflammatory activity with an IC_{50} value of 225.845 ± 5.81 ug/ml, along with notable iron chelating ability with an IC_{50} of 577.43 ± 23.15 ug/ml. These findings highlight the aerial parts of nettle as a rich source of phenolic compounds with potent antioxidant and anti-inflammatory properties, reinforcing its traditional use in herbal medicine and supporting its potential for the development of therapeutic agents.

Keywords: Antioxidant, Anti-inflammatory, Nettle, Protein denaturation

Enhanced Pechini Sol-Gel Synthesis of NiO Nanoparticles Using Eruca Sativa Extract: Photocatalytic and Antibacterial Applications

Hayet Missouni[1], Djanette Blizak Meriem[2], Souheyla Toubal[2], Imane Djouabi[1]

[1]N-Body and Structure of Matter Laboratory, Higher Normal School of Kouba Echeikh Mohamed, Elbachir Elibrahimi, 16308 Vieux-Kouba, Algeirs, Algeria
[2]Bioinformatics, Applied Microbiology and Biomolecules Research Laboratory (BMAB), University M'Hamed Bougara of Boumerdes, Algeria
Corresponding author: Hayet Missouni (e-mail: Hayette2015@gmail.com)

Abstract

This study focuses on the fabrication of NiO nanoparticles using an improved Pechini sol-gel method enhanced with the plant extract of Eruca sativa, comparing two approaches for synthesizing Nickel Oxide Nanoparticles (NiO-NPs): the green approach using natural, environmentally friendly sources, and the conventional approach using chemical solutions. These nanoparticles were characterized by X-ray diffraction and tested for their photocatalytic activity in degrading Methylene Blue (MB) dye under UV light. The findings reveal that NiO-NPs synthesized using the green method exhibit more uniform crystal phases and smaller particle sizes than those synthesized conventionally, which showed greater variability in crystal size and shape. To provide further insight, we reviewed the degradation mechanisms through experimental results and references from the literature. The synthesized NiO-NPs demonstrated over 65% degradation efficiency under UV light, making them highly effective for environmental applications in water purification. The degradation process generates reactive oxygen species (ROS) that break down the dye molecules, further highlighting the potential of NiO nanoparticles for water purification. Additionally, the antibacterial efficacy of NiO-NPs was tested against *Bacillus cereus* (Gram-positive) isolated from milk. Using the disc diffusion method, the nanoparticles demonstrated significant inhibitory effects, with the size of inhibition zones indicating enhanced antibacterial potential. These results highlight the dual functionality of NiO-NPs synthesized via green methods, offering sustainable solutions for environmental purification and antimicrobial applications.

Keywords: Nanoparticles, Nickel oxide, Sustainable nanotechnology, Environmental Applications, Antibacterial activity

Algerian Lemon Balm: Chemical Composition and Antioxidant Capacity of Hydroethanolic Extract from the Aerial Parts

Nedjla Derbal[1], Hakima Belattar[1], Zineb Bouamrane[1]

[1]Department of Natural Science and Life, University Centre Abdelhafid Bouussouf, Mila, Algeria
Corresponding author: Nedjla Derbal (e-mail: n.derbal@centre-univ-mila.dz)

Abstract

Lemon balm under the scientific name *Melissa officinalis* L is one of the most used medicinal plants, growing in the Mediterranean region, western Asia, southwestern Siberia, and northern Africa. This plant is well known as a herbal tea for its aromatic, digestive and antispasmodic and sedative properties. In the present work, we are interested to determine the phenolic compounds and antioxidant activity of *Melissa officinalis* L of Algerian origin. The qualitative analyse of the hydroethanolic extract of *Melissa officinalis* L by phytochimecal screening showed a great source of a wide range of active chemical compounds. *Melissa officinalis* L presented high contents in polyphenols, tannins, coumarins, terpènoids and flavonoids with a total absence of anthocyanins, free quinones and alkaloids. This was confirmed by considerable extraction yield with a value of 15.96%. The antioxidant activity was evaluated in *vitro* by ferric reducing antioxidant power (FRAP) tests. At 2000 mg/ml, the hydroethanolic extracts was showed a high inhibition percentages with a better reducing capacity of 2.28. Therefore, based in our study the *Melissa officinalis L*, can be used to extract and purify phytochemicals with potentially beneficial effects on health and to prevent oxidative processes.

Keywords: Melissa officinalis, FRAP, Phenolic compounds, Antioxidant activity

A Descriptive Study of Pathologically Confirmed Patients with Breast Cancer in the Region of Bejaia, Algeria

Mostaphaoui Yasmine[1], Menad Rafik[1,2], Moudilou Elara N'tima[3], Bencharif Chahla[4]

[1]Laboratory of Valorization and Bioengineering of Natural Resources, Department of Natural and Life Sciences, Faculty of Sciences, University of Algiers, Algiers, Algeria

[2]Laboratory of Research on Arid Areas, Small Vertebrates Reproduction, Faculty of Biological Sciences, Houari Boumediene University of Sciences and Technology, Algiers, Algeria

[3]Sciences and Humanities, Lyon Catholic University, Lyon, France

[4]Anatomy and Pathology Laboratory, CHU Khelil Amrane, Bejaia, Algeria

Corresponding author: Mostaphaoui Yasmine (e-mail: y.mostaphaoui@univ-alger.dz)

Abstract

Breast cancer is the most common pathology among women in Algeria. Clinical and pathological characteristics of this cancer among this population are not widely reported. The aim of our study was to report clinical and pathological characteristics of women's BC in the region of Bejaia, Algeria. This retrospective study analyzed 20 patients diagnosed with primary invasive breast cancer of no special type, aged between 34 and 77, who underwent mastectomy. Patients' detailed characteristics data were obtained from their records such as HER2, ERα, PgR, Ki-67 immunohistochemical status and scoring, grade, age and lymph node metastasis. Histological and intrinsic (molecular) subtype classification was done according to the latest WHO edition of breast tumors classification. The median age at diagnosis was 58.1 ± 15.9. Only 10% of the study population was made up of men while 90% were women. 75% of the tumors were classified as grade II, while 20% were classified as grade III. Furthermore, the left breast accounted for 55% of the tumor locations. Lymph node status was graded considering the number of metastatic reginal lymph nodes, only 35% of the cases were positive. The tumors were divided into five intrinsic subtypes, with a Ki-67 average of $33,4 \pm 19,8$. The most common subtype was luminal B HER2 negative (35%), followed by luminal A (25%), HER2 enriched (15%), triple negative (15%), and luminal B HER2 positive (10%). Estrogen and testosterone hormone receptor status were primarily positive.

Keywords: Invasive breast cancer, Bejaia, Pathology, Immunohistochemistry

Visceral Leishmaniasis and Poverty in the Middle East and North Africa Region

Mohammed-Yassine Takzima[1], Mohamed Echchakery[1,2], Mohamed Hafidi[1], Loubna El Fels[1]

[1]Laboratory of Microbial Biotechnologies, Agrosciences and Environment (BioMAgE), Faculty of Science Semlalia, Cadi Ayyad University, Marrakech, Morocco

[2]Laboratory of Health Sciences and Technologies Epidemiology and Biomedical Unit, Higher Institute of Health Sciences Hassan Premier University, Settat, Morocco

Corresponding author: Mohammed-Yassine Takzima (e-mail: mohammed.takzima@gmail.com)

Abstract

The World Health Organization (WHO) considers leishmaniasis a group of neglected tropical diseases (NTDs) affecting 12 to 15 million people in 88 countries; it represents a serious health problem in the Middle East and North Africa region (MENA). Several studies worldwide show that there is a link between poverty and the risk of developing visceral leishmaniasis. To demonstrate this relationship, we compared the number of visceral leishmaniasis (VL) cases reported between (2005 and 2021) against the poverty rate of the MENA countries. The data were extracted from WHO epidemiological bulletins and the World Bank data. As a result of data analysis, the poverty rates of 2.15 and 3.65 dollars are correlated to the VL prevalence with a p-value highly significant (Pearson's r = 0.482; p-value = < .001 and Pearson's = 0.448; p-value = 0.002 respectively). Consequently, public investment in treating and controlling VL can reduce the disease burden and alleviate poverty in the MENA region.

Keywords: Visceral leishmaniasis, Poverty, MENA, Middle East, North Africa

Phenolic Content and Antioxidant Activity of Ethyl Acetate Extract of *Pistacia Atlantica* Seeds

Younes Douffa[1], Nadjat Azzi[1], Nour El Houda Belabas[1], Haifaa Laroui[1], Thoraya Guemmaz[1], Karima Saffidine[1], Fatima Zerargui[1], Abderrahmane Baghiani[1]

[1]Laboratory of Applied Biochemistry, Department of Biochemistry, Faculty of Nature and Life Sciences, Farhat Abbas University of Setif 1, 19000 Setif, Algeria
Corresponding author: Younes Douffa (e-mail: younesdouffa2022@gmail.com)

Abstract

Antioxidants are molecules that help protect cells from damage caused by free radicals, which can lead to oxidative stress and contribute to various diseases such as cancer, cardiovascular disease and diabetes. Phenolic compounds of medicinal plants can neutralize free radicals in the body and reduce the risk of chronic diseases. For this reason, this work aimed to quantify the total polyphenols (TPC) and flavonoids (TFC) contents of ethyl acetate extract (EAES) from *Pistacia atlantica* seeds, as well as their antioxidant activity using total antioxidant capacity (TAC) and hydroxyl radical scavenging (OH·) assays. The results showed that TPC and TFC amounts were 266.34 ± 15.5 mg GAE/g and 62.7 ± 0.42 µg QE/mg, respectively. This extract exhibited a strong TAC EC_{50} of 18.23 ± 0.23 µg/mL and has the ability to scavenge free radical with IC_{50} of 0.50 ± 0.02 mg/ml. These results suggest that EAES could be considered a potential source of natural antioxidant that contributes to therapeutic benefits.

Keywords: Antioxidant, Flavonoids, Free radicals, Polyphenols, *Pistacia atlantica*

Phytochemical Analysis, Anti-Inflammatory, and Analgesic Activities of a Cypress Methanolic Extract

Thoraya Guemmaz[1], Nour El Houda Belabas[1], Nadjat Azzi[1], Younes Douffa[1], Haifaa Laroui[1], Fatima Zerargui[1], Karima Saffidine[1], Abderrahmane Baghiani[1]

[1]Laboratory of Applied Biochemistry, Department of Biochemistry, Faculty of Nature and Life Sciences, Ferhat Abbas University of Setif 1, 19000 Setif, Algeria
Corresponding author: Thoraya Guemmaz (e-mail: thorayaguem@gmail.com)

Abstract

Nonsteroidal and steroidal antiinflammatory drugs are classes of medication used to treat pain, fever, and other inflammatory processes, but their use causes undesired and sometimes serious side effects. Therefore, finding new and effective antiinflammatory drugs that can reduce pain and inflammation with lower adverse effects is crucial. Recently, there has been a growing interest in the search for natural antiinflammatory products derived from plants. This study focuses on the chemical analysis of *Cupressus sempervirens* L. leaves methanolic extract (CS) by HPLC and evaluation of its anti-inflammatory and analgesic effects. Quantitative analysis by HPLC revealed the richness of CS in catechin, epicatechin, quercitrin and ferulic acid. The acute toxicity test in male mice showed that CS does not exert any toxic effect with the 2 g/kg dose (LD50 > 2 g/kg). The antiinflammatory activity, *in vivo*, was tested in xylene-induced ear edema, while the antinociceptive effect was tested with the pain model induced by acetic acid-induced writhing response. Results showed that, in xylene-induced ear edema, oral administration of CS (100, 300, and 500 mg/kg) significantly reduced the edema. In antinociceptive experiment, the pretreatment with CS produced important analgesic activity. In the above assays, the extract demonstrated significant antiinflammtory activities. These findings revealed that *C. sempervirens* leaves could be used as a promising source of natural compounds for therapeutic uses.

Keywords: *Cupressus sempervirens* L, Ear edema, Xylene, Acetic acid, Antinociceptive effect

Antioxidant Activity of Two Date Fruits Cultivar in First Ripening Stage

Amel Barkat[1,2], Hayat Trabsa[2,3], Abderahmane Baghiani[3], Abdelnacer Agli[4,5]

[1]Promoting Innovation in Agriculture in Arid Regions (PIAAR), Biskra, Algeria
[2]Department of Natural Sciences and life, Faculty of Exact Sciences Natural and Life Sciences, University of Mohamed Khider, Biskra, Algeria
[3]Laboratory of Applied Biochemistry, Faculty of Nature and Life Sciences, University Ferhat Abbas, Setif, Algeria
[4]Laboratory of Nutrition and Food Technologies, Constantine, Algeria
[5]Institute of Nutrition, Food and Agri-Food Technologies, Constantine, Algeria
Corresponding author: Amel Barkat (e-mail: amel.barkat@univ-biskra.dz)

Abstract

Bioactive compounds are known for their several activities, and have different health benefits. Date fruits in their different ripening stages, are rich with these bioactive compounds, and the variation in phenolic content among different cultivars can influence their antioxidant activity. This study aimed to evaluate the quantity of total phenolic content and their antioxidant activity of two date fruits cultivars (Deglet Nour and Mech Degla) in the first repining stage (Loulou stage). The samples of date fruits were collected from west in Biskra, extracted using decoction for 20min and the phenolic content was measured using Folin-Ciocalteu method. The antioxidant activity was tested using DPPH scavenging essay. The results revealed no significant differences in extraction yield of both Deglet Nour and Mech Degla cultivars (Deglet Nour 7.7% and Mech Degla 9.1%) using Mann-Whitney U test $\rho = 0.333 > 0.05$. For phenolic content, a significant variation was noticed, where Deglet Nour gave higher phenolic content comparing to Mech Degla (157.1 and 123.8 µg GAE/mg extract respectively) based on T test ($\rho = 0 < 0.05$). However, no significant variation was noticed in DPPH scavenging assay according to Mann-Whitney U test ($1 > 0.05$), respectively IC50 for Deglet Nour was 10.8 µg/ml and IC50 for Mech Degla was 21.1 µg/ml. In conclusion, this study highlights that date fruits in Loulou stage has a noticeable antioxidant capacity due to its higher total phenolic content.

Keywords: Deglet Nour, Mech Degla, Total phenolic content, DPPH scavenging assay

Impact of Early Maladaptive Schemas on Perceived Stress and Moderating Role of Resilience in Nursing Students

Ilham Rhzali[1], Hanane Khalki[2], Samira Boulbaroud[2], Fatima-Zahra Azzaoui[1]

[1]Laboratory of Biology and Health, Faculty of Science, Ibn Tofail University, Kenitra, Morocco
[2]Laboratory of biotechnology and Sustainable Development of Natural Ressources, Polydisciplinary Faculty, Sultan Moulay Slimane University, Mghila, Beni Mellal, Morocco

Corresponding author: Ilham Rhzali (e-mail: rhzaliilham@gmail.com)

Abstract

Nursing education entails navigating challenging academic coursework and demanding clinical environments, which may significantly impact students' psychological well-being. This study aimed to investigate the relationship between early maladaptive schemas (EMS), stress, and resilience among nursing students. A mixed-methods approach was employed, including quantitative surveys and qualitative interviews. Participants completed self-administered surveys assessing EMS, perceived stress, and resilience. Pearson correlation analysis examined the relationships between variables, while thematic analysis elucidated qualitative data. Findings revealed moderate levels of EMS among nursing students, with prevalent domains including Abandonment/Instability, Mistrust/Abuse, and Emotional Deprivation. Participants reported moderate levels of perceived stress, with clinical experiences emerging as significant stressors. Positive correlations were found between EMS domains and perceived stress, highlighting the impact of maladaptive cognitive-emotional patterns on stress experiences. Resilience moderated this relationship, with higher resilience buffering the negative effects of EMS on stress levels. Qualitative interviews revealed experiences of EMS, stressors in nursing education, coping mechanisms, and factors contributing to resilience. This study advances understanding by employing comprehensive assessment tools, examining resilience's moderating role, and providing insights for tailored interventions to support nursing students' well-being and success. Limitations include the cross-sectional design and reliance on self-report measures. Future research should employ longitudinal designs and objective measures to further elucidate these relationships. Overall, this study contributes valuable insights into cognitive-emotional factors influencing stress and resilience among nursing students.

Keywords: Nursing students, EMS, Clinical experiences, Psychological well-being, Cognitive-emotional factors

1,3-Dipolar Reaction Study by Means of Density Functional Theory Approaches

Boulanouar Messaoudi[1,2]

[1]Higher School of Applied Sciences of Tlemcen, 13000 Tlemcen, Algeria
[2]Toxicomed Laboratory, University of Abou Bekr Belkaid, 13000 Tlemcen, Algeria
Corresponding author: Boulanouar Messaoudi (e-mail: messaoudiboulanouar@gmail.com)

Abstract

Since its discovery, cycloaddition reactions have known a tremendous attention in organic synthesis. This kind of reactions has gained such success because of the possibility of forming cycloadducts with heteroatoms as it is called heterocyclic compounds. This latter can be found in many disciplines and are very important not only in industry but also in natural products, biology, pharmacy and drugs, medicine and many other fields of daily interests. Among cycloaddition reactions, 1,3-dipolar reactions are one of the most important. This type needs a multiple bond reactant which would react with another molecule known as 1,3-dipole. The reaction generally conducts to different stereoisomers. This makes of it a good subject of regioselectivity and stereoselectivity. In this work, a reaction type was studied in order to reveal the formation of the obtained products by means of some theoretical approaches such as global and local reactivity indices under density functional theory DFT.

Keywords: Dipolar reaction, B3LYP, Cycloadduct, Regioselectivity

Synthesis, Biological Activity, and Enantioseparation of Iminonaringenine

Mohamed Nadjib Rebizi[1], Salah-Eddin Rahmani[1]

[1]Organic Chemistry and Natural Substances Laboratory, Faculty of Exact Sciences and Computer Science, University of Djelfa, PO Box 3117, 17000 Djelfa, Algeria
Corresponding author: Mohamed Nadjib Rebizi (e-mail: mn.rebizi@univ-djelfa.dz)

Abstract

In this work it was interested in the synthesis, biological activity and the chiral separation of enantiomers and diastereomers of Iminonaringenine. The various syntheses are performed based on condensation reactions of primary amines and diamines the structures of these compounds have been proved by spectroscopic methods IR, UV, RMN1H and RMN13C. These products have undergone varied biological activities, such as antibacterial activities, antioxidant and antifungal. As regards the antibacterial effect, we used five bacterial strains: Staphylococcus aureus, Bacillus subtilis, Listeria monocytogenes Escherichia coli, Pseudomonas aeroginosa. The results allowed us to say that the majority of the synthesized products have an inhibitory power all the tested micro-organisms. The antifungal tests against Fusarium oxysporum f.sp. albedinis were negative. The results of antioxidant activity the DPPH and β-carotene have been shown that these derivatives presented a very important activity on free radicals. The HPLC enantiomeric separation of fourteen Iminonaringenine was accomplished in the normal phase and organic polar mode, using six polysaccharides derived chiral stationary phases (Chiralcel OD-H, Chiralcel OD, Chiralcel OJ, Chiralpak AD, Chiralpak IA and Chiralpak IB) and various n-alkane/alcohol mobile phases. The enantioseparation of these new prepared shows that the chiral recognition mechanism of each stationary phase has been suggested, and based on the chemical nature and conformation of the chiral selector.

Keywords: Iminonaringenine, HPLC, Biological activities, Enantioseparation, DPPH

Molecular Pharmacology of Anti-Rheumatic Biomolecules: A Review

Sara Ouari[1], Nadia Benzidane[1], Noureddine Bribi[2]

[1]Laboratory of Applied Biochemistry, Faculty of Nature and Life Science, University Ferhat Abbes Setif 1, Setif, Algeria
[2]Laboratory of Plant Biotechnology and Ethnobotany, Faculty of Nature and Life Sciences, University of Bejaia, Bejaia, Algeria
Corresponding author: Sara Ouari (e-mail: ouari.sarra@univ-setif.dz)

Abstract

Modern pharmacological studies have demonstrated the anti-arthritic effect of various biomolecules extracted from medicinal plants, many molecular mechanisms are involved in the etiology of Rheumatoid arthritis (RA); increasing attention has been focused on ethnological medicinal plants and the use of combined molecules to target the different molecular pathways involved in synovial hyperplasia, inflammatory response, and the cartilage and bone destruction. Aconite decoction, largely used in traditional Chinese medicine, has an anti-rheumatic function, this alkaloid reduces high expression of toll-like receptor 2 (TLR2), tumor necrosis factor receptor-associated factor 6 (TRAF6) and Faslg which regulate the different strength of a peripheral T cell subset. Total flavonoid of Astragalus membranaceus improve bone destruction by up-regulating OPG expression and down-regulating RANKL expression which lead to a non-activation of NF-κB p65 (involved in arthritis progression and inflammatory mediator production), hence a remarkably anti-arthritic effect. Triptolide (an active ingredient extracted from Tripterygium wilfordii) inhibits the migration and invasion of fibroblast-like synoviocytes (FLSs) by blocking the activation of JNK-MAPK pathway leading to an inhibition of MMP-9 activation and cytoskeleton rearrangement. Salvianolic acid B ("Sal-B" a phenolic compound present in Salvia miltiorrhiza) reduced apoptosis via modulating cell-growth-related proteins (p53 and p21) and inhibiting caspases-dependent apoptosis contributing to repression of pro-inflammatory cytokines release (MCP-1, IL-6 and TNF-α), it also up-regulated miR-142-3p signaling hence desactivating NF-κB and JNK pathways indicating its anti-inflammatory property. This review disscuss the molecular pathways involved in treatment of RA using of herbal plants to avoid the side effects that generally occur in allopathic treatments

Keywords: Rheumatoid arthritis, Molecular pathways, Natural products, Medicinal plants, In vitro & in vivo models

1. INTRODUCTION

The use of medecinal plants have evolved over centries for the treatment of various health challenges, and it continues to expand across the world [1]. Rheumatoid arthritis (RA) a chronic autoimmune disease that principally attacks synovial joints [2], still require extensive research for the development of new treatments controlling the inflammation, reducing joint damage and pain, to improve patients' quality of life [3]. The pathogenesis of RA involves abnormal activation of fibroblast-like synoviocytes (FLS) as an initial event of synovial inflammation [2, 3], an overexpression of proinflammatory molecules (TNF-α and IL-1β) promoting the production of prostaglandin E_2 (PGE_2) by RA synoviocytes, thus facilitating angiogenesis and bone resorption [4], attracting other immune cells to produce generalized effects such as pain, fever, and discomfort [5]. Natural compounds derived from traditionally used medicinal herbs targetting the signaling mechanisms of inflammation have been the focus of the latest researchs work [6], In the present review, we report the molecular pharmacology of anti-inflammatory and anti-rheumatic compounds from natural sources, exploring the mechanism of interaction by performed experiments: enzyme-linked immunosorbent assay (ELISA), polymerase chain reaction (PCR) or flow cytometry (FCM).

2. MATERIAL AND METHOD

A literature search related to natural molecular treatment of RA was conducted using Google Scholar Database with a combination of keywords. Studies published from 2020 to 2024 were selected as recent advances in the field, evidence of biomolecules effectiveness has been summarized according to their mechanism of action, in vitro and in vivo studies were included; ancient articles were used for bibliography.

3. RESULTS

3.1. NF-κB Signaling Network

NF-kB signaling is a master regulator of autoimmune diseases and inflammatory response [7], responsible of the regulation of thousands of primary and secondary response genes including cytokines, chemokines, transcription factors, antimicrobial peptides, and interferon (IFN)-stimulated genes (ISGs) [8]. In RA, the inflammatory process is mediated by M1 macrophages both in peripheral blood and in synovial tissue [9] it detects various microbial components, pathogen-associated molecular patterns (PAMPs) and damage-associated molecular patterns (DAMPs), via pattern recognition receptor (PRRs) including toll-like receptors (TLRs), RIG-I-like receptors, NOD-like receptors (NLRs), C-type lectin-like receptors and cytosolic DNA sensors [8, 10]. The main types of synovial cells: Fibroblast-like synoviocytes (FLS) and macrophage-like synovial cells (MLS) are important participants in the pathogenesis of RA [11] in pathogenic conditions, FLS migrate into the cartilage and bone, produces RANKL which binds to the receptor activator of NF-κB (RANK) on osteoclast precursors, inducing osteoclast differentiation, activation, and production, thus, these cells induce bone destruction [12]. On the other hand, TLR4-ligand induces macrophages M1 polarization (an imbalance between M1 and M2 macrophages), after receptor configuration change, IKK is activated, which leads to phosphorylation of the complex IκB/NF-κB (formed by two units: p65-p50), phosphorylated IκB is ubiquitined and degraded by the 26S proteasome, NF-κB is then activated, thus, M1 polarization is promoted secreting several proinflammatory cytokines, such as tumor necrosis factor-α (TNF-α), IL-6, IL-1β, IL-23 and others [13]. İmmunohistochemistry results reported by Liu et al., revealed that flavonoids, isolated from Astragalus membranaceus, suppressed Freund's complete adjuvant (FCA)-induced arthritis in rats by suppressing NF-κB p65 over-expression, increasing the OPG/RANKL ratio improving bone resorption [14], Wang et al., also confirmed by molecular study that baicalin (a flavonoid extracted from the root of Scutellaria radix) suppresses NF-κB p65 protein expression and phosphorylation in synovial tissue and human-derived synoviocytes [15]. Endale et al., study results showed that quercetin had an anti-RA effect on LPS-induced RAW264.7 cells achieved by inhibiting inhibit RANKL production, inhibiting IKK/NF-kB complex dissociation and by that inhibiting monocyte-to-osteoclast formation and the production of inflammatory mediators (TNF-a, IL-1b, IL-6, and macrophage colony stimulating factor) [16]. Inhibiting this pathway blocked the production of pro-inflammatory cytokines, such as IL-1, IL-6, IL-12, TNF-α and chemokines, involved in the inflammatory processes, inhibit the RANK ligand-induced differentiation of monocytes/macrophages into the bone-resorbing osteoclasts, and by that contributes to bone resorption [8].

3.2. JNK/MAPK Signaling Pathway

The mitogen-activated protein kinase (MAPK) signaling pathway is very important in the regulation of RA FLSs migration and invasion [17]. When activated, RA FLSs mimic tumor cells; they proliferate in an anchorage-independent manner, escape apoptosis, migrate to the cartilage and bone, activate osteoclasts, leading to cartilage degradation and bone destruction [18]. Yang et al., study reported that triptolide treatment (extracted from Tripterygium wilfordii) caused an in vivo and in vitro reduction of RA FLSs invasiveness into the cartilage, by reducing the phosphorylation of JNK, blocking the MAPK pathway, decreasing the activation of MMP-9 and cytoskeleton rearrangement which leaded to the decrease of the migration and invasion of RA FLSs, preventing joint damage [19]. Molecular study results of Pan et al., demonstrated that Kaempferol (a flavonoid extracted from Kaempferia rotunda) had a similiar effect to triptolide, it reduced RA FLS invasiveness through the inhibition of several MAPK pathways (reducing the phosphorylation of ERK, JNK and p38), reducing the expression of MMP-1, MMP-3, MMP-9 and MMP-13 which are essential for osteoclastogenesis [17, 20], thus, it plays a protective effect against bone destruction.

3.3. JAK/STATs Signaling Pathway

The JAK/STAT signaling pathway can be segmented into three main components: receptor-associated tyrosine kinase, JAK tyrosine kinase, and STAT transcription factor [12]. In RA JAK1/STAT3 signaling is mediated by IL-6 family cytokines, which stimulate activation and production of osteoclast via osteoblast lineage cells [21]. Elevated STAT3 expression contributes to the inhibition of programmed cell death, blocking apoptosis in RA-FLS, thus, promotes RA synovial thickening. Results study of Lin et al., demonstrated that triptolide could also inhibit JAK2/STAT3 signaling pathway, inhibiting the proliferation of FLSs and the expression of inflammatory cytokines (IL-1b, IL-6, and VEGF) [22]. Lee et al., molecular study results of an animal model of arthritis, showed that epigallocatechin-3-gallate (a polyphenol extracted from green tea) inhibits osteoclastogenesis and Th17 cell activation, and increase the number of Foxp3+ Treg, through the inhibition of STAT3 activation, inhibiting mTOR and activating HIF-1a [23]. Targeting this pathway could improve synovial hyperplasia and bone destruction.

3.4. MiRNAs Regulation

MiRNAs are a group of small non-coding RNAs of about 18–22 nucleotides in length, that can repress gene expression at the post-transcriptional level [24], They are related to the regulation of various processes including T cell activation, cell infiltration and inflammation regulation [2]. Meng et al., showed that, miR-142-3p was up-regulated by Salvianolic acid-B (extracted from Salvia miltiorrhiza) in LPS-induced inflammation, repressing the activation of NF-κB and JNK pathways, thus, attenuating the release of pro-inflammatory cytokines in MH7 A cells [3]. Wen et al., molecular study results showed that triptolide enhanced miR-31-5p expression dicreasing CDK1 expression, thus, suppressing the proliferation of RA-FLS, as well as the production of cytokines (IL-1β, IL-6, IL-4, and IL-10) [25]. Molecular targets and treatment results are summerized in Table 1.

Table 1. Molecular targets of herbal biomolecules

Biomolecules	Source	Signaling Pathways	Molecular Treatment Results	References
Flavonoids	Flavonoid from Astragalus membranaceus	NF-κB	↓ NF-κB p65 expression, ↑ OPG/RANKL ratio, ↑ bone resorption.	[14]
Baicalin	Flavonoid from Scutellaria radix	NF-κB	× NF-κB p65 protein expression, ↑ bone resorption.	[15]
Quercetin	Flavonoid	NF-κB	↓ RANKL production × osteoclast formation, ↓ IKK/NF-kB complex dissociation, ↓ Production of inflammatory mediators.	[16]
Triptolide	Terpenoid from Tripterygium wilfordii	JNK/MAPK	↓ JNK phosphorylation × MAPK pathway, ↓ MMP-9 activation ↓ FLSs invasiveness into the cartilage, ↑ bone resorption, ↓ Synovial hyperplasia.	[19]
		JAK/STAT	× JAK2/STAT3 × FLS proliferation × Expression of inflammatory cytokines (IL-1b, IL-6, and VEGF).	[22]
			↑ miR-31-5p expression ↓CDK1 expression, × RA-FLS proliferation × Cytokines production (IL-1β, IL-6, IL-4, and IL-10)	[25]
Kaempferol	Flavonoid from Kaempferia rotunda	JNK/MAPK	↓ ERK, JNK and p38 phosphorylation, × MAPK pathways ↓ MMP-1, MMP-3, MMP-9 and MMP-13 expression, ↓ RA FLS invasiveness, × osteoclastogenesis.	[20]

Epigallocatechin-3-gallate	Polyphenol from Green tea	JAK/STAT	× STAT3 activation, × mTOR and ↑ HIF-1a, ↑ Foxp3+ Treg, × Th17 cell activation, × osteoclastogenesis.	[23]
Salvianolic acid-B	Polyphenol from Salvia miltiorrhiza	NF-κB and JNK	↑ miR-142-3p, × NF-κB and JNK pathways, × the release of pro-inflammatory cytokines	[3]

3. CONCLUSION

In this review we summary the biomolecules multiple targets of the pathways involved in the pahogenesis of RA and their mechanisms of action. Studies conducted in vitro on arthritis induced in multiple cells type and in vivo in multiple arthritis induced models were consulted. the popular targeting signaling pathways were NF-κB, MAPK and JAK/STAT, some molecules also targets miRNA that regulates these pathways. All the molecules reported had a great curative effect in the treatment of RA, treating clinical symptoms. Therefore, developing efficient and low-toxic active substances from traditional plants is an important development direction for treating RA.

References

[1]   X.-H. Wu, B. Dou, N.-Y. Sun, J. Gao, and X.-L. Liu, "Astragalus saponin IV promotes osteogenic differentiation of bone marrow mesenchymal stem cells via miR-21/NGF/BMP2/Runx2 pathway," *Acta Histochem.*, vol. 122, no. 4, art. no. 151549, May 2020, doi: 10.1016/j.acthis.2020.151549.

[2]   Y. Wang et al., "Novel anti-inflammatory target of geniposide: Inhibiting Itgβ1/Ras-Erk1/2 signal pathway via the miRNA-124a in rheumatoid arthritis synovial fibroblasts," *Int. Immunopharmacol.*, vol. 65, pp. 284–294, Dec. 2018, doi: 10.1016/j.intimp.2018.09.049.

[3]   D. Meng, J. Li, H. Li, and K. Wang, "Salvianolic acid B remits LPS-induced injury by up-regulating miR-142-3p in MH7A cells," *Biomed. Pharmacother.*, vol. 115, art. no. 108876, Jul. 2019, doi: 10.1016/j.biopha.2019.108876.

[4]   H. Wang, B. Dong, Z. Zheng, Z. Wu, W. Li, and J. Ding, "Metastasis-associated protein 1 (MTA1) signaling in rheumatoid synovium: Regulation of inflammatory response and cytokine-mediated production of prostaglandin E2 (PGE2)," *Biochem. Biophys. Res. Commun.*, vol. 473, no. 2, pp. 442–448, Apr. 2016, doi: 10.1016/j.bbrc.2016.03.027.

[5]   A. Khan et al., "Anti-Inflammatory and anti-rheumatic potential of selective plant compounds by targeting TLR-4/AP-1 signaling: A comprehensive molecular docking and simulation approaches," *Molecules*, vol. 27, no. 13, art. no. 13, Jan. 2022, doi: 10.3390/molecules27134319.

[6]   I. Naz, M. S. Masoud, Z. Chauhdary, M. A. Shah, and P. Panichayupakaranant, "Anti-inflammatory potential of berberine-rich extract via modulation of inflammation biomarkers," *J. Food Biochem.*, vol. 46, no. 12, Dec. 2022, doi: 10.1111/jfbc.14389.

[7]   M. G. Dorrington and I. D. C. Fraser, "NF-κB signaling in macrophages: Dynamics, crosstalk, and signal integration," *Front. Immunol.*, vol. 10, art. no. 705, Apr. 2019, doi: 10.3389/fimmu.2019.00705.

[8]   T. Liu, L. Zhang, D. Joo, and S.-C. Sun, "NF-κB signaling in inflammation," *Signal Transduct. Target. Ther.*, vol. 2, no. 1, art. no. 1, Jul. 2017, doi: 10.1038/sigtrans.2017.23.

[9]   M. Cutolo, R. Campitiello, E. Gotelli, and S. Soldano, "The role of M1/M2 macrophage polarization in rheumatoid arthritis synovitis," *Front. Immunol.*, vol. 13, May. 2022, doi: 10.3389/fimmu.2022.867260.

[10]   E. Platanitis and T. Decker, "Regulatory networks involving STATs, IRFs, and NFκB in inflammation," *Front. Immunol.*, vol. 9, art. no. 2542, Nov. 2018, doi: 10.3389/fimmu.2018.02542.

[11]   Z. Wu et al., "Fibroblast-like synoviocytes in rheumatoid arthritis: Surface markers and phenotypes," *Int. Immunopharmacol.*, vol. 93, art. no. 107392, Apr. 2021, doi: 10.1016/j.intimp.2021.107392.

[12]   Y. Tong, X. Li, Q. Deng, J. Shi, Y. Feng, and L. Bai, "Advances of the small molecule drugs regulating fibroblast-like synovial proliferation for rheumatoid arthritis," *Front. Pharmacol.*, vol. 14, Jul. 2023, doi: 10.3389/fphar.2023.1230293.

[13]   Y. Song et al., "Characteristics, polarization and targeted therapy of mononuclear macrophages in rheumatoid arthritis," *Am. J. Transl. Res.*, vol. 15, no. 3, pp. 2109–2121, Mar. 2023.

[14] X.-Y. Liu et al., "Protective effects of total flavonoids of Astragalus against adjuvant-induced arthritis in rats by regulating OPG/RANKL/NF-κB pathway," *Int. Immunopharmacol.*, vol. 44, p. 105–114, Mar. 2017, doi: 10.1016/j.intimp.2017.01.010.

[15] H.-Z. Wang et al., "Inhibitory effect of baicalin on collagen-induced arthritis in rats through the nuclear factor–κb pathway," *J. Pharmacol. Exp. Ther.*, vol. 350, no. 2, pp. 435–443, Aug. 2014, doi: 10.1124/jpet.114.215145.

[16] M. Endale et al., "Quercetin disrupts tyrosine-phosphorylated phosphatidylinositol 3-kinase and myeloid differentiation factor-88 association, and inhibits MAPK/AP-1 and IKK/NF-κB-induced inflammatory mediators production in RAW 264.7 cells," *Immunobiology*, vol. 218, no. 12, pp. 1452–1467, Dec. 2013, doi: 10.1016/j.imbio.2013.04.019.

[17] X. Yu et al., "Kaempferol attenuates wear particle-induced inflammatory osteolysis via JNK and p38-MAPK signaling pathways," *J. Ethnopharmacol.*, vol. 318, art. no. 117019, Jan. 2024, doi: 10.1016/j.jep.2023.117019.

[18] E. Neumann et al., "Migratory potential of rheumatoid arthritis synovial fibroblasts: Additional perspectives," *Cell Cycle*, vol. 9, no. 12, pp. 2286–2291, Jun. 2010, doi: 10.4161/cc.9.12.11907.

[19] Y. Yang et al., "Triptolide inhibits the migration and invasion of rheumatoid fibroblast-like synoviocytes by blocking the activation of the JNK MAPK pathway," *Int. Immunopharmacol.*, vol. 41, pp. 8–16, Dec. 2016, doi: 10.1016/j.intimp.2016.10.005.

[20] D. Pan et al., "Kaempferol inhibits the migration and invasion of rheumatoid arthritis fibroblast-like synoviocytes by blocking activation of the MAPK pathway," *Int. Immunopharmacol.*, vol. 55, pp. 174–182, Feb. 2018, doi: 10.1016/j.intimp.2017.12.011.

[21] N. Kondo, T. Kuroda, and D. Kobayashi, "Cytokine networks in the pathogenesis of rheumatoid arthritis," *Int. J. Mol. Sci.*, vol. 22, no. 20, art. no. 20, Jan. 2021, doi: 10.3390/ijms222010922.

[22] J. Lin et al., "Triptolide inhibits expression of inflammatory cytokines and proliferation of fibroblast-like synoviocytes induced by IL-6/sIL-6R-mediated JAK2/STAT3 signaling pathway," Curr. Med. Sci., vol. 41, no. 1, pp. 133–139, Feb. 2021, doi: 10.1007/s11596-020-2302-1.

[23] S.-Y. Lee et al., "Epigallocatechin-3-gallate ameliorates autoimmune arthritis by reciprocal regulation of T helper-17 regulatory T cells and inhibition of osteoclastogenesis by inhibiting STAT3 signaling," *J. Leukoc. Biol.*, vol. 100, no. 3, pp. 559–568, Sep. 2016, doi: 10.1189/jlb.3A0514-261RR.

[24] Y. Zhang, M. Yang, H. Xie, F. Hong, et S. Yang, "Role of miRNAs in rheumatoid arthritis therapy," Cells, vol. 12, no. 13, art. no. 1749, Jun. 2023, doi: 10.3390/cells12131749.

[25] J. Wen et al., "Triptolide inhibits cell growth and inflammatory response of fibroblast-like synoviocytes by modulating hsa-circ-0003353/microRNA-31-5p/CDK1 axis in rheumatoid arthritis," *Int. Immunopharmacol.*, vol. 106, art. no. 108616, May 2022, doi: 10.1016/j.intimp.2022.108616.

α-Amylase and Antifungal Activity of a Medicinal Plant from Algeria Ammoides

Roumeila Zerrouk[1,2], Sihem Boudermine[2], Tarek Boudiar[3]

[1]Department of Chemistry, Faculty of Science, University 20 August 1955, Algeria
[2]Laboratory of Physical Chemistry of Surfaces and Interfaces, Faculty of Sciences, University 20 August 1955, Algeria
[3]Quality Analysis Laboratory, National Biotechnology Research Center (CRBT), Algeria
Corresponding author: Roumeila Zerrouk (e-mail: r.zerrouk@univ-skikda.dz)

Abstract

Apiaceae is a family of mostly aromatic flowring plants and commonly known as the celery, consist of about 55 genera and 130 species, is an endemic plant1 traditionally used as an infusion to treat headache, fever, diarrhea, and vitiligo and is also added as a spice in some recipes. This contribution concerns the biological evaluation of a species of the apiaceae family. After extraction of the aerial parts of the plant, tests were carried out on the different biological activities α-amylase and antifungal of its extracts in solvents of increasing polarity. Phytochemical screening is identification of different classes of phytoconstituents present in various parts of a plant. Plants are rich in a wide variety of secondary metabolites such as flavonoids content, phenolic content (total flavnoid (216.3194 ± 1.3258) and total phenol (187.895 ± 0.87)). The results suggest that extract of a plant might be promising for the treatment or prevention of many diseases associated with oxidative damage. Further researches needed to identify and isolate the active principles present in this extract which could be useful for pharmaceutical purposes.

Keywords: Medicinal plant, Apiaceae family, Antifungal, α-amylase, Biological

Exploring Arthropods as an α-Chitin and β-Chitin Sources for Circular Economy Applications

Samia Elouali[1,2], Samira Benali[2], Jean-Marie Raquez[2], Mohammed Rhazi[1]

[1]Interdisciplinary Laboratory in Bio-Resources, Environment and Materials, Higher Normal School, Cadi Ayyad University, 4000 Marrakech, Morocco
[2]Laboratory of Polymeric and Composite Materials (LPCM), Center of Innovation and Research in Materials and Polymers (CIRMAP), University of Mons (UMONS), 7000 Mons, Belgium
Corresponding author: Samia Elouali (e-mail: samia.ELOUALI@umons.ac.be)

Abstract

Chitin is a natural biopolymer found in arthropods exoskeleton, it has a garnered significant attention due to its biocompatibility, biodegradability and antimicrobial properties [1, 2]. Its applications are extensive, with uses in cosmetics, agriculture, water treatment and nets fishing industries [2]. In this work, chitins were extracted from arthropods known as sources of alpha and beta chitin. Our focus was to obtain chitin under its native form as characterized by high acetylation, crystallinity, and resistance to degradation. An original, efficient, and eco-friendly extraction method using autoclave process, has been thereby developed. The extracted chitin samples underwent characterization using various techniques, including Nuclear Magnetic Resonance, Fourier Transform Infrared Spectroscopy, X-ray Diffraction, Energy-Dispersive X-ray Spectroscopy, Thermogravimetric Analysis, and Scanning Electronic Microscopy. We obtained α-chitin from *Hermetia illucens* breeding waste and shrimp exoskeletons, and β-chitin from cuttlefish bone and squid feather. The crystallinity index ranged from 51.5% to 57.3%, as confirmed by the honeycomb and fibrillar structure observed on SEM, with yields ranging from 20% to 100% and DTG_{max} between 341°C and 396°C. These chitins will be subsequently exploited for circular economy applications, particularly in wastewater treatment.

Keywords: Chitin, Arthropods, Eco-friendly process

References

[1] U. Dave, E. Somanader, P. Baharlouei, L. Pham, and M. A. Rahman, "Applications of chitin in medical, environmental, and agricultural industries," *J. Mar. Sci. Eng.*, vol. 9, art. no. 1173, 2021.
[2] F. Khoushab and M. Yamabhai, "Chitin research revisited," *Mar Drugs.*, vol. 8, no. 7, pp. 1988–2012, 2010.

Tuning the Plasmonic Properties of Gold Nanoparticles via Nd:YAG Laser Ablation in Liquid for Ethylene Glycol Sensing Application

Latifatul Aisyah Nabila[1], Nurul Hidayat[1,2], Ahmad Taufiq[1]

[1]Department of Physics, Universitas Negeri Malang, Malang, Indonesia
[2]Center for Science and Engineering, Universitas Negeri Malang, Malang, Indonesia
Corresponding author: Nurul Hidayat (e-mail: nurul.hidayat.fmipa@um.ac.id)

Abstract

Ethylene glycol (EG) has been widely used in many industries, varying from antifreeze liquids to coatings, due to its versatility. Detection of EG levels in solution is important to prevent serious health risks due to exposure to EG vapor, such as kidney failure, pulmonary edema, and death. This study aims to develop a localized surface plasmon resonance (LSPR) based sensor utilizing gold nanoparticles (AuNPs) to detect the concentration of EG in solution. Morevover, the LSPR properties of AuNPs were tuned by changing the Nd:YAG laser energy, from 200 mJ to 400 mJ, during the laser ablation process. Meanwhile, the wavelength and frequency of Nd:YAG laser were set constant at values of 1064 nm and 4 Hz, respectively. Ultraviolet–visible (UV-Vis) analysis results showed that the interaction of AuNPs with EG solution at various concentrations resulted in dual changes in absorbance peak and LSPR wavelength shift. The absorbance peak tended to decrease, while the wavelength shifted to a larger direction with an increase in EG concentration. The sensitivities of of AuNPs to EG solutions were 0.010 a.u./EG% and 0.104 nm/G% for amplitude and spectral modalities, respectively. The developed LSPR-based sensor demonstrated potential to detect EG levels in solution with high accuracy and opens new opportunities in the development of more sensitive and effective solution sensors.

Keywords: Gold nanoparticles, Localized surface plasmon resonance, Nd:YAG laser ablation in liquid, Ethelyne glycol sensor

1. INTRODUCTION

Ethylene glycol (EG) is an organic chemical compound that is commonly used in various industries. It is commonly utilized as a key ingredient in antifreeze liquids, textiles, plastics, and coatings due to its excellent chemical properties [1]. In the fields of chemistry and nanotechnology, the detection of EG levels in solutions plays an important role in investigating chemical interactions, catalytic reactions, and other properties of materials such as nanoparticles on EG-containing solutions. However, most of the current research only focused on developing gas-based sensors to detect EG vapor [2–4]. In this sense, high concentration of EG vapor is toxic and severe EG poisoning may cause major health risks and death [5]. On the other hand, research on solution-based sensors that utilize changes in optical properties due to EG interactions is rarely reported. In fact, detection of EG levels in solution is also critical to prevent the dangerous increase in its vapor concentration. Therefore, the use of plasmonic nanomaterials, for example gold nanoparticles (AuNPs), for EG sensing applications can be an alternative, AuNPs increase the detection sensitivity through the Localized Surface Plasmon Resonance (LSPR) phenomenon. Later, the plasmonic material will interact with EG molecules in solution, this can cause changes in the spectrum of absorbed light so that it can be used to detect the concentration of EG solution.

Until now, AuNPs have been commonly used in various applications because they have unique properties. The plasmonic effect of AuNPs allows optical properties to be tailored based on their size and shape, resulting in better light absorption [6]. Unfortunately, in the fabrication of AuNPs, many studies have been implementing conventional chemical methods where hazardous chemicals cannot be avoided [7]. Hence, there is an urgent need to employ cleaner and more environmentally friendly approach to synthesize AuNPs. Herein, Nd:YAG laser ablation in liquid is introduced to fabricate AuNPs without the need for additional chemicals in the sense that they do not produce hazardous waste [8], [9]. Therefore, the objective of this study is to develop an EG solution sensor using AuNPs synthesized using Nd:YAG laser technology. UV-Vis spectroscopic analysis was conducted to analyze optical properties of the synthesized AuNPs as well as their interaction with different concentrations of EG solutions.

2. MATERIALS AND METHODS

2.1. Materials

The main materials used in this study were 1 g of pure gold plate (99.999%), ethylene glycol (EG) and deionized water (DIW). The materials used for the synthesis of gold nanoparticles (AuNPs) only required the pure gold plate and DIW. Meanwhile, EG was used for sensing purposes.

2.2. Synthesis of AuNPs

This study began with the synthesis of AuNPs using the Nd:YAG laser ablation in liquid method. Pure gold plate was initially sonicated for 10 minutes to remove contaminations, especially from dust or dirt. The sonicated gold was then placed in a glass beaker containing 20 mL of DIW. Next, the Nd:YAG laser was set at a wavelength of 1064 nm with laser energy variations of 200 mJ, 250 mJ, 300 mJ, 350 mJ, and 400 mJ. Other controlled synthesis parameters were repetition rate of 4 Hz, laser beam diameter of 3 mm, and ablation time of 20 minutes. The sonication was always done prior to lasing process at each Nd:YAG laser energy. The synthesis of AuNPs using Nd:YAG laser is illustrated in Figure 1.
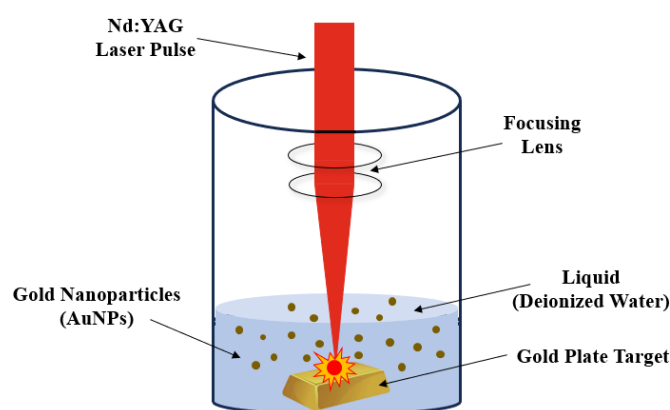
Figure 1. Ilustration of AuNPs synthesis using Nd:YAG laser

2.3. Characterization and Optimization of Synthesized AuNPs

The characterization was conducted using UV-Vis spectroscopy (Analytik Jena, Specord 200 Plus). This characterization aimed to analyze the plasmonic properties of AuNPs at each variation of laser energy. For UV-Vis test, the produced AuNPs colloidal solutions were diluted in DIW with volume ratio of 1:1 to prepare samples in such a way that its absorbance is detectable by the UV-Vis spectrometer. Next, the optimized sample was selected based on the highest absorption intensity, indicating the optimum plasmonic properties of AuNPs.

2.4. EG Sensing Evaluation

The optimized AuNPs were then mixed with EG, in which the EG concentrations in AuNPs nanocolloidal solution varied at 0%, 10%, 20%, 30%, 40%, 50%, 60%, 70%, 80%, and 90%. The plasmonic behaviours of AuNPs-EG solutions were recorded by means of UV-Vis. The EG sensing sensitivity by AuNPs was calculated by taking the linear regression of absorption-EG concentration and wavelength-EG concentration graphs.

3. RESULTS AND DISCUSSION

3.1. Effect of Nd:YAG Laser Energy

UV-Vis characterization was done to observe the plasmonic properties of AUNPs samples, where different in pulsed Nd:YAG laser energies, as depicted in Figure 2. The analysis results showed that the LSPR peaks occurred at wavelengths of 542 nm, 534 nm, 529 nm, 537 nm, and 537 nm respectively for samples with laser energies of 200 mJ, 250 mJ, 300 mJ, 350 mJ, and 400 mJ. The corresponding absorbance peaks of the respective samples were 0.2739, 0.3689, 0.5467, 0.3341, and 0.3067 (a.u.).

As seen in Figure 2a, the synthesized AuNPs using laser energy of 300 mJ showed the best plasmonic behaviour. This was indicated by the LSPR peak at the lowest wavelength, i.e. 529 nm, and highest LSPR peak, i.e. 0.55. The

LSPR wavelength could be related with the size and optical properties of the nanoparticles. A shift to shorter wavelengths (blueshift) tended to indicate a smaller nanoparticle size [10]. In addition, AuNPs synthesized with 300 mJ laser energy exhibited the highest absorbance peak (see Figure 2b). A higher absorbance peak indicated that the nanoparticles absorb more light, which might be affected by the concentration, size, shape, or distribution of particles in the sample [11]. Therefore, the synthesized AuNPs with 300 mJ laser was selected as the EG sensor.
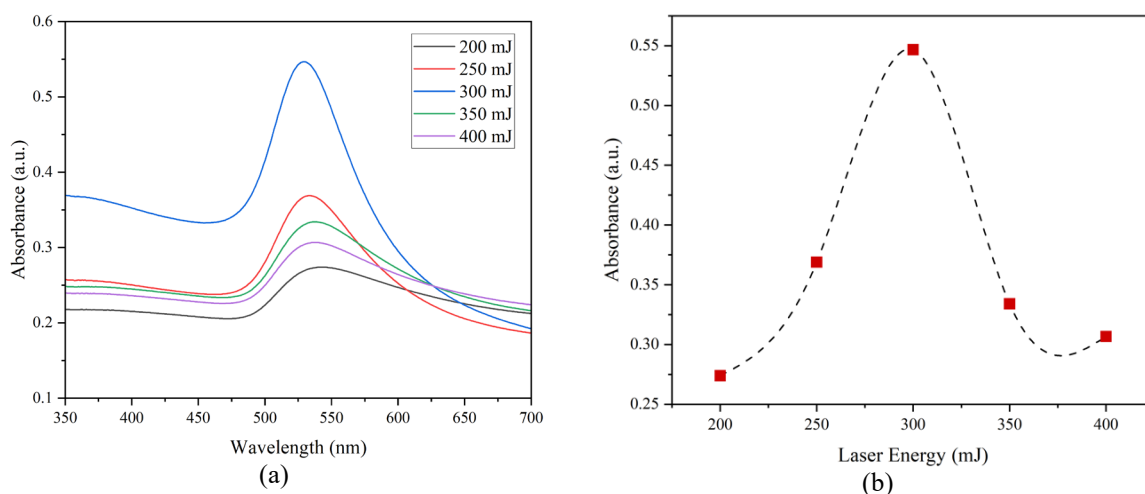
Figure 2. (a) UV-Vis spectra and (b) optimization of AuNPs produced at different Nd:YAG laser energies

3.2. EG Sensing Evaluation

Figure 3(a) shows the color difference of AuNPs solution with various concentrations of EG. The color of the solution gradually fades as the amount of EG added to the AuNPs solution increases. Based on the UV-Vis spectral analysis, Figure 3(b), it can be seen that the peak absorbance decreased with increasing EG concentration. In addition, there was also a wavelength shift that tended to be linear. The decrease in absorbance might be due to the decrease in nanoparticles concentration, or the higher the concentration of EG. This led to less numbers of AuNPs formed, which in turns decreased the absorbance of UV-Vis spectra. Meanwhile, the wavelength shift could be caused by the size of the nanoparticles [13].
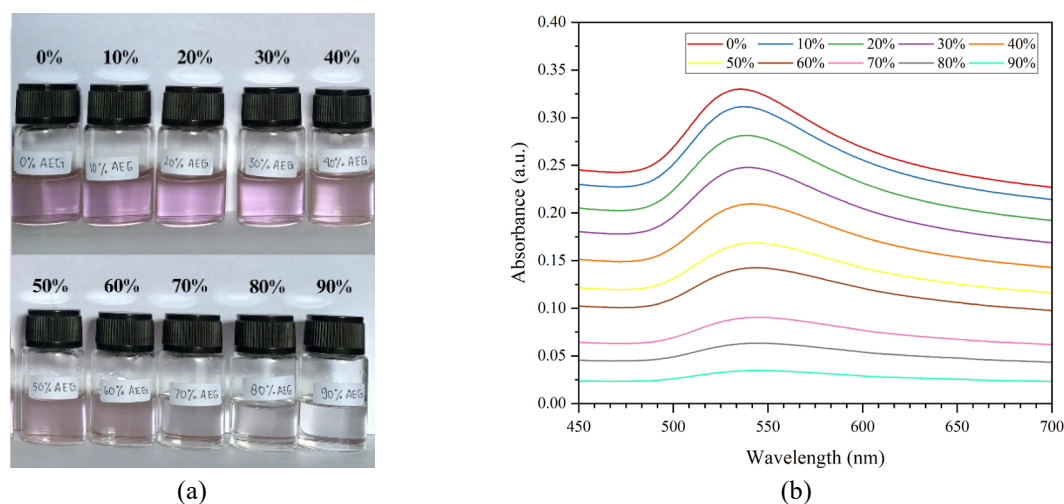
Figure 3. (a) AuNPs containing EG with various concentrations and (b) their UV-Vis spectra

Figure 4 shows the fitting results in this study, which clearly indicated a decrease in relative absorbance and a wavelength shift as the EG concentration increases. The relative absorbance change can be represented by the linear equation $y = -0.010x \pm 0.0003$ with $R^2 = 0.99$ while the wavelength shift is represented by the equation $y = 0.104x \pm 0.0090$ with $R^2 = 0.95$. Based on UV-Vis analysis, the sensitivity of AuNPs mixed with EG, when viewed from the absorbance peak, was 0.010 a.u./%EG, or when viewed from the wavelength shift was 0.104 nm/%EG. For both amplitude- and apectral-modalities, the detection range was from 0% to 90% of EG solutions. These results indicated that AuNPs had potential as an optical sensor that is sensitive to environmental changes, especially in detecting variations in EG concentraFtion or changes in refractive index in solution.
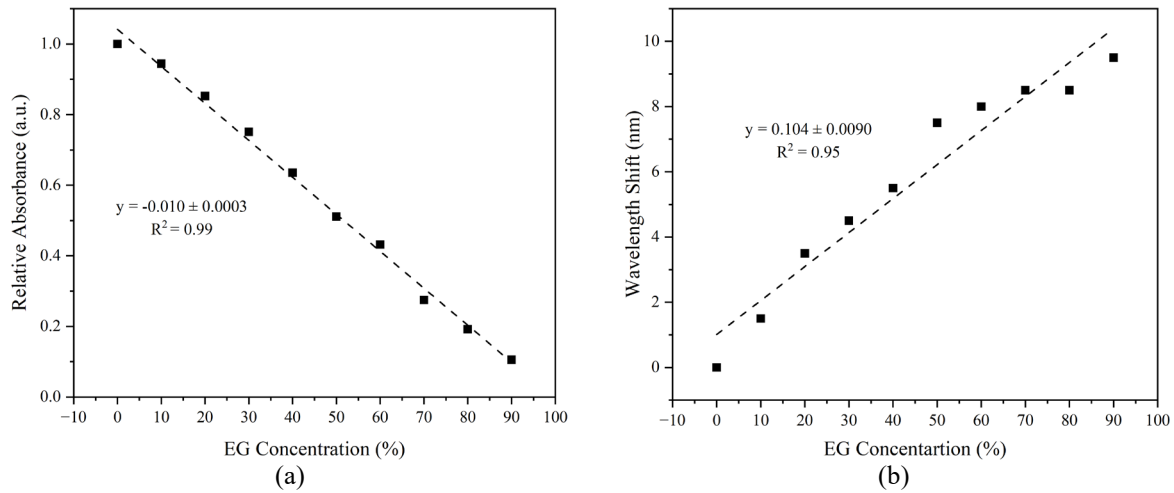
Figure 4. Linear fittings for sensitivity analyses based on (a) amplitude-modality and (b) spectral-modality of EG sensors using plasmonic AuNPs

3.3. Possible EG Sensing Mechanisms Using Plasmonic AuNPs

AuNPs have strong LSPR properties, in which the collective oscillation of electrons on the nanoparticle surface resonates with light at a specific wavelength. Based on the optimization data (Figure 2a), it can be seen that the LSPR on the optimized AuNPs (laser energy of 300 mJ) occured at a wavelength of 529 nm. After mixing with EG, the wavelength was shifted to 538 nm, see Figure 3(right). The position of the LSPR peak depends on various factors, such as the size, shape of the nanoparticles, and refractive index of the surrounding medium [14], [15].

The possible sensing mechanisms of the LSPR-based sensor using AuNPs to detect EG solution could be based on amplitude-modality, spectral-modality, or dual-modalities (see Figure 5). In AuNPs solutions containing EG, incoming light triggers collective oscillations of free electrons on the AuNPs surface. This interaction is strongly influenced by the refractive index of the solution around the AuNPs, where more concentrated EG has a higher refractive index. Consequently, an increase in the concentration of EG in solution causes a change in the LSPR effect and results in a measurable LSPR wavelength shift. As the concentration of EG in the solution increases, there is a shift of the LSPR peaks or changes in absorbance peaks. In this study, dual-response, where both amplitude and wavelength of UV-Vis spectra were simultaneously observed.
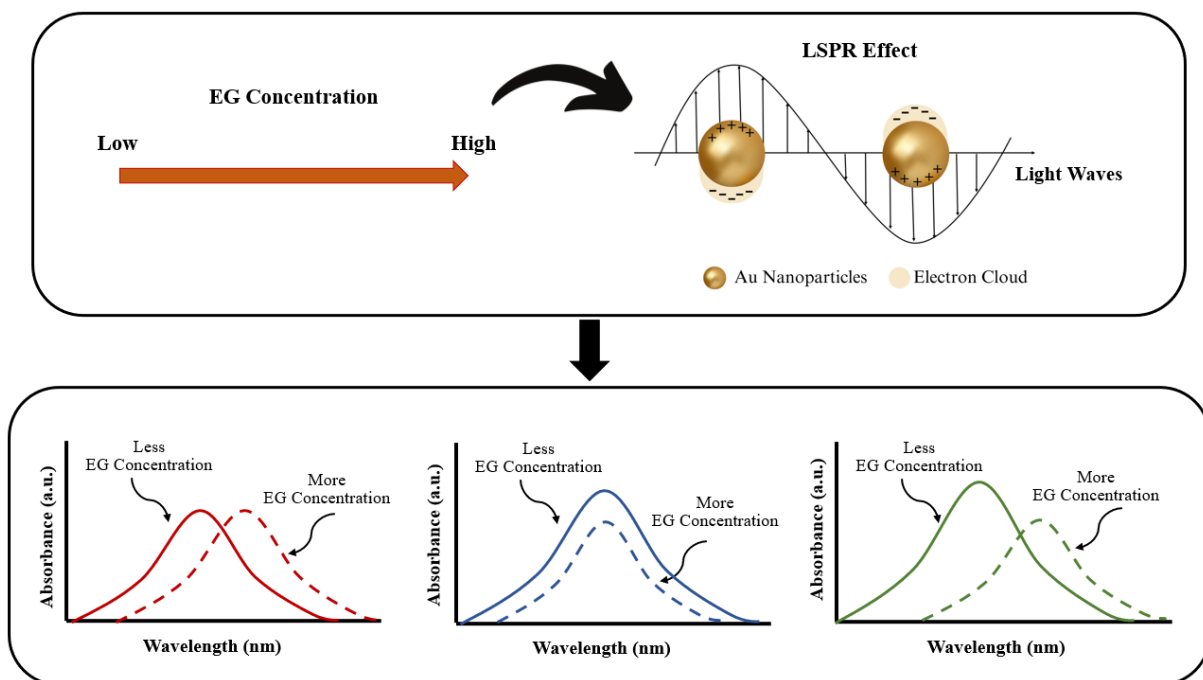
Figure 5. Possible mechanisms for sensing EG solution using LSPR-based of AuNPs

4. CONCLUSION

This paper presented the potential of AuNPs for EG sensing applications. The AuNPs were produced using Nd:YAG pulsed laser ablation in water where the AuNPs was optimized at laser energy of 300 mJ. The optimized AuNPs exhibited highest LSPR peak at 529 nm. Based on the UV-Vis test results, the interaction of AuNPs with EG at various concentrations showed changes both in the absorbance peak and wavelength shift. The increase of EG concentraions in the AuNPs samples yielded to linearly decrease the absorbance peak, and at the same time, shifted the LSPR wavelengths to higher values. The sensitivities of the LSPR-based sensor to detect EG solution were 0.010 a.u./%EG (based on amplitude-modality) and 0.104 nm/%EG (based on spectral-modality).

Acknowledgments

References

[1]   V. Rostovtseva, I. Faykov, and A. Pulyalina, "A review of recent developments of pervaporation membranes for ethylene glycol purification," *Membranes*, vol. 12, no. 3, art. no. 312, Mar. 2022, doi: 10.3390/membranes12030312.

[2]   J. S. Wei, S. Y. Ma, Y. H. Cai, C. Y. Xu, J. M. Liu, and H. T. Jiang, "A high-performance ethylene glycol sensor based on fibrous $ErFeO_3$ prepared by electrostatic spinning," *Ceramics International*, vol. 49, no. 20, pp. 32611–32618, Oct. 2023, doi: 10.1016/j.ceramint.2023.07.228.

[3]   S. Liu, G. Zhang, W. Zhang, N. Tian, Q. Sun, and Z. Wu, "High-performance ethylene glycol sensor based on imine covalent organic frameworks," *Nanomaterials*, vol. 13, no. 24, art. no. 3103, Dec. 2023, doi: 10.3390/nano13243103.

[4]   J. Ding, H. Dai, H. Chen, Y. Jin, H. Fu, and B. Xiao, "Highly sensitive ethylene glycol gas sensor based on ZnO/rGO nanosheets," *Sensors and Actuators B: Chemical*, vol. 372, art. no. 132655, Dec. 2022, doi: 10.1016/j.snb.2022.132655.

[5]   W. Wan, Y. Li, X. Ren, Y. Zhao, F. Gao, and H. Zhao, "2D SnO_2 Nanosheets: Synthesis, characterization, structures, and excellent sensing performance to ethylene glycol," *Nanomaterials*, vol. 8, no. 2, art. no. 112, Feb. 2018, doi: 10.3390/nano8020112.

[6]   X. Hu, Y. Zhang, T. Ding, J. Liu, and H. Zhao, "Multifunctional Gold Nanoparticles: A novel nanomaterial for various medical applications and biological activities," *Front. Bioeng. Biotechnol.*, vol. 8, art. no. 990, Aug. 2020, doi: 10.3389/fbioe.2020.00990.

[7]   P. B. Santhosh, J. Genova, and H. Chamati, "Green synthesis of gold nanoparticles: an eco-friendly approach," *Chemistry*, vol. 4, no. 2, pp. 345–369, Apr. 2022, doi: 10.3390/chemistry4020026.

[8]   I. Y. Khairani, G. Mínguez-Vega, C. Doñate-Buendía, and B. Gökce, "Green nanoparticle synthesis at scale: a perspective on overcoming the limits of pulsed laser ablation in liquids for high-throughput production," *Phys. Chem. Chem. Phys.*, vol. 25, no. 29, pp. 19380–19408, 2023, doi: 10.1039/D3CP01214J.

[9]   N. Fouad, A. Mahmoud, F. Abdel Samad, Y. Abd El-Salam, M. Ashour, R. Apsari, and T. Mohamed, "Utilizing the 2nd harmonic Nd: YAG laser ablation in liquid for the production of copper oxide quantum dots: Influence of laser fluence and ablation duration," *Physica B: Condensed Matter*, vol. 694, art. no. 416453, Dec. 2024, doi: 10.1016/j.physb.2024.416453.

[10]   R. B. P. Rivera *et al.*, "Influence of the Gold Nanoparticle Size on the Colorimetric Detection of Histamine," *ACS Omega*, vol. 9, no. 31, pp. 33652–33661, Aug. 2024, doi: 10.1021/acsomega.4c02023.

[11]   S. Lavanya, G. Paramasivam, and G. Maragathavalli, "Comparison of Optical and Morphological Analysis of Chemically Synthesized Silver Nanoparticles using Nucleation and Growth method," in *2022 14th International Conference on Mathematics, Actuarial Science, Computer Science and Statistics (MACS)*, Karachi, Pakistan, Nov. 2022, pp. 1–5. doi: 10.1109/MACS56771.2022.10023299.

[12]   G. Liu, H. Mu, F. Zhang, Y. Zeng, X. Bao, Z. Nie, and Q. Bao, "Nonlinear optics and photonics applications of two-dimensional materials," in *Fundamentals and Applications of Nonlinear Nanophotonics*, N. C. Panoiu, Eds.: Elsevier, 2024, pp. 393–440. doi: 10.1016/B978-0-323-90614-2.00007-9.

[13]   A. R. Shafiqa, A. Abdul Aziz, and B. Mehrdel, "Nanoparticle optical properties: Size dependence of a single gold spherical nanoparticle," *J. Phys.: Conf. Ser.*, vol. 1083, art. no. 012040, Aug. 2018, doi: 10.1088/1742-6596/1083/1/012040.

[14]   W.-S. Chang, J. W. Ha, L. S. Slaughter, and S. Link, "Plasmonic nanorod absorbers as orientation sensors," *Proc. Natl. Acad. Sci. U.S.A.*, vol. 107, no. 7, pp. 2781–2786, Feb. 2010, doi: 10.1073/pnas.0910127107.

Tuning the plasmonic properties of gold nanoparticles via Nd:YAG laser ablation in liquid for ethylene glycol sensing application

ICMUSTED 2024

[15]   Y. A. Hong and J. W. Ha, "Enhanced refractive index sensitivity of localized surface plasmon resonance inflection points in single hollow gold nanospheres with inner cavity," *Sci Rep*, vol. 12, no. 1, art. no. 6983, Apr. 2022, doi: 10.1038/s41598-022-11197-6.

An Interior-Point Methods for Linear Complementarity Problem Based on a New Hyperbolic Kernel Function

Youssra Bouhenache[1], Wided Chikouchee[1]

[1]Mathematics, Mouhamed Seddik Ben Yahia, Jijel, Algeria
Corresponding author: Youssra Bouhenache (e-mail: youssrabouhenache1997@gmail.com)

Abstract

Kernel functions play an important role in the amelioration of the computational complexity of interior-point algorithms for solving optimization problems. In this work, we present a primal-dual interior-point method for linear complementarity problem based on a kernel function with a hyperbolic parametric barrier term. By using several new technical lemmas, we derive the currently best-known iteration bounds for large-update methods, namely, $O\left(\sqrt{n}\log(n)\log\left(\dfrac{n}{\varepsilon}\right)\right)\cdot$ Finally, some numerical results are provided to show the practical behavior of the new proposed kernel function.

Keywords: Linear complementarity problems, Kernel function, Interior point methods

Investigation of Structural, Electronic, Magnetic, and Elastic Characteristics of New KTaSn Half-Heusler Compound for Spintronic Devices

Sabir Makhlouf[1], Malika Labidi[1], Abdelaziz Amara[1]

[1]Laboratory of LEREC, Department of Physics, Faculty of Sciences, Badji Mokhtar - Annaba University 12, 23000 Annaba, Algeria
Corresponding author: Sabir Makhlouf (e-mail: sabir.makhlouf@univ-annaba.dz)

Abstract

In this study, the density functional theory (DFT) was employed to study the structural, electronic, magnetic and elastic characteristics of the KTaSn half-Heusler compound. This HH identified as a half-metal compound. The calculations using GGA-mBJ approximation showed a direct band gap energy of 1.28 eV in spin-down states. We found higher density of states that leads to greater thermal power in the material as well as a large number of electronic states, this can enhance thermoelectric properties. The total magnetic moment is of 2 µB. The Ta atom makes a substantial contribution to the overall magnetic moments. The Elastic constants have indicated dynamic stability, anisotropic and ductile nature of the compound. The metallic character may be in the bonding of the compound. Our results indicate their application in spintronic devices.

Keywords: DFT, Half-metal, Magnetic, Elastic, Spintronic

Structural and Mechanical Properties of Zinc-Strontium-Lithium Phosphate Glass Doped with Carboxymethyl Cellulose

Siti Norfariza Farhana Binti Mohd Razak[1], Nur Hazwani Binti Mohd Yusoff[1], Nurhafizah Binti Hasim[1], Nur Hidayah Binti Ahmad[1], Norshahirah Binti Mohamad Saidi[1], Mohd Fuad Bin Mohamad[1]

[1]Advanced Optical Materials Research Group, Faculty of Science, Universiti Teknologi Malaysia, Johor, 81310 Skudai, Malaysia
Corresponding author: Nurhafizah Binti Hasim (e-mail: nurhafizah.h@utm.my)

Abstract

A series of phosphate glass doped with carboxymethyl cellulose (CMC) with the composition (40-x) P_2O_5-ZnO-Li_2O–SrO-xCH$_2$CO$_2$H where $(0.0 \leq x \leq 0.5 \text{ mol\%})$ was prepared by melt–quenching technique. The characterization of the glass which are structural, and mechanical properties are characterized by using Fourier transform infrared (FTIR) spectroscopy, Raman spectroscopy, ultrasonic testing and Vickers Hardness. The FTIR and Raman spectra of the phosphate glass were used to evaluate the effect of CMC on its structural properties. Both spectra indicated that the glass structure had been slightly changed by the addition of CMC. The mechanical properties of ultrasonic elastic properties were measured by using ultrasonic testing. From the values obtain from ultrasonic wave velocities, elastic properties were calculated and tabulated. The increase in polar bonding in the modifiers is responsible for the rise in ionicity of the glass. The results of the study showed that CMC addition improved the mechanical and structural properties of the glass system, suggesting that this is a workable method for enhancing glass performance.

Keywords: Phosphate glass, Carboxymethyl cellulose, FTIR, Raman spectra, Vickers hardness

Some Physical Properties of Sn95X5 (X = Zn, Cd, Sb, and Ag) Alloys Rapidly Solidified by Melt Spinning Technique

Teysir Alzamil[1]

[1]Physics Department, Aleppo University in the Liberated Areas, Azaz, Syria
Corresponding author: Teysir Alzamil (e-mail: ztrtmama@gmail.com)

Abstract

We prepared a group of binary metal alloys (Sn95X5, where: X=Zn, Cd, Sb, and Ag) using rapid solidification method, by single-roller melt spinning technique. We studied some of the structural, thermal, electrical and mechanical properties of these alloys, and the results showed, that the Sn95Zn5 alloy has the smallest melting temperature (474.8K) and the largest value of enthalpy change (62.8 kJ/kg) compared to the rest of the studied alloys. As for the Sn95Cd5 alloy, the results showed that it has the smallest value of density (7.02 g/cm3) and the smallest value of young's modulus of elasticity (18 GPa). The results also showed that the Sn95Ag5 alloy is characterized by the smallest electrical resistivity (12x10-8 Ohm.m) and the largest value of the young's modulus of elasticity (51 GPa) and the coefficient of internal friction (10.6x10-2) too, compared to the rest of the mixtures studied

Keywords: Alloy, Rapid solidification, Melt spinning, Physical properties

1. INTRODUCTION

Metals and metal alloys are crucial to most traditional and modern industries. Historically, they were prepared using traditional methods where the molten metal was allowed to cool in molds. This process evolved with the introduction of rapid solidification techniques, which provide different properties to the same alloy [1]. Various methods utilizing rapid solidification of the molten metal have been developed, one of which is the melt spinning technique. In this method, the molten metal is poured onto a rapidly rotating wheel made of copper or aluminium, where it absorbs the heat and solidifies in a very short time [2].

Studying the physical properties of rapidly solidified alloys which prepared by melt spinning technique is significant due to the potential applications of these alloys in various fields, including orthopedic implant materials. The rapid solidification process, as demonstrated in similar studies, leads to microstructural refinement and the formation of specific phases, which can significantly impact the mechanical properties of the alloys. Furthermore, the stabilization of the supercooled liquid, as discussed in [3] is a critical aspect that can be influenced by the cooling rates and chemical compositions of the alloys.

Tin is characterized by its unique properties and exists in three phases depending on the temperature. The most common phase is the beta phase, where tin appears as a shiny silver metal with a relatively low melting point, making it widely used in industries requiring relatively low temperatures. When mixed with other elements, it forms alloys with specific properties for various applications. For example, the tin-lead alloy is a key material in soldering electronic circuits [4].

Sn-based alloys exhibit unique characteristics and properties that make them suitable for various applications, especially within the context of rapidly solidified alloys. Research on Mg-Sn alloys has shown that the content of tin significantly influences the phase composition of the alloy. For instance, an increase in tin content leads to a greater presence of the Mg2Sn phase due to the substantial solubility limit of Sn in Mg. This indicates that the behaviour and composition of Sn-based alloys can be tailored by adjusting the tin content, offering potential for customized properties and performance [5].

Furthermore, the addition of tin to aluminium-silicon alloys has been found to have a significant impact on their microstructure and functional properties. Studies on Al-Si-Cu alloys have demonstrated the potential of tin as an alloying element, with a focus on understanding its influence on mechanical properties and the method of interaction with other additives in the alloy [6]. These findings underscore the importance of considering tin as a key factor in the development and customization of Sn-based alloys for specific applications.

Another's studies have been conducted on metal alloys based on tin examined the effect of rapid solidification on the structure and properties of Sn-Cd alloys, including their electrical and mechanical properties [7]. Dali et al. investigated the effect of creep on the Sn-Sb binary alloy [8]. Osorio et al. studied the mechanical properties of the Sn-Ag binary alloy [9]. While Kamal and Al-Ashram focused on the valence electron concentration of the same alloy [10]. The Sn-Zn binary alloy was also studied by Kamal and Al-Ashram for its valence electron concentration [11], and Garcia et al. examined its mechanical properties for use as a soldering alloy [12].

2. METHOD

We prepared the alloys using tin, zinc, antimony, cadmium, and silver, with a purity of 99.8% for each element. The elements were weighed using an electronic balance, then placed in a porcelain crucible and heated until completely melted, then they were left in the furnace for one hour at appropriate temperature. The molten metal was then poured onto an aluminium wheel rotating at 1345 RPM, forming metal strips of varying lengths. We studied the thermal properties using differential thermal analysis (DTA), the electrical properties were measured using a double bridge method, and determined the mechanical properties using kinetic response techniques.

3. RESULTS AND DISCUSSION

We measured the density of the alloys and calculated the unit cell volume for each alloy. Figure 1 shows the density variations for the studied alloys.it is clear from the figure that the smallest density value was for the tin-cadmium alloy, while the largest value was for the tin-silver alloy. Figure 2 illustrates the changes in unit cell volume for the studied alloys.it is appear that the smallest unit cell volume was for the tin-cadmium alloy, and the largest was for the tin-antimony alloy.
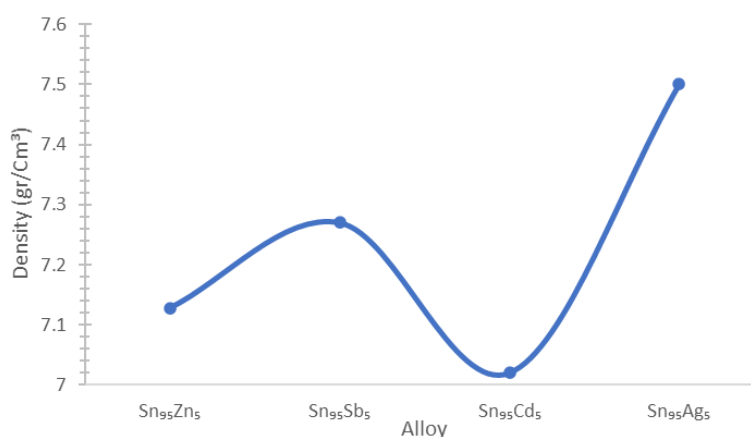
Figure 1. Density of the alloys
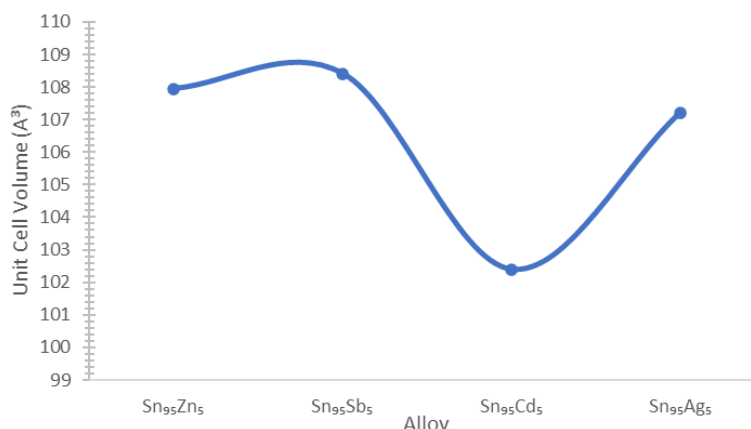
Figure 2. Unit cell volume of the alloys

Figure 3 displays the changes in electrical resistivity for the studied alloys. We note from the figure that the smallest value of the resistivity was for the tin-silver alloy, while the largest value was for the tin-antimony alloy. This is attributed to silver's higher electrical conductivity compared to the other elements in the alloys.
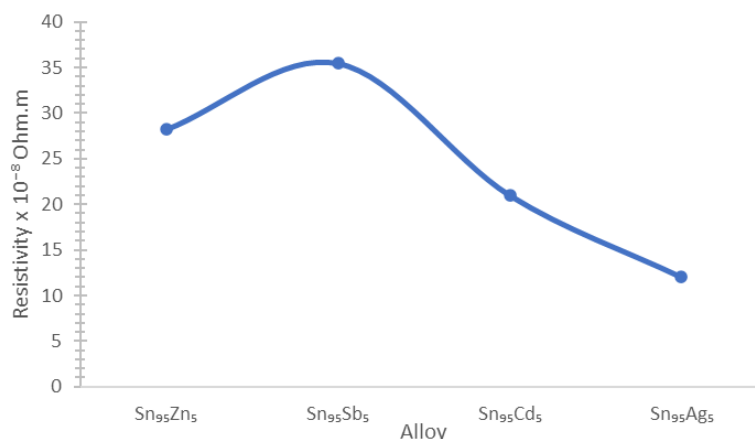
Figure 3. The resistivity of the alloys

Figure 4 shows the changes in melting temperature, Liquidus, and solidus of the studied alloys, according to the figure it's clear that the tin-zinc alloy exhibited the lowest liquidus temperature, the smallest melting range, while the tin-cadmium alloy has the smallest solidus temperature. This may be due to zinc atoms being smaller than other atoms, therefore, it is located within the tin crystal structure more effectively. Figure 5 shows the enthalpy difference for the alloys. We note that the tin-zinc alloy has the largest value, and the tin- silver alloys has the smallest value of the enthalpy difference.
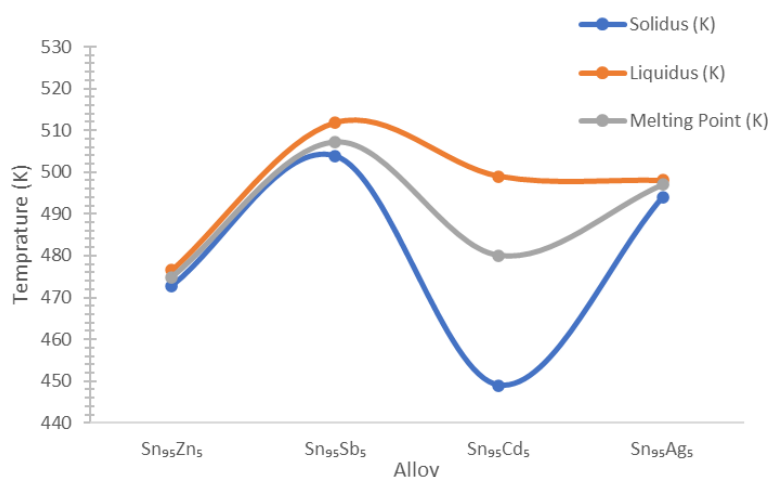
Figure 4. Solidus, liquids, and melting temperature of the alloys
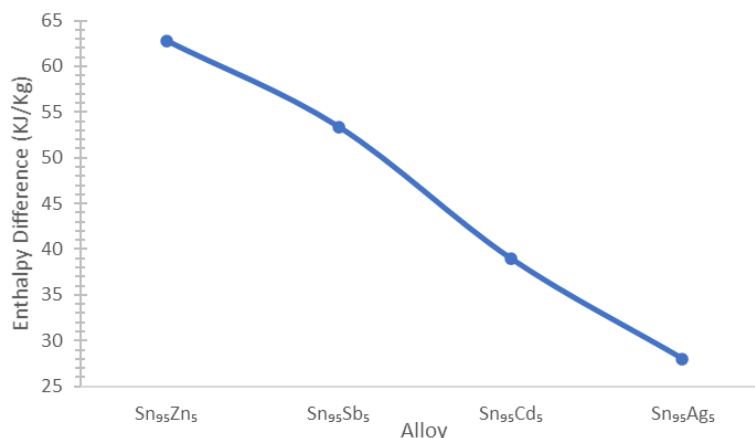
Figure 5. The enthalpy difference of the alloys

In the study of mechanical properties, Figures 6 shows the internal friction of the alloys, we observed that the tin-silver alloy had the highest values for the internal friction, while the smallest internal friction was found in the tin-

417

antimony alloy. Figure 7 illustrate young's modulus for the alloys, the smallest Young's modulus was in the tin-cadmium alloy, while the largest young's modulus was for the tin-silver alloy.
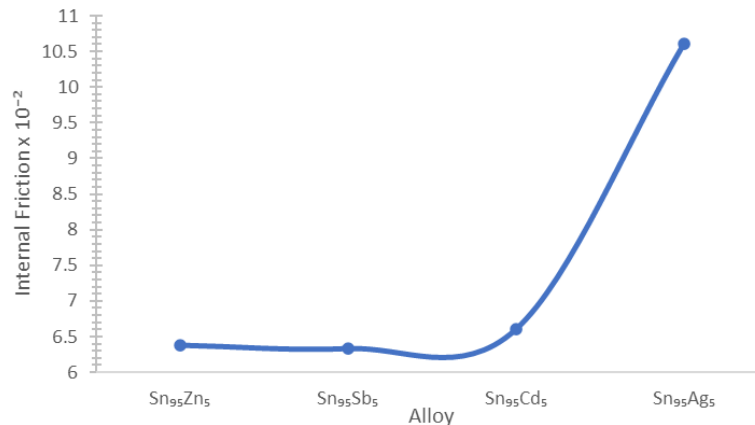
Figure 6. Internal friction of the alloys
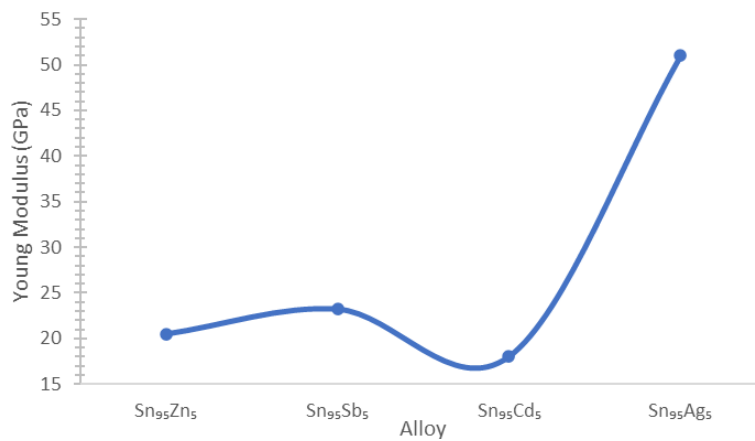
Figure 7. Young's modulus of the alloys

All the results of structural, thermal, electrical and mechanical properties are found in the Table 1.

Table 1. Structural, thermal, electrical, and mechanical properties

Alloy	$Sn_{95}Zn_5$	$Sn_{95}Sb_5$	$Sn_{95}Cd_5$	$Sn_{95}Ag_5$
Solidus (K)	472.8	503.9	449	494
Liquidus (K)	476.5	511.8	499	498
Melting Point (K)	474.8	507.3	480	497
Resistivity x 10^{-8} Ohm.m	28.217	35.492	21	12
Enthalpy Difference (KJ/Kg)	62.8	53.4	39	28
Unit Cell Volume (A^3)	107.946	108.409	102.4	107.2
Density (gr/Cm^3)	7.128	7.27	7.02	7.5
Internal Friction x 10^{-2}	6.381	6.334	6.6	10.6
Young Modulus (GPa)	20.472	23.219	18	51

4. CONCLUSION

In conclusion, the study on the physical properties of Sn5%X Alloys rapidly solidified by melt spinning technique has provided valuable insights into the behavior of these alloys. The results showed, that the Sn95Zn5 alloy has the smallest melting temperature (474.8K) and the largest value of enthalpy change (62.8 kJ/kg) compared to the rest of the studied alloys. As for the Sn95Cd5 alloy, the results showed that it has the smallest value of density (7.02 g/cm3) and the smallest value of young's modulus of elasticity (18 GPa). The results also showed that the Sn95Ag5 alloy is characterized by the smallest electrical resistivity (12x10-8 Ohm.m) and the largest value of the

young's modulus of elasticity (51 GPa) and the coefficient of internal friction (10.6x10-2) too, compared to the rest of the mixtures studied.

The findings underscore the significance of the melt spinning technique in producing rapidly solidified alloys with unique properties, and the research contributes to the field by shedding light on the physical properties of the alloys. Moreover, the suitable applications of these alloys, particularly in the context of their use in various industrial applications. Furthermore, the study's results will aid in advancing the design and development of Sn-based metallic alloys, thereby opening new avenues for further exploration and innovation in this domain.

References

[1] F. J. Hong and H. H. Qiu, "Experimental study on rapid solidification process using a novel ultrasound technique," *Experimental Thermal and Fluid Science*, vol. 30, pp. 17–26, 2005.

[2] M. Rajabi, A. Simchi, and P. Davami, "Microstructure and mechanical properties of Al–20Si–5Fe–2X (X = Cu, Ni, Cr) alloys produced by melt-spinning," *Materials Science and Engineering A*, vol. 492, pp. 443–449, 2008.

[3] K. Mlynarek-Zak, I. Dhiman, K. Matus, M. Kadziolka-Gawel, W. Lonski, A. Radon, T. Czeppe, and R. Babilas, "Structural characterization of newly-developed Al (79) Ni (5) Fe (5)Y(11) and Al (79) Ni (11) Fe (5)Y(5) alloys with amorphous matrixes," *Nature,Scientific Reports*, vol. 13, art. no. 21322, 2023.

[4] W. Yang, M. Liu, J. Feng, J. Wu, J. Mao, Z. Du, X. Ke, X. Zhang, and Y. Zhan, "Solid state phase equilibria of an Al–Sn–Y ternary system," *Materials*, vol. 12, no. 3, art. no. 444, 2019.

[5] R. Rajendran and S. Dondapati, "Insights of microstructural features and their effect on degradation and the in vitro bioactivity response of as-cast Mg-Sn alloys for orthopedic implant applications," *Materials*, vol. 15, no. 18, art. no. 6327, 2022.

[6] J. Kozana, M. Piekos, A. Garbacz-Klempka, and M. Perek-Nowak, "The effect of tin on microstructure and properties of the Al-10 wt.% Si alloy," *Materials*, vol. 15, no. 18, art. no. 6350, 2022.

[7] M. Kamal, A. B. El-Bediwi, and T. Al-Ashram, "The effect of rapid solidification on the structure, decomposition behavior, electrical and mechanical properties of the Sn–Cd binary alloys," *Journal of Materials Science: Materials in Electronics*, vol. 15, pp. 211–217, 2004.

[8] A. A. El-Daly, Y. Swilem, and A. E. Hammad, "Creep properties of Sn–Sb based lead-free solder alloys," *Journal of Alloys and Compounds*, vol. 47, pp. 98–104, 2009.

[9] W. R. Osorio, D. R. Leiva, L. C. Peixoto, L. R. Garcia, and A. Garcia, "Mechanical properties of Sn–Ag lead-free solder alloys based on the dendritic array and Ag3Sn morphology," *Journal of Alloys and Compounds*, vol. 562, pp. 194–204, 2013.

[10] M. Kamal, A. B. El-Bediwi, T. El-Ashram, and M. E. Dorgham, "The role of valence electron concentration on the structure and properties of rapidly solidified Sn-Ag binary alloys," *Materials Sciences and Applications*, vol. 3, pp. 179–184, 2012.

[11] M. Kamal, A. B. El-Bediwi, T. El-Ashram, and M. E. Dorgham, "Verification of hume-rothery condition of phase stability in rapidly solidified Sn-Zn binary alloys," *Journal of Ovonic Research*, vol:7, no. 4, pp. 73–82, 2011.

[12] L. R. Garcia, W. R. Osorio, L. C. Peixoto, and A. Garcia, "Mechanical properties of Sn–Zn lead-free solder alloys based on the microstructure array," *Materials Characterization*, vol. 61, pp. 212–220, 2010.

The Cauchy Problem of Ostrovsky Equation in Anisotropic Gevrey Spaces

Feriel Boudersa[1], Abdellaziz Mennouni[1]

[1]Department of Mathematics, University of Batna 2 Mostafa Ben Boulaid Fisdis, Batna, Algeria
Corresponding author: Feriel Boudersa (e-mail: ferielboudersa181095@gmail.com)

Abstract

We study the Cauchy problem of the Ostrovsky equation $\partial_t u - \beta \partial_x^3 u - \gamma \partial_x^{-1} u + u \partial_x u = 0$, with $\beta\gamma < 0$. By establishing a bilinear estimate on the anisotropic Bourgain space $X_{s,w,b}^{\delta_1,\delta_2,\sigma}$, we prove that the Cauchy problem of this equation is locally well-posed in the anisotropic Gevrey space $G_{s,w}^{\delta_1,\delta_2,\sigma}(R)$ for any $s > -5/8$ and some $\omega \in (0,1/2)$.

Keywords: Ostrovsky equation, Cauchy problem, Well-posedness, Bilinear estimate, Anisotropic Gevrey space

The Combined Effects of Concave-Convex Nonlinearities to a New Class of Fractional Kirchhoff-Schrodinger-Poisson Systems

Hamza Boutebba[1]

[1]Department of Mathematics, University of 20 August 1955, Skikda, Algeria
Corresponding author: Hamza Boutebba (e-mail: boutskiham@gmail.com)

Abstract

The main purpose of this work is to establish the existence of nontrivial solutions to a new class of fractional Kirchhoff-Schrodinger-Poisson systems involving the combined effects of nonlinearities. To achieve this result, we utilize variational methods based on the critical point mountain pass theorem under the Cerami condition.

Keywords: Kirchhoff-type systems, mountain pass theorem, Cerami condition, Variational methods

Theoretical Study of Legendre Polynomials and Block-Pulse Functions Operational Matrix Algorithm and Its Application to the Stochastic Equation

Sara Youcef Achira[1]

[1]Department of Sciences and Computer Science, University of Hassiba Benbouali, Chlef, Algeria
Corresponding author: Sara Youcef Achira (e-mail: youcefachirasara98@gmail.com)

Abstract

In this paper, we propose a numerical method based on Legendre polynomials and block-pulse functions operational matrix algorithm to find numerical solutions for stochastic equation. First, we defined block-pulse functions and hybrid functions of Legendre polynomials that we gave the relation between Legendre polynomails and block pulse functions (Operational matrix). Then this operator, the ordinary operational matrix, is used to transform the solution of stochastic equations into the solution of algebraic equations of a system

Keywords: Stochastic equations, Fractional Brownian motion, Operational matrix method, Legendre polynomails

Schrodinger Equation Approximate Eigensolutions for the Generalized Cornell Plus Inverse Trigonometric Scarf-Type Potential

Amal Ladjeroud[1,2], Badredine Boudjedaa[1,3]

[1]Department of Mathematics and Computer Sciences, University Center Abdelhafid Boussouf, Mila, Algeria
[2]Laboratory of Applied Mathematics and Didactics, ENS Assia Djabar, Constantine, Algeria
[3]Laboratory of Natural Sciences and Materials, University Center Abdelhafid Boussouf, Mila, Algeria
Corresponding author: Amal Ladjeroud (e-mail: a.ladjeroud@centre-univ-mila.dz)

Abstract

Approximate eigensolutions of Schrodinger equation are found, for the radial generalized Cornell plus inverse trigonometric scarf-type potential, in the framework of quasi-exactly solvable problems. It is shown that by using an appropriate approximation scheme, the radial equation can be put in the biconfluent Heun's equation form, where the approximate eigensolutions and the corresponding energy eigenvalues are obtained in closed form.

Keywords: Schrodinger equation, Approximate eigensolutions, The radial generalized Cornell potential, Inverse trigonometric scarf-type potential, Biconfluent Heun's equation

On the p-Variation and Lax-Friedrichs Scheme

Aimen Daoudi[1], Stéphane Junca[2]

[1]Côte d'Azur University, Nice, France
[2]Kasdi Merbah Ouargla University, Algeria
Corresponding author: Aimen Daoudi (e-mail: aimen.daoudi@univ-cotedazur.fr)

Abstract

This work focuses on the efficient computation of p-variation. For $p > 1$, this semi-norm is associated with fractional regularity $s = \dfrac{1}{p} < 1$ and the fractional BV space BV^s. It is well-known in probability theory and has recently gained significance in the context of hyperbolic partial differential equations. The primary motivation of this paper is to calculate p-variation efficiently for numerical schemes of hyperbolic conservation laws. The p-variation is a nonlocal semi-norm. Initially, based on its definition, the cost of computing the p-variation for a piecewise constant function with N data points appears to be exponential with respect to N. However, we introduce new algorithms featuring polynomial costs, building on the recent one provided by Vygantas Butkus and Rimas Norvaiša. Then we apply one of these algorithms using the Lax-Friedrichs scheme with hyperbolic conservation laws, where we observe the variation of p-variation.

Keywords: p-variation, Fractional BV spaces, Conservation laws, Lax-Friedrichs scheme

Global Asymptotic Stability of Nonlinear Difference Equations Using Semi-Cycle Analysis

Seyma Yesilusta[1]

[1]Department of Mathematics, Zonguldak Bulent Ecevit University, Zonguldak, Türkiye
Corresponding author: Seyma Yesilusta (e-mail: seymayesilusta@gmail.com)

Abstract

One of the fundamental structures of applied mathematics is the difference equations used to understand the behavior of models defined in discrete time periods, to reveal their properties and to analyze them. Difference equations are also used to build real-life mathematical models. Difference equations help to understand many areas from biology to medicine, from economics to physics. In other words, they are a part of discrete mathematics that describes changes in small time periods. Difference equations are known as the first theory to emerge with the systematical development of mathematics. Having emerged as the discrete analogues of differential equations, difference equations are a field of mathematics with a rich application area. Difference equations found in economy, biology, signal processing, computer engineering, genetics, medicine, ecology and digital control some of its application fields.

In this study, we provide a comprehensive review of global asymptotic stability in second-order rational difference equations. We will explore theoretical foundations, computational methods, and practical applications across diverse fields. By synthesizing insights from existing literature and recent advancements, we aim to offer a thorough overview of state-of-the-art techniques and approaches in this area. The aim of this study is to equip researchers and practitioners with a comprehensive understanding of the tools available for analyzing the stability of second-order rational difference equations, as well as to encourage further exploration and development of new methods. This review serves as both a reference and a guide for those interested in the mathematical modeling and analysis of dynamic systems exhibiting complex stability behavior. In this context, the following rational difference equation is investigated: $x_{n+1} = \dfrac{x_n x_{n-1} + a}{x_n + x_{n-1}}$ and $n = 0,1,2,\dots$. Here $a \in [0,\infty)$ and initial values $x_{-1}, x_0 \in (0,\infty)$, and the asymptotic stability of the solutions to this equation is also investigated.

Keywords: Global asymptotic stability, Semi-cycle, Equilibrium point, Solution, Difference equations

Analysis Study of the Polymeric Materials Weldability by Friction Stir Welding Process

El Bahri Ould Chikh[1], Abdelnour Zaim[2], Laid Aminallah[2]

[1]Department of Mechanics, Mascara University, Mascara, Algeria
[2]Department of Mechanics, Relizane University, Relizane, Algeria
Corresponding author: El Bahri Ould Chikh (e-mail: b.ouldchikh@univ-mascara.dz)

Abstract

Friction stir welding is a solid-state joining process which was first used for welding of aluminum and its alloys and is now employed for welding of other materials such as polymers and composites. The welding parameters play a major role in the determination of the weld quality. In this study, the aim was to examine the weldability of a high density polyethylene (HDPE) using the technique of friction stir welding FSW and effect of process parameters on mechanical properties of welded plates. A choice parametric was carried out to optimize the operating parameters such as rotational speed, advance speed and the tool geometry. Monotonic tensile tests were used to evaluate the quality of the joint and compare the mechanical properties between HDPE specimen and a test specimen of a welded by FSW. It appears from this study that the FSW introduces a fragility of joints characterized by a significant decrease in fracture strain. The weldablity is significantly affected by the rotation speed and the advance speed of the tool.

Keywords: Welding, FSW, Behavior low, Tensile tests, Polymer

Impact of Ground Motion Selection Strategies on the Seismic Response of Reinforced Concrete Structure

Abdelhamid Abdelmalek[1,2], Bouderba Bachir[2], Benahmed Baizid[1]

[1]Development Laboratory in Mechanics and Materials, University of Djelfa, Djelfa, Algeria
[2]Mechanical Engineering Materials and Structures Laboratory, Department of Civil, Mechanical and Transportation Engineering, Tissemsilt University, Tissemsilt, Algeria
Corresponding author: Abdelhamid Abdelmalek (e-mail: abdelmalek.abdelhamid@univ-djelfa.dz)

Abstract

This study investigates the impact of seismic record selection strategies on the time-history response of reinforced concrete (RC) structures. Five real earthquake records were selected from the NGA-West2 strong ground motion database provided by the Pacific Earthquake Engineering Research Center (PEER). The analysed structure is a five-story reinforced concrete building founded on S3-class soil (soft soil with 200 m/s < Vs30 ≤ 400 m/s) according to the Algerian Earthquake Regulation. The selected records have moment magnitudes (Mw) ranging between 5.5 and 7.5. The *SeismSelect* and *SeismMatch* software tools were employed for seismic record selection and scaling. Adjusted accelerograms obtained through these techniques were used for dynamic time-history analyses. Two matching techniques were applied: the PGA-based scaling method and the spectrum-matching method. Results, in terms of displacements and internal forces, were compared to those obtained using the modal spectral method. The PGA-based method produced maximum displacements and internal forces that exceeded the spectral method's results by 20%. Conversely, the spectrum-matching method showed maximum values that were 19% lower than the spectral method's results.

Keywords: Record selection, Scaling, Target spectrum, Time-history response, Reinforced concrete structure

Hybrid and Floating Photovoltaic Systems: Insights into Efficiency, Challenges, and Future Potential

Zulkifli Mohd Yusop[1], Siti Atirah Ibrahim[1], Muhamad Zalani Daud[1], Mohd Afifi Jusoh[1]

[1]Faculty of Ocean Engineering Technology, Universiti Malaysia Terengganu, 21030 Kuala Nerus, Terengganu, Malaysia
Corresponding author: Zulkifli Mohd Yusop (e-mail: zulkifli.yusop@umt.edu.my)

Abstract

The increasing global demand for renewable energy and the challenges posed by traditional photovoltaic systems have driven the development of floating photovoltaic (FPV) technologies. This paper presents a comprehensive review of FPV systems, examining their efficiency, environmental impacts, and technological advancements. FPV systems offer significant advantages over on-ground photovoltaic (OPV) systems, including enhanced efficiency through water cooling, reduced land use, and mitigation of water evaporation. The integration of hybrid FPV (HFPV) systems with other renewable energy sources, such as hydropower and wind, further enhances their potential by addressing the intermittent nature of solar energy and optimizing resource utilization. Key findings highlight the comparative performance of FPV and OPV systems, the environmental considerations unique to water-based installations, and the technical innovations in system components like floating platforms and anchoring systems. Despite higher initial costs, FPV systems demonstrate long-term financial and environmental benefits, making them a viable solution for sustainable energy generation. This study underscores the necessity of continued research to overcome challenges such as durability in harsh environments and potential ecological impacts.

Keywords: Floating photovoltaic system, Renewable energy technologies, System control and optimization, Embedded system

Breast Cancer Detection Using a Hexagonal Slotted Microstrip Patch Antenna with an Electromagnetic Signal

Souheyla Ferouani[1], Bouchra Moulfi[1], Fatima Zahra Moussa[1], Safaa Moulfi[1]

[1]Electronic and Telecom Department, University of Ain Temouchent, Ain Temouchent, Algeria
Corresponding author: Souheyla Ferouani (e-mail: souhilaferouani@gmail.com)

Abstract

Breast cancer detection using microwaves is a promising method that can complement traditional screening techniques. By offering a non-invasive approach that is potentially more comfortable and less expensive, it has the potential to improve early detection rates and increase the chances of successful treatment. However, further research and development are required to overcome technical challenges and validate the clinical effectiveness of this technology. This article aims to design and implement a hexagonal slotted patch antenna with dimensions of $37.6 \times 38 \times 1.5$ mm^3 for breast tumor detection, utilizing electromagnetic wave radiation to differentiate between healthy and cancerous tissues. The proposed antenna is optimized to operate in the microwave range at a frequency of 2.45 GHz, within the ISM band for medical applications. This non-invasive and potentially low-cost technique enables early tumor detection through microwave imaging or analysis of the reflected signal. The main challenges include achieving precise calibration and sufficient resolution to identify small tumors. This technology holds promise for enhancing breast cancer screening as a complement to traditional methods. The results obtained with the proposed antenna, including the reflection coefficient, H-field, E-field, and surface current, demonstrate that it is well-suited for such medical applications.

Keywords: Hexagonal patch antenna, Breast cancer, Screening, Radiation, Microwave imaging

A Frequency-Reconfigurable Pentagonal Microstrip Antenna Array

Khouloud Mohammed Belhadj[1], Souheyla Ferouani[2], Djalal Ziani Kerarti[3]

[1]Smart Structure Laboratory SSL of Temouchent, Department of Electronic and Telecommunications, University of Ain Temouchent, Belhadj Bouchaib, Ain Temouchent, Algeria
[2]LTT Laboratory of Tlemcen, Department of Electronic and Telecommunications, University of Ain Temouchent, Belhadj Bouchaib, Ain Temouchent, Algeria
[3]Department of Post Graduated and Specialties, LARATIC Laboratory at National Institute of Telecommunications and ICT of Oran, Oran, Algeria
Corresponding author: Khouloud Mohammed Belhadj (e-mail: khouloud.mohammedbelhadj@univ-temouchent.edu.dz)

Abstract

Reconfigurable antennas are essential and indispensable components in modern wireless communication systems. Thanks to their operational degrees of freedom, such as frequency agility, steerable radiation patterns, and polarization diversity, they offer enhanced performance. Intelligent micro-strip antenna arrays are also widely used in telecommunication systems, as they enable numerous functionalities that cannot be achieved with a single element. In this work, we propose to simulate a frequency-agile two-element pentagonal patch antenna array using eight PIN diodes and five modes of operation, with the CST simulation software. Integrating these eight PIN diodes into the patch results in the following frequencies: 2.21 and 5.35 GHz in M1 mode; 2.22, 4.01, 4.94, and 5.335 GHz in M2 mode; 2.13 and 5.31 GHz in M3 mode; 3.555 and 5.255 GHz in M4 mode; and 3.285 and 5.28 GHz in M5 mode. This design is suitable for various applications, such as S-band, radar, Wi-Fi 5, Wi-Fi 6, C-band, 3G-UMTS, 5G, and WiMAX. The simulation results are very satisfactory in terms of S11 parameters, gain, and bandwidth for all applications.

Keywords: Reconfigurable antennas, CST, Micro-strip antenna array, S11, C-band

Elliptical Pin Fin Heat Sink: Passive Cooling Control

Fatima Zohra Bakhti[1], Mohamed Si-Ameur[2]

[1]Mechanical Engineering Department, Faculty of Technology, University Med Boudiaf, 28000 M'sila, Algeria
[2]Mechanical Engineering Department, Faculty of Technology, University of Batna 2, 05000 Batna, Algeria
Corresponding author: Fatima Zohra Bakhti (fatimazohra.bakhti@univ-msila.dz)

Abstract

The aim of this study is to examine by means of three-dimensional numerical simulations the thermal-fluid features in elliptical pin fin heat sink. The passive heat transfer enhancement technique is used to comprehend and control the cooling process. This passive methodology is based on pin fins arrangement, hydrodynamic and geometrical parameters. The present numerical results are confronted with experimental measurements in open literature which used one-dimensional model to explore the thermal field. A good agreement was found especially around the optimal fins dimensions. A parametric study has been carried out to deeply analyse the three-dimensional thermal-fluid fields of the heat sink for various key parameters range such the Reynolds number (Re = 50–250) and the aspect ratio (γ = H/d = 5.1–9.18). Some new observations and results are obtained thanks to numerical simulations as tool of investigation. It is shown that the fins circumferential temperature is almost uniform. Furthermore, a better cooling is obtained when the Reynolds number increases mainly when the inlet velocity u_0> 0.3m/s. The most suitable value of the aspect ratio is attained for γ = 8.16, which ensure an optimal cooling process of the pins. A new global Nusselt number correlation was developed for engineering applications.

Keywords: Mixed convection, Heat sink, Elliptical pin fins, Cooling device, CFD

1. INTRODUCTION

With the rapid advancement of electronic technology, devices have become significantly smaller while their performance has markedly improved. However, this trend has inevitably led to an increased heat generation per unit volume. In this context, the primary challenge for manufacturers is to ensure efficient cooling. Excess heat, if not adequately dissipated, can shorten a device's lifespan and compromise its functionality. Air heat sinks remain the preferred solution in the electronics industry, primarily due to their affordability and reliability. The objective is to identify an optimal configuration that delivers higher thermal efficiency while maintaining the system's temperature within the manufacturer's specified limits. To design an effective heat sink with superior thermal performance, both numerical and experimental studies are essential to evaluate heat transfer characteristics under various conditions and with different pin-fin array arrangements. This area of research has garnered interest not only from academic laboratories but also from industrial entities. A review of the open literature has identified the following scientific contributions. Chapman et al. [1] investigated forced convection heat sinks in great detail experimentally, analysing various pin fin geometries, including square, circular, and elliptical shapes. Their findings demonstrated that elliptical pin fins exhibited superior thermal performance compared to rectangular pin fins, highlighting their efficiency in heat dissipation under forced convection conditions. Kobus and Oshio [2, 3] conducted a comprehensive study on pin-fin heat sinks using both theoretical and experimental approaches. Their research identified an optimal fin spacing by analysing the influence of various fin parameters. Additionally, their detailed theoretical model demonstrated strong agreement with experimental results. Similarly, Sahiti et al. [4, 5] performed numerical simulations to assess the impact of pin fin shapes on thermal performance and pressure drop. Among six evaluated shapes, the elliptical profile emerged as the most effective, offering the best balance between thermal efficiency and reduced pressure drop.

Seyf and Layeghi [6] examined forced convective heat transfer in heat sinks featuring an elliptical pin-fin cross-section. Their findings revealed that integrating metallic foam into the heat sink significantly enhances thermal efficiency, albeit with a moderate increase in pressure drop. Deshmukh and Warkhedkar [7] conducted an extensive literature review on the thermal efficiency of heat sinks with various pin-fin shapes, addressing all three modes of heat transfer: natural, forced, and mixed convection. Chen and Jan [8] utilised a 3D numerical approach in COMSOL to investigate forced convection in cylindrical and plate-fin heat sinks. Their study concluded that cylindrical fins outperform plate fins in terms of heat dissipation. Deshmukh and Warkhedkar [9]

conducted experimental research on mixed convection around elliptical pin fins. They developed a theoretical model to evaluate the influence of various parameters, including the heat sink's void fraction, aspect ratio, and longitudinal and transverse fin pitch, on its thermal performance. Matsumoto et al. [10] combined numerical and experimental methods to investigate natural convection in five types of pin-fin heat sinks. Their study examined the effects of fin count and geometric parameters on thermal efficiency. Liu et al. [11] performed a comparative analysis of the hydrodynamic and heat transfer performance of heat sinks featuring staggered arrangements of elliptical, circular, and diamond-shaped fins within a rectangular channel. Yadav and Pandey [12] performed a numerical study of convective heat transfer in heat sinks with various fin shapes, including cylindrical, elliptical, sprocket, kite, channeled, and triangular, using the COMSOL Multiphysics software. Their findings showed that heat transfer from pin fins increases with higher inlet velocity. Notably, the kite and elliptical fin shapes demonstrated a significant impact on the Nusselt number and heat transfer coefficient, indicating superior thermal performance compared to other shapes. The characteristics of heat transfer and flow field of a water-cooled pin-fin heat sink were numerically studied by Rezaee et al. [13]. They investigated the effects of pin length and longitudinal pitch on both heat transfer performance and pressure drop, providing insights into how these parameters influence the overall efficiency of the heat sink.

The present work focuses on the numerical study of mixed convection in a heat sink with elliptical pin fins. Using high-resolution 3D numerical simulations, the complete geometry of the heat sink is analyzed to achieve greater precision and better reflect real-world configurations. Both qualitative and quantitative analyses are conducted to explore the thermal and dynamic fields. The qualitative analysis is based on 3D flow visualizations to observe vortex interactions and how the flow behavior changes with varying fin geometrical dimensions, while the quantitative analysis highlights key thermal parameters. The primary objective is to understand the flow topology and improve the passive cooling process, minimizing pressure drop through optimal fin geometry and hydrodynamic inlet conditions (flow rate, Reynolds number, etc.). Additionally, the study aims to develop a new numerical database that complements the experimental work of Deshmukh and Warkhedkar [9], providing more detailed and precise results that are difficult to obtain experimentally. Specifically, the effects of fin aspect ratio and inlet velocity on thermal resistance, Nusselt number, and fin efficiency are thoroughly investigated.

2. MATHEMATICAL MODELLING

2.1 Physical Models

Figures 1 and 2 illustrated the heat sink which is investigated in this paper. In order to confront numerical results against experimental measurements available in the open literature especially the work of Deshmukh and Warkhedkar [9], the target configuration is described as follows. The heat sink consists of 14x7 fins having an elliptic cross-section with inline arrangement and for semi-minor axis a=8mm and semi-major axis b=12mm.
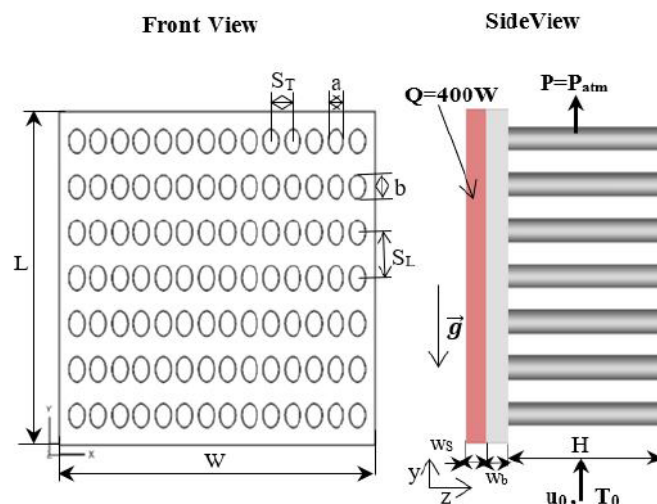
Figure 1. Designed geometry of pin-fin heat sink

The pins-fins sections are attached to a solid volume of parallelepiped form with dimensions (W x L x w_b=164mm x 164mm x 12mm). S_L=22.5mm and S_T=11.25mm are respectively the longitudinal and transversal pitches between the fins. The heat sink is made on the basis of Aluminium alloy (K=202.4 W/m.K), it is attached to an electronic component of Sillicium (K=130 W/m.K), which produces a heat flux Q=400W. The coolant fluid flows along the y-axis according to the inlet condition.
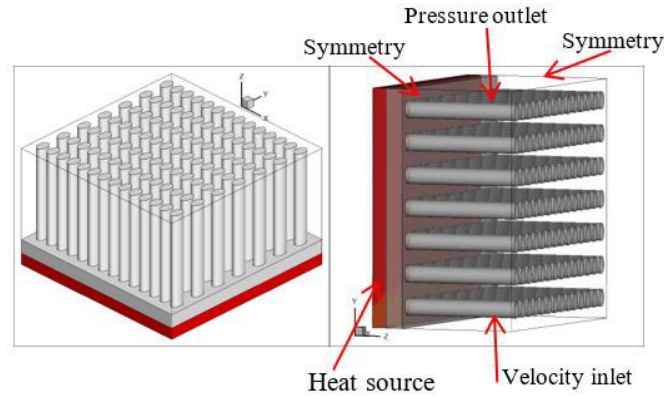
Figure 2. Isometric view of studied heat sink

2.2 Governing Equations and Boundary Conditions

The below equations, let to elaborate a three-dimensional numerical model to study steady air incompressible flow with mixed convective heat transfer by means of numerical simulations. All the fluid thermophysical properties are considered constant in the range of the temperature variation. However, the density varies according to the Boussinesq approximation. Following the considerations above, the governing equations of mass, momentum and energy conservation are written in vector form as follows:

Continuity equation:

$$\nabla \cdot \vec{u} = 0 \tag{1}$$

Momentum equation:

$$\vec{u} \cdot \nabla \vec{u} = -\frac{1}{\rho_0} \overrightarrow{\nabla p} + v \cdot \nabla \vec{u} + \vec{g} \cdot \beta \cdot (T - T_0) \tag{2}$$

Energy equation for fluid:

$$\vec{u} \cdot \overrightarrow{\nabla} T = \frac{K_f}{\rho_0 \cdot C_p} \Delta T \tag{3}$$

Energy equation for solid:

$$K_s \cdot \Delta T + \rho_s = 0 \tag{4}$$

where, $\vec{u}$ is the vector field of flow velocity, the velocity of x, y and z-coordinate are represented as u, v and w, correspondingly; the density of heat transfer fluid is defined as ρ; v is the kinematic viscosity; p is the pressure value of heat transfer fluid; Cp is defined as the specific heat capacity in the constant pressure; β is the thermal expansion coefficient; K_f and K_s are the heat conductivity of heat transfer fluid and solid.

2.3. Boundary Conditions

The boundary conditions at inlet, outlet, and symmetry as well as inside of computational domain are given below:

Inlet flow condition (velocity-inlet):

$$u = w = 0, \ v = u_0, \ T = T_0 = 293.16K \tag{5}$$

Outlet condition (pressure outlet):

$$\frac{\partial u}{\partial x} = \frac{\partial v}{\partial x} = \frac{\partial w}{\partial x} = \frac{\partial T}{\partial x} = 0, \; P = 0 \qquad (6)$$

At planes $x = 0$ and $x = W$, we chose a symmetry conditions:

$$\frac{\partial u}{\partial x} = \frac{\partial v}{\partial x} = \frac{\partial w}{\partial x} = \frac{\partial P}{\partial x} = \frac{\partial T}{\partial x} = 0 \qquad (7)$$

A heat source $\dot{q}_s$ is generated inside of the electronic component.

$$\dot{q}_s = \frac{Q}{V} \qquad (8)$$

$Q = 400$ W, $V = 164$ mm $\times$ 164 mm $\times$ 10 mm $= 268960$ mm^3 and $\dot{q}_s = \dfrac{400}{268960 \times 10^{-9}} = 1487210 \; \text{W}/\text{m}^3$.

- The top surface of pin fin ($z = H$) is well insulated.
- The contour of the base of the heat sinks and the electronics component are supposed to be adiabatic
- The heat flux between the interface of the fluid and the solid walls is coupled and its continuity between the interface of the solid and the liquid is given as:

$$K_s \left.\frac{\partial T}{\partial n}\right|_{wall} = K_f \left.\frac{\partial T}{\partial n}\right|_{wall} \qquad (9)$$

2.4. Numerical Procedure

In this 3D parametric study, numerical experiments are conducted to evaluate the thermal performance of the heat sink under varying aspect ratios of the pin fins and different inlet hydrodynamic conditions. The geometries and meshes are designed using Gambit software, which serves as a pre-processor for the FLUENT commercial code. The finite volume method is applied to discretize the governing equations (1-4) and the boundary conditions by integrating over finite control volumes. The QUICK (Quadratic Upstream Interpolation for Convective Kinetics) scheme is employed for discretizing the convection and diffusion terms. The resulting algebraic equations are solved using the SIMPLE (Semi-Implicit Method for Pressure-Linked Equations) algorithm. Convergence is achieved when the normalized residuals for the continuity and momentum equations are less than 10^{-3}, while the residual for the energy equation is set to 10^{-6}.

3. RESULTS AND DISCUSSIONS

3.1. Temperatures Fields of the Heat Sink

Figure 3 presents the temperature contour in the pin-fin heat sink for an aspect ratio $\gamma = 8.16$. It is observed that, for all inlet velocities ($u_0 = 0.1$ m/s, 0.2 m/s, 0.4 m/s, and 0.5 m/s), the temperature distribution along the circumference of the fins remains nearly uniform. The temperature difference between consecutive pin-fin lines progressively decreases in the flow direction, from the bottom of the heat sink up to the seventh row of fins. This behavior is attributed to the gradual increase in vertical velocity, which helps maintain efficient cooling throughout the system.

The thermal performance of the heat sink is evaluated based on the temperature difference ΔT between the inlet and exit of the heat sink. Figure 4 illustrates the variation of ΔT with inlet velocity u_0 and fin aspect ratio γ. It is evident that ΔT decreases as both u_0 and γ increase.

The convective heat transfer rate is directly influenced by the aspect ratio γ, which corresponds to the height of the fins. Using taller fins (higher aspect ratio) provides a larger surface area for heat exchange, thereby increasing the heat transfer rate. Additionally, as the inlet surface area increases, the air mass flow also increases, as shown in Figure 5. As a result, the outlet air temperature decreases progressively for higher inlet velocities, particularly when $u_0 > 0.3$ m/s.

(a) $u_0 = 0.1$ m/s

(b) $u_0 = 0.2$ m/s

(c) $u_0 = 0.4$ m/s

(d) $u_0 = 0.5$ m/s
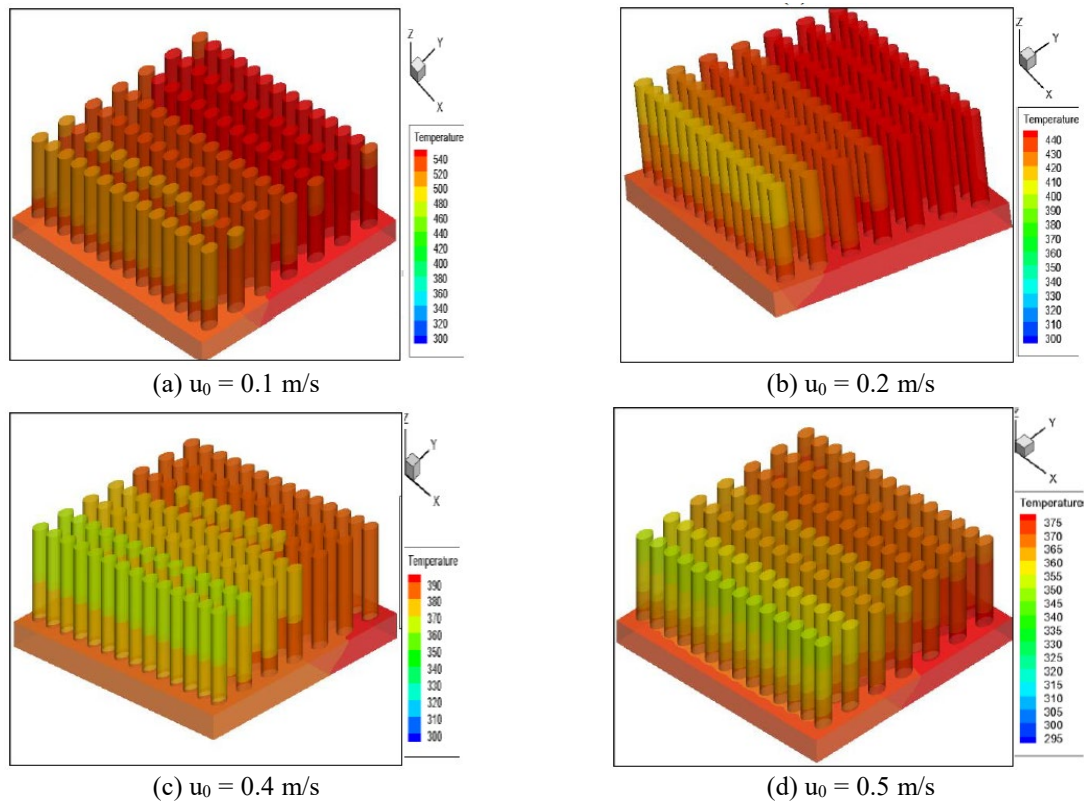
Figure 3. Contours of static temperature in the solid heat sink for $\gamma = 8.16$
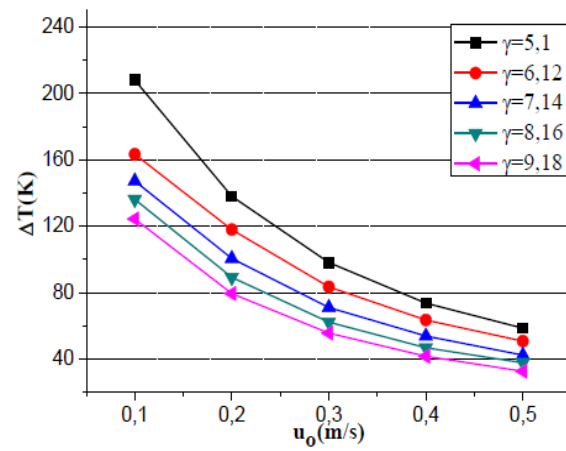
Figure 4. Temperature difference variation versus inlet velocity and aspect ratio γ
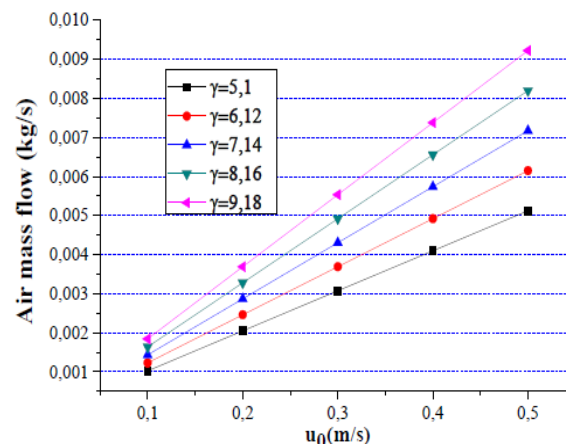
Figure 5. Air mass flow variation with inlet velocity and aspect ratio γ

3.2. Vector Velocity and Path Lines

Figure 6 display the velocity vector plots for $\gamma = 8.16$ at the mid-plane ($z = 0.04$) for various inlet velocity values. The velocity profile at the entry of the heat sink remains uniform. However, as fluid particles approach the pins and flow over them, the direction of the velocity vector changes. It is also noticeable that the velocity increases in the longitudinal direction between the pins, which is attributed to the reduction in the cross-sectional area of the fluid passage. In this region, the friction coefficient remains significant. The acceleration of the fluid enhances the heat transfer by convection. Additionally, the velocity profile is distorted as the fluid nears the heated fins, leading to three-dimensional thermal-fluid fields.

(a) $u_0 = 0.1$ m/s

(b) $u_0 = 0.2$ m/s

(c) $u_0 = 0.4$ m/s

(d) $u_0 = 0.5$ m/s
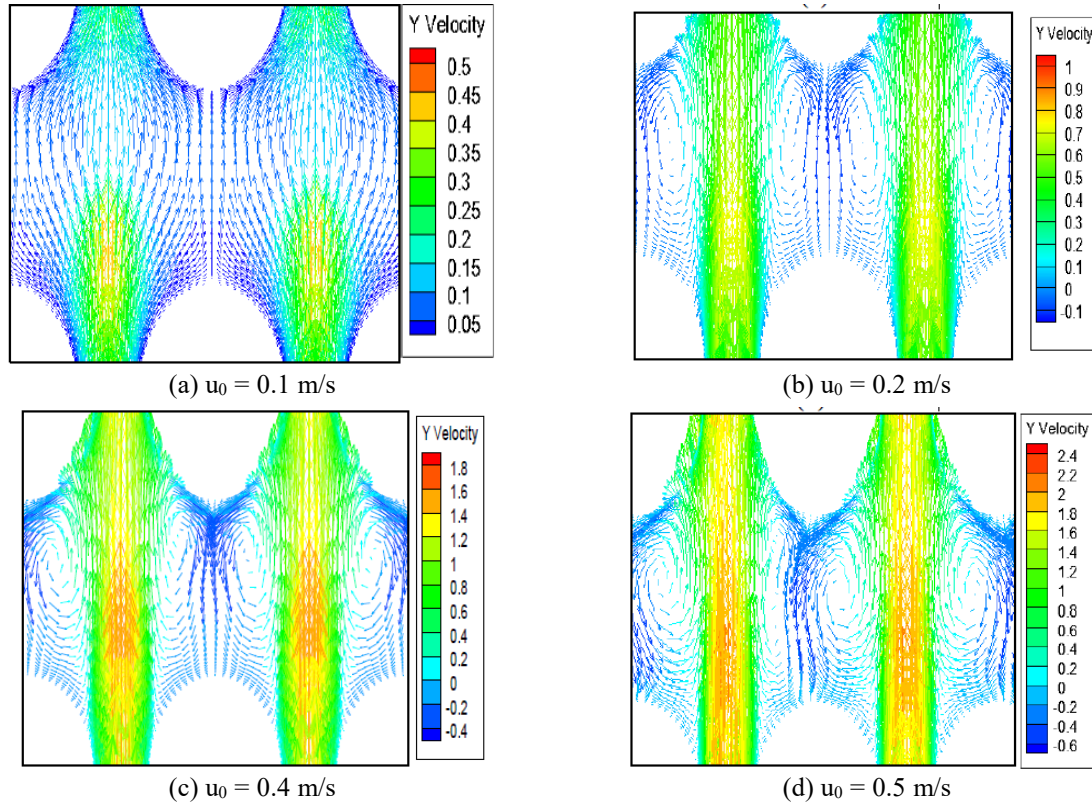
Figure 6. Velocity vectors in the plane z = 0.04 for γ = 8.16

3.3. Thermal Resistance

For a more comprehensive evaluation of the thermal performance of the fins, Figure 7 presents the thermal resistance for different pin heights and inlet velocities. It is observed that the thermal resistance decreases as both the inlet velocity u_0 and the fin aspect ratio γ increase. This indicates that higher velocities and taller fins improve the heat dissipation efficiency of the heat sink, leading to a reduction in thermal resistance.
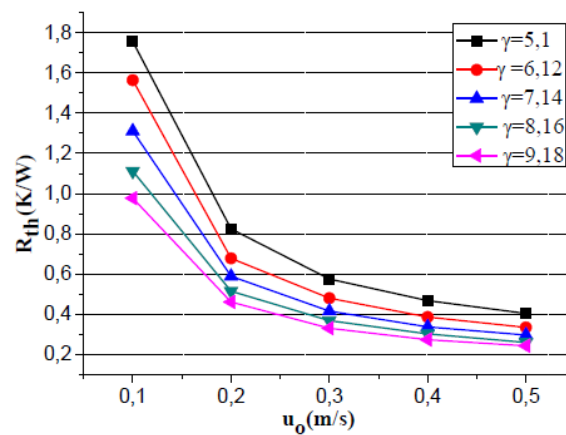
Figure 7. Thermal resistance variation versus the inlet velocity

3.4. Nusselt Number

Figure 8 illustrates the variation of the Nusselt number with inlet velocity for all pin-fin arrangements. It is evident that the mean Nusselt number increases as the air flow rate increases, reinforcing the conductive-convective heat transfer process between the fins and the fluid flow within the heat sink.
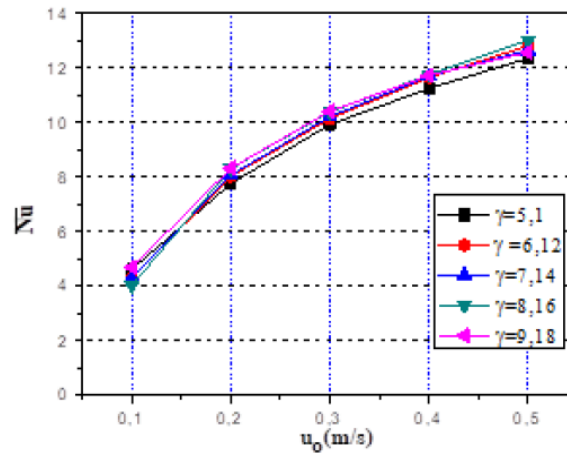
Figure 8. Mean Nusselt number variation versus the inlet velocity

Figure 9 further shows that as the fin height increases, the Nusselt number also increases for all aspect ratios (γ = 5.1 to 8.16). However, detrimental effects are observed for $\gamma > 8.16$. This can be attributed to the temperature gradients near the tips of the pin fins. Specifically, for $\gamma > 8.16$, the thermal resistance causes a significant temperature drop near the fin tips, leading to a reduction in thermal performance. Therefore, the optimal fin aspect ratio appears to be around $\gamma = 8.16$.
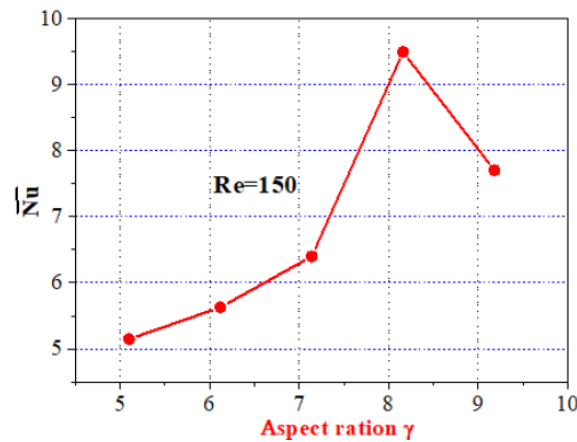
Figure 9. Mean Nusselt number variation versus the aspect ratio

This optimum is exactly the same for both the two approaches; the present numerical simulation and the experimental investigation [9], although their experimental model involves numerous simplifications. However, our approach is more precise as all the governed equations are solved in three dimensional numerical computations.

Obviously the heat flux inside the fins is not unique and dispersed for all the system. The new observations presented above are due to 3D numerical simulations as tool of investigation. The Nusselt number could be correlated as a polynomial function such as equation:

$$\overline{Nu_d} = a_1 + b_1 \cdot R e_d - c_1 \cdot R e_d^2 \qquad (10)$$

Coefficients Data: $a_1 = 0.36987$, $b_1 = 0.07494$, and $c_1 = 1.21936 \cdot 10^{-4}$

Where, $50 \leq Re_d \leq 250$.

4. CONCLUSION

In this study, the cooling process of a heated electronic component is investigated using 3D numerical simulations. A parametric analysis was conducted to examine the effects of various hydrodynamic parameters (inlet velocity and Reynolds numbers) and the geometrical dimensions of the pin fins. The finite volume method, along with the SIMPLE algorithm, was employed to solve the thermal-fluid equations. The numerical results were compared with experimental measurements of pin-fin heat sinks, showing a good agreement. Simulations were performed over a wide range of independent parameters, specifically Reynolds numbers Re=50−250 and fin aspect ratios γ = 5.1−9.18. Based on this 3D study, both the dynamical and thermal fields were analysed qualitatively and quantitatively through numerical visualizations and profiles of significant physical quantities. The results show that the circumferential temperature of the fins remains almost uniform. Moreover, enhanced cooling performance is observed with increasing inlet velocity.

An optimal fin aspect ratio of γ = 8.16 was determined, which provides the best heat dissipation while maintaining a satisfactory pressure drop. Additionally, a new correlation describing the evolution of the Nusselt number with Reynolds number in this thermal system was developed. The numerical experiments presented here reveal more detailed insights, particularly regarding the topology of the thermal-fluid fields, compared to laboratory experiments. These findings contribute to a better understanding of the cooling mechanisms, potentially leading to improved control over heat dissipation and, consequently, longer device lifespan.

References

[1]   C. L. Chapman, S. Lee, and B. L. Schmidt, "Thermal performance of an elliptical pin fin heat sink," in *Proceedings of 1994 IEEE/CHMT 10th Semiconductor Thermal Measurement and Management Symposium (SEMI-THERM)*, 1994, pp. 24–31.

[2]   C. J. Kobus and T. Oshio, "Development of a theoretical model for predicting the thermal performance characteristics of a vertical pin-fin array heat sink under combined forced and natural convection with impinging flow," *International Journal of Heat and Mass Transfer*, vol. 48, no. 6, pp. 1053–1063, 2005.

[3]   C. J. Kobus and T. Oshio, "Predicting the thermal performance characteristics of staggered vertical pin fin array heat sinks under combined mode radiation and mixed convection with impinging flow," *International Journal of Heat and Mass Transfer*, vol. 48, no. 13, pp. 2684–2696, 2005.

[4]   N. Sahiti, A. Lemouedda, D. Stojkovic, F. Durst, and E. Franz, "Performance comparison of pin fin in-duct flow arrays with various pin cross-sections," *Applied Thermal Engineering*, vol. 26, no. 11–12, pp. 1176–1192, 2006.

[5]   N. Sahiti, F. Durst, and P. Geremia, "Selection and optimization of pin cross-sections for electronics cooling," *Applied Thermal Engineering*, vol. 27, no. 1, pp. 111–119, 2007.

[6]   H. R. Seyf and M. Layeghi, "Numerical analysis of convective heat transfer from an elliptic pin fin heat sink with and without metal foam insert," *Journal of Heat Transfer*, vol. 132, no. 7, pp. 071401-1–071401-9, 2010.

[7]   P. A. Deshmukh and R. M. Warkhedkar, "Thermal performance of pin fin heat sinks – A review of literature," *International Review of Mechanical Engineering (IREME)*, vol. 5, no. 4, pp. 726–732, 2011.

[8]   C. T. Chen and S. H. Jan, "Dynamic simulation, optimal design and control of pin-fin heat sink processes," *Journal of the Taiwan Institute of Chemical Engineers*, vol. 43, no. 1, pp. 77–88, 2012.

[9]   P. A. Deshmukh and R. M. Warkhedkar, "Thermal performance of elliptical pin fin heat sink under combined natural and forced convection," *Experimental Thermal and Fluid Science*, vol. 50, pp. 61–68, 2013.

[10]   Z. G. Liu, N. Guan, C. W. Zhang, and G. L. Jiang, "The flow resistance and heat transfer characteristics of micro pin-fins with different cross-sectional shapes," *Nanoscale and Microscale Thermophysical Engineering*, vol. 19, no. 3, pp. 221–243, 2015.

[11]   S. Yadav and K. M. Pandey, "A comparative thermal analysis of pin fins for improved heat transfer in forced convection," *Materials Today: Proceedings*, vol. 5, no. 1, pp. 1711–1717, 2018.

[12]   M. Rezaee, M. Khoshvaght-Aliabadi, A. A. Abbasian Arani, and S. H. Mazloumi, "Heat transfer intensification in pin-fin heat sink by changing pin-length/longitudinal-pitch," *Chemical Engineering & Processing: Process Intensification*, vol. 141, art. no. 107544, 2019.

[13]   W. A. Khan, J. R. Culham, and M. M. Yovanovich, "Fluid flow around and heat transfer from elliptical cylinders: Analytical approach," *Journal of Thermophysics and Heat Transfer*, vol. 19, no. 2, pp. 178–185, 2005.

Experimental Investigation of a High-Order Technique Combined with Electrical Signal Analysis for Fault Detection in Electrical Drives

Azeddine Ratni[1], Djamel Benazzouz[1], Ali Damou[1], Mohammed Tsebia[2]

[1]Solid Mechanics and Systems Laboratory, University of Boumerdes, Boumerdes, Algeria
[2]Signals and Systems Laboratory, University of Boumerdes, Boumerdes, Algeria
Corresponding author: Azeddine Ratni (e-mail: a.ratni@univ-boumerdes.dz)

Abstract

Early and accurate fault detection in electrical drives is essential for reducing downtime and minimizing maintenance costs in industrial systems. Traditionally, higher-order spectral analysis, a technique used to analyze spectral features, has been widely applied for mechanical fault detection in motors based on vibrational signals. However, this paper proposes an innovative approach that applies higher-order spectral analysis to electrical signals, specifically the stator current, for the detection of mechanical faults such as broken rotor bars in electrical drives. By leveraging the electrical signal, this method offers several advantages, including simplified sensor configurations, lower costs, and the ability to detect faults with greater sensitivity and accuracy. The experimental results validate the effectiveness of using the electrical signature for fault diagnosis, demonstrating its potential for predictive maintenance and enhanced reliability of electrical drive systems. This research emphasizes the practical advantages of electrical signal-based fault detection, offering a valuable tool for motor diagnostics across a wide range of industrial applications.

Keywords: Higher-order spectral techniques, Fault diagnosis, Electrical Drives, Signal processing, Broken rotor bars

Nanocrystalline NiO Thin Films: Optical Characteristics

Djanette Meriem Blizak[1]

[1]Laboratory of Bioinformatics, Applied Microbiology and Biomolecules, M'hamed Bougara University of
Boumerdes, Algeria
Corresponding author: Djanette Meriem Blizak (e-mail: d.blizak@univ-boumerdes.dz)

Abstract

Nickel oxide (NiO) thin films are widely studied for their electrochemical stability, affordability, and potential applications in electrochromic devices. This research investigates the optical properties of nanocrystalline NiO thin films on glass substrate, produced using the spin-coating method. The films were prepared through a sol-gel process and annealed at 300 °C to achieve the desired structure. Optical characterization was carried out through absorbance and transmittance measurements in the 300–800 nm wavelength range, supported by Raman and FTIR spectroscopy. The results indicate that film thickness significantly influences the optical behavior of NiO thin films. Thicker films exhibited higher absorbance and lower transmittance, with visible light transmittance decreasing from 65% to 45% as thickness increased. The optical band gap values ranged from 3.78 eV to 3.62 eV, decreasing with increased thickness. Spectroscopic analyses confirmed a nanocrystalline structure with Ni-O bonds and residual moisture, while Raman data identified antiferromagnetic behavior and carbon presence in thicker films. These findings enhance the understanding of NiO thin films for optoelectronic applications.

Keywords: NiO thin films, Nanocrystalline structure, Spin-coating, Optical properties

K-Fold Cross-Validation for Enhancing Predictive Accuracy of Gradient Boosting Machine for Blasting Induced Fly Rock

Mohammed Bouhannache[1], Hamza Cheniti[1]

[1]Department of Mining Engineering, Metallurgy, and Materials, National Higher School of Technology and Engineering, Annaba, Algeria
Corresponding author: Mohammed Bouhannache (e-mail: m.bouhannache@etu.ensti-annaba.dz)

Abstract

This study focuses on the development and evaluation of predictive models for fly rock distance resulting from blasting operations in limestone quarries. Data was collected from 61 blasts at three limestone quarries in M'sila, Algeria, 10 controllable parameters are used as the input variables, and the measured fly rock distance is the output variable. The dataset was divided into training (49 datasets, 80% of the total) and testing (12 datasets, 20% of the total) groups. The training portion was used to develop and fine-tune predictive models with the integration of K-fold cross-validation to enhance performance and prevent overfitting. Model performance was assessed using the coefficient of determination (R^2) and the root mean-squared error (RMSE). The results demonstrate that models trained with K-fold cross-validation significantly outperformed those without it, illustrate higher R^2 values and lower RMSE, that emphasizing the effectiveness of K-fold cross validation in improving predictive accuracy and preventing overfitting.

Keywords: Cross validation, K-fold cross validation, Gradient boosting machine, Rock blasting, Fly rock

1. INTRODUCTION

A fundamental issue in supervised learning is the model's ability to generalize to new, unseen data. A primary challenge here is overfitting While it is often straightforward to create a model that fits the training data precisely, such models may struggle to perform well on new data due to limited generalization [1].

The causes of the overfitting phenomenon can be complex and multifaceted [2], to address challenges related to the learning process and model selection, various resampling methods are employed. One of the most widely used is cross-validation, particularly K-fold cross-validation, which involves repeatedly sampling from a training set to refit the model on different subsets. This approach provides valuable insights into the model's performance and robustness, helping to reduce overfitting and improve generalization [3].

In this study, we apply the gradient boosting machine (GBM) algorithm to predict fly rock in blasting operations, focusing on its effectiveness in generalizing across datasets. To examine the influence of resampling on model performance, we compare the results of the GBM algorithm when applied with and without K-fold cross-validation. Without K-fold CV, the model achieves high accuracy on training data but shows limited accuracy on testing data, suggesting overfitting. By introducing K-fold CV, the model performs consistently well on both training and testing datasets, showcasing the benefits of resampling methods for improved generalization. Through this approach, we demonstrate with real data the efficiency of K-fold cross-validation in enhancing the performance and reliability of predictive models like GBM.

2. METHODOLOGY

2.1. GBM

The GBM is a tree-based model that was introduced by Jerome H. Friedman [4]. Enhancing prediction accuracy involves sequentially creating numerous models, with a focus on training situations that pose challenges in estimation. During the boosting process, instances that are challenging to predict accurately using the preceding base models occur more frequently in the training data compared to instances that are successfully estimated. Each subsequent base model is designed to rectify the errors created by its preceding base models [4–7].

The choice of loss functions can be arbitrary, but for better understanding, if the error function is the traditional squared-error loss, the learning process would lead to consecutive error-fitting. Typically, the researcher has the freedom to select the loss function, as there exist a wide range of pre-existing loss functions and the option to create a custom loss function tailored to the specific task [7]. According to this principle. This study used a traditional loss function, where the concept underlying this loss function is to impose penalties on major deviations from the desired outputs while disregarding smaller differences [8]:

$$\Psi\left(y,f\right)_{L_2} = \frac{1}{2}\left(y-f\right)^2 \tag{1}$$

Where the variable y denotes the actual observed value, while f represents the predicted value generated by the model. The term $\left(y-f\right)$ captures the error or residual between the actual and predicted values. To penalize larger errors more significantly, the squared error $\left(y-f\right)^2$ is applied, while the factor $1/2$ is used to simplify the derivative calculation during optimization. In the case of the L_2 loss-function, its derivative is the residual $\left(y-f\right)$, which implies that the GBM algorithm simply performs residual refitting.

2.2. K-Fold Cross Validation

K-fold cross-validation is a commonly used subsampling method for assessing a predictive model's generalization ability and reducing the risk of overfitting. In this method, the available dataset is divided into k non-overlapping subsets (or "folds") of approximately equal size. The process involves training the model on k-1 of these subsets combined as the training set, while the remaining subset is used as the validation set for performance evaluation. This step is repeated k times, with each subset serving as the validation set once. This ensures that every data point is used for both training and validation, contributing to a comprehensive assessment of the model's performance. The folds are created by randomly sampling without replacement from the dataset [1, 9], Figure 1 illustrate K-fold cross validation, with 10 folds:
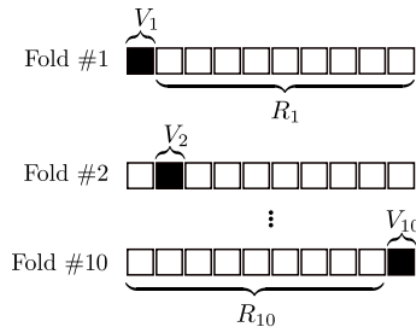
Figure 1. K-fold cross validation with 10 folds [1]

2.3. Application of GBM Algorithm in Real Data

The data collected is a total of 61 blasts from three limestone quarries located in the province of M'sila, Algeria. These quarries, which supply limestone for cement production, have a combined annual mining production of approximately 6 million tons.

Various blasting parameters were measured, including bench height, stemming, hole spacing, powder factor, maximum charge per delay, and the percentage of Anfo in the total explosive quantity, which influences the explosive's pushing strength. Additionally, the distance of fly rock from the muck pile was recorded.

In this study, the database collected from blasting operations is divided into two principle groups: the training and testing portions. Approximately 49 datasets (80% of the total database) are selected for the training class of the models, in which the 49 datasets are used to improve the performance of prediction models by integrating K-fold cross validation, while the remaining 12 blasting data (20% of the total database) are addressed to the testing class for the validation of the models.

Moreover, to control the performance of each model, two metric criteria are established, the coefficient of determination (R^2) offers an idea of how well the model fits the data (best score is 1, 0 is the worst), the root mean-squared error (RMSE) offers an idea of how wrong all predictions are (best score is 0).

$$R^2 = 1 - \frac{\sum_i \left(y_i - \overline{y}_i \right)}{\sum_i} \tag{2}$$

$$RMSE = \sqrt{\frac{\sum_{i=1}^{N} \left(\overline{y}_i - y_i \right)}{N}} \tag{3}$$

Where N represents the number of samples in the stage of training or testing, in our case, y_i represents the observed distance of Fly rock value, $\hat{y}_i$ is the predicted distance of Fly rock value of the model, $\overline{y}_i$ represents the average of the observed Fly rock distance values.

4. RESULTS AND DISCUSSION

In this section, for developing GBM model a classic loss function was selected which is commonly used in practice is the squared error l_2 loss, in this regard to provide the best degree of predictive accuracy, there are four hyper-parametres in developing GBM should be tuned, the step size reduction or learning rate which has usually a positive value range between 0 and 1 and the smaller can achieve to a more accuracy of the model with into account the number of iterations as summarized [10] and subsample or fraction of data used to add the randomization of datasets for each iteration step to avoid over fitting and also augment the performance of predictive model, respectively, 07, 100, 0.1, and 0.8 selected value for max depth n-estimators learning rate and subsample for both whene the GBM model training with and without cross validation as it shown in Table 1. Also, Table 1 clearly presents the defferents results of performance of the gbm model specifically in the testing results with R^2 (0.99 and 1) RMSE (2.07 and 0.06) in the case whene used cross validation in the learning process, instead R^2 (0.99 and 0.22) RMSE (2.11 and 15.94).

Furthermore, Figures 2 and 3 respectively illustrate a comprehensive analysis of the correlation between the predicted and actual fly rock distance values for the GBM model when K-fold cross-validation is used during the learning process, as well as when it is absent for both training and testing data. As shown in the figures, the distribution of actual versus predicted points closely aligns with the perfect fit line when K-fold cross validation is applied, indicating strong model performance. However, in the absence of K-fold cross-validation, the testing data revealed some discrepancies and inappropriate point locations, highlighting potential issues with model generalization.

Table 1. Statistical values for learning model

Learning GBM model	Training		Testing	
	RMSE	R^2	RMSE	R^2
With K-fold cross validation	2.07	0.99	0.06	1
Without K-fold cross validation	2.11	0.99	15.94	0.22
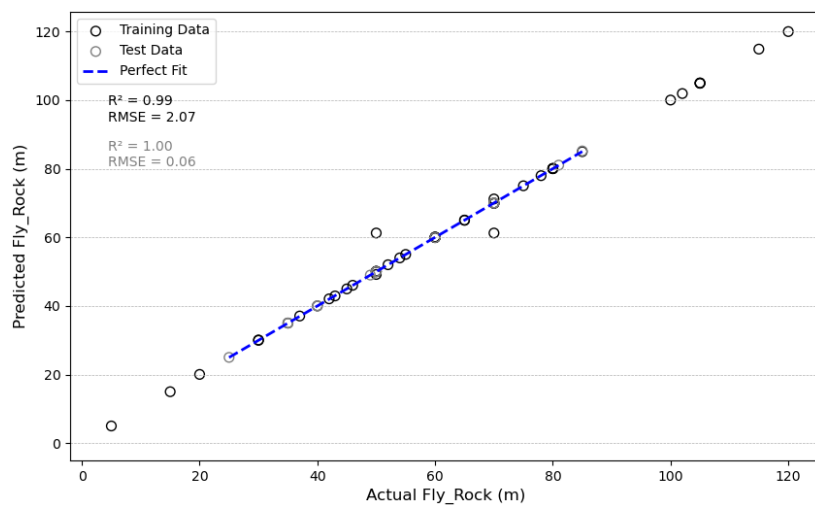
Figure 2. Comprehensive analyses of correlation between predicted and measured (actual) fly rock distance values for GBM model with k-fold validation
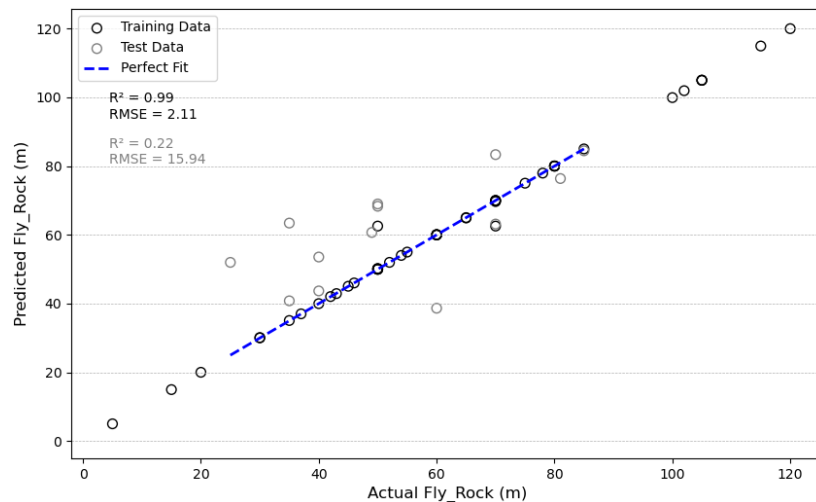
Figure 3. Comprehensive analyses of correlation between predicted and measured (actual) fly rock distance values for GBM model without k-fold validation

5. CONCLUSION

The results presented in this study underscore the efficiency of using K-fold cross-validation in developing predictive models such as the GBM model. By comparing the performance metrics with and without K-fold cross-validation, it is evident that applying this technique significantly enhances the model's ability to generalize, reducing the risk of overfitting. The high R^2 values (0.99 and 1) and low RMSE (0.06 and 2.07) obtained during testing when K-fold cross-validation was applied demonstrate robust predictive accuracy and a close alignment with the perfect fit line. In contrast, the absence of K-fold cross-validation led to reduced performance, with notable discrepancies in testing data points and an increase in decrease in R^2 (0.22) and RMSE (15.94). These findings highlight that K-fold cross-validation is a vital component in the learning process, ensuring reliable model performance and the avoidance of overfitting, thereby improving the predictive accuracy and robustness of the GBM model.

Acknowledgments

References

[1]   D. Berrar, *Cross-Validation*, *Elsevier eBooks*, 2018, pp. 542–545. doi: 10.1016/b978-0-12-809633-8.20349-x.

[2]   X. Ying, "An overview of overfitting and its solutions," *Journal of Physics Conference Series*, vol. 1168, art. no. 022022, Feb. 2019, doi: 10.1088/1742-6596/1168/2/022022.

[3]   G. James, D. Witten, T. Hastie, R. Tibshirani, and J. Taylor, "Resampling methods," in *Springer Texts in Statistics*, 2023, pp. 201–228. doi: 10.1007/978-3-031-38747-0_5

[4]   J. H. Friedman, "Greedy function approximation: A gradient boosting machine," *The Annals of Statistics*, vol. 29, no. 5, Oct. 2001, doi: 10.1214/aos/1013203451.

[5]   J. H. Friedman, "Stochastic gradient boosting," *Computational Statistics & Data Analysis*, vol. 38, no. 4, pp. 367–378, Feb. 2002, doi: 10.1016/s0167-9473(01)00065-2.

[6]   C. Xie, H. Nguyen, X.-N. Bui, Y. Choi, J. Zhou, and T. Nguyen-Trang, "Predicting rock size distribution in mine blasting using various novel soft computing models based on meta-heuristics and machine learning algorithms," *Geoscience Frontiers*, vol. 12, no. 3, art. no. 101108, Dec. 2020, doi: 10.1016/j.gsf.2020.11.005.

[7]   Y. Zhang and A. Haghani, "A gradient boosting method to improve travel time prediction," *Transportation Research Part C Emerging Technologies*, vol. 58, pp. 308–324, Apr. 2015, doi: 10.1016/j.trc.2015.02.019.

[8]   A. Natekin and A. Knoll, "Gradient boosting machines, a tutorial," *Frontiers in Neurorobotics*, vol. 7, Jan. 2013, doi: 10.3389/fnbot.2013.00021.

[9]   T. Yan, S.-L. Shen, A. Zhou, and X. Chen, "Prediction of geological characteristics from shield operational parameters by integrating grid search and K-fold cross validation into stacking classification algorithm," *Journal of Rock Mechanics and Geotechnical Engineering*, vol. 14, no. 4, pp. 1292–1303, Apr. 2022, doi: 10.1016/j.jrmge.2022.03.002.

[10]   S. Touzani, J. Granderson, and S. Fernandes, "Gradient boosting machine for modeling the energy consumption of commercial buildings," *Energy and Buildings*, vol. 158, pp. 1533–1543, Nov. 2017, doi: 10.1016/j.enbuild.2017.11.039.

Prediction of Penetration Resistance for Fine-Grained Soils Using Artificial Neural Networks

Haseeb Ullah Kashif[1], Naveed Ahmad[1]

[1]Civil Engineering, University of Engineering and Technology, Taxila, Pakistan
Corresponding author: Haseeb Ullah Kashif (e-mail: haseeb3833@gmail.com)

Abstract

For predicting the standard penetration resistance (SPT-N) values of soil, the present work successfully analysed the procedure involved in building an artificial neural networks (ANNs) model using the relevant data set. Determining the SPT-N values of a certain soil, it may be an expensive, and lengthy procedure that requires a lot of work to be done in the field. There are many opportunities for the field circumstances to change, which could lead to the test findings being fabricated. One hundred experimental test results, including factors such as % of sand, silt and clay, plastic index (PI), liquid limit (LL), moisture content, and SPT-N values are used to create the experimental database. With the help of the modified MATLAB code, ANNs models are created, trained, verified, and tested using various combinations of the crucial soil parameters listed above. Performance of model assessed by correlation coefficient (R), mean squared error (MSE) and mean absolute error (MAE) to provide best model. With the comparison between predicted and the experimental output values, the effectiveness of the created prediction models is assessed, and results show that there is a linear relationship between both values as coefficient of determination R^2 is near to 1. Furthermore, the reduction in MSE and MAE by 0.8453% and 4.8% respectively along with enhanced R and R^2 of 0.92 and 0.85 shows the effectiveness of model. ANNs model for predicting different soil engineering characteristics are generated by modifying the given parameters that are introduced to the model.

Keywords: MATLAB, ANNs, SPT-N values, R, MSE

1. INTRODUCTION

In situ tests and site investigation are used for analysis and design of structure by determining the soil's strata. In other words, penetration resistances can be used to group and describe the subsurface. Inspection of soil by SPT-N value is common in construction projects and it considered as the most usual soil investigation method. There are numerous advantages to this approach [1].It is an important test at the field. In addition to other laboratory tests that are carried out to gain further information about the properties of soils [2]. There are a lot of empirical equations which have been formulated and used in the past to determine soil strength by using different independent variables [3].

It is also able to mitigate this constraint by allowing for better representation of the site conditions, thereby enhancing the accuracy of the forecasts. The efficacy of such approaches is normally somewhat low because of the variability in the soil properties and the significant number of factors that may affect its strength [4]. Soft computing- based machine learning and artificial intelligence-based modelling are in trending from the last decade. This method based on logic of human capability for learning and identification of certain pattern in data even if the data are uncertain and imprecise in nature, proved good in every field. For instance, it is shown in various investigations that machine learning techniques are adopted in geotechnical engineering for the prediction of soil characteristics accurately [5]. Out these techniques, ANNs are a subfield of artificial intelligence (AI) which are being found as an important technique for modelling and forecasting of such systems like soil behaviour [6].

ANNs for prediction must be built up with a complex network of perceptron's which are laid down in many layers. There are three types of layers including output layers; hidden layers; and input layer [7]. ANNs are optimal tool categorizing complex occurrences in soil mechanics due to its applicability to identifying non-linear relationship and trends [8]. The objective of present work to construct a framework of an ANNs model to accurately predict and assess the characteristics of fined grained soil [9]. This study uses MATLAB to create an analytical tool called the Multilayer Feedforward Backpropagation (MFFBP) neural network [10]. The importance of back propagation networks has increased due to the shortcomings of existing techniques. Back propagation has many layers and neuron in each layer. The number of layers which are hidden and neurons in every layer of concealment will

depend on the problem's severity, inputs, and outputs. [11]. With this tool, scientists can quickly address a variety of difficult industrial challenges by varying the input and output parameters. Once the problem's nature has been established, we can look for the best method or strategy to plane. Certainly, apply one or more different artificial neural network learning methods and structures toward every previously stated trait [12].

Behaviour of soil, settlement analysis, liquefaction, stability of slope, mapping and classification of soil, bearing capacity of pile prediction are all often modelled by ANNs in geotechnical engineering [13]. Steel, concrete, and wood are among the most common civil engineering materials that exhibit significantly greater homogeneity and isotropy than this. The geographical range of these materials and the complication of geotechnical activities naturally lead to a simplification of traditional engineering design methodologies. A technology called ANNs is useful for simulating complex problems which are unclear about the connectivity of model variables [14].

2. MATERIAL AND METHOD

For experimental and modelling reasons, around 100 test samples were collected in the lab from different places with different geological and climatic characteristics are involved in this study. Dataset was constructed by gathering percentages of sand, silt and clay, moisture content and Atterberg limits except plastic limit as input parameters and SPT-N values as a predictive outcome. Table 1 below displays the findings from the soil datasets statistical analysis.

Table 1. Statistics of the dataset

	Sand (%)	Silt and Clay (%)	Liquid Limit (%)	Plastic Index (%)	Moisture Content (%)	Standard Penetration Resistance
Maximum	49	99	28.89	7	27.7	43
Minimum	1	50	22.11	4.57	17.23	11
Mean	11.88	82.97	25.578	5.7098	15.8119	19.01
Standard Deviation	10.96201	13.86106	1.695765	0.850024	6.147894	9.546198

The database's various input and output parameters' correlation matrix is displayed in next table 2 that supplied under [15]. The relationship matrix shows the correlation coefficient which are known as "r" of the included parameters. Positive number in a correlation table indicated that there was positive correlation among the different variables. Oppositely, minus sign proves the two variables are inversely related [16].

Table 2. The database's parameters' correlation matrix

	Sand (%)	Silt and Clay (%)	Liquid Limit (%)	Plastic Index (%)	Moisture Content (%)	Standard Penetration Resistance
Sand (%)	1					
Silt And Clay (%)	-0.8	1				
Liquid Limit (%)	-0.41	0.32	1			
Plastic Index (%)	-0.01	0.04	0.33	1		
Moisture Content (%)	-0.34	0.41	0.14	-0.18	1	
Standard Penetration Resistance (Blow)	0.34	-0.25	-0.16	0.19	-0.5	1

ANNs are capable of learning, estimating, classifying, generalizing, and approximating data as well as making predictions based on inputs and outputs parameters. This is of particular importance to these operations because of the flexibility provided by the network and the ability to retain knowledge through training. The layers of neurons in ANNs are bonded by weighted connections [13]. This is because according to the distinction between target and projected outputs the model changed these weights during training. Therefore, for their ability to determine error using predictor and target values, Feedforward Backpropagation Neural Networks (FBPNNs) methods were selected for that study [5].

There are many methods by which overfitting of model in artificial neural network can be avoided, one of these is that entire database is divided into three parts that are training, validation and testing. However, to minimize the training errors, gradient descent is used to revise the bias and weight during training process. Overtraining may

occur, in which the network conforms too closely to the training data, and thus performs poorly on data not seen during training. MATLAB split data between training set, validation, and subset being tested.

Figure 1. Number of sample for training, testing and validation
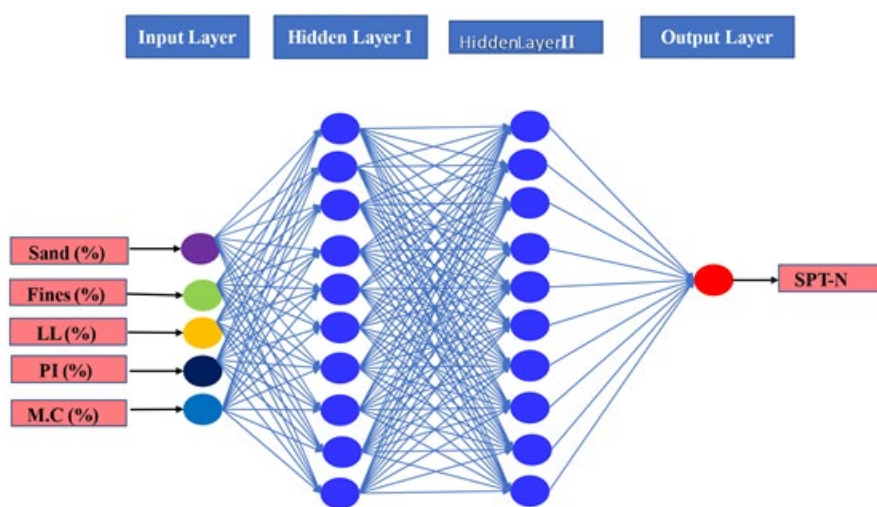
Figure 2. Architectural diagram of ANNs model

3. RESULTS

The proposed model based on ANNs is built by using one hundred set of data points obtained from different sites within a region to determine the SPT-N values of soil. Sand, silt and clay, plasticity index, liquid limit and moisture content percentages are among its five input parameters and the SPT-N values are its sole output parameter. The MATLAB software is used to create the ANNs model, and the "divide rend" function is used to divide the database into training, validation and testing subsets. Figure 3 below shows the performance of the training, validation and testing stage for the whole run of the model. Over the course of seven epochs, the learning and training of model has been completed.
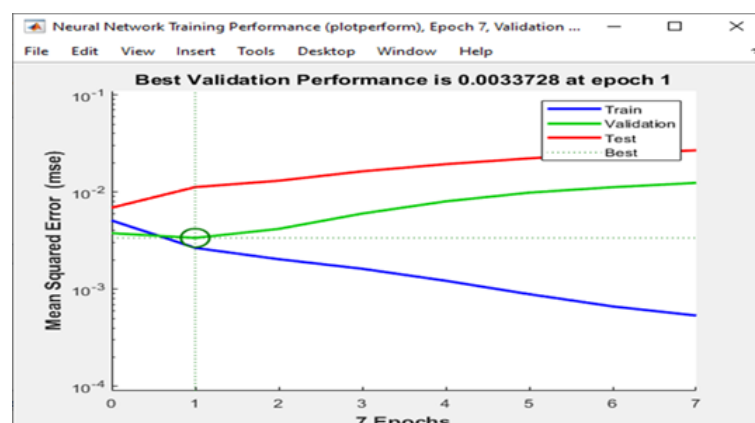
Figure 3. Neural Network training performance

Regression results in training, testing and validation simulations show the effectiveness of the model in identifying the relationships among output and input variables of soil in Figure 4.
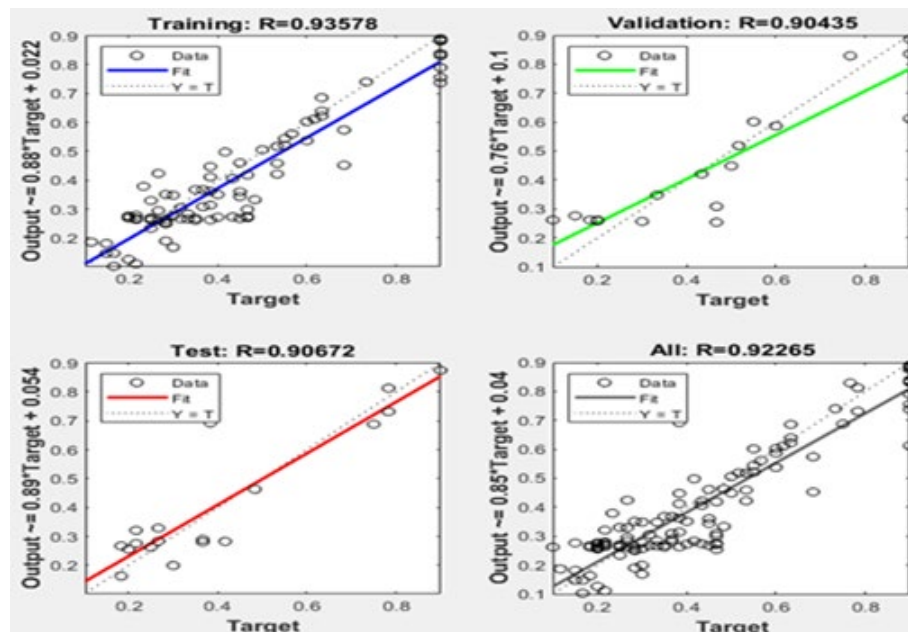
Figure 4. Regression Curve for Artificial neural network model

4. DISCUSSION

In this section, the original output values are compared with the predicted values. Model's scatter plots between the original SPT-N values at ordinate and the predicted SPT-N values on abscissa show the linear fitting line or linearity.
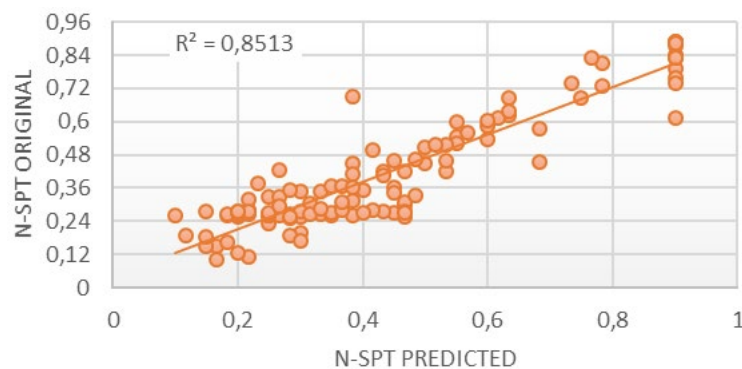
Figure 5. Comparison of experimental and ANNs predicted SPT-N values
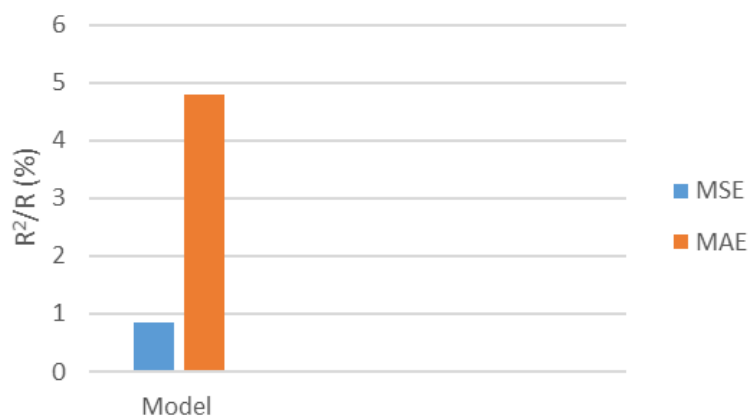
Figure 6. Coefficient of determination (R2) and coefficient of relation (R)

In a regression analysis, the statistical metric such as R^2 and R, conveys the direction and magnitude of a linear relationship between two variables. The regression model and the data match each other better when the R and R^2 numbers are greater. This means that the independent variable or variables can account for most of the variance in the dependent variable. Figure 6 below shows how well our ANNs model performs with the R^2 and R values for the suggested ANNs model being 0.85 and 0.92, respectively. The ability of the model to predict the standard SPT-N values of soil was evaluated in the current study using other performance indices as additional performance measures shown below in Figure 7.
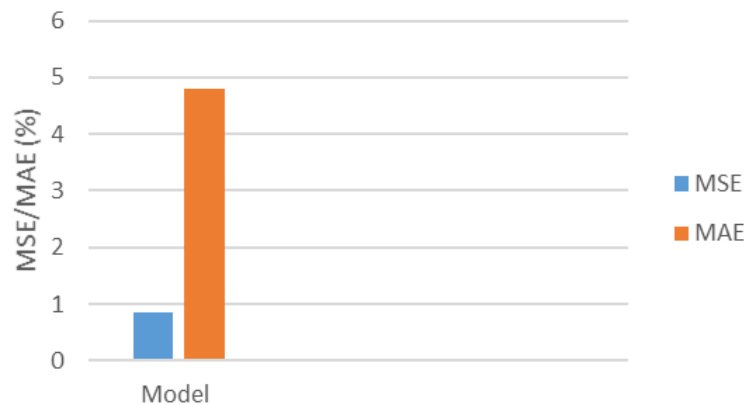
Figure 7. Mean square error (MSE)and mean absolute error (MAE) values

When the MSE is lower (0.8453%), the squared differences between the model2s predictions and the actual values are typically insignificant. A lower MAE which is (4.8%) suggests that, on average, there aren't many absolute differences between the expected and actual values. This suggests that the model regularly forecasts values that are near to the actual values and that there is little bias or distortion.

5. CONCLUSION

In ANNs it is very mandatory to divide the full datasets into subsets training, testing and validation to increase generality and reduce over-fitting. It also allows segmentation of the ANNs model for training purposes and for effective monitoring of the models' performance. Input pass through FBPNNs during training process. Depending on the results achieved, the anticipated output is checked with target values to estimate the net error. To minimize on errors weights and bias are adjusted using the "gradient descent" approach.

The predictions from the created ANNs model were then contrasted with the goal values from the experimental investigation. To prove the relationship between the target and expected values, they plotted the data points on fitting Line. They also reported other measures, for instance, Coefficient of determination for optimization purposes. When tested with other parameters which are shown in Figure 6 shows higher values like 0.85 and 0.92 which indicate proposed ANNs model is quite effective. In addition, MAE and MSE show that developed model is accurate and genuine. Towards the end of the paper, in the conclusions section, the author presents the most important findings of the study.

References

[1]   B. Tarawneh, "Predicting standard penetration test N-value from cone penetration test data using artificial neural networks," *Geoscience Frontiers*, vol.8, no. 1, pp. 199–204, Jan. 2017, doi: 10.1016/J.GSF.2016.02.003.

[2]   S. A. Nugroho, H. Fernando, and R. Suryanita, "Estimation of standard penetration test value on cohesive soil using artificial neural network without data normalization," *IAES International Journal of Artificial Intelligence*, vol. 11, no. 1, pp. 210–220, Mar. 2022, doi: 10.11591/IJAI.V11.I1.PP210-220.

[3]   ASTM, "Test method for unconfined compressive strength of cohesive soil," Jul. 2016, doi: 10.1520/D2166_D2166M-16.

[4]   A. Esposito, M. Faundez-Zanuy, F. C. Morabito, and E. Pasero, "Some Note on Artificial Intelligence," *Smart Innovation, Systems and Technologies*, vol. 151, pp. 3–8, 2020, doi: 10.1007/978-981-13-8950-4_1.

[5]   G. James, D. Witten, T. Hastie, and R. Tibshirani, *An Introduction to Statistical Learning with Applications in R Second Edition*, 2021.

[6]   I. Yilmaz, "Evaluation of shear strength of clayey soils by using their liquidity index," *Bulletin of Engineering Geology and the Environment*, vol. 59, no. 3, pp. 227–229, 2000, doi: 10.1007/S100640000056.

[7]   N. J. Higham, "Computing the nearest correlation matrix—A problem from finance," *IMA Journal of Numerical Analysis*, vol. 22, no. 3, pp. 329–343, Jul. 2002, doi: 10.1093/IMANUM/22.3.329.

[8]   S. Jones, D. Johnstone, and R. Wilson, "An empirical evaluation of the performance of binary classifiers in the prediction of credit ratings changes," *J Bank Financ*, vol. 56, pp. 72–85, Jul. 2015, doi: 10.1016/J.JBANKFIN.2015.02.006.

[9]   A. Goel, A. K. Goel, and A. Kumar, "The role of artificial neural network and machine learning in utilizing spatial information," *Spatial Information Research*, vol. 31, no. 3, pp. 275–285, Jun. 2023, doi: 10.1007/S41324-022-00494-X/TABLES/3.

[10]   A. D. Dongare, R. R. Kharde, and A. D. Kachare, *Introduction to Artificial Neural Network*, 2008.

[11]   M. H. Kutner, C. Nachtsheim, J. Neter, and W. Li, *Applied Linear Statistical Models*, McGraw-Hill Irwin, 2005.

[12]   Z. Juan, "Introduction to artificial neural network (ANN) methods: What they are and how to use them," [Online]. Available: https://www.researchgate.net /publication/251626579_Introduction_to_Artificial_ Neural_Network_ANN_Methods_What_They_Are_and_How_to_Use_Them (Accessed: Dec. 03, 2024).

[13]   E. Yaghoubi, E. Yaghoubi, A. Khamees, and A. H. Vakili, "A systematic review and meta-analysis of artificial neural network, machine learning, deep learning, and ensemble learning approaches in field of geotechnical engineering," *Neural Comput Appl*, vol. 36, no. 21, pp. 12655–12699, Jul. 2024, doi: 10.1007/S00521-024-09893-7/FIGURES/16.

[14]   M. A. Shahin, M. B. Jaksa, and H. R. Maier, "Artificial neural network applications in geotechnical engineering," [Online]. Available: https://www.researchgate.net/publication/245498369_Artificial_Neural _Network_ (Accessed: Dec. 03, 2024).

[15]   N. Papernot, P. Mcdaniel, S. Jha, M. Fredrikson, Z. B. Celik, and A. Swami, "The limitations of deep learning in adversarial settings," in *2016 IEEE European Symposium on Security and Privacy, EURO S and P 2016*, pp. 372–387, May 2016, doi: 10.1109/EUROSP.2016.36.

[16]   A. Kumar, V. Singh, S. Singh, R. Kumar, and S. Bano, "Prediction of unconfined compressive strength of cement–lime stabilized soil using artificial neural network," *Asian Journal of Civil Engineering*, vol. 25, no. 2, pp. 2229–2246, Feb. 2024, doi: 10.1007/S42107-023-00905-W/METRICS.

Recycling Construction Waste to Obtain a Cellular Insulation Material

Fayrouz Benhaoua[1], Djalila Aoufi[2], Nacira Stiti[1], Younes Lamri[1], Abdelouaheb Djeddou[1], Mahdia Toubane[1], Razika Tala-Irgil[1]

[1]Research unit Materials, Processes and Environment UR-MPE, Faculty of Engineering, University M'Hamed Bougara, 35000 Boumerdes, Algeria

[2]Research Center in Industrial Technologies-CRTI, Echahid Mohammed Abassi, Cheraga, 16014 Algiers, Algeria

Corresponding author: Fayrouz Benhaoua (e-mail: f.benhaoua@univ-boumerdes.dz)

Abstract

In this study, our objective is to significantly contribute to environmental protection by adopting an innovative approach to recycling certain types of construction waste, such as used plaster and window glass, to develop a revolutionary new eco-friendly material for building thermic insulation. This material also helps reduce the energy consumption required for air conditioning. To achieve this, we mixed up to 10% plaster powder with window glass powder, adding 1% $CaCO_3$ foaming agent to the powdery mixture to obtain a porous structure. The different mixtures are pressed using a hydraulic press into pellets at a pressure of 100 KN to ensure optimal cohesion. Subsequently, these pellets underwent thermal treatment at a temperature of 800°C for 10 minutes, resulting in cellular material samples. To evaluate the quality and performance of our materials, we utilized various physicochemical analysis techniques such as X-ray diffraction (XRD), differential scanning calorimetry (DSC), porosity measurement, mechanical strength characterization, etc. The results obtained demonstrate that our foams exhibit high porosity, exceeding 81%, as well as compression resistance exceeding 5 MPa. These results position our material as a high-quality construction insulation, offering both exceptional performance and a reduced ecological footprint, contributing to a more sustainable future for our planet.

Keywords: Environmental, Construction waste, Cellular material

Separation of Benzene – Cyclohexane Mixture Using Intensified Extraction Process by Pyridinium-Based Ionic Liquids

Mohammed Djamel Eddine Allali[1], Hassiba Benyounes[1], Nesrine Amiri[2]

[1]Laboratory of Physical Chemistry of Materials, Catalysis and Environment, University of Sciences and Technology of Oran Mohamed Boudiaf, Oran, Algeria
[2]Process Engineering, University of M'Hamed Bougara Boumerdes, Boumerdes, Algeria
Corresponding author: Mohammed Djamel Eddine Allali (e-mail: allali.meddjamel@gmail.com)

Abstract

The separation of cyclohexane from benzene is the most challenging tasks in the petrochemical industry due their close boiling points and the formation of azeotrope. For this reason, the conventional distillation is not suitable for their separation. Hence, the liquid-liquid extraction is most widely used process for low concentration benzene with the advantages of high selectivity and low energy consumption compared to extractive distillation. Recently, a new type of environmentally friendly solvent has been introduced as a promising alternative such as ionic liquids (ILs) to enhance the performance of the extraction process, because of their high selectivity, less volatility and reduced toxicity compared to the conventionnel solvents such as sulfolane. This work aims to design an extraction process for the separation of the azeotropic mixture benzene – cyclohexane using pyridinium based ILs as an alternative to sulfolane. The modelling of the liquid – liquid equilibrium (LLE) of the ternary systems benzene + cyclohexane + solvents was performed using the non-random two- liquid thermodynamic model (NRTL). The calculated LLE data using the fitted binary interaction parameters of NRTL model are in good agreement with those experimental collected from the literature. The results shows that the obtained values of selectivity and distribution coefficient for benzene - cyclohexane are higher using the ILs and that the extraction process using ILs is more efficient.

Keywords: Liquid-liquid extraction, Ionic liquid, Thermodynamic model, Azeotropic mixture

Performance Evaluation of PV/Wind/Wave Hybrid System for Green Hydrogen Generation for Kuala Terengganu, Malaysia

Mohd Afifi Jusoh[1], Mohd Zamri Ibarahim[1], Zulkifli Mohd Yusop[1], Muhamad Zalani Daud[1], Aliashim Albani[1], Muhammad Syarifuddin Yahya[1]

[1]Renewable Energy & Power Research Interest Group (REPRIG), Eastern Corridor Renewable Energy Special Interest Group, Faculty of Ocean Engineering Technology, Universiti Malaysia Terengganu, 21030, Kuala Nerus, Terengganu, Malaysia
Corresponding author: Mohd Afifi Jusoh (e-mail: afifi@umt.edu.my)

Abstract

This study presents a comprehensive analysis of a hybrid renewable energy system that integrates solar photovoltaic (PV), wind turbine (WT) and wave energy converter (WEC) systems for green hydrogen production in Kuala Terengganu, Malaysia. The hybrid system aims to mitigate the intermittency of individual renewable energy sources by leveraging the complementary nature of solar, wind, and wave energies. The performance of the system was evaluated over a one-year period under real climatic conditions, with an emphasis on energy production, system efficiency, and hydrogen output. The results demonstrate that the hybrid system produced a total of 265.6 MWh of electricity annually, which was used to drive a proton exchange membrane (PEM) electrolyser for hydrogen generation. The analysis revealed that the PV system contributed 85.4% of the total energy, followed by the WT and WEC systems contributing 12.2% and 2.4%, respectively. The consistent operation of the electrolyser resulted in an annual hydrogen production of approximately 5,694 kg, highlighting the system's potential for sustainable hydrogen production. The study underscores the importance of integrating multiple renewable energy sources to enhance the reliability and stability of energy supply for hydrogen production, contributing to the global efforts towards achieving net-zero emissions.

Keywords: Green hydrogen production, Hybrid renewable energy, Solar photovoltaic, Wind turbine, Wave energy converter

Nano Terahertz Patch Antenna for Wireless Body Area Network Applications

Bouchra Moulfi[1], Souheyla Ferouani[1], Fatima Zahra Moussa[1], Safaa Moulfi[1]

[1]Department Electronic and Telecommunications, University Belhadj Bouchaib (of Ain Temouchent), Temouchent, Algeria
Corresponding author: Bouchra Moulfi (e-mail: bouchramoulfi @gmail.com)

Abstract

In this paper, a nano terahertz antenna for on-body wireless body area network (WBAN) applications is designed. The antenna features a gold patch with a thickness of 4 μm, while Roger RO 3210 (εr = 10.8) is selected as the substrate material, with a thickness of 5 μm. The antenna's dimensions are 26.84 μm × 14.96 μm (width × length), and it is intended for integration on the human body for medical applications, such as measuring and monitoring various physiological parameters using sensors to assess an individual's overall health status. The design achieved a return loss of -45 dB and a gain of 3 dBi at a frequency of 2.31 THz.

Keywords: Nano patch antenna, Terahertz transmission; Wireless Body Area Network, Return loss, medical applications

1. INTRODUCTION

In recent years, the advancement of technology and the emergence of the wireless body area network (WBAN) standard (802.16.6) in 2012 [1] have brought significant improvements to the lives of patients requiring continuous monitoring and care. The integration of miniature sensors and actuators has enabled the remote observation of various human vital organ activities, including measurements of oxygen levels, ECG, EEG, and other physiological functions [2, 3]. This has transformed the way medical professionals can monitor patients, allowing for a more seamless, real-time tracking of vital signs without the need for patients to remain confined to clinical environments. WBAN technology offers an automatic and efficient service by utilizing a network of small, distributed nodes that communicate wirelessly. These nodes can be positioned on the body (ON-body), near the body (OFF-body) [4], or even implanted within the body (IN-body) [5], depending on the specific medical application. Each node is essentially composed of a small antenna that facilitates integration into the patient's environment or clothing, promoting ease of movement and comfort for the patient. The compact nature of these antennas ensures minimal intrusion, while their low energy consumption and low power requirements make them ideal for long-term use in wearable or implantable medical devices. In our research, we aim to utilize the optical spectrum, particularly the terahertz spectrum, which spans from 0.1 to 10 THz [6], to explore novel solutions for WBAN technology. The terahertz spectrum offers unique advantages for high-speed, high-frequency data transmission, which is crucial for the rapid communication required in health monitoring systems. Many recent studies have focused on this frequency range, investigating innovative designs such as graphene-based antennas [7, 8], and lens-based antennas [9, 10]. These cutting-edge designs demonstrate the potential for improved performance in terms of size, power efficiency, and data transmission capabilities, making them well-suited for applications in WBAN. By leveraging the properties of the terahertz spectrum, we hope to contribute to the growing body of research aimed at enhancing WBAN systems for medical use, particularly in areas such as remote health monitoring, where reliable, low-power, and high-performance communication systems are essential for improving patient care and outcomes.

This paper presents the design and analysis of a rectangular patch antenna with slots operating in the terahertz frequency band, using CST Microwave Studio technology. Gold is used for both the patch and ground plane, while Roger RO3210 (εr = 10.8) with a thickness of 5 μm serves as the dielectric substrate. The antenna's performance is evaluated for WBAN, specifically for on-body applications, where it can measure and monitor various physiological parameters through sensors, contributing to the overall health status monitoring of individuals. The antenna has dimensions of 26.84 × 14.96 μm² and operates at a frequency of 2.31 THz. The proposed nano patch antenna achieves a return loss of -47 dB and a gain of 3 dB.

2. ANTENNA DESIGN

In this section, we outline the design process of a nano patch antenna (as shown in Figure 1). The antenna is constructed using a Roger RO 3210 substrate, which has a dielectric constant (εr) of 10.8 and a thickness (h) of 5 μm. A gold patch, with a thickness of 4 μm, is used for both the patch and ground plane components due to its excellent conductivity properties, which are critical for high-performance antenna designs at terahertz frequencies. The antenna is fed by a 50 Ω microstrip line, which ensures efficient impedance matching and minimizes signal reflections.
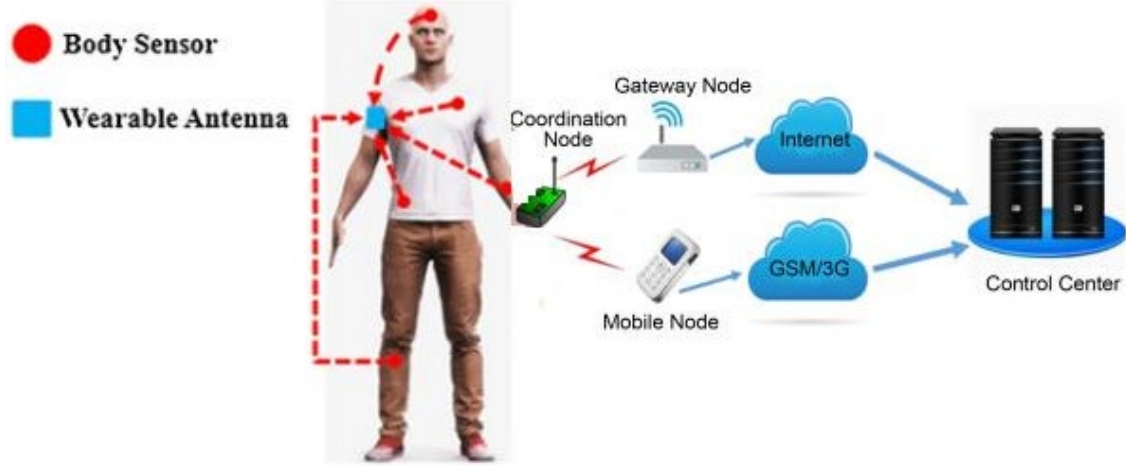
Figure 1. Wireless body area network application

The dimensions of the patch are carefully calculated using a standard design equation for rectangular patch antennas, which takes into account the operating frequency, the dielectric constant of the substrate, and the physical properties of the materials used. These calculations are crucial to achieving the desired operating frequency and optimal performance for WBAN applications, specifically for on-body communication systems [11]. The antenna's design is tailored to function efficiently in the terahertz frequency band, specifically at 2.31 THz, which offers significant advantages in terms of data transmission speed and signal resolution, particularly for medical and health-monitoring applications.

$$w = \frac{3 \times 10^8}{2\,fr\left(\dfrac{\varepsilon_r + 1}{2}\right)^{0.5}} \tag{1}$$

$$L = \left(\frac{3 \times 10^8}{2f_r\left(\varepsilon_{eff}\right)^{0.5}}\right)10^6 - 2\delta l \tag{2}$$

$$\varepsilon_{eff} = \frac{\varepsilon_r + 1}{2} + \frac{\varepsilon_r - 1}{2}\left(1 + 12\frac{h}{w}\right)^{-0.5} \tag{3}$$

$$l = L - 2\delta L \tag{4}$$

$$Lg = l + 2L + 6h \tag{5}$$

$$Wg = w + 6h \tag{6}$$

Where, w : the width of the antenna, ε_r : the dielectric constant of the substrate used, f_r : the resonance frequency, h : height of the antenna, l : the length of the line, L_g : length of the substrate, and W_g : width of the substrate.

To ensure that the designed antenna operates effectively at the targeted frequency, we will utilize a matching technique referred to as the patch slate technique, as depicted in Figure 2. This approach is crucial for optimizing

the antenna's performance by enhancing impedance matching between the antenna and the feeding line. Impedance matching is essential in antenna design, as it minimizes signal reflections and maximizes the transfer of power from the feed line to the antenna, thereby improving overall efficiency.

(a)   (b)
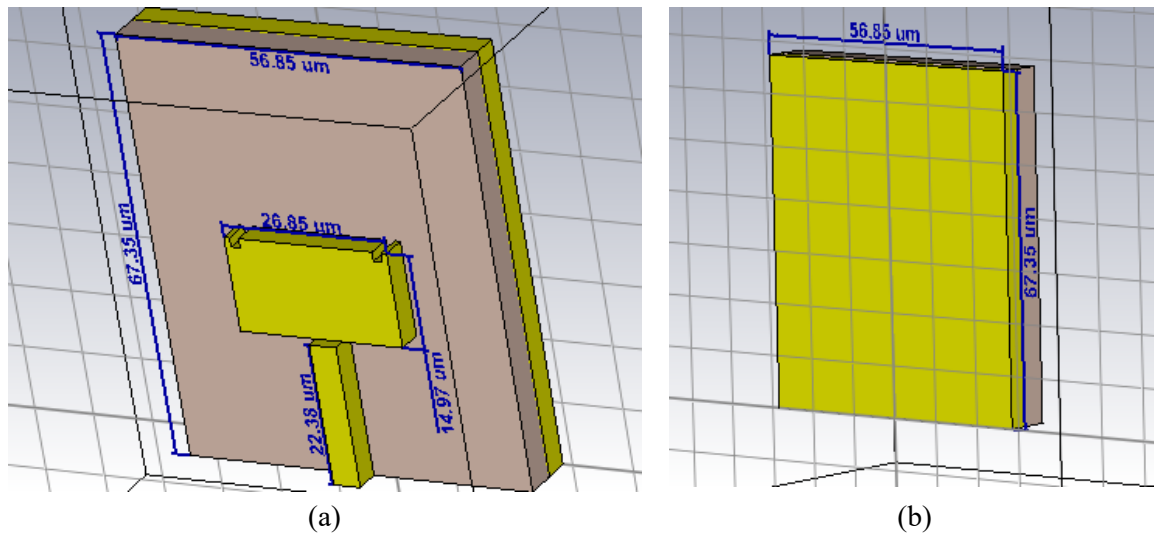
Figure 2. The rectangular gold patch antenna, (a) front view and (b) rear view

3. SIMULATION AND RESULT

3.1. Reflexion Coefficient S11

Figure 3 illustrates a reflection coefficient of -45.17 dB, along with a bandwidth of 94.326 GHz at a frequency of 2.31 THz. This indicates that the antenna exhibits excellent impedance matching at the target frequency, as a reflection coefficient of -45.17 dB signifies minimal signal reflection, allowing most of the input power to be effectively radiated. The substantial bandwidth of 94.326 GHz further highlights the antenna's capability to operate efficiently across a range of frequencies, which is advantageous for various applications in WBAN. This performance characteristic is critical for ensuring reliable communication and accurate monitoring of physiological parameters in medical settings.
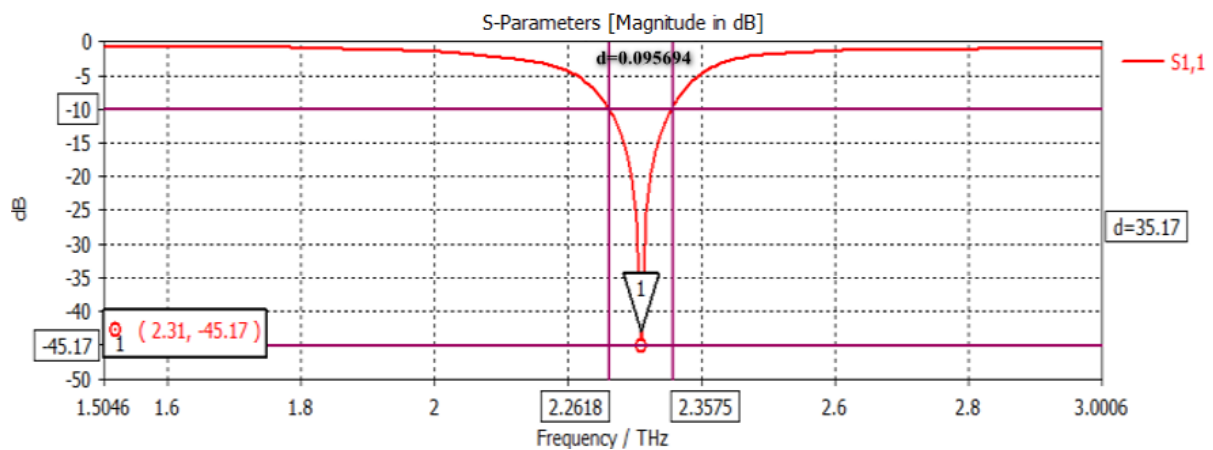
Figure 3. The reflexion coefficient S11 of proposed terahertz nano antenna

3.2. Radiation Pattern (Gain)

Figure 4 presents a gain value of 3.19 dB, demonstrating an omnidirectional radiation pattern at a frequency of 2.31 THz, as illustrated in Figure 2. This omnidirectional behavior indicates that the antenna radiates power uniformly in all horizontal directions, making it well-suited for applications where signal coverage is required across multiple angles. The gain of 3.19 dB signifies a moderate level of efficiency, indicating that the antenna effectively transmits and receives signals within its operational environment.

(a)

(b)
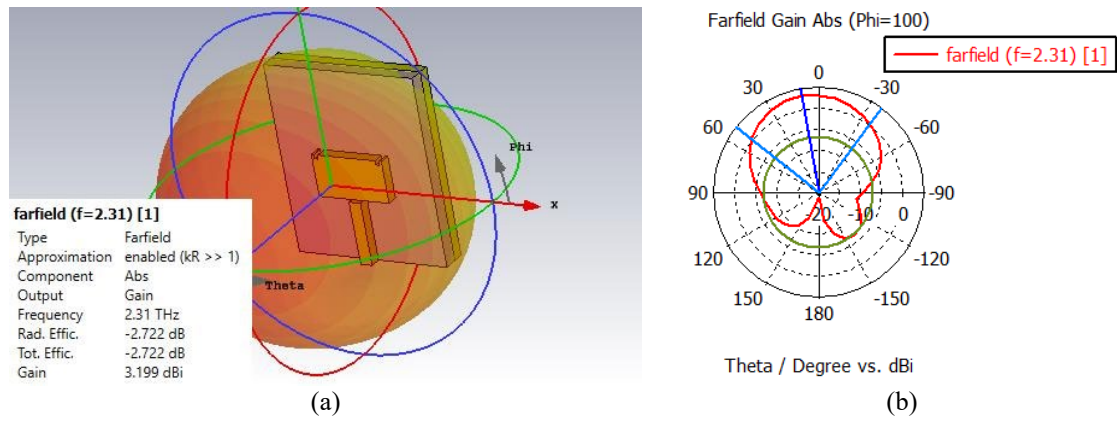
Figure 4. (a) 3D radiation pattern and (b) polar radiation pattern
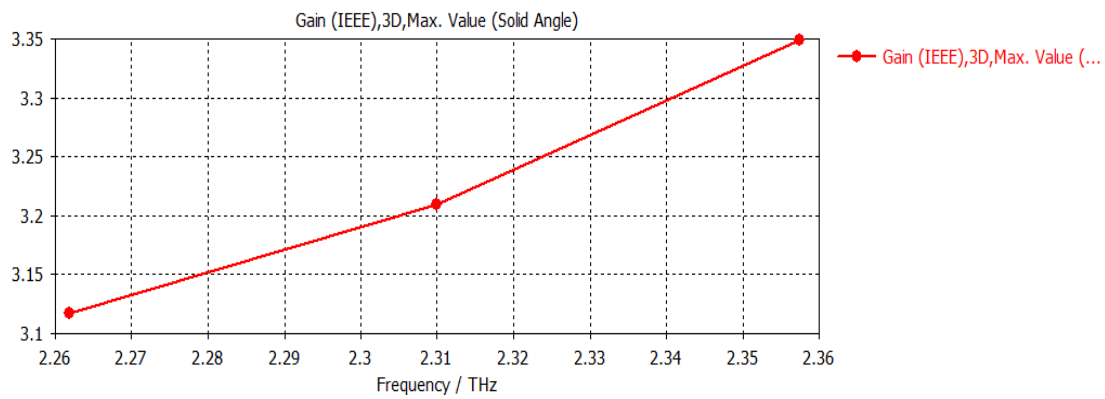
Figure 5. Gain of the proposed antenna

3.3. Voltage Standing Wave Ratio (VSWR)

The VSWR is measured to be less than 2, as depicted in Figure 6. A VSWR value below 2 indicates good impedance matching between the antenna and the transmission line, which is essential for minimizing signal reflections and ensuring efficient power transfer. This level of VSWR suggests that the antenna operates effectively within the desired frequency range, contributing to improved performance in applications such as WBAN. Maintaining a low VSWR is crucial for optimizing the antenna's functionality and enhancing its ability to accurately transmit and receive signals, which is particularly important in medical and health-monitoring contexts.
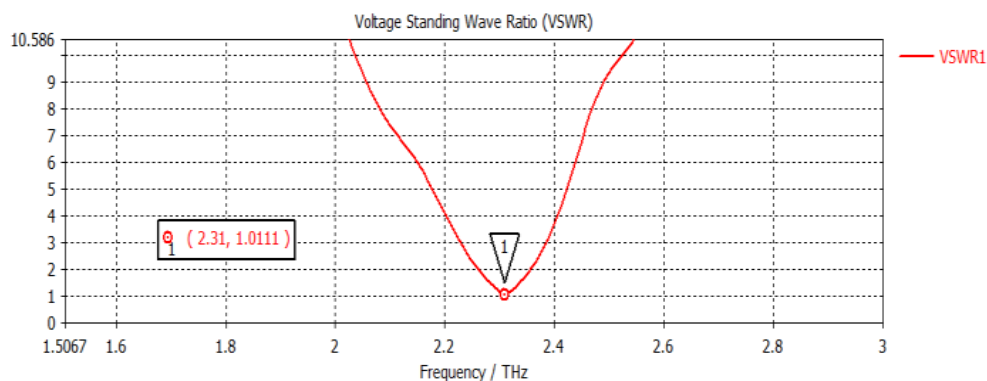
Figure 6. VSWR of our proposed antenna at frequency 2.31THz

3.4. Current Density

The current density of the proposed antenna is illustrated in Figure 7. This figure provides insight into the distribution of electrical current across the antenna's surface, highlighting areas of higher current concentration. Analyzing the current density is essential for understanding the antenna's performance characteristics, including its radiation efficiency and overall effectiveness. Regions with increased current density typically correlate with enhanced radiation and improved gain, which are vital for optimal operation at the desired frequency of 2.31 THz.

By evaluating the current density, we can further refine the antenna design to ensure efficient energy distribution, ultimately leading to better performance in WBAN applications and other related medical monitoring systems.
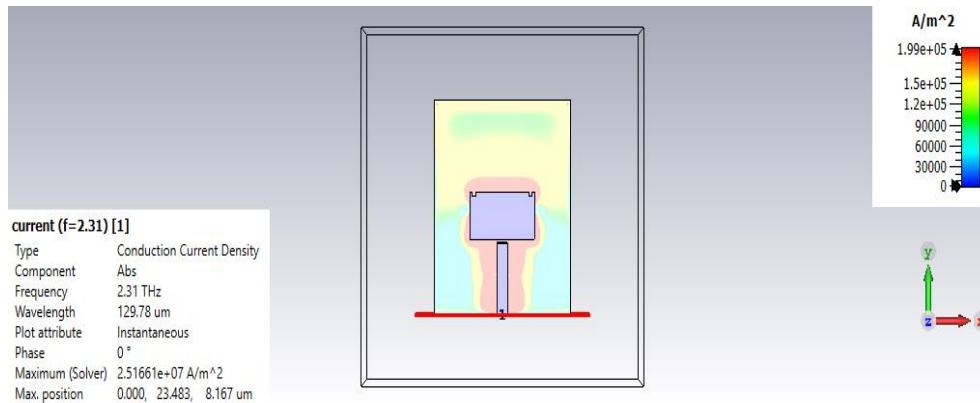
Figure 7. Current density of our proposed antenna at frequency 2.31THz

4. COMPARAISON RESULTS

A comparison between several results of research papers is given in Table 1:

Table 1. Comparison of proposed work with previous literatures

	fr (GHz)	S11 (dB)	Gain (dBi)
Proposed antenna	2310	-45.17	3.199
[12]	852	-20	2.5
[13]	2.45	-20.18	1.8
[14]	2.4	-26	2.5

Table 1 presents a comparison of various results from research papers, highlighting that the S11, gain, and directivity achieved in our proposed antenna design are superior to those reported in the referenced studies. Notably, these improvements are achieved with a significantly smaller antenna size, which enhances its suitability for integration onto the human body for WBAN applications. This compact design not only facilitates seamless integration but also ensures comfort for users, making it an ideal choice for continuous health monitoring and physiological parameter tracking in medical settings. The combination of excellent performance metrics and a small footprint underscores the potential of our antenna design in advancing WBAN technology.

5. CONCLUSION

In this paper, we utilized CST Microwave Studio simulation software to design a rectangular nano patch antenna with slots, employing gold as the material for both the patch and ground plane. The antenna operates at a frequency of 2.31 THz and exhibits a gain of 3.19 dBi, along with a reflection coefficient of -45 dB. These characteristics indicate that the proposed antenna delivers outstanding performance in terms of efficiency and signal quality. Additionally, its compact size facilitates easy integration onto the human body, making it well-suited for WBAN applications. The combination of excellent performance metrics and a small footprint highlights the potential of our antenna design for effective health monitoring and physiological parameter tracking in medical settings.

References

[1]   V. Das and S. Rawat, "Modified rectangular planar antenna with stubs and defected ground structure for THz applications," *Optik*, vol. 242, art. no. 167292, Sep. 2021, doi: 10.1016/j.ijleo.2021.167292.

[2]   M. Bouchra, S. Ferouani, and Z. K. Djalal, "Design of optical gold printed antenna in terahertz band for on body WBAN applications," *Microw. Rev.*, vol. 28, no. 1, pp. 9–13, 2022.

[3]   S. Mirhadi, "Single-layer, dual-port, and dual-mode antenna with high isolation for WBAN communications," *IEEE Antennas Wirel. Propag. Lett.*, vol. 21, no. 3, pp. 531–355, Mar. 2022, doi: 10.1109/LAWP.2021.3137961.

[4]   X. Tong, C. Liu, X. Liu, H. Guo, and X. Yang, "Switchable on-/off-body antenna for 2.45 GHz WBAN applications," *IEEE Trans. Antennas Propag.*, vol. 66, no. 2, pp. 967–971, 2018, doi:

10.1109/TAP.2017.2780984.

[5]   Fajr, A. Rajawat, and S. H. Gupta, "Design and optimization of THz antenna for onbody WBAN applications," *Optik*, vol. 223, art. no. 165563, Dec. 2020, doi: 10.1016/j.ijleo.2020.165563.

[6]   Y. Denizhan Sirmaci, C. K. Akin, and C. Sabah, "Fishnet based metamaterial loaded THz patch antenna," *Opt. Quantum Electron.*, vol. 48, no. 2, pp. 1–10, 2016, doi: 10.1007/s11082-016-0449-6.

[7]   M. Bouchra, F. Souheyla, K. DjalalZiani, and W. Moulessehoul, "Design of a novel nanometric graphene pentagone patch antenna array for terahertz transmission," in *2021 International Conference on Information Systems and Advanced Technologies (ICISAT)*, Tebessa, Algeria, 2022, doi: 10.1109/ICISAT54145.2021.9678495.

[8]   B. Moulfi, S. Ferouani, and D. Ziani Kerarti, "Wide band nano circular graphene printed antenna for terahertz transmission with DGS," *Telecommunications and Radio Engineering*, vol. 81, no. 2, pp. 37–48, 2022.

[9]   Y. He, Y. Chen, L. Zhang, S. W. Wong, and Z. N. Chen, "An overview of terahertz antennas," *China Commun.*, vol. 17, no. 7, pp. 124–165, 2020, doi: 10.23919/J.CC.2020.07.011.

[10]   S. Ebrahimi, "Microfluidic as liquid lens for THz reconfigurable antenna and gain enhancement with sensing application," *Optik*, art. no. 167705, Jul. 2021, doi: 10.1016/j.ijleo.2021.167705.

[11]   R. Bala and A. Marwaha, "Investigation of graphene based miniaturized terahertz antenna for novel substrate materials," *Eng. Sci. Technol. an Int. J.*, vol. 19, no. 1, pp. 531–537, 2016, doi: 10.1016/j.jestch.2015.08.004.

[12]   T. Khajawal, Q. Rubani, A. Rajawat, and S. H. Gupta, "Performance analysis and optimization of band gap of terahertz antenna for WBAN applications," *Optik.*, vol. 243, art. no. 167387, Oct. 2021, doi: 10.1016/j.ijleo.2021.167387.

[13]   U. Afruz, "Design of wearable microstrip patch antenna for wireless body area network," in *2021 24th International Conference on Computer and Information Technology (ICCIT)*, Dhaka, Bangladesh, 2021.

[14]   A. S. Sayem, R. B. V. B. Simorangkir, K. P. Esselle, A. Lalbakhsh, D. R. Gawade, B. O'Flynn, and J. L. Buckley, "Flexible and transparent circularly polarized patch antenna for reliable unobtrusive wearable wireless communications," *Sensors*, vol. 22, no. 3, art. no. 1276, Feb. 2022.

Slotted Miniature Patch Antenna for Wi-Fi 5 and Wi-Fi 6 Applications

Fatima Zahra Moussa[1], Souheyla Ferouani[1], Bouchra Moulfi[1]

[1]Dept. Electronic and Telecommunications, Ain Temouchent University, Ain Temouchent, Algeria
Corresponding author: Fatima Zahra Moussa (e-mail: moussafatima12@hotmail.com)

Abstract

This paper presents the design of a miniature dual-band hexagonal patch antenna for Wi-Fi 5/ Wi-Fi 6 applications. A rectangular slot has been incorporated into the ground plane to achieve miniaturization. The antenna demonstrates return losses of -24.22 dB at 5.2 GHz and -14.7 dB at 7.74 GHz, with corresponding bandwidths of 230 MHz and 390 MHz. The achieved gains are 2.6 dB and 3.2 dB, respectively. The overall antenna size has been reduced by 27.43%, from 32.22 x 48.13 mm² to 26.42 x 42.59 mm².

Keywords: Hexagonal patch antenna, Slot, Miniaturization, Wi-Fi 5, Wi-Fi 6

1. INTRODUCTION

In recent years, the telecommunications sector has benefited greatly from the technological progress. The needs for high-speed, high-reliability, and low-latency Wi-Fi communication are growing rapidly [1]. 802.11ac, also known as Wi-Fi 5, is a wireless network standard. It offers significant speed and performance improvements over its predecessor. Wi-Fi 5 operates in the 5 GHz frequency band and supports wider channels, enabling higher data transfer rates [2]. Therefore, the Wi-Fi 6 (the sixth generation of Wi-fi), also known as 802.11ax, is the latest generation of Wi-Fi technology. It was officially introduced in 2019 [3]. The Wi-Fi 6 cover a bandwidth of 5.925 GHz - 7.125 GHz, with 14 × 80 or 7 ×160 MHz channels similar to Wi-Fi 5 [4]. As Wi-Fi 6 became more widespread, new devices started supporting this standard, allowing users to take advantage of the enhanced performance, especially in busy environments like offices, public spaces, and smart homes with multiple connected devices [5].

The microstrip patch antenna is an electronic device consisting of a ground plane, a dielectric substrate and the radiating patch. Microstrip patch antennas have been widely used for many years, and offer a number of advantages and better prospects [6]. For many years now, microstrip patch antennas have been indispensable elements of any wireless communication system, thanks to their advantages and improved prospects [7]. In telecommunications, miniature antennas play a crucial role in our increasingly connected and portable world. They are designed to take up little space while maintaining efficient communication performance [8]. In order to meet the miniaturization requirements of mobile units, today's mobile communication system applications generally require smaller antennas, while reducing their size and improving their bandwidth is becoming a major design consideration for practical applications of microstrip antennas [9].The small volume, low profile, compact design and light weight of a miniature microstrip antenna make it easy to integrate with other devices, and it has a wide range of applications in many fields of technology [10]. These include wireless networks (Wi-Fi, LAN, and Bluetooth), satellite applications, cognitive radio systems, military applications, and global positioning system (GPS) [11]. there are several techniques for miniaturizing printed antennas, which are essential to make them suitable for integration into compact electronic devices and wireless devices [12], the most common ones are: Loading of high dielectric material in substrate of an antenna, using double-layered substrate in micro strip patch antenna [13], Introducing slots and modifications of the ground plane [14, 15], and use of metamaterials [16]. The need for smaller antennas with better performance is always present. These include miniaturized versions of various antenna types, including patch antennas, printed monopoles, planar inverted F-shaped antennas (PIFAs), among others [17].

In this paper, a new slotted bi-band hexagonal miniature microstrip patch antenna is proposed for Wi-Fi 5 and Wi-Fi 6 applications. The slot technique has been used to miniaturize the proposed hexagonal antenna with insertion of a rectangular-shaped slot on ground plane. The proposed antenna has an omnidirectional radiation pattern and covers the Wi-Fi 5 and Wi-Fi 6 bands (5 GHz to 7.97 GHz). The simulation results obtained are competitive with those described in the literature.

2. ANTENNA DESIGN

The printed hexagonal antenna shown in the Figure 1 is designed on a Rogers RT-5880 ($\varepsilon r = 2.2$) substrate of 1.75 mm thickness, using CST MWS software. The antenna is fed by microstrip line feed in order to resonate at 5.2 GHz for Wi-Fi 5/Wi-Fi 6 applications. The dimensions of our proposed antenna are shown in Table 1.
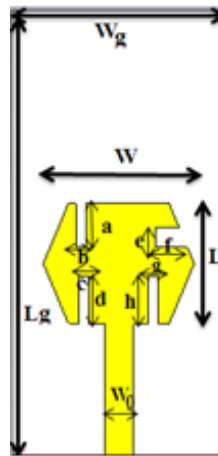
Figure 1. Proposed hexagonal antenna

Table 1. Dimension of the hexagonal proposed antenna

Parameters	Dimensions
W	22.8 mm
L	18.54 mm
Wg	32.22 mm
Lg	48.13 mm
W0	4.3 mm
a	4.5 mm
b, c, g	1.5 mm
d, h	7.5 mm
e	3 mm
f	3.85 mm

Figure 2 shows the result of simulation in term of return loss which gives a value of -32.59 dB at 5.2 GHz. Voltage standing wave ratio (VSWR) is presented by Figure 3 with value around 1.04 which is very satisfactory.
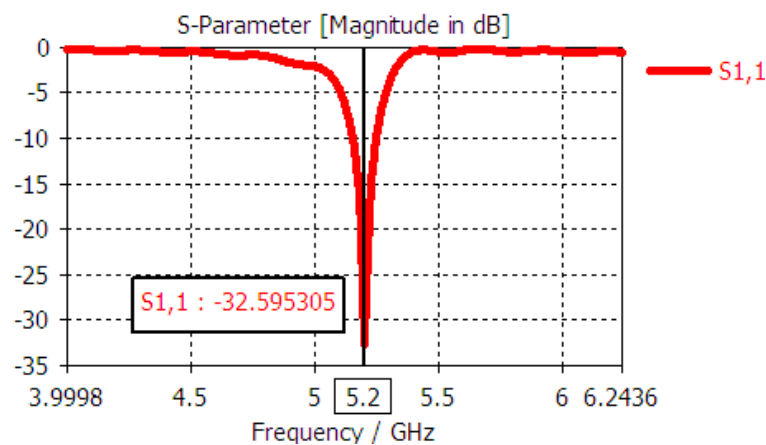
Figure 2. Return loss of the hexagonal proposed antenna
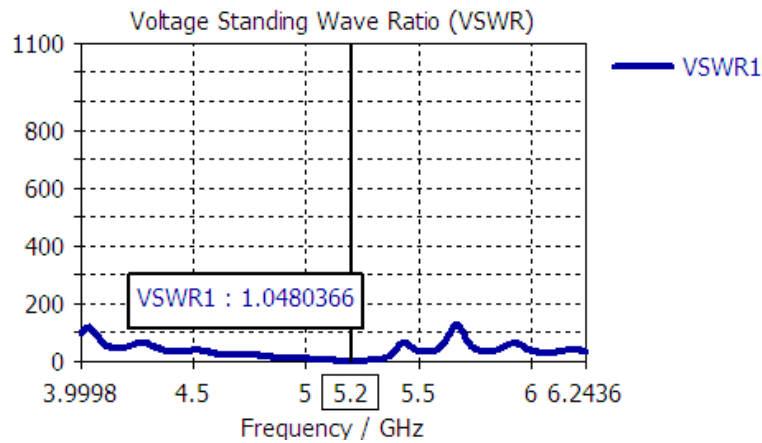
Figure 3. VSWR of the hexagonal proposed antenna

The Figure 4 shows the gain of the hexagonal proposed antenna with the value of 4.84 dB at 5.2 GHz resonant frequency. Then Figure 5 presents the radiation pattern which is quasi-omnidirectional.
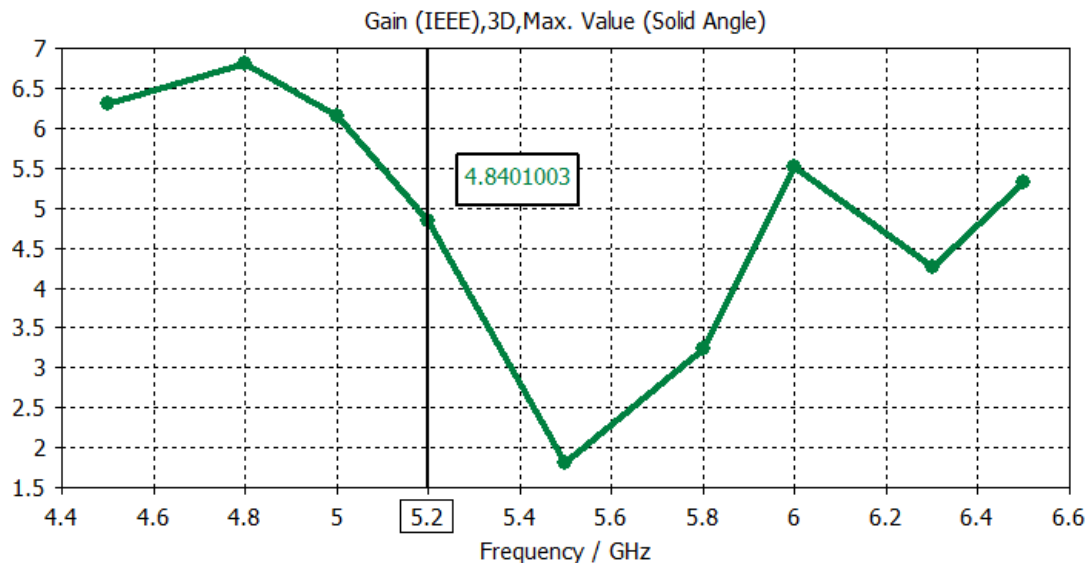
Figure 4. The gain of the hexagonal proposed antenna

| (a) | (b) | (c) |
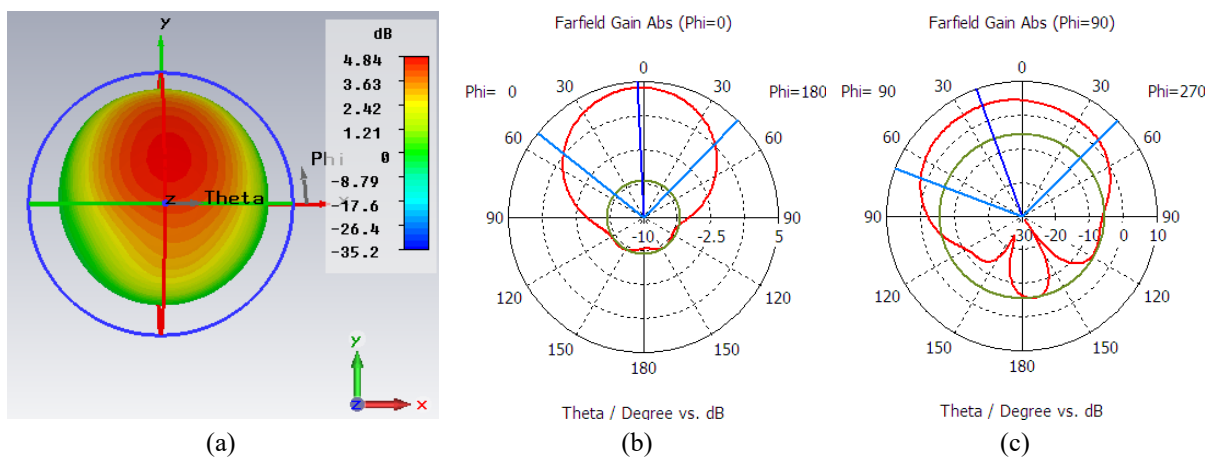
Figure 5. Radiation pattern of the hexagonal proposed antenna: (a) 3D, (b) polar, and (c) polar

3. MINIATURE ANTENNA

In order to miniature our hexagonal antenna size, slotted technique is used. We inserted a rectangular shaped-form on ground plane. The finale geometry is shown by Figure 6 and its dimensions are presented in Table 2. Several

parametric studies have been carried out on the variation in patch width and length, these results are presented in Figure 7.

(a)   (b)
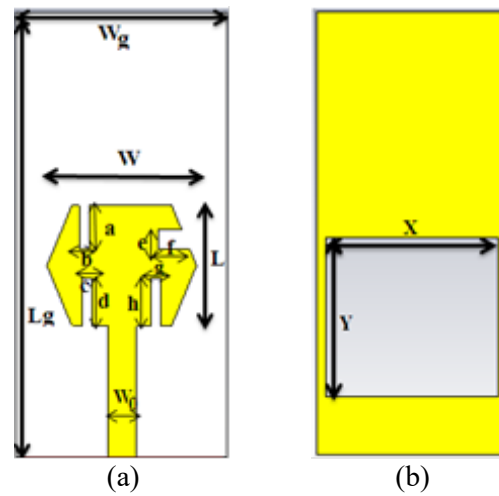
Figure 6. The slotted miniature hexagonal antenna, (a) top view, (b) bottom view

Table 2. Final dimensions of miniature hexagonal antenna

Parameters	Dimensions
W	17 mm
L	14 mm
Wg	26.42 mm
Lg	42.59 mm
W0	4.3 mm
a	4.5 mm
b, c, g	1.5 mm
d, h	7.5 mm
e	3 mm
f	3.85 mm
X	24 mm
Y	22.15 mm
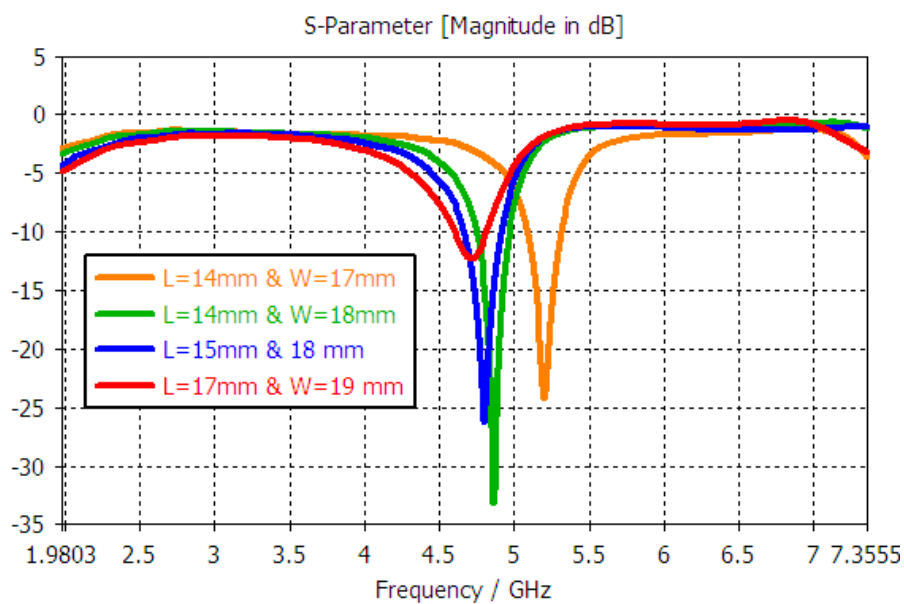
Figure 7. Width and length variation

The return loss of slotted antenna after simulation is shown in Figure 8. It was observed that antenna operated at 2 different frequency 5.2 GHz and 7.74 GHz. The miniature hexagonal antenna exhibited return loss of -24.22 dB and -14.7 dB respectively. A bandwidth around 250 MHz and 390 MHz are obtained which is satisfactory for Wi-Fi 5 and Wi-Fi 6 applications.
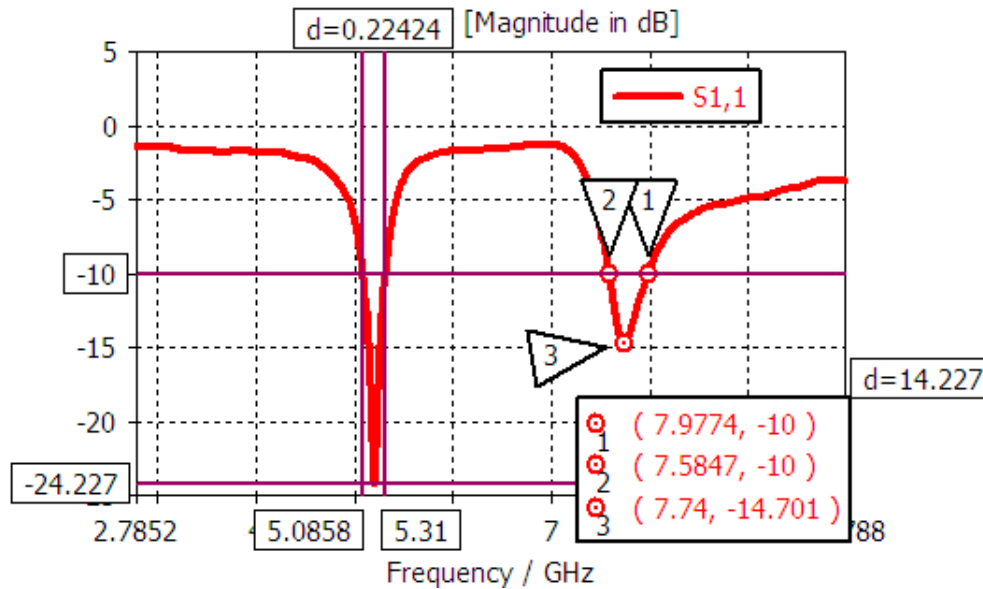
Figure 8. Return loss of the slotted hexagonal miniature antenna based on the slot technique at resonant frequencies 5.2 GHz and 7.74 GHz respectively

The VSWRs of slotted hexagonal miniature antenna obtained after simulations are shown in Figure 9. It has a value of 1.13 and 1.45 for 5.2 GHz and 7.74 GHz respectively.
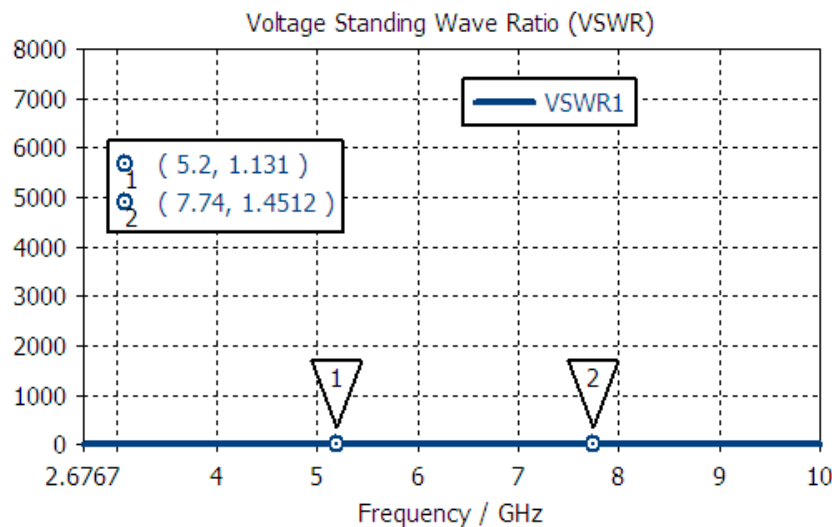
Figure 9. VSWRs of the slotted hexagonal miniature proposed antenna at resonant frequencies 5.2 GHz and 7.74 GHz respectively

The simulated Gains of slotted hexagonal miniature antenna are as shown in the Figure 10. From simulated plot it was observed that Gains of the miniature hexagonal antenna are about 2.6 dB and 3.2 dB at the operating frequencies of 5.2 GHz and 7.74 GHz respectively which is very satisfactory for Wi-Fi applications.

Three-dimensional and Two-dimensional radiation patterns of slotted miniature hexagonal antenna after simulation are shown in Figures 11 and 12. we obtained and omnidirectional radiation patterns which is very satisfactory for Wi-Fi 5 and Wi-Fi 6 applications.
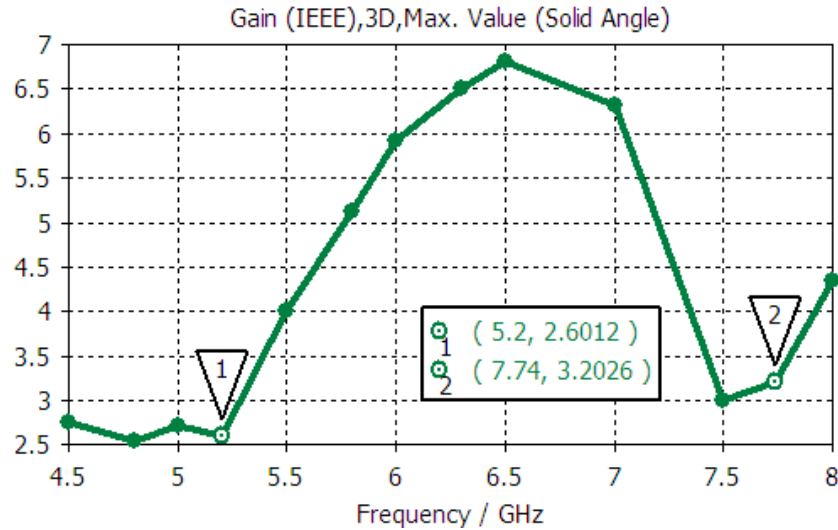
Figure 10. The gains of the slotted hexagonal miniature antenna at resonant frequencies 5.2 GHz and 7.74 GHz respectively

(a)   (b)   (c)
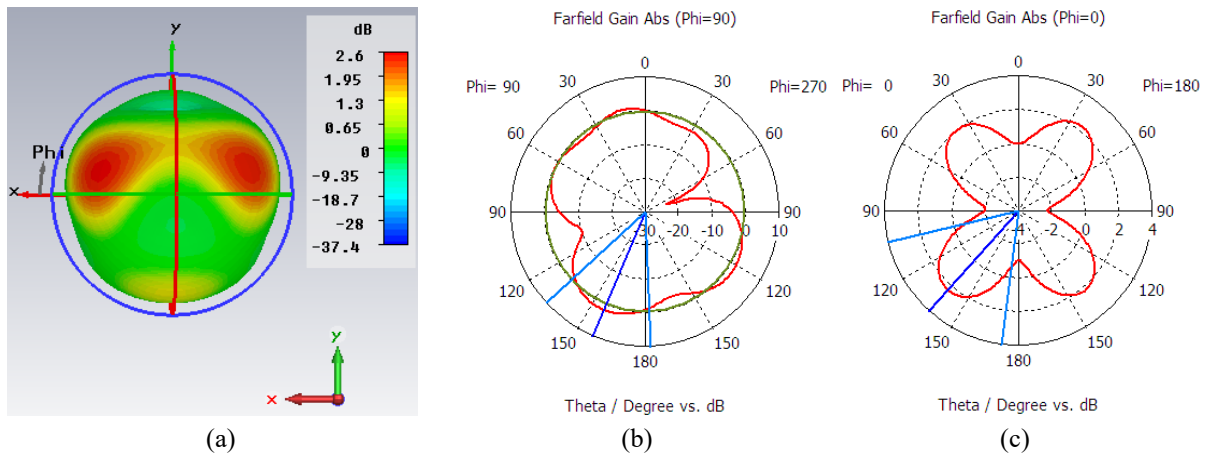
Figure 11. Radiation pattern of the hexagon proposed antenna: (a) 3D, (b) polar, and (c) polar at the resonant frequency 5.2 GHz

(a)   (b)   (c)
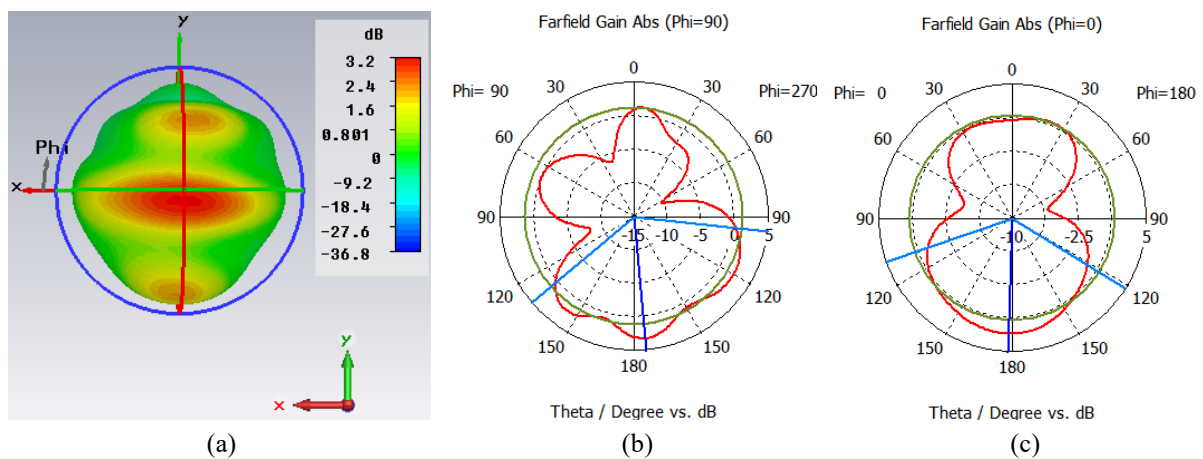
Figure 12. Radiation pattern of the hexagon proposed antenna: (a) 3D, (b) polar, and (c) polar at the resonant frequency 7.74 GHz

4. CONCLUSION

In the present paper, a miniature hexagon-shaped patch antenna fed by a microstrip line feed, has been investigated. The antenna has a dimension of 26.42 x 42.59   etched on a Roger RT-5880 type substrate with a relative

permittivity of 2.2. CST MWS software was used to simulate parameters such as reflection coefficient, gain, and radiation pattern, which present satisfactory results. The proposed antenna exhibits a dual wideband; the first band operates at 5.2 GHz while the second one operates at 7.74 GHz covering Wi-Fi 5/ Wi-Fi 6 applications. The qualified miniaturized slot antenna is a suitable solution for Wi-Fi 5/Wi-Fi 6 applications.

To take this work a step further, practical fabrication and measurements are required to validate these results. Also, improvements can be made such as improving the gain by designing an antenna array to make the antenna suitable for all available Wi-Fi bands.

References

[1]   Y. M. Al Hyasat, Y. S. Faouri, and D. Abualnadi, "Multi-function dual UWB patch antenna for modern communications," in *Int. Telecommun. Conf. ITC-Egypt 2022 - Proc.*, 2022, pp. 1–4, doi: 10.1109/ITC-Egypt55520.2022.9855695.

[2]   Y. M. Hyasat, D. Abualnadi, and Y. S. Faouri, "Two elements ultra wideband MIMO antenna for 5G communications, WiFi-5 and WiFi-6 applications," in *14th Int. Conf. Commun. COMM 2022 - Proc.*, 2022, vol. 1, pp. 1–4, doi: 10.1109/COMM54429.2022.9817255.

[3]   C. Min and Z. Jinhao, "The application of WiFi 6 technology in underground mine," *IOP Conf. Ser. Earth Environ. Sci.*, vol. 687, no. 1, art. no. 012153, 2021, doi: 10.1088/1755-1315/687/1/012153.

[4]   W. C. Jhang and J. S. Sun, "Small antenna design of triple band for wifi 6E and wlan applications in the narrow border laptop computer," *Int. J. Antennas Propag.*, vol. 2021, no. c, pp. 4–11, 2021, doi: 10.1155/2021/7334206.

[5]   Y. M. Al Hyasat, Y. S. Faouri, D. I. Abualnadi, and M. K. Abdelazeez, "Two element UWB array antenna for 5G communications, WiFi-5 and WiFi-6 applications," in *2022 IEEE Int. Symp. Antennas Propag. Usn. Radio Sci. Meet. AP-S/URSI 2022 - Proc.*, 2022, no. 1, pp. 1048–1049, doi: 10.1109/AP-S/USNC-URSI47032.2022.9886746.

[6]   F. Mahbub, S. B. Akash, S. A. K. Al-Nahiun, R. Islam, R. R. Hasan, and M. A. Rahman, "Microstrip patch antenna for the applications of wlan systems using S-band," in *2021 IEEE 11th Annu. Comput. Commun. Work. Conf. CCWC 2021*, 2021, pp. 1185–1189, doi: 10.1109/CCWC51732.2021.9376114.

[7]   N. Sharma, B. Jain, P. Singla, and R. R. Prasad, "Rectangular patch microstrip antenna: A survey," *Int. Adv. Res. J. Sci. Eng. Technol.*, vol. 1, no. 3, pp. 144–147, 2014.

[8]   A. Kaur, G. Singh, and M. Kaur, "Miniaturized multiband slotted microstrip antenna for wireless applications," *Wirel. Pers. Commun.*, vol. 96, no. 1, pp. 441–453, 2017, doi: 10.1007/s11277-017-4177-4.

[9]   S. Rathod, A. Shah, D. Rathod, M. Dhakane, and P. Deosarkar, "Dual band slotted hexagonal microstrip antenna," in *Proc. - 1st Int. Conf. Comput. Commun. Control Autom. ICCUBEA 2015*, 2015, pp. 220–222, doi: 10.1109/ICCUBEA.2015.211.

[10]   J. Prasojo and R. Sarno, "Hexagonal patch microstrip antenna with parasitic element for vehicle communication," in *Proc. - 2020 Int. Semin. Appl. Technol. Inf. Commun. IT Challenges Sustain. Scalability, Secur. Age Digit. Disruption, iSemantic 2020*, 2020, pp. 340–345, doi: 10.1109/iSemantic50169.2020.9234242.

[11]   I. Singh and V. S. Tripathi, "Micro strip patch antenna and its applications: A survey," *International Journal of Computer Applications in Technology*, vol. 2, no. 5, pp. 1595–1599, 2011.

[12]   A. A. Rakholiya and N. V Langhnoja, "A review on miniaturization techniques for microstrip patch antenna," *International Journal of Advance Research and Innovative Ideas in Education*, no. 2, pp. 4281–4287, 2017.

[13]   D. Upadhyay and R. P. Dwivedi, "Antenna miniaturization techniques for wireless applications," in *IFIP Int. Conf. Wirel. Opt. Commun. Networks (WOCN)*, 2014, pp. 1–4, doi: 10.1109/WOCN.2014.6923083.

[14]   T. Aathmanesan, "Novel slotted hexagonal patch antenna for sub-6 GHz 5G wireless applications," *Ictact J. Microelectron.*, vol. 6, no. 4, pp. 1010–1013, 2021, doi: 10.21917/ijme.2021.0176.

[15]   F. Z. Moussa, S. Ferouani, Y. Belhadef, and G. Abdellaoui, "New design of miniature rectangular patch antenna with DGS for 5G mobile communications," in *Proc. - 2021 Int. Conf. Inf. Syst. Adv. Technol. ICISAT 2021*, 2021, no. 4, pp. 1–5, doi: 10.1109/ICISAT54145.2021.9678464.

[16]   F. Z. Moussa, S. Ferouani, and Y. Belhadef, "New design of metamaterial miniature patch antenna with dgs for 5G mobile communications," *Microw. Rev.*, vol. 28, no. 2, pp. 9–16, 2022.

[17]   M. U. Khan, M. S. Sharawi, and R. Mittra, "Microstrip patch antenna miniaturisation techniques: A review", *IET Microw. Antennas Propag.*, 2015, vol. 9, no. 9, pp. 913–922, doi: 10.1049/iet-map.2014.0602.

Machine Learning Based Weather Type Classification

Mustafa Alptekin Engin[1], Latif Akcay[1]

[1]Department of Electrical and Electronics Engineering, Bayburt University, Bayburt, Türkiye
Corresponding author: Mustafa Alptekin Engin (e-mail: maengin@bayburt.edu.tr)

Abstract

The accurate classification of weather types is of paramount importance in a multitude of fields, including transportation, agriculture, and disaster management. This study assesses the potential of machine learning in classifying weather types using a synthetic and balanced dataset comprising 13,200 samples across four distinct weather categories. The four weather types are defined as follows: Rainy, Sunny, Cloudy and Snowy. The findings demonstrate the potential of synthetic data augmentation to address real-world dataset imbalances and enhance model generalisation. Among the various machine learning architectures employed, the Ensemble Bagged Tree (EBT) classifier was identified as the most effective method, attaining a test accuracy of 91.9%. This substantiates the efficacy of ensemble methods in processing high-dimensional meteorological data. Furthermore, comparative analyses with other models demonstrate the resilience of the advanced algorithms in handling non-linear feature relationships.

Keywords: Weather type classification, Machine learning, Ensemble bagged tree

1. INTRODUCTION

The accurate forecasting of weather types is of paramount importance in a plethora of sectors, including but not limited to daily activities, transportation, agricultural practices, and disaster management. The early and accurate modelling and classification of weather provides numerous benefits, including the ability to take necessary precautions in various areas and to enhance the decision-making process [1]. Traditional weather forecasting, which is based on expert-driven physical models and has a high computational workload, is an effective method, but it is challenging due to the necessity of considering numerous parameters [2]. Concurrently with developments in data science, machine learning is emerging as a highly effective tool for addressing problems characterised by large-scale and high-dimensional data. In recent years, machine learning algorithms have been employed with increasing frequency to enhance the process of weather forecasting without the need for human intervention [3]. This approach enables the discovery of relationships between parameters that are difficult to detect, thus facilitating the attainment of successful results in the weather forecasting process [4]. However, the performance of machine learning-based classifiers is adversely affected by the limited and unstable real-world meteorological data. To address this challenge, it is possible to enhance the precision of forecasts for infrequent meteorological occurrences by enabling models to be trained on a more extensive and balanced data set through the utilisation of synthetic databases. The use of synthetic data is also endorsed in the literature as a means of overcoming the imbalanced dataset problem and improving model performance [5]. In this study, we utilise a synthetically generated database to simulate weather data, with the objective of investigating classifier performance on machine learning using a database comprising a total of 13,200 instances, distributed across four different weather labels: Rainy, Sunny, Cloudy, and Snowy [6]. The database contains an equal number of data points for each weather condition. Among the different machine learning-based methods used, the Ensemble Bagged Tree classifier achieved an accuracy of 91.9%. Therefore, while the study demonstrates the potential of synthetic databases in weather forecasting, it also emphasises the adaptability of machine learning algorithms to different data types. In this context, the findings are in line with similar studies in the literature [7, 8].

2. MATERIAL AND METHOD

A visual representation of the study's process stages is provided in Figure 1.

Figure 1. Process steps of the presented method

2.1. Dataset

In this study, the publicly available Weather Type Classification dataset, obtained through Kaggle, a sharing platform for machine learning and related applications, was used [6]. The variables in the database are described in Table 1 and include temperature, humidity, wind speed, precipitation, cloud cover, atmospheric pressure, ultraviolet (UV) index, season, visibility and weather type. The total number of cases in the database for which these values are mentioned is 13,200.

Table 1. Variables in the database and their descriptions

Variable	Data Type	Description
Temperature	Numeric	The temperature is expressed in degrees centigrade, with values ranging from extremely cold to extremely hot.
Humidity	Numeric	Percent moisture in air
Wind speed	Numeric	The wind speed is expressed in kilometres per hour.
Precipitation	Numeric	The proportion of precipitation in a given area is expressed as a percentage.
Cloud cover	Categorical	A description of the cloud cover (clear, cloudy, overcast, partly cloudy).
Atmospheric pressure	Numeric	Atmospheric pressure expressed in hectopascals (hPa)
UV index	Numeric	The ultraviolet (UV) index is a measure of the strength of ultraviolet radiation.
Season	Categorical	The season during which the data were generated is indicated (spring, autumn, winter, summer)
Visibility (km)	Numeric	The visibility in kilometres is indicated, including values that are either very low or very high.
Location	Categorical	This denotes the geographical position where the data was obtained (coastal, mountain, inland).
Weather type	Categorical	The target variable for classification is indicative of the prevailing meteorological conditions (cloudy, rainy, sunny, snowy).

Figure 2 provides a visual representation of the percentage and amount of data in the categorical columns of the database. In advance of further analysis, the categoric data stored within the database were transformed into numerical values.
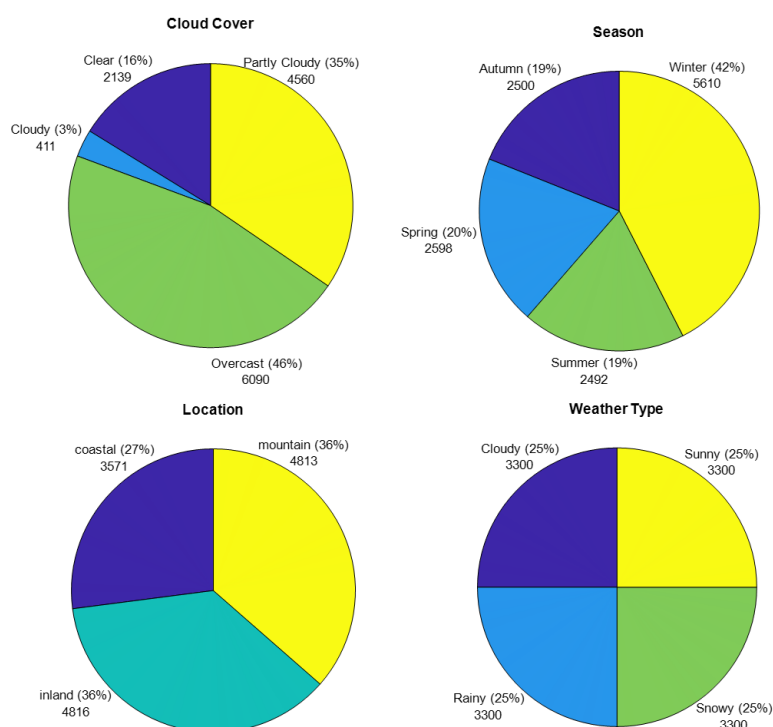
Figure 2. Distribution of categorical data in the database

2.2. Classification Process

The initial stage of the study entails the division of the data set into two distinct subsets, with the first subset comprising 90% of the data and the second subset comprising 10%. These subsets will be utilized in the subsequent training and testing phases, respectively. Subsequently, a variety of machine learning-based classification models were developed through the utilisation of the 10-fold cross-validation approach. These models included the Ensemble Bagged Tree (EBT), Trilayered Neural Network (TNN), Cubic Support Vector Machine (Cubic SVM), Naïve Bayes (NB), Fine K-Nearest Neighbours (KNN), Quadratic Discriminant (QDA), and Linear Discriminant Analysis (LDA). Subsequently, the efficacy of the derived classification models was assessed utilising test data. The data employed for the purposes of training the model were not subsequently utilised for testing purposes, thereby ensuring that the evaluation was conducted in a blind and fair manner. Then, in order to compare the performance of the obtained models, the confusion matrix and the accuracy value obtained from this matrix were calculated.

Table 2. Confusion matrix

Confusion Matrix		Actual	
		Positive	Negative
Prediction	Positive	True Positive (TP)	False Positive (FP)
	Negative	False Negative (FN)	True Negative (TN)

The confusion matrix, as detailed in Table 2, represents the actual and predicted label values in relation to each other. The calculation of the classification accuracy using this matrix is presented in Equation 1. The accuracy of a classification model can be calculated as the ratio of the sum of correctly predicted values to the total number of predictions. This metric is both successful and sufficient for comparison on a balanced database.

$$Accuracy = \frac{TP + TN}{TP + TN + FP + FN} \tag{1}$$

3. RESULTS

The validation and test accuracy values of the classification methods employed in the study are presented in Table 3. The EBT classifier was identified as the most effective method in both the validation and test phases.

Table 3. Comparison of different classification methods

Method	Validation Accuracy	Test Accuracy
EBT	91.2	91.9
TNN	90.9	91.1
Cubic SVM	90.4	90.9
NB	89.9	90.0
Fine KNN	89.4	89.4
QDA	88.0	88.3
LDA	83.7	83.0

The validation and test confusion matrices of the EBT classifier, which is the most successful method for classifying cloudy, rainy, sunny, and snowy weather conditions, are presented in Figure 3. In these matrices, the value 1 corresponds to cloudy conditions, 2 to rainy conditions, 3 to snowy conditions, and 4 to sunny conditions.
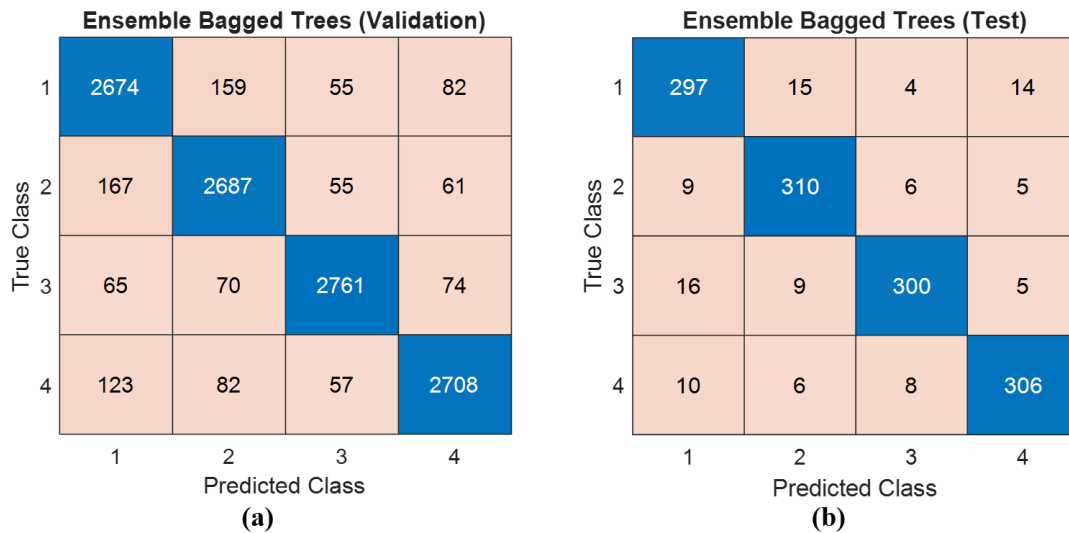
Figure 3. Confusion matrix of the EBT classifier: (a) Validation and (b) test

The receiver operating characteristic (ROC) curves, which illustrate the true positive rate (TPR) in relation to the false positive rate (FPR), are presented in Figure 4. These curves have been generated using the test results of the EBT classifier and represent the true positive rate versus the false positive rate for different classification score thresholds. The area under the curve (AUC) value is defined as the integral of a ROC curve with respect to the FPR between 0 and 1. The AUC value in the range 0 to 1 is a measure of the overall quality of the classifier, with large values indicating successful classifier performance.
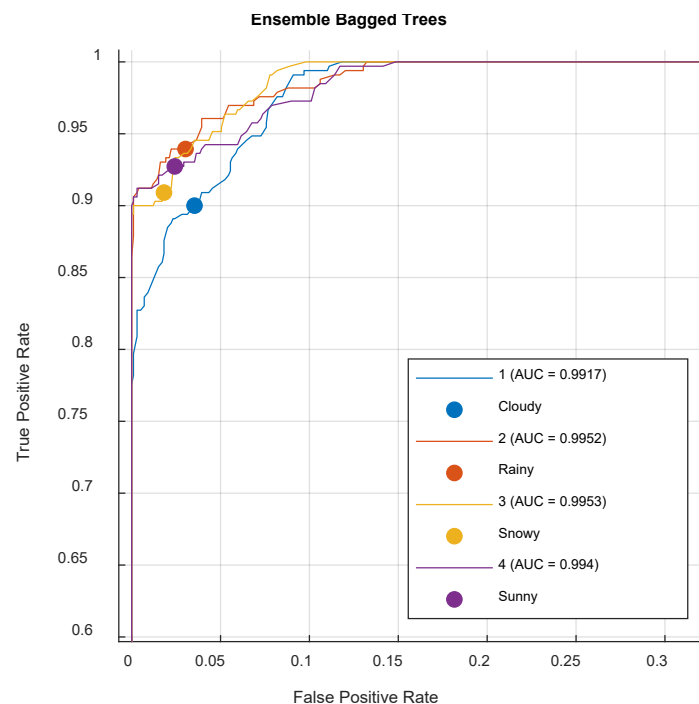
Figure 4. ROC curves of the test results of the EBT classifier

4. CONCLUSION

This study explores the application of machine learning for the classification of weather types, utilising a range of algorithms and evaluating their performance across validation and test datasets. The Ensemble Bagged Trees (EBT) method demonstrated the highest accuracy among the examined models, achieving 91.2% accuracy on the validation set and 91.9% on the test set. This serves to illustrate the efficacy of ensemble methods in discerning intricate patterns within the data and their capacity to generalise effectively to samples that have not been previously observed. Furthermore, the Tri-Layered Neural Network (TNN) and Cubic SVM models exhibited

comparable performance, attaining accuracies of 91.1% and 90.9%, respectively, on the test set. These findings indicate that neural networks and support vector machines may offer a viable alternative to ensemble methods, particularly when considering computational resources and scalability. Conversely, more straightforward models such as Naive Bayes (NB) and Linear Discriminant Analysis (LDA) demonstrated comparatively lower accuracy. This suggests that the relationships between features and weather classes are likely to be non-linear, necessitating the use of more sophisticated techniques for effective modelling. The confusion matrices for both the validation and test sets demonstrated that the majority of classification errors occurred between similar weather types, such as "Rainy" and "Snowy." This indicates the necessity for additional feature engineering to more effectively differentiate between these overlapping classes. The receiver operating characteristic (ROC) analysis confirmed the model's strong discriminative ability, with all classes achieving an area under the curve (AUC) value above 0.99, thereby further validating the robustness of the proposed approach. In conclusion, the findings of this research demonstrate that ensemble-based methods, such as EBT, provide a reliable solution for weather type classification tasks, achieving a fine balance between accuracy and generalisation. Further work could concentrate on optimising the hyperparameters of these models, incorporating additional features and exploring ensemble combinations of top-performing models with a view to enhancing classification performance. Furthermore, the utilisation of larger and more diverse datasets could serve to mitigate class overlap and enhance overall robustness.

References

[1]   J. Hidalgo and R. Jougla, "On the use of local weather types classification to improve climate understanding: An application on the urban climate of Toulouse," *PLoS One*, vol. 13, no. 12, art. no. e0208138, 2018.

[2]   T. Weusthoff, "Weather Type Classification at MeteoSwiss - Introduction of new automatic classifi-cations schemes," *Arbeitsberichte der MeteoSchweiz*, vol. 46, 2011.

[3]   M. Safia, R. Abbas, and M. Aslani, "Classification of weather conditions based on supervised learning for Swedish cities," *Atmosphere (Basel)*, vol. 14, no. 7, art. no. 1174, 2023.

[4]   M. AbdulRaheem, J. B. Awotunde, A. E. Adeniyi, I. D. Oladipo, and S. O. Adekola, "Weather prediction performance evaluation on selected machine learning algorithms," *IAES Int. J. Artif. Intell. (IJ-AI)*, vol. 11, no. 4, art. no. 1535, 2022.

[5]   N. V. Chawla, K. W. Bowyer, L. O. Hall, and W. P. Kegelmeyer, "SMOTE: Synthetic minority over-sampling technique," *J. Artif. Intell. Res.*, vol. 16, pp. 321–357, 2002.

[6]   N. Narayan, (2024, Jun. 23). "Weather Type Classification," *Forecast with Precision: Simulated Data for Predicting Weather Types* [Online]. Available: https://www.kaggle.com/datasets/nikhil7280/weather-type-classification/data. [Accessed: 2024, Nov. 30].

[7]   S. Wadhwa and R. G. Tiwari, "Machine learning-based weather prediction: A comparative study of regression and classification algorithms," in *2023 International Conference in Advances in Power, Signal, and Information Technology (APSIT)*, 2023.

[8]   I. Oshodi, "Machine learning-based algorithms for weather forecasting," *International Journal of Artificial Intelligence and Machine Learning*, vol. 2, no. 2, pp. 12–20, 2022.

A Historiography Study: Sudanese Historians During and After the Anglo-Egyptian

Maab Ahmed[1]

[1]Humanities Department, Yildiz Technical University, Istanbul, Türkiye
Corresponding author: Maab Ahmed (e-mail: maabbaldo@gmail.com)

Abstract

Currently, Sudan is passing through a pivotal historical period that will reshape society and individual structure, and this will require us to reread the history and investigate it, to be able to convey and write the present events accurately for future generations. Sudanese historians during and after the era of the Anglo-Egyptian occupation from 1899 to 1970 will be examined in this research paper by drawing attention to their historical background, sources, and methodologies, focusing on prominent historians and their perspectives. The researcher argues that by knowing the historical writing methods they had followed and their deficiencies and understanding the historiography of this occupation, historians will be able to convey the long-lasting repercussions of colonialism on people, to reflect it on the country's future development. To conclude that Sudanese historians were exceedingly influenced by their political and religious backgrounds, which clearly impacted their methods of documenting events. The research urges that in order to achieve a philosophical, methodical and intellectual rigorous level of historical writing in Sudan's history, intellectuals and historians should transcend the dilemma imposed upon them since the colonial period. Sudanese historians are also required to acknowledge and accept the culture of others while renewing the vision of authenticity and tradition in a contemporary manner.

Keywords: Sudan, Historians, Dilemma, Colonialism, Historiography

1. INTRODUCTION

The Political, and economic aspects and strategic location of Sudan were the main reasons behind the Anglo-Egyptian occupation of Sudan. The majority of historians agree that historical events cannot be traced to a single cause and should be many [1], during that period Britain and Egypt interests emerged in this region for numerous reasons that led to the colonization of Sudan [2]. The British and Egyptian authorities sought to retake control of the area after the Mahdist rebellion in Sudan in the late 19th century from 1881 to 1885, which was an uprising due to taxes imposed by the Turco-Egyptian rule, and it was the first national religious revolution that reformed public opinion against the occupier in Sudan [3]. Britain sought to protect its strategic interests in Africa, preserve trade lines to the East, and maintain its control over the Nile waterways due to its imperial aspirations [4, 5] they aimed to secure dominance over this vital resource and protect their own interests. The shared interests between both nations were a mutually reinforcing reason for Sudan's establishment of a strategic presence and its economic potential [6]. One of the compelling factors for both colonial powers was the endowment of abundant resources and fertile lands. The potential for economic growth through resource extraction and agricultural development was an attractive reason for British and Egyptian interests [7]. As a result of that agreement by Britain and Egypt, Sudan was transformed into a condominium with shared political and administrative duties between Britain and Egypt in 1899. Britain continued to hold a large amount of power over Sudan's affairs as a senior partner, while Egypt was still seen as a secondary partner. Especially regarding security and finances because at the same time Egypt was a British colony, and the Egyptian motivation to participate in the Sudan occupation was to maintain control over the Nile and its headwaters [8]. By putting its hands in Sudan, Egypt sought to keep its rights from the River Nile, Britain extended its influence in the entire Nile Valley to fulfill Egyptian's requirements and to keep the Suez Canal in Egypt, without allowing the other European great powers to intervene. Coupled with keeping all Red Sea coasts in Sudan and Egypt into its power and accomplishing its empire [9].

Thus, rereading the historical background and reasons behind the Anglo-Egyptian occupation will help us for better interpretation of the dynamics of power and resistance at this time in Sudanese history. The objective of this paper is to examine how historical documents and narrative stories of the Anglo-Egyptian occupation in the Sudan have been interpreted by utilizing both primary and secondary sources. Regarding the historical frame, this study will primarily concentrate on the role of historians and their deficiencies in the period of Anglo-Egyptian occupation in Sudan and after, from 1899 to 1970. Furthermore, it attempts to track the development of historical

perspectives to comprehend how many historians have affected our understanding of the occupation through their study and analysis. Methodologically, the historiography of the Anglo-Egyptian occupation period and after will be analyzed and evaluated, using a historical methodology that requires assessing primary sources which include Archives, government records, letters, diaries, newspapers, other modern sources and it might require first-person interviews and perspectives. The secondary sources will include writings, books, articles, and pertinent critical historical studies, using evaluation tools, interpretations, and historiographical discussions offered by these secondary sources of the historiography of the Anglo-Egyptian [1]. For more than fifty years, Sudan was under occupation, which permanently changed Sudanese society, politics, and economics [10]. One of the societal transformations that colonialism entered was the imposition of Western culture and education by missionaries [7]. At the time of the occupation, missionaries—particularly Christian missionaries—had a significant impact in Sudan's community. They built schools, hospitals, and other institutions that had massive effects on cultural dynamics, healthcare, and education. Religious practices in Sudan were also impacted by the presence of missionaries, especially in the south of the country, because the Islamic presence there was frail at that time due to the minority of advocates to spread Islam there, religion was the main reason which caused the country's division into two parts in 2011 [11]. Conversely, a crucial reason for the North Sudanese rejection of the occupation was the colonizer's attempt to introduce the Christian religion into society, since Islam entered Sudan through the Arab traders, the North Sudanese have been distinguished by their strong Islamic faith, which greatly influenced their culture and identity formation and later was the main cause of the emergence of nationalism against colonial invader's foreign customs [3].

Another change brought by the colonizers was in the social dynamics itself because before the occupation Sudan was organized along a tribal system people used to live in small traditional villages', but with the colonial entry, the ethnic and religious groups in Sudan had to comply with the colonial system. Occasionally, colonial authority favored one group over others according to its interests, which led to shifts in the balance of power and intergroup relations. Moreover, launching Western education and new governance systems influenced social stratification and class formation [3]. Before colonial Sudan education system relied on traditional Quranic memorization schools, which were replaced with British schools and curriculum institutions to graduate brilliant administrators, economists, and politicians without the intellectual contribution required for societal development [3]. Although the Sudanese elite (Thinkers, leaders of thought in politics, historians, and sociologist) played insignificant roles in changing or stopping society's restructuring in the colonial period, yet they still played intricate roles in the country's politics. Some of them worked with the colonial government, acting as middlemen between the colonial authorities and the native populace, and others opposed colonial rule and rose to prominence in the nationalist movement as proponents of Sudan's independence by supporting and guiding the people's uprising against oppression and colonial domination [9].

1.1. Historical Writing Resource During and After the Anglo- Egyptian Occupation of Sudan

As history is continuously derived from its origins to sum the total community experience in the past, understanding how it is transmitted and what these sources are is crucial. Mary Rampolla, in her book (A Pocket Guide to Writing in History), published in 2012, defined the historical sources as historical material that serves as evidence of a particular historical event. Thus, history reaches us through the narratives of those who participated in or witnessed its occurrences, which historians rely on to interpret and describe the past. This definition clarifies that all members of society are able to write history as long as they witnessed the events. However, surely historical writing requires other aspects as well, and it varies according to the narrators and their background, such as the historiography of Sudan, which has been written and reached us by non-Sudanese writers who were contemporary to the events. Since the modern history period in Sudan which began with the Turko-Egyptian rule from 1821 up to the current present, sources for writing Sudan's history have depended mainly on the writers from outsiders - traders, missionaries, and colonizers- who were the first to document the conditions and the history of Sudan during different periods.

Indeed, from the ancient time in the history of Sudan, since the kingdom of Kush, 300 BCE and 600 BCE, inscriptions and writings found in the temples remain primarily unknown and thoroughly misunderstood. Most of the events, names of kings, and information we possess derived from external sources non-Sudanese writers and civilizations, such as ancient Egyptian hieroglyphics and Roman, Persian, and Assyrian writings [12]. The significant challenge with this historical transmission is that it conveys major events but does not focus on all aspects of Sudan's life. Thus, the primary sources for writing the history of Sudan were non-Sudanese writers, mostly European or foreign researchers who relied on their writing for what they witnessed. Despite any personal description and perspective toward the events that they witnessed and contemporaries, their writings hold significant value because they were based on facts and information corroborated by those who experienced these events alongside them in Sudan, which makes their works a vital resource for Sudanese researchers and historians

to know and collect the origins of phenomena and societal motivations until today [13]. Collecting documents and books from various foreign writers was the first aspect that Sudanese historians used as a source, but according to the historical methodology, this is a secondary resource. The second central aspect that Sudanese historians greatly rely on is narrators of oral resources to uncover certain truths about the past. Oral resources are essential lies in their ability to fill the gaps in historical knowledge that cannot be addressed through written documents only. This type of historical writing resources the oral narratives and employs a scientific methodology to verify events and ensure their accuracy through analysis, comparison, and contextual circumstances, as well as biographies of the narrators [14].

1.2. Historians During the Anglo-Egyptian Occupation of Sudan

Oddly enough, what has been written about Sudan's history before and during the Anglo-Egyptian occupation, other than the pens of its people in the north and south, exceeds what the Sudanese writers and historians have written; before the occupation these writings return to the early modern period in European history, which was known as an exploration era from 1500 to 1780, where many European travelers to explore Africa. The most prominent of them in this regard is the Scottish traveler (James Bruce), who traced the origins of the Blue Nile began from Egypt through Sudan until Ethiopia in 1770; he wrote about Sudan in the first editions of his book, which appeared in 1790, and he was the second European that took this trip in the deep of Africa [3]. He was preceded by writings edited by the French traveler (Charles Poncet) and his companion (Father Brendan); they arrived in Sudan in February 1699, where they stayed for about three months. Then, the writings of (Krump the Bifarian), who remained in the region for about a year and a half in 1702 [12]. Thus, the beginnings of documenting and writing about modern Sudan's history Initiated with them because there was a gap and dark period that was undocumented in Sudan's history after Islam entered and before the Turkish-Egyptian invasion of Sudan, which began in 1820. However, European studies and writing about Sudan continued through successive historical periods until today, and it increased during the Anglo-Egyptian occupation of Sudan [15]. Additionally to that, as it is known history main objective is to document all aspects of civilization, categorize events and describe decline and prosperity, golden and dark periods through eras; in other words, it suggests that civilization dynamics oscillate between Struggles then rushes to flourish and vice versa [13]. At the same time, historical processes do not cease; they are continuous and unbroken.

This starkly contradicts Sudan's history, which relies on non-Sudanese writers to write about specific aspects according to their experience. This leads to a narrative characterized by the historian's background with possible wrong interpretations, creating unconnected episodes across various historical periods and lacking a cohesive connection among them. Besides, it is essential to mention that most of these writers came to the country either as conquering invaders within European military campaigns, missionaries of Christianity, or as travelers and tourists. Notable among those who wrote, ruled, and chronicled the history of Sudan during the Anglo-Egyptian occupation: Rudolf Carl von Slatin, entitled Slatin Pasha, wrote his book The "Fire and Sword" in 1895, describing the situations in Sudan before the occupation and during and the events that he recognized. Lord Cromer, also known as Evelyn Baring, who announced from Omdurman city in Sudan the beginning of the Anglo-Egyptian occupation in Sudan and the first who raised the Britain and Egyptian flags in Sudan, covered in his book about Sudan, explained some administrative decisions, documents and facts about that period. Addition to them, also there was Ronald Wingate, was the second governor-general of the Anglo-Egyptian Sudan in his book "Wingate of the Sudan" in 1955. According to Gabriel Warburg, "Wingate was the architect who created the British version of the legend of the Mahdiya, aiming to convince British public opinion and decision-makers that British intervention was essential in order to liberate the suffering Sudanese from Mahdist oppression" [4]. There were a few Sudanese historians during the Anglo-Egyptian occupation who did not document any social or economic historical events during that period because all their writings focused on the country's liberation. So they began writing, documenting and reflected on historical events they witnessed in the last years of the occupation and after the independence. Therefore, Sudan's history documenting and writing exceedingly relied on non-Sudanese external writers, Europeans, Egyptians, and others during the Anglo-Egyptian occupation, particularly the memoirs of explorers and colonizers, who are not historians; they arrived in Sudan for other purposes, chronicled their experiences, and conveyed their perspectives on social and economic life as well. They obviously obscured certain aspects of the national and social history of the country according to their own agendas and interests, creating a narrative way that positions Sudan's history as if it was a mere continuation and as an episode of the history of the Ottomans and British Empire rather than as a distinct narrative of the history of the Sudanese in Sudan what result in numerous gaps and disjointed episodes in the recounting of Sudan's history [14].

In general, Sudanese intellectuals and writers were significantly scarce and tended to be in the fields of literature (poetry, stories, plays, etc.), political and economic. During the Anglo-Egyptian occupation of Sudan, several prominent writers and intellectuals played crucial roles in shaping public opinion and resistance to colonial rule.

Their writings encompassed various genres, including literature, journalism, and political commentary, and reflected their views on the occupation. In history, many Sudanese historians who were a few, preferred to show great interest in writing about the history of religion, such as the Sufi heritage movements and their intellectual influences. Also, due to the rapid changes in the country's rulers and political movements and uprisings, historians have shown a massive interest in political history writing. These efforts to resist the colonial regime played a pivotal role in shaping the Sudanese national identity. The rise of nationalism and loyalty increased the rejection of the colonizer, represented by belonging and adhering to the Islamic religion, speaking the Arabic language, and rejecting colonial western culture. The imposition of colonial authority also sparked resistance. The struggle against colonialism fostered a sense of unity and solidarity among Sudanese of different backgrounds, eventually contributing to the push for independence [13]. However, writing in social history, which focused on daily life, customs, traditions, and social structure, did not receive the same level of attention from Sudanese historians during the Anglo-Egyptian occupation of Sudan, after independence historians started to write in all fields [16].

One of the notable figures during the occupation was Makki Shubaika (1905-1980). He defined history as a chain of events occurring within a specific time, shaped by particular individuals; another description he points out was incidents of facts at a specific time by a certain human being. He added that historical documents, events, and figures upon which one historian relies might be identical to another historian. Yet, each historian's narrative and writing emerges distinct, which was shaped by their interpretation. Here, the differences between historians arise not only in accuracy and fidelity in conveying historical events as they are but also in historians' perspectives. Therefore, the Sudanese historian should exercise caution in conveying events from their original sources and presenting them as they are. The point of contention is not the availability of historical material; instead, it is the historian who is different, influenced by the environment, educational background, era, beliefs, and individual character [16]. This indicates that Sudan historical issue was not in the sources or the way events were chronicled but instead in the way the Sudanese narrators and historians thought, as they were educated and grew up in British system schools that prioritized graduating assistants in the colony's affairs to promote their own agendas and interests and not for serving their country. Shabeika authored many books about the Anglo-Egyptian administration of Sudan. In one of his books (British Policy in Sudan 1882-1902), published in 1949 in English, he examined the reasons and motivations for British intervention in Sudan. He concluded that the main two reasons were to expand the British Empire and protect the River Nile's valley from French and Italian encroachment. From historical Writing resource, he used the primary resources by collecting many documents in this book from the Egyptian archive [16]. He also wrote (Sudan's Future) published in 1959, which relied on narration only from the beginning of the British entry into Egypt until the independent of Sudan. This book was extensively supported by Sudanese historians and added to historical documents because it contains many facts and events that Shabeika collected from contemporary people. He wrote using a historical narrative method. He held political perspectives that were reflected in his writing. He was one of the first intellectuals who called for the liberation of Sudan from occupation and unification with Egypt. His historical resources relied on primary resources by accessing original documents, even he often travelled to Egypt and Britain to ensure the validity of the documents, sources, and reports. Shabeika's methodology was characterized by simplicity, as he was a contemporary witness to the Anglo-Egyptian occupation and its events. Through his books, he provided a different historical writing method, giving historians after him a new perspective on documenting the country's history far away from relying on the books of non-Sudanese travellers and historians, which was a Sudanese historian dilemma. In his works, he also presented historical perspectives impartiality, acknowledging strengths and flaws without critique, which was a novel approach at the time. His writings were encouraged by Sudanese readers and beyond, as he conveyed Sudanese history in a manner that authentically reflected the Sudanese spirit [18].

1.3. Historians in the Post-Occupation

As mentioned before, Sudanese historians were significantly scarce during the Anglo-Egyptian occupation. For this reason and to understand the historical situation of the country profoundly, the researcher wanted to address some historians from the post-occupation period who lived through the last periods of colonialism before the country's independence and obtain insights shaped by both the colonial and post-colonial eras. Following Sudan's independence in 1956, intellectuals, writers and historians' perspectives evolved as they engaged with the cultural legacy of the country after occupation, the challenges of nation-building, and the quest for a new Sudanese identity. Several literary and intellectual figures continued to shape the discourse on colonialism and its aftermath [13]. Consequently, with the arouse of national awareness, the continued growth of the nationalist movement in Sudan had a direct impact on the emergence of Sudanese historians and intellectuals, who moved toward adopting a new systematic method of writing history that covers all aspects and topics about Sudan which have been neglected or overlooked by foreign historians. The impact of Sudanese historians significantly appeared in the diversity of topics and the freedom of expression, which restored balance and totality to the writing of Sudanese history. In addition to that, they presented the culture and the authenticity of the folk heritage, emphasizing the richness and

depth of Sudan's cultural heritage, which demonstrates that historical writing and documenting history from the perspectives of the people themselves is crucial in rooting national culture and alleviating estrangement from it. Prominent among them was the works of distinguished Sudanese historians, beginning with their elder, Professor Youssef Fadl, a historian and researcher on Arab presence and Arabization in Sudan, he uses a critical method to investigate other historians' books. He condemned the limited education offered to Sudanese after replacing traditional Quranic memorization schools with British curriculum institutions by opening the first college in Sudan, established in 1902, and restricted education primarily to administrative and accounting roles to produce a workforce serving the colonial regime [16]. Muhammad Ibrahim Abu Salim, a historian, and a politician, was interested and a specialist in the history of religion and politics in Sudan; on Mahdist publications and the intellectual movement during the Mahdist period, he enriched this scholarly history landscape [17]. Abu Salim's historical research is indispensable for any researcher in the history of Sudan, as it is rooted primarily in documents and rigorous scientific analysis, enriched by expertise and complete neutrality, steering clear of common historical inaccuracies; which was evident in his book, Sudanese Personality, published in 1979, where he skillfully analyzes Sudanese characters and all the influences that shaped them. The historian and document expert Dr. Abu Salim remained committed to rigorous historical methodology in his writings until his death. Many books he published in modern critical methods.

Another notable figure who carefully should be considered because of his remarkable scientific method and historical perspective contributions is Muhammad Abū al-Qāsim Ḥājj Ḥamad (1941-2004), who described himself as an Islamic thinker, philosopher, writer, and Sudanese strategic researcher rather than a historian. His famous book (Sudan: Historical Dilemma and Future Prospects) positioned him in the category of new historians because of his unique method, description, and critical perspective, which were previously unseen in Sudanese writings. Intensely, he criticized colonial roles and their decisions on many occasions, for instance, in the exploitation of tribal chiefs (Sheikhs) to consolidate British rule in the country, adding that the British government aimed to reduce the role of religion in society by sending Christian missionaries and utilizing the influence of tribal elders (Sheikhs) to gather support as well as minimize Egyptian intermediaries by fostering false nationalism concepts among the Sudanese to promote its interests, allowing to involve Sudanese in governance through local administration, such as roles of administrative accountants and assistants to the ruling authority [13]. Most of the writings of Sudanese historians relied exceedingly on presentation and description without analysis until the historian Ḥājj Ḥamad came in his book (Sudan: Historical Dilemma and Future Prospects) the second and third versions were published in 1996 and broke this direction by relying on critical assessment, issuing judgments, and supporting or opposing historical events that were characterized by a bias towards particular individuals or groups. He highlighted the nature complex of the Sudanese personality, which needs to unify its efforts by opening objective discussions about the current situation and the future with a more accepting mentality and receptive to other's opinions. Hajj Hamad's historical perspective aims to free the Sudanese people from the impasse (dilemma as he describes in his book) within which they had been trapped.

2. CRITICIZING

Sudan's issue with history is not in glorification but in an attempt to understand the past events in a specific way to discover historical dialectical paths and deal with history with indicators and connotations that have taken to inform and draw the future, and not just deal with history by taking lessons and preaches. Most contemporary writings about Sudan were characterized by superficiality and simplification for a few reasons: Either because historians suffer from the complexities of Sudan in their profound comprehensiveness because of the varying forms of governance and rulers in Sudan during and after occupation, and the persistence of dilemmas or crises that are a transmission of issues from one generation to the next remains unresolved among Sudanese historians, with each era blaming its predecessor [13]. Or because the historians bias themselves in favor of certain tendencies that tend to attempt peripheral influence without focusing on the fundamental issues that the historian should address regarding Sudan's events and contradictions.

Researcher agreed with Ḥājj Ḥamad's perspective when he argued that Sudanese historians had wasted time merely responding to describing crises while neglecting the deeper roots of the issues embedded within society. Instead of that, they focused on political issues in specific social groups [13]. Main reason to be considered as well is the Sudanese identity, which emerged after the social freedom people experienced after the occupation up to today, they stuck between whether they were Arab or African, Communist or Islamist, whether they were centered or decentralized politically. Sudanese society could develop only by overcoming these binaries. Another factor to mention is the influence that the Sudanese historians and intellectuals faced in the transitional period; they struggled to convey their ideas, this period was a gap and a decisive transitional phase. It was that gap that historian caught on between European modernity, which came with the Anglo-Egyptian occupation and its educational system, and their community traditions and customs that restricted their writing methods to simplicity.

3. RESULTS AND RECOMMENDATIONS

The research emphasizes the necessity of impartially researching and writing to convey actual events in all topics related to Sudan's history. To this day, only one historical Sudanese figure embodies the values of courage and sacrifice for the people: Al-Mahdi, who fought against and expelled the Turko-Egyptian rule in 1885. From this perspective, writing about biographies of prominent Sudanese will provide inspiring examples for confronting present fears and fostering hope for a bright future. Figures such as: Thinkers, leaders of thought in politics and economics and all fields, pioneers of political resistance movements against colonialism and occupation in the past and present, advocates of social change and reform, and innovators in fields such as poetry, literature, arts, and traditional technology, among others [13]. Historians need to understand and accept the culture of others (the colonizer) while renewing the vision of authenticity and tradition in a contemporary manner, subjecting the new colonizer's cultures to the same criteria as the authentic imitative perspectives [18]. Otherwise, the historian would remain confused regarding the social reality, religious roots, and national framework. This dialectic appeared with complete clarity in the personality of the historians in the era they lived.

Additionally, Sudanese historians were required to write impartially by avoiding political and personal perspectives, which was challenging them because their writing was most often directed toward a group or to reshape specific historical periods in a way that fits the present reality [13]. Sudanese historians during and after the Anglo-Egyptian occupation suffered from a state of intellectual schizophrenia, leading them to face a split between writing about current events in their present to glorify and grow the society and writing about their past. Or to write their opinion on the modern ideologies of socialism and liberalism. In this dilemma, Sudanese historians took a passive stance on analyzing and criticizing the past because there were gaps; as Ḥājj Ḥamad mentioned, there were rapid events in their lives that made their vision toward past events superficial, so they believed they could write about their present in opposition against their traditional, regressive past without forcing them to subject it to any critical revision [13]. As a result, Sudanese historians choose to write from the past what remains and emphasize their greatness and authenticity from what they witness and according to their background without providing a shred of evidence or try returning to the origin before writing history, and that should change in the current historian's generations who will write and convey present events.

4. CONCLUSION

The research concluded that two primary historical resources were used to write Sudan's history. It also found that historians were exceedingly influenced by their political and religious backgrounds, which impacted their methods of documenting events and focused on specific historical aspects in transmitting events. The research recommended that to achieve comprehensive intellectual and historical development in Sudan's history transmission, historians should transcend the dilemma imposed upon them since the colonial period. Sudanese historians are also required to acknowledge and accept the culture of others while renewing the vision of authenticity and tradition in a contemporary manner. Additionally, what sought to present in this paper, as presented and clarified, it seems clear that written material about Sudan's history in the Anglo-Egyptian occupation period was broadly available, especially in foreign references. However, the central issue lies in the fact that Sudanese researchers and historians have not been well utilized these studies objectively fully and have not extended them to the philosophically and intellectually rigorous levels required; instead, they contented themselves with simple writings that lacked cognitive foundations and critical analysis in understanding the accurate Sudanese structuring and used a methodical, philosophical approach to historical writing [7]. By studying the historiography of this period, Sudanese historians can be able to comprehend the various perspectives and stories, look at the roots of the issues by recognizing the meaning of events that can be narrated in our current reality, and the ability to compare the periods and similar events. Especially in this contemporary challenging time, which requires the full preparation of skilled scientific historians to convey and write about this crucial period. What Sudan is going through these days requires presenting all the shortcomings that faced the Sudanese historians in the past and some recommendations to avoid them during this pivotal period in Sudanese history. Seeking to reach the ability to understand and avoid the failures of past historians, enabling the creation of a balanced history that describes, comprehends, and learns from the past to shape the future.

REFERENCES

[1]   M. Rampolla, *A Pocket Guide to Writing in History*, 7th ed. Bedford: Martin's Publication, 2012.

[2]   J. A. Smith, *Sudan: The Anglo-Egyptian Condominium Reappraised. In Colonialism and Its Forms of Knowledge: The British in India,* 1st ed. New Jersey: Princeton University Press, 2005.

[3]   G. Warburg, *The Sudan Peace Process: Challenges and Future Prospects*, 1st ed. Washington: United States Institute of Peace Press, 2004.

[4]   M. W. Daly, *Empire on the Nile: The Anglo-Egyptian Sudan, 1898-1934*, 1st ed. Cambridge: Cambridge University Press, 1992.

[5]   P. M. Holt, *The Mahdist State in Sudan, 1881-1898: A Study of Its Origins, Development, and Overthrow*, 1st ed. Oxford: Clarendon Press, 1958.

[6]   A. G. Saad, "Sudan: Colonial rule, 1898–1956," in *The Making of Modern Sudan: The Life and Letters of Sir Douglas Newbold*, R. M. Baten and D. W. White, Eds. London: Faber & Faber, 2015, pp. 73–90.

[7]   P. Brown, "The scramble for Africa," in *American Economic Association*, 2012, pp. 64–67.

[8]   H. J. Sharkey, *Living with Colonialism: Nationalism and Culture in the Anglo-Egyptian Sudan*, 1st ed. Berkeley: University of California Press, 2003.

[9]   A. L. Stoler, *Carnal Knowledge and Imperial Power: Race and the Intimate in Colonial Rule*, 1st ed. Berkeley: University of California Press, 2002.

[10]   H. A. Elhag, "The Sudanese identity and the Anglo-Egyptian condominium rule (1898–1956) towards a postcolonial reading," in *Conf. Middle Eastern Studies*, Cambridge, UK, 2019, pp. 113–120.

[11]   R. Hill, *A History of the Sudan: From the Coming of Islam to the Present Day*, 1st ed. London: Weidenfeld & Nicolson, 2000.

[12]   M. A. bu Ḥājj Ḥamad, *Sudan: Historical Dilemma and Future Prospects*, 2nd ed. Lebanon: Dar Abn Hazm, 1996.

[13]   A. M. Osman, "Sudanese voices: Archiving oral histories of the colonial era," *British Journal of Middle Eastern Studies*, vol. 48, no. 1 pp. 1–23, 2021.

[14]   E. O'Ballance, *The Sudan: War and Slavery in the Late 20th Century*, 1st ed. London: Pearson1998.

[15]   M. I. Abu Salim, *Writers, Scholars, and Historians in Sudan History,* 1st ed. Lebanon: Dar Al-Jabal, 1991.

[16]   O.A. Al-Tom, *Colonialism and Resistance: A Study of the Anglo-Egyptian Occupation in Sudan*, 1st ed. Khartoum: Khartoum University Press, 1979.

[17]   G. Warburg, "The wingate literature revisited: The Sudan as seen by members of the Sudan political service during the condominium: 1899–1956," *Middle Eastern Studies*, vol. 41, no. 3, pp. 373–389, Mar. 2006.

[18]   M. A. Salih, *The Sudan: From Subsistence to Wage Labour*, 1st ed. Edinburgh: Edinburgh University Press, 2008.

The Impact of Digitalization on Business Management: A Case Study of SMEs in Tirana, Albania

Anxhela Bakiasi[1], Mariglend Pepmarku[2]

[1]Department of Management, Faculty of Economy, University of Tirana, Albania
[2]International Baccalaureate (IB) Business Management Teacher, Albania
Corresponding author: Anxhela Bakiasi (e-mail: bakiasianxhela1@gmail.com)

Abstract

Digitalization is reshaping the way businesses operate, offering new pathways to improve efficiency, reduce costs, and enhance competitiveness. This study explores the impact of digital technologies on small and medium enterprises (SMEs) in Tirana, Albania, focusing on how these businesses integrate digital tools into their management practices. Employing a mixed methodology that combines a comprehensive literature review with a case study approach, the research draws on data collected through 50 questionnaires completed by SME representatives in Tirana. The findings reveal both the opportunities and challenges presented by digitalization. Opportunities include streamlined operations, enhanced communication, and expanded market access, while challenges encompass limited digital skills, resource constraints, and the difficulty of aligning traditional business models with modern technological demands. Using the framework proposed by Parviainen et al. (2017), the study contextualizes these findings within the socio-economic realities of Tirana, providing valuable insights into the digital transformation process of SMEs in this region. This research highlights the critical need for capacity building, investment in infrastructure, and the development of supportive policies to foster digital adoption among SMEs. By bridging the gap between theoretical perspectives and real-world applications, the study offers actionable recommendations for businesses and policymakers aiming to accelerate digital progress in Albania's evolving business landscape.

Keywords: Digitalization in SMEs, Business management transformation, Technological adoption challenges, SMEs in Tirana, Digital tools integration

Maternal Perceptions of Psychosocial Support and Family Well-Being: Exploring Connections

Nino Kitoshvili[1]

[1]Department of Psychology, School of Social Sciences, University of Georgia, Tbilisi, Georgia
Corresponding author: Name Surname (e-mail: N.kitoshvili@ug.edu.ge)

Abstract

Understanding the dynamics of family well-being is essential in contemporary research, particularly in diverse cultural contexts like Georgian society. This study examines how a mother's perception of psychosocial support influences various facets of family dynamics. The research aims to explore correlations between maternal perceptions of support and outcomes related to child well-being, marital dynamics, and overall family functioning. Data from 167 families in Georgia were analyzed. Measures included maternal perception of support, child well-being, marital conflict, family functioning, and financial perceptions. Statistical analyses were conducted to assess relationships between variables. The study confirms the influential role of maternal perceptions of support in shaping family dynamics in Georgian society. These findings underscore the need for targeted interventions to strengthen family support systems and enhance overall well-being. This research contributes empirical evidence to the understanding of family dynamics in a cultural context, informing policy and interventions aimed at promoting family well-being.

Keywords: Family dynamics, Maternal perception, Psychosocial support, Child well-being, Marital conflict

Communication in Fashion Media – Analysis and Comparision

Martina Hendija[1], Ivana Salopek Čubrić[1]

[1]Department of Textile Design and Management, Faculty of Textile Technology, University of Zagreb, Zagreb, Croatia
Corresponding author: Ivana Salopek Čubrić (e-mail: ivana.salopek@ttf.unizg.hr)

Abstract

Today, the fashion media has a strong influence on the culture of fashion, clothing and the creation of fashion laws. It is difficult to assess who is dictating fashion today, designers and big fashion houses, influencers and bloggers or consumer society itself. Fashion changes have become so fast that it is difficult to follow them, therefore the fast fashion industry is barely able to respond to these increasingly rapid changes. The standard of product quality is significantly reduced, and the moral and ethical codes of business and environmental sustainability are called into question. The fashion media that is in symbiosis with the fashion industry lacks critical reporting on the fashion industry today. The paper systematically investigates and presents the history of fashion and clothing, the theory of fashion and media in general, and the origin, development and fashion media today. The experimental part is based on concrete examples of fashion media, which are researched, compared and analysed through different parameters. The sampling method was used to determine the fashion media that will be researched - fashion magazines (Vogue, Harper's Bazaar and Elle); fashion platforms (The Business of Fashion (BOF), Highsnobiety, and Hypebeast) and social networks (Facebook, Instagram, and Tik Tok).

Keywords: Communication, Fashion, Journalism, Media, Social network, Digital

1. INTRODUCTION

Mass media i.e. means of mass communication, is a collective name for means of communication, means of public communication and institutions that act on a large number of readers, listeners and viewers. Traditional mass media are increasingly connected with computer technology, so new interactive media are emerging, such as the Internet - which is no longer a typical mass media, because production and distribution are subject to institutionalization and commodification, and the audience is dislocated in time and/or space. This is why the term mass media is increasingly being replaced by the term communication media. Mass media are the result of technological innovations (printing machine, camera, radio wave transmission, computers, digitization) [1].

1.1. Media – from Traditional to Digital

The book was the first medium of mass communication. In today's era, it has lost its monopoly on the dissemination of knowledge and superiority in education, but it has retained its exclusivity. Newspapers and magazines, as the next media of mass communication, are included in traditional printed media such as posters, books, comics, etc., but they differ from them in terms of frequency and specific publication schedule, informative content, paid advertisements, commercials, and target audience. They are intended for the general public, they are mostly published every day, once a week or once a month. They are financed by advertising and selling printed copies.

Today, radio, film and television are also traditional electronic media, but electronic. Newspapers and magazines are distributed through newsstands, specialty stores, subscriptions, and mail, and TV and radio programs are broadcast over the air, cable networks, or satellite. The reach is quite large, local, regional or global, the limitation is usually the language area. The communication of all traditional media with the audience is one-way, there is no direct feedback from the audience, and the costs of production and distribution are quite high.

Digital media works with the help of the Internet. The Internet is a global network, it is the communication event of this century. With the help of the Internet, the flow of information is very fast. With digital media, information is available immediately. Digital formats are websites, social networks, streaming services and various applications. Communication with users is two-way. Users have the option of commenting, sharing, "liking" and direct communication with media authors and other users. Content is distributed over the Internet and is available to users around the world, often in real time. The costs of distributing digital content are generally favorable.

Digital media use data about users for precise "targeting" of content and advertisements according to the interests and behavior of the user, so that often the user does not even have to search for the content, but it is imposed on him. All digital media are dependent on the coverage of the user's location by the Internet network and on technological support (mobile phone, computer, ...). The arrival of digital (new) media raises the question of whether the survival of traditional media is threatened. Digital books, newspapers and magazines are available on the Internet at the click of a mouse, so it is questionable whether printed editions will survive. On this issue, Labaš optimistically concludes "that new media do not simply replace the media that preceded them, but together with them lead to transformational processes, or include them through the phenomenon that McLuhan called re-mediation, that is, acceptance of one medium as the content of another medium" [2].

1.2. Media and Fashion

Traditional fashion media today include fashion magazines. The first forms of fashion communication that may be related to fashion journalism were used in royal circles and the French newspaper "Mercule Galant" was the first to publish a special edition dedicated to the fashion in 1672. In the second half of the 19th century, Harper's Bazaar, Vogue and Cosmopolitan, the journal that are the leaders in fashion even nowadays, saw the light of day [3]. In the traditional printed form, fashion journals are published mostly once a week, once every 2 weeks, once a month or quarterly. They are present in different countries and written in the official language of the country where they are published. They follow and report on fashion trends around the world and advertise products related to the world of fashion. Today, fashion magazines have primarily progressed in their visual identity, the quality of printing and the speed of production is at a much higher level than twenty years ago and is continuously improving. It strives to be made from renewable sources, from recycled paper and in quantities of sales frames. They regularly flirt with digital media, they have their own digital pages where they publish content from printed editions, release new sub-issues and/or articles, editorials and advertisements. In this way, today fashion magazines are present every day and are becoming more and more read. In accordance with the demand, the scope of topics, fashion editorials, creations, collections expands, and all of this consequently leads to greater circulation and sales, not only of the magazine but also of the fashion clothing items they advertise. Some of the most famous fashion magazines published in printed form are: Vogue, Harper's Bazaar, Elle, Marie Claire, GQ, Vanity Fair, In Style, Cosmopolitan, Grazia, W Magazine, Dazed and D Magazine. Fashion newspapers: The New York Times Fashion Section, The Guardian Fashion and The Daily Telegraph Fashion.

Today's digital fashion media includes a wide range of different formats and platforms, from traditional printed fashion magazines, through films, series and television shows, to modern digital platforms and social networks. Fashion media promote fashion innovations, communicate with the public and directly influence consumer decisions. New fashion identities are created, bought, consumed and re-created. The model of the socially acceptable identity of an individual today relies mainly on the values of capitalist society: power, money, brands and consumption. That vicious circle turns very quickly. The role of the media in this process is multiple. They not only create new identities through the exchange of information, but with their contents they cause a constant demand for new identities and enable their easy integration into new value systems [4]. The connection between fashion and media exists on several levels. Fashion shows from the main fashion cities are shown in the daily news, and other major fashion events and fashion spectacles are followed. Fashion magazines analyze the styles of celebrities, offering their readers tips on how to copy them. Designers need celebrities as much as celebrities need designers, both designers and celebrities need the media to promote their products - designers clothes, and celebrities themselves. The monopolized nature of the fashion media has a strong influence on the culture of fashion and the creation of fashion laws; from fashion magazines to fashion blogs that lack critical reporting on the fashion industry today.

2. METHOD

In this research, different methods were used to arrive at relevant results relevant to the topic. The sample method, description method, observation and comparison method, statistical method and analysis method were used. For the research, nine fashion media were selected. The fashion media were chosen randomly from among the global fashion media that are doing well in today's era:

i.   fashion magazines (Vogue, Harper's Bazaar and Elle)
ii. fashion platforms (The Business of Fashion (BOF), Highsnobiety and Hypebeast) and
iii. social networks (Facebook, Instagram and Tik Tok).

The main parameters of the observation and comparison of our sample are as follows:

a. Purpose / role,
b. Format,
c. Distribution and access to content,
d. Frequency of going out,
e. Time for production,
f. Target audience – age, gender, financial status,
g. Access to the audience,
h. Space availability,
i. Content and coverage of topics,
j. Writing style,
k. Representation of the text,
l. Representation of photographs,
m. Representation of advertisements,
n. Appearance / design,
o. Engagement / personalization,
p. Interactivity / feedback,
q. Brands and advertising,
r. Number of followers / subscribers,
s. Authority and credibility,
t. Business/ profit / profit.

3. RESULTS

The results of the investigation are elaborated taking into account the defined main parameters:

3.1. Purpose / Role

The main purpose / role of all observed fashion media is primarily to convey to the reader information about fashion, fashion events and styles with accompanying pictorial content.

3.2. Format

Traditional fashion magazines Vogue, Harper's Bazaar and Elle are published in printed form, and more recently also in digital form. BoF, Highsnobiety, Hypebeast are in the format of digital fashion platforms, and they also publish several printed editions throughout the year. Facebook, Instagram and Tik Tok function exclusively in digital form, as social networking platforms and mobile applications.

3.2. Distribution and Access to Content

Vogue, Harper's Bazaar and Elle are distributed in print form globally, at authorized sales points (newsstands, bookstores) and by subscription. Digital editions can be accessed through their familiar apps or pages, as well as through various digital platforms. Subscription required. They are also present on social networks such as Instagram, Facebook, Twitter and YouTube. BoF is available on its digital platform, with a subscription. Hypebeast and Highsnobiety are available without subscription on their digital platform, in which web sales are integrated. Hypebeast also operates through its own mobile application. Social networks Facebook, Instagram and Tik Tok enable instant publication and distribution of content through their digital platforms and mobile applications. All digital media are available anytime and anywhere if there is internet coverage and technical support (smartphone, personal computer, ...).

3.3. Frequency of Going Out

Traditional magazines have a precisely defined cycle of publishing a printed copy. Vogue, Harper's Bazaar and Elle are published monthly in print, their digital magazine is also monthly, but the content on their sites and social networks is updated more often, sometimes in real time. BoF, Highsnobiety, Hypebeast continuously publish content on their website, sometimes in real time. Printed Bof is published 4 times a year, Highsnobiety several times a year, and Hypebeast 2 times a year. Advertising through social networks is present in real time and depends solely on the advertiser.

3.4. Time for Production

Vogue, Harper's Bazaar and Elle have a month to produce from issue to issue. Printed BoF takes 3 months, Hypebeast even 6 months, while digital fashion platforms and social networks have a much shorter production time, publications are often in real time and improvisation is present.

3.5. Target Audience – Age, Gender, and Financial Status

Print Vogue, Harper's Bazaar and Elle focus on an older, mostly highly educated and affluent audience with an interest in high fashion. Digitally, they are also targeting a younger, mostly female audience. BoF is tailored to professionals and fast-paced industrial dynamics, targeting entrepreneurs and marketing professionals. Highsnobiety and Hypebeast are aimed at a younger population that loves branded street fashion. They are also focused on the male audience. Facebook, Instagram and Tik Tok gather a wide audience, mostly young and in the case of Facebook, the middle-aged population.

3.6. Access to the Audience

Vogue, Harper's Bazaar and Elle focus on high fashion, luxury and sophistication. They engage their audience with luxurious editorials, interviews and carefully crafted articles on fashion, beauty, culture, travel and lifestyle. BoF cultivates a professional approach, offering fashion industry news, in-depth analysis and credible informative articles. On the other hand, Highsnobiety and Hypebeast have a more relaxed approach, offering fast news and analysis, fashion advice and a web shop, focusing on street fashion and culture, providing content that is close to a younger audience. Facebook, Instagram and Tik Tok enable the creation and distribution of content by users, resulting in greater interaction, instant content and faster changes in trends. In addition, they offer the option of shopping, thereby further encouraging the reaction of users and connecting them with brands and products in real time.

3.7. Space Availability

All printed editions have spatial limitations in terms of the number of printed pages, while fashion platforms and digital networks have no limitations in this regard.

3.8. Content and Coverage of Topics

Contemporary editions of Vogue, Harper's Bazaar and Elle are mostly oriented towards fashion and beauty, personal stories of celebrities, cultural comments. In some editions, we also find topics on tourist destinations, advice on health, career and topics of feminism, LGBTQ+ rights, topics on ecology and social justice. The topics are general social and adapted mainly to the female population. BoF covers topics from the world of fashion, textile industry and marketing in a scientific way. To analyze business strategies, corporate changes, financial results, market trends, trends in fashion design, production and consumer behavior. It reports on the impact of technology on the fashion industry, including e-commerce, digital innovation and sustainability. Interviews industry leaders and provides career and professional development advice,... Highsnobiety and Hypebeast mainly cover topics from the world of street and sports fashion, interview designers and focus on promotion and sales. Facebook and Instagram are social networks and cover the entire spectrum of current topics, and readers are also co-creators of content. Tik tok publishes viral content mainly by influencers and brands, short videos on various topics, mostly fashion and beauty tips, promotional and sales materials.

3.9. Writing Style

The writing style is most formal in BoF and the print editions of Vogue, Harper's Bazaar and Elle. BoF fosters an analytical, informative, professional and expert formal writing style. Vogue, Harpers Bazaar and Elle write in a detailed, sophisticated and modern formal style. Highsnobiety and Hypebeast write in a relaxed and modern, but still formal style. With social networks, the writing style depends on who is writing, but it is mostly casual and informal.

3.10. Representation of the Text

The smallest percentage, up to 10% - Tik Tok. Followed by Instagram, Vogue and Harper's Bazaar with 10-20%. From 20 to 30% of the total text content can be found in Elle, Hipebeast and Facebook. In Highsnobiety, the representation of text is 20-40%, and the highest percentage of text representation is found in BoF, 50-70%. BoF, unlike the others, mainly focuses on in-depth articles and analytical reports. Instagram and Tik Tok use complex algorithms to personalize content for each user, so their content representation can vary significantly.

3.11. Representation of Photographs

The smallest representation of visual elements is used by BoF, 20-30%. In Vogue, Harpers Bazaar and Elle, in print and online versions, as well as in Highsnobiety and Hypebeast, it is difficult to separate advertisements from photographs. There you get different information, but approximately 40 to 50% of the content is covered by photos. If we were to look at total visuals, together with native advertisements, the percentage would be up to 80%. On Facebook, 50-60% of the feed is occupied by photos, on Instagram, 60 to 70% of the content is wasted on visuals in the form of photos and videos. Tik Tok is a video oriented platform and they make up 70-80% of the total content.

3.12. Representation of Advertisements

With advertisements, we come to the same problem as with visuals, it is often difficult to distinguish the advertisement from the visual element, the magazine photo. Ads make up 10-20% of content on BoF and Tik Tok, 15-20% on Facebook, 20-30% on Instagram, Highsnobiety and Hypebeast. The traditional magazines Vogue, Harper's Bazaar and Elle contain the most advertisements. Elle 30-40%, Vogue and Harper's Bazaar even 50-70%.

3.13. Appearance / Design

Minimalism prevails in all print and digital media, as a current style and reflection of society and times. Design also depends on the region of release, as fashion media adapts to market interests.

3.14. Engagement / Personalization

The greatest engagement and personalization is invested and achieved by fashion media on Facebook, Instagram and Tik Tok, and the smallest is with classic printed fashion magazines Vogue, Harper's Bazaar and Elle.

3.15. Interactivity / Feedback

Social networks Facebook, Instagram and Tik Tok receive the most feedback from the audience. Direct communication between the content distributor and the audience takes place on social networks.

3.16. Brands and Advertising

Vogue, Harper's Bazaar and Elle advertise famous fashion brands and designers, luxury fashion goods. Vogue (Chanel, Prada, Hermès, Fendi, Michael Kors Collection, Tom Ford, ...), Harper's Bazaar (Louis Vuitton, Wolford, Bottega Veneta, Balenciaga, Ferragamo, Emilio Cavallini, Missoni, Prada, Dior, Fendi, Etro, Falke, ...), Elle (Gucci, Prada, Dior, Fendi, Ferragamo, Balenciaga, Marc Jacobs, Saint Laurent, Alaïa, ...).

Highsnobiety and Hypebeast specialize in sports fashion brands and street fashion. Highsnobiety (Stüssy, Bode, Marni, Bottega Veneta, Martine Rose, Arc'teryx, Moncler, The North Face, Dickies, Levi's, ...), Hypebeast (Supreme, Off-White, Palace, Balenciaga, Nike, Adidas, Fear of God, A Bathing Ape).

BoF does not run commercial campaigns directly, but regularly collaborates with brands in a variety of ways, including partnerships for content, research and analysis (Louis Vuitton, Chanel, Gucci, Balenciaga, Prada, Nike and Adidas).

On Facebook, Instagram and Tik Tok, everything is advertised, from well-known fashion brands, up-and-coming designers, and mostly consumer goods and large sales platforms such as About You, Zalando, BestSecret, etc.

3.17. Number of Followers / Subscribers

- Vogue - 30 globally, 21 print editions, 11 digital editions, 89 social networks / in millions / month.
- Harper's Bazaar – 10.6 global, 3.5 print editions, 7 digital versions, 20.1 social networks / in millions / month.
- Elle – 33 globally, Hearst C.: 4.9 print editions, 8 digital versions, 23.5 social networks / in millions/ month.
- BoF – 964,300 page visits/month.
- Highsnobiety – 19,065 followers/month.
- Hipebeast – 17.8 million followers/month.

Social networks are more complex, their users are not all tied to fashion media:

- Facebook – 3,065 million active users/month.
- Instagram – 2,000 million active users/month.
- Tik Tok – 1,582 million active users/month.

3.18. Authority and Credibility

Vogue, Harper's Bazaar and Elle, in that order, have the most credibility among the fashion media. BoF, Highsnobiety, Hypebeast, also in that order, also have an enviable reputation, and Facebook, Instagram and Tik Tok are the platforms with the least credibility and authority in the fashion industry.

3.19. Business / Profit / Profit

Traditional magazines use luxury advertising campaigns and collaborations with famous designers and also rely on the sale of printed copies. Digital media use membership programs, exclusive content, e-commerce and analytics as a source of revenue. Social networks enable direct sales and branded content collaboration through options such as "Shop Now" on Instagram and TikTok. Through sponsorships, influencers earn a certain income by advertising a certain product in the best possible way to attract as many people as possible to buy that product.

4. CONCLUSION

The methodology employed in this research provided a thorough examination of the selected fashion media and the evolution of their roles in the modern digital landscape. By using a diverse set of methods like sample selection, observation, comparison, statistical analysis, and more, the study was able to holistically assess both traditional and digital fashion platforms. The analysis of parameters such as purpose, format, distribution, audience, engagement, and business models across three categories of fashion media (traditional magazines, fashion platforms, and social networks) demonstrates the shifts in how fashion content is produced, consumed, and monetized today.

Key findings include the persistence of traditional media like Vogue, Harper's Bazaar, and Elle in maintaining authority and credibility while adapting to digital formats. Fashion platforms such as BoF, Highsnobiety, and Hypebeast have bridged the gap between high fashion and streetwear culture, leveraging real-time digital interactions. Social networks (Facebook, Instagram, TikTok) have redefined audience engagement, providing unparalleled interactivity and instant feedback. Ultimately, this study highlights the broadening scope of fashion media, from highly curated print editions to dynamic, user-driven digital ecosystems. Each category plays a crucial role in shaping the global fashion narrative, from exclusive high fashion coverage to more democratized, user-generated content, while offering varied opportunities for brands, designers, and influencers to engage audiences and drive business outcomes.

References

[1]   N. Zgrabljić Rotar, *Media Literacy and Civil Society*, Media Centar, 2005.
[2]   L. Pajazetović, "Analysis: who and what are fashion bloggers in Croatia," Diploma thesis, University of Rijeka, 2017.
[3]   I. Salopek Čubrić and S. Bartolić. "Fashion journalism - historical overview and evolution from print to digital media," in *Proceedings of International Symposium on Current Developments in Science, Technology and Social Sciences*, Ankara: ISPEC, pp. 432-440.
[4]   L. Špinderk, "The role of media in creating fashion trends", Bachelor thesis, University North, 2016.

Exploring the Relationship Between Organizational Justice and Job Satisfaction: The Case of the Banking Sector in Albania

Petrit Dollani[1], Arjola Hoti[2]

[1]Faculty of Economics, University of Tirana – Albania & Warsaw School of Economics, Poland
[2]Faculty of Economics, University of Tirana, Albania
Corresponding author: Petrit Dollani (e-mail: petrit.dollani@unitir.edu.al)

Abstract

This study aimed to explore the relationship between organizational justice and job satisfaction, as perceived by employees in the banking sector of Albanian capital city - Tirana. Organizational justice has been considered as a mix of three components - distributive justice, procedural justice and interactional justice. A standard questionnaire used internationally in similar previous studies has been deployed and a sample of 147 employees was randomly chosen from 76 branches of five biggest commercial banks operating in Tirana. The study revealed a relationship between organizational justice and job satisfaction, age and banking experience, meanwhile no relation was found with regard to gender of employees.

Keywords: Organizational justice, Job satisfaction, Banking sector, Albania

1. INTRODUCTION

Over the past 30 years, organizational justice has been extensively researched, particularly in organizational contexts by psychologists and management researchers. The concept of justice is essential to understanding a wide range of human behavior in the organizational environment. Organizational justice, a term coined by Greenberg refers to employees' perception of fairness in the workplace. It has shown to be related to several results such as job satisfaction, motivation, turnover intention, work performance, etc. [1].

Employees of any organization are relatively satisfied, if they find that rewards have been distributed fairly for the efforts and output given in the job place. When employees feel that they are treated fairly by the organization in every aspect, they tend to show more positive attitude and job satisfaction. Issues, such as the allocation of monetary resources, the employment of employees in organizations, the formulation of policies and the implications of policies that affect the decision maker and the people who are affected by such decisions require special attention in relation to justice [2].

Organizational justice is mentioned in this study as an expression of the state in which employees recognize comprehensive equality as the rules of the institution, techniques and policies that are related to work. People seek justice in the work environment, in terms of the procedures used to set the reward, distribution of reward that make them satisfied or committed to their work or organization.

Organizational justice is conceptualized as a variety of different elements. The three main aspects of organizational justice are distributive justice (distributive justice), procedural justice (procedural justice), and interactional justice (interactional justice). Distributive justice is defined as honesty in giving results among employees based on fairness, equality and need.

Perceptions about distributive justice are largely shaped by comparisons. Indeed, employees evaluate their reward and position by making a comparison with people in the same layer within the organization or with people who have a similar position outside the organization [3].

Procedural justice refers to the participants' perception of the fairness of the rules and procedures that govern a process. While distributive justice suggests that satisfaction is a function of outcome, procedural justice suggests that satisfaction is a function of process. Among the traditional principles of procedural justice are impartiality, voice or opportunity to be heard, and reasons for decisions. Procedural justice defines some specified principles that regulate the roles of participants within the decision-making process. Procedural issues such as the neutrality of the process, the treatment of participants as well as the credibility of the decision-making body are important

for increasing perceptions of procedural justice. Thus, procedural justice is the perceived fairness of policies and procedures used to make decisions [4].

Bies and Moag [5] contributed into the organizational justice literature by focusing attention on the importance of the quality of interpersonal treatment of people when procedures are implemented. They developed the notion of interactional justice defined as the quality of interpersonal treatment received while adopting organizational procedures, referred to these aspects as "interactional justice." In general, interactional justice reflects concerns about the fairness of dictated non-procedural aspects of interaction. However, research has identified two sub-categories of interactional justice: informational justice and interpersonal justice. These two sub-categories of justice have considerable overlap. However, research shows that they should be considered separately, as each has differential effects on perceptions of justice [6].

Job satisfaction is often perceived as a behavioral variable that measures the degree to which employees like various aspects of their work. This is an important area of research, because job satisfaction is related to enhanced work performance, positive values, high levels of employee motivation, as well as low rates of absenteeism, turnover, etc. Although job satisfaction is influenced by many external factors, it remains something internal that has to do with feelings of the employees [7].

2. MATERIAL AND METHOD

Keeping in mind the lack of studies in this field in Albania, this paper aims, first, to try to measure the perceived degree of organizational justice and job satisfaction among the employees of a group of subjects in the banking sector. Second, we aim to investigate if there is any relationship between organizational justice and job satisfaction, and third, to verify, if there is any relationship between organizational justice and variables such as: gender, age and banking experience.

In our study we formulated two research questions:

- Is there any relationship between employee characteristics such as age, gender, and banking experience with organizational justice?
- Is there any relationship between organizational justice (in its three dimensions) and job satisfaction?

As a survey instrument, we used the questionnaire created by Niehoff and Moorman [6]. The answers to the questions were given on a Likert scale from 1-5, where 1- Do not agree at all, 2- Disagree, 3- Neutral, and 4- Agree, 5- Strongly agree. We proceeded further by using Cronbach's Alpha reliability coefficient to verify the internal consistency of the instrument. Initially, 15 individuals were surveyed in the pilot phase and for the entire sample a total of 147 individuals, which comprise about 10% of the total number of employees in all branches of the five largest banks operating in the capital of Albania - Tirana.

The variables used to measure distributive justice were working hours, pay level, workload, rewards and job responsibilities. For procedural justice, the variables used were prejudice, sensitivity, information, communication, consistency and disagreement. While interactional justice was measured by perceptions of consideration, respect, sensitivity, ethics and concern.

3. RESULTS

In terms of demographic findings, 38.3% of the respondents were male and the rest - 61.7% were female. Regarding the age group of the respondents, it turns out that the highest number is represented by the age group 25-34 years with 50%, followed by the age group less than 25 years and 35-44 years with 20% and the last one more than 44 years 10%. Regarding the banking experience from the questionnaire, the following data were collected: 26.7% have 3-4 years, 25% have 5-6 years, 16.7% have 1-2 years and 10% less than a year and more than 8 years.

The reliability coefficient for distributive justice in this study resulted in 0.954, for procedural justice 0.818 and for interactional justice 0.973. The reliability coefficient of the collected answers for this study is in each case obviosly greater than 0.7 - the lowest limit accepted by the literature for the validity of questionnaires. This shows that the questions were properly understood by the users and no doughts appear with regard to the reliability of the data.

In the descriptive data of the questions related to distributive justice, referring to the mean (from 1 to 5) it results that the question with the highest mean has the question "I think that my work responsibilities are quite fair" (M = 3.2, Sd = 1.424) and the lowest mean has the question "In general, the rewards I receive are quite fair". (M = 2.6, Sd = 1.50). Regarding procedural justice, it results that the question with the highest mean has the question "All work-related decisions are applied consistently to all affected employees" (M = 3.33, Sd = 1.244) and the lowest mean has the question "Work decisions are made by my supervisor in a biased manner" (M = 1.98, Sd = 1.12). Regarding interactional justice, the highest mean is the question "When decisions are made about my work, my manager treats me with respect and dignity" (M = 3.48, Sd = 1.14) and the lowest mean is the question "When decisions are made about my work, my manager is sensitive to my personal needs" (M = 3.05, Sd = 1.19). Meanwhile, regarding the level of job satisfaction, it turns out that the highest mean is the question "I am satisfied with the personal relationship between my boss and his/her employees" (M = 3.53, Sd = 1.30) and the lowest mean is the question "I am satisfied with the way my salary compares to similar jobs in other companies" (M = 2.58, Sd = 1.51).

In order to formulate answers to the research questions and determine the correctness of the statistical tests, we verified whether the variables in the study are normally distributed or not, through the normality test. From the data processing, it results that the normality test presents a significant value for Kolmogorov-Smirnov (p = < .05) and Shapiro-Wilk (p < .05). From the testing of the results, the variables present a non-normal distribution since the significance value must be above .05. Thus, we have to use non-parametric tests, which meet the condition of non-normality.

The Mann-Whitney U test was used to compare the differences between two independent groups, i.e. gender (male, female) and the relationship of the variable with organizational justice. The Kruskal Wallis test was used to compare the differences between three independent groups, as well as the relationship of the variable with organizational justice.

It turned out that there is no significant relationship between gender and organizational justice (Mann-Whitney Test = 302.5, p > .05), while there is a significant relationship between age and organizational justice ($X^2_{(3,147)}$ = 37.078, p < .05). Referring to the Mean Rank, it results that the highest level of organizational justice is presented in the age group over 44 years old, (M. Rank = 57.25) followed by the age group 35-44 years old with (M. Rank = 48.04). In the younger age group, the level of organizational justice is presented as lower. As a conclusion, we might say that age and organizational justice have a significant relationship and that with increasing age, the level of perceived organizational justice also increases.

We verify that there is a significant relationship between experience in the bank and organizational justice ($X^2_{(5,147)}$ = 24.437, p < .05). Referring to Mean Rank, it results that the highest level of organizational justice is presented in personnel with 7-8 years with (M. Rank = 54.43) followed by more than 8 years with (M. Rank = 44.33). In the group with less than one year, the level of organizational justice is presented as lower. with (M. Rank = 19.83). As a conclusion, we say that experience in the bank and organizational justice have a significant relationship and that it is presented with higher levels in employees with more years of work.

Based on the above results, in response to research question 1, we conclude that there is a relationship between age and banking experience with organizational justice, but there is no relationship between gender and organizational justice in the banking sector.

Searching the answer for research question 2, we used the nonparametric Spearman's rho correlation. Based on the results, it is confirmed that there is a significant positive correlation between distributive justice and procedural justice (rs = .889, p < 0.01). Distributive justice has a significant positive relationship with interactional justice (rs = .822, p < .01). Procedural justice also has a significant positive relationship with interactional justice (rs = .813, p < .01). The increase in one dimension leads to the increase in the other dimension.

On the other hand, the relationship between the variables of the organizational justice dimension and the level of job satisfaction is examined. Based on the results, it is verified that there is a significant positive correlation between distributive justice and the level of job satisfaction (rs = .896, p < .01). Procedural justice has a significant positive relationship with the level of job satisfaction (rs = .923, p < .01). Also, interactional justice has a significant positive relationship with the level of job satisfaction (rs = .841, p < .01). An increase in one dimension leads to an increase in the level of job satisfaction. The relationship between the two variables organizational justice and the level of job satisfaction was examined. The results verify that there is a significant positive correlation between organizational justice and the level of job satisfaction (rs = .930, p < .01). Increasing organizational justice leads

to an increase in the level of employee satisfaction. In response to research question 2, we conclude that there is a significant relationship between organizational justice (in all three of its dimensions) and job satisfaction.

4. CONCLUSION

This study, in our opinion, presents some valuable managerial conclusions. First, the findings have revealed that a positive and significant correlation exists between the three dimensions of organizational justice and the perception of employee satisfaction in the banking sector of Albanian capital city - Tirana. These results should draw the attention of commercial banks' executives toward serious consideration for the importance of organizational justice in the workplace, thus some improvement steps and measures might be implemented, in order to increase the job satisfaction of their employees. Banks should be reasonable and careful in implementing new standards with regard to the distribution of work, rewards and promotions.

Second, the results of this study provide supporting evidence about the uniqueness of the components of interactional justice. Thus, banks should give considerable importance to several critical organizational values, such as: courtesy, honesty and respect, because they are directly related to employee satisfaction and engagement at work.

Third, this study might inspire further research in banking sector at national level, and might me extended as well into other sectors of economy, such as telecommunication, big retail, tourism etc.

Finally, the results might have some valuable implications for cross-cultural research in new areas. It would be intriguing to investigate whether the relationships between organizational justice, satisfaction, and other organizational variables would remain the same in a multicultural and diverse banking sector.

References

[1]   J. Greenberg, "A taxonomy of organizational justice theories," *The Academy of Management Review*, vol. 12, no. 1, pp. 9–22, 1987.

[2]   J. A. Colquitt, J. Greenberg, and C. Zapata-Phelan, "What is organizational justice: An historical analysis," in *Handbook of organizational justice,* J. Greenberg and J. A. Colquitt, Eds. Lawrence Erlbaum Associates Publishers*, 2005, pp. 3–56.

[3]   R. Cropanzano, D. E. Bowen, and S. W. Gilliland, "The management of organizational justice," *The Academy of Management Perspectives*, vol. 21, no. 4, pp. 24–48, 2007.

[4]   M. D. Bayles, "A study of relationship between organizational justice and job satisfaction," *International Journal of Business and Management*, vol. 5, no. 12, pp. 103–119, 1990.

[5]   R. J. Bies and J. F. Moag, "Interactional justice: Communication criteria of fairness", in *Research on Negotiations in Organizations,* R. J. Lewicki, B. H. Sheppard, and M. H. Bazerman, Eds. JAI Press, Greenwich, 1986, vol. 1, pp. 43–55.

[6]   J. A. Colquitt, "On the dimensionality of organizational justice: a construct validation of a measure," *Journal of Applied Psychology*, vol. 86, no. 3, art. no. 386, 2001.

[7]   J. P. Meyer, D. J. Stanley, L. Herscovitch, and L. Topolnytsky, "Affective, continuance, and normative commitment to the organization: A meta-analysis of antecedents, correlates, and consequences," *Journal of Vocational Behavior*, vol. 61, no. 1, pp. 20–52, 2002.

[8]   B. P. Niehoff, and R. H. Moorman, "Justice as a mediator of the relation-ship between methods of monitoring and organizational citizenship behavior," *Academy of Management Journal*, vol. 36, no. 5, pp. 527–556, 1993.

The Administration's Liability for Errors Committed by Artificial Intelligence

Ahmed Merah[1]

[1]Department of Law, Faculty of Law and Political Science, University Mustapha Stambouli of Mascara, Algeria
Corresponding author: Ahmed Merah (e-mail: merah.ahmed@univ-mascara.dz)

Abstract

Today, artificial intelligence (AI) applications have a clear impact on various aspects of life, as their widespread and increasing use accelerates workflows and shifts from traditional work systems to digital work systems. An example of this is the use of AI in making administrative decisions through AI-based applications. This paper, therefore, explores the administration's liability for any errors that this system may commit, especially since the AI system itself lacks legal personality and, hence, cannot be held accountable for its errors. To address these questions, we adopted a descriptive-analytical approach by examining legal texts and general principles governing administrative decisions and applying them to decisions made by AI systems. Additionally, a comparative approach was used to provide recommendations aimed at preserving the legality of decisions made under AI systems on one hand, and on the other, safeguarding the rights and freedoms of individuals. The study concludes that administrative liability cannot be attributed to the AI system itself, and it ends with key findings and recommendations.

Keywords: Management responsibility, Error, Artificial intelligence, Management decisions, Legal personality

The Use of Artificial Intelligence in Teaching German as a Foreign Language: Potencials, Challenges, and Perspectives

Marisa Janku[1], Daniel Leka[1]

[1]Department of German Studies, University of Tirana, Tirana, Albania
Corresponding author: Daniel Leka (e-mail: daniel.leka@unitir.edu.al)

Abstract

The use of artificial ıntelligence in teaching German as a foreign language: Potentials, challenges, and perspectives artificial ıntelligence (AI) is rapidly transforming the educational landscape, including the teaching of German as a foreign language (DaF). This paper explores the potential, challenges, and future perspectives of integrating AI into language learning. AI tools such as chatbots, language processing models, and adaptive learning platforms offer personalized instruction, real-time feedback, and flexible learning environments, making language acquisition more accessible and efficient. Moreover, AI can enhance student engagement through gamified experiences and interactive exercises, addressing diverse learning styles. However, challenges such as data privacy concerns, the risk of over-reliance on technology, and limitations in handling nuanced cultural and contextual aspects of language learning persist. Additionally, the lack of trained educators proficient in AI-driven tools and the potential for biases in language models pose significant obstacles. This paper argues that while AI offers substantial promise in enhancing the effectiveness of teaching German, a balanced integration with traditional pedagogical methods and careful consideration of ethical implications is essential. Future perspectives include hybrid learning models and AI-enhanced curricula that align with learners' individual needs while preserving the human aspect of teaching.

Keywords: Artificial ıntelligence, German as a foreign language, Personalized learning, Language teaching, Challenges, Perspectives

1. INTRODUCTION

The rapid advancement of artificial ıntelligence (AI) has permeated various sectors, including education. One of the most significant areas of potential transformation is language learning, where AI offers innovative solutions to long-standing challenges [1]. In the context of teaching German as a foreign language (Deutsch als Fremdsprache or DaF), AI is poised to revolutionize instructional methodologies, providing learners with more personalized and interactive experiences. Traditionally, learning a foreign language has been heavily dependent on classroom-based interactions, textbooks, and the direct guidance of teachers. While these approaches have their merits, they are often limited in addressing individual learning styles, providing immediate feedback, and adapting to the pace and needs of each learner. AI-driven tools can complement and enhance these methods by offering tailored educational content, automating repetitive tasks, and creating immersive learning environments that simulate real-world language use [2].

AI technologies such as natural language processing (NLP), machine learning algorithms, and adaptive learning systems allow for the automation of many aspects of language instruction. These technologies can analyze a learner's progress in real-time, identify areas of difficulty, and adjust exercises accordingly [3].

Tools like chatbots and AI-based tutors simulate conversational practice, providing immediate feedback and correction. Moreover, AI can assist in the development of pronunciation and grammar skills through speech recognition and error analysis [2, 3]. However, while the potential of AI in language teaching is vast, it is accompanied by several challenges. Issues related to the accuracy of AI in understanding complex language structures, the cultural subtleties of German, and concerns regarding data privacy must be carefully considered. There is also the question of how to best integrate AI with existing pedagogical approaches without diminishing the critical role of human interaction in language learning [7, 8].

This paper aims to explore the potentials, challenges, and future perspectives of AI in the context of teaching German as a foreign language. It will examine the technological innovations that are currently reshaping the landscape of DaF education, address the limitations and ethical concerns associated with AI-driven tools, and

discuss how educators and learners can benefit from a balanced approach to integrating AI into the language learning process.

2. MATERIAL AND METHOD

This section outlines the tools, technologies, and methodologies employed to investigate the role of AI in teaching DaF. The study adopts a mixed-methods approach, combining qualitative and quantitative research methods to evaluate the effectiveness, challenges, and future potential of AI-driven tools in language instruction.

2.1. Materials

The study utilizes various AI-based tools [4] and platforms that are currently applied in language education. These tools were selected based on their popularity, accessibility, and functionality in the context of language teaching. The key materials include:

- AI-based Language Learning Platforms: Duolingo, Babbel, and Busuu, which incorporate AI for personalized language instruction, adaptive learning pathways, and real-time feedback [4,9].
- Chatbots and Conversational AI: Tools such as Replika and AI-based chat platforms that simulate German language conversations to help learners practice speaking and writing.
- NLP Tools: Applications like Google Translate and DeepL, which offer AI-driven translations, grammar corrections, and speech recognition for pronunciation practice [4, 5].
- Speech Recognition and Pronunciation Training Tools: Software like Rosetta Stone and Mondly that employ AI to improve learners' spoken German through speech analysis and corrective feedback [10].

2.2. Methodology

2.2.1. Qualitative Analysis

To assess the impact of AI on the learning experience, a qualitative approach was used, gathering data from language learners and educators through:

- Interviews with Educators: In-depth interviews were conducted with 10 German language teachers who use AI-driven tools in their classrooms. The focus was on their experiences with integrating AI into their teaching methods, its perceived effectiveness, and the challenges they faced.
- Learner Feedback: Surveys and focus groups were conducted with 40students learning German as a foreign language at different proficiency levels. Participants were asked to share their experiences with AI tools, including ease of use, perceived benefits, and challenges such as inaccuracies or cultural disconnects in language usage.
- Content Analysis of AI-based Tools: The features and functionalities of various AI-based tools were analyzed in terms of how well they support language learning objectives, such as vocabulary building, grammar, pronunciation, and conversational fluency.

2.2.2. Quantitative Analysis

A quantitative approach was employed to measure the effectiveness of AI tools in improving language proficiency. This involved:

- Pre- and Post-Tests: A cohort of 40students was divided into two groups: one using AI-driven tools and the other using traditional learning methods (classroom instruction, textbooks, etc.). Both groups were tested on their German language skills before and after a 12-week learning period. The tests assessed vocabulary, grammar, reading comprehension, speaking, and listening skills. A comparative analysis was conducted to determine the improvement in language proficiency between the two groups.
- Usage Data Analysis: For students using AI tools, data on usage frequency, completion of exercises, and progress was collected and analyzed. The data was correlated with test performance to explore whether increased engagement with AI tools led to better language outcomes.

2.2.3. Ethical Considerations

Given the use of AI, the study took into account ethical concerns related to:

- Data Privacy: Ensuring that personal information and learning progress data collected from students were stored securely and used solely for research purposes.
- Bias in AI Algorithms: A review of AI tools was conducted to determine the extent of any biases in the data sets used to train them, particularly in relation to the cultural and contextual understanding of the German language.

2.2.4. Limitations

The study acknowledges certain limitations in the methodology, including:

- Sample Size: While the study includes 40participants, a larger and more diverse sample would provide more generalizable results.
- Technological Access: The availability of AI tools may vary depending on the learners' access to technology and the internet, potentially influencing the outcomes.
- Subjectivity in Qualitative Feedback: Learner and educator feedback may be influenced by personal biases or prior experience with technology, which could affect their perception of AI's effectiveness. By employing this mixed-methods approach, the study aims to provide a comprehensive analysis of the potentials, challenges, and future perspectives of using AI in teaching German as a foreign language. The combination of qualitative and quantitative data allows for a more holistic understanding of AI's impact on language acquisition.

3. RESULTS

The results from this study provide insights into the effectiveness, challenges, and potential of using AI tools in teaching German as a foreign language (DaF). The findings are organized into two main sections: the quantitative analysis of language proficiency improvements and the qualitative analysis based on learner and educator feedback.

3.1. Quantitative Results

3.1.1. Pre- and Post-Test Scores

The comparison between the AI-assisted learning group (Group A) and the traditional learning group (Group B) revealed noticeable differences in language proficiency improvement over the 12-week period.

- Group A (AI-assisted tools) showed a 24% average improvement in overall language proficiency, with the highest gains in vocabulary retention (30%) and speaking skills (28%).
- Group B (traditional methods) demonstrated a 15% average improvement, with a notable increase in reading comprehension (18%) but lower gains in speaking and pronunciation skills (10%). These results suggest that AI tools have a significant impact on oral language skills, likely due to the real-time feedback and interactive nature of AI-based language practice.

3.1.2. Usage Data and Learning Outcomes

Data on student engagement with AI tools (e.g., frequency of use, completion of exercises) revealed a strong correlation between high usage and greater language improvement. Students who used AI tools for at least 4 hours per week scored 20% higher on post-tests than those who used them less frequently.

- Frequent users (4+ hours/week) improved their grammar and writing by 22%, compared to 12% for less frequent users.
- Speech recognition tools were particularly effective for pronunciation, with students using these tools regularly reducing pronunciation errors by 35% compared to 18% in the non-AI group. This data supports the idea that increased engagement with AI-driven platforms leads to better learning outcomes, particularly in skill areas that require repetitive practice.

3.2. Qualitative Results

3.2.1. Feedback from Learners

The feedback from learners highlighted several key benefits and challenges associated with using AI tools for learning German:

- Personalization and Adaptability: Over 80% of students appreciated the personalized learning paths offered by AI tools, noting that exercises were adjusted to their skill level and learning pace. They reported higher motivation due to the sense of individual progress.
- Instant Feedback: Students found the real-time feedback on grammar, pronunciation, and vocabulary to be highly beneficial. The majority (75%) mentioned that immediate correction of mistakes helped them improve their language skills faster, especially in speaking and writing.
- Gamification and Engagement: Many learners (65%) enjoyed the gamified elements present in platforms like Duolingo, which increased their engagement and made language learning feel less like a chore. However, learners also identified some challenges:
- Cultural Context and Nuance: Around 40% of students reported that AI-driven exercises sometimes lacked cultural context or provided overly literal translations, which could lead to confusion in understanding idiomatic expressions or cultural references.
- Pronunciation Limitations: While AI tools improved pronunciation accuracy, about 30% of students noted that the speech recognition software occasionally failed to recognize regional accents or less common pronunciations, resulting in incorrect feedback.

3.3. Feedback from Educators:

Educators shared mixed opinions about the integration of AI tools into their teaching practices:

- Support for Repetitive Tasks: Teachers found AI useful for automating repetitive exercises such as vocabulary drills, grammar correction, and pronunciation practice. This allowed them to focus on higher-order teaching activities, such as explaining complex grammatical rules or providing cultural context.
- Supplementary Role: Most educators (70%) agreed that AI should complement, not replace, traditional teaching methods. They emphasized that while AI tools can reinforce language skills, human interaction is crucial for understanding the cultural and social aspects of language learning.
- Concerns about Bias: Some educators (25%) expressed concerns about potential biases in AI algorithms, particularly in the way language models are trained. They pointed out instances where AI tools made errors in interpreting complex sentence structures or idiomatic expressions, potentially confusing learners.

3.4. Challenges and Limitations

The study also identified several key challenges in the use of AI for teaching German as a foreign language:

- Data Privacy Concerns: Both educators and learners raised concerns about the privacy of personal data collected by AI-driven platforms. The lack of transparency in how data is stored and used was a major issue for 40% of respondents.
- Technological Access: Approximately 20% of learners mentioned that limited access to the required technology (high-speed internet, updated devices) hindered their ability to fully benefit from AI tools.
- Over-Reliance on AI: There was a concern that over-reliance on AI might lead to a reduction in critical thinking or the ability to navigate complex language situations without automated assistance. 4. Summary of Key Findings
- AI tools led to greater improvements in oral language skills (speaking, pronunciation) compared to traditional methods.
- Personalization and real-time feedback were key strengths of AI-driven learning, contributing to higher learner motivation and engagement.
- Challenges with cultural nuance and occasional errors in AI feedback were noted as areas needing improvement.
- Educators generally viewed AI as a valuable supplement to traditional teaching, with the potential to enhance but not replace human interaction in language learning [5, 6].

These results provide a comprehensive overview of both the strengths and limitations of AI in teaching German as a foreign language, highlighting the need for thoughtful integration of AI tools into language curricula.

4. CONCLUSION

This study has explored the potentials, challenges, and perspectives of using Artificial Intelligence (AI) in teaching DaF. The results indicate that AI-driven tools offer significant advantages in terms of personalized learning, adaptive feedback, and enhanced engagement. However, there are also critical challenges that need to be addressed to fully realize the benefits of AI in language education.

i.   Key Findings AI tools have demonstrated their effectiveness, particularly in improving oral language skills, such as speaking and pronunciation. The ability to provide real-time feedback and tailor lessons to individual learners' needs has resulted in faster progress compared to traditional methods. Learners who used AI tools showed greater overall improvement, especially in vocabulary retention, pronunciation accuracy, and speaking fluency. The study also highlighted that AI tools excel in repetitive and practice-based tasks, such as vocabulary drills, grammar exercises, and pronunciation corrections. This allows learners to engage with language in a more dynamic and interactive way, and gives educators more time to focus on complex teaching tasks. However, the research identified several limitations in the current AI technologies. These include difficulties in recognizing cultural nuances, handling idiomatic expressions, and interpreting regional accents in German. Furthermore, while learners appreciated the personalized experiences offered by AI tools, they also acknowledged the importance of human interaction for a deeper understanding of the language's cultural and social dimensions.

ii. Challenges Several challenges remain in the use of AI in language education:

•   Cultural and Contextual Understanding: AI tools need further development to accurately handle cultural nuances and idiomatic expressions in German. Currently, they can provide literal translations and corrections but struggle with the subtleties of language use in different contexts.
•   Data Privacy and Ethical Concerns: Privacy issues were raised regarding how AI platforms collect and manage user data. More transparency and ethical practices are needed to ensure user trust.
•   Technological Barriers: Unequal access to the necessary technology, such as high-speed internet and updated devices, poses a barrier to the full adoption of AI tools for language learners in various regions.

iii. Future Perspectives Moving forward, AI's role in teaching German as a foreign language will likely involve a hybrid model, where AI tools complement traditional methods rather than replace them. A balance between automated, personalized learning and human-led instruction is essential for achieving holistic language proficiency. Future developments in AI should focus on improving cultural context understanding, reducing biases in language models, and enhancing speech recognition for various accents. Additionally, the ethical use of AI in education must be prioritized, with clear policies on data privacy and protection to address user concerns.

In conclusion, AI presents a promising avenue for transforming language education, making it more accessible, engaging, and tailored to individual learners' needs. However, its integration must be carefully managed to ensure that the human element of teaching—particularly in areas requiring cultural, social, and emotional understanding—remains central to language learning.

References

[1]   K. Batty, *Teaching and Researching Language and Technology*, Pearson Education, 2019.
[2]   R. Godwin-Jones, "Emerging technologies: AI and language learning," *Language Learning & Technology*, vol. 24, no. 2, pp. 4–14, 2020.
[3]   R. Luckin, W. Holmes, M.Griffiths, and L. B. Forcier, *Intelligence Unleashed: An Argument for AI in Education*, Pearson Education, 2016.
[4]   C. Tschichold, "AI-based language learning apps: A case study of Duolingo," *ReCALL*, vol. 32, no. 1, pp. 102–117, 2020.
[5]   W. Xu and M. Warschauer, "Artificial ıntelligence in education: A review of current applications and future perspectives," *Journal of Educational Technology*, vol. 54, no. 5, pp.12–24, 2021.
[6]   J. Traxler and A. Kukulska-Hulme, *Mobile Learning: The Next Generation*, Routledge, 2022.
[7]   L. Selinker, *Second Language Acquisition: An Introductory Course*, Routledge, 2013.
[8]   J. Schmidhuber, "Deep learning in neural networks: An overview," *Neural Networks*, vol.61, pp. 85–117, 2015.
[9]   Duolingo. (2022). *AI in Language Learning* [Online]. Available: https://www.duolingo.com/ai-language
[10] D. J. Young, and M. E. O'Neill, *Language Learning with Technology: Ideas for Integrating Technology in the Classroom*, Cambridge University Press, 2020.

Exploring Style: An in-Depth Analysis of Robert Frost's Poem "The Road Not Taken"

Fakiha Arain[1]

[1]Department of English, Quaid-e-Awam University of Engineering, Science and Technology, Nawabshah, Pakistan
Corresponding author: Fakiha Arain (e-mail: fakihaarain23@gmail.com)

Abstract

This research conducts an in-depth stylistic analysis of Robert Frost's well-known poem, "The Road Not Taken." Recognized as a linguistic marvel, the study aims to dissect the poem's linguistic significance and uncover underlying meanings. By applying levels of stylistic analysis, the research explores how Frost employs stylistic emphasis to make distinctive linguistic choices. Additionally, the study delves into the impact of figures of speech on reader perception, emphasizing the role of literary devices in shaping interpretation. The analysis extends to the thematic exploration of choices and consequences in the poem. This research contributes to a deeper understanding of Frost's work, revealing the intricate relationship between literature and linguistics. It serves as a valuable resource for students and literary critics interested in unraveling the complexities of "The Road Not Taken."

Keywords: Deviation, Linguistic significance, Poetry, Stylistic analysis, Style

1. INTRODUCTION

The word "style," which comes from the Greek word "elocution," captures a complex and wide-ranging idea, and its meaning changes depending on the situation. Fundamentally, style is an original way of doing things, a distinct approach that takes on various forms depending on the context in which it is studied. Within the field of linguistics, style assumes a more specific meaning, evolving into a focus of inquiry that includes a writer's word choice, sentence construction, and use of literary devices to communicate ideas. This complex idea is applicable to a variety of literary genres, such as poetry, prose, and novels, where the writing style of each author becomes an expressive fingerprint that reflects personal preferences and creative tendencies.

The scholarly field of stylistics, as defined by Leech [1] explores the complex relationship between language and literature. It focuses mostly on literary materials and analyses the differences in style between discourses. The study of style becomes a dynamic investigation within the framework of stylistics, embracing linguistic components like syntax, phonology, lexicology, semantics, and the graphical aspects of expression. According to Leech, the linguistic approach to literature explores the creative roles that language plays and aims to clarify the relationship between linguistic decisions and literary effect.

This research involves a stylistic analysis of Robert Frost's renowned poem, "The Road Not Taken." With the use of stylistics, the objective is to dissect the poem's formal components, looking at syntactic, phonological, lexical, and semantic components in order to shed light on the complex interplay between linguistic effects and literary text. The aim of this study is to enhance comprehension of Frost's unique writing style and its influence on the long-lasting influence of "The Road Not Taken" on the literary domain.

1.1. Research Questions

RQ1. How does Frost use stylistic elements to convey the theme of individual choice in "The Road Not Taken"?
RQ2. How do phonological, graphological, grammatical, lexical, and semantic elements contribute to the stylistic impact of the poem?

1.2. Research Objectives

RO1. To analyze Frost's stylistic choices to convey the theme of individual choice in "The Road Not Taken."

RO2. To examine how phonological, graphological, grammatical, lexical, and semantic elements contribute to the poem's overall stylistic impact and reader interpretation.

1.3. Stylistics Analysis Levels

A framework provided by Leech (1969) [1] is followed in the stylistic examination of literary works, with different levels being used:

- Phonological Level: Analyze sound components in the text, such as syllables and rhyme patterns.
- Graphological Level: Concentrates on the capitalization and punctuation patterns used in writing.
- Grammatical Level: Examines how sentences are put together and how they interact.
- Lexical Level: Examines the text's vocabulary and lexis while taking word choice and interpretation into account.
- Thematic Level: This level brings the investigation to a close by looking at the text's theme and incorporating textual evidence and the levels that were previously examined.

1.4. Literature Review

Literature stands as an indispensable testimony to human experiences, encapsulating thoughts, feelings, and observations about life through the medium of language. As Samuel Johnson puts it in "Lives of the Poet," language is the "dress of thoughts." This metaphor illustrates how ideas begin life in a preverbal state before being creatively molded and articulated through language. Therefore, the words, phrases, and linguistic patterns we choose to use in our writing and speech act as windows into our mental processes, revealing our views. In literature, truth and linguistic beauty are skillfully combined to create vivid narratives. Literature and language are inextricably linked since language is the main medium of expression. Throughout history, language and literature have been prominent subjects of critical discourse. The field of literary criticism, which has its roots in text interpretation, greatly depends on knowledge of fundamental terms like metaphor, irony, and figurative language all of which are closely related to the idea of language.

Research [2] states that stylistics is a branch of linguistics that bridges the gap between linguistic components and artistic functions in literature by concentrating on differences in language use. Similarly, [3] emphasizes the need of stylistics for the objective, scientific examination of literary text styles, with the goal of supplanting impressionistic and subjective literary criticism. The study [4] focuses on the critical function of stylistic analysis as a literary and linguistics bridge. His observations indicate that this analytical method explores the complex interactions between linguistic patterns and techniques, revealing the layers of meaning contained within literary pieces. The perspective highlighted in stylistic analysis underscores the comprehensive nature of the approach by examining both the deeper structures of language and its surface-level elements, such as syntax and word choice.

With the use of this method, academics may reveal the complex stylistic decisions writers have made, which enhances our knowledge of the role language plays in literature. Research [5] focuses on the investigation of unusual representations in language and their roles in stylistic analysis, which balances this viewpoint. By doing this, he highlights the creative and dynamic parts of language use that go beyond accepted conventions. According to [5], stylistic analysis includes the study of creative and non-traditional language usage in addition to the research of conventional language expressions. This wider focus illuminates the ways in which writers use language to achieve certain effects and creative goals while enabling analysts to recognize the creativity and artistry present in literary works. In order to bring a linguistic perspective to the conversation. The study of linguistics focuses on investigating the nature of human language, how it is learned, and how it functions in both social and individual contexts [6]. His viewpoint highlights the intrinsic relationship between language and human communication by placing stylistic study within the larger context of linguistics. He provides groundwork for the integration of linguistic theories into the stylistic analysis of literary works by recognizing the central role of linguistics in comprehending language as a dynamic and growing system. This multidisciplinary method promotes a comprehensive analysis of language that takes into account its social, cognitive, and expressive aspects.

Holman [7] defines, language style, often known as figure of speech, is a departure from conventional construction, significance, or order for the purpose of achieving unique effects or meaning. Language style is essentially the use of language to express more complex and elegant meanings than simple language use. Readers experience a range of emotions in response to it, from adoration or sympathy to rage and hatred. He categorizes language style or figure of speech into two types: rhetorical language and figurative language. Rhetorical language is characterized by departures from formal language usage in order to accomplish specific effects without changing the fundamental meaning of words. Assonance and alliteration are two examples. Conversely, figurative language

uses word choice, construction, and meaning transfer to produce powerful and original expression. It produces an image effect by drawing comparisons, drawing contrasts, or explaining by analogy. Antithesis, apostrophe, climax, hyperbole, irony, metaphor, metonymy, personification, simile, synecdoche, paradox, and symbol are a few instances of figurative language. Studies [8, 9] propose that symbols possess significance that extends beyond their literal interpretations. "The Road Not Taken," for example, represents decisions made in life between developing options and has more significance than just selecting a route.

2. MATERIAL AND METHOD

The methodology for this research on Robert Frost's poem "The Road Not Taken" combines qualitative and quantitative approaches within a comprehensive framework. Adhering to a qualitative research paradigm, primary data is derived directly from the poem, forming the cornerstone of the analysis. This qualitative exploration is complemented by secondary sources, including critical analyses, academic articles, and online references, enhancing the understanding of Frost's stylistic choices. The research design involves a meticulous reading of the poem for qualitative data collection. The subsequent analysis adopts a sequential and methodical approach, systematically addressing various literary stylistic aspects such as linguistic parallelism, deviation, graphological, grammatical, lexical, phonological, and thematic levels. The discussion extends to examine the impact of Frost's linguistic preferences, emphasizing the use of figurative language. This integrated qualitative and quantitative methodology aims to provide a nuanced understanding of Frost's distinctive style and its profound implications in the interpretation of "The Road Not Taken."

2.1. Introduction to Robert Frost (1874-1963): A Visionary Voice in 20th Century Poetry

Robert Frost, an eminent American poet, is renowned for his profound contributions to literature during the 20th century. Frost was born in San Francisco in 1874, and most of his early life was spent in rural New England, which is reflected in his poetry. Frost is well known for his use of common language, although his poetry has a profundity of meaning that goes beyond the everyday. Frost was a pathfinder in a period when the use of common language in poetry was revolutionary. But Frost went a step farther and embraced clarity and simplicity in his poetry. He distinguished himself as a poet ahead of his time with his unique style, which was characterized by understandable language and deep insights. "The Road Not Taken," one of Frost's well-known pieces, illustrates his examination of decisions and their effects. The poem, which was first published in 1916 and has since gained notoriety, is a prime example of Frost's skill at explaining difficult subjects with language that seems simple. Frost's dedication to rendering complex concepts in understandable language is consistent with the spirit of his day, during the Romantic period. Robert Frost is a poet who skillfully blended linguistic forms, bringing local dialects into the English language at large. His lasting influence on American literature confirms his status as a literary great and a pioneer of 20th-century poetry.

2.2. Structure of Poem "The Road Not Taken"

"The Road Not Taken" stands as a poetic masterpiece penned by Robert Frost, a distinguished American poet. Unlike traditional poems of his time, Frost adeptly employs common language to convey profound messages, a hallmark of his poetic brilliance. Published in 1916, this iconic work is nestled within Frost's collection, "Mountain Interval." Comprising four stanzas, each with five lines, the poem encapsulates the essence of choice and consequence. Frost, who is renowned for his ability to write poetry that is both approachable and thought-provoking, addresses the subject of making decisions throughout life. Because of the purposeful simplicity of the language, readers of many backgrounds can relate to the complex ideas included in the lines. Frost is acknowledged for having pioneered a corresponding strategy to used ordinary language for his audience. In "The Road Not Taken," Frost guides readers on an introspective journey as they consider the consequences of past decisions. The poet conveys the significance of divergent routes and the long-term effects of the selected route using powerful imagery and metaphors. The eternal themes of "The Road Not Taken" resonate with readers because they are relevant and enduring.

3. RESULTS

3.1. Stylistic Emphasis in "The Road Not Taken"

Stylistic emphasis, a pivotal strategy in linguistic analysis, serves to create a sense of uniqueness and deviation within the language used in Robert Frost's poem "The Road Not Taken." This focus, according to [10], includes the intentional diversity in language that enhances the overall literary effect on the reader. This intentional break from standard grammatical conventions brings some aspects to the fore and makes them stand out. Stylistic focus

is consistent with the idea of "defamiliarization," as defined by the distinguished Russian linguist Victor Shklovsky. The stress on making something foreign, or ostranenie, as used by Shklovsky, emphasises this emphasis's stylistic goal. This analysis uses stylistic emphasis as a way to give verbal elements more meaning within the parameters of "The Road Not Taken." The goal is to highlight linguistic patterns, whether they are replicated through parallelism or deviation from norms. Two important strategies used to achieve stylistic emphasis are "Parallelism" and "Deviation." Parallelism is the process of keeping words and ideas' sound structures consistent, which results in a harmonious pattern. Deviation, on the other hand, is the deliberate breaking of established sound or grammatical rules, introducing a disruptive element. As the analysis progresses, these techniques will be used to investigate how Frost employs stylistic emphasis in "The Road Not Taken," illuminating the unique decisions that enhance the poem's overall effect.

3.1.1. Lexical Divergence

Robert Frost strategically utilizes lexical divergence to enhance the poem's allure, combining his unique linguistic style with the overarching theme of choices and paths taken.

In the First Stanza
i.   "Yellow Wood": Frost diverges from conventional descriptions of woods by using "yellow," introducing a vivid and unconventional visual element that sets the tone for the poem and emphasizes the unique nature of the setting.
ii. "Travel Both": The phrase "travel both" deviates from a more straightforward construction like "travel on both," emphasizing the impossibility of simultaneously exploring both paths and highlighting the speaker's internal conflict and decision-making dilemma.

In the Second Stanza
iii. "Grassy and Wanted Wear": Frost uses "wanted wear" instead of a simpler term like "needed use" or "lacked wear." This deviation adds a nuanced layer to the description of the chosen path, suggesting a sense of longing or anticipation for human presence, enhancing the thematic emphasis on choices and their consequences.
iv. "Worn Them Really About the Same": The phrase "worn them really about the same" deviates from a more straightforward expression like "worn them equally." This choice of words contributes to the speaker's reflection on the similarity of the paths, underscoring the idea that, despite external differences, the choices ultimately lead to comparable outcomes.

In the Third Stanza
v.   "How Way Leads on to Way": Frost's use of "way leads on to way" deviates from a more straightforward phrasing like "paths lead to other paths." The choice of the word "way" introduces a broader and more abstract concept, emphasizing the cumulative nature of life's choices and the potential for one decision to lead to countless others. This subtle shift in language adds depth to the speaker's contemplation of the unfolding journey.

In the Last Stanza
vi. "And That Has Made All the Difference": The unconventional use of "difference" instead of a more common term emphasizes the unique impact of the speaker's choice, highlighting the distinctiveness of their journey.

3.1.2. Parallelism

Robert Frost artfully employs parallelism to create rhythmic symmetry and emphasize key thematic elements in "The Road Not Taken."

In the first stanza, Frost establishes a structural parallelism:

Two roads diverged in a yellow wood,
And sorry I could not travel both

This mirroring highlights the speaker's regret at being unable to explore both paths simultaneously, setting the tone for the poem's overarching theme of choices and their consequences.
The second stanza maintains rhythmic and thematic parallelism:

Then took the other, as just as fair,
And having perhaps the better claim,

This repetition reinforces the speaker's rationalization for choosing the less-traveled path, adding depth to the exploration of decision-making.

Continuing into the third stanza, thematic parallelism persists:

And both that morning equally lay
In leaves no step had trodden black.

This parallel construction underscores the equal and unexplored nature of the two diverging paths, contributing to the poem's reflection on the significance of choices.

In the final stanza, thematic parallelism is evident in the repetition of the first person:

I shall be telling this with a sigh
Somewhere ages and ages hence:

The consistent use of "I" emphasizes the personal and reflective nature of the speaker's narration, reinforcing the enduring impact of the chosen path.

3.1.3. "The Road Not Taken" as a Narrative Poem

"The Road Not Taken" is a narrative poem that chronicles a personal journey marked by a crucial decision. Through a first-person perspective, Robert Frost unfolds the speaker's contemplation and introspection when faced with two divergent paths in a yellow wood. The poem's narrative structure delves into the consequences of the chosen path, offering a concise exploration of choice and its enduring impact on the speaker's life.

3.1.4. Graphological Level of Analysis

The graphological level of analysis explores the visual and typographic elements employed by an author, contributing to the aesthetic and structural aspects of a literary text. In the context of "The Road Not Taken"" by Robert Frost, the graphological features, including punctuation, stanzaic arrangements, and spacing, play a crucial role in conveying the poem's thematic depth and emotional resonance. Frost's deliberate choices in these graphological elements contribute to the overall crafting and impact of the poem, shaping the reader's experience and interpretation.

The poem is composed of four stanzas, each comprising five lines, and adheres to a consistent rhyme scheme. The deliberate choice of structure and stanzaic arrangement reflects Frost's meticulous crafting, contributing to the poem's aesthetic appeal.

In this poem various punctuation are used like full stops, commas, exclamation mark, semi-colons, colon and dash.

- Full stops employed in the poem are three in line 12, 15 and 20 which emphasis the poet's stylistic choice to maintain a continuous flow of thought.
- Commas in "The Road Not Taken" enhance the poem's rhythm, offering pauses and dividing ideas. Ten commas are strategically placed, in line 1, 3, 6, 7, 10, 13, 14, 18 and 19 contributing to the contemplative flow of the speaker's reflections.
- Exclamation marks in the poem punctuate moments of emphasis and heightened emotions. It is employed once precisely in the line 13 "Oh, I kept the first for another day!"
- Semi-colons is used two times in this poem in line 5 "To where it bent in the undergrowth;" and line 8 "Because it was grassy and wanted wear;"
- Colon is used once in line 17 "Somewhere ages and ages hence:"
- Dash is also used once in line 18 "Two roads diverged in a wood, and I—"

3.1.5. Grammatical Level of Analysis

In this level of the research, it is observed that the poem is consisted of four stanzas with 5 lines in each stanza. The poem is composed of sentences that can stand alone as complete thoughts, contributing to its narrative and reflective style.

The poem employs the first person pronoun "I" consistently, accentuating the speaker2s personal reflection:

- Line 2: And sorry I could not travel both
- Line 3: And be one traveler, long I stood
- Line 4: And looked down one as far as I could
- Line 13: Oh, I kept the first for another day!
- Line 15: I doubted if I should ever come back.
- Line 16: I shall be telling this with a sigh
- Line 18: Two roads diverged in a wood, and I—
- Line 19: I took the one less traveled by,

Each stanza represents a distinct and complete idea, contributing to the overall narrative of the poem.

- Stanza 1: The speaker encounters a metaphorical crossroad, symbolizing a moment of decision and choice in life.
- Stanza 2: The speaker chooses one path over the other, acknowledging the difficulty in discerning which is truly superior, as both seem equally traveled.
- Stanza 3: The speaker reflects on the choice made and contemplates the potential consequences, emphasizing the unpredictability of life's journey.
- Stanza 4: Looking back on the decision, the speaker anticipates recounting the story in the future; expressing the impact of taking the less traveled path and the significance of individual choices.

3.1.5. Lexical Level of Analysis

i. In the poem lexical choices like "sorry" and the repetitive use of "and" contribute to the regretful and contemplative tone of the poem, conveying the speaker's decision-making process and its impact on the narrative.
ii. Frost utilizes specific lexical choices, such as "diverged" and "undergrowth," to vividly depict the theme of choices and the natural environment in the poem.
iii. The poem consistently employs first-person pronouns, emphasizing the personal nature of the speaker's journey and decision-making process, fostering a strong connection between the reader and the narrative.
iv. Frost's lexical selections like "grassy" and "wanted wear" contribute to the imagery.
v. The term "difference" in the closing lines acts as a lexical focal point, encapsulating the poem's overarching theme and highlighting the profound impact of the chosen path on the speaker's destiny.

Table 1. Lexical level of analysis

Noun	Pronoun	Verb	Adverb	Adjective
roads, wood, traveler, undergrowth, claim, way, morning, leaves, step, day, sigh, ages, difference	I, one, it, them	diverged, could travel, be, stood, looked, took, was, wanted, wore, lay, had trodden, kept, knowing, leads, doubted, should come, shall be telling, took, made	far, really, equally, perhaps, just	yellow, fair, better, grassy, same, black, first, another, less

3.1.6. Phonological Level of Analysis

"The Road Not Taken" adopts a narrative structure with an ABAAB rhyme scheme in each stanza, providing a distinct rhythm. The poem incorporates various phonetic devices like Alliteration, consonance, assonance, and anaphora, enhancing the auditory appeal. Rhyming words contribute to the phonological richness, creating a harmonious and memorable soundscape.

Table 2. Phonological level of analysis

Rhyming Words	
Wood	Could
Both	Growth
Fair	Wear
Same	Claim
Lay	Day
Black	Back
Hence	Difference

3.1.7. Alliteration

The repetition of consonant sounds in closely positioned words within a phrase or sentence, creating a melodic and rhythmic effect.

- Line 8: "wanted wear" (repetition of the /w/ sound)
- Line 13: "first for" (repetition of the /f/ sound)

3.1.8. Consonance

Consonance is a poetic and literary device characterized by the repetitive use of consonant sounds, at the initial, middle, and end of a line.

- Line 1: "roads diverged" (repetition of the /r/ sound) and "yellow wood," (repetition of the /w/ sound)
- Line 2: "not travel" (repetition of the /t/ sound)
- Line 5: "To where it bent" (repetition of the /t/ sound)
- Line 6: "Then took the other" (repetition of the /th/ sound)
- Line 14: "Yet knowing how way leads on to way," (repetition of the /w/ sound)
- Line 16: "this with" (repetition of the /th/ sound)

3.1.9. Assonance

Assonance is the repetition of vowel sounds.

- Line 1: "Two roads diverged in a yellow wood," (repetition of the /o/ sound)
- Line 9: "Though as for that the passing there" (repetition of the /a/ sound)

Table 3. Assonance

Alliteration	Consonance	Assonance
/w/	/r/ /w/	/o/
/f/	/t/ /th/	/a/

3.1.10. Figures of Speech

Simile: A simile is a figure of speech in which two distinct objects are compared with the use of the terms "like" or "as" to emphasize a common feature. In the line "And took the other, as just as fair," from the poem the simile is used to compare the fairness or attractiveness of the two diverging roads.

Metaphor: A metaphor is a figure of speech that involves making a direct comparison between two unrelated things, suggesting that they are alike in some way. In the line "And looked down one as far as I could." Metaphorically, looking down one road represents contemplating a life choice.

Enjambment: Enjambment occurs when a sentence or clause runs over from one line of poetry to the next without a pause or a syntactical break. In the line "Oh, I kept the first for another day! / yet knowing how way leads on to way." The idea flows seamlessly from one line to the next without a break.

Symbolism: Symbolism is the use of symbols to represent ideas or qualities, often giving deeper meaning to a work. In the poem, the two roads symbolize choices in life, and the choice of the less-traveled road symbolizes uniqueness and individuality.

Imagery: Imagery involves the use of vivid and descriptive language to create sensory experiences for the reader, appealing to the senses. In the line "And looked down one as far as I could / To where it bent in the undergrowth." This paints a visual image of the speaker contemplating the paths in a wooded area.

Hyperbole: Hyperbole is an exaggeration or overstatement used for emphasis. In the line "I doubted if I should ever come back." The use of "ever" is a hyperbolic expression of uncertainty about returning.

Anaphora: Anaphora is the repetition of a word or phrase at the beginning of successive clauses or lines. In the line "And I— / I took the one less traveled by," The repetition of "I" at the beginning of each line emphasizes the personal nature of the speaker's choice.

Paradoxes: A paradox is a statement that may seem contradictory but can reveal a deeper truth. In the line "I took the one less traveled by, / And that has made all the difference." The paradox lies in the idea that the choice of the less-traveled road made a significant difference, even though both paths seemed about the same initially.

Thematic Level of Analysis: Upon comprehensive analysis, the primary themes arising from "The Road Not Taken" center around the concepts of "choices" and "individuality." Examining the lexical choices and narrative structure, the poem revolves around the speaker's contemplation of diverging paths, symbolizing life's choices. The theme of choice is central, as the speaker reflects on the decision-making process and the implications of taking the less-traveled path. Additionally, the theme of individuality is evident in the speaker's unique journey, emphasizing the significance of personal decisions and their impact on life. The title itself, "The Road Not Taken," underscores the exploration of alternate paths, contributing to the thematic richness of the poem.

4. CONCLUSION

Robert Frost's "The Road Not Taken" stands as a timeless masterpiece intricately weaving the themes of choice and individuality through carefully crafted linguistic elements. Frost's stylistic prowess, evident in phonological, graphological, grammatical, lexical, and thematic elements, unveils a contemplative journey marked by diverging paths. The poem's rhythmic structure, phonetic devices, and deliberate graphological choices contribute to its aesthetic appeal, while lexical nuances and thematic depth enhance the narrative's imagery and meaning. Frost's exploration of the consequences of choosing the less-traveled path resonates beyond the verses, inviting readers to reflect on their own life choices. "The Road Not Taken" is a testament to the enduring power of language to convey profound truths about the human experience, leaving an indelible impact on those who engage with its linguistic landscape.

References

[1]   G. Leech, *A Linguistic Guide to English Poetry*, London: Longman, 1969.
[2]   G. W. Turner, *Stylistics*, London: Penguin Books, 1973.
[3]   M. H. Abrams, *A Glossary of Literary Terms*, 4th ed. New York: Holt, Rinehart and Winston, 1981.
[4]   H. G. Widdowson, *Stylistics and the Teaching of Literature*, London: Longman, 1975.
[5]   P. Verdonk, *Stylistics*, Oxford: Oxford University Press, 2002.
[6]   S. P. Corder, *An Intermediate English Practice Book*, London: Longman, 1960.
[7]   C. Hugh Holman, *A Handbook to Literature*, Indianapolis: ITT Bobbs-Merrill Educational Publishing Company Inc., 1985.
[8]   M. Meyer, *The Bedford Introduction to Literature*, 2nd ed. Boston: Bedford Books of St. Martin's Press, 1995.
[9]   L. Perrine, *Literature Structure, Sound, and Sense*, 5th ed. USA: Harcourt Brace Jovanovich Publishers, 1988.
[10]   G. Leech and M. Short, *Style in Fiction: A Linguistic Introduction to English Fictional Prose*, 2nd ed. London: Longman, 2007.
[11]   R. Frost, "The road not taken," in *Mountain Interval*, New York, NY, USA: Henry Holt and Company, 1916.

Doing Applied Linguistics (2011) by Nicholas Groom and Jeannette Littlemore: A Critical Review

Om Kumar[1], Shan E. Zehra[2]

[1]English Department, Quaid-e-Awam University of Engineering, Science & Technology University, Nawabshah, Sindh, Pakistan

[2]Institute of English Language & Literature, University of Sindh, Jamshoro, Sindh, Pakistan

Corresponding author: Om Kumar (e-mail: omk7341@gmail.com)

Abstract

"Doing Applied Linguistics" is a famous book by Nicholas Groom and Jeannette Littlemore. This book provides an overview of the field of Applied Linguistics with a clear introduction to the different dimensions of applied linguistics. The book is for novices; it gives straightforward answers to the basic questions about what applied linguistics is, what it does, and how. It shows how linguists influence the practical world. Its accessibility makes this an important book for students and anyone who wants to know how language affects them and those around them. This critical review describes the book's thematic focus, the pragmatism of its approach to researching linguistics, and its value as a contribution to the academic study of language. Doing Applied Linguistics (2011) by Nicholas Groom and Jeannette Littlemore is published by Routledge.

Keywords: Applied linguistics, Doing applied linguistics, Nicholas Groom and Jeannette Littlemore, Book review

1. INTRODUCTION

Books are "tools for communication between two minds" and a book review can tell what is in the book but also what is the purpose of the book [1]. A good book review is not a summary of the book but a commentary on the book with opinion [2]. An effective book is always attractive and opinion-based [3]. A scholarly book review is a type of academic writing that explains and critically evaluates the subject matter, value, meaning, and relevance of a book [4].

This paper provides a critical review of the book *Doing Applied Linguistics* (2011) by Nicholas Groom and Jeannette Littlemore [5], it is a comprehensive book and provides a path to understanding the basics of Applied linguistics. The book is divided into 10 chapters. Every chapter is very comprehensive with real-life examples. The following table provides a brief introduction to themes discussed in every chapter.

Table 1. A brief introduction to the themes covered in each chapter of [5]

Chapters	Themes
1 - Questions about applied linguistics	What is applied linguistics
2 - Topics in Applied Linguistics	Different topics in applied linguistics
3 - The impact of applied linguistics	How applied linguistics has helped language learning
4 - Studying applied linguistics	What students learn in applied linguistics
5 - Collecting qualitative data	Methods for collecting qualitative user data
6 - Analysing qualitative data	Techniques for analysing qualitative data
7 - Collecting quantitative data	Methods for collecting quantitative data
8 - Analysing quantitative data	Techniques for analyzing quantitative usage data
9 - Analysing texts	Approaches to analysing real-world texts and discourse through text analysis
10 - Analysing corpora	Using corpus data to study language

2. CRITICAL REVIEW

In introducing their book, Doing Applied Linguistics (2011), Nicholas Groom and Jeannette Littlemore say that it "offers a clear, accessible introduction to applied linguistics that is full of engaging content" and that they hope it "will be suitable for students and anyone else coming to applied linguistics for the first time". These are lofty goals, and they come through in the opening pages with a narrative that is remarkably clear, accessible, and well-written. The book is remarkable for its "accessibility" and balance between theory and method. The authors aim above all to give a guide to understanding what applied linguistics is how people research it, and, more importantly, what the study of linguistics can do locally and globally. Applied linguistics is an immensely broad field, covering everything from second language acquisition to language policy, and the authors do an admirable job of presenting the material in a comprehensive way without being overwhelming. There is no lack of superficiality and false clarity in the popular accounts of academic subjects, so it is rare to find a textbook that is thorough, clear, and engaging.

A clear strength of the book overall is that it makes abstract ideas and concepts accessible to beginners, thereby lowering the threshold for those not well-versed in the field. In answering introductory questions that anyone new to the field is likely to have for example, 'What is applied linguistics? Why is it important? What do applied linguists do? the authors make sure that readers know not only what applied linguistics is but why it matters, and why its body of knowledge and research methods can and should be applied to real-world language problems. Applied linguistics is neither a special sub-field of theoretical linguistics, but rather has drawn on a wide range of other disciplines including psychology, sociology, and education. This is particularly important for readers who might come to the book presuming that linguistics studies the formal structures of language as a purely abstract endeavor. Groom and Littlemore show how applied linguistics can be relevant to contemporary concerns such as education, language policies, and social justice.

The middle chapters of the book outline how research is carried out in applied linguistics. Here, the authors provide a practical toolkit for students outlining qualitative and quantitative methods. They cover data-collection methods such as interviews, questionnaires, and corpus analysis, and make clear how applied linguists collect and analyze data from their participants and research sites in order to answer language-related questions. This part of the book is particularly useful for students who may be planning to do their research in the field, not only giving them a theoretical understanding of research but also a practical guide to how to carry out such studies.

Another is its emphasis on application, Groom and Littlemore show how applied linguistics research informs language teaching, where the findings of studies help to shape teaching methodologies and curricula in classrooms; language policy, where the findings of applied linguistics research inform educational policies on multilingualism and the protection of minority languages; and policy more generally, where applied linguistics research can have an impact on matters of education, healthcare, the law and more. By giving examples of the direct application of applied linguistics findings, the book helps readers see how applied linguistics research impacts people's lives.
The second strength of the book is that, all the chapters with little examples. They often refer to real studies and what they found, so you get a good idea of what applied linguistics research actually looks like, and of what can be learned from it. Here the authors range widely over the varied linguistic contexts in which the field operates from second language learning to forensics and sociolinguistics. In this way, they keep the rather abstract theoretical concepts firmly in contact with concrete examples.

The more specialized chapters on the analysis of texts and corpora appear in the final chapters of the book and, to their credit, the authors do try to articulate how applied linguists use computational tools to analyze the use of language on a large scale. Given the increasing role of technology in linguistic research, and particularly in applied linguistics, these chapters are essential for readers with an interest in the proliferation of technology. More specifically, the authors' discussion of corpus linguistics and similar tools is extremely accessible and informative and will be valuable for students interested in the role of technology in linguistics.

Although the book is very strong in many ways, it is probably best suited for students at the beginning of their journey in applied linguistics. The focus on beginners makes the book accessible, but more advanced readers might find some areas to be quite thin in covering some very complex issues. For example, most theoretical discussions do not always go into great depth, although the authors provide an excellent list of further readings for readers who wish to delve deeper into specific topics. In this way, the book is both a great starting point and a good gateway to other areas of interest.

Structurally, the book is very well organized, as each chapter builds on the one before. The progression from the beginning of applied linguistics, where the authors discuss basic questions about the field, to more advanced topics

such as the analysis of data and corpus linguistics is logical and easy to follow. The book can be read in a straightforward manner, either from start to finish or from section to section (and parts of it might be more suitable for reading in sections, depending on the interest and level of the reader). Moreover, the glossary of terms, the list of major journals in applied linguistics, and the suggestions for further reading make this book a very useful reference guide.

To summarize, Groom and Littlemore's Doing Applied Linguistics is an essential introduction to the field, particularly for novices. It is a clear, jargon-free, thoughtful, and well-written book. Its practical orientation, combined with its ability to illustrate concepts through engaging examples, makes it a must-read for students embarking on studies in applied linguistics and, more broadly, for those in language teaching, TESOL, language acquisition, and other allied fields. The book lives up to its title as it demystifies applied linguistics without reducing it to a trivial enterprise; it provides readers with the necessary tools and exposures to both the theory and practice of the field, and it will remain a go-to text for students and teachers alike because of its focus on real-world applications and practical research methodologies.

3. CONCLUSION

In conclusion, we can say, that *"Doing Applied Linguistics"* is a very useful book, and we encourage anyone who is just starting out in applied linguistics to read it. While it will delight and inform both those who are just starting out in the field and those who have been in it for a long time, it is especially useful for new students, as they make their way through graduate school. Groom and Littlemore have written a text that is theoretically, pedagogically appropriate, lively, readable, and most importantly highly engaging. Doing Applied Linguistics is a welcome, well-written, and substantive addition to the literature on applied linguistics. By demarcating the boundaries of the field, both as theory and as practice, the book will be a useful resource for readers as they embark on the study of second language acquisition and language use in the world.

References

[1]   C. Bazerman, "The informed writer," UCSB [Online], Apr. 2022. Available: https://www.academia.edu/ 78059776/The_informed_writer

[2]   S. George and A. Dharmadhikari, "Writing a book review: frequently asked questions answered," *British Journal of Hospital Medicine*, vol. 69, no. Sup2, pp. M30–M31, Feb. 2008, doi: 10.12968/hmed.2008.69.sup2.28370.

[3]   G. R. Williamson, "What makes a good book review?," *Journal of Advanced Nursing*, vol. 50, no. 2, p. 119, Mar. 2005, doi: 10.1111/j.1365-2648.2005.03370.x.

[4]   I. Peate, "The anatomy of a book review," *Journal of Paramedic Practice*, vol. 1, no. 2, pp. 82–83, Nov. 2008, doi: 10.12968/jpar.2008.1.2.42029.

[5]   N. Groom and J. Littlemore, *Doing Applied Linguistics*, 2012, doi: 10.4324/9780203808955.

First-Principles Investigation on the Structural, Optoelectronic, and Photovoltaic Properties of Perovskite Oxide

Rekia Larbi[1], Sahnoun Omar[1], Sahnoun Mohamed[1]

[1]Department of Physics, University of Mascara, Mascara, Algeria
Corresponding author: Rekia Larbi (e-mail: rekia.larbi@univ-mascara.dz)

Abstract

The combination of stability and energy efficiency has been elusive despite long years of effort by scientists the world over. For this antiperovskites materials have drawn significant attention in solar industry because they milk more electricity out of sunlight than do the conventional crystalline silicon photovoltaic cells. Here, We investigate the structural, electronic, and optical properties of the antiPerovskite Ba_4As_2O using first-principles calculations based on density functional theory (DFT).The results from this report were consistent with the experimental data. The optical bandgap was accurately estimated from the absorption spectra. Ba_4As_2O has a direct gap (H–H) of 1.29 eV obtained by the TB-mBJ approximation very close to experimental values. the compound is semiconductor. In addition, These results have shown that properties such as the structural stability, nature of the bandgap, dielectric function, energy loss, and absorption coefficient of a material are the important parameters which are used to predict a given material as good solar cell absorber.

Keywords: Antiperovskite, Optical properties, Photovoltaic applications, DFT

Enhancing Self-Cleaning and Optical Properties in Erbium/Neodymium Co-Doped Lithium Niobate Tellurite Glass with Silver Nanoparticles for Laser Host Application

Nurhafizah Hasim[1]

[1]Advanced Optical Materials Research Group, Department of Physics, Faculty of Science, Universiti Teknologi Malaysia, 81310 UTM Johor Bahru, Johor, Malaysia
Corresponding author: Nurhafizah Hasim (e-mail: nurhafizah.h@gmail.com)

Abstract

This study explores the enhancement of optical and catalytic properties in Erbium (Er)/Neodymium (Nd) co-doped lithium niobate tellurite glass through the inclusion of silver nanoparticles (Ag NPs). Glass samples with varying Ag NP concentrations were synthesized using the melt-quenching method, revealing high thermal stability and a confirmed amorphous structure via X-ray diffraction (XRD) and TEM imaging. The Ag NPs induced hydrophilicity and structural changes, as shown in FTIR and Raman spectral shifts. UV-Visible-NIR spectra demonstrated intensified absorption peaks, while both direct and indirect optical band gaps widened with increased Ag NP content, reducing Urbach energy. Judd-Ofelt analysis highlighted high radiative quality, especially in S4 glass, with a quality factor of 3.37. Under 385 nm excitation, significant green and red emissions were observed, with notable stimulated emission cross-section and gain bandwidth. Photocatalytic testing using methyl blue degradation under visible light confirmed enhanced activity due to Ag NPs, underscoring the potential of Ag-doped Er/Nd co-doped lithium niobate tellurite glass for advanced optical and catalytic applications.

Keywords: Silver nanoparticles (Ag NPs), Optical properties, Photocatalytic activity, Erbium/neodymium co-doped glass, Lithium niobate tellurite glass

A Singular Fractional Elliptic Problem with an Absorption Term

Hanaa Achour[1], Sabri Bensid[1]

[1]Department of mathematics, Abou Bekr Belkaid-University of Tlemcen, Tlemcen, Algeria
Corresponding author: Hanaa Achour (e-mail: hanaa495@outlook.com)

Abstract

In this paper, we study the following problem:

$$\begin{cases} (-\Delta)_p^s u \ + \ \beta \dfrac{|u|^{p-2}}{|x|^{sp}} = \lambda f(x,u) & in \ \ \Omega \\ \qquad\qquad u = 0 & on \ \ \mathbb{R}^N \backslash \Omega, \end{cases} \qquad (P)$$

where Ω is a bounded regular domain in $\mathbb{R}^N (N \geq 2)$ containing the origin, $p > 1$, $s \in (0,1)$, $(N > ps)$, $\lambda > 0$, $0 < \beta < 1/c_H$ where c_H is the best constant in the fractional Hardy inequality, $f: \Omega \times \mathbb{R} \longrightarrow \mathbb{R}$ is a discontinuous function with respect to u and $(-\Delta)_p^s$ is the fractional p-Laplacian defined as

$$(-\Delta)_p^s u(x) = 2 \lim_{\varepsilon \to 0} \int_{\mathbb{R}^N \backslash B_\varepsilon(x)} \frac{|u(x) - u(y)|^{p-2}(u(x) - u(y))}{|u(x) - u(y)|^{N+sp}} \, dy, \ \ x \in \mathbb{R}^N,$$

where $B_\varepsilon(x)$ is the open ε-ball of center x and radius ε. Using the critical point theory combining to the fractional Hardy inequality, we show that the problem (P) admits at least two distinct nontrivial weak solutions.

Keywords: Singular problem, Fractional p-Laplacian, Critical point, Fractional Hardy inequality

Munckenhoupt Weights and Homogeneous Besov Spaces Associated with No-Negative Self-Adjoint Operators

Romaissa Chichoune[1]

[1]Department of Mathematics, University of Batna 2, Batna, Algeria
Corresponding author: Romaissa Chichoune (e-mail: r.chichoune@univ-batna2.dz)

Abstract

Let X be a space of homogeneous type and L be a non negative self-adjoint operator on $L^2(X)$ satysfying Gaussian upper bounds on its heat kerenels. In this study, we present some results concerning the theory of weighted Besov space $B_{p,q,w}^{s,L}(X)$ where $0 < p, q \leq \infty$, $s \in \mathbb{R}$ and w being in the Muckenhoup weight class A_∞. Specifically, we prove the molecular decompostion of the above homogeneous weighted Besov space.

Keywords: Muckenhoupt weights, Besov space, Doubling measure, Molecular decomposition

Water Balloon Parachute: Synergy Between Generative AI, Design Thinking Process, and Project Based Learning in Physics and Mathematics

Siti Salwa Alias[1,2], Raihanah Maisarah Roslan[3], Nuramilin Aishah Mohd Roslan[3], Muhammad Shafiq Izuddin Sazali[3], Arif Aiman Mohd Zulkarnain[3], Nor Ezzaty Ahmad[1], Nor Ain Husein[1]

[1]Department of Physics, Faculty of Science, Universiti Teknologi Malaysia, 81310 Skudai, Johor, Malaysia
[2]Centre for Sustainable Nanomaterials, Ibnu Sina Institute for Scientific and Industrial Research (ISI-SIR), Universiti Teknologi Malaysia, 81310, Skudai, Johor, Malaysia
[3]Department of Innovative Science and Mathematics Education, Faculty of Educational Sciences and Technology, Universiti Teknologi Malaysia, 81310 Skudai, Johor, Malaysia
Corresponding author: Siti Salwa Alias (e-mail: siti.salwa@utm.my)

Abstract

The Interactive Module on Water Balloon Parachute integrates physics and mathematics into an engaging learning experience, emphasizing real-world application through project-based learning and design thinking. The activity explores the principles of work and energy, leveraging deduction reasoning and artificial intelligence tools such as Tracker and Canva. Participants calculate key metrics like gravitational acceleration, potential and kinetic energy, and power, fostering a deep understanding of physical laws such as Newton's laws of motion and conservation of energy. By analysing free-falling motion with and without parachutes, students observe the transformation of energy forms and the impact of variables like mass and height on descent dynamics. This module underscores the synergy between several physics and mathematical topics, aligning with Sustainable Development Goal 4: Quality Education. The interactive approach develops critical and creative thinking, enhances problem-solving skills, and improves digital literacy—essential for modern learners. Furthermore, students collaboratively design parachute prototypes to optimize outcomes, fostering teamwork and innovation aligned with Goal 9: Industry, Innovation, and Infrastructure. By linking learning outcomes to real-world challenges, such as safe cargo landing technologies, this activity not only enriches scientific inquiry but also introduces a philosophy of sustainable, applied learning. The integration of generative AI tools ensures a forward-thinking educational experience, preparing students for dynamic and technology-driven environments. This innovative approach to education exemplifies how physics and mathematics, rooted in empirical exploration, can inspire constructive solutions for global challenges, ensuring lasting educational impact.

Keywords: Water balloon parachute, Physics, Mathematics, Generative AI, Project-based learning

Decay Rate of Timoshenko System with Only Microtemperature Effects and No Thermal Diffusivity

Brahim Kilani[1], Marwa Boudeliou[1]

[1]Laboratory of Mathematics, Dynamics and Modelization, Badji Mokhtar-Annaba University, Algeria
Corresponding author: Brahim Kilani (e-mail: kilbra2000@yahoo.fr)

Abstract

In this work, we study the asymptotic behavior of a thermoelastic Timoshenko system with dissipation due only to microtemperature effects and no thermal diffusivity. Under an appropriate new assumption about the coefficients of the system and by using the energy method, we prove that the unique dissipation due to microtemperatures is strong enough to stabilize the system exponentially.

Keywords: Exponential decay, Timoshenko system, Microtemperature dissipation, Energy method, Exponential stability

DFT Computations of Schiff Base Ligand and Its Ni(II) and Cu(II) Complexes

Zakia Messasma[1]

[1]Department of Chemistry, Faculty of Sciences, Ferhat Abbas University of Setif, Algeria
Corresponding author: Zakia Messasma (e-mail: zakia.messasma@gmail.com)

Abstract

Schiff base ligand was prepared by using methoxy substituted amine and 5 bromosalicylaldehydic in methanolic solution. Then, its Cu- and Ni- complexes were also prepared under same experimental conditions. The electronic properties were quantified by density functional theory (DFT) calculations using DFT- B3LYP/6-31 G (d,p) level basis set. The molecular structures, geometrical parameters, chemical reactivity (HOMO, LUMO, and a Gap (EHOMO-ELUMO...)), stability, molecular electrostatic potential (MEP) and Mulliken atomic charges were computed to identify the chemical reactive sites on the molecular surface. The computational study by DFT is well correlated with their experimental results.

Keywords: Schiff bases ligands, DFT calculation, HOMO, LUMO, Gap

Optical Parameter of New Glasses Base Antimony Oxide

Hanane Bouden[1]

[1]Laboratory of Photonic Physics and Multifunctional Nanomaterials, University Mohamed Khiderof Biskra, Algeria

Corresponding author: Bouden Hanane (e-mail: hanane.bouden@univ-biskra.dz)

Abstract

Heavy metal oxide (HMO) glasses have recently had high research activities due to their good physical and chemical properties. They possess low phonon energy, refractive index higher than traditional glasses like borosilicate and phosphate glasses, and a chemical durability better than fluoride glasses. Further, they are transparent in near, middle infrared and visible spectra, which put them at the first-choice materials for photonics, optoelectronics, sensors, and nonlinear optical devices.

New ternary glasses with composition of (90-x) Sb_2O_3-10PbO–xMoO, for x = 10, 20, and 30 mol%, have been prepared by a melt quenching method. The absorption spectra in the UV-VIS region have been recorded. And also, the calculation of each optical parameter and physique A good stability against devitrification has been confirmed by differential scanning calorimetry (DSC). The glasses density measurement exhibits density increases with rising MoO_3 content in the glass.

Keywords: New ternary glasses base antimony oxide, Melt quenching method, Optical parameter and physique

Plasmonic Optimization of Laser-Ablated Gold Nanoparticles for Ethylene Glycol Detection

Ana Mardiana[1], Nandang Mufti[1], Nurul Hidayat[1,2]

[1]Department of Physics, Faculty of Mathematics and Natural Sciences, Malang State University, Jl. Semarang 5, Malang 65145, Indonesia
[2]Center for Science and Engineering, Malang State University, Jl. Semarang 5, Malang 65145, Indonesia
Corresponding author: Nurul Hidayat (e-mail: nurul.hidayat.fmipa@um.ac.id)

Abstract

This study aims to develop an ethylene glycol sensor based on localized surface plasmon resonance (LSPR) effect of gold nanoparticles (AuNPs). AuNPs exhibit excellent plasmonic properties, making them sensitive and versatile for various sensing applications. Herein, AuNPs were prepared using green synthesis approach using a Nd:YAG pulsed laser ablation in deionized water. The plasmonic properties of AuNPs was optimized by modifying the laser beam diameters, from 2 mm to 6 mm. Based on the experimental results, the AuNPs produced with a laser beam diameter of 5 mm showed the best LSPR characteristic as they showed the highest absorbance peak of 0.567 at wavelength of 529 nm. Furthermore, the sensitivity level of the EG sensor was evaluated by detecting the response of AuNPs to the addition of EG at different concentrations. The results of ultraviolet–visible (UV-Vis) data analysis suggested a change in the LSPR absorbance peak, implying that the sensor exhibited amplitude-modality response. The AuNPs sensitivity on EG solutions, with linear range of 0-5%, was 0.006 a.u./%EG. This study is expected to contribute and new breakthroughs in the field of nanotechnology for the development of EG sensors in solution based on the LSPR effect on AuNPs.

Keywords: Localized surface plasmon resonance, Gold nanoparticles, Nd:YAG pulsed laser ablation, Ethylene glycol sensor

1. INTRODUCTION

Ethylene glycol (EG) is a chemical compound that has the formula $C_2H_6O_2$ with odorless and colorless characteristics. In general, EG is used in various industries, such as raw materials for making polyester fibers, antifreeze fluids, and as solvents in various industries because it has good chemical properties [1]. Despite its superiorities for many applications, EG in high concentrations is potentially dangerous [2]. At high concentrations, EG is toxic which can cause poisoning with a high risk to human health and even death [2]. Current studies on EG detection mostly only implemented in gas form, while detection of EG concentration in solution form is less explored [3–5]. In fact, detection of EG concentration in solution form is very important, considering the potential danger of EG to human health. Therefore, one solution to this problem is to use AuNPs as an EG sensor based on the LSPR effect. AuNPs exhibit superior plasmonic properties [6], making them aplicable in various sensing applications.

When embedded in sensing systems, like optical fiber-based sensors, LSPR effect of AuNPs improves theer sensitivity, which is key to the development of effective and efficient sensors [7]. Most previous studies focus on the synthesis of AuNPs using chemical synthesis methods. Unfortunately, chemical methods are not environmentally friendly as hazardous chemicals or waste cannot be avoided [8]. Consequently, a more environmentally friendly synthesis method is needed. One of the clean synthesis methods is the pulsed laser ablation using the Nd:YAG laser. It does not require additional chemicals and does not produce hazardous waste [9–11]. Thus, this study aims to synthesize AuNPs using Nd:YAG laser ablation method and apply the AuNPs to detect EG. This study is expected to contribute to the development of reliable and environmentally friendly EG sensors.

2. MATERIALS AND METHODS

2.1. Materials

In the experimental process of this study, gold plate (with purity more than 99.999), ethylene glycol (EG), and deionized water (DI water). The laser ablation in liquid is considered as clean synthesis approach as it only required gold plate and DI water during the process. EG and DIW were used to prepare EG solutions with different concentrations.

2.2. AuNPs Synthesis Using Nd:YAG Laser Ablation

The AuNPs synthesis process was carried out using the Nd:YAG laser ablation method using the following parameters: a laser wavelength of 1064 nm, a frequency of 4 Hz, and a laser energy of 200 mJ. Meanwhile, the laser beam diameters were varied at 2 mm, 3 mm, 4 mm, 5 mm and 6 mm. To form the AuNPs colloidal solution, a medium of 20 mL DIW was used. The AuNPs synthesis process lasted for 20 minutes for each laser beam diameter. Prior to synthesis, the gold plate was sonicated for 10 minutes to remove any dust or impurities. The gold plate in DIW was placed under the Nd:YAG laser head and remains stationary during the synthesis process. The illustration of this AuNPs synthesis process is shown in Figure 1.
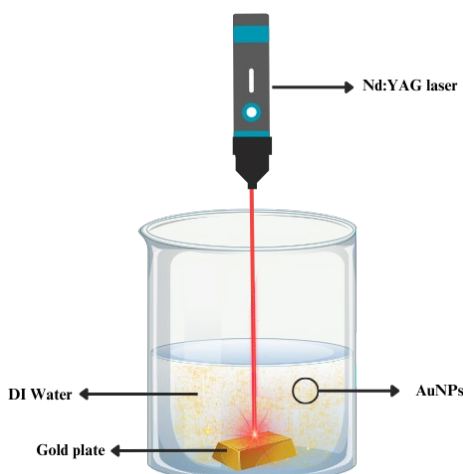
Figure 1. Synthesis of AuNPs using Nd:YAG laser ablation in liquid approach

After the synthesis process was complete, the colloidal AuNPs were put into vials and wrapped using aluminum foil paper with the aim of maintaining the stability of AuNPs colloids so that agglomeration does not occur quickly. Furthermore, AuNPs were characterized by UV-Vis test to investigate their plasmonic properties. Before testing, AuNPs were diluted using DIW in a ratio of 1:1. The UV-Vis instrument (Analytik Jena, Specord 200 Plus) having wavelength range between 190 to 1100 nm.

2.3. Evaluation of EG Sensor Using AuNPs

AuNPs nanocolloidal solution containing EG with concentrations of 1%, 2%, 3%, 4%, and 5% were tested using the UV-Vis spectroscopy. The UV-Vis test is carried out to determine the peak absorbance value and to determine whether or not there is a shift in wavelength. The UV-Vis data were used to evaluate the interaction between AuNPs and EG based on the plasmonic properties of AuNPs.

3. RESULTS

3.1. Optimization of AuNPs Synthesis

The optimization of AuNPs synthesis was carried out by varying the diameter of the laser beam diameter. This was done to alter the LSPR effects, read by UV-Vis spectra in terms of peak positions and absorbance. Figure 2 shows the AuNPs produced by Nd:YAG laser ablation, where Figure 2(a) shows colloidal AuNPs before dilution, Figure 2(b) shows colloidal AuNPs after dilution in DIW, Figure 2(c) shows the UV-Vis spectrum of AuNPs, and Figure 2(d) shows the optimization graph of AuNPs. The UV-Vis test results indicated that the AuNPs samples synthesized at laser beam diameters of 2, 3, 4, 5, and 6 mm had LSPR peak positions at wavelengths of 525, 532, 526, 529, and 532 nm, with absorbance values of 0.261; 0.295; 0.519; 0.566; and 0.434 respectively. The LSPR peak positions of AuNPs produced in this study were consistent with other reports [12].

From the optimization analysis, it was revealed that AuNPs synthesized using a laser beam diameter of 5 mm showed the best performance, characterized by the highest absorbance value of 0.566. The analysis showed that

the absorbance value increased from 0.261 at laser beam diameter of 2 mm to 0.295 at laser beam diameter of 3 mm. This trend continued until the maximum absorbance value reached 0.566 at a laser beam diameter of 5 mm. In contrast, the absorbance dropped when the laser beam diameter was 6 mm. LSPR absorbance peak strongly relates to the ability of the nanoparticles to absorb light. Increasing the concentration of AuNPs causes the number of collectively oscillating particles to increase, resulting in higher absorbance [13]. AuNPs with high absorbance can improve detection sensitivity, as the strong plasmon resonance allows for better interaction with target molecules [14, 15]. Thus, the higher absorbance values of AuNPs reflect an increase in their plasmonic properties [13].
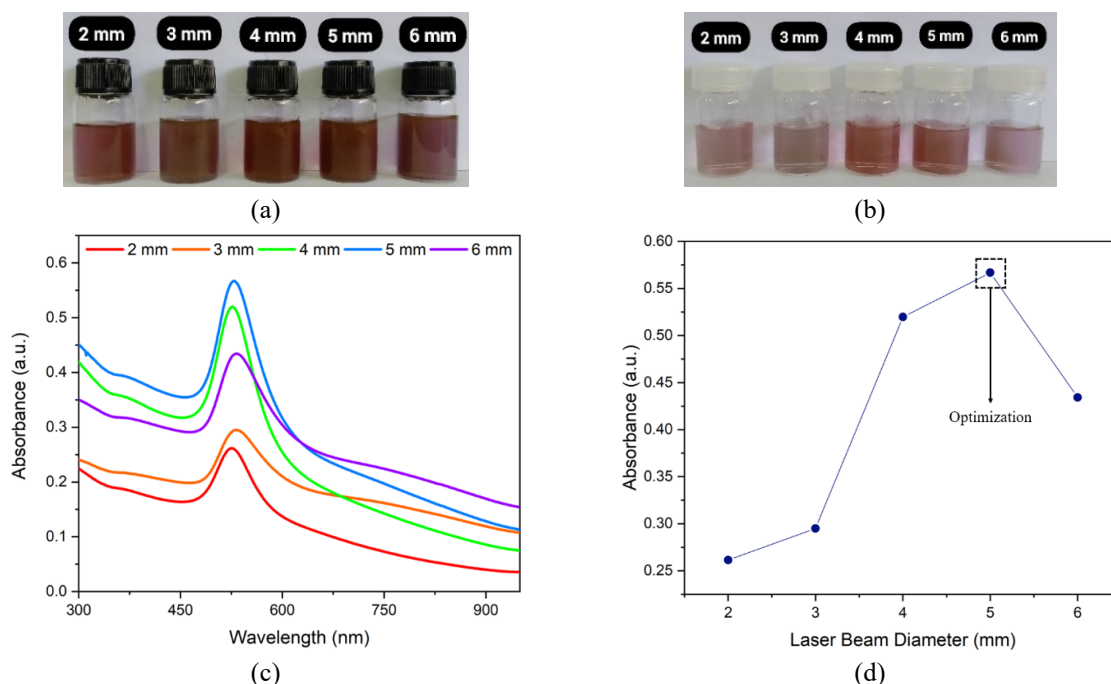
Figure 2. AuNPs produced by Nd:YAG laser ablation (a) before dilution and (b) after dilution in DI water for UV-Vis characterization. (c) AuNPs UV-Vis spectra and (d) their optimization graph

3.2. Evaluation of EG Sensor Using AuNPs
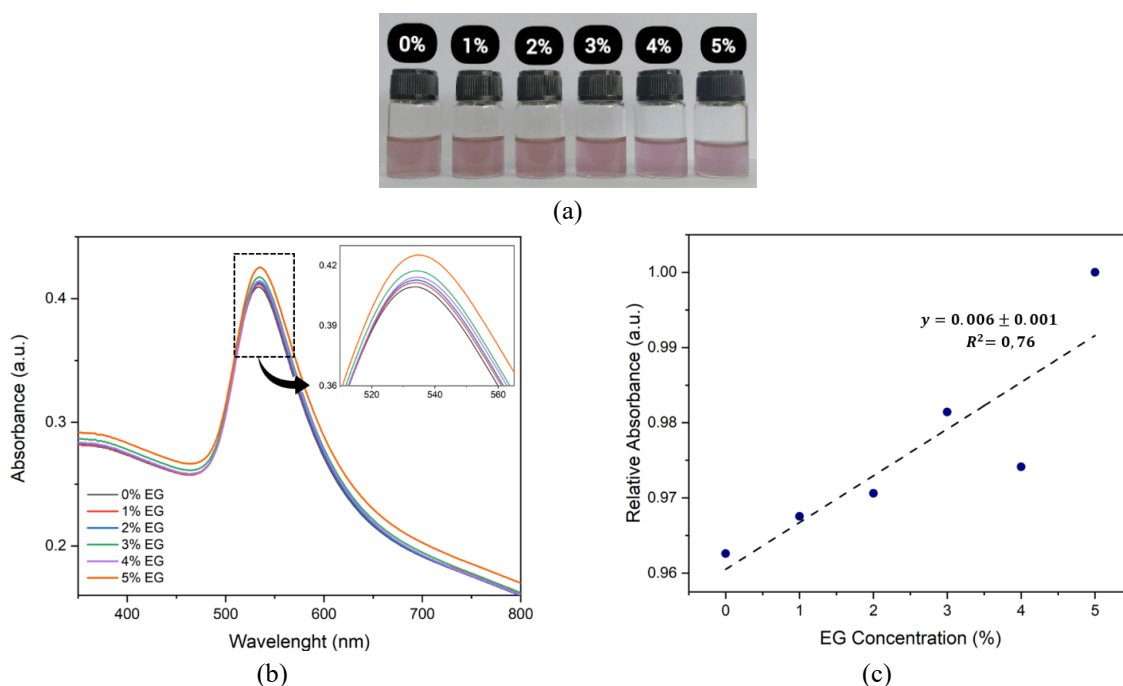
Figure 3. (a) Characterization of AuNPs mixed with EG (b) UV-Vis test analysis results, and (c) linearity of relative absorbance against EG addition

Figure 3(a) shows the response of AuNPs to ethylene glycol (EG) was tested by mixing EG solution into the optimized AuNPs colloid with EG concentrations of 0%, 1%, 2%, 3%, 4%, and 5%. To determine the response of AuNPs due to the addition of EG at various concentrations, UV-Vis testing is required. Based on the UV-Vis test results shown in Figure 3(b), the response of AuNPs due to the addition of EG shows a change in absorbance. The absorbance values were follows, 0.261; 0.295; 0.519; 0.566; and 0.434 respectively for AuNPs containing 0%, 1%, 2%, 3%, and 5% EG. Figure 3(c) shows the changes in absorbance values presented in a relative absorbance linearity graph, with the equation $y = 0.006 \pm 0.001$ dengan $R^2 = 0.76$. Based on the UV-Vis analysis results, AuNPs could detect EG with sensitivity of 0.006 a.u/% and linear range of 1–5%.

4. CONCLUSION

Herein, the laser beam diameter optimization of AuNPs laser using Ns:YAG laser ablation method was investigated. In addition, the optimized AuNPs was applied for EG sensing. The results indicated that the optimum laser beam diameter for the synthesis of AuNPs was 5 mm, where the resulting nanoparticles had an LSPR peak at a wavelength of 529 nm. Furthermore, the interaction of AuNPs with EG at various concentrations was observed. It was found that the change in absorbance peak value predominantly increased with the increase of EG concentration. From these absorbance changes, the sensitivity of the LSPR-based EG sensor in this study reached 0.006 a.u/% with the detection range between 1% and 5%. These findings indicated the potential use of AuNPs in analytical applications that require accurate detection of low concentrations of EG.

References

[1]   T. Shimizu and M. Inui, "Novel aspects of ethylene glycol catabolism," *Appl Microbiol Biotechnol*, vol. 108, no. 1, art. no. 369, Dec. 2024, doi: 10.1007/s00253-024-13179-2.

[2]   J. S. Wei, S. Y. Ma, Y. H. Cai, C. Y. Xu, J. M. Liu, and H. T. Jiang, "Sensor etilen glikol berkinerja tinggi berdasarkan ErFeO3 berserat yang disiapkan dengan pemintalan elektrostatik," *Ceramics International*, vol. 49, no. 20, pp. 32611–32618, Oct. 2023, doi: 10.1016/j.ceramint.2023.07.228.

[3]   J. Ding, H. Dai, H. Chen, Y. Jin, H. Fu, and B. Xiao, "Highly sensitive ethylene glycol gas sensor based on ZnO/rGO nanosheets," *Sensors and Actuators B: Chemical*, vol. 372, art. no. 132655, Dec. 2022, doi: 10.1016/j.snb.2022.132655.

[4]   M. D. Wakade *et al.*, "Nano NaA thick film: Excellent EG vapors sensor," *Materials Today: Proceedings*, vol. 92, pp. 933–937, 2023, doi: 10.1016/j.matpr.2023.04.546.

[5]   M. M. Liu, S. Y. Ma, L. Wang, Y. H. Cai, and N. N. Ma, "Highly sensitive and selective glycol gas sensor based on SmFeO3 microspheres," *Ceramics International*, vol. 49, no. 1, pp. 1108–1113, Jan. 2023, doi: 10.1016/j.ceramint.2022.09.086.

[6]   N. H. Anh *et al.*, "Gold nanoparticle-based optical nanosensors for food and health safety monitoring: recent advances and future perspectives," *RSC Adv.*, vol. 12, no. 18, pp. 10950–10988, 2022, doi: 10.1039/D1RA08311B.

[7]   J. Ou, Z. Zhou, Z. Chen, and H. Tan, "Optical Diagnostic Based on Functionalized Gold Nanoparticles," *IJMS*, vol. 20, no. 18, art. no. 4346, Sep. 2019, doi: 10.3390/ijms20184346.

[8]   L. A. Dykman and N. G. Khlebtsov, "Methods for chemical synthesis of colloidal gold," *Russ. Chem. Rev.*, vol. 88, no. 3, pp. 229–247, Mar. 2019, doi: 10.1070/RCR4843.

[9]   A. Khumaeni, W. S. Budi, and H. Sutanto, "Synthesis and characterization of high-purity gold nanoparticles by laser ablation method using low-energy Nd:YAG laser 1064 nm," *J. Phys.: Conf. Ser.*, vol. 909, art. no. 012037, Nov. 2017, doi: 10.1088/1742-6596/909/1/012037.

[10] H. Barbosa, M. Neumann, and C. Cavalheiro, "Photochemical Synthesis of Gold Nanoparticles by Irradiation of Gold Chloride with the 2nd Harmonic of a Nd:YAG Laser," *J. Braz. Chem. Soc.*, pp. 813–818, 2019, doi: 10.21577/0103-5053.20180213.

[11] N. Jamaludin *et al.*, "Effect of laser energy and wavelength on average size of gold nanoparticles synthesized by pulsed laser ablation in deionized water," *J. Phys.: Conf. Ser.*, vol. 1484, no. 1, art. no. 012029, Apr. 2020, doi: 10.1088/1742-6596/1484/1/012029.

[12] P. Khajegi, "Optical properties of gold nanoparticles: Shape and size effects," *IJOP*, vol. 15, no. 1, pp. 41–48, Jan. 2021, doi: 10.52547/ijop.15.1.41.

[13] E. I. Fazrin, A. I. Naviardianti, S. Wyantuti, S. Gaffar, and Y. W. Hartati, "Review: Sintesis dan karakterisasi nanopartikel emas (AuNP) serta konjugasi AuNP dengan DNA dalam aplikasi biosensor elektrokimia," *PENDIPA Journal of Science Education*, vol. 4, no. 2, pp. 21–39, Jun. 2020, doi: 10.33369/pendipa.4.2.21-39.

[14] X. Zhao, H. Zhao, L. Yan, N. Li, J. Shi, and C. Jiang, "Recent developments in detection using noble metal nanoparticles," *Critical Reviews in Analytical Chemistry*, vol. 50, no. 2, pp. 97–110, Mar. 2020, doi: 10.1080/10408347.2019.1576496.

[15] Y. Wy, H. Jung, J. W. Hong, and S. W. Han, "Exploiting plasmonic hot spots in Au-based nanostructures for sensing and photocatalysis," *Acc. Chem. Res.*, vol. 55, no. 6, pp. 831–843, Mar. 2022, doi: 10.1021/acs.accounts.1c00682.

[15] Y. Wy, H. Jung, J. W. Hong, and S. W. Han, "Exploiting plasmonic hot spots in Au-based nanostructures for sensing and photocatalysis," *Acc. Chem. Res.*, vol. 55, no. 6, pp. 831–843, Mar. 2022, doi: 10.1021/acs.accounts.1c00682.

Removal Pharmaceutical Wastewater Using Green Hydrothermal Synthesised Nanostructured Zinc Oxide Photocatalyst

Nur Aqilah Kamaludin[1], Nur Nabila Abd Aziz[1], Siti Salwa Alias[1,2], Juan Matmin[2,3], Nik Ahmad Nizam Nik Malek[2,4]

[1]Department of Physics, Faculty of Science, Universiti Teknologi Malaysia, 81310 Skudai, Johor, Malaysia
[2]Centre for Sustainable Nanomaterials, Ibnu Sina Institute for Scientific and Industrial Research (ISI-SIR), Universiti Teknologi Malaysia, 81310, Skudai, Johor, Malaysia
[3]Department of Chemistry, Faculty of Science, Universiti Teknologi Malaysia, 81310 Skudai, Johor, Malaysia
[4]Department of Bioscience, Faculty of Science, Universiti Teknologi Malaysia, 81310 Skudai, Johor, Malaysia
Corresponding author: Siti Salwa Alias (e-mail: siti.salwa@utm.my)

Abstract

Pharmaceutical waste such as amlodipine has caused major environmental problems due to the inefficiency of the pharmaceutical waste removal system. However, the study obtained that amlodipine is facing pharmaceutical disposal issues by using the incineration process. Photocatalysts are materials that change the rate of a chemical reaction on exposure to light. Nanostructure ZnO is a photocatalysis material based on the larger initial rates of activities and its absorption efficiency of solar radiations that can be produced using several methods such as hydrothermal. Green hydrothermally methods offer an eco-friendly alternative for synthesising ZnO. Plant extracts, such as *Pandanus amaryllifolius* (*P. amaryllifolius*), have proven to be effective as reducing agents that enhances both the morphological structure and optical properties of ZnO. In this experiment green synthesis has been use as reducing and capping agent to prepare powder of zinc oxide (ZnO) and the size, shape, and morphology of the nanostructures ZnO can all be precisely controlled through the process of green hydrothermal synthesis. Zinc oxide was selected because of its inherent photoactivity and stability, which make it a good option for more complex oxidation processes. We advanced our experiment by conducting analyses like X-ray diffraction (XRD), Fourier-transform infrared spectroscopy (FTIR), ultraviolet-visible spectroscopy (UV-Vis), Raman spectroscopy, thermogravimetric analysis (TGA) and photoluminescence (PL) spectroscopy to investigate the ZnO's structural, thermal, optical and compositional properties. Next, we furthered the experiment by investigating the photocatalytic activity of green ZnO nanostructure embedded with basil seed, aiming to enhance their efficiency and sustainability. From this study, the sustainability of pharmaceutical disposal technology could ensure better quality of environment and water for the future generations.

Keywords: Pharmaceutical waste, Green hydrothermal, *P. amaryllifolius*, ZnO, Photocatalyst, Green adsorbent

Defining Priorities of the Polar Research Institute Using ANP Decision Support Tool

Ozgun Oktar[1], Burcu Ozsoy[1]

[1]Maritime Faculty, Istanbul Technical University, Istanbul, Türkiye
Corresponding author: Ozgun Oktar (e-mail: oktaro@itu.edu.tr)

Abstract

Scientific research in polar regions offers critical insights into global issues, particularly concerning past, present, and future climate change. Although the first Turkish researcher conducted studies in Antarctica in 1967, it was not until 2017, under the Turkish Presidency, that the National Polar Program was formally established. Despite the program's strategy document outlining priority research areas, the organizational structure of the Polar Research Institute has yet to be fully aligned with these objectives. This study seeks to identify the key organizational priorities for a Polar Research Institute in Türkiye by utilizing the analytic network process (ANP) as a decision-making framework. Drawing on a survey of national and international experts, the research evaluates various relevant criteria to guide the institute's strategic focus. The findings underline that scientific research should remain the Institute's core mission, supported by robust logistical infrastructure. Moreover, postgraduate education emerges as a critical component for building the human capital necessary to advance polar research. Based on these insights, the study proposes recommendations for refining the Institute's organizational framework to better support Türkiye's strategic polar research goals.

Keywords: Analytic network process, ANP, Decision support tool, Management, Polar research

Effect of (Al, Ag, and F) Dopants on Morphological and Electrical Properties of ZnO Thin Films

Djedjiga Haouanoh[1], Mahdia Toubane[2], Razika Tala Ighil[3]

[1]UR-MPE Unit, University M`Hamed Bougara Boumerdes, 35000 Boumerdes, Algeria
[2]Institute of Electrical and Electronic Engineering, University M`Hamed Bougara Boumerdes, 35000 Boumerdes, Algeria
[3]Physics Department, Faculty of Sciences, University M'Hamed Bougara Boumerdes, 35000 Boumerdes, Algeria
Corresponding author: Djedjiga haouanoh (e-mail: dhaoua2017@gmail.com)

Abstract

Zinc oxide layers very important in photovoltaic applications, ZnO thin films doped (Al, Ag, and F) are deposited by the gel dip coating technique on glass substrates, the effect of three dopants is remarked that on the morphological and electrical properties. The spectrum of Raman noticed that the presence of two basic phonon modes of the hexagonal ZnO structure, wish are located at 105.35 cm^{-1} and 446.07 cm^{-1}, we also observed that the presence of two asymmetric multi-phonon peaks located at 566.47 cm^{-1} and 1135.86 cm^{-1}. The SEM images indicate that the nature of dopants effect on the ZnO surfaces, the image ZnO-Al Layer shows the presence nanometers nanowires, concerning ZnO-Ag layer shows the presence of nanoparticles and the presence of nano-bricks on the ZnO-F surface. The Al doped ZnO film has a minimum resistivity of the other Ag and F doped ZnO layers.

Keywords: Photovoltaic, Morphological, Electrical, Nanowires, Nano-bricks, Resistivity

Electrical Conductivity Characterization of $Bi_4V_2O_{11}$ Doped with Sulfur Prepared by Hydrothermal Process

Abdelmajid Agnaou[1], Wafaa Mhaira[1], Rachida Essalim[1], Fabrice Mauvy[2], Mustapha Zaghrioui[3], Tatiana Chartier[3], Maati Alga[1], Mohamed Zamama[1], Abdelaziz Ammar[1]

[1]Laboratory of Materials Science and Process Optimization, Faculty of Sciences-Semlalia, Cadi Ayyad University, Av. My Abdellah, B.P. 2390, Marrakech, Morocco
[2]University of Bordeaux, UMR 5026, 87, Av. Dr A. Schweitzer, 33608 Pessac, France
[3]GREMAN Laboratory, University of Tours, 41000 Blois, France
Corresponding author: Abdelmajid Agnaou (e-mail: a.agnaou.ced@uca.ac.ma)

Abstract

The $Bi_4V_{2-x}S_xO_{11+\delta}$ (BiSVOx) compounds ($0.0 \leq x \leq 0.5$) prepared by the hydrothermal method have been characterized using techniques such as X-ray diffraction, Raman spectroscopy, FT-IR spectroscopy, thermogravimetric analysis and scanning electron microscopy. This synthesis method has been shown to have an important influence, especially on the crystallinity and morphology of these materials. The obtained BiSVOx phase crystallizes with the tetragonal structural type γ-$Bi_4V_2O_{11}$. The spherical particles of the nanoparticles characterize the morphology of the synthesized powders. The stability of the BiSVOx samples was checked at temperatures up to 1000 °C using DTA/TGA analysis. The conductivity of these compounds was measured using electrochemical impedance spectroscopy. In contrast to the general observation of BiMeVOx, the conductivity increases with the increase of the substitution ratio. The highest conductivity values were obtained for the sample with composition $x = 0.4$.

Keywords: BiSVOx, XRD, Hydrothermal process, Ionic conductivity

High-Sensitivity Surface Plasmon Resonance Based Sensor for HIV Detection

Mohamed Esseddik Ouardi[1,2], Kada Abdelhafid Meradi[1,2], Fatima Tayeboun[1,3]

[1]Laboratory of Materials Sciences and Applications (LSMA), University of Ain Temouchent, Ain Temouchent, Algeria
[2]Institute of Science and Technology, University of Ain Temouchent, Ain Temouchent, Algeria
[3]University Djillali Liabes, Sidi Bel Abbes, Algeria
Corresponding author: Mohamed Esseddik Ouardi (e-mail: mohamed.ouardi@univ-temouchent.edu.dz)

Abstract

A highly sensitive surface plasmon resonance sensor for HIV detection is proposed and investigated in this paper. The structure of this sensor is made of layers including silicon (Si), silicon dioxide (SiO2), graphene and silver over a BK7 prism, the detection of HIV infected blood sample relies on the refractive index of it which is different from normal blood sample's. In order to obtain good results, geometrical parameters are adjusted for the best sensitivity. The studied sensor performs well, the sensitivity is equal to 207 deg/RIU. The proposed sensor might be a useful tool for the detection of HIV infections in blood samples. The transfer matrix method was used to simulate and investigate the sensor's performances.

Keywords: Surface plasmon resonance, Biosensor, HIV, Blood

Total Polyphenol Content and Antioxidant Activity of Date Palm Seeds in Adrar Region of Algeria

Omar Fandougouma[1,2], Khadidja Djaafri[3], Halima Kina[3]

[1]Higher School of Saharan Agriculture, Adrar, Algeria
[2]Laboratory of Saharan Natural Resources, Faculty of Natural and Life Sciences, University of Adrar, Adrar, Algeria
[3]Department of Matter Sciences, University of Adrar, Adrar, Algeria
Corresponding author: Omar Fandougouma (e-mail: o.fandougouma@esas-adrar.edu.dz)

Abstract

In the Adrar region of Algeria, a wide variety of date palms (*Phoenix dactylifera* L.) comprising over 2000 species can be found. Our comprehensive study, which aims to evaluate the nutritional content and biological activity of the seeds of these local date varieties, has practical implications for agriculture and nutrition. By analysing flavonoid polyphenols and DPPH oxidation activity in four prevalent date cultivars in the Adrar oases: H'mira, Takerbouchet, Tinaceur, and Tegazza, we have provided valuable insights into the nutritional properties of these local date varieties. We utilised a Soxhlet extractor with a methanol/water solvent to extract polyphenols from the seeds and determined the total polyphenol content using the Folin-Ciocalteu method. Additionally, we quantified the flavonoid content using aluminium chloride. The general polyphenol content was determined to be 17.311 ± 0.644, 51.287 ± 8.173, 61.829 ± 1.493, and 125.183 ± 3.735 mg GAE/g dry matter for the four date varieties, while the flavonoid values were 72 ± 13.333, 202 ± 8.819, 510.889 ± 8.388, and 442 ± 26.458 mg QE/g dry matter for H'mira, Takerbouchet, Tinaceur, and Tegazza, respectively. Furthermore, the IC50 values of DPPH oxidation activity were 2.283 ± 0.168, 3.227 ± 0.114, 1.061 ± 0.188, and 0.568 ± 0.001 ml/mg for H'mira, Takerbouchet, Tinaceur, and Tegazza, respectively, demonstrating the thoroughness and reliability of our research.

Keywords: *Phoenix dactylifera* L., Date seeds, Total polyphenol, Flavonoid, DPPH

Exploring Piperazine Derivatives: Novel Insights and Therapeutic Prospects in Cancer Research

Ikram Bouziane[1], Yousra Mdarhri[1], Fatima Zohra Lenda[1], Mohamed Chabbi[1]

[1]Department of Chemistry, Abdelmalek Essaadi University, Faculty of Science and Technology, Tangier, Morocco
Corresponding author: Ikram Bouziane (e-mail: ikram.bouziane@etu.uae.ac.ma)

Abstract

Piperazine derivatives, known for their diverse pharmacological properties, are currently being explored as promising therapeutic agents in cancer research. These compounds, with their unique chemical structures, have shown significant potential in targeting various cancer-related pathways, making them an area of growing interest in the search for more effective cancer treatments. Research efforts are increasingly focused on understanding how piperazine derivatives interact with key molecular targets involved in tumor growth, metastasis, and resistance to conventional therapies. Early studies have indicated that these derivatives may exhibit anticancer properties, such as inhibiting cell proliferation, inducing apoptosis, and modulating tumor microenvironments. Furthermore, piperazine derivatives are being evaluated for their ability to overcome drug resistance, which remains a significant challenge in cancer treatment. Their potential to sensitize cancer cells to existing therapies and improve treatment outcomes is particularly promising. In addition to their direct anticancer effects, piperazine derivatives may also serve as effective adjuvants in combination therapies, enhancing the overall efficacy of cancer treatments. This abstract underscores the exciting potential of piperazine derivatives in cancer therapeutics, offering novel approaches to enhance the effectiveness of current treatments while overcoming the limitations posed by drug resistance and tumor heterogeneity.

Keywords: Piperazine derivatives, Drug resistance, Therapeutic treatments, Cancer therapeutics

A Novel Corrosion Inhibitor for Carbon Steel Revealed by Gravimetric Analysis

Benhadria Naceur[1,2], Tarik Attar[1,3], Abbes Benchadli[3], Esma Choukchou-Braham[3]

[1]Higher School of Applied Sciences of Tlemcen, ESSA-Tlemcen, BP 165, RP Bel Horizon,
13000 Tlemcen, Algeria
[2]Laboratory of Chemistry of Materials (LCM), University of Oran 1 Ahmed Ben Bella, Oran, Algeria
[3]ToxicoMed Laboratory, University of Abou Bekr Belkaid, BP 119, 13000 Tlemcen, Algeria
Corresponding author: Benhadria Naceur (e-mail: nacben1974@gmail.com)

Abstract

The study examined the effectiveness of expired syrup as a corrosion inhibitor for carbon steel (C-steel) in an acidic environment. Using the weight loss method, the research assessed how the concentration of the inhibitor, temperature, and exposure duration affected both corrosion inhibition efficiency and the corrosion rate. The results demonstrated that the expired drug significantly inhibits corrosion, achieving a maximum inhibition efficiency of 96.03% at a concentration of 1.25% (v/v) over 6 hours at a temperature of 303 K. The inhibition efficiency showed a tendency to stabilize with increased concentration and immersion time. Findings revealed that the inhibition efficiency (IE%) of Sulpuren improved with rising concentration and reduced temperature, with the corrosion rate of carbon steel decreasing as the Sulpuren concentration increased from 0.25% to 1.25% v/v. The adsorption of the inhibitor on the metal surface follows the Langmuir isotherm model, involving both physical adsorption (physisorption) and chemical adsorption (chemisorption) processes. The adsorption is spontaneous, and the dissolution of the metal is an endothermic process. The activation energy values suggest the formation of a protective layer on the metal surface, which serves as a barrier against the corrosive effects of sulfuric acid (H_2SO_4). Additionally, the metal dissolution process is associated with a gas-phase reaction, specifically the evolution of hydrogen gas.

Keywords: Gravimetric method, Weight loss, Corrosion rate, Inhibition, Isotherm

Jet-Vortex Above-Bit Arrangement for Drilling Production Wells

Denys Panevnyk[1]

[1]Department of Oil and Gas Machines and Equipment, Ivano-Frankivsk National Technical University of Oil and Gas, Ivano-Frankivsk, Ukraine
Corresponding author: Denys Panevnyk (e-mail: den.panevnik@gmail.com)

Abstract

The efficiency of the traditional vortex near-bit systems is limited by the reduction of the drilling fluid consumption at the well bottom, part of which is directed to the near-bit area to create a low-pressure zone. The creation of a vortex zone in the near-bit area while maintaining the required drilling fluid consumption at the well bottom can be achieved by using the well assembly developed by the author, which includes a parallel connection of jet pumps and a vortex nozzle. The pressure reduction in the vortex area is described by the Euler integral. Based on the finite element method and the Solidworks Flow Simulation program, a three-dimensional geometric model and a grid fluid model were built, diagrams of kinematic and hydrodynamic parameters were obtained, and the nature of the flow distribution in the proposed near-bit vortex-ejection system was analyzed. The initial data for the calculation were the performance of the drilling pump and the pressure in the annulus above the level of the device. Visualization of the flow lines on the outer surface of the device shows that the maximum intensity of the circulation currents is observed between the levels of the vortex nozzle and the suction holes of the jet pumps. The calculated pressure characteristics demonstrate the possibility of operating a high-pressure jet pump in the mode of negative values of the ejection coefficient. The value of the pressure reduction in the above-bit area when using the vortex-ejection system increases by 98.6 %, and the flow rate at the well bottom increases by 23.9 %. The total flow rate of the drilling fluid in the bottomhole circulation circuit when using the vortex-ejection system exceeds the productivity of the drilling pump by 49.3 %.

Keywords: Ejector system, Jet pump, Vortex region, Euler equation, Finite element method

1. INTRODUCTION

Global economic growth contributes to the growth of world consumption of hydrocarbons and determines the need to involve hard-to-recover oil and gas reserves in the development. In particular, it is necessary to note the existence of a persistent tendency to increase the depth of drilling production wells [1], which leads to an increase in the pressure on the bottomhole, repeated grinding of drill cuttings, deterioration of the removal of cuttings and a decrease in the technical and economic indicators of drilling. An increase in pressure in the bottomhole zone of the well, associated with an increase in its depth, has an extremely negative effect on the preservation of the natural permeability of the productive horizon during its primary opening [2]. Traditional methods of reducing pressure on the productive horizon during its primary opening involve the use of balanced drilling technologies that prevent the loss of circulation of drilling fluid and damage to the productive formation in oil and gas wells located both onshore [3] and in the coastal zone [4]. In contrast to the methods of implementing balanced drilling technologies, the use of above-bit jet pumps [5] and vortex nozzles [6] allows reducing the pressure directly in the near-wellbore zone of the well, maintaining its constant value throughout the entire channel of the annular space. In the practice of using above-bit jet pumps for implementing direct well flushing, ejection systems of the injection-suction [7] and injection type [8] are used. Suction-discharge ejector systems are used to reduce the pressure at the bottomhole, and injection systems are used to intensify the local bottom hole circulation of drilling fluid. The main disadvantage of using suction-discharge ejector systems is the increased probability of operating the jet pump in the cavitation mode. The use of vortex devices to reduce the pressure at the bottomhole involves feeding part of the flow created by the surface drilling pump to the above-bit vortex nozzle. This reduces the flow rate of drilling fluid supplied to the bottom hole and worsens the quality of its cleaning. Reducing the pressure while maintaining a constant flow rate of drilling fluid at the bottomhole can be achieved by combining vortex nozzles and injection-type jet pumps in a single above-bit assembly.

The aim of the research, the results of which are presented in this paper, is the development and study of the working process of a vortex-ejection above-bit device intended for the primary opening of oil and gas-bearing horizons.

2. MATERIAL AND METHOD

A combined vortex-ejection near-bit arrangement, which ensures the creation of a vortex region in the above-bit region without reducing the consumption of drilling fluid at the bottomhole, is shown in Figure 1.
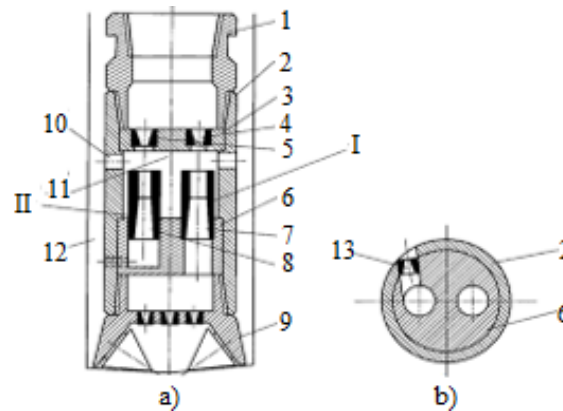
Figure 1. The design of the device for drilling a) and vortex nozzle b) 1 – Upper sub, 2 – Above-bit sub, 3, 6 – Upper and lower bases, 4, 5 – Working nozzles, 7, 8 – Mixing chambers with diffusers, 9 – Bit, 10 – Radial holes, 11 – Receiving chamber, 12 – Annulus channel, 13 – Vortex nozzle, I – Low-pressure jet pump, and II – High-pressure jet pump

The device consists of an upper sub 1 placed in the lower part of the drill pipe column, an above-bit sub 2, in which an upper base 3 with working nozzles 4, 5 and a lower base 6 with mixing chambers and diffusers 7, 8 are placed. The working nozzle 4 and the mixing chamber with diffuser 7 form a jet pump I, and the working nozzle 5 and the mixing chamber with diffuser 8 form a jet pump II. A bit 9 is placed in the lower part of the above-bit sub 2. The above-bit sub 2 contains radial openings 10 connecting the receiving chamber 11 of the jet pumps I, II with the channel of the annular space 12. The working nozzles 4, 5 of the jet pumps I, II communicate with the cavity of the upper sub 1 and the channel of the drill column. The diffuser 7 of the jet pump I is connected to the flushing system of the bit 9, and the diffuser 8 of the jet pump II is connected to the vortex nozzle 13 and the annular space channel 12. The axis of the vortex nozzle 13 is offset relative to the axis of symmetry of the device and the well axis. The mixing chamber with the diffuser 8 of the jet pump II has a smaller diameter compared to the mixing chamber with the diffuser 7 of the jet pump I. The ratio of the diameters of the mixing chamber and the working nozzle determines the magnitude of the pressure created by the ejection system: the jet pump I is low-pressure, and the jet pump II is high-pressure. Low-pressure jet pump I, due to suction of the ejected flow, increases the flow rate of the flushing fluid in the flushing system of the bit 9 and at the well bottom, as a result of which the required intensity of its flushing is maintained after directing part of the total flow with the flow rate to the working nozzle 5 of the jet pump II.
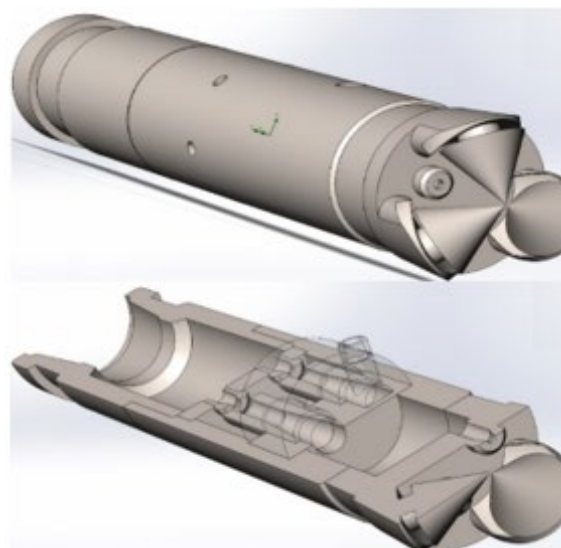
Figure 2. Three-dimensional model of a device for drilling wells, developed on the basis of the Solidworks software package

High-pressure jet pump II increases the flow rate of the flushing fluid, which is directed to the vortex nozzle 13, as a result of which the value of the pressure reduction at the well bottom increases.

The pressure drop in the vortex region is described by the Euler integral (which is a special case of the Lagrange equation), since the Bernoulli equation is valid only for points of one streamline. Given the concept of "flow circulation", the equation for determining the magnitude of the pressure drop in the vortex field can be obtained in the form

$$\Delta P_0 = \frac{\rho V^2}{2}\left(1 - \frac{r_0}{r_w}\right),$$
(1)

where ρ is the density of the drilling fluid; V is the linear velocity of the vortex flow on the well wall; r_w, r_0 are the radii of the well and the point in the vortex field at which the pressure drop is determined, respectively.

To determine the operating mode of the above-bit ejection system, including a parallel connection of low-pressure and high-pressure jet pumps with different pressures of mixed flows, the finite element method can be used. To build the geometric model shown in Figure 2, the product of SolidWorks Corporation – Solidworks was used, which is a software package aimed at automating the design and technological preparation of the production of highly complex products.

3. RESULTS

Based on the results of the simulation modeling, diagrams of the distribution of kinematic and dynamic parameters in the hydraulic system of the near-bit device were obtained (Figure 3).
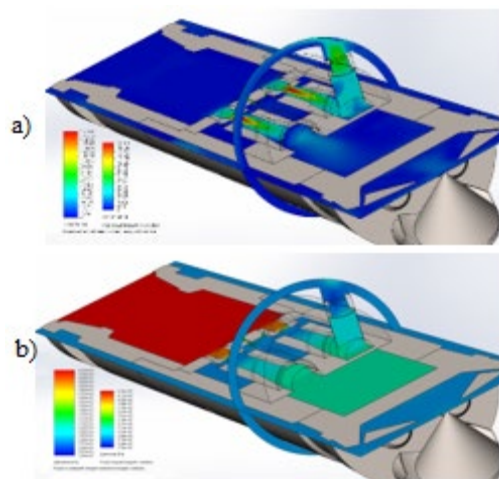
Figure 3. Diagrams of the distribution of velocities a) and pressures b) in the above-bit ejection system

Analysis of the diagrams shown in Figure 3 demonstrates a decrease in pressure at the outlet of the vortex nozzle and in the adjacent annular region. The distribution of kinematic and hydrodynamic parameters shown in Figure 3 is subsequently used to determine the flow rates and pressures in typical sections of the ejection system elements. The nature of the arrangement of the flow lines on the outer surface of the above-bit ejection system (Figure 4) confirms the formation of circulation flows in the annular space of the well (flow lines at the outlet of the bit flushing system nozzles are not shown) above the level of the vortex nozzle.

The maximum intensity of circulation flows is observed between the levels of the vortex nozzle and the suction holes of the jet pumps. Circulation flows of lower intensity are maintained throughout the entire length of the device body above the level of the suction holes of the jet pumps. The current lines emanating from the flushing nozzles of the bit, upon reaching the level of the vortex nozzle, change the direction of movement and are drawn into the vortex flow.

When using the vortex nozzle and drilling bit flushing nozzles of the same diameter in the prototype design, 75 % of the drilling fluid pumped by the drilling pump is supplied to the well bottom, and 25 % is supplied to the above-bit zone (to create a vortex region). When using the proposed device, the drilling fluid consumption in the drilling

bit nozzles is 98.9 % of the drilling pump performance, and the pressure reduction value in the vortex region increases by 98.6%.
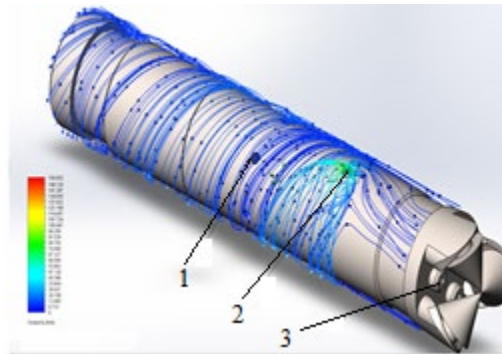
Figure 4. Trajectories of streamlines on the surface of the ejection system: 1 – Suction holes of jet pumps, 2 – Outlet hole of vortex nozzle, and 3 – Nozzles of the bit flushing system

The total drilling fluid consumption is almost twice (by 49.3%) higher than the drilling pump performance. Thus, the simultaneous creation of a vortex region and an increase in the drilling fluid consumption in the well bottomhole circulation circuit are ensured.

4. CONCLUSION

In the process of modeling the working process of the above-bit ejection system, it was found that the use of a parallel connection of jet pumps and a vortex nozzle in a joint well assembly allows for an increase in the efficiency of the primary opening of the productive horizon:

- Compared to the prototype design, the flow rate of flushing fluid at the well bottom increases by 23.9 %, which improves the quality of its cleaning and increases the technical and economic indicators of drilling,
- The value of pressure reduction in the above-bit area increases by 98.6 %. At the same time, the conditions for rock destruction are improved and the mechanical drilling speed increases. The creation of a low-pressure area during the primary opening of the productive horizon allows for the preservation of its natural permeability and a decrease in the amount of unrecovered oil,
- The total flow rate in the bit flushing system and the vortex nozzle exceeds the productivity of the drilling pump by 49.3 %. In this section, the importance and effects of the study should be clearly stated. In the conclusion part, the results should not be repeated.

The task of subsequent studies is to verify the obtained results in a field test. In this section, the importance and effects of the study should be clearly stated. In the conclusion part, the results should not be repeated.

References

[1]   Y. I. Kryzhanivskyi, O. Y. Vytyaz, V. V. Tyrlych, R. S. Hrabovskyi, and V. I. Artym, "Evaluation of the conditions of drill pipes failure during tripping operations," *SOCAR Proceedings*, vol. 1, pp. 36–48, Mar. 2021, doi: 10.5510/OGP20210100478.

[2]   M. C. Halim, H. Hamidi, and A. R. Akisanya, "Minimizing formation damage in drilling operations: a critical point for optimizing productivity in sandstone reservoirs intercalated with clay," *Energies*, vol. 15, no. 162, pp. 1–30, Jan. 2022, doi: 10.3390/en15010162.

[3]   W. Zhang, W. Dang, W. Zhang, X. Sun, and Z. Zhu, "Underbalanced drilling optimum methodology," in *10th Chinese Geosynthetics Conference & International Symposium on Civil Engineering and Geosynthetics (ISCEG 2020)*, Chengdu, CN, 2020, pp. 1–4, doi: 10.1051/e3sconf/202019803004.

[4]   M. M. Huque, S. Imtiaz, A. Rahman, and M. Hossain, "Kick detection and remedial action in managed pressure drilling: A review", *SN Applied Sciences*, vol. 2, pp. 1–29, Jun. 2020, doi: 10.1007/s42452-020-2962-2.

[5]   E. I. Kryizhanivskiy and D. A. Panevnik, "The study on the flows kinematics in the jet pump's mixing chamber," *Naukovyi Visnyk NHU – Scientific Bulletin of NMU*, no. 1, pp. 62–68, Mar. 2019, doi: 10.29202/nvngu/2019-1/7.

[6]   X.-Y. Chen, T. Cao, K.-A. Yu, D.-L. Gao, J. Yang, and H.-S. Wei, "Numerical and experimental investigation on the depressurization capacity of a new type of depressure-dominated jet mill bit,"

Petroleum Science, vol. 17, pp. 1602–1615, Jun. 2020, doi: 10.1007/s12182-020-00472-8.

[7] E. I. Kryzhanivskyi and D. A. Panevnyk, "Improving use efficiency above-bit jet pumps," *Socar Proceeding*, vol. 2, pp. 112–118, Jun. 2020, doi: 10.5510/OGP20200200437.

[8] A. P. Melnikov and N. A. Buglov, "Parameter substantiation of supra bit jet pump for productive formation opening," *Socar Proceeding*, vol. 2, pp. 112–118, Jun. 2021, doi: 10.21285/2686-9993-2021-44-4-433-440.

Clay-Hydrochar Composites: A Sustainable Material for Solar Photocatalysis of Methylene Blue

Jalila Hanyny[1], Zaina Izghri[1], Abdelrani Yaacoubi[1], Layla El Gaini[1], Abdelaziz Bacaoui[1]

[1]Laboratory of Applied Chemistry and biomass, Department of Chemistry, Faculty of Science Semlalia, University Cadi Ayyad, Marrakech, Morocco
Corresponding author: Jalila Hanyny (e-mail: j.hanyny.ced@uca.ac.ma)

Abstract

Nowadays, our country as many countries in the word threatens a significant water stress, so consequently, effective wastewater treatment become one of its major challenges. Heterogeneous photocatalysis is one of advanced oxidation processes that showed high removal efficiencies of refractory pollutants from water. Clay-hydrochar composites have emerged as promising and sustainable materials for solar photocatalysis, particularly in the degradation of pollutants. This study investigates the efficiency of clay-hydrochar composites in harnessing solar energy for the photocatalytic degradation of Methylene Blue, a widely used dye in various industries. The composites were prepared by hydrothermal carbonization, combining the unique properties of clay and hydrochar. The composite was characterized by XRD, SEM, EDS, ICP, and FT-IR. The experimental results show a significant photocatalytic activity, because the addition of naturel clay improve the specific characteristics of hydrochar, which increase reactive sites. This can be attributed to the presence of iron, Ti and other minerals showcasing the potential of these composites as efficient and eco-friendly catalysts for wastewater treatment applications.

Keywords: Solar photocatalysis, Clay, Hydrochar, Degradation, Wastewater treatment

Design and Characterization of Topical Nanosystems for Photodynamic Therapy

Daniela Maza Vega[1,2], R. Daniel Cacciari[3], Cristian Lillo[4,5,6], Silvia Del Valle Alonso[1,2], María Jimena Prieto[1,2], Fernando Alvira[2,7], Paula Caregnato[3], Mónica C. Gonzalez[3], Jorge Montanari[4,5,6]

[1]Laboratory of Bio-Nanotechnology, Department of Science and Technology, National University of Quilmes (UNQ), Bernal, Argentina
[2]Structural Biology and Biotechnology Group (GBEyB), IMBICE (CONICET CCT-La Plata), La Plata, Argentina
[3]Institute of Theoretical and Applied Physical Chemistry (INIFTA), CONICET CCT-La Plata, Faculty of Exact Sciences, National University of La Plata, La Plata, Argentina
[4]Laboratory of Biotechnological Application Nanosystems (LANSAB), National University of Hurlingham (UNAHUR), Hurlingham, Argentina
[5]Scientific Research Commission of the Province of Buenos Aires (CIC), La Plata, Buenos Aires, Argentina
[6]National Scientific and Technical Research Council (CONICET), Autonomous City of Buenos Aires, Argentina
[7]Laboratory of Simulations, Automatic Control, Biophotonics, and Nanotechnology, Department of Science and Technology, National University of Quilmes (UNQ), Bernal, Argentina
Corresponding author: Daniela Maza Vega (e-mail: dmazavega@gmail.com)

Abstract

Skin diseases require innovative approaches to improve treatments, particularly in overcoming the stratum corneum (SC) barrier. This study combines lipid matrices with photochemistry-based therapies to enhance drug delivery and induce cytotoxicity. First, carbon quantum dots (CQD) were synthesized from spinach leaves (Spinacia oleracea) using a top-down method. Fluorescence and absorbance spectra were analyzed to identify optimal excitation and emission windows for photodynamic therapy, which generates reactive oxygen species (ROS) toxic to parasites or infected cells upon exposure to visible light. The CQD exhibited a size of approximately 50 nm and a zeta potential of -28.8 mV. Three key wavelengths were identified: 350 nm (corresponding to the CQD themselves) and 418 and 620 nm (associated with chlorophyll residues expected to be located on the nanoparticle surface). Emission spectra at these wavelengths revealed peaks at 475 and 675 nm. The fluorescence quantum yield (QY) and singlet oxygen QY were approximately 2% and 30%, respectively, with minimal production of superoxide anion. CQD were incorporated into ultradeformable ethosomes, designed to transiently disrupt the SC barrier, enabling the photodynamic agents to penetrate the skin and reach the viable epidermis and dermis. The incorporation of CQD into formulations using ethanol, water, or both solvents was evaluated, comparing size, zeta potential, membrane stability, and encapsulation efficiency. The best-performing ethosomal formulation had a size of 108±1 nm, a zeta potential of -9.7 mV, and was confirmed to be in a liquid-crystalline phase. It demonstrated biocompatibility with J774.A1 macrophage cells and an encapsulation efficiency of 38%. This promising ethosomal formulation, integrating CQD, shows potential for enhanced skin penetration and photodynamic activity, offering a novel therapeutic strategy for treating parasites or infected cells.

Keywords: Carbon quantum dots, Ethosomes, Drug delivery, Photodynamic therapy

Elaboration and Characterization of PVA-g-PAA Graft Copolymers and PVA-g-PAA/Fe$_2$O$_3$: CuO Composites

Radja Megherbi[1], Hadjer Addou[2], Halima Benallou[1], Amina Arbaoui[1], Mohamed Karmaoui[3]

[1]Materials Engineering Department, University of Science and Technology of Oran M-B, Oran, Algeria
[2]Physical Chemistry Department, University of Science and Technology of Oran M-B, Oran, Algeria
[3]Chemical Engineering Department, University of Science and Technology of Oran M-B, Oran, Algeria
Corresponding author: Radja Megherbi (e-mail: m_radjaa@yahoo.fr)

Abstract

The PVA is of considerable interest to researchers. However being a water-soluble polymer. PVA has poor resistance to water, also not plasticizing. This has prompted scientific research to work on modifying PVA in order to improve its properties. One of the most important methods for modifying PVA is grafting copolymerization. The objective of this study is to develop and characterize thin films of composites based on polyvinyl alcohol grafted with polyacrylic acid. Acrylic acid (AA) was introduced to balance PVA problems. AA is soluble in water and miscible with most organic solvents. The composites were developed by inserting nanoparticles of metal oxides such as copper oxide (CuO) and iron oxide III (Fe$_2$O$_3$) into the matrix. The analyzes used to study the characteristics of these films are FTIR, RMN^{1}H, RMN^{13}C, thus the study of the kinetics of the rate of swelling, the biodegradation test, then the effect of the addition of the charges on the electrical conductivity. For the composites obtained, we can find on the kinetic curves a maximum value of the degree of swelling more or less accentuated according to the amount of added charge (CuO, Fe$_2$O$_3$). The first change in swelling rate is in quantities of the load, where there is an increase in swelling rate as the quantity of the load is low. The strong increase in the system reflects the hypersensitivity of the swelling phenomenon to the load. PVA-g-PAA/CuO film (2%) has a higher swelling rate than other films. We have obtained a very high maximum swelling in the basic solution. These results may explain that the highly hydrophilic character of carboxylic acid functions (COOH group) promotes the swelling of these films. The conductivity of the composite depends on the conductivity of the polymer and concentration of the charge incorporated within the polymer matrix. Moreover, it depends on the orientation, distribution, shape and size of nanoparticles in the polymer matrix. Thus, the addition of conductive or semiconductor nanoparticles can modify the electrical behavior of the polymer matrix which initially behaves as insulating materials.

Keywords: Polyvinyl alcohol PVA, Polyacrylic acid PAA, Nanoparticles; Metal oxide, Biodegradability

Luminescence Enhancement in Eu^{3+}, Sm^{3+} Co-Doped $Li_2B_4O_7$ Phosphor

Rekia Belhoucif[1,2], Abdelkader Lalmi Benmaiza[1], Lyes Benharrat[3]

[1]Laboratory of Quantum Electronics, Faculty of Physics, University of Sciences and Technology Houari Boumediene, 16111 Algiers, Algiera
[2]Coating, Materials and Environment Laboratory, University of M'hamed Bougara Boumerdes, Boumerdes, Algeria
[3]Research Center in Semiconductors Technology for Energy-CRTSE, 16038 Algiers, Algeria
Corresponding author: Rekia Belhoucif (e-mail: r.belhoucif@univ-boumerdes.dz)

Abstract

Eu^{3+}, Sm^{3+} co-doped $Li_2B_4O_7$ was synthesized using quentching melt technique. X-ray Diffraction (XRD), Photo-Luminescence (PL), and Photo-Luminescence Excitation (PLE) were used to characterize the phase impurities, and spectroscopic properties, respectively. The red emission intensity of Eu^{3+} is considerably enhanced due to the energy transfer from Sm^{3+}. The enhancement's mechanism is attributed to the increase in quantum efficiency of the $^5D_0$ state of Eu^{3+} rather than the increase in the absorption of Eu^{3+}. This finding has opened an opportunity to use Sm^{3+} in reducing the cost of consuming Eu^{3+} in lighting technologies. The spectroscopic results that were obtained such as large stimulated emission cross-section at 614 nm, high branching ratios and quantum efficiencies suggest that these present glass can be a candidate for visible red lasers materials and optical devices.

Keywords: Quentching melt, PL-PLE, Quantum efficiency, Stimulated emission cross, Branching ratios

Characterization of Pristine Bismuth Manganite Thin Films Deposited on Glass Substrates by Sol Gel Technique

Ouiza Allouane[1], Mahdia Toubane[2], Ryma Ben-Mammar[3], Katia Ayouz[4], Redouane Douali[5], Nadir Beldjoudi[1]

[1]Department of Physics, USTHB University, Algiers, Algeria
[2]Department of Physics, UMBB University, Boumedes, Algeria
[3]Department of Physics, UMMTO University, Tizi Ouzou, Algiers
[4]CRTSE Research Center, Algiers, Algeria
[5]University of Littoral-Côte d'Opale, France
Corresponding author: Ouiza Allouane (e-mail: allouane_pg@yahoo.fr)

Abstract

BiMnO3 thin films were deposited onto glass substrate by sol-gel dip coating method. The films annealing at 500 ℃ for 1h are characterized by X-ray diffraction (XRD), scanning electron microscopy (SEM), UV visible spectrophotometer and photocatalytic test degradation of methylene blue solution. The evolution of structural, optical properties and methylene blue (MB) photodegradation of the as-deposited films was investigated. Monoclinic structure is shown via X-ray diffraction. The morphological description reveals films that are continuous and smooth. Finally, we have presented optical parameters including absorption response in order to compute the gap energy Eg of these layers.

Keywords: $BiMnO_3$, Multiferroic, Gap energy, Sol-gel technique

Green Synthesis of Tin Oxide (SnO₂) Nanoparticles from Ficus Carica Leaf Extract for Murexide Degradation

Toubal Badreddine[1]

[1]Department of Material Sciences, University of Algiers 1, Benyoucef Benkhedda, Algeria
Corresponding author: Toubal Badreddine (e-mail: b.toubal@univ-alger.dz)

Abstract

In this study, an eco-friendly, green synthesis, approach was adopted to synthesize tin oxide (SnO_2) nanoparticles (NPs) from Ficus Carica leaf extract. Tin (II) chloride ($SnCl_2 \cdot 2H_2O$) is the precursor used to prepare NPs of SnO_2. The annealed SnO_2 NPs at 500 ºC were analysed using various physicochemical characterization techniques, including XRD, FTIR, UV-Vis, and SEM. The XRD spectrum reveals that the rutile phase of SnO_2 NPs is obtained at this calcination temperature (500 ºC). The particles size from XRD spectrum using Debye-Scherrer equation is found to be 17.87 nm. The chemical functional groups of metal-oxygen (Sn-O), Alkane (-C=C-), Carbonyl (-C=O) and hydroxyl (H-O) are presented in FTIR spectrum of SnO_2 NPs. The SEM image shows that the shape morphology of the prepared SnO_2 NPs is spherical. The SnO_2 nanoparticles exhibited efficiency degradation of Murexide dye under visible light. Furthermore, the kinetic of prepared SnO_2 nanoparticles affirmed the complete degradation of Murexide dye after only 30 min.

Keywords: Green synthesis, Ficus Carica, SnO_2 nanoparticles, Murexide degradation

1. INTRODUCTION

The rising levels of toxins, chemicals and dyes in water bodies represent a threat to the environment and its welfare. The scientific committee seeks to ensure universal access to safe and affordable drinking water, enhance water quality through pollution reduction, and increase water-use efficiency in all sectors [1, 2]. One way to addressing these issues is to exploit the fascinating world of green chemistry. This approach is considered and used due to its effectiveness, sustainability and rapid efficiency [2, 3]. The use of plant extracts in synthesis is an environmentally beneficial strategy that reduces dependency on toxic chemicals. In addition, this method offers multiple benefits, including cost reduction, decreased greenhouse gas emissions [4, 5]. Using deionized water as solvent, a leaf extract as capping agent, and fewer chemical reagents, led to a more sustainable and environmentally friendly synthesis approach [6, 7]. Furthermore, these substances can be utilized in the fabrication of tin oxide (SnO_2) nanoparticles [8]. Among many other metal oxides, scientists are interested in Tin oxide (SnO_2) due to its low electrical sheet resistance, high stability and high transparency [2, 3]. Tin oxide (SnO_2) is an n-type semiconductor with a 3.6 eV band gap energy and outstanding electrical and optical properties, including good conductivity and transparency cells [9]. it is commonly employed as Catalyst supports, gas-sensing materials, optoelectronic devices, transparent conductive electrodes, and photovoltaic cells. SnO_2 has characteristics that make it suitable, for purifying water and fighting bacteria [4]. The improved photocatalytic activity of SnO_2 NPs, assisted by their high surface area and low electron-hole recombination rate, enables the effective breakdown of hazardous pollutants such as dyes, medicines, and other industrial chemicals. The SnO_2 nanoparticles could potentially eliminate all contaminants from water suggesting a method, for water treatment purposes [10, 11].

The aim of this study is to synthesize SnO_2 nanostructures by a green chemical approach and to explore their application in dye water degradation against Murexide. The study also considers the selection of Ficus Carica leaf extract and the annealed temperature for the process of synthesis.

2. MATERIAL AND METHOD

2.1. Preparation of Ficus Carica Leaf extract

The synthesis of pristine SnO_2 was conducted from Ficus Carica leaves. First they were freshly collected and washed several times with deionized water (DI) in order to eliminate all dust particles and impurities, then left to dry in Biophysics Laboratory of the university for 3 weeks. After the leaves were completely dried and brittle at touch, they were ground using a ceramic mortar until a fine, cornstarch-like powder was obtained. The leaf extract

was prepared by adding 20 g of Ficus Carica leaves powder to 600 mL of DI then heating at 55 °C until the majority of the precipitate was dissolved. The solution was then filtered using Whattman no 1 filter and a vaccum pump (N820 Labo Port) as a mean to accelerate the filtering process. A pure brown leaf extract was obtained with no green precipitate at the bottom.

2.2. Preparation of SnO₂ NPs

An amount of tin chloride dihydrate ($SnCl_2 \cdot 2H_2O$) was dissolved in 120 mL of F. Carica leaf extract and 62.5 ml of distilled water. The leaf extract acts as a surfactant that reduces the solution into SnO_2 nanoparticles. The mixture was left on a heating magnetic stirrer at 300 rpm for 24 hours at 50 °C then poured in 50 mL eppendorfs and centrifuged at 4500 rpm for a set of three 3 minutes long cycles. The precipitate was continuously washed using four cycles of deionized water (DI) and one cycle with methanol solution (50% DI+ methanol). The resulting precipitate was dried in an oven at 90 °C and the dried powder was annealed at 500 °C for 2 hours.

2.3. Characterization Studies

To study the structural properties of the resulting SnO₂ NPs, the XRD spectrum is obtained from the PANalytical XRD diffractometer, with monochromator radiation ($\lambda_{CuK\alpha}$ = 1.54187 Å) in the range of 2θ = 15–90°. NICOLET 380 transform infrared spectroscope FTIR analysis is used to identify organic and inorganic functional groups present in SnO₂NPs. The Thermo-Scientific Scanning Electron Microscope with a built-in Energy Dispersive X-ray spectroscope was used to analyze the SnO₂ surface morphology. The HACH DR 6000 spectrophotometer was used to evaluate the photocatalytic degradation of Murexide dye present in water solutions after multiple cycles of direct sunlight exposure.

2.4. Photocatalytic Activityof SnO₂ NPs

Pristine tin oxide NPs were used as a photocatalyst for Murexide solutions and the degradation of dye was done as follows. 100 ml was claimed from the dye wastewater barrel and put in 200 ml Bechers for SnO₂ photocatalyst NPs. The solutions were stirred magnetically in the dark for 30 minutes to allow adsorption and desorption processes between the photocatalyst and the dye solutions. After stirring, the solutions were exposed to direct solar light for numerous cycles.

3. RESULTS

3.1. XRD Analysis of SnO₂ NPs
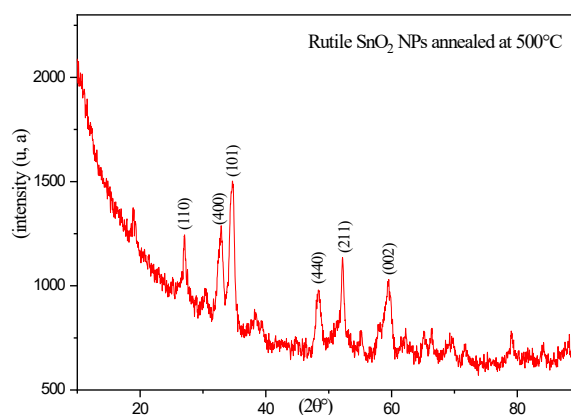
Figure 1. XRD spectrum of pristine SnO₂ NPs obtained from Ficus. Carica leaf extract and annealed at 500 °C

The XRD spectrum of SnO₂ nanoparticles annealed at 500 °C for 2h is shown in Figure 1. The rutile tetragonal Phase of SnO₂NPs has been revealed [12, 13]. According to JCPDS cards 01-072-1147, 00-003-0439, and 00-013-0082. The diffracted planes were determined with respect to the following diffracting angles respectively at 27.07° (110); 32.48 (400); 34.77° (101); 48.47 (440); 52.21° (211); and 59.60° (002). The average particle size is found to be 17.87nm. The size was determined using the following Debye-Scherrer Equation:

$$D = \frac{k \cdot f}{\beta \cdot \cos\theta} \tag{1}$$

Where k is constant (0.9), λ is the wavelength corresponding to CuKα source (1.540 Å), θ is the Bragg angle and β is the full width of the half maximum.

3.2. FTIR Analysis of SnO₂ NPs

Figure 2 exhibits the FTIR spectrum of SnO₂ NPs synthesis from Ficus. Curica leaf extract. The functional group of metal oxide (Sn-O) was observed respectively at 600.69 cm^{-1} and 665.81cm^{-1} [14, 15]. On the other hand, the functional groups of F. Carica leaf extract corresponds to different organic compounds such as Alkane (-C=C-), Carbonyl (-C=O) and hydroxyl (H-O) relatively appear in same determine area respectively at 1350-1590 cm^{-1}, 1600-1990 cm^{-1} , 2280-2398 cm^{-1} and 3500-3900 cm^{-1} in the spectrum [16, 17].
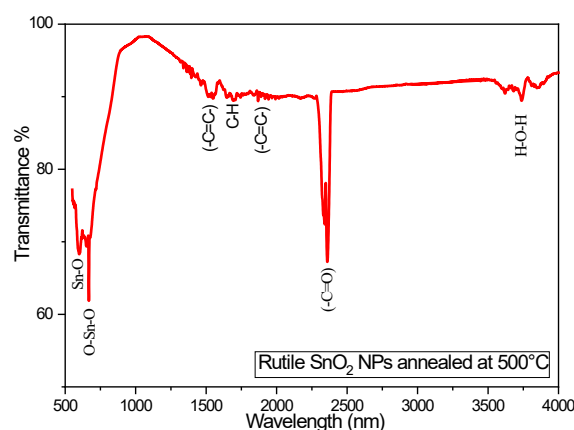
Figure 2. FTIR spectrum of pristine SnO₂ NPs obtained from Ficus. Carica leaf extract and annealed at 500 ºC

3.2. SEM Analysis of SnO₂ NPs

SEM image of SnO₂ nanoparticles obtained from Ficus. Curica leaf extract is presented in figure 3. The image reveal clearly homogenous and spherical particles with a smooth, sponge-looking surface texture, which proves the high adsorption quality of SnO₂NPs.
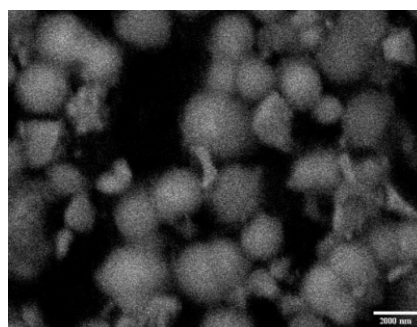
Figure 3. SEM image of pristine SnO2 NPs obtained from Ficus. Carica leaf extract and annealed at 500 ºC

3.3. Photocatalytic Activity of SnO₂ NPs

Figure 4 depicts photocatalytic degradation of Murexide using pristine SnO₂ NPs obtained from Ficus. Carica leaf extracts and annealed at 500 ºC. It is clear to note that after the first 30 minutes, the absorbance shifts to a lower intensity and the solution's observed colour gradually fades after 30 minutes of solar exposure. This faster degradation of Murexide dye can be correlated to the crystallinity enhancement and reduces defects, which enhances charge carrier mobility and reduces electron-hole recombination rates, and consequently, increases the photocatalytic efficiency which provides more active sites for the photo-degradation reactions [18, 19]. The basic mechanism of photocatalytic reactions can be explained as follows. When a photocatalyst is exposed to light with an energy equal to or greater than its band gap energy, electrons migrate from the valence band (VB) to the conduction band (CB), forming holes in the VB [2, 5]. Photogenerated holes and electrons undergo oxidation and reduction with water and dissolved oxygen, producing reactive oxygen species (ROS) including hydroxyl radicals (OH) and superoxide radical anions (O₂) [9, 18]. Superoxide radical anions combine with h+ to produce HO₂ radicals, which then collide with electrons to form hydrogen peroxide anions (HO^{-2}). They react with hydrogen ions to form molecules of hydrogen peroxide (H₂O₂) [13, 14].
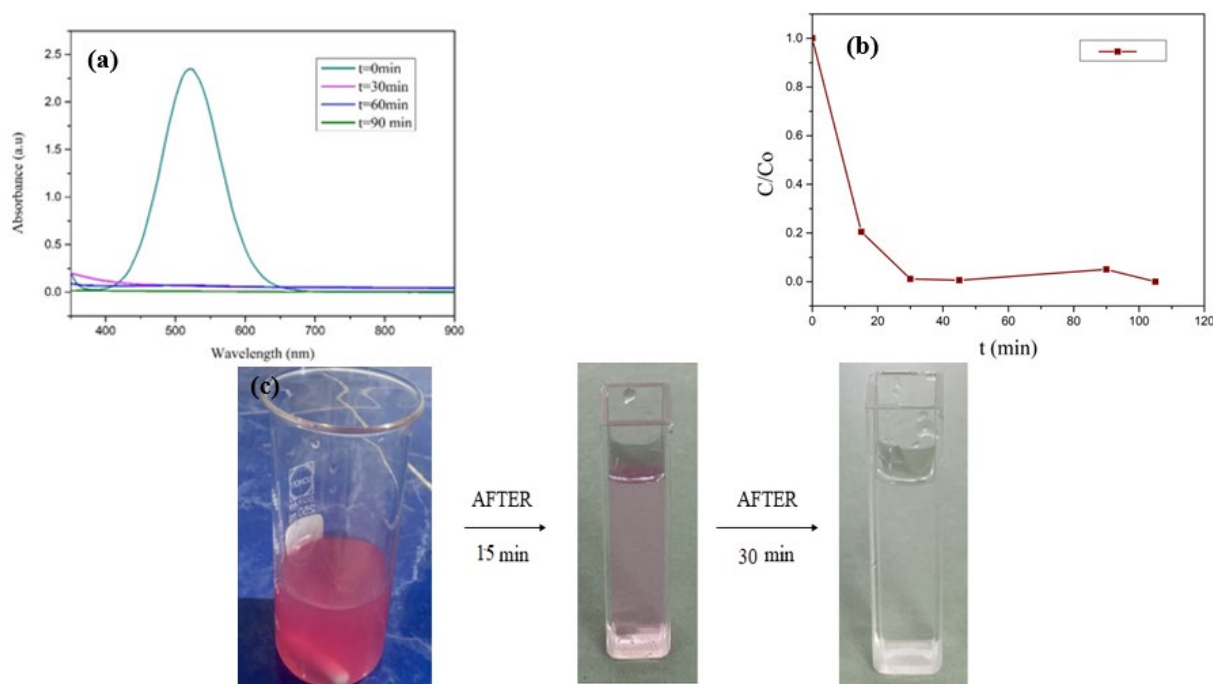
Figure 4. Photo-degradation of Murexide dye using pristine SnO_2 NPs obtained from Ficus. Carica leaf extract: (a) The UV-Vis absorption spectrum of Murexide dye, (b) ratio of dye concentrations, and (c) colour degradation after 30 minutes

4. CONCLUSION

This study investigates the green synthesis of pristine SnO_2 nanoparticles using Ficus. Carica leaf extract and evaluates their potential applications against Murexide dye. The study successfully demonstrates the formation of SnO_2 nanoparticles within rutile phase. Photocatalytic experiments showed that annealed SnO_2 nanoparticles at 500 ºC exhibited an efficiency degradation of Murexide under visible light. the kinetic of prepared SnO_2 nanoparticles affirmed the degradation of Murexide dye which is probably due to decreased electron-hole recombination rate, increased surface area, and improved crystallinity.

References

[1] S. P. Patil "Ficuscarica assisted green synthesis of metal nanoparticles: A mini review," *Biotecknology Reports*, vol. 28, art. no. e00569, Nov. 2020.

[2] Bhawna, A. K. Choudhary, A. Gupta, S. Kumar, P. Kumar, R. P. Singh, et al., "Synthesis, antimicrobial activity, and photocatalytic performance of Ce doped SnO_2 nanoparticles," *Frontiers in Nanotechnology*, vol. 2, art. no. 595352, Nov. 2020.

[3] Y. L. Tiki, L. D. Tolesa, A. H. Tiwikrama, and T. F. Chala, " Ginger (zingiber officinale)-mediated green synthesis of silver doped tin oxide nanoparticles and evaluation of its antimicrobial activity," *ACS Omega*, vol. 9, pp. 11443–11452, Feb. 2024.

[4] A. M. Hamdi, S. E. Laouini, S. Meneceur, G. H. Gamil, I. Kir, and A. A. A. Johar "Green synthesis of SnO_2 nanoparticles from laurusnobilis l. extract for enhanced gelatin-based films and CEF@SnO_2 for efficient antibacterial activity," *Food and Bioprocess Technology*, vol. 17, pp. 1364–1382, May 2024.

[5] E. Gribov, E. Koshevoy, I. Chikunova, and V. Parmon "Template-assisted SnO_2: Synthesis, composition, and photoelectrocatalytical properties," *Catalysts*, vol. 13, no 1, art. no. 168, Jan. 2023.

[6] D. Borah, P. Saikia, J. Rout, D. Gogoi, N. N. Ghosh, and C. R. Bhattacharjee "Sustainable green synthesis of SnO_2 quantum dots: a stable, phase-pure and highly efficient photocatalyst for degradation of toxic dyes," *Materials Today Sustainability*, vol. 26, art. no. 100770. Jun. 2024.

[7] R. Kumar, S. Gokul, F. Ran, S. Sambasivam, K. A. Alrashidi, and R. Thangappan "Green synthesis of g-C3N4 decorated with SnO_2 nanocomposites using a novel ananascomosus crown extract for boosted performance of asymmetric supercapacitors," *Energy Storage*, vol. 98, Part B, art. no. 113231, Sep. 2024.

[8] Ch. Sun, J. Yang, M. Xu, Y. Cui, W. Ren, J. Zhang, et al., "Recent intensification strategies of SnO_2-based photocatalysts: A review," *Chemical Engineering*, vol. 427, art. no. 131564, Jan. 2022.

[9] S.F. Alshahateet, R.M. Altarawneh, W. M Altawarh, S. A. Altrawneh, S. Altaweel, K. Azzaoui, et al.,

"Catalytic green synthesis of tin (IV) oxide nanoparticles for phenolic compounds removal and molecular docking with EGFR tyrosine kinase," *Scientific Reports*, vol.14, art. no. 6519, Apr. 2024.

[10] I. Buniyamin, N. A. Asli, K. A. Eswar, S. A. I. A. Syed AbdKadir, A. Saiman, M. Y. Idorus, et al., "Biosynthesis of tin (IV) oxide nanoparticles (SnO2 NPs) via chromolaena odorata leaves: the influence of heat on the extraction procedure," *Science and Mathematics Letters*, vol. 12, no 2, pp. 142–150, Jul. 2024.

[11] A. Alsulimani, S. M. Abdullah, A. A. Jerah, A. M. Hendi, and A. Farasani "Green synthesis of chitosan-coated tin dioxide nanoparticles using moringaoleifera flower extract against breast cancer via the caspase-dependent apoptotic pathway," *Pharmacognosy Magazine*, 2024, doi: 10.1177/09731296241276588.

[12] J. J. Mini, S. Khan, M. Aravind, T. Mol, A. A. A. Bahajjaj, H M. Robert, et al., "Investigation of antimicrobial and anti-cancer activity of thermally sensitive SnO$_2$ nanostructures with green-synthesized cauliflower morphology at ambient weather conditions," *Environmental Research*, vol. 245, art. no. 117878, Mar. 2024.

[13] Z. Saeed, M. Pervaiz, A. Ejaz, S. Hussain, S. Shaheen, B. Shehzad, et al., "Garlic and ginger extracts mediated green synthesis of silver and gold nanoparticles: A review on recent advancements and prospective applications," *Biocatalysis and Agricultural Biotechnology*, vol. 53, art. no. 102868, Oct. 2023.

[14] B. P. Narasaiah, P. Banoth, A. Sohan, B.K. Mandal, A.G. B. Dominguez, L. D. L. S. Valladares, et al., "Green biosynthesis of tin oxide nanomaterials mediated by agro-waste cotton boll peel extracts for the remediation of environmental pollutant dyes," *ACS Omega*, vol. 7, no. 18, pp. 15423−15438, Apr. 2022.

[15] M. S. Gari, B. P. Narasaiah, A. Pandurengan, B. Mandal, and M. Natarajan "Synthesis and antioxidant activity of some novel 4H-chromene derivatives catalysed by biogenic tin oxide nanoparticles," *Biointerface Research Applied Chemistry*, vol. 13, no. 6, art. no. 521, Feb. 2023.

[16] A. S. Aloufi "Assessment of structural, optical, and antibacterial properties of green Sn (Fe: Ni) O2 nanoparticles synthesized using Azadirachta indica leaf extract," *Bioinorganic Chemistry and Applications*, vol. 2023, no. 1, art. no. 5494592, Feb. 2023.

[17] Y. Uday, H. Manjunatha, Y. Vidya, S. Manjunatha, R. Soundar, and K. Sridhar "Multifunctional properties of tin oxide nanoparticles synthesized by green and chemical approach," *Current Applied Physics*, vol. 55, pp. 9–15, Nov. 2023.

[18] G.K. Dalapati, H. Sharma. A. Guchhait, N. Chakrabarty, P. Bamola, Q. Liu, et al., "Tin oxide for optoelectronic, photovoltaic and energy storage devices: A review," *Materials Chemistry A*, vol. 9, no. 31, pp. 16621–16684, Jun. 2021.

[19] A. Rana, K. Yadav, and S. Jagadevan, "A comprehensive review on green synthesis of nature-inspired metal nanoparticles: mechanism, application and toxicity," *Cleaner Production*, vol. 272, art. no. 122880, Nov. 2020.

Green Synthesis of Zinc Oxide Nanoparticles: An Eco-Friendly Approach

Asma Bessaad[1,2], Badreddine Toubal[1], Mahdia Toubane[2], Kaouther El Kourd[1]

[1]Department of Material Sciences, University of Algiers 1, Benyoucef Benkhedda, Algeria
[2]Research Unit on Materials Processes & Environment URMPE, University M'hamed Bougara Boumerdes, Algeria
Corresponding author: Asma Bessaad (e-mail: a.bessaad@univ-alger.dz)

Abstract

Green synthesis of zinc oxide nanoparticles (ZnO NPs) has garnered significant attention for its sustainable and environmentally friendly methodology, utilizing natural agents such as plant extracts to produce nanomaterials without harmful chemicals. This approach not only minimizes environmental impact but also enhances the biocompatibility and safety of the nanoparticles for various applications. The synthesis process typically involves extracting phytochemicals from plants, which act as both reducing and stabilizing agents, resulting in ZnO NPs with unique structural properties. However, one of the primary challenges of green synthesis is achieving uniform particle size and morphology, as variations in biological extracts can lead to inconsistencies. Despite these challenges, ZnO NPs synthesized through green methods have demonstrated promising properties, including enhanced antibacterial activity, making them suitable for applications in biomedicine, sensors, and photocatalysis. This study investigates the influence of different plant extracts on the synthesis and characterization of ZnO NPs, highlighting their potential for innovation in sustainable nanotechnology. By focusing on green synthesis techniques, this research emphasizes the importance of developing eco-friendly methods that not only yield effective nanomaterials but also align with principles of sustainability and environmental responsibility in scientific research.

Keywords: ZnO NPs, Eco-friendly, Green synthesis, Plant extracts, Structural property, Nanotechnology

Impact of Different Immobilization Techniques on Probiotic Viability

Tanja Krunic[1]

[1]Innovation Centre Faculty of Technology and Metallurgy, University of Belgrade, Belgrade, Serbia
Corresponding author: Tanja Krunic (e-mail: tkrunic@tmf.bg.ac.rs)

Abstract

Immobilization is a valuable method recognized for use in the food industry. Immobilization of probiotics brings many benefits as the probiotics are protected from external factors in a carrier, allowing them to better withstand the time and conditions of production and storage. In addition, immobilized probiotics can survive conditions such as low pH, and the presence of digestive enzymes and bile salts in the human gastrointestinal tract. The technology of probiotic immobilization meets an important requirement: bacterial cells must stay alive. This requirement has been crucial in selecting the appropriate immobilization technology and carrier used for immobilization. Alginate is the most commonly used hydrogel for immobilization. Its low price, wide availability, and mild crosslinking conditions make it a good choice for the immobilization of living cells. This work compared extrusion and spray dry techniques. Encapsulation efficiency for probiotic immobilization in alginate carrier using extrusion technique is about 95% compared to 75% for spray drying. Also, the product yield of the extrusion technique is almost 100%, compared to 70% for spray drying. To have a broader picture, it is necessary to compare the fermentable activity of the encapsulated culture, as well as the stability of the product during storage. Probiotics encapsulated by extrusion technique showed slightly better fermentation activity and approximately the same stability during storage compared to probiotics encapsulated by spray dry technique. From the previously mentioned it can be concluded that extrusion is a better option for probiotic immobilization than spray dry technique.

Keywords: Alginate, Extrusion, Spray dry, Encapsulation efficiency, Fermentation activity

Acknowledgments

Supported Nickel Catalyst: Exploring Advanced Hybrid Material with Synergistic Properties

Wahiba Amrane[1], Mohamed Karmaoui[2]

[1]Physical Chemistry, University of Science and Technology of Oran-Mohamed Boudiaf (USTO-MB), Oran, Algeria
[2]Chemical Engineering, University of Science and Technology of Oran-Mohamed Boudiaf (USTO-MB), Oran, Algeria
Corresponding author: Wahiba Amrane (e-mail: saveway.hibess@gmail.com)

Abstract

Targeted approaches are continually being developed to enhance the performance and efficiency of metal oxide nanoparticles. Doping with noble or non- noble metals, grafting metal oxides on polymers, and supporting metal oxides on porous materials are among the possible strategies to combine the properties of metal oxides, and those of supported materials. In this work, we report the synthesis of Nickel oxide supported on polyaniline polymer, and metal organic framework materials via a solvothermal method, as well as their synergistic effect on catalysis process. The supported catalysts were characterized using several advanced analytical techniques, including UV-Vis spectroscopy, Fourier transform infrared spectroscopy (FTIR), thermogravimetric analysis (ATG), and scanning electron microscopy (SEM).

Keywords: Polyaniline, Nano-hybrid materials, Nickel oxide, Solvothermal method, Characterization

Phenolic Compounds in Solanum Tuberosum Peel and Their Antioxidant Activities and FTIR Spectroscopy

Tassadit Sahki[1], Fatiha Brahmi[1], Fatima Djenad[1], Yasmine Achat[1], Lila Makhlouf-Boulekbache[1], Khodir Madani[2]

[1]Biomathematics, Biophysics, Biochemistry, and Scientometrics Laboratory, University of Bejaia, 06000, Algeria

[2]Center for Research in Agro-Food Technologies, 06000 Bejaia, Algeria

Corresponding author: Tassadit Sahki (e-mail: tassadit.sahki@univ-bejaia.dz)

Abstract

Potato (solanum tuberosum) peels contain a significant amount of phenolic compounds, which are recognized for their potent antioxidant properties. These bioactive compounds make potato peels valuable in both health-related and food processing applications. Among the various phenolic acids found in potato peels, chlorogenic acid is the most abundant, followed by other notable phenolic acids like caffeic, gallic, and protocatechuic acids. Each of these compounds contributes to the peel's antioxidant capacity, which involves neutralizing free radicals that can cause cellular damage. The antioxidant activity of these compounds has been extensively studied. For instance, potato peel extracts can effectively scavenge free radicals such as DPPH and ABTS, both of which are common indicators used in antioxidant assays. These tests demonstrate the ability of phenolic compounds to mitigate oxidative stress, which is linked to several health benefits, including anti-cancer, anti-inflammatory, and anti-aging effects. To further understand the bioactivity of phenolic compounds, FTIR is commonly used. FTIR helps to identify the molecular structure and functional groups present in the phenolic compounds, giving researchers insight into how these compounds work at a chemical level. This analysis is essential for determining the compounds' effectiveness in neutralizing free radicals. In conclusion, potato peels are an excellent source of phenolic compounds with substantial antioxidant capacity. Their potential applications range from natural food preservatives to ingredients in health-promoting products. These findings support the use of potato peel extracts as a sustainable and valuable by-product in various industries, particularly in enhancing food shelf-life and promoting overall health. Numerous studies have validated these antioxidant properties, reinforcing their importance in both the food and health sectors.

Keywords: Potato peels, Bioactive compounds, DPPH, Antioxidant activity, FTIR

Investigation of Structural and Optical Characteristics of Fe-Doped ZnO Nanoparticles Co-Precipitation Method

Roguai Sabrina[1]

[1]Department Science of the Matter, Abbes Laghrour University Khenchela, Algeria
Corresponding author: Sabrina Roguai (e-mail: rog.sabrina@yahoo.fr)

Abstract

Fe-doped ZnO nanoparticles with varying concentrations of iron (0.00, 0.02, 0.05, and 0.10) were synthesized using the chemical co-precipitation method. This method provides a simple and efficient way to incorporate dopants into ZnO's crystal structure, enhancing its properties for various applications. The impact of iron doping on the structural, morphological, and optical characteristics of ZnO nanoparticles was systematically investigated through X-ray diffraction (XRD), scanning electron microscopy (SEM), and UV-Visible spectroscopy. XRD analysis confirmed that both the pure and Fe-doped ZnO nanoparticles maintained a single-phase wurtzite crystal structure, indicating that iron was successfully incorporated into the ZnO lattice without the formation of secondary phases. The crystallite size was found to decrease with increasing Fe content, which can be attributed to the substitution of Zn^{2+} ions by smaller Fe^{3+} ions, leading to lattice distortion and hindering grain growth. SEM imaging provided insights into the surface morphology of the nanoparticles, revealing that the nanoparticles tended to form aggregates, with individual particles exhibiting a range of sizes. These aggregates were likely the result of the coalescence of smaller nanoparticles, and the size distribution appeared to vary depending on the level of Fe doping. UV-Visible spectroscopy demonstrated a notable effect of iron doping on the optical properties of ZnO. As the concentration of Fe increased, a reduction in the energy band gap was observed. This band gap narrowing is likely due to the introduction of Fe-related states within the band structure, which modifies the electronic transitions. The reduction in the band gap with increasing Fe concentration suggests potential applications of Fe-doped ZnO nanoparticles in photocatalysis and optoelectronic devices.

Keywords: Fe-doped ZnO nanoparticles, Co-precipitation method, Structural, Microstructural, Optical properties

Spray Deposition and Characterization of Cerium Oxide Thin Films as Optically Passive Counter Electrodes for Electrochromic Devices

Abdellatif El-Habib[1], Samir Haloui[1], Abdessamad Aouni[1], Mustapha Diani[1], Mohammed Addou[1]

[1]Department of Physics, Abdelmalek Essaadi University, Tangier, Morocco
Corresponding author: Abdellatif El-Habib (e-mail: eabdellatif@uae.ac.ma)

Abstract

Electrochromic devices are systems that change color or transparency when an electric voltage is applied, used in applications like smart windows and displays for controlling light and energy efficiency. Cerium oxide (CeO_2) serves as an optically passive counter electrode in electrochromic devices due to its high transparency in the visible spectrum, chemical stability, and good ionic conductivity. Its redox activity enhances performance in electrochemical applications, allowing light to pass through without interference while facilitating effective ion transport. Nanostructured thin films of Cerium Oxide (CeO_2), doped with Neodymium (Nd), were successfully deposited onto glass and ITO substrates using the spray pyrolysis method. The structural, morphological, optical, and electrochemical properties of these films were systematically studied. X-ray diffraction (XRD) confirmed the formation of a single-phase polycrystalline cubic fluorite structure of CeO_2. The crystallite size and microstrain of the thin films were found to depend on the level of Nd doping. Raman spectroscopy and UV–Vis–NIR analyses revealed a red-shift, peak broadening, and asymmetry in the F2g Raman mode, as well as a red-shifted energy gap. Scanning electron microscopy (SEM) images showed nanograin formation in the films, and energy-dispersive spectroscopy (EDS) confirmed the elemental composition. Electrochemical measurements indicated that Nd doping enhanced the electrochemical properties of CeO_2. Furthermore, the Nd-doped CeO_2 thin films remained fully transparent during the intercalation and deintercalation of Li^+ ions. These significant findings expand the potential applications of this oxide, particularly in supercapacitors and electrochromic devices.

Keywords: Cerium oxide, Doping, Thin film, Spray pyrolysis, Electrochemical properties

Green Synthesis of Magnesium Oxide Nanoparticles: The Influence of Lanthanum and Eucalyptus Extract

Fares Chabira[1,2], Toubane Mahdia[1,2], Tala-Ighil Razika[1,3], Ismail Pir[4], Mohamed Bououdina[4]

[1]Research Unit on Materials Processes & Environment URMPE, University M'hamed Bougara of Boumerdes, 35000 Boumerdes, Algeria
[2]Department of Physics, Faculty of Sciences, University M'hamed Bougara of Boumerdes, 35000 Boumerdes, Algeria
[3]Institute of Electrical & Electronic Engineering, University M'hamed Bougara of Boumerdes, 35000 Boumerdes, Algeria
[4]Energy, Water and Environment Lab, College of Humanities and Sciences, Prince Sultan University Riyadh, 11586, Saudi Arabia
Corresponding author: Fares Chabira (f.chabira@univ-boumerdes.dz)

Abstract

Magnesium oxide (MgO) is a versatile oxide material according to its broad applications, such as in catalysis, hazardous waste treatment, antimicrobial materials, refractory materials, and superconductor materials. In this study, magnesium oxide (MgO) nanoparticles were synthesized through a simple hydrothermal process. Magnesium sulfate served as the magnesium source, while lanthanum chloride ($LaCl_3$) and eucalyptus extract were employed as dopants to modify the structural and functional properties of the nanoparticles, with a specific focus on evaluating the effect of eucalyptus extract on the synthesis and properties of MgO NPs. Homogeneous precursor solutions were prepared and transferred into a Teflon-lined stainless-steel autoclave, where they were subjected to hydrothermal treatment at 130°C. Following this, the resulting products were calcined at 350°C to obtain the final MgO nanoparticles. The synthesis process yielded three distinct samples: pure MgO, MgO doped with lanthanum, and MgO doped with lanthanum and eucalyptus extract. The structural and morphological characteristics of these nanoparticles were investigated using X-ray diffraction (XRD) and electron microscopy techniques. X-ray diffraction analysis indicates the formation of pure high-quality MgO phase with an average crystallite size in the range 5.25 – 6.80 nm. Electron microscopy revealed a consistent plate-like morphology across all samples. These nanomaterials will offer high potential as antimicrobial materials and purifying waste water, highlighting their versatility and applicability in environmental and health-related fields.

Keywords: Magnesium oxide (MgO), Nanoparticles, Eucalyptus extract, Hydrothermal

Output Voltage Regulation of an LLC Resonant Inverter Based on Control

Chaimaa Youcef Achira[1], M'hamed Helaimi[1]

[1]Department of Electrotichnique, University of Hassiba Benbouali, Chlef, Algeria
Corresponding author: Chaimaa Youcef Achira (e-mail: chaimaayoucef61@gmail.com)

Abstract

The importance of tension waves in the industrial sector through its various applications such as correlation with electrical machines, which allow changing the speed of electric motors, in addition to providing uninterrupted energy and the support of electrical equipment has made it the target of many different studies of its control techniques. And thanks to the technological renaissance in the field of electronics, waves mean the conversion of direct current into Alternating current with controlled frequency. This study is related to the study and simulation of an electric tension wave, as the first chapter is devoted In the mathematical modeling of this corrugators, in the second chapter, we introduced some techniques for controlling the corrugators And the types of technologies used in the industrial sector, and we simulated control techniques On an inverter with control techniques on Matlab Simulink simulation program original results The simulations are identical, demonstrating our success in simulating the inverter and implementing the control technique with pulse width modulation Suspicions decrease.

Keywords: Tension waves, Controlled frequency, Pulse width modulation, Matlab

Performance Comparison of RISC-V and TTA Processors for Ascon

Latif Akcay, Mustafa Alptekin Engin

[1]Electrical - Electronics Engineering Department, Bayburt University, Bayburt, Türkiye
Corresponding author: Latif Akcay (e-mail: lakcay@bayburt.edu.tr)

Abstract

Cryptography is the fundamental building block of modern digital security, facilitating the development of applications such as secure communication, data integrity, and authentication. The deployment of lightweight cryptography methods, such as the Ascon algorithm, is vital in resource-constrained environments, including the Internet of Things (IoT) and embedded systems. Ascon was selected as a finalist in the National Institute of Standards and Technology (NIST) Lightweight Cryptography standardization process. It has been optimized for efficiency, low power consumption, and minimal memory usage, which makes it an ideal choice for devices with limited processing resources. The advent of open-source hardware architectures constitutes a significant transformation in the domain of embedded systems, facilitating innovation and enhancing accessibility. Notable examples in this field include RISC-V and transport triggered architecture (TTA). The modular and extensible instruction set architecture of RISC-V is widely used in academia and industry to develop cost-effective and customizable processors. On the other hand, TTA offers optimisation and energy efficiency through a very long instruction word (VLIW)-like computation methodology. This paper compares the performance of the Ascon algorithm on popular 32-bit and 64-bit RISC-V processors and Transport Triggered Architecture processors in various configurations. Despite the standardized ecosystem, broad tool support, and flexibility inherent to RISC-V, analysis using reference Ascon software and standard TTA and RISC-V instructions demonstrated that TTA processors exhibit superior computational performance than RISC-V cores. This is attributed to their capacity to effectively utilize instruction-level parallelism (ILP). Furthermore, the results demonstrate that TTA processors require less hardware resources in the FPGA implementation and can operate at higher clock frequencies.

Keywords: Lightweight cryptography, Embedded systems, Security-performance tradeoff, Comparative analysis, Performance benchmarking

1. INTRODUCTION

In today's digital age, the increasing use of technologies such as the Internet of Things (IoT) has made data security a critical priority. However, IoT devices and other embedded systems have limited compatibility with traditional cryptography due to constraints in processing power, memory capacity and energy resources [1]. Lightweight cryptography [2], developed to address these challenges, aims to provide a high level of security with low resource consumption. In this context, lightweight cryptography plays a critical role in a wide range of applications, from IoT devices to medical sensors, smart home devices to industrial automation systems.

Ascon is a lightweight encryption algorithm designed for devices for low power consumption and limited hardware resources [3]. It is specifically designed to ensure data security in IoT devices and embedded systems and is optimised for authenticated encryption and message hashing. Offering high performance in both software and hardware applications, Ascon has proven its reliability by winning the National Institute of Standards and Technology (NIST) Lightweight Cryptography competition [4]. By providing a perfect balance between efficiency and security, Ascon has an important role in setting modern security standards [5].

In the context of modern electronic design processes, there has been a notable shift towards the adoption of open-source processor architectures [6]. Open-source architectures offer a compelling combination of flexibility, customisability and community-driven innovation, making them an attractive choice for both academic research and industrial projects. In particular, embedded systems and IoT devices stand to gain significantly from such architectures. An open source approach allows for the creation of custom hardware and software solutions that can be tailored to meet the specific security, cost and performance requirements of these systems. Two notable architectures in this field, RISC-V [7] and transport triggered architecture (TTA) [8], address different application areas with their distinct design philosophies. RISC-V offers a modular, portable and widely supported open

standard architecture, while TTA provides energy efficiency and performance optimisation through greater control and customisation in processor design.

In this paper, a comparison of the performance of RISC-V and TTA processors based on the Ascon encryption algorithm is discussed. In addition to the performance analysis, the hardware implementations of both architectures on FPGA are examined. The main objective of the study is to reveal the advantages and disadvantages of these two architectures in terms of security, speed, and hardware resource utilisation for embedded systems and IoT applications. Thus, the research results will serve as a guide to understand which architecture is more suitable in specific application scenarios. This comparison contributes to the literature providing an important perspective on processor designs optimised for lightweight cryptography. In this regard, there are many studies on optimizing RISC-V and TTA processors for cryptography applications [9–14].

Rest of the paper is organized as follows: The Ascon cipher and the compared processor architectures are explained in the second section together with the test method. The results are shared and evaluated in the third section, while the fourth section concludes the paper.

2. MATERIAL AND METHOD

2.1. Ascon Cipher

Ascon is an encryption family designed to meet the contemporary data security requirements in resource-limited systems. The initial version was developed in 2014 and submitted to the CAESAR (Competition for Authenticated Encryption: Security, Applicability and Robustness) competition by a team of cryptographers [15]. After that, it was determined as a standard in the final round of the NIST Lightweight Cryptography standardization project [4].

The Ascon family consist of authenticated ciphers (Ascon-AEAD128, Ascon-AEAD128a, Ascon-AEAD80pq), cryptographic hash (Ascon-Hash256), and extendable output functions (Ascon-XOF128, Ascon-CXOF128). The structure of the algorithm is based on a sponge construction with a combination of substitution-permutation networks (SPN) and simple bitwise operations [3]. The authenticated encryption process involves five stages. Firstly, the key and nonce are loaded into a state register, which is then subjected to multiple rounds of the SPN. Subsequently, the associated data is absorbed (XORed) into the state and processed using the permutation function. Thereafter, the plaintext is XORed into the state block-by-block. Each block of plaintext is extracted from the state to form the ciphertext. Following the processing of each block, the state is updated using the permutation function. Finally, the key is XORed into the state, and the permutation function is applied one last time to update the state.

2.2. The RISC-V Instruction Set Architecture

RISC-V is an open-source and royalty-free instruction set architecture (ISA) based on the classical RISC design philosophy [7]. It was developed with the intention of providing a flexible framework that could be utilised in both academic research and industrial contexts. RISC-V is characterised by a modular design comprising a fundamental instruction set and optional extensions, including integer arithmetic (I), multiplication and division (M), atomic operations (A), floating-point (F and D), and vector processing (V). The modular approach permits the implementation of flexible solutions tailored to specific use cases, ranging from simple embedded systems to high-performance supercomputers. RISC-V International is a non-profit organization that manages, promotes and develops the ISA. It ensures the ISA remains open, royalty-free and freely available for use by researchers, developers, companies and hardware manufacturers worldwide.

In this study, we chose two popular 32-bit and 64-bit RISC-V platforms for performance comparison with the TTA cores: Pulpissimo [16], and CVA6 [17]. Pulpissimo is powered by a 32-bit, 4-stage, in-order RISC-V core, CV32E40P, which implements the integer arithmetic (I), multiplication and division (M), and compressed (C) instruction sets (RV32IMC) along with custom several ISA extensions such as: hardware loops, post-incrementing load and store instructions, bit-manipulation instructions, etc. On the other hand, CVA6 has a 64-bit, 6-stage, application-class RISC-V core, CV64A60, that implements the RV64GC (I, M, A, F, D, C) instruction sets. Both Pulpissimo and CVA6 are widely used, FPGA and ASIC-proven system-on-chip (SoC) designs.

2.3. Transport Triggered Architecture

TTA is an open-source and free processor design methodology designed and developed by Tampere University, Finland. Even though it has a similar computation philosophy to the very long instruction word (VLIW) architecture, it stands out with distinctive features. TTA achieves instruction level-parallelism (ILP) similarly to

VLIW architectures but in a more modular and flexible way. While VLIW relies on a compiler to schedule multiple independent operations in a single, large instruction, TTA only requires the compiler to handle data movement instructions. Each "move" instruction specifies the source and destination of the data, and computation occurs automatically as a side effect of this transfer. Since multiple transport buses can operate concurrently, multiple moves can be issued simultaneously, enabling the concurrent triggering of different operations in separate functional units. This design exposes ILP more explicitly than traditional architectures, as each move corresponds directly to data flow, which inherently reflects parallel execution. The architectural design comprises transport buses, functional units (FUs), register files (RFs), load-store units (LSUs) and a simplified global control unit (GCU). The FUs operate independently, executing their operations automatically when input data is available. The transport buses enable concurrent data movement between the FUs. A diagrammatic representation of the internal structure of TTA processors is provided in Figure 1.
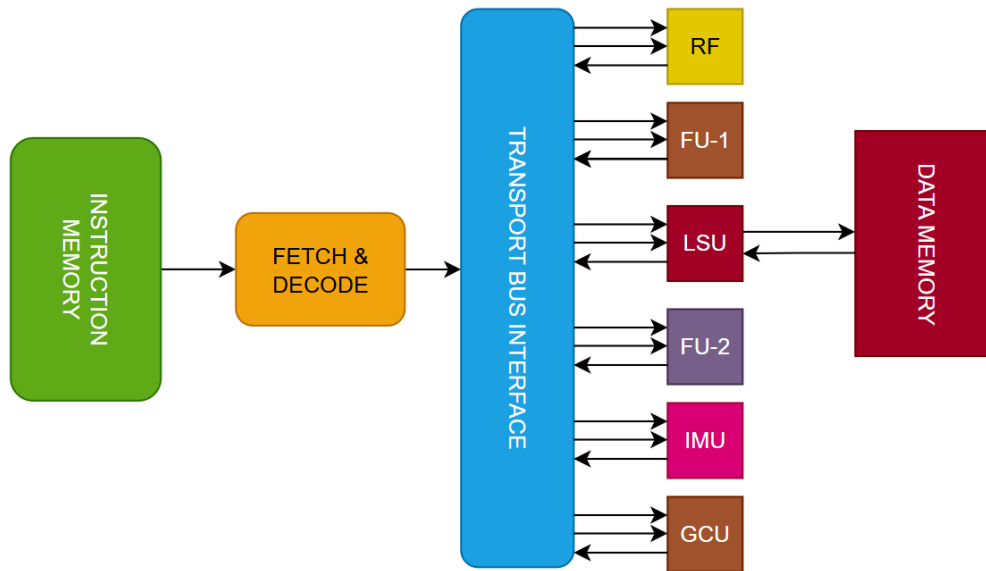
Figure 1. Internal structure of TTA processors

In this study, we used 64-bit TTA processor for performance comparison with the RISC-V cores. The reason for this is that the reference software implementation of the Ascon encryption algorithm [18] performs calculations on 64-bit data.

2.4. Test Method

Using the Ascon reference C implementation, the testbench was first compiled for the Pulpissimo platform using the 32-bit RISC-V GCC toolchain. The Pulpissimo platform provides helper scripts for users to simulate test code on the processor. In this way, performance data was obtained by running the Ascon testbench on the Pulpissimo platform. Similarly, the CVA6 platform offers Verilator-based rapid test facilities. This time the Ascon testbench code was compiled using the 64-bit RISC-V GCC toolchain and run on the CVA6 platform. It should be noted that the code running on CVA6 is actually running on a proxy kernel. In order to analyse the delays caused by this situation, performance data was generated by considering only the sections where the Ascon code was executed.

The test process of TTA processors was carried out with completely different tools to RISC-V processors. OpenASIP [9], an open source integrated design environment developed for the design, testing, and hardware implementation of TTA processors, was used. After the tool was installed, general purpose TTA processors with various configurations were designed. In order to make a meaningful comparison with RISC-V processors, custom operations were not used. Instead, only operations similar to RISC-V instructions were included in the FUs. Ascon testbench was compiled separately with the designed processors and then run on Proxim, OpenASIP's cycle-accurate simulation tool. Thus, performance data for all configurations were obtained in terms of total number of clock cycles (NoC).

First of all, we used a minimal 64-bit TTA core provided as a sample design in OpenASIP. The minimal 64-bit core has a single arithmetic-logic FU which contains general-purpose TTA operations such as ADD, AND, XOR, SHIFT, etc. It also has a distinct FU contains multiplication and multiply-and-add operations. In Figure 2, the structure of the core is represented. We designed separate configurations with fewer FUs than the minimal 64-bit processor and named them according to the number of transport buses. The configuration with a single FU

containing general-purpose operations and one transport bus was named GP-C1, while the configuration with two buses was similarly codenamed GP-C2. We also developed separate configurations with a second FU containing frequently repeated operations in the Ascon encryption algorithm, and similarly named them GP-C2-DA and GP-C4-DA according to the number of transport buses. The core GP-C2 is shown in Figure 3.
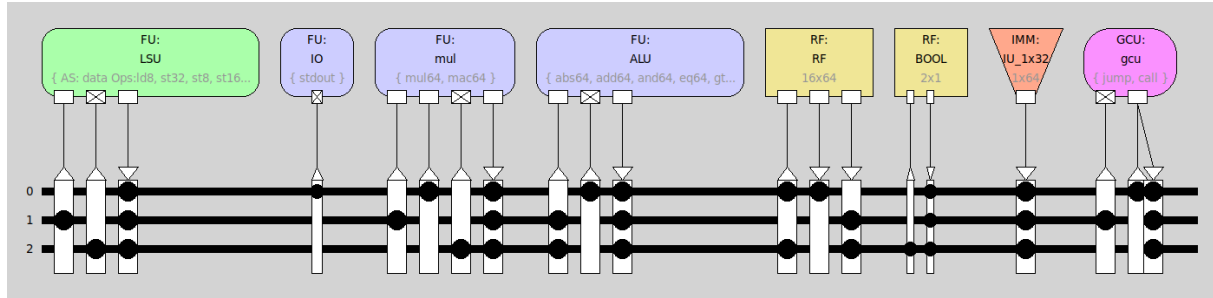
Figure 2. Minimal 64-bit TTA processor model provided by OpenASIP
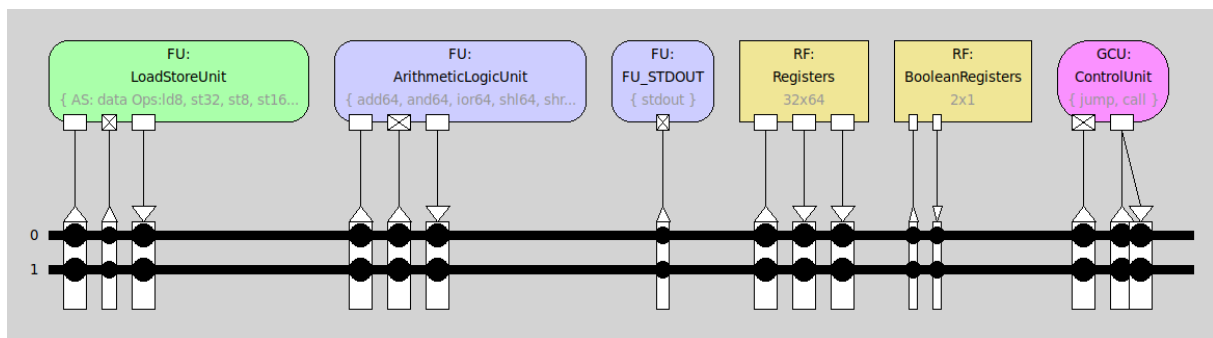
Figure 3. GP-C2 processor configuration

3. RESULTS

We give the performance comparison according to the core configurations in Table 1. The term IWL refers to the Instruction word length for each processor. As a natural consequence of the structure of the architecture, the IWL in TTA processors is generally considerably longer than in RISC processors. The performance results are quite remarkable. It is clearly seen that TTA processors offer a very high performance advantage over their RISC-V competitors for the Ascon encryption algorithm. When TTA processors are compared among themselves, it can be concluded that the increase in the number of transport buses contributes positively to performance up to a certain point. However, the performance contribution of more than three transport buses is very limited for this configuration. In the processors using dual ALUs, it was observed that the performance improved slightly. To create a hardware perspective, we synthesised some of the cores for FPGA and reported the results in Table 2. For a fair comparison, the synthesis was performed by removing the floating-point units of the RISC-V processors.

Table 1. Performance comparison of RISC-V and TTA processors for the Ascon-AEAD128

Processor	IWL	Bus Count	Core Configuration	NoC
CV32E40P	32	N/A	RV32IMC	103263
CV64A60	64	N/A	RV64GC	63855
Minimal-64	84	3	Single ALU + mul, mac	6788
GP-C1	75	1	Single ALU	17652
GP-C2	150	2	Single ALU	10947
GP-C3	225	3	Single ALU	6627
GP-C4	300	4	Single ALU	6597
GP-C2-DA	150	2	Dual ALU	9035
GP-C4-DA	300	4	Dual ALU	5243

Table 2. Comparison of FPGA resource utilizations

Processor	LUT	FF	DSP	f_{max} (MHz)
CV32E40P	7595	2970	7	20
CV64A60	9567	4729	16	40
GP-C2	3054	2627	0	108
GP-C4-DA	4348	3682	0	104

4. CONCLUSION

Lightweight cryptology is critical for today's rapidly evolving IoT systems. Ascon, with its security guarantees and hardware-friendly structure, is likely to be widely used as a standard in this area for many years to come. In this paper we compare two processor architectures for Ascon that are similar in their open source and free licences, but completely different in their computational approach. Although the RISC-V architecture has many advantages such as ubiquity, support, forward compatibility, etc., the TTA processors are found to be more prominent in terms of performance and efficiency due to their effective implementation of ILP and flexible structure.

References

[1] A. Hameed and A. Alomary, "Security issues in IoT: A survey," in *2019 International Conference on Innovation and Intelligence for Informatics, Computing, and Technologies (3ICT)*, Sakhier, Bahrain, 2019, pp. 1-5, doi: 10.1109/3ICT.2019.8910320.

[2] E. R. Naru, H. Saini, and M. Sharma, "A recent review on lightweight cryptography in IoT," in *2017 International Conference on I-SMAC (IoT in Social, Mobile, Analytics and Cloud) (I-SMAC)*, Palladam, India, 2017, pp. 887-890, doi: 10.1109/I-SMAC.2017.8058307.

[3] C. Dobraunig, M. Eichlseder, F. Mendel, and M. Schläffer, "Ascon v1.2: Lightweight authenticated encryption and hashing," *Journal of Cryptology*, vol. 34, no. 3, 2021, doi:10.1007/s00145-021-09398-9.

[4] K. Mohajerani, L. Beckwith, A. Abdulgadir, J.-P. Kaps, and K. Gaj, "Lightweight champions of the world: Side-channel resistant open hardware for finalists in the NIST lightweight cryptography standardization process," *ACM Trans. Embed. Comput. Syst.*, 2024, doi:10.1145/3677320.

[5] M. Sonmez Turan et al., Status Report on the Final Round of the NIST Lightweight Cryptography Standardization Process, (National Institute of Standards and Technology, Gaithersburg, MD), NIST Interagency or Internal Report (IR) NIST IR 8454., 2023, doi: 10.6028/NIST.IR.8454.

[6] R. Antoniou, J. Bonvoisin, P.-Y. Hsing, E. Dekoninck, and D. Defazio, "Defining success in open source hardware development projects: A survey of practitioners," *Des. Sci.*, vol. 8, no. e8, 2022, doi:10.1017/dsj.2021.30.

[7] K. Asanović and D. A. Patterson, "Instruction sets should be free: The case for risc-v," EECS Department, University of California, Berkeley, Tech. Rep. UCB/EECS-2014-146, 2014.

[8] L. Akcay and B. Ors, "Comparison of RISC-V and transport triggered architectures for a postquantum cryptography application," *Turk. J. Of Electr. Eng. Comput. Sci.*, vol. 29, no. 1, pp. 321–333, 202, doi: 10.3906/elk-2003-27.

[9] L. Akcay and B. O. Yalcin, "Lightweight ASIP design for lattice-based post-quantum cryptography algorithms," *Arab. J. Sci. Eng.*, 2024, doi: 10.1007/s13369-024-08976-w.

[10] L. Akcay and B. O. Yalcin, "Analysing the potential of transport triggered architecture for lattice-based cryptography algorithms," *Int. J. Embed. Syst.*, vol. 15, no. 5, art. no. 404, 2022, doi: 10.1504/IJES.2022.127164.

[11] L. Akcay and B. Ors, "Custom TTA operations for accelerating kyber algorithm," in *2021 13th International Conference on Electrical and Electronics Engineering (ELECO)*, 2021, doi: 10.23919/ELECO54474.2021.9677863.

[12] J. Wei, W. Guo, H. Liu, and Y. Tan, "A unified cryptographic processor for RSA and ECC in RNS," in *Communications in Computer and Information Science*, Berlin, Heidelberg: Springer Berlin Heidelberg, 2013, pp. 19–32, doi: 10.1007/978-3-642-41635-4_3.

[13] H. Cheng, J. Großschädl, B. Marshall, D. Page, and T. Pham, "RISC-V instruction set extensions for lightweight symmetric cryptography," *IACR Transactions on Cryptographic Hardware and Embedded Systems*, pp. 193–237, 2022.

[14] E. Tehrani, T. Graba, A. S. Merabet and J.-L. Danger, "RISC-V extension for lightweight cryptography," in *2020 23rd Euromicro Conference on Digital System Design (DSD)*, Kranj, Slovenia, 2020, pp. 222–228, doi: 10.1109/DSD51259.2020.00045.

[15] F. Abed, C. Forler, and S. Lucks, "General classification of the authenticated encryption schemes for the CAESAR competition," *Comput. Sci. Rev.*, vol. 22, pp. 13–26, 2016, doi: 10.1016/ j.cosrev.2016.07.002.

[16] P. D. Schiavone, D. Rossi, A. Pullini, A. Di Mauro, F. Conti, and L. Benini, "Quentin: An ultra-low-power PULPissimo SoC in 22nm FDX," in *2018 IEEE SOI-3D-Subthreshold Microelectronics Technology Unified Conference (S3S)*, Burlingame, CA, USA, 2018, pp. 1–3, doi: 10.1109/S3S.2018.8640145.

[17] F. Zaruba and L. Benini, "The cost of application-class processing: Energy and performance analysis of a Linux-ready 1.7-GHz 64-bit RISC-V core in 22-nm FDSOI technology," *IEEE Transactions on Very Large Scale Integration (VLSI) Systems*, vol. 27, no. 11, pp. 2629–2640, Nov. 2019, doi: 10.1109/TVLSI.2019.2926114.

[18] Ascon Team. (2023). *Reference, optimized, masked C and ASM implementations of Ascon* [Online]. *GitHub*. Available: https://github.com/ascon/ascon-c

Heat Transfer Analysis of Rotating Casson Blood-based Carbon Nanofluid in Channel

Wan Nura'in Nabilah Noranuar[1], Ahmad Qushairi Mohamad[1], Lim Yeou Jiann[1], Sharidan Shafie[1]

[1]Department of Mathematical Sciences, Faculty of Science, Universiti Teknologi Malaysia, 81310 Johor Bahru, Johor, Malaysia
Corresponding author: Ahmad Qushairi Mohamad (e-mail: ahmadqushairi@utm.my)

Abstract

This study aims to investigate the thermal characteristics of Casson nanofluid flow, incorporating carbon nanotubes (CNTs), under the influence of rotational effect over a vertically moving channel. The heat transfer behavior of the nanofluid is analyzed using the Tiwari and Das model, as well as Xue model. The base fluid is human blood, modelled as a Casson fluid, with single-wall carbon nanotubes (SWCNTs) serving as the nanoparticles. The problem is mathematically formulated using a set of governing equations in their dimensional form, along with the corresponding initial and moving boundary conditions. To simplify the governing equations, dimensionless variables are applied to convert the equations into a dimensionless form. Closed form solutions for the flow and energy transfer are derived using the Laplace transform method, and the results are presented in graphical and tabular formats. The study finds that the rotating effect induces primary and secondary velocity components, which are particularly significant in medical applications, such as the design of artificial circulatory devices. Furthermore, both the primary and secondary velocities, as well as temperature profile, increase with a higher SWCNTs volume fraction, thereby enhancing the performance of blood in oxygen transport and drug delivery.

Keywords: SWCNTs, Casson blood fluid, Rotating fluid, Moving Channel, Laplace transform method

Analysing Transmission Dynamics of Chagas Disease with Diapause and Developmental Delays

Manel Sbia[1], Tewfik Mahdjoub[1]

[1]Nonlinear Analysis and Applied Mathematics, Abou-Bekr Belkaid University, Tlemcen, Algeria
Corresponding author: Manel Sbia (e-mail: manel.sbia17@gmail.com)

Abstract

Chagas disease, a vector-borne illness caused by Trypanosoma cruzi, remains a significant public health challenge in many regions of the world. Recent studies have observed developmental delays in certain triatomine vectors. In this work, we introduce these delays into our mathematical model to better understand their impact on the spread of Chagas disease. This approach aims to shed light on how these biological mechanisms influence transmission dynamics, potentially guiding improved control strategies.

Keywords: Chagas disease, Diapause, Delay differential equation, Population dynamics, Triatomines

Superhydrophobic Coating Based on Nanostructured ZnO Thin Films

Zehira Belamri[1]

[1]Phase Transformations Laboratory, Department of Physics, University Freres Mentouri Constantine 1, 25000
Constantine, Algeria
Corresponding author: Zehira Belamri (e-mail: belamri.zehira@umc.edu.dz)

Abstract

In this work, ZnO thin film is prepared by spraying a solution of zinc acetate precursor prepared with distilled water at optimized conditions for aluminum substrate temperature and solution concentration in one step. The sample was characterized by scanning electron microscopy (FEG-SEM) equipped with energy dispersive X-ray analysis (EDX), X-ray diffraction (XRD), and Raman spectroscopy. The wettability property of the synthesized film was evaluated by measuring the contact angle between the surface of the film and a deposited water drop (WCA). Structural analysis confirms that hexagonal Wurtzite ZnO thin film is polycrystalline, and has (002) preferential orientation. FEG-SEM observation confirms the coexistence of ZnO micro-nanostructure. The wettability study reveals that the surface of ZnO thin film prepared with distilled water is superhydrophobic. The obtained results shows that the superhydrophobic ZnO thin film was successfully deposited on the aluminum substrate using a low-cost spray pyrolysis technique that requires no high temperature annealing. The studied thin films can be used to limit the presence of water and frost in the automotive and aeronautical fields.

Keywords: Superhydrophobic, Nanostructures, One step, Wettability, ZnO thin film

Multiscale Modeling of Structural Stability and Mechanical Properties of TeAuF$_4$ (Te = Na, K, Rb) Materials

Ishak Mebarkia[1]

[1]Quantum Electronics Laboratory, Department of Radiation Physics, Faculty of Physics, University of Science and Technology Houari Boumediene, El Alia, Bab Ezzouar, 16111 Algiers, Algeria
Corresponding author: Ishak Mebarkia (e-mail: ishak.mebarkia@usthb.edu.dz)

Abstract

This study provides an in-depth theoretical exploration of the structural and mechanical properties of alkali metal tetrafluoroaurate compounds NaAuF$_4$, KAuF$_4$, and RbAuF$_4$ using ab-initio calculations based on density functional theory (DFT) with the pseudopotential plane wave approach. The calculated structural parameters exhibit a strong consistency with previously reported experimental values, demonstrating the reliability of our computational methods. These compounds are identified as naturally ductile, as confirmed by the computed elastic constants, which highlight their mechanical robustness and potential suitability for various applications. To further investigate the elastic properties, we analyze multiple anisotropy indices, emphasizing the materials' significant elastic anisotropy. The analysis employs 3D visualizations, introducing new perspectives on the directional dependencies of these properties. This approach offers a comprehensive framework for understanding the complex elastic behavior of these compounds. In the absence of prior detailed studies on these materials, our findings serve as a benchmark for future experimental validation. Thus, this theoretical groundwork paves the way for upcoming experimental investigations that may build upon these results, potentially guiding future applications in fields that demand materials with high elastic stability and unique anisotropic characteristics.

Keywords: Ab-initio calculations, Elastic constants, Mechanical properties, TeAuF$_4$ ternary compounds

1. INTRODUCTION

Inorganic fluoride single crystals, known for their strong ionic bonds, are promising candidates for a range of advanced applications due to their stability, unique structural properties, and high resistance to chemical reactions. These properties make them particularly suitable for applications in optoelectronics, catalysis, and electrochemistry [1, 2]. Among inorganic fluorides, alkali metal complex fluorides, such as the alkali metal tetrafluoroaurates (TeAuF$_4$, where Te = Na, K, Rb), have garnered attention for their structural and mechanical versatility and wide applicability in catalytic and electronic devicesass of alkali metal complex fluorides includes compounds that are often used in high-performance technologies, as they possess interesting optical and magnetic characteristics, along with notable chemical stability [3].

In light of their importance, our research focuses on alkali metal tetrafluoroaurates (TeAuF$_4$) due to their potential in diverse applications, such as organic synthesis and industrial catalysis, where they are valued for their catalytic activity and structural resilience. Previous theoretical studies have explored the main physical properties of certain alkali metal tetrafluoridobromates (TeBrF$_4$) and alkali metal tetrafluoroaurates (TeAuF$_4$) with Te = Na, K, Rb, though comprehensive mechanical analysis has been lacking [4, 5].

Alkaltrafluoroaurates are typically formed by pairing an alkali metal cation (Te = Li, Na, K, Rb, or Cs) with the tetrafluoroaurate anion (AuF$_4$). They are often observed to have a yellow to golden-brown tint, attributed to the interaction between the gold and fluoride ions. Beyond aesthetics, their unique chemical composition opens doors to applications in fields like catalysis, electronics, magnetism, and photovoltaics. This compound class showcases versatility by forming advanced materials and functional alloys, with applications ranging from energy storage to electrochemical devices.

Structurally, alkali metal tetrafluoroaurates exhibit varying crystal structures: LiAuF$_4$ adopts a monoclinic crystal structure with the space group P2/c (No. 13) [6, 7], while NaAuF$_4$, KAuF$_4$, and RbAuF$_4$ crystallize in a tetragonal structure under the I4/mcm space group (No. 140) [6–9]. The CsAuF$_4$ compound shows orthorhombic symmetry with an Immm space group (No. 71) [10]. Despite substantial interest in the chemical synthesis and

characterization of these materials, no experimental work has been conducted on their mechanical properties [11–15].

To bridge this knowledge gap, we undertake a theoretical analysis of the structural and mechanical properties of tetragonal alkali metal tetrafluoroaurates TeAuF$_4$ (Te = Na, K, Rb) through first-principles calculations within the density functional theory (DFT) framework. This investigation aims to provide foundational insights that may support future experimental efforts and inspire further studies on these intriguing compounds.

2. MATERIAL AND METHOD

In this study, ab-initio calculations were carried out using the Cambridge Serial Total Energy Package (CASTEP) codeerates based on the pseudopotential plane wave (PP-PW) method within the framework of density functional theory (DFT) [16]. The Generalized Gradient Approximation (GGA) with the Perdew-Burke-Ernzerhof (PBE-sol) exchange-correlation functional is selectately describe the solid-state interactions within the materials studied [17]. Specific valence electron configurations were applied to each element to enhance the precision of pseudoatomic computations, including Rb ($5s^1$), K ($4s^1$), Na ($3s^1$), Au ($6s^1$), and F ($2s^2\ 2p^5$).

To ensure computational accuracy, a Monkhorst-Pack k-point grid with a 4x4x2 mesh was used for Brillompling [18]. A plane-wave basis set cut-off energy of 30 Ha (Hartree) was applied, balancing computational efficiency and precision. Structural parameter optimizations were achieved through the Broyden-Fletcher-Goldfarb-Shanno (BFGS) algorithm [19, 20], known for its robustness in convergence. Moreover, the Ultra-Soft Pseudopotential Generated on the Fly (OTFG-USPP) approximation was employed to improve calcuciency and minimize errors compared to fully converged all-electron DFT calculations [21].

For the calculation of elastic constants, the strain-stress method, as implemented within CASTEP, was used [16]. This method involves applyirains to the crystal lattice along specific crystallographic directions, causing deformation, and then calculating the resulting stress. The relationship between applied strain and resultant stress, based on Hooke's law, allows for the derivation of the elastic constants by fitting the stress-strain data to a linear model. Specifically, uniaxial strains were applied along the c-axis (out-of-plane), while shear strains were introduced in the basal plane (a-b plane) [22].

Hydrostatic pressure effects were simulated byally compressing and expanding the crystal lattice, with small variations in volume corresponding to ±1–5% changes in lattice constants. This approach allowed us to analyze structural responses under varied hydrostatic pressures, providing a detailed understanding of the material's resilience under different stress conditions.

3. RESULTS

3.1. Structural Properties

At room temperature, the TeAuF$_4$ (Te = Na, K, Rb) ternary compounds adopt a tetragonal crystal structure, classified under the space group I4/mcm (No. 140). Within this structural arrangement, the unit cell is composed of four formula units (Z = 4), where Na, K, and Rb atoms occupy the Wyckoff position 4a (0, 0, 1/4) while the Au atom is located at the Wyckoff position 4d (0, 1/2, 0), as depicted in Figure 1.
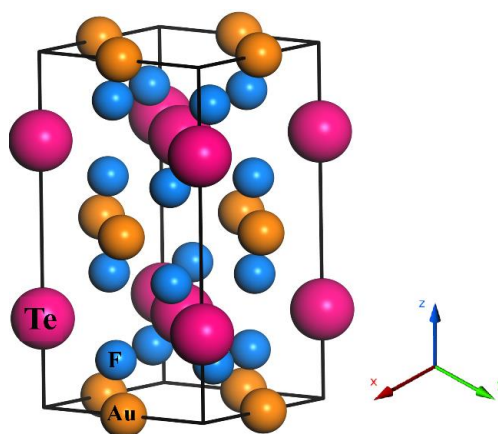

Figure 1. The unit cell of TeAuF$_4$ (Te = Na, K, and Rb) materials

To thoroughly examine the structural properties and gain insights into the lattice framework, we systematically relax the tetragonal ratio (c/a) and internal atomic coordinates (x_F, y_F, and z_F) across a range of volumes. This optimization allows for the precise determination of key structural parameters, including lattice constants (a and c) and the specific coordinates of the fluorine atom at the 16l Wyckoff site (x_F, y_F, and z_F). The final values obtained through this analysis are compiled in Table 1, facilitating a comprehensive comparison with available experimental data.

Table 1. The equilibrium lattice parameters (Å) for TeAuF$_4$ (Te = Na, K, and Rb) ternary compounds

Compounds	References	a (Å)	c (Å)	c/a	V_0 (Å^3)	x_F	y_F	z_F
NaAuF$_4$	This work	5.67	10.45	1.84	335.804	0.172	0.672	0.130
	Experiment [6]	5.64	10.49	1.86	333.683	0.177	0.677	0.135
KAuF$_4$	This work	6.05	1.88	1.87	414.752	0.161	0.661	0.120
	Experiment [6]	5.99	1.92	1.90	408.316	0.167	0.667	0.124
	Experiment [9]	5.99	1.93	1.90	408.316	0.167	0.667	0.118
RbAuF$_4$	This work	6.26	11.78	1.88	461.216	0.156	0.656	0.115
	Experiment [6]	6.18	11.85	1.92	452.580	0.162	0.662	0.119
	Experiment [7]	6.18	11.91	1.93	455.166	0.155	0.655	0.113

The results demonstrate an impressive consistency between our computed and experimentally reported structural parameters across all examined compounds, indicating the robustness and accuracy of our optimized configurations. This agreement highlights the reliability of the chosen computational approach in predicting structural details. Notably, this study represents, to the best of our knowledge, the first theoretical investigation of these TeAuF$_4$ (Te = Na, K, Rb) ternary compounds, with no prior theoretical work on their structural characteristics. This foundational exploration is expected to support and guide future experimental studies on these materials.

3.2. Mechanical Properties

The elastic constants and polycrystalline moduli of crystals provide key insights into their mechanical characteristics, such as stability, stiffness, strength, hardness, and brittleness or ductility, as well as certain physical properties including phonon spectra, Debye temperature, and sound velocities. For the compounds NaAuF$_4$, KAuF$_4$, and RbAuF$_4$, calculated elastic constants confirm elastic stability, meeting the criteria [23]: $C_{11} > |C_{12}|$; $(C_{11} + C_{12}) C_{33} > 2(C_{13})^2$; $C_{44} > 0$; and $C_{66} > 0$. Given the tetragonal structure of these compounds, six elastic stiffness constants C_{11}, C_{12}, C_{13}, C_{33}, C_{44}, and C_{66} were calculated, as detailed in Table 2. The values satisfy the aforementioned stability criteria, underscoring the robustness of the elastic properties and structural stability in the studied compounds.

Table 2. The elastic stiffness constants C_{ij} (GPa) for TeAuF$_4$ (Te = Na, K, and Rb) materials

Compounds	C_{11}	C_{12}	C_{13}	C_{33}	C_{44}	C_{66}
NaAuF$_4$	51.71580	28.85730	32.71620	60.29265	12.98810	18.39195
KAuF$_4$	27.73630	13.55175	16.74140	38.13905	12.14230	11.94490
RbAuF$_4$	23.02935	12.06035	16.99595	35.22720	15.77370	7.66030

The Voigt [24] and Reuss [25] approximations were utilized to compute the polycrystalline moduli, specifically the bulk modulus (B) and shear modulus (G), using these equations:

$$B_V = \frac{2(C_{11} + C_{12}) + C_{33} + 4C_{13}}{9} \tag{1}$$

$$B_R = \frac{(C_{11} + C_{12})C_{33} - 2C_{13}^2}{C_{11} + C_{12} + 2C_{33} + 4C_{13}} \tag{2}$$

$$G_V = \frac{2C_{11} - C_{12} - 2C_{13} + C_{33} + 6C_{44} + 3C_{66}}{15} \tag{3}$$

$$G_R = \frac{15}{\dfrac{18B_V}{(C_{11}+C_{12})C_{33}-2C_{13}^2} + \dfrac{6}{(C_{11}-C_{12})} + \dfrac{6}{C_{44}} + \dfrac{3}{C_{66}}} \tag{4}$$

Using Hill's approximation [26], the overall bulk modulus B, shear modulus G, Young's modulus E, and Poisson's ratio v were derived:

$$B = \frac{B_V + B_R}{2} \tag{5}$$

$$G = \frac{G_V + B_R}{2} \tag{6}$$

$$E = \frac{9BG}{3B+G} \tag{7}$$

$$v = \frac{3B-2G}{6B+2G} \tag{8}$$

The polycrystalline moduli for the ternary compounds TeAuF₄ (Te = Na, K, and Rb), as shown in Table 3, reveal a decreasing trend in the bulk modulus B from Na to Rb, correlating with an increase in volume V. This observation aligns with Cohen's approximation $B{\sim}V^{-1}$ [27], supporting the reliability of our results.

Table 3. The calculated values of polycrystalline moduli (in GPa) for TeAuF₄ (M = Na, K, and Rb) materials

Compounds	B_V	B_R	G_V	G_R	B	G	E	v
NaAuF₄	39.14485	38.65595	13.50260	13.07910	38.90040	13.29085	35.79584	0.34663
KAuF₄	20.85342	20.04204	10.35104	9.75028	20.44773	10.05066	25.90725	0.28883
RbAuF₄	19.26560	17.52881	10.19045	8.12692	18.39720	9.15868	23.56551	0.28651

To assess the ductility of these compounds, Pugh's criterion [28], which indicates ductility when the B/G ratio is above 1.75 was applied. The calculated B/G ratios (2.93 for NaAuF₄, 2.03 for KAuF₄, and 2.01 for RbAuF₄) confirm their ductile nature. Frantsevich's criterion [29], which associates ductility with a Poisson's ratio v greater than 0.26, further substantiates this conclusion, as each compound's v exceeds this threshold. The elastic anisotropy was evaluated using the universal anisotropic index A^U [30]:

$$A^U = 5\frac{G_V}{G_R} + \frac{B_V}{B_R} - 6 \geq 0 \tag{9}$$

Additionally, the bulk anisotropy A_B and shear anisotropy A_G are given by [31]:

$$A_B = \frac{B_V - B_R}{B_V + B_R} \tag{10}$$

$$A_G = \frac{G_V - G_R}{G_V + G_R} \tag{11}$$

Table 4 summarizes these indices, highlighting the significant anisotropic nature of MAuF₄ (M = Na, K, and Rb) compounds. The increasing trend in anisotropy from NaAuF₄ to RbAuF₄ implies heightened directional dependence in elastic properties across this series. Notably, the bulk modulus demonstrates a lesser directional reliance compared to the shear modulus, as indicated by the lower compression anisotropy A_B values, which adds further depth to our understanding of directional variations in the elastic properties of these compounds.

Table 4. The anisotropic indices the ternary compounds TeAuF$_4$ (M = Na, K, and Rb)

Compounds	A^U	A_B	A_G
NaAuF$_4$	0.17455	0.00628	0.01593
KAuF$_4$	0.34856	0.01984	0.02989
RbAuF$_4$	1.36865	0.04720	0.11265

To visualize this anisotropy, the polycrystalline moduli were plotted in three-dimensional space (Figure 2) using the following relations [4]:

$$B = \frac{1}{S} \tag{12}$$

$$E = \frac{1}{S'} \tag{13}$$

$$G = \frac{3}{9S' - S} \tag{14}$$

$$v = \frac{1}{2}(1 - \frac{S}{3S'}) \tag{15}$$

where S and S' represent the elastic compliance constants depend of the directional cosines in the x, y, and z axes.
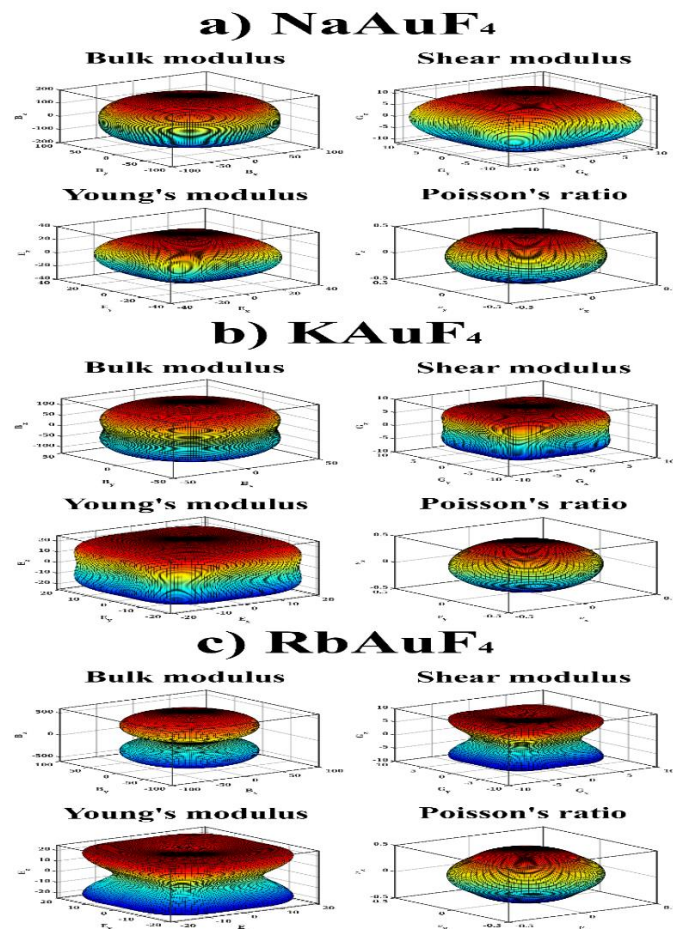

Figure 2. 3D plot of the different polycrystalline moduli anisotropy for TeAuF$_4$ (M = Na, K, and Rb) materials

In summary, NaAuF$_4$ exhibits the lowest elastic anisotropy, while RbAuF$_4$ shows the highest. Bulk modulus and Poisson's ratio exhibit weaker anisotropy than Young's and shear moduli across all compounds, corroborating the trends in Table 4.

4. CONCLUSION

The pseudopotential plane-wave approach and the generalized gradient approximation were utilized in this study within the framework of density functional theory to examine the structural and mechanical properties of the alkali metal tetrafluoroaurates NaAuF$_4$, KAuF$_4$, and RbAuF$_4$ ternary compounds. The following summarizes the outcomes achieved:

- The findings on structural properties align well with experimental data, confirming the reliability of the theoretical approach used.
- The results of elastic constants and polycrystalline moduli indicate that these materials exhibit ductile behavior with clear elastic anisotropy.
- A systematic trend was observed in the bulk modulus and volume, with a decreasing bulk modulus correlating to an increasing atomic radius from Na to Rb, consistent with Cohen's approximation.
- The ductility of the compounds was supported by Pugh's criterion and Frantsevich's criterion, with all compounds demonstrating a favorable Poisson's ratio, further confirming their ductile nature.
- Elastic anisotropy was evaluated, with RbAuF$_4$ displaying the highest degree of anisotropy across the compounds. The bulk modulus exhibited weaker directional dependence compared to the shear and Young's moduli, revealing nuanced insights into the mechanical characteristics of these compounds.

This comprehensive study highlights the structural stability, ductility, and elastic anisotropy of the NaAuF$_4$, KAuF$_4$, and RbAuF$_4$ compounds, providing valuable insights for their potential applications in fields that require materials with specific mechanical properties. Future studies could explore their thermal properties and electronic behaviors to broaden the scope of their practical applications.

References

[1] P. Capper. (2022, Apr. 26). *Bulk crystal growth of electronic, optical and optoelectronic materials* [Online]. Available: https://books.google.com/books?hl=en&lr=&id=ZqTkCF6Ra9kC&oi=fnd&pg=PR7&ots=CZwOWJnDM5&sig=hT0FCNm2AIbW86xXSONZ4zzYMjg

[2] A. J. Stevenson, H. Serier-Brault, P. Gredin, and M. Mortier, "Fluoride materials for optical applications: Single crystals, ceramics, glasses, and glass–ceramics," *J. Fluor. Chem.*, vol. 132, no. 12, pp. 1165–1173, Dec. 2011, doi: 10.1016/J.JFLUCHEM.2011.07.017.

[3] S. Stepleton. (2021, Jul. 07). *Synthesis of complex fluorides for optical applications* [Online]. Available: https://tigerprints.clemson.edu/all_dissertations/418

[4] I. Mebarkia, A. Manallah, and R. Belghit, "The first foreseen of structural, mechanical, electronic and optical properties of novel alkali metal tetrafluoridobromate ABrF4 (A=Na, K and Rb)," *Phys. B Condens. Matter*, vol. 624, art. no. 413450, 2022, doi: 10.1016/j.physb.2021.413450.

[5] I. Mebarkia, "First-principles study of structural , elastic , and optoelectronic properties of alkali metal tetrafluoroaurate materials MAuF 4 (M = Na , K , and Rb)," *Indian J. Phys.*, vol. 4, 2024, doi: 10.1007/s12648-024-03188-2.

[6] R. Hoppe and R. Homann, "Neue untersuchungen an fluorkomplexen mit dreiwertigem silber und gold," *Zeitschrift fur Anorg. und Allg. Chemie*, vol. 379, no. 2, pp. 193–198, Dec. 1970, doi: 10.1002/ZAAC.19703790210.

[7] U. Engelmann and B. G. Muller, "Darstellung und struktur der tetrafluoroaurate(III) MI[AuF4] mit MI = Li, Rb," *Zeitschrift fur Anorg. und Allg. Chemie*, vol. 598, no. 1, pp. 103–110, Jun. 1991, doi: 10.1002/ZAAC.19915980110.

[8] R. Hoppe and W. Klemm, "Uber fluorokomplexe des palladiums und des goldes," *ZAAC - J. Inorg. Gen. Chem.*, vol. 268, no. 4–6, pp. 364–371, 1952, doi: 10.1002/zaac.19522680415.

[9] A. J. Edwards and G. R. Jones, "Fluoride crystal structures. Part VIII. Neutron diffraction studies of potassium tetrafluorobromate(III) and potassium tetrafluoroaurate(III)," *J. Chem. Soc. A Inorganic, Phys. Theor. Chem.*, pp. 1936–1938, Jan. 1969, doi: 10.1039/J19690001936.

[10] R. Schmidt and B. G. Muller, "Einkristalluntersuchungen an Cs[AuF4], Cs[Au2F 7] und U2F7[AuF4]," *Zeitschrift fur Anorg. und Allg. Chemie*, vol. 630, no. 13–14, pp. 2393–2397, 2004, doi: 10.1002/zaac.200400123.

[11] H. D. Bartunik, W. Potzel, R. L. Mossbauer, and G. Kaindl, "Resonance spectroscopy of γ-radiation on Au (I) and Au (III) compounds," *Zeitschrift fur Physik*, vol. 240, no. 1. pp. 1–16, 1970, doi:

10.1007/BF01400165.

[12] G. K. Shenoy, "Mossbauer-effect isomer shifts," *Mossbauer Spectrosc. Appl. to Inorg. Chem.*, pp. 57–76, 1984, doi: 10.1007/978-1-4899-0462-1_5.

[13] F. Mohr, "The chemistry of gold-fluoro compounds: A continuing challenge for gold chemists," *Gold Bull.*, vol. 37, no. 3–4, pp. 164–169, 2004, doi: 10.1007/BF03215208.

[14] M. A. Ellwanger et al., "Taming the high reactivity of gold(III) fluoride: Fluorido gold(III) complexes with N-based ligands," *Chem. - A Eur. J.*, vol. 23, no. 54, pp. 13501–13509, 2017, doi: 10.1002/chem.201702663.

[15] F. A. Redeker, M. A. Ellwanger, H. Beckers, and S. Riedel, "Investigation of molecular alkali tetrafluorido aurates by matrix-isolation spectroscopy," *Chem. - A Eur. J.*, vol. 25, no. 66, pp. 15059–15061, 2019, doi: 10.1002/chem.201904335.

[16] S. J. Clark et al., "First principles methods using CASTEP," *Zeitschrift fur Krist.*, vol. 220, no. 5–6, pp. 567–570, 2005, doi: 10.1524/zkri.220.5.567.65075.

[17] J. P. Perdew et al., "Restoring the density-gradient expansion for exchange in solids and surfaces," *Phys. Rev. Lett.*, vol. 100, no. 13, pp. 1–4, 2008, doi: 10.1103/PhysRevLett.100.136406.

[18] H. J. Monkhorst and J. D. Pack, "Special points for Brillouin-zone integration Monkhorst and Pack," *Physical Review B*, vol. 13, no. 12. pp. 5188–5192, 1976.

[19] T. H. Fischer and J. Almlof, "General methods for geometry and wave function optimization," *J. Phys. Chem.*, vol. 96, no. 24, pp. 9768–9774, 1992, doi: 10.1021/j100203a036.

[20] B. G. Pfrommer, M. Côté, S. G. Louie, and M. L. Cohen, "Relaxation of crystals with the quasi-Newton method," *J. Comput. Phys.*, vol. 131, no. 1, pp. 233–240, 1997, doi: 10.1006/jcph.1996.5612.

[21] K. Lejaeghere, V. Van Speybroeck, G. Van Oost, and S. Cottenier, "Error estimates for solid-state density-functional theory predictions: An overview by means of the ground-state elemental crystals," *Crit. Rev. Solid State Mater. Sci.*, vol. 39, no. 1, pp. 1–24, 2014, doi: 10.1080/10408436.2013.772503.

[22] T. C. Chibueze, C. E. Ekuma, A. T. Raji, F. I. Ezema, and C. M. I. Okoye, "Tetragonal and uniaxial strains in pristine and doped half-Heusler AuMnSn alloy," *J. Alloys Compd.*, vol. 848, p. 156186, 2020, doi: 10.1016/j.jallcom.2020.156186.

[23] F. Mouhat and F. X. Coudert, "Necessary and sufficient elastic stability conditions in various crystal systems," *Phys. Rev. B - Condens. Matter Mater. Phys.*, vol. 90, no. 22, pp. 1–3, 2014, doi: 10.1103/PhysRevB.90.224104.

[24] W. Voigt, *Lehrbuch der Kristallphysik*. 1966, doi: 10.1007/978-3-663-15884-4.

[25] A. Reuss, "Berechnung der fließgrenze von mischkristallen auf grund der plastizitätsbedingung fur einkristalle," *ZAMM - J. Appl. Math. Mech. / Zeitschrift fur Angew. Math. und Mech.*, vol. 9, no. 1, pp. 49–58, Jan. 1929, doi: 10.1002/zamm.19290090104.

[26] R. Hill, "The elastic behaviour of a crystalline aggregate," *Proc. Phys. Soc. Sect. A*, vol. 65, no. 5, pp. 349–354, May 1952, doi: 10.1088/0370-1298/65/5/307.

[27] M. L. Cohen, "Calculation of bulk moduli of diamond and zinc-blende solids," *Phys. Rev. B*, vol. 32, no. 12, pp. 7988–7991, 1985, doi: 10.1103/PhysRevB.32.7988.

[28] S. F. Pugh, "XCII. Relations between the elastic moduli and the plastic properties of polycrystalline pure metals," *London, Edinburgh, Dublin Philos. Mag. J. Sci.*, vol. 45, no. 367, pp. 823–843, 1954, doi: 10.1080/14786440808520496.

[29] I. N. Frantsevich. (1982, Dec.). "Elastic constants and elastic moduli of metals and insulators," *Ref. B.* [Online]. Available: https://ci.nii.ac.jp/naid/10004038718

[30] S. I. Ranganathan and M. Ostoja-Starzewski, "Universal elastic anisotropy index," *Phys. Rev. Lett.*, vol. 101, no. 5, pp. 3–6, 2008, doi: 10.1103/PhysRevLett.101.055504.

[31] H. Zhai, X. Li, and J. Du, "First-principles calculations on elasticity and anisotropy of tetragonal tungsten dinitride under pressure," *Mater. Trans.*, vol. 53, no. 7, pp. 1247–1251, 2012, doi: 10.2320/matertrans.M2011373.

Nanoemulsions: Formulation Strategies and Characterization Techniques

Yousra Mdarhri[1], Ikram Bouziane[1], Mohamed Chabbi[1]

[1]Department of Chemistry, Abdelmalek Essaâdi University, Tangier, Morocco
Corresponding author: Yousra Mdarhri (e-mail: yousra.mdarhri@gmail.com)

Abstract

Nanoemulsions are nanoscale colloidal dispersions with droplet sizes typically ranging from 20 to 200 nm. They offer advantages such as enhanced stability, solubility, and bioavailability of active compounds, making them valuable in pharmaceuticals, cosmetics, and food industries. These systems are kinetically stable and capable of encapsulating both hydrophilic and lipophilic compounds. Nanoemulsion formulation involves selecting oils, surfactants, co-surfactants, and water based on their compatibility and application. Preparation methods include high-energy techniques like high-pressure homogenization and ultrasonication, as well as low-energy approaches like phase inversion temperature and spontaneous emulsification. Characterization techniques, such as dynamic light scattering, electron microscopy, zeta potential analysis, and rheological studies, ensure the quality and stability of nanoemulsions. Challenges like scalability, surfactant toxicity, and stability persist, but advancements in biodegradable surfactants and application-specific designs continue to drive innovation. This review discusses formulation strategies, characterization methods, and future trends shaping the field.

Keywords: Nanoemulsions, Formulation, Stability

Thermal Analysis of Low-Density Polyethylene Composites Reinforced with Copper and Zinc

Mohamed Belhamiani[1], Jihad Guendouz[1], Wahid Oudad[1]

[1]Mechanical Engineering Department, University of Ain Temouchent, Algeria
Corresponding author: Mohamed Belhamiani (e-mail: mohammed.belhamiani@univ-temouchent.edu.dz)

Abstract

This study examines the thermal properties of low-density polyethylene (LDPE) composites reinforced with copper (Cu) and zinc (Zn) nanoparticles, using differential scanning calorimetry (DSC). The findings indicate that adding Cu reduces the melting and crystallization temperatures of LDPE, likely due to interactions between the Cu nanoparticles and the polymer matrix. In contrast, introducing Zn into composites with 20% Cu increases these temperatures, possibly due to the interaction of Zn^{2+} ions with the polymer. The crystallinity curves show a decrease in the crystallinity percentage (C%) with Cu addition, but an increase when Zn is present. Further research is needed to fully understand the underlying mechanisms.

Keywords: LDPE, copper, Zinc, DSC

Thermal Stress Effects on Structures Repaired with Composite Patches: A Numerical Analysis

Laid Aminallah[1], Ali Merdji[1], El Bahri Ould Chikh[1], Ismail Drai[1]

[1]Department of Mechanical Engineering, University of Mustapha Stambouli Mascara, Mascara, Algeria
Corresponding author: Laid Aminallah (e-mail: laid.aminallah@univ-mascara.dz)

Abstract

In this study, the finite element method is used to analyze the effect of thermal residual stresses resulting from adhesive curing on the performance of bonded composite repairs in aircraft structures. The stress intensity factor at the crack tip is chosen as the fracture criterion to estimate the performance of the repairs. The results obtained show that the presence of thermal residual stresses significantly reduces repair performance and consequently decreases the fatigue life of cracked structures. This study not only highlights the detrimental impact of thermal residual stresses on repair integrity but also emphasizes the necessity for advanced modeling techniques in predicting the long-term behavior of repaired aircraft structures under operational conditions.

Keywords: Bonded composite repair, Stress intensity factor, Thermal stresses, Adhesive, Finite element method

Advancing Clinical Diagnosis Through High-Resolution Ophthalmic Imaging with Deep Learning Innovations

Rania Saoudi[1]

[1]ETA Laboratory, Department of Electronics, University of Mohamed El Bachir El Ibrahimi, Bordj Bou Arreridj, Algeria
Corresponding author: Name Surname (e-mail: rania.saoudi@univ-bba.dz)

Abstract

Acquiring high-resolution (HR) medical imaging in clinical fields such as X-ray, CT, MRI, and retinal imaging presents significant challenges. These challenges often result in low-resolution (LR) images, which can lead to misinterpretations and hinder accurate diagnoses due to hardware limitations, long scanning times, and high costs. To address these issues, the field of medical imaging has increasingly explored the use of super-resolution (SR) methods, particularly those based on deep learning techniques. This paper introduces a novel deep learning approach that incorporates an Advanced Hybrid Feature Extraction Module. This module employs a dual feature extraction domain with attention mechanisms, operating in both spatial and transform domains. The innovative model is designed to capture local features from the spatial domain while simultaneously extracting global features from the frequency domain within a hierarchical multi-scale framework, allowing the model to capture features across various scales. We incorporate attention mechanisms to enhance the model's ability to select and prioritize the most important features, ensuring that critical information is emphasized during the feature extraction process. Our methodology was specifically applied to retinal fundus imaging (RFI), demonstrating substantial improvements over existing SR baseline techniques. Experimental results indicate superior performance in terms of image quality metrics and visual quality, making our model a suitable tool for retinal fundus image super-resolution (RFI SR) in clinical evaluations.

Keywords: Medical imaging, Super-resolution, Deep learning, Spatial and transform domains, Retinal fundus imaging

Combustion Efficiency and Environmental Characteristics of Olive Pomace Fuel Systems

Zaina Izghri[1], Imad Rabichi[1], Jalila Hanyny[1], Abdelaziz Ounas[1], Fatima Ezzahra Yaacoubi[1], Chaima Sekkouri[1], Karima Ennaciri[1], Abdelaziz Bacaoui[1], Abdelrani Yaacoubi[1]

[1]Laboratory of Applied Chemistry and Biomass, Unity of Methodology and Environment, Faculty of Sciences Semlalia, Cadi Ayyad University, 40000 Marrakech, Morocco
Corresponding author: Zaina Izghri (e-mail: zaina.izghri.cmm@gmail.com)

Abstract

This study investigates the combustion performance and gas emission characteristics of two-phase olive pomace, an agricultural residue with significant potential as a renewable biomass fuel. The research comprehensively analyzes the thermal degradation processes, combustion efficiency, and environmental implications of this biomass feedstock. Through systematic experimental procedures, we evaluated combustion parameters including temperature profiles, burning rates, and emission concentrations of key pollutants such as carbon monoxide (CO), carbon dioxide (CO_2), NOx and SO_2. Experimental results demonstrated that two-phase olive pomace exhibits complex combustion dynamics, with combustion efficiency varying between 78–85% depending on moisture content and particle size. Notably, the biomass showed lower sulfur emissions compared to traditional fossil fuels, presenting a potentially more environmentally sustainable alternative. Gas emission analysis revealed moderate levels of nitrogen oxides (NOx) and relatively consistent carbon compound release patterns. The findings contribute critical insights into the thermochemical conversion potential of olive pomace, highlighting its prospects as an alternative biomass fuel source. These results have significant implications for agricultural waste management, renewable energy strategies, and mitigating greenhouse gas emissions in the agro-industrial sector.

Keywords: Ccombustion efficiency, Two-phase olive pomace, Gas emissions, Thermochemical conversion

Preliminary Observations on the Habitat of Two Mediterranean Endemic Birds in Algeria

Amira Bouderbala[1], Mohcen Menaa[2], Salah Telailia[1], Lamia Boutabia[1]

[1]Laboratory Agriculture and Ecosystem Functioning, Department of Agronomy, Faculty of Nature and Life Sciences, Chadli Bendjedid University, 36000 El Tarf, Algeria
[2]Department of Biology, Faculty of Nature and Life Sciences, Mohammed Cherif Messaadia University, 41000 Souk-Ahras, Algeria
Corresponding author: Amira Bouderbala (amiraboude24@gmail.com)

Abstract

The Mediterranean Basin, celebrated as one of the world's most significant biodiversity hotspots, is home to a remarkable array of endemic species across various taxonomic groups. Among its avian diversity, *Curruca sarda* (Marmora's Warbler) and *Curruca deserticola* (Tristram's Warbler) stand out as emblematic species of the region. This study aims to characterize the habitats of these two species in Algeria, focusing on *C. sarda* during its migration in November 2023 in the arid Metlili region (Batna) and *C. deserticola* during its breeding season in spring 2024 in the semi-arid Merahna region (Souk Ahras). Results indicate that Metlili is dominated by xerophytic vegetation such as *Juniperus phoenicea*, *Artemisia herba-alba*, and *Macrochloa tenacissima*, critical for *C. sarda* during its migratory stopover. In Merahna, *C. deserticola* is associated with Aleppo pine (*Pinus halepensis*) forests interspersed with Holm oak (*Quercus ilex*), mastic tree (*Pistacia lentiscus*), and rosemary (*Rosmarinus officinalis*). Statistical analysis identified the density of small trees as a significant factor influencing the presence of *C. deserticola* ($p < 0.05$). These findings highlight distinct ecological preferences: *C. sarda* relies on arid habitats during migration, while *C. deserticola* depends on semi-arid forests for breeding. The study underscores the need to conserve arid and semi-arid ecosystems to ensure the survival of these species and provides a foundation for further research into bird-environment interactions.

Keywords: Mediterranean biodiversity, Habitat, Curruca sarda, Curruca deserticola

Insecticidal Potential of Basil Essential Oil (*Ocimum Basilicum* L.)

Nacira Amara[1], Sabrina Amara[2], Souad Touati[3], Hadjer Guettaf[1], Ichrak Rahali[1]

[1]Biology Department, Saad Dahleb Blida 1 University, Blida, Algeria
[2]Institute of Architecture and Urban Planning, Saad Dahleb Blida 1 University, Blida, Algeria
[3]Technical and Scientific Research Centre for Physical and Chemical Analysis (CRAPC), Tipaza, Algeria
Corresponding author: Nacira Amara (e-mail: naciraamara973@gmail.com)

Abstract

This study aims to explore the use and valorization of essential oil (EO) extracted from the aerial part of basil (*Ocimum basilicum*) from the Oued Alleug (Blida, Algeria). The objectives of this work are to characterize the chemical composition of *Ocimum basilicum* EO and to evaluate its bio-insecticide activity against the green aphid (*Aphis spiraecola*), a pest for crops. The EO of the aerial part of *Ocimum basilicum*, extracted by the hydro-distillation technique, was analyzed using a gas chromatograph coupled with a mass spectrometer (GC-MS). The activity of this EO was evaluated by the *in vitro* contact toxicity method. Four doses of the formulated EO: D1 (50 µl/ml), D2 (100 µl/ml), D3 (150 µl/ml), and D4 (200 µl/ml), were applied to the infested orange leaves. The EO provided an extraction yield of 0.75%. The chemical analysis of the EO revealed the presence of two major compounds which are: Linalool (25.42%) followed by (+)–Carvotanacetone (8.43%). The evaluation of the insecticidal effect of *Ocimum basilicum* EO against green aphids shows remarkable efficacy. After 48 hours of exposure, the mean mortality rate corrected for Aphis spiraecola populations for the four doses varied between $43.9 \pm 0.85\%$ and $100 \pm 0.15\%$. The LD50 and LD90 values recorded are 67µl/ml and 144µl/ml respectively. According to the results obtained, the EO formulated from *Ocimum basilicum* represents a promising alternative to synthetic products and without risk for the environment.

Keywords: *Ocimum basilicum* (L), Essential oil, *Aphis spiraecola*, Insecticidal, GC-MS

Exploring the Relationship Between Polyphenol Content and Antioxidant Activity in Mustard Seed and Its By-Products: An in Vitro Study

Siham Beddar[1], Hafid Boudries[1], Meriem Amrane-Abider[2], Yasmine Achat[1], Fatima Djenad[1], Sabrina Idir[1]

[1]Laboratory of Biomathematics, Biochemistry, Biophysics and Scientometrics, Faculty of
Nature and Life Sciences, University of Bejaia, Bejaia 06000, Algeria
[2]Agri-Food Technologies Research Center, Targa Ouzemour, University Campus, Bejaia, 06000, Algeria
Corresponding author: Siham Beddar (e-mail: siham.beddar@univ-bejaia.dz)

Abstract

Agricultural production, agro-industrial food processing, considered as one of the largest sectors around the world, is of primary importance to all national economies. The increase in the world population is leading to a sharp increase in the food production demand in the upcoming years. Under these circumstances, high volumes of food industry wastes attract increasing socioeconomic, political, and scientific attention. Hence, focusing on the use of different consolidated biotechnological processes and methodologies as suitable strategies for food by-products management and valorization, highlighting them as potential bioresources because they still gather high compositional and nutritional value, owing to their richness in functional and bioactive molecules with human health benefits. In this regard, the present study focuses on the recovery of polyphenols from white mustard seeds and its byproduct using ultrasound extraction, followed by the measurements of their content of total polyphenols and flavonoids with spectrophotometric methods, also the Antioxidant activity was measured by Applying the 2,2-diphenyl-1-picrylhydrazyl (DPPH) and 2,2'-azinobis-(3-ethylbenzothiazoline-6-sulfonic acid) (ABTS) radical decolorization, followed by studying the correlation among them, results showed that white mustard seed and its byproduct have a significant content in phenolic compounds, besides the two tested samples exhibit a considerable antioxidants activity. Generally, these results highlight the value of natural antioxidants driven from agro-industrial food processing, which seems to be a good alternative to synthetic antioxidants also reducing economic expenses and waste disposal.

Keywords: Mustard, Byproduct, Bioactives compounds, Antioxidant activity, Correlation

Curcumin-Based Nanocomposite for the Bioactive Coloration of Cotton

Hassam Mehmood[1], Arruje Hameed[2], Tahir Farooq[1]

[1]Department of Biochemistry, Government College University Faisalabad, Pakistan
[2]Department of Applied Chemistry, Government College University Faisalabad, Pakistan
Corresponding author: Tahir Farooq (e-mail: tahirfarooqfsd@gmail.com)

Abstract

The textile industry's extensive use of synthetic dyes and compounds has significantly contributed to environmental pollution. To address this issue, it is necessary to develop eco-friendly and sustainable methods and materials for the dyeing and coloration of textiles. Utilizing bioactive natural compounds to create nanotech materials for the functional coloration of cotton/textiles is a promising approach. Accordingly, in our recent study, we have developed a nanocomposite (NC) based on nano-curcumin, ZnO NPs and chitosan NPs for the bioactive coloration of cotton. The prepared CS-ZnO-Cur NC was characterized using SEM, XRD, and FT-IR and subsequently used as bioactive coloring and finishing agents. The prepared NC was evaluated for antioxidant, antibacterial, and antifungal properties validating its bioactive potential. Further, the non-toxic and eco-friendly nature of the prepared NC was validated by evaluating its potential for growth regulation in wheat seeds.

Keywords: Sustainable agriculture, Eco-friendly nanocomposite, Eco-textiles, Bioactive coloration, Nanopriming

Urban Sustainability Through Vertical Farming: A Review of Techniques and Benefits

Zeenat Khan[1], Daud Khan[2]

[1]Department of Biotechnology, Capital University of Science and Technology, Islamabad, Pakistan
[2]Department Civil Engineering, Capital University of Science and Technology, Islamabad, Pakistan
Corresponding author: Zeenat Khan (e-mail: zeenatkhan2613@gmail.com)

Abstract

In today's rapidly urbanizing world, food insecurity has become an increasingly pressing issue, significantly exacerbated by the challenges of traditional agricultural practices. Urbanization has resulted in a substantial decline in agricultural production, with estimates suggesting an annual reduction of 7.24%, thereby threatening food availability for millions, particularly in resource-constrained regions like Sub-Saharan Africa. Vertical farming emerges as a viable solution to this crisis, leveraging innovative agricultural techniques to boost productivity and align with the goal of eradicating hunger by 2030. This literature review aims to explore the potential of vertical farming in enhancing food security, utilizing insights from articles published in esteemed journals over the past two decades. Initially, the review examines the correlation between urbanization and food insecurity, followed by a detailed discussion on the various vertical farming techniques, such as hydroponics, aeroponics, and aquaponics, which can reduce water consumption by up to 90% and increase crop yields by 20-30%. The analysis highlights the multifaceted benefits of urban farming, including a potential reduction of transportation-related carbon emissions by 70% and improved access to fresh produce by 25%. Ultimately, the review underscores the urgent need for further exploration of vertical farming practices on a larger scale to address food insecurity effectively and promote sustainable urban ecosystems.

Keywords: Urbanization, Food insecurity, Vertical farming, Sustainable development, Innovative techniques

1. INTRODUCTION

Urbanization poses a serious threat to food security by degrading agricultural land, with projections indicating a potential loss of 3.7% of global cultivated land by 2030 [1]. This trend leads to two viewpoints among scholars: one asserts that urban growth diminishes agricultural space and weakens food supply, while the other suggests it could enhance food production [2]. However, evidence overwhelmingly indicates that urbanization results in a 7.24% annual decline in agricultural output, exacerbating food insecurity, particularly in resource-limited regions like Sub-Saharan Africa [3]. Increasing populations further heighten food demand, leading to malnutrition. Vertical farming emerges as a viable solution, utilizing urban spaces for crop cultivation in controlled environments, thereby improving productivity and reducing reliance on traditional land [4]. Integrating vertical farming with supportive policies can effectively address the challenges of urbanization and population growth, advancing food security and the Sustainable Development Goals [5], especially the goal of eradicating hunger by 2030.

Vertical farming (VF) offers a ground breaking solution to the challenges faced by urban agriculture in light of increasing urban populations and rising food demands [6]. This approach involves building multi-story structures filled with stacked layers of growing beds, utilizing advanced greenhouse technologies to manage environmental conditions like light and humidity, which allows for high-density food production while requiring significantly less land than traditional farming methods [7]. VF can transform underused urban areas, such as rooftops and warehouses, into productive agricultural spaces, effectively addressing food security challenges, especially in "food deserts" where fresh produce is limited [8]. By utilizing techniques such as hydroponics, aeroponics, and aquaponics, VF enhances resource efficiency and boosts crop yields while decreasing water usage by up to 90% and eliminating the need for harmful pesticides [9]. Locating these farms within cities not only reduces transportation costs and lowers carbon emissions but also creates local job opportunities and encourages healthier eating habits [10]. With global population projections suggesting that around 9 billion people will live in urban areas by 2050 [11], vertical farming stands out as a crucial strategy for ensuring a consistent, nutritious food supply and fostering sustainable urban ecosystems.

Urban vertical farming has become an essential solution to the challenges posed by traditional urbanization, particularly regarding rising resource consumption and environmental deterioration [12]. As cities grow, the transition from compact designs to sprawling developments has resulted in significant ecological issues, such as water scarcity and diminished biodiversity [13]. Urban farming effectively addresses these challenges by supporting local food production, improving food security, and encouraging community involvement while decreasing transportation emissions and restoring ecological balance [14]. Government initiatives focused on developing interconnected green spaces further enhance this approach, promoting urban agriculture as a means to increase sustainability [15]. During the COVID-19 pandemic, the resilience of localized food systems highlighted the importance of shorter supply chains and self-sufficiency [16]. The diverse benefits of urban farming, including reduced carbon emissions and better access to fresh produce, emphasize its potential to foster healthier and more sustainable urban environments.

Given the significant rise in urbanization, the risk of food insecurity is increasingly unavoidable [17]. To address this challenge, it is essential to explore potential solutions, with vertical farming emerging as the most promising option [18]. Urban vertical farming has become a vital response to the issues posed by traditional urbanization, such as resource depletion and environmental degradation [19]. By utilizing innovative agricultural practices, it improves food security and sustainability in rapidly expanding urban areas. To achieve this goal, numerous articles published in reputable journals over the last two decades have been reviewed. Initially, the examination focuses on how population growth drives urbanization and ultimately leads to food insecurity. The phenomenological aspects of vertical farming are detailed, highlighting its three distinct techniques. After a comprehensive study of vertical farming, it becomes evident that this approach enhances food security and fosters the development of sustainable urban ecosystems. With the global population projected to reach around 9 billion by 2050, with 80% residing in urban areas, vertical farming emerges as a crucial strategy for ensuring a reliable and nutritious food supply, paving the way for healthier and more sustainable urban communities. Finally, the integration of vertical farming within sustainable development is discussed, emphasizing its benefits and impacts.

2. URBANIZATION KEY DRIVER OF FOOD INSECURITY

Urbanization poses a significant threat to food security by negatively impacting both the quantity and quality of cultivated land, which is essential for sustainable human development [17]. Research suggests that by 2030, around 3.7% of the world's cultivated land will be lost due to urban expansion [20]. This phenomenon has led to two main perspectives among scholars regarding its effect on food production [21]. One viewpoint highlights a negative correlation, asserting that the growth of urban areas diminishes the amount of cultivated land, thereby reducing the space available for food cultivation and weakening food supply capabilities [22]. The migration of rural populations to urban centers exacerbates this problem, leading to the abandonment of large areas of farmland and a decline in regional food production [23]. Furthermore, urbanization contributes to soil pollution and intensifies competition for water resources, further limiting food production [24]. On the other hand, some studies propose a positive or balanced relationship, suggesting that urbanization may enhance food production. Nonetheless, the overwhelming evidence points to the harmful effects of urbanization on food security, as the loss of agricultural land and the degradation of soil quality make it increasingly difficult to meet the growing global food demand [25]. This situation has resulted in heightened food insecurity in many regions, as shown by various studies quantifying the adverse impacts of rapid urbanization on agricultural output [26]. Overall, the evidence indicates that urbanization has led to a significant decline in agricultural production, with estimates suggesting a decrease of up to 7.24% annually in regions affected by rapid urban expansion, ultimately exacerbating food insecurity for millions.

The relationship between population growth and food insecurity is concerning. As populations increase, the demand for food often exceeds supply, especially in resource-limited areas [27]. Bremner's research in Africa illustrates this problem, indicating that rising population levels lead to more severe food scarcity, resulting in malnutrition for millions, particularly children in Sub-Saharan Africa [28]. Hall and Molotoks identified population growth as a significant factor driving food insecurity and malnutrition, with the FEEDME model highlighting the global implications of unchecked population increases on food availability [29]. As food production struggles to meet the demands of growing populations, the risk of widespread food insecurity rises, particularly in vulnerable regions facing acute shortages and high levels of malnutrition [30]. Tackling these challenges requires innovative and sustainable solutions. Vertical farming has emerged as a viable strategy to mitigate the negative impacts of urbanization and population growth on food security [31]. This method utilizes vertical spaces in urban areas to cultivate crops in controlled environments, significantly reducing the need for arable land and lowering water consumption [32]. Vertical farming enhances agricultural productivity and provides a sustainable alternative to traditional farming, which is increasingly limited by urban expansion and population pressure [33]. Coupled with political stability and supportive policies to address rapid population growth,

urbanization, and water scarcity, vertical farming could be pivotal in achieving food security and advancing global initiatives such as the Sustainable Development Goals (SDGs) [34], particularly the objective of ending hunger by 2030 (Figure 1). Urbanization has reduced agricultural production by an estimated 7.24% annually in affected areas, worsening food insecurity for millions. Meanwhile, rising populations threaten food scarcity, particularly in resource-limited regions like Sub-Saharan Africa. Vertical farming offers a promising solution to enhance productivity and support the goal of eradicating hunger by 2030.
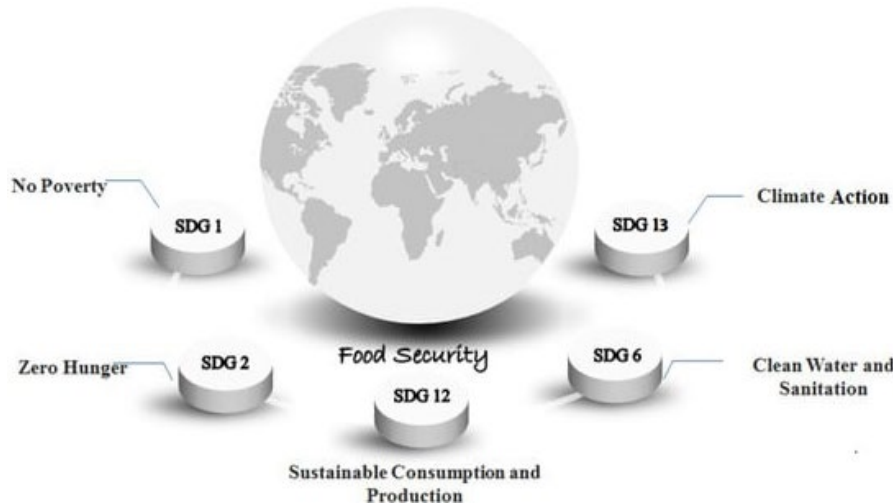

Figure 1. Food security and sustainable development [34]

3. VERTICAL FARMING AND URBAN FOOD SECURITY

Vertical farming (VF) offers an innovative solution to the pressing issues faced by urban agriculture, particularly as urban populations rapidly increase and the demand for food rises [32]. This cutting-edge method involves constructing multi-story buildings filled with stacked layers of growing beds, where advanced greenhouse technologies allow for precise regulation of environmental variables like light, temperature, and humidity [6]. By creating optimal conditions for plant growth, VF facilitates high-density food production while using significantly less land than traditional farming methods [35]. As urban areas expand and arable land decreases, VF becomes essential, maximizing the use of available space and ensuring that fresh produce is accessible to city dwellers [36]. In contrast to conventional agriculture, which relies on extensive farmland and faces climate-related vulnerabilities, vertical farming can flourish in urban environments by transforming underutilized spaces such as rooftops, warehouses, and abandoned structures into productive agricultural centers [36]. The importance of vertical farming is amplified by several interconnected factors, including urban density, ecosystem sustainability, climate change, economic viability, health implications, and food security. As cities grow, the need for accessible, nutrient-rich food sources intensifies, particularly in "food deserts," where fresh produce is scarce [8]. Vertical farms can tackle these food security challenges directly by providing locally grown crops that lessen the dependency on long-distance transport, thus reducing the carbon emissions linked to food distribution. Additionally, VF employs technologies like hydroponics and aeroponics, which conserve vital resources, utilizing up to 90% less water than traditional farming and decreasing the need for harmful pesticides and fertilizers that can harm soil health and contribute to pollution.

Moreover, vertical farming generates economic advantages by creating job opportunities in urban areas and boosting local economies. By situating vertical farms within city limits, food can be sold directly to consumers, cutting transportation costs by up to 60% and making fresh produce more affordable [31]. The incorporation of advanced technologies in VF not only increases productivity but also trains a new generation of urban farmers familiar with modern agricultural practices. This evolution fosters a reconnection between city residents and sustainable farming, promoting healthier eating habits and lifestyles [7]. Additionally, VF plays a vital role in mitigating climate change impacts by reducing reliance on traditional farming practices that contribute to greenhouse gas emissions, while providing a resilient food production system capable of adapting to extreme weather conditions [37]. In summary, vertical farming serves as a comprehensive solution to urgent urban challenges related to food production, environmental sustainability, and public health. By optimizing land use and promoting innovative agricultural techniques, VF enhances food security and contributes to developing sustainable urban ecosystems [10]. With the global population expected to reach approximately 9 billion by 2050 80% of whom will live in urban areas vertical farming presents a critical strategy for ensuring a reliable and nutritious food supply, paving the way for healthier and more sustainable urban communities.

3.1. Techniques of Vertical Farming

Vertical farming (VF) employs advanced agricultural systems designed for the rapid growth and intentional production of crops by carefully managing ambient conditions and nutritional solutions. Utilizing cutting-edge greenhouse technologies, VF enhances yields while significantly reducing water usage [33]. These high-tech farms are meticulously designed to provide each plant with precisely calibrated nutrients and optimal light exposure. One of the critical advantages of VF is its ability to function without toxic herbicides and pesticides, leading to healthier produce while also boosting nutritional value [9]. Vertical farming can be classified into three primary methods: hydroponics, aeroponics, and aquaponics, each offering unique benefits and applications (Figure 2). Hydroponics, the most prevalent technique, enables soil-less plant growth by utilizing water as a medium for nutrient distribution, thus eliminating many soil-related issues such as pests and diseases [38]. This method also allows for more straightforward control of fertilizer and pH levels, making it an environmentally friendly and efficient choice for urban agriculture.
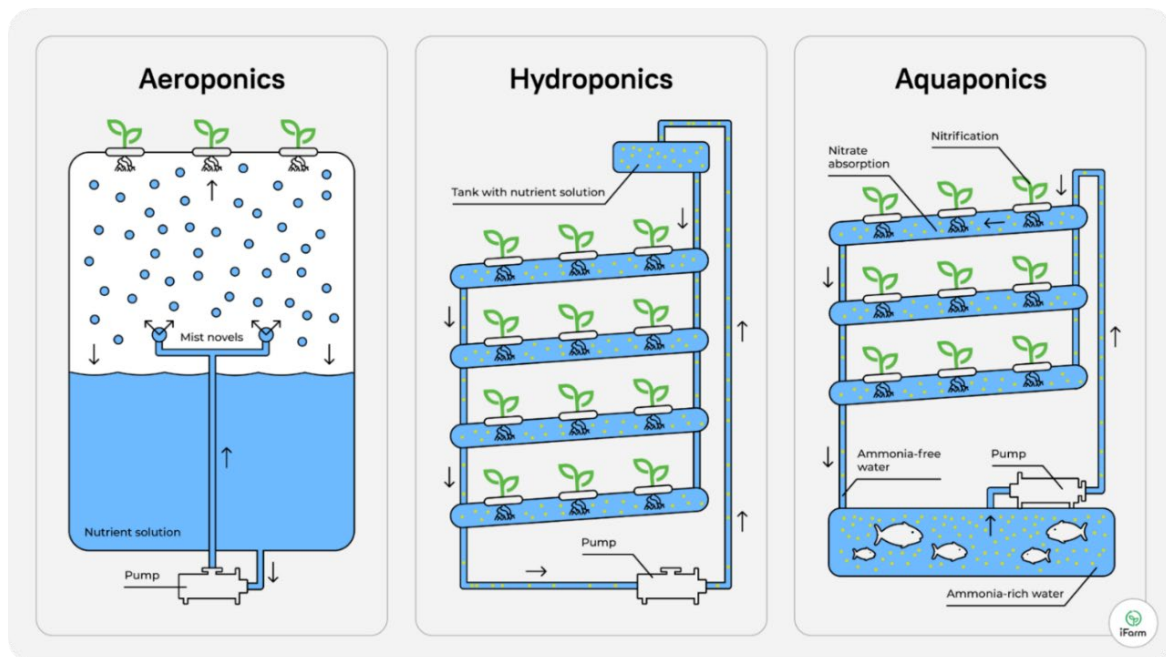

Figure 2. Methods of vertical farming [38–40]

Aquaponics further integrates hydroponics with fish farming, creating a sustainable, symbiotic system where fish waste provides nutrients for plants, while plants filter and purify the water for fish [39]. This circular resource flow exemplifies sustainable food production, significantly reducing the need for fertilizers and artificial chemicals while optimizing water use [39]. Aeroponics, on the other hand, employs a misting system to deliver nutrients directly to plant roots without soil or large quantities of water [11]. While it requires meticulous monitoring and maintenance to prevent root damage and bio-debris clogging the misting nozzles, it can reduce water usage by up to 95% and occupy significantly less space than traditional farming methods [40]. Each of these techniques showcases the potential of vertical farming to address urban food production challenges, making it a promising avenue for sustainable agriculture in densely populated areas. Vertical farming techniques, including hydroponics, aeroponics, and aquaponics, can reduce water usage by up to 90% compared to traditional farming methods while simultaneously increasing crop yields by 20-30%, making them essential solutions for sustainable food production in urban environments facing rapid population growth.

4. URBAN VERITCAL FARMING AND SUSTAINABILITY

Urban farming has emerged as a pivotal strategy in addressing the challenges posed by traditional urbanization models, particularly those that arose after the mid-twentieth century [41]. The original compact urban design, which fostered a high quality of environmental integrity and sociability, has transitioned to low-density industrial estates characterized by sprawling developments that lack integrated planning [42]. This shift has led to increased consumption of vital resources such as water, energy, and materials, with studies indicating that urban areas consume 75% of the world's natural resources, thereby placing immense pressure on ecosystems [43]. The expansion of cities has exacerbated environmental issues, including the proliferation of informal settlements and the degradation of rural landscapes, which further contributes to urban heat islands and loss of biodiversity [44].

Table 1. Benefits and impacts of vertical farming

No	Benefits	Social Impact	Economic Impact	Environmental Impact	References
1	Reducing travel distances for food	Fresher, locally sourced cuisine enhances health.	Decreases energy, packaging, and fuel costs.	Reduces air pollution and improves air quality.	[41]
2	Reducing water usage	Increases access to safe drinking water for residents.	Cost savings and improved efficiency in land use.	Lowers runoff from traditional farms.	[42]
3	Recycling organic waste	Enhances food quality and consumer health.	Transforms waste into valuable resources, contributing to revenue.	Minimizes landfill waste and its environmental impact.	[43]
4	Creating employment opportunities	Fosters local community engagement and networks.	Boosts local economies through job creation.	Reduces environmental impacts by minimizing commuting.	[44]
5	Reducing use of fertilizers and pesticides	Promotes healthier food and consumer well-being.	Decreases costs associated with chemical inputs.	Improves environmental health and sustainability.	[45]
6	Enhancing productivity	Saves time and reduces repetitive labor.	Increases agricultural yields and efficiency.	Requires less space for cultivation, preserving land.	[46]
7	Protection against climate-related events	Improves food security by diversifying local supplies.	Mitigates economic losses due to natural disasters.	Reduces environmental damage during climate events.	[47]
8	Year-round product availability	Increases access to fresh produce throughout the year.	Supports continuous economic activity in local markets.	Allows for seasonal adaptability in agricultural production.	[47]
9	Utilizing renewable energy	Improves air quality and community health.	Reduces operational costs through energy efficiency.	Lowers reliance on fossil fuels and carbon emissions.	[48]
10	Integrating nature into urban spaces	Enhances mental health and reduces stress.	Creates local job opportunities in green sectors.	Increases urban biodiversity and ecological health.	[49]
11	Promoting green and high-tech industries	Encourages education and development of skilled workers.	Generates employment in emerging fields like biotechnology.	Minimizes environmental damage with sustainable practices.	[50]
12	Reducing traditional agricultural activities	Improves public health through modern farming techniques.	Reduces economic burdens on conventional farming methods.	Preserves natural ecosystems and prevents overexploitation.	[16]
13	Restoring dilapidated structures	Fosters community interaction and social networks.	Revitalizes local economies and enhances property values.	Cleans up urban environments, reducing blight and stigma.	[14]

As cities continue to grow, they often fail to maintain a balance between resource inflow and outflow, leading to significant ecological disturbances, such as soil erosion and water scarcity [45]. This alarming trend underscores the urgent need for innovative solutions that prioritize sustainability and mitigate the adverse effects of urban sprawl [46]. Urban farming not only offers a viable alternative for enhancing food security but also promotes

community engagement, reduces transportation emissions, and restores ecological integrity, making it an essential component in the pursuit of sustainable urban development.

To counteract the detrimental impacts of urbanization, numerous governmental initiatives worldwide are focused on enhancing sustainability within urban contexts [47]. One key strategy is the establishment of a green matrix, comprising interconnected green spaces that integrate urban, peri-urban, and agricultural areas [48]. This approach not only addresses pressing ecological concerns but also fosters social cohesion and economic development through urban agriculture (Table 1). By promoting local food production, urban farming can enhance food security, improve access to fresh produce, and cultivate community involvement, ultimately yielding physical, psychological, and social benefits for residents [49]. Additionally, urban farming initiatives have demonstrated significant environmental advantages, such as enhanced biodiversity, reduced pollution, and improved urban microclimates. During the COVID-19 pandemic, the vulnerabilities of global food supply chains became apparent, highlighting the importance of localized food systems [16]. Urban farming presents a viable solution by shortening supply chains and fostering self-sufficiency, thereby contributing to a more resilient and sustainable urban landscape [50]. The multifaceted benefits of urban farming quantitatively demonstrate its potential to enhance urban sustainability; for instance, studies indicate that localized food production can reduce transportation-related carbon emissions by up to 70%, while community gardens have been shown to increase access to fresh produce by 25%, ultimately leading to improved public health outcomes and economic resilience.

5. CONCLUSION

This review paper investigates the potential of vertical gardening to mitigate food insecurity, utilizing insights from articles published in reputable journals over the past two decades. The goal is to consolidate existing information regarding urbanization, food insecurity, and vertical farming. The study yields several key conclusions:

- Urbanization has caused agricultural production to decline by an estimated 7.24% annually in affected regions, worsening food insecurity for millions. At the same time, increasing populations threaten food availability, particularly in resource-limited areas like Sub-Saharan Africa. Vertical farming offers a promising approach to boost productivity and align with the goal of eradicating hunger by 2030.
- By maximizing land use and implementing innovative agricultural techniques, vertical farming (VF) enhances food security and aids in the development of sustainable urban ecosystems. With the global population projected to reach approximately 9 billion by 2050, with 80% living in urban areas, vertical farming emerges as a vital strategy for ensuring a consistent and nutritious food supply, paving the way for healthier and more sustainable urban communities.
  - o Vertical farming techniques, such as hydroponics, aeroponics, and aquaponics, can decrease water usage by up to 90% compared to traditional farming practices while simultaneously increasing crop yields by 20-30%. These methods are crucial for sustainable food production in rapidly urbanizing environments.
- The various benefits of urban farming quantitatively underscore its potential to enhance urban sustainability; for instance, studies indicate that localized food production can reduce transportation-related carbon emissions by up to 70%, and community gardens have been shown to increase access to fresh produce by 25%, leading to improved public health outcomes and greater economic resilience.

The findings are promising, suggesting that further exploration of its application on a larger scale is necessary. Detailed investigations and experimental research could facilitate the successful implementation of vertical farming in real-life settings, ultimately bolstering food security.

Acknowledgments

References

[1] H. Fatima, H. Man, M. Ameen, I. Aslam, T. Athar, S. S. Hussain Shah, and G. H. Abbasi, "Soil security to address potential global issues," in *Environmental Nexus for Resource Management*, pp. 81–113, CRC Press, 2024.

[2] P. Khatri, P. Kumar, K. S. Shakya, M. C. Kirlas, and K. K. Tiwari, "Understanding the intertwined nature of rising multiple risks in modern agriculture and food system," *Environment, Development and Sustainability*, vol. 26, no. 9, pp. 24107–24150, 2024.

[3] J. E. Reeger, "Rice roots for drought tolerance: functional roles and genetic components of root anatomical and architectural traits in oryza sativa," Ph.D. Diss., The Pennsylvania State University, 2020.

[4] O. B. Akintuyi, "Vertical farming in urban environments: A review of architectural integration and food security," *Open Access Research Journal of Biology and Pharmacy*, vol. 10, no. 2, pp. 114–126, 2024.

[5] D. D. Avgoustaki and G. Xydis, "How energy innovation in indoor vertical farming can improve food security, sustainability, and food safety?" in *Advances in Food Security and Sustainability*, vol. 5, pp. 1–51, Elsevier, 2020.

[6] D. Petrovics and M. Giezen, "Planning for sustainable urban food systems: an analysis of the up-scaling potential of vertical farming," *Journal of Environmental Planning and Management*, vol. 65, no. 5, pp. 785–808, 2022.

[7] R. M. Lefers, M. Tester, and K. J. Lauersen, "Emerging technologies to enable sustainable controlled environment agriculture in the extreme environments of Middle East-North Africa coastal regions," *Frontiers in Plant Science*, vol. 11, art. no. 801, 2020.

[8] K. Al-Kodmany, "The vertical farm: A review of developments and implications for the vertical city," *Buildings*, vol. 8, no. 2, art. no. 24, 2018.

[9] R. Kumar, A. Fayaz, and M. Kaundal, "Vertical Farming: The future of controlled-environment agriculture and food-production system," *Current Journal of Applied Science and Technology*, vol. 42, no. 48, pp. 74–86, 2023.

[10] F. C. Coelho, E. M. Coelho, and M. Egerer, "Local food: Benefits and failings due to modern agriculture," *Scientia Agricola*, vol. 75, pp. 84–94, 2018.

[11] Y. Abe, K. Yamada, R. Tanaka, K. Ando, and M. Ueno, "Dynamic living space: toward a society where people can live anywhere in 2050," *Futures*, vol. 161, art. no. 103363, 2024.

[12] M. S. Udaykumar, M. Patil, and L. Suman, "Vertical farming: Way for urban food security," *International Journal of Environment and Climate Change*, vol. 14, no. 7, pp. 529–539, 2024.

[13] D. Wu, L. Zheng, Y. Wang, J. Gong, J. Li, and Q. Chen, "Characteristics of urban expansion in megacities and its impact on water-related ecosystem services: A comparative study of Chengdu and Wuhan, China," *Ecological Indicators*, vol. 158, art. no. 111322, 2024.

[14] A. Siegner, J. Sowerwine, and C. Acey, "Does urban agriculture improve food security? Examining the nexus of food access and distribution of urban produced foods in the United States: A systematic review," *Sustainability*, vol. 10, no. 9, art. no. 2988, 2018.

[15] E. J. Cilliers, L. Lategan, S. S. Cilliers, and K. Stander, "Reflecting on the potential and limitations of urban agriculture as an urban greening tool in South Africa," *Frontiers in Sustainable Cities*, vol. 2, art. no. 43, 2020.

[16] K. Kent, F. Gale, B. Penrose, S. Auckland, E. Lester, and S. Murray, "Consumer-driven strategies towards a resilient and sustainable food system following the COVID-19 pandemic in Australia," *BMC Public Health*, vol. 22, no. 1, art. no. 1539, 2022.

[17] M. G. Abebe, "Impacts of urbanization on food security in Ethiopia. A review with empirical evidence," *Journal of Agriculture and Food Research*, art. no. 100997, 2024.

[18] Z. Akbari, A. Y. Hesar, N. Siamian, C. Fürst, R. Värnik, and H. Azadi, "Feasibility of using vertical farming in northern Iran: A multiple necessity," *Journal of Environmental Management*, vol. 354, art. no. 120232, 2024.

[19] R. de Sousa, L. Bragança, M. V. da Silva, and R. S. Oliveira, "Challenges and solutions for sustainable food systems: The potential of home hydroponics," *Sustainability*, vol. 16, no. 2, art. no. 817, 2024.

[20] S. Angel, J. Parent, D. L. Civco, A. Blei, and D. Potere, "The dimensions of global urban expansion: Estimates and projections for all countries, 2000–2050," *Progress in Planning*, vol. 75, no. 2, pp. 53–107, 2011.

[21] F. Taheri, M. Forouzani, M. Yazdanpanah, and A. Ajili, "How farmers perceive the impact of dust phenomenon on agricultural production activities: A Q-methodology study," *Journal of Arid Environments*, vol. 173, art. no. 104028, 2020.

[22] T. Gomiero, "Soil degradation, land scarcity and food security: Reviewing a complex challenge," *Sustainability*, vol. 8, no. 3, art. no. 281, 2016.

[23] E. Ustaoglu and M. J. Collier, "Farmland abandonment in Europe: An overview of drivers, consequences, and assessment of the sustainability implications," *Environmental Reviews*, vol. 26, no. 4, pp. 396–416, 2018.

[24] S. Barthel, C. Isendahl, B. N. Vis, A. Drescher, D. L. Evans, and A. van Timmeren, "Global urbanization and food production in direct competition for land: Leverage places to mitigate impacts on SDG2 and on the earth system," *The Anthropocene Review*, vol. 6, no. 1–2, pp. 71–97, 2019.

[25] R. Lal, "Restoring soil quality to mitigate soil degradation," *Sustainability*, vol. 7, no. 5, pp. 5875–5895, 2015.

[26] A. A. Hatab, M. E. R. Cavinato, A. Lindemer, and C.-J. Lagerkvist, "Urban sprawl, food security, and

agricultural systems in developing countries: A systematic review of the literature," *Cities*, vol. 94, pp. 129–142, 2019.

[27] D. McLaughlin and W. Kinzelbach, "Food security and sustainable resource management," *Water Resources Research*, vol. 51, no. 7, pp. 4966–4985, Jul. 2015.

[28] S. Moreland and E. Smith, "Climate change, food security, and population in Sub-Saharan Africa: Modeling the linkages," *The International Journal of Climate Change: Impacts and Responses*, vol. 4, no. 2, art. no. 29, 2013.

[29] M. Ferré Gras, "Desarrollo de una web segura," 2023.

[30] H. Kakaei, H. Nourmoradi, S. Bakhtiyari, M. Jalilian, and A. Mirzaei, "Effect of covid-19 on food security, hunger, and food crisis," in *COVID-19 and the Sustainable Development Goals*, pp. 3–29, Elsevier, 2022.

[31] R. de Sousa, L. Bragança, M. V. da Silva, and R. S. Oliveira, "Challenges and solutions for sustainable food systems: The potential of home hydroponics," *Sustainability*, vol. 16, no. 2, art. no. 817, 2024.

[32] D. Despommier, "Farming up the city: The rise of urban vertical farms," *Trends in Biotechnology*, vol. 31, no. 7, pp. 388–389, 2013.

[33] K. Al-Kodmany, "The vertical farm: A review of developments and implications for the vertical city," *Buildings*, vol. 8, no. 2, art. no. 24, 2018.

[34] S. Kousar, F. Ahmed, A. Pervaiz, and Š. Bojnec, "Food insecurity, population growth, urbanization and water availability: The role of government stability," *Sustainability*, vol. 13, no. 22, art. no. 12336, 2021.

[35] K. Al-Kodmany, "The vertical farm: Exploring applications for peri-urban areas," in *Smart Village Technology: Concepts and Developments*, pp. 203–232, 2020.

[36] S. Sharma, B. Shree, D. Sharma, S. Kumar, V. Kumar, R. Sharma, and R. Saini, "Vegetable microgreens: The gleam of next generation super foods, their genetic enhancement, health benefits and processing approaches," *Food Research International*, vol. 155, art. no. 111038, 2022.

[37] T. Mizik, "Climate-smart agriculture on small-scale farms: A systematic literature review," *Agronomy*, vol. 11, no. 6, art. no. 1096, 2021.

[38] S. Mourouzidou, G. K. Ntinas, A. Tsaballa, and N. Monokrousos, "Introducing the power of plant growth promoting microorganisms in soilless systems: A promising alternative for sustainable agriculture," *Sustainability*, vol. 15, no. 7, art. no. 5959, 2023.

[39] K. C. Shreejana, R. Thapa, A. Lamsal, S. Ghimire, K. Kurunju, and P. Shrestha, "Aquaponics a modern approach for integrated farming and wise utilization of components for sustainability of food security: A review," *Archives of Agriculture and Environmental Sciences*, vol. 7, pp. 121–126, 2022.

[40] X. Yang, Y. Luo, and P. Jiang, "Sustainable soilless cultivation mode: Cultivation study on droplet settlement of plant roots under ultrasonic aeroponic cultivation," *Sustainability*, vol. 14, no. 21, art .no. 13705, 2022.

[41] M. Jain, "Mitigation of urbanization ill-effects through urban agriculture inclusion in cities," in *New forms of urban agriculture: An Urban ecology perspective*, pp. 39–56, Singapore: Springer Nature Singapore, 2022.

[42] P. Sanches, F. L. de Oliveira, and G. Celani, "Green and compact: A spatial planning model for knowledge-based urban development in peri-urban areas," *Sustainability*, vol. 13, no. 23, art. no. 13365, 2021.

[43] S. B. Wassie, "Natural resource degradation tendencies in Ethiopia: A review," *Environmental Systems Research*, vol. 9, no. 1, pp. 1–29, 2020.

[44] T. Hailu, E. Assefa, and T. Zeleke, "Land use transformation by urban informal settlements and ecosystem impact," *Environmental Systems Research*, vol. 13, no. 1, art. no. 32, 2024.

[45] L. Chen, P. Han, and G. Zhang, "Use of an ecological compensation model in water resource development: A case study from Shaanxi Province, China," *Water*, vol. 16, no. 19, art. no. 2851, 2024.

[46] A. I. Almulhim and P. B. Cobbinah, "Urbanization provocateur: Reaching urban planning-led development in Saudi Arabia," *Land Use Policy*, vol. 147, art. no. 107365, 2024.

[47] A. I. Almulhim, A. Sharifi, Y. A. Aina, S. Ahmad, L. Mora, W. L. Filho, and I. R. Abubakar, "Charting sustainable urban development through a systematic review of SDG11 research," *Nature Cities*, vol. 1, pp. 1–9, 2024.

[48] M. Baxevani, D. Tsiotas, G. Kolkos, E. Zafeiriou, and G. Arabatzis, "Peri-urban and urban green space management and planning: The case of Thessaloniki, Greece," *Land*, vol. 13, no. 8, art. no. 1235, 2024.

[49] S. Sarah and S. Nurhayati, "Enhancing family food security through experiential learning-based training in organic food cultivation," *Jurnal Simki Pedagogia*, vol. 7, no. 1, pp. 84–94, 2024.

[50] Y. Yusriadi, A. Cahaya, M. C. B. Umanailo, and S. Z. Bin Tahir, "Perspectives of rural farming households on home gardens as an agroforestry for food security: A qualitative study in Indonesia," *African Journal of Food, Agriculture, Nutrition and Development*, vol. 24, no. 2, pp. 25645–25661, 2024.

Scale Insects in Orange Orchards of Guelma Province, Algeria: Diversity, Abundance, and Climatic Influences

Omar Khaladi[1, 2], Amira Bouderbala[3]

[1]Department of Ecology and Environmental Engineering, Faculty of Natural and Life Sciences, Earth and Universe Sciences, University of 8 May 1945 Guelma, BP 401, Guelma, 24000, Algeria
[2]Laboratory of Silicates, Polymers, and Nanocomposites, University 8 May1945 Guelma, BP 401, Guelma, 24000, Algeria
[3]Laboratory of Agriculture and Ecosystem Functioning, Faculty of Nature and Life Sciences, Department of Agronomy Sciences, University Chadli Bendjedid, El Tarf, Algeria
Corresponding author: Omar Khaladi (e-mail: omarkhbiopest@hotmail.fr)

Abstract

Scale insects are major pests of citrus crops in the Mediterranean basin, but their impact is often underestimated due to a lack of data in certain countries. In Algeria, this study aimed to inventory the scale insect species affecting orange orchards in three regions of Guelma Province (northeastern Algeria) during the winter-spring seasons from 2014 to 2018. Samples were collected from the cardinal directions of the trees and the center of the canopy. A total of 17 species were identified, among which *Aonidiella aurantii*, *Parlatoria ziziphi*, and *Coccus pseudomagnoliarum* were dominant, while *Lepidosaphes beckii*, *Saissetia oleae*, and *Saissetia coffeae* were rare. Richness estimators, including Chao 1, Chao 2, Jackknife 1, and Bootstrap, suggested the potential presence of up to 21 species, with a theoretical richness of 20.15±0.96 species. Climatic correlation analysis revealed a positive relationship between species abundance and relative humidity, and a negative relationship with average temperature, while species diversity remained unchanged. This study highlights the diversity of scale insects and the influence of climatic conditions on their population dynamics.

Keywords: Scale insects, Inventory, Algeria, Richness estimators, Orange orchards

Green Synthesis of Silver Nanoparticles Mediated by Essential Oil: Characterization and Antifungal Activity Against Plant Pathogens

Laila Reklaoui[1], Abdellatif El-Habib[2], Samir Haloui[2], Zine El Abidine Bzazou Elouazzani[1], Abderazzak Rfaki[3], Hassan Ghazal[3], Haiat Essalmani[1], Said Barrijal[1]

[1]Laboratory of Biotechnological Valorization of Microorganisms, Genomics, and Bioinformatics, Faculty of Sciences and Techniques, Abdelmalek Essaadi University, 90000 Tangier, Morocco
[2]Materials, Systems and Energy Engineering Laboratory (MaSEEL), Faculty of Sciences and Techniques of Tangier, Abdelmalek Essaadi University, Tetouan, Morocco
[3]National Center for Scientific and Technical Research CNRST, 10000 Rabat, Morocco
Corresponding author: Laila Reklaoui (e-mail: l.reklaoui@uae.ac.ma)

Abstract

This study presents a sustainable, cost-effective, and eco-friendly method for synthesizing silver nanoparticles (AgNPs) using silver nitrate and the essential oil of *Origanum compactum* as a natural reducing agent, aimed at combating phytopathogenic fungi. The essential oil was extracted and characterized through gas chromatography-mass spectrometry (GC-MS) prior to its role in the synthesis. A solution of $AgNO_3$ was prepared, and the essential oil, diluted in acetone for enhanced integration, was gradually added dropwise at 70°C under constant stirring. The formation of silver nanoparticles was indicated by a color change from yellow to brown. The synthesized AgNPs were characterized using UV-Vis spectroscopy, scanning electron microscopy (SEM), Raman spectroscopy, and dynamic light scattering (DLS), confirming their size, shape, and stability. GC-MS analysis revealed the presence of key compounds in the essential oil, including pulegone (25.79%), borneol (23.28%), and α-terpineol (9.86%), known for their antimicrobial properties and their role in reducing and stabilizing AgNPs. SEM analysis showed the nanoparticles to be predominantly spherical, while Raman spectroscopy confirmed interactions between the essential oil and the AgNPs at the molecular level. The antifungal efficacy of the AgNPs was assessed using the poisoned food technique against three significant tomato pathogens: *Fusarium oxysporum* f. sp. *radicis-lycopersici*, *Rhizoctonia solani*, and *Botrytis cinerea*. The AgNPs exhibited strong antifungal activity, with inhibition rates reaching up to 94% at a concentration of 100 ppm. This green synthesis approach offers notable advantages, including improved safety, environmental sustainability, and potential for application in sustainable agriculture.

Keywords: Green synthesis, Silver nanoparticle, Essential oil, Antifungal activity, Nanotechnology

Validation of *Pandanus Amaryllifolius* Phytochemicals Compound as Reducing Agent in Green Synthesis of Ag-Doped ZnO by Computational Method

Siti Rashidah Abdol Razid[1], Siti Salwa Alias[2,3], Juan Matmin[1,3], Fazira Ilyana Abdul Razak[1,3]

[1]Department of Chemistry, Faculty of Science, Universiti Teknologi Malaysia, 81310 Skudai, Johor, Malaysia
[2]Advanced Optical Materials Research Group (AOMRG), Department of Physics, Faculty of Science, Universiti Teknologi Malaysia, 81310 Skudai, Johor, Malaysia
[3]Centre for Sustainable Nanomaterials, Ibnu Sina Institute for Scientific and Industrial Research (ISI-SIR), Universiti Teknologi Malaysia, 81310, Skudai, Johor, Malaysia
Corresponding author: Siti Salwa Alias (e-mail: siti.salwa@utm.my)

Abstract

Electricity generation predominantly relies on fossil fuels, which account for 86% of global production and release approximately 7.8 billion metric tons of greenhouse gases annually. To address these environmental and energy challenges, green hydrogen produced via renewable-powered photocatalysis presents a promising carbon-neutral solution. By efficiently utilizing sunlight to split water, this approach reduces fossil fuel dependency, curbs greenhouse gas emissions, and aligns with sustainability goals, energy security, and climate change mitigation efforts. Zinc oxide (ZnO) has gained attention as a promising photocatalyst for water splitting due to its stability, non-toxicity, and cost-effectiveness. However, its wide bandgap of ~3.2 eV restricts light absorption to ultraviolet (UV) wavelengths, limiting its efficiency. To overcome this, silver (Ag) nanoparticles are incorporated into ZnO, influencing the surface plasmon resonance (SPR) to enable visible light absorption and improve photocatalytic performance. Green synthesis methods offer an eco-friendly alternative for fabricating Ag-doped ZnO, eliminating the need for hazardous chemicals. Plant extracts, such as *Pandanus amaryllifolius* (*P. amaryllifolius*), have proven to be effective as reducing agents that enhances both the morphological structure and optical properties of ZnO. Previous studies highlight that flavonoids and phenolic acids in *P. amaryllifolius* are key to its reducing capabilities. In this study, the reduction potential of phytochemicals in *P. amaryllifolius* was analysed using density functional theory (DFT) with the B3LYP functional and 6-311G basis set to evaluate their HOMO-LUMO gaps and dipole moments. FORcite software was employed to perform adsorption studies of these phytochemicals on ZnO surfaces, calculating adsorption energies to evaluate their interactions and potential to enhance photocatalytic activity. Among the phytochemicals, quercetin and gallic acid demonstrated an excellent performance in reducing the band gap of ZnO and Ag-doped ZnO, enhancing photocatalytic efficiency and offering a sustainable pathway for green hydrogen production.

Keywords: *P. amaryllifolius*, Reducing agent, Ag-doped ZnO, Computational method, Photocatalytic water splitting

Production of Vegan and Reduced-Calorie Mayonnaise Using Aquafaba and Pectin Derived from Fruit Waste

Sebahat Oztekin[1]

[1]Department of Food Engineering, Bayburt University, Bayburt, Türkiye
Corresponding author: Sebahat Oztekin (e-mail: ozakca.sebahat@gmail.com)

Abstract

The development of sustainable, vegan, and calorie-reduced mayonnaise addresses the increasing consumer demand for healthier and environmentally friendly food options. This study explored the formulation of plant-based mayonnaise using aquafaba from chickpea cooking water as a natural emulsifier and pectin gel from fruit waste as a fat substitute. Traditional mayonnaise, with approximately 70–80% fat content, is unsuitable for individuals with egg allergies or vegan diets due to its reliance on egg yolk and oil. Aquafaba successfully replaced egg yolk, providing emulsifying properties and ensuring desired texture and stability, while pectin gels effectively reduced fat content, maintaining creaminess and structural integrity. Rheological analysis revealed that increasing substitution levels weakened the structural network, with reductions in elastic (G') and viscous (G") modulus. The M25 formulation, containing 25% substitution, was the most preferred in sensory evaluations, retaining taste, texture, and overall acceptability comparable to the control. Higher substitution levels (M75 and M100) showed noticeable declines in sensory and structural quality, with M75 achieving acceptable stability and texture, whereas M100 exhibited significant structural breakdown. This innovative approach supports sustainable waste management by recycling chickpea water and fruit waste, aligning with zero-waste principles and reducing food loss. Additionally, it promotes eco-friendly production processes and offers a sustainable, cost-effective, and lower carbon footprint alternative to animal-based proteins. The findings demonstrate the potential for developing plant-based, healthier products that cater to diverse dietary needs while contributing to global sustainability goals.

Keywords: Aquafaba, Vegan mayonnaise, Pectin, Light and plant-based mayonnaise, Fruit waste

1. INTRODUCTION

In the new century, hunger is the most fundamental global issue, and reducing poverty is one of the priority sustainable development goals identified by the United Nations. To feed the world's population today, agricultural activities must be increased, and all nutritionally rich agricultural products must be utilized without loss. Considering that insufficient access to protein is one of the most significant causes of global hunger, legumes are among the most valuable food sources. To ensure the sustainability of legumes, alternative new methods for recycling their waste based on these multifunctional properties are being sought [1]. Aquafaba is a liquid that forms during the cooking of chickpeas or other legumes and is known as canned chickpea water. This liquid can be used as an egg substitute in mayonnaise production. Aquafaba contains plant-based protein and starch, and its structure is similar to egg whites, making it suitable for playing the emulsifying role in mayonnaise. It can be recycled for use as a food raw material in various processes, contributing to reduced food waste [1–3]. Secondly, pectin, a natural polysaccharide obtained from fruit waste, has gelling properties. In this context, pectin gels can be used as thickeners and stabilizers in mayonnaise. Pectin derived from fruit waste can also serve as a sustainable component [4].

Aquafaba, the viscous wastewater obtained from chickpeas and other legumes, contains significant amounts of carbohydrates, protein, and saponin and is used as a rheological additive in various food processes [5]. For example, aquafaba derived from chickpea cooking water has been used as a functional ingredient in vegan and vegetarian diets, replacing eggs in cakes (at an optimum rate of 25% aquafaba) [6]. Additionally, studies have shown that chickpea aquafaba can replace eggs in the production of vegan mayonnaise analogs [2, 3, 7]. However, these studies included the use of oils such as canola, rapeseed, and sunflower in addition to aquafaba. In our study, the use of pectin gels instead of oil makes this work unique. Other studies have also explored the use of pectin as a fat substitute, particularly in cookie and bakery product formulations [4, 8, 9]. Inspired by these studies, pectin gels can be used to fulfill the functional properties of fat. In this context, aquafaba, with its emulsifying properties, and pectin, by substituting some functions of fat, can provide the desired texture and stability. This approach could enable the production of a new generation of plant-based, vegan, and low-calorie mayonnaise. However, it is

essential to work on production processes and develop appropriate formulations by determining the correct ratios of components [3].

The United Nations Sustainable Development Goals (SDGs) aim to end hunger (SDG 2.4.1) and halve food waste (SDG 12.3) by 2030 [10, 11]. In this regard, the production of plant-based, vegan, nutritious, and low-calorie food products could represent a step towards achieving these goals.

2. MATERIAL AND METHOD

2.1. Preparation of Aquafaba from Chickpea Cooking Water

Chickpeas were soaked in tap water at a chickpea-to-water ratio of 1:3 (w/v) for 24 hours and then drained. The hydrated chickpeas were boiled in a pressure cooker with a chickpea-to-water ratio of 1:1.5 (weight/volume) for 1 hour. The cooking water was subsequently separated, stored at 4 ℃, and used to obtain chickpea aquafaba. Before incorporating it into the mayonnaise mixture, the pH of the aquafaba was adjusted to 4.9 [3].

2.2. Extraction of Pectin from Various Fruit Wastes

Peels of oranges, and tangerines were frozen at -18 ℃ for 48 hours and then subjected to lyophilization (-55 ℃, 4 Pa). The freeze-dried fruit waste was ground into powder and mixed with ethanol, incubated at 70 ℃ for 20 minutes, and filtered. This process was repeated three times. The residue (10 g) was added to an oxalic acid/ammonium oxalate solution (pH 4.6, 400 mL) and heated at 85 ℃ for 1 hour before being filtered again. The filtrate was treated with 96% ethanol at a ratio of 1:3 and centrifuged at $14,500 \times g$ for 10 minutes. The ethanol washing process was repeated several times. Finally, the precipitate was dried at 50 ℃ for 24 hours to produce pectin [8].

2.3. Preparation of Pectin Gels

Pectin gels were prepared by mixing pectin (30%; w/w) with distilled water at room temperature for 10 minutes at 650 rpm [8].

2.4. Preparation of Mayonnaise Formulations

The formulations for mayonnaise preparation are presented in Table 1 and Table 2 [3].

Table 1. Formulations of mayonnaise samples

Ingredients	Control	M25	M50	M75	M100
Sunflower oil (control)	187.5	0	0	0	0
Egg yolk (control)	30	0	0	0	0
Pectin gel addition	0	210	202.5	195	187.5
Aquafaba addition	0	7.5	15	22.5	30
Vinegar	26	26	26	26	26
Salt	3	3	3	3	3
Sugar	3.5	3.5	3.5	3.5	3.5

Table 2. Description of mayonnaise formulations

Sample	Description
Control	Mayonnaise sample prepared with egg yolk and sunflower oil.
M25	Mayonnaise containing 25% aquafaba as a replacement for egg yolk.
M50	Mayonnaise containing 50% aquafaba as a replacement for egg yolk.
M75	Mayonnaise containing 75% aquafaba as a replacement for egg yolk.
M100	Mayonnaise containing 100% aquafaba as a replacement for egg yolk.

The visual related to the production of vegan and calorie-reduced mayonnaise made with aquafaba and pectin extracted from fruit waste is presented in Figure 1.
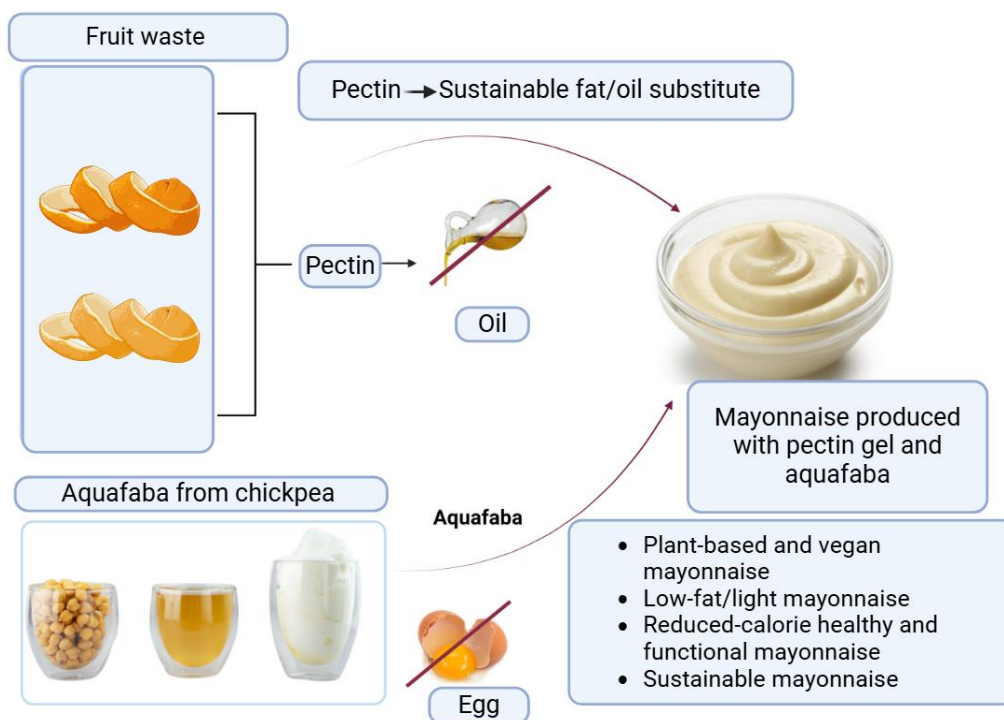
Figure 1. Production of vegan mayonnaise using aquafaba and pectin derived from fruit waste

2.5. Rheological Measurements

The steady shear viscosity will be measured using a rheometer at 25 ^{o}C over a shear rate range of 0.1-100 s^{-1} [8].

2.6. Sensory Analysis

Ten semi-trained panelists evaluated the sensory attributes of mayonnaise samples, including appearance, color, texture, odor, taste, and overall acceptability, using a five-point hedonic scale, with varying ratios of egg substitutes [12].

2.7. Statistical Analysis

Statistical analyses, including variance analysis (ANOVA), standard deviations, means, and coefficient of variation, will be performed using SPSS software based on the results of the tests conducted in the study ($p < 0.05$).

3. RESULTS

Figure 2 shows the values of G' (elastic modulus) and G" (viscous modulus) as a function of strain ($\gamma 0$, %). It was observed that G' and G" values decreased with increasing aquafaba levels. The rheological analysis showed that the G' and G" of the mayonnaise samples decreased with the replacement of oil and egg yolk by pectin gel and aquafaba. In the control group, the presence of oil and egg yolk provided a strong structural network, resulting in higher G' and G" values. However, as the aquafaba and pectin gel levels increased, the absence of oil weakened the elastic and viscous properties, leading to a softer and more fluid-like structure. At higher substitution levels, particularly in the M75 and M100 samples, strain softening became evident, indicating the breakdown of the structural network under deformation. Overall, the results highlight that oil plays a key role in maintaining the viscoelastic properties of mayonnaise, while pectin gel and aquafaba, despite their contributions, are insufficient to replicate the structural stability provided by oil and egg yolk.

Figure 3 shows the sensory analysis results of the produced vegan and pectin-based mayonnaise samples. The sensory analysis results revealed that the substitution of oil and egg yolk with aquafaba and pectin gel negatively impacted the sensory attributes of mayonnaise samples as the substitution level increased. The control sample, which contained oil and egg yolk, received the highest scores for all attributes, particularly texture and overall acceptability, indicating superior sensory quality. The M25 sample, with 25% aquafaba substitution, showed relatively similar results to the control, with only slight declines in texture and appearance. However, as the substitution level increased to 50% (M50), texture and overall acceptability began to noticeably decrease, despite

color and odor remaining consistent. The M75 and M100 samples, with 75% and 100% substitution, exhibited the lowest scores across all attributes, particularly texture and appearance, highlighting significant structural weakening and reduced consumer preference. Overall, the findings suggest that while low levels of aquafaba and pectin gel substitution (M25) can maintain acceptable sensory properties, higher substitution levels fail to replicate the desirable qualities provided by oil and egg yolk.
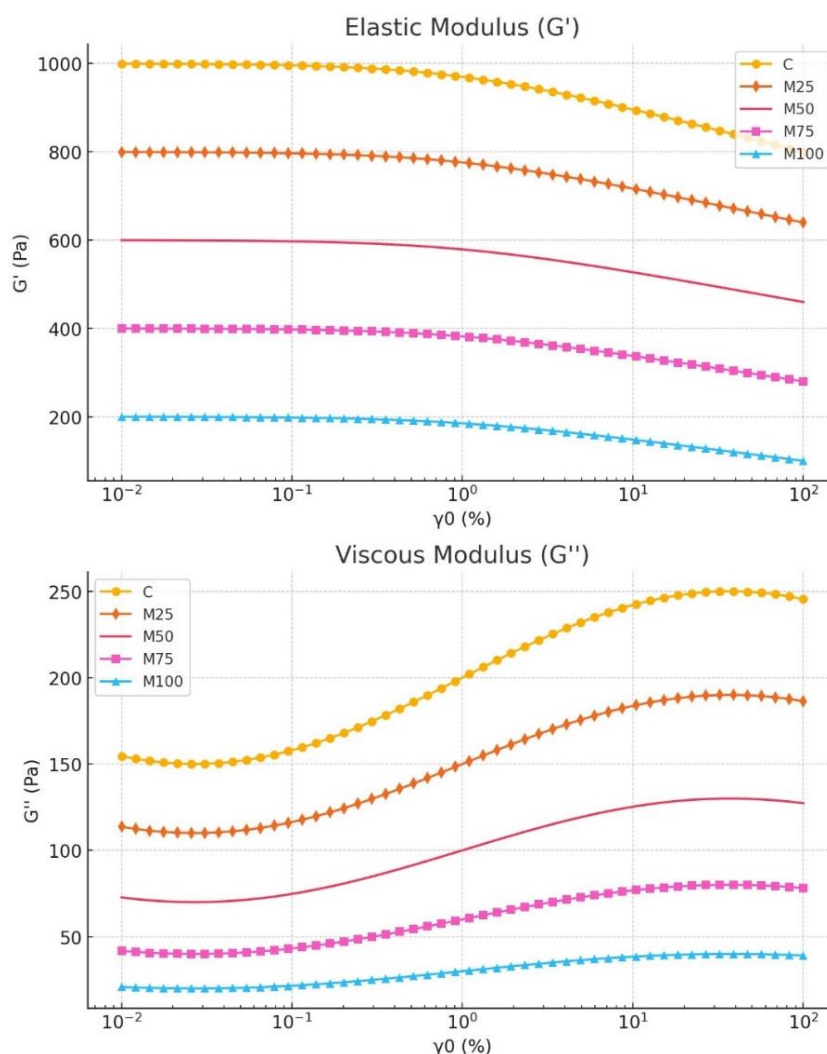

Figure 2. Strain sweep plots of mayonnaise samples as a function of aquafaba substitution levels (0%, 25%, 50%, 75%, and 100%) at 6.28 rad/s. Elastic modulus and viscous modulus are shown as a function of strain (γ_0, %)
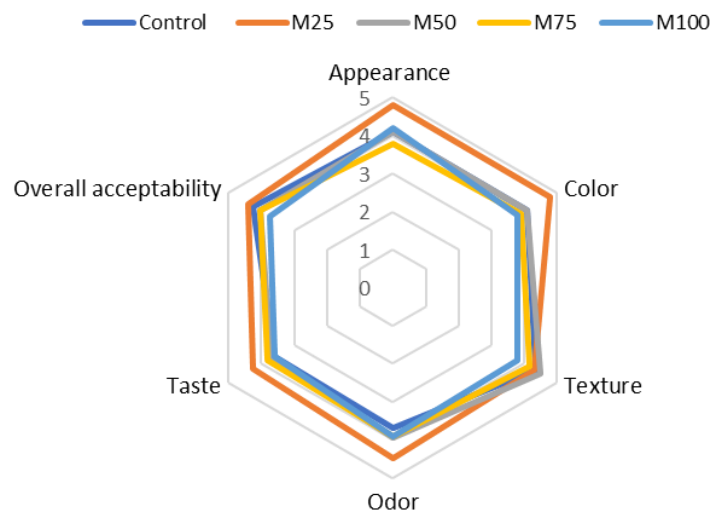

Figure 3. Sensory analysis of prepared mayonnaise samples

4. CONCLUSION

This study demonstrated the potential for producing sustainable, vegan, and calorie-reduced mayonnaise by replacing egg yolk and oil with aquafaba and pectin gel. Aquafaba provided emulsifying properties, while pectin reduced fat content. Higher substitution levels significantly impacted rheological and sensory properties. Rheological analysis showed reduced elastic (G') and viscous moduli (G") at higher substitutions, indicating a weaker structural network. Formulations with up to 75% substitution (M75) retained acceptable stability and texture, but M100 experienced structural breakdown. Sensory analysis identified M25 as the most preferred, maintaining taste, texture, and acceptability similar to the control. Higher substitutions (M75 and M100) resulted in noticeable declines, especially in texture. In conclusion, M25 achieved the best balance of sustainability, sensory quality, and stability, highlighting the need for further optimization at higher substitution levels.

References

[1]   E. Erem, N. C. Icyer, N. B. Tatlisu, M. Kilicli, G. H. Kaderoglu, and O. S. Toker, "A new trend among plant-based food ingredients in food processing technology: Aquafaba," *Crit. Rev. Food Sci. Nutr.*, vol. 63, no. 20, pp. 4467–4484, Aug. 2023.

[2]   V. Raikos, H. Hayes, and H. Ni, "Aquafaba from commercially canned chickpeas as potential egg replacer for the development of vegan mayonnaise: Recipe optimisation and storage stability," *Int. J. food Sci. Technol.*, vol. 55, no. 5, pp. 1935–1942, 2020.

[3]   I. Ozcan, E. Ozyigit, S. Erkoc, S. Tavman, and S. Kumcuoglu, "Investigating the physical and quality characteristics and rheology of mayonnaise containing aquafaba as an egg substitute," *J. Food Eng.*, vol. 344, art. no. 111388, 2023.

[4]   P. Sharma, K. Osama, V. K. Gaur, A. Farooqui, S. Varjani, and K. Younis, "Sustainable utilization of Citrus limetta peel for obtaining pectin and its application in cookies as a fat replacer," *J. Food Sci. Technol.*, vol. 60, no. 3, pp. 975–986, 2023.

[5]   Y. He, V. Meda, M. J. T. Reaney, and R. Mustafa, "Aquafaba, a new plant-based rheological additive for food applications," *Trends food Sci. Technol.*, vol. 111, pp. 27–42, 2021.

[6]   M. Aslan and N. Ertas, "Possibility of using "chickpea aquafaba" as egg replacer in traditional cake formulation," *Journal*, vol. 24, no. 1, pp. 1–8, 2020.

[7]   Y. He, S. K. Purdy, T. J. Tse, B. Tar'an, V. Meda, M. J. T. Reaney, and R. Mustafa, "Standardization of aquafaba production and application in vegan mayonnaise analogs," *Foods*, vol. 10, no. 9, art. no. 1978, 2021.

[8]   J. Lim, S. Ko, and S. Lee, "Use of Yuja (Citrus junos) pectin as a fat replacer in baked foods," *Food Sci. Biotechnol.*, vol. 23, pp. 1837–1841, 2014.

[9]   C. Zheng, W. Huang, Y. Zou, W. Huang, G. Zhang, and P. Fei, "Preparation of amidated pectins through enzymatic method: Structures, hydrogel properties and its application potential in fat substitutes," *Food Res. Int.*, vol. 160, art. no. 111719, 2022.

[10]   A. Ciurzyńska, P. Ciesluk, M. Barwinska, W. Marczak, A. Ordyniak, A. Lenart, and M. Janowicz, "Eating habits and sustainable food production in the development of innovative "healthy" snacks," *Sustainability*, vol. 11, no. 10, p. 2800, 2019.

[11]   UN (2022). *The sustainable development goals (SDGs), United Nations* [Online]. Available: https://sdgs.un.org/goals.

[12]   T. Altug and Y. Elmaci, *Gidalarda Duyusal Degerlendirme*, Meta Basim Matbaacilik, 2005.